Proceedings from the 20th Annual SCMR Scientific Sessions

Washington, DC, USA. February 1-4, 2017

Published: February 1, 2017

C001

The Role of Cardiovascular Magnetic Resonance Imaging in Determining Cardiac Anatomy in Surgical Planning for the Successful Separation of Thoracoomphalophagus Conjoined Twins

Jennifer G. Co-Vu, MD[1]Dhana Rajdershekar, MD[2], Suzanne Mastin, MD[2], Andrew Pitkin, MD[2], Shane Chatfield, RT[2], Saleem Islam, MD[2], Mark Bleiweis, MD[2]

1. *University of Florida, Gainesville, FL*
2. *University of Florida, FL*

Description of Clinical Presentation: A 32-year-old G3P2 female was referred to our center at 22 weeks gestation for fetal evaluation of her conjoined twins. Fetal echocardiography revealed Twin A has D-transposition of great arteries (dTGA) and ventricular septal defect (VSD), and Twin B with normal intracardiac anatomy. There is possible fusion of the right atrium of Twin A and the left atrium of Twin B. Fetal MRI at 23 weeks gestation revealed that portions of the heart, sternum, diaphragm and liver were shared, and bowel loops were commingled. The twins were delivered via elective C-section at 35 5/7 weeks with no complications. After obtaining imaging from multiple modalities including cardiovascular magnetic resonance (CMR), numerous multidisciplinary team meetings were held for preoperative planning. The twins were separated at 2 months of age and intraoperative findings confirmed the CMR findings and the operation was successful. Twins are currently recovering very well postoperatively.

Diagnostic Techniques and Their Most Important Findings: Immediate postnatal imaging, including a transthoracic echocardiogram confirmed the prenatal diagnosis. Due to the twins' position (conjoined facing each other), transthoracic imaging windows were extremely limited. The interatrial connection between the twins was difficult to delineate, including the position of the systemic venous structures of Twin A and the pulmonary venous structures of Twin B in reference to the interatrial connection. It was also difficult to ascertain the cardiac position. Because of diagnostic uncertainty, at 9 days of age, a cardiovascular magnetic resonance (CMR) imaging and magnetic resonance angiography was performed on a Siemens Avanto scanner (Erlangen, Germany) at 1.5 T, under general anesthesia. The findings show Twin A has levocardia, Twin B has dextroposition. Twin A's heart has dTGA with a membranous VSD. Twin B's heart has normal atrioventricular and ventriculoarterial concordance. The right atrium of Twin A is connected to the left atrium of Twin B. There is bilateral superior vena cavae in Twin B. The systemic and pulmonary venous drainage on both babies are separate with no connections. With steady state free precession imaging, it was seen that there were widely patent foramen ovale on both twins. Both twins also have patent ductus arteriosus. There was one pericardial sac shared by both babies with small pericardial effusion. Extracardiac findings include a single diaphragm, a fused liver with asymmetric hepatic vasculature that leads to variable liver parenchyma perfusion with a central watershed zone. The majority of the hepatic artery flow to the liver is supplied by Twin B with diminutive Twin A hepatic artery branches supplying only the liver parenchyma most proximal to the Twin A. There was an asymmetric decreased renal perfusion with delayed excretion in Twin A. The bowel and mesentery of both twins crosses midline.

Learning Points from this Case: CMR is an extremely important imaging modality in thoracoomphalophagus conjoined twins, as it is proven in this case to provide answers when there is diagnostic uncertainty in transthoracic echocardiogram. Transthoracic imaging is extremely difficult in this type of conjoined twins since the babies are facing each other with attachment in the thorax and abdomen, thereby limiting the ability to obtain optimal and diagnostic imaging windows. With CMR, multiplanar imaging and 3D reconstruction and animation were available to better delineate very complex cardiac anatomical structures. With the guidance of the images derived from CMR, patients were positioned in the OR table where the cardiac apices were pointing anterior, and the conjoined atria posterior to the OR table, as deemed optimal by the Cardiothoracic and Pediatric Surgical teams. With the 3-D printed heart, the cardiac structures can be seen better and the surgeons know precisely where to do their incisions, and where to divide the interatrial connection. Extracardiac anatomy was also well seen in the same scan as the CMR, which provided very relevant information in surgical planning. The cardiothoracic and pediatric surgical teams relied heavily on the images from the CMR and CT in preoperative planning for this highly complex surgery, and both played an important role in the success of the separation of this set of conjoined twins.

C002

An Example of the Improved Diagnostic Utility of Black Blood Delayed Enhancement (FIDDLE) in a Patient with Complete Transposition of the Great Arteries

Michael J. Campbell, MD, MHA[1]Stephen Darty, RT-N,MR; BSRS[2], Piers Barker, MD[3], Han Kim, MD[1], Raymond j. Kim, MD[2]

1. Duke University, Durham, NC
2. Duke University Medical Center, NC
3. Duke Cardiovascular Magnetic Resonance Center, Durham, NC

Description of Clinical Presentation: An asymptomatic 13 year old male with complete transposition of the great arteries/intact ventricular septum status post an arterial switch operation presented for a routine biannual CMR exam. His arterial switch operation was performed during infancy at an outside hospital. Two years prior to the current evaluation, he underwent CMR at our institution with traditional delayed enhancement imaging and no hyperenhancement was appreciated (Fig. 1). On the most recent CMR exam a novel black blood delayed enhancement technique (FIDDLE, Flow-Independent Dark blood Delayed Enhancement) was utilized and a sub-endocardial myocardial infarction was noted (Fig 2). The patient underwent cardiac catheterization with coronary angiography. The coronary artery anatomy was circumflex arising from the right coronary artery. Severe proximal right coronary artery stenosis was identified (Fig. 3).

Diagnostic Techniques and Their Most Important Findings: The patient's previous CMR employed SSFP single shot delayed enhancement imaging and hyperenhancement was not appreciated (Fig. 1). On the more recent exam FIDDLE imaging was performed and Figure 2 is a FIDDLE image at an identical slice position to Figure 1. Sub-endocardial hyperenhancement of the inferolateral wall is clearly seen in Figure 2. This would be consistent with right coronary artery pathology in a patient whose circumflex coronary artery arises from the right coronary artery. With the knowledge that the infarct is present, repeat evaluation of Figure 1 reveals some thinning of the inferolateral wall but hyperenhancement is not well appreciated. In retrospect, the infarction was likely present on the previous CMR but was not detected because of the limited sensitivity of traditional delayed enhancement imaging when evaluating sub-endocardial infarctions.

Learning Points from this Case: Coronary artery stenosis can occur as a complication of the arterial switch operation in patients with complete transposition of the great arteries. The CMR evaluation of these patients should include imaging for myocardial infarction. FIDDLE is a novel black blood delayed enhancement technique which has improved sensitivity for the detection sub-endocardial infarctions. This is an excellent illustration of the usefulness of this technique in patients with congenital heart disease.

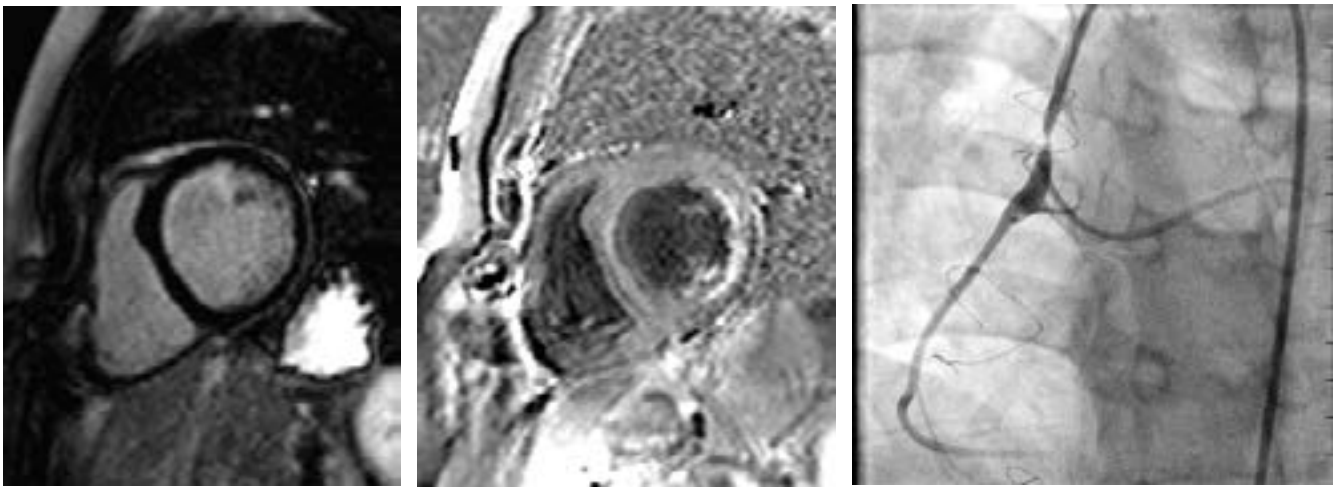

C003

Uhl's Anomaly - Absence of right ventricular myocardium

Bharti Sharma, MD [1]Madhusudan Ganigara, MD [2], Nitin Rao, MD[3], Santosh Uppu, MD[4]

1. STAR Hospitals, Telangana, India
2. Icahn School of Medicine at Mount Sinai, NY
3. Star Hospitals, Hyderabad, Telangana, India
4. The Mount Sinai Hospital, NY

Description of Clinical Presentation: A 4-year old child with no significant family history was referred for cardiac evaluation secondary to failure to thrive, dyspnea on exertion and easy fatigability that was progressive since infancy, and an incidental murmur. Child was underweight, had a quiet precordium and a holosystolic murmur at the left lower sternal border. The electrocardiogram showed sinus rhythm, right axis deviation, enlarged right atrium (RA) and paucity of right ventricular (RV) forces in the precordial leads. Chest X-ray showed moderate cardiomegaly with right atrial enlargement. Echocardiography demonstrated marked dilation of the right cardiac chambers. Tricuspid valve was normal without leaflet displacement but with severe low pressure regurgitation. Right ventricular systolic function was severely impaired.

Diagnostic Techniques and Their Most Important Findings: Cardiac MRI was performed to further evaluate, it showed severely dilated RA, thin walled, dilated and akinetic RV with absent trabeculations, and normal left ventricular size and function. Continuous antegrade flow was noted across the pulmonary artery with biphasic pattern. Late Gadolinium enhancement showed near complete absence of RV myocardium with some areas of preserved muscle in the basal anteroinferior regions (Figure 1). These findings along with absence of fibro-fatty infiltration within the myocardium suggested Uhl's anomaly. Single ventricle palliation by excluding right ventricle and creation of a bidirectional Glenn was considered but not performed due to unclear prognosis. The child was started on oral aspirin and is being followed clinically.

Learning Points from this Case: Uhl's anomaly is an extremely rare congenital cardiac disorder with complete/near complete absence of RV free wall myocardium. It is believed to be caused by selective but unrestrained apoptosis of the RV myocytes after complete cardiac development. Arrhythmogenic RV dysplasia is a differential diagnosis and has to be excluded in order to make this diagnosis. Cardiac MRI helps by evaluating the myocardium and characterizing the tissue

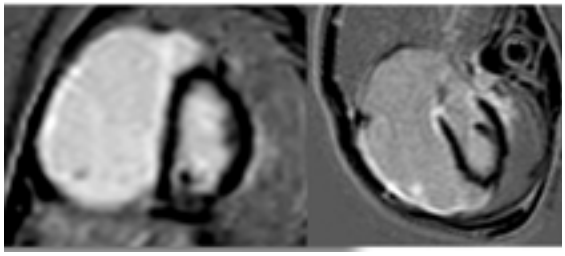

C004

Scimitar syndrome: An unnatural history of a baffling baffle

Anuj Pareek, Medical Doctor[1] Rebecca Beroukhim, MD[2], Sunil Ghelani, MD, MBBS[3], Puja Banka, MD[4]

1. Aarhus University Hospital, Aarhus C, Midtjylland, Denmark
2. Harvard Medical School and Massachusetts General Hospital, Boston, MA
3. Boston Children's Hospital, Boston, MA
4. Boston Children's Hospital, MA

Description of Clinical Presentation: A 12-year-old girl with Scimitar syndrome had previously undergone coil embolization of a large aortopulmonary collateral to the right lung at the age of 2 months and surgical repair with baffling of the Scimitar vein to the left atrium at the age of 4 years. She was referred for cardiovascular MRI (CMR) evaluation as part of a routine surveillance. At the time of referral she was asymptomatic with echocardiographic findings notable for mild tricuspid regurgitation with low right ventricular pressures. The pulmonary venous baffle could not be well visualized.

Diagnostic Techniques and Their Most Important Findings: A comprehensive CMR examination including steady-state free precession cine imaging, gadolinium-enhanced angiography, and phase-contrast velocity mapping was performed. The examination revealed that the hepatic veins drained appropriately to the right atrium (RA), but the inferior vena cava (IVC) was incorporated into the Scimitar vein baffle and connected to the left atrium (LA). There was severe narrowing of the baffle and an extensive network of intrahepatic dilated venous channels allowing the IVC and Scimitar vein to decompress through the liver to the RA. This resulted in a small net left-to-right shunt with a Qp:Qs of 1.1. There was moderate tricuspid regurgitation with a regurgitant fraction of 26%. The right ventricle (RV) was mildly dilated with an indexed end-diastolic volume of 110 ml/m2 (z-score 2.6) and normal function. Left ventricular size and function were normal.

Patient was lost to follow-up and returned nearly 6 years later for a clinical evaluation. In the interim she had remained asymptomatic with a stable echocardiogram and low right ventricular pressures. Follow-up CMR examination showed worsening baffle obstruction but the remaining findings remained largely unchanged with a Qp:Qs of 1.2, 20% tricuspid regurgitation, and a mildly dilated RV (116 ml/m2, z-score 3). Of the MPA flow, 52% was noted to drain via the Scimitar vein.

Learning Points from this Case: This case demonstrates the utility of CMR in post-operative assessment of congenital heart disease, especially in the setting of restricted echocardiographic windows. It also highlights the strength of CMR in noninvasive assessment and longitudinal follow-up of the physiology and hemodynamic burden of residual lesions. CMR may also be helpful in pre-operative three-dimensional assessment of complex vascular anatomy such as Scimitar syndrome to help guide placement of complex baffles.

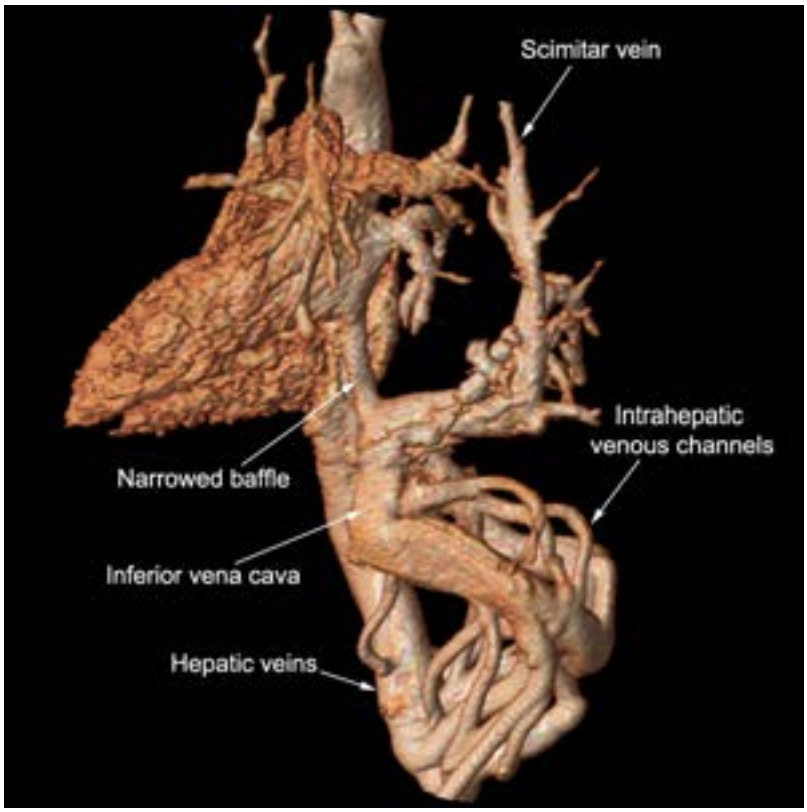

C005

Three atrioventricular valves? Three is too much!

Deepa Prasad, MBBS MD[1] Ashwin Prakash, M.D.[2]

1. Boston Children's Hospital, Boton, MA
2. Boston Children's Hospital, Boston, MA

Description of Clinical Presentation: A 14 month old male from Southeast Asia, with a presumed diagnosis of double inlet left ventricle, hypoplastic right ventricle (RV), D-looped transposition of great arteries, large ventricular septal defect (VSD), overriding tricuspid valve and valvar pulmonic stenosis, was referred to our institution for possible biventricular repair. He had not undergone any surgeries and was offered single ventricle palliation at the outside institution. Upon arrival to our institution, he was cyanotic with baseline saturations of 80-85% in room air.

Diagnostic Techniques and Their Most Important Findings: He underwent echocardiogram, cardiac catheterization and MRI for evaluation of suitability of biventricular repair. Echocardiogram showed unusual atrioventricular valve morphology, possibly consisting of 3 separate valve orifices. Cardiac MRI revealed atrial situs solitus, atrioventricular concordance, D-looped good sized ventricles, double outlet right ventricle, mildly stenotic bicuspid pulmonary valve, right pulmonary artery hypoplasia, bilateral SVC, a large VSD that involved both atrioventricular and conoventricular components (Figures 1 and 2). Both atrioventricular valves straddled the interventricular septum. The tricuspid valve straddled through the atrioventricular canal component of VSD, with most of the flow directed to the LV. Mitral valve also straddled through the conoventricular component of the VSD with chordal attachments to the RV free wall. Mitral inflow was predominantly directed to the LV. LV was mildly dilated and RV was normal in size with indexed end diastolic volume of 104 ml/m2 and 62 ml/m2 respectively. Biventricular function was normal.

Learning Points from this Case: This was a complex case of bilateral straddling atrioventricular valves, large VSD and double outlet right ventricle, which was felt to be unsuitable for biventricular repair at the outside institution. Based on the comprehensive multimodality imaging, we determined that a staged biventricular repair was feasible. He subsequently underwent first staged repair, consisting of bilateral bidirectional Glenn, arterial switch, resection of the atrial septum and partitioning of atrium with autologous pericardium leaving the right sided portion of the tricuspid valve to receive the IVC blood and the left sided portion of the tricuspid valve along with the mitral valve to receive the pulmonary venous blood, and pulmonary artery banding. His post-operative course was unremarkable and he is currently doing well. The next staged surgical repair is anticipated in 1 year. This case illustrates the usefulness of CMR and multimodality imaging in surgical planning and decision making regarding staged palliation vs. biventricular pathway.

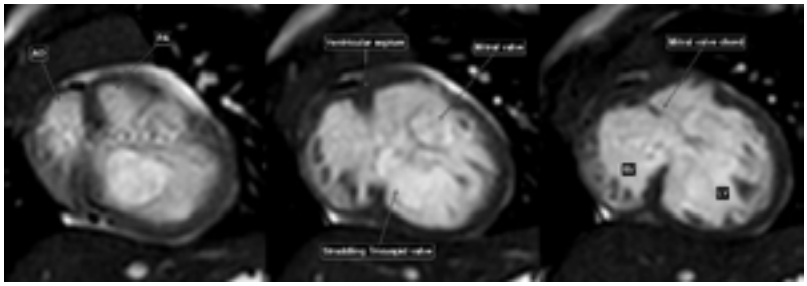

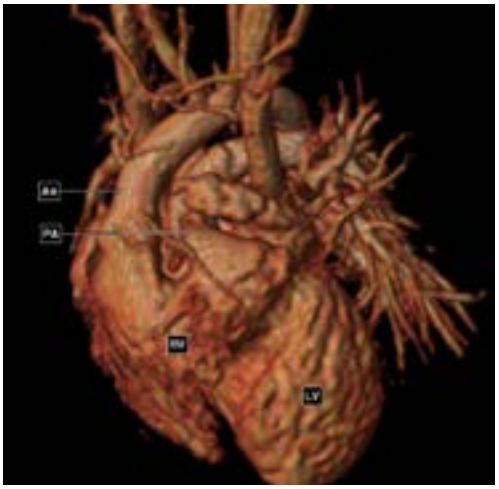

C006

Noninvasive Diagnosis of Coronary-cameral Fistula in a child with Tricuspid and Pulmonary atresia: Advantages of Gadofosveset-enhanced MRI

Nam Ju Lee, MD, MMS[1] Harold Litt, MD-PhD[2], Matthew A. Harris, MD[3]

1. *Johns Hopkins School of Medicine, Baltimore, MD*
2. *Perelman School of Medicine of the University of Pennsylvania, Philadelphia, PA*
3. *Children's Hospital of Philadelphia, Perelman School of Medicine of the University of Pennsylvania, Philadelphia, PA*

Description of Clinical Presentation: A 6-year-old boy with tricuspid and pulmonary atresia had underwent Blalock-Taussing shunt placement along with left pulmonary artery patch arterioplasty and duct ligation right after birth, bilateral bidirectional Glenn at age of 7 months, and extracardiac nonfenestrated Fontan procedure at age of 3 years.

On cardiovascular exam, he had a quiet precordium with a normal apical impulse and a regular rhythm on auscultation. He has a single S1 and a single S2. No clicks, gallops, or rubs were noted. He had a grade 3/6, holosystolic, almost continuous murmur in the left upper sternal border or mid sternal border and also a 2/4, diastolic murmur in the same region, which radiates all over his chest. Baseline ECG demonstrated normal sinus at a rate of 70 bpm with right ventricular hypertrophy.
The patient underwent cardiac MRI for post surgery functional and anatomical evaluation.

Diagnostic Techniques and Their Most Important Findings: At cardiac MRI, a functional single ventricle was noted in the form of pulmonary atresia with intact ventricular septum and severe tricuspid valve hypoplasia. There was severe right ventricular hypertrophy with a diminutive RV cavity. Single ventricular function was within normal range. There was mild central and proximal LPA stenosis with moderate systemic to pulmonary collateral flow (Qp/Qs: 0.9).A 3D Navigator-gated, inversion recovery, FLASH (Nav_IR_Flash) sequence following Time Resolved Imaging with Stochastic Trajectories (TWIST) was performed after injection of 0.12 ml/kg Gadofevoset at a flow rate of 1.5 ml/sec (TR 309.8ms, TE 1.6ms, TI 260ms, BW 496 Hz, FA 18 degrees, TT 600ms) followed by a sterile saline flush of 1 ml/kg. There was aneurysmal dilation of the left coronary artery, measuring up to 9 mm, which was emptying into the proximal right ventricle. The right coronary artery had a fistulous connection to the right ventricle distally. These findings had been previously demonstrated at preoperative cardiac catheterization, however, no intervention was undertaken as it was considered high risk.

Learning Points from this Case: MRI has been limited in its clinical application in infants or young children because of fast heart rates, small vessel size, and respiratory motion. However, Gadofosveset (Ablavar) is an intravascular contrast agent, providing extended intravascular enhancement compared to traditional extracellular MR contrast agents. This allows comprehensive evaluation of CHD by providing simultaneous visualization of the coronary arteries, great vessels, and heart without confounding background contrast enhancement or radiation exposure. The safety and tolerability of Gadofosveset and its accuracy for evaluation of vascular disease have been established by multiple studies.

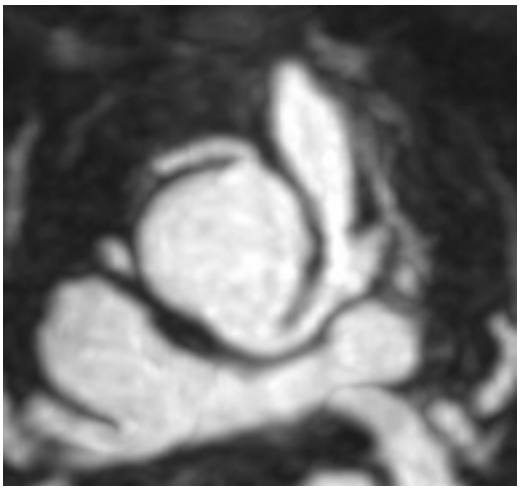

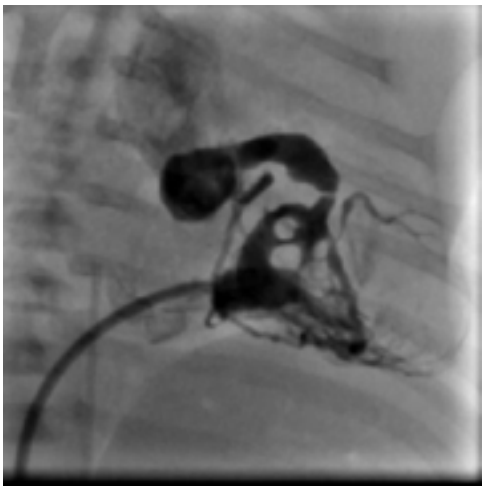

C007

LPA sling with aberrant right subclavian artery- A rare vascular anomaly

Madhusudan Ganigara, MD [1]James Starc, MD[2], Simon Lee, MD[3], Anas Abdul Kayoum, MD[1], James Nielsen, MD[4], Santosh Uppu, MD[5]

1. Icahn School of Medicine at Mount Sinai, NY
2. The Mount Sinai Hospital, New York, NY
3. Northwestern University Feinberg School of Medicine, IL
4. Stony Brook Medicine, New York, NY
5. The Mount Sinai Hospital, NY

Description of Clinical Presentation: Four month-old boy presented with inspiratory stridor noted since birth. He had multiple presentations to the emergency department that were managed as possible laryngomalacia with gastroesophageal reflux disease. He gradually dropped off his growth curve over 2 months. There were no gastrointestinal (GI) symptoms or cyanosis. On exam he was noted to have an inspiratory stridor with minimal tachypnea. Evaluation with upper GI series showed a persistent extrinsic compression defect only at the posterior and left lateral margin of the upper esophagus. Esophagoscopy was performed later that confirmed the previously described posterior compression, bronchoscopy showed minimal compression of the bilateral proximal bronchi.

Diagnostic Techniques and Their Most Important Findings: Magnetic resonance angiography was then performed to evaluate for possible vascular anomalies. It revealed a left pulmonary artery (LPA) sling and left aortic arch with an aberrant right subclavian artery coursing posterior to the esophagus. The LPA originates from the posterior aspect of the right pulmonary artery and then courses between the trachea and esophagus. Echocardiogram showed normal intracardiac anatomy. The LPA was surgically divided and reimplanted to the main pulmonary artery and the aberrant right subclavian artery was reimplanted to the distal ascending aorta via median sternotomy. The child had an uneventful postoperative course. At follow up 8 months later, child remains asymptomatic and is following his expected growth curve.

Learning Points from this Case: Left pulmonary artery sling along with the aberrant right subclavian artery is a very rare combination, LPA sling is caused when the proximal part of the left sixth arch regresses or fails to develop its normal connections to the left lung bud and instead a collateral vessel to left lung develops. Children presenting with airway symptoms in early infancy can mimic variety of common conditions including bronchiolitis, laryngomalacia and gastroesophageal reflux disease. A high index of suspicion is required to suspect multiple coexisting vascular anomalies; routine upper GI imaging may not be adequate to recognize this combination especially when the anterior esophageal indentation is not seen as in our case and the posterior esophageal indentation was a red herring. Magnetic resonance angiography is an ideal tool to evaluate suspected vascular anomalies.

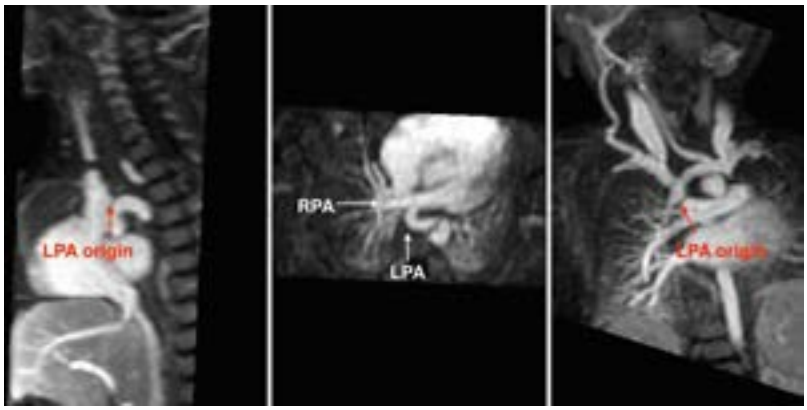

C008

Infected Myocardial Calcific Deposit: Value of Multimodality Imaging

Rajesh Janardhanan, MD, FACC[1] Preethi William, MD[2], Bijin Thajudeen, MD[2]

1. Banner University Medical Center, Tucson, Tucson, AZ
2. Banner University Medical Center, Tucson, AZ

Description of Clinical Presentation: A 55-year-old male with prior renal transplant, ESRD on hemodialysis, anemia of chronic disease, biventricular dysfunction (EF of 25%) presented with septic shock. Laboratory tests showed leukocytosis. The alkaline phosphatase and parathormone levels were significantly elevated. Blood culture grew methicillin-resistant *Staphylococcus aureus*.

Diagnostic Techniques and Their Most Important Findings: A transthoracic echo revealed a highly mobile, bright mass in the left atrium **[Figure 1]**. A real-time 3D transesophageal echocardiogram (RT-3DTEE) showed a large 2.2 cm x 1.2 cm bright, highly mobile echo density attached to the muscular ridge separating the left atrial appendage and left superior pulmonary vein **[Figure 2]**. Cardiac MRI demonstrated low signal intensity on T1 and T2 weighting **[Figure 3]** suggesting the mass likely to be a myocardial calcific deposit. Since patient was deemed a high-risk surgical candidate, the mass was treated conservatively with 6 weeks of intravenous antibiotics. Aggressive attempts to normalize the bone mineral metabolism disorder were also undertaken.

Learning Points from this Case: In our patient with septicaemia and a mobile mass on transthoracic echo, infective endocarditis was the primary concern. RT-3DTEE confirmed the presence of the mass adjacent to the left atrial appendage, but was unable to provide further tissue characterization. Cardiac MRI confirmed it to be a myocardial calcific deposit. There was most likely superadded infection in this patient with septic shock

The calcification in the left atrium is likely secondary to dystrophic calcification. At the same time, the elevated serum alkaline phosphatase and parathyroid hormone concentrations suggest altered bone mineral metabolism which act as promoter of metastatic calcification. Calcium deposition often involves the valves, left ventricular free wall, septum as well as the left atrial appendage. Presence of these calcified lesions can result in turbulent blood flow inducing endothelial injury, which can act as a nidus for development of thrombosis or infective endocarditis. Management decisions of these calcific lesions depend on history, size & location of mass, obstructive or non-obstructive, embolic potential, systemic or constitutional symptoms and surgical risk profile.

We present an unusual case of dystrophic as well as metastatic calcification involving the left atrium in an ESRD patient who developed superimposed infective endocarditis. Multimodality imaging, especially cardiac MRI was helpful in the accurate diagnosis and management in our patient with an infected myocardial calcific deposit. Attempts to normalize the bone mineral metabolism disorder in ESRD patients is prudent to control pathological ectopic bio-mineralization.

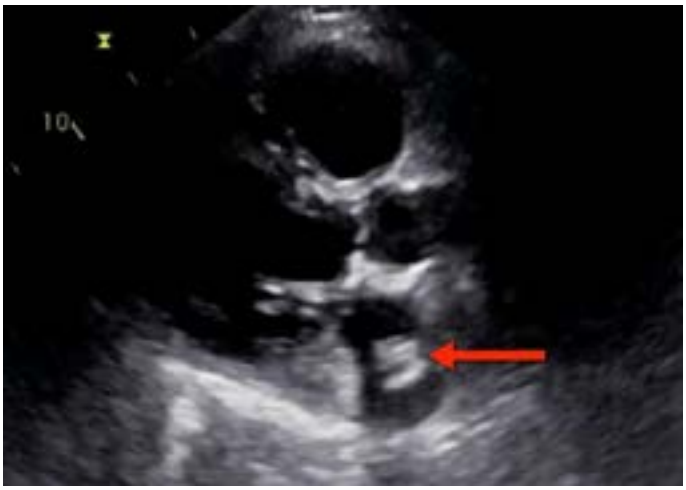

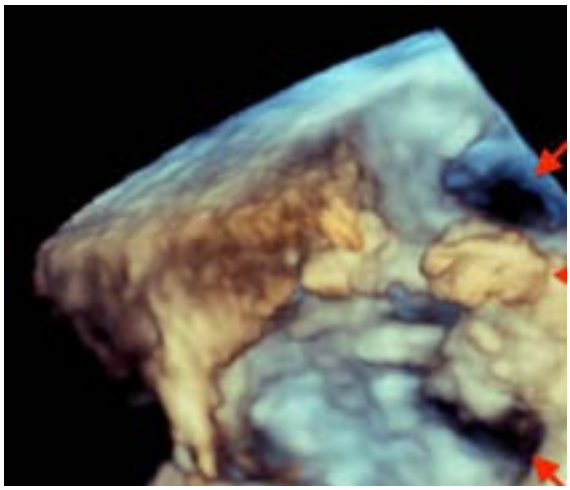

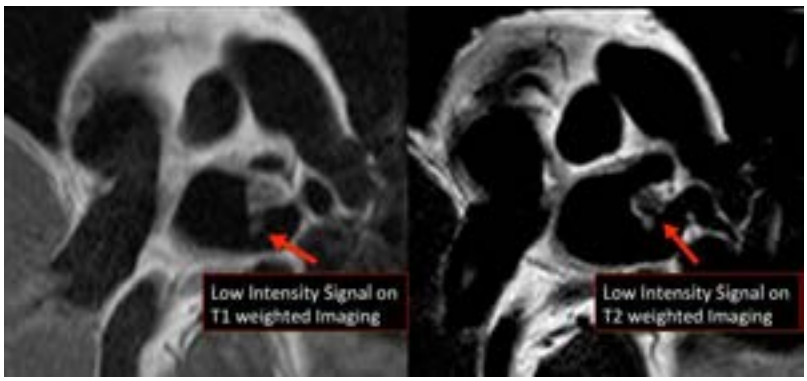

C009

A complex phenomenon or plain bad luck - viral myocarditis in Becker's muscular dystrophy

Shivani G. Patel, MBBS[1], Howard Hsu, MD[2]

1. Boston Children's Hospital, Chicago, IL
2. University of Nebraska Medical Center, Omaha, NE

Description of Clinical Presentation: A 12 year old boy with known Becker's muscular dystrophy presented with sudden history of sharp chest pain, shortness of breath, bilateral arm pain and tingling. He did not have any history of recent illnesses. An electrocardiogram showed marked elevation of ST segments in the lateral leads and a troponin I level that was extremely elevated at 35 which subsequently increased to 70 in the next 24 hours. His baseline cardiac function was known to be within normal limits by prior echocardiograms. His only medication was Enalapril for cardiac remodeling.

Diagnostic Techniques and Their Most Important Findings: An echocardiogram showed normal left ventricular systolic function and no evidence of regional wall motion abnormalities. A cardiac magnetic resonance (CMR) examination was performed to evaluate coronary anatomy and evidence of ischemia. It showed a significant diffuse, subepicardial hyperenhancement of the entire lateral wall extending into the mid and apical anterior and inferior walls. The left ventricle was normal in size and shape, with severely depressed systolic function (ejection fraction 29%) and regional wall motion abnormalities matching the distribution of the delayed hyperenhancement. The right ventricle was normal in size with borderline reduced systolic function (RVEF 38%). There was no evidence of ischemic myocardial damage or anomalous coronary anatomy. Over the next 3 days, the ST segment changes resolved and his troponin level decreased to baseline. Repeat echocardiography was essentially unchanged from that at admission. He was discharged home on Enalapril. Coxsackie B3 antibody was noted to be elevated to 1:320 with normal being 1:10. A repeat CMR exam in about 2 months showed significant improvement in the left ventricular function and resolution of the late gadolinium enhancement seen on the prior exam.

Learning Points from this Case: The clinical findings of ischemia with chest pain, ST segment and troponin elevation were a diagnostic dilemma in a child with underlying Becker's muscular dystrophy. The CMR finding of subepicardial delayed hyperenhancement was fundamental in ruling out an ischemic cause of the cardiomyopathy, given the subendocardial sparing and presence of normal coronary anatomy. This diagnostic CMR prevented further invasive investigation in the form of a cardiac catheterization. Also, the lack of delayed hyperenhancement on a follow up CMR was vital in eliminating muscular dystrophy and pinpointing viral myocarditis as a cause of his transient cardiomyopathy**.**

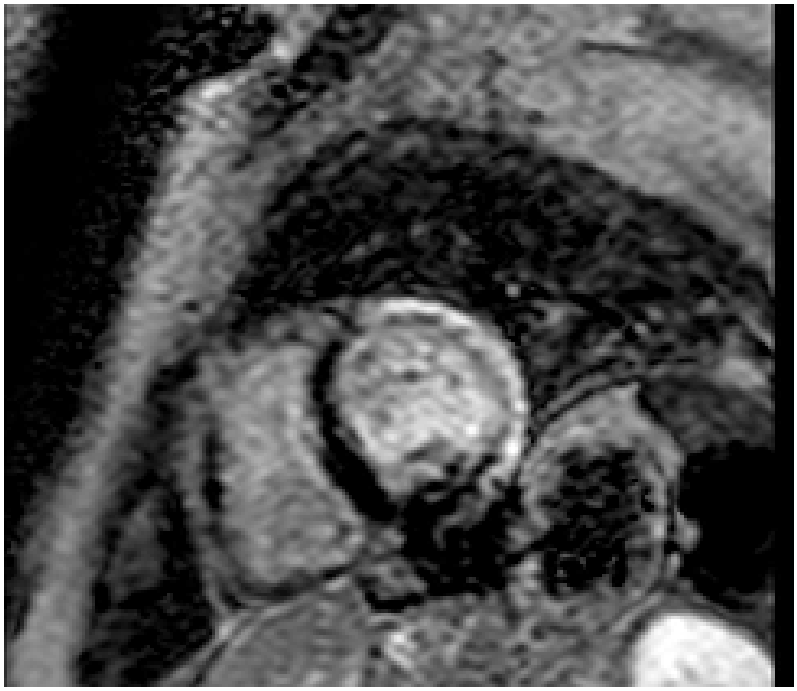

C010

A Case of Adhesive Mediastinopericarditis post Orthotopic Cardiac Transplant

Syed R. Latif, MD[1] Chirag A. Shah, MD[2], Demetrius Dicks, MD[3], David J. Hur, M.D.[4], Steffen Huber, M.D.[5], Judith L. Meadows, MD[6], Isabel Oliva, MD[7], Hamid Mojibian, M.D.[5], Pramod Bonde, MD FACS[6], Lauren A. Baldassarre, MD[5]

1. *Yale University, Hamden, CT*
2. *Yale-New Haven Hospital, Hamden, CT*
3. *Yale University School of Medicine, NEW HAVEN, CT*
4. *Yale School of Medicine, New Haven, CT*
5. *Yale University, CT*
6. *Yale School of Medicine, CT*
7. *YALE UNIVERSITY, MADISON, CT*

Description of Clinical Presentation: A 59 year-old female with a history of a non-ischemic cardiomyopathy status post orthotopic cardiac transplantation twenty years prior presented for cardiac magnetic resonance (CMR) imaging for evaluation of heart failure symptoms with preserved left ventricular (LV) ejection fraction. Her past medical history was also significant for coronary artery disease status post recent drug-eluting stent to the left anterior descending artery and significant left and right sided heart failure symptoms for which she was hospitalized multiple times over the past year. Her chest x-ray and computed tomography scan demonstrated a calcified pericardium and echocardiography showed biatrial enlargement, preserved LV systolic function and mildly decreased right ventricular function. CMR was obtained at that time which showed a thickened and enhanced pericardium, pericardial adhesions, and ventricular interdependence consistent with constrictive cardiomyopathy (Images 1 and 2). Constrictive physiology was subsequently confirmed via cardiac catheterization. The patient then underwent pericardiectomy. Intraoperative video demonstrated immediate improvement of cardiac function upon release of pericardial adhesions. Gross pathology was also consistent with thickened and fibrotic pericardium. The patient demonstrated improvement of her hemodynamics post operatively and subsequent repeat CMR at that time no longer demonstrated evidence of constrictive physiology.

Diagnostic Techniques and Their Most Important Findings: CMR imaging was performed on a 1.5-Tesla clinical scanner (Aera, Siemens Healthcare, Erlangen, Germany). The pre-operative CMR included cine SSFP, tagging, and delayed enhancement which demonstrated pericardial thickening, adhesions to the chest wall and diaphragm, and pericardial enhancement. Additionally, real time cine imaging with deep inspiratory maneuver demonstrated flattening of the septum consistent with ventricular interdependence. Overall, these findings were consistent with constrictive cardiomyopathy and adhesive mediastinopericarditis. A limited post-operative CMR was performed without contrast and included cine SSFP, tagging, and real time cine imaging which did not show evidence of constrictive physiology.

Learning Points from this Case: Adhesive mediastinopericarditis is a subset of constrictive pericarditis that is attributed to the development of adhesions between not only the visceral and parietal pericardium but also adhesions to surrounding intrathoracic structures such as the chest wall, diaphragm, and lungs. This case demonstrates the value of CMR for visualization of the entire pericardium and surrounding structures and for pre-operative planning for pericardiectomy as well as post-operative assessment.

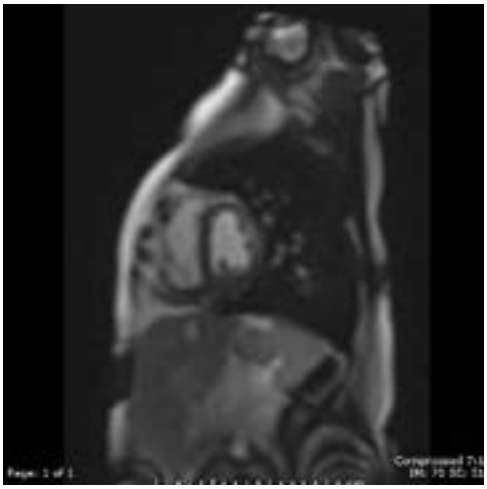

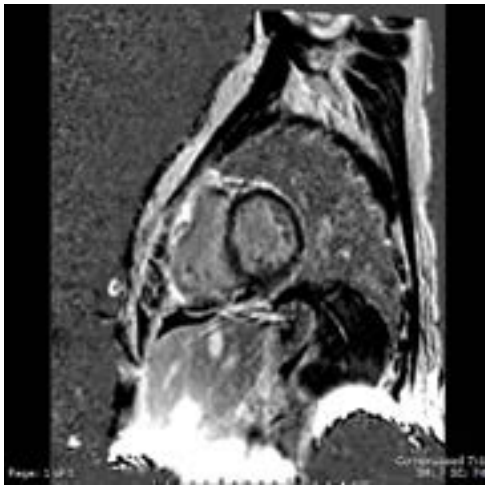

C011

Löffler Endocarditis: Multimodality Imaging Approach (Case Review with Histopathologic Correlation)

Harold Goerne[1]Sachin Saboo[2], Prabhakar Rajiah[2], Shirley Yan, M.D.[2], Ronald Peshock[2], Suhny Abbara[2]

1. UT Southwestern Medical Center, Dallas, TX
2. UT Southwestern Medical Center, TX

Description of Clinical Presentation:

- 57-year-old Vietnamese woman with persistent asthma for 5-6 years and urticaria.
- She presented to emergency department with shortness of breath and constant chest tightness for past 5 days.
- She has long standing hypereosinophilia.

Diagnostic Techniques and Their Most Important Findings:

- Transthoracic echocardiogram (TTE) revealed apical LV wall thickening concerning for Apical Hypertrophic Cardiomyopathy. Diffusely increased endocardial echogenicity in mid and apical LV wall was seen.
- Cardiac Catheterization revealed severely elevated left heart filling pressure and non-obstructive coronary artery disease with minimal stenosis in proximal LAD (20%) and proximal CX (20%) and mild stenosis in mid LAD (40%).
- Cardiac Magnetic Resonance Imaging (MRI) images revealed diffuse thickening with three-layered LV wall configuration (normal myocardium, inflamed endocardium, and laminar thrombus), endocardial delayed enhancement and LV apical arrowhead configuration. Normal LVEF 65%, mildly depressed RVEF 41%, restrictive LV pattern, shortening of the rapid early filing phase of LV with Peak Filling Rate 224 ml/s, absent left atrial kick, severe reduced left ventricle longitudinal shortening was seen.
- Non-gated Contrast Chest Computed Tomography (CT) performed for evaluation of RV perforation complication during catheterization revealed diffuse myocardial thickening with mid and apical LV predominance and low attenuation in subendocardial myocardium which can be seen with combination edema and cardiac pulsation artifact.
- Histopathology study reported inflamed fibrous tissue, likely endocardial tissue reveals numerous eosinophils, lymphocytes, plasma cells and rare neutrophils identified. No myocytes are identified within this tissue fragment. A small fragment of unremarkable adipose tissue is also noted. The morphologic findings are consistent with eosinophilic endomyocarditis (Loeffler endocarditis).

Learning Points from this Case:

- The challenge of TTE in few cases is the difficult to distinguish between tissues, like in this case Apical Hypertrophic Cardiomyopathy from Hypereosinophilic (Löffler) Endocarditis.
- MRI provides pathognomonic features for this condition and is turning into reference standard for non-invasively confirm the diagnosis, assess ventricular functions (both systolic and diastolic), and provide excellent delineation of the layers (normal myocardium, abnormal inflamed endocardium, laminar thrombus, blood pool) with good spatial and temporal resolution.
- Non-gated chest CT can be limited in assessment of subendocardial inflammatory process besides its limitation in evaluation of small laminar LV thrombus in current case and measurement of myocardial and endocardial thickness.
- Histopathology confirmed the diagnosis revealed by MRI.

http://www.ConferenceAbstracts.com/uploads/cfp2/attachments/LDFAIBDN/LDFAIBDN--218726-1-ANY.pdf

http://www.ConferenceAbstracts.com/uploads/cfp2/attachments/LDFAIBDN/LDFAIBDN--218726-2-ANY.pdf

http://www.ConferenceAbstracts.com/uploads/cfp2/attachments/LDFAIBDN/LDFAIBDN--218726-3-ANY.pdf

C012

49 Year-Old Congolese Man with Myocardial Cysts

Daniel W. Groves, MD[1] Tendoh Timoh, MD[1], Evan A. Nelson, MD[2], Marcus Y. Chen, MD[2], Amy D. Klion, MD[3], Andrew E. Arai, MD[2]

1. National Heart, Lung and Blood Institute, National Institutes of Health, MD
2. National Heart, Lung and Blood Institute, National Institutes of Health, Bethesda, MD
3. National Institute of Allergy and Infectious Diseases, National Institutes of Health, Bethesda, MD

Description of Clinical Presentation: A 49 year-old man with a history of hypertension and myocardial cysts was referred for evaluation for possible filarial infection. He was born in the Republic of the Congo, but he fled the country during the Civil War. He settled in an abandoned refugee camp in the Democratic Republic of the Congo (DRC), where he lived for 13 years in rudimentary conditions, taking care of sheep and goats, until being relocated to the United States. Chest radiography performed in DRC as part of tuberculosis screening revealed an enlarged cardiac silhouette. Cardiac imaging on arrival in the United States demonstrated multiple myocardial cysts and reduced left ventricular systolic function. At the time of the referral, he denied chest discomfort, shortness of breath, or peripheral edema.

Diagnostic Techniques and Their Most Important Findings: Electrocardiogram showed sinus rhythm, first-degree atrioventricular block, nonspecific interventricular conduction delay, and left ventricular hypertrophy. Echocardiogram demonstrated a complicated cystic structure in the anteroseptal wall with calcified regions noted within this lesion. This large cystic region did fill with echocardiographic contrast but a blood supply was not identified. On cardiac MRI, the left ventricle was mildly dilated with moderately reduced left ventricular systolic function (LVEF 37%). There were three large cystic cavities in the basal-to-mid anteroseptal and anterior wall which were in continuity with each other. Two of the cysts had characteristics similar to blood while the middle cyst had a significantly shorter T1 time indicating that it may be partially filled with thrombus. Velocity-encoded phase contrast imaging demonstrated that the most basal cyst filled directly from the aortic root during diastole. On first-pass perfusion imaging, the cysts enhanced 1-2 heart beats after arrival of contrast in the aortic root. The cystic structures appeared encapsulated, and the capsule enhanced on late gadolinium enhancement imaging. A cardiac CT performed following MRI demonstrated calcification of portions of the cyst capsule and a communication between the left Sinus of Valsalva and the most basal cyst. Given the cystic appearance of the lesion with calcifications and the significant exposure history, the patient was diagnosed with cardiac echinococcosis.

Learning Points from this Case:

1. Isolated cardiac echinococcosis is extremely rare but has been reported in the literature.
2. Careful inspection of the aortic root with velocity-encoded phase contrast imaging demonstrated diastolic blood flow from the sinus of Valsalva into the most basal cyst in the anteroseptal and anterior wall. Flow during systole may not be present due to either a high pressure within the cyst during myocardial contraction or closure of the communication by an aortic valve leaflet.
3. First-pass perfusion imaging confirmed a communication from the blood pool to the myocardial cysts as the cysts brighten shortly after the left ventricle and aorta.

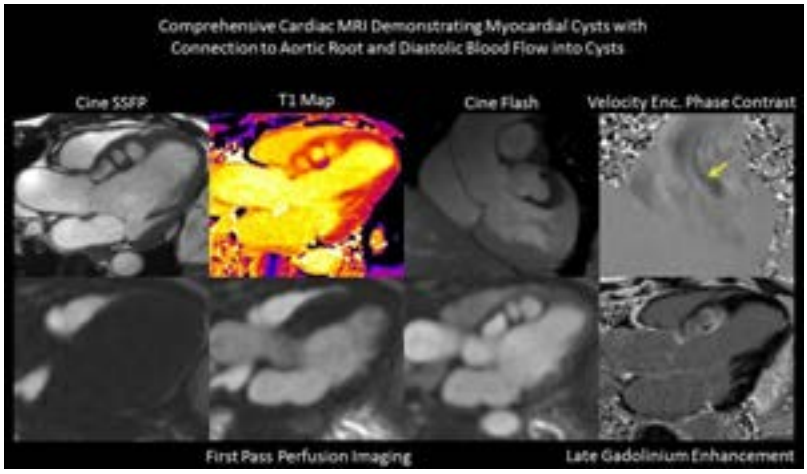

C013

Clinical Applications of CMR in Rheumatic Cardiomyopathy, When Myocardial Fibrosis Matters.

Lilia M. Sierra-Galan, MD[1] Angel L. Alberto-Delgado, MD[2], Ana-Camila Flores-Ventura, MD[3]

1. *American British Cowdray Medical Center, Mexico City, Distrito Federal, Mexico*
2. *Central Military Hospital, Mexico, City, Distrito Federal, Mexico*
3. *Hospital de Diagnóstico. Clínica de Radiología BMP., San Salvador, San Salvador, El Salvador*

Description of Clinical Presentation: A 57-years-old woman with previous history of systemic hypertension, diabetes mellitus type 2, and mitral valve disease; arrived to our Institution due to a reduction in NYHA functional class and effort-related chest pain. A series of diagnostic test were performed and surgical valvular replacement was proposed to the patient which done succesfully, the native valves and biopsies of different sites of the left atrium and the left ventricle were sent to Pathology Department and the patient was discharged from the Hospital in excellent clinical conditions.

Diagnostic Techniques and Their Most Important Findings: An EKG in the ER showed normal sinus rhythm, heart rate of 75 bpm (figure 1). The echocardiogram performed showed LV concentric hypertrophy, normal global and regional wall motion, LVEF 61%, normal RV size and function, and moderate left atrium enlargement, LAVI 47cc/$m^2$and mildly enlargement right atrium, no thrombus were noted. Cusps and tendinae chordae of the mitral valve were calcified and thickened, with domed opening and moderate mitral regurgitation. A tricuspid thickened aortic valve with free edge cusps and normal opening but with moderate aortic regurgitation. Normal appearance of tricuspid valve with moderate regurgitation. A normal opening pulmonic valve with moderate regurgitation. PSAP of 42 mmHg (Figure 2). An invasive coronary angiography showed a non-significant ostial lesion in a posterolateral branch, the rest of the coronary arteries were normal; and the invasive PSAP was 63/24 (39) mmHg and PCP of 10mmHg (Figure 3). CMR showed normal global and regional LV function with mildly reduced RV global function with no regional wall motion abnormalities, LA was moderately to severely enlarge with no thrombus, mild biventricular hypertrophy, severe mitral stenosis with an area of 0.55 mm^2 and gradient of 17 mmHg, a regurgitant orifice of 15.7 mm^2 which causes moderate regurgitation. A tricuspid aortic valve mildly thickened and normal opening with a regurgitant orifice of 8.5 mm^2 which causes moderate to severe regurgitation. Pulmonary artery hypertension of non-quantify severity. A non-ischemic LGE pattern was noted. (Figure 4: A-J). Myocardial biopsy showing extensive myocardial fibrosis in the sites identified by LGE - CMR (Figure 4: K).

Learning Points from this Case: CMR allows better assessment of valvular diseases when multiple valves are involved and the patho-physiology includes mechanisms, stenosis and regurgitation, it also demonstrates more accurately the possible ethiology of the valvular disease thru the clear visualization of the valve and the measurements by planimetry independent of mathematical models to assume them. Tissue characterization unique properties of CMR have the advantage of showing the presence, pattern, location and magnitude of myocardial fibrosis, which provides important prognostic information to guide the proper treatment of the patient.

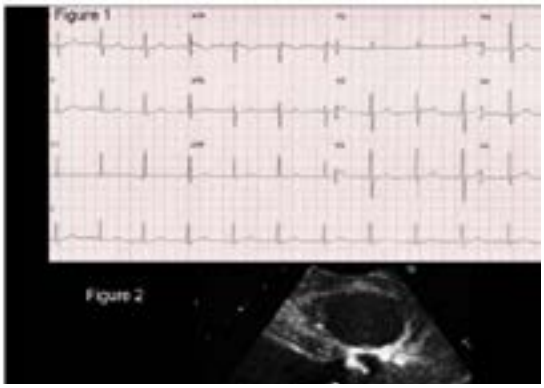

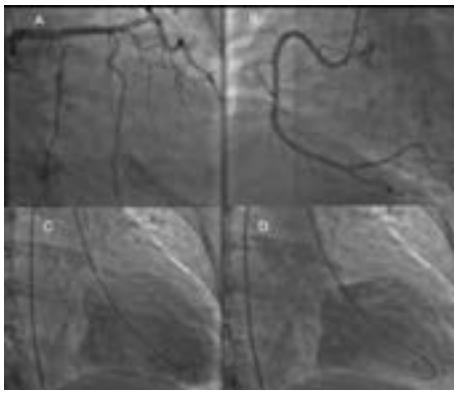

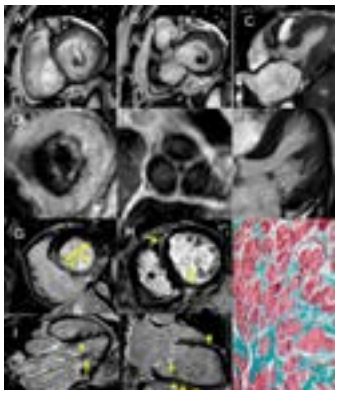

C015

Utilization of a Wideband Protocol to Attenuate Intracardiac Device Artifact

Jonathan Taylor[1], Amita Singh, MD[2], Keigo Kawaji, Ph.D.[3], Roderick Tung, MD[4], Amit R. Patel, MD[5]

1. *University of Chicago Medical Center, Country Club Hills, IL*
2. *University of Chicago Medical Center, Chicago, IL*
3. *University of Chicago, Chicago, IL*
4. *University of Chicago Medical Center, IL*
5. *University of Chicago, IL*

Description of Clinical Presentation: A 39 year old man with dilated cardiomyopathy and previous ventricular tachycardia (VT) treated with dual-chamber intracardiac device (ICD) implantation presents with VT. He had no obstructive coronary disease, and was maintained on an optimal heart failure medication regimen. He was referred for cardiac magnetic resonance (CMR) to localize myocardial scar to determine the best approach for possible ventricular tachycardia ablation procedure.

Diagnostic Techniques and Their Most Important Findings: The patient presented for CMR with late gadolinium enhancement imaging. Initial steady-state free-procession (SSFP) survey views demonstrated significant "clover"-shaped metallic artifact overlying the majority of the right and left ventricle, sparing a small portion of the lateral wall. The patient was repositioned with his arms extended above his head, which resulted in significant cranial displacement of the ICD-artifact (Fig 1A-1B). Pre-contrast phase sensitive inversion recovery images were obtained using a wideband protocol at three specific frequency shifts (-1500Hz, 0 Hz and +1500Hz) to identify the optimal frequency which minimized hyperintensity artifact related to the ICD(Fig 2). After injection of gadolinium, a standard T1-weighted Look-Locker sequence was obtained at an inversion time of 230milliseconds. Traditional late gadolinium enhancement (LGE) imaging revealed epicardial LGE in the mid-anterior wall, suspicious for scar. (Fig 3, red arrows). A second inversion sequence using the wideband protocol was performed with a frequency shift of +1500Hz, as determined by the pre-contrast frequency scouts. Wideband images demonstrated no late enhancement, suggesting the initial LGE imaging was artifact (Fig 4). Given the absence of myocardial scar, the patient did not undergo invasive ablative therapy and his antiarrhythmic regimen was intensified.

Learning Points from this Case: The assessment for myocardial scar using LGE is a critical risk-stratification tool to identify patients at risk for sudden cardiac death (SCD), as well as all cause mortality in the non-ischemic cardiomyopathy population. Standard of care would dictate that these patients receive ICD therapy to reduce their risk of SCD, which is invoked as a major limitation to CMR evaluation for LGE due to device-associated artifact. Wideband protocols have been reported to "lift" the artifact associated with ICD generators, by minimizing the hyperintensity artifact which results from the frequency shift caused by the ICD generator itself. While still investigational, our results demonstrate the importance of patient positioning to minimize ICD artifact, and the utility of wideband protocols to clarify the presence of myocardial scar in the setting of ICD related artifact. In this case, imaging results changed management by avoiding the need for an invasive ablation for non-scar mediated VT in a young patient with significant comorbidities.

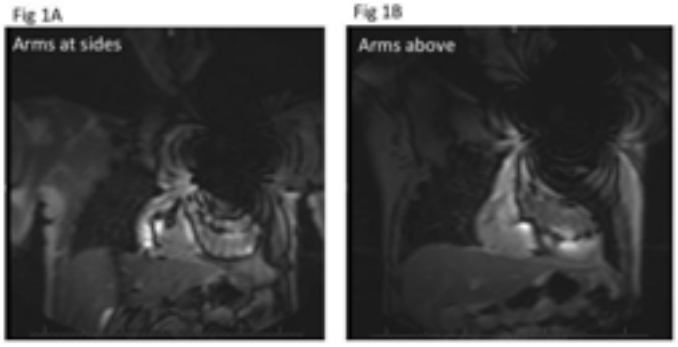

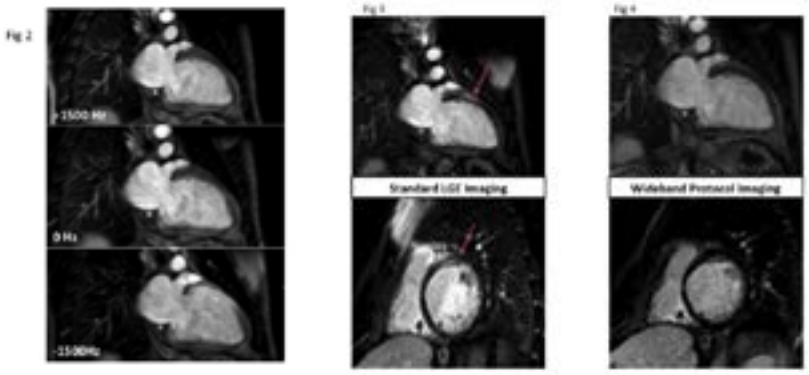

C016

MRI-Conditional Subcutaneous ICD System: the Diagnostic Performance of Cardiac MRI is Still Preserved

Santo Dellegrottaglie, MD; PhD[1]Maurizio Malacrida, MS[2], Paolo Gallo, MD[3], Carmine Pascale, RT[3], Valter Bianchi, MD[4], Pasquale Guarini, MD[3], Antonio D'Onofrio, MD[4]

1. *Clinica Villa dei Fiori, Acerra (Naples,), Italy, Campania, Italy*
2. *Boston Scientific Italia, Lombardia, Italy*
3. *Clinica Villa dei Fiori Acerra, Naples, Campania, Italy*
4. *Monaldi Hospital, Naples, Campania, Italy*

Description of Clinical Presentation: A 52-year-old male patient with a known history of hypertrophic cardiomyopathy (HCM), recent unexplained syncope and an abrupt increase in wall thickness at follow-up echocardiography (from 18 mm to 38 mm at septal level within 2 years) was referred for a cardiac MRI evaluation.

Diagnostic Techniques and Their Most Important Findings: MRI confirmed a severely hypertrophied septum (end-diastolic maximal wall thickness = 39 mm), with large areas of late-gadolinium enhancement. Considering the significant risk for sudden cardiac death, a S-ICD (EMBLEM™ full body 1.5T MR-conditional S-ICD, Boston Scientific) was implanted for primary prevention. The lead was placed in the lower left parasternal area and the generator in a left-side lateral chest pocket. About 18 months later, a new non-contrast cardiac MRI examination was prescribed to accurately assess disease progression. Both cardiac MRI studies were performed using a 1.5T whole body scanner (Achieva, Philips) and a 16-channel torso coil. The scanner was equipped with a user interface (ScanWise, Philips) for automatic scan parameter selection applicable in case of patients with MRI conditional implants. No adverse effects were noticed during the follow-up MRI study. No malfunctions of S-ICD were detected. Multi-segment gradient-echo sequences were used to obtain cine images in the post-implantation study and the diagnostic value of the acquired images was not affected by relevant artifacts. From these images, the maximal wall thickness measured at the septal level was 40 mm. Overall, the image quality of cine images acquired post S-ICD implantation was good and only mildly reduced when compare with the pre-implantation images (**Figure 1.** Left panels - pre-implantation study: Diastolic frames from cine gradient-echo images in standard cardiac planes for the left ventricle. Right panels - post-implantation study: Corresponding images obtained in the same cardiac planes than the pre-implantation study, showing only mildly reduced image quality and preserved diagnostic power).

Learning Points from this Case: In our case, even though a S-ICD generator was implanted on the left-side of the lower chest, thus in close proximity to cardiac apex, the image quality and the diagnostic value of the cardiac MRI examination was preserved. Of interest, the S-ICD might result in low risk of image distortion as none of the system components is in the heart. Whether this finding will be confirmed in large series of patients, apparently, S-ICD does not preclude the possibility to use cardiac MRI for a proper follow-up of the underlying cardiac disease.

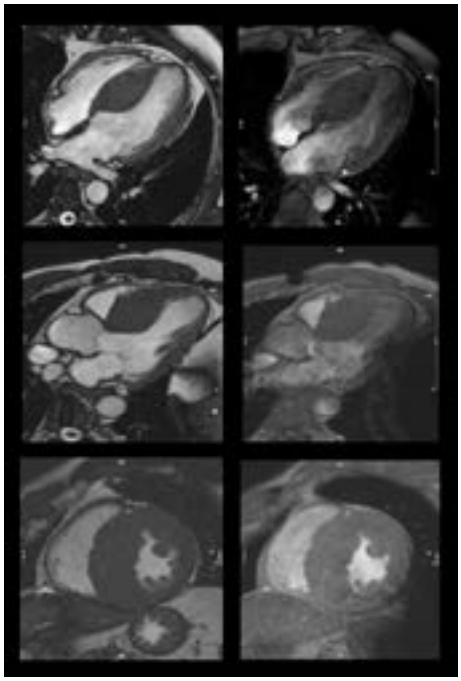

C017

Diffuse myocardial inflammation in a young patient presenting with ventricular tachycardia

Joao R. Inacio, MD[1] Daniel Juneau, MD[2], Girish Dwivedi, MD[3], Regina De La Mora Cervantes, MD[1], Carole Dennie, MD[1]

1. *The Ottawa Hospital/ University of Ottawa, ON, Canada*
2. *University of Ottawa Heart Institute, ON, Canada*
3. *The Ottawa Heart Institute, ON, Canada*

Description of Clinical Presentation: A 37-year old male developed sudden dyspnea, chest pain and palpitations while playing hockey. At the Emergency Department he had a monomorphic ventricular tachycardia (VT), successively cardioverted to sinus rhythm.

The patient's history included occasional bouts of joint paint for the last 3 years involving the hands, knees and ankles joints. There were no joint symptoms or abnormalities in the clinical exam at presentation.
Laboratory investigations were positive for rheumatoid factor, anti-cyclic citrullinated peptide and C-reactive protein.

Diagnostic Techniques and Their Most Important Findings: Echocardiography showed normal biventricular function and no regional wall motion abnormalities. Coronary angiography was normal.

Whole body ^{18}F-FDG PET-CT and cardiac PET (^{18}F-FDG and ^{82}Rb perfusion) showed mildly hypermetabolic lymph nodes in the mediastinum and lung hila, and multifocal patchy myocardial uptake, highly suggestive of active inflammatory lesions from cardiac sarcoidosis.

Cardiac magnetic resonance (CMR) confirmed normal global and regional bi-ventricular systolic function and volumes. Late-gadolinium enhancement (LGE) images reveled patchy subepicardial and mid myocardial enhancement in the basal and mid lateral, anterior and inferior segments of the left ventricle. Linear mid myocardial enhancement was also present in the basal septum. The features were interpreted as compatible with non-specific myocarditis or sarcoidosis.

A single-chamber ICD for secondary prevention was implanted and an oral beta-blocker was started.
Right ventricle (RV) voltage guided endomyocardial biopsy of the basal septum of the RV showed focal nonspecific chronic inflammation and no specific features of sarcoidosis or other specific diagnosis.

During the first year after acute presentation progressive incapacitating episodes of polyarthritis, a left-sided pleural exudative effusion and pleural thickening developed. Pleural biopsies demonstrated chronic granulomatous pleuritis with areas of coagulative-type of necrosis. Overall clinical, serological and pathological findings were consistent with rheumatoid arthritis (RA) involving the pleural and the myocardium.

Treatment with NSAIDS, corticosteroids, methotrexate and leflunomide resulted in significant clinical improvement of arthritis, pleural effusion and no recurrent sustained ventricular arrhythmias during 5 years of follow-up.

Learning Points from this Case:

1. Rheumatoid arthritis is a common autoimmune condition presenting with symmetric polyarticular arthritis and extra-articular systemic complications
2. Cardiac manifestations of RA occur in up to 60% of patients and include pericarditis, myocarditis, ischemic heart disease and heart failure, impacting prognosis
3. Diffuse or focal fibrosis and inflammation can all be identified reliably with CMR in RA patients, using LGE, T2-weighted, T1-mapping and ECV sequences
4. Myocarditis secondary to RA has a non-specific LGE pattern, most commonly patchy non-ischemic mid-wall enhancement, that overlaps with other causes of myocarditis

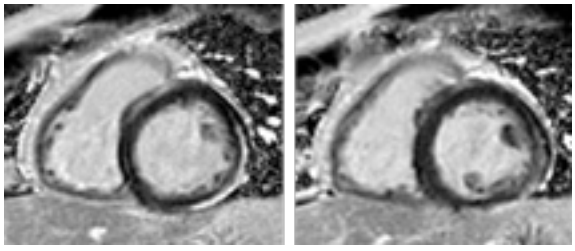

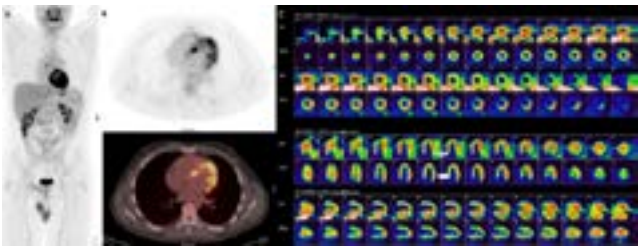

C018

Improved DENSE Strain Imaging Using a Reduced Field of View in a Patient with Heart Failure and a Cardiac Implantable Electronic Device

Kenneth C. Bilchick, MD, MS[1]Xiaoying Cai, BS[2], Daniel A. Auger, Ph.D[2], Frederick H. Epstein, Ph.D.[3]

1. *UVA Health System, Charlottesville, VA*
2. *University of Virginia, Charlottesville, VA*
3. *University of Virginia, VA*

Description of Clinical Presentation: A patient with heart failure and an MR-conditional implantable loop recorder (ILR) was undergoing CMR including strain imaging with Displacement Encoding with Stimulated Echoes (DENSE) prior to implantation of a cardiac resynchronization therapy (CRT) defibrillator. The strain data were acquired in order to assess left ventricular (LV) regional dyssynchrony, characterize the sequence of mechanical activation, and inform the optimal LV lead implantation site. In the present era, a number of different cardiac implantable electronic devices (CIEDs) have been approved for conditional use in the MRI environment, including ILRs, pacemakers, and implantable cardioverter defibrillators (ICDs); however, the optimal method for reducing off-resonance artifacts and optimizing image quality has not yet been determined. The conventional DENSE technique utilizes a spiral acquisition trajectory, which can be associated with signal loss from off-resonance effects and is directly related to the length of each spiral readout.

Diagnostic Techniques and Their Most Important Findings: A recently developed DENSE sequence with outer-volume-suppression was used on a 3T MRI system. The method prepares displacement encoding slices selectively in 2 dimensions and allows imaging with a (FOV) focused on the region of interest. With a smaller FOV, not as much data are needed to support a fully sampled image. As a result, the length of the spiral readout can be reduced significantly, which also decreases metallic artifacts. 2D cine DENSE datasets were acquired for a basal slice of the LV with both a full FOV and a reduced FOV. The lengths of the spiral readouts were 6 ms and 3.4 ms for the full FOV and reduced FOV acquisitions, respectively. Other parameters were: FOV = 340 mm for the full FOV acquisition and 180 mm for the reduced FOV acquisition, 6 spiral interleaves per image, and 2 interleaves per heartbeat. Total imaging occurred over 14 heartbeats per breath-hold. Circumferential strains for each segment from the two acquisitions were analyzed and compared. As shown in the Figure, imaging quality with the reduced FOV (F-J) was better than with the full FOV (A-E) with respect to magnitude (A, F) and phase (B,G) images, and the septal dropout from the device artifact was eliminated with the reduced FOV imaging. Furthermore, the strains in the septal region were more accurate with the reduced FOV, as shown in the strain versus time curves (E,J) and the strain maps (D,I).

Learning Points from this Case: Reduced field of view imaging for DENSE on a 3T scanner resulted in artifact-free imaging in this patient with a CIED. As a result, accurate strain could be determined even in the septal myocardium near the device. This has important implications for CMR strain imaging in the many patients with MR-conditional CIEDs. Artifact-free DENSE strain imaging promises to be very useful for many patients. In particular, high-quality assessment of global and regional strain with DENSE in patients with heart failure and MR-conditional ICDs is now possible.

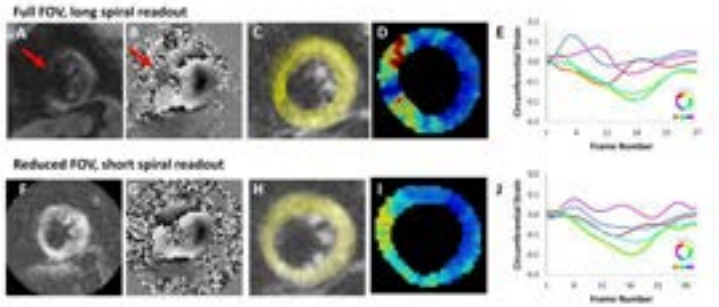

C019

Case of Apical Hypertrophic Cardiomyopathy Presentiing with Ventricular Arrythmmia.

Srujal Patel, M.D.[1]Rajeev Fernando, M.D.[2]

1. *University of Louisville School of Medicine, Department of Cardiovascular Medicine, Louisville, KY*
2. *University of Louisville School of Medicine, Department of Cardiovascular Medicine, louisville, KY*

Description of Clinical Presentation: A 54-year-old man presented with resuscitated sudden cardiac death (SCD) due to ventricular fibrillation. An EKG showed deep T wave inversions in the precordial leads (Figure1a). Selective coronary arteriography demonstrated normal coronary arteries. However, left ventriculography (LVG) showed spade shaped configuration in end-systole (Figure1b). Transthoracic echocardiogram (TTE) could not visualize the left ventricular (LV) apex adequately. TTE with microbubble contrast revealed apical trabeculations and hypertrophy. Cardiac magnetic resonance imaging (CMR) confirmed the findings of apical hypertrophic cardiomyopathy (HCM). He underwent ICD implantation for secondary prevention of SCD.

Diagnostic Techniques and Their Most Important Findings: CMR was performed on a 1.5 T GE scanner with a cardiac coil. Cine images at end diastole displayed asymmetric hypertrophy of the LV apex with 2 apical segments with wall thickness > 1.5 cm, and ratio of > 1.3 cm when compared to the basal segment. Systolic images demonstrated the classic spade like configuration in the long axis views. Late gadolinium enhancement (LGE) uncovered limited patchy fibrosis in the apical lateral wall (figure 2).

Learning Points from this Case: TTE is the initial imaging technique to identify structural heart disease in patients after resuscitated SCD. However, poor acoustic windows in intubated patients, body habitus, COPD and technical skill often limit the ability for high quality images (Figure 1c). Microbubble contrast agents can improve LV opacification in a substandard image. However, our patient's suspected diagnosis could not be confirmed, despite EKG evidence of deep T wave inversions and spade shaped LV cavity on the LVG. CMR has superior contrast resolution for cine imaging of chamber size, wall thickness, and systolic function. LGE identifies fibrosis within the hypertrophied and dysfunctional myocardial segments[1]. In early stages of apical HCM, fibrosis may be limited to the anterior and lateral apical walls[2]. Fibrosis becomes extensive and homogeneous with progressive disease. Therefore, CMR with LGE can risk stratify patients for intervention and invaluable in identifying structural heart disease in resuscitated SCD patients[3,4].

References:

1. Rickers C, Wilke NM, et al.Utility of cardiac magnetic resonance imaging in the diagnosis of hypertrophic cardiomyopathy. Circulation. 2005, 112: 855-61.
2. Suzuki J, Shimamoto R, Nishikawa J, et al.. Morphological onset and early diagnosis in apical hypertrophic cardiomyopathy: a long term analysis with nuclear magnetic resonance imaging. *J Am Coll Cardiol* 1999;33(1):146–151.
3. Eriksson MJ, Sonnenberg B, Woo A, et al. Long-term outcome in patients with apical hypertrophic cardiomyopathy. J Am Coll Cardiol. 2002;39:638–645.
4. Kwon DH, Setser RM, Popovic´ ZB, et al. Association of myocardial fibrosis, electrocardiography and ventricular tachyarrhythmia in hypertrophic cardiomyopathy: a delayed contrast enhanced MRI study. Int J Cardiovasc Imaging 2008;24:617–25.

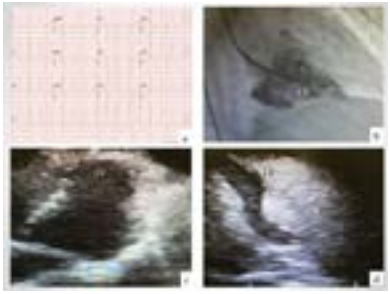

C020

An Unusual Manifestation of Cardiac Sarcoidosis: Utility of Comprehensive Cardiovascular Magnetic Resonance Imaging

Gregory B. Ang, MD[1] Venkateshwar Polsani, MD[2], Ameen F. Person, MD[3], Naveen Rajpurohit, MD[4]

1. Kaiser Permanente, Atlanta, GA
2. Piedmont Heart Institute, Atlanta, GA., Atlanta, GA
3. Kaiser Permanente, GA
4. Sanford Cardiovascular Institute, Sioux Falls, SD

Description of Clinical Presentation: A 54-year-old female with no previous cardiac history was referred to the cardiology clinic for evaluation of chest pain. An electrocardiogram showed normal sinus rhythm with nonspecific intraventricular conduction delay. Nuclear myocardial perfusion imaging showed a reversible inferior perfusion defect, and an echocardiogram showed regional wall motion abnormalities involving the basal septal and inferior walls. The patient then underwent cardiac catheterization which showed normal coronary arteries.

Diagnostic Techniques and Their Most Important Findings: Due to abnormal wall motion and myocardial perfusion imaging, the patient was referred for cardiovascular magnetic resonance (CMR) imaging, which showed a focally aneurysmal right ventricular free wall and a calculated RVEF of 44%, suggestive of arrhythmogenic right ventricular cardiomyopathy (Figure 1). However, multiple focal wall motion abnormalities were also noted in the left ventricle. Late gadolinium enhancement (LGE) imaging revealed transmural scarring involving the basal anteroseptal and inferoseptal walls; subepicardial scarring involving the basal to mid inferior wall; subendocardial scarring involving the basal anterolateral and inferolateral walls, the mid anterolateral wall, and apical lateral wall; transmural scarring involving the basal to mid right ventricular free wall; and subendocardial scarring involving the right ventricular side of the interventricular septum (Figure 2). There was no evidence of fibrofatty infiltration based on dark-blood imaging (Figure 3); parametric mapping showed prolonged myocardial T1 and T2 relaxation times (Figure 4).

The patient underwent right ventricular endomyocardial biopsy, which confirmed the presence of infiltrative non-necrotizing granulomas consistent with sarcoidosis (Figure 5). She was subsequently treated with corticosteroids and underwent prophylactic implantation of a dual-chamber implantable cardioverter-defibrillator.

Learning Points from this Case: Cardiac sarcoidosis is known to present with protean manifestations, making clinical diagnosis challenging. Cardiac sarcoidosis mimicking arrhythmogenic right ventricular cardiomyopathy (ARVC) remains a rare occurrence as described in isolated case reports in the literature. Despite the use of CMR, a number of cases were still misdiagnosed, resulting in delay or withholding of appropriate therapy. As suggested by others, a high index of suspicion should be present if left ventricular involvement and the LGE scarring pattern is suggestive of cardiac sarcoidosis. The sensitivity of endomyocardial biopsy may be limited by the patchy myocardial involvement seen in cardiac sarcoidosis. CMR's high spatial resolution is useful in both right ventricular scar characterization and localization, thus potentially guiding endomyocardial biopsy and enhancing its sensitivity. This case highlights the importance of comprehensive CMR imaging to characterize the disease process and differentiate cardiac sarcoidosis from alternative pathologic conditions.

http://www.ConferenceAbstracts.com/uploads/cfp2/attachments/LDFAIBDN/LDFAIBDN--221185-1-ANY.pdf

C022

59-Year-Old Male Returning from Eritrea with Fevers and Chest Pain

Daniel W. Groves, MD[1] Andrew E. Arai, MD[2], W. Patricia Bandettini, MD[1]

1. National Heart, Lung and Blood Institute, National Institutes of Health, MD
2. National Heart, Lung and Blood Institute, National Institutes of Health, Bethesda, MD

Description of Clinical Presentation: A 59-year-old male smoker with no significant past medical history presented after recently returning from a trip to Eritrea. During this trip, his children had a diarrheal illness. On the evening prior to presentation, he developed a fever, chest, shoulder, and back discomfort and had emesis. He also developed a headache, but he took ibuprofen which helped him fall back asleep. The following morning, he had another episode of emesis. He continued to have fevers, chills, and nausea before presenting to an urgent care clinic. A troponin returned positive, and he was transferred to the emergency room. Early in his admission, he was referred for a cardiac MRI to evaluate for myocarditis.

Diagnostic Techniques and Their Most Important Findings: Initial electrocardiogram showed sinus rhythm and left ventricular hypertrophy with strain pattern. On cardiac MRI, his left ventricle was normal in size with mild left ventricular hypertrophy. Regional wall motion abnormalities were present in the basal to mid inferior and inferolateral walls. Left ventricular ejection fraction was 54%. On the native T2 steady-state free precession images, T1 and T2 parametric maps, there was a subepicardial region in the inferior and inferolateral wall with elevated signal intensity. On late gadolinium enhancement (LGE) imaging, there was subepicardial enhancement in the inferior and inferolateral wall with a region of subendocardial sparing predominantly in the inferolateral wall. This region in the subendocardium of the inferolateral wall without enhancement could represent normal myocardium or epicardial coronary artery obstruction. The early gadolinium enhancement images taken less than 10 minutes following gadolinium injection were key to establish the diagnosis. These early gadolinium enhancement images demonstrate a severe rest perfusion defect, and this subendocardial region of hypoenhancement in the inferolateral wall was still present on LGE imaging.

Contrary to the pre-CMR diagnosis, the cumulative CMR findings were consistent with a myocardial infarction. Following these findings, the patient underwent coronary angiography which showed a complete occlusion of an obtuse marginal branch and a severe stenosis at the bifurcation of the proximal left anterior descending artery and first diagonal branch. He was referred for coronary artery bypass graft surgery.

Learning Points from this Case:

1. The native images (T2 steady-state free precession, T1 and T2 parametric maps) demonstrated a subepicardial region in the inferior and inferolateral wall of elevated signal intensity in a pattern that could be consistent with myocarditis.
2. However, early gadolinium enhancement imaging was consistent with a severe rest perfusion defect which helped confirm myocardial infarction as the diagnosis rather than myocarditis.
3. The subendocardial region in the inferolateral wall that appears normal on pre-contrast images could be due to intramyocardial hemorrhage. T2* imaging in this region would have been helpful to confirm intramyocardial hemorrhage.

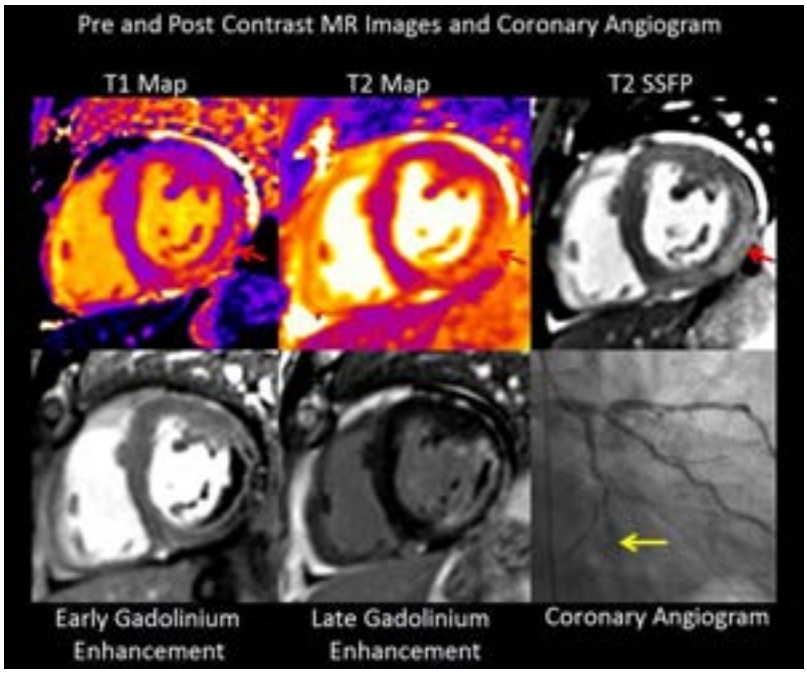

C023

Characterization of right atrial mass using advanced CMR imaging – mDixon and parametric mapping

Tomas Lapinskas, MD[1] Tamar Bigvava, MD[2], Rolf Gebker, MD, PhD[3], Stephan Jacobs, MD[3], Remigijus Zaliunas, MD, PhD[1], Burkert Pieske, MD, PhD[3], Sebastian Kelle, MD, PhD[3]

1. *Lithuanian University of Health Sciences, Kaunas, Kauno Apskritis, Lithuania*
2. *Tbilisi Heart and Vascular Clinic, Tbilisi, T'bilisi, Georgia*
3. *German Heart Institute Berlin, Berlin, Berlin, Germany*

Description of Clinical Presentation: A 49-year-old man presented with episodes of dizziness during head and neck movements and increased fatigue. His medical and family history as well as physical examination was normal. Transthoracic echocardiography (TTE) demonstrated a large mass in the right atrium (RA) attached to the interatrial septum. Transesophageal echocardiography (TEE) showed partial obstruction of the superior vena cava.

Diagnostic Techniques and Their Most Important Findings: Cardiovascular magnetic resonance (CMR) was performed to determine specific mass characteristics using a 1.5 T scanner (Achieva, Philips Healthcare, Best, The Netherlands) with a 32-channel cardiac surface coil. Single breath-hold three dimensional (3D) ECG-gated multi-echo chemical shift-based (mDixon) and single breath-hold two dimensional (2D) modified Look-Locker inversion recovery (MOLLI) sequences were used for advanced CMR imaging. The mass had high signal intensity on fat only and low signal intensity on water only images. Native T1 mapping showed homogeneous and significantly lower T1 values (274 ms) for the tumor than for the normal myocardium (1013 ms). The T1 values of the tumor were similar to the T1 of subcutaneous fat tissue (289 ms). The extracellular volume fraction (ECV) of the mass was lower than that of the myocardium (17.8 % vs. 32.4 %, respectively). Pre-contrast T2 mapping showed higher values for the tumor than for normal myocardium. Following these advanced tissue characterization findings, the cardiac mass was diagnosed as a benign lipoma. The diagnosis was confirmed after surgery and histological evaluation.

Learning Points from this Case: The diagnosis of primary cardiac tumors is frequently challenging. Echocardiography remains the first choice imaging modality, providing high sensitivity in detecting cardiac masses. However, it cannot determine composition of the tumor tissue. Current CMR protocols recommended for cardiac masses are insufficiently specific whereas accurate diagnosis is extremely important. Recently developed advanced tissue characterization techniques could be suitable for differential diagnosis of cardiac masses without the need of histological evaluation. Fat-water separation (mDixon) and parametric (T1 and T2 relaxation) mapping techniques may allow improvement in noninvasive characterization of cardiac masses in the future.

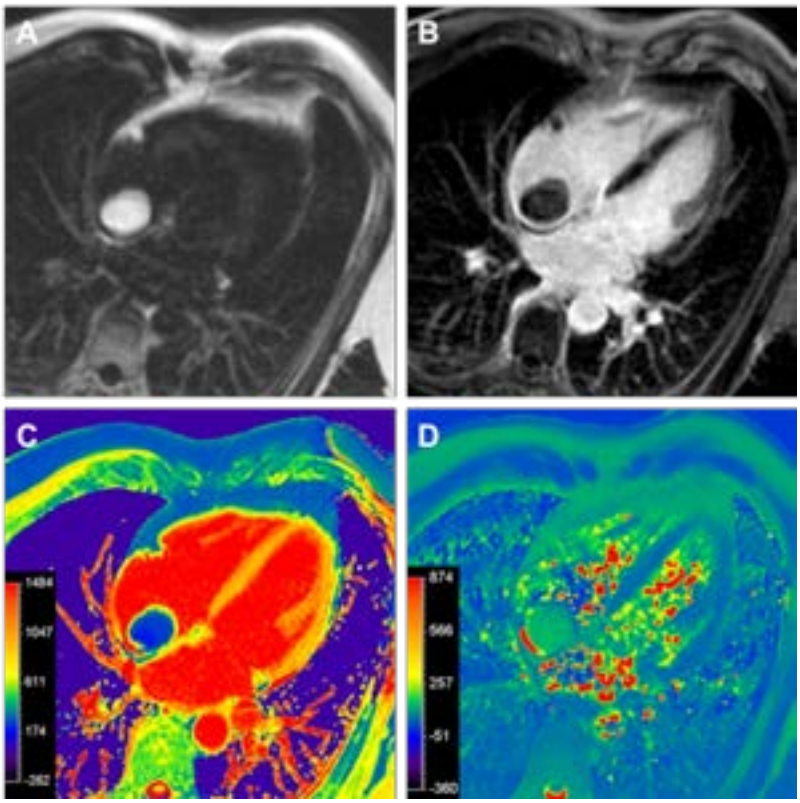

C024

A different context for microvascular obstruction: end-stage cardiomyopathies instead of acute myocardial infarction

Giulia Benedetti, MD[1] Katia Menacho-Medina, MD[2], Stefania Rosmini, MD, PhD[2], Charlotte Manisty, PhD MBBS[3], James Moon, MBBS, MD, MRCP[4], Anna Herrey, MD PhD MRCP[2]

1. *Barts Heart Centre, London, England, United Kingdom*
2. *Barts Heart Centre, England, United Kingdom*
3. *Barts Heart Centre and university college, London, England, United Kingdom*
4. *Barts Heart Center, The Cardiovascular Magnetic Resonance Imaging Unit and The Center for Rare Cardiovascular Diseases Unit, St Bartholomew's Hospital, West Smithfield, London, UK, England, United Kingdom*

Description of Clinical Presentation: A 58-year-old female with an echo diagnosis of hypertrophic cardiomyopathy presented with troponin positive chest pain. Coronary angiography revealed unobstructed coronary arteries, repeat echocardiography showed impaired left ventricular (LV) function (EF 30-35%) with global hypokinesis but preserved right ventricular (RV) function. The patient was newly found to be in atrial fibrillation (AF).

Diagnostic Techniques and Their Most Important Findings: Cine imaging (real-time due to coarse AF) demonstrated a dilated LV with variable wall thickness from thinned segments and segments with residual hypertrophy and a maximum wall thickness of 13mm (figure 1a). LV function was poor (EF 35%) with regional hypokinesis of the thinned segments (figure 1b). Slow flow was noted in the LV and both atria. Tissue characterization showed diffusely high native myocardial T1 (1200ms, MOLLI) (figure 2) and extensive scarring on late gadolinium enhancement (LGE), involving approximately 70-80 % of LV myocardium, sparing only the basal and lateral segments. There was extensive RV involvement. A number of dense hypo-vascular areas were noted close to and within areas of high signal intensity in the LV myocardium, similar to microvascular obstruction (MVO) (figure 3), which is usually seen in acute myocardial infarction. No thrombus was seen in LV or the atria.

Learning Points from this Case: Hypertrophic cardiomyopathy is a familiar condition causing chest pain, shortness of breath, diastolic dysfunction and, most importantly, sudden death. However, at any one time, 3 to 5% of HCM patients have heart failure from progressive disease ('burnt out' or 'end-stage' HCM) with systolic impairment. This is caused by scar visible by LGE. LGE is a good predictor of heart failure.

Here, the scarring was extensive and, in the context of troponin positive chest pain, had extensive areas of compromised microvascular integrity. MVO associated with acute infarctions, conveys a poor prognosis. It is conceivable a similar MVO role in end-stage HCM. This end-stage pattern has been seen associated with others heart muscle diseases with hypertrophy eg - Anderson-Fabry Disease and glycogen storage disease (GSD) including Danon disease and AMP-protein kinase deficiency– with a final common pathway of scar, and sometimes MVO.

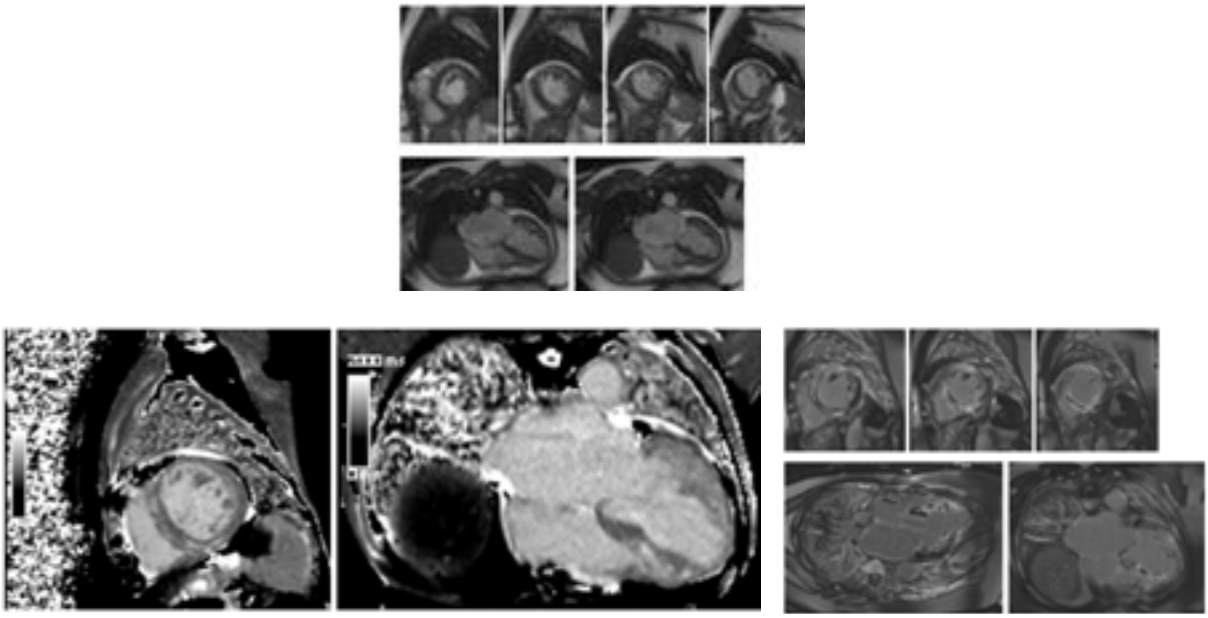

C025

Pseudo cardiac amyloidosis; where ECV map makes the difference

Ana Martinez-Naharro, MD[1] Daniel S. Knight, MBBS MRCP(UK)[2], Tushar Kotecha, MBChB[3], Giulia Zumbo, MD[3], Gerry Coghlan, MD, MRCPI, FRCP[4], James Moon, MBBS, MD, MRCP[5], Peter Kellman, PhD[6], Marianna Fontana, MD, PhD[3]

1. *National Amyloidosis Centre, University College London, London, England, United Kingdom*
2. *Royal Free London NHS Foundation Trust, London, England, United Kingdom*
3. *National Amyloidosis Centre, University College London, England, United Kingdom*
4. *Royal Free Hospital, England, United Kingdom*
5. *Barts Heart Center, The Cardiovascular Magnetic Resonance Imaging Unit and The Center for Rare Cardiovascular Diseases Unit, St Bartholomew's Hospital, West Smithfield, London, UK, England, United Kingdom*
6. *Laboratory of Cardiac Energetics, National Institutes of Health/NHLBI, Bethesda, MD, United States., MD*

Description of Clinical Presentation: A 44 year-old gentleman with background of Chuvash polycythaemia and pulmonary hypertension was referred for a cardiac MRI for assessment of biventricular function. His past medical history also included type 2 diabetes mellitus and sleep apnoea.

Diagnostic Techniques and Their Most Important Findings: Cine SSFP imaging showed RV dilatation with moderately impaired systolic function and evidence of increased RV afterload. Interestingly, LV tissue characterization showed elevated native myocardial T1 value (MOLLI, 1136ms), altered gadolinium kinetics with myocardium and blood nulling at the same time and possible diffuse subendocardial late gadolinium enhancement. These findings raised suspicion of cardiac amyloidosis. However, when an extracellular volume (ECV) map was generated, the myocardium had normal appearance and value (28%) making a diagnosis of cardiac amyloidosis unlikely. Of note the blood had unusually low ECV value (35%) reflecting the high haematocrit (Figure 1).

Learning Points from this Case: The ECV of the myocardium reflects the volume of distribution of contrast in the myocardium. The ECV of the blood is the volume of distribution of contrast in the blood that can be calculated as 1-haematocrit. This patient had Chuvash polycythaemia and presented with a haematocrit of 0.65. Therefore the blood ECV was unusually very low and therefore similar to the myocardial ECV. An equal volume of distribution of contrast in the blood and myocardium is usually found in diseases with very high myocardial volume of distribution (i.e. cardiac amyloidosis or very extensive fibrosis). In this case we are seeing the opposite: the haematocrit is very elevated, causing reduction in the blood volume of distribution of contrast, making it very similar to the myocardial volume of distribution. This also explains the altered gadolinium kinetics and the similar nulling point on LGE imaging of the blood and myocardium. The ECV maps showed the reason for the LGE appearance and helped to reach the correct diagnosis.

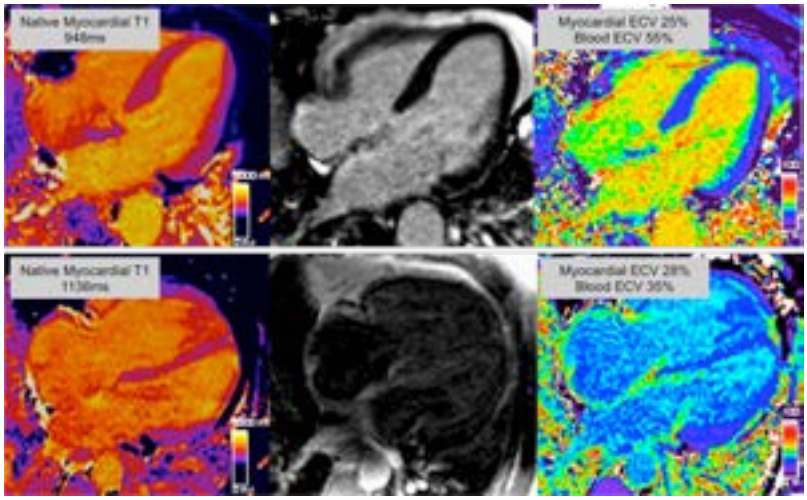

C026

Elevated T2 values and Microvascular Obstruction: a diagnostic challenge

Manish Ramlall, BSc(Hons)MedSci, MBchB[1]Derek Hausenloy, MD, PhD[2], James Moon, MBBS, MD, MRCP[3]

1. *University College London, London, England, United Kingdom*
2. *The Hatter Cardiovascular Institute, Institute of Cardiovascular Science, University College London; Cardiovascular and Metabolic Disorders Program, Duke-National University of Singapore, N/A, Singapore*
3. *Barts Heart Center, The Cardiovascular Magnetic Resonance Imaging Unit and The Center for Rare Cardiovascular Diseases Unit, St Bartholomew's Hospital, West Smithfield, London, UK, England, United Kingdom*

Description of Clinical Presentation: A 66-year old man with a history of anti-phospholipid (APL) syndrome, recurrent deep vein thromboses (DVT), interstitial lung disease (ILD), renal impairment and hypertension presented with chest pain at rest radiating to his back. It was relieved by lying flat and after taking pain-killers. His ECG showed T-wave inversion in leads V3-V6. His troponin T levels were elevated at around 600ng/L. His initial investigations including CTPA, CT aortogram and invasive coronary angiography did not show any significant abnormalities.

He subsequently had an out-patient CMR scan which showed increased T2-STIR signal in the sub-epicardial mid-to-apical anterolateral wall. There was corresponding elevated T1(MOLLI) values up to 1100ms. Gadolinium enhancement showed microvascular obstruction (MVO) in the apical septal wall early-phase and patchy enhancement in the apical segments in the late-phase. There was also mid-lateral and apical hypokinesia with mildly impaired left ventricular function. He was diagnosed of myocarditis.

He re-presented to hospital 3 months later with a recurrence of chest pain. His troponin and inflammatory markers were raised. He was on a course of steroids and colchicine but was slow to respond. He was transferred to the nearest tertiary centre for further assessment.

A more detailed history revealed that he was thought to have possible systemic lupus erythromatosus (SLE) on the basis of APL syndrome, renal dysfunction, ILD and positive anti-dsDNA. Given there was no evidence of disease activity, SLE was thought to be an unlikely cause of myocarditis. He suffered from 2 DVTs and had been on life-long warfarin. This was changed to Rivaroxaban a few month prior.

His initial angiogram was reviewed and showed sluggish flow in the left anterior descending artery. It was felt that he was more likely to have suffered a myocardial infarction.

Diagnostic Techniques and Their Most Important Findings: The patient had a second CMR scan which showed elevated T2 values of up to 84ms (normal < 55ms) in the apical segments. There was an area of MVO as previously described. There was thinning of the mid-lateral and apical segments with significant hypokinesia. Left ventricular function was mildly impaired (50%). He then had an FDG-PET scan which revealed acute myocardial inflammation and no evidence of large vessel vasculitis. Increased tracer uptake was identified in the entire lateral wall as opposed to elevated T2 values limited to the mid-apical segments on CMR. The patient subsequently had a myocardial biopsy which showed multiple foci of recent haemorrhagic myocardial necrosis with established fibrosis. There was small vessel mural thickening but no active myocarditis. These appearances were suggestive of SLE. He is currently on steroid therapy and is due to have a repeat CMR scan in the coming months.

Learning Points from this Case:

1. Consider myocardial vasculitis as a cause of elevated T2 values.
2. MVO can be due to vasculitis or micro-emboli rather than atheromatous disease in the major coronary arteries.

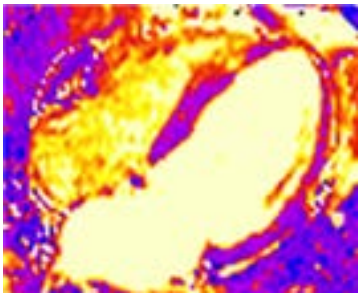
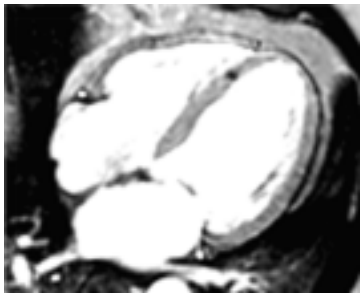
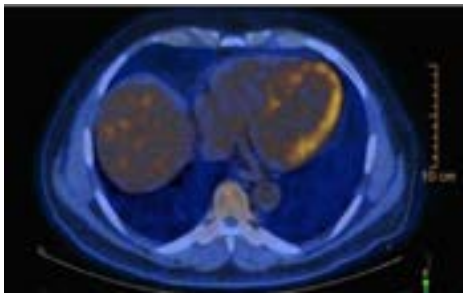

C027

Atypical late gadolinium enhancement pattern in hematopoietic stem cell transplant recipient: what is this?

Yeseul Jo, M.D.Jung Im Jung, M.D., Ph. D.

Department of Radiology, Seoul St. Mary's Hospital, College of Medicine, The Catholic University of Korea, N/A, Republic of Korea

Description of Clinical Presentation: A 49-year-old male was admitted for dyspnea that started 3 weeks ago. He had received allogeneic peripheral blood stem cell transplantation (HSCT) for acute myeloid leukemia 8 months ago.

His echocardiography showed normal left ventricular ejection fraction (LVEF) but high LV filling pressure was noted as restrictive physiology.

Diagnostic Techniques and Their Most Important Findings: Coronary CT angiography was performed, and it showed no significant coronary artery stenosis. Both ventricular walls were diffusely thick, raising the possibility of infiltrative cardiomyopathy. Mild pulmonary edema and bilateral pleural effusions were associated.

Cardiac magnetic resonance (CMR) imaging showed abnormal wall thickening of ventricles (wall thickness=18mm) as well. On the cine images, evidence of regional wall motion abnormality was not definite. On late gadolinium enhancement (LGE) images, there were linear faint enhancement at mesocardium of interventricular septum, epicardial enhancement at infero-septal wall of LV, and patchy gray enhancement at lateral wall of LV base. Diffuse enhancement of RV free wall was suspected. Myocardial T2 mapping showed increased value (47-49ms (reference value in our hospital (Ref); 39.6 ± 7.4ms)). T1 mapping and extracellular volume (ECV) values were also higher than normal range (1431-1599ms (Ref; 1315±39ms) and 28.9-44% (Ref; 24.2±3.8%)). There were regional variations of T1, T2, and ECV values across the 16 segments of the left ventricle. Segments with myocardium showing enhancement had higher T1, T2, and ECV values than the other segments, which were already higher than normal range.

Learning Points from this Case: CMR findings were atypical, and it was difficult to make a specific diagnosis. Cardiac graft versus host disease was thought to be a possible diagnosis because of ventricular hypertrophy, atypical enhancement pattern, and increased T1, T2, and ECV values. Differential diagnoses included amyloidosis, infiltrative cardiomyopathy, or myocarditis. Leukemic recurrence was not included in the differential diagnoses at first because the laboratory findings were normal.

Endomyocardial biopsy was performed at RV wall. There was interstitial infiltration of atypical cells with high N/C ratio, suggestive of leukemic (AML) infiltration.

This case demonstrates an isolated cardiac relapse of acute leukemia without concomitant bone marrow involvement, which is very rare. Unlike concomitant relapse, the isolated cardiac relapse lesion appears as diffuse infiltration rather than a locally invasive intracavitary mass. However, imaging findings are nonspecific, so we have to suspect leukemic infiltration in cases of CMR abnormality presented in patients with HSCT.

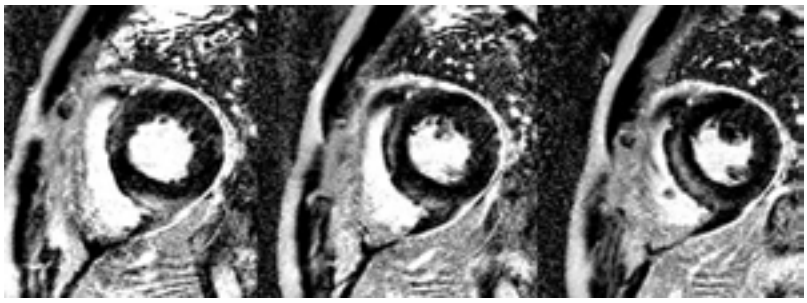

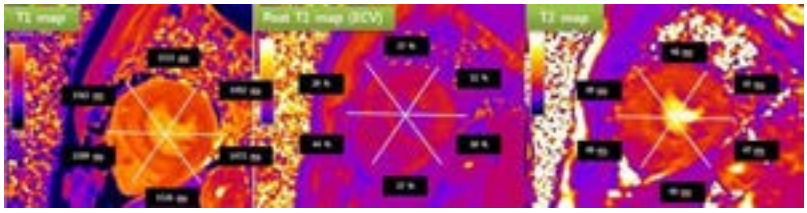

C028

Presumed viral myocarditis, utility of T1/T2 mapping?

Sudip K. Saha, MD

Mid Atlantic Permanente Group, Mclean, VA

Description of Clinical Presentation: A forty-one year old man presented with a one month duration of worsening chest pain, orthopnea, and dyspnea on minimal exertion. Approximately 6 weeks prior to presentation he had a viral respiratory illness. He had no significant past medical history and was on no medications. No known sick contacts or recent travel history. A transthoracic echocardiogram showed depressed global left ventricular systolic function with an estimated LVEF of 30-35%. He was referred for cardiac MRI for further characterization of his newly diagnosed cardiomyopathy.

Diagnostic Techniques and Their Most Important Findings: Techniques: Cardiac MRI was performed on a Philips 1.5 T scanner with a commercial 5-element cardiac-surface coil. Cine images were acquired in a contiguous LV short-axis orientation with an ECG-gated, breath-hold, steady-state free-precession sequence with full LV coverage (8-mm slice thickness, 2-mm interslice gap, in-plane spatial resolution 2 × 2 mm, 30 ms temporal resolution). EGE- CMR was performed 3 minutes after and LGE-CMR was performed 15 minutes after the intravenous administration of 0.2 mmol/kg gadolinium-DTPA (Magnevist; Schering, Berlin, Germany) with a 2-dimensional breath-hold, segmented inversion-recovery sequence (inversion time optimized by the Look-Locker sequence [inversion time scout] to null normal myocardium) acquired in the same orientation (short-axis stack) as the cine images. T2 weighted images of the myocardium and short tau inversion recovery (T2-STIR) were also analyzed. Quantitative T1 and T2 mapping as well as ECV measurement was performed.

Important findings: The patient was confirmed to have a cardiomyopathy and met two Lake Louise Criteria for myocarditis based on the presence of myocardial edema (myocardial/skeletal muscle signal intensity ratio > 2) and early gadolinium enhancement. Quantitative T1 and T2 mapping revealed increased global T1 time (1161 ms, institutional normative values 1017-1157 ms) and increased global T2 time (64 ms, institutional normative values 37-59 ms) as well as an increased extracellular volume (0.48, institutional normative value of < 0.28). The patient was medically managed for heart failure with the resolution of his symptoms. Five months later, an abbreviated repeat cardiac MRI was performed to evaluate his cardiomyopathy which showed near normalization of left ventricular systolic function, absence of any early or late gadolinium enhancement, and decreased global T1 and T2 times (1035 ms and 48 ms, respectively).

Learning Points from this Case: Cardiac MRI is a powerful tool in the characterization of non-ischemic cardiomyopathies. It can help provide more definitive diagnosis of conditions such as myocarditis which were previously presumptively diagnosed. Quantitative T1 and T2 mapping remain largely experimental tools with challenges of standardization. However, T1 and T2 mapping can provide information on a wide variety of disease processes and may help track sub-clinical changes in a various clinical contexts such as myocarditis.

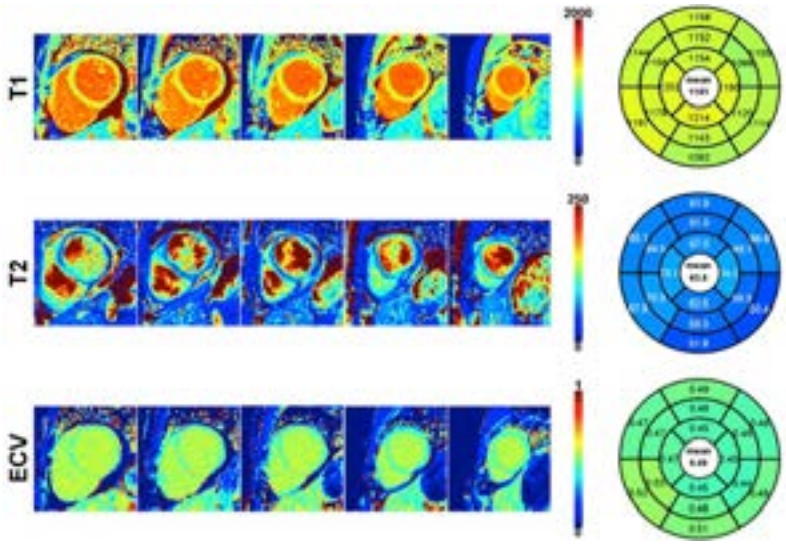

C029

A Case of Lung Cancer, Myocardial Infarction and a Cardiac Mass: The Added Value of CMR

Akhil Narang, MD[1] Kirk T. Spencer, MD[2], Karima Addetia, MD[2]

1. *University of Chicago, Chicago, IL*
2. *University of Chicago, IL*

Description of Clinical Presentation: A previously healthy 34 year-old female was diagnosed with lung cancer after presenting with hip pain from a metastatic lesion. Chest computerized tomography (CT) noted a left ventricular (LV) filling defect **(Figure A)** and transthoracic echocardiography (TTE) revealed an LV mass in the anterior wall **(B)**. During the hospitalization, the patient experienced an inferior STEMI. Coronary angiogram revealed filling defects in the right coronary artery without underlying atherosclerosis **(C)**. Pathological analysis of the aspirate obtained during coronary angiogram revealed thrombus. A cardiac MRI (CMR) was obtained to further characterize the LV mass.

Diagnostic Techniques and Their Most Important Findings: CMR was used to evaluate signal properties and morphology of the LV mass. Steady-state free precession cine sequences revealed a normal LV ejection fraction (62%) with hypokinesis of the inferior wall. An 18x25 mm mass was noted on the anterior wall **(D and E)**. T1-weighted imaging demonstrated isointense signal of the mass when compared to the myocardium while T2-weighted imaging showed a hyperintense signal in the mass suggestive of edema **(F)**. The mass did not suppress on fat-suppression imaging **(G)**. First-pass perfusion revealed contrast uptake in the mass consistent with vascularity **(H)**., Late-gadolinium enhancement (LGE) was noted within the mass likely representing ongoing cell necrosis **(I)**. The CMR findings strongly suggested that the mass was a metastatic lesion. Interval lung mass biopsy revealed non-small cell lung carcinoma. The patient was treated with Coumadin for hypercoagulable coronary occlusion and underwent chemotherapy. At six-month follow-up, the LV mass has decreased in size.

Learning Points from this Case: The incidence of cardiac metastasis from lung cancer is lower than other organs. Treatment of cardiac metastasis depends on the risk for adverse events. Multiparametric CMR imaging allow for integration of multiple parameters to delineate the etiology of cardiac masses. In this case, as CT and TTE suggested tumor versus thrombus, more accurate diagnosis of the LV mass was necessary. Tissue characterization with T1 and T2-weighted imaging takes advantage of differences in signal intensity to differentiate between various tissue types. The combination of isointense T1-weighted signal and hyperintense T2-weighted signal within the mass suggested the presence of edema due to active inflammation from a tumor. First-pass perfusion demonstrated heterogeneous contrast uptake within the mass suggesting vascularity and excluded simple thrombus or cyst. LGE allowed differentiation between areas of fibrosis/scar and living tissue. LGE noted within the cardiac mass confirmed the presence of focal cellular necrosis. The constellation of findings on CMR, together with the lung biopsy results, confirmed the cardiac mass was metastatic cancer with superimposed thrombus. This diagnosis was reached without the need for biopsy. CMR is a robust tool that allows for accurate characterization over CT and TTE.

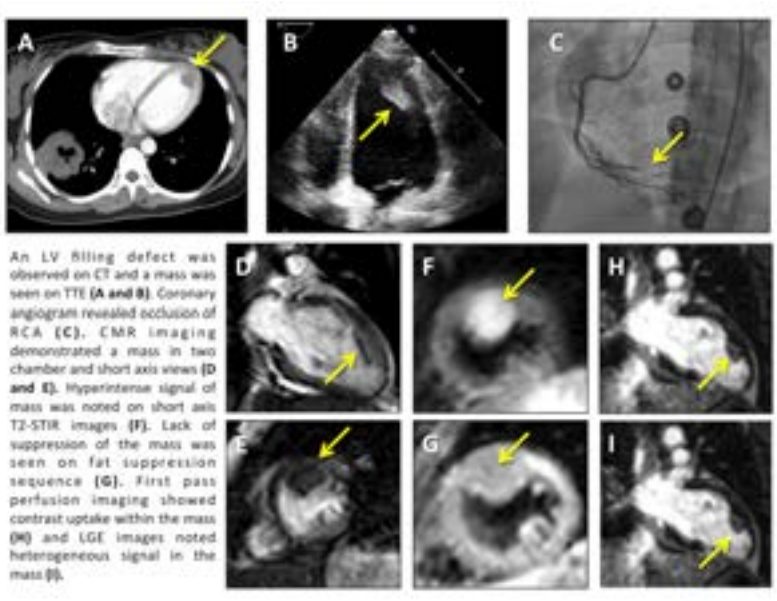

An LV filling defect was observed on CT and a mass was seen on TTE **(A and B)**. Coronary angiogram revealed occlusion of RCA **(C)**. CMR imaging demonstrated a mass in two chamber and short axis views **(D and E)**. Hyperintense signal of mass was noted on short axis T2-STIR images **(F)**. Lack of suppression of the mass was seen on fat suppression sequence **(G)**. First pass perfusion imaging showed contrast uptake within the mass **(H)** and LGE images noted heterogeneous signal in the mass **(I)**.

C030

Myocardial perfusion mapping in a patient with apical hypertrophic cardiomyopathy

Kristopher Knott, MBBS MA[1]Anish N. Bhuva, MRCP MBBS[2], Paul Scully, MBBS MRes[3], Hui Xue, PhD[4], Charlotte Manisty, PhD MBBS[5], James Moon, MBBS, MD, MRCP[6], Peter Kellman, PhD[7], Anna Herrey, MD PhD MRCP[8], Anna Herrey, MD, PhD, FRCP[8]

1. *Barts Heart Centre, London, England, United Kingdom*
2. *Barts Heart Centre and Institute of Cardiovascular Science, UCL., England, United Kingdom*
3. *Barts Heart Centre, N/A, United Kingdom*
4. *National Heart Lung and Blood Institute (NHLBI), National Institutes of Health, Bethesda, MD*
5. *Barts Heart Centre and university college, London, England, United Kingdom*
6. *Barts Heart Center, The Cardiovascular Magnetic Resonance Imaging Unit and The Center for Rare Cardiovascular Diseases Unit, St Bartholomew's Hospital, West Smithfield, London, UK, England, United Kingdom*
7. *Laboratory of Cardiac Energetics, National Institutes of Health/NHLBI, Bethesda, MD, United States., MD*
8. *Barts Heart Centre, England, United Kingdom*

Description of Clinical Presentation: A 76 year old gentleman with a history of apical hypertrophic cardiomyopathy (HCM) described a several month history of chest tightness when he was reviewed in cardiomyopathy clinic. It was associated with exertion and cold weather. The ECG showed deep T wave inversion in the precordial and lateral leads and voltage criteria for left ventricular hypertrophy. Recent transthoracic echocardiogram showed apical hypertrophy with a provocable apical cavity gradient of 20mmHg. He was referred for cardiovascular magnetic resonance (CMR), including stress perfusion to rule out an epicardial coronary stenosis.

Diagnostic Techniques and Their Most Important Findings: As per protocol, initial SSFP cine imaging revealed apical hypertrophy (maximal wall thickness 14mm) with systolic apical cavity obstruction. Adenosine was administered at 140mcg/kg/min with appropriate heart rate increment and symptoms consistent with adequate stress. This was repeated after 4 minutes at rest followed by late gadolinium enhancement imaging. Visually perfusion imaging showed a circumferential apical perfusion defect. Furthermore, myocardial blood flow was quantified at voxel level and represented on a myocardial perfusion colour map (Figure 1). This revealed 82% maximal decrease in blood flow relative to normal myocardium and a clear gradient in the perfusion defect from base to apex within the area of maximal hypertrophy suggesting microvascular ischaemia rather than epicardial coronary disease. Late gadolinium enhancement showed diffuse mid wall enhancement co-localising with the perfusion defect (Figure 2).

The patient was subsequently started on vasodilatory therapy with a good symptomatic response.

Learning Points from this Case: Reduced myocardial blood flow (MBF) and myocardial perfusion reserve (MPR) in cardiomyopathy is well documented and associated with a worse prognosis. Up until recently, quantifying perfusion has been time consuming and labour intensive making it unsuitable for routine clinical use. PET imaging has demonstrated the importance of absolute quantification as a prognostic tool but the availability, radiation and cost of PET is often prohibitive. Myocardial perfusion mapping by CMR therefore offers potential as a prognostic and diagnostic tool in the assessment of patients with cardiomyopathy to measure MBF and MPR.

http://www.ConferenceAbstracts.com/uploads/cfp2/attachments/LDFAIBDN/LDFAIBDN--214984-1-ANY(1).pdf

http://www.ConferenceAbstracts.com/uploads/cfp2/attachments/LDFAIBDN/LDFAIBDN--214984-2-ANY.pdf

C031

Use of MRI flow measurements to optimise heart rate in a paced patient with functional single Ventricle

Srinivas Ananth Narayan, MD, MRCPCH[1]Henry Chubb, MRCP MRCPCH[2], Eric Rosenthal, MD FRCP[3], Aaron Bell, MB.ChB[4]

1. *King's College London, England, United Kingdom*
2. *Kings college London, England, United Kingdom*
3. *Evelina London Children's Hospital, England, United Kingdom*
4. *Guy's & St Thomas' Hospital NHS Foundation Trust, London, England, United Kingdom*

Description of Clinical Presentation: An 8y boy was referred for evaluation of exercise limitation and assessment of Fontan circulation, in the presence of a permanent pacemaker (PPM). He had hypoplastic left heart syndrome with restrictive atrial septum (mitral stenosis and aortic stenosis variant) and bilateral superior caval veins. His Fontan palliation was achieved by 3y of age, complicated by prolonged chylothorax and cerebral infarcts causing hemiparesis, from which he recovered. At 7y he developed intra-atrial re-entry tachyarrhythmia, with a background of slow nodal rhythm. Electrophysiological study which identified multiple mechanisms of atrial tachyarrhythmia. A trans venous PPM (Advisa SR MRI™ SureScan® Model A3SR01 with Capsurefix MRI™ 5076 lead in lateral tunnel; MRI Conditional; set at AAIR at 85bpm) was implanted to allow aggressive beta blockade.

Diagnostic Techniques and Their Most Important Findings: Echocardiography demonstrated good function of the dominant right ventricle, trivial tricuspid regurgitation, no flow in the fenestration and unobstructed Fontan tunnel, with pacing lead in-situ. Cardiac MRI was performed under general anaesthetic on a Philips Achieva 1.5T MRI Unit. Standard pre-MRI pacing checks were performed and pacemaker set to MR 'safe' mode (AOO 85 bpm). Imaging planes were defined using a real-time Interactive sequence (Balanced-FFE, TE 1·05 ms, TR 2·1 ms, matrix 128x128) and bSSFP cine images and 3D volume (TR/TE = 3.7/1.86 ms, matrix 320 × 320), Free breathing phase contrast flow sequence (TE/TR 3/5 ms, matrix 128×256, FOV 250–350 mm, 40 phases) were obtained. Significant artefact related to the presence of the generator box and pacing lead precluded accurate measurement of structures proximal to the pacing system within the 3D SSFP volume and flow measurements for the SVC and IVC. After confirming echo findings, Aortic flow measurements were repeated after changing the rate of the pacemaker first to 75 and then to 100 bpm. The child was taken out of the MRI scanner and the table moved beyond the 5-Gauss line in order to enable each change PPM parameters. The localiser and reference scans were repeated before rechecking the aortic flow (Table 1). PPM rate was set at rate of optimal aortic flow.

Learning Points from this Case: This case illustrates the use of MRI phase contrast flow imaging in optimising the cardiac output by adjusting the rate of the pacemaker in pacemaker dependent patients. Although the rate is adjusted in controlled conditions with the patient under general anaesthesia, it gives a framework to estimate the cardiac output in differing heart rates and this could help optimise the rate for the patient. This could be one of the parameters which would help optimal function of his cardiovascular system.

Further studies with larger number of patients in different centres may allow more general recommendations for the base rate in Fontan patients and may also give information on the influence of heart rate on cardiac output on these patients.

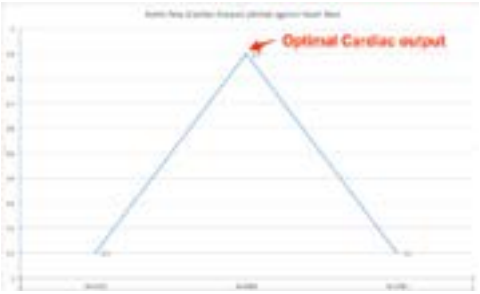

Table 1: Flow values in Aorta at selected Heart Rates

Max Velocity	Cardiac output		Regurgitation fraction	Backward Flow		Forward Flow		Effective Flow		PC Flows
m/s	l/min/m^2	l/min	%	ml/beat/m^2	ml/beat	ml/beat/m^2	ml/beat	ml/beat/m^2	ml/beat	(HR)
0.6	2.7	2.1	3%	1	1	38	29	36	28	Ao (075)
0.6	3.8	2.9	0%	0	0	44	34	44	34	Ao (085)
0.6	2.7	2.1	5%	1	1	29	22	27	21	Ao (100)

C032

Exercise perfusion imaging in the setting of exertional chest pain

Alexandra Channing, MD[1]Kevin K. Whitehead, MD PhD[2], Matthew A. Harris, MD[3]

1. *Children's Hospital of Philadelphia, New York, NY*
2. *Children's Hospital of Philadelphia, Philadelphia, PA*
3. *Children's Hospital of Philadelphia, Perelman School of Medicine of the University of Pennsylvania, Philadelphia, PA*

Description of Clinical Presentation: 19 year old male with familial hypertrophic cardiomyopathy (HCM) presented with sharp, exertional chest pain. His ECG and echocardiogram demonstrated stable left ventricular hypertrophy (LVH) without concern for ischemic change however given his underlying diagnosis he was referred for cardiac MRI (CMR) with exercise perfusion imaging.

Diagnostic Techniques and Their Most Important Findings: An exercise CMR with perfusion was performed consisting of TrueFISP and HASTE static axials, real-time and segmented cine, velocity mapping, resting and exercise perfusion and viability. The patient had normal cardiac anatomy with preserved resting LV ejection with severe LVH without dilation. The LV end-diastolic volume was 71 cc/m^2, LV ejection fraction was 73%, LV mass was increased at 190 g/m^2. The ventricular septum and superior walls had maximal diastolic thickness of 3 cm. At rest, there was mild systolic anterior motion of the mitral valve, mild LV outflow tract(LVOT) obstruction to a peak velocity of 2.2 m/s and no significant valve regurgitation. Exercise CMR was performed to assess ventricular function and perfusion. The patient had no symptoms during exercise to a peak heart rate of 155 bpm. Real-time cine imaging in the short-axis view demonstrated preserved LV ejection without increased LVOT obstruction during exercise however there were regional wall motion abnormalities consisting of decreased thickening of the ventricular septum. Perfusion stress imaging demonstrated significant septal and inferior wall sub-endocardial perfusion defects extending from base to apex (Figure 1). Post-gadolinium delayed enhancement imaging demonstrated significant enhancement at the anterior and inferior septal regions and patchy enhancement of the lateral wall (Figure 2).

Learning Points from this Case: 19 year old male with familial HCM with mild LVOT obstruction and no arrhythmias who had chest pain consistent with a musculoskeletal etiology. Exercise CMR demonstrated significant HCM with fibrotic changes and areas of ischemia during exercise. The literature has focused on the use of exercise CMR to assess flows, ventricular function and volumes. Our case demonstrates that exercise CMR can also be performed safely and effectively to provide important diagnostic information in pediatric patients at risk for myocardial perfusion defects. It has benefits over adenosine stress CMR as it replicates the physiological and mechanical changes that take place during exercise whereas adenosine stress testing tends to reflect vasodilatory changes. Additionally, exercise CMR has advantages over exercise stress testing by other imaging modalities that include reproducibility and accuracy of ventricular volume measurements at maximal exercise (La Gerche et al.Circ Cardiovasc Imaging.2013;6:329-338). Despite the limitations of exercise CMR, which include motion artifact and the challenges of balancing spatial and temporal resolution–we are able to show that the images can be high quality and of diagnostic value.

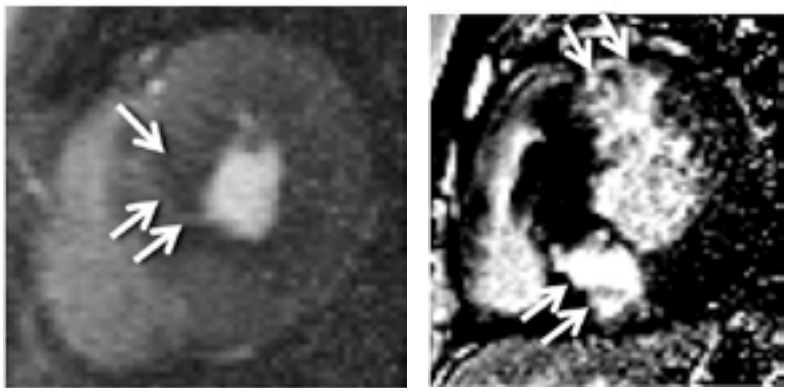

C033

"Going in Circles"- Circular Shunt Physiology in a Patient with Hypoplastic Left Heart Syndrome after the Fontan Operation

Oluwatosin O. Fatusin, MD/MPH[1] Gabriela Liberato, MD[2], Sunil Ghelani, MD, MBBS[1]

1. *Boston Children's Hospital, Boston, MA*
2. *Boston Children's Hospital, MA*

Description of Clinical Presentation: AL is a 10 year old with prenatal diagnosis of aortic stenosis and evolving hypoplastic left heart syndrome (HLHS) who underwent both fetal and post-natal balloon aortic valvuloplasty. At 7 days of age, he underwent a modified stage 1 procedure (partial atrial septectomy, aorto-pulmonary anastomosis, and right ventricle to pulmonary artery shunt), surgical aortic valvuloplasty, mitral valve repair, and resection of endocardial fibroelastosis. Due to continued severe left ventricular diastolic dysfunction he underwent a series of palliative operations culminating in a fenestrated Fontan circulation at age 2.

Since then, he is noted to have an unusual circumstance of significant flow through a moderately hypoplastic left heart with moderate native aortic regurgitation and mitral regurgitation. In clinic, his saturation was 88% on room air with a grade 3-4/6 systolic ejection murmur at the left mid sternal border and a grade 2/4 diastolic murmur.

Diagnostic Techniques and Their Most Important Findings: On echocardiogram, he has an unrestrictive atrial septal defect, mild mitral and tricuspid regurgitation, moderate native aortic regurgitation, no neo-aortic regurgitation, mildly depressed biventricular function, and an unobstructed Fontan pathway with patent fenestration.

An MRI was requested to delineate his anatomy and quantify the degree of regurgitation across the native aortic valve and mitral valve, given concerns for circular shunt physiology creating an inefficient cardiac workload.

Using free-breathing phase velocity flow measurements cardiac output, fenestration flow, and valvar regurgitation fractions were calculated (Figure 1). There was more retrograde flow across the native aortic valve than antegrade. Flow across the mitral valve was all retrograde consistent with severe left ventricular diastolic dysfunction. Presence of a circular shunt was demonstrated at 0.7 L/min (20% of cardiac output).

Using breath-held cine SSFP short-axis stack ventricular volume and ejection fractions showed a mildy dilated right ventricle (120 ml/m$^{2)}$ with normal ejection fraction (52%). The left ventricle was hypoplastic (35 ml/m2) with normal ejection fraction (59%).

Late gadolinium imaging showed a thin, circumferential layer of subendocardial enhancement in the left ventricle consistent with residual endocardial fibroelastosis.

Learning Points from this Case: Ventricles in the Fontan circulation have various sources of volume overload including aorto-pulmonary collaterals, valve regurgitation, and unusual circular shunts as described above. As well, these patients can be cyanotic due to a number of anatomic reasons including patent fenestration, baffle leaks, and veno-venous collaterals. Cardiac MRI can help identify these lesions and quantify the volume load and degree of shunting using phase velocity flow mapping as shown. In addition, since severe diastolic dysfunction may exist in presence of normal systolic function, MRI can assess for myocardial fibrosis that may be contributing, as evident by the endocardial fibroelastosis seen.

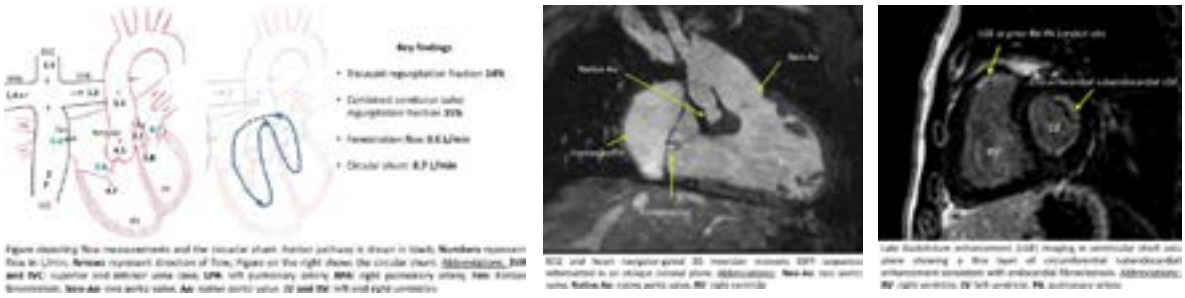

C034

Exercise stress perfusion imaging in an unusual case of anomalous origin of the left coronary artery from the pulmonary artery (ALCAPA) in an adolescent female

Michael P. DiLorenzo, MD[1]Matthew A. Harris, MD[2], David M. Biko, MD[3], Sara L. Partington, MD[4], Mark A. Fogel, MD[1], Kevin K. Whitehead, MD PhD[1]

1. *Children's Hospital of Philadelphia, Philadelphia, PA*
2. *Children's Hospital of Philadelphia, Perelman School of Medicine of the University of Pennsylvania, Philadelphia, PA*
3. *The Children's Hospital of Philadelphia, Philadelphia, PA*
4. *Hospital of the University of Pennsylvania and Children's Hosptial of Philadelphia, Philadelphia, PA*

Description of Clinical Presentation: A 15 year old female with no significant past medical history presented to the outpatient cardiology clinic with a new murmur on routine physical examination. She was otherwise asymptomatic. An echocardiogram performed at that time demonstrated a concern for a coronary cameral fistula to the right ventricular outflow tract and an ECG demonstrated T wave inversions. With these findings, she was referred for further cardiac imaging.

Diagnostic Techniques and Their Most Important Findings: CMR with a dual contrast protocol with gadavist and gadofosveset trisodium was performed. First-pass myocardial perfusion with gadavist at rest and bike exercise stress was performed. No perfusion defects or regional wall motion abnormalities were present at rest. At peak exercise, there were no regional wall abnormalities, though there was evidence of circumferential subendocardial hypoperfusion. Delayed enhancement was not demonstrated on viability imaging. IR FLASH sequences with gadofosveset trisodium demonstrated normal location of the right coronary artery but showed an anomolous origin of the left coronary artery from the pulmonary artery (ALCAPA), with the left coronary specifically arising from the right pulmonary artery (PA) with a stenotic course. This finding was later confirmed on angiography by cardiac catheterization, and the patient underwent successful coronary reimplantation without complication.

Learning Points from this Case: We present an unusual case of ALCAPA diagnosed in an asymptomatic adolescent with no significant areas of scar on viability imaging. The lack of scarring or symptoms may be related to the left coronary artery stenosis preventing coronary steal. Further, this case demonstrates the utility of exercise stress CMR as part of a comprehensive exam that includes defining the coronary anatomy and identifying areas of hypoperfusion and potential ischemia. Stress perfusion imaging may prove beneficial in the workup of patients presenting with coronary anomalies.

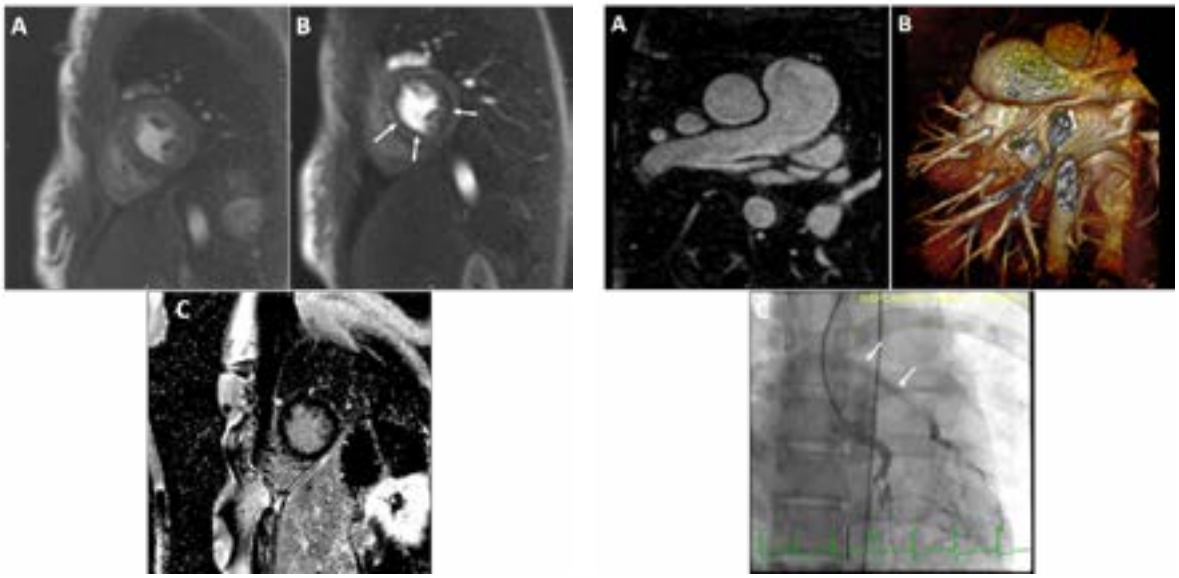

C035

Congenital Heart Disease Detected Based on Distorted Arterial Input Function found during Quantitative Analysis of a CMR First Pass Perfusion Study

Artur Gevorgyan[1]Li-Yueh Hsu, DSc[2], Arlene Sirajuddin, MD[2], Evan A. Nelson, MD[3], W. Patricia Bandettini, MD[4], Andrew E. Arai, MD[5]

1. *National Institutes of Health, MD*
2. *National Institutes of Health, Bethesda, MD*
3. *National Heart, Lung and Blood Institute, National Institutes of Health, Bethesda, MD*
4. *National Heart, Lung and Blood Institute, National Institues of Health, MD*
5. *National Institues of Health, Bethesda, MD*

Description of Clinical Presentation: A 74 year old female presented with a chief complaint of dyspnea on exertion. She was felt to have NTHA Class II dyspnea and her symptoms were interpreted as non-anginal. She had no prior cardiac diagnoses. The patient had a left bundle branch block (LBBB) on ECG. An echocardiogram showed a mildly dilated left ventricle with an ejection fraction of 50%. Further evaluation included a normal stress myocardial perfusion SPECT study. A stress perfusion CMR scan was ordered next to evaluate for ischemia and an etiology for left ventricular dysfunction.

Diagnostic Techniques and Their Most Important Findings: On cine MRI, the LV was mildly dilated left ventricle, LVEF was 41%, and had abnormal septal motion consistent with LBBB. There was mild bilateral left atrial enlargement. The right ventricle was mildly enlarged but had normal global function. Late gadolinium enhancement was normal. First pass perfusion imaging was performed with a dual bolus acquisition protocol. Stress and rest perfusion looked qualitatively normal. Localizer images revealed an anomalous left upper pulmonary vein draining into the left brachiocephalic vein. A few weeks later, the ratio of pulmonary (Qp) and systemic (Qs) flow was Qp/Qs 1.4. Independently during quality assurance of the perfusion quantification, the arterial input function (AIF) was noted to be distorted. The arterial input function had a prolonged tail of high signal intensity prolonging the first pass of the AIF (Figure). Raw images showed high signal intensity in both the right and left ventricles throughout the acquisition after arrival of contrast in the left ventricular cavity. These findings are consistent with a left to right shunt through the anomalous pulmonary vein.

Learning Points from this Case:

1. Partial anomalous pulmonary venous drainage of the left upper lobe occurs in about 0.4-0.7% of individuals and can be confused with a persistent left superior vena cava on thoracic imaging.
2. Unlike a persistent left superior vena cava which generally does not have pathological significance, partial anomalous pulmonary venous drainage of the left upper lobe is a left to right shunt and therefore is intrinsically pathological. While a Qp/Qs ratio of 1.4 does not necessarily need surgical correction, it can explain right ventricular enlargement.
3. To the best of our knowledge, this is the first case detected on the basis of quality assurance of the arterial input function during quantitative analysis of first pass perfusion CMR. The distortion of the arterial input function violates assumptions of indicator dilution theory and may lead to unreliable myocardial perfusion results.

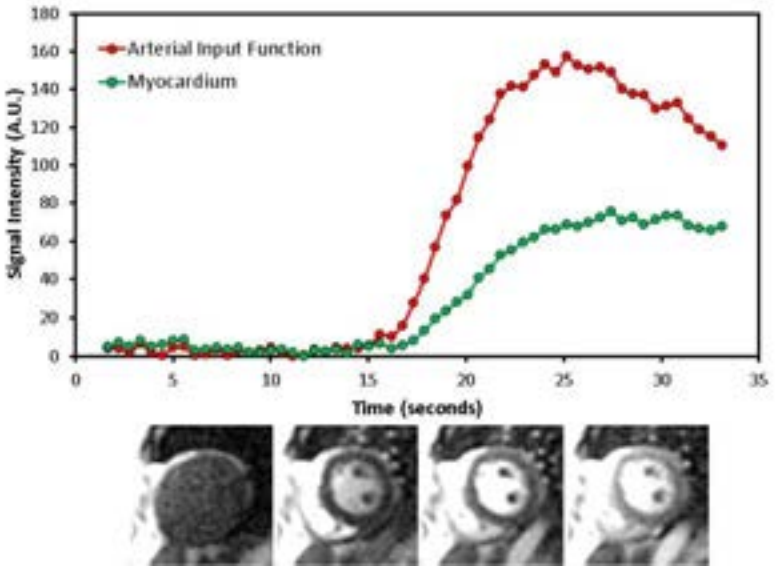

C036

Diagnostic Challenges in Cardiac Sarcoidosis

Shant Manoushagian, MD[1] Rene Alvarez, MD[2], Scott Simpson, DO[2], Chandra Dass, MD[2], William Van Decker, MD[3], Pravin Patil, MD[3]

1. Lewis Katz School of Medicine at Temple University, Philadelphia, PA
2. Temple University Hospital, PA
3. Lewis Katz School of Medicine at Temple University, PA

Description of Clinical Presentation: A 48 year old asymptomatic Caucasian male with no medical history had a right bundle branch block (RBBB) and first degree atrioventricular (AV) block on routine electrocardiogram (ECG). On echocardiogram, the right ventricle (RV) was mildly dilated and hypokinetic. Exercise nuclear stress testing revealed excellent exercise tolerance, no ischemia, and RV enlargement with fixed perfusion defects in the inferior septal wall of the left ventricle (LV). Cardiac magnetic resonance imaging (cMRI) showed late gadolinium enhancement (LGE) of the RV and inferoseptum. The patient was referred to an advanced heart failure center for possible cardiac sarcoidosis (CS). Repeat cMRI redemonstrated LGE in the same territories. Positron emission tomography (PET) showed myocardial uptake involving the entire RV with multiple metabolically active lymph nodes and lung nodules. Endomyocardial biopsy was negative for sarcoid, but supraclavicular lymph node biopsy revealed sarcoidosis. The patient was started on oral corticosteroids for presumed CS.

Diagnostic Techniques and Their Most Important Findings: **ECG** – first degree AV delay; RBBB. **Echocardiogram** – mild RV enlargement and hypokinesis; normal LV size and function. **Exercise Stress Testing with Myocardial Perfusion Imaging using Technetium–99m Sestamibi** – Bruce stage 5, 15 METs; no ischemia on ECG or nuclear imaging; RV enlargement; fixed perfusion defects in the inferior and inferior septal walls of the LV with normal function. **cMRI** – Extensive LGE of RV extending into septal segments of the LV (Figure 1). **PET with fluorine-18-fluorodeoxyglucose (FDG)** – high metabolic activity involving the entire RV with relative sparing of the LV; metabolically active hilar, mediastinal, and supraclavicular lymph nodes and lung nodules (Figure 2). **Myocardial Biopsy** – multiple specimens from RV septal wall showed hypertrophic cardiomyocytes with focal interstitial fibrosis; no inflammatory infiltrate, recent myocardial infarction, granuloma, myofiber disarray, or deposition of amyloid or iron. **Supraclavicular Lymph Node Biopsy** – positive for sarcoid

Learning Points from this Case: This case is an example of an atypical presention of CS and highlights its diagnostic challenges. This patient does not follow the usual demographic for sarcoidosis and has an unusual distribution of myocardial involvement. The Japanese Ministry of Health and Welfare (JMHW) criteria **(Table 1)** are currently used for diagnosing CS; our patient does not meet these criteria despite a high degree of suspicion. Myocardial biopsies may confirm the diagnosis but are often falsely negative due to skip lesions as is likely the case here. Findings on adjunctive imaging in this patient increased suspicion for CS despite the negative myocardial biopsy and prompted the treatment team to initiate steroid therapy. This case highlights the utility of cMRI and PET in diagnosing CS and underscores the need for more sensitive diagnostic criteria.

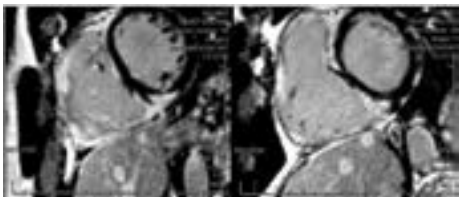

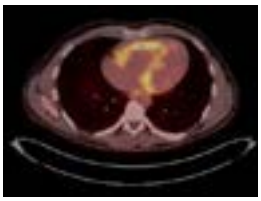

Table 1 – Japanese Ministry of Health and Welfare Criteria for Diagnosis of Cardiac Sarcoidosis

Histological Diagnosis - Endomyocardial biopsy specimens demonstrating non-caseating epithelioid granulomas with histological or clinical diagnosis of extra-cardiac sarcoidosis
Clinical Diagnosis - Endomyocardial biopsy specimens do not demonstrate non-caseating epithelioid granulomas, but extra-cardiac sarcoidosis is diagnosed histologically or clinically - Have at least two of the four major criteria, OR one in four major criteria + two or more of the five minor criteria
Major Criteria - Advanced AV block - Basal thinning of interventricular septum - Positive Gallium-67 uptake in the heart - Depressed left ventricular ejection fraction <50%
Minor Criteria - Abnormal ECG findings (ventricular arrhythmias, multifocal or frequent PVC's, complete RBBB, axis deviation, abnormal Q waves - Abnormal Echo - wall motion abnormality, morphological abnormality (aneurysm or wall thickening or ventricular dilation) - Perfusion defects on nuclear imaging (thallium-201, technetium 99m SPECT) - Delayed gadolinium enhancement on CMR - Interstitial fibrosis or monocyte infiltration on cardiac biopsy

C037

Left Dominant Arrhythmogenic Cardiomyopathy

Pravin Patil, MD[1]Shant Manoushagian, MD[2], Daniel Dries, MD[1], Joshua Cooper, MD[1], Chandra Dass, MD[1], William Van Decker, MD[1]

1. Lewis Katz School of Medicine at Temple University, PA
2. Lewis Katz School of Medicine at Temple University, Philadelphia, PA

Description of Clinical Presentation: A 37 year old woman presented with recurrent shortness of breath and non-sustained ventricular tachycardia. On her index hospitalization she was provisionally diagnosed with perimyocarditis with elevation of her troponin. Cardiac testing revealed moderate global LV hypokinesis and normal RV size and function. Cardiac magnetic resonance (CMR) confirmed biventricular function and revealed multifocal areas of late gadolinium enhancement (LGE) in the LV with a pattern suggesting myocarditis. She was optimized on medical therapy. She was discharged with a wearable defibrillator and returned with an appropriate shock for ventricular tachycardia and underwent ICD implantation. She has an extensive family history of cardiomyopathy. Her father and paternal uncle both suffered sudden death in their 30s with reported "rhythm problems." Her sister also has an unknown cardiomyopathy and has a defibrillator. Her daughter has right-sided heart failure and is being considered for heart transplantation. Given the strong family history above, our patient underwent genetic testing that included a conduction disease and arrhythmogenic cardiomyopathy panel. Testing was ARVC positive for desmoplakin (DSP) Tyr198fs, a class I mutation. Clinically she has continued to struggle with ventricular arrhythmias despite aggressive pharmacologic therapy, though complicated by issues with hyperthyroidism. Her LV systolic function remains moderately depressed with normal RV size and function. She has an AICD for secondary prevention of sudden death. She is actively being evaluated for ablative therapy and advanced heart failure therapies.

Diagnostic Techniques and Their Most Important Findings: Diagnostic workup notably included routine 2D echocardiography, cardiac magnetic resonance and genetic testing. Echocardiography revealed moderate diffuse LV hypokinesis with an LVEF 40%, no significant valvular disease and normal RV size and systolic function. Cardiac magnetic resonance confirmed biventricular function as assessed by echocardiography. There was multifocal patchy epicardial and pericardial LGE in a non-vascular distribution suggesting perimyocarditis **(Figure 1)**. There were no associated areas of T2 signal to suggest myocardial edema. Genetic testing was performed using conduction disease and arrhythmogenic cardiomyopathy panels (Transgenomic®) demonstrating a deleterious class I desmoplakin mutation, Tyr198fs.

Learning Points from this Case: The most common presentation of arrhythmogenic cardiomyopathy is that of ARVC. Left dominant arrhythmogenic cardiomyopathy (LDAC) is likely under-appreciated. In this case, CMR made note of significant LGE, but the diagnosis of LDAC was only made after genetic testing data revealed a frameshift desmoplakin mutation. This case and diagnostic workup highlight the utility of genetic testing in evaluating certain cardiomyopathies and assessing risk of sudden death.

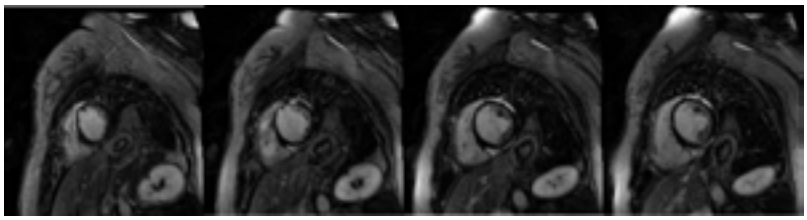

C038

Hypertrophic cardiomyopathy masquerading as cardiac amyloidosis

Tushar Kotecha, MRCP(UK) MBChB[1] Ana Martinez-Naharro, MD[2], Daniel S. Knight, MBBS MRCP(UK)[3], Rohin Francis, MBBS[4], Giulia Zumbo, MD[4], Peter Kellman, PhD[5], Marianna Fontana, MD, PhD[4]

1. *Royal Free London NHS Foundation Trust, Bushey, Hertfordshire, England, United Kingdom*
2. *National Amyloidosis Centre, University College London, London, England, United Kingdom*
3. *Royal Free London NHS Foundation Trust, London, England, United Kingdom*
4. *National Amyloidosis Centre, University College London, England, United Kingdom*
5. *Laboratory of Cardiac Energetics, National Institutes of Health/NHLBI, Bethesda, MD, United States., MD*

Description of Clinical Presentation: This 60-year old gentleman was referred to our centre with a 6-month history of progressive breathlessness. He was a smoker with a past history of hypertension and was had recently been found to be in atrial fibrillation (AF). Echocardiography performed at his local hospital had identified severe left ventricular (LV) hypertrophy with preserved radial and reduced longitudinal function. Echo and CMR locally were thought to be highly suggestive of cardiac amyloidosis, with symmetric concentric hypertrophy, typical strain pattern on echo and altered gadolinium kinetics with subendocardial late gadolinium enhancement (LGE) on CMR. However, other investigations had failed to show extra-cardiac evidence of amyloidosis.

Diagnostic Techniques and Their Most Important Findings: He underwent repeat CMR at our centre (Figure 1). Imaging showed severe symmetric hypertrophy (maximal wall thickness 30mm at mid-septum) and increased LV mass. There was good radial function (LV ejection fraction 73%), preserved apical contraction and severely reduced longitudinal function. There was inferior insertion point LGE but also diffuse sub-endocardial LGE more prominent at the level of the inferoseptum, inferior, inferolateral and lateral walls. Importantly, native T1, T2 and ECV were normal in the remote myocardium. Whilst the cine imaging showing symmetrical hypertrophy and reduced longitudinal function was consistent with cardiac amyloidosis, the pattern of LGE was atypical. In this case, the T1 maps and ECV were essential to demonstrate that the increased mass was due to myocyte hypertrophy rather than expansion of the extracellular space. These finding were therefore in keeping with a diagnosis of hypertrophic cardiomyopathy.

Learning Points from this Case: This case demonstrates that, where traditional imaging techniques show atypical features, mapping sequences can play an important role in differentiating the underlying cause of cardiomyopathy.

http://www.ConferenceAbstracts.com/uploads/cfp2/attachments/LDFAIBDN/LDFAIBDN--222361-1-ANY.pdf

C039

Apical variant hypertrophy in Anderson Fabry Disease

Bharath Sathya, MD[1] Andrew E. Arai, MD[2]

1. National Institutes of Health, Bethesda, MD
2. National Institues of Health, Bethesda, MD

Description of Clinical Presentation: A 53-year-old female presented with complaints of dyspnea and lightheadedness on exertion. Her past medical history was significant for Anderson Fabry disease and heart failure with preserved ejection fraction. She was currently on enzyme replacement therapy. Physical examination was notable for a 2/6 systolic ejection murmur auscultated loudest at the apex without radiation. ECG demonstrated sinus rhythm and left ventricular hypertrophy associated with deep anterior and anterolateral T wave inversions.

Diagnostic Techniques and Their Most Important Findings: A transthoracic echocardiogram noted severe left ventricular hypertrophy with hyperdynamic left ventricular systolic function and no significant left ventricular outflow tract (LVOT) gradient. CMR was performed on a 3T Siemens Magentom Skyra. Short axis steady state free precession (SSFP) cine imaging showed marked mid and apical left ventricular hypertrophy with a maximum measured septal thickness of 16.7 mm. The left ventricle was hyperdynamic and exhibited systolic cavity obliteration of the mid to apical LV cavity. The 4-chamber SSFP cine MRI demonstrated a spade shaped left ventricle. Late gadolinium enhancement (LGE) imaging utilizing segmented phase sensitive inversion recovery demonstrated abnormal intermediate enhancement in the basal inferolateral segment. Native T1 measurements obtained in selected short axis and 4 chamber views showed an average of 1249. The normal T1 value on a 3T scanner in our lab was 1247 +/- 50. The only sector with abnormally low T1 was the basal inferoseptum (1164-1203 ms). Velocity encoded phase contrast imaging demonstrated flow acceleration in the left ventricular outflow tract at the level of the aortic valve with velocity encoding set at 170 cm/second.

Learning Points from this Case: 1) Anderson Fabry disease is an underdiagnosed etiology in suspected hypertrophic cardiomyopathy. A study by Elliot et al. demonstrated that 0.5% of patients with unexplained severe left ventricular hypertrophy carried the alpha-galactosidase mutation. Typical findings in the apical variant of cardiac Fabry disease include significant left ventricular hypertrophy from to mid left ventricle to apex, and fibrosis in the basal inferolateral segment on late gadolinium imaging. In a study by Deva et al., 5% of patients with known cardiac involvement in Anderson Fabry disease (AFD) were recognized to have the apical variant. 2) Prior studies have demonstrated that T1 measurements obtained in Anderson Fabry disease patients are significantly lower than in normal volunteers. In this case, the patient had an average T1 measurement within the normal range. It is possible that these values could represent treatment effect from enzyme replacement. However, there is a paucity of data regarding the effect of treatment on myocardial T1 measurements.

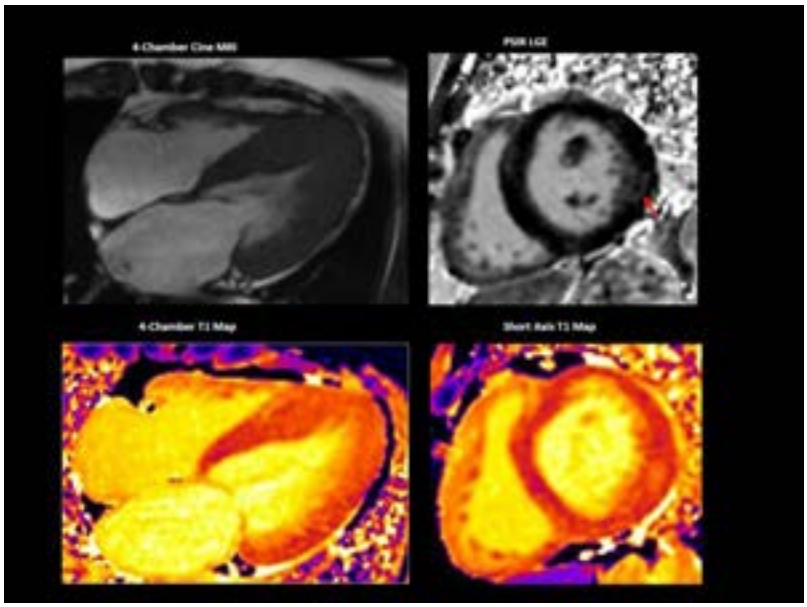

C040

CASE: MRI characteristics of myocardial involvement in Churg-Strauss vasculitis

Purvi Parwani, MBBS[1] Karen Ordovas, MD, MAS[2]

1. University of california, San Francisco, CA
2. University of California San Francisco, San Francisco, CA

Description of Clinical Presentation: 58 year old female with recurrent sinusitis, nasal polyposis and adult onset asthma presented to emergency room with typical chest pain. She didn't any traditional risk factors of coronary artery disease like diabetes, hypertension, family history of CAD or smoking. She denied any other cardiac symptoms. Her BP was 150/90 with a pulse of 64. physical examination were within normal limits

Diagnostic Techniques and Their Most Important Findings: Patient was found to have hypereosinophilia (27.8% of total WBC, abs eosinophil of 2000) but perinuclear anti-neutrophil cytoplasmic antibody was negative. The diagnosis of churg-staruss vasculitis was made. An electrocardiogram showed sinus rhythm with a rate of 65 beats per minute. The echocardiogram showed normal biventricular function with impaired LV relaxation and small pericardial effusion. Cardiac catheterization didn't show any coronary artery disease. Cardiac MRI was done. SSFP cine and late gadolinium enhanced(LGE) sequences were acquired in the short axis, horizontal and long axis planes. Cardiac MRI revealed normal LV and RV function without any regional hypokinesis but diffuse subendocardial and midwall enhancement of the anterolateral, inferolateral, and inferior walls of the left ventricle.

Learning Points from this Case: Myocardial involvement in Churg-Strauss syndrome detected by LGE imaging may be observed even when findings by echocardiography are still normal. CMR can therefore serve as a more sensitive means to detect early cardiac involvement and help clinicians decide when treatment should be instituted or modified.

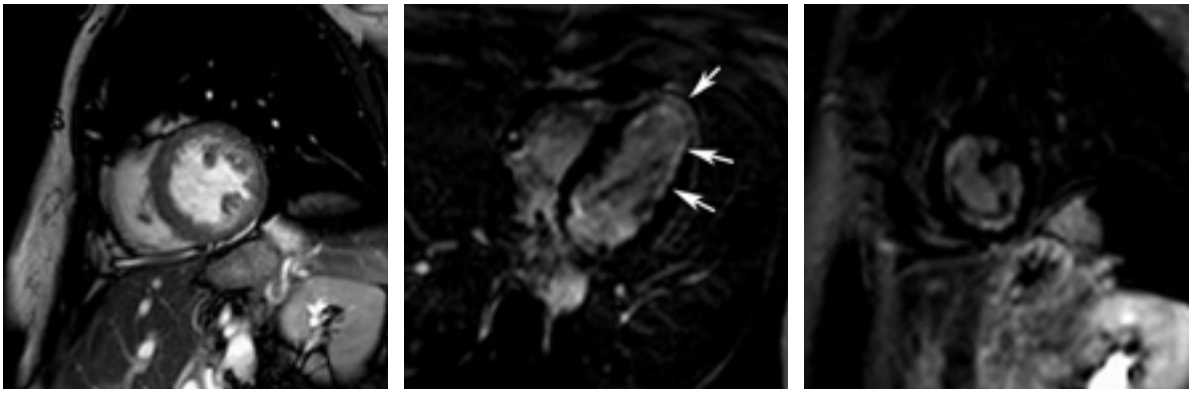

C041

A Pain in the Neck: Differentiating Between an Aneurysm and a Pseudoaneurysm of the Left Ventricle Post-Myocardial Infarction

Weiyi Tan, MD, MPH[1] Peyman Benharash, MD[1], Shelley Shapiro, MD. Ph.D[1], Alberta L. Warner, MD[1], Kim-Lien Nguyen, M.D.[2]

1. David Geffen School of Medicine at UCLA, VA Greater Los Angeles Healthcare System, Los Angeles, CA
2. Division of Cardiology, David Geffen School of Medicine at UCLA and VA Greater Los Angeles Healthcare System, CA

Description of Clinical Presentation: A 73-year old man was admitted to the hospital with shortness of breath and lower extremity edema for two days. Three months prior to admission, the patient suffered from a late-presenting anterior ST-elevation myocardial infarction (STEMI) with placement of four drug-eluting stents. He was discharged home in stable condition with no signs of heart failure . On admission, he presented to the emergency room with complaints of dyspnea on exertion and lower extremity swelling. On examination, the patient had vital signs within normal limits. His exam was unremarkable except for jugular venous distension to 10 cm of water, mild bilateral pitting edema of the lower extremities, and a laterally displaced apical impulse. Labs revealed a BNP of 1115 pg/mL. Echocardiogram showed severely reduced left ventricular systolic function with aneurysmal apex and layered thrombus. An EKG-gated CT angiogram of the chest confirmed the existence of a large aneurysm at the apex of the left ventricle (Figure 1A), but differentiation between a true aneurysm versus pseudoaneurysm of the left ventricle was challenging. The next day, cardiac magnetic resonance (CMR) imaging with and without contrast was performed (Figure 1C-D, Figure 2, Figure 3A-B). The patient was referred for aneurysmectomy and Dor procedure. Pathology samples from the surgery confirmed the diagnosis of a pseudoaneurysm (lack of myocardium or endocardium around the aneurysmal segment) and need for high risk surgery (up to 30% mortality) (Figure 3C).

Diagnostic Techniques and Their Most Important Findings: CMR: EKG-gated and real time cine imaging along with LGE. A large left ventricular aneurysm with contained rupture (pseudoaneurysm) was present and involved the entire apex. Dense thrombus, cellular debris, and fluid within the pericardial sac. The pericardium was thick with hyperenhancement. The neck of the pseudoaneurysm measured 5.1-5.9cm. The basal-mid left ventricle walls were viable with a transmural myocardial infarction involving the mid to apical left ventricle.

Learning Points from this Case: This case highlights the difficulty of differentiating between a true aneurysm and a pseudoaneurysm of the left ventricle after a myocardial infarction. The distinction between true aneurysm versus pseudoaneurysm is vital to the patient's long-term outcome, as pseudoaneurysms that are treated with medical therapy alone have a high risk of rupture and a mortality of almost 50%.[i] The best imaging strategy may have been echo as the initial screening tool followed by CMR for additional tissue characterization. In this case, CMR is a value added imaging modality that facilitates differentiation between true aneurysms and pseudoaneurysms. Findings such as a hyperenhanced pericardium, detection of a complex left ventricular thrombus, and lack of myocardium located at the aneurysmal site may point towards the diagnosis of a pseudoaneurysm.[ii]

[i] Frances, et al., JACC Vol. 32, No. 3 September 1998:557–61 [ii] Konen, et al., Radiology 2005; 236:65–70

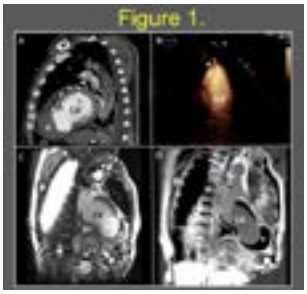

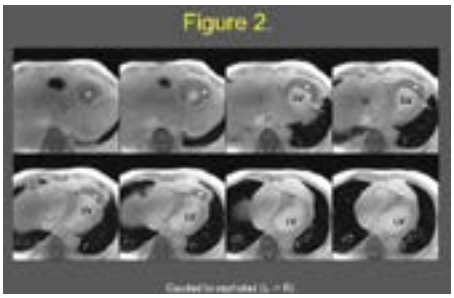

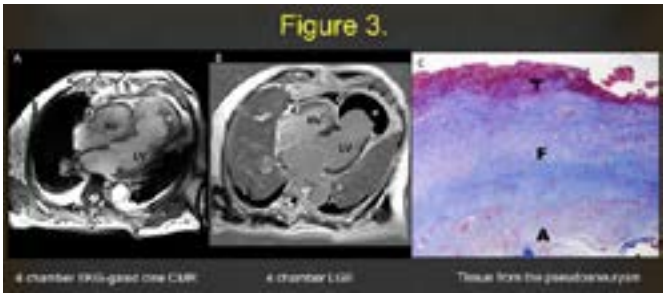

C042 23

Year Old Male Presenting for Dilated Cardiomyopathy Evaluation

Evan A. Nelson, MD[1] Christine Mancini, RT[2], Andrew E. Arai, MD[1], Sujata M. Shanbhag, MD, MPH[3]

1. National Heart, Lung and Blood Institute, National Institutes of Health, Bethesda, MD
2. Suburban Hospital, MD
3. NIH/NHLBI, Bethesda, MD

Description of Clinical Presentation: A 23 year old male who was previously healthy presented to a primary care physician for a routine evaluation. At that time he was noted to have a wide left bundle branch block on his EKG and was sent to a cardiologist for further workup. His initial workup included a normal exercise stress nuclear test. He also had a TTE which showed severely reduced left ventricular function and a dilated left ventricular chamber. He was placed on low doses of carvedilol and lisinopril due to borderline low systolic blood pressure. On subsequent follow up TTEs, the patient's ejection fraction had increased to 35% and ICD was considered however the patient was reluctant. He sought a second cardiology opinion which lead to a cardiac MRI for a more accurate ejection fraction calculation and evaluation of late gadolinium enhancement for scar quantification.

Diagnostic Techniques and Their Most Important Findings: His cardiac MRI findings were diagnostic for left ventricular non-compaction cardiomyopathy (LVNC). The non-compacted myocardium was very prominent in both the long a short axis SSFP cine imaging. The non-compacted to compacted myocardium ratios were as high as 5 in the mid-inferolateral wall. The papillary muscle architecture was poorly formed and the trabeculations from all of the myocardial segments appeared to coalesce to form a central connection point. This central connection point was slow to enhance on early gadolinium enhancement imaging, however was brightly enhanced on the late gadolinium imaging due to the heavy amount of scarring in this area. Additionally, there was dense fibrosis at the base and mid portion inferoseptum on late gadolinium enhancement imaging. There was no evidence of intra-cardiac thrombus.

Learning Points from this Case: 1. Cardiac MRI can reveal diagnoses not apparent on transthoracic echocardiography. 2. The central connection point which exhibited marked fibrosis on late gadolinium enhancement imaging has not previously been described in the literature. 3. The extent and severity of late gadolinium enhancement correlates with severity of the cardiomyopathy in LVNC. 4. In the setting LVNC, there have been no direct correlations between the presence of late gadolinium enhancement and arrhythmic events which may be a worthwhile area of future research.

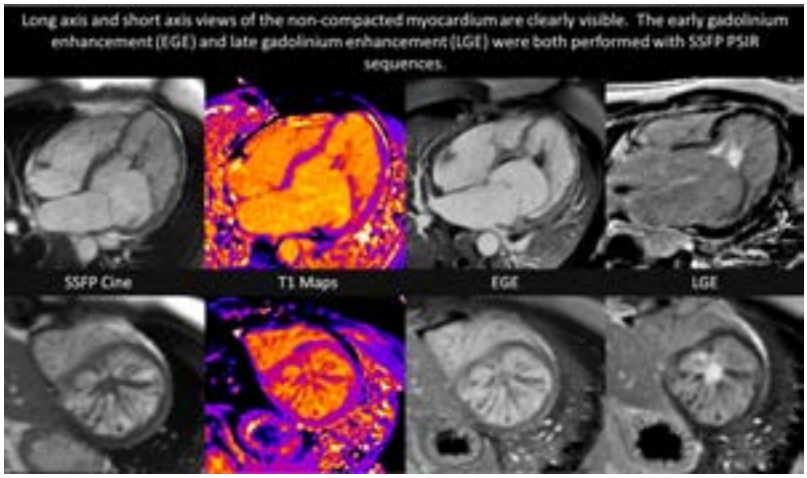

C043

Multimodality imaging of protracted complications of aortopathy in Ehlers Danlos syndrome

Zohya Khalique, MBBS[1] Evangelia Nyktari, MD[2], Raad Hashem Mohiaddin, MD PhD[3]

1. NIHR Cardiovascular Biomedical Research Unit, Royal Brompton Hospital, London, England, United Kingdom
2. Royal Brompton Hospital, England, United Kingdom
3. Royal Brompton Hospital and Imperial; College London, London, England, United Kingdom

Description of Clinical Presentation: A 24 year old man presented with retrosternal chest pain. His index CMR scan showed a dilated sinus of Valsalva with a cusp-cusp diameter of 49mm. He was consequently diagnosed with vascular Ehlers Danlos syndrome (EDS) and underwent a freestyle root and aortic valve implantation. However a year later he had developed aortic valve infective endocarditis, necessitating a redo perimount AVR. Tissue from his first aortic valve grew the fungus purpureocillium lilacinum. He had on-going pyrexia and underwent both PET and CT imaging. He had developed a mycotic aneurysm of his infrarenal aorta, with a retroperitoneal abscess, requiring surgical removal and drainage. A right common iliac aneurysm was also identified. Two years later he was admitted with sudden right foot numbness and pain, due to lower limb emboli. He underwent a femoral embolectomy and left to right femoral to femoral cross over graft. The removed clot grew purpureocillium lilacinum and hence the patient was started on lifelong voriconazole. Further PET-CT suggested no further active infection. He was considered free of fungal infection and reassured, until his next presentation.

Diagnostic Techniques and Their Most Important Findings: On re-presentation his echocardiogram detected a large mass in the ascending aorta, requiring further assessment. His CMR demonstrated one complex false aneurysm at the anterior mid ascending aorta and another posteriorly at the level of the aortic root. The anterior aneurysm has a narrow neck to which a large mobile mass (39mm x 10mm) was attached. A second smaller mass was adjacent to the AVR (Figure 1). These had low signal intensity in T1 and T2 weighted images and did not enhance with gadolinium contrast. Hence they were reported as being more consistent with thrombi than vegetation. CT also confirmed the aneurysms. His brain MRI showed multiple abscesses as shown in Figure 3. His brain CT reported ventricular haemorrhage, features of raised intracranial pressure and tonsillar herniation. The patient died two days later.

Learning Points from this Case: Ehlers-Danlos syndrome is a disorder of abnormal collagen with a mean lifespan of 48 years and expected complication rate of 80%, often fatal due to arterial rupture. We show a case of multiple aneurysms associated with mycotic thrombi as another complication, sadly associated with early death at the age of 28 years. CMR is invaluable in the assessment of vascular complications of EDS and is unique in enabling tissue characterisation, in this case distinguishing thrombi from other masses.

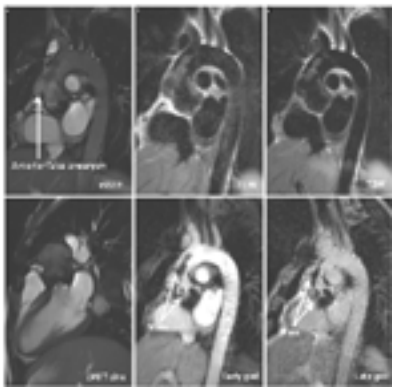

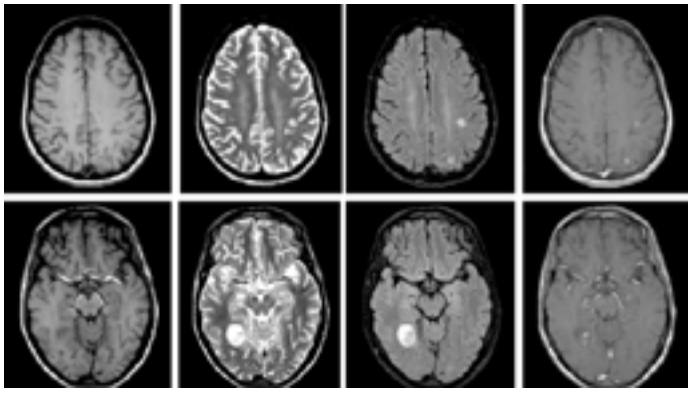

C044

CMR Images Dictate and Help Execute Treatment Plan in Catheterization Lab

Nimisha Aggarwal, M.D.[1]Adrienne E. Campbell-Washburn, PhD[2], Joshua Kanter, MD[3], Kanishka Ratnayaka, MD[4], Anitha John, M.D.[5], Laura Olivieri, M.D.[6]

1. *Children's National Health System, DC*
2. *National Heart, Lung, and Blood Institute, National Institutes of Health, MD*
3. *Children's National Medical Center, DC*
4. *Rady Children's Hospital, CA*
5. *Children's National Healthy System, DC*
6. *Children's National Medical Center, Washington, DC*

Description of Clinical Presentation: The patient is 17-year-old male with history of bicuspid aortic valve and severe coarctation of the aorta who is status post stent angioplasty 3 years prior. At that time, he had near interruption of his aorta with a severe narrowing to less than 1.5mm in diameter. He had a Cordis XL 3110 stent placed within the coarctation with no residual stenosis identified, and a resultant diameter of 14mm. He presented 3 years later for possible dilation of the stent. He underwent a cardiac MRI prior to his catheterization which demonstrated a complex pseudoaneurysm extending from the superior aspect of the stent to the inferior aspect. In light of these CMR findings, the patient underwent covered stent angioplasty in the catheterization lab under x-ray fused with MR (XFM) guidance.

Diagnostic Techniques and Their Most Important Findings: The complex pseudoaneurysm was suspected based on T2-TSE imaging, where the stent appeared to "float" in the lumen of the aorta (Figure A). Findings were confirmed on magnetic resonance angiography despite the artifact from the metal stent (Figure B-1); however, the pseudoaneurysm was not obvious on the 3D SSFP imaging due to artifact from the stent (Figure B-2). The pseudoaneurysm was treated through placement of a covered stent within the previously placed stent to exclude the aneurysmal segment. The pseudoaneurysm coursed from the anterior and superior rim of the stent and wrapped around to the posterior and inferior rim. This made the placement of the covered stent challenging, as the transverse aortic arch and left subclavian artery were at risk for compromise. During the placement and deployment of the stent within the catheterization lab, a 3D digital image was overlaid onto the fluoroscopy screen using the XFM technique (Figure C). This enhanced visualization of the pseudoaneurysm while selecting and positioning the covered stent.

Learning Points from this Case: CMR done prior to cardiac catheterization in this case was a pivotal part of the diagnosis and management plan. The positioning of the covered stent was aided by the XFM images and thus led to a positive outcome for the patient. The fact that the pseudoaneurysm could clearly be seen with MRA and not with 3D-SSFP technique must also be noted. It is possible the diagnosis would have been missed if only 3D-SSFP images were acquired.

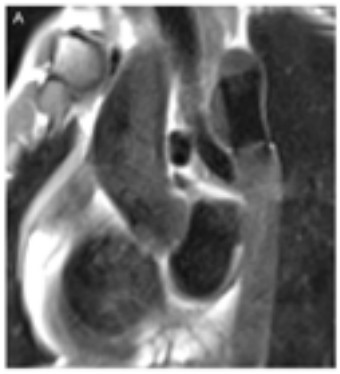

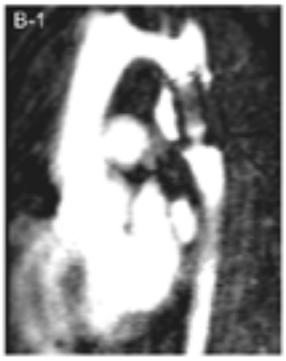

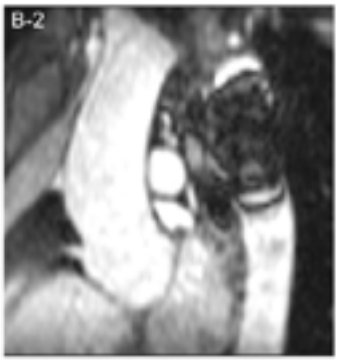

C045

Primary aortic intimal sarcoma initially presenting as low extremity thromboembolism

Yeseul Jo, M.D.Jung Im Jung, M.D., Ph. D.

Department of Radiology, Seoul St. Mary's Hospital, College of Medicine, The Catholic University of Korea, N/A, Republic of Korea

Description of Clinical Presentation: A 74-year-old male came to our emergency department with chief complaint of right leg numbness. The numbness started suddenly in the morning involving both legs with tingling sensation, and the symptom of left leg only lasted few minutes. His right foot was cold and pale, and the physical examination showed pulseless right dorsalis pedis artery.

Diagnostic Techniques and Their Most Important Findings: Lower extremity artery 3D CT was performed. The bilateral anterior and distal posterior tibial arteries were not opacifed after contrast injection and showed abrupt cutoff, which suggested thromboembolism. Also, an about 1.1X4.6 cm sized irregular filling defect was noted at the left lateral aspect of mid-descending thoracic aorta. To differentiate thrombus from tumor, thoracic aorta MR angiography (MRA) was done. The filling defect in the thoracic aorta showed high signal intensity on T2 weighted images and peripheral enhancement after gadolinium contrast injection, suggesting tumor rather than thrombus. PET-CT showed FDG uptake of the mass (SUV max 4.6), suggesting malignancy.

Learning Points from this Case: Right posterior artery thrombectomy was firstly performed. The pathological study showed thrombus with some atypical cells, which led to suspicion of malignancy. The resection of the mass and graft interposition of thoracic aorta was done subsequently. Histological examination revealed poorly differentiated intimal sarcoma.

Acute thromboembolism is commonly caused by atherosclerotic, but the possibility of tumor in the proximal artery should be considered. Aortic intimal sarcoma is an aggressive tumor with extremely low incidence. It is mostly accompanied by embolic phenomena. MRA of the aorta is the most sensitive imaging modality for the detection of the tumor. MRA study can differentiate tumor from atheromatous plaque by enhancement and reveal the extent of the tumor and involvement of the adjacent structures without invasive procedure.

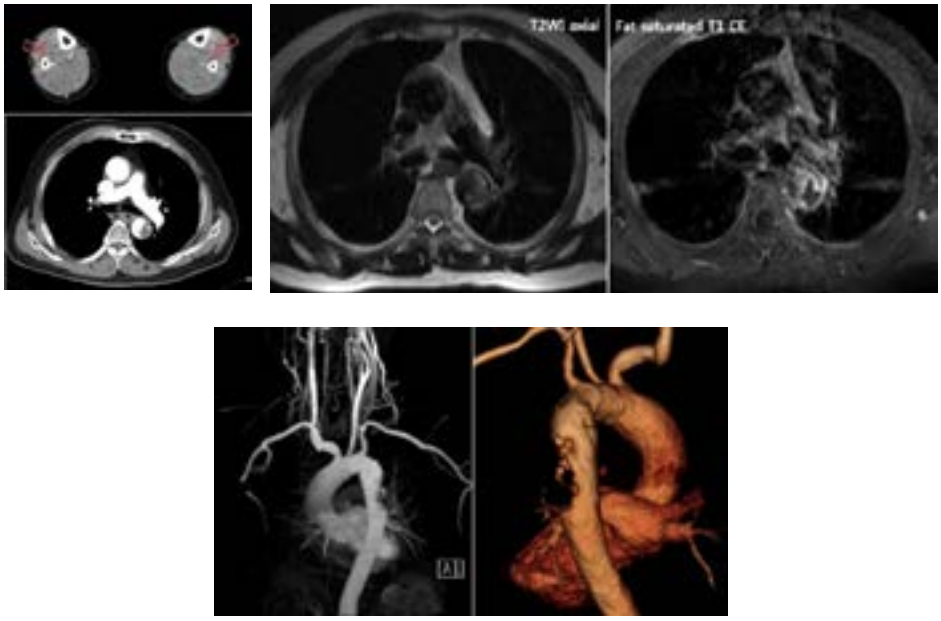

C046

Non malignant superior venacava syndrome and utility of gadofoveset in imaging of superior venacava and bypass grafts.

Vimalkumar Veerappan Kandasamy, MDRajeev R. Fernando, MD

University of Louisville, Louisville, KY

Description of Clinical Presentation: 44-year-old male with past medical history of Alport syndrome leading to end statge renal disease presented with right upper extremity and facial swelling for 11 months. Previously, he underwent living related kidney transplantation in 1992 with transplant failure in 1998 and subsequent cadaveric renal transplant in 2010. He had multiple failed central venous catheters for dialysis in both the subclavian veins including Cannon catheters, tunneled catheters and failed AV fistulas. CT chest with IV contrast demonstrated brachio-cephalic vein (BCV) occlusion and initially underwent venoplasty and BCV stent. He had recurrence of symptoms and venography showed occluded stent for which he underwent catheter directed thrombolysis with no resolution of occlusion or symptoms. Transesophageal echocardiography showed severely dilated superior venacava (SVC) and thickened pericardium. Operative room exploration showed the junction of the BCV, right subclavian vein, and SVC were completely occluded with extensive superficial collateral veins. Due to the extent of obstruction, it was not possible to remove the obstructed segment and primarily reconstruct the SVC. Subsequently, a 10 mm ring Gore-Tex(polytetrafluroethylene) graft was used to anastomose the right internal jugular vein (RIJV) to the right atrial appendage(RAA). Patient had an uneventful post operative course. He also underwent anterior pericardiectomy for pericardial thickening and calcification. During the follow-up, MRA was done to look for graft patency and the anastomotic sites and rule out thoracic outlet compression of the graft. We discuss below the novel technique we utilized in imaging of the SVC graft.

Diagnostic Techniques and Their Most Important Findings: MRA showed dilated RIJV, ocluded left IJV. A graft was seen from the RIJV to the RAA. The graft coursed anteriorly just behind the sternum and finally terminates at the RAA. Gadofoveset enhanced images showed - the stent in the left BCV was occluded. The proximal and distal anastomotic sites of the RIJV to the RAA were patent. The body of the graft appeared patent.

Color Doppler ultrasound has high sensitivity and specificity for detecting catheter associated thrombus, however SVC cannot be directly imaged due to acoustic shadowing by the overlying ribs. We utilized a novel approach using gadofoveset contrast agent, which is a gadolinium based contrast agent which is reversibly bound to albumin and imaging can be performed upto 1 hour after a single low dose injection. Gadofoveset is approved by FDA for use in Aortoilliac occlusive disease in adults with known or suspected peripheral vascular disease. Recent trial by Kim et al, showed that, gadofoveset enhanced MRV resulted in adequate visualization of the thoracic vessels including central veins, pulmonary arteries and thoracic aorta in equilibrium phase in healthy volunteers.

Learning Points from this Case: Catheter-induced SVC syndrome is a rare but very serious complication in patients. Gadofoveset enhanced MRA can be used for imaging of the central veins.

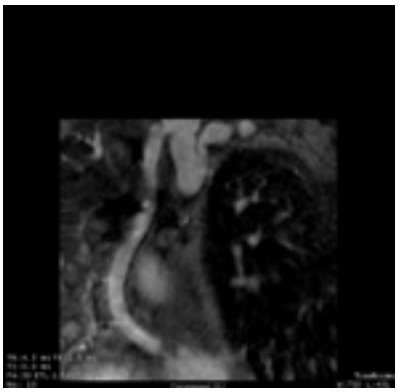

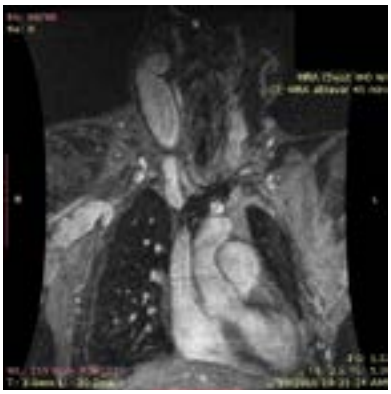

C047

Infiltrative aortitis causing sinus of Valsalva pseudoaneurysm in a patient with lymphocytic variant hypereosinophilic syndrome

Tushar Acharya, MD[1]Paneez Khoury, MD [2], Arlene Sirajuddin, MD[3], Marcus Y. Chen, MD[1], Andrew E. Arai, MD[4], W. Patricia Bandettini, MD[5]

1. *National Heart, Lung and Blood Institute, National Institutes of Health, Bethesda, MD*
2. *National Institute of Allergy and Infectious Diseases, National Institues of Health, Bethesda, MD*
3. *National Institutes of Health, Bethesda, MD*
4. *National Institues of Health, Bethesda, MD*
5. *National Heart, Lung and Blood Institute, National Institues of Health, MD*

Description of Clinical Presentation: An 18-year-old African-American male with marked eosinophilia since 2006, severe atopic dermatitis, reactive airway disease, food allergies, and lymphadenopathy was found to have a clonal T-cell (CD3-, CD4+) infiltration of the skin, lymph nodes, bone marrow and blood and diagnosed with lymphocytic variant hypereosinophilic syndrome (LHES). Until recently, he had been active and played competitive sports without dyspnea, palpitations or syncope. He had been on chronic steroid therapy for the eosinophilia for three years with waxing and waning skin disease. He had been treated with corticosteroids, imatinib, interferon-alpha and topical corticosteroids with limited success in controlling the eosinophilia.

Diagnostic Techniques and Their Most Important Findings: A routine echocardiogram showed an echo-dense region around the aortic annulus. Cardiac CT found an 11 x 11 x 5 mm outpouching of the posterior aspect of the left sinus of Valsalva consistent with a pseudoaneurysm. The pseudoaneurysm wall separating the left coronary sinus from the left atrium was ~6 mm thick. On CMR, the thick wall of the pseudoaneurysm was comprised of non-fatty tissue based on signal intensities on cine MRI, Dixon fat/water separation images, T1-weighted images and black blood fat-suppressed T2-weighted turbospin echo images. The prolonged T1 and T2 were consistent with either edematous or hypervascular tissue that could represent inflammation. No fistula or flow from the pseudoaneurysm to the left atrium was detected on velocity-encoded phase contrast imaging. The aortic valve cusps and left main ostium were not involved. Additional clinical questioning after the CT and CMR revealed moderately severe but atypical chest pain episode in 2010. Retrospective review of an echo from 2012 and chest CT from 2010 showed a similar but smaller density in the same location, suggesting a chronic process. Clinical correlation suggested inflammatory eosinophilic infiltration of the aortic root to be the most likely etiology for pseudoaneurysm formation. Endocarditis was ruled out with negative cultures. The patient was treated aggressively with high dose steroids and mepolizumab with a subsequent reduction of absolute eosinophil count (7530/uL at the time of identification of pseudoaneurysm; 1780/uL two months later; 890/uL four months later). The inflammatory lesion improved on imaging after reduction of eosinophil counts following two months of therapy.

Learning Points from this Case:

1. Sinus of Valsalva pseudoaneurysm is a rare manifestation of an eosinophilic syndrome.
2. CMR is a useful diagnostic tool for inflammatory/infiltrative conditions of the aortic root. CMR can evaluate anatomy, detect or exclude fistulas between the aortic root and cardiac chambers, and offers tissue characterizations that can point to active local inflammation.
3. CMR is an excellent imaging modality for characterizing and following aortic root abnormalities particularly in a patient that is allergic to CT contrast and is less invasive than transesophageal echocardiography.

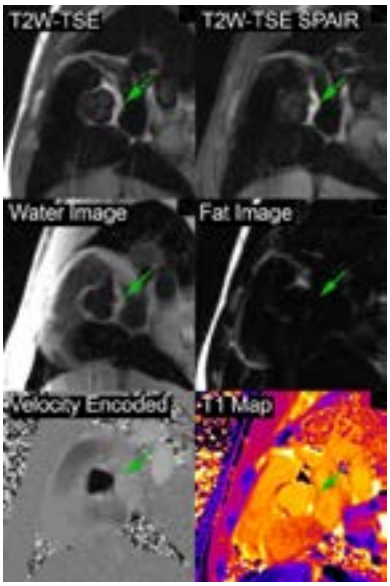

C048

Acute Aortic Syndrome Diagnosed with Noncontrast Magnetic Resonance Imaging

Piyush Sovani, MD[1] Monvadi B. Srichai, MD, MS[2]

1. Medstar Georgetown University Hospital, Washington, DC
2. Medstar Georgetown University Hospital, DC

Description of Clinical Presentation: A 79 year-old Caucasian woman with hypertension presented to the emergency department with 2 weeks of worsening lower extremity edema and dyspnea on exertion. Physical exam was notable for tachycardia with irregularly irregular rhythm and lower extremity pitting edema.

Diagnostic Techniques and Their Most Important Findings: Her electrocardiogram (EKG) showed atrial fibrillation with rapid ventricular response (Figure 1). Laboratory studies demonstrated severe renal insufficiency. Transthoracic echocardiogram (TTE) howed mildly dilated left ventricle with moderate systolic dysfunction with ejection fraction of 35-40%, and normal aortic root size but severely dilated ascending aorta measuring 5.9 cm in maximal diameter (Figure 2). Computerized tomography (CT) scan was deferred due to severe renal insufficiency. Transesophageal echocardiography (TEE) was considered risky due to acute heart failure and possible incomplete evaluation of the ascending aorta due to technique. Therefore, noncontrast cardiac magnetic resonance imaging and angiography (MRI/MRA) was performed, and demonstrated a type A aortic dissection extending from sinotubular junction to before the aortic arch (Figure 3), with aneurysmal dilation of 6.4 cm at the mid ascending level and partial thrombosis of the false lumen. There was no involvement of the coronaries.

Learning Points from this Case: Rapid, accurate diagnosis of acute aortic syndromes is important to facilitate patient management. This case demonstrates the important role of cardiac magnetic resonance imaging in diagnosing acute aortic syndromes, particularly for patients with renal insufficiency. TTE is a very useful technique that can be performed at the bedside and may screen for the proximal 4 to 8 mm of the ascending aorta to above the sinotubular junction. The distal ascending aorta and arch are not well visualized and require alternative techniques for evaluation of acute aortic syndromes. TEE allows for visualization of both the ascending and descending aorta and portions of the arch with high accuracy for detection of acute aortic syndromes. TEE can also be performed at the bedside but requires adequate sedation, which can be difficult in unstable patients. CT is the preferred modality to evaluate for aortic dissection in the emergencies, given its high accuracy, wide availability, and 3 dimensional volumetric imaging of the entire aorta. However, accurate diagnosis requires use of iodinated contrast with increased risk for nephrotoxicity. Cardiac MRI is highly accurate for detection of aortic syndromes providing information on aortic dimensions, hemodynamic assessments, and potential wall shear stress. MRI does not require radiation or contrast administration to generate image contrast. Noncontrast MRA techniques are increasingly used to provide similar 3-dimensional volumetric information as CT with contrast. Our patient underwent emergent replacement of her ascending aorta with a graft and resuspension of the aortic valve and was discharged to a rehabilitation facility in stable condition.

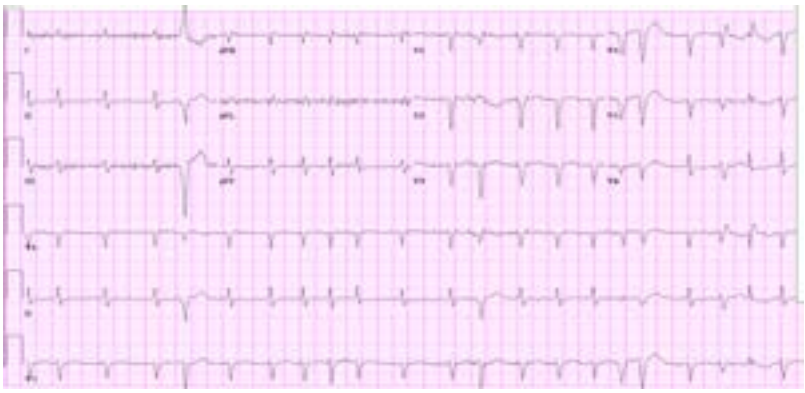

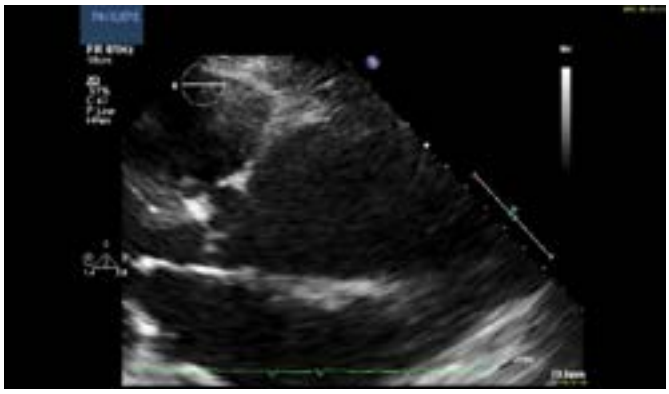

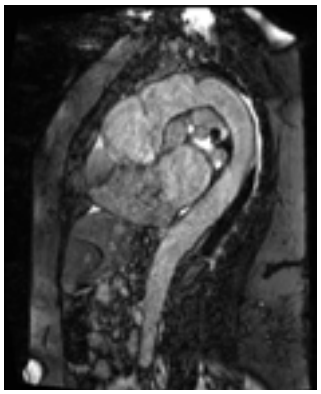

C049

A case of midaortic syndrome due to Neurofibromatosis Type 1

Satyam Veean, BS[1]Gyanendra Sharma, MD[2], William Bates, MD[1], Jayanth H. Keshavamurthy, MD[3]

1. Augusta University, GA
2. Medical College of Georgia at Augusta University, GA
3. Medical College of Georgia at Augusta University, Augusta, GA

Description of Clinical Presentation: We report a case of a 9-year-old female with history of Neurofibromatosis type 1 (NF1) found to have incidental hypertension upon physical exam. She was asymptomatic and had no family history of NF1. She remained hypertensive in all four extremities even after medical treatment. CT angiogram confirmed narrowing of the abdominal aorta above the bifurcation and atrophic left kidney. Treatment with a graft to bypass the stenotic segment was performed. During follow up cardiac MRI, severe aortic insufficiency is noted along with patent abdominal aortic graft segment.

Diagnostic Techniques and Their Most Important Findings: Cardiac MRI showed left ventricle normal in size with wall motion and function. Left ventricular ejection fraction was 59% and LV end diastolic volume was 203 mL. There were no perfusion defects or abnormal areas of enhancement on delayed inversion recovery images to suggest scar or fibrosis. There was severe aortic insufficiency with regurgitation fraction of 71%. The thoracic aorta measures 2.8 cm at the sinus of Valsalva. The ascending thoracic aorta measures 2.0 cm. A bicuspid aortic valve is present. MRI of the abdomen showed a patent graft unchanged in caliber since the prior exam in 2014.

Learning Points from this Case: Midaortic syndrome (MAS) is a rare entity that affects children and young adults. It is characterized by progressive narrowing of the abdominal aorta and its major branches. The usual presentation is most commonly with hypertension, renal failure, and intermittent claudication.

MAS can be attributed to Neurofibromatosis type 1, Williams syndrome, Takayasu arteritis, or Turner's syndrome.

NF1 has many phenotypes. A rare phenotype is NF1 vasculopathy, with prevalence of up to 6% in NF1 patients. The loss of neurofibromin, encoded by the NF1 gene, regularly expressed by endothelial cells to regulate cell proliferation, may lead to unregulated smooth muscle proliferation. NF1 vasculopathy can take the form of mid-aortic syndrome or coarctation of the abdominal aorta.

Midaortic syndrome can be treated medically and/or via endovascular or surgical methods. Surgery is superior in providing long-term patency rates before re-intervention.

MAS is commonly associated with the finding of a bicuspid aortic valve. Our patient had a bicuspid valve and she progressively became symptomatic. Her cardiac MRI showed significant insufficiency. Most cases of MAS and bicuspid aortic valve require surgery to ameliorate the problem.

It is also important to note that this patient has been followed up for 13 years status post graft placement for her abdominal coarctation. The graft remains patent and shows the superiority of surgery in treatment of this disease.

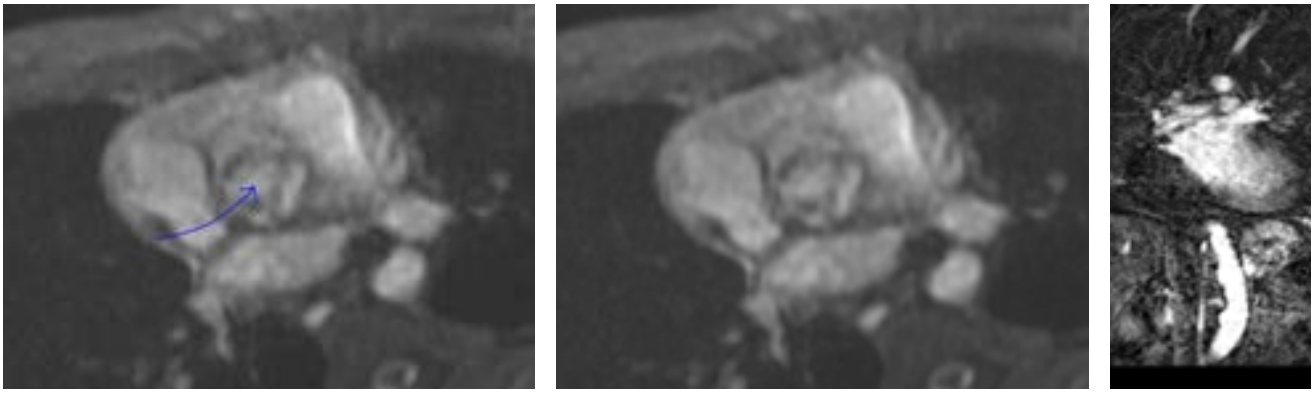

C050

Unusual case of a young male with a large thrombus in the heart

Naveen Rajpurohit, MD[1] Venkateshwar Polsani, MD[2], Robi Goswami, MD[3], Ashish Kabra, MD[4]

1. *Sanford Cardiovascular Institute, Sioux Falls, SD*
2. *Piedmont Heart Institute, Atlanta, GA., Atlanta, GA*
3. *Piedmont Heart Institute, Atlanta, GA*
4. *Piedmont Heart, Atlanta, GA*

Description of Clinical Presentation: A 27 year of male with past medical history of recurrent axillary cysts presented to his primary care physician for a routine physical exam. Patient was an avid traveler and had lived for prolonged periods in South America. He did not have any complaints and his clinical exam was unremarkable. An electrocardiogram (ECG) was performed as part of routine cardiac evaluation (Figure 1). The ECG showed normal sinus rhythm with inverted T waves in the antero-lateral leads.

Diagnostic Techniques and Their Most Important Findings: A transthoracic echocardiogram was performed to rule out apical variant hypertrophic cardiomyopathy. The echocardiogram showed a homogenous echogenic mass filling the left ventricular apex (Figures 2). Left ventricular wall motion was normal. A complete blood count was obtained that revealed a normal leucocyte count with eosinophilia (relative eosinophilic count 44%). A presumptive diagnosis of hypereosinophilia syndrome was made due to the high eosinophil counts and characteristic echocardiographic findings. A cardiac magnetic resonance imaging (MRI) was performed (Figures 3, top pics) which confirmed the findings of a homogenous mass in the left ventricular apex. In addition, delayed enhanced images showed a central area of thrombus surrounded by areas of fibrosis lining the endocardium (Figures 3, bottom pics). Secondary causes of hypereosinophila were excluded. The patient had a bone marrow biopsy performed that resulted in the diagnosis of chronic eosinophilic leukemia (CEL). Fluorescence in situ hybridization (FISH) analysis on bone marrow sample was positive for FIP1L1-PDGFRA fusion and negative for BCR/ABL translocation (Philadelphia chromosome).

Learning Points from this Case: Chronic eosinophilic leukemia is a rare chronic disorder with clonal eosinophil overproduction in the bone marrow, which results in marked and sustained peripheral blood eosinophilia. Eventually this leads to eosinophilic infiltration and functional damage of peripheral organs. Detection of FIP1L1-PDGFRA fusion gene and absence of BCR/ABL translocation (Philadelphia chromosome) supports the diagnosis of CEL. As seen in our case patients with FIP1L1-PDGFRA (+) CEL are more likely to have cardiac involvement at presentation. Cardiac involvement with hypereosinophilia syndromes evolves through three stage, although these stages may overlap. The first stage is the acute necrotic stage which may be clinically silent; The second is an intermediate phase characterized by thrombus formation along damaged endothelium; And the third stage is characterized by heart failure due to restrictive cardiomyopathy and/or cordae tendinae compromise leading to mitral and tricuspid regurgitation. Cardiac MRI may diagnose cardiac manifestations at all the stages including the initial asymptomatic stage. Our patient was in the intermediate phase at presentation. Patients with CEL with FIP1L1-PDGFRA fusion gene have good hematological response to Imatinib mesylate.

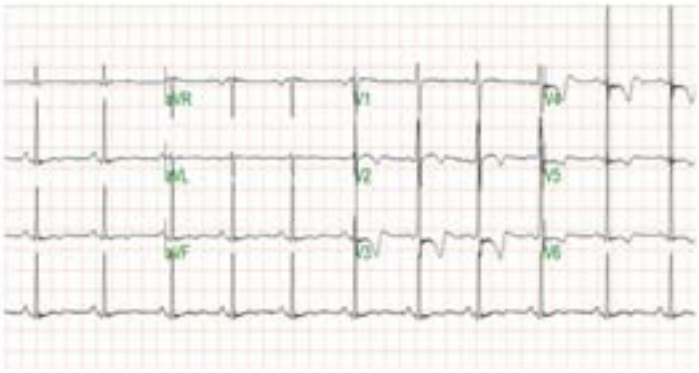

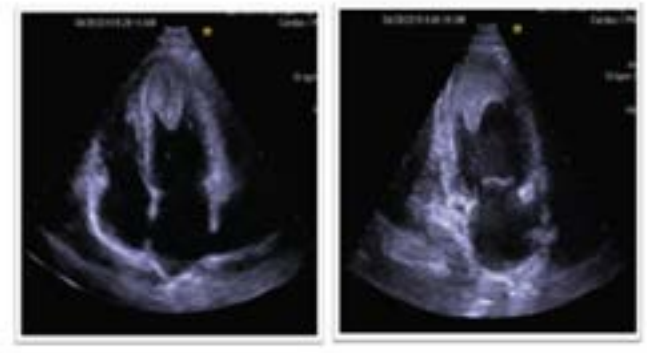

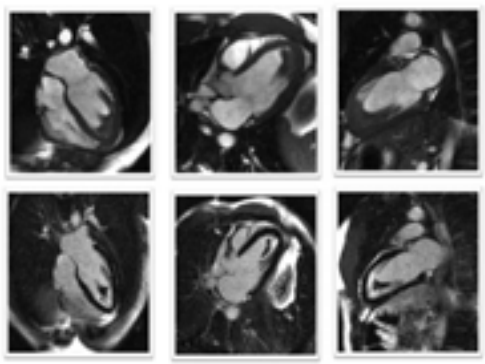

C051

Atrial Mass Post-Percutaneous Coronary Intervention: Diagnosis and Management

Andrew E. Kott, M.D.[1]Mita B. Patel, MD[2], Dhiraj Baruah, MBBS, MD[3], Aimee Welsh, MD[1], Kaushik Shahir, MD[1], Jason C. Rubenstein, MD[1]

1. *Medical College of Wisconsin, Milwaukee, WI*
2. *Medical College of Wisconsin, WI*
3. *Medical College of Wisconsin, brookfield, WI*

Description of Clinical Presentation: A 70 year-old man with a history of coronary artery disease status post coronary artery bypass surgery presented to an outside hospital facility with a non-ST elevation myocardial infarction. Coronary angiography revealed a culprit lesion in the distal left main coronary artery extending into the proximal left circumflex coronary artery. Percutaneous coronary intervention with a drug-eluting stent was performed. Post-procedural transthoracic and transesophageal echocardiography revealed a 45 x 39 mm mass in the posterior left atrium thought to be consistent with an atrial myxoma. He was transferred to our facility in stable condition for further evaluation. Cardiac MRI was performed (details below) demonstrating a retro-atrial hematoma. After discussion with cardiac surgery, the patient was managed conservatively with resolution of the hematoma over the course of several months.

Diagnostic Techniques and Their Most Important Findings: Cardiac MRI with off-label administration of gadolinium contrast was performed revealing a 65 x 83 mm mass in the posterior left atrium with mass effect within the left atrium. Steady-state free precession cine, bright and black blood, black blood with fat saturation, first-pass contrast, long inversion time and delayed enhancement imaging were performed to characterize the mass (Figure 1). The characteristics of the mass were most consistent with a hematoma (isointense to myocardium with focal areas of hyperintense signal on black and bright blood imaging, hypointense on T2 weighted imaging, no first-pass perfusion, hypointense on long TI imaging). Follow-up serial imaging revealed gradual resolution of the hematoma (Figure 2).

Learning Points from this Case:

1. This case illustrates an uncommon but important complication to recognize post-PCI.
2. Cardiac MRI was vital in the identification and subsequent management of this patient's mass.

http://www.ConferenceAbstracts.com/uploads/cfp2/attachments/LDFAIBDN/LDFAIBDN--219135-1-ANY(1).pdf

http://www.ConferenceAbstracts.com/uploads/cfp2/attachments/LDFAIBDN/LDFAIBDN--219135-2-ANY.pdf

C052

Primary Cardiac Leiomyoma presenting as a Large Left Ventricular Mass

Madhusudan Ganigara, MD [1]Bharti Sharma, MD [2], Michelle de Padua, MD[3], Br Jagannath, DNB[4], Nitin Rao, MD[5]

1. *Icahn School of Medicine at Mount Sinai, NY*
2. *STAR Hospitals, Telangana, India*
3. *Apollo Health City Campus Hyderabad, Telangana, India*
4. *Star Hospitals, Telangana, India*
5. *Star Hospitals, Hyderabad, Telangana, India*

Description of Clinical Presentation: A 6-month-old boy presented with congestive cardiac failure. Transthoracic echocardiogram revealed a large mass involving the lateral wall of the left ventricle with moderate left ventricular dysfunction. The ventricular inflow and outflow tracts were unobstructed, and valve function was preserved.

Diagnostic Techniques and Their Most Important Findings: Cardiac magnetic resonance imaging (MRI) with a 1.5T MR scanner [Philips Acheiva; Philips, Best, Netherlands] showed a large tumor measuring 40 mm in the longest axis, involving the basal- and mid-left ventricular free wall and extending into the cardiac cavity (Figure 2). The tumor mass was isointense on T1 and T2 weighed imaging with enhancement on delayed gadolinium enhancement imaging, suggesting an intramural cardiac fibroma (Figure 2). There was an hypointense region at the centre of the tumor on delayed enhancement imaging that likely represents area of non-perfusion or central necrosis.

The child underwent sub-total resection of the tumor using median sternotomy and lateral ventriculotomy, under cardiopulmonary bypass. Complete resection was not performed as the tumor was considered to form part of the left ventricular free wall. Histopathology revealed a benign spindle cell neoplasm measuring 55 x 33 x 18 mm. Immunohistochemistry was positive for vimentin and smooth muscle actin, and negative for S100 protein and desmin, confirming a primary cardiac leiomyoma. At 6-month follow up, the child was asymptomatic with normal ventricular function and unchanged residual tumor size on Echocardiography.

Learning Points from this Case: Cardiac leiomyomas are exceedingly rare and are usually described in the context of an adult woman with primary uterine leiomyoma with cardiac extension. To our knowledge, this is only the third case report describing a primary cardiac leiomyoma in children. They mimic the tissue characteristics of the more common tumor, cardiac fibroma on cardiac MRI. The definitive diagnosis is only possible after histopathological analysis. The decision to resect largely depends on the clinical picture. In view of the paucity of literature on long-term outcomes, these children need close clinical follow–up and observation.

http://www.ConferenceAbstracts.com/uploads/cfp2/attachments/LDFAIBDN/LDFAIBDN--218565-1-ANY.pdf

http://www.ConferenceAbstracts.com/uploads/cfp2/attachments/LDFAIBDN/LDFAIBDN--218565-2-ANY.pdf

C053

An unusual cause of Right Atrial mass

Luke H. Dancy, MD[1]Mohammad Albarjas, MD MRCP[2], Daniel Sado, BM, MRCP[1]

1. Kings College Hospital, London, England, United Kingdom
2. King's College Hospital NHS Foundation Trust, London, England, United Kingdom

Description of Clinical Presentation: An 81 year old Gentleman presented with pain over his left Humerus, giving a concurrent history of breathlessness. His initial investigation focused on a musculoskeletal cause although a routine Transthoracic Echocardiogram was arranged to evaluate his Dyspnea.

Diagnostic Techniques and Their Most Important Findings: A left humeral X-ray deomnstrated a single osteosclerotic lesion in the mid shaft.

A routine transthoracic echocardiogram demonstrated an echodense mass in the right atrium.

A Cardiac MRI was performed to further characterise the mass. Spin Echo Axial Stack images demonstrated circumferentiially thickened adventitia with the Aortic Arch and Descending Aorta. The Kidneys, although not well visualised appeared abnormal. Two distict large masses were seen in the Right Atrium and Right atrial appendage. The larger extended up into the Superior Vena Cava causing near complete caval obstruction. Due to frequent ventricular ectopics and poor breath hold, dedicated T1 and T2 imaging was not undertaken. Following administration of Gadolinium (Gadovist 0.1mmol/l), there was early uptake up of contrast into both the masses and the thickened descending aorta. The masses went on to late enhance. Along with this, a completed inferior infarct was present.

Further imaging was performed with a CT scan of the abdomen to assess the kidneys. This showed bnormal soft tissue encroaching the corticomedullary zone, which extends into the renal pelvis and the proximal ureters. There is also bilateral perinephric cuffing of soft tissue.

X-rays of all of the long bones was performed. This found patchy sclerosis (confluent in parts) of the metaphyses of the distal femora and proximal tibia bilaterally.

Renal Biopsy showed Fibrofatty tissue with areas of fat necrosis and accumulated histiocytes. There are also chronic inflammatory cell infiltrates. No evidence of malignancy is seen.

A Diagnosis of Erdheim Chester Disease was made.

Learning Points from this Case:

1. Infiltration of the Descending Aorta is rare and shoud raise suspision of rare or unusual conditions
2. Histiocytosis related conditions are multisystem infiltrative disoreders and should be considered in the differential of such imaging findings.
3. Erdheim Chester is rare, but recongition of the pattern of infiltration on MRI in conjunction with X-ray imaging will prompt biopsy and correct diagnoses

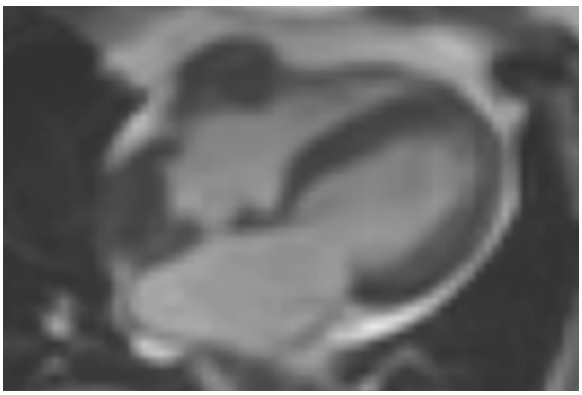
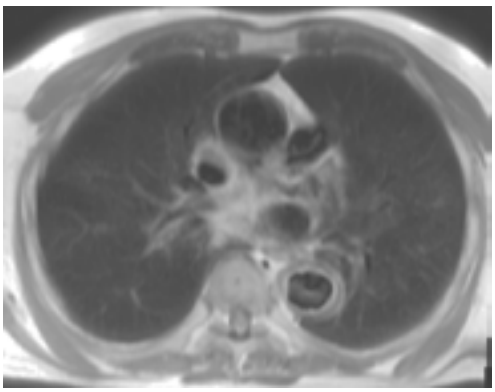
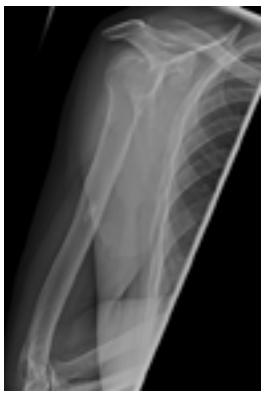

C054

An intracardiac presentation of hepatocellular carcinoma

Harjot Singh, M.D.[1]Harsimar Singh, M.D.[2], Vamsi Pavuluri, M.D.[2], Madhavi Kadiyala, M.D.[2]

1. St. Francis Hospital, Long Island City, NY
2. St. Francis Hospital, NY

Description of Clinical Presentation: 73 year old female presenting with with progressive shortness of breath on exertion, increased abdominal girth and bilateral lower extremity swelling for 2 months. Her history was significant for Diabetes, hypertension, hyperlipidemia, stroke and thrombocytopenia. Her echocardiogram revealed a large mass in the IVC, right atrium and right ventricle and cardiac MRI was ordered for further characterization.

Diagnostic Techniques and Their Most Important Findings: Cardiac MRI showed a large bilobed heterogeneous mass measuring 6 x 5.5 cm that occupies the entire right atrium and extending into the right ventricle. The mass extended into the inferior vena cava (IVC) and into the right atrium. The signal intensity of the mass was isointense on T1 weighted images and hyperintense on T2 weighted images. There was minimal gadolinium uptake on first pass perfusion and heterogeneous hyperenehancement on the delayed gadolinium images. These findings are consistent with a tumor with vascularity. The mass did not appear to encroach on the cardiac walls. Tissue characteristics were not typical of a thrombus although thrombotic components on the mass could not be excluded. MRI of the abdomen was also done to further characterize the liver, which showed nodular cirrhotic hepatic appearance. A hepatic mass was noted that distended the hepatic veins and extended into the IVC along with portal vein thrombus. The mass is most likely a hepatocellular carcinoma (HCC) given the MRI findings, it's origin, underlying cirrhosis of the liver and an elevated alpha fetoprotein level of 15948 ng/ml.

Learning Points from this Case: HCC with intracardiac involvement is rare and is found in about 2% of cases. It frequently invades the vascular system and is almost always a continuous extension from the hepatic vein into the heart. Isolated metastasis is extremely rare. Tissue characterization by cardiac MRI is helpful in differentiating tumor from thrombus. Additionally, the first pass perfusion and the pattern of uptake give additional information about the mass composition and vascularity.

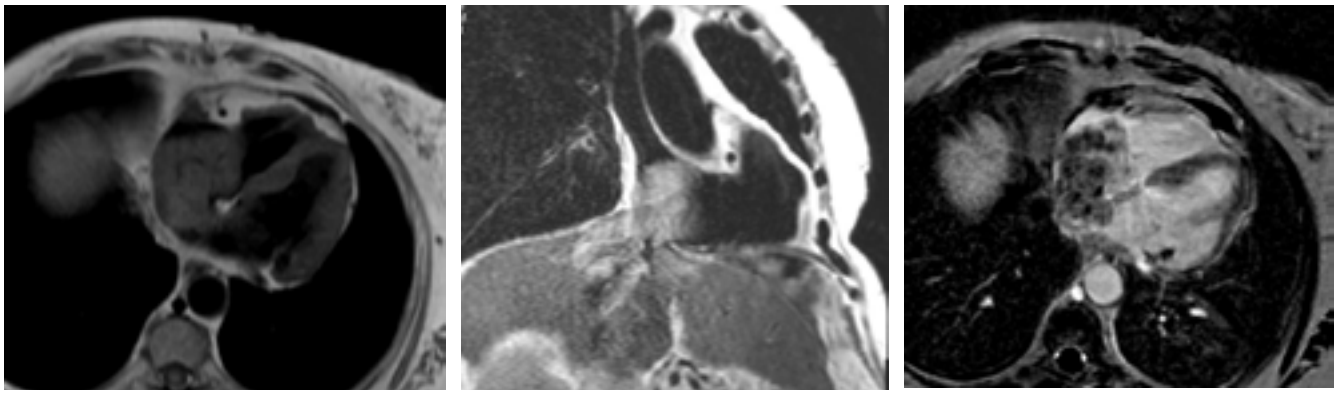

C055

A zebra or a horse of a different color?

Hanita Shai, MD

Boston children's hospital, Brookline, MA

Description of Clinical Presentation: A 5 month old baby with known tuberous sclerosis (TS) mutation and a large left ventricular (LV) free wall tumor presented with a resuscitated cardiac arrest and documented ventricular fibrillation. Echocardiogram showed a stable, large tumor without inflow or outflow obstruction and with normal ventricular and valvar function (Figure 1). Ongoing complex ventricular arrhythmias were noted and eventually controlled with amiodarone and propranolol. Although a rhabdomyoma was suspected in the setting of a known TS mutation, fibroma could not be fully excluded given the rhythm disturbances and tumor morphology. Cardiac magnetic resonance (CMR) examination was, therefore, performed for tissue characterization.

Diagnostic Techniques and Their Most Important Findings: CMR showed a large (~2 x 4 cm) tumor, located in the LV free wall extending from mid cavity to apex with signal characteristics most consistent with a rhabdomyoma. Specifically, the tumor was homogeneous, with no cystic elements. It was isointense compared to myocardium on T1- and slightly hyperintense on T2-weighted imaging. There was mild perfusion of the tumor on first pass perfusion imaging. On delayed enhancement imaging, minimal enhancement of the tumor was noted (Figure 2). Given these findings, surgical tumor resection was deferred and a conservative approach was followed with placement of an epicardial defibrillator for secondary prevention. At two year follow-up, the patient remained asymptomatic with no events or device related complications, and echocardiography demonstrated complete resolution of the rhabdomyoma (Figure 3).

Learning Points from this Case: In this child with an atypically high arrhythmia burden in the setting of a suspected rhabdomyoma, CMR provided valuable insight into tumor type, thereby avoiding a challenging and unnecessary cardiac surgery. This case demonstrates the power of CMR tissue characterization in diagnosis of cardiac tumors, and its potential role in guiding management, especially in atypical cases.

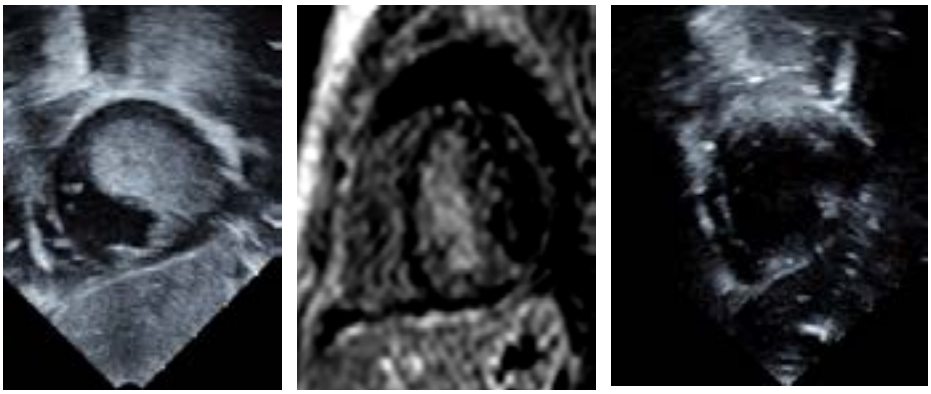

C056

Cardiovascular CT and MR Imaging of Cardiac Lymphangioma

Ruma Madhu Sreedharan, DNB,MNAMS

GMC, Trivandrum, Trivandrum, Kerala, India

Description of Clinical Presentation: A 24 year old female presented to the out patient department with chest discomfort and pain. ECG, physical examination, blood routine was unremarkable. The patient was sent for Chest Radiograph which demonstrated cardiomegaly. Echocardiography revealed a multiseptated mass arising from the atrioventricular groove compressing Right Atrium (RA) and Right Ventricle (RV).She was sent for taking a cardiac CT and Cardiac MRI Scan.

Diagnostic Techniques and Their Most Important Findings: CT scan showed a large multiseptated lesion centered around the anterior atrio ventricular groove compressing the RV It was hypodense with central area showing water density (5-20 HU) and multiple thin enhancing septations. No areas of calcification or fat density or solid areas was demonstrated. It was seen anterior to RA, RV. The mass was seen compressing and infiltrating RV myocardium with associated mild pericardial effusion. RCA was seen arising from right coronary sinus and seen coursing through the lesion and appear stretched out with good contrast opacification. Left Main, LAD appear compressed by the mass effect but the lumen was patent with no stenosis. The lesion measured 15.1 x 8 x 12cm in its maximum transverse, anteroposterior, and craniocaudal diameters, respectively and appears confined to the boundary of pericardium. Superiorly the lesion was seen extending up to the root of great vessels and inferiorly extending up to the diaphragm. Anteriorly reaching upto the posterior surface of the sternum. She was advised MRI scan for assessing cardiac function. Lesion appeared hyperintense in T1WI, T2WI, and STIR and not suppressed in FAT sat sequence. Lesion showed multiple thin septations (2 mm) which appeared hypointense in all sequences. After contrast administration the subtraction images showed the enhancement of the wall and the septations. No solid enhancing areas were seen within the lesion. . No abnormal myocardial wall signal intensity was seen. In Delayed gadolinium scans there were no trans mural or subendocardial enhancement. The preoperative differentials were pericardial lymphangioma, pericardial cyst. Biopsy was not undertaken due to encasement of RCA and branches. Hence surgery done with excision of the mass and Saphenous RCA graft. The mass was seen partly adherent to the RA RV free wall and hence only partly could be excised. A straw colored fluid was aspirated. The biopsy report came as Cardiac Lymphangioma.

Learning Points from this Case: Although cardiac Lymphangioma is a rare benign cardiac tumor, it can have varied clinical picture and can present at any age from infancy to adulthood. The clinical manefestations may vary from mild chest discomfort to cardiac tamponade. Cardiac CT and MRI can help surgens to plan surgery, assess the anatomical details, nature of the mass and asscoiated findings. Case was presented due to the rarity of the lesion as well as one of the largest Cardiac lymphangioma being reported so far.

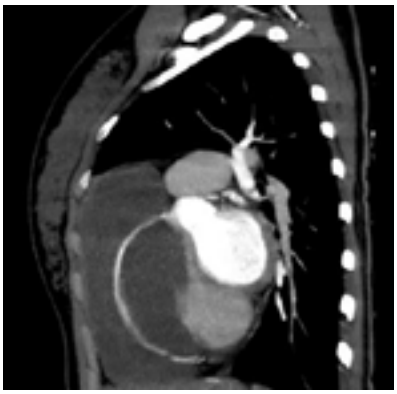

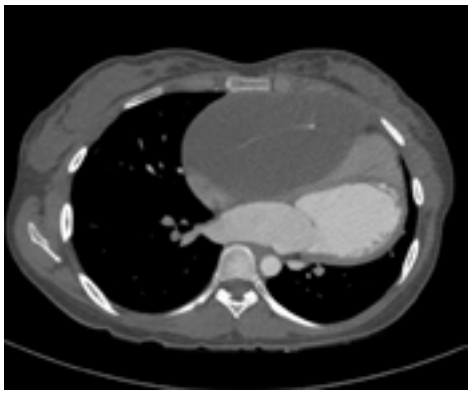

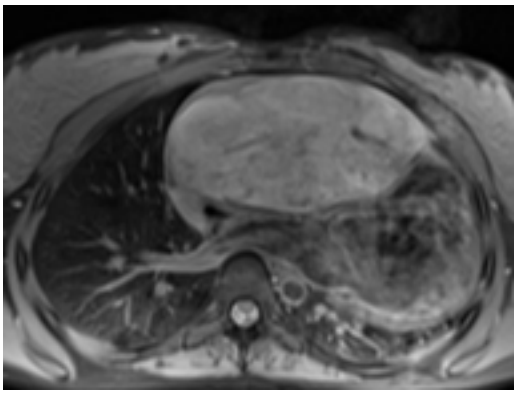

C057

Patient-specific 3D printing enables biventricular surgical repair in a complex case of heterotaxy syndrome

Nick Byrne, MPhys, MSc[1], Mari N. Velasco Forte, MD [2]Gareth J. Morgan, MB BCh BaO MPhil MRCPCH[3], Christoph Kiesewetter, Dr[4], Tarique Hussain, MD, PhD[5], Israel Valverde, MD[6], David Anderson[7], Yaso Emmanuel

1. *Guy's and St. Thomas' NHS Foundation Trust / King's College London, England, United Kingdom*
2. *King's College London, London, England, United Kingdom*
3. *University of Colorado, Aurora, CO*
4. *Guy's & St Thomas NHS Foundation Trust, London, England, United Kingdom*
5. *Dept. of Pediatrics, UT Southwestern Medical Center, TX*
6. *King's College London, Andalucia, Spain*
7. *Evelina London Children's Hospital, England, United Kingdom*

Description of Clinical Presentation: A 35 year-old woman diagnosed with Kartagener's and heterotaxy syndromes was referred for cardiac surgery owing to symptoms of heart failure. She had midline liver, polysplenia and complex systemic and pulmonary venous drainage. There was no atrial septum giving the appearance of a common atrium with left atrial isomerism; bilateral SVCs (right SVC to coronary sinus, left SVC to left-sided atrium), interrupted IVC with azygos continuation to right SVC, hepatic veins to left-sided atrium, pulmonary veins draining centrally in the common atrium.

After previous cardiac surgeries (at 2 and 34 years) failed to achieve full repair, she developed heart failure symptoms, becoming increasingly desaturated and tired upon daily activity.

Diagnostic Techniques and Their Most Important Findings: The previous surgical septation of the atrium proved to be difficult to interpret on multiplanar reformatted 3D bSSFP images (diastolic phase, respiratory navigated, ECG triggered, sagittal orientation; repetition time ms/echo time ms: 3.4/1.7; flip angle: 90°; 150 overcontiguous slices; acquired isotropic, resolution: 1.3 mm^3; acquisition window: 100 msec) and cine images (breath-hold acquisition, ECG triggered, axial and sagittal acquisition, repetition time ms/echo time ms: 3/1.5, flip angle: 60°, 12-15 contiguous slices of 10 mm thickness).

Diagnostic catheterisation and transoesophageal echocardiogram followed. A dehiscence of the patch was thought the most likely cause of the patient's status. It was not until the heart was reproduced in a flexible, 3D printed model that our surgeon gained a faithful understanding of the case. Whole heart anatomy was segmented from bSSFP data (further details in full report). In vitro surgical simulation suggested that the presumed patch dehiscence was actually a lack of roof between the coronary sinus and the pulmonary venous atrium. Consequently, the right SVC with azygos continuation was entirely committed to the pulmonary venous atrium.

Learning Points from this Case: When coupled with previous surgical intervention, the congenital abnormalities of this case resulted in a structurally complex picture. By conventional tomographic or volume-rendered presentation of imaging data alone, our surgical team could not affect a sufficient spatial understanding of the case. In its absence, the failure of two previous attempts at surgical repair favoured the Kawashima procedure. However, after in vitro surgical simulation, the team achieved biventricular repair, routing all systemic venous flow towards the right ventricle. Simulation used a 3D printed presentation of imaging data. The patient-specific model provided a fully 3D, tactile appreciation of anatomy which, owing to its complexity, the surgeon could not understand from an interpretation of tomographic CMR images nor from discussion with the imaging cardiologist.

Even at a large tertiary referral centre with a vastly experienced surgical team, surgical care can be enhanced through the use of 3D printed models of cardiovascular anatomy.

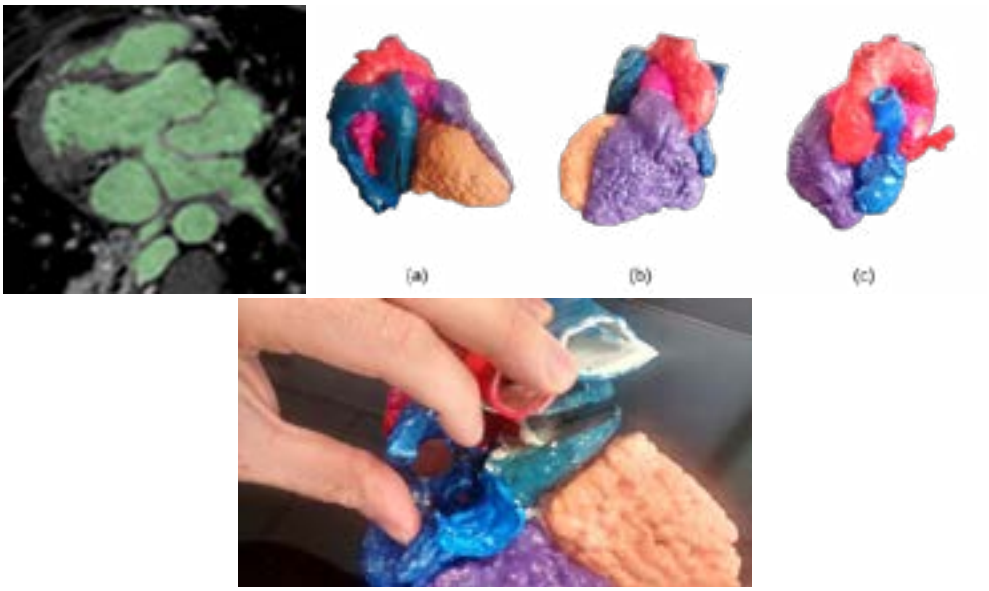

C058

Ruptured Sinus of Valsalva aneurysm: Incremental value of Cardiac Magnetic Resonance imaging in Diagnosis and Management

Anub G. John, MD[1]RAJEEV Fernando, MD[2]

1. *University of Louisville, KY*
2. *University of Louisville, Louisville, KY*

Description of Clinical Presentation: 57 year old man presented with a four week history of dyspnea on exertion associated with fatigue and lower extremity edema. Physical examination was significant for elevated jugular venous pressure, precordial continuous murmur, loud P2 and pedal edema. Transthoracic echocardiography (TTE) was suggestive of Gerbode ventricular septal defect (VSD). He was unable to tolerate transesophageal echocardiography (TEE).

Diagnostic Techniques and Their Most Important Findings: Cardiac MRI (Table1, Figure2) confirmed the presence of aneurysmal dilatation of the non-coronary sinus of Valsalva. Cine imaging demonstrated the defect in the non-coronary sinus of Valsalva and the wind-sock deformity of the ruptured flap. Inplane flow mapping showed continuous shunting of blood from the aorta to the right atrium. Throughplane flow mapping demonstrated Qp:Qs = 1.5:1. MRA identified a 7mm x 8mm defect in the non-coronary sinus. There was no VSD on cine imaging or MR angiography ruling out Gerbode VSD. MRI also showed closed proximity of the ruptured site to the non-coronary leaflet of the aortic valve and the septal leaflet of the tricuspid valve, precluding interventional closure of the defect. Selective coronary arteriography showed non obstructive coronary artery disease. Aortogram (Figure 1) showed contrast extravasation from the aorta into the right atrium. Left ventriculogram did not demonstrate contrast extravasation at the ventricular level. However, after contrast opacification of the ascending aorta, the right atrium was opacified. Intra-cardiac echocardiography (ICE) showed classic wind sock appearance of sinus of valsalva rupture at the non-coronary sinus communicating with right atrium (Figure1). Color Doppler showed continuous shunt from the aorta to the right atrium. It also confirmed close proximity of the septal leaflet of the tricuspid valve with the defect making it unsuitable for percutaneous closure. Patient underwent successful double pericardial patch surgical repair.

Learning Points from this Case: SOVA is a rare cardiac anomaly (0.15–3.5%) that can be congenital or acquired. Acquired causes include infective endocarditis, trauma, iatrogenic, degenerative and connective tissue diseases. SOVA mostly involves right (75%) sinus, followed by non-coronary (20%) and left (< 5%) sinus of Valsalva. CMR can clearly show the origin above the aortic annulus, delineate the saccular shape and characterize the asymmetry in aortic root dilatation. It can further exclude co-existent lesions such as VSD & aortic regurgitation. Flow imaging will often demonstrate a continuous shunt, accurately determine the receiving chamber and quantify shunt fraction. It is particularly useful when ultrasound based methods are unavailable (ICE), not tolerated (TEE) or non-diagnostic (TTE). Our case study demonstrates the incremental value of CMR in diagnosing SOVA giving anatomical, hemodynamic and functional assessment preoperatively.

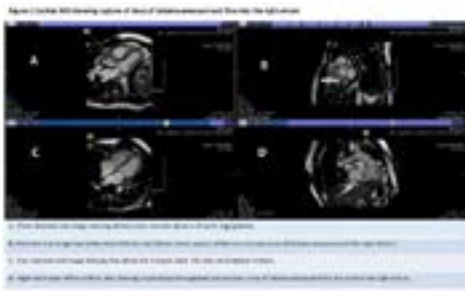

C059

Late presentation of atrial tachyarrhythmia in a patient with Fontan revision

Nilanjana Misra, MBBS, FAAP

Cohen Children's medical Center of NY, New Hyde Park, NY

Description of Clinical Presentation: 34 y/o female with a history of double inlet left ventricle {S, L, L}, who underwent a late, single staged Atrio-Pulmonary Fontan procedure in 1989 when she immigrated to USA at 8 years of age. Given palpitations but no documented arrhythmia, a dilated atrium on cardiac catheterization and future consideration of pregnancy, she underwent Fontan revision in 2001 with an extracardiac Fontan and plication of the right atrium. She had a successful pregnancy in 2009. In August 2015, she presented to adult cardiology with palpitations and was found to have intra-atrial re-entrant tachycardia (IART) with 3:1 conduction. She was successfully cardioverted and placed on Metoprolol and Coumadin. She presented with recurrent IART 2 months later and was again cardioverted. She was then referred to our adult congenital team.

Diagnostic Techniques and Their Most Important Findings: Transthoracic echocardiogram showed patent extracardiac Fontan, dilated right atrium (RA) and moderate subaortic obstruction at the bulboventricular foramen (BVF) level (PSIG of 50 mm Hg).

Cardiac MRI was recommended and showed the following:

- Double inlet left ventricle with left-sided, subaortic, hypoplastic right ventricle (L-loop ventricles) and leftward anterior aorta (L-transposition of the great arteries). No pulmonary valve seen.
- Widely patent extracardiac Fontan conduit with patent IVC end and patent Glenn anastomosis with no fenestration. Branch pulmonary arteries were widely patent with no evidence of stenosis. Estimated QpR: QpL was 44%: 56%.
- Severely dilated RA with swirling flow noted on cine imaging but no obvious thrombus seen. There was no interatrial communication. RA was still connected to the branch pulmonary arteries and thereby connected to the Fontan circuit.
- There was no atrioventricular connection between RA and LV suggesting patch closure of the right valve.
- Coronary sinus opened into the RA.
- There was narrowing of the BVF with a dephasing jet of stenosis.
- Mild to moderately dilated ascending aorta (2.6 x 3.2 cm) with trivial aortic regurgitation (RF of 5%).
- No aortopulmonary or venovenous collaterals seen.
- Left ventricular volumes were on the lower end of normal (LVEDVi: 53 mL/m2, z: -1.99) with normal ejection fraction of 68%.
- No significant shunt with Qp/Qs of 0.98:1
- She underwent a cardiac catheterization that showed severe obstruction at the BVF with PSEG of 90 mm Hg and normal Fontan pressures of 10 mm Hg.

Learning Points from this Case: Persistent atriopulmonary connections following a Fontan revision is almost unheard of. CMR helped diagnose the cause of the dilated right atrium leading to recurrent IART. Patient underwent Fontan re-revision with closure of RA-PA communication, atrial septectomy, right atrial resection, MAZE procedure, relief of LVOT obstruction and placement of a permanent epicardial dual chamber pacemaker. She has done well subsequently. This case highlights the importance of CMR in defining the anatomy in adults with congenital heart disease, thus assisting in proper surgical and clinical management of the patient.

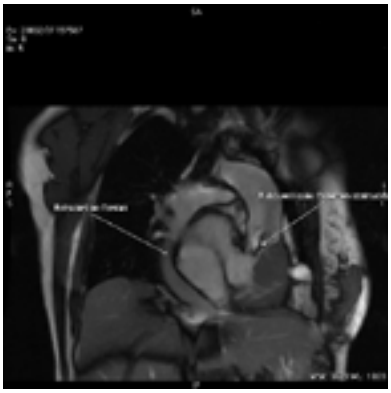
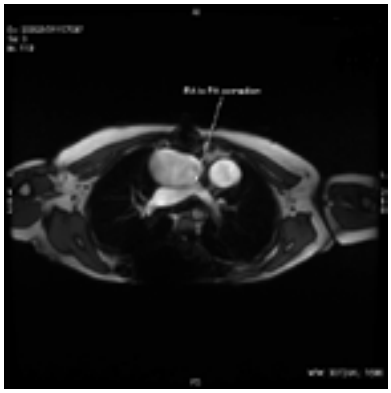
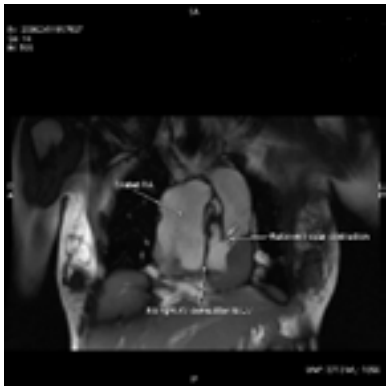

C060

Unexplained shortness of breath following surgical repair of partial anomalous pulmonary venous return

Rukmini R. Komarlu, MD

Cleveland Clinic Children's Hospital, Beachwood, OH

Description of Clinical Presentation: A 24 year old female presented to the ED with history of pre-syncope and transient bilateral vision loss while throwing a softball around in the yard. She also had worsening shortness of breath of 2 months duration. She was diagnosed with partial anomalous pulmonary venous return of the right upper and right middle pulmonary veins to the right superior vena cava 5 months prior to presentation and had undergone baffling of the anomalous veins through creation of atrial septal defect 4 months prior to presentation. Immediately following her surgery she had done well, but from the past 2 months had become more symptomatic. CTA of the head was negative for stroke. An echocardiogram could not assess the surgical repair due to limited acoustic windows. A CMR was ordered for assessment of her surgical repair and to delineate the cause of progressive shortness of breath.

Diagnostic Techniques and Their Most Important Findings: CMR revealed that the right upper and middle pulmonary veins drained via a common ostium into the left atrium via the surgically created intra-atrial baffle. The baffle had a long tunnel before entering the left atrium that appeared significantly narrowed. There was a small baffle leak noted in the superior portion of the atrial septum with Qp/Qs of 1.04. The SVC baffle was significantly narrowed as well. The azygous vein had been ligated as part of the surgical repair. There was normal biventricular size and systolic function and no pericardial effusion. Differential pulmonary blood flow revealed: right lung 46%; left lung 54%.

The patient underwent cardiac catheterization which confirmed the findings of severe long segment stenosis of the right upper/middle pulmonary vein baffle, stenosis of the superior vena cava and residual leak in the superior portion of the baffle. She underwent stenting of the baffle of the right upper pulmonary vein with overlapping stents and stenting of the stenosis of the inferior portion of the superior vena cava with excellent result and significant reduction in SVC gradient.

Learning Points from this Case: Pulmonary venous baffle obstruction and stenosis of the superior vena cava are some of the complications that can occur following repair of partial anomalous pulmonary venous return. What is unusual in this case is that these complications developed relatively early following the surgery. In this patient who presented with progressive shortness of breath and pre syncopal symptoms, cardiac MRI was crucial in delineating the baffle obstruction and stenosis of the superior vena cava. Correct diagnosis of this postoperative complication was essential for optimal management of this patient.

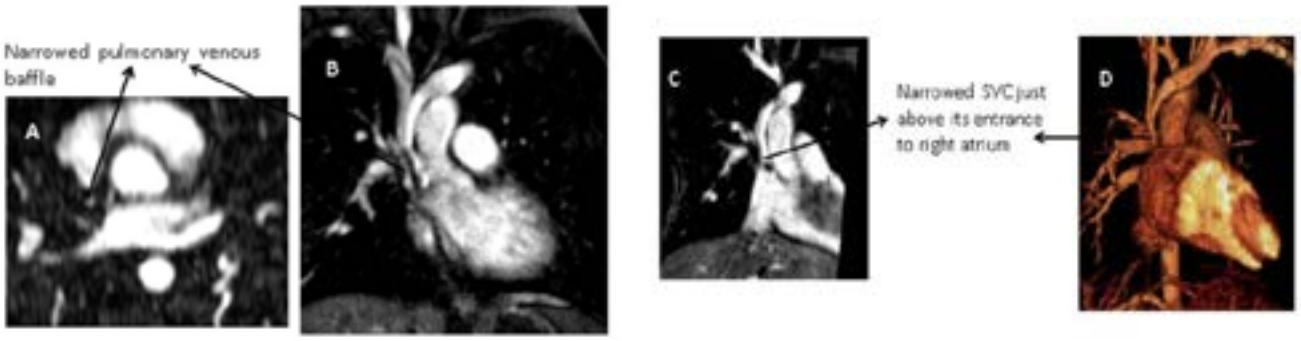

C061

The unusual suspect of a pulmonary hypertension referral for 'low gradient left to right shunting patent ductus arteriosus'

Bram Ruijsink, MD[1] Alessandra Frigiola, MD, PhD[2]

1. King's College London, England, United Kingdom
2. Guys and St Thomas Hospital NHS Foundation Trust, England, United Kingdom

Description of Clinical Presentation: A 52 year old lady was referred to a tertiary adult congenital heart disease centre with a suspected diagnosis of pulmonary hypertension in the context of a patent ductus arteriosus. The patient initially presented to her local hospital with progressive increasing shortness of breath on exertion (less than 300 yards on the flat); an echocardiogram revealed a low velocity flow into the main pulmonary artery. On the clinical examination the patient had an obese habitus (BMI 37), normal blood pressure, saturations, and jugular venous pressure; respiratory rate was regular at 20 per minute. There were no signs of cyanosis and no signs of heart failure. Chest auscultation was unremarkable and there were normal first and second heart sounds. ECG showed sinus rhythm with normal QRS duration and axis. An echocardiogram was performed which showed normal biventricular size and function, structurally and functionally normal valves. The right ventricle did not appear hypertrophied. There was a low velocity flow into a dilated main pulmonary artery, which was interpreted as a patent ductus arteriosus. Based on these contrasting features of the clinical examination and echocardiographic findings, the patient was referred for a cardiac MRI and a diagnostic right and left heart catheterisation.

Diagnostic Techniques and Their Most Important Findings: A cardiac MRI scan revealed a structurally and functionally normal intracardiac anatomy but a severe aneurysm of the main pulmonary artery. A ductus arteriosus could not be found and it became clear that the jet seen on echocardiography was swirling flow due to severe dilatation of the pulmonary artery itself. Patient underwent cardiac CT in order to exclude bronchial compression and to assess the lung parenchyma. The scan showed normal coronary artery, mild bronchiectasis consistent with gastro-oesophageal reflux, and mild compression of the main left bronchus due to the giant pulmonary artery. A cardiopulmonary exercise test showed a reduced level of fitness (peak VO2 10 ml/min/kg, 56% of predicted) with a normal heart rate and blood pressure response. The anaerobic threshold was not reached due to shortness of breath. A lung function test revealed a mild restrictive defect in keeping with the body habitus. Overnight oximetry did show mild REM-related sleep apnoea (OSA) and hypoventilation. The patient was then referred for respiratory rehabilitation and mandibular advancement splint as treatment for her OSA whereas proton pump inhibitors have been used as a treatment for her gastro-oesophageal reflux.

Learning Points from this Case: In patients with a dilated main pulmonary artery, swirling flow can mimic a low gradient left to right shunting patent ductus arteriosus. This can lead to misdiagnosis and unnecessary and potentially harmful invasive diagnostic tests. Sole evidence of low flow patent ductus arteriosus without supporting physical, ECG and echocardiographic findings of pulmonary hypertensions should alert for potential pitfalls in diagnostic assessment.

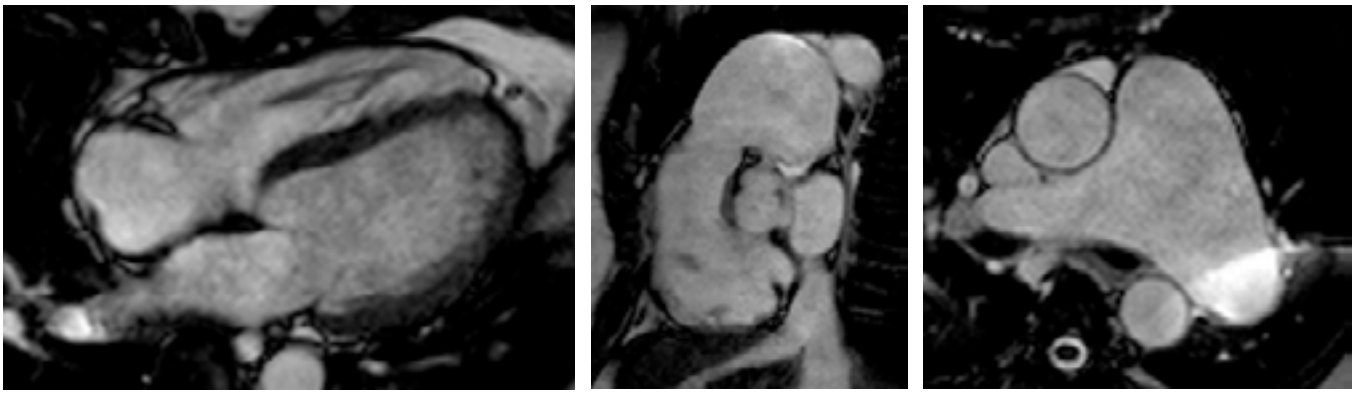

C062

From Tunisia to New York City: Uncontrolled Hypertension in an Adult with Repaired Coarctation

Lynn Zaremski, MD[1]Nadine Choueiter, MD[2], Ali N Zaidi, MD[3]

1. Montefiore Medical Center, NY
2. The Pediatric Heart Center, The Children's Hospital at Montefiore, Albert Einstein College of Medicine, NY
3. Montefiore Heart and Vascular Care Center, Albert Einstein College of Medicine, NY

Description of Clinical Presentation: A 39-year-old male with a history of aortic coarctation, surgically repaired at 15 years of age in Tunisia presented with uncontrolled hypertension to the Adult Congenital Heart Disease Program. No surgical reports were available. He denied any chest pain, claudication or syncope. He was on lisinopril and metoprolol for hypertension. His physical exam revealed no murmurs and normal femoral pulses. On BP evaluation the RUE BP was 152/92 mmHg and the LUE BP was 124/86 mmHg. The RLE BP was 174/108 mmHg.

Diagnostic Techniques and Their Most Important Findings: An echocardiogram showed mild flow acceleration in the distal aortic arch with a peak velocity of 1.5 m/sec, the LV mass index was 99.6 g/m^2 with normal biventricular global systolic function. The aortic isthmus was not well visualized. A cardiac magnetic resonance (CMR) study was obtained to delineate arch anatomy. It demonstrated an interrupted aortic arch type A with an interposition graft between the aortic isthmus and the descending aorta. The aortic arch was stenosed between the left common carotid artery and the left subclavian artery (1.7 cm), at both the proximal and distal ends of the graft (2.1 cm).

Cardiac catheterization corroborated the CMR findings and showed multiple pressure gradients throughout the arch:

a. 20 mm Hg gradient between the proximal transverse arch and the distal arch at the origin of the left subclavian artery
b. 5 mm Hg gradient between the distal arch and the proximal end of the graft, and
c. 5 mm Hg gradient between the graft and the descending aorta with a 2-4 mm narrowing in the proximal and distal conduit ends.

Learning Points from this Case: Re-coarctation is an important diagnosis to consider in patients with uncontrolled hypertension after coarctation repair. The physicians interpreting CMR studies in patients post-coarctation repair should closely evaluate the aortic arch for the precise location and degree of narrowing. In this case CMR clearly defined the aortic arch anatomy, type of surgical repair, as well as sites and degree of stenosis without the use of ionizing radiation. This was essential in guiding further surgical management. Given the complex arch anatomy and multiple areas of arch stenosis, the patient underwent an extra-anatomic aorto-aortic bypass graft with no complications. He was discharged on amlodipine and atenolol. The hypertension resolved and his BP remained controlled at follow up six months later.

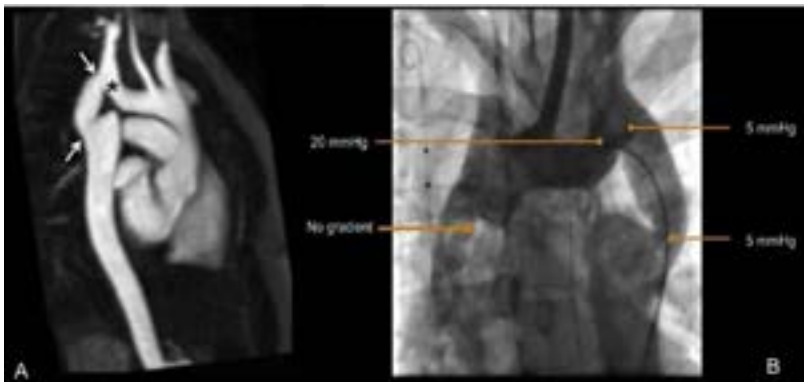

C063

Late presentation of a common congenital condition: why TOF should be always in your differential

Marta Alhama-Belotto, MD[1] Amitabh C. Pandey, MD[2], Laura Lavrencik, RT[1], Nicholas Pinto, RT[1], Kyle McBride, RT[1], Roman Szkopiec, MD[3], Charles Liu, MD[1], Martin Kendall, MD[1], Allen Johnson, MD[4], George Wesbey, MD[1], Jorge A. Gonzalez, M.D.[5]

1. *Scripps Clinic, CA*
2. *Scripps Clinic, San Diego, CA*
3. *Scripps Health, CA*
4. *Scripps Clinic, La Jolla, CA*
5. *Scripps Clinic Division of Cardiovascular Diseases, La Jolla, CA*

Description of Clinical Presentation: The patient is a 61 year-old Hispanic female with history of longstanding hypertension who was referred to cardiology by his primary care physician for increasing fatigue and shortness of breath. She denied any problems during her lifetime until 1 year ago when dyspnea on exertion started. On physical exam was found to have a 3/6 harsh murmur present throughout the precordium with radiation to the carotids and a single heart sound. ECG showed NSR with RVH. Chest x-ray showed a dilated left pulmonary artery. Subsequently, a transthoracic echocardiogram (TTE) was obtained and showed a VSD with left to right shunt, severe pulmonic stenosis, dilated and thickened RV, severe PHTN with RVSP of 143 mmHg and an overriding aorta consistent with Tetralogy of Fallot (TOF).

Diagnostic Techniques and Their Most Important Findings: Cine images show a large membranous VSD (19 mm x 20 mm) (Fig.1) with left to right shunting, severe pulmonic and infundibular stenosis (Fig.2) and a hypoplastic main and right pulmonary artery (Fig.3). Short axis and RV cine images show a dilated hypertrophic RV. Delayed enhancement images show RV insertion site LGE. The systolic function of both ventricles was preserved. Qp/Qs was calculated at 3.6 by phase contrast analysis.

Learning Points from this Case: Most patients with TOF are diagnosed at birth and childhood, usually before the 1st year of life. In a series of adult patients with TOF published by Atik et al. showed that this late presentation is rare. During a period of 20 years only 39 cases with TOF diagnosed in adulthood presented at their Heart Hospital in Sao Paulo, Brazil. The mean age at time of diagnosis was 27 years, with all the patients complaining of shortness of breath (NYHA Class II, III or IV). Furthermore, epidemiological studies have shown that only 2% of all patients with TOF reach the 4th decade of life without a diagnosis. These statistics show how rare these cases are. The most important factor in predicting long term survival in patients with TOF is the degree of infundibular/pulmonic stenosis, pulmonic regurgitation and the compliance of the right ventricle. As we can see in this patient, the balance between right sided pressures, pulmonic stenosis, RV compliance and physiology of the VSD, were in "perfect harmony" until the patient's sixth decade of life.

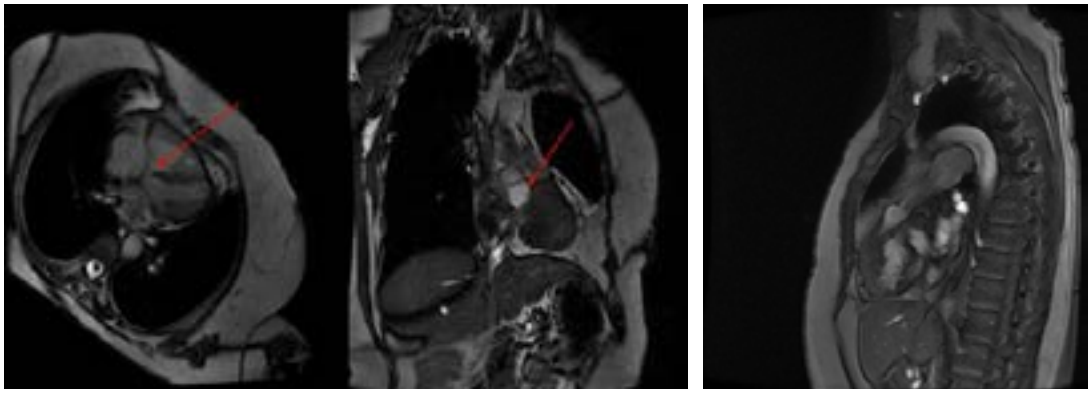

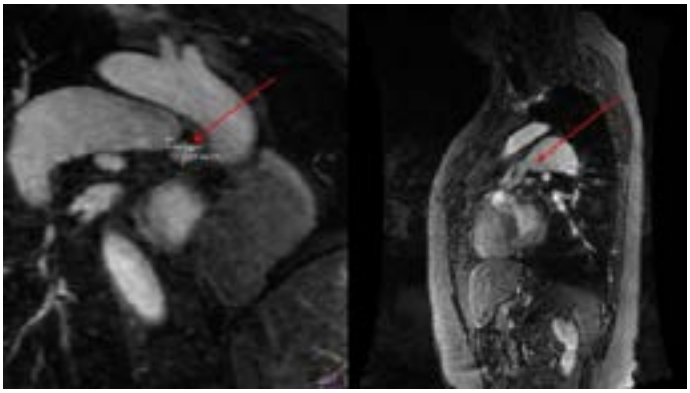

F001

Non-contrast-enhanced imaging of radiofrequency ablation lesions in normal and infarcted myocardium

Michael A. Guttman, MS[1]Susumu Tao, MD, PhD[2], Aravindan Kolandaivelu, MD[3], Sarah Fink, BA[4], Henry Halperin, MD, MA[5], Daniel A. Herzka, PhD[6]

1. *The Johns Hopkins University, School of Medicine, MD*
2. *Johns Hopkins University, school of medicine, Baltimore, MD*
3. *Johns Hopkins University School of Medicine, MD*
4. *Johns Hopkins University, MD*
5. *Johns Hopkins University, Baltimore, MD*
6. *Johns Hopkins University School of Medicine, Baltimore, MD*

Background: Interventional treatment of arrhythmia using radiofrequency ablation (RFA) is currently performed using x-ray fluoroscopy guidance. However, lack of soft tissue contrast presents a problem for monitoring of treatment, i.e. determining whether ablation has resulted in tissue necrosis. MRI provides excellent soft tissue contrast and typical methods of visualizing RFA lesions involve enhancement from injected gadolinium contrast agent. Unfortunately, the enhancement varies with time, which obscures interpretation of the images, significantly the differentiation between necrotic and edematous tissues. Non-contrast-enhanced T1-weighted (T1w) imaging has been under investigation as an alternative. We present work on the visualization of RFA lesions in healthy swine and animals with myocardial infarction (MI).

Methods: Healthy Swine (N=6): Both left and right ventricles (LV, RV) were ablated. Imaging was performed after RFA using a free-breathing navigator-gated 3D inversion recovery sequence for T1-weighting. A long TI (~700 ms) was used to maximize contrast between lesions and normal myocardium, requiring 2-beat triggering for higher heart rates. Typical imaging parameters were: flip=25 deg, TR/TE=5.4/2.7 ms, pixel size=1.1x1.1x2.5 mm, BW=250 Hz/pixel, 32-40 slices, scan time=10-15 min. Additional higher resolution images (pixel size=1.1x1.1x2.2 mm interpolated to 1.1 mm isotropic) required ~20 minutes. Delayed contrast-enhanced (DCE) imaging with similar resolution was also performed.

Swine with MI (N=3): MI was induced by 120 min balloon occlusion of the LAD. Eight weeks post-MI, DCE imaging was performed to produce a substrate map. RFA was targeted at infarct border zones using electro-anatomical mapping and the substrate map. Immediately after RFA, animals were imaged as above.

Results: Healthy Swine: In all experiments, RFA lesions were clearly evident in the non-contrast T1w scans in both LV and thin RV walls (Fig. 1A,B). Lesion core is hyperenhanced and surrounded by a hypointense ring. TI between 700-900 ms produced best contrast between lesion and normal myocardium, with the lower range providing better blood suppression, improving lesion conspicuity. Contrast was sufficient to create 3D volume renderings using cropping and window/level adjustment (Fig. 1C).

Swine with MI: Scar tissue appeared hypointense in the T1w images, while RFA lesions appeared hypointense in early phase DCE, allowing differentiation between acute RFA lesions and chronic scar (Fig. 2). Using both sets of images, co-display of substrate (chronic scar) and treatment (acute RFA lesions) was possible using color labeling and 3D volume rendering (Fig. 3).

Conclusions:

- Non-contrast-enhanced, free breathing, T1w imaging produces readily visible contrast between RFA lesions and normal myocardium, in the LV and thin RV walls, making 3D volume rendering for lesion visualization feasible.
- T1w imaging with long TI allows differentiation between acute RFA lesions and preexisting scar from MI.

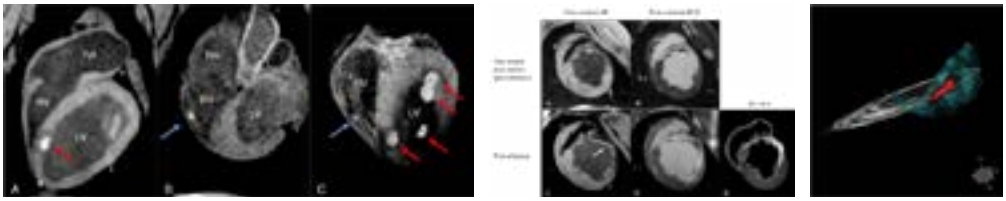

F002

Assessment of radiofrequency ablation lesions over time using non-contrast-enhanced imaging

Susumu Tao, MD, PhD[1]Michael A. Guttman, MS[2], Sarah Fink, BA[3], Aravindan Kolandaivelu, MD[4], Daniel A. Herzka, PhD[5], Henry Halperin, MD, MA[6]

1. *Johns Hopkins University, school of medicine, Baltimore, MD*
2. *The Johns Hopkins University, School of Medicine, MD*
3. *Johns Hopkins University, MD*
4. *Johns Hopkins University School of Medicine, MD*
5. *Johns Hopkins University School of Medicine, Baltimore, MD*
6. *Johns Hopkins University, Baltimore, MD*

Background: Radiofrequency ablation (RFA) is broadly performed for treatment of cardiac arrhythmias. The inability of current methods to accurately determine the therapeutic effects of RFA contributes to sub-optimal success rates. Delayed contrast enhanced (DCE) imaging using gadolinium contrast agents is typically used to assess RFA lesions. However, the amount of gadolinium enhancement is different for acute and chronic lesions, and varies with time after injection, making it difficult to predict the chronic extent of lesions from their acute appearance. Non-contrast-enhanced T1-weighted (T1w) imaging has been reported to allow accurate assessment of acute RFA lesions. We aimed, therefore, to estimate the change over time observed with T1w imaging after RFA.

Methods: Under IACUC approval, 7 lesions were created in the left-ventricular endocardium of 2 swine using a 3.5 mm-tip irrigated catheter at 30 W for 60 sec. Imaging was performed 0, 7, 14, and 21 days post-ablation at 1.5 T. Typical imaging parameters for the free-breathing navigator-gated 3D inversion recovery T1w sequence were: flip=25 deg, TR/TE=5.4/2.7 ms, TI = 700 ms, pixel size=1.1x1.1x2.5 mm, BW=250 Hz/pixel, 32-40 slices, scan time=10-15 min. DCE imaging with similar resolution was also performed. After *in-vivo* imaging at day 21, high-resolution (0.5x0.5x0.5 mm) contrast-enhanced *ex-vivo* imaging was performed at 3.0 T. Image Intensity Ratio (IIR) was calculated as the maximum signal of lesion divided by mean signal of normal myocardium for T1w images. Lesion volume and transmurality were measured at all time points and all acquisitions.

Results: All lesions demonstrated a hyperintense core and hypointense rim with T1w images (Fig. 1). IIR decreased insignificantly over time (Fig. 2A). The volume of hyperintense lesion core decreased 17% from day 0 to day 21 ($p=0.040$, Fig. 2B). Hyperintense volumes on T1w and DCE at day 21 were correlated with volumes on *ex-vivo* ($r^2=0.92$; $p=0.0004$, $r^2=0.98$; $p < 0.0001$, respectively, Fig. 3). At day 21, T1w imaging underestimated lesion volume by 20% ($-121\pm89 mm^3$, $p=0.011$) and DCE overestimated volume by 39% ($+232\pm135 mm^3$, $p=0.0039$) relative to *ex-vivo*. One transmural lesion observed *ex-vivo* was classified as transmural in both of T1w and DCE imaging at day 0 and 21. However, three non-transmural lesions were incorrectly classified as transmural in DCE imaging at day 0.

Conclusions: Non-contrast-enhanced T1w imaging may be better than DCE for estimating acute and chronic lesion size, and identifying relevant acute lesion characteristics such as transmurality. Chronic lesions exhibit consistent enhancement and decreasing volume over time.

http://www.ConferenceAbstracts.com/uploads/cfp2/attachments/LDFAIBDN/LDFAIBDN--222564-1-ANY(1).pdf

http://www.ConferenceAbstracts.com/uploads/cfp2/attachments/LDFAIBDN/LDFAIBDN--222564-2-ANY(1).pdf

http://www.ConferenceAbstracts.com/uploads/cfp2/attachments/LDFAIBDN/LDFAIBDN--222564-3-ANY(2).pdf

F003

Increased efficiency catheters for MRI-guided Electro-physiology (EP); initial results

Ehud J. Schmidt, PhD[1]Jose De Arcos Rodriguez, PhD[2], Junichi Tokuda, PhD[2], Jeffrey Schweitzer, MS[3], Gregory Olson, BS[4], Joseph Ting, PhD[5], Erin McKenna, MBA[6], William Stevenson, MD[2], Charles L. Dumoulin, PhD[7], Mikayel Dabaghyan, Phd[2]

1. *Brigham and Women's Hospital, Newton, MA*
2. *Brigham and Women's Hospital, Boston, MA*
3. *St. Jude Medical, St. Paul, MN*
4. *St. Jude Medical, Plymouth, MN*
5. *Catapult Product Development Inc., Waltham, MA*
6. *Boston Biomedical Innovation center, Cambridge, MA*
7. *Cincinatti Chiildren's Hospital Medical Center, Cincinatti, OH*

Background: Major advantages of MRI-guided thermal ablation, such as for treatment of atrial fibrillation or ventricular tachycardia, are the ability to accurately navigate to desired locations and then monitor therapy delivery. Ongoing human trials are validating its clinical utility. However, the durations of MRI-guided procedures far exceed those performed in the conventional EP lab. We previously developed the means to perform Voltage-Device-Tracking (VDT)-based positional localization in MRI [1]. VDT-tracking, which also works outside MRI, allows registration-free transfer of a patient from the MRI to a conventional interventional-suite, so portions of the procedure can be performed outside MRI. We also developed intra-cardiac MRI imaging catheters [2], with improved imaging SNR, relative to (diagnostic) surface cardiac arrays, so they can shorten the MRI imaging sessions. **Objectives:** Improve the MRI-guided EP workflow by using a novel catheter set; 1. A dual VDT/MR-Tracking (MR-T) deflectable EP catheter for rapid navigation and mapping 2. A sensitive Intra-Cardiac MRI (ICMRI) catheter, for motion-compensated heart imaging.

Methods: An irrigated 7-Fr deflectable EP ablation catheter with 5 VDT electrodes interleaved with 4 MR-T coils [Fig. 1] was developed by St. Jude Medical (SJM, Minnetonka, MN). It includes MRI radio-frequency heat-mitigation elements on both the VDT and MR-T channels. Real-time software transfer of MR-Tracking locations from a Siemens MRI to the SJM NavX-Velocity workstation was developed for rapid VDT to MRI coordinate-frame registration. An ICMRI catheter (sheath) [Fig. 2] was also developed by Catapult (Waltham, MA), including a tuned/matched printed-circuit imaging coil that expands from 5 to 35 mm diameter, a tetrahedral-array (MR-TA) of printed-circuit tuned/matched MR-T coils, and a lumen that encompasses the EP ablation catheter. A prospective motion-compensated 2D/3D GRE or SSFP MRI sequence utlizing the MR-TA for motion detection was developed for 3T Siemens MRIs. Testing was performed in human-size saline-filled phantoms, and in swine models.

Results: The new EP catheter provided susceptibility-free MR imaging at 3T, and its interleaved MR-T/VDT electrodes permitted rapid registration from the VDT to MRI coordinate frames. The new ICMRI provides a robust intra-cardiac imaging coil, which offers 10X SNR improvement within a 50x50 mm FOV, covering the entire swine Left Atrium. IMCRI's MR-TA permits artifact-free motion-compensated imaging.

Conclusions: Initial phantom and animal use of a new catheter set was demonstrated, demonstrating its ability to accelerate and simplify the MRI-guided EP workflow. **References**: [1] Schmidt, MRM. '14, [2] Chen, JCMR '15

Acknowledgements: NHLBI U54HL119145, NIBIB P41EB015898

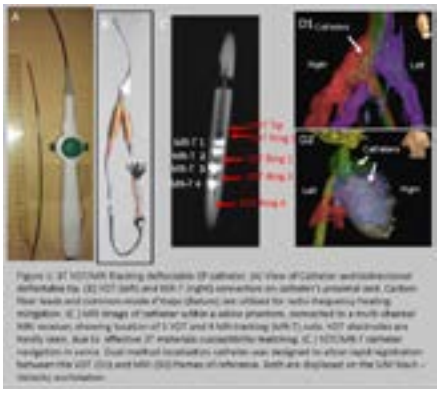

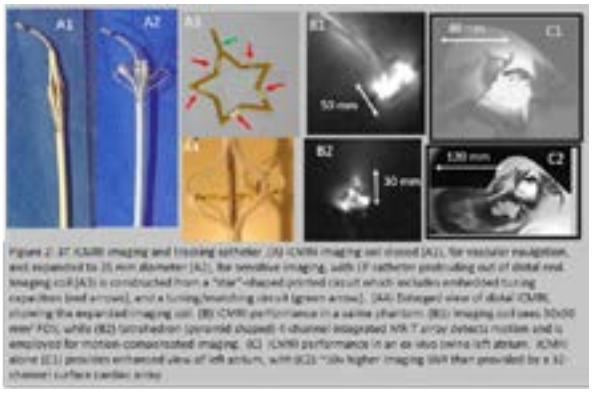

F004

Noise reduction techniques for 3D Motion Correction on intra-cardiac active MR-tracked devices

Jose De Arcos Rodriguez, PhD[1] Wei Wang, Ph.D.[2], Ravi Teja. Seethamraju, Ph.D.[3], Ehud J. Schmidt, PhD[4]

1. *Brigham and Women's Hospital, Boston, MA*
2. *Brigham and Women's Hospital, MA*
3. *Siemens Healthcare, Malden, MA*
4. *Brigham and Women's Hospital, Newton, MA*

Background: Intra-cardiac (IC) imaging catheters can potentially acquire faster high-resolution heart images, since they employ smaller-diameter RF coils, which are also brought closer to the target, relative to surface coils; however, they suffer from higher motion-sensitivity. We previously developed [1] MR- tracking-based motion compensation, which delivered 3D rigid-body (translation/rotation) motional- characteristics using a tetrahedral-shaped micro-coil array integrated within the IC catheter. Accurate measurement of motion is challenging due to the small array length (~18mm) and ~11% (~2mm) standard-deviation (SD) in coil-location. Currently, noise-related fluctuations in tracking-coil locations lead to large errors in the motional estimate, leading to image artifacts.

Objectives: To improve the performance and robustness of motion-correction methods under realistic (noisy) conditions by implementing a noise-adaptive algorithm.

Methods: Motion simulations. We implemented and tested novel strategies using scanner workflow simulations based on both real and simulated data (Figure 1). To ensure robustness, we made our algorithm adaptive; utilizing a learning time-period to measure the dimensions of the extended tetrahedron and the noise level of each coil, which allowed rejecting data from noisy coils and detecting periods of non-rigid-body motion. To reduce the noise's effects on motion estimation, we characterized separately rotational and translational noise thresholds using the motion SD. Additionally, a set of different filtering methods was analyzed to optimize their performance (Figure 2). Finally, the system was forced to behave as a rigid-body, so that during periods when noise induced translation estimates were greater than one SD, this data was rejected, and the motion of the system was extrapolated using the mean filtered translation. **Experiments with an MRI-compatible motional platform.** We built translational and rotational motional platforms to test the new algorithm features by applying displacements and rotations to a gel phantom which included a 4-microcoil tetrahedron-shaped inclusion. The experiments were performed in a 3T Siemens Verio, using a custom sequence which interleaved MR-tracking and imaging segments. Motion detected by the tetrahedron's tracking coils was processed by our algorithm and then used for prospective correction of the subsequent imaging segment.

Results: The maximum improvement using the mean filter was 16%, 33%, in translation and rotation, respectively. When noisy coils were included in the system, the rejection filter improved the performance by up to 20%, 50%.

Conclusions: New methods to improve the performance of MR-tracked motion-compensated imaging have been tested, enabling improved MR-tracked high-resolution imaging of the heart during interventional MRI-guided procedures.

Funding: NHLBI/U54HL119145, NIBIB/P41EB015898 **References**: [1]Qin L, MRM'13, [2]Kabsch W, ActaCryst'76

http://www.ConferenceAbstracts.com/uploads/cfp2/attachments/LDFAIBDN/LDFAIBDN--222696-1-ANY(2).pdf

http://www.ConferenceAbstracts.com/uploads/cfp2/attachments/LDFAIBDN/LDFAIBDN--222696-2-ANY.pdf

F005

RF-induced heating of commercial guidewires in clinically relevant configurations

Adrienne E. Campbell-Washburn, PhD[2]Daisy J. Xu[1], Dumitru Mazilu, PhD[2], Gary Melvin[3], Anthony Z. Faranesh, PhD[2], Robert J. Lederman, MD[2]

1. *National Heart, Lung, and Blood Institute, National Institutes of Health, Rockville, MD*
2. *National Heart, Lung, and Blood Institute, National Institutes of Health, MD*
3. *National Institutes of Arthritis and Musculoskeletal and Skin Diseases, National Institutes of Health, MD*

Background: MRI-guidance is appealing for cardiac catheterization procedures, but clinical translation has been limited by the unavailability of safe guidewires for the MRI environment [1, 2]. RF-efficient imaging methods have been investigated to reduce safety concerns of RF-induced heating in guidewires [3]. Here, we characterize heating of commercial guidewires in configurations relevant to clinical catheterization procedures.

Methods: Experiments were performed on a clinical 1.5T scanner (Aera, Siemens, Erlangen). A home-built positioning apparatus was used to secure commercial guidewires (.035"/145cm Nitrex, Covidien, Plymouth, MN and 0.035"/150cm Glidewire, Terumo, Somerset, NJ) and fiber-optic temperature probes (Opsens, Quebec, Canada) at precise locations in an ASTM 2182 phantom (Fig 1). Temperature was monitored at multiple positions during 2 minutes of continuous scanning with spiral gradient echo (GRE) (TE/TR = 0.86/5.16 ms, 16 interleaves, flip angle=10°) and standard Cartesian bSSFP (TE/TR = 1.29/2.86 ms, flip angle=45°) real-time imaging sequences (transmit voltage = 400V).

Results: The positioning apparatus enabled good repeatability over 3 separate measurements at the tip of a straight guidewire (ΔT= 4.6°C, 3.7°C, 3.4°C, coefficient of variation=15.9%). The Nitrex guidewire generated more heating compared to the Glidewire (ΔT_{Nitrex}=5.0°C, $\Delta T_{Glidewire}$=1.0°C). Relative position between the guidewire and catheter (7F Arrow, Teleflex, Morrisville, NC) influenced guidewire tip heating (Table 1A) with maximum temperature when the guidewire was extended 1cm from the catheter tip (ΔT= 15.4°C). A second location of increased temperature was observed at contact points in looped configurations (Fig 2). The temperature at both the tip and the loop increased with the number of guidewire loops (Table 1B). Furthermore, temperature at the loop decreased as the loop contact point was separated (ΔT_{0cm}= 2.3°C, ΔT_{3cm}= 1.8°C, ΔT_{5cm}= 1.5°C, ΔT_{8cm}= 1.0°C). Importantly, in all conditions tested, negligible heating was observed using spiral GRE imaging (Table 1).

Conclusions: This work aimed to study guidewire heating in clinically relevant configurations with looping and catheter placement. Looping can occur in the pericardium, in the ventricles, and during prolapse at the valves. In addition, guidewires are used to guide and exchange catheters in clinical procedures. Heating exceeded 15°C with standard bSSFP imaging, but remained < 0.6°C with spiral GRE in all conditions. MRI-guided cardiovascular interventions using RF-efficient imaging sequences could become clinically feasible following careful characterization of guidewire heating.

Funding: NHLBI DIR (Z01-HL006039, Z01-HL005062).

References: [1] Rogers T and Lederman RJ, Current cardiology reports **17**(5):31 (2015), [2] Konings MK et al, JMRI **12**(1):79-85 (2000), [3] Campbell-Washburn AE et al, JCMR **17**:114 (2015).

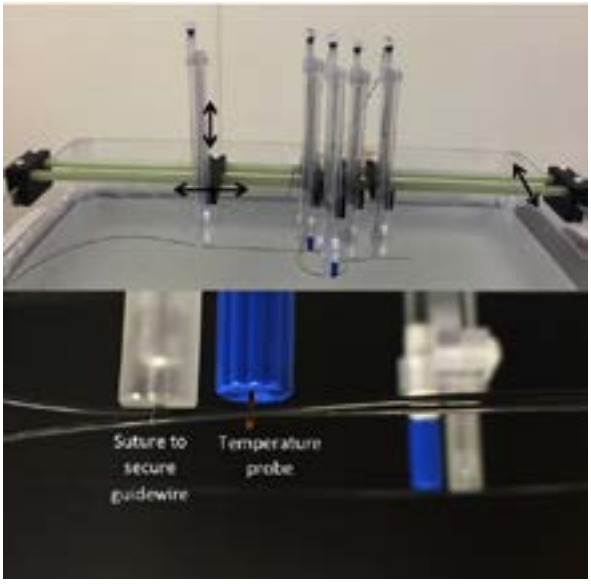

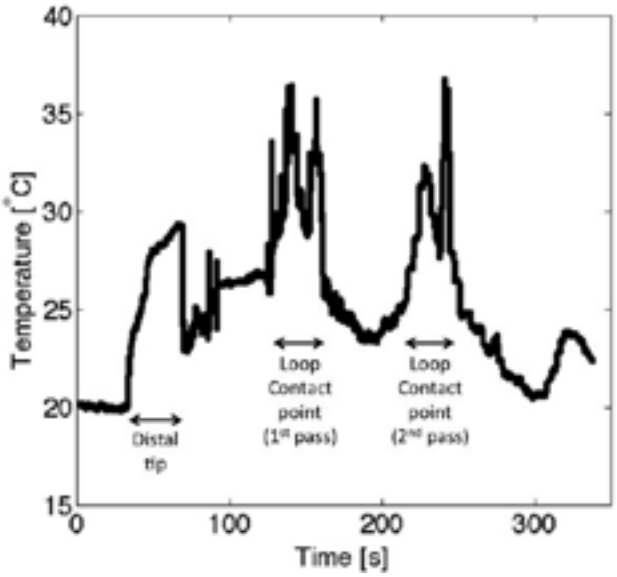

Table 1: A) ΔT at guidewire tip (Nitrex) during 2 minutes of continuous scanning with catheter positioned proximal to guidewire tip (10cm, 5cm, 2cm, 1cm), aligned with tip (0 cm), and distal to guidewire tip (guidewire tip inside catheter lumen, -2cm and -5cm). B)ΔT measured simultaneously the guidewire tip and loop connection point (Nitrex) during 2 minutes of connection point for single loop, double loop, triple loop and quadruple loop.

Spiral GRE	Cartesian bSSFP	**A.**
N/A	3.82 °C	10cm (catheter proximal)
0.22 °C	4.92 °C	5cm (catheter proximal)
0.25 °C	6.56 °C	2cm (catheter proximal)
0.55 °C	15.44 °C	1cm (catheter proximal)
0.60 °C	10.92 °C	0cm (tips aligned)
0.24 °C	0.24 °C	-2cm (catheter distal)
0.28 °C	0.21 °C	-5cm (catheter distal)

Guidewire loop		Guidewire tip		**B**
Spiral GRE	Cartesian bSSFP	Spiral GRE	Cartesian bSSFP	
0.51 °C	2.31 °C	0.29 °C	2.27 °C	Single loop
0.25 °C	3.83 °C	0.26 °C	7.09 °C	Double loop
0.27 °C	4.02 °C	0.26 °C	7.37 °C	Triple loop
0.27 °C	4.02 °C	0.26 °C	8.17 °C	Quadruple loop

F006

Fontan circulation shows deranged haemodynamics with 4D flow CMR

Malenka M. Bissell, DPhil, MD[1] Victoria Stoll, DPhil, BMBCh[2], Aaron T. Hess, PhD[3], Jonatan Eriksson, PhD[4], Carl-Johan G. Carlhäll, MD, PhD[5], Saul Myerson, MD, FRCP[6], Stefan Neubauer, MD, FRCP[7]

1. *Oxford University, Leeds, England, United Kingdom*
2. *Oxford University, Oxford, England, United Kingdom*
3. *OCMR, University of Oxford, England, United Kingdom*
4. *Divsion of Cardiovascular Medicine, Department of Medical and Health Sciences, Linköping University, Linköping, Sweden, Ostergotlands Lan, Sweden*
5. *Linköping university, Ostergotlands Lan, Sweden*
6. *NA, Oxford, England, United Kingdom*
7. *University of Oxford, England, United Kingdom*

Background: Routine assessment of the Fontan circulation with cardiovascular magnetic resonance imaging (CMR) includes ventricular function assessment. Recent advances in 4D flow CMR now facilitate additional detailed assessment of left ventricular intra-cardiac flow patterns and kinetic energy (KE). This has shown to be abnormal in adults with dilated cardiomyopathy and low normal ejection fraction. We therefore hypothesised that haemodynamic changes may already be apparent in the ventricle in Fontan patients prior to a decline in ejection fraction.

Methods: 8 Fontan patients (2 atrio-pulmonary Fontan connection and 6 total cavopulmonary connection) and 8 healthy volunteers (age 14-35 years, mean 22 years) prospectively underwent 4D flow CMR at 3 Tesla. For 4D flow CMR analysis the ventricular volume was divided into 4 functional components: direct flow, delayed ejection flow, retained inflow and residual volume. For each individual components the volume was calculated and expressed as percentage of end diastolic volume and the kinetic energy was calculated over the cardiac cycle and measured at end diastole.

Results: Ejection fraction was comparable in Fontan patients and healthy volunteers (57% vs 67%). In the functional component analysis, Fontan patients had significantly increased residual volume 64% vs 36%; $p < 0.05$) and reduced direct flow (43% vs 51%; $p < 0.05$) compared to healthy volunteers. This was less apparent in the 2 Fontan circulations with an isolated left ventricle. The kinetic energy profiles were similar in both groups.

Conclusions: Ventricular 4D flow CMR assessment is feasible in complex congenital heart disease. While Fontan patients show less direct flow and increased residual volumes than healthy volunteers, kinetic energy values were normal. This is in contrast to adults with cardiomyopathies and may suggest that the anatomical ventricular geometry has a bigger impact on the circulatory component of blood flow than kinetic energy profiles.

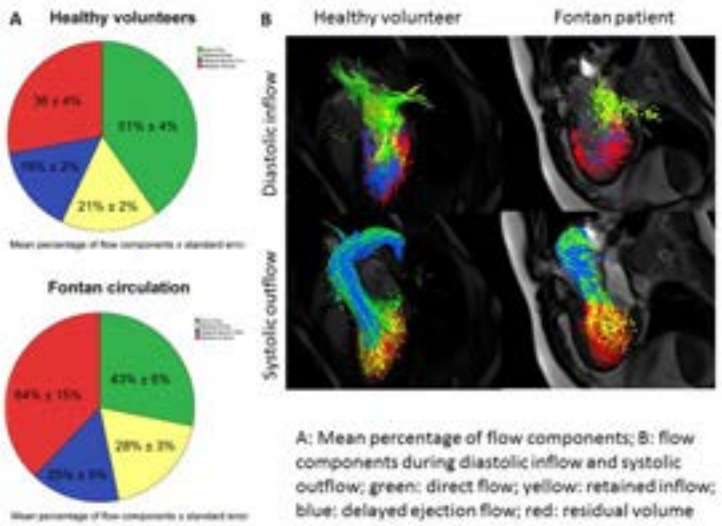

A: Mean percentage of flow components; B: flow components during diastolic inflow and systolic outflow; green: direct flow; yellow: retained inflow; blue: delayed ejection flow; red: residual volume

F007

Evaluation of right ventricular function in Fontan physiology using feature tracking magnetic resonance strain, strain rate and wall motion delay

Akio Inage, MDNaokazu Mizuno

Division of Pediatric Cardiology, Tokyo, N/A, Japan

Background: Patients are commonly affected by ventricular dysfunction after Fontan palliation. Reliable quantification of ventricular function was hampered by complex ventricular anatomy and physiology. Cine-based feature tracking strain (FTS) is a new technique to assess cardiac function from cardiac magnetic resonance (CMR). The objective of this study was to investigate into FTS in single right ventricle subjects after Fontan palliation undergoing CMR.

Methods: Right ventricular end-diastolic and end-systolic volumes (SVEDV and SVESV), stroke volume (SV), and ejection fraction (EF) were measured offline (Medis QMass advanced edition, the Netherlands) as conventional function parameters. Offline global longitudinal and circumferential strain/SR (GLS/GLSR and GCS/GCSR), and radial strain/SR were performed (TomTec Image Arena, Germany) using FTS. As well, anterior to posterior wall motion delay (>130ms; APWMD) analysis was calculated on the short-axis view at the basal level, and bilateral wall motion delay (>90ms; BLWMD) on the 4-chamber view at the basal and mid levels.

Results: 25 Fontan subjects with right ventricular morphology (mean age 18.4+/-9.6 years, post Fontan period 15.3+/-8.4 years) underwent a CMR study. Basal GCS/GCSR (-11+/-9 %, -0.8+/-0.5 1-s) were lower than it at the mid (-17+/-6 %, -1.1+/-0.5 1-s; p=0.02) and apical (-26+/-9 %, -1.9+/-1.0 1-s; p=0.001 and 0.003) levels. There were correlations between SVEDV and GCS/GCSR (r=0.71). But, no correlations with GLS/GLSR. At the mid and apical levels, there were correlations between GCS/GCSR and SVESV, and EF (r=0.68 to 0.79 and r=0.51 to 0.77). There was also correlation between GLSR and SV (r=0.71). Basal GCS/GCSR were correlated with grade of atrioventricular valve regurgitation assessed by echocardiography (mild; r=0.53, moderate; r=0.63, severe; r=0.65). BLWMD was found for 17 cases (67%) at the basal and 14 cases (56%) at mid levels, and APWMD for 6 cases (22%) at the basal level.

Conclusions: In Fontan patients there is moderate correlation between strain/SR and measures of ventricular size and ejection. However, there were no correlations GLS/GLSR and SVEDV. Annular dysfunction suggested by correlation of low basal GCS/GCSR with grade of atrioventricular valvular regurgitation, and basal BLWMD. Analysis of regional strain/SR may helpful in understanding myocardial mechanics with Fontan physiology in further studies.

F008

Cardiac Magnetic Resonance Tissue Tracking In Single Ventricle Fontan Patients

Stephanie Ambach[1] Vien Truong, MD[1], John Jefferies, MD[2], Wojciech Mazur, MD[3], Michael Taylor, MD, PhD[2], Ryan Moore, MD[2]

1. *The Christ Hospital Health Network, Cincinnati, OH*
2. *Cincinnati Children's Hospital Medical Center, Cincinnati, OH*
3. *The Christ Hospital Health Network, Mason, OH*

Background: Total cavopulmonary connection has been the preferred palliation for patients with univentricular hearts of varied morphologies. Systolic performance of single ventricle is an important determinant of survival in Fontan patients. The purpose of this study was to investigate single ventricular contractility by CMR derived strain using tissue tracking. (CMR TT).

Methods: Twenty eight single ventricle patients status post Fontan procedure (14 patients with left ventricular morphology, 9 patients with right ventricular morphology and 5 undetermined morphology), 10 to 57 years of age, were studied 14 ± 7 years after Fontan procedure. Mid ventricle circumferential and and global longitudinal strain was calculated using CMR TT. (Circle Cardiovascular Inc.) These strain values were compared with strain from 30, age matchednormal patients. Ejection fraction of the single ventricle was preserved in all patients with mean EF of 55%.

Results: There was no significant difference between global longitudinal strain ($P = 0.12$) and mid ventricle circumferential strain at mid-cavity between patients and controls ($P = 0.48$), regardless of single ventricle morphology

Conclusions: Longitudinal strain and circumferential strain at mid cavity are preserved in patients after remote Fontan procedure, irrespective of single ventricle morphology when compared to normal LV. Single ventricles with RV and undetermined morphology adapted to function as systemic ventricles without evidence of systolic dysfunction as measured by myocardial strain

Ventricular strain value

P	Single Ventricle (n=28)	Normal (n=30)	
0.45	21 (14-25)	19 (14-32)	Median age (IQR)-yr
0.62	15	18	Sex (female)
0.07	54.68 ± 7.02	58.03 ± 4.11	EF
0.12	-15.50 ± 4.19	-16.97 ± 2.60	Longitudinal strain
0.48	-17.35 ± 4.33	-16.67 ± 2.77	Circumferential strain (mid-cavity)

Continuous variable are expressed as mean ± standard deviation with normal distribution and median and interquartile range with non-normal distribution. IQR, interquartile range; yr, year; EF, ejection fraction

F009

A novel imaging method, vortex flow mapping using cine magnetic resonance imaging, revealed that vortex flow in the Fontan route is associated with supraventricular tachycardia after Fontan operation

Tatsunori Takahashi, MD[1] Michinobu Nagao, MD, PhD[2], Yumi Shiina, MD PhD[3], Keiko Toyohara[4], Daiji Takeuchi, MD,Ph.d[5], Tomomi Nishimura, MD[6], Kota Taniguchi, MD[1], Kei Inai, MD., PhD.[7], In-Sam Park, Associate professor[8]

1. *Tokyo Women's Medical University, Tokyo, Japan*
2. *Tokyo Women's Medical University, Shinjuku-ku, Tokyo, Japan*
3. *Cardiovascular center, St.Luke's International Hospital, N/A, Japan*
4. *Tokyo Women's Medical University, N/A, Japan*
5. *Tokyo Womens Medical University, Tokyo, Japan*
6. *TOKYO WOMEN'S MEDICAL UNIVERSITY, N/A, Japan*
7. *Tokyo Women's Medical University, Tokyo, Tokyo, Japan*
8. *Department of Pediatric Cardiology, Tokyo Women's Medical University, Shinjuku-ku, Tokyo, Japan*

Background: Supraventricular tachycardia (SVT) occasionally affects patients who have undergone an atriopulmonary connection (APC)-type Fontan procedure and causes deterioration in their hemodynamics. We developed a novel method to visualize and quantitate vortex flow (VF) in the right atrium (RA) by using images derived from cine magnetic resonance imaging (MRI) (Vortex Flow Map, VFM). The aim of this study was to evaluate the association between SVT and VF.

Methods: APC type Fontan patients who underwent cine MRI between 2007 and 2016 were enrolled. Patients with massive baffle leak with pulmonary blood flow—systemic blood flow ratio of less than 0.9 were excluded. Using the VFM method, we visualized the radial-directed VF in an arbitrary slice of the RA that provided maximal RA area in trans-axial , sagittal and coronal sequences, and quantitated the strength of VF in the range of −20% to 50%. The VFM area ratio was calculated using the following formula: [(area with VFM > 30%) / (whole RA area)]. Volumetric and phase contrast data derived from cardiac MRI, history of SVT, and data of low voltage area (LVA, < 0.5 mV) in the RA wall on a voltage map were acquired from medical records.

Results: A total of 25 APC Fontan patients were enrolled [age, 25(12-45), 9 males (36%)]. Trans-axial, sagittal and coronal VFM area ratio range were 0-0.53 (median 0.23), 0-0.53 (median 0.20), and 0-0.62 (median 0.28), respectively. Trans-axial and sagittal VFM area ratio had good correlations with ventricular stroke volume index (L/min/m^2) derived from a phase contrast method (r=0.68, p < 0.01/r=0.64, p < 0.01, respectively). There was no correlation between VFM area ratio and RA ejection fraction (RAEF) or RA volume index (mL/m^2). Eight (32%) patients were affected by SVT. The median VFM area ratio was significantly higher in patients with SVT than in those without SVT (0.30 vs 0.13, respectively, p25% of the RA wall revealed a significantly higher prevalence rate of SVT and lower RAEF than that in those with a small LVA (On each trans-axial, sagittal and coronal slices, LVA and high VFM (>30% of VFM) areas corresponded in 8/11 (73%), 7/11 (64%), 7/11 (64%) cases, respectively.

Conclusions: In patients with APC Fontan circulation, vortex flow may injure the RA wall, subsequently inducing SVT.

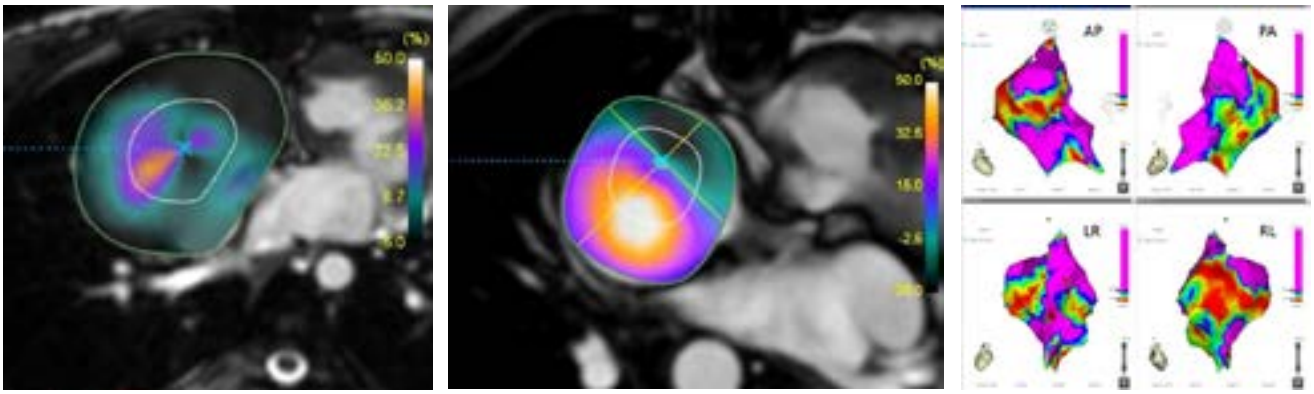

F010

The impact of systemic-to-pulmonary collateral flow (SPCF) in patients after Fontan operation assessed with 4D flow MRI.

Abdullah M. AL Bulushi, MD[1]Mona Salehi Ravesh, PhD[1], Dominik Daniel. Gabbert, PhD[1], Michael Jerosch-Herold, PhD[2], Anne Schöber[1], Philip Wegner, MD[1], Gunther Fischer, MD[1], Jens Scheewe, MD[3], Tim Attmann, MD[3], Ines Kristo, MD[1], Hans-Heiner Kramer, MD[1], Carsten Rickers, MD[1]

1. *Department of Congenital Heart Disease and Paediatric Cardiology, University Hospital Schleswig-Holstein UKSH, Schleswig-Holstein, Germany*
2. *Department of Radiology, Brigham & Women`s Hospital & Harvard Medical School, Boston, United States., MA*
3. *Department of Cardiovascular Surgery, University Hospital Schleswig-Holstein UKSH, Schleswig-Holstein, Germany*

Background: Systemic-to-pulmonary collaterals (SPC) are found frequently in patients with single ventricle (SV) physiology but the hemodynamic relevance of SPC flow (SPCF) is unclear. The aim of this study was to quantify SPCF in patients with Fontan-circulation utilizing novel MRI flow measurements. Furthermore, we compared SPCF with catheter findings and sought to identify associations for collateral development.

Methods: 61 patients with SV post total cavo-pulmonary circulation (TCPC) physiology underwent comprehensive CMR and conventional catheterization (age: 9.0 ± 1.2 years). Aanatomical measurements of the pulmonary arteries and veins and phase contrast cine 3D flow imaging ("4D flow") were performed in all patients. A dedicated software was used for quantification of SPCF for both lungs and color coded 4D-visualization of blood flow (GT-Flow™, Gyrotools Inc., Zurich). SPCF was graded from 0 to 3 for both lungs from catheter angiography and compared to MRI measurements.

Results: SPCF was present in all patients. SPCF was 23.2 ± 8.44% of Qp (pulmonary venous return) with 9% in the right and 47% in the left lung. Overall, in 34% of cases collateral flow was considered significant with both methods. Pulmonary artery cross-sectional area showed significant inverse correlation with SPCF ($r=0.29$, $p=0.02$). There was no correlation between the SPC flow and ventricular dimensions: end-diastolic and end-systolic volume ($r=0.13$, $p=0.3$ and $r=0.08$, $p=0.6$, respectively), suggesting that there is no hemodynamic burden due to SPCF. Additionally, by using the invasive catheterization data, we did not find any correlation between the SPCF and SV end-diastolic pressure, as well as mean pulmonary artery pressure. A comparison between 4D-velocity acquisitions and cardiac catheterization grading of SPCF showed significant correlation and agreement ($r=0.82$, $p < 0.001$).

Conclusions: Patients with small left pulmonary artery (LPA) cross-sectional area are prone to develop SPCF. 4D flow MRI identified significant SPCF in more than one third of patients in Fontan-circulation which was not hemodynamically relevant for the single ventricle. There is no correlation between the SPC flow and ventricular dimensions.

F011

Blood Oxygen Level Dependent (BOLD) Cardiovascular Magnetic Resonance (CMR) as Predictor of Cardiac Prognosis in Asymptomatic Chronic Kidney Disease (CKD) Patients

Ranjit Shah, MBBS, FRACP[2]Susie Parnham, FRACP, PhD[1], Jonathan Gleadle, FRACP, DPhil[3], Anand Ganesan, MBBS, PhD[3], Richard Woodman, PhD[4], Carmine De Pasquale, FRACP, PhD[3], Joseph Selvanayagam, FRACP, DPhil[5]

1. *Flinders Medical Centre, Bedford Park, South Australia, Australia*
2. *South Australian Health and Medical Research Institute, Adelaide, SA, Australia, Prospect, South Australia, Australia*
3. *Flinders Medical Centre, South Australia, Australia*
4. *Flinders University, South Australia, Australia*
5. *Flinders University, Adelaide, SA, Australia, South Australia, Australia*

Background: Current invasive and non-invasive diagnostic approaches are poorly predictive of future cardiovascular events, and in particular the risk of sudden cardiac death (SCD). We hypothesized that blunted myocardial oxygenation response to stress (defined by negative BOLD Signal Intensity (SI) Change value) could be an independent predictor for cardiovascular events in asymptomatic CKD patients.

Methods: Participants with pre-existing CKD (CKD+) with no established coronary artery disease underwent BOLD CMR scanning at 3 Tesla. BOLD images were acquired at rest and with adenosine stress. BOLD Signal Intensity Change was assessed semi-quantitatively. Patients were prospectively followed for major adverse cardiac events (MACE), defined as cardiovascular death, myocardial infarction, ventricular arrhythmia and pulmonary oedema.

Results: The mean follow-up was 20± 12 months. Ten patients (26%) had MACE (p= 0.01): four (10%) deaths, four (10%) non-fatal myocardial infarctions, two (5%) heart failure. [8 out of 20 (44%) in CKD patients with negative BOLD SI Change had MACE versus 1 out of 16 (6%) in CKD patients without negative BOLD SI Change had MACE, p= 0.026)]. On multivariate analysis, the negative BOLD SI Change value was independently associated with MACE (Hazard Ratio 19.48, 95% CI 1.28 - 295.44, p= 0.03). CKD patients with negative BOLD SI Change value had reduced MACE-free survival compared to CKD patients with positive BOLD SI Change value (p =0.03).

Conclusions: Blunted myocardial oxygenation response to stress could be a predictor of major adverse cardiovascular events in patients with CKD. Non-contrast BOLD CMR is a promising prognostic tool to assess silent myocardial ischaemia in CKD patients.

Further studies in larger patient populations are warranted.

F013

Increased myocardial native T1 and extracellular volume in Duchenne muscular dystrophy carriers

Preeti Ramachandran, MD[1] Justin Tretter, M.D.[2], Ryan Moore, MD[3], Peace Madueme, M.D., M.S.[4], Mantosh Rattan, MD[3], John Jefferies, MD[3], Michael Taylor, MD, PhD[3]

1. *Cincinnati Children's Hospital and Medical Center, Cincinnati, OH*
2. *Cincinnati Children's Hospital Medical Center, Blue Ash, OH*
3. *Cincinnati Children's Hospital Medical Center, Cincinnati, OH*
4. *Cincinnati Children's Hospital Medical Center, OH*

Background: Female Duchenne muscular dystrophy (DMD) carriers are at risk for cardiomyopathy and cardiac dysfunction. Studies have shown both dysfunction and myocardial fibrosis using late gadolinium enhancement (LGE) in these patients. Our primary goal was to investigate the presence of diffuse ECM expansion using ECV (extracellular volume) mapping in this cohort. Correlation of ECV with global systolic performance by left ventricular ejection fraction (LVEF) was assessed.

Methods: A single center retrospective observational study of nineteen gene positive female DMD carriers (mean age 42 years, range 32-59 years) who underwent CMR assessment from Jan 2015 – July 2016 was performed. All patients underwent routine CMR study including T1 mapping with a modified Look Locker (MOLLI) sequence before and after contrast administration. T1 and ECV maps of the mid left ventricular myocardium were generated and contoured to estimate global ECV.

Results: A majority of the DMD carriers had elevated LV myocardial pre contrast T1 and ECV independent of the presence of LGE and/ or normal LVEF. Mean pre contrast T1 values in DMD carriers with LGE was elevated at 1059ms (range 982-1191ms) and for DMD carriers without LGE was 1056ms (range 950-1089ms).Mean ECV in patients with LGE was 0.34 and in patients without LGE was 0.31. Eight patients had elevated ECV (mean 0.31) with normal LVEF. The correlation coefficient between ECV and LVEF in this study group was - 0.45 ($R^2 = 0.20$, $P>0.05$).

Conclusions: DMD carriers have abnormal pre contrast T1 and ECV values. This suggests that DMD carriers similar to their sons are at risk for diffuse ECV expansion and progressive fibrosis despite the absence of LGE or overt left ventricular dysfunction. Future prospective studies with larger sample studies are warranted to establish ECV mapping as a potential non-invasive biomarker for sub-clinical myocardial disease in this population.

DMD carriers with LGE (N=8)	DMD Carriers (N=19)	
44.4+/-8.4	42.4+/-6.5	Age (Years)
1.8+/-0.2	1.9+/-0.5	Body surface area (m^2)
53.8+/-7.8	67+/-16	Heart rate (bpm)
44 +/-2	44+/-3	Estimated Hematocrit (%)
45+/-4	54.5+/-4.7	LVEF[a] (%)
88.7+/-9.4	87.4+/-15.2	Indexed LVEDV[b] (ml/m^2)
44.2+/-9.8	39.8+/-10.4	Indexed LVESV[c] (ml/m^2)

[a]Left ventricular ejection fraction; [b]Left ventricular end diastolic volume; [c]left ventricular end systolic volume

F014

Facioscapulohumeral Muscular Dystrophy (FSHD) – Detection of Fat and Fibrosis in the myocardium in patients with preserved LVEF

Edyta Blaszczyk, MD[1]Florian von Knobelsdorff-Brenkenhoff, MD[2], Stephanie Funk, MD[1], Luisa Schmacht[1], Ulrike Grieben, MD[3], Peter Kellman, PhD[4], Simone Spuler, MD[5], Jeanette Schulz-Menger, MD[6], Agnieszka Töpper, MD[7]

1. *Working Group on Cardiovascular Magnetic Resonance, Experimental and Clinical Research Center, a joint cooperation between the Charité Medical Faculty and the Max-Delbrueck Center for Molecular Medicine and HELIOS Hospital Berlin Buch, Berlin, Berlin, Germany*
2. *Working Group on Cardiovascular Magnetic Resonance, Experimental and Clinical Research Center a joint cooperation between the Charité Medical Faculty and the Max-Delbrueck Center for Molecular Medicine HELIOS Klinikum Berlin Buch, Germany, Berlin, Germany*
3. *Muscle Research Unit, Experimental and Clinical Research Center a joint cooperation between the Charité Medical Faculty and the Max-Delbrueck Center for Molecular Medicine, Berlin, Germany., N/A, Germany*
4. *Laboratory of Cardiac Energetics, National Institutes of Health/NHLBI, Bethesda, MD, United States., MD*
5. *Charité Universitätsmedizin Berlin, Berlin, Germany*
6. *Working Group on Cardiovascular Magnetic Resonance, Experimental and Clinical Research Center a joint cooperation between the Charité Medical Faculty and the Max-Delbrueck Center for Molecular Medicine HELIOS Klinikum Berlin Buch, Germany, Berlin, Germany*
7. *Working Group on Cardiovascular Magnetic Resonance, Experimental and Clinical Research Center a joint cooperation between the Charité Medical Faculty and the Max-Delbrueck Center for Molecular Medicine HELIOS Klinikum Berlin Buch, Department of Cardiology and Nephrology, Berlin, Germany., Berlin, Berlin, Germany*

Background: Cardiac involvement in muscle disorders is of growing interest in cardiology. FSHD is an autosomal dominant disease with an incidence of 1:15.000, usually affecting facial and shoulder girdle muscles[1]. The myocardial involvement in FSHD seems to be underestimated. The aim of this study is to identify myocardial tissue injury applying CMR in FSHD patients with preserved LVEF.

Methods: 56 patients with genetically confirmed diagnosis of FSHD were prospectively enrolled and compared with 30 healthy age-matched controls (table 1). Patients with other cardiovascular or malign diseases were excluded. Healthy controls underwent the same protocol. Scans were performed at 1.5T (Siemens). LV was assessed by state of the art SSFP cine-imaging. Tissue differentiation was based on native and contrast-media enhanced imaging using short and long axis. Fat imaging: multi-echo sequence for fat/water separation[2]. T1-mapping using MOLLI before and after 0.15 mmol/kg bw gadobutrol. Late gadolinium enhancement (LGE) imaging was identified to assess focal fibrosis. Results were compared to healthy volunteers. ECV was calculated in FSHD. Analysis was performed using CVI42 (circle cvi).

Results: Focal myocardial fibrosis was found in 15 patients (26%, 12 men) (fig.1 A). Fat deposits were identified in 9 patients (16%, 6 men) (fig.1 B). There was no fat or fibrosis in healthy controls. LGE positive patients were older (54±13 vs. 46±15 years, p=0.037), but LVEF did not differ (63±4 vs. 63±5% p=0.704). Interestingly native T1 was not only significantly higher in LGE positive segments but also in the adjacent regions (fig.2). Native T1 was not sex-dependent in healthy controls. Remarkably T1 as well as ECV was not only significantly higher in all female FSHD patients compared to FSHD men, but also in FSHD female without focal fibrosis (table 2). There was no difference in heart rate between FSHD males and females (77±18 vs. 75±13 p=0.477).

Conclusions: In FSHD, focal and diffuse fibrosis as well as focal fat are detectable in the left ventricular myocardium already in patients with preserved LVEF. Sex differences are identifiable applying mapping. These findings may help to identify patients at higher risk and to predict a further remodeling.

1. Tawil R et al. Neurology 2015;85:357-64
2. Kellman et al. Myocardial Fat Imaging. Current cardiovascular imaging reports 2010;3:83-91.

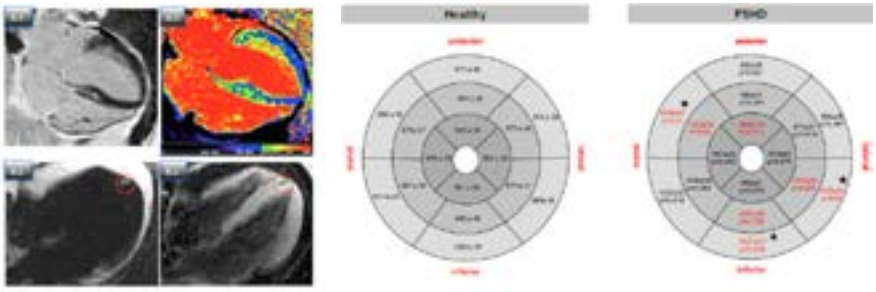

Table 1. Demographics of patients and healthy volunteers

p-value	Healthy	FSHD	Parameter
	30 [15|15]	56 [38|18]	n [male/female]
p =0.36	45±14	48±15	Age [years]
p =0.17	65±5	63±5	LVEF [%]

Table 2. Mapping reveals sex differences in patients without focal fibrosis

	women	men	Parameter*
	Healthy	**Healthy**	
p = 0.222	990±32	977±33	**T1 native**
	FSHD all	**FSHD all**	
p = 0.003	1012±29	989±26	**T1 native**
p = 0.010	28±3	26±3	**ECV**
	FSHD without LGE	**FSHD without LGE**	
p = 0.010	1014±77	993±26	**T1 native**
p = 0.084	28±6	26±4	**ECV**

*All values are given for a midventricular slice

F015

Left ventricular systolic function and the pattern of LGE independently predict adverse cardiac events in muscular dystrophy patients – extended study results

Anca R. Florian[1] Alexandru Patrascu[2], Markus A. Engelen[3], Johannes Waltenberger, Prof. Dr.[3], Sabine Roesch[2], Udo Sechtem, Prof. Dr.[3], Ali Yilmaz, Prof. Dr.[3]

1. *University Hospital Muenster, Muenster, Nordrhein-Westfalen, Germany*
2. *Robert-Bosch Hospital Stuttgart, Baden-Wurttemberg, Germany*
3. *University Hospital Muenster, Nordrhein-Westfalen, Germany*

Background: Cardiac involvement characterized by a non-ischemic, myocarditis-like pattern of left ventricular (LV) myocardial fibrosis is a frequent cause of morbidity and mortality in patients with Duchenne (DMD) and Becker (BMD) muscular dystrophy (MD) - as it may be associated with dilated cardiomyopathy, progressive heart failure and arrhythmias.
In a previous study, we could show that cardiovascular magnetic resonance (CMR)-based LV ejection fraction (LV-EF) and a "transmural" pattern of late gadolinium enhancement (LGE) are independent predictors for the occurrence of secondary adverse cardiac events such as heart failure and ventricular arrhythmias - but not for the very low number of hard primary endpoints (cardiac death/transplantation) during an average 4-year follow-up period. In the present study, we re-evaluated our previous results in an extended cohort of MD patients with a longer follow-up time.

Methods: The current study population comprised N=111 male patients (age 30±15yrs) with genetically-proven MD (27 DMD and 84 BMD). All patients underwent a multi-parametric CMR study comprising cine- and LGE-CMR (1.5-Tesla) at study inclusion and were followed up for possible adverse cardiac events. The study endpoint was defined as a combination of cardiac death and/or cardiac transplantation and/or one of the following: hospitalization for heart failure, un-/sustained ventricular tachycardia (VT), ventricular fibrillation (VF) and/or ICD implantation.

Results: The mean follow-up time was 68±29 months. At baseline, mean LV end-diastolic volume (LV-EDV) was 85±34 ml/m², mean LV ejection fraction (LVEF) 53±13% and 58 (52%) patients demonstrated an impaired LV systolic function. Presence of LGE was documented in N=74 (67%) patients – almost all showing a non-ischemic pattern of LGE. During follow-up, four deaths and one heart transplantation were observed. The pre-defined combined endpoint was encountered in 34 (31%) patients. Compared to patients without any events, those with at least one combined endpoint were older (39±12yrs vs. 26±15yrs, $p < 0.001$), had more often BMD (91% vs. 69%, p=0.015), had lower LVEF (40±12% vs. 58±9%, $p < 0.0001$) and RVEF (50±12% vs. 56±9%, p=0.008), increased LV-EDV (109±41ml/m² vs. 75±24ml/m², $p < 0.0001$) and showed more frequently presence of LGE (94% vs. 55%, $p < 0.0001$). In a multivariable model including age, type of MD, LV-EF and either LGE presence/extent/pattern, LV-EF (HR, 95% CI: 0.92, 0.89-0.95, $p < 0.001$) and a transmural pattern of LGE (HR, 95% CI: 2.21, 1.04-4.66, p=0.038) were the only independent predictors for the combined endpoint.

Conclusions: In the current extended analysis, an impaired LV systolic function and a "transmural" pattern of myocardial fibrosis independently predicted the occurrence of adverse cardiac events – including hard endpoints such as cardiac death - in DMD/BMD patients.

F016

CMR-guided endomyocardial biopsy in an in vivo porcine model

Patrick Behm, MD[1]Mareike Gastl, MD[1], Annika Jahn, vet[2], Sascha Krueger, PhD[3], Andrea Rohde, BS[4], Steffen Weiss, PhD[3], Bernhard Schnackenburg, PhD[5], Sager Martin, DVM[6], Klaus Düring, PhD[7], Hélène Clogenson, PhD[7], Patrick Horn, MD[4], Ralf Westenfeld, MD[4], Malte Kelm, MD[8], Mirja Neizel-Wittke, MD[1], Florian Bönner, MD[4]

1. *Division of Cardiology, Pulmonology and Vascular Medicine, Heinrich Heine University, Düsseldorf, Medical Faculty, Germany, Düsseldorf, Nordrhein-Westfalen, Germany*
2. *Division of Cardiology, Pulmonology and Vascular Medicine, Heinrich Heine University, Düsseldorf, Medical Faculty, Germany; Central facility for animal research, Heinrich Heine University, Düsseldorf, Germany, Nordrhein-Westfalen, Germany*
3. *Innovative Technologies, Philips, Technology GmbH, Hamburg, Germany, Hamburg, Germany*
4. *Division of Cardiology, Pulmonology and Vascular Medicine, Heinrich Heine University, Düsseldorf, Medical Faculty, Germany, Nordrhein-Westfalen, Germany*
5. *Philips GmbH Marked DACH, Hamburg, Germany, Hamburg, Hamburg, Germany*
6. *Central Animal Research Facility, Heinrich-Heine-University, Düsseldorf, Germany., Nordrhein-Westfalen, Germany*
7. *MaRVis Medical, Hannover, Germany, Nordrhein-Westfalen, Germany*
8. *Division of Cardiology, Pulmonology and Vascular Medicine, Heinrich Heine University, Düsseldorf, Medical Faculty, Germany; Cardiovascular Research Institute Düsseldorf (CARID), Heinrich Heine University Düsseldorf, Medical Faculty, Germany, Nordrhein-Westfalen, Germany*

Background: Endomyocardial biopsy (EMB) is regarded as the diagnostic gold standard in cardiomyopathies with new onset heart failure. Fluoroscopy-guided EMB has the disadvantage of 1) revealing little information on cardiac anatomy and lesions, which leads to a considerable sampling error and 2) imperfect simultaneous complication monitoring. These shortcomings may be overcome by Cardiovascular Magnetic Resonance (CMR)-guided EMB. The aim of the present study was to investigate basic feasibility of interventional CMR (iCMR) lesion guided EMB in an *in vivo* porcine-model.

Methods: *Ex vivo* experiments for evaluation of dotation strength dependent artifact shape and device performance were conducted on explanted pig hearts (n=4). *In vivo* iCMR consisted of technical feasibility assessment (n=2), and feasibility assessment of lesion (acute myocardial infarction, AMI) guided EMB (n=4). iCMR was performed 7 days after AMI on a 1.5 Tesla MRI-System (Achieva, Philips, Best, Netherlands) equipped with an Interventional MRI Suite (iSuite) research prototype (Philips-Research,Hamburg). All devices used (biotom,sheath:ITP,Bochum,Germany; guide-wire:MaRVis,Hannover,Germany) were passively visualized via susceptibility artefacts. Real-time imaging (RT) was performed with a single-shot-balanced-SSFP-sequence (voxel size:1.7x1.8x8 mm³, temporal resolution:0.4s) and myocardial lesions were identified under RT with a single-shot-T2-weighted-TSE (sshT2) and a single-shot-inversion-prepared balancedSSFP-LGE (sshLGE) sequence. Experiments were conducted as follows: generation of a road map (3D-balancedSSFP), switching to RT with iSuite, introduction of guidewires via arterial or venous introducer sheaths and forwarding into the respective cavity. The guide-sheath was then introduced over the wire followed by angulation maneuvers in the left (LV) or right ventricle (RV). Finally, the biotom was introduced for EMB of remote and lesion areas. Biopsies were assessed histologically.

Results: From *ex vivo* experiments a rather continuous dotation of a larger distal portion of the guide-sheath was found to be preferable over single dots placed close to the tip. This led to the following *in vivo* artifact diameters under RT with optimal visibility: guidwire~2.7mm, guidesheath~7.4mm and biotom~3.2mm. All pigs survived the procedure. Targeted EMB of AMI lesions via RV and LV was feasible in 4/4 cases (Fig.1A). Histology revealed appropriate EMB size and quality (Fig.1B). Signal-to-noise ratio of sshT2- and sshLGE in myocardial-lesions was 124±35 and 67±51 respectively, whereas Contrast-to-noise ratio was 81±30 and 57±44. In 1 pig, repetitive biopsy of the free wall provoked EMB associated pericardial effusion, which was immediately detected under RT-Imaging (Fig.1C).

Conclusions: Initial results promise basic feasibility of *in-vivo* CMR-guided RV and LV-biopsy. Furthermore, real time lesion targeting opens a new avenue to a broad spectrum of EMB indications.

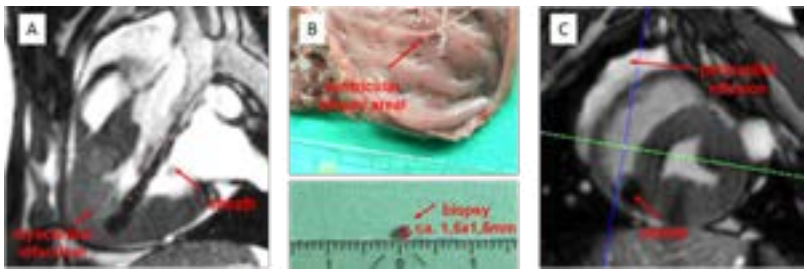

F017

Detection of acute myocarditis using T1- and ECV mapping does not differ between early and late post-contrast imaging

Magnus Lundin, MD[1] Liya Vishnevskaya, MD[2], Peder Sörensson, MD, PhD[2], Peter Kellman, PhD[3], Andreas Sigfridsson, PhD[4], Martin Ugander, MD, PhD[5]

1. *Karolinska institutet, Stockholms Lan, Sweden*
2. *Karolinska University Hospital, Stockholms Lan, Sweden*
3. *Laboratory of Cardiac Energetics, National Institutes of Health/NHLBI, Bethesda, MD, United States., MD*
4. *Karolinska Institute, Stockholm, Stockholms Lan, Sweden*
5. *Karolinska Institutet, Stockholms Lan, Sweden*

Background: Prior studies have shown that early post contrast T1-weighted imaging can be useful for detecting myocarditis. We aimed to evaluate if early or late post-contrast cardiovascular magnetic resonance (CMR) imaging using T1 mapping was better at detecting acute myocarditis.

Methods: Controls and patients referred for evaluation of acute myocarditis underwent 1.5T CMR (Siemens Aera). Modified Look-Locker inversion recovery (MOLLI) T1 mapping was performed before, and 4 minutes (early) and 23 minutes (late) after intravenous contrast (gadoteric acid, 0.2 mmol/kg). Affected myocardium was defined as an increased native T1 compared to remote myocardium in the same individual. Regions of interest for T1 measurement were placed in skeletal muscle, in the left ventricular (LV) blood pool, and midmurally in 6 LV short-axis segments. Extracellular volume fraction (ECV) and relative enhancement (ECV myocardium / ECV skeletal muscle) were calculated from T1 maps.

Results: In patients (n=20, age 39±18 years, 80% male), native T1 was greater in affected myocardial segments than in remote segments by (median (interquartile range)), 77 (56-89) ms. ECV late post contrast was greater in affected than remote myocardium (mean±SEM, 30±1% vs 26±1%, p< 0.001). The difference in ECV between affected and remote myocardium did not differ between early and late post contrast (3.7±0.5 % points vs 4.4±0.6 % points, p=0.07), see Figure. Relative enhancement in affected segments was 16±2% higher than remote segments early, and this did not differ late post contrast (17±2%, p=0.55). Compared to controls (n=20, age 51±16 years, 30% male), remote myocardium in patients did not differ in early ECV (p=0.44), late ECV (p=0.81), early relative enhancement (p=0.59), or late relative enhancement (p=0.11), while native T1 was slightly higher (1007±16 vs 990±23 ms, p=0.01).

Conclusions: The ability to detect both focal and diffuse abnormalities in acute myocarditis using T1 mapping did not differ between early and late post-contrast imaging. These findings differ from prior studies using relative enhancement with early post-contrast T1-weighted imaging (Lake Louise Criteria). These differences are likely explained by the fact that T1 mapping has better contrast sensitivity late post-contrast compared to T1-weighted imaging.

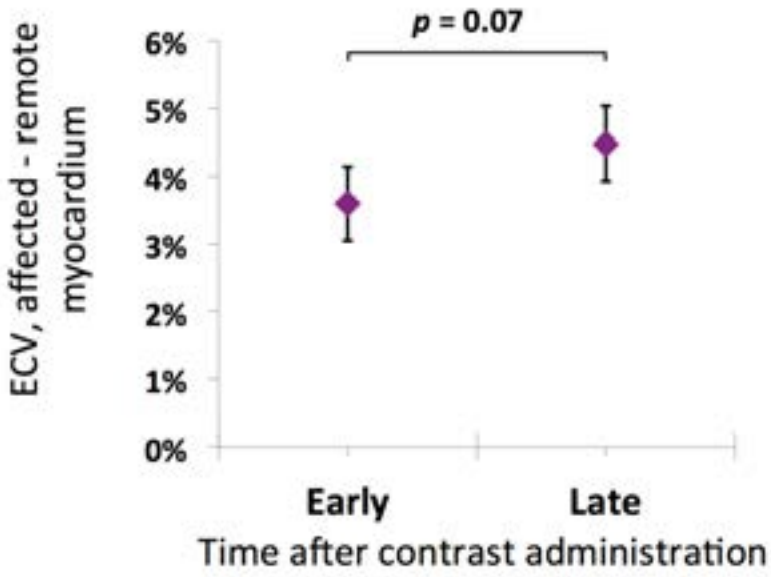

F018

Prevalence of late gadolinium enhancement in pediatric patients with clinical myocarditis and normal ejection fraction

Marc V. Lee, MD[1] Jeffrey A. Towbin, MD[2], Asim Choudhri, MD[3], Jason Johnson, MD, MHS[4]

1. University of Tennessee Health Science Center, Memphis, TN
2. Le Bonheur Children's Hospital, St. Jude Children's Research Hospital, University of Tennessee Health Science Center, Memphis, TN
3. Le Bonheur Children's Hospital, TN
4. Le Bonheur Children's Hospital, University of Tennessee Health Science Center, TN

Background: Myocarditis is an inflammatory cardiomyopathy with presentations ranging from subacute illness to fulminant heart failure. Although regarded as the diagnostic gold standard, endomyocardial biopsy is invasive and subject to sampling error. In pediatric patients, myocarditis is usually diagnosed with a combination of clinical history, ECG, laboratory tests, and imaging. As in adults, cardiac MRI has become a useful modality in children with suspected myocarditis. Late gadolinium enhancement (LGE) signifies cardiomyocyte damage and can be present even in patients with preserved systolic function. The objective of this study is to describe LGE in pediatric patients with clinical diagnosis of myocarditis with no evidence of systolic dysfunction on echocardiogram.

Methods: A retrospective case series was performed at a tertiary care children's hospital including all children up to 18 years old with clinical myocarditis based on clinical history, abnormal ECG, or laboratory data (elevated inflammatory markers, troponin, or BNP) from 2013 - 2016. Patients who initially underwent echocardiogram followed by cardiac MRI within 30 days of presentation were included. Measurements of systolic and diastolic function were measured by echocardiogram. The prevalence of LGE, left and right ventricular volumes, left ventricular mass, and left atrial volumes were measured.

Results: During the study period, 13 children who met inclusion criteria were diagnosed with clinical myocarditis on the basis of history, positive laboratory findings, and imaging. Median age was 15 years old (interquartile range (IQR), 11-17 years) and 77% male. Of these, 10 had normal (>55%) ejection fraction (EF) on echocardiogram. Diastolic dysfunction (abnormal E/A ratio) by echocardiogram was present in 80% of patients with normal EF. Viral myocarditis was presumed to be the etiology in 12 cases (Coxsackie titers positive in 75%). In patients with normal EF, median left ventricular end diastolic volume indexed was 77 ml/m^2 (IQR, 70.5-99.5 ml/m^2) and mass indexed was 56.2 g/m^2 (IQR, 50.9-65.2 g/m^2). LGE was noted in 7 patients with normal EF (70%) and in all 3 patients with decreased EF (Figure 1). Median peak troponin was 5.7 ng/mL in patients with LGE (IQR 2.4-10.5 ng/mL).

Conclusions: Myocardial LGE is common in pediatric patients with clinical myocarditis and normal EF. The prognosis of children with LGE and a normal EF is currently unknown. Cardiac MRI for viability is indicated in all patients with clinical myocarditis regardless of the systolic function.

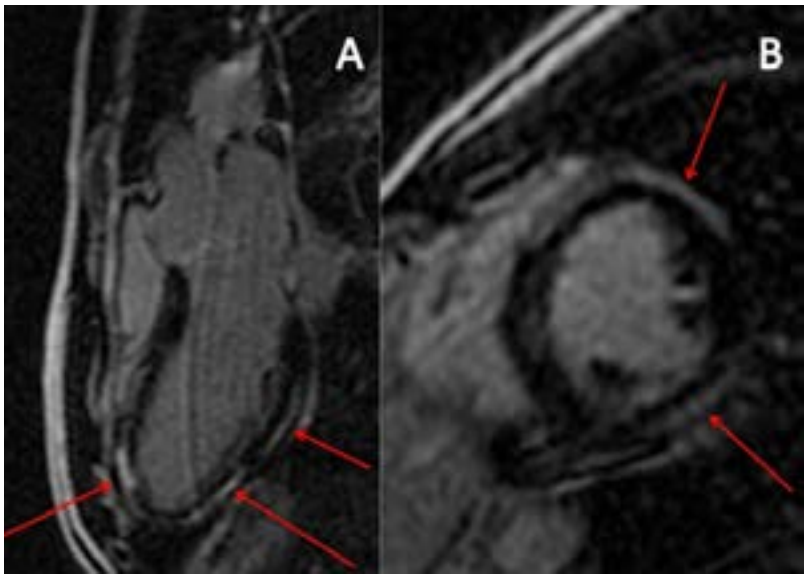

F019

Comparison of diagnostic accuracy of the Lake-Louise Criteria and a combined Mapping approach to detect active myocarditis – a direct comparison

Jeanette Schulz-Menger, MD[1]Johannes Schueler, MD[1], André Rudolph, MD[1], Florian von Knobelsdorff-Brenkenhoff, MD[2], Andreas Greiser, Ph.D[3], Peter Kellman, PhD[4]

1. *Working Group on Cardiovascular Magnetic Resonance, Experimental and Clinical Research Center a joint cooperation between the Charité Medical Faculty and the Max-Delbrueck Center for Molecular Medicine HELIOS Klinikum Berlin Buch, Germany, Berlin, Germany*
2. *Working Group on Cardiovascular Magnetic Resonance, Experimental and Clinical Research Center a joint cooperation between the Charité Medical Faculty and the Max-Delbrueck Center for Molecular Medicine HELIOS Klinikum Berlin Buch, Germany, Berlin, Germany*
3. *Siemens Healthcare GmbH, Erlangen, Germany, Erlangen, Bayern, Germany*
4. *Laboratory of Cardiac Energetics, National Institutes of Health/NHLBI, Bethesda, MD, United States., MD*

Background: CMR has the unique capability to differentiate myocardial injury and disease activity in myocardial inflammation. There is an increasing use of quantitative mapping techniques to overcome technical challenges of conventional imaging. Currently, the Lake Louis criteria (LLC) are mainly used to diagnose active inflammation applying CMR [1]. We aimed to compare LLC with a combined mapping approach.

Methods: 18 prospective patients with clinically defined acute myocarditis (inclusion criteria: new onset of chest pain or dyspnea, aberrations in electrocardiography (ECG) or dysrhythmias, elevated biomarkers, exclusion of coronary artery disease) who underwent clinical CMR (LLC-CMR) at 1.5 Tesla in four different hospitals were included. CMR was performed according to the in-house standard based on LLC.

The scientific CMR study included parametric mapping techniques and was performed at one single site (Map-CMR) using a 1.5T MR (Siemens) [2].Both protocols included cine-imaging, T2-weighted edema imaging (STIR) and LGE covering the whole left ventricle. LLC-CMR included early enhancement (EE) including relative (EGER) and global enhancement (GRE). Map-CMR included native T2 Mapping and native T1 Mapping (MOLLI 5(3)3). Cut-offs for detection of active inflammation were global T2 > 52.3 ms and T1 > 980.7 ms [2].Data were analyzed using CVI42 (Circle cvi).

Results: All 18 patients completed all examinations (age 30.06±10.9, 14 men). The technical performance of the protocols was different and especially tissue differentiation in LLC-CMR was affected by technical challenges hampering semi-quantification (table 1).

Cine and LGE had diagnostic quality in all scans. LLC-CMR was performed 4.1 ± 2.1 days and Map-CMR 7.2 ± 3.1 days after symptoms onset. Time-delay was 3.1 ± 2.9 days. There were no significant differences between both examinations in T2ratio, EF, LVEDV or LVM (table 2). Detection of focal fibrosis was similar (14/18) in both. So far, both scans were comparable to prove their capability for detection of active inflammation.

Active myocardial inflammation was detected as followed:

1. LLC-CMR: 72% when using 2 of 3 criteria. In 89% when using 1 of 3 criteria without counting for LGE, the latter reflects activity only. Eight (50%) where based on EE only, but EE was the less accepted technique.
2. MAP-CMR: 83% when using T2 mapping only, 89% when using T1 and T2 mapping.

Whereas STIR and EE had a good quality in the study center, the techniques suffered from technical impairments in other settings.

Conclusions: While assessment of disease activity is possible with both approaches, mapping sequences are more stable and provide an alternative for assessment of disease activity. Further investigation and harmonization for the establishment of reliable cutoffs are needed.

References:

1 Friedrich et al JACC 2009

2 Schueler et al SCMR 2016

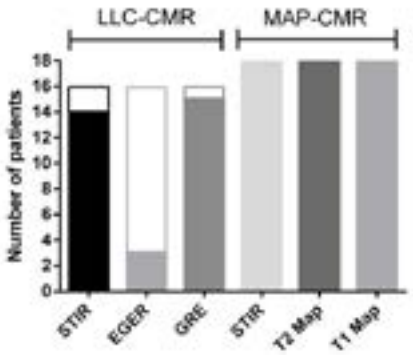

Table 1. Summary of LLC-CMR and MAP-CMR. Performance of T2-ratio, early gadolinium enhancement ratio (EGER), global relative enhancement (GRE), late enhancement (LGE) and parametric mapping

not performed	negative	positive	diagnostic	Modality
2	4	10	14/18	LLC CMR T2 ratio > 1.9 or focal lesion
2	2	1	3/18	EGER ≥ 4.0
2	1	14	15/18	GRE > 45 %
0	4	14	18/18	LGE (both examinations)
0	3	15	18/18	MAP-CMR T2 ratio > 1.9 or focal lesion
0	3	15	18/18	T2 Map > 52.3 ms
0	2	16	18/18	T1 Map > 980.7 ms

Table 2. Comparison of T2 Ratio, ejection fraction (EF), left ventricular end-diastolic volume (LVEDV) and mass (LVM) of examinations

p	MAP-CMR	LLC-CMR	
0.075	2.16 ± 0.18	2.03 ± 0.2	T2 ratio
0.079	59.0 ± 6.6	55.4 ± 8.8	EF in %
0.214	162 ± 39	178 ± 38	LVEDV in ml
0.521	141 ± 27	145 ± 24	LVM in g

F020

Ferumoxytol-enhanced MRI (FEMR) detects early stages of acute myocarditis

Yuko Tada, MD, PhD[1] Atsushi Tachibana, RT, MS[2], Phillip Yang, MD[2], Michael V. McConnell, MD, MSEE[2], Rajesh Dash, MD, PhD[2]

1. Stanford University School of Medicine, Palo Alto, CA
2. Stanford University School of Medicine, CA

Background: Diagnostic utility of MRI is limited during the early stages of myocarditis. Ferumoxytol is a clinically available ultra-small paramagnetic iron oxide, which can be taken up by inflammatory cells and cause MRI signal loss. This study examines whether ferumoxytol-enhanced MRI (FEMR) detects early stages of rodent acute myocarditis.

Methods: Lewis Rats (n=12) were induced with experimental autoimmune myocarditis, employing porcine cardiac myosin fraction. The rats were evaluated at early- (Day 14) and peak-phase (Day 21) of myocardial inflammation using 3T MRI (GE Signa). Cardiac function and LV mass were evaluated by cine-MRI. After gadolinium-DTPA (1mg/kg) was administered, early (EGE) and late (LGE) gadolinium enhancement were obtained. Then, ferumoxytol (300μmolFe/kg) was administered intravenously and dephasing signal loss was evaluated by gradient echo MRI (GRE) 6- and 24-hours later. Immunohistochemistry was performed on *ex vivo* rodent hearts.

Results: On day 21 following induction of myocarditis, LV mass/body weight (LVM/BW) was significantly increased in the myocarditis (n=6) vs. control groups (n=6): 3.06±0.40 vs. 1.19±0.03 mg/g, $p \leq 0.01$. Similarly, LV ejection fraction (EF) was decreased in the myocarditis group: 52.0±4.0% vs. 66.5±6.1%, $p \leq 0.01$. Distinct negative dephasing signal with FEMR was observed 6 hours after ferumoxytol administration (Figure 1A), which persisted at 24 hours (Figure 1B). The region of inflammation by FEMR was 42.8±8.7% of LV mass, which was larger than both EGE (36.3±6.2%, $p > 0.05$) and LGE (24.8±4.8%, $p > 0.05$). Histologically, iron particles were observed in the region of active myocardial inflammation, however, they were absent in the region of advanced myocardial necrosis. Day 14 data showed less of an increase in LVM/BW (2.58±0.72 mg/g, $p > 0.05$) and LGE (15.9±6.3%,$^{*}p < 0.05$) demonstrated less extensive detection of myocarditis compared to FEMR. These results suggest that FEMR can detect the early hyperemic phase of myocardial inflammation.

Conclusions: FEMR acquisition at 6 hours detects early stages of myocarditis to enhance detection and enable appropriate therapeutic intervention.

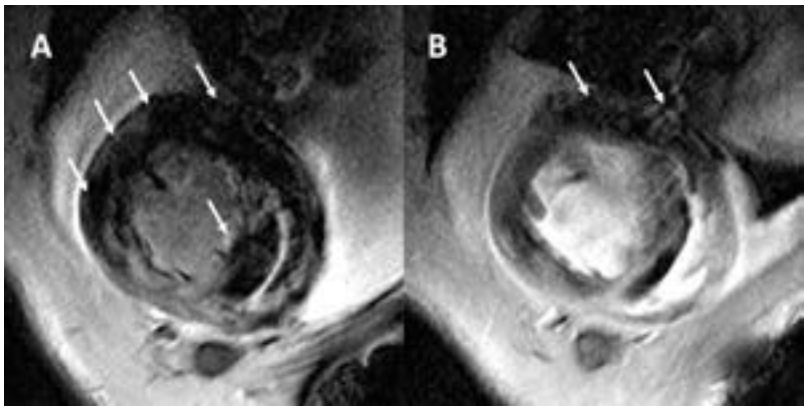

F021

T-Wave Abnormalities as ECG Signature of Myocardial Edema in NST-Elevation Acute Coronary Syndromes

Andrea Cardona, MD[1] Giuseppe Ambrosio, MD, PhD[2], Karolina Zareba, M.D.[3], Stephen Schaal, MD[1], Subha Raman, M.D.[4]

1. *Ohio State University, Columbus, OH*
2. *University of Perugia School of Medicine, Perugia, Umbria, Italy*
3. *The Ohio State University Wexner Medical Center, Columbus, OH*
4. *The Ohio State University Wexner Medical Center, OH*

Background: Persistent T-wave abnormalities (TWAs) are often seen during the acute phase of non ST-segment elevation acute coronary syndromes (NSTE-ACS), but their pathophysiological significance has not been established. We hypothesized that persistent TWAs in NSTE-ACS correspond to the presence of myocardial edema by T2 cardiac magnetic resonance (CMR).

Methods: In 82 prospectively-enrolled patients with NSTE-ACS, 12-lead electrocardiography (ECG) and CMR with T2-weighted imaging (T2W) and late gadolinium enhancement were acquired before invasive coronary angiography. TWAs were defined as presence of inverted or biphasic T-wave in ≥ 2 leads on the ECG acquired closest in time to CMR examination. Myocardial edema by CMR was defined as ≥ 2 T2-positive left ventricular segments.

Results: Patients were studied at a median 24 (IQ 17 – 50) hours after admission. Of 79 patients with adequate T2W-CMR, 36 (46%) showed TWAs on ECG. The prevalence of myocardial edema was higher in those with vs. without TWAs (32/36 [89%] vs. 20/43 [47%], $p < 0.001$). TIMI risk score, hemodynamics, ejection fraction, major cardiovascular risk factors, time-to-CMR, and troponin plasma concentrations, were similar in the 2 groups. By univariable logistic regression analysis, wall motion score index, and myocardial edema at CMR were the only variables significantly associated with TWA presence. By multivariable logistic regression analysis (adjusted for age and sex) edema at CMR was the only independent predictor of T-wave abnormalities (OR=14.6; 95% CI 2.9-73.2; $p < 0.001$). TWA yielded 89% positive predictive value, with a specificity of 85%, and a sensitivity of 61% to predict edema at CMR.

Conclusions: This is the first demonstration that standard 12-lead ECG T-wave abnormalities seen during the acute phase of NSTE-ACS are related to the presence of myocardial edema. Presence of TWAs is a simple, highly specific, and moderately sensitive marker of myocardial edema. The electrophysiological mechanisms and treatment implications of this underlying pathophysiology warrant further investigation.

F022

Cardiac Diffusion Imaging : Quantitative assessment of Apparent Diffusion Coefficient (ADC) changes in Infarct, Border and Remote regions after acute myocardial infarction.

Alban Chazot[1] Kevin Moulin, PhD[2], Antoine Gerbay[3], Florian Espinosa, MD[4], Magalie Viallon, PhD Dr[5], Pierre Croisille, MD PhD[6]

1. *CHU Saint Etienne, Lyon 05, N/A, France*
2. *Department of Radiological Sciences, University of California, Los Angeles, CA, USA., CA*
3. *Hopital Nord CHU Saint Etienne, Rhone-Alpes, France*
4. *Uni Lyon, UJM-Saint-Etienne, CHU Saint-Etienne, L'Etrat, Rhone-Alpes, France*
5. *CREATIS UMR CNRS 5220 - INSERM U1206/ Hopital Universitaire de Saint-Etienne, Rhone-Alpes, France*
6. *Univ Lyon, UJM-Saint-Etienne, INSA, CNRS UMR 5520, INSERM U1206, CREATIS, Saint-etienne, Rhone-Alpes, France*

Background: After myocardial infarction, the exact role and clinical relevance of inflammatory processes is a central interest in ischemia-reperfusion characterization, and has motivated recent developments of quantitative MRI methods such as T1 and T2 mapping. Diffusion in the brain has proven to be a key differentiator of paramount importance for patient management, with complementary information of ADC and T2 when describing interplay and time variations between inter and intracellular water. The motivation is therefore high to explore the potential of DWI-related biomarkers after myocardial infarction. We investigated the feasibility of cardiac Diffusion Weighted Imaging (cDWI) and the potential added value of ADC mapping as an alternative noninvasive approach to quantify inflammation and explore water redistribution (edema) in acute and chronic MI patients.

Methods: We studied 29 STEMI patients (62±11 yo) treated by PPCI within 12 hours after symptom onset. Imaging was performed between 2 and 10 days after AMI. 15 Chronic MI patients (>3 months; 63±12 yo) and 10 normal subjects were also studied on the same clinical 1.5-T magnet and used as controls. End-systolic acquisitions were performed using an acceleration motion compensation (AMC) SE-EPI diffusion sequence with slice-following prospective motion correction to allow free breathing acquisition. Acquisition parameters were: b =200 mm^2 s^{-1}, 6-directions, 6mm-slices, 5 TDs(averages), 5 slices. CMR protocol included LV function assessment, native T1 and T2 mapping in matching short-axis slices, as well as post-gadolinium 3D-LGE sequences and post-injection T1 MOLLI. TRACE, and ADC maps were calculated. Using conventional CMR imaging (cine, T2, LGE) as reference, Regions of interest (ROIs) were traced in infarct (LGE+), border (LGE-) and remote regions on matching slices of ADC, T1 and T2 maps.

Results: ADC was markedly increased in infarct ($2.58\pm.0.3x10^{-3}mm^2/s$, $p < .001$) compared to border ($1.91\pm.0.1x10^{-3}mm^2/s$, $p < .001$) and remote regions($1.53\pm.0.1x10^{-3}mm^2/s$), but decreased in no-reflow regions ($0.64\pm0.3x10^{-3}mm^2/s$). This 57±16% and 24±11% signal increase relative to remote regions, was larger than corresponding %signal changes in T2 (46.8±22% and 12±14%) and T1 (29.8±16.9% and 14.7±17%) maps.

Conclusions: In AMI patients, DW-Trace images provide excellent intrinsic dark-blood T2-weighted images. Increased signal intensity (known as T2 shine-through effect) help in identifying infarct inflammatory lesions that coincides with T1 and T2 abnormalities. ADC is providing an additional information (free from T2 shin-through effect) by quantifying water diffusion, known to reflect changes in water and electrolyte concentration in the extracellular space. ADC maps are measures that could refine exploration of water redistribution between myocardial compartments.

http://www.ConferenceAbstracts.com/uploads/cfp2/attachments/LDFAIBDN/LDFAIBDN--222587-1-ANY.pdf

F023

Non-contrast T1 CMR relaxometry technique to demonstrate widespread tissue injury during acute myocardial infarction

Amardeep Ghosh Dastidar, MBBS(Hons), MRCP[1]Elisa McAlindon, PhD[2], Estefania De Garate, MD[1], Iwan Harries, MBBS, MRCP[3], Giulia Pontecorboli, MD[3], Gareth Morgan[4], Charlie Moret[4], Anna Baritussio, MD[1], Chiara Bucciarelli-Ducci, MD, PhD[1]

1. *NIHR Bristol Cardiovascular Biomedical Research Unit, Bristol, England, United Kingdom*
2. *Heart and Lung Centre, New Cross Hospital, Wolverhampton, England, United Kingdom*
3. *NIHR Bristol CVBRU, England, United Kingdom*
4. *University of Bristol, England, United Kingdom*

Background: In patients with acute ST elevation myocardial infarction (STEMI), myocardial tissue injury is not restricted to the territory supplied by the culprit artery but it affects also the remote myocardium supplied by unaffected arteries. The aim was to investigate the non contrast native T1 characteristics in infarcted and remote myocardium in acute STEMI comparing it with chronic MI and normal healthy volunteers.

Methods: We studied a total of 80 subjects: 30 patients (mean age 61±10years and 70% males) with STEMI and successful revascularisation by percutaneous coronary intervention (day 2), 30 patients (mean age 67±10years and 80% males) with chronic MI (>2months) and 20 healthy volunteers (with no previous medical history). Each patient underwent clinical CMR at 1.5 T, SSFP cines, T1 mapping (MOLLI) pre contrast and late gadolinium enhancement imaging. The healthy volunteers underwent native T1 and SSFP cines only (no contrast). The native T1 values were evaluated in each of the 16 AHA myocardial segments.

Results: Out of 480 myocardial segments in acute STEMI patients, 143 were affected and the rest were unaffected (remote) (no regional wall motion abnormality, no oedema and no late gadolinium enhancement). The mean native T1 of the remote myocardium in acute STEMI was significantly lower compared to infarcted myocardium (1054±65msec vs 1153±85ms, $p < 0.0001$). However when compared to 320 normal myocardial segments from healthy volunteers and 337 remote segments from chronic MI patients, the mean native T1 in the remote acute STEMI myocardium was significantly higher (1054±65msec vs 1028 ± 48msec, $p < 0.0001$ and 1054±65msec vs 1031 ± 31msec, $p < 0.0001$ respectively). The mean native T1 in remote myocardium in chronic MI was not different from healthy normal myocardium (1031 ± 31msec vs 1028 ± 48msec p=0.42). Figure 1

Conclusions: This is the first study looking at the impact of acute STEMI on remote myocardium via non contrast advanced CMR (T1 mapping) relaxometry technique. Our study highlights that in acute STEMI the remote myocardium is also affected which normalises over time. These findings may have significant future implications in the treatment of acute STEMI, including targeting the remote myocardial inflammation.

http://www.ConferenceAbstracts.com/uploads/cfp2/attachments/LDFAIBDN/LDFAIBDN--222334-1-ANY.pdf

F024

Reperfusion Hemorrhage Leads to Crystallized Iron Deposits and Promotes M1 Macrophage Polarization in Convalescent Myocardial Infarction

Ivan Cokic, MD[1] Avinash Kali, PhD[2], Richard LQ Tang, MD[2], Hsin-Jung Yang, PhD[2], Andreas Kumar, MD, MSc[3], Frank S Prato, PhD[4], Joseph Francis, B.V.Sc., Ph.D[5], Eduardo Marban, MD, PhD[6], Rohan Dharmakumar, PhD[2]

1. *Cedars-Sinai Medical Center: BIRI, Los Angeles, CA*
2. *Cedars-Sinai Medical Center: BIRI, CA*
3. *Northern Ontario School of Medicine, Sudbury, ON, Canada*
4. *Lawson Health Research Institute, University of Western Ontario, ON, Canada*
5. *Louisian State University, LA*
6. *Cedars-Sinai Medical Center: Heart Institute, CA*

Background: Reperfusion hemorrhage (RH) following acute myocardial infarction (AMI) has been associated with adverse LV remodeling which leads to heart failure, however, the mechanism by which RH exerts adverse long-term effects is not well understood. The latest data shows that hemorrhagic AMI (h-AMI) evolves into regions of persistent iron deposits (PID) that are associated with prolonged recruitment of monocytes/macrophages throughout the convalescent phase of MI. The physicochemical characteristics of PID and the phenotype of these macrophages, however, have not been characterized. Herein, we hypothesized that h-AMI leads to crystallized iron deposits, which in turn drive macrophages in convalescent MI (CMI) to a preferentially pro-inflammatory (M1) phenotype.

Methods: Ten canines were subjected to 3 hours of LAD occlusion followed by reperfusion. CMR was performed on day 5 and 8-weeks post-MI in a 3T clinical MRI system. ECG-triggered breath-held 2D cine-SSFP images, T2*-weighted images (multiple gradient-echo, 6 TEs = 2.0ms–9.5ms with ΔTE=1.5ms, flip angle=10°), and LGE images were acquired along the short-axis direction with full LV coverage. Commonly used imaging parameters for a ll the scans were: resolution = 1.4 x 1.4 x 6 mm^3. All quantitative image analyses were performed using a commercially available software. LV remodeling was determined based on end-diastolic sphericity index (EDSI) from cine-SSFP images. Hearts were explanted following the 8 weeks post-MI CMR and Transmission Electron Microscopy (TEM) was performed to determine iron crystallinity. Energy-dispersive X-ray spectroscopy was used to identify the chemical composition of the iron crystals. Iron-driven macrophage polarization was determined histologically.

Results: Significant T2* losses were observed within the MI territories in all 10 canines at 5 days and 8 weeks post-MI (Figure 1). Relative to remote myocardium, mean T2* value the infarcted regions were significantly decreased compared to the remote myocardium. Both infarct and iron volumes measured in acute phase was a significant predictors of change in EDSI between acute and chronic phases ($p < 0.01$ all cases). Iron deposits within CMI were found within macrophages as aggregates of nanocrystals (~2.5 nm diameter) in the ferric state (Figure 2). Histological evaluation of CMI revealed extensive co-localization of PID (Perls' stain) with newly recruited macrophages (MAC387 marker), CD163 (marker of iron-specific macrophage activation), as well as the proinflammatory cytokines (TNF-α, IL-1β) within the scar territory (Figure 3).

Conclusions: Crystallized iron deposits from h-AMI promote macrophage polarization preferentially to a pro-inflammatory, M1, phenotype within CMI. Given the deleterious nature of M1 macrophages, therapeutic strategies to combat post h-AMI adverse remodeling should take into account the prolonged iron-driven inflammation.

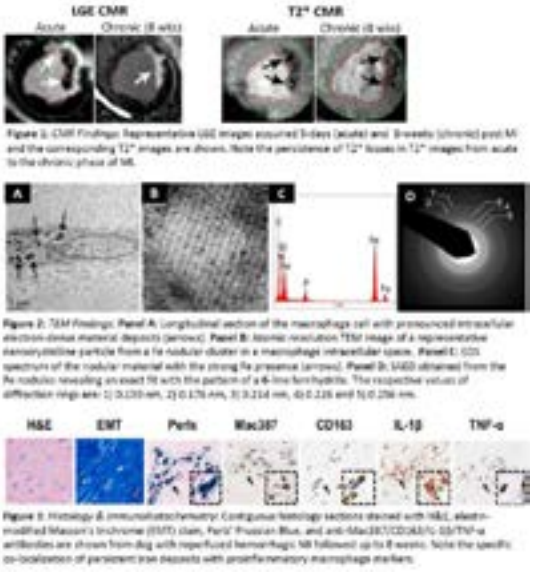

F025

Assessment of LV function and infarct in Spontaneous Coronary Artery Dissection Study, UK

Abtehale Al-hussaini, MBBS,BSC, MRCP.[1]Dave Adlam, BM DPhil[2], Gerry P. McCann, MBChB, MD[3], Joanne Wormleighton, DCR(R)[4], Gaurav S. Gulsin, MBChB(Hons) MRCP(UK)[5], Eylem Levelt, DPhil[6], Daniel Swarbrick[7], Fadi Magdy[8]

1. *Cardiovascular Sciences, Glenfield Hospital, University Hospitals of Leicester NHS Trust, Leicester United Kingdom, Leicester, England, United Kingdom*
2. *University of Leicester, Leicester, England, United Kingdom*
3. *The University of Leicester, Leicester, United Kingdom, Leicester, England, United Kingdom*
4. *Glenfield Hospital, University Hospitals of Leicester NHS Trust, Leicester, England, United Kingdom*
5. *The University of Leicester, Nottingham, England, United Kingdom*
6. *University of Leicester, England, United Kingdom*
7. *The University of Leicester, England, United Kingdom*
8. *Leicester University, Leicester, England, United Kingdom*

Background: Spontaneous coronary artery dissection (SCAD) is an unusual but increasingly recognized cause of acute coronary syndrome and sudden cardiac death mainly in young women, in the absence of conventional cardiac risk factors. The pathophysiology remains poorly understood with controversy regarding the optimal management of SCAD. Aim: We report the first and largest CMR series from the SCAD UK study (http://scad.lcbru.le.ac.uk/), illustrating outcomes and prognosis in terms of functional LV assessment and infarct size.

Methods: Cardiac MRI and peripheral arterial MR-angiography performed using our dedicated 3T cardiovascular research scanner provides a detailed assessment of LV function, Late Gadolinium Enhancement (LGE), any remote arteriopathies. Pulse wave velocity and aortic compliance are assessed using semiautomatic aortic tracking during the cardiac cycle. Cardiac images include HASTE and localiser sequence, CINE images using TRUFISP and CINE SAX. Delayed contrast imaging is acquired following an MRA of the aorta.

Results: In this cohort of 100 SCAD patients from the SCAD UK registry, the follow up median time is 380 days. None had any cardiovascular risk factors and athermatous SCAD on angiography. The mean age was 40.6 years, with exclusively female cases. 85% had LAD SCAD involving the mid to distal segment. 10% of the cases were multivessel SCAD, and in 8 % had recurrent SCAD. There was almost at equal split of patients treated conservatively following angiography and those who were revasculrised with stenting or surgery. The mean EF was 57 %. On assessment of LV function between the different management arms including conservative therapy, PCI and CABG, there was no significant difference in LV Ejection fraction or function. However there was more extensive myocardial injury in patients who received non-conservative therapy with infarct in non-SCAD vessel territory.

Conclusions: SCAD remains to be under diagnosed with no guidelines yet in place for management of SCAD. The natural history of SCAD includes complete resolution and healing suggesting conservative approach as the best strategy. This is the first MRI series in SCAD demonstrating insight into the outcome and prognosis of this condition but also that related to various management strategies, with limited infarct in conservatively managed SCAD. This may help comprehend the pathophysiology of SCAD, and vessel healing which may be associated with improved long-term prognosis. Also this stipulates a consensus for clinical guidance in conservatively managing SCAD and the role of MRI in assessment and follow up of rare coronary disease.

http://www.ConferenceAbstracts.com/uploads/cfp2/attachments/LDFAIBDN/LDFAIBDN--223096-1-ANY.pdf

http://www.ConferenceAbstracts.com/uploads/cfp2/attachments/LDFAIBDN/LDFAIBDN--223096-2-ANY.pdf

F026

Incremental benefit of functional, volumetric and tissue characterisation techniques in the differentiation of HCM and athlete's heart

Peter P. Swoboda, PhD[1] Adam K. McDiarmid, MD[2], Bara Erhayiem, BMBS[2], Philip E. Haaf, PhD[3], David A. Broadbent, MSc[4], Laura E. Dobson, MD[2], David Ripley, MBChB[2], Tarique Musa, MBBS[2], Stephen Page, MD[4], John P. Greenwood, PhD[2], Sven Plein, MD PhD[5]

1. *University of Leeds, Leeds, England, United Kingdom*
2. *University of Leeds, England, United Kingdom*
3. *University Hospital Basel, N/A, Switzerland*
4. *Leeds Teaching Hospitals NHS Trust, England, United Kingdom*
5. *St. Thomas' Hospital, London; King's College London; University of Leeds, England, United Kingdom*

Background: Athletic training can lead to changes in cardiac structure and function which can be difficult to different from hypertrophic cardiomyopathy (HCM), in particular in individuals with indeterminate wall thickness, generally defined as 12-15mm. Recent developments in non-invasive cardiac imaging allow for rapid and reproducible assessment of tissue composition and function of hypertrophied regions. We planned to test the incremental benefit of several cardiovascular magnetic resonance (CMR) methods in the differentiation of HCM from athlete's heart; including maximum wall thickness, T1 mapping, late gadolinium enhancement (LGE), regional strain analysis and LV cavity size.

Methods: 59 HCM patients and 52 athletes underwent 3.0T CMR including short axis cine imaging with whole heart coverage, Modified Look-Locker Inversion (MOLLI) T1 maps and LGE imaging. For the most hypertrophied segment in each patient regional circumferential strain by feature tracking, native T1, extracellular volume (ECV) and presence of LGE were quantified. Receiver operator characteristics (ROC) curves were created for each parameter for the whole cohort and for those with maximum wall thickness (MWT) of 12-15mm.

Results: In athletes as MWT increased there was a significant decrease in ECV (F=8.64, P=0.001) and increase in LV end-diastolic volume (EDV) (F=4.52, P=0.02). There was no association with circumferential strain (Ecc) (F=0.24, P=0.79), Figure 1. In HCM as MWT increased there was a significant increase in ECV (F=4.24, P=0.009) and decrease in Ecc (F=3.01, P=0.04). There was no association with LV EDV (F=0.66, P=0.58).

The tissue characterisation parameter with the best diagnostic accuracy for HCM was ECV of the thickest segment (area under curve (AUC) 0.942, PThere were 18 athletes and 18 HCM patients with MWT 12-15mm. In these subjects the AUC for ECV, EDV and Ecc remained significant (0.981, 0.917, 0.694). However only ECV provided a significant incremental benefit over MWT (difference in AUCs 0.182, P=0.02).

There were 18 athletes and 18 HCM patients with MWT 12-15mm. In these subjects the AUC for ECV, EDV and Ecc remained significant (0.981, 0.917, 0.694). However only ECV provided a significant incremental benefit over MWT (difference in AUCs 0.182, P=0.02).

Conclusions: It is possible to differentiate athlete's heart from HCM by volumetric measurement, regional tissue characterisation or strain assessment. Of the CMR parameters tested ECV measured by T1 mapping had the highest incremental benefit over MWT, particularly in subjects with hypertrophy of 12-15mm.

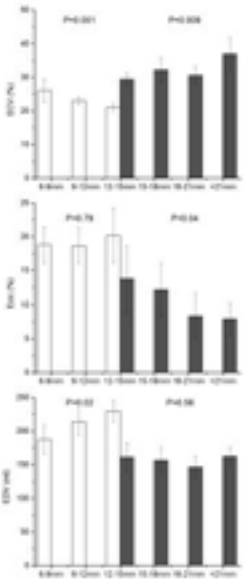

Diagnostic accuracy from ROC analysis of individual imaging characteristics in descending order of AUC.

P value	95% CI	Area under curve	
<0.001	0.959 - 0.998	0.979	Maximal wall thickness (MWT)
<0.001	0.902 - 0.983	0.942	ECV in MWT segment
<0.001	0.948 - 0.824	0.886	LV EDV
<0.001	0.946 - 0.816	0.881	LV ESV
<0.001	0.813 - 0.947	0.880	Native T1 in MWT segment
<0.001	0.768 - 0.922	0.845	LGE anywhere in LV
<0.001	0.731 - 0.89	0.810	Ecc in MWT segment
<0.001	0.682 - 0.86	0.771	LGE in MWT segment
<0.001	0.652 - 0.835	0.743	LV ejection fraction
0.001	0.575 - 0.777	0.676	Left atrial volume
0.004	0.556 – 0.761	0.659	Diastolic Strain Rate in MWT segment
0.07	0.495 - 0.705	0.600	Systolic strain rate in MWT segment
0.33	0.446 - 0.661	0.554	LV mass

Diagnostic accuracy from ROC analysis of individual imaging characteristics in descending order of AUC.

P value	95% CI	Area under curve	
	0.959 - 0.998	0.979	Maximal wall thickness (MWT)
	0.902 - 0.983	0.942	
		0.886	LV EDV
		0.881	LV ESV
		0.880	Native T1 in MWT segment
		0.845	LGE anywhere in LV
		0.810	Ecc in MWT segment
		0.771	LGE in MWT segment
		0.743	LV ejection fraction
		0.676	Left atrial volume
		0.659	Diastolic Strain Rate in MWT segment
		0.600	Systolic strain rate in MWT segment
		0.554	LV mass

ECV in MWT segment
LV EDV
LV ESV
Native T1 in MWT segment
LGE anywhere in LV
Ecc in MWT segment
LGE in MWT segment
LV Ejection Fraction
Left atrial volume
DSR in MWT segment
SSR in MWT segment
LV Mass

F027

Endogenous T1rho mapping in hypertrophic cardiomyopathy

Michael Solomon, BS[1] Patricia O'Donnell, RT(R)(MR)[1], Jacqueline Meeks, MBA, RT(R)(MR)[1], Anjali T. Owens, MD[1], Harold Litt, MD-PhD[2], Yuchi Han, MD[3], Walter R. Witschey, PhD[3]

1. *University of Pennsylvania, PA*
2. *Perelman School of Medicine of the University of Pennsylvania, Philadelphia, PA*
3. *University of Pennsylvania, Philadelphia, PA*

Background: Hypertrophic cardiomyopathy (HCM) is a cardiovascular disease of genetic origin characterized in some patients by infiltrative myocardial fibrosis on late gadolinium enhanced (LGE) MRI. However, many HCM patients do not have late enhancement and the presence of LGE has poor specificity for prediction of clinical outcomes. Gadolinium based contrast agents (GBCAs) are contraindicated in many patients due to poor renal function and persistent GBCA observed in brain tissue is concerning. T1ρ is an endogenous contrast method that sensitizes the MR signal to fibrosis with a moderate radiofrequency pulse. The purpose of this study was to investigate T1ρ MRI in HCM patients and correlate fibrotic area with enhancement on LGE and native T1 maps.

Methods: Patients with HCM (n=32) and a control group (n=10) consented to pre-contrast T1 and T1ρ mapping and LGE MRI at three slice positions (basal, mid, apical). T1ρ MRI was performed with a motion and heart rate corrected single-shot balanced steady-state free precession (bSSFP) sequence (8 spin lock times (TSL), B1=500 Hz) and T1 maps with modified Look-Locker sequence using a 5-(3)-3 acquisition scheme. In a subset of patients with visible LGE enhancement (HCM+; n=11), T1ρ and T1 fibrosis area were correlated with LGE images at 1-5 standard deviation (SD) and full-width half maximum (FWHM) signal intensity thresholds. Average mean bias, variance, and Pearson's r were calculated to correlate percentage of fibrotic myocardium (%, fibrosis area/remote myocardium) with LGE.

Results: Fig 1A shows T1ρ, T1 and LGE images from 3 patients with extensive, moderate and no LGE enhancement and in 1 control subject. As shown in Fig 1B, there was excellent correlation between 3SD T1ρ and FWHM LGE fibrotic area ($r=0.94$; $p < 0.05$) and good correlation between 3SD T1 and LGE ($r=0.87$; $p < 0.05$). Mean bias between T1ρ, T1 and LGE was low (T1ρ=0.7±2.8% and T1 = 1.4±2.2%). T1ρ=91.9±19.1 ms in enhancing regions (T1 =1212.6±127.4) and 60.0±5.4 ms in remote tissue (T1=966.2±38.1). T1ρ in all segments tended to decrease among groups (HCM+: 68±1.1; HCM-:66.5±1.1; control=63.5±1.2).

Conclusions: Our principal findings were that 1) T1ρ maps had excellent correlation with LGE in HCM patients and 2) T1ρ enhancement in infiltrative fibrosis was 50-55% above unenhanced regions at 3SD theshold. The physiologic mechanism for enhancement may be an increase in water tumbling rate in fibrotic tissue (reduced dipole-dipole broadening), spin lock suppression of background relaxation rate enhancement and increased sensitivity to 1H chemical exchange.

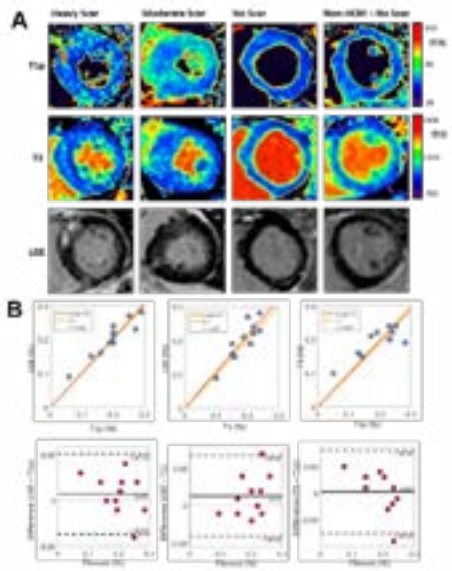

F028

Quantification of late gadolinium enhancement in the end-stage phase of hypertrophic cardiomyopathy with or without ventricular dilatation

Sainan Cheng, MDShihua Zhao, PhD

National Center for Cardiovascular Diseases of China, Chinese Academy of Medical Sciences and Peking Union Medical College, Beijing, China (People's Republic)

Background: End-stage hypertrophic cardiomyopathy (ES-HCM) is a recognized part of the HCM disease spectrum. Previous literatures have described the clinical and CMR expression. But the precise extent of LGE and its prognostic value in ES-HCM patients remain unknown, especially in those without ventricular dilatation. We quantitatively evaluated the extent of LGE and sought to explore the prognostic value of LGE for ES-HCM.

Methods: Of 2228 consecutive HCM patients, 63 showed systolic dysfunction (left ventricular eject function less than 50%). ES-HCM patients were divided into those with ventricular dilatation (D-ES, n=40) and those with normal ventricular size (N-ES, n=23). All of the patients were assessed by ultrasound and CMR. LGE were semi-automatic measured with the gray-scale threshold method at 5 SD above the mean signal intensity of normal myocardium. Regional LGE analyses were performed using 17-segments model.

Results: The left ventricular eject function of D-ES (27.9±8.8)% were significantly less than that of N-ES (35.0±7.5)% ($p<0.05$). LGE in D-ES were more extensive. The volume fraction of LGE was significantly larger in D-ES (36.3±14.6)% than in N-ES (21.4±8.7)% ($p<0.05$). Over the follow-up period of 21.62±13.41 months, 17 patients experienced cardiovascular death/heart transplant events (13 in D-ES, 4 in N-ES). Log-rank test found no significant difference between 2 groups in cardiovascular death/heart transplant events ($c2=1.211$, $p=0.271$). There was a significantly correlation between LGE volume fraction and cardiovascular death/heart transplant events (HR:1.69, $P<0.05$).

Conclusions: ES-HCM is an uncommon presentation of the clinical spectrum of HCM. ES-HCM patients with ventricular dilatation had a higher LGE volume fraction than those with normal ventricular size, which usually expressed as restrictive phenotype. Besides, extensive LGE measured by quantitative contrast enhanced CMR provides additional information for assessing cardiovascular death or heart transplant events among ES-HCM patients, regardless of whether the ventricular dilatation or not.

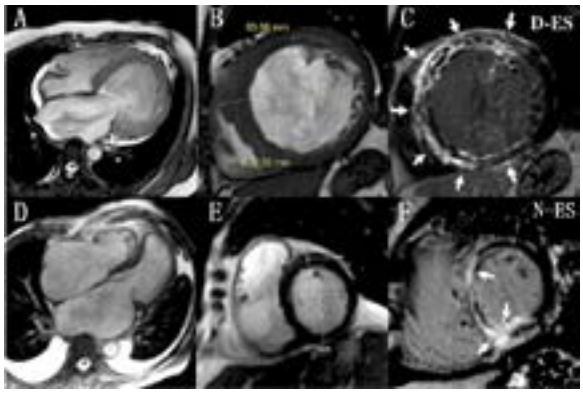

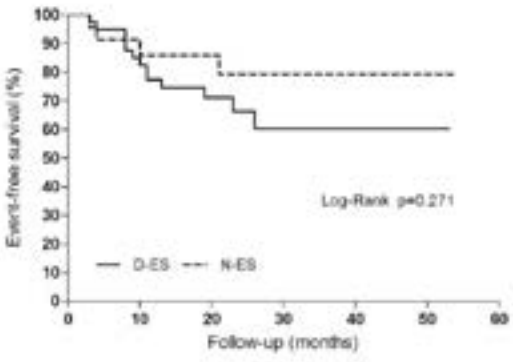

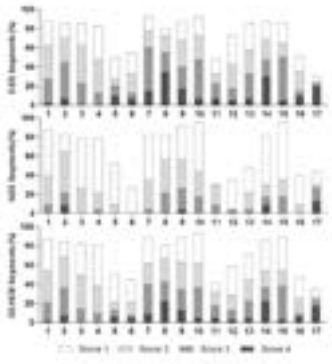

F029

An initial evaluation of STEAM and M012 spin echo diffusion tensor imaging in hypertrophic cardiomyopathy patients

Zohya Khalique, MBBS[1] Andrew D. Scott, PhD[2], Pedro F. Ferreira, PhD[3], Margarita Gorodezky, MSc[4], Rick Wage, DCR (R)[4], Sonia Nielles-Vallespin, PhD, MSc[5], David N. Firmin, PhD[4], Dudley J. Pennell, MD[6]

1. *NIHR Cardiovascular Biomedical Research Unit, Royal Brompton Hospital, London, England, United Kingdom*
2. *NIHR Cardiovascular Biomedical Research Unit, The Royal Brompton Hospital, Sydney Street, London, SW3 6NP, UK, England, United Kingdom*
3. *Cardiovascular Biomedical Research Unit, The Royal Brompton Hospital, Sydney Street, London, SW3 6NP, UK, England, United Kingdom*
4. *NIHR Cardiovascular Biomedical Research Unit, Royal Brompton Hospital, England, United Kingdom*
5. *NIH, MD*
6. *Royal Brompton Hospital and Imperial College, London, England, United Kingdom*

Background: Stimulated echo acquisition mode (STEAM) is an established technique for diffusion tensor (DT)-CMR [1]. More recently second order motion compensated spin-echo (SE) imaging has shown some benefits when compared to STEAM, but only in healthy volunteers at 1.5T in systole [2, 3]. Here we present initial data comparing mean diffusivity (MD), fractional anisotropy (FA), helix angle (HA) and second eigenvector angle (E2A) in patients with hypertrophic cardiomyopathy (HCM) using both STEAM and SE in systole and diastole at 3T.

Methods: Four patients with HCM (2 male, 30-71years) underwent CMR imaging including DT-CMR at 3T (Siemens, Skyra). SE and STEAM images were acquired using b_{main}=450smm^{-2} and b_{ref} =150smm^{-2}, 6 directions and 2.8x2.8x8mm^3 (1.4x1.4x8mm^3 reconstructed), SENSE x2, field of view 360x135mm. STEAM imaging used TE=23ms, TR=2RR-intervals and SE imaging used TE=75ms, TR=1RR-interval. Images of a mid-ventricular short-axis slice were acquired until 8 STEAM or 16 SE averages of acceptable quality were obtained. DT-CMR data were processed using custom MATBLAB software.

Results: The median (range) maximal wall thickness was 23 (16 –31) mm and ejection fraction was 73 (63 – 78) %. DT-CMR data was obtained in all patients. On average 10 breath holds were required for each cardiac phase using STEAM, 11 for SE in systole and 14 for SE in diastole. Figure 1 shows example DT-CMR parameter maps. This patient had variable duration of diastasis, resulting in poor quality SE data in diastole. Figure 2 plots average left ventricular DT-CMR parameters and provides healthy volunteer data for reference. Parameters are also summarised in Table 1. MD was higher and FA was lower using SE in both systole and diastole. HA gradient was steeper for STEAM. E2A was similar in SE and STEAM; with E2A higher in systole than diastole.

Conclusions: This is the first time SE DT-CMR has been demonstrated in a patient population. The elevated MD and reduced FA using SE in this cohort accords with a previous comparison in healthy subjects [3] and is a result of the shorter SE diffusion times. E2A appears elevated in systole compared to diastole (in keeping with previous STEAM data in HCM [4]), regardless of sequence. Work is on-going to further compare these two DT-CMR sequences in a larger cohort of HCM patients with aged matched healthy controls.

References

1. Reese MRM 1995.DOI:10.1002/mrm.1910340603
2. Stoeck MRM 2015. DOI:10.1002/mrm.25784
3. Von Deuster MRM 2015. DOI:10.1002/mrm.25998
4. Ferreira JCMR 2014. DOI: 10.1186/s12968-014-0087-8

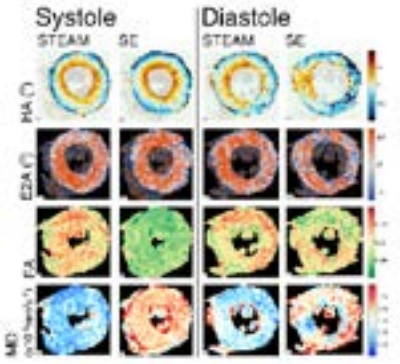

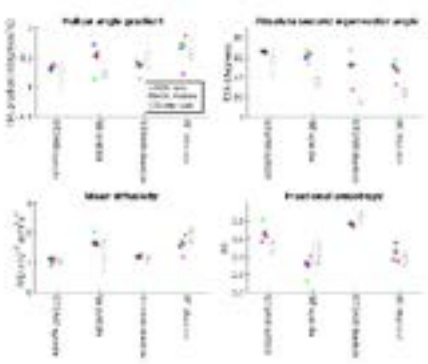

Table 1: Diffusion parameters obtained by both SE and STEAM at end systole and diastasis [mean (range)].

SE diastole	STEAM diastole	SE systole	STEAM systole	
1.63 (1.18-1.91)	1.19 (1.15-1.26)	1.64 (1.58-2.03)	1.05 (0.88-1.14)	Mean diffusivity ($x10^{-3}mm^2s^{-1}$)
0.43 (0.37-0.47)	0.58 (0.56-0.59)	0.35 (0.27-0.40)	0.53 (0.48-0.61)	Fractional anisotropy
-0.30 (-0.77 – -0.14)	-0.63 (-0.85 – -0.57)	-0.46 (-0.87 – -0.28)	-0.66 (-0.75 – -0.61)	Helical angle gradient (°/%)
49 (33-57)	53 (27-68)	62 (54-66)	66 (65-67)	Absolute second eigenvector angle (°)

F030

Evaluation of mechanisms responsible for discrepancies in maximal left ventricular wall thickness between cardiac magnetic resonance imaging and echocardiography in hypertrophic cardiomyopathy

Waseem Hindieh, MD, FRCPCAdaya Weissler-snir, MD, Harry Rakowski, MD, FRCPC, Raymond Chan, MD, FRCPC

Toronto General Hospital, ON, Canada

Background: Maximal left ventricular wall thickness (LVWT) by echocardiography (echo) has been shown to be independently associated with sudden cardiac death in hypertrophic cardiomyopathy (HCM). Prior studies have shown that wall thickness measurements by echo may at times be significantly discrepant with those by cardiac magnetic resonance (CMR). We sought to compare maximal LVWT measurements between echo and CMR as well as document mechanisms responsible for significant discrepancies.

Methods: One hundred seventy five consecutive genotyped HCM patients who underwent echo and CMR imaging within 6 months at Toronto General Hospital were included. LVWT was assessed using parasternal long and short axis by 2-dimensional echo and short axis by CMR. Maximal LV wall thickness was defined as the greatest dimension at any site within the LV myocardium at end-diastole. A significant discrepancy in maximal LVWT between both imaging modalities was arbitrarily defined as a WT difference of at least 20% of the smaller absolute WT measured by either echo or CMR, since this difference would be generally considered clinically significant when used in SCD risk determination.

Results: Mean maximal LVWT by echo was similar to CMR (20.9 mm vs. 20.5 mm, $p=0.49$). Maximal LVWT by echo and CMR showed a strong correlation ($r=0.72$, $p < 0.001$). Bland-Altman plot demonstrated equal distribution of discrepancy along the full range of measured LVWT. However, 56 patients (32.0%) were identified to have significant (≥20%) measurement discrepancy, where echo significantly underestimated (n=24, 13.7%) or overestimated (n=32, 18.3%) maximal LVWT compared with CMR. Underestimation was mainly due to the inability by echo to capture the appropriate plane for maximal hypertrophy in the correctly identified LV segment, occurring in 9 patients (16.1%), and poor acoustic windows leading to misidentification by echo of the most hypertrophied LV segment, occurring in 15 patients (26.8%). Reasons for overestimation of LVWT by echocardiogram include the inappropriate inclusion of right ventricular myocardium (n=21, 37.5%) and plane obliquity (n=11, 19.6%). In 32 (18.2%) patients, discrepancy in maximum LVWT occurred at diagnostic (15 mm) or prognostic cut-offs (30 mm).

Conclusions: Despite apparently good correlation between measured LVWT between echo and CMR within the cohort, there was discordance amongst a significant subgroup of patients, some of which may lead to important changes in clinical decision making.

http://www.ConferenceAbstracts.com/uploads/cfp2/attachments/LDFAIBDN/LDFAIBDN--219575-1-ANY.pdf

http://www.ConferenceAbstracts.com/uploads/cfp2/attachments/LDFAIBDN/LDFAIBDN--219575-2-ANY.pdf

http://www.ConferenceAbstracts.com/uploads/cfp2/attachments/LDFAIBDN/LDFAIBDN--219575-3-ANY.pdf

Baseline characteristics

P-value	Patients with WT discrepancy N=56	Patients with no WT discpreancy N= 119	All patients N=175	
0.42	55.6 (15.8)	57.6 (14.9)	56.9 (15.2)	Age, years (SD)
0.81	41 (73.2)	85 (71.4)	126 (72.0)	Male, n (%)
0.98	1.96 (0.26)	1.96 (0.25)	1.96 (0.26)	Body surface area, m^2
0.53	18 (32.1)	44 (40.0)	62 (35.4)	Hypertension, n (%)
0.14	3 (5.4)	15 (12.6)	18 (10.3)	Diabetes Mellitus, n (%)
0.53	4 (7.1)	12 (10.1)	16 (9.1)	Coronary artery disease, n (%)
0.65	16 (28.6)	38 (31.9)	54 (30.9)	Dyslipidemia, n (%)
0.74	3 (5.4)	5 (4.2)	8 (4.6)	Stroke/TIA, n (%)
0.58	8 (14.3)	21 (17.6)	29 (16.6)	Atrial fibrillation, n (%)
0.11	 41 (73.2) 10 (17.9) 5 (8.9)	 71 (59.7) 32 (29.6) 16 (13.4)	 112 (64.0) 42 (24.0) 21 (12.0)	NYHA functional class, n (%) I II III
0.33	13 (23.2)	37 (31.1)	50 (28.6)	Genopositive, n (%)
0.99 0.29	 20.9 (6.0) 19.9 (5.0)	 20.9 (4.7) 20.8 (4.9)	 20.9 (5.1) 20.5 (5.0)	LV wall thickness Echo, mm (SD) CMR, mm (SD)
0.56	164.3 (57.8)	170.6 (68.1)	168.6 (64.8)	LVM, g (SD)
0.54	83.7 (24.9)	86.7 (31.1)	85.7 (29.2)	LVM index, g/m^2 (SD)
0.35	171.0 (48.6)	164.3 (41.9)	166.4 (44.2)	LVEDV, ml (SD)
0.46	86.4 (20.2)	84.2 (16.6)	84.6 (17.6)	LVEDV indexed, ml/m^2 (SD)
0.75	64.6 (26.3)	63.4 (21.2)	63.8 (22.9)	LVESV, ml (SD)
0.55	33.2 (12.4)	32.0 (9.6)	32.4 (10.5)	LVESV indexed, ml/m^2 (SD)
0.62	62.8 (8.0)	62.2 (6.9)	62.4 (7.3)	Ejection fraction, % (SD)

TIA – transient ischemic attack; NYHA – New York Heart Association; LV – left ventricle; echo- echocardiography; CMR – cardiac magnetic resonance; LVM – left ventricular mass; LVEDV – left ventricular end diastolic volume; LVESV – left ventricular end systolic volume; WT - wall thickness

F032

Real-time cardiovascular magnetic resonance using 60-channel acquisition for the assessment of cardiac exercise reserve

Thu-Thao Le, PhD[1] Jennifer A. Bryant, PhD[1], Alicia Ting Er, BSc[1], Bao Ru Leong, BSc[1], Yiying Han[1], Pei Yi Ho, BSc[1], Boyang Su, PhD[1], Declan O'Regan, MBBS, PhD[2], Stuart Alexander Cook, MBBS, PhD[1], Calvin Woon-Loong Chin, MD, PhD[1]

1. *National Heart Centre Singapore, N/A, Singapore*
2. *MRC Clinical Sciences Centre, England, United Kingdom*

Background: Exercise cardiovascular magnetic resonance (CMR) has huge potential for clinical application but its development has been hindered by equipment compatibility and sequence development issues. We developed a supine in-scanner exercise protocol combined with 60-channel real time image acquisition and tested this in elite athletes from healthy volunteers.

Methods: Free-breathing real-time CMR imaging (1.5T Aera, Siemens; 60-channel cardiac coil) was performed in 16 healthy volunteers (7 males; median age 26 [25 – 33] years) and 11 elite athletes (5 males; median age 29 [28 – 39] years). The exercise protocol comprised of supine, in-scanner cycling on a cycle ergometer (Lode BV, the Netherlands), with an initial workload of 25W followed by 25W increments every minute. In 20 individuals, exercise capacity was evaluated against cardiopulmonary test (CPET). Scan-rescan reproducibility was assessed in five individuals.

Results: The CMR-exercise protocol demonstrated excellent scan-rescan reproducibility (difference in cardiac index: -0.2 [-0.8 to 0.1] L/min/m^2, p = 0.102). CMR-derived cardiac index (CI) correlated closely with CPET-derived CI (r = 0.826, p < 0.001) (Figure A) and CPET VO2 max (r = 0.635, p = 0.003). Elite athletes had higher exercise capacities compared to healthy individuals as assessed using change from baseline to peak exercise in (1) indexed stroke volumes (52 [35 – 77] % versus 16 [5 – 30] % , p = 0.002) (Figure B) and (2) cardiac index (290 [200 – 330] % versus 170 [140 – 210] %, p = 0.002). Receiver operating characteristic curve analysis of peak indexed stroke volume had an area under the curve of 0.95 (95% CI 0.87 – 1.00, p < 0.001) to differentiate athletes from healthy volunteers.

Conclusions: We have developed an in-scanner exercise protocol of using 60-channel acquisition enabled real-time CMR imaging that is easy to implement and is a highly reproducible technique for assessing cardiac performance.

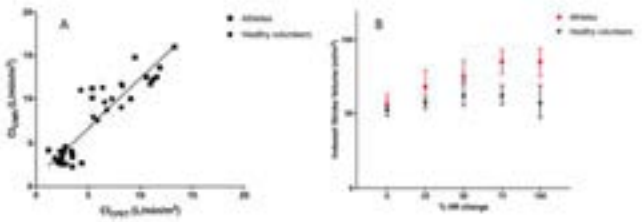

Linear regression of cardiac index values measured from CMR and estimated from CPET at rest and peak exercise (A) and Changes in indexed stroke volume with heart rate (B)

F033

Pulmonary vascular resistance and intracardiac shunt quantification during real-time MRI guided cardiac catheterization

Toby Rogers, BM BCh, PhD[1] Kanishka Ratnayaka, MD[1], Jaffar M. Khan, BM BCh[2], Annette Stine, RN[1], Laurie Grant, RN[1], William Schenke, BS[1], Jonathan Mazal, MS[1], Michael Hansen, PhD[3], Anthony Z. Faranesh, PhD[4], Robert J. Lederman, MD[4]

1. *National Institutes of Health, MD*
2. *NHLBI, NIH, Washington, DC*
3. *National Heart, Lung, and Blood Institute, Bathesda, MD*
4. *National Heart, Lung, and Blood Institute, National Institutes of Health, MD*

Background: We have previously described right heart catheterization using real-time MRI guidance and MRI-safe balloon catheters. During real-time MRI-guided cardiac catheterization, quantification of pulmonary and systemic cardiac output required for calculation of pulmonary vascular resistance (PVR) and intra-cardiac shunt (Qp:Qs) is feasible using phase-contrast MRI. We compared PVR and shunt calculations obtained using MRI with conventional cath lab calculations using the Fick principle.

Methods: We calculated pulmonary and systemic cardiac output using the Fick principle and phase contrast MRI simultaneously in consecutive patients undergoing real-time MRI-guided right heart catheterization at our institution. Transpulmonary pressure gradient, required for PVR calculation, was transduced through a MRI-safe balloon catheter navigated to the pulmonary arteries under direct real-time MRI visualization. We performed a Bland-Altman analysis to compare agreement between the two techniques.

Results: 100 subjects underwent MRI-guided cardiac catheterization. 96 paired PVR calculations (phase contrast MRI and Fick principle) and 90 paired intra-cardiac shunt calculations were obtained. The mean difference (or bias) between MRI and Fick was -0.02 Wu/m^2 for indexed PVR with limits of agreement -2.6 and 2.5 Wu/m^2. The bias between MRI and Fick was 0.13 for Qp:Qs with limits of agreement -0.8 and 1.1.

Conclusions: In conclusion, there is good agreement between PVR and intra-cardiac shunt calculations obtained using phase contrast MRI and Fick principle during real-time MRI-guided cardiac catheterization.

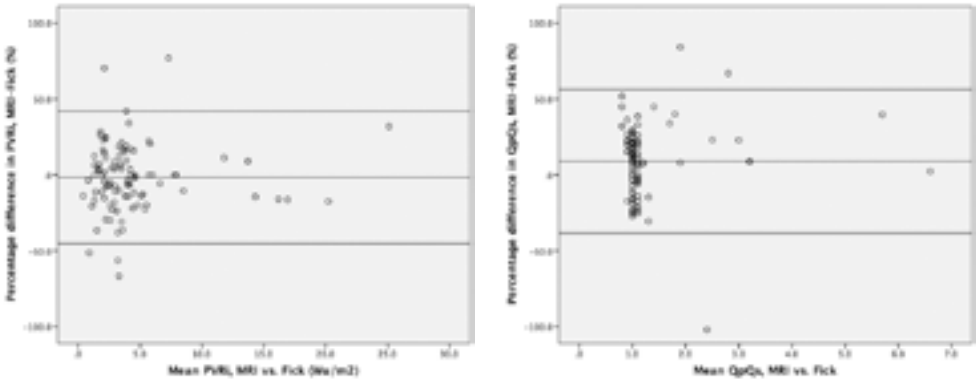

F034

Measuring invasive blood pressure by catheters guided solely by Cardiovascular Magnetic Resonance by using a new MRI conditional guidewire for post-market surveillance purposes

Christian Meierhofer, Dr. Dr.[1]Kristina Belker[2], Susanne Naumann[2], Stefan Martinoff, MD[3], Heiko Stern, Prof. Dr.[2], Nerejda Shehu, Dr.[2], Naira Mkrtchyan, Dr.[2], Andreas Eicken, Dr.[2], Peter Ewert, Prof. Dr.[2]

1. Pediatric Cardiology and Congenital Heart Disease, German Heart Center Munich, Munich, Bayern, Germany

2. Pediatric Cardiology and Congenital Heart Disease, German Heart Center Munich, Bayern, Germany

3. German Heart Center Munich, Bayern, Germany

Background: Blood pressure or pressure gradients cannot be evaluated accurately by routine cardiovascular magnetic resonance (CMR). Pressure gradients are usually measured using invasive fluid-filled catheters guided by fluoroscopy in conventional catheter-laboratories. First clinical approaches have also been made using so-called hybrid cardiovascular magnetic resonance fluoroscopy suites.

In previous studies we tested the feasibility of measuring blood pressure using fluid-filled catheters solely by CMR guidance. Here we provide data of the first series of patients (n=15) of the post market clinical follow-up (PMCF) with the CE marked MRI conditional MRWire (Nano4imaging, Aachen, Germany).

Methods: Patients scheduled for routine clinical CMR for combined diagnostic and/or interventional catheterization by fluoroscopy were included into the study. Fifteen patients have been scanned so far, a total of 25 patients will be included for the PMCF till October 2016. All patients had a congenital heart defect and a dedicated question has to be answered by catheterization in the CMR setting such as determining right ventricular pressure, pressure in the pulmonary artery or pressure gradients in the right ventricular outflow tract or in the aorta. The PMCF study sponsor was Nano4imaging (Aachen, Germany).

Results: Dedicated pressure and pressure gradients were measured successfully by fluid-filled catheters guided solely by CMR using an MRI conditional guidewire (MRWire, Nano4imaging, Aachen, Germany) No guidewire-related adverse events occurred. Only in two patients the clinical question could not be answered completely due to severe anatomic difficulties preventing to reach the target region.

Conclusions: This study shows that invasive blood pressures can be measured routinely using fluid-filled catheters solely by CMR guidance. Partial transition of such diagnostic procedures from the cathlab to the CMR can be considered.

Patients' characteristics

Clinical question	Diagnosis	Sex	Age	Patient
Pressure RV	Tricuspid atresia, Fontan prodedure, RA-RVOT homograft, now: homograft stenosis	male	38 yrs	#1
Pressure gradient CoA	CoA, arterial hypertension, now: re-CoA	male	28 yrs	#2
Pressure gradient RVOT	Valvular AR and AR, Ross procedure, now: Contegra-graft stenosis	male	14 yrs	#3
Pressure gradient TCPC	Pulmonary atresia, TCPC (extracardial conduit), now: severe AR, TCPC tunnel stenosis	male	18 yrs	#4
Pressure RA	Chronic pulmonary embolism, PAPVR upper left pulmonary vein	female	55 yrs	#5
Pressure RV, pressure gradient RVOT	TOF, residual VSD, Shelhigh-conduit, now: Shelhigh stenosis, residual-VSD	male	36 yrs	#6
Pressure RV and PA	VSD (outlet), PAPVR/ASD II, atrial fibrillation, arterial hypertension	male	55 yrs	#7
Pressure RV	Pulmonary stenosis, ASD II, valvuloplasty, transannular patch repair, ASD closure, now: severe pulmonary regurgitation and RV dilation	male	19 yrs	#8
Pressure PA	Situs inversus, azygos continuation, PAPVR, pulmonary artery hypertension	female	28 yrs	#9
Pressure RA and RV	Ebstein's anomaly, TVR (bio), Re-TVR (bio), VSD-closure, tricuspid valve stenosis valve, resudual VSD; TVR (interventionel, Sapien 26mm)	male	45 yrs	#10
Pressure RV and PA	TOF; late VSD-closure, RV-PA conduit,ischemic heart disease, now: RV-PA stenosis	female	78 yrs	#11
Pressure RV	Combined valvular AS and AR, Ross procedure, now RVOT obstruction pulmonary regurgitation, RV enlargement	female	49 yrs	#12
Pressure RV	Valvular pulmonary stenosis	male	28 yrs	#13
Pressure RV	Pulmonary atresia, VSD, PDA, Waterston-Anastomosis, RV-PA allograft, now: allograft stenosis and regurgitation, severe AR, aortic dilation	male	39 yrs	#14
Pressure gradient CoA	DORV (Taussig-Bing), CoA. Correction of CoA, banding pulmonary artery, dilatation of Re-CoA. Correction (Kawashima), VSD-closure, now: Re-CoA	male	28 yrs	#15

RA (right atrium), RVOT (right ventricular outflow tract), RV (right ventricle), CoA (coarctation), AS (aortic stenosis), AR (aortic regurgitation), TCPC (total cavopulmonary connection), PAPVR (partial aberrant pulmonary venous return), TOF (teralogy of Fallot), VSD (ventricular septal defect), ASD (atrial septal defect), PA (pulmonary artery), TVR (tricuspid valve replacement), PDA (persistent ductus arteriosus), DORV (double outlet right ventricle).

F035

Intracardiac MR Oximetry in Patients with Cardiovascular Disease: Preliminary Comparison with Right Heart Catheterization

Juliet Varghese, PhDRizwan Ahmad, PhD, Subha Raman, MD, MSEE, Lee Potter, PhD, Orlando Simonetti, PhD

The Ohio State University, OH

Background: Estimation of blood oxygen saturation (O2 sat) by T2 oximetry is limited by the use of technique-specific in vitro calibration that may not be accurate across patients, or patient-specific in vitro calibration that is impractical to perform [1,2]. We previously demonstrated a method to determine O2 sat using multiple quantitative blood T2 measurements at variable inter-echo spacings to eliminate the need for separate calibration [3]. In this study, we evaluated the technique in a preliminary cohort of cardiovascular disease (CVD) patients by comparing against their reference invasive O2 sat.

Methods: Nine CVD patients (51.44 ± 19.66 years, four females) clinically indicated for invasive right heart catheterization and cardiac MRI participated in the study. Four short-axis T2 maps including both arterial (left ventricle, LV) and venous (right ventricle, RV) blood were acquired at τ_{180} = 12, 15, 20 and 25 ms respectively at 1.5T. The resulting eight blood T2 measurements (four venous and four arterial), arterial O2 sat obtained with a pulse oximeter, and hematocrit on the day of MRI, were jointly processed to fit the Luz-Meiboom model. The unknown venous O2 sat and other three nuisance parameters of the model (T_{2O}, τ_{ex} and α) were estimated using a non-linear least-squares fit. Venous O2 sat was then compared against the invasive reference.

Results: Example T2 maps acquired in one patient are shown in Figure 1. The time between MRI and invasive measurements ranged from four hours to one week. The average hematocrit levels were 40.34 ± 6.56 % (range, 30.7% – 48.4%). Venous O2 sat estimated from MRI against the invasive measurement for each patient is compared in Figure 2; the mean values of estimated nuisance parameters are given in Table 1. The average absolute mean difference between MRI and invasive O2 sat measurements was 4.44 ± 3.24 % (range, 1% - 11%). A paired t-test between the two measurements showed no statistically significant difference (p = 0.29).

Conclusions: The proposed method overcomes the major limitation of T2 based oximetry, i.e., the need for a calibrated model. The result of this preliminary evaluation in patients by direct comparison against invasive O2 sat is promising. The largest difference of 11% was observed in Patient 3, whose MRI and catheter measurements were acquired under different hemodynamic conditions and with a time difference of one week. Future validation studies should ideally perform the two O2 sat measurements on the same day to avoid hemodynamic variations. The results of this preliminary study will serve to further optimize and improve the accuracy of the proposed oximetry technique, and thereby allow rapid translation into a clinically useful CMR diagnostic tool in the evaluation of heart failure, pulmonary hypertension and congenital heart disease.

References:

1. Wright et al. JMRI 1991, 1(3):275-283.
2. Lu et al. MRM. 2008, 60(2):357-363.
3. Varghese et al. JCMR 2016, 18(Suppl 1):W29.

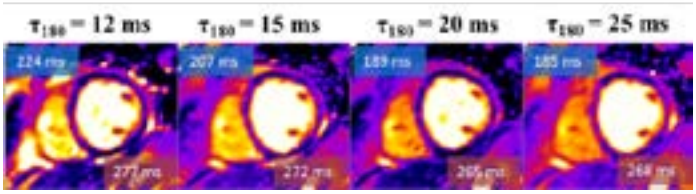

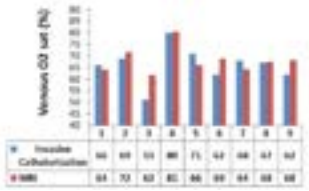

Table 1: Mean ± Standard Deviation and Range of Nuisance Parameters Estimated in Patients from the Fitting of Blood T2 to the L-M Model

Range	*Mean ± SD*	*Nuisance Parameters*
214.39 – 272.58	249.95 ± 20.05	T_{2o} (ms)
2.12 – 6.83	3.65 ± 1.55	τ_{ex} (ms)
0.27 – 0.6	0.49 ± 0.11	α (ppm)

F036

Multiyear 4D flow MRI Follow-up Suggests Associations of Baseline Aortic Hemodynamics with Progressive Aortic Dilation with Bicuspid and Trileaflet Aortic Valve Patients

Ozair Rahman, MD[1]Emilie Bollache, PhD[2], Alex J. Barker, PhD[2], Jeremy D. Collins, MD[3], James Carr, MD[3], Michael Markl, PhD[4]

1. *Northwestern University, Feinberg School of Medicine, Chicago, IL*
2. *Northwestern University Feinberg School of Medicine, Chicago, IL*
3. *Northwestern Memorial Hospital, Chicago, IL*
4. *Northwestern University, Chicago, IL*

Background: Patients with bicuspid aortic valve (BAV) are known to be at higher risk for the development of aortopathy (aortic dilatation, aneurysm, and dissection) compared to patients with trileaflet aortic valves (TAV). Previous 4D flow MRI studies have shown that valve mediated changes in aortic hemodynamics, such as elevated peak velocity (PV) or altered wall shear stress (WSS), are associated with aortic dilatation. However, there is limited data on the potential value of these parameters to predict which patients may be at risk for development of aortopathy. In this multi-year follow-up study, we assessed long-term changes in ascending aortic (AAo) WSS and PV and their association with progressive aortic dilatation.

Methods: A retrospective IRB approved and HIPAA compliant study was conducted in patients with BAV (n=20, age: 44±12 years) or TAV (n=20, age: 69±5 years) and dilated aorta, as well as TAV patients without aortic dilation ('controls', n=9, age: 50±15 years), who underwent two aortic 4D flow MRI exams (follow-up duration: 2.70±0.62 years for BAV; 1.70±0.77 years for TAV; 1.09±0.48 years for controls). 4D flow MRI data analysis included the 3D segmentation of the thoracic aorta and subsequent quantification of systolic PV and calculation of 3D WSS maps in the AAo. Systolic WSS was quantified as the average over the entire AAo wall surface. In addition, aortic diameters at the sinus of Valsalva (SOV) and mid AAo (MAA) as well as AAo volume were determined at baseline and follow-up using Contrast Enhased Magnetic Resonance Angiograms.

Results: AAo diameters and volumesincreased for both BAV (P=0.001) and TAV (P=0.01) patients while AAo size was unchanged for controls (see Table). This increase in aortic dilatation was accompanied by a significant increase in AAo PV (P=0.02) and decrease in WSS (P < 0.0001) in BAV patients, while no changes were observed in TAV patients and controls (Figure). Notably, longitudinal aortic volume changes significantly correlated with baseline PV in BAV patients (r=0.51, P=0.02). In addition, progressive dilatation was significantly correlated to baseline WSS in both BAV (r=0.46, P=0.04) and TAV (r=0.46, P=0.04) patients.

Conclusions: The significant associations between baseline WSS and volume change in BAV and TAV patients suggest the involvement of hemodynamics as a potential predictive parameter for progressive aortic dilation. We speculate that the reduction of WSS at follow-upin BAV patients could be representative of adaptive remodeling (vessel dilation) to return WSS values closer to those typically found in the normal control population.

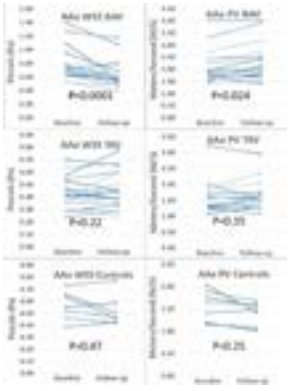

(B) *statically significant compared to Baseline	BAV (N=20)		TAV (N=20)		Controls (N=9)	
	Baseline	Follow-up	Baseline	Follow-up	Baseline	Follow-up
Age (yrs)	44±12	47±12	58±14	60±14	49±14	50±15
MAA (cm)	4.0±0.5	4.1±0.5*	3.8±0.6	3.87±0.5	3.2±0.4	3.2±0.5
SOV (cm)	4±0.4	4.1±0.4*	4.2±0.4	4.27±0.5	3.4±0.3	3.5±0.3
AAo Volume (ml)	123±31	130±31*	104±25	106±24*	78±20	74±22
Wall Shear Stress (Pa)	0.81±0.25	0.65±0.24*	0.48±0.13	0.46±0.16	0.55±0.11	0.53±0.13
Peak Velocity (m/s)	2.15±0.72	2.29±0.85*	1.62±0.48	1.67±0.45	1.54±0.32	1.44±0.28

F037

Impact of Aortic Valve Stenosis on the Expression of Aortic 3D Wall Shear Stress: New Insights from 4D Flow MRI in 618 subjects

Alex J. Barker, PhD[1] Pim van Ooij, PhD[2], Jeremy D. Collins, MD[3], James Carr, MD[3], Cynthia Rigsby, MD FACR[4], Michael Markl, PhD[5]

1. *Northwestern University Feinberg School of Medicine, Chicago, IL*
2. *Amsterdam Medical Center, N/A, Netherlands*
3. *Northwestern Memorial Hospital, Chicago, IL*
4. *Ann & Robert H Lurie Children's Hospital of Chicago, Chicago, IL*
5. *Northwestern University, Chicago, IL*

Background: The cause of life threatening ascending aortic (AAo) aneurysms are poorly understood, particularly in the presence of valve disease such as bicuspid aortic valve (BAV) or aortic valve stenosis (AS). The aim of this study was to investigate 3D aortic wall shear stress (WSS) patterns in groups known to be at risk of aneurysm formation by testing: 1) whether BAV cusp fusion morphology has a distinct expression of regionally elevated WSS in the aorta, and, 2) how AS alters aortic hemodynamics and WSS.

Methods: 618 subjects (272 with BAV, 290 with aortic dilatation and tricuspid aortic valve [TAV], & 56 healthy controls) underwent CMR, including 4D flow MRI of the thoracic aorta (resolution=2.2-4.2×1.7–2.9×2.2-4.0mm^3; temporal resolution=32.8–43.2ms, venc=150–450cm/s). 2D CINE SSFP was used to categorize BAV fusion patterns by right-left coronary valve cusp fusion (RL-BAV) or right-noncoronary fusion (RN-BAV). Data analysis employed 3D WSS atlases to depict and quantify distinct group-specific 3D WSS changes in the aorta [1]. 3D aorta segmentation was performed using 3D PC-MRA images (Mimics, Materialise, Belgium). Aortic stenosis was defined as systolic peak velocity >3m/s in the vena contracta region. 3D systolic WSS was mapped onto the aorta surface. For each group mean, WSS was regionally quantified in the AAo.

Results: Demographics are summarized in table 1. WSS atlases for the different groups are shown in figure 1. Compared to controls, BAV patients without AS demonstrated regionally elevated WSS (red color). Different BAV cusp fusion patterns resulted in distinct differences in 3D WSS patterns (figure 1 top row, table 2): for RL-BAV patients, WSS was regionally elevated along the entire right-anterior part of the AAo ($p < 0.001$) while RN-BAVs were elevated at the distal anterior AAo ($p < 0.001$). Patients with TAV and dilated aorta showed reduced WSS ($P < 0.001$) throughout the AAo. AS resulted in significantly increased WSS ($p < 0.001$) for all groups (figure 1 lower row, table 2). Notably, regions with elevated WSS were larger and differences between BAV cusp fusion patterns were less pronounced.

Conclusions: The findings demonstrate that: 1) BAV is associated with elevated aortic WSS even for normal valve function (no AS) and BAV cusp fusion morphology significantly impacts the distribution of 3D WSS; 2) 3D WSS in TAV patients with aortic dilatation is significantly reduced; 3) in patients with AS, differences between valve phenotypes is not apparent.

Funding: NIH R01 HL115828 and K25 HL119608 **References:** 1. van Ooij P, et al. MRM 2015;73:1216-1227.

	Controls	BAV patients		TAV patients	
		RL-BAV	RN-BAV		P
All subjects					
N (% female)	56 (34%)	211 (25%)	61 (34%)	290 (29%)	-
Age (years)	43 ± 13	48 ± 14	49 ± 14	58 ± 14	<0.001
No AS					
N (% female)	-	168 (24%)	38 (42%)	269 (24%)	-
Age (years)	-	46 ± 13	44 ± 12	58 ± 14	<0.001
SOV diameter (cm)	-	4.0 ± 0.5	3.8 ± 0.5	4.1 ± 0.5	<0.001
MAA diameter (cm)	-	3.9 ± 0.7	3.8 ± 0.7	3.9 ± 0.8	0.8
Peak systolic velocity (m/s)	-	1.8 ± 0.4	1.9 ± 0.5	1.5 ± 0.4	<0.001
AS (>3m/s)					
N (% female)	-	43 (30%)	23 (22%)	21 (24%)	-
Age (years)	-	57 ± 14	57 ± 12	62 ± 15	0.4
SOV diameter (cm)	-	3.8 ± 0.5	4.0 ± 0.6	3.7 ± 0.5	0.11
MAA diameter (cm)	-	3.9 ± 0.6	4.1 ± 0.6	4.0 ± 0.5	0.33
Peak systolic velocity (m/s)	-	3.9 ± 0.7	3.6 ± 0.6	4.1 ± 0.8	0.11

Table 1: Demographics, aortic dimensions and peak systolic velocity for 618 study participants

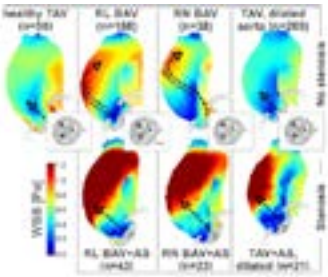

Figure 1: 3D WSS atlases (cohort averaged 3D WSS mapped onto the respective group-specific aorta geometry) for all subject groups in left-anterior view of the thoracic aorta illustrate the spatial distribution of the cohort-averaged 3D WSS on the aorta surface. In patients with no or mild AS (top row), WSS in BAV patients was regionally elevated compared to controls. In addition, differences in ascending aortic 3D WSS patterns for RL-BAV and RN-BAV cusp fusion types can clearly be appreciated. In contrast, patients with TAV and dilated aorta showed reduced WSS throughout the aorta. In subjects with moderate to severe AS, WSS was markedly elevated in the ascending aorta for all patient groups (RL-BAV, RN-BAV, TAV and dilated aorta). Color coding = WSS magnitude.

regional WSS [Pa]	controls	No AS			Moderate to severe AS		
		RL-BAV	RN-BAV	TAV	RL-BAV	RN-BAV	TAV
posterior proximal AAo	0.75±0.20	0.84±0.20	0.80±0.20	0.58±0.19	1.10±0.32	1.20±0.34	1.05±0.21
anterior proximal AAo	0.65±0.16	0.83±0.21	0.70±0.14	0.59±0.22	1.25±0.28	1.02±0.19	1.01±0.19
posterior distal AAo	0.67±0.15	0.78±0.20	0.66±0.16	0.52±0.19	0.97±0.32	0.96±0.33	0.90±0.28
outer distal AAo	0.63±0.18	0.98±0.35	0.92±0.29	0.49±0.24	1.66±0.38	1.47±0.40	1.47±0.28

p-values	No AS vs. controls			Moderate to severe BAV vs. TAV	
	RL-BAV	RN-BAV	TAV	RL-BAV	RN-BAV
posterior proximal AAo	0.04#	0.32*	<0.001#	<0.001#	<0.001#
anterior proximal AAo	<0.001#	0.44*	<0.001#	<0.001#	<0.001#
posterior distal AAo	<0.001*	0.70*	<0.001*	<0.001*	<0.001*
anterior distal AAo	<0.001#	<0.001*	<0.001#	<0.001#	<0.001#

p-values	Moderate/severe AS BAV vs. TAV	
	RL-BAV	RN-BAV
posterior proximal AAo	0.27*	0.19#
anterior proximal AAo	0.36*	0.36#
posterior distal AAo	0.82*	0.91*
anterior distal AAo	0.25*	0.50*

* 2-sided t-test
\# Mann-Whitney test

Table 2: Results of regional quantification of mean wall shear stress (WSS) in the ascending aorta (AAo).

F038

Quantification of Ischemic Mitral Regurgitation with Cardiovascular Magnetic Resonance and Its Association with Outcomes

João L. Cavalcante, MD[1] Kenia Kusunose, MD PhD[2], Nancy A. Obuchowski, PhD[3], Zoran B. Popovic, MD PhD[3], James D. Thomas, MD[4], Milind Y. Desai, MD[3], Scott D. Flamm, MD MBA[3], Brian P. Griffin, MD[3], Deborah H. Kwon, MD[3]

1. *University of Pittsburgh - UPMC, Pittsburgh, PA*
2. *Tokushima University Hospital, N/A, Japan*
3. *Cleveland Clinic, OH*
4. *Northwestern University Hospital, IL*

Background: Ischemic mitral regurgitation (IMR) is associated with poor outcomes in patients with advanced ischemic cardiomyopathy (ICM). Its quantification by echocardiography is challenging and severity assessment controversial. Although cardiac magnetic resonance (CMR) can accurately quantify and risk stratify patients with primary mitral regurgitation, its role in secondary IMR and association with clinical outcomes in ICM patients is unknown. We sought to use CMR imaging to quantify IMR and identify the cutoff associated with increased likelihood of the combined endpoint of one-year all-cause mortality and/or heart transplant.

Methods: Consecutive patients with advanced ICM and baseline CMR with quantification of IMR were included. IMR was quantified by calculating the mitral regurgitant volume as the difference between the LV stroke volume (as determined by endocardial segmentation of cine images) and forward aortic flow volume using breath-held phase-contrast imaging. The mitral regurgitant fraction was calculated as (mitral regurgitant volume/LV stroke volume) x 100%. Time-dependent ROC analysis was used to find optimal cut points for mitral regurgitant fraction; the Cox models were used to test whether the resulting stratification added value over standard risk stratification.

Results: We evaluated 578 patients (age 62±11 years, 76% males), mean LVEF was 25±10%, mean LV end-systolic volume index was 108 ± 47 ml/m^2 and mean mitral regurgitant fraction of 18±17%. A total of 112 patients received surgical mitral valve repair or replacement, 291 patients received coronary revascularization, and 267 were medically treated. Over a median follow-up time of 58 months, 190 patients experienced the combined endpoint. Progressive IMR severity quantified by phase-contrast CMR was associated with higher likelihood of combined endpoint (HR=1.22, 95% CI 1.07, 1.40, p=0.0027). Mitral regurgitant fraction of ≥ 20% was already associated with worse combined endpoint suggesting that even lower severity of IMR carries a worse outcome in this population (HR=1.51; 95% CI 1.12-2.05, p=0.008, **Figure 1**). On multivariable analysis, after controlling for age, diabetes, use of ACE-inhibitor, and treatment received, mitral regurgitant fraction (either as a continuous or as a dichotomous variable), was independently associated with the combined endpoint.

Conclusions: Quantification of IMR severity by CMR allows for risk-stratification of ICM patients. Since this is a heterogeneous population, in whom surgical correction of IMR has not been shown to alter outcomes, future prospective studies are necessary to confirm our findings and to determine the role of CMR in selecting the appropriate patients with ICM and IMR who could derive a survival benefit from correction of IMR.

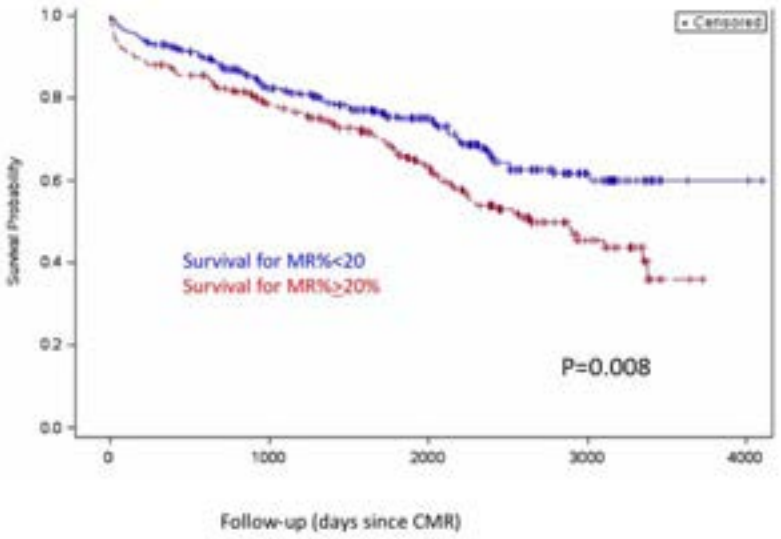

F039

Isolated pulmonary regurgitation causes decreased right ventricular longitudinal function and compensatory increased septal pumping in a porcine model.

Sascha Kopic, MD, PhD[1], Marcus Carlsson, MD, PhD[1]Einar Heiberg, PhD[2], Håkan Arheden, MD, PhD[3], Philipp Bonhoeffer, MD[4], Mads Ersbøll, MD, PhD[5], Niels Vejlstrup, MD, PhD[6], Lars Søndergaard, MD; DMSc[7]

1. *Lund University, Department of Clinical Sciences Lund, Clinical Physiology, Skane University Hospital, Lund, Sweden, Skane Lan, Sweden*
2. *Lund University, Department of Clinical Sciences Lund, Clinical Physiology, Skane University Hospital, Lund, Sweden; Lund University, Faculty of Engineering, Department of Biomedical Engineering, Lund, Sweden, Skane Lan, Sweden*
3. *Lund University, Department of Clinical Sciences Lund, Clinical Physiology, Skane University Hospital, Lund, Sweden, Lund, Skane Lan, Sweden*
4. *n/a, Toscana, Italy*
5. *Bispebjerg Hospital, Department of Cardiology, Holte, Hovedstaden, Denmark*
6. *Rigshospitalet, Hovedstaden, Denmark*
7. *Rigshospitalet, Copenhagen, Hovedstaden, Denmark*

Background: Longitudinal ventricular contraction, i.e. the movement of the atrio-ventricular plane towards the apex during ventricular systole, has evolved into an increasingly important parameter in the assessment of overall cardiac performance. Furthermore, it has been shown that the degree of its impairment in the left ventricle (LV) is a strong predictor of adverse cardiac events. Right ventricular (RV) longitudinal function is impaired in patients with pulmonary regurgitation (PR) following corrective surgery for Tetralogy of Fallot (TOF). However, it remains controversial whether these changes are a byproduct of corrective surgery and concomitant scarring, or whether they are primarily inherent to PR. The aim of this study was therefore to assess the relationship between longitudinal, lateral and septal pumping in a porcine model of isolated PR. Understanding the pathophysiological changes underlying PR may lead to improved risk stratification and may aid in the clinical management of TOF patients with regard to timing of corrective interventions for PR.

Methods: Piglets were divided into control (n=8) and treatment (n=11) groups. Animals in the treatment group received a metal stent over the pulmonary valve via percutaneous intervention, inducing free PR. PR was maintained for two (n=7) or three (n=4) months, respectively, before animals were subjected to cardiac magnetic resonance imaging (CMR) on a 1.5T scanner. Control animals were imaged at corresponding time points. CMR analysis yielded global cardiovascular parameters and the contribution of longitudinal, lateral and septal contraction to corresponding ventricular stroke volumes (SV), as described previously.

Results: PR amounted to 43.0 ± 3.0% (SEM) of right ventricular stroke volume (RVSV) in treated animals. Animals with PR demonstrated a significantly lower longitudinal contribution to RVSV (longitudinal RVSV), compared to animals without PR (59.6 ± 2.7% *vs.* 73.7 ± 3.7%; p=0.008). Furthermore, we observed a marked compensatory increase in septal contribution to RVSV (septal RVSV) in animals suffering from PR (11.4 ± 1.7% *vs.* -3.3 ± 1.3%; p < 0.0001). The LV showed concomitant counter-regulation with an increased longitudinal LVSV (87.8 ± 4.7% *vs.* 70.0 ± 2.0%; p=0.004) and a decreased septal LVSV (-26.0 ± 3.7% *vs.* 3.2 ± 1.5%; p < 0.0001) in animals with PR.

Conclusions: Our findings suggest that decreased longitudinal function in the RV is a result of PR and corresponding RV volume overload, rather than a byproduct of surgery. Interestingly, we observed a concomitant increase in longitudinal LVSV, which has not been observed in TOF patients. This most likely reflects compensation for the strongly negative septal LVSV and may be attributable to an acute adaptive mechanism following 2-3 months of free-flowing PR. Measurement of longitudinal RVSV may aid risk stratification and facilitate timing choice for interventional correction of PR in TOF patients.

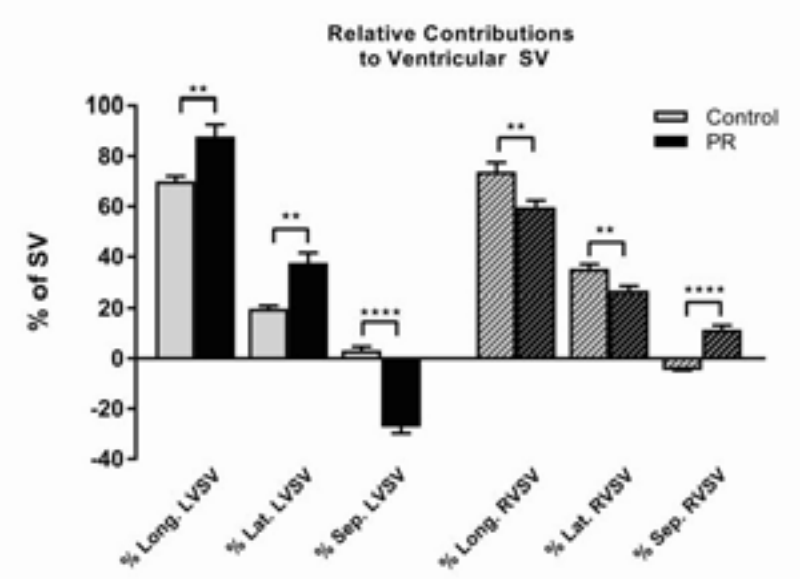

F040

Model-Based Therapy Planning accurately predicts postoperative Blood Flow Profiles in the Ascending Aorta after Aortic Valve Replacement

Sarah Nordmeyer, M.D.Marcus Kelm, M.D., Florian Hellmeier, Jan Bruening, Leonid Goubergrits, Joao Fernandes, Simon Suendermann, M.D., Pavlo Yevtushenko, Felix Berger, M.D., Volkmar Falk, M.D., Titus Kuehne, M.D.

Deutsches Herzzentrum Berlin, Berlin, Germany

Background: Model-based therapy planning holds great promise for optimizing outcome after heart valve surgery, yet has remained a yearned-for goal. In this study we aimed to validate accuracy of model-based prediction of blood flow profiles in the ascending aorta after aortic valve replacement.

Methods: In ten patients with aortic valve disease virtual treatment of aortic valve replacement and modifications of the ascending aorta was performed according and next to the actual surgical procedure. Model-based predictions of postoperative blood flow profiles in the ascending aorta was performed in the virtual treatment group using computational fluid dynamics and preoperative information derived from magnetic resonance imaging (e.g. 4D VEC MRI). Predicted outcome was compared to actual post-operative imaging assessment of the surgically treated patients. Parameters included peak flow velocities across the valve, wall shear stress and blood flow profiles (helicity, vorticity, eccentricity, and secondary flow degree).

Results: Predicted vs. actual aortic arch anatomy were comparable (28.3±5.7 mm vs. 29.6±7 mm, p=0.1) as well as peak velocities across the valve (2.97±1.1 vs. 2.7±0.7 m/s; p=0.4). Wall shear stress (17.3±12.3 Pa vs. 16.7±16.84 Pa; p = 0.8), secondary flow degree (0.44±0.32 Pa vs. 0.49±0.23 Pa; p = 0.3) and blood flow patterns (helicity p = 0.8, vorticity p = 0.2, eccentricity p = 0.3) were not significantly different between predicted and actual measurements.

Conclusions: Model-Based therapy planning was able to accurately predict postoperative blood flow profiles in the ascending aorta after aortic valve replacement. This may open up so far unknown options for improvements in patient care and surgical strategy planning through individually targeted interventions.

F041

Cardiac CEST MRI with Dual-Echo Readout for B0 Correction: A Preliminary Reproducibility Study for Assessment of Metabolic Activity in the Heart

Zhengwei Zhou, MS,[1]Xiaoming Bi, PhD[2], Debiao Li, PhD[3]

1. *Cedars-Sinai Medical Center, Los Angeles, CA*
2. *Siemens Healthcare, CA*
3. *Biomedical Imaging Research Institute, Cedars-Sinai Medical Center, Los Angeles, CA, CA*

Background: It has been shown that cardiac CEST technique can measure the distribution of creatine, an important substrate in the ATP synthesis system, thereby detecting myocardial metabolic abnormalities in cardiac dysfunctions[1,2]. However, B_0 field variations, mostly caused by respiratory motion within the acceptance window in a navigator-gated acquisition, especially on the edge of heart-lung interface, can induce errors of the CEST signal[3]. In this work, we developed a cardiac CEST dual-echo technique which not only acquires CEST-weighted image, but also enables acquisition of B_0 map for each saturation frequency offset. CEST reproducibility with the technique was assessed.

Methods: Fig. 1 shows the workflow of the proposed cardiac CEST dual-echo technique. As illustrated in the sequence diagram (Fig. 1a), images were acquired using dual-echo readout to allow simultaneous acquisition of B_0 map and CEST-weighted image. Figure 1b shows the analysis of images acquired at each CEST saturation frequency offset. After B_0 correction for each CEST-weighted image, MTR_{asym} was calculated as $MTR_{asym} = (S(-2\ ppm)–S(+2\ ppm))/S_0$, where S_0 is the signal intensity of the reference image. Five healthy volunteers were scanned on a 3T Siemens Verio clinical scanner. CEST saturation frequency offsets range from -3.6 ppm to 3.6 ppm with a step size of 0.3 ppm. Imaging parameters are: 3 CEST saturation pulses (flip angle 2700º and duration of 80 ms at duty cycle of 50%); FOV: 350 x 280 mm^2; Spatial resolution: 2.7 x 2.2 x 8.0 mm^3; TE1: 0.99 ms; TE2: 2.37 ms; Partial Fourier: 6/8; iPAT: 2. Two mid-ventricular slices were acquired in each volunteer.

Results: Fig.2 represents the B_0 map acquired using cardiac CEST dual-echo sequence. Average and standard deviation of B_0 maps acquired at different saturation frequency offsets were shown in Fig. 2b and 2c, respectively. It is clear that there is more variation of the B_0 map in the lateral wall. This is mostly because B_0 field changes rapidly in this region and it is more sensitive to respiratory motion. Therefore, it is important to correct for B_0 field for each image acquired at different CEST saturation frequency offsets. Fig. 3(a) shows one representative MTR_{asym} map acquired using the proposed method. One ROI was drawn in the septal region and mean MTR_{asym} value was calculated. The Bland-Altman plot of the MTR_{asym} values from two measurements was shown in Fig. 3(b). The y axis is the percentage difference, defined as Difference/Average*100. The limits of agreement were -4.32±17.41%.

Conclusions: We developed a cardiac CEST dual-echo method and performed reproducibility studies in healthy volunteers. Preliminary results suggest that cardiac CEST with B_0correction is reproducible. The proposed method needs to be tested in patients to assess its ability to detect mild myocardial metabolic abnormalities. [1] Haris, M., et al. Nat. Med 2014. [2] Zhou, Z., et al. JCMR 2016. [3] Singh, A., et al. MRM 2012.

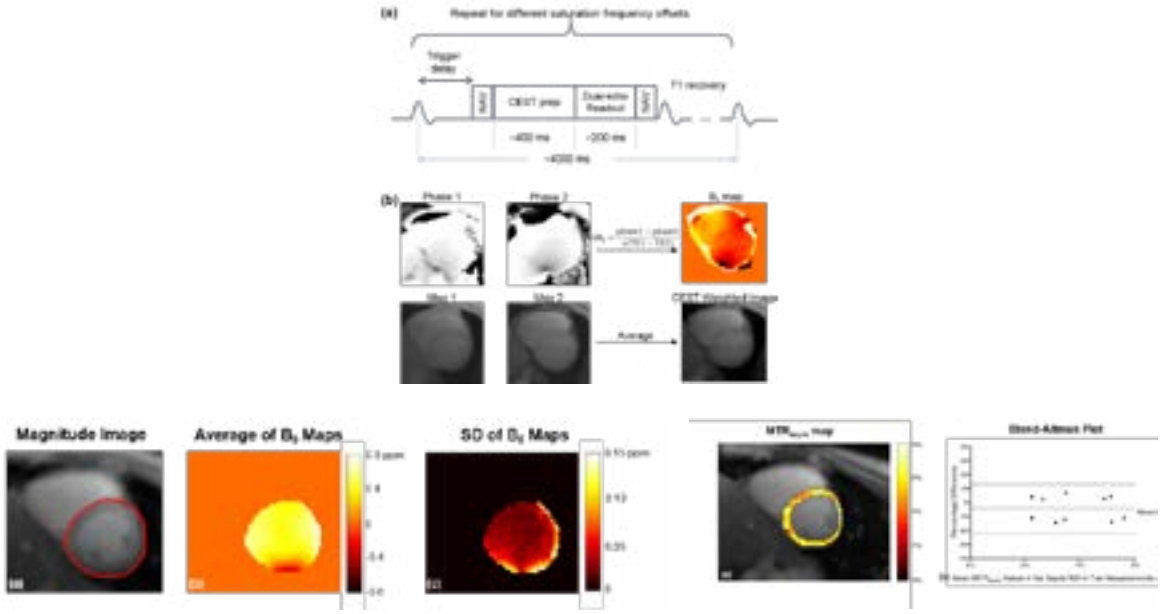

F042

Hyperpolarized magnetic resonance imaging of cardiac inflammation and repair following myocardial infarction

Andrew Lewis, MRCP[1]Jack Miller, DPhil[2], Oliver Rider, DPhil[2], Robin Choudhury, MD[2], Stefan Neubauer, MD, FRCP[3], Carolyn Carr, DPhil[2], Damian Tyler, PhD[2]

1. *University of Oxford Centre for Clinical Magnetic Resonance, Oxford, England, United Kingdom*
2. *University of Oxford, Oxford, England, United Kingdom*
3. *University of Oxford, England, United Kingdom*

Background: Myocardial infarction (MI) remains a major killer despite highly optimised primary reperfusion systems, highlighting a need for novel therapeutic approaches administered in the days following the event. The healing myocardium undergoes a macrophage driven inflammatory response which may be one such therapeutic target, though clinical exploration has been hampered by the absence of imaging biomarkers. We hypothesised that metabolic reprogramming in activated inflammatory cells within healing myocardium could be detected by using hyperpolarized [1-^{13}C]pyruvate magnetic resonance imaging.

Methods: Experimental myocardial infarction was induced in rodents prior to hyperpolarized [1-^{13}C]pyruvate magnetic resonance imaging at days 3 or 7, using a 7T MR system and a custom-designed ^{13}C imaging sequence. Separate *in vitro* [1-^{13}C]pyruvate spectroscopic experiments were performed using macrophage-like cell suspensions and an 11.7T magnet. The resulting [1-^{13}C]lactate signals from these cell and rodent models were compared to immune cell number, phenotype, and cytokine levels measured using flow cytometry, ELISA and qPCR.

Results: MI caused intense [1-^{13}C]lactate signal in healing myocardial segments at both day 3 (paralleling the maximal 'inflammatory' phase of the macrophage response) and also at day 7 ('reparative' phase), compared to sham operated controls (Figure 1a). Mechanistically, macrophage depletion using clodronate liposomes abrogated the lactate signal at both day 3 and day 7, suggesting that macrophage driven inflammation is causative (Figure 1a&b). Hyperpolarized [1-^{13}C]pyruvate MR spectroscopy in macrophage-like cell suspensions confirmed that cellular activation and polarization using lipopolysaccharide almost doubles hyperpolarized lactate label flux rates *in vitro*; blockade of glycolysis with 2-deoxyglucose in activated cells normalised lactate label flux (Figure 1c) and also markedly inhibited the production of key pro-inflammatory cytokines without cytotoxicity. Systemic administration of 2-deoxyglucose following rodent cryoinfarction normalised hyperpolarized [1-^{13}C]lactate signal in healing myocardial segments and also improved inflammatory cytokine levels in both the infarct and border zones at day 3. Ongoing work will determine the effect of this 'MR visible' immunomodulatory approach upon longer term myocardial remodelling and systolic function.

Conclusions: High hyperpolarized [1-^{13}C]lactate signal in the days following myocardial infarction is caused by macrophage driven inflammation, and reflects not just the number of inflammatory cells infiltrating the myocardium but also the inflammatory phenotype of those cells. Hyperpolarized MRI therefore provides a novel method for the detection of myocardial inflammation with high translational potential as both a biomarker and potential novel pharmacological target.

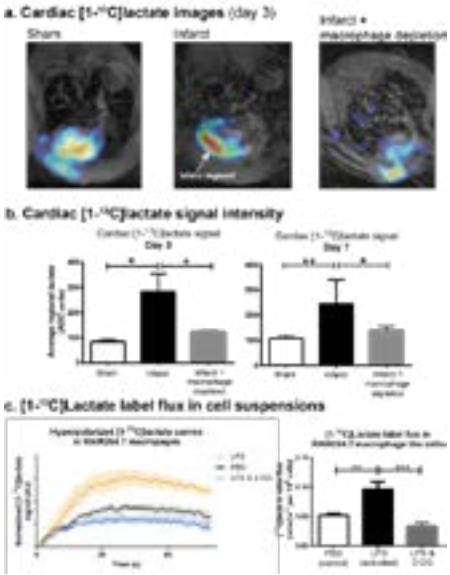

F043

Obesity is Associated with a Compensatory Increase in the Pseudo-First-Order Rate Constant of the Creatine Kinase Reaction

Jennifer Rayner, BMBCh, BA(Hons)[1] William Clarke, DPhil[1], Mark A. Peterzan, BSc(Hons) MRCP(UK)[1], Stefan Neubauer, MD, FRCP[2], Christopher T. Rodgers, DPhil[1], Oliver Rider, DPhil[1]

1. *University of Oxford, Oxford, England, United Kingdom*
2. *University of Oxford, England, United Kingdom*

Background: Using phosphorus magnetic resonance spectroscopy (^{31}P MRS), it has been shown that obesity is associated with impaired myocardial energetics (a reduced phosphocreatine (PCr) to adenosine triphosphate ratio (PCr/ATP)). The most likely mechanism for the reduced PCr/ATP in obesity is a loss of the total creatine pool, in proportion to the loss of PCr, as occurs in many other diseases of left ventricular hypertrophy. However, unlike in heart failure where PCr/ATP is similarly reduced, LV systolic function in obesity is usually preserved, suggesting that the rate of ATP delivery to the contractile apparatus may in fact be maintained. We hypothesised that in order to preserve ATP delivery rates in obesity, the forward rate constant of the CK reaction would be increased as a compensatory mechanism for the reduced creatine pool size.

Methods: 29 participants were recruited into 2 groups - 22 obese with BMI 36.3±5.0, and 7 normal weight (BMI 22.6±2.8). All underwent CMR imaging at 3T to determine left ventricular geometry (mass, end-diastolic volume (EDV)) and ejection fraction (LVEF). The pseudo-first-order rate constant of the creatine kinase reaction (CK k_f) was determined by Triple Repetition time Saturation Transfer (TRiST) 1D-CSI ^{31}P MRS, which determines CK k_f as: $k_f = (1/T_1')(1-M'_0/M_0^{control})$. T_1' and M_0' were measured with a short TR (2s) and a long TR (10s) acquisition, both with DANTE saturation of γ-ATP. To compensate for the effects of spill-over irradiation on PCr during γ-ATP saturation, a third acquisition (TR ~ 15s) is performed to measure M_0 while applying control saturation at +2.5 ppm yielding M_0 control.

Results: There were no differences between LV EDV, mass or LVEF between the 2 groups (all $p < 0.05$). The resting pseudo-first-order CK forward rate constant (k_f) was higher in obese participants than normal weight (CK k_f 0.19 ± 0.10 s^{-1} vs 0.09 ± 0.05 s^{-1}; p=0.003, fig 1), despite no difference in heart rate (63±4 vs 55±4, p = 0.215) or rate pressure product (7453±831 vs 8083±1029, p=0.170). In addition, resting myocardial CK k_f increased in proportion to both body mass index (r=0.380, p=0.042, Fig 2) and body fat percentage (r=0.424, p=0.024, Fig 3).

Conclusions: We have studied the effect of obesity on the kinetics of the CK reaction in the human heart for the first time, demonstrating that the rate of the creatine kinase reaction is higher in obesity than in normal weight individuals. This may reflect a compensatory increase in resting creatine kinase activity to maintain ATP delivery rates in the setting of reduced creatine pool size.

http://www.ConferenceAbstracts.com/uploads/cfp2/attachments/LDFAIBDN/LDFAIBDN--218477-1-ANY.pdf

http://www.ConferenceAbstracts.com/uploads/cfp2/attachments/LDFAIBDN/LDFAIBDN--218477-2-ANY.pdf

http://www.ConferenceAbstracts.com/uploads/cfp2/attachments/LDFAIBDN/LDFAIBDN--218477-3-ANY.pdf

F044

The Pseudo-First-Order Rate Constant of the Creatine Kinase Reaction is More Closely Related to Functional Capacity than Resting Left Ventricular Ejection Fraction

Jennifer Rayner, BMBCh, BA(Hons)[1] William Clarke, DPhil[1], Mark A. Peterzan, BSc(Hons) MRCP(UK)[1], Stefan Neubauer, MD, FRCP[2], Christopher T. Rodgers, DPhil[1], Oliver Rider, DPhil[1]

1. *University of Oxford, Oxford, England, United Kingdom*
2. *University of Oxford, England, United Kingdom*

Background: In systolic heart failure, myocardial ATP delivery rates are reduced. However, in earlier stages of disease, as creatine pool depletion occurs (and a subsequent fall in PCr/ATP) an increase in the rate constant of the creatine kinase reaction (CK k_f) may act to compensate for this and maintain ATP delivery rates. In this case, the ability of the CK reaction rate to increase further to meet energetic demands might be reduced, which may equate to a limitation of exercise capacity. As a result, we hypothesised that an elevated resting CK k_f would reflect a reduced ability to increase ATP delivery further during exercise and would be related to a more limited exercise tolerance.

Methods: 29 participants across a spectrum of exercise-induced symptoms underwent cardiac magnetic resonance imaging at 3T for LV structure and ejection fraction (LVEF). In addition the pseudo-first order rate constant of the creatine kinase reaction (CK k_f) was determined by Triple Repetition time ST (TRiST) 1D-CSI ^{31}P magnetic resonance spectroscopy, which computes as $k_f = (1/T'_1)(1-M'_0/M_0^{control})$. T_1' and M_0' were measured with a short TR (2s) and a long TR (10s) acquisition, both with DANTE saturation of γ-ATP. To compensate for the effects of spill-over irradiation on PCr during γ-ATP saturation, a third acquisition (TR ~ 15s) was performed to measure M_0 while applying control saturation at +2.5 ppm yielding M_0 control. All patients underwent maximal cardiopulmonary exercise testing (CPET) and six minute walk testing (6MWT).

Results: Across a range of exercise capacity (peak VO_2 13-47ml/min/kg), resting LVEF did not significantly correlate with either 6MWT (r= -0.308, p= 0.118; fig 1A) or peak VO_2 (r= -0.337, p= 0.099) in this relatively small sample. However, CK k_f was inversely correlated with both peak VO_2 (r= -0.390, p= 0.054, Fig 1C) and 6MWT (r= -0.470, p=0.013, Fig 1B). CK k_f did not correlate with resting LVEF (r= 0.058, p= 0.763).

Conclusions: We have demonstrated for the first time that higher resting CK k_f in human myocardium is associated with reduced exercise tolerance. This may reflect a compensatory increase of the resting CK reaction rate in order to maintain ATP delivery and preserve function, at the expense of flexibility to augment further when required, thereby reducing overall exercise capacity.

http://www.ConferenceAbstracts.com/uploads/cfp2/attachments/LDFAIBDN/LDFAIBDN--218491-1-ANY(1).pdf

http://www.ConferenceAbstracts.com/uploads/cfp2/attachments/LDFAIBDN/LDFAIBDN--218491-2-ANY.pdf

http://www.ConferenceAbstracts.com/uploads/cfp2/attachments/LDFAIBDN/LDFAIBDN--218491-3-ANY.pdf

F045

Diastolic Dysfunction in Obesity is More Related to Metabolic Processes than to Concentric Hypertrophy

Jennifer Rayner, BMBCh, BA(Hons)[1], Oliver Rider, DPhil[1]Rajarshi Banerjee, MRCP DPhil[2], Cameron Holloway, FRACP Dphil [3], Andrew Lewis, MRCP[4], William Clarke, DPhil[1], Mark A. Peterzan, BSc(Hons) MRCP(UK)[1], Jane M. Francis, DCR(R) DNM[5], Christopher T. Rodgers, DPhil[1], Stefan Neubauer, MD, FRCP[6]

1. *University of Oxford, Oxford, England, United Kingdom*
2. *Perspectum Diagnostics, Oxford, England, United Kingdom*
3. *St Vincent's Hospital Sydney, New South Wales, Australia*
4. *University of Oxford Centre for Clinical Magnetic Resonance, Oxford, England, United Kingdom*
5. *University of Oxford, OX39DU, England, United Kingdom*
6. *University of Oxford, England, United Kingdom*

Background: Obesity is associated with diastolic dysfunction, and is one of the leading causes of heart failure with preserved ejection fraction. Myocardial relaxation is determined by a combination of active, energy-consuming metabolic processes and intrinsic properties determining LV stiffness. Whether these processes are related to each other, and the relative contribution of each to diastolic dysfunction in obesity is currently unknown.

Methods: 80 adult subjects (48 male) with no cardiovascular risk factors across a wide range of body mass indices (18.4-53.0 kg/m^2) underwent 1.5T MRI for abdominal visceral fat (cm^2) and LV geometry (LV mass: volume ratio, LVMVR), and at 3T ^{31}P and ^{1}H magnetic resonance spectroscopy for PCr/ATP and myocardial triglyceride content (MTGC), respectively. Insulin resistance was calculated from fasting glucose and insulin (HOMA-IR). Peak diastolic strain rate (PDSR) was assessed using feature tracking.

Results: Increasing visceral obesity was related to diastolic dysfunction as determined by reduced PDSR (r -0.46, p=0.001), reduced PCr/ATP ratio (r -0.50, p < 0.001), increased MTGC (r 0.46, p < 0.001) and concentric LV remodelling (r 0.37, p < 0.001). In addition, increasing LV concentric remodelling (LVMVR, r -0.28, p=0.01), insulin resistance (HOMA, r -0.26, p=0.03), PCr/ATP (r 0.38, p=0.001) and MTGC (r - 0.42, p < 0.001) were also related to diastolic function. Stepwise multivariable regression of these variables showed that MTGC (β -0.2, p=0.008), PCr/ATP (β -0.22, p=0.04) and LVMVR (β -0.61, p=0.04) were all independent predictors of diastolic function (model R^2 0.36 p < 0.001). Moderated multiple regression (dependent variable PDSR, independent variable visceral fat, moderators PCr/ATP, MTGC and LVMVR, Figure 1) was performed with 10,000 sample bootstrapping of indirect effects. This confirmed the mediating roles of PCr/ATP, MTGC and LVMVR in the relationship between visceral fat and PDSR. The direct effect of visceral fat became non-significant (β -0.006, p=0.42) suggesting full mediation. Of the negative effect of visceral fat on diastolic function, 40% was explained by increased MTGC, 39% by reduced PCr/ATP and 21% by LV concentric remodelling. MTGC and PCr/ATP were not related (r -0.17, p=0.13).

Conclusions: Energy-consuming active metabolic processes appear to be more important than geometric remodelling in determining the impact of obesity on diastolic function, with myocardial lipid (40%) and myocardial energetics (39%) accounting for more of the negative effect than LV concentric remodelling (21%). Not only is this a fascinating observation in itself, but it suggests that targeting these metabolic processes could be an attractive strategy to treat diastolic dysfunction in obesity.

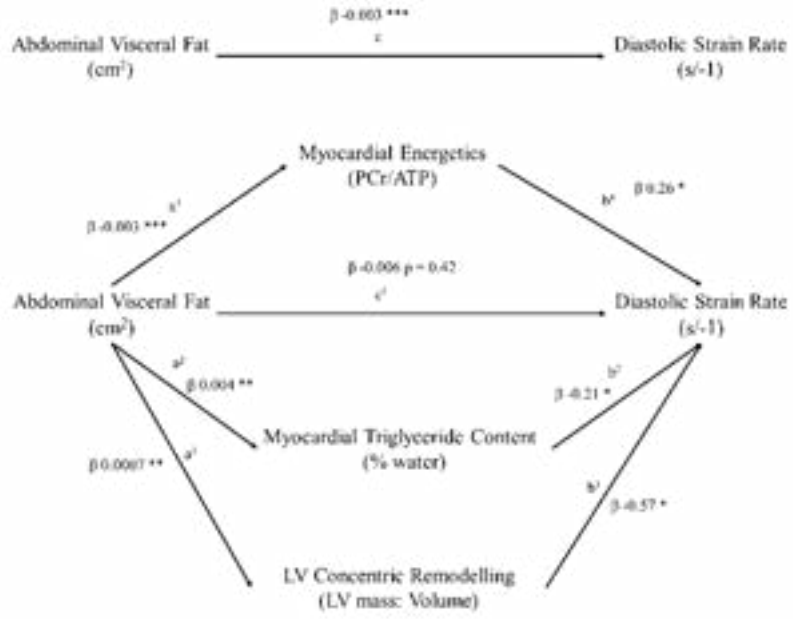

F046

Self-Gated Golden Angle Spiral CINE MRI for Coronary Endothelial Function Assessment

Gabriele Bonanno, PhD[1] Allison G. Hays, MD[1], Robert G. Weiss, MD[1], Michael Schär, PhD[2]

1. Johns Hopkins University School of Medicine, MD
2. Johns Hopkins University, MD

Background: The coronary endothelium maintains vascular tone and attenuates inflammation in non-diseased vascular tissue[1]. Abnormal coronary endothelial function (CEF) is a marker for sub-clinical atherosclerotic disease and an independent predictor of cardiovascular events[2]. Recently, a non-invasive, reproducible method to quantify CEF was introduced that combined isometric handgrip exercise (IHE) with ECG-triggered MRI[3,4]. However, CEF measures are sometimes hindered by previously-required ECG-triggering in the MRI scanner. The ECG signal may be distorted during the acquisition, potentially leading to failed studies, and the number of cardiac phases is defined and fixed before the scan.
In response, we propose a novel cardiac *self-gating* technique in combination with a golden-angle spiral acquisition and iterative reconstruction (**SG-GA**). If available, the technique can apply ECG-determined triggers for retrospective gating (**ECG-GA**). The SG-GA method was tested in comparison to ECG-GA and gold-standard ECG-triggered spiral cine[3] (**ECG-STD**).

Methods: The self-gating signal is extracted from independent component analysis of the k-space center[5] acquired at the beginning of each spiral arm. After filtering, peak analysis of the signal is performed to identify self-gating triggers. CEF data were obtained in 6 healthy volunteers, after fasting, at rest and during IHE stress from cross-sectional images of the right and left coronary arteries in a 3T scanner (Philips).

Breath-held ECG-STD was acquired as reference[3]. The golden-angle[6] variable-density 2D spiral[7] sequence was matched for scan time and resolution. The same data were reconstructed with the SG-GA and ECG-GA methods with iterative-SENSE[8] in GPI[9].
For CEF assessment, lumen cross-sectional area (CSA) change between rest and IHE, was quantified after deblurring[11] using a FWHM algorithm (Cine, GE). For image quality, vessel sharpness (VS%) was quantified[12]. Statistics: Bonferroni-corrected one-way ANOVA.

Results: RR times detected with self-gating (***x***) showed high correlation with those from the ECG (***y***): Pearson's correlation coefficient 0.89±0.12, accuracy $\mu(|x-y|)$=9.8±7.5ms and precision $\sigma(x-y)$=12.4±11.2ms (Figure 1). Good image quality was obtained throughout; Figure 2.

Bland-Altman plots for CSA showed fair agreement of SG-GA and ECG-GA with ECG-STD (C.I. 95% ~ 3.6 mm^2 for both), Figure 3A-B. ECG-GA CSA measures at rest were significantly higher than ECG-STD measures (p=0.009). However, CSA change measured with the SG-GA and ECG-GA was not statistically different from the one measured with ECG-STD (p=0.91), and in agreement with literature[4].

VS% was significantly higher for SG-GA when compared to ECG-STD (p=0.04), Figure 3C.

Conclusions: The proposed cardiac self-gated MRI technique provides high image quality and CEF measures in agreement with the published standard sequence while without the need for ECG-triggering.

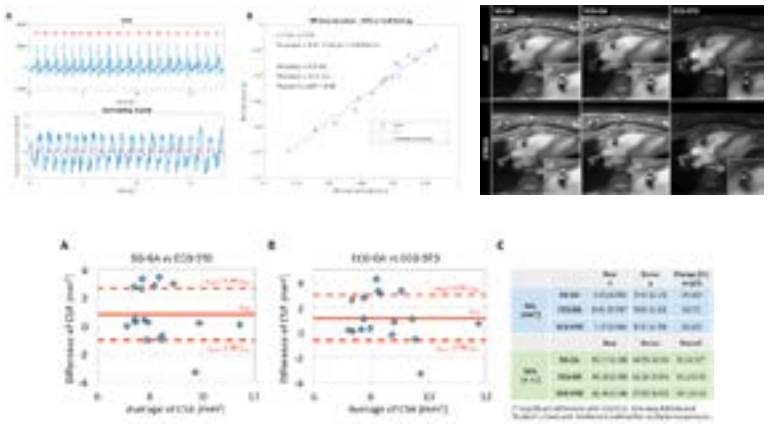

References

1. Ludmer PL, Selwyn AP, Shook TL, et al. Paradoxical Vasoconstriction Induced by Acetylcholine in Atherosclerotic Coronary Arteries. N Engl J Med. 1986;315(17):1046-1051.
2. Schächinger V, Britten MB, Zeiher AM. Prognostic impact of coronary vasodilator dysfunction on adverse long-term outcome of coronary heart disease. Circulation. 2000;101(16):1899-1906.
3. Hays AG, Hirsch GA, Kelle S, Gerstenblith G, Weiss RG, Stuber M. Noninvasive visualization of coronary artery endothelial function in healthy subjects and in patients with coronary artery disease. J Am Coll Cardiol. 2010;56(20):1657-1665.
4. Hays AG, Iantorno M, Soleimanifard S, et al. Coronary vasomotor responses to isometric handgrip exercise are primarily mediated by nitric oxide: a noninvasive MRI test of coronary endothelial function. Am J Physiol Heart Circ Physiol. 2015;308(11):H1343-H1350.
5. Bonanno G, Piccini D, Maréchal B, Zenge MO, Stuber M. A New Binning Approach for 3D Motion Corrected Self-Navigated Whole-Heart Coronary MRA Using Independent Component Analysis of Individual Coils. Proc Intl Soc Magn Reson Med Volume 23. Milan, Italy; 2014. p 936.
6. Winkelmann S, Schaeffter T, Koehler T, Eggers H, Doessel O. An optimal radial profile order based on the Golden Ratio for time-resolved MRI. IEEE Trans Med Imaging. 2007;26(1):68-76.
7. Pipe JG, Zwart NR. Spiral trajectory design: A flexible numerical algorithm and base analytical equations: Spiral Trajectory Design. Magn Reson Med. 2014;71(1):278-285.
8. Pruessmann KP, Weiger M, Börnert P, Boesiger P. Advances in sensitivity encoding with arbitrary k-space trajectories. Magn Reson Med. 2001;46(4):638-651.
9. Zwart NR, Pipe JG. Graphical programming interface. Workshop on data sampling and image reconstruction. In: Proceedings of the Workshop Series of ISMRM. Sedona, Arizona; 2013.
10. Jackson JI, Meyer CH, Nishimura DG, Macovski A. Selection of a convolution function for Fourier inversion using gridding [computerised tomography application]. IEEE Trans Med Imaging. 1991;10:473-478.
11. Noll DC, Pauly JM, Meyer CH, Nishimura DG, Macovski A. Deblurring for non-2D Fourier transform magnetic resonance imaging. Magn Reson Med. 1992;25(2):319-333.
12. Etienne A, Botnar RM, Van Muiswinkel AM, Boesiger P, Manning WJ, et al. (2002) “Soap-Bubble” visualization and quantitative analysis of 3D coronary magnetic resonance angiograms. Magn Reson Med 48: 658-666.

F047

A patient-specific MRI-based 3D computational modeling study of right coronary flow changes during vasodilator therapy in pulmonary hypertension

Miguel S. Vieira, MD[1]Christopher J. Arthurs, DPhil[1], Mari N. Velasco Forte, MD [2], Bram Ruijsink, MD[3], Kuberan Pushparajah, MD [4], Carlos Alberto Figueroa, PhD[5]

1. *King's College London, London, England, United Kingdom*
2. *King's College London, London, England, United Kingdom*
3. *King's College London, England, United Kingdom*
4. *Guy's & St Thomas' Hospital NHS Foundation Trust, Evelina London Children's Hospital, England, United Kingdom*
5. *University of Michigan & King's College London, MI*

Background: Previous work suggests right coronary artery (RCA) flow is impaired in pulmonary hypertension (PH) proportionally to the increased right ventricular (RV) afterload, even in the absence of luminal stenosis. Limited data is available on the relevance of these changes to the assessment/management of PH. Computational modeling permits investigation of multiple patient-specific PH scenarios via virtual interventions in order to gain mechanistic insight on the same individual. We have created an image-based computational model that allows studying the impact of RV extra-vascular compression (EVC), a surrogate of RV afterload, upon RCA flow as would occur due to PH advanced vasodilator therapy.

Methods: A closed-loop multidomain fluid-structure interaction model of the systemic and pulmonary circulation of an infant with isolated post-capillary PH secondary to congenital aortic stenosis was created. The model was informed by patient-specific data on flow, pressure and ventricular function from a hybrid cardiac MRI-catherization study. 3D-geometry of the systemic and pulmonary major vessels including the coronaries was segmented from a dual-phase 3D-bSSFP MRI (figure 1). A 3-element Windkessel was coupled at each vessel outlet to model the downstream vasculature. At both aortic/pulmonary valves, a 0D-heart model with patient-specific time-varying left/right ventricular elastance functions, derived from segmentation of the invasive pressure and MRI volume curves, were imposed. The coupled momentum method was used to model blood flow in 3D-deformable arteries. A validated model of coronary metabolic autoregulation ensured physiological coronary flow. Several scenarios virtually investigating decreasing levels of RVEVC experienced by the RCA due to pharmacological intervention were performed to explore flow changes.

Results: RCA diastolic flow dominates with increasing RVEVC becoming morphologically akin to LCA flow (figure 2). There is a strong correlation between the RCA peak systolic to peak diastolic flow ratio (PSPD) and RVEVC (R^2=0.974), with increases in PSPD with decreasing levels of RV afterload (figure 3). Therefore, we hypothesize that morphologic RCA flow waveform changes may be indicative of the severity of PH. Within the typical RV afterload changes of 5-10% seen with pharmacological intervention, RCA flow changes are relatively small (0.4-0.8%). PSPD should be investigated for inclusions in models to assess the efficacy of PH advanced therapy.

Conclusions: Biphasic RCA flow pathomorphology with dominant diastolic coronary perfusion occurs in PH and is relieved with decreasing RVEVC in a computational model of PH. This patient-specific computational model can be used to gain insight into pathophysiological biomechanical adaptations in coronary flow as a potential disease biomarker in PH.

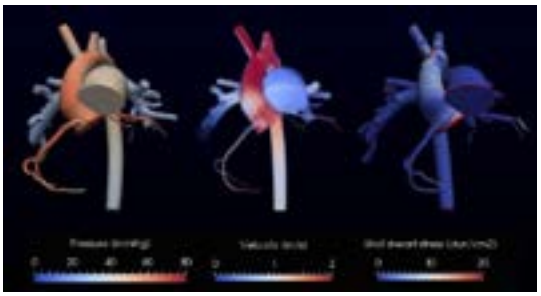

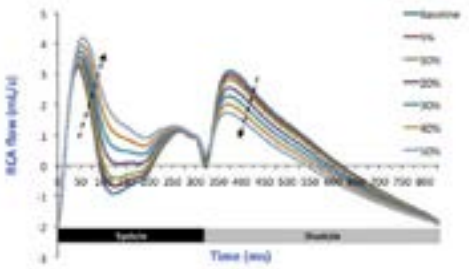

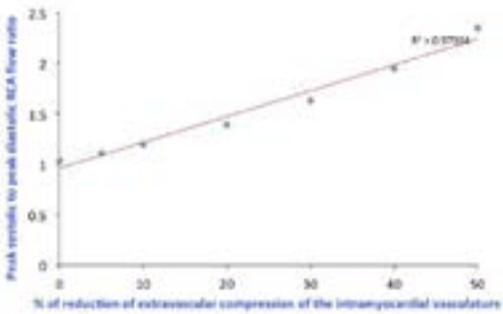

F048

Diagnostic performance of comprehensive 3.0T CMR with stress in detecting coronary artery disease: High additive value of free-breathing coronary MRA.

Mineka Yamazoe, MD[1]Masaki Ishida, MD[1], Akimasa Yamada, MD[2], Yoshitaka Goto, MD[3], Mio Uno, MD[4], Wakana Makino, MD[1], Motonori Nagata, MD[3], Yasutaka Ichikawa, MD[1], Kakuya Kitagawa, MD[5], Hajime Sakuma, MD[6]

1. *Radiology, Mie, Japan*
2. *Radiology, Tsu, Mie, Japan*
3. *Department of Radiology, Mie University Hospital, Tsu, Mie, Japan*
4. *Department of Radiology Mie university hospital, Tsu, Mie, Japan*
5. *Department of Radiology Mie university hospital, Mie, Japan*
6. *Department of Radiology, Mie University Hospital, Mie, Japan*

Background: Cardiac MRI (CMR) including stress-rest perfusion (PERF) and late gadolinium enhancement CMR (LGE) have shown to provide accurate detection of myocardial ischemia and infarction. Recently, the diagnostic performance of 3.0T contrast-enhanced free-breathing coronary MRA (CMRA) in detecting significant coronary artery disease (CAD) has been substantially improved. However, the additive value of CMRA to PERF and LGE remains uncertain at 3.0T. The purpose of this study was to evaluate the diagnostic value of comprehensive assessment of LGE, PERF and CMRA using 3.0T MR imager for detecting significant CAD.

Methods: 416 consecutive patients with known or suspected CAD were prospectively referred for comprehensive 3.0T CMR including PERF, LGE and CMRA. 77 of 416 patients (age, 79 ± 9 years) who underwent catheter coronary angiography within 3 months from CMR were retrospectively evaluated. The presence or absence of abnormality suggestive of CAD on LGE, PERF and CMRA and the combination of LGE/PERF and LGE/PERF/CMRA was assessed by binary reading and by using 5-point scale, separately, by two independent observers. CMR images were displayed side-by-side for the combinations. In case of disagreement, consensus by two observers was sought. Significant CAD was defined as luminal narrowing of >50% on catheter coronary angiogram. The vessels with stents (n=35) were excluded from analysis.

Results: The success rate of CMRA was 97.6% (406/416). CMRA was diagnostic for all coronary arteries except for segments with stents. The vessel-based prevalence of significant CAD was 35.9%on coronary angiography. On the vessel based analysis, the area under the ROC curves (AUC) for LGE/PERF/CMRA (0.903) was significantly higher than that for LGE/PERF (0.826 p=0.016) and that for LGE only (0.593, $p < 0.0001$) (Figure 1). The sensitivity, specificity, accuracy and inter-observer agreement for LGE/PERF/CMRA, LGE/PERF and LGE only were summarized in Table 1. LGE/PERF/CMRA exhibited an excellent sensitivity (91.7%) which was significantly higher than that by LGE/PERF (72.2%, p=0.0026), while the specificity was similar between LGE/PERF/CMRA and LGE/PERF (84.7% and 90.3%, p=0.1185). Inter-observer agreement for LGE/PERF/CMRA (K=0.812) was greater than that for LGE/PERF (K=0.706).

Conclusions: The results of the current study demonstrated that the diagnostic performance of 3.0T comprehensive CMR including stress and rest perfusion CMR and LGE CMR can be significantly improved by adding free-breathing contrast enhanced coronary MRA for the detection of significant CAD with an improved inter-observer agreement.

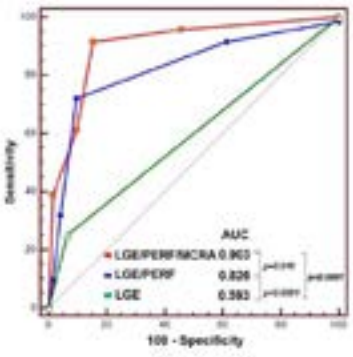

	Sensitivity (%)	Specificity (%)	Accuracy (%)	K
LGE	25.0	93.5	68.4	-
LGE/PERF	72.2	90.3	84.8	0.706
LGE/PERF/CMRA	91.7	84.7	87.2	0.812

$^{a}p<0.0001$, $^{b}p=0.0026$, $^{c}p=0.0347$, $^{d}p=0.0002$

F049

Lipid insensitive free-breathing self-navigated coronary MR angiography at 3T using a novel water excitation method

Jessica A.M. Bastiaansen, PhD[1] Davide Piccini, PhD[2], Ruud van Heeswijk, PhD[3], Jerome Yerly, PhD[4], Matthias Stuber, PhD[5]

1. *Department of Radiology, University Hospital (CHUV) and University of Lausanne (UNIL), Lausanne, Vaud, Switzerland*
2. *Advanced Clinical Imaging Technology, Siemens Healthcare, Vaud, Switzerland*
3. *Department of Radiology, University Hospital (CHUV) and University of Lausanne, Vaud, Switzerland*
4. *CIBM / CHUV / UNIL, Fribourg, Switzerland*
5. *CHUV, University of Lausanne, Geneve, Switzerland*

Background: Robust and homogeneous lipid suppression is mandatory for coronary MRA since coronary arteries are commonly embedded in fat. Incomplete fat suppression hinders a correct visualization of the coronary vessels, and complicates the use of advanced motion correction methods. Therefore, we developed a novel lipid insensitive binomial off-resonant excitation (LIBRE) pulse for respiratory self-navigated whole-heart coronary MRA at 3T, and assessed image quality in comparison to commonly used lipid-suppression methods in healthy volunteers.

Methods: LIBRE pulses were implemented in a prototype respiratory-self-navigated free-breathing 3D radial MRI sequence with T2 preparation (Fig 1a)[1-3]. LIBRE was optimized in simulations and phantoms, its efficacy compared with conventional methods in vitro, before performing contrast-free coronary MRA in (n=10) healthy volunteers on a 3T clinical scanner. Data were 1D motion-corrected using the projection image of the thorax [1]. One data set was reconstructed using respiratory-motion-resolved k-t-sparse SENSE [5]. Three scans were performed in volunteers: 1) conventional fat saturation (FS), 2) conventional binomial water excitation (WE), 3) the LIBRE pulses. Signal-to-noise ratios (SNR) of phantom agar and oil compartments were computed in ImageJ. SNR of blood, myocardium and fat, blood-myocardium and blood-fat contrast-to-noise ratio (CNR) were computed (SoapBubble [4]) together with the vessel sharpness of the right coronary artery (RCA). Statistics included a paired two-tailed student's t-test corrected for multiple comparisons.

Results: Simulations show a range of LIBRE parameters (Fig 1b) for optimal fat suppression that were confirmed in experiments in vitro (Fig 1c). Its flexible design allows pulse durations as short as 1.4 ms and in vitro LIBRE enables more effective fat nulling than WE (Fig 1c-d, $p < 0.05$) or FS (Fig 1d, $p < 0.05$).

In vivo, LIBRE achieves a near complete suppression of the chest fat (Fig 2a) and also lead to a high contrast between the coronary lumen blood-pool and epicardial fat (Fig 2b&e). Further, they provide a clean tracking signal for the self-navigation algorithm (data not shown).

A distinct visual difference among the three methods in reformatted images of the RCA is apparent (Fig 2b). These visual findings are corroborated by quantitative endpoints (SNR, CNR, Fig 2d-e) that were significantly improved for the LIBRE method ($p < 0.05$). RCA vessel sharpness also increased by 30% for LIBRE (Fig 2f, $p < 0.05$). Excellent image quality with a high degree of fat suppression was also obtained using respiratory-motion-resolved reconstruction (Fig 2c).

Conclusions: LIBRE pulses achieve improved fat saturation for coronary imaging at 3T, higher CNR of blood/myocardium and increased vessel sharpness, leading to improved visualization of the coronary arteries compared with conventional methods. Respiratory and cardiac self-navigation may particularly benefit from the improved efficacy of this novel pulse.

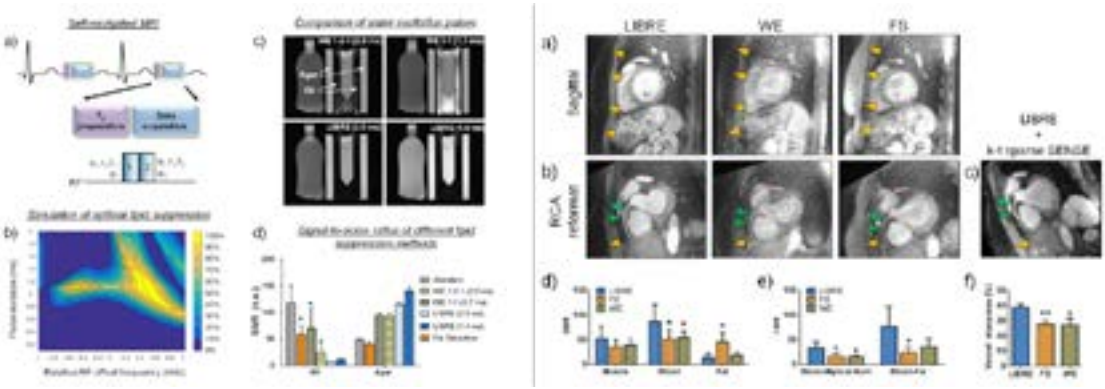

References [1] Piccini *et al*., Radiology 270:378-386 (2014). [2] Piccini *et al*., Magn Reson Med 68:571-579 (2012). [3] Nezafat *et al*., Magn Reson Med 55:858-864 (2006). [4] Ebsenne *et al*., Magn Reson Med 48:658-666(2002) [5] Piccini *et al*., Magn Reson Med. In Press (2016)

Acknowledgements Center for biomedical imaging, Lausanne, Switzerland (CIBM), Nanotera

F050

Magnetic Resonance Angiography to Assess Anomalous Coronary Arteries in Children at 3-Tesla: Diagnosis, Risk Stratification, and Interobserver Reliability.

Steve Muyskens, M.D., F.A.C.C.[1] Keegan Olmstead, B.S.[2], Tyler Hamby, Ph.D.[3], Lisa Roten, M.D.[1]

1. *Cook Children's Medical Center, Fort Worth, TX*
2. *University of North Texas Health Science Center - Texas College of Osteopathic Medicine, TX*
3. *Cook Children's Medical Center, TX*

Background: Anomalous aortic origin of the coronary arteries (AAOCA) is the second most common cause of sudden cardiac death (SCD) in young athletes. The prevalence, pathophysiology, and optimal method of evaluating AAOCA are unknown. The reliability of coronary magnetic resonance angiography (MRA) in assessing AAOCA, and the use of contrast enhanced coronary MRA in children at 3-Tesla has not been well described. We present our institutional experience using a 3-dimensional (3D) IR-FLASH sequence with slow gadolinium infusion and respiratory navigation at 3-Tesla to diagnose and risk stratify AAOCA in children.

Methods: A retrospective review was conducted of all MRA patients referred for possible AAOCA between January 1, 2011 and May 9, 2016. Patients with complex congenital heart disease were excluded. Coronary anomalies with an intramural or interarterial course were classified as high risk, and a high aortic origin or intraseptal course were classified as low risk. Completed studies were anonymized and evaluated by two blinded independent observers for image quality, diagnosis of AAOCA, intramural course, and interarterial course using a Likert-scale formatted response. Reliability analyses, utilizing kappa, assessed diagnostic agreement between raters. MRA and surgical findings were compared in patients with AAOCA repair.

Results: Fifty-nine patients were referred for suspected AAOCA (median age 13.79 years, range 5.19 – 19.84, 73% male). One case was not completed secondary to ventricular ectopy. For 58 successfully acquired angiograms, 31 were high risk, 11 were low risk, and 16 were normal. Overall image quality was rated good to excellent. The two raters showed excellent agreement on image quality, $\kappa = .85$ (93%), diagnosis of AAOCA, $\kappa = .81$ (91%), and diagnosis of proximal interarterial course, $\kappa = .81$ (88%). There was moderate agreement about diagnosis of intramural course, $\kappa = .63$ (74%). For all 11 cases with surgical repair, the combined MRA ratings correctly diagnosed the presence of AAOCA and interarterial course. The presence of an intramural course was correctly rated in all 9 cases, while the absence of an intramural course was correctly rated in 1 of 2 cases.

Conclusions: Coronary MRA using 3D IR-FLASH with slow contrast infusion at 3-Tesla showed high inter-rater reliability for diagnosing and characterizing AAOCA in pediatrics. Furthermore, findings were validated at time of surgical repair. This protocol is an effective means to examine AAOCA in pediatric patients and help stratify those who may be at high risk of SCD.

O001

ECV Imaging In Left Ventricular Hypertrophy: Cell And Matrix Expansion Have Disease-Specific Relationships

Thomas Treibel, MBBS.MRCP(UK)[1] Rebecca Kozor, MBBS[2], Katia Menacho-Medina, MD[1], Marianna Fontana, MD, PhD[3], Viviana Maestrini, MD[4], Silvia Castelletti, MD[5], Stefania Rosmini, MD, PhD[1], Sabrina Nordin, MBBS[1], Amna Abdel-Gadir, MBBS. MRCP(UK)[6], Anish Bhuva, MRCP MBBS[1], Heerajnarain Bulluck, MBBS[7], Anna Herrey, MD PhD MRCP[1], Charlotte Manisty, PhD MBBS[8], James C Moon, MD[1]

1. *Barts Heart Centre, England, United Kingdom*
2. *Royal North Shore Hospital, Sydney, New South Wales, Australia*
3. *National Amyloidosis Centre, University College London, England, United Kingdom*
4. *Sapienza University of Rome, Lazio, Italy*
5. *UCL, N/A, Italy*
6. *University College London and Barts Heart Centre, London, England, United Kingdom*
7. *University College London, England, United Kingdom*
8. *Barts Heart Centre and university college, London, England, United Kingdom*

Background: Cardiac remodeling in health and disease is categorized histologically into cellular (cell death/hypertrophy) and extracellular matrix (fibrosis/infiltration) processes, whereas cardiac imaging traditionally combines both compartments into left ventricular mass (LVM). We used CMR extracellular volume fraction (ECV) to dichotomize LVM into cellular and matrix components across conditions with left ventricular hypertrophy (LVH) as well as healthy volunteers.

Methods: 168 subjects underwent CMR with T1 mapping (ShMOLLI) at 1.5T: Healthy volunteers (HV, n=30), young athletes (YA, n=28), severe aortic stenosis awaiting valve replacement (AS, n=30), Fabry Disease (FD, n=20), hypertrophic cardiomyopathy (HCM, n=30), and cardiac amyloidosis (n=30, all ATTR). ECV was derived from pre- and post-contrast short axis T1 maps and blood hematocrit. To obtain matrix and cell volume, ECV and (1-ECV) were multiplied by the LV myocardial volume (LVM/1.05g), respectively.

Results: LVM progressively increased from health and physiological hypertrophy (HV<YA<AS<HCM<FD<ATTR, $p < 0.001$; Table 1). For each etiology apart from amyloid, cell and matrix volumes correlated strongly (R^2=0.6 to 0.8, all $p < 0.01$; Figure 1), each etiology with a slightly different regression slope: Athletes displayed greater cell hypertrophy than HV, whereas matrix expansion predominated in the other diseases compared to HV, with increasing contribution across the diseases: FD<AS<HCM<ATTR. In ATTR amyloid, LVM was predominantly driven by ECM expansion.

Conclusions: With hypertrophy, most diseases have slightly more matrix expansion than cellular hypertrophy – with two exceptions: firstly, athletes (cell>matrix) and secondly amyloid (matrix>cell). Assessing this ratio gives insight into LVH disease biology.

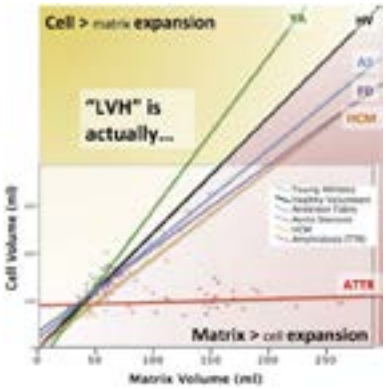

Patient characteristics

Cardiac Amyloidosis	**Fabry** Disease	Hypertrophic Cardiomyopathy	Aortic Stenosis	Young Athletes	Healthy Volunteers	
30	20	30	30	28	30	n
76±7	51±9	50±16	74±6	31±4	41±11	Age (years)
93%	75%	57%	66%	46%	44%	Male
257±57	233±92	207±94	187±33	167±42	98±26	LV mass (g)
60.5±7.8	29.8±4.0	33.1±5.2	28.5±2.5	26.8±2.8	28.0±2.9	ECV (%)
99±20	163±64	139±65	134±24	123±34	71±20	Cell volume (ml)
158±50	69±29	68±32	53±10	44±9	27±7	Matrix volume (ml)

O002

Regression of cardiac AL amyloid following chemotherapy demonstrated by cardiovascular magnetic resonance

Ana Martinez-Naharro, MD[1] Amna Abdel-Gadir, MBBS.MRCP(UK)[2], Thomas Treibel, MBBS.MRCP(UK)[3], Giulia Zumbo, MD[4], Daniel S. Knight, MBBS MRCP(UK)[5], Stefania Rosmini, MD, PhD[3], Thirusha Lane, MD[4], Shameem Mahmood, FRCPath[4], Sajitha Sachchithanantham, FRCPath[6], Carol Whelan, MD[4], Helen Lachmann, MD[4], Ashutosh Wechalekar, MD[4], Peter Kellman, PhD[7], Julian Gillmore, MD, PhD[4], James Moon, MBBS, MD, MRCP[8], Philip Hawkins, PhD[4], Marianna Fontana, MD, PhD[4]

1. *National Amyloidosis Centre, University College London, London, England, United Kingdom*
2. *University College London and Barts Heart Centre, London, England, United Kingdom*
3. *Barts Heart Centre, England, United Kingdom*
4. *National Amyloidosis Centre, University College London, England, United Kingdom*
5. *Royal Free London NHS Foundation Trust, London, England, United Kingdom*
6. *University College London, National Amyloidosis Centre, N/A, United Kingdom*
7. *Laboratory of Cardiac Energetics, National Institutes of Health/NHLBI, Bethesda, MD, United States., MD*
8. *Barts Heart Center, The Cardiovascular Magnetic Resonance Imaging Unit and The Center for Rare Cardiovascular Diseases Unit, St Bartholomew's Hospital, West Smithfield, London, UK, England, United Kingdom*

Background: Cardiac involvement in immunoglobulin light chain (AL) amyloidosis is the major determinant of survival; Cardiac response to chemotherapy is conventionally assessed by serum brain natriuretic peptide (NT-proBNP) and echocardiography, but neither quantify amyloid burden. The aim of this study was to evaluate cardiac AL amyloid serially using cardiovascular MR (CMR) including extracellular volume measurement (ECV), which is the site of the amyloid deposits.

Methods: 31 patients with cardiac AL amyloidosis who had chemotherapy were studied serially using ECG, echocardiography, ^{123}I-labeled serum amyloid P component (SAP) scintigraphy, NT-proBNP measurements and CMR with T1 mapping and ECV measurements (mean interval 20±11months).

Results: Nineteen patients achieved a complete or very good partial haematological response (CR n=10; VGPR n=9). Twelve patients attained a partial response (PR) or no response (NR). Among patients in CR or VGPR there was regression of amyloid in 12 (92%) compared to 1 (8%) patient who achieved a PR or NR ($p < 0.01$) as evidenced by reduction in the ECV. Changes in the ECV consistent with regression of amyloid were concordant with the reduction in amyloid volume and in 5 patients with changes in late gadolinium enhancement pattern. Overall there was significant reduction in NT-proBNP concentration, LV mass, left atrial area and improvement in diastolic function in patients whose amyloid burden decreased. Regression of cardiac amyloid by CMR correlated with regression of amyloid in other organs measured by SAP scintigraphy.

Conclusions: CMR with T1 mapping and ECV measurements demonstrates that cardiac AL amyloid deposits frequently regress following chemotherapy that substantially suppresses clonal light chain production.

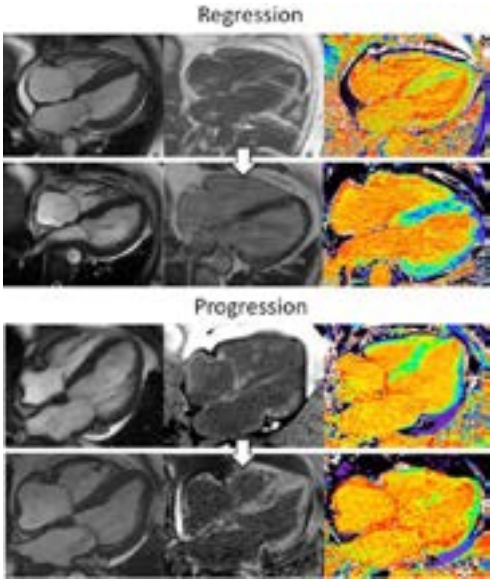

O003

Dual identity of the interventricular septum with in vivo diffusion tensor imaging

Pedro F. Ferreira, PhD[1]Sonia Nielles-Vallespin, PhD, MSc[2], Andrew D. Scott, PhD[3], Zohya Khalique, MBBS[4], Dudley J. Pennell, MD[5], David N. Firmin, PhD[6]

1. *Cardiovascular Biomedical Research Unit, The Royal Brompton Hospital, Sydney Street, London, SW3 6NP, UK, England, United Kingdom*
2. *NIH, MD*
3. *NIHR Cardiovascular Biomedical Research Unit, The Royal Brompton Hospital, Sydney Street, London, SW3 6NP, UK, England, United Kingdom*
4. *NIHR Cardiovascular Biomedical Research Unit, Royal Brompton Hospital, London, England, United Kingdom*
5. *Royal Brompton Hospital and Imperial College, London, England, United Kingdom*
6. *NIHR Cardiovascular Biomedical Research Unit, Royal Brompton Hospital, England, United Kingdom*

Background: The right and left ventricle form separately in early stages of cardiogenesis, resulting in a dual inter-ventricular septum (IVS) [1]. In the fully formed human heart, the two ventricles are coupled together and its shape and curvature are defined by biventricular pressure and volume. In this work we compare the myocyte and sheetlet microstructure in the IVS and free-wall in healthy and HCM hearts with in vivo diffusion tensor imaging (DTI).

Methods: DTI data of a mid-ventricular slice from 19 healthy and 13 HCM hearts scanned during the systolic pause was used. A STEAM sequence: 6 diffusion directions at b = 600 and 150 s/mm2, fat saturation, TR=2RR-intervals, TE=23 ms, SENSE (2 x acceleration), echo train duration 13 ms, reconstructed spatial resolution = 1.4 × 1.4 mm2, 10–15 averages. Diffusion tensor orientation parameters for the primary (HA, myocyte orientation) and secondary (E2A, sheetlet orientation) eigenvectors were calculated. Three left ventricular regions were delineated based on the HA image: The free-wall, distal to the RV. The septal segment containing only the same myocyte orientations as the free-wall, considered to be the LV septum (ROI1). Finally, the entire interventricular septal wall (ROI2) (figure 1).

Results: The LV septum comprises approximately 80% of the total IVS thickness. The range of HA angles of the entire IVS wall (ROI2) is significantly higher than the free-wall (table 1). Both the free-wall and entire septum show smooth transmural transition of myocyte orientations, although with the higher range of HAs in the IVS, the myocytes wrap back to positive angles on the RV side, not seen on the epicardium of the free wall (figure 2). Additionally, there are consistently lower E2As for the epicardial layer, especially for the RV side when considering the entire IVS (figure 1 & 3).

Conclusions: DTI has shown that the right-side of the IVS has myocyte orientations not seen in the free-wall, and lower E2As. There was no obvious interventricular border, although these microstructural differences may indicate an RV identity to this region. Cardiac MR analysis quite often involves the delineation of the LV. Even though there is no clear delineation of the septal LV, even microstructurally, the dual identity of the IVS must be considered, as there are clear implications for many different MR derived parameters.

References: [1]- Franco D et al.*Dev Biol* (2006): 366

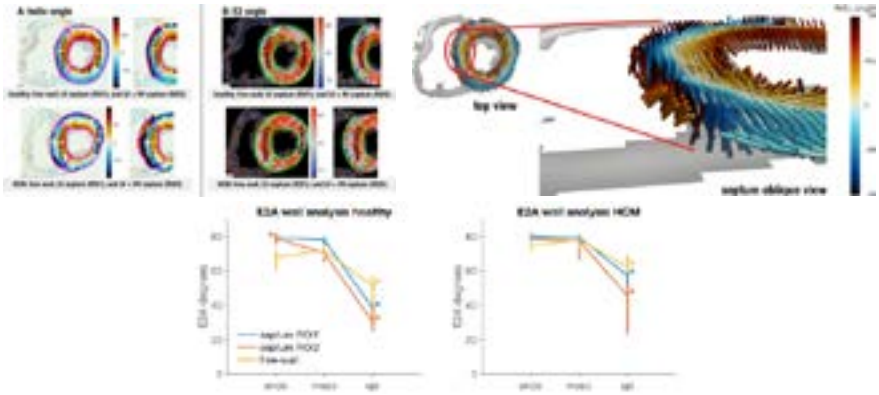

Wall thickness and HA range

HA range (degrees)				Wall thickness (mm)				
p value	HCM	p value	controls	p value	HCM	p value	controls	
0.33	104 [14]	0.19	96 [17]	0.54	18.1 [3.8]	0.88	11.0 [1.3]	septum ROI1
0.006	115 [23]	< 0.001	119 [16]	0.006	21.7 [4.0]	< 0.001	13.4 [4.6]	septum ROI2
-	99 [13]	-	91 [20]	-	17.2 [4.2]	-	10.7 [1.8]	free-wall

Median [interquartile range] wall thickness and HA range for ROI1, ROI2, and free-wall. ROI2 which comprises the entire IVS is significantly different to the free-wall for all measures.

O004

A MRI-based Algorithm for Pattern Recognition and Machine Learning of 3D Myocardial Strains for Classifying Disease Status in Dilated Cardiomyopathy

Julia Kar, PhD[1]Michael K. Pasque, MD[2], Brian P. Cupps, PhD[2], Daniel Koerner, none[3], Jennifer Bell, RN[1], Heidi Craddock, RN[1]

1. *Washington University, MO*
2. *Washington University, St. Louis, MO*
3. *Missouri State, MO*

Background: To develop an automated pattern recognition and machine learning system for predicting disease status (progressive failure or recovery) in non-ischemic, non-valvular dilated cardiomyopathy (DCM), implemented via a support vector machine (SVM) algorithm that was initially trained with regional myocardial multi-parametric (3D) strain predictors and physician assigned binary classifications of disease status.

Methods: Three-dimensional displacement data in DCM patients (N=31) were acquired with Navigator-gated 3D Spiral DENSE and Spatial Modulation of Magnetization (SPAMM) sequences in a 1.5 T MRI machine. Images from both sequences were analyzed with the MR Analytical Software System (MASS) for semi-automated boundary detection and automated meshfree Radial Point Interpolation Method (RPIM) was used to compute LV myocardial strains. A SVM-based pattern recognition system, with a non-linear radial basis function kernel, was created with 3D myocardial strains from 16 left-ventricular sub-regions as predictors and physician-based diagnosis of failure/recovery as the classifier. A residual sum of squares sequential feature selection algorithm ensured that an optimal combination of strain-based predictors were selected for generating the model. K-fold (k=3) cross-validation tests were conducted to assess the accuracy of the SVM model. The accuracy, sensitivity, specificity and the area under the receiver operator curve (ROC) from all folds were computed to test the effectiveness of classification.

Results: A 34-dimensional hyperplane of separation was generated following sequential feature selection , which separated the heterogeneous strains related to progressive failure in DCM from its counterparts in recovery. K-fold cross-validation results showed overall predictive accuracy of 0.97 ± 0.02, sensitivity of 0.82 ± 0.09, specificity of 0.92 ± 0.07 and 0.97 ± 0.03 for area under the ROC curves.

Conclusions: A SVM-based machine learning algorithm, initially trained with regional multi-parametric strain predictors and physician-based binary classifications of disease progression, could lead to the creation of a strain-based pattern recognition model that can predict the status of recovery or failure in new DCM patients.

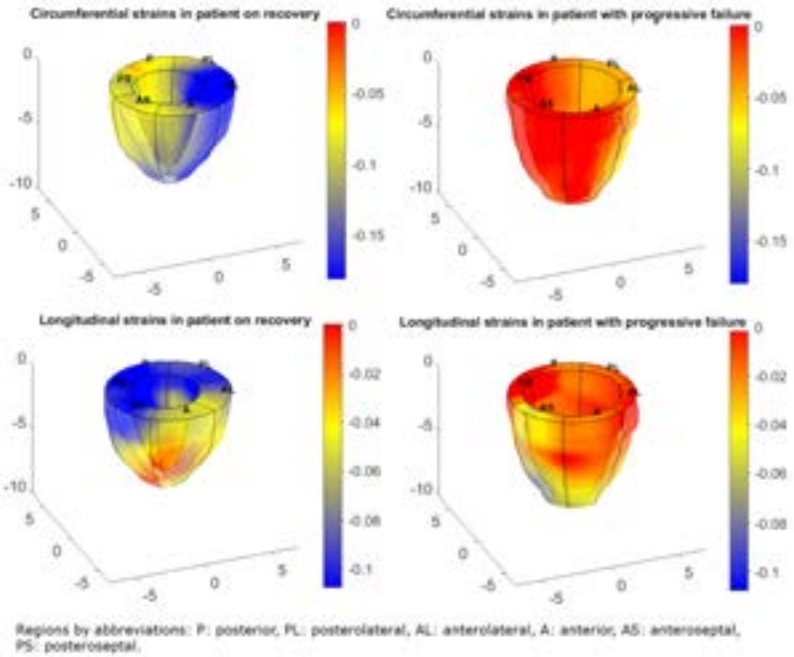

O005

Prediction of Adverse Cardiovascular Outcomes in Patients with Mild Dilated Cardiomyopathy using Cardiovascular Magnetic Resonance

Brian Halliday, BSc (Hons) MBChB (Hons)[1]Ankur Gulati, MD[2], Aamir Ali, MBBS[2], Monika Arzanauskaite[3], Simon Newsome, MA MSc[4], Amrit Lota, BMBCh BA[5], Vassilis Vassiliou, MBBS[2], Upasana Tayal, BMBCh[2], Stuart Cook, PhD[6], Dudley J. Pennell, MD[7], John Cleland, MD PhD[6], Sanjay Prasad, MD[7]

1. *Royal Brompton Hospital and National Heart and Lung Institute, Imperial College London, London, England, United Kingdom*
2. *Royal Brompton Hospital, England, United Kingdom*
3. *Royal Brompton Hospital, London, England, United Kingdom*
4. *London School of Hygiene and Tropical Medicine, England, United Kingdom*
5. *NIHR Royal Brompton Cardiovascular Biomedical Research Unit and National Heart and Lung Institute, Imperial College London, England, United Kingdom*
6. *Imperial College, London, England, United Kingdom*
7. *Royal Brompton Hospital and Imperial College, London, England, United Kingdom*

Background: Dilated cardiomyopathy (DCM) is a common cause of heart failure and sudden death. Pharmacological therapy reduces morbidity and mortality in patients with reduced left ventricular ejection fraction (LVEF) and is recommended in guidelines for patients with a LVEF < 40%. However, patients with a LVEF≥40% remain at risk of adverse outcomes. We aimed to identify markers of adverse cardiovascular (CV) outcomes from cardiovascular magnetic resonance (CMR) in patients with DCM and a LVEF≥40% with the aim of being able to prioritise those at greatest risk.

Methods: We prospectively investigated markers of adverse cardiovascular outcomes in consecutive patients with DCM and a LVEF≥40% referred for CMR imaging between 2000 and 2011. The primary composite end-point was CV death, CV hospitalisation and transplantation. All outcome events were adjudicated by a panel of physicians blinded to the CMR results. Left atrial volume was calculated by the biplane area-length method by two operators and indexed against body surface area (LAVi). Mid-wall fibrosis was determined by a blinded expert operator.

Results: In total, 432 patients (273 male, median LVEF 50%, median right ventricular ejection fraction (RVEF) 57%, median LAVi 52.8ml/m^2, median age 50 years) were followed-up for a median of 4.5 years. There were 20 CV deaths (16 sudden cardiac death and 4 deaths secondary to heart failure), 2 cardiac transplantations and 51 unplanned CV hospitalisations. In univariable analyses the presence of mid-wall fibrosis (HR 3.1; 95% CI 1.9-4.8; p < 0.0001) (Figure 1) and higher LAVi (per 10ml/m^2 increase: HR 1.19; 95% CI 1.10:1.28; p < 0.0001) (Figure 2) predicted the occurrence of the primary end-point while higher left ventricular ejection fraction (LVEF; per 10% increase: HR 0.41; 95% CI 0.26:0.64; p=0.0001) was associated with freedom from the primary end-point. This remained the case after adjustment for these variables in multivariable analysis together with NYHA class, age and gender (LAVi: per 10ml/m^2 increase: HR 1.17, 95% CI 1.09:1.25, p < 0.0001; LGE: HR 2.9, 95% CI 1.8:4.7, p < 0.0001; LVEF: per 10% increase: HR 0.48, 95% CI 0.29:0.82, p=0.007). RVEF was not associated with the primary end-point in univariable analysis.

Conclusions: Mid-wall fibrosis, elevated LAVi and reduced LVEF predict adverse cardiovascular outcomes in patients with dilated cardiomyopathy and LVEF>40%. Patients with these features should undergo close clinical follow-up and pharmacological therapy may be considered at an earlier stage.

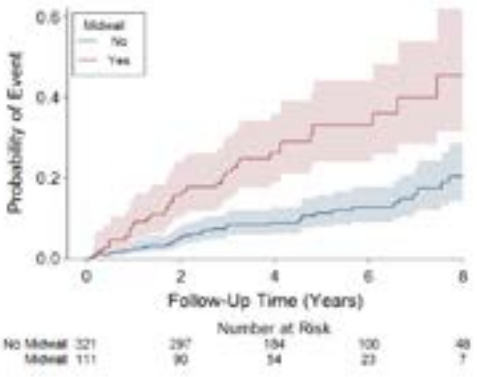

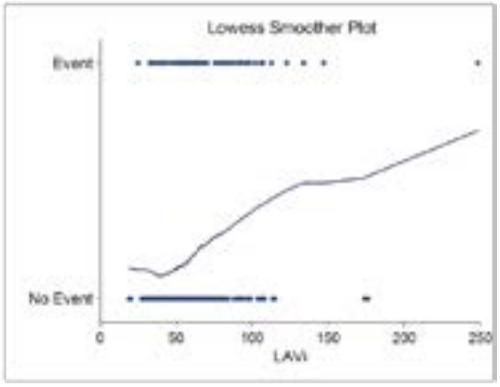

O006

Early changes of native T1 time predict development of subsequent anthracycline-induced cardiomyopathy with impaired systolic function

Fabian Muehlberg, MD[1]Stephanie Funk, MD[2], Leonora Zange, MD[1], Alexander Schulz[2], Florian von Knobelsdorff-Brenkenhoff, MD[3], Edyta Blaszczyk, MD[2], Saeed Ghani, MD[4], Annette Reichardt, MD[4], Jeanette Schulz-Menger, MD[5]

1. *Working Group on Cardiovascular Magnetic Resonance, Experimental and Clinical Research Center, a joint cooperation between the Charité Medical Faculty and the Max-Delbrueck Center for Molecular Medicine and HELIOS Hospital Berlin Buch, Berlin, Berlin, Berlin, Germany*
2. *Working Group on Cardiovascular Magnetic Resonance, Experimental and Clinical Research Center, a joint cooperation between the Charité Medical Faculty and the Max-Delbrueck Center for Molecular Medicine and HELIOS Hospital Berlin Buch, Berlin, Berlin, Germany*
3. *Cardiology at Clinic Agatharied, University of Munich, Hausham, Bayern, Germany*
4. *HELIOS Clinic Berlin-Buch, Berlin, Berlin, Germany*
5. *Working Group on Cardiovascular Magnetic Resonance, Experimental and Clinical Research Center a joint cooperation between the Charité Medical Faculty and the Max-Delbrueck Center for Molecular Medicine HELIOS Klinikum Berlin Buch, Germany, Berlin, Germany*

Background: Anthracyclines are the mainstay of treatment of a variety of malignancies. However, the clinical use of these drugs is limited by its cardiotoxicity, which can lead to severe anthracyline-induced cardiomyopathy (aCMP). Aim of this study was to assess the value of subclinical changes in functional and morphologic myocardial MR parameters to predict subsequent development of aCMP.

Methods: Sarcoma patients prepared for anthracycline-based chemotherapy (300-450mg/m^2 doxorubicin-equivalent) were screened and prospectively enrolled. Study individuals received at least three CMR studies (before treatment, 48 hours after first anthracycline treatment and upon completion of treatment). Native T1 mapping (MOLLI 5s(3s)3s), T2 mapping, and extracellular volume (ECV) maps were acquired in addition to a conventional CMR with SSFP-cine imaging at 1.5 Tesla (SIEMENS, Germany). Patients were given 0.2mmol/kg gadoteridol for ECV quantification and LGE imaging. CVI42® (Circle CVI, Canada) was used for post-processing. Development of relevant aCMP was defined as drop of left ventricular ejection fraction (LVEF) by >10%.

Results: 26 patients with mean age of 61.2±13.5 years were enrolled. 54% were female. Eight patients developed aCMP with LVEF reduction >10% between baseline CMR and CMR at the end of chemotherapy (Figure 1). Baseline LVEF was not different between patients with and without subsequent aCMP (63.7±6.1% vs. 59,7±9.3%, p=0.30). When assessed 48 hours after first dose of antracyclines, patients with subsequent aCMP had significantly lower native myocardial T1 times compared to before therapy (998.1±36.8ms vs. 953.6±26.7ms, p=0.001) than patients who did not develop aCMP (986.3±52.4ms vs. 975.3±49.4ms, p>0.05) (Figure 2). There was a positive correlation (r^2=0.48) of change of T1 after first anthracycline treatment and change of LVEF over the entire course of chemotherapy (Figure 3). LVEF increased at 48 hours after start of therapy in patients who did not develop aCMP (59.7±9.3% before treatment vs. 64.1±7.2% after first treatment, p=0.01) while LVEF in patients with development of subsequent aCMP did not increase (63.7±6.1% vs. 63.2±8.1%, p>0.05). Heart rate, T2 times, ECV and left atrial volume did not change after first treatment in either group and showed no difference between the groups (Table 1). No patient developed new LGE under chemotherapy.

Conclusions: Early decrease of native myocardial T1 times 48 hours after first treatment with anthracyclines can predict the development of subsequent aCMP several months later. Non-contrast CMR may provide a valuable tool to screen for patients at high risk for developing aCMP in the future.

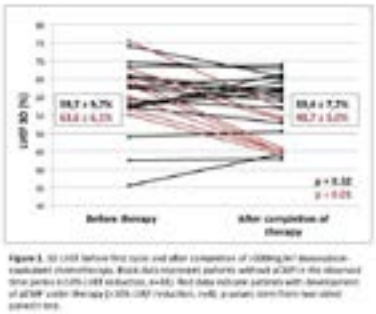

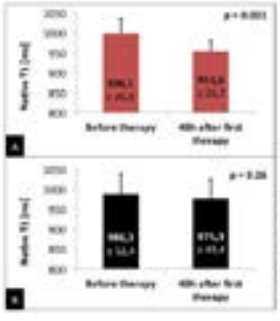

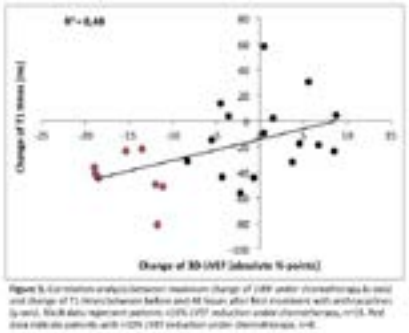

Table 1 - Mean ± SD of functional and morphologic parameters before and 48 hours after first treatment with anthracyclines.

Patients without subsequent aCMP				**Patients with subsequent aCMP**				
p values	**48 hours after first therapy**	**Before chemotherapy**		**p values**	**48 hours after first therapy**	**Before chemotherapy**		
p = 0.02	171.7 ± 46.3	156.3 ± 40.3		p > 0.05	165.6 ± 35.0	151.9 ± 29.6	*[ml]*	**LV-EDV**
p = 0.01	64.1 ± 7.2	59.7 ± 9.3		p > 0.05	63.2 ± 8.1	63.7 ± 6.1	*[%]*	**LV-EF**
p > 0.05	80.0 ± 28.7	73.0 ± 20.8		p > 0.05	78.3 ± 13.9	70.6 ± 15.9	*[ml]*	**LA volume**
p > 0.05	54.3 ± 2.8	53.0 ± 3.9		p > 0.05	55.6 ± 1.5	54.1 ± 2.7	*[ms]*	**T2**
p > 0.05	27.1 ± 1.8	27.6 ± 6.5		p > 0.05	29.6 ± 2.6	26.9 ± 5.2	*[%]*	**ECV**
p > 0.05	66.1 ± 10.7	67.9 ± 15.2		p > 0.05	71.3 ± 11.3	69.5 ± 11.7	$[min^{-1}]$	**Heart rate**

O007

Burden of Trabecular and Papillary-Muscle Volume is Not Associated with Incident Adverse Cardiovascular Disease Events

Michael L. Chuang, MD[1]Philimon N. Gona, PhD[2], Saadia Qazi, DO, MPH[3], Carol J. Salton, AB[4], Christopher J. O'Donnell, MD MPH[5], Warren J. Manning, MD[6]

1. *Framingham Heart Study, Framingham, MA*
2. *University of Massachusetts Boston, Framingham, MA*
3. *Boston VA Healthcare, MA*
4. *Beth Israel Deaconess Medical Center, MA*
5. *Boston VA Healthcare, Boston, MA*
6. *Beth Israel Deaconess Medical Center, Boston, MA*

Background: Hypertrabeculation of the left ventricle is a component of left ventricular (LV) noncompaction (LVNC), a cardiomyopathy associated with arrhythmias and cardiac dysfunction, but it is unclear whether LVNC is a distinct disease entity, a morphologic trait common to multiple diseases, or even an extreme normal anatomical variation. We sought to determine whether a high proportion of trabecular and papillary-muscle (TPM) volume relative to LV end-diastolic volume (EDV) was predictive of incident adverse cardiovascular disease (CVD) events in a community-dwelling cohort.

Methods: 1494 Framingham Offspring cohort members (65±9y, 46.8% men) underwent ECG-gated, contiguous multislice LV short-axis bSSFP CMR during 2002-2006 with quantification of TPM volume by custom software using thresholds based on signal intensities of standard (compacted) LV myocardium and the LV bloodpool. LV EDV was determined from manually traced endocardial borders. Proportional burden of TPM was TPM volume/LVEDV, converted to a percentage (%TPM); this obviated the need to index to body or ventricular size. Clinical covariates were collected at the adjacent Offspring cycle-7 examination (1998-2001). Adverse CVD events during follow-up comprised CVD death, myocardial infarction, unstable angina, ischemic stroke, and first admission for heart failure. Seventy Offspring with prevalent (prior to CMR) CVD were excluded. We used multivariable-adjusted Cox proportional hazards models to assess whether %TPM augmented traditional CVD risk factors (age, sex, systolic blood pressure, total and HDL cholesterol, diabetes, smoking, hypertension treatment) for prediction of CVD events.

Results: Women had greater %TPM than men (23.0±3.9 vs 21.1±4.4%, $p < 0.0001$). Over a median 8.4-year follow-up, there were 71/1424 (5.0%) incident CVD events. Offspring experiencing an adverse CVD event had minimally lower %TPM than event-free participants, but differences were borderline with respect to significance among both men (19.9±4.4 vs 21.1±4.4%, p=0.059) and women (21.7±3.7 vs. 23.1±3.8%, p=0.047). Cox models showed greater age (hazard ratio, HR=1.09/year, 95% confidence intervals 1.06 – 1.12) was most strongly associated with incident CVD events, while HDL cholesterol was protective (HR=0.76/10mg/dl, 95%CI 0.63 – 0.93). The addition of %TPM to the Cox model did not affect results, and %TPM itself was nonsignificant (HR=0.97, 95%CI=0.91 – 1.03).

Conclusions: Over 8.4-year follow-up among middle-aged and older community-dwelling adults, %TPM was not predictive of incident adverse CVD events.

O008

In vitro and in vivo effects of CMR on circulating leukocytes

William R. Critchley, BSc MRes[1]Anna Reid, MBChB(Hons) MRCP[2], John P. Stone, BSc MSc[3], Alexandra Ball, MBChB[3], Triin Major, BSc MSc[3], David Clark, BSc[4], Nick Waldron[2], Christien Fortune[2], Jakub Lagan, LEKARZ MRCP[5], Gavin Lewis, MBChB[2], Josephine Naish, PhD[3], Erik B. Schelbert, MD, MS[6], Matthias Schmitt, MD PhD[2], James E. Fildes, PhD[3], Christopher A. Miller, MBChB PhD[2]

1. *University of Manchester, Manchester, England, United Kingdom*
2. *University Hospital of South Manchester, England, United Kingdom*
3. *University of Manchester, England, United Kingdom*
4. *Alliance Medical University Hospital of South Manchester CMR Unit, England, United Kingdom*
5. *University Hospital of South Manchester, Liverpool, England, United Kingdom*
6. *University of Pittsburgh; Heart and Vascular Institute of UPMC, PA*

Background: Since investigators have proposed that CMR should have restrictions similar to those of ionizing imaging techniques, we investigated the acute effect of CMR on leukocyte DNA integrity and cell counts *in vitro*, and in a large cohort of patients *in vivo*. CMR has been reported to induce T cell death via loss of DNA integrity, as evidenced by increased histone H2AX phosphorylation (γ-H2AX) combined with a reduction in circulating T cells post-CMR.

Methods: *In vitro* study: Peripheral blood mononuclear cells (PBMC) were isolated from peripheral blood of 5 healthy volunteers. Each sample was divided and γ-H2AX expression and absolute leukocyte counts were quantified using multiparameter flow cytometry under the following conditions: 1) immediately following PBMC isolation, 2) after a standard CMR viability scan (1.5T Siemens Avanto; 40 minute duration), 3) after standing on the benchside as a temperature and time control. *In vivo* study: Blood samples were taken from consecutive consenting patients immediately before and after a standard clinical viability scan (1.5T Siemens Avanto). All patients received 0.1mmol/kg Gadovist. Samples were analysed for T cell count and γ-H2AX expression using flow cytometry.

Results: CMR scanning was associated with a trend towards an increase in DNA damage (determined via γ-H2AX expression, a marker of DNA double strand breaks) in leukocytes and decrease in absolute leukocyte numbers *in vitro* (Figure 1). The *in vivo* study included 64 patients; 37 (58%) male, age 51±16years, body surface area 2.0±0.3m2. Scan duration 42±11minutes. Scan diagnosis: normal (23; 36%), IHD (10; 16%), cardiomyopathy (26, 40%). CMR was not associated with a significant change in γ-H2AX expression (pre-CMR 8678±3088, post CMR 8412±2734, p=0.47). However there were significant inter-patient variations in T cell DNA damage with both large increases and large decreases seen in γ-H2AX expression following CMR (Figure 2). There was a significant reduction in circulating T cells following CMR (pre-CMR 48% (range 9-72%), post-CMR 44% (4-72%), p=0.02).

Conclusions: In the largest study to date, CMR was not associated with DNA damage *in vivo*. γ-H2AX expression did vary markedly between individuals, therefore studies using γ-H2AX as a marker of DNA damage in small cohorts should be interpreted with caution. CMR was associated with a statistically significant reduction in viable leukocytes, although the clinical relevance of the magnitude, which is small in comparison to natural variation, is unclear. Further work is warranted to contextualize these findings and delineate their impact.

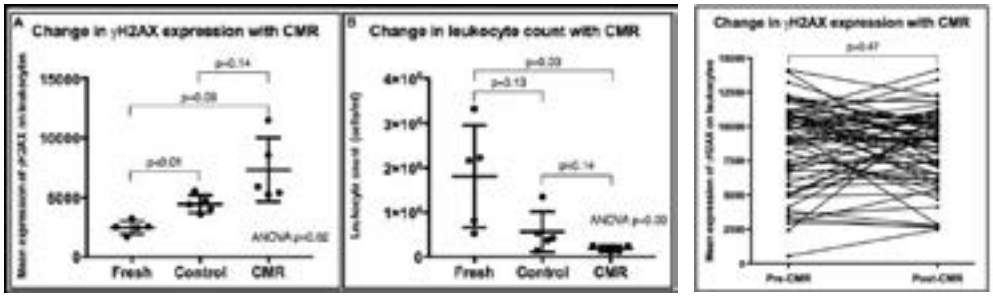

O009

MRI assessment of coronary endothelial nitric oxide synthase (eNOS) function using T1 mapping

Sophia X. Cui, B.S.Frederick H. Epstein, Ph.D.

University of Virginia, VA

Background: Endothelial dysfunction occurs in many types of cardiovascular diseases. As an early and sensitive biomarker of disease, it has been called a "barometer" of cardiovascular health [1]. Endothelial nitric oxide synthase (eNOS)-mediated production of NO plays a central role in the process, controlling vessel diameter and maintaining low microvascular permeability. We hypothesized that native T1 mapping of the healthy heart and microvasculature during NOS inhibition would detect elevated myocardial T1 corresponding to increased interstitial water content resulting from increased microvascular permeability. In contrast, a blunted change in myocardial T1 between baseline and NOS inhibition would be indicative of coronary eNOS dysfunction.

Methods: Wild type male C57Bl/6 mice (n=6) and eNOS-/- mice (n=7) underwent MRI studies using a 7T system (Clinscan, Bruker). T1 mapping was performed in a mid-ventricular short-axis slice at baseline and at 5, 12 and 20 minutes after intravenous injection of 4mg/kg LNAME, a NOS inhibitor that rapidly increases coronary microvascular permeability in rodents [2]. The T1-mapping method used fuzzy-clustering of spiral k-space data to ensure heart rate independence as previously described [3], and was accelerated using sparse sampling and compressed-sensing to reduce the scan time to 7 minutes. To exclude that the increase in T1 is due to vasodilatory effects, gadolinium-DTPA-enhanced first-pass perfusion MRI was performed in a separate imaging session in WT mice (n=6) at baseline and 5 minutes after IV injection of LNAME.

Results: Figure 1 shows example R1 (1/T1) maps of the heart acquired before and 5 minutes after injection of LNAME in WT and eNOS-/- mice, demonstrating a decrease in R1 in response to NOS inhibition in WT mice but not in eNOS-/- mice. Figure 2 summarizes data from all the mice and shows that NOS inhibition with LNAME causes a transient and significant increase in myocardial T1 in WT mice but not in eNOS-/- mice. First pass perfusion MRI in WT mice measured similar perfusion at baseline (6.2 ± 0.4 ml/g/min) and 5 minutes after LNAME (6.1 ± 0.6 ml/g/min), suggesting no vasodilation.

Conclusions: Inhibition of NOS with LNAME caused an increase in myocardial T1 in WT mice. As LNAME increases coronary microvascular permeability [2], the increased T1 is likely due to an increase in myocardial water content. The increase in myocardial T1 due to NOS inhibition was completely blunted in eNOS-/- mice, demonstrating that the LNAME-induced T1 increase is mediated through eNOS. Future work will investigate the potential of LNAME T1 mapping to detect coronary eNOS dysfunction in mouse models of diabetes and other heart diseases. **References** 1. Vita JA, et al., Circulation, 2002. 106(6): p. 640-2. 2. Filep JG, et al., Br J Pharmacol, 1993. 108(2): p. 323-6. 3. Vandsburger MH, et al., MRM 2010; 63(3):648-657.

Acknowledgements Funding: NIH R01 EB001763 and AHA pre-doctoral fellowship 16PRE29750008.

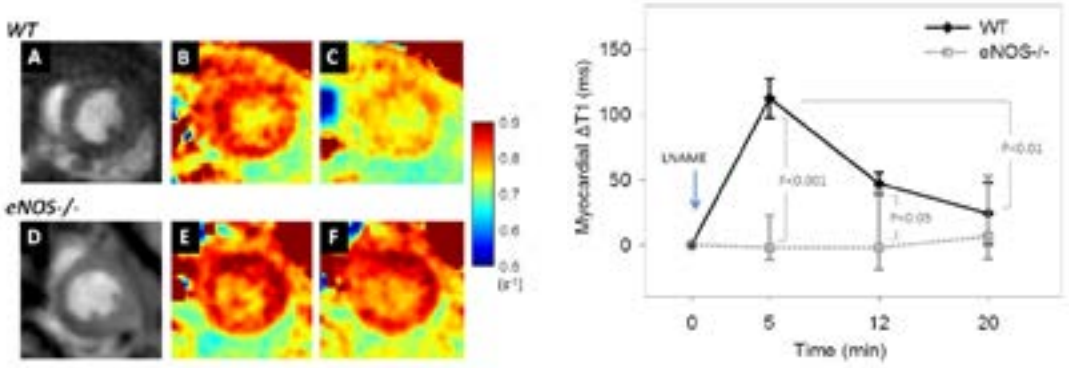

O010

Wideband late gadolinium enhancement (LGE) imaging in patients with implanted cardiac devices gives important clinical insights: robust free-breathing protocol with motion correction and 2D FLASH PSIR

Anish N. Bhuva, MRCP MBBS[1]Redha Boubertakh, PhD[2], Alex McLellan, PhD MBBS[3], Patricia Feuchter, MSc (MRI) Radiology[4], Neha Sekhri, FRCP PhD[5], Richard Schilling, FESC FRCP[3], Peter Kellman, PhD[6], James Moon, MBBS, MD, MRCP[7], Charlotte Manisty, MBBS PhD[8]

1. *Barts Heart Centre and Institute of Cardiovascular Science, UCL., London, England, United Kingdom*
2. *Barts Health NHS Trust, London, England, United Kingdom*
3. *Barts Heart Centre, England, United Kingdom*
4. *Barts Heart Centre, London, England, United Kingdom*
5. *St Bartholomews Hospital, West Smithfield, EC1A 7BE, England, United Kingdom*
6. *Laboratory of Cardiac Energetics, National Institutes of Health/NHLBI, Bethesda, MD, United States., MD*
7. *Barts Heart Center, The Cardiovascular Magnetic Resonance Imaging Unit and The Center for Rare Cardiovascular Diseases Unit, St Bartholomew's Hospital, West Smithfield, London, UK, England, United Kingdom*
8. *Barts Heart Centre and University College London, England, United Kingdom*

Background: Many patients with the greatest clinical need for high quality LGE imaging have implanted cardiac devices, however metallic artifacts using standard sequences pose a significant challenge. Prior work in LGE imaging to mitigate artifacts combined a wide bandwidth inversion and navigated 3D acquisition to achieve thin slices to minimize signal loss caused by dephasing. We employed a different approach to achieve a sequence that was robust in a clinical environment and explored its impact on patient care.

Methods: Sequence: Key features were: a wideband (WB) IR pulse (adiabatic, +/- 1.9kHz); 4mm 2D slices to reduce through-plane dephasing; single-shot FLASH readout; free-breathing respiratory motion correction (MOCO) with 24 averages to improve SNR; and phase sensitive inversion recovery (PSIR) achieving insensitivity to inversion time (alpha=9º optimised for infarct to remote contrast using Bloch simulation) (Figure 1). **Patients:** Patients with implantable cardiac devices (including MR non-conditional) referred for CMR for clinical indications were scanned according to our local standard operating procedure (based on national guidelines and the Magnasafe Registry). WB-MOCO LGE approach was used primarily, with comparator conventional PSIR FLASH LGE (often in inspiration rather than expiration), or free breathing MOCO SSFP. The best conventional image and the WB-MOCO LGE were assessed, with artifact rated on a scale of 1 to 4 (1=no artifact, 4=completely obscured).

Results: Of the 24 patients (age 55±18 years, 16 male), 7 had ICDs, 4 cardiac resynchronisation devices, 10 pacemakers and 3 implantable loop recorders. 8 (33%) devices were non-conditional, and all generators were left-sided. There were no clinical complications and no changes to device parameters post scanning. With conventional LGE imaging, 19 (79%) patients had artifact, with greater than half of LV segments affected in 13 (54%) patients. WB-MOCO LGE completely removed hyperintensity artifact in 17 out of 19 (89%) patients and improved image quality in the remaining two patients. Overall, CMR resulted in a new diagnosis in 11 (46%) patients and a management change in 17 (71%) patients (Figure 2). This included 91% of defibrillator patients (CRTD and ICD) in whom only the WB-MOCO LGE images were diagnostic. Examples of significant unexpected findings were a large apical thrombus (in a patient awaiting LV VT ablation); myocardial infarction, HCM, and embolic infarction.

Conclusions: The WB-MOCO LGE sequence permits high quality LGE imaging in device patients, providing new clinically important diagnoses in this at-risk population and almost completely removing image artifact. 2D FLASH readout with MOCO averaging enables fast robust image acquisition, thereby optimising clinical workflow.

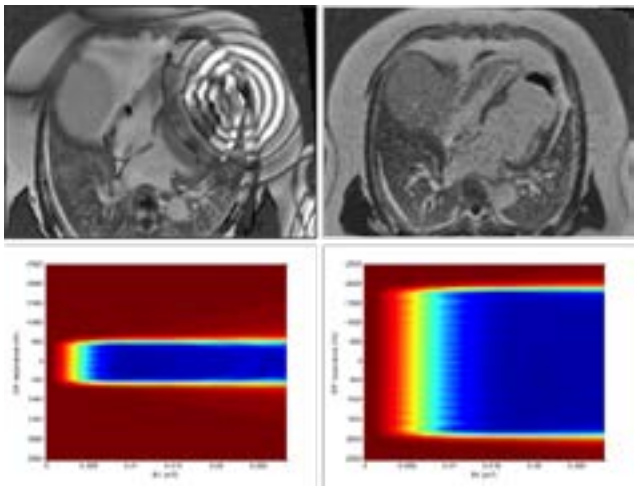

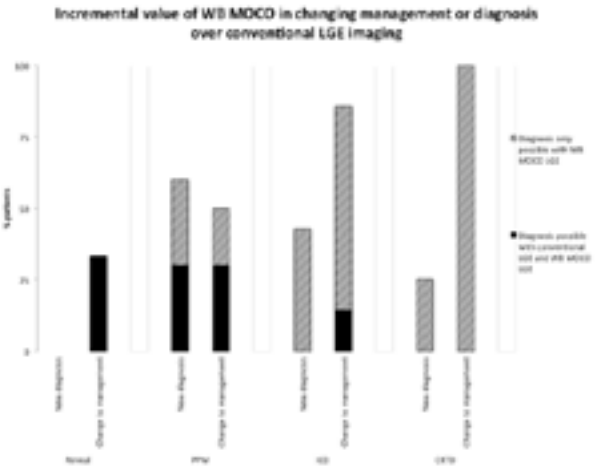

O011

Validation of Diffusion Tensor CMR-based Myocardial Fiber Orientation Mapping of Intact Hearts using Optically Transparent Tissue Preparation with 3D Optical Microscopy

Christopher Nguyen, PhD[1] Sang-Eun Lee, MD[2], Jongjin Yoon, MD, PhD[3], Hyuk-Jae Chang, MD, PhD[2], Sekeun Kim[3], Chul Hoon Kim, MD, PhD[3], Namsik Chung, MD, PhD[4], Debiao Li, PhD[5]

1. *Cedars-Sinai Medical Center, CA*
2. *Severance Cardiovascular Hospital, Yonsei-Cedar Sinai Integrative Cardiovascular Imaging Research Center, Yeonsei University Health System, Seoul, South Korea, N/A, Republic of Korea*
3. *Yonsei University College of Medicine, N/A, Republic of Korea*
4. *Yonsei University College of Medicine, Seoul, N/A, Republic of Korea*
5. *Biomedical Imaging Research Institute, Cedars-Sinai Medical Center, Los Angeles, CA, CA*

Background: The myocardium consists of a complex 3-dimensional (3D) microstructure and has been shown to be perturbed in the presence of myocardial disease [1]. Recently, diffusion tensor magnetic resonance imaging (DT-CMR) was introduced which can characterize the 3D tissue microstructure in intact myocardium [2]. However, previous histologic validation of DTI has been limited since traditional pathology allows only for 2D optical microscopy after potentially destructive tissue sectioning [3]. We present a novel approach to validate the derivation of the myocardial fiber orientation (MFO) using DT-CMR with 3D histology using a non-destructive, transparent-tissue preparation technique (CLARITY [4]).

Methods: Validation of the approach was performed ex vivo in normal (n=7) and ischemic (n=8) mouse hearts after fixation. All hearts were scanned with a gold standard DT-CMR (single spin echo, 12 directions, b=1000 s/mm^2, TR=8750ms, TE=36ms, NEX=5, 125x125x300um^3, scan time=14hrs) sequence on a 9.4T Bruker (BioSpec 94/20 USR, Bruker Biospin) scanner. After CMR, the hearts were fixed and processed with CLARITY. After 1 month of CLARITY, 3D optical fluorescence imaging (638nm wavelength, 4.4x4.4x7.8um^3, 5x objective lens) of the hearts were performed on an optical system (Light Sheet Z1, Carl Zeiss Microscopy Co) covering the entire left ventricle (LV). DT-CMR images were processed to estimate self-diffusion tensors with primary eigenvectors assumed to be parallel to MFO. Optical images were processed with a 3D structural tensor analysis [5] to derive MFO. Voxelwise helix angle (HA) and global HA transmurality (HAT) were calculated and compared between both imaging modalities for each subject after co-registration of with standard non-rigid, mutual information cost function.

Results: Voxelwise HA comparison between the two modalities demonstrated substantial and signficiant ($p < 0.05$) correlation for normal (R^2=0.77) and ischemic (R^2=0.75) groups. Correlation of global HAT was also significant ($p < 0.05$) substantial (R^2=0.80) between both modalities across all subjects and within normal (R^2=0.81) and ischemic (R^2=0.70) groups. Normal HAT (DT-CMR: 1.31±0.20°/% transmural depth (TD) vs optical: 1.36±0.27°/%TD) was significantly ($p < 0.05$) larger than ischemic HAT (DT-CMR: 0.79±0.13°/%TD vs optical: 0.84±0.26°/%TD) for both modalities.

Conclusions: DT-CMR fundamentally reflects myocardial fiber orientation in ex vivo conditions showing concordance with CLARITY-based 3D optical imaging in intact normal and ischemic myocardium.

References: [1] Sosnovik, Circulation 2012. [2] Mekkaoui, JCMR 2014 [3] Scollan Am J Physio 2010 [4] Chung Nature 2014 [5] Budde, NeuroImage 2016.

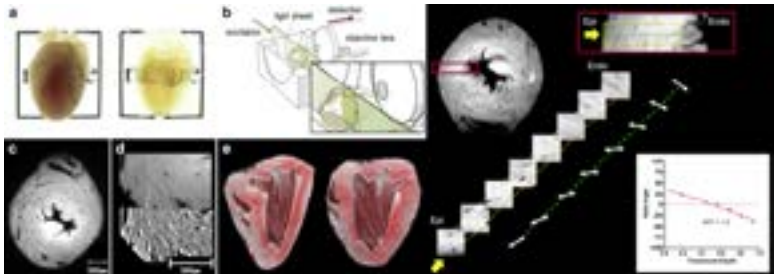

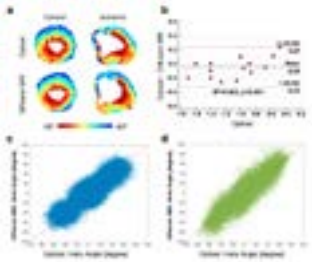

O012

3D myocardial t1 mapping using a saturation recovery acquisition

Giovanna Nordio, Biomedical Engineering[1]Markus Henningsson, PhD[2], Amedeo Chiribiri, MD, PhD[2], Adriana Villa, MD[2], Torben Schneider, PhD[3], Rene Michael. Botnar, PhD[1]

1. *King's College London, London, England, United Kingdom*
2. *King's College London, England, United Kingdom*
3. *Health Systems, Philips, Guildford, England, United Kingdom*

Background: Quantitative T1 mapping is an effective non-invasive method to detect and visualize both diffuse and local myocardial fibrosis.[1] The Modified Look-Loocker (MOLLI)[2] and the Saturation-recovery Single Shot Acquisition (SASHA)[3] sequences are 2D techniques that are limited in spatial resolution and time efficiency. Here we propose a high-resolution multi-shot 3D SASHA sequence combined with a 1D-hemidiaphragmatic navigator, which allows for volumetric coverage of the heart in free-breathing. The imaging sequence has been tested and validated on a T1 phantom and in healthy subjects.

Methods: The 2D SASHA sequence was modified to make the sequence compatible for 3D segmented k-space acquisition. First the segments of the "infinity" image, without any magnetization preparation, were acquired, followed by interleaved segmented acquisitions with preceding saturation pulse and increasing saturation delays (figure 1a). To compensate for respiratory motion a 1D hemi-diaphragmatic navigator was used: for the shortest saturation time (TS) the position between the saturation pulse and the navigator was swapped (figure 1b). Three "pause" heart cycles were added between the acquisitions of the segments without magnetization preparation to allow for complete recovery of the magnetization. Phantom and in-vivo data from 10 healthy subjects were acquired on a 1.5T Philips Ingenia MR system (Philips, Best, The Netherlands). The acquisition parameters for the 3D SASHA sequence included: TR/TE=3.2/1.6; FA=35°; subject specific mid-diastolic trigger delay; image resolution=1.4x1.4x8mm; FOV=300x300x90mm. Ground truth T1 measurements in a T1 phantom were acquired with an inversion recovery spin-echo (IRSE) sequence. Subsequently, the 3D SASHA sequence was compared to 2D MOLLI and 2D SASHA in healthy subjects. T1 image analysis of the SASHA T1 maps was performed offline with customized software (MATLAB, R2014a, The MathWorks; Natick, MA).

Results: The Blank-Altman analysis shows good agreement between IRSE and 3D SASHA sequences in terms of accuracy (figure 2a), with improved precision for 3D compared to 2D SASHA. Both 2D SASHA and 3D SASHA correlate extremely well with the IRSE sequence (r=0.9997) (figure 2b-c). Mean and standard deviation of the myocardial T1 values in healthy subjects measured with 2D SASHA and 3D SASHA sequences are in agreement within the range of their standard deviation (1181.3±32ms and 1153.6±28ms), while T1 values derived from 2D MOLLI are considerably lower (881±40ms) (figure 3).

Conclusions: The proposed 3D SASHA T1-mapping technique allows the acquisition of high-resolution myocardial T1 maps of the whole left ventricle in free breathing with improved accuracy compared to 2D MOLLI sequence and with improved precision compared to 2D SASHA.

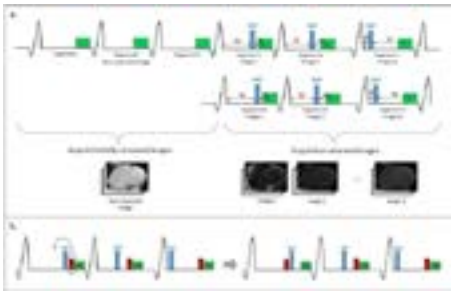

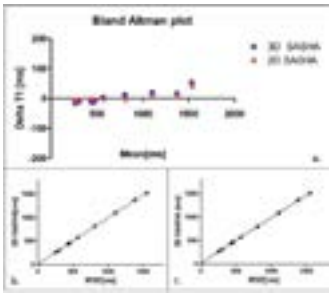

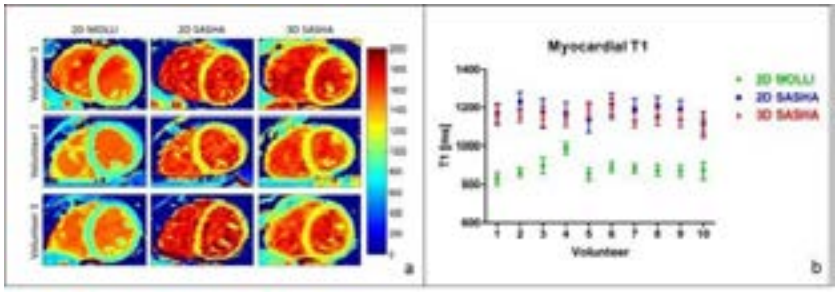

O013

Phase-Contrast MRI with Hybrid One- and Two-sided Flow-Encoding and Velocity Spectrum Separation (HOTSPA)

Da Wang, MS[1] Jiaxin Shao, PhD[2], Daniel Ennis, PhD[2], Peng Hu, PhD[2]

1. university of california los angeles, Los Angeles, CA
2. university of california los angeles, CA

Background: To develop and evaluate an M_1-space (gradient first moment) undersampling phase-contrast MRI (PC-MRI) technique with hybrid one- and two-sided flow-encoding (FE) and velocity spectrum separation (HOTSPA) for accelerated blood flow and velocity measurement.

Methods: In conventional 4D-flow MRI, the duration of each cardiac phase is 4*TR*views-per-segment (VPS). In the HOTSPA technique, each cardiac phase is shortened by 50% to 2*TR*VPS. This is achieved by applying two-sided FE in the z-direction (i.e. $+FE_z$ and $-FE_z$) and encoding two orthogonal in-plane FE directions (i.e. X+Y and X-Y directions) alternatively in two consecutive cardiac phases as shown in Fig. 1. If one applies a temporal Fourier transform of the HOTSPA 4D flow data with alternating FE directions, the temporal spectra for the three orthogonal flow directions are shifted away from each other and can be easily separated using a temporal filter. Thus, HOTSPA can accelerate PC-MRI by encoding 3D velocities using only 2TRs instead of 4TRs as in reference four-point PC-MRI. The specific theory and workflow are shown in Figure 2. More details about the technique are recently published in Wang D. et. al. MRM 2016 Aug 9. doi: 10.1002/mrm.26366. Six volunteers were scanned at the common carotid arteries (CCAs) using two sequences: 1) reference four-point PC-MRI with 3D FE plus the FC data, i.e. 4D flow FC/3FE; 2) our HOTSPA strategy with 3D FE, i.e. 4D HOTSPA. The sequences parameters are: TE/TR=3.6-3.9/6.2-6.4 ms, Flip Angle=20°, VENC=100-110 cm/s, FOV=256*176*20 cm^3, Acquired matrix size=256*176*8, VPS=4.

Results: Fig. 3a-b show examples of through-plane mean velocity and peak velocity measurement in one slice of the 4D flow data comparing two different measurements: the 4-VPS 4D FC/3FE (red), and the 4-VPS 4D HOTSPA (blue). The 4D HOTSPA technique generated up to 40% higher peak velocity compared with standard 4D FC/3FE. As shown in Figure 3c, the total volumetric flow measurements agree well between 4D HOTSPA and 4D FC/3FE (-0.02 mL bias with [-0.3 0.3] mL 95% Confidential Interval). The peak velocity from 4-VPS HOTSPA (average = 98.0 cm/s, range: 73.7-125.6 cm/s) was significantly higher than the 4-VPS standard 4D FC/3FE (average = 83.2 cm/s, range: 60.2-109.6 cm/s) ($P < 0.05$, one-side paired t-test).

Conclusions: In this work, we propose a new and more efficient flow encoding and velocity calculation strategy for PC-MRI using a temporal modulation technique to double the temporal resolution or reduce the scan time by 50%. This is the first study to examine a temporal modulation strategy for an under-sampled M_1-space. Our strategy can be combined with conventional acceleration techniques, i.e. parallel imaging and compressed sensing, to further shorten the scan time of PC-MRI. The proposed HOTSPA technique achieves nearly two-fold acceleration of PC-MRI while maintaining accuracy for total volumetric flow and peak velocity quantification.

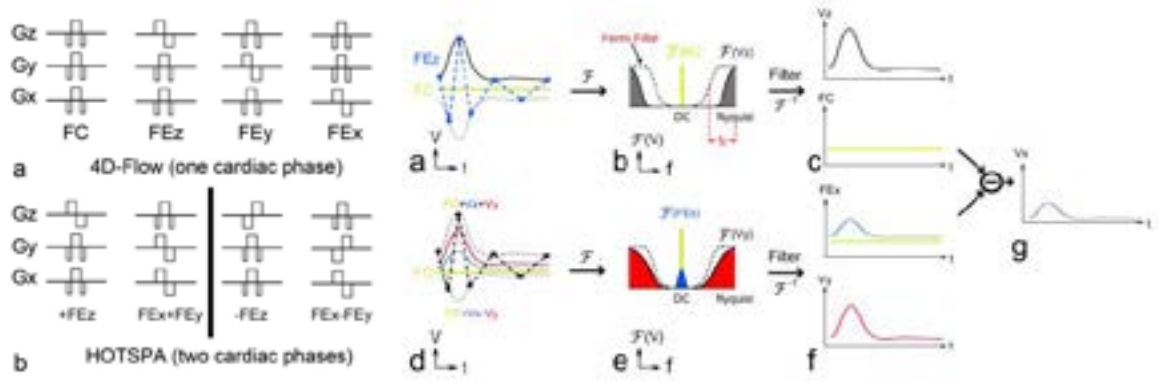

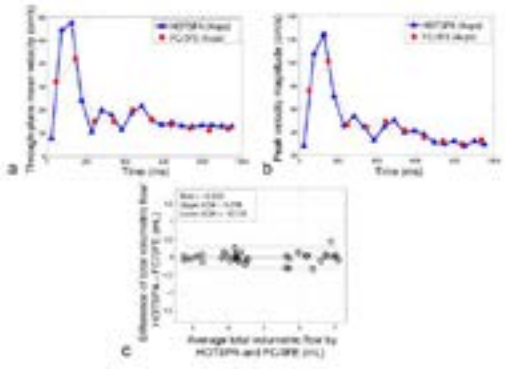

O014

Validation of Fully Automatic Absolute Myocardial Perfusion Quantification by Cardiac Magnetic Resonance Imaging versus Invasive Fractional Flow Reserve in Swine

Daniel W. Groves, MD[1]Shawn Kozlov, BS[2], Joni L. Taylor, BS[2], Sarah K. Yang, BS[2], Li-Yueh Hsu, DSc[2], Andrew E. Arai, MD[2]

1. National Heart, Lung and Blood Institute, National Institutes of Health, MD
2. National Heart, Lung and Blood Institute, National Institutes of Health, Bethesda, MD

Background: In an animal model without microvascular disease, fractional flow reserve (FFR) should correspond to a myocardial blood flow (MBF) ratio between an ischemic and remote zone. Since there is a near linear relationship between pressure and MBF during maximal vasodilation, we hypothesized that quantitative cardiac magnetic resonance (CMR) perfusion imaging could predict invasive pressure measurements of FFR based on a CMR MBF ratio.

Methods: Twenty-seven adenosine stress FFR experiments during computer-regulated partial left anterior descending (LAD) coronary occlusions were completed in 10 swine. Gadolinium-enhanced first pass, free-breathing perfusion images were acquired on a 3T MRI scanner. The quantification program was implemented as a standalone software application to automatically process raw perfusion images. MBF was quantified at the pixel level in units of $ml \cdot min^{-1} \cdot g^{-1}$. Each experiment provided 2 data-points: Ischemic zone and Control zone MBF ratio. These were calculated as follows: Ischemic zone MBF ratio = the entire LAD zone MBF / basal remote zone MBF, and Control zone MBF ratio = mid-to-apical remote zone MBF / basal remote zone MBF. The MBF ratios were compared to invasive FFR.

Results: Automatic perfusion quantification took approximately 1–2 minutes per slice. Ischemic zone FFR was normally distributed around 0.75 ± 0.13 for the LAD coronary occlusions and thus straddled diagnostically important thresholds. CMR MBF ratio correlated with FFR ($r=0.86$, $p < 0.0001$). Using a diagnostic threshold of 0.80 for both FFR and CMR MBF ratio, the sensitivity and specificity was 89% (AUC 0.96, $p < 0.0001$). The positive and negative predictive values were 80% and 94%, respectively.

Conclusions: Fully automatic quantification of absolute myocardial perfusion at a pixel level in units of $ml \cdot min^{-1} \cdot g^{-1}$ are capable of distinguishing FFR(+) from FFR(-) coronary stenoses.

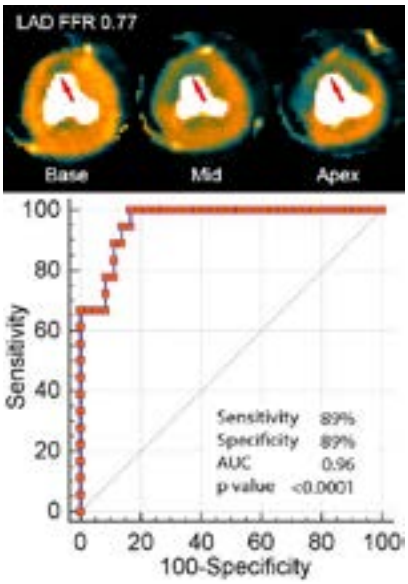

O015

Longitudinal Evaluation of Aortic Hemodynamics in Marfan Syndrome: New Insights from a Multi-Year 4D Flow MRI Follow-Up Study

Julia Geiger, MD[1] Daniel Hirtler, MD[2], Kristina Gottfried, MD[3], Ozair Rahman, MD[4], Emilie Bollache, PhD[5], Alex J. Barker, PhD[5], Brigitte Stiller, MD[2], Michael Markl, PhD[6]

1. *Department of Radiology, Northwestern University, Chicago, IL*
2. *Dept.of Pediatric Cardiology and Congenital Heart Disease, University Hospital Freiburg, Baden-Wurttemberg, Germany*
3. *Dept. of Anaesthesiology, University Hospital Mainz, Rheinland-Pfalz, Germany*
4. *Northwestern University, Feinberg School of Medicine, Chicago, IL*
5. *Northwestern University Feinberg School of Medicine, Chicago, IL*
6. *Northwestern University, Chicago, IL*

Background: Marfan syndrome (MFS) is a genetic disorder of the connective tissue leading to cardiovascular pathologies associated with high morbidity and mortality.The aim of this 4D flow MRI follow-up study was to investigate longitudinal changes in aortic hemodynamics (systolic wall shear stress (WSS), peak velocity, flow patterns) in adolescent patients with MFS in comparison with healthy volunteers.

Methods: 4D flow MRI (venc=200cm/s, TE=2.4-3.7ms, TR=4.8-6.1ms, temporal resolution=38.4-48.4ms) of the thoracic aorta was performed twice (baseline scan t1/ follow-up scan t2) in 19 adolescent MFS patients (age at t1: 12.7±3.6, t2: 16.2±4.3 years) with a mean follow-up duration of 3.5±1.2 years. Cross-sectional 4D flow data of 10 healthy volunteers (mean age: 24±3.8 years) served as a control group. Data analysis included correction of phase offset errors due to eddy currents, Maxwell terms, and velocity aliasing (Matlab, USA) as well as 3D segmentation of the thoracic aorta (Mimics, Materialise, Leuven, Belgium). Aortic blood flow visualization was performed by color-coded 3D pathlines (EnSight, CEI, Apex, USA). Secondary flow patterns (helices/vortices) were graded on a 3 point scale (none, moderate, severe; blinded reading, 2 observers). Systolic 3D WSS was calculated along the entire aortic wall and quantified in 10 aortic segments (fig. 1a-b). Aortic peak systolic velocities were obtained from generated velocity maximum intensity projections (MIPs; fig. 1c). Z-Scores of the aortic root (as an indicator for the standard deviations from the mean) were assessed based on echocardiographic measurements.

Results: MFS patients revealed significant lower mean systolic WSS in the proximal inner descending aorta (DAo) compared with volunteers (0.78±0.15N/m^2) at baseline t1 (0.60±0.18N/m^2; p=0.01) and follow-up t2 (0.55±0.16N/m^2; p=0.001). In the MFS group, segmental mean WSS did not change significantly between t1 and t2, except for a significant decrease in the proximal inner DAo segment (p=0.02, fig. 2). There were significant relationships ($p < 0.05$) between the segmental WSS in the proximal inner DAo and helix/vortex grading (fig. 3) at both t1 and t2 (r=-0.51; r=-0.55). In addition, WSS was significantly different between the inner and outer proximal DAo segment at both scans, conversely to volunteers ($p < 0.001$). Peak systolic flow velocity in the ascending aorta decreased significantly between t1 and t2 (p=0.02), but was not different compared with volunteers (fig. 2). Patients' z-scores were stable over time (t1: 2.11, t2: 2.05). No correlations between Z-scores and WSS or velocity were found.

Conclusions: MFS patients have lower segmental WSS in the inner proximal DAo segment which correlates with increased localized aberrant vortex/helix flow at one of the most critical sites for aortic dissection. These hemodynamic changes are already present at young age and tend to be more pronounced in the course of time.

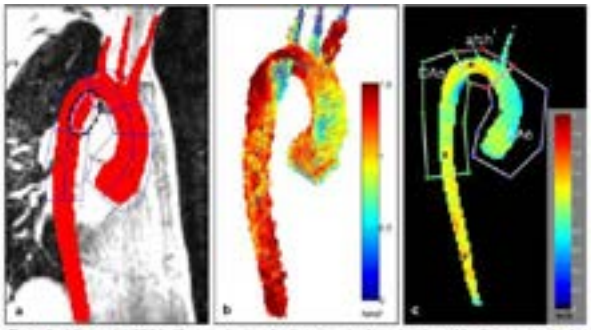

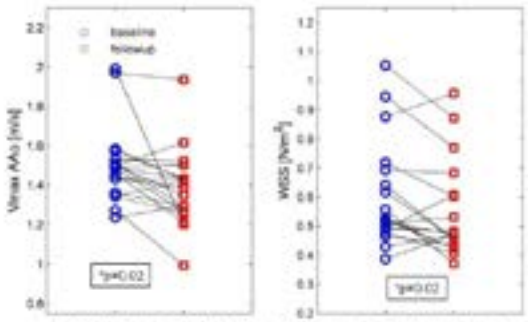

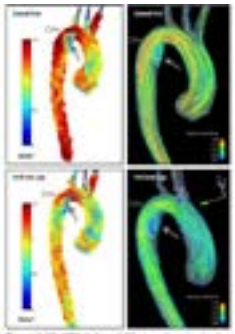

O016

Extracellular volume fraction in transposition of the great arteries with a systemic right ventricle: Myocardial fibrosis may not account for clinical heart failure.

Craig S. Broberg, MD, MCR[1] Anne M. Valente, MD[2], Andrew J. Powell, M.D.[3], Jonathan Holt, BS[4], Luke Burchill, MBBS Phd[4], Michael Jerosch-Herold, PhD[5]

1. *Oregon Health and Science University, Portland, OR*
2. *Boston Children's Hospital; Brigham and Women's Hospital, Boston, MA*
3. *Harvard Medical School and Boston Children's Hospital, Boston, MA*
4. *OHSU, OR*
5. *Department of Radiology, Brigham & Women`s Hospital & Harvard Medical School, Boston, United States., MA*

Background: Myocardial dysfunction and clinical heart failure are common in adults with transposition of the great arteries (TGA) with a systemic right ventricle (RV). Myocardial fibrosis has been implicated in the pathophysiology of this condition, and can be assessed by calculating the extra-cellular volume fraction (ECV) by cardiac magnetic resonance (CMR).

Methods: We prospectively measured ECV in patients with TGA with a systemic RV and age-matched controls, together with same-day blood sampling and 6-minute walk test. Measurements were repeated after one year. A Look-Locker sequence through a single mid-ventricular short-axis plane before and 3, 7, and 15 minutes after gadolinium contrast injection was used to quantify T1 for the systemic ventricle (RV for TGA and left ventricle (LV) for controls). ECV was calculated using T1 values from the compacted myocardium and the hematocrit. Baseline ECV and 1 year change in ECV were correlated with other clinical variables and outcome.

Results: The mean ECV for the RV (28.6±4.4%) in TGA subjects (n=55, age 34±10 years, 42% female) was significantly higher than the ECV for the LV (26.1±2.8%) in controls (n=22, age 40±11 years, 41% female) (p=0.0145). There was no significant segmental variation in ECV. ECV was not associated with age and was not different in L-TGA (N=10) vs. D-TGA (n=45). TGA subjects with an abnormally high ECV (n=15, 27%) had a higher b-type natriuretic peptide (BNP) (456± 650 vs. 151±173 pg/mL, p=0.009). 6-minute walk distance was unexpectedly higher (546±89 vs. 460±117 m, p=0.025). They did not differ by age, functional class, medication use, history of atrial arrhythmia, ventricular volume or ejection fraction, or circulating collagen fragments. In the 28 TGA subjects restudied after 1 year, ECV did not change significantly (mean difference 0.7±2.7%, p=0.18 on paired t-test). During clinical follow-up (median 3.3 years), ECV was not significantly different for those with heart failure endpoints (death or need for advanced therapy, N=13) or an arrhythmia event (N=3).

Conclusions: Myocardial fibrosis measured by CMR ECV is common in TGA patients with a systemic RV and associated with a higher BNP, but not other markers of cardiovascular dysfunction or outcome. Our results suggest that myocardial fibrosis may not be a strong factor in clinical deterioration and raise further questions regarding the role of standard heart failure pharmacotherapy directed at fibrosis.

p value	ECV abnormal	ECV normal	
	15	40	N
0.094	38.1±5.4	32.8±11.4	Age (years)
0.045	3 (20%)	20 (50%)	Female (N, %)
0.17	1 (3%)	9 (23%)	L-TGA (N, %)
0.76	87±22	96±27	RVEDVi (ml/m2)
0.84	54±15	54±11	RVEF (%)
0.023	5.3±1.3	4.5±1.1	ln b-natriuretic peptide
0.025	546±89	460±117	6 minute walk distance
0.59	4.1±3.3	4.5±1.4	procollagen 3 NT (ug/l)

O017

4D flow MRI derived kinetic energy measures are associated with disease progression in children with repaired tetralogy of Fallot

Maria Joh[1]Michael Rose, B.S.E[2], Kelly Jarvis, MS[3], Susanne Schnell, PhD[4], Alex J. Barker, PhD[5], Cynthia Rigsby, MD FACR[6], Michael Markl, PhD[4], Joshua D. Robinson, MD[5]

1. *Northwestern University Feinberg School of Medicine, IL*
2. *Ann & Robert H. Lurie Children's Hospital of Chicago, IL*
3. *Northwestern University McCormick School of Engineering, IL*
4. *Northwestern University, Chicago, IL*
5. *Northwestern University Feinberg School of Medicine, Chicago, IL*
6. *Ann & Robert H Lurie Children's Hospital of Chicago, Chicago, IL*

Background: Conventional MRI assessment with repaired tetralogy of Fallot (TOF) relies heavily on morphologic and simplified global functional parameters (e.g. ventricular volumes and ejection fraction) which reflect late disease expression. Our aim was to assess whether 4D flow MRI derived right ventricular (RV) and pulmonary artery (PA) kinetic energy (KE) measures: 1) differentiate pediatric patients with repaired TOF from controls and 2) are associated with disease progression.

Methods: In this retrospective case-control cohort study, pediatric patients status-post TOF repair (n=21) and controls (n=24) underwent 4D flow MRI for assessment of in-vivo 3D blood flow. Informed consent was obtained for performing 4D flow per a prospective IRB-approved, HIPAA-compliant protocol. 4D flow data analysis included phase offset error correction (velocity aliasing, Maxwell terms, eddy currents) and calculation of 3D PC-MR angiograms. Systolic and diastolic 3D RV and PA segmentation was performed (Figure 1A). For each voxel inside a segmentation volume, kinetic energy (KE) was calculated (KE = 1/2 mv^2; m = mass, or voxel volume multiplied by blood density 1.05 g/mL; v = absolute velocity). Total KE_{RV} and KE_{PA} were determined as the sum of the KE of all voxels within the respective segmentation, and calculated for peak systole and diastole. KE maps were generated for each time point by projecting mean KE on a 2D plane transecting the RV and PA, respectively (Figure 1B). To normalize for patient size, total KE_{RV} and KE_{PA} were indexed to body surface area (BSA).

Results: Across the cardiac cycle, KE_{PA} was increased in TOF vs. controls (median 12.5 [IQR 8-18.4] vs. 8.2 [6.1-10.4] mJ/m^2, $p < 0.01$ during peak systole; 2.3 [1.3-4] vs. 1.4 [1-1.9] mJ/m^2, $p < 0.01$ during peak diastole; see Table 1 and example KE maps in Figure 2). Elevated diastolic KE_{RV} and KE_{PA} correlated with increased RV end-diastolic volume (EDV) (R^2=0.33, $p < 0.001$; R^2=0.50, $p < 0.001$; Figure 3A&B). Diastolic KE_{PA} exhibited a non-linear relationship with RVEDV, with an inflection point near 120 ml/m^2. Higher systolic KE_{RV} and KE_{PA} strongly correlated with increased RV stroke volume (R^2=0.58, $p < 0.001$; R^2=0.60, $p < 0.001$; Figure 3B&C), denoting elevated KE at higher cardiac outputs. Similarly, KE_{RV} and KE_{PA} correlated with systolic KE_{RV} and KE_{PA} (Figure 3E&F).

Conclusions: 4D flow MRI energetic measures, such as KE, were abnormal in repaired TOF compared to controls and have a direct relationship with traditional measures of disease progression. As a non-invasive and comprehensive method for measuring RV myocardial demand and TOF disease progression, KE biomarkers may help to refine criteria for reintervention in TOF.

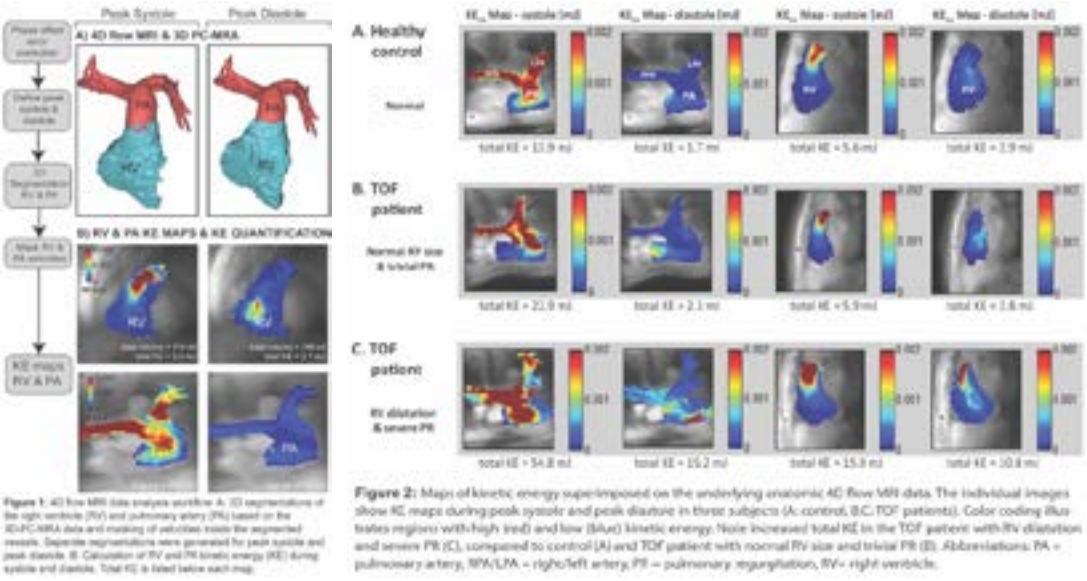

Figure 2: Maps of kinetic energy superimposed on the underlying anatomic 4D flow MRI data. The individual images show KE maps during peak systole and peak diastole in three subjects (A: control, B,C: TOF patients). Color coding illustrates regions with high (red) and low (blue) kinetic energy. Note increased total KE in the TOF patient with RV dilatation and severe PR (C), compared to control (A) and TOF patient with normal RV size and trivial PR (B). Abbreviations: PA = pulmonary artery, RPA/LPA = right/left artery; PR = pulmonary regurgitation, RV= right ventricle.

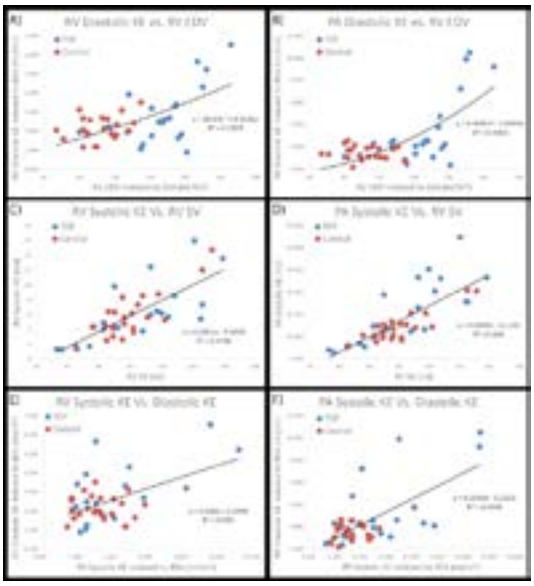

Table 1: Patient & control characteristics, standard MRI measurements and 4D MRI derived energetic calculations.

p value	Controls n=24	TOF s/p repair n=21	
0.18	15.8 (14.5 - 17.5)	13.8 (9.9 - 18)	Age
0.12	58 (46.8 - 65.4)	48 (27.9 - 64.5)	Weight (kg)
0.25	1.62 (1.44 - 1.71)	1.62 (1.06 - 1.76)	BSA (m^2)
Standard MRI parameters			
N/A	N/A	23 (10 - 38)	PR fraction flow 2D (%)
<0.01	0 (-3 - 3)	19 (7 - 37)	PR fraction stroke volume comparison (%)
<0.01	92 (82 - 101)	128 (116 - 139)	RVEDV index (ml/m^2)
<0.01	41 (39 - 50)	70 (62 - 75)	RVESV index (ml/m^2)
<0.01	50 (46 - 53)	59 (55 - 66)	RV stroke volume index (mL/m^2)
<0.01	54 (50 - 57)	47 (43 - 53)	RV ejection fraction (%)
0.27	87 (79 - 95)	91 (83 - 97)	LVEDV index (ml/m^2)
<0.01	35 (32 - 39)	41 (38 - 49)	LVESV index (ml/m^2)
0.37	51 (45 - 54)	49 (42 - 54)	LV stroke volume index (mL/m^2)
<0.01	58 (56 - 61)	55 (48 - 58)	LV ejection fraction (%)
4D MRI parameters			
Systole			
0.92	5.1 (3.8 - 6.8)	5.4 (3.9 - 7.6)	KE_{RV} (mJ)
0.27	13 (9.4 - 15)	15 (8.8 - 32)	KE_{PA} (mJ)
0.5	3.3 (2.4 - 4.4)	3.4 (2.6 - 4.9)	KE_{RV} index (mJ/m^2)
<0.01	8.2 (6.1 - 10)	12.5 (8 - 18.4)	KE_{PA} index (mJ/m^2)
Early diastole			
0.78	3.4 (2.8 - 4.5)	3.6 (1.9 - 5.9)	KE_{RV} (mJ)
0.13	2.4 (1.6 - 2.9)	2.5 (2 - 5.6)	KE_{PA} (mJ)
0.18	2.1 (1.7 - 2.7)	2.5 (1.8 - 3.5)	KE_{RV} index (mJ/m^2)
<0.01	1.4 (1 - 1.9)	2.3 (1.3 - 4)	KE_{PA} index (mJ/m^2)

Abbreviations: BSA = Body surface area, KE = kinetic energy, LV= left ventricle, PA = pulmonary artery, PR = pulmonary regurgitation, RVEDV = right ventricular end-diastolic volume, RVESV = right ventricular end-systolic volume

O018

How Can Situs Inversus Totalis Hearts Work: From Genes, Myocardial Micro-architecture, to Cardiac Function

Yijen L. Wu, Ph.D.[1]Sameh Tadros, MD[2], Fang-Cheng Yeh, MD, PhD[3], Cecilia Lo, PhD[4]

1. *Deapartment of Developmental Biology, University of Pittsburgh and Rangos Research Center Imaging Core, Children's Hospital of Pittsburgh of UPMC, Pittsburgh, PA, USA, Pittsburgh, PA*
2. *Pediatric Radiology, Children's Hospital of Pittsburgh of UPMC and Department of Radiology, University of Pittsburgh, PA*
3. *Department of Neurological Surgery, University of Pittsburgh, PA*
4. *Department of Developmental Biology, University of Pittsburgh, PA*

Background: Situs inversus totalis (SIT) is a congenital condition in which the major visceral organs are completely reversed from the normal situs solitus (SS). SIT is highly associated with ciliopathy such as primary ciliary dyskinesia (PCD). The SIT hearts are thought to be equivalent to normal hearts, however, few pathology accounts found that SIT hearts were organized differently. The goal of this study is to elucidate the micro-architecture of the SIT hearts and its mechanic consequences in both mutant mice and human patients.

Methods: ***Animal model:*** Mutant mice with homozygous ciliopathy gene mutations, such as Pkd1L1, Daw1(Wdr69) and Ccdc164(Drc1) genes that displayed either SIT or SS situs were imaged. ***Human patients:*** PCD patients with SIT and SS are recruited. **Cardiac MRI:** *In vivo* cine and tagging MRI, and *ex vivo* multi-shell diffusion MRI in mice were acquired with Bruker 7-Tesla Avance III system. Cine and tagging MRI for human patients were acquired with GE 1.5T system. Strain, rotation, and torsion were derived from tagging MRI with HARP software (Myocardial Solutions, Inc.).

Results: Individuals with homozygous PCD gene mutations, both in humans and mice, can display 3 types of situs – SS, SIT, and heterotaxy. Figure 1 shows multi-slice tagging MRI for a SIT mutant mouse (Fig. 1 A-L), a patient with SS (Fig.1M) and a patient with SIT (Fig. 1N). The normal heart rotates clockwise at the base and counter-clockwise at the apex to bring about the "wringing motion". Figure 2 shows rotation analysis for various mutant mouse hearts. Both homozygous SIT (Fig. 2 B-D) and SS (Fig.2E) mutants have very different rotation patterns from the normal WT control (Fig.2 A). SS and SIT mutants have additional "twists", which are out-of-phase from the WT control, suggesting that they have different myocardial organization. Diffusion MRI was used to delineate myocardial fiber organization of homozygous SIT and SS hearts. Conventional DTI was insufficient in defining myocardial fibers in SIT mutants. We implemented a new multi-shell diffusion MRI (Fig.3) that is capable of capturing myocardial fiber organization of various mutant hearts. Quantitative anisotropy (QA) is calculated from the peak orientations on a spin distribution function. Larger QA indicates high coherent compact fiber bundle. WT has significantly higher QA (Fig.3J), indicating that myocardial fiber bundles are far more coherent in the WT heart (left) than mutant hearts.

Conclusions: Our results showed that PCD homozygous mutant hearts, both SS and SIT, are not the same as WT hearts.

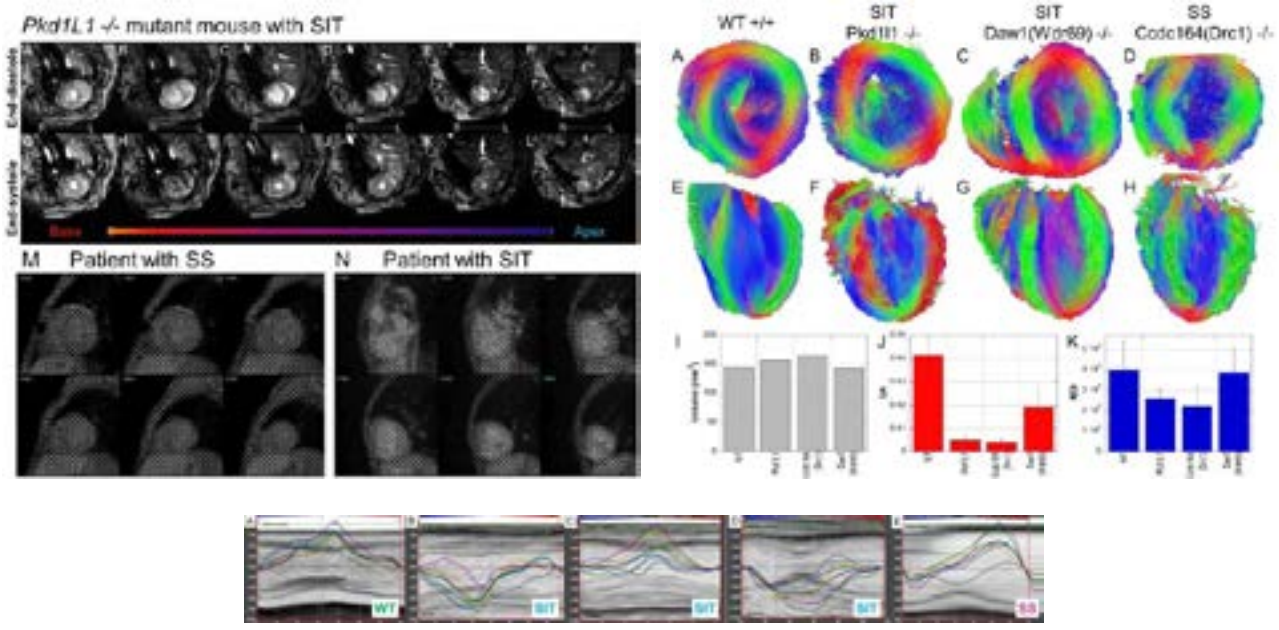

O019

Impact of the Cone Operation in Ebstein Anomaly on Ventricular Size, Function, and Synchrony: a Cardiac Magnetic Resonance Study

Rebecca Beroukhim, MD[1] Linyuan Jing, PhD[2], Abba Mejia-Spiegeler, LLB[3], David Harrild, MD, PhD[4], Sitaram Emani, MD[5], Brandon K. Fornwalt, MD, PhD[6], Andrew J. Powell, M.D.[7]

1. *Harvard Medical School and Massachusetts General Hospital, Boston, MA*
2. *Geisinger Health System, State College, PA*
3. *Geisinger Health System, Danville, PA*
4. *Harvard Medical School and Boston Childrens Hospital, Boston, MA*
5. *Harvard Medical School, Boston Childrens Hospital, Boston, MA*
6. *Geisinger Health System, PA*
7. *Harvard Medical School and Boston Children's Hospital, Boston, MA*

Background: Ebstein anomaly is characterized by displacement of the effective tricuspid annulus into the right ventricle (RV), tricuspid regurgitation (TR), and RV dilation. The cone operation involves repositioning the tricuspid valve leaflets at the true annulus, and right atrial and RV plication. To better understand the pathophysiology and surgical treatment of Ebstein anomaly, we used cardiovascular magnetic resonance (CMR) to study the impact of the cone procedure on ventricular size, function, and synchrony.

Methods: All patients who underwent a cone operation for Ebstein anomaly at a single institution and had both pre- and post-operative CMR studies were retrospectively identified and included. Ventricular volumes were prospectively re-measured to ensure consistency. LV circumferential and longitudinal strain (global and segmental) were measured from cine short- and long-axis views using a custom displacement-based feature tracking algorithm applied to the endocardial borders [1]. To quantify dyssynchrony, cross-correlational temporal offsets (TOs) were computed for 72-96 short-axis segmental curves encompassing the LV, and a patient-specific reference curve was determined using a quality threshold clustering algorithm [2]. An LV dyssynchrony index was calculated as the standard deviation of the TOs. To further investigate the contribution of the septum to LV dyssynchrony, the median TO of the ventricular septum was quantified.

Results: Twenty-one patients (38% male) were included with a mean age at cone operation of 16±9 years, a median time between CMRs of 2.5 years (range 0.25-7.2), and no significant change in heart rate between CMRs (p=0.38). Pre and post-operative values are shown in the Table. With the expected decrease in TR, indexed RV end-diastolic volume (EDV), end-systolic volume (ESV), and stroke volume significantly decreased while ejection fraction (EF) was unchanged. For the LV, indexed EDV, ESV, and stroke volume all increased while EF, global circumferential strain, and global longitudinal strain were unchanged. Regional analysis revealed a significant improvement in LV basal septal strain (Table, Figure 1). Although QRS duration increased after the operation, there was a significant reduction in the LV dyssynchrony index, likely attributable to earlier activation of the septum and anterior wall compared to pre-operation (Figure 2).

Conclusions: In patients with Ebstein anomaly, the cone operation leads to a reduction in TR and RV stroke volume, an increase in LV stroke volume, better LV basal septal strain, and enhanced LV synchrony. Beyond simply relieving the TR, the operation thus appears to improve ventricular-ventricular interaction. Future studies should address whether the extent of improvement relates to postoperative outcome.

References:

[1] Jing et al, European Heart Journal - Cardiovascular Imaging 2014;15:1333-1343

[2] Suever et al, Journal of Magnetic Resonance Imaging 2014;39:958-65

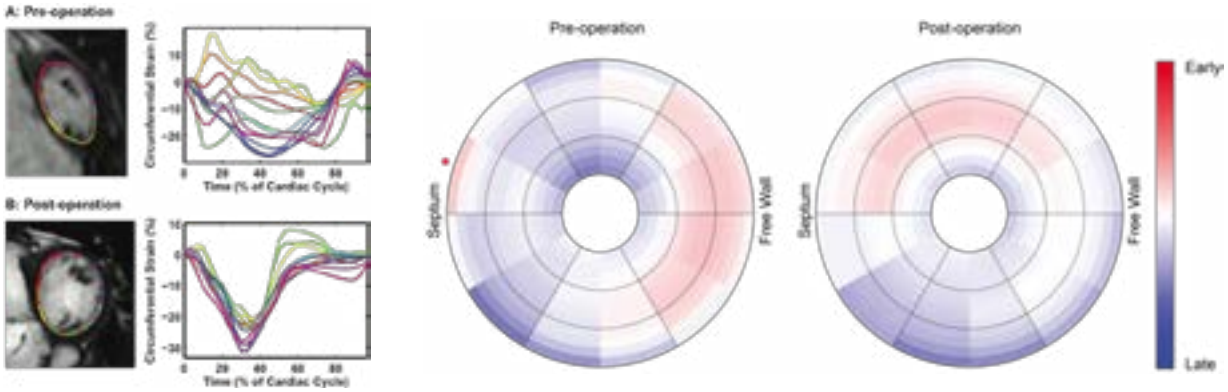

Values Before and After the Cone Operation (mean ± SD)

P value	Postop	Preop	Variable
<0.0001	86 ±14	68 ± 14	LV EDV index (ml/m^2)
0.0007	38 ± 11	31 ± 10	LV ESV index (ml/m^2)
<0.0001	48 ± 6	37 ± 7	LV stroke volume index (ml/m^2)
0.0005	91 ± 27	70 ± 27	LV mass index (g/m^2)
0.41	56 ± 7	55 ± 8	LV ejection fraction (%)
0.0001	141 ± 65	237 ± 110	RV EDV* index (ml/m^2)
0.001	89 ± 61	141 ± 80	RV ESV index (ml/m^2)
<0.0001	52 ± 8	96 ± 37	RV stroke volume index (ml/m^2)
0.003	29 ± 13	36 ± 15	RV mass index (g/m^2)
0.13	40 ± 9	43 ± 9	RV ejection fraction (%)
<0.0001	9 ± 10	50 ± 20	Tricuspid regurgitant fraction (%)
0.51	-26 ± 4	-26 ± 4	LV global circumferential strain
0.29	-19 ± 4	-20 ± 4	LV global longitudinal strain
0.06	-25 ± 4	-22 ± 5	Entire septum strain
0.004	-21 ± 5	-16 ± 7	Basal septum strain
0.14	-25 ± 4	-23 ± 4	Mid septum strain
0.74	-30 ± 5	-30 ± 5	Apical septum strain
0.38	83 ± 16	86 ± 13	Heart rate (bpm)
<0.0001	141 ± 28	115 ± 23	QRS duration (msec)
0.02	22 ± 10	32 ± 17	LV dyssynchrony index (msec)
0.02	29 ± 12	46 ± 26	LV dyssynchrony index (msec) ÷ RR (sec)
0.02	25 ± 10	38 ± 20	LV dyssynchrony index (msec) ÷ √RR (sec)
0.06	1.4 ± 12	-8 ± 16	Ventricular septum median TO (msec) ÷ √RR (sec)

LV = left ventricular; RV = right ventricular; EDV = end-diastolic volume; ESV = end-systolic volume; TO = temporal offset. *RV volumes include the atrialized portion of the RV

O020

The relationship between right ventricular extracellular volume measurements and clinical outcomes in patients with repaired tetralogy of Fallot

Kate Hanneman, MD[1] Bernd J. Wintersperger, MD[2], Elsie T. Nguyen, MD, FRCPC[2], Andrew M. Crean, MD MRCP[3], Paaladinesh Thavendiranathan, MD, MS[4], Camilla Kayedpour, MD[5], Rachel Wald, MD[6]

1. *Department of Medical Imaging, University of Toronto, ON, Canada*
2. *Department of Medical Imaging, University of Toronto, Toronto, ON, Canada*
3. *Toronto General Hospital, Toronto, ON, Canada*
4. *Toronto General Hospital and University of Toronto, Toronto, ON, Canada*
5. *Toronto General Hospital, ON, Canada*
6. *Division of Cardiology, University of Toronto, ON, Canada*

Background: Cardiac magnetic resonance (CMR) imaging is routinely used to evaluate patients with repaired tetralogy of Fallot (rTOF). Segmental myocardial fibrosis is known to be present in rTOF, however the role of extracellular volume (ECV) measurements as a marker of diffuse interstitial fibrosis has not been studied extensively. The aim of this study is to quantify right ventricular ECV (RVECV) in patients with repaired tetralogy of Fallot (rTOF), and to investigate its association with ventricular size and function and clinical outcomes.

Methods: We prospectively recruited adults for measurement of ECV by pre- and 15 minutes post-gadolinium T1 measurements (MOLLI) using a 1.5-T scanner in 39 patients with rTOF (34.6±9.5 years, 44% female) between September 2014 and May 2016. Three short-axis T1 maps were analyzed at base, mid and apex. Left ventricular ECV (LVECV) was determined by averaging segmental values, and RVECV was calculated by averaging values from anterior, lateral and the diaphragmatic RV wall segments. All available clinical data, including cardiopulmonary exercise testing results, were recorded within 12 months of CMR. Major adverse events were defined as death, cardiac surgical/catheter intervention, heart failure requiring admission for escalation of therapy or arrhythmia requiring medical and/or device therapy.

Results: RVECV was significantly higher than LVECV (43.3±0.8 ms vs. 27.2±0.6 ms, $p < 0.001$), and values correlated positively ($r=0.60$, $p < 0.001$). RVECV correlated with RV mass ($r=0.40$, $p=0.016$), RVEF ($r= -0.42$, $p=0.011$), and indexed RVEDV ($r=0.37$, $p=0.028$). RVECV did not correlate significantly with pulmonary regurgitation, LVEDV, LV mass or peak aerobic capacity on cardiopulmonary exercise testing. A major adverse event was documented in 12/39 patients (31%): death n=1 (3%), pulmonary valve replacement n=4 (10%), heart failure requiring admission for escalation of therapy n=1 (3%), and arrhythmia requiring intensification of medical therapy and/or device therapy n=6 (15%). The association between RVECV and major adverse events (OR 1.16, 95%CI [1.002, 1.35], $p=0.047$) remained statistically significant even after controlling for patient age and indexed RVEDV (OR 1.17, 95%CI [1.004, 1.35], $p=0.044$). There was a significant association between RVECV and tachyarrhythmia (OR 1.31, 95%CI [1.03, 1.68], $p=0.029$).

Conclusions: In this cohort, increased RVECV was associated with major adverse events. RVECV correlated positively with LVECV, indexed RVEDV, and RV mass and negatively with RVEF. These results may lead to further studies exploring the potential role for RVECV in risk stratification within the adult population with rTOF.

O021

Synthetic Hematocrit Derived from the Longitudinal Relaxation of Blood Can Lead to Clinically Significant Errors in Measurement of Extracellular Volume Fraction

Frank J. Raucci, Jr., M.D., Ph.D.[1]Jason T. Christensen, M.D.[1], Lazaro E. Hernandez, M.D.[2], Larry W. Markham, M.D.[1], Meng Xu, M.S.[3], James C. Slaughter, Dr.PH.[3], David A. Parra, M.D.[1], Jonathan H. Soslow, M.D., M.S.C.I.[4]

1. *Vanderbilt University Medical Center, Division of Pediatric Cardiology, Nashville, TN*
2. *Joe DiMaggio Children's Hospital, Hollywood, FL*
3. *Vanderbilt University Medical Center, Department of Biostatistics, Nashville, TN*
4. *Vanderbilt University Medical Center, Nashville, TN*

Background: Extracellular volume fraction (ECV) is altered in pathologic cardiac remodeling and predicts death and arrhythmia. ECV can be quantified using cardiac MRI (CMR) T1 mapping but calculation requires a measured hematocrit (Hct). The longitudinal relaxation of blood has been used in adults to generate a synthetic Hct (estimate of true Hct) but has not been validated in pediatrics.

Methods: Fifty-three children and young adults [42 Duchenne muscular dystrophy (DMD) and 11 controls] underwent CMR with T1 mapping using modified Look-Locker inversion recovery (MOLLI) sequences. The subjects had a measured Hct the same day as CMR. Native and post-contrast T1 were determined in blood pool, septum, and free wall of mid-LV, avoiding areas of late gadolinium enhancement. Synthetic Hct and ECV were calculated. Intraclass correlation coefficient (ICC) and linear regression were used to compare measured and synthetic Hct as well as ECV from both locations.

Results: The mean age was 15.0 ± 5.6 years and mean left ventricular ejection fraction (LVEF) was 56% ± 8% (range 27-74). The mean measured Hct was 41.6% ± 2.8% compared to the mean synthetic Hct of 43.2% ± 2.9 (ICC 0.44 [0.24, 0.60]). Mean measured mid-free wall ECV was 31.0% ± 5.1% and mean synthetic mid-free wall ECV was 30.2% ± 5.2% (ICC 0.95 [0.92, 0.97]). The mean measured mid-septal ECV was 29.9% ± 4.8% and mean synthetic mid-septal ECV was 29.1% ± 4.5% (ICC 0.94 [0.91, 0.96]). Correlations were not affected by heart rate. Correlations were higher in controls, likely due to narrower ranges of Hct and ECV. While the ICC was strong, differences between measured and synthetic ECV ranged from -2.4% to 5.5% in the septum and -3.3% to 5.5% in the free wall. Using our laboratory's normal cut-off of 28.5%, for the mid-septal synthetic ECV, there were 12 patients incorrectly categorized as normal (false negative) and 3 false positives. Similarly, based on mid-free wall ECV, there were 11 false negatives and 2 false positives. Figure 1 demonstrates scatterplots with regression fits for measured vs synthetic (A) Hct, (B) mid-septal ECV, and (C) mid-free wall ECV.

Conclusions: Our data suggest that the use of synthetic Hct for the calculation of ECV results in miscategorization of individual patients. This difference may be less significant once synthetic ECV is calculated and averaged over a large research cohort. However, we recommend formal measurement of Hct in children and young adults for clinical CMRs.

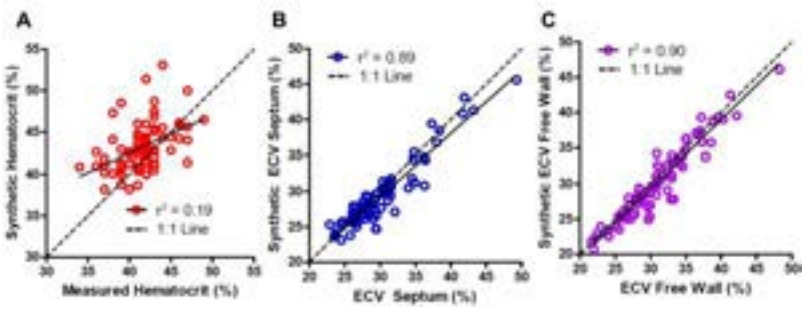

O022

Non-contrast perfusion imaging in the human heart using flow intra-voxel incoherent motion (fIVIM)

Kévin Moulin, PhD[1] Eric Aliotta, M.S.[2], Daniel B. Ennis, PhD[3]

1. *UCLA, Los Angeles, CA*
2. *UCLA, CA*
3. *Department of Radiological Sciences, University of California, Los Angeles, CA, USA., CA*

Background: Myocardial perfusion imaging is central to evaluating cardiac health, but existing contrast-based methods are contraindicated for patients with poor renal function. Contrast-free myocardial perfusion methods [1], such as the intra-voxel incoherent motion (IVIM) model [2], can separate the effects of perfusion and diffusion in diffusion weighted imaging (DWI). Current IVIM methods, however, require DWI signals with both low b-values (weighted by diffusion and perfusion) and high b-values (solely diffusion weighted) to separate the two effects. Recent work in the brain [3] has shown that perfusion and diffusion effects can be separated using velocity (i.e. flow) compensated diffusion encoding gradient waveforms. In this study, we propose flow-IVIM (*fIVIM*), which can generate perfusion maps in the heart using only low b-values (≤100s/mm²) via subtraction of DWI with and without flow compensation.

Methods: Healthy volunteers (N=7) were imaged on a 3T scanner (Prisma, Siemens). Two diastolic measurements were made with flow compensation (FC) and with no flow compensation (NC) using (TE=49ms, TR=4000ms, 2x2x5mm, end-respiratory triggered DW-EPI) at four b-values (0, 35, 65, 100 s/mm²) with flow encoding strengths α (0, 0.5, 0.76, 0.94s/mm for NC and 0s/mm for FC). Six diffusion encoding directions, and five averages were acquired in a single short-axis slice (250 total images, ~12-minutes). As shown in Figure 1, NC DWI were subtracted from FC DWI and used in the proposed fIVIM model: $F(b,\alpha)=f\cdot e^{-b\cdot D_b}(1-e^{-\alpha^2\cdot V_b^2/2})$ Similarly to [4], a global fit was achieved to calculate the perfusion fraction (f) and the micro-circulatory velocity (V_d) by aggregating the LV pixels for each subject. A second fit was realized pixel-wise to generate f maps. Blood diffusivity was set as constant D_b=1.75s/mm² [5].

Results: The fIVIM model demonstrated very good accuracy with a low residual to the overall fit (4.3±4.3%). Across the volunteers we found that f=15.2±5.4% and V_d=3.45±0.7mm/s in the LV myocardium. Perfusion fraction (f) maps (Figure 2) appeared homogenous with a lower mean (f=12.6±2.3%) (Figure 3) but a higher residual (29±5.1%) compared to global approach.

Conclusions: In this study, f and V_d were estimated in the human heart using only 4 b-values, compared to >9 usually used in classical IVIM [3,4,6]. Also a lower maximum b-value was used (compared with 400s/mm² in classical IVIM), which significantly reduces sensitivity to bulk motion. The proposed fIVIM method is thus a promising non-contrast perfusion method.

References:

(1) P. Martirosian et al., Eur J Nucl Med Mol Imaging, 2010

(2) D. Le Bihan et al., Radiology, 1986

(3) A. Ahlgren et al., NMR in biomedicine, 2016

(4) B.M. Delattre et al., Invest Radiol, 2012

(5) A. Wetscherek et al., MRM, 2014

(6) K. Moulin et al., MRM, 2016

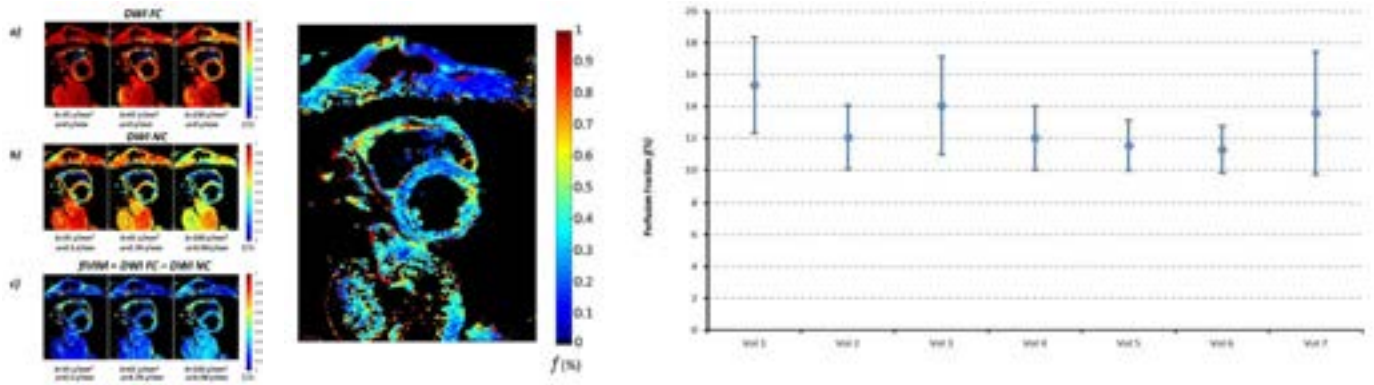

O023

Purely-systolic T1 mapping using an ungated spoiled steady-state approach: Towards reducing the confounding effect of intra-myocardial blood volume on native T1

Behzad Sharif, PhD[1] Zulma Sandoval, PhD[1], Daniel Berman, MD[2], C. Noel Bairey Merz, MD[3]

1. *Cedars-Sinai Medical Center, Los Angeles, Los Angeles, CA*
2. *Cedars-Sinai Medical Center, Los Angeles, CA*
3. *Cedars Sinai Medical Center, Los Angeles, CA*

Background: Recently, it has been established that a major contributor to native myocardial T1 is intra-myocardial water content [1], mainly driven by intra-myocardial blood volume (MBV). MBV depends on various physiologic factors and may act as a confounder for detecting myocardial fibrosis based on native T1. Hence, minimizing the dependence of native T1 on MBV can enhance its role as a reliable marker of fibrosis. To this end, we developed and tested an *ungated free-breathing T1 mapping* method that, in contrast to MOLLI-based methods, avoids any magnetization preparation – enabling it to capture "purely systolic" T1 maps. Since MBV is reduced during systole vs. diastole, this approach has the potential to reduce its confounding effect on T1.

Methods: Fig. 1 describes the proposed scheme, which continuously acquires data using a spoiled steady-state approach with alternating 3D/2D excitation (see caption) and without ECG gating or breath holding. Data acquisition was performed twice with two different flip angles (FAs) and a fixed TR= 5 ms (FA = 10° and 3°; scan time for each FA: 45 sec). Image reconstruction employed a self-gating approach using the acquired 3D readouts (*separating* systolic/diastolic readouts) followed by radial SENSE reconstruction using the 2D readouts (in-plane resolution: 1.8x1.8 mm). FA mapping was performed using an improved version of a previous method [2] to account for B1+ inhomogeneity (12-sec ungated scan). The reconstructed images and the relative FA map were used to generate a pixel-wise T1 map using the DESPOT1 method [3]. Healthy volunteers (n=9) were studied at 3T using the proposed method and the vendor-provided MOLLI sequence for native T1 mapping of the mid ventricular slice in systole and diastole.

Results: Fig. 2 shows representative results for the proposed method including raw images for the two FAs and the FA map in (a), and the T1 maps in (b) with comparison to MOLLI. In the studied subjects, there was a significant difference between systolic vs. diastolic septal T1 for the proposed method (1126 vs. 1233, respectively; $p < 0.01$) consistent with reduced MBV contribution for systolic T1. Overall, the diastolic septal T1 was not significantly different between MOLLI vs. the proposed method (1219 vs. 1233, respectively; p = n.s.).

Conclusions: We have proposed a hybrid 3D/2D *steady-state* approach for T1 mapping that eliminates the need for ECG-gating or breath-holding and, most notably, magnetization preparation. The latter feature has the potential to reduce the confounding effect of MBV on native T1 *by limiting the T1-fitting data to systole* (with lower MBV vs. diastole) and avoiding contamination of the fitting data by diastolic MBV dynamics. The promising results (high image quality and close agreement vs. MOLLI) point to the potential of this approach for accurate ungated free-breathing T1 mapping.

References:

[1] Mahmod & Piechnik et al. JCMR 2014;16.

[2] Chung & Axel et al. MRM 2010;64.

[3] Deoni et al. MRM 2003;49.

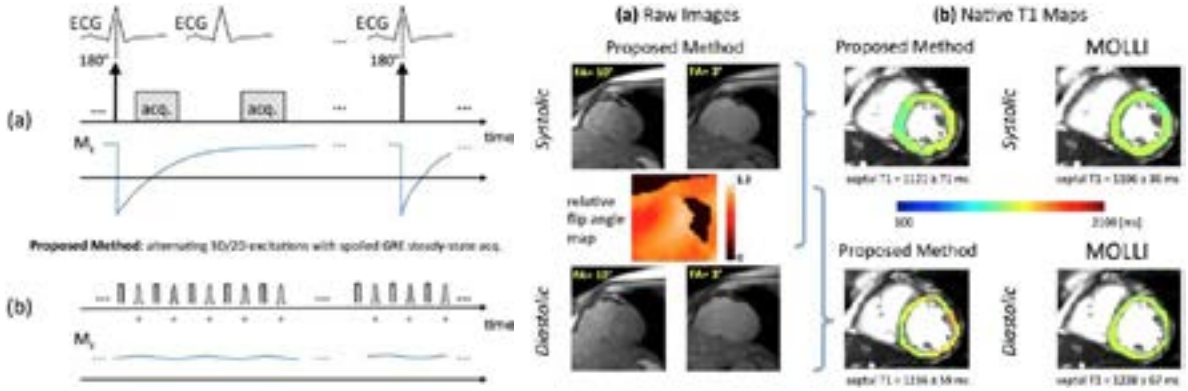

O025

CMR Validation of the Porcine Ameroid Occluder Model

Matthew J. Van Houten, MS[1] Yang Yang, PhD[2], David K. Glover, PhD, ME[1], Li-Ming Gan, MD professor[3], Mark Yeager, MD, PhD[1], Michael Salerno, MD, PhD[2]

1. *University of Virginia, Charlottesville, VA*
2. *University of Virginia, VA*
3. *Department of cardiology,Sahlgrenska University hospital, Hovås, Blekinge Lan, Sweden*

Background: 15.5 million patients in the US have coronary artery disease (CAD), which is responsible for 1 in 7 deaths [1]. Adenosine (Ado) stress CMR perfusion imaging can quantify absolute perfusion and myocardial perfusion reserve (MPR) in CAD with higher spatial resolution than PET, the only clinically-available technique for quantitative myocardial perfusion imaging. Porcine models offer insight to the development of perfusion abnormalities in chronic CAD. To date, there are limited studies using quantitative CMR perfusion imaging to evaluate these models. We created a progressive chronic coronary occlusion in the Yucatan pig model using ameroid occlusion of the left circumflex (LCX) artery and developed a quantitative adenosine protocol for evaluating the temporal evolution of perfusion defects in this model.

Methods: 10 Yucatan mini-pigs underwent ameroid-occlusion of the LCX to induce a chronic coronary obstruction. Resting and stress blood flow was measured using a Doppler flow probe placed around the LCX, 4 animals underwent a dose range experiment to determine the dose of Ado resulting in maximal hyperemia. CMR stress and rest perfusion imaging was performed using a spiral pulse sequence before surgery, then 1 week, 3 weeks, and 6 weeks following ameroid occlusion on a 1.5 T scanner (Siemens Avanto) using a 4 minute infusion of Ado at 300 mcg/kg/min). Perfusion images were acquired for 90 heartbeats at 3 short-axis slices during an injection of Magnevist at 0.075 mmol/kg [2]. Rest imaging was performed 30 minutes following stress imaging to allow adequate time for contrast wash-out. Pixel-wise perfusion quantification was performed in MATLAB. ROIs were drawn in the remote myocardium, and if present, in perfusion defects in the LCX territories. The perfusion defects were coded as “infarct” or “ischemia” using LGE images obtained at the same slice positions to identify myocardial infarction. Statistical analysis was performed in MATLAB and SAS using linear-mixed effect models.

Results: 7 of the 10 animals developed perfusion abnormalities by the 3rd week, and 6 animals developed an infarct. Figure 1 shows ischemia without infarction in one animal at the 3 week time point. The remote regions had higher stress flow and MPRs than the ischemic or infarct regions at 3 weeks and 6 weeks (Fig 2 and table 1). The ischemic and infarct region stress flows and MPRs were not significantly different from one another.

Conclusions: We developed a model of progressive CAD and evaluated the temporal evolution of the development of quantitative perfusion defects. Flow was significantly reduced in the infarct and ischemic regions at weeks 3 and 6. While the majority of animals developed a perfusion defect in the LCX territory, some animals also developed infarction. This model will serve as a platform for understanding the development of perfusion abnormalities in chronic occlusive CAD.

References:

1. Mozaffarian et al. Circ. (2015)
2. Salerno et al. MRM (2011)

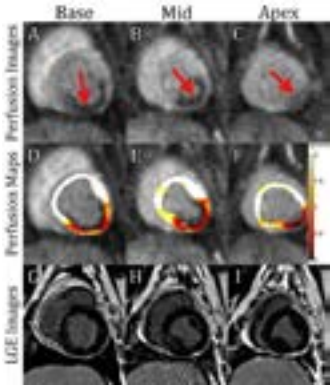

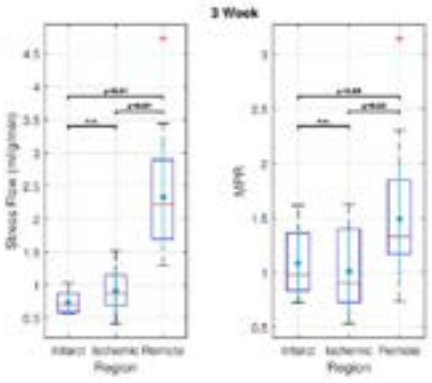

The remote region had significantly higher stress flows and MPRs than the ischemic and infarct regions at three weeks.

MPR	Stress Flow (mg/ml/min)	n	
1.5 ± 0.50	2.3 ± 0.78	30	Remote
1.0 ± 0.38	0.91 ± 0.34	15	Ischemic
1.1 ± 0.32	0.73 ± 0.17	13	Infarct

O026

In Vivo Cardiomyocyte Orientation Mapping with Diffusion Tensor MRI using Convex Optimized Diffusion Encoding (CODE)

Eric Aliotta, M.S.[1]Kévin Moulin, PhD[2], Luigi E. Perotti, PhD[1], Holden Wu, PhD[1], Daniel B. Ennis, PhD[3]

1. UCLA, CA
2. UCLA, Los Angeles, CA
3. Department of Radiological Sciences, University of California, Los Angeles, CA, USA., CA

Background: Recent developments in motion compensated diffusion encoding (*Stoeck, et al*. MRM 2015, *Nguyen, et al*. MRM 2013) have enabled high quality mapping of cardiomyocyte orientations *in vivo* using Diffusion Tensor Imaging (DTI). Convex Optimized Diffusion Encoding (CODE) optimizes motion compensated (MOCO) DTI pulse sequence timing for high resolution DTI with short TEs and consequently high SNR (*Aliotta, et al*. MRM2016) but has yet to be validated for mapping cardiomyocyte orientations. The ***objectives*** of this study were: 1) to measure cardiomyocyte orientations *in vivo* in healthy pigs using CODE DTI; 2) to validate the results with post-mortem *ex vivo* DTI; and 3) to demonstrate feasibility in human volunteers.

Methods: Healthy female Yorkshire pigs (N=3) were imaged on a 3T scanner (Siemens Prisma) in an IRB approved study. *In vivo* DTI was acquired using first and second order MOCO(M_1=M_2=0) CODE DTI (CODE-M_1M_2) (b=350s/mm^2, 10 directions, 2.0x2.0x8.0mm). Free-breathing imaging was triggered to end-expiration and mid-systole. Eight short axis slices were acquired with eight signal averages to improve SNR (scan time: 8 minutes per slice). After euthanasia, the heart was excised and imaged using "gold standard" readout segmented DTI (Porter, et al. MRM 2009) with b=1000s/mm^2, 30 directions, 1.0x1.0x1.0mm spatial resolution, 105 slices and 5 signal averages (scan time: 10 hours). Healthy volunteers (N=6) were also imaged after obtaining informed consent using a protocol matched to the *in vivo* porcine acquisitions. For all studies, diffusion tensors were reconstructed at each voxel using linear least squares and helix angles (HA) were calculated and binned by percent wall depth in increments of 10% for an *in vivo* mid-ventricular slice matched to *ex vivo*.

Results: DTI, reconstructed cardiomyocyte orientation maps, and HA maps are shown in Figure 1. Excellent qualitative agreement was observed between *in vivo* and *ex vivo* maps in swine as was good quantitative agreement between *in vivo* and *ex vivo* transmural distributions of HA (Figure 2). No significant difference was observed between *in vivo* and *ex vivo* HA distributions (mean ΔHA=-5.8±7.7°, p=N.S.) nor between differences in HA pitch (slope of transmural HA gradient; $pitch_{in\text{-}vivo}$=-1.4±1.4°/%vs. $pitch_{ex\text{-}vivo}$=-1.3±0.7°/%, p=N.S.). HA values measured in humans were qualitatively consistent across volunteers (Figure 3) and were in line with those measured in pigs (pitch=-1.3±1.0°/%).

Conclusions: CODE-M_1M_2 DTI produced high-quality *in vivo* maps of cardiomyocyte orientation and HA that show good agreement with *ex vivo* imaging. In vivo human results are consistent with previous work (*Nielles-Vallespin et al*, MRM 2012). Further work is needed to optimize the protocol for total scan time but this preliminary validation indicates that CODE-M_1M_2 DTI provides accurate *in vivo* microstructural information in free-breathing scans with reasonable durations.

http://www.ConferenceAbstracts.com/uploads/cfp2/attachments/LDFAIBDN/LDFAIBDN--218956-1-ANY.pdf

http://www.ConferenceAbstracts.com/uploads/cfp2/attachments/LDFAIBDN/LDFAIBDN--218956-2-ANY(1).pdf

http://www.ConferenceAbstracts.com/uploads/cfp2/attachments/LDFAIBDN/LDFAIBDN--218956-3-ANY(2).pdf

O027

ECG Triggering at Ultra-High Field Using a Conventional 3-Lead Trigger Device

Daniel Stäb, Dr.[1]Juergen Roessler, Dr.[2], Kieran O'Brien, Dr.[3], Christian Hamilton-Craig, Dr.[4], Markus Barth, Prof. Dr.[5]

1. *The University of Queensland, Brisbane St Lucia, Queensland, Australia*
2. *Siemens Healthcare GmbH, Bayern, Germany*
3. *Siemens Healthcare, Queensland, Australia*
4. *The Prince Charles Hospital, Brisbane, Queensland, Australia, Queensland, Australia*
5. *The Universtity of Queensland, Brisbane, Australia, Queensland, Australia*

Background: Cardiac magnetic resonance (CMR) at ultra-high field (UHF) has the potential to provide improved spatial resolution and new opportunities for tissue characterization or metabolic imaging. While essential for CMR, electrocardiographic (ECG) triggering can be impacted by the magneto-hydrodynamic (MHD) effect. Scaling with B_0, the MHD is particularly pronounced at higher fields meaning synchronization issues have been reported for numerous UHF CMR studies (1-3).

Methods: In this work, we investigate the performance of a 3-lead ECG trigger (Siemens Healthcare, Erlangen, Germany) and a state-of-the-art trigger algorithm (4-5) for cardiac synchronization at 7T.

6 healthy volunteers were examined on a non-commercial 7T whole-body research MRI scanner (Siemens Healthcare, Erlangen, Germany) under institutional review board permission equipped with a 8/32-channel Tx/Rx cardiac array (MRI Tools, Berlin, Germany).

To ensure accurate triggering, ECG electrodes were placed following the manufacturer's instructions, and in conjunction with a senior electrophysiology cardiac scientist. The trigger algorithm was calibrated by observing the subject's ECG outside the magnet for approximately 30s. This learning phase allows the algorithm to store the shape of the rising edge of the R-wave without the MHD effect being present. Inside the magnet and in presence of the MHD effect, the algorithm continuously compares the learnt shape to the incoming ECG and initiates trigger events based on several conditions (4-5).

Cine images were acquired using a two-dimensional gradient-echo sequence, and images were assessed visually. The trigger performance was evaluated qualitatively based on recorded ECG signals.

Results: A representative section of the recorded ECG signal time curves is shown in Fig. 1. Despite severe MHD-based signal distortions, trigger events were initiated accurately. Vectorcardiograms (Fig. 2) also demonstrate a high trigger fidelity. The histograms in Fig. 3 analyse the spacing between succeeding trigger events in greater detail. The very small number of shorter or longer RR-intervals indicates low false positive and false negative rates. The images were free of visible trigger-related artefacts.

Conclusions: By means of an accurate subject preparation and by including a learning phase outside of the magnetic field, reliable ECG triggering is feasible at ultra-high field using a standard 3-lead trigger device. The employed trigger algorithm provided sufficient accuracy for high-fidelity cardiac imaging despite severe ECG signal distortions by the MHD effect. Future work will evaluate the algorithm quantitatively in larger cohorts and patients with cardiac arrhythmia.

References:

[1] Suttie,NMR Biomed 2012;25:27–34.

[2] Frauenrath,JCMR 2010;12:67.

[3] Krug,JCMR 2013;15:W19.

[4] Frank,US Patent 2010/0191134 A1.

[5] Knesewitsch,JCMR 2013;15:3.

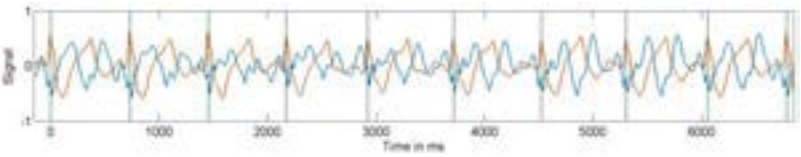

http://www.ConferenceAbstracts.com/uploads/cfp2/attachments/LDFAIBDN/LDFAIBDN--220471-2-ANY.pdf

http://www.ConferenceAbstracts.com/uploads/cfp2/attachments/LDFAIBDN/LDFAIBDN--220471-3-ANY.pdf

O028

Are synthetic haematocrit values derived from blood T1 a good substitute for blood samples to achieve accurate ECV calculation?

Pierre Croisille, MD PhD[1] Charles De Bourguignon, Master[2], Alban Chazot[3], Magalie Viallon, PhD Dr[4]

1. *Univ Lyon, UJM-Saint-Etienne, INSA, CNRS UMR 5520, INSERM U1206, CREATIS, Saint-etienne, Rhone-Alpes, France*
2. *Centre Hospitalier Universitaire de Saint-Étienne, Rhone-Alpes, France*
3. *CHU Saint Etienne, Lyon 05, N/A, France*
4. *CREATIS UMR CNRS 5220 - INSERM U1206/ Hopital Universitaire de Saint-Etienne, Rhone-Alpes, France*

Background: CMR is the only non-invasive method that permits quantification of extracellular volume fraction (ECV) : ECV is calculated using T1 mapping from the ratio of changes in signal in myocardium and blood before and after contrast injection, but also needs correction for the blood hematocrit (Hct). It was recently proposed to generate a synthetic ECV using blood native T1 that would ease ECV map calculation without the need for venous Hct sampling[1] : a linear relationship existing between Hct and relaxation rate constant of native R_1(blood), as already reported also in other various MRI applications including ASL[2]. However, it remains unclear if synthetic-Hct is reliable enough to be considered as a surrogate for blood sample Hct measurement.

Methods: We prospectively studied 53 outpatient subjects (35males/18females; 53±20 yo) referred for routine CMR with gadolinium injection. We performed and compared in each patient 4 different Hct measures: 1) outpatient laboratory-based measures performed within days before CMR-imaging (Lab-Hct); 2) same day venous blood sample drawn *before* imaging (before-Hct), 3) same day venous blood sample *during* imaging, immediately drawn after MOLLI sequence and set as the reference method (during-Hct) 4) synthetic-Hct calculated from Blood T1 (Base, mid, apex) as performed by Treibel et al[1]. Same day on-site Hct measures (K2-EDTA, 2x75microl) at MR-bedside were performed using spun packed cell volume (PCV) reference method (ICSH recommendations) using an Heamatocrit 200 centrifuge (Hettich Lab, Germany).

Results: Using synthetic-Hct (calculated from T1 blood values averaged across levels) , the systematic absolute difference (bias) was 3.5% Hct [95%CI: 10.2,-3.1] ($p < 0.0001$), with a coefficient of repeatability (CR) or least detectable difference of 6.8 Hct %. Bias was also observed to vary according to the slice level used, from 3.9% [11.1,-3.2] at basal level to 3.2% [9.1,-2.7] at mid level. Note the smaller but significant bias observed with Lab-Hct measures (2.7% [6.2;-0.87]) and even with blood samples drawn before imaging (before-Hct samples; 2.2% [6.9;-2.5]).

Conclusions: Among all clinical scenarios evaluated to obtain Hct values for online ECV map calculation, synthetic-Hct appeared unfortunately the less reliable approach due to both systematic bias (inaccuracy) and lack of precision (partly caused also by T1 imprecision). Hematocrit is also unfortunately influenced by many pre-analytical physiological and environmental factors, including time of the day, fasting conditions, and interestingly changes in position that are recognized to induce postural pseudoanemias[3] from standing to lying and illustrated here by the difference between same day on-site measures performed before and during CMR examination.

References: 1-Treibel (JACC 2016); 2-Lu (MRM 2004); 3-Jacob (Mayo Clin Proc 2005)

O029

Non-ECG, Free-Breathing Joint Myocardial T1-T2 Mapping Using CMR Multitasking

Anthony G. Christodoulou, PhD[1]Christopher Nguyen, PhD[2], Jaime L. Shaw, MS[1], Yibin Xie, PhD[1], Nan Wang, B.S.[2], Debiao Li, PhD[3]

1. *Cedars-Sinai Medical Center, CA*
2. *Cedars-Sinai Medical Center, Los Angeles, CA*
3. *Biomedical Imaging Research Institute, Cedars-Sinai Medical Center, Los Angeles, CA, CA*

Background: Quantitative mapping of myocardial T1 and T2 show promise for diagnosis of myocardial infarction, ischemia, edema, and more [1]. T1 and T2 maps are typically acquired using ECG-triggering and breath-holding, which lead to heart-rate sensitivity and patient discomfort (or when unsuccessful, mis-triggering and/or respiratory motion artifacts). This work describes a method achieving non-ECG, free-breathing joint T1-T2 mapping using the cardiovascular low-rank tensor (LRT) imaging framework [2] for CMR multitasking (simultaneous imaging of multiple dynamics such as cardiac/respiratory motion, T1 recovery, T2 decay, etc.).

Methods: The proposed method employed hybrid T2prep/IR magnetization preparation and a continuous-acquisition single-slice 2D radial sequence with a golden-angle ordering scheme modified to collect LRT subspace training data [2]. T1-T2 contrast was achieved using a T2prep/IR preparation pulse (Fig. 1). Each prep pulse was followed by 5° FLASH readouts every 3.6 ms for 2.45 s; the prep pulse duration was cycled through 12, 20, 30, 40, and 50 ms. The process was repeated for a total duration of 85 s. Real-time low-rank matrix images [3] were reconstructed first for image-based cardiac/respiratory binning. LRT image reconstruction was then performed with 15 cardiac bins, five respiratory bins, five T2prep durations, and 344 inversion times (3.6, 10.7, 17.8, ..., 2446 ms).

Data were collected on a 3T Siemens Verio from n=5 healthy volunteers. To assess T1-T2 accuracy and repeatability, three scans each were collected of: diastolic T1 maps from ECG-triggered, breath-held SSFP MOLLI 5(3)3 [4]; diastolic T2 maps from ECG-triggered, breath-held T2prep-SSFP mapping [5]; and multiphase T1-T2 maps from the proposed non-ECG, free-breathing method, all at 1.7 mm in-plane spatial resolution.

Results: Fig. 2 shows diastolic and systolic T1-T2 maps from LRT, a diastolic T1 map from MOLLI, and a T2 map from T2prep-SSFP, all for the subject with median repeatability. Table 1 summarizes statistical findings from the three methods. The proposed method underestimated diastolic T1 compared to MOLLI with reduced precision (coefficient of variation: 5.4% vs. 0.6%), but yielded values within the range previously reported in the literature [6]. This apparent bias may be an effect of the preparation scheme differences (T2prep/IR vs. IR) or from sequence differences (FLASH vs. SSFP). The proposed method yielded similar T2 measurements to T2prep-SSFP.

Conclusions: We have presented a method for non-ECG, free-breathing joint T1-T2 mapping using LRT imaging, allowing T1 and T2 measurement at multiple cardiac and respiratory phases. Measurements were within the range reported in the literature, and were repeatable to 5.4% for T1 and 6.9% for T2. These initial results show great promise for non-ECG, free-breathing multiparameter mapping.

References:

1. Blume *JMRI* 2009
2. Christodoulou *ISMRM* 2016
3. Christodoulou *TBME* 2013
4. Xue *MRM* 2013
5. Giri *JCMR* 2009
6. von Knobelsdorff-Brenkenhoff *JCMR* 2013

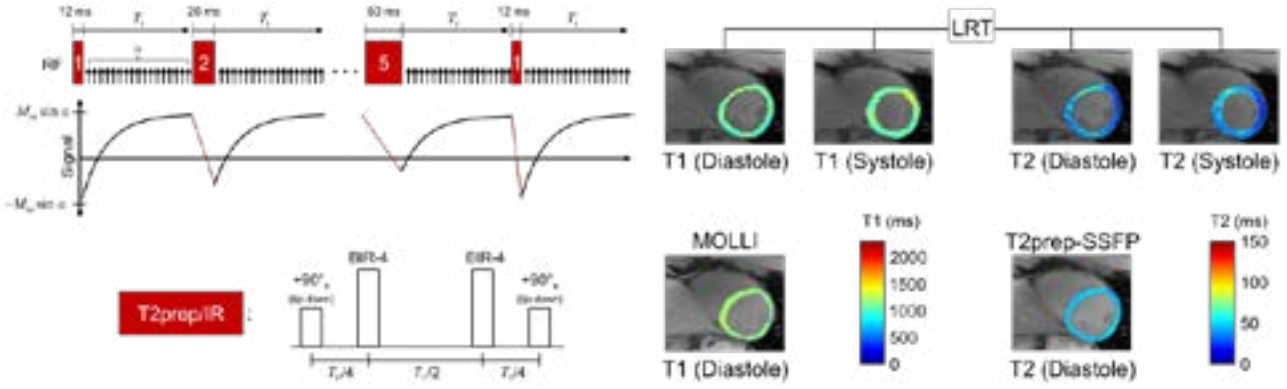

Table 1: Summary of measurement statistics

Coeff. of variation	Within-subject standard deviation	Values	Measurement	Method
5.4%	57	1054 ± 61	Mean myocardial T1 (ms)	LRT CMR Multitasking
6.9%	3.5	50 ± 7.3	Mean myocardial T2 (ms)	
0.6%	7.9	1252 ± 47	Mean myocardial T1 (ms)	MOLLI
3.3%	1.7	51 ± 3.0	Mean myocardial T2 (ms)	T2prep-SSFP

O030

Building Understanding Of The Myocardial Phenotype: ECV, LGE And Biopsy Measure Complementary But Overlapping Aspects – A 133 Biopsy Severe Aortic Stenosis Study

Thomas Treibel, MBBS.MRCP(UK)[1]Begoña López, PhD[2], Arantxa González, PhD[2], Katia Menacho-Medina, MD[1], Rebecca Schofield, MBChB, MRCP[1], Marianna Fontana, MD, PhD[3], Steven K. White, MBChB[4], Javier Díez, PhD[2], James C Moon, MD[1]

1. *Barts Heart Centre, England, United Kingdom*
2. *Universidad de Navarra: Cima Centro de Investigación Médica Aplicada, Pamplona, Pamplona, Navarra, Spain*
3. *National Amyloidosis Centre, University College London, England, United Kingdom*
4. *East Kent Hospitals University NHS Trust, England, United Kingdom*

Background: Historically, insights on cardiac fibrosis in aortic stenosis (AS) have been obtained from histology. Recently, late gadolinium enhancement (LGE) and extracellular volume fraction (ECV) by cardiovascular magnetic resonance (CMR) have emerged as promising non-invasive biomarkers of cardiac fibrosis. The aim of this study was to compare the performance of LGE, ECV and histology to assess myocardium in severe AS.

Methods: 133 patients with severe, symptomatic AS accepted for surgical aortic valve replacement (age 70±10 years, 55% male, AVAi 0.40±0.13cm^2/m^2) underwent CMR with LGE and T1 mapping (MOLLI) for ECV quantification, echocardiography, blood biomarker analysis and intra-operative left ventricular biopsies (quantified as collagen volume fraction, CVF). Biopsies (by needle and scalpel) yielded tissue including endocardium (n=53) and without (n=80); these were compared to myocardium from ten controls (age 60±7 years, 70% male).

Results: The endocardial biopsies revealed a fibrosis gradient from superficial to deep. This had: a massive fibrotic layer thickening the endocardium; abundant microscopic scars in the subendomyocardium (Figure 1), and the faint reinforcement of the perimyseal collagen in the whole myocardial interstitium. CVF was elevated in severe AS (11.5±8.6% vs 1.95±0.20% in controls, $p < 0.001$) with higher CVF in endocardial than in non-endocardial biopsies (15.0±12.0% vs 9.0±6.7%, $p < 0.001$). LGE correlated with CVF in all samples (r=0.499; $p < 0.001$) and in endomyocardial samples (r=0.708; $p < 0.001$), but ECV did not (Table 1). Both LGE and ECV correlated with NT-proBNP and hs-Troponin T in all samples and in endomyocardial samples, with the stronger correlations of ECV with NT-proBNP, and of LGE with hs-Troponin T. ECV was the only parameter predicting six minute walk test distance.

Conclusions: In AS measured by histology, multifocal replacement fibrosis (mainly subendomyocardial microscars) predominates over perimyseal fibrosis. Whereas LGE captures fibrosis and tracks hs-Troponin T best, ECV tracks NT-proBNP and patients' functional limitation best. These findings suggest that LGE is a marker of the reparative fibrotic response to ischemia and cardiomyocyte damage whereas ECV is a marker of the response of the cardiomyocyte to hemodynamic stress – thus ECV appears more a measure of functional cardiomyocyte phenotype than our current mainstream concepts of fibrosis.

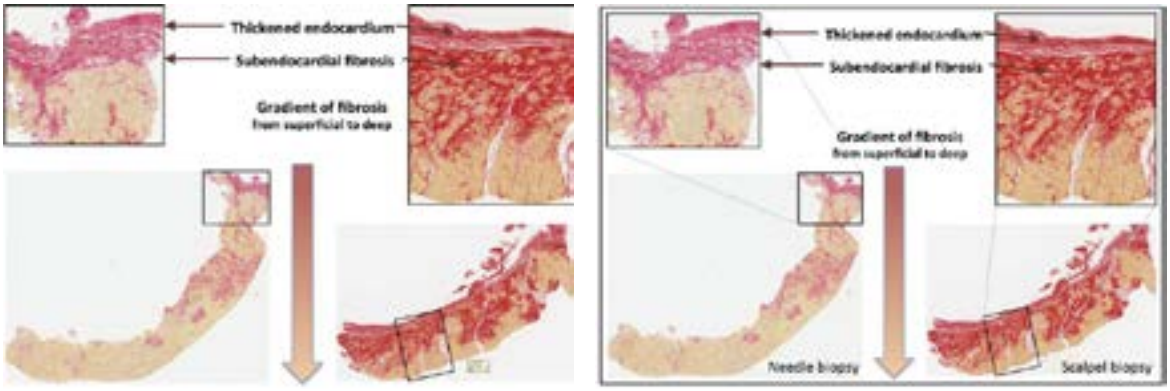

Correlations between imaging and biopsy markers of fibrosis

NT-proBNP	CVF	LGE	ECV	
r=0.460 *p<0.001*	r=0.499 *p<0.001*		r=0.255 *p<0.01*	**LGE**
r=0.236 *p<0.05*		r=0.499 *p<0.001*	NA	**CVF**
	r=0.236 *p<0.05*	r=0.460 *p<0.001*	r=0.554 *p<0.001*	**NT-proBNP**
r=0.552 *p<0.001*	r=0.268 *p<0.01*	r=0.451 *p<0.001*	r=0.364 *p<0.001*	**hs-Troponin-T**

O031

Myocardial T2* Changes Periodically over the Cardiac Cycle and is Prolonged in Patients with Hypertrophic Cardiomyopathy versus Healthy Controls: A 7.0 Tesla MRI Study

Till Huelnhagen, Dipl.-Ing.[1]Fabian Hezel, PhD[1], Teresa Serradas Duarte, MSc[1], Bert Flemming, MD[2], Erdmann Seeliger, MD[2], Marcel Prothmann, MD[3], Jeanette Schulz-Menger, MD[4], Thoralf Niendorf, PhD[1]

1. *Berlin Ultrahigh Field Facility, Max Delbrueck Center for Molecular Medicine, Berlin, Germany, Berlin, Germany*
2. *Institute for Physiology, Charité University Medicine, Berlin, Germany, Berlin, Germany*
3. *Working Group on Cardiovascular Magnetic Resonance, Experimental and Clinical Research Center, a joint cooperation between the Charité Medical Faculty and the Max-Delbrueck Center for Molecular Medicine and HELIOS Hospital Berlin Buch, Berlin, Berlin, Germany*
4. *Working Group on Cardiovascular Magnetic Resonance, Experimental and Clinical Research Center a joint cooperation between the Charité Medical Faculty and the Max-Delbrueck Center for Molecular Medicine HELIOS Klinikum Berlin Buch, Germany, Berlin, Germany*

Background: Ultrahigh field MR enables temporally resolved myocardial T2* mapping which benefits probing myocardium at different physiological states[1]. Myocardial T2* is commonly regarded as surrogates for myocardial tissue oxygenation[2], but the factors influencing T2* are manifold[3]. Meaningful interpretation of T2* requires identification of influential factors and their contributions. This study examines the relationship of myocardial T2* and cardiac macromorphology and investigates it's capability to distinguish healthy myocardium from myocardium affected by hypertrophic cardiomyopathy (HCM).

Methods: Six healthy volunteers (4 male,age=50.0±12.4,BMI=23.9±2.9kg/m^2) and six patients with confirmed HCM (4 male,age=52.7±17.5,BMI=25.2±1.9 kg/m^2) were examined using a 7T whole body MR system (Siemens Healthcare,Erlangen,Germany) equipped with a 16 channel RF-transceiver array. For CINE T2* mapping a cardiac triggered interleaved multi-echo gradient-echo technique was employed[1] (Fig.1). Prior to T2* fitting, images were de-noised and co-registered. Ventricular septal wall thickness (SWT), left ventricular inner radius and septal T2* were analyzed.

Results: Mean SWT was 7.3±1.2mm in controls and 14.1±2.5mm in patients. Mean septal T2*=13.7±1.1ms and T2*=17.45±1.4ms were obtained. Mean end-systolic SWT=9.8±1.4 mm (SWT=16.6±1.8 mm) and mean T2*=15.0 ± 2.1ms (T2*=17.7±1.2ms) were observed in controls (patients). Mean end-diastolic SWT=6.2±1.2mm (SWT=13.0±3.1mm) and T2*=13.4±1.3ms (T2*=16.2±2.5ms) were found. SWT and T2* were significantly higher in patients. A systolic increase and diastolic decrease of T2* were observed in both groups. The diastolic T2* decrease was less steep in patients (Fig.2). Pearson correlation analysis yielded a significant strong positive correlation (R=0.97,P < 0.001) of septal T2* and SWT (Fig.3).

Conclusions: Septal T2* changes periodically across the cardiac cycle and is increased in HCM. Septal T2* correlates with SWT. While temporal changes of myocardial T2* have been attributed to changing myocardial blood volume fraction (MBVF) [4], two main factors are assumed to cause the T2* increase in HCM. Improved tissue oxygenation in HCM is unlikely. Instead, first, T2 was reported to be elevated in HCM[5] which also increases T2*. Second, reduced myocardial perfusion and ischemia are common in HCM[6], effectively reducing MBVF resulting in T2* increase. These conditions are also associated with a higher risk for a poor outcome. Hence our results suggest that myocardial T2* mapping could be beneficial for understanding cardiac (patho)physiology in vivo and support risk stratification in HCM.

References:

[1]Hezel et al.(2012)PLoSOne 7(12):e52324

[2]Friedrich et al.(2013)JCMR 15:43

[3]Christen et al.(2012)MRM 67(5):1458

[4]Huelnhagen et al.(2016)MRM, doi:10.1002/mrm.26312

[5]Abdel-Aty et al.(2008)JMRI 28(1):242,[6]Johansson et al.(2008)Int J Card 126(2):252.

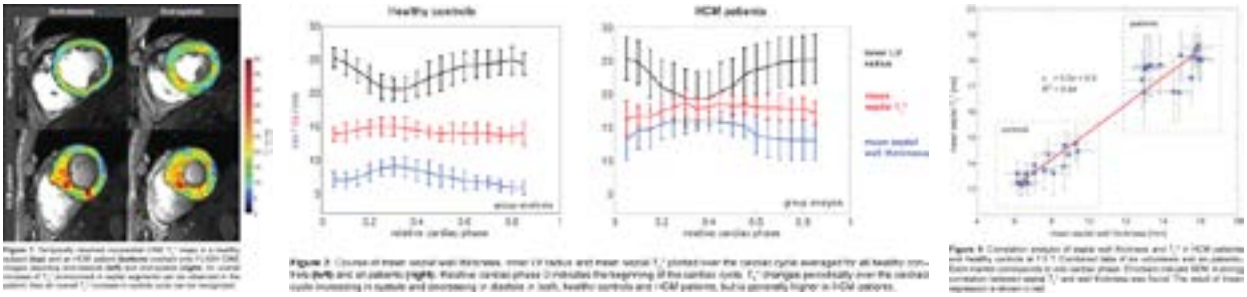

O032

Doxorubicin-associated cardiac tissue remodeling followed by CMR of myocardial extracellular volume and myocyte size in breast cancer patients.

Thiago Ferreira de. Souza, MD[1]Felipe Osorio Costa, MD[2], Tomas Neilan, MD, MPH[3], Ravi Shah, MD[4], Lício Velloso, MD,PhD[5], Wilson Nadruz, Jr., MD, PhD[6], Fabricio P. Brenelli, PhD, MD[6], Otávio Coelho, MD, PhD[7], Michael Jerosch-Herold, PhD[8], Coelho-Filho R. Otavio, MD, PhD, MPH[1]

1. *State University of Campinas, Campinas, Sao Paulo, Brazil*
2. *State University of Campinas - UNICAMP, Sao Paulo, Brazil*
3. *Massachusetts General Hospital, Newton, MA*
4. *BIDMC, MA*
5. *University of Campinas, Campinas, Sao Paulo, Brazil*
6. *State University of Campinas, Sao Paulo, Brazil*
7. *State University of Campinas - ENCAMP, Sao Paulo, Brazil*
8. *Department of Radiology, Brigham & Women`s Hospital & Harvard Medical School, Boston, United States., MA*

Background: Doxorubicin (DOX) persists as a key component of chemotherapy regimens in adult malignancies, though cardiovascular disease remains a leading cause of morbidity and mortality among these patients. The mechanism of DOX-induced heart damage is not entirely understood. Experimental studies showed that cardiac atrophy, accompanied by augmented interstitial myocardial fibrosis and decreased myocyte size, is a common tissue phenotype after DOX. The goal of this study was to characterize DOX-associated remodeling by CMR ECV and intracellular lifetime of water (tau) in breast cancer patients.

Methods: Twenty-seven breast cancer (BC) women (mean-age 52±9 years, BMI 27±4 kg/m2), without heart-failure, underwent CMR imaging (3T-Achieva, Philips) before and 3 times serially (medium days after DOX:v-1:70, v-2:154,v-3:364) after adjuvant DOX (4-cycles of 60 mg/m2). CMR included LV-function, T1 mapping pre and post gadolinium and LGE imaging. Biomarkers were obtained before and 72 hours after each DOX-cycle.

Results: BC-patients had normal baseline LVEF (69±4%), LVMass-index (51±9g/m2) without occurrence of LGE. After DOX, LVEF (v-1:60±7,v-2:56±4 and v-3:54±7%) and LVMass-index (v-1:44±5, v-2:42±4, v-3:38±7g/m2) significantly decreased (all $p < 0.01$). While DOX-therapy was associated with a progressive expansion of ECV (baseline:0.32±0.07, v-1:0.33±0.05, v-2:0.35±0.05, v-3:0.36±0.04), tau significantly decreased (baseline:0.17±0.02, v-1:0.14±0.05, v-2:0.13±0.05, v-3:0.13±0.08, all $p < 0.05$, figure1). ECV showed a positive association with time after DOX ($r=0.5$, $p < 0.01$) and a negative association with time after DOX with tau($r=-0.6$, $p < 0.001$). Interestingly tau positively correlated with LVEF, suggesting that less myocyte atrophy was associated with better systolic function after DOX ($p < 0.05$). LVMass-index showed a positive association with tau, and a negative association with ECV, suggesting a loss of LVMass due to diffuse replacement fibrosis, which causes an increase of ECV, with simultaneous adjustment for changes in cardiomyocyte size (figure3).
Radiation-therapy also had a significant effect on LV mass index($p=0.005$). Serial ultra-sensitive troponin after each DOX-cycle showed a positive significant association with time after DOX ($p < 0.001$) but no association was seem with LVMass index or LVEF.

Conclusions: DOX-therapy was associated with a significant decline in both LVEF and LVMass. DOX was associated with signs of cardiac atrophy, documented by decrease of LVMass. The loss of LV mass was driven by both a reduction in cardiomyocyte size, and an expansion of the extra-cellular volume due to diffuse replacement fibrosis, despite the absence of LGE. This study demonstrates that CMR offers the potential to enhance the understanding of LV remodeling in DOX.

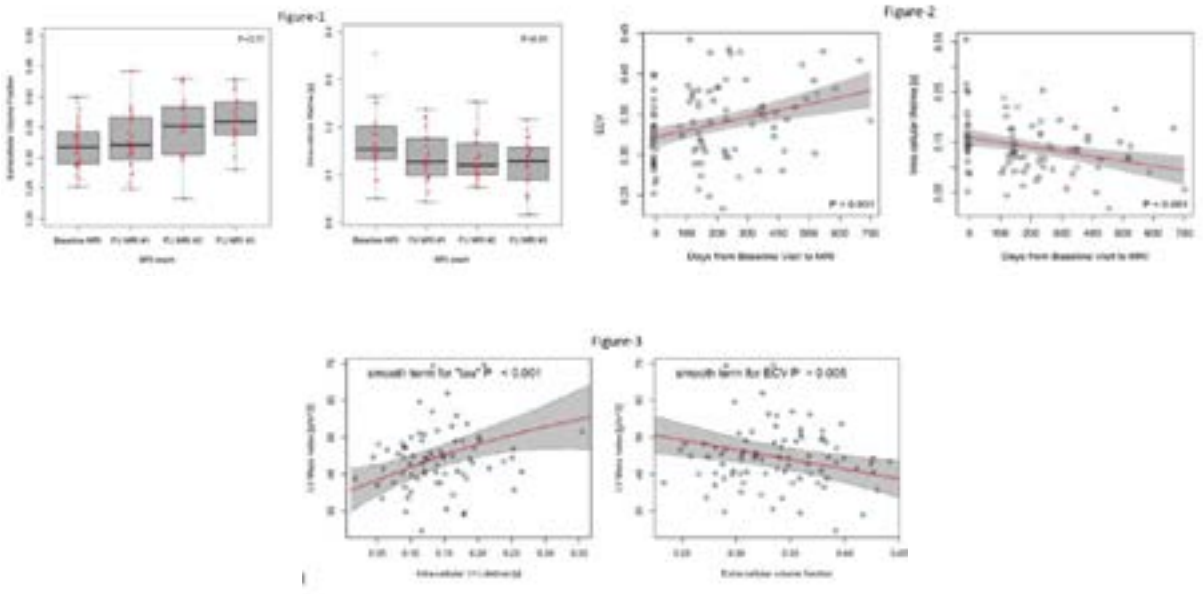

O033

Comparative Prognostic Value of Myocardial Strain Derived From Deformation-Tracking, Feature-Tracking or DENSE CMR: the British Heart Foundation MR-MI Study.

Kenneth Mangion, MD[1] David Carrick, PhD[2], Jaclyn Carberry, BScMedSci[3], Ahmed Mahrous Abouzaid, MRCP, MD[4], Christie McComb, PhD[5], Hao Gao, PhD[6], Xiaoyu Luo, PhD, MSc [1], Hany Eteiba, MD[7], Mitchell Lindsay, MD[7], Margaret McEntegart, MBChB PhD[2], Stuart Hood, MD FRCP[8], Mark Petrie, MD[9], Keith G. Oldroyd, MD (Hons); FRCP[7], Stuart Watkins, MD, FRCP[2], Andrew Davie, MB ChB[7], Xiaodong Zhong, PhD[10], Caroline E Haig, PhD[11], Colin Berry, PhD FRCP[1]

1. *University of Glasgow, Glasgow, Scotland, United Kingdom*
2. *Golden Jubilee National Hospital, Glasgow, Scotland, United Kingdom*
3. *BHF Glasgow Cardiovascular Research Centre, University of Glasgow, Scotland, United Kingdom*
4. *West of Scotland Deanery, Scotland, United Kingdom*
5. *NHS Greater Glasgow and Clyde / University of Glasgow, Glasgow, Scotland, United Kingdom*
6. *School of Mathematics and Statistics, University of Glasgow, Scotland, United Kingdom*
7. *Golden Jubilee National Hospital, Scotland, United Kingdom*
8. *NHS Greater Glasgow and Clyde, Scotland, United Kingdom*
9. *Glasgow University, Scotland, United Kingdom*
10. *Siemens Healthcare, GA*
11. *Robertson Centre for Biostatistics, Glasgow, Scotland, United Kingdom*

Background: Infarct size assessed early after acute ST-segment elevation myocardial infarction (STEMI) may over-estimate the true extent of infarction, which may limit its utility as a prognostic biomarker. Myocardial strain derived from Displacement ENcoding with Stimulated Echoes (DENSE) cardiac magnetic resonance (CMR) provides information on myocardial contractility with high precision and accuracy. Compared with feature-tracking, deformation tracking may be more closely representative of contractility. We aimed to compare the prognostic value of peak circumferential strain (E_{cc}) derived from a novel deformation tracking cine-strain method, feature-tracking, and DENSE.

Methods: We undertook a prospective, single centre cohort study (ClinicalTrials.gov identifier NCT02072850). Participants provided written informed consent (ethics reference 10/S0703/28) and underwent CMR at 1.5 T (Avanto, Siemens Healthcare, Erlangen, Germany) 2 days and 6 months post-MI. CMR included cine (balanced steady-state free precession), 2D-cine EPI DENSE, and delayed-enhancement phase-sensitive inversion-recovery pulse sequence 10-15 minutes after IV injection of 0.15 mmol/kg of gadoterate meglumine (Dotarem, Guebert S.A., Villepinte, France).The myocardial mass of late gadolinium (LGE) was quantified using computer-assisted planimetry, utilising the 5 SD technique and expressed as % LV mass.

Mid-left ventricular acquisitions were analysed using an inhouse b-spline deformable method (Matlab), feature-tracking (TomTec Imaging Systems, Germany), and CIM_2D DENSE (University of Auckland, New Zealand).

During longer term follow-up, spontaneous serious adverse cardiovascular events (major adverse cardiac events (MACE), all-cause death or heart failure (ACD/HF) were independently assessed by cardiologists blind to the baseline data. Statistical analysis was performed using SPSS and R and directed by a statistician independent of the research group.

Results: 323 patients (58.6 ± 13.2y age, 237(73%) male, 118 (37%) anterior MI, 30(9%) diabetes, 304 (94%) with normal flow (TIMI 3) post-PCI), underwent CMR, of these, 259 had DENSE acquired. Of these 259 subjects, 21 patients (8%) experienced a MACE and 22 patients (8%) experienced ACD/HF at a minimum of 3 years follow-up. DENSE and baseline LGE had reasonable power for prediction of adverse events. For MACE, using ROC analysis, optimal cut-offs for DENSE was -10.51%, LGE 24.05g, for ACD/HF, using ROC analysis optimal cut-offs for DENSE was -10.40%, and LGE 24.20g (figure 1). Using Cox-regression analysis, DENSE offered an incremental prognostic benefit over baseline infarct size to predict MACE (Table 2).

Conclusions: DENSE-derived E_{cc} offers an incremental prognostic benefit over infarct size revealed by LGE to predict MACE, and using a cut-off of -10.51% can identify STEMI patients at higher risk of events.

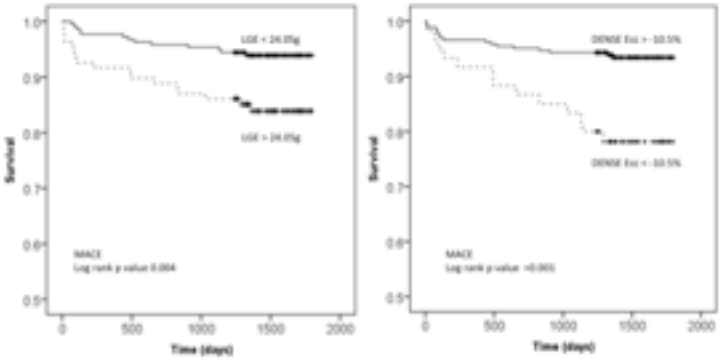

Table 1. Receiver Operator Characteristics curves for baseline scar and circumferential strain for MACE and ACD/HF outcomes.

ACD/HF (n=22)		MACE (n=21)		
p-value	AUC	p-value	AUC	
0.037	0.635	0.028	0.644	Baseline infarct size (%LV mass)
0.006	0.678	0.001	0.712	DENSE E_{cc}
0.335	0.562	0.117	0.603	Deformation tracking E_{cc}
0.488	0.545	0.348	0.562	Feature-tracking E_{cc}

AUC- area under curve, MACE- major adverse cardiovascular events, ACD/HF- all cause death or hospitalisation for heart failure .

Table 2. Cox-regression for major adverse cardiovascular events (MACE) and for all-cause death/ heart failure (ACD/HF) (n=259)

ACD/HF		**MACE**		
p-value	HR (95% CI)	p-value	HR (95% CI)	
0.007	1.040 (1.011-1.070)	0.008	1.040 (1.010- 1.070)	Infarct Size at Baseline
				Sequential adding DENSE derived circumferential strain
0.145	1.023 (0.9920 1.055)	0.227	1.019 (0.988- 1.052)	Infarct Size at Baseline
0.28	1.146 (1.015- 1.294)	0.012	1.175 (.036-1.334)	Circumferential Strain (DENSE)
				Sequential adding deformation-tracking derived circumferential strain
0.044	1.040 (1.001- 1.081)	0.115	1.031 (0.993-1.070)	Infarct Size at Baseline
0.997	1.000 (0.850- 1.177)	0.487	1.061 (0.899- 1.252)	Circumferential Strain (deformation tracking)
				Sequential adding feature-tracking derived circumferential strain
0.017	1.043 (1.008- 1.080)	0.021	1.042 (1.006- 1.079)	Infarct Size at Baseline
0.987	0.987 (0.913- 1.068)	0.846	0.992 (0.916-1.075)	Circumferential Strain (FT)

AUC- area under curve, MACE- major adverse cardiovascular events, ACD/HF- all cause death or hospitalisation for heart failure .

O034

Quantification of Cardiac Output with Phase Velocity Mapping in Patients with Pulmonary Hypertension: A Comparison between Cardiac Magnetic Resonance and Right Heart Catheterization

Jose Ricardo Po, M.D, Shimaa S. Khidr, MDMatthew S. Tong, D.O., Talha Meeran, M.D., Alekhya Potluri, M.D., Mark Doyle, Ph.D., Amresh Raina, M.D.

Allegheny General Hospital, Pittsburgh, PA

Background: Cardiac output (CO) has remained a strong diagnostic and prognostic indicator of cardiovascular morbidity and mortality. Since the practical utility of the thermodilution (TD) and Fick method has been mainstreamed by the PA catheter in the 1970s, it has remained the most reliable method for measuring CO. However, confounders include the practicality of oxygen consumption measurements, valvular regurgitation, and technical variabilities. CMR phase velocity mapping (PVM) is a non-invasive, quick, highly reproducible acquisition. CO was previously validated in 23 patients for RHC. In PH, many confounders are applied in this cohort, especially related to oxygen requirement/consumption. The objective of our study is to determine the accuracy of CMR compared to RHC in measuring CO in patients with PH.

Methods: We retrospectively identified patients with PH who underwent CMR and RHC within one month. Demographic and hemodynamic measurements were obtained. Invasive CO were calculated using the Fick principle and TD. Measurement of cardiac output by CMR was performed by phase velocity mapping (PVM) of the proximal aorta. Correlation coefficients of the cardiac output measurement were calculated. Bland-Altman analysis was performed to assess the bias and differences between pairs of measurements.

Results: 102 cases were analyzed (mean age: 60 years, SD: 12.7). 71 (70%) were females and 69 (68%) were WHO group I. Heart rate comparison during CMR and RHC showed an average 7 beat difference and 9% change from baseline. There was very good correlation between PVM-Fick (r = 0.72) and PVM-T D (r = 0.74). Bland-Altman analysis showed PVM-Fick had a mean difference of 0.43 and SD of 1.09 L/min, PVM-TD had a mean difference of 1.25 and SD of 1.24 L/min, and Fick-TD had a mean difference of 0.79 and SD of 1.26 L/min. For same day PVM and RHC, analyses were similar (PVM-Fick mean = 0.37, SD = 1.18, r = 0.72; PVM-TD mean = 1.17, SD = 1.14, r = 0.78; Fick-TD mean = 0.74, SD = 1.22). The same day SV-Fick mean difference was 4 cc, similar to the original validation paper. Ranking of contribution to SD showed that PVM contributed the least variation followed by Fick then TD.

Conclusions: Compared to invasive RHC, non-invasive PVMs correlates well with Fick and TD in one month and same day analyses, however it is superior in terms of having the least amount of variation. This relates to high reproducibility of PVMs without discerning the need for oxygen consumption/requirements in invasive measurements.

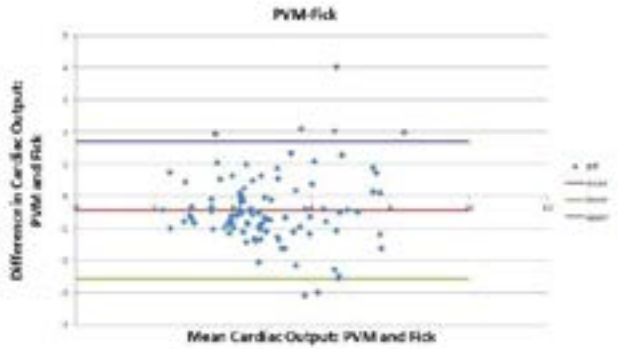

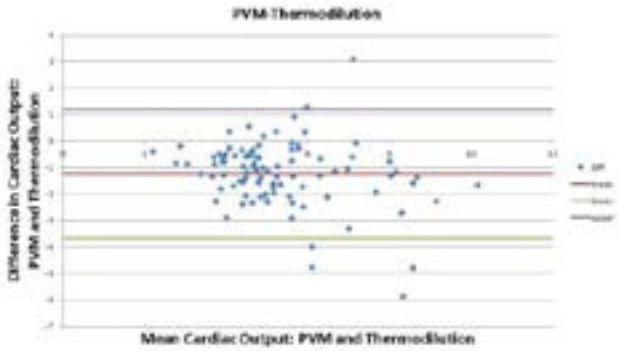

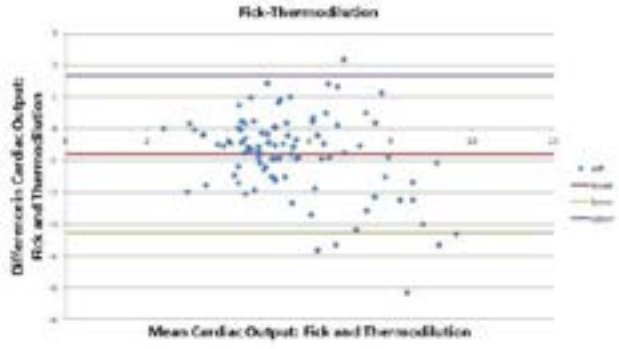

O035

High-risk coronary plaque characteristics by T1-weighted CMR identify ischemia-causing lesions: comparison with invasive fractional flow reserve (FFR)

Yibin Xie, PhD[1]Sang-Eun Lee, MD[2], Anthony G. Christodoulou, PhD[1], Zixin Deng, MS[1], Jianing Pang, PhD[3], Christopher Nguyen, PhD[1], Qi Yang, PhD[1], Daniel Berman, MD[4], Hyuk-Jae Chang, MD, PhD[2], Debiao Li, PhD[5]

1. *Cedars-Sinai Medical Center, CA*
2. *Severance Cardiovascular Hospital, Yonsei-Cedar Sinai Integrative Cardiovascular Imaging Research Center, Yeonsei University Health System, Seoul, South Korea, N/A, Republic of Korea*
3. *Siemens Healthcare, Chicago, IL*
4. *Cedars-Sinai Medical Center, Los Angeles, CA*
5. *Biomedical Imaging Research Institute, Cedars-Sinai Medical Center, Los Angeles, CA, CA*

Background: Fractional Flow Reserve (FFR) is the gold standard for identifying coronary lesions that cause ischemia (Tonino et al, NEJM 2009). Although coronary hyper-intensive plaques (CHIPs) on dark-blood T1-weighted MRI are associated with future major events (Noguchi et al, JACC 2015), their relationship with lesion-specific ischemia remains unclear. We recently developed an improved acquisition scheme, Coronary Atherosclerosis T1-weighted Characterization (CATCH), providing integrated anatomical reference, shortened scan time, improved spatial resolution and coverage (Xie et al, JACC CVI 2016). This study utilized CATCH to evaluate the association between CHIPs and lesion ischemia by FFR.

Methods: Using the previously published CATCH protocol (Xie et al, JACC CVI 2016), we studied 40 consecutive patients (28 men and 12 women, mean age: 61±9) with new-onset or recurrent stable angina for whom coronary catheterization was planned. After receiving CATCH scans pre- and post-contrast enhancement, patients underwent invasive coronary angiography (ICA) and FFR measurements. Pre- and post-contrast Plaque-to-Myocardial Ratio (PMR) was quantified in 55 lesions blinded to invasive imaging results and compared with location-matched FFR data. PMR was dichotomized using the receiver-operating characteristics (ROC) analysis to determine the optimal thresholds for discrimination of ischemia (FFR ≤0.80). Incremental discrimination of ischaemia by PMR was evaluated by area under the curve (AUC) analysis of ROC. Logistic regression analysis was employed to evaluate the predictors of ischemia.

Results: Figure 1 shows two representative patient study cases in comparison. With the identical level of intermediate luminal stenosis (50%), the CHIP (PMR=2.0) was causal of ischemia (FFR=0.66), whereas non-CHIP (PMR=0.9) was not hemodynamically significant (FFR=0.86). Figure 2 is the global ROC analysis showing increased AUC with the inclusion of pre- and post-contrast PMR compared with stenosis along. Table 1 summarizes the regression statistics showing added predictive ability provided by PMR for the detection of ischemia.

Conclusions: Preliminary clinical results suggested that coronary plaque hyperintensity on dark-blood T1-weighted MRI provides independent improvement for the identification of ischemia-causing lesions compared with stenosis evaluation alone. Further study with a larger sample size is warranted and currently underway.

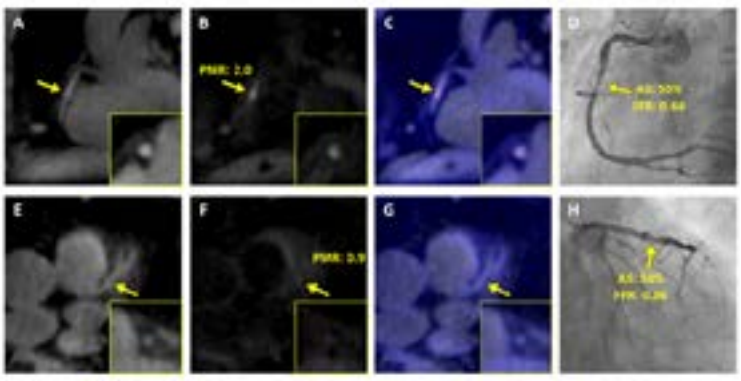

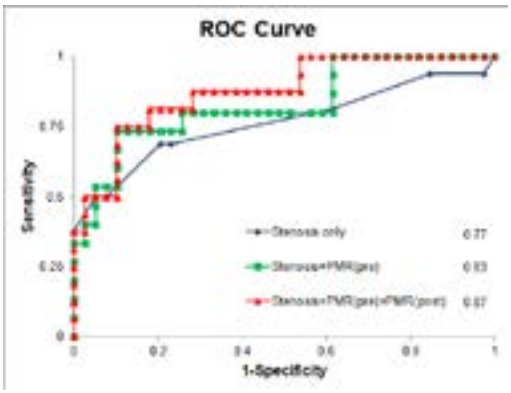

Comparison of different models for discriminating lesion-specific ischemia

Stenosis+PMR(pre)+PMR(post)	Stenosis+PMR(pre)	Stenosis only	Model
24.73	20.17	12.33	Global X^2
<0.0001	<0.0001	0.0004	Wald test *p*-value

O036

Prevalence and Prognostic Significance of Unrecognized Myocardial Scar in 30,000 Patients Followed for Ten Years

Han Kim, MD[1]Dina Labib, MD[2], Dipan Shah, MD[3], John Heitner, MD[4], Anna Lisa Crowley, MD[5], Igor Klem, MD[6], Faisal Nabi, MD[7], Michele Parker, MS[8], Raymond j. Kim, MD[2], Robert M. Judd, PhD[9]

1. *Duke University, Durham, NC*
2. *Duke University Medical Center, NC*
3. *Houston Methodist, Weill Cornell Medical College, Houston, TX*
4. *New York Methodist Hospital, NY*
5. *Duke University, NC*
6. *Duke University Medical Center, Durham, NC*
7. *Houston Methodist DeBakey Heart & Vascular Center, Houston, TX*
8. *Duke Cardiovascular MR Center, Durham, NC*
9. *Duke University Medical center, Durham, NC*

Background: Prior CMR studies have suggested that myocardial scarring increases mortality even without overt symptoms of irreversible injury, for example due to unrecognized myocardial infarction (UMI) in patients with coronary artery disease (CAD), or replacement scarring in non-ischemic cardiomyopathy. However, studies are single center or include relatively small numbers of patients. To our knowledge, no large-scale multicenter studies have addressed the prevalence and prognostic significance of unrecognized myocardial scar in patients undergoing routine CMR.

Methods: Analysis was performed on a cloud-based system that is currently receiving de-identified searchable data from electronically-signed clinical reports with full DICOM datasets performed at three U.S. hospitals from 1-Jan-05 through 31-Dec-15. Data from 31,389 consecutive CMR exams were included. All patients with a history of MI and/or abnormal contractile function were excluded. Normal contractile function was defined as normal wall motion scores in all 17 myocardial segments. Scar was defined as the presence of delayed enhancement in post-contrast images. Scar pattern (CAD or non-CAD) was defined by the physician's interpretation in the electronically signed final report. For assessment of vital status, an automated query of the social security death index was performed at each site. This data was then updated to the cloud and made available for analysis.

Results: Of 31,389 consecutive patients undergoing clinical CMR for routine purposes, 12,391 patients had normal wall motion scores and no history of MI (indications: cardiomyopathy 15%; ischemia evaluation 14%; vascular 18%; viability assessment 12%; arrhythmia 22%). Patient demographics are shown in the Table. Of these 12,391 patients, unrecognized scar was present in 1,794 (14.5%). LVEF was normal in patients without (63±8%) and with scar (65±10%). Although scar size was variable (mean 4.2±6.4% of LV mass), scar burden was at least moderate in 21%, involving >5% of LV mass. Overall, patients were followed for a median of 5.0 (3.0, 7.1) years, during which 1623 patients died (8.3%). The mortality rate for patients with scar was 2.8%/year compared to 1.4%/year for those without scar ($p < 0.0001$, Figure)

Conclusions: This investigation is the largest multicenter CMR study of unrecognized scar. One in seven patients (14.5%) with normal contractile function and no history of MI undergoing routine CMR testing have unrecognized myocardial scar. Annualized mortality rate in those with scar was double that those without scar, despite both groups having normal LVEF.

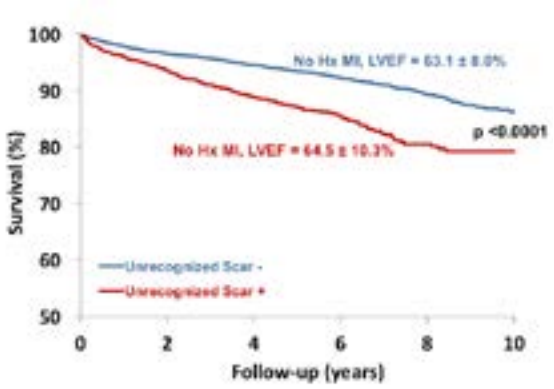

Patient Demographics

n=12,391	Characteristics
54.8 ± 16.7 years	Age (mean ± SD)
50.6%	Male gender
15.4%	Diabetes mellitus
51.1%	Hypertension
38.5%	Hyperlipidemia
7.5%	Smoking
28.5%	Family history of CAD
7.3%	History of heart failure
63.4% ± 8.4%	LV ejection fraction

O037

MRI prospective survey on heart and liver iron and cardiac function in Thalassemia Major patients treated with Deferasirox versus Deferiprone and Desferrioxamine in monotherapy

Antonella Meloni, PhD[1]Laura Pistoia, MSc[2], Liana Cuccia, MD[3], Maria Rita Gamberini, MD[4], Vincenzo Caruso, MD[5], Vincenzo Positano, MSc[2], Gennaro Restaino, MD[6], Stefania Renne, MD[7], Ada Riva, MD[8], Alessia Pepe, MD, PhD[2]

1. *Fondazione G. Monasterio CNR Regione Toscana, Pisa, Toscana, Italy*
2. *Fondazione G. Monasterio CNR Regione Toscana, Toscana, Italy*
3. *ARNAS Civico "Benfratelli-Di Cristina", Palermo, Sicilia, Italy*
4. *Azienda Ospedaliero-Universitaria "S. Anna", Ferrara, Emilia-Romagna, Italy*
5. *Presidio Ospedaliero Garibaldi-Centro - ARNAS Garibaldi, Catania, Sicilia, Italy*
6. *Fondazione di Ricerca e Cura "Giovanni Paolo II", Campobasso, Molise, Italy*
7. *Presidio Ospedaliero "Giovanni Paolo II", Lamezia Terme, Calabria, Italy*
8. *Ospedale "SS. Annunziata" ASL Taranto, Taranto, Puglia, Italy*

Background: No prospective data are available about the efficacy of deferasirox versus deferiprone and desferrioxamine in monotherapy. Our study aimed to prospectively assess the efficacy of deferasirox versus deferiprone and desferrioxamine in monotherapy in a large cohort of thalassemia major (TM) patients by quantitative Magnetic Resonance (MR).

Methods: Among the 2551 TM patients enrolled in the MIOT (Myocardial Iron Overload in Thalassemia) network we selected those with an MR follow up study at 18±3 months who had been received one chelator alone between the 2 MR scans. We identified three groups of patients: 235 treated with DFX, 142 with DFP and 162 with DFO. Iron overload was measured by T2* multiecho technique. Liver T2* values were converted into liver iron concentration (LIC) values. Biventricular function parameters were quantitatively evaluated by cine images.

Results: Excellent/good levels of compliance were similar in the DFX (98.7%) vs DFP (96.3%) and DFO (97.5%) groups. Among the patients with myocardial iron overload at baseline, in all three groups there was a significant improvement in the global heart T2* value (DFX: +4.58±5.91ms P‹0.0001, DFP: 8.53±6.97ms P‹0.0001 and DFO: +3.93±5.21 ms P‹0.0001) and a reduction in the number of pathological segments (DFX: -4.49±4.55 P‹0.0001, DFP: -8.08±5.5.84 ms P=0.001 and DFO: -3.65±3.81 ms P‹0.0001). In DFP and in DFO groups there was a significant improvement in left ventricular ejection function (LVEF) (+4.86±6.99% P=0.044 and +3.87±7.48% P=0.004, respectively). Only in the DFP group there was a significant improvement in right ventricular ejection function (RVEF) (6.69±4.61% P=0.001). The improvement in the global heart T2* was significantly lower in the DFX versus the DFP group , but it was not significantly different in the DFX versus the DFO group (Figure 1). The improvement in the LVEF was significantly higher in both DFP and DFO groups than in the DFX group while the improvement in the RVEF was significantly higher in the DFP than in DFX group (Figure 2). Among the patients with hepatic iron at baseline (LIC3≥mg/g dw) the changes were not significantly different in DFX versus the other groups.

Conclusions: Prospectively in a large clinical setting of TM patients, DFX monotherapy was significantly less effective than DFP in improving myocardial siderosis and biventricular function and it was significantly less effective than DFO in improving the LVEF.

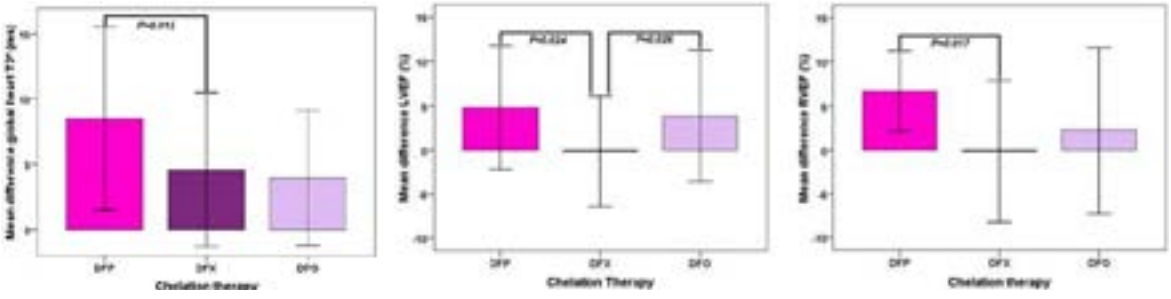

O038

Prediction of all-cause mortality from clinical CMR-derived left ventricular ejection fraction: 15 years of data from a large regional health system

Gregory J. Wehner, BS[1] Christopher M. Haggerty, PhD[2], Jonathan D. Suever, PhD[3], Linyuan Jing, PhD[4], Joseph B. Leader, BA[2], Brandon K. Fornwalt, MD, PhD[2], Joseph Neil A. Manus, BS[2]

1. *University of Kentucky, KY*
2. *Geisinger Health System, PA*
3. *Geisinger Health System, Bellefonte, PA*
4. *Geisinger Health System, State College, PA*

Background: Despite the widespread use of cardiovascular magnetic resonance to assess cardiac function for multiple decades, no study has evaluated the ability of clinically reported left ventricular ejection fraction (LVEF) derived from CMR to predict important outcomes such as all-cause mortality. We utilized nearly 15 years of CMR acquisitions and mortality outcomes from a large regional health system to assess the ability of clinical CMR-derived LVEF to predict all-cause mortality. We hypothesized that, similar to previous studies using echocardiography and ventriculography, CMR-derived LVEF would be a significant predictor of all-cause mortality with improved survival for higher LVEFs, up to an LVEF near 45%.

Methods: Electronic medical records from approximately 1.35 million patients were reviewed to identify all instances where LVEF was measured clinically using CMR. Mortality status and either date of death or last living encounter date were obtained from the medical records. The presence of confounding diagnoses at the time of CMR (Table 1) was assessed from *International Classification of Disease, Ninth and Tenth Revisions* (ICD-9, ICD-10) codes. Cox proportional hazard and Kaplan-Meier survival analyses were performed to assess the ability to predict all-cause mortality. Patients were stratified into intervals of LVEF spanning 10 absolute percentage points (i.e. LVEF < 20%, 20%≤LVEF < 30%, etc).

Results: We identified 2870 CMR studies over 2596 unique patients with clinically reported LVEF. Mean follow-up interval was 5.4 ± 3.8 years (median: 5.1, range: 0.0 – 14.2). The endpoint of all-cause mortality was reached after 727 (25%) CMR studies over 671 (26%) unique patients. After adjustments for confounders, LVEF was a significant predictor of all-cause mortality (Table 2). The highest hazard ratio was observed in the lowest (< 20%) LVEF interval (hazard ratio = 2.86, 95% confidence interval: 2.01 - 4.07). The hazard ratio steadily declined with increasing LVEF up to the 50–60% interval. There was no significant difference in the hazard ratio among the three highest LVEF intervals (starting at 50–60%). Kaplan-Meier curves demonstrated the ability of LVEF to stratify survival, particularly among lower LVEF intervals (Figure 1).

Conclusions: Based on nearly 15 years of historical CMR and outcomes from over 2500 patients in a large regional health system, clinical CMR-derived LVEF is a significant predictor of all-cause mortality. In particular, CMR-derived LVEF can be used to stratify patients according to their risk of all-cause mortality, with improved survival for higher LVEFs, up to an LVEF near 50%.

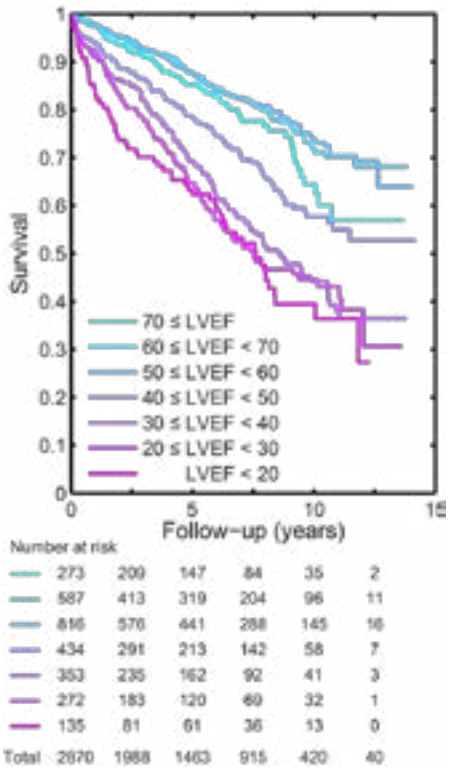

Table 1. Characteristics of the population of CMR Studies

Mean ± SD or N (%)	
56 ± 17	Age (years)
1767 (62)	Male sex
29 ± 6	BMI (kg/m^2)
340 (12)	Previous myocardial infarction
780 (27)	Baseline hypertension
364 (13)	Baseline diabetes
235 (8)	Baseline atrial fibrillation/flutter
248 (9)	Congenital heart defect
1491 (52)	Positive smoking history
50 ± 16	LVEF (%)

Table 2. Cox Proportional Hazards Analysis

P-value	Hazard Ratio (95% CI)	Age (years)
0.011	0.19 (0.05 - 0.69)	Age < 18
0.035	0.42 (0.19 - 0.94)	18 ≤ Age < 30
<0.001	0.31 (0.16 - 0.61)	30 ≤ Age < 40
<0.001	0.36 (0.24 - 0.56)	40 ≤ Age < 50
	1.00 (referent)	50 ≤ Age < 60
<0.001	1.74 (1.36 - 2.23)	60 ≤ Age < 70
<0.001	2.88 (2.26 - 3.69)	70 ≤ Age < 80
<0.001	4.99 (3.66 - 6.81)	80 ≤ Age
		BMI (kg/m^2)
0.022	1.93 (1.10 - 3.40)	BMI < 18.5
	1.00 (referent)	18.5 ≤ BMI < 25
0.002	0.71 (0.57 - 0.88)	25 ≤ BMI < 30
0.013	0.73 (0.57 - 0.93)	30 ≤ BMI < 35
0.588	0.90 (0.63 - 1.30)	35 ≤ BMI < 40
0.663	0.92 (0.63 - 1.34)	40 ≤ BMI
0.272	1.11 (0.92 - 1.34)	Male sex
0.513	0.99 (0.95 - 1.02)	CMR date (per year)
0.843	0.97 (0.75 - 1.26)	Previous myocardial infarction
0.060	1.22 (0.99 - 1.49)	Baseline hypertension
<0.001	1.68 (1.34 - 2.11)	Baseline diabetes
0.555	1.09 (0.82 - 1.44)	Baseline atrial fibrillation
0.317	0.82 (0.55 - 1.21)	Congenital heart defect
<0.001	1.42 (1.18 - 1.71)	Positive smoking history
		LVEF (%)
<0.001	2.86 (2.01 - 4.07)	LVEF < 20
<0.001	2.33 (1.72 - 3.16)	20 ≤ LVEF < 30
<0.001	2.00 (1.51 - 2.63)	30 ≤ LVEF < 40
0.004	1.51 (1.14 - 1.99)	40 ≤ LVEF < 50
0.512	1.09 (0.84 - 1.41)	50 ≤ LVEF < 60
	1.00 (referent)	60 ≤ LVEF < 70
0.287	1.20 (0.86 - 1.67)	70 ≤ LVEF

O039

Physiological atrial remodelling associated with variation in physical activity level in a large-scale population study: Results from the UK Biobank

Nay Aung, MD, MRCP[1]Mihir M. Sanghvi, MB BS, BSc[2], Filip Zemrak, MD MRCP[1], Kenneth Fung, MBBS BSc[3], Jose Miguel Paiva, MSc[1], Elena Lukaschuk, MSc[4], Aaron Lee, PhD, MBBS[1], Valentina Carapella, DPhil[5], Stefan K. Piechnik, PhD, MScEE[6], Stefan Neubauer, MD, FRCP[6], Steffen E. Petersen, MD DPhil MPH FRCP[1]

1. *Barts Heart Center, The Cardiovascular Magnetic Resonance Imaging Unit and The Center for Rare Cardiovascular Diseases Unit, St Bartholomew's Hospital, West Smithfield, London, UK, England, United Kingdom*
2. *William Harvey Research Institute, NIHR Cardiovascular Biomedical Research Unit at Barts, Queen Mary University of London, Charterhouse Square, London EC1M 6BQ, UK, England, United Kingdom*
3. *Barts Heart Center, The Cardiovascular Magnetic Resonance Imaging Unit and The Center for Rare Cardiovascular Diseases Unit, St Bartholomew's Hospital, West Smithfield, London, UK, London, England, United Kingdom*
4. *University of Oxford, Oxford, England, United Kingdom*
5. *University of Oxford, Oxford, United Kingdom, England, United Kingdom*
6. *University of Oxford, England, United Kingdom*

Background: Morphological and functional adaption of cardiovascular structures in response to physical training is well-established in high performance athletes. A few studies have also reported the relationship between moderate physical activity and an increase in ventricular mass and cavity dilatation akin to athlete's heart in community-based population. The aim of this study was to examine in a general population the effects of different levels of physical activity on atrial structures and function.

Methods: We performed a cross-sectional analysis of the data from the UK Biobank which is a large scale population-based cohort study of more than 500,000 UK residents aged 40-69 years at baseline recruited between 2006-10. Left and right atrial (LA and RA) maximal, minimal and stroke volumes and ejection fraction were derived from balanced study-state free precession long-axis cine images of 5,065 cardiac magnetic resonance imaging (CMR) studies acquired between 2014-15. CMR variables were indexed to body surface area. The data on clinical characteristics, medical history and physical activity level were obtained from standardized questionnaires. Physical activity score in *'Metabolic Equivalent of Task (MET)-minutes per week'* was calculated using the conversion formula recommended by International Physical Activity Questionnaire (IPAQ) - Short Form. The relationship between atrial parameters and physical activity level was assessed by multiple linear regression models adjusted for covariates selected for their known or possible influence on cardiac structures.

Results: The studied cohort was 59±7 years old and 47% male. In multivariate regression, there was a positive correlation between physical activity level and LA maximal volume, LA stroke volume, RA maximal and minimal volumes after adjusting for age, gender, ethnicity, Townsend deprivation index, education, job class, smoking and alcohol drinker status, systolic blood pressure, heart rate, medications for hypertension, diabetes and hyperlipidaemia, presence of diabetes, respiratory or cardiovascular diseases (β coefficient 0.1 – 0.2, p-value < 0.05) (Table 1 and 2). A small negative association between increment in physical activity and LA ejection fraction was also found (β coefficient -0.2, p-value < 0.03). There was a significant interaction between gender and physical activity for LA ejection fraction - female gender was associated with a more rapid decline in LA ejection fraction after adjusting for all other covariates (p-value for interaction = 0.03) (Figure 1).

Conclusions: Incremental physical activity level was associated with a small but statistically significant bi-atrial remodelling in community-dwelling middle-aged adults. Gender was a significant effect modifier for association between LA ejection fraction and physical activity level.

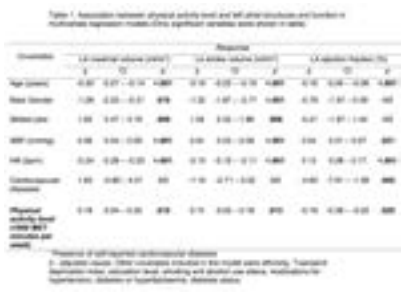

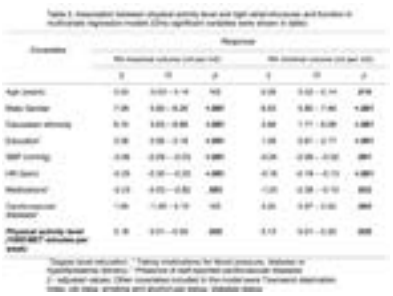

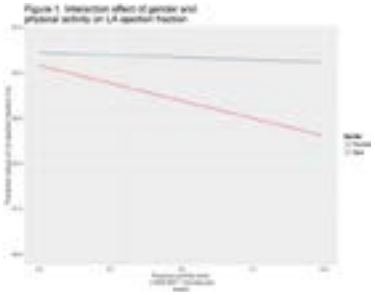

O040

Myocardial T1 times vs. Extracellular Volume Fraction: A Comparison of Prognostic Significance

Eric Y. Yang, MD PhD[1]Mohamad Ghosn, PHD[2], Mohammad A. Khan, MBBS[3], Nickalaus L. Gramze, MD[2], Grant W. Pickett, MD[2], Stephen J. Pickett, MD[2], Patrick Green, MD[2], Doreen Berko, BA[4], Gerd Brunner, MS/Ph.D.[5], Faisal Nabi, MD[6], Vijay Nambi, MD PhD[7], Sherif F. Nagueh, MD[2], Christie M. Ballantyne, MD[5], William A. Zoghbi, MD[2], Dipan J. Shah, MD[2]

1. *Houston Methodist Hospital, TX*
2. *Houston Methodist DeBakey Heart & Vascular Center, TX*
3. *Houston Methodist DeBakey Heart & Vascular Center, Sugar Land, TX*
4. *Methodist DeBakey Heart & Vascular Center, TX*
5. *Baylor College of Medicine, TX*
6. *Houston Methodist DeBakey Heart & Vascular Center, Houston, TX*
7. *Michael E. DeBakey Veteran Affairs Medical Center, TX*

Background: Cardiac magnetic resonance (CMR) permits the quantification of myocardial native T1 relaxation times and extracellular volume fraction (ECV). Both CMR markers have been associated with various cardiac pathologies, but only ECV has been strongly linked with outcomes. Comparisons of the prognostic significance of these markers have been limited. We examined the associations between ECV derived without late gadolinium enhancement (LGE)-involved wall segments, native T1 times, and cardiac events in a population of patients referred for CMR.

Methods: Mid short axis T1 maps were derived from imaging on a 1.5T or 3.0T scanner with modified Look-Locker inversion-recovery sequences before and 15 minutes following intravenous gadolinium-based contrast administration. T1 maps were divided into 6 cardiac segments, each classified as LGE absent or present. Global native T1 and ECV were derived from T1 maps using the area-weighted average of only LGE-absent segments. ECV was considered high if measured >30%, the upper 95% bounds of a reference group without known cardiac disease (n=28), stratified for magnet strength. Native T1 was considered abnormal if greater than the upper 95% bounds of the same reference group, stratified for magnet strength. Patients were dichotomized based on either elevated ECV or native T1. Subsequent cardiac admission and all-cause death were ascertained by electronic medical record review, follow up phone call, or Social Security Death Index search. Their relationship with ECV and native T1 were examined separately and as a combined endpoint with Cox proportional hazard models.

Results: Of 1,604 serial patients with T1 maps, 1,047 were eligible after exclusions (listed in Table 1) and followed over a median 10.5 (interquartile range 5.4, 21.4) months. Patients with high ECV had an increased risk for death (hazard ratio [HR] 2.60, 95% confidence interval [CI] 1.78 to 3.79), cardiac admissions (HR 1.97, 95%CI 1.48 to 2.61), and combined endpoint (HR 2.14, 95% CI 1.69 to 2.70) (Figure 1). Patients with high native T1 had an increased risk for a combined endpoint (HR 1.29, 95%CI 1.02 to 1.63) but not for death (HR 1.36, 95%CI 0.93 to 1.97) or cardiac admissions (HR 1.24, 95%CI 0.93 to 1.65) (Figure 2). After adjustments for covariates, only the relationship between ECV and outcomes persisted (Table 2).

Conclusions: Myocardial extracellular volume fraction measures, censored for late gadolinium enhancement, were more strongly associated with cardiac outcomes than native T1 times. ECV may have more clinical utility than native T1 times as a cardiac risk marker among patients referred for cardiac magnetic resonance.

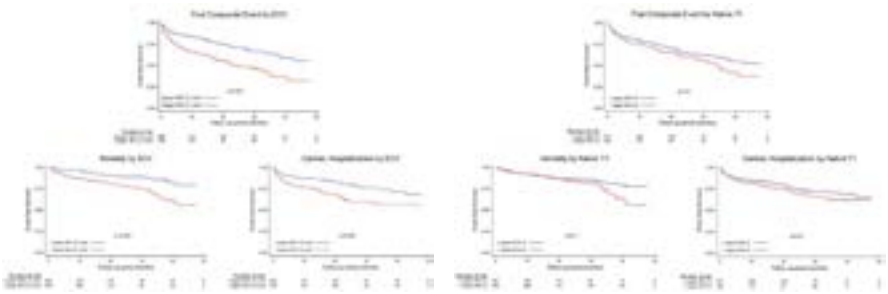

Baseline characteristics, medication use, and CMR characteristics

n=1,047	Variable*
58.5 (15.7)	Age (yrs)
57.2	Male (%)
73.5	White (%)
13.6	Black (%)
2.6	Asian (%)
10.4	Other race (%)
64.4	Hypertensive (%)
9.2	Current Smoking (%)
29.8	Former Smoking (%)
52.3	Dyslipidemic (%)
22.6	Diabetic (%)
15.2	Prior MI (%)
28.6 (6.7)	Body mass index (kg/m^2)
38.9	Inpatient (%)
126.3 (17.0)	Systolic BP (mm Hg)
73.7 (12.9)	Diastolic BP (mm Hg)
74.4 (15.2)	Pulse (bpm)
Medications*	
47.1	RAAS blocker (%)
58.8	Beta blocker (%)
43.6	Aspirin use (%)
10.6	Thienopyridine (%)
46.3	Statin (%)
38.6	Diuretic (%)
Cardiac magnetic resonance characteristics*	
80.8 (34.2)	LV EDVi (mL/m^2)
38.3 (31.9)	LV ESVi (mL/m^2)
42.5 (14.2)	LV SVi (mL/m^2)
57.6 (18.4)	LV EF (%)
77.3 (28.9	LV MMi (gm/m^2)
0 (0, 4)	Scar burden (%)†
1017.8 (56.5)	Native T1 (ms) at 1.5T (n=535)
1220.9 (60.6)	Native T1 (ms) at 3.0T (n=512)
29.7 (4.3)	ECV (%)

Exclusions: Intracardiac mass (n=68), infiltrative cardiomyopathy (n=30), imaging technical issues (n=18), and missing ECV data (n=200), missing follow-up data (n=209) *All values are mean (standard deviation) or proportions unless otherwise stated †Values are median (interquartile range)

ECV = extracellular volume fraction; LGE = late gadolinium enhancement; MI = myocardial infarction; BP = blood pressure; RAAS = renin-angiotensin-aldosterone system; LA Voli = indexed left atrial volume; LV = left ventricular; EDVi = indexed end diastolic volume; ESVi = indexed end systolic volume; SVi = indexed stroke volume; EF = ejection fraction; MMi = indexed myocardial mass

Outcomes, event rates, and adjusted hazard ratios.

Native T1 High n=394	Native T1 Low n=653	ECV High n=379	ECV Low n=668	Variable
121 (25.3)	160 (19.4)	148 (33.1)	133 (15.6)	First composite event (number, event-rate / 1000 person-months)
1.17 (0.91, 1.49)	1.00 (Ref)	1.52 (1.18, 1.96)	1.00 (Ref)	Adjusted hazard ratio (95% CI)
50 (8.8)	62 (6.6)	67 (12.1)	45 (4.7)	Mortality (number, event-rate / 1000 person-months)
1.22 (0.82, 1.80)	1.00 (Ref)	1.74 (1.17, 2.61)	1.00 (Ref)	Adjusted hazard ratio (95% CI) *
82 (17.1)	112 (13.6)	98 (21.9)	96 (11.2)	Cardiac admissions (number, event-rate / 1000 person-months)
1.11 (0.83, 1.49)	1.00 (Ref)	1.49 (1.10, 2.02)	1.00 (Ref)	Adjusted hazard ratio (95% CI) *

*Adjusted for age, gender, black race, inpatient status, systolic BP, pulse, body mass index, diabetes, hypertension, prior MI, and MRI scanner type.

O041

Prognostic Value of Extracellular Volume Fraction Quantification in Patients with Non-ischemic Non-infiltrative Cardiomyopathy.

Tomas Vita, MD[1] Coelho-Filho R. Otavio, MD, PhD, MPH[2], Siddique A. Abbasi, MD[3], Ethan Rowin, MD[4], Tomas Neilan, MD, MPH[5], Hoshang Farhad, MD[6], Eri Watanabe, MD, PhD[7], Francois-Pierre Mongeon, md[6], Michael M. Givertz, MD[6], Ron Blankstein, MD[6], Michael Steigner, MD[6], Michael Jerosch-Herold, PhD[8], Raymond Kwong, MD[6]

1. *Brigham and Womens Hospital, Cambridge, MA*
2. *State University of Campinas, Campinas, Sao Paulo, Brazil*
3. *Brown University, Providence, RI*
4. *Tufts Medical Center, MA*
5. *Massachusetts General Hospital, Newton, MA*
6. *Brigham and Womens Hospital, Boston, MA*
7. *Tokyo Women's Medical University, Tokyo, Japan*
8. *Department of Radiology, Brigham and Women's Hospital, MA*

Background: Left ventricular ejection fraction (LVEF) is the current diagnostic standard prognosis for patients with non-ischemic cardiomyopathy. The amount of fibrosis, detected by late gadolinium enhancement (LGE) on cardiac MRI (CMR), has been validated as an independent predictor factor. It is well establish that the presence of LGE predicts outcomes as death, ventricular tachycardia and heart failure (HF) admissions. However, it remains unclear whether there are additional CMR parameters provide prognostic information beyond LVEF and LGE. Conventional imaging techniques cannot robustly quantify the full spectrum of extracellular cardiac matrix (ECM) expansion. ECM expansion often may not be evident on LGE CMR or other modalities. Quantifying ECM and myocardial intracellular volume expansion (ECV) may ultimately provide independent prognostic value to improve care through targeted treatment. Our aim was to evaluate ECV expansion as a predictor of mortality, HF hospitalizations and heart transplant independently of LVEF and LGE.

Methods: Population: We included 360 individuals referred for CMR for assessment of etiology of cardiomyopathy. All patients had LVEF 80 ml/m^2 as an entry criteria. Individuals with documented coronary artery disease, LGE in a pattern consistent with myocardial infraction, evidence of infiltrative disease or moderate to severe valvulopathy were excluded.

Statistical Analysis: Multivariable Cox regression analysis was performed using a stepwise selection of variable forcing age, gender, LVEF, RVEF and LGE mass quantification a priori. ECV Measurements: T1 measurements were performed with a cine Look-Locker sequence nonslice-selective adiabatic inversion pulse, followed by segmented gradient-echo acquisition for 13 cardiac phases/times after inversion, spread over 2 cardiac cycles. End Points: All cause mortality, HF hospitalizations and heart transplant.

Results: Among 360 patients (age 50±20yrs; LVEF 37±15%), LGE was positive in 45% of the cohort and 115 (32%) had abnormal ECV values. There were 33 deaths, 37 HF hospitalizations and 11 heart transplants. The composite endpoint of death and CHF was 64. When diving ECV by quartiles there was more than 7-fold increase in annualized event (Figure 1-A). Among individuals with LVEF < 30% stratified by ECV quartiles there was a significant increase of events as the ECV increase (Figure 1-B). On multivariable Cox regression analysis ECV remains significant (HR 1.03; p=0.03) after adjustment

Conclusions:

1. Extracellular volume measurements by CMR provide incremental risk stratification in patients with non-ischemic cardiomyopathy, which is especially evident among those with LVEF < 30%
2. The risk of major adverse events increases with increasing quartiles of ECV

http://www.ConferenceAbstracts.com/uploads/cfp2/attachments/LDFAIBDN/LDFAIBDN--220723-1-ANY.pdf

http://www.ConferenceAbstracts.com/uploads/cfp2/attachments/LDFAIBDN/LDFAIBDN--220723-2-ANY.pdf

O042

Relations of Aortic Stiffness with Cardiovascular Risk Factors and Left Ventricular Remodeling

Connie Tsao, MD, MPH[1] Philimon N. Gona, PhD[2], Martin Larson, ScD[3], Michael L. Chuang, MD[4], Gary Mitchell, MD[5], Christopher J. O'Donnell, MD MPH[6], Warren J. Manning, MD[1]

1. *Beth Israel Deaconess Medical Center, Boston, MA*
2. *University of Massachusetts Boston, Framingham, MA*
3. *Department of Mathematics and Statistics, Boston University, Framingham, MA*
4. *Framingham Heart Study, Framingham, MA*
5. *Cardiovascular Engineering, Inc, Norwood, MA*
6. *Boston VA Healthcare, Boston, MA*

Background: Greater aortic stiffness is associated with adverse cardiovascular disease (CVD) outcomes including heart failure. Altered ventriculo-arterial relations may underlie these associations. We evaluated relations of proximal aortic stiffness with CVD risk factors and measures of left ventricular (LV) remodeling and function.

Methods: Framingham Heart Study Offspring participants (n=1727, 60±9 yrs, 53% F) underwent cardiovascular magnetic resonance (CMR) at 1.5T (2002-2006) including short axis ECG-gated cine SSFP images to assess LV function and phase contrast images of the ascending and descending thoracic aorta at the level of the pulmonary artery bifurcation to assess aortic stiffness. Aortic flow waveforms were visually inspected and resampled to 1 ms temporal resolution using cubic spline interpolation. Percent aortic strain was defined as (max-min aortic cross-sectional area)/min area x 100, with lower strain=greater stiffness. Aortic pulse wave velocity (PWV) was defined as distance across aortic arch/aortic pulse wave transit time, with higher PWV=greater aortic stiffness. Sex-pooled analysis of covariance was used to relate natural log-transformed % strain and PWV (dependent variables) with 1-SD increase in CVD risk factors and CMR measures of LV structure and function.

Results: Higher aortic stiffness was associated with the clinical CVD risk factors of age, higher heart rate, greater diastolic blood pressure, and smoking (**TABLE**). Higher aortic stiffness was also related to CMR measures of higher LV end-diastolic volume index, greater LV mass/LV end-diastolic volume (but not relative wall thickness), and lower myocardial contraction fraction. Aortic stiffness was not associated with sex, systolic blood pressure, or LV mass index, stroke volume, or ejection fraction.

Conclusions: In this cross-sectional study of adults in the community, proximal aortic stiffness was associated with several CVD risk factors and adverse LV structural remodeling and systolic function. Further investigation may elucidate the effect of modification of these factors on aortic stiffness and CVD outcomes including heart failure.

Log Aortic arch PWV, Est B±SE	**Log % Descending aorta strain,** Est B±SE	**Log % Ascending aorta strain,** Est B±SE	
			Risk factors
0.025±0.001**	-0.014±0.002**	-0.016±0.002**	Age, yr
-0.012±0.02	0.087±0.034	-0.044±0.034	Sex, M
-0.050±0.01**	-0.031±0.018	0.061±0.017**	Body Mass Index, kg/m^2
0.015±0.012	-0.132±0.016**	-0.083±0.016**	Heart rate, bpm
0.010±0.015	-0.011±0.022	-0.007±0.022	Systolic blood pressure, mm Hg
0.033±0.015*	0.018±0.02	-0.034±0.02	Diastolic blood pressure, mm Hg
0.139±0.037**	0.03±0.05	-0.085±0.051	Smoking
			CMR variables
0.021±0.012	-0.019±0.022	0.005±0.021	LVMI, g/m^2
0.005±0.011	0.018±0.019	0.066±0.019**	LVEDVI, ml/m^2
0.010±0.010	-0.040±0.019*	-0.058±0.018**	LVM/LVEDV
0.006±0.010	-0.013±0.018	-0.033±0.018	RWT
-0.008±0.012	0.021±0.021	0.04±0.021	Stroke volume, ml
-0.015±0.010	0.014±0.018	-0.027±0.017	LVEF, %
-0.020±0.011	0.052±0.019*	0.039±0.018*	MCF

*0.001 **p≤0.001

Estimated B expressed as log unit increment of outcome variable (aortic stiffness) per standard deviation increment of continuous predictor variable or presence of categorical variable.

Aortic stiffness variables were natural log-transformed. Mean ± SD of ln ascending aorta strain = 2.39±0.50; ln(descending aorta strain)= 2.69±0.54; ln(PWV)= 2.14±0.42.

Models with each of the strain variables as outcomes included age, sex, body mass index, systolic blood pressure, diastolic blood pressure, diabetes, total/HDL cholesterol, current smoking, history of antihypertensive medication use, and prevalent CVD; separate models were run for risk factors alone and CMR variables adjusting for the risk factors.

LVEDV= Left ventricular end-diastolic volume. LVEF= Left ventricular ejection fraction. LVM = LV mass. MCF= myocardial contraction fraction. PWV = pulse wave velocity. RWT= relative wall thickness. Smoking = current cigarette smoking.

O043

Resting perfusion is not needed for clinical interpretation of adenosine perfusion CMR

Eike Nagel, MD, PhD[1]Konstantinos Bratis, MD, PhD[2], Chrysantos Grigoratos, M.D.[3], Melanie Le[4], Iris Burck, Dr.[5], Julian Wichmann, MD[6], Thomas Vogl, MD[7], Andreas Zeiher, MD, PhD[7], Valentina O. Puntmann, MD, PhD[8]

1. *University Hospital Frankfurt; Institute for Experimental and Translational Cardiovascular Imaging; DZHK Centre for Cardiovascular Imaging, Frankfurt, N/A, Germany*
2. *St George's NHS Trust, London, England, United Kingdom*
3. *MRI Lab, Fondazione G. Monasterio/CNR Regione Toscana, Pisa, Toscana, Italy*
4. *Institute for Experimental and Translational Cardiovascular Imaging, University Hospital Frankfurt, Hessen, Germany*
5. *Universum Hospital Germany, Hessen, Germany*
6. *Goethe University Hospital Frankfurt, Hessen, Germany*
7. *Goethe University Hospital Frankfurt, N/A, Germany*
8. *Institute of experimental and translational cardiovascular imaging, Frankfurt, N/A, Germany*

Background: Resting perfusion imaging has been advocated as an integral part of rest/stress adenosine perfusion imaging mainly to overcome artifacts. However, resting perfusion imaging requires additional contrast injection and significantly prolongs scan time. Many centres do not perform rest perfusion imaging routinely any more. Aim of the study is to systematically evaluate the value of rest perfusion imaging for clinical diagnoses.

Methods: 200 patients who underwent clinically indicated stress/rest perfusion imaging (80 Philips Achieva 3T, RxTx; 90 Philips Achieva 1.5T; 30 Siemens Avanto Fit 1.5T all equipped with 32-channel coils; SSFP imaging; parallel imaging, Philips: kt-blast, 0.075 mmol Gadobutrol/kg body weight for each scan) were assessed by 2 blinded observers. Observers were asked to assess each segment for the presence and transmural extent of inducible ischeamia as well as the presence of an artifact based on the stress scan in combination with late gadolinium enhancment (LGE) imaging only. Artifacts were graded as no artifact, clear artifact of questionable artifact and classified into a) positioning artifact, b) dark rim artifact, c) breathing artifact, d) arrhythmia/mistriggering artifact and e) unknown artifact. Resting scans were then provided to 1) reclassify the presence of ischaemia and 2) solve questionable artifacts on the stress scan.

Results: 3200 segments were analysed. 77.2% had no artifact, 23.6% clear artifacts and 9.2% questionable artifacts (7% questionable dark rim and 2.2% unknown artifacts). In 34 segments (1.1% of all segments) the resting scan helped to better classify the artifact. None of the questionable dark rim artifacts were better understood after assessing the rest scan. No change of clinical interpretation was necessary in any segment. For more detail see figure 1.

Conclusions: Resting perfusion helps to better understand 1.1% of all segments (11.5% of all segments with artifacts) but does not add to clinical interpretation. In routine examinations resting perfusion has become obsolete.

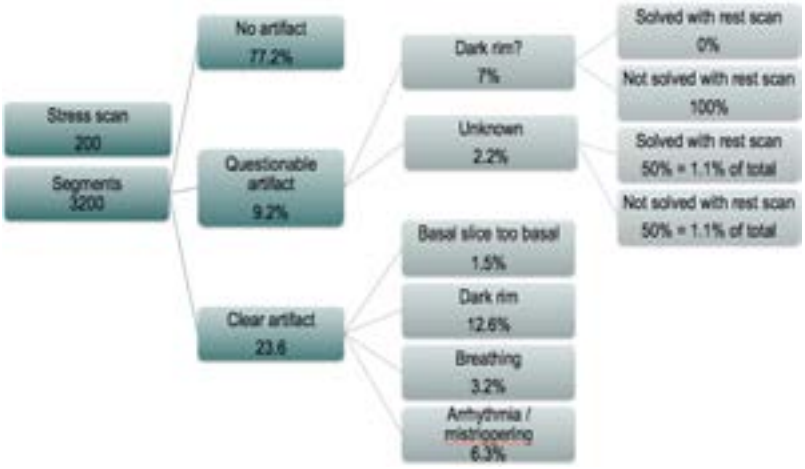

O044

Iron-Induced Foam Cell Formation is the Hallmark of Early Fat Infiltration in Healing Hemorrhagic Myocardial Infarction

Ivan Cokic, MD[1]Avinash Kali, PhD[2], Hsin-Jung Yang, PhD[2], Richard LQ Tang, MD[2], Joseph Francis, B.V.Sc., Ph.D[3], Rohan Dharmakumar, PhD[2]

1. *Cedars-Sinai Medical Center: BIRI, Los Angeles, CA*
2. *Cedars-Sinai Medical Center: BIRI, CA*
3. *Louisian State University, LA*

Background: Myocardial fat deposition has been frequently observed in regions of old myocardial infarction. The mechanism of this fatty degeneration has conventionally been attributed to the process of "lipomatous metaplasia" (LM). LM describes the replacement of scar tissue by metaplastic adipose tissue as part of the healing cascade after myocardial infarction (MI). To the best of our knowledge, no studies have yet been undertaken to elucidate the mechanisms underlying the LM in the post-MI setting. Since iron plays an important role in macrophage foam cell formation, we hypothesized that fatty infiltration of myocardial scar following MI can in part be attributed to macrophage foam cell formation in the scar regions containing persistent iron deposits.

Methods: Ten canines were subjected to 3-hour occlusion of the LAD artery, followed by reperfusion. All dogs underwent T2* and Late Gadolinium Enhancement (LGE) CMR on day 5 post-MI in a 3T clinical MRI system. T2*-weighted (multiple gradient-echo, TR=12ms, 6 TEs = 2.0ms–9.5ms with ΔTE=1.5ms, flip angle=10°) and the Late Gadolinium Enhancement were acquired along the short-axis direction covering the entire LV. Commonly used imaging parameters for all the scans were: resolution = 1.4 x 1.4 x 6 mm^3. All qualitative image analyses were performed using the cvi42 (Circle Cardiovascular Imaging Inc.). Animals were recovered and followed for 6 months post-MI at which time the hearts were explanted for histopathological analysis of macrophage markers within fat and iron-laden scar territories.

Results: All dogs exhibited the presence of intramyocardial hemorrhage in acute MI, as evidenced by CMR (Figure 1). Histopathological studies demonstrated both iron and fat deposits within all chronic myocardial infarctions. Interestingly, sparse fat deposits within scar tissue showed strong positive staining for CD36 (indicating foam cell formation) and were exclusively co-localized with iron deposits and $CD163^+$ macrophages (indicating iron-specific macrophage activation) (Figure 1).

Conclusions: Our data demonstrates that the process of fatty infiltration of myocardial infarctions begins with macrophage foam cell formation in the scar regions containing persistent iron deposits. The present study is the first to suggest that fatty degeneration of myocardial infarctions is driven by processes other than lipomatous metaplasia.

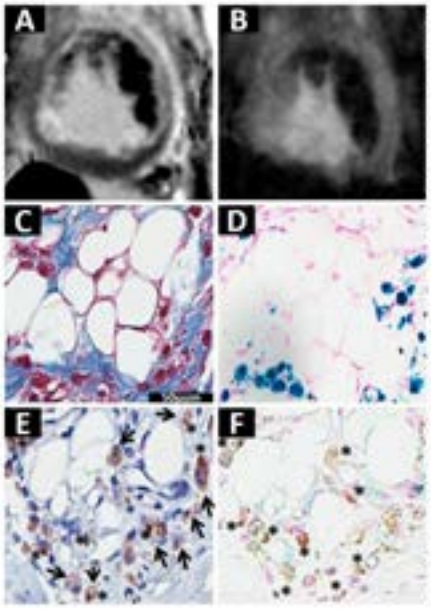

Figure 1: Representative LGE (**A**) and T2* (**B**) CMR acquired 5 days after MI and corresponding ex-vivo histology sections at 6 months post-MI stained with elastin-modified Masson's trichrome stain (**C**), Prussian Blue (**D**), anti-CD36 (**E**) and anti-CD163 (**F**) antibodies.

Panel C: Isolated fat depots (white globules) are found within an old myocardial infarction (blue).

Panel D: Persistent iron deposits (blue) co-localize with fat depots (white globules) in scar tissue.

Panel E: CD163-positive macrophages (arrows; pink) co-localize with iron (asterisks; brown) and fat (white globules) deposits.

Panel F: Fat depots (white globules) and iron-laden territories (asterisks; brown) stained positive for CD36 (green) indicating macrophage-derived foam cell formation.

O045

Extracellular Volume as a Risk Marker for Mortality in Patients With Ischemic Coronary Artery Disease

Vinay Acharya, DO[1] Eric Y. Yang, MD PhD[2], Mohamad Ghosn, PHD[3], Mohammad A. Khan, MBBS[4], Nickalaus L. Gramze, MD[3], Vijay Nambi, MD[5], Faisal Nabi, MD[6], Dipan J. Shah, MD[3], Grant W. Pickett, MD[3], Stephen J. Pickett, MD[3], Patrick Green, MD[3], Gerd Brunner, MS/Ph.D.[5], Christie M. Ballantyne, MD[5]

1. *Houston Methodist Hospital, Houston, TX*
2. *Houston Methodist Hospital, TX*
3. *Houston Methodist DeBakey Heart & Vascular Center, TX*
4. *Houston Methodist DeBakey Heart & Vascular Center, Sugar Land, TX*
5. *Baylor College of Medicine, TX*
6. *Houston Methodist DeBakey Heart & Vascular Center, Houston, TX*

Background: Coronary artery disease is frequently associated with myocardial infarction (MI) resulting in myocyte replacement fibrosis. Extracellular volume fraction (ECV) allows for quantification of extracellular matrix expansion in remote noninfarcted myocardium which may be a result of left ventricular (LV) remodeling. Whereas the presence of MI is a marker of vulnerability in patients with CAD, the role of ECV has not been well established. We examined the association of ECV with clinical outcomes in a patient population with established CAD.

Methods: From an initial cohort of 1604 patients who underwent T1 mapping, 257 were selected with significant CAD, confirmed on angiography or functional testing. Patients underwent T1 mapping using a modified Look-Locker (MOLLI) sequence before and approximately 15 minutes after administration of gadolinium contrast. ECV was computed from a mid-ventricular short axis view excluding any late gadolinium enhancement segments (either CAD or non-CAD pattern). From a reference group of normal volunteers, an upper 95% confidence limit of 30% was determined for elevation in ECV. Using this cutoff, we divided patients into elevated ECV (n=122) and "normal" ECV (n=145) groups. We assessed for subsequent mortality and HF hospitalization.

Results: Baseline characteristics were similar for both groups except for age, systolic blood pressure, dyslipidemia, and diabetes. Over a median follow-up of 10.0 (interquartile range 3.0, 19.1) months, 40 deaths and 61 HF hospitalizations occurred. Mortality was increased in patients with elevated ECV (unadjusted hazard ratio [HR] 2.00 [95% confidence interval (CI) 1.06, 3.80], p=0.03). On univariate Cox proportional hazard model analysis, age, diastolic blood pressure, and indexed right ventricular stroke volume were significant predictors of death. When adjusted for these covariates, elevated ECV remained a significant predictor of mortality (HR 1.94 [1.02, 3.68], p=0.04). No significant difference was seen with the survival analyses for HF hospitalizations.

Conclusions: Elevated ECV in patients with definitive CAD was associated with increased mortality. ECV may have a role as a risk marker for mortality in patients with ischemic CAD.

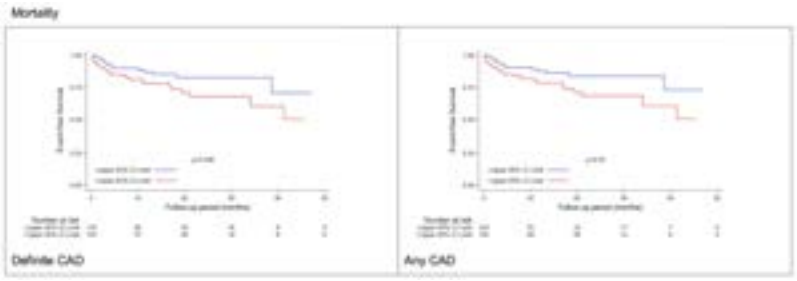

O046

Adenosine stress and rest native splenic T1 predicts the "splenic switch-off" sign without the need for gadolinium – a novel method to assess stress adequacy before first-pass perfusion imaging

Alexander Liu, MBBS, MRCP[1]Rohan S. Wijesurendra, MB BChir, MRCP[1], Rina Ariga, MBBS, MRCP[2], Masliza Mahmod, MBChB, DPhil[2], Eylem Levelt, DPhil[2], Andreas Greiser, Ph.D[3], Mario Petrou, PhD[4], George Krasopoulos, MD PhD[4], John C. Forfar, MD, PhD[4], Rajesh K. Kharbanda, MBChB, PhD[4], Keith M. Channon, MD, FRCP[2], Stefan Neubauer, MD, FRCP[2], Stefan K. Piechnik, PhD, MScEE[2], Vanessa M. Ferreira, MD, DPhil[2]

1. *University of Oxford, Oxford, England, United Kingdom*
2. *University of Oxford, England, United Kingdom*
3. *Siemens Healthcare GmbH, Erlangen, Germany, Erlangen, Bayern, Germany*
4. *Oxford Heart Centre, England, United Kingdom*

Background: Inadequate adenosine stress response is the commonest cause of false-negative CMR perfusion scans, which may lead to suboptimal diagnosis and treatment. The recently proposed marker of adequate stress, the "splenic switch-off" sign, detects reductions in splenic blood flow during adenosine stress perfusion (spleen appears dark), but can only be assessed after gadolinium first-pass perfusion, when it is too late to optimize the stress response. Reduction in splenic blood volume during adenosine stress is expected to shorten the native splenic T1, which we hypothesize can predict the "splenic switch-off" sign, *without* the need for gadolinium.

Methods: 212 subjects underwent adenosine stress CMR: 1.5T (n=104: 75 patients and 29 healthy controls); 3T (n=108: 86 patients and 22 healthy controls). Native $T1_{spleen}$ was assessed using heart-rate-independent ShMOLLI prototype sequence at rest and during adenosine stress (140µg/kg/min, 4minutes, IV) in 3 short-axis slices (basal, mid-LV, apical). This was compared with changes in peak splenic perfusion signal intensity (ΔSI_{spleen}) and the "splenic switch-off" sign on conventional stress/rest gadolinium first-pass perfusion imaging. $T1_{spleen}$ values were obtained blinded to splenic perfusion data, both were derived using regions of interest carefully placed with avoidance of artefacts and partial-volume effects (figure 1).

Results: Normal resting $T1_{spleen}$ were 1102±66ms (1.5T) and 1352±114ms (3T), slightly higher than in patients (1083±59ms, p=0.04; 1295±105ms, p=0.01, respectively). Resting $T1_{spleen}$ decreased significantly during adenosine stress (mean $\Delta T1_{spleen}$ ~ -40ms), independent of field strength, age, gender and cardiovascular diseases (including coronary artery disease, atrial fibrillation, type 2 diabetes mellitus, severe aortic stenosis and hypertrophic cardiomyopathy). While $\Delta T1_{spleen}$ correlated strongly with ΔSI_{spleen}on perfusion (R=0.70, $p < 0.001$, figure 2A); neither showed significant relations with changes in conventional hemodynamic markers during stress (heart rate and systolic blood pressure). By ROC analysis, $T1_{spleen}$ reduction of ≥30ms during adenosine stress accurately predicted the "splenic switch-off" sign (AUC 0.93, $p < 0.001$), with high sensitivity (94%), specificity (88%), and diagnostic accuracy (90%), figure 2B.

Conclusions: We successfully developed and implemented a novel method for assessing adenosine stress adequacy using splenic T1-mapping, independent of conventional hemodynamic parameters. We showed for the first time that splenicT1 reduction of ≥30ms during adenosine stress accurately predicted the "splenic switch-off" sign, without the need for gadolinium. Splenic T1-mapping can be performed "on-the-fly" during adenosine stress (figure 3), and holds promise to facilitate stress response optimization before gadolinium first-pass perfusion imaging.

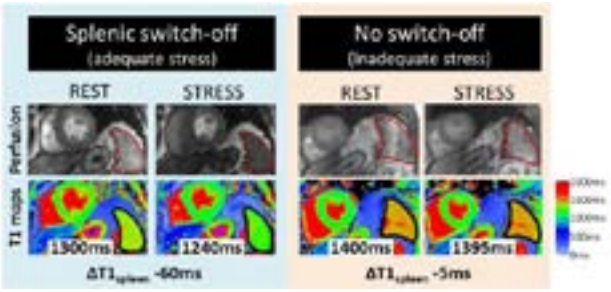

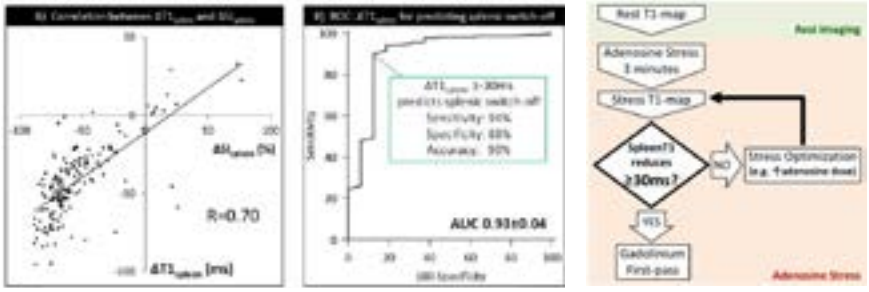

O047

Prognostic Utility of Circumferential Strain on Left Ventricular Outcomes in Patients with an Acute ST-Elevation Myocardial Infarction (STEMI): the British Heart Foundation MR-MI Study.

Kenneth Mangion, MD[1] David Carrick, PhD[2], Christie McComb, PhD[3], Hao Gao, PhD[4], Xiaoyu Luo, PhD, MSc [1], Margaret McEntegart, MBChB PhD[2], Hany Eteiba, MD[5], Mitchell Lindsay, MD[5], Mark Petrie, MD[6], Xiaodong Zhong, PhD[7], Stuart Hood, MD FRCP[8], Keith G. Oldroyd, MD (Hons); FRCP[5], Stuart Watkins, MD, FRCP[2], Andrew Davie, MB ChB[5], Caroline E Haig, PhD[9], Colin Berry, PhD FRCP[1]

1. *University of Glasgow, Glasgow, Scotland, United Kingdom*
2. *Golden Jubilee National Hospital, Glasgow, Scotland, United Kingdom*
3. *NHS Greater Glasgow and Clyde / University of Glasgow, Glasgow, Scotland, United Kingdom*
4. *School of Mathematics and Statistics, University of Glasgow, Scotland, United Kingdom*
5. *Golden Jubilee National Hospital, Scotland, United Kingdom*
6. *Glasgow University, Scotland, United Kingdom*
7. *Siemens Healthcare, GA*
8. *NHS Greater Glasgow and Clyde, Scotland, United Kingdom*
9. *Robertson Centre for Biostatistics, Glasgow, Scotland, United Kingdom*

Background: The prognostic significance of circumferential strain (E_{cc}) revealed by cardiac magnetic resonance (CMR) in patients following an acute ST-elevation myocardial infarction (STEMI) is uncertain. We hypothesised that an in-house developed intensity-based b-spline deformable registration method deriving E_{cc} from cine imaging would be more strongly linked to left ventricular (LV) surrogate outcomes revealed by CMR than feature-tracking software derived E_{cc} and comparable to a reference method (Displacement ENcoding with Stimulated Echoes-DENSE).

Methods: A prospective single centre cohort study was performed. The study had ethics approval (reference 10-S0703-28) and was publically registered (ClinicalTrials.gov identifier NCT02072850). Participants underwent CMR at 1.5 T (Avanto, Siemens Healthcare, Erlangen, Germany) 2 days and 6 months post-MI. The CMR protocol included cine-imaging (balanced steady-state free precession), 2D-cine EPI DENSE and delayed-enhancement phase-sensitive inversion-recovery pulse sequence 10-15 minutes after IV injection of 0.15 mmol/kg of gadoterate meglumine (Dotarem, Guebert S.A., Villepinte, France). Age and sex-matched healthy volunteers also underwent a similar CMR protocol. The myocardial mass of late gadolinium (LGE) was quantified using computer-assisted planimetry, utilising the 5 SD technique and expressed as % LV mass. Global peak circumferential strain was derived from spatially co-registered mid-left ventricular acquisitions using an in-house b-spline deformable method (Matlab), feature-tracking software (TomTec Imaging Systems, Germany), and CIM_2D DENSE (University of Auckland, New Zealand). Statistical analysis was performed using SPSS software and R. Multivariate regression models were used to analyse the relationship between E_{cc} utilising the 3 modalities and 1) change in LVEF, accounting for baseline LVEF, 2) change in indexed LVEDV, accounting for baseline indexed LVEDV, and 3) final infarct size, accounting for logged baseline infarct size. A statistician independent of the research group directed the statistical analyses.

Results: 323 patients and 33 age- and sex- matched volunteers (Table 1) underwent the same CMR protocol. (Table 1). Cine-derived strain data were available in all (100%) subjects but DENSE was not acquired in 64 (20%) patients. On multivariate regression analyses (Table 2), E_{cc} derived from DENSE had the highest adjusted-R square values for change in LVEF, and change in indexed LVEDV. The model utilising deformation-tracking had the highest adjusted-R square value for final infarct size, implying greater prognostic value.

Conclusions: E_{cc} is predictive of change in LV outcomes in the longer term in patients after an acute STEMI, even after accounting for baseline parameters. Cine-strain derived from deformation tracking and feature tracking had similar prognostic value.

Table 1. Demographics and left ventricular parameters of the patients and the healthy volunteers.

p-value	Healthy Volunteers (n=33)	Patients (n=323)	
0.776	59.2 ± 11.5	58.6 ± 13.2	Age (years)
0.872	72%	73%	Sex (male)
<0.001	64.9 ± 5.1	55.5 ± 9.6	LVEF (%)
<0.001	65.4 ± 10.5	79.5 ± 14.6	LVEDV-indexed to BSA (ml/m^2)
<0.001	23.9 ± 6.3	36.6 ± 12.8	LVESV- indexed to BSA (ml/m^2)
<0.001	-16.7 ± 1.9	-13.0 ± 3.5	Deformation Tracking- E_{cc} (%)
<0.001	-29.8 ± 4.1	-21.5 ± 6.5	Feature tracking- E_{cc} (%)
<0.001	-19.3 ± 2.2	-13.3 ± 3.8	DENSE E_{cc} (%)

LVEF- left ventricular ejection fraction, LVEDV- left ventricular end diastolic volume, LVESV- left ventricular end systolic volume, E_{cc}- Circumferential strain

Table 2. Prognostic multivariate models utilising the 3 different strain techniques to predict MRI surrogate outcomes.

Feature-tracking			Deformation-tracking			DENSE			
p-value	B	Adjusted R square	p-value	B	Adjusted R square	p-value	B	Adjusted R square	Patients n=259
0.136	-0.168	0.224	0.013	-0.557	0.237	<0.001	-0.444	0.252	Change in LVEF (%) (Accounting for Baseline LVEF)
0.030	0.156	0.014	<0.001	0.980	0.051	<0.001	0.926	0.068	Change in LVEDVi (%) (Accounting for Baseline LVEDVi)
<0.001	0.328	0.623	<0.001	0.718	0.633	<0.001	0.459	0.613	Final Infarct Size (% LV mass) (Accounting for logged baseline infarct size)

LVEF- LV ejection fraction, LVEDVi – indexed LV end diastolic volume, B- regression co-efficient

O048

Assessment Of Myocardial Viability By Native T1 Mapping: Comparison With Late Gadolinium Enhancement Technique

Amardeep Ghosh Dastidar, MBBS(Hons), MRCP[1] Giulia Pontecorboli, MD[2], Iwan Harries, MBBS, MRCP[2], Estefania De Garate, MD[1], Charlie Moret[3], Gareth Morgan[3], Anna Baritussio, MD[1], Elisa McAlindon, PhD[4], Chiara Bucciarelli-Ducci, MD, PhD[1]

1. NIHR Bristol Cardiovascular Biomedical Research Unit, Bristol, England, United Kingdom
2. NIHR Bristol CVBRU, England, United Kingdom
3. University of Bristol, England, United Kingdom
4. Heart and Lung Centre, New Cross Hospital, Wolverhampton, England, United Kingdom

Background: Viability assessment is a key aspect in the management of ischaemic heart disease (IHD). Targeted revascularization of viable myocardium improves clinical outcomes. Late gadolinium enhancement (LGE) or low dose dobutamine are the conventional cardiac magnetic resonance (CMR) methods for viability assessment. Native T1 mapping technique is highly sensitive to changes in myocardial tissue. We tested the hypothesis that T1 mapping can differentiate between viable and non-viable myocardium in IHD without the use of gadolinium contrast/dobutamine.

Methods: 20 normal healthy controls, 60 patients with known myocardial infarction (MI) (30 chronic >2months from MI and 30 acute day 2 STEMI) underwent conventional CMR (1.5-T, Siemens Avanto) to assess left ventricular function (cine) and the presence and extent of MI (LGE) using a scale of 0-4 for the 16 AHA segment (0=no scar, 1= 1-24%, 2=25-49%, 3=50-74%s and 4=>75% scar thickness) by a level 3 observer. A scar score of 2 or less (< 50% wall thickness) was deemed viable. These were compared with the corresponding native T1 mapping images (validated MOLLI sequence, motion corrected). T1 values were derived by drawing region of interest in each segment (Argus software).

Results: A total of 1,280 segments were analysed (320 in healthy controls and 960 in MI patients). The T1 values (1028 ± 48 ms) in healthy controls were similar to remote myocardium in chronic MI (1031 ± 31ms, p=ns) whilst high native T1 values were found in the remote myocardium in acute MI (1054 ± 65ms, p=0.0001). The mean segmental T1 values for scar score 0-4 were 1031±31ms, 1070±33ms, 1103±32ms, 1164±58ms, 1206±118ms respectively in chronic MI and 1054±65ms, 1103±65ms, 1175±81ms, 1151±56ms and 1168±71ms respectively in acute MI. (Figure 1a, b) ROC analysis of 960 segments showed that for myocardial viability assessment, native T1-mapping demonstrated excellent diagnostic performance compared to LGE as the gold standard (area-under-the-curve (AUC) - 0.9, 95%CI 0.87- 0.93, p < 0.0001). Subgroup ROC analysis of native T1 in chronic compared to acute MI showed a superior diagnostic accuracy of native T1 as a marker of viablity in chronic MI (AUC 0.94, 95%CI 0.89- 0.99, p < 0.0001, vs AUC – 0.85, 95%CI 0.81- 0.88, p < 0.0001). (Figure 1c,d & e) A T1 threshold of 1098ms most optimally differentiated viable from non-viable segments with a sensitivity and specificity of 85%.

Conclusions: Native T1 mapping can differentiate between normal, viable, and non-viable myocardium with distinctive T1 profiles especially in chronic MI. T1 mapping holds promise for viability assessment without the need for gadolinium contrast/dobutamine.

http://www.ConferenceAbstracts.com/uploads/cfp2/attachments/LDFAIBDN/LDFAIBDN--222429-1-ANY.pdf

O049

A Porcine Model of Hemorrhagic Myocardial Infarction Leads to Persistent Iron Deposition in the Chronic Post-MI Setting: Serial Cardiac MRI Studies with Ex-vivo Histological Validation

Ivan Cokic, MD[1]James F Dawkins, DVM[2], Hsin-Jung Yang, PhD[3], Eduardo Marban, MD, PhD[2], Rohan Dharmakumar, PhD[3]

1. *Cedars-Sinai Medical Center: BIRI, Los Angeles, CA*
2. *Cedars-Sinai Medical Center: Heart Institute, CA*
3. *Cedars-Sinai Medical Center: BIRI, CA*

Background: Several studies have now shown that hemorrhagic acute myocardial infarction (h-AMI) leads to persistent iron deposition in the convalescent phase of infarction. Recent reports also indicate that these infarcts have worse remodeling, prolonged iron-driven pro-inflammatory process, and altered electrophysiological parameters compared to infarcts without iron deposits. So far, iron deposits within infarct scars have been demonstrated in dogs and humans. Whether this phenomenon occurs in pig models of infarction, which is commonly used in translational cardiac studies, has not been proven. We hypothesize that h-AMI in pigs leads to persistent iron deposition, whose presence in the scarred myocardium can detected with T2* CMR.

Methods: Ten Yucatan minipigs, subjected to myocardial ischemia/reperfusion injury (90 minutes to 2.5 hours of left anterior descending artery occlusion followed by reperfusion), underwent T2* and LGE CMR at 3T on day 5 and week 8 post-MI. T2*-weighted images (multiple gradient-echo, 6 TEs = 2.0ms–9.5ms with ΔTE=1.5ms, flip angle=10°) and LGE images were acquired along the short-axis direction with full LV coverage. Commonly used imaging parameters for all the scans were: resolution = 1.4 x 1.4 x 6 mm^3. All quantitative image analyses were performed using a commercially available software. Subsequently, hearts were explanted and excised for histological assessment for persistent iron deposition.

Results: Mean T2* of hemorrhagic MIs (hemo+, n=5) was 18±3ms in acute phase and 17±2ms in chronic phase of post-MI period. In non-hemorrhagic MIs (hemo-, n=5) the mean T2* was significantly higher (36±4 ms in the acute and 35±4ms the chronic MIs) compared to hemo+ infarcts ($p < 0.001$, for both). Prussian blue (PB) staining confirmed that all h-AMIs lead to localized iron deposition within chronic MI scars (elastin-modified Masson's trichrome (EMT) stain) (Figure).

Conclusions: Our findings confirmed that reperfused h-AMI in pigs, like in humans and dogs, lead to persistent iron deposition. We propose that a pig model of h-AMIs can provide opportunities for examining late effects of persistent iron deposits related to adverse LV remodeling and ventricular arrhythmias.

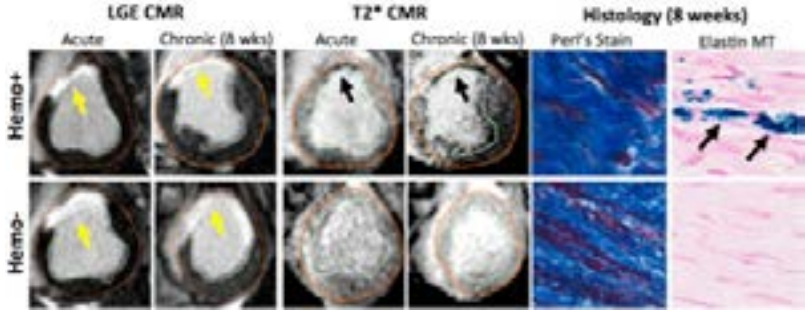

O050

Cardiac MRI Practice: An Analysis of 2012-2014 Medicare Provider Utilization and Payment Data

James W. Goldfarb, PhD[1]Nathaniel Reichek, MD[2], Jie Cao, MD[3]

1. St Francis Hospital, Roslyn`, NY
2. St Francis Hospital, Roslyn, NY
3. St Francis Hospital, NY

Background: Cardiac magnetic resonance (CMR) imaging appropriateness criteria are well documented, but outside of professional society membership and voluntary registries, little information is known about the practitioners and practice of cardiovascular CMR in the United States of America. The goal of this study is to document and describe practitioners who provide services to the US Medicare population and their CMR practice. In 2014, Medicare provided health insurance to over 54 million Americans; 45 million people age 65 and older and 9 million younger people with disabilities.

Methods: A retrospective cross-sectional analysis of Medicare physician payments from a publically available database was performed. CMR services were identified using the Healthcare Common Procedure Coding System (HCPCS): (75557-75565). Characteristics of physicians, CMR exams and reimbursement as well as trends from 2012 to 2014 were analyzed. Statistics were calculated for the number of providers, number of services, payment, geographic location and type of facility.

Results: From 2012 to 2014, the number of CMR providers increased 24% to 389. The total amount paid to these healthcare providers in 2014 was 2.4 million US dollars; a 1.2% decrease compared to 2012. There was a 19% increase in the number of CMR procedures to 18,101. Mean number of providers and payments are shown geographically in Figure 1. In contrast, there were more than a million nuclear cardiology scans with payments of 700 million dollars and more than 10 million echocardiography scans with more than 1 billion dollars of physician payments. The majority of CMR scans were performed with contrast (>80%). Payments to providers remained constant while the number of scans increased due to a 5-10% decrease in provider payments per scan and a shift from the outpatient office to the hospital setting. The vast majority of practitioners were identified as Cardiologists or Diagnostic Radiologist. Diagnostic Radiology saw a 35% growth in the number of practitioners while Cardiology had a 10% growth. In 2014, there were slightly more Radiologist providers, but Cardiologists performed 20% more CMR scans. More men than women provided CMR services (~15% Female). The gender disparity was similar for Radiology and Cardiology.

Conclusions: Cardiac MR utilization increased (~20%) and payment per scan decreased from 2012 to 2014. Usage was split between Cardiology and Diagnostic Radiology. Cardiac MRI usage remains a small fraction of overall cardiovascular imaging.

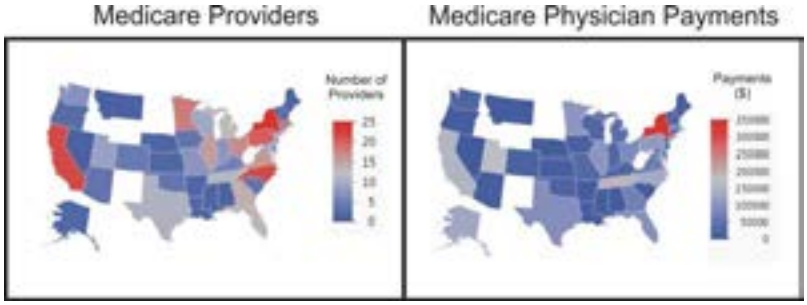

2014 US Medicare CMR Physician Payment Summary

389	Providers
185 (48%)	Radiologists
178 (46%)	Cardiologists
46.5	Number of Studies per Provider
$ 261.6	Payment per Procedure (Outpatient Office; Technical and Professional Fees)
$ 107.6	Payment per Procedure (Facility; Professional Fee)

O051

Motion-compensated spiral simultaneous multi-slice myocardial perfusion

Yang Yang, PhD[1] Li Zhao, PhD[2], Xiao Chen, PhD[3], Daniel S. Weller, PhD[4], Klaus Hagspiel, MD[1], Patrick Norton, MD[1], Christopher M. Kramer, MD[1], Michael Salerno, MD, PhD[1]

1. *University of Virginia, VA*
2. *Beth Israel Deaconess Medical Center, Boston, MA*
3. *Medical Imaging Technologies, Siemens Healthineers, NJ*
4. *University of Virginia, Charlottesville, VA*

Background: Contrast-enhanced first-pass myocardial perfusion is a valuable noninvasive technique to evaluate patients with known or suspected CAD. Conventional CMR perfusion techniques have limitations for achieving high spatial-temporal resolution and whole heart coverage. Simultaneous multi-slice (SMS) techniques utilizing multi-band RF pulse to excite multiple slices simultaneously have the potential to significantly improve the sampling efficiency. We have previously demonstrated high image quality and diagnostic utility of variable-density spiral perfusion imaging with 3 slices coverage. We proposed to incorporate the SMS technique into this spiral pulse sequence to achieve 6 slices coverage without additional acquisition time or significant loss in SNR.

Methods: We proposed an approach where the phase of one slice was modulated by alternating angles (Fig 1a and f) to achieve incoherent aliasing pattern (Fig 1c and h), and the excitation phase was incremented by the golden-angle between heart-beats to further improve the temporal incoherency. The perfusion images were reconstructed using a rigid motion-compensated L1-SPIRiT technique. To test this strategy, we retrospectively reconstructed 10 data sets with simulated SMS acquisition using the proposed scheme. The reconstructed images were assessed quantitatively by normalized root mean square error (NRMSE) and structural similarity index (SSIM). In addition, prospective SMS spiral perfusion imaging was performed in 4 patients undergoing clinically ordered CMR studies with gadolinium on a 1.5T Aera Siemens scanner. Sequence parameters included: FOV 340mm, TE 1.0ms, TR 8ms, SRT 80ms, FA 26^{o}, 64ms per two slices, 6 slices with 10mm thickness, 2mm in-plane resolution. Image quality of the prospectively acquired studies was graded on a 5-point scale (5 excellent, 1 poor) by a cardiologist.

Results: Fig 1 (d,i) shows direct reconstruction of the SMS simulated data from retrospective experiment. It demonstrated minimal interference of the data from each slice on the other slice. L1-SPIRiT reconstruction easily recovers images each slice with no significant SNR loss (e,j). The NRMSE was 2.57±0.35% and SSIM was 0.89±0.07 for the 10 retrospective cases which demonstrated high quality images of minimum error and the maximum similarity to the gold-standard images acquired from each slice location independently. Fig 2 and 3 show 6 slices perfusion images prospectively acquired using the spiral-SMS technique during first pass. The average image score from prospectively acquired studies was 3.8±0.5 demonstrating good image quality.

Conclusions: We demonstrated the successful application of an SMS spiral perfusion technique. The sampling efficiency is improved to achieve twice the slice coverage with no additional acquisition time and high image quality. Further validation will be required in patients undergoing adenosine stress CMR.

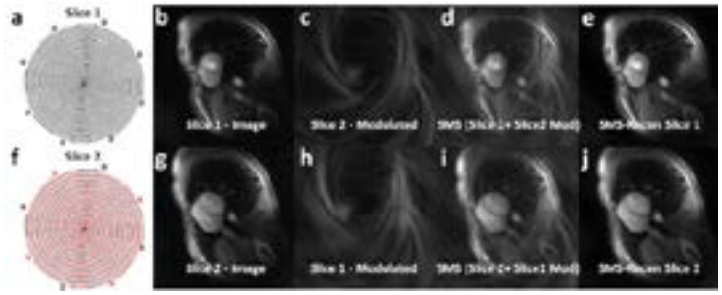

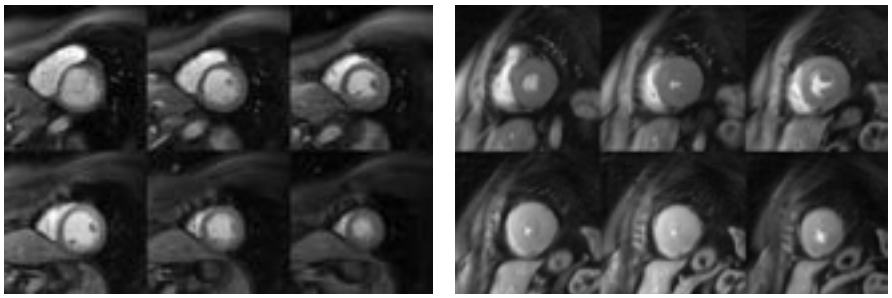

O052

Free-Breathing, Non-ECG-Gated, Continuous Myocardial T1 Mapping with Cardiac MR Multitasking

Jaime L. Shaw, MS[1] Anthony G. Christodoulou, PhD[2], Behzad Sharif, PhD[3], Debiao Li, PhD[4]

1. *Cedars-Sinai Medical Center/UCLA, CA*
2. *Cedars-Sinai Medical Center, CA*
3. *Cedars-Sinai Medical Center, Los Angeles, Los Angeles, CA*
4. *Biomedical Imaging Research Institute, Cedars-Sinai Medical Center, Los Angeles, CA, CA*

Background: T1 mapping is known to detect both focal and diffuse myocardial fibrosis, important in cardiovascular disease [1]. Currently used techniques utilize both ECG gating and breath-holds/navigators with low imaging efficiency and/or respiratory motion artifacts. We remove the need for ECG gating and respiratory monitoring with cardiac MR multitasking, a continuous technique using a low-rank tensor (LRT) imaging framework, here used for inversion recovery (IR) T1 mapping [2,3]. The aim of this work is to validate free-breathing, non-ECG-gated T1 mapping in healthy subjects against standard MOLLI T1 mapping.

Methods: The proposed continuous 2D acquisition utilizes a golden-angle radial FLASH scheme modified to also collect interleaved low-rank tensor auxiliary data used for temporal subspace estimation [2,3]. IR pulses are applied at set intervals to achieve T1 recovery. Sequence parameters: scan time: 1 min., 2.5 s between IRs, 24 IRs, TE/TR: 1.6/3.6ms, flip angle: 5°, FOV: 270x270mm^2, in-plane resolution: 1.7x1.7mm^2, slice thickness: 8 mm. First, real-time low-rank matrix images [4] were reconstructed for image-based cardiac and respiratory binning. Next, LRT reconstruction was performed using an explicit tensor subspace constraint estimated from the auxiliary data and a dictionary of T1 curves with 344 inversion time (TI) images (range: 3.6-2,476ms), with 15 cardiac and 5 respiratory bins. Pixel-wise T1 maps were created at an end-expiration respiratory phase and a diastolic cardiac phase. For both methods, T1 was measured with an ROI in the septum. Repeatability was assessed as within-subject variance by the coefficient of variation (CV). Ten healthy subjects were scanned at 3T (Siemens Verio) with the proposed method in a single mid-ventricular slice as well as a resolution-matched breath-hold, ECG-gated, MOLLI 5(3)3 [5] with online motion correction. Both methods were repeated 3 times.

Results: Fig. 1 shows TI images as well as T1 maps for the proposed method and MOLLI. T1 values for both methods are not significantly different (MOLLI: 1259.3±45.9 Proposed: 1246.7±24.6 p=0.53) and are within the published normal range at 3T (Fig. 2). Both methods demonstrate low CVs within 3 repetitions, demonstrating good repeatability (MOLLI: 1.16%, Proposed: 2.48%). Fig. 3 demonstrates the ability of the proposed method to quantify T1 in both diastole and systole from the same scan while MOLLI required 2 separate breath-hold scans.

Conclusions: The proposed free-breathing, non-ECG-gated, T1 mapping technique produces T1 values similar to MOLLI with good repeatability and within the range of reported values. The proposed technique also enables T1 quantification throughout the cardiac cycle and at multiple respiratory phases. Our findings show promise for myocardial T1 mapping free of ECG-gating and breath-holds or respiratory navigators.

References

1. Puntmann *Circ Res.* 2016
2. Shaw *ISMRM* 2016
3. Christodoulou *ISMRM* 2016
4. Christodoulou *TBME* 2013
5. Xue *MRM* 2013

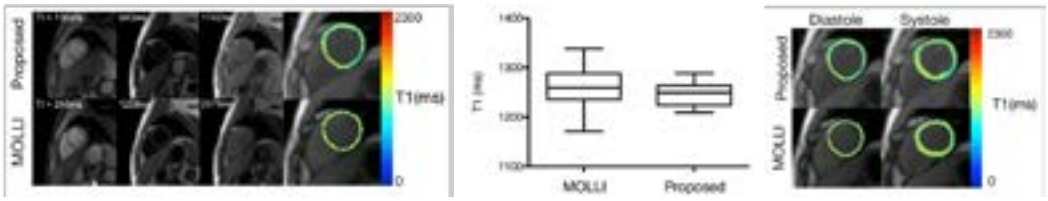

O053

Semi-automated quantification of aortic arch length and stiffness in CMR using a 3D cylindrical active surface

Thomas Dietenbeck, PhD[1] David Rosenbaum, MD, PhD[2], Damian Craiem, Eng[3], Alban Redheuil, MD, PhD[2], Nadjia Kachenoura, PhD[1]

1. *Sorbonne Universités, UPMC Univ Paris 06, INSERM UMRS 1146, CNRS UMR 7371, Laboratoire d'Imagerie Biomédicale, Ile-de-France, France*
2. *Sorbonne Universités, UPMC Univ Paris 06, INSERM UMRS 1146, CNRS UMR 7371, Laboratoire d'Imagerie Biomédicale, Paris, Ile-de-France, France*
3. *Universidad Favaloro (IMETTyB), Buenos Aires, Argentina*

Background: Aortic stiffness is a well-recognized predictor of cardiovascular risk and is commonly assessed through aortic pulse wave velocity (PWV). In cardiovascular magnetic resonance imaging (CMR), aortic PWV estimation requires the measurement of aortic arch length which is often performed in multiple 2D axial and sagittal oblique views to take into account the complex aortic arch geometry.

Methods: We studied 77 individuals (40 men and 37 women, age 50±12y): 23 healthy volunteers and 54 patients with essential hypertension who underwent 3D CMR of the aorta and aortic phase contrast imaging to estimate ascending to descending aorta transit time. The proposed method segments the thoracic aorta volume using explicit active contours where the aortic surface is defined in a cylindrical coordinate system. The computation of the aortic centerline and the definition of aortic anatomical segments required manual initialization of 7 anatomical landmarks from the sino-tubular junction to the celiac trunk. Evaluation of the method was performed by comparing the measured aortic arch length against manual measurements, obtained from the combined analysis of sagittal oblique and axial planes covering the aortic arch. The PWV calculated using both the manual and automatic aortic length measurements were also compared against carotid-femoral PWV (cf-PWV) measured with applanation tonometry.

Results: Mean aortic length using our method vs. manual segmentation was 130.5±19mm vs. 112.9±17mm in the control group and 139.6±20mm vs. 120.9±23mm in the hypertensive group. Our method was shown to correlate well with the manual reference in terms of arch length ($r = 0.75$, $p < 0.001$; Bland-Altman (BA) mean bias [limits]: 9.5mm [-20.3; 39.2]) and PWV ($r = 0.96$, $p < 0.001$; BA mean bias [limits]: 0.58m/s [-1.56; 2.72]). Equivalent correlations of aortic PWV with cf-PWV were found for both aortic length methods (automated: $r = 0.52$, $p < 0.001$; manual: $r = 0.57$, $p < 0.001$). The mean analysis time was around 5min (2-3min to load the data and setting the landmarks and 2min for the centerline extraction and aortic segmentation) for a Matlab implementation of the software.

Conclusions: The proposed method enables fast and semi-automated segmentation of the aorta from a single CMR 3D dataset, providing its centerline length for the estimation of aortic PWV. Such measurements were comparable to the manual aortic length and PWV measurements, which required a time consuming definition of the centerline. Furthermore, such volumetric approach will ultimately enable the extraction of advanced morphological indices such as segmental volumes, arch tortuosity and aortic tapering for further evaluation of aortic physiological changes.

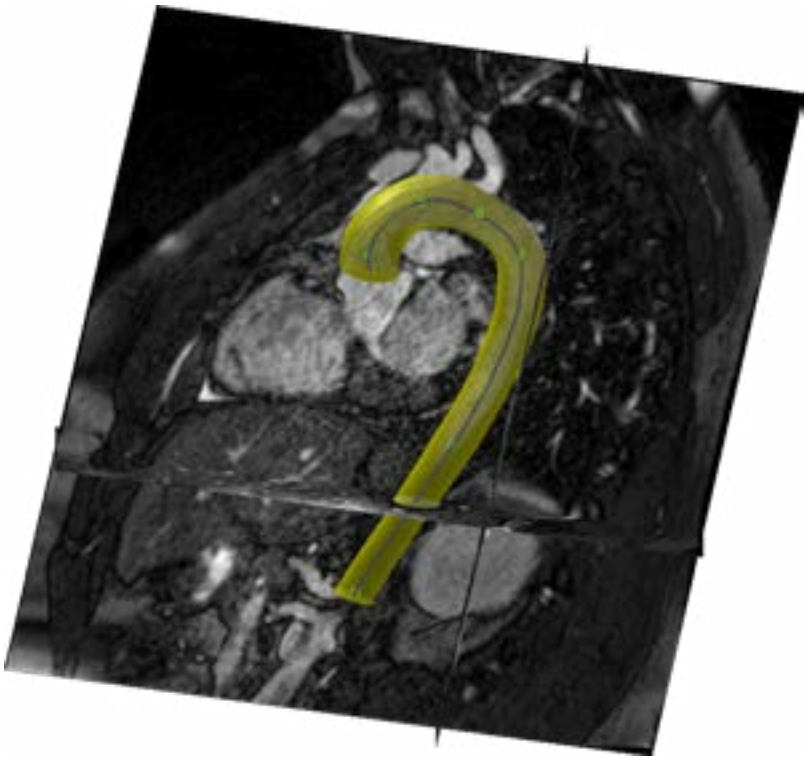

O054

To screen or not to screen? Long-term cost effectiveness of CMR screening for unrecognised myocardial infarctions

Jonathan Siverskog, M.Sc.[1] Jannike Nickander, MD[2], Erik B. Schelbert, MD, MS[3], Raquel Themudo, MD, PhD[4], Martin Henriksson, PhD[5], Martin Ugander, MD, PhD[6]

1. *Linköping University, Linköping, N/A, Sweden*
2. *Karolinska Institute, Stockholm, Stockholms Lan, Sweden*
3. *University of Pittsburgh; Heart and Vascular Institute of UPMC, PA*
4. *Department of Clinical Physiology, Karolinska Institutet and Karolinska University Hospital, Stockholms Lan, Sweden*
5. *Department of Medical and Health Sciences, Linköping University, N/A, Sweden*
6. *Karolinska Institutet, Stockholms Lan, Sweden*

Background: Cardiac magnetic resonance (CMR) imaging using late gadolinium enhancement (LGE) has been shown to detect unrecognised myocardial infarction (UMI) in 20% of 70 year olds screened from the general population. Individuals with UMI have an increased mortality similar to patients with recognized myocardial infarction and 60% are not taking any medication for secondary prevention. Hence, identifying unmedicated 70 year olds with UMI by CMR and initiating treatment with secondary prevention medications (statins, aspirin, angiotensin converting enzyme inhibitors, beta blockers) may improve health outcomes. The aim of this study was to compile available evidence and assess the cost effectiveness of CMR screening for UMI using decision-analytic modelling.

Methods: A Markov simulation model was employed to estimate long-term healthcare costs, life expectancy (life years) and quality-adjusted life years (QALYs) with a screening or no screening strategy. With screening, unmedicated 70-year-olds were invited to CMR and secondary preventive medication was initiated in those identified with UMI. Published sources were used to estimate key input parameters such as attendance rates to CMR, mortality risk with UMI, and the risk reduction associated with secondary preventive treatment. Results are presented as cost-effectiveness ratios reported in Euros (EUR). Extensive sensitivity analyses were performed in order to determine which parameters had the greatest impact on cost effectiveness and to identify key areas for further research.

Results: Compared to no screening, a CMR screening program was associated with 9.44 vs 9.37 QALYs (12.59 vs 12.51 life years). Lifetime costs of the screening and no screening strategy were EUR 951 and EUR 250, respectively. The cost per QALY of screening was EUR 11317 per QALY (EUR 8224 per life year). Sensitivity analyses revealed that the results were most sensitive to baseline mortality risk and mortality risk reduction associated with secondary preventive treatment. An analysis of the cost per CMR exam indicated that the cost per QALY varied linearly from EUR 7000 to EUR 16000 with cost per CMR exam ranging from EUR 200 to EUR 800.

Conclusions: Previously unknown estimates of long-term costs and health outcomes of a CMR screening program for UMI are presented. Although associated with uncertainty, the conservatively applied model indicates that CMR screening can be cost effective to such an extent that it is associated with a cost per QALY below conventional thresholds for cost effectiveness. The range of cost per CMR exam appears feasible for an abbreviated scanning protocol (≤15 minutes) focused on LGE infarct imaging. The analysis shows that it is justified to undertake a pilot screening study to resolve the uncertainties around cost effectiveness of CMR screening for UMI.

O055

Cardiac MR Fingerprinting with Simultaneous Multi-Slice Imaging for T1 and T2 Quantification

Jesse I. Hamilton, B.S.[1] Yun Jiang, B.S.[2], Dan Ma, Ph.D.[2], Wei-Ching Lo, M.S.[2], Mark Griswold, Ph.D.[3], Nicole Seiberlich, Ph.D.[2]

1. *Case Western Reserve University, Cleveland Heights, OH*
2. *Case Western Reserve University, OH*
3. *Case Western Reserve University; University Hospitals, OH*

Background: MR Fingerprinting (MRF) has previously been demonstrated for mapping myocardial T_1, T_2, and M_0. MRF has also been combined with simultaneous multi-slice (SMS) techniques for neuroimaging. This project increases the efficiency of cardiac MRF by combining SMS and a sparse reconstruction to generate maps of T_1 and T_2 for 3 slices in one breathhold.

Methods: An ECG-triggered FISP MRF sequence was employed with variable flip angles (4- 15deg), a constant TR of 5.1ms, and a 250ms diastolic acquisition window. Data were sampled along a variable density spiral with 0^{th} moment compensation and a golden angle rotation between interleaves. SMS excitation was achieved by changing the RF phase according to a POMP schedule. The dictionary contained 6000 entries with T_1 50-4000ms and T_2 5-500ms. A different dictionary was simulated for each slice that accounted for the slice-specific RF phase. Parameter maps were generated by solving an L-1 minimization problem. Data consistency was enforced using the acquired slice-collapsed and undersampled k-space. Additionally, an L-1 term penalized signal timecourses that did not match well with any entries in the dictionary and was calculated as follows. The k-space data were demodulated by the RF phase, gridded, and matched to the dictionary. The goodness of fit ,defined as one minus the inner product with the best matching dictionary element, was summed over all pixels and all slices to yield the L-1 term. The minimization was solved using the ADMM algorithm.

Three volunteers were scanned at 3T (Skyra, Siemens Medical Solutions). MRF data were acquired with MB=3 (scan time 10 heartbeats, 8mm slice thickness, 16mm slice gap). Single slice MRF acquisitions were performed at the same positions.

Results: MRF maps acquired with MB=3 collected in 10 heartbeats are presented in Figure 1. Figure 2 shows maps from single slice acquisitions at approximately the same positions. The mean T_1 and T_2 measurements in the septal wall were comparable for the SMS and singleband acquisition; representative results from one volunteer are shown in Table 1. With SMS, the mean T_2 measurements were 0-5ms lower, and slightly higher standard deviations for both parameters were obtained.

Conclusions: SMS can be combined with cardiac MRF to quantify T_1 and T_2 up to MB=3. Future work will explore improving the T_1 and T_2 precision and extending the technique to whole-heart mapping in one breathhold.

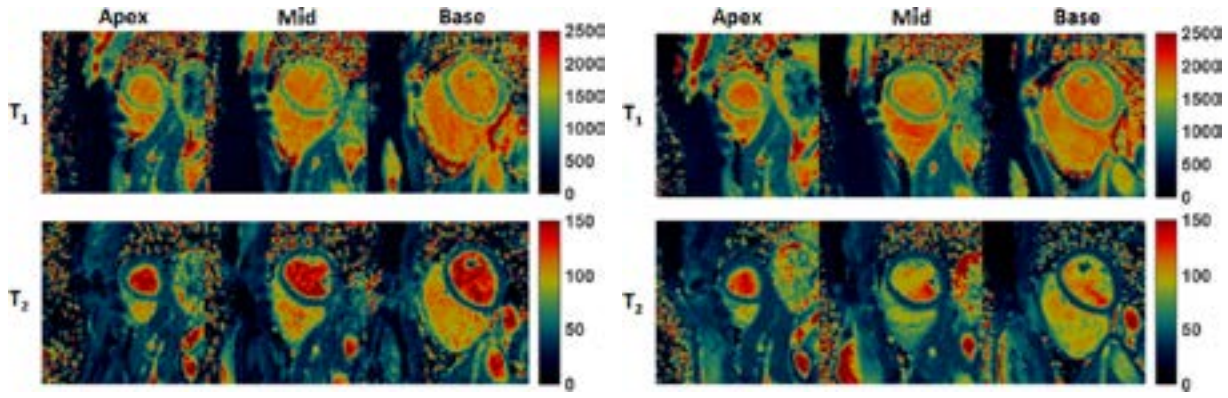

SMS MRF Myocardial T1 and T2 Measurements

T_2 (ms) Single Slice	T_1 (ms) Single Slice	T_2 (ms) MB=3	T_1 (ms) MB=3	Slice
42.1±1.7	1218±67	47.9±3.5	1277±67	Apex
39.7±1.7	1217±38	43.7±3.4	1203±65	Mid
40.4±2.6	1209±35	41.8±3.6	1193±78	Base

O056

Arrhythmia insensitive LGE with REPAIR: stabilizing variable signal regrowth by variable flip angles

Chenxi Hu, PhD[1]Steffen Huber, M.D.[1], Maolin Qiu, PhD[1], Gigi Galiana, PhD[2], Hamid Mojibian, M.D.[1], Lauren A. Baldassarre, MD[1], Dana C. Peters, PhD[1]

1. *Yale University, CT*
2. *Yale University, New Haven, CT*

Background: When 3D high resolution late gadolinium enhancement (LGE)[1] is used in patients with arrhythmia, image quality is impaired by the variable time between inversion pulses (due to RR variation), which yields ghosting artifacts and image blurring. Previous solutions explored using 2-RR acquisition, adding a 90° saturation[2], or dynamically changing TI[3]. In this work, we propose a dynamically saturated LGE sequence. The nonselective saturation pulse, referred to as **R**egrowth **E**qualization **P**ulse for **A**rrhythmias in **I**nversion **R**ecovery (**REPAIR**), changes its flip angle dynamically based on the previous RR interval.

Methods: Figure 1 shows the pulse sequence and the corresponding signal evolution. The standard LGE generates a fluctuating signal strength due to a variable signal regrowth time during arrhythmia. This problem is resolved in REPAIR LGE by applying a saturation pulse (alpha ≤ 90) immediately before the inversion to reduce Mz to a predetermined baseline value (for a target T1). The flip angle of the REPAIR pulse is calculated by Bloch equation modeling of the signal evolution in response to a varying RR. Within the pulse sequence, after each ECG trigger, the sequence reads from the scanner the previous RR interval and calculates the flip angle in real time. In conjunction with this, Bloch equations were used to calculate the optimal TI for this modified LGE sequence, given an estimated myocardial T1.

Phantom studies were conducted with REPAIR LGE for a range of post-contrast T1 values, and programmed arrhythmia, using following parameters: TR/q/vps/BW/RRmin/RRmax = 8.06ms/10°/33/200Hz/Px/400ms /1900ms. Several arrhythmia patients (RR: 600-1100ms) were imaged with LGE and REPAIR on a 1.5T scanner (Siemens Aera), after providing written informed consent. The target T1 for REPAIR was chosen to be 350 ms. Other parameters were: TR/q/vps/BW = 5.12ms/15°/27/399Hz/Px.

Results: Figure 2 shows phantom and in vivo imaging results. REPAIR (2(B)) generates dramatically fewer ghosts compared to LGE (2(A)) for a range of T1 values. Figure 2(C-F) demonstrates the reduced ghosting and blurring with REPAIR LGE in vivo. Figure 3 shows that REPAIR LGE has a slightly lower SNR and CNR, a similar myocardial nulling, but reduced ghosting and blurring compared to standard 3D LGE.

Conclusions: REPAIR LGE is less sensitive to arrhythmia and leads to better image quality, enabling assessment of left atrial scar in patients with ongoing arrhythmia. 1. Marrouche, JAMA 2014; 2. Weingartner, MRM 2014; 3. Keegan, MRM 2015

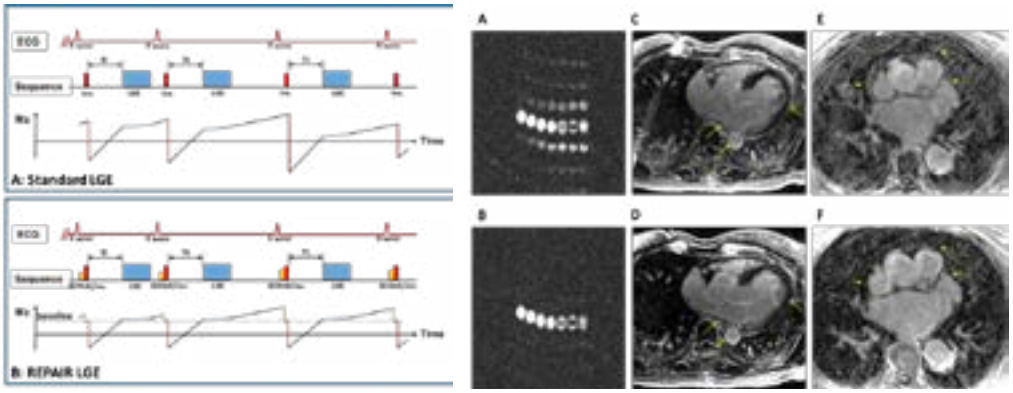

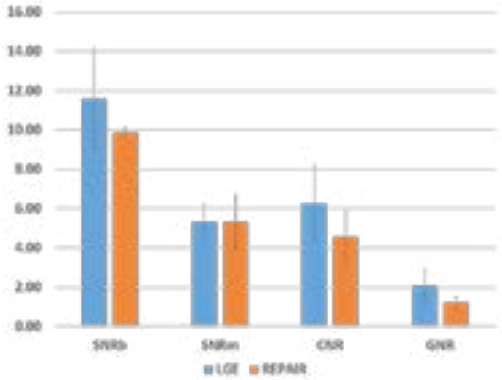

O058

T1, extracellular volume and myocardial blood flow mapping: a multiparametric mapping approach in cardiac amyloidosis

Ana Martinez-Naharro, MD[1] Daniel S. Knight, MBBS MRCP(UK)[2], Tushar Kotecha, MBChB[3], Rohin Francis, MBBS[3], Giulia Zumbo, MD[3], Thomas Treibel, MBBS.MRCP(UK)[4], Jannike Nickander, MD[5], Raquel Themudo, MD, PhD[6], Julian Gillmore, MD, PhD[3], Martin Ugander, MD, PhD[7], James Moon, MBBS, MD, MRCP[8], Hui Xue, PhD[9], Peter Kellman, PhD[10], Philip Hawkins, PhD[3], Marianna Fontana, MD, PhD[3]

1. *National Amyloidosis Centre, University College London, London, England, United Kingdom*
2. *Royal Free London NHS Foundation Trust, London, England, United Kingdom*
3. *National Amyloidosis Centre, University College London, England, United Kingdom*
4. *Barts Heart Centre, England, United Kingdom*
5. *Karolinska Institute, Stockholm, Stockholms Lan, Sweden*
6. *Department of Clinical Physiology, Karolinska Institutet and Karolinska University Hospital, Stockholms Lan, Sweden*
7. *Karolinska Institutet, Stockholms Lan, Sweden*
8. *Barts Heart Center, The Cardiovascular Magnetic Resonance Imaging Unit and The Center for Rare Cardiovascular Diseases Unit, St Bartholomew's Hospital, West Smithfield, London, UK, England, United Kingdom*
9. *National Heart, Lung, and Blood Institute, Bethesda, MD*
10. *Laboratory of Cardiac Energetics, National Institutes of Health/NHLBI, Bethesda, MD, United States., MD*

Background: Cardiac involvement is the main driver of outcome in systemic amyloidosis, but the relationship between amyloid deposits and cellular injury is not well understood. The simple explanation of physical, mechanical replacement of parenchymal tissue seems insufficient, and preliminary studies support the hypothesis that myocardial hypoperfusion could contribute to cell damage in amyloidosis. The aim of this study was: 1) To assess feasibility of fully automated pixel-wise rest myocardial blood flow (MBF) mapping in cardiac amyloidosis during routine clinical scans; 2) To assess the prevalence of myocardial hypoperfusion and correlation with amyloid deposits and disease severity.

Methods: Patients (n=56) with systemic amyloidosis and healthy volunteers (n=16) were recruited. All subjects underwent CMR at 1.5T (Siemens) with standard SSFP cine imaging, Phase Sensitive Inversion Recovery Reconstruction Late Gadolinium Enhancement (PSIR-LGE), T1 mapping, Extracellular Volume (ECV) mapping and rest MBF mapping.

Results: The pixel-wise MBF maps for all slices were generated automatically in all patients within 2.5 minutes after image acquisition. Myocardial perfusion was globally reduced in patients with cardiac amyloidosis compared to healthy volunteers (0.66±0.26ml/min/g vs 0.84±0.19ml/min/g, $p < 0.05$)Myocardial perfusion inversely correlated with amyloid burden measured as extracellular volume fraction ($r = -0.46$, $p < 0.001$) (figure 1) and with the transmurality of LGE (no LGE 0.88±0.18ml/min/g, subendocardial LGE 0.73±0.28ml/min/g and transmural LGE 0.58±0.20ml/min/g, $p < 0.01$) (figure 2). There was a correlation between myocardial perfusion and markers of systolic dysfunction (EF, $r = 0.39$, $p < 0.001$), current reference prognostic markers in cardiac amyloidosis. There was no significant correlation between myocardial perfusion and native T1 values ($r = -0.07$, $p=0.59$).

Conclusions: Myocardial perfusion can be measured in cardiac amyloidosis during routine clinical scans with fully automated MBF mapping. Myocardial hypoperfusion at rest is highly prevalent in subjects with cardiac amyloidosis, and correlates with the degree of amyloid infiltration and disease severity.

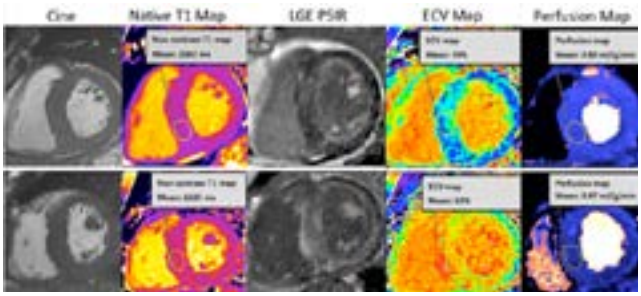

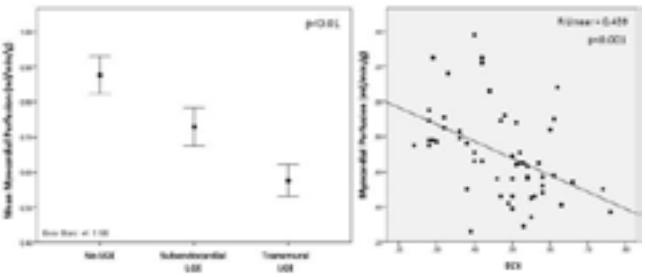

O059

CMR Perfusion Imaging Objectively Diagnoses Microvascular Ischaemia – Novel Validation against Invasive Index of Microvascular Resistance (IMR)

Alexander Liu, MBBS, MRCP[1]Rohan S. Wijesurendra, MB BChir, MRCP[1], Joanna M. Liu, MBBS[2], John C. Forfar, MD, PhD[3], Keith M. Channon, MD, FRCP[2], Stefan Neubauer, MD, FRCP[2], Stefan K. Piechnik, PhD, MScEE[2], Rajesh K. Kharbanda, MBChB, PhD[3], Vanessa M. Ferreira, MD, DPhil[2]

1. *University of Oxford, Oxford, England, United Kingdom*
2. *University of Oxford, England, United Kingdom*
3. *Oxford Heart Centre, England, United Kingdom*

Background: Microvascular ischaemia affects ~50% of all patients with coronary artery disease (CAD) and impairs clinical outcomes independent of epicardial-CAD. It remains a diagnostic challenge, which hinders targeted therapy. Although CMR myocardial perfusion reserve index (MPRI) has been shown to be reduced in patients with suspected microvascular disease, the underlying pathophysiology remains unclear. We hypothesised that MPRI is related to changes in coronary microvascular resistance, as determined by invasive index of microvascular resistance (IMR).

Methods: 75 subjects (50 known CAD patients and 25 age/sex-matched healthy controls) underwent CMR to assess LV function (cines), ischaemia (adenosine stress/rest gadolinium first-pass perfusion) and infarction (LGE). Patients had CMR at 1.5T (n=25) or 3T (n=25); controls had CMR at 1.5T. Subsequently, all 50 patients underwent invasive coronary angiography with pressure-wire assessment of fractional flow reserve (FFR), coronary flow reserve (CFR) and IMR in 3 coronary arteries. CMR images were analysed according to AHA-16-segments, by observers blinded to clinical information, coronary angiography and FFR/IMR/CFR data. MPRI was derived as the ratio of signal-intensity up-slope gradients during stress/rest perfusion. IMR was defined as mean transit-time of intra-coronary saline injection × distal coronary pressure, during adenosine stress (Fig 1).

Results: Segments downstream of significant epicardial stenosis (FFR < 0.8) in patients had lower MPRI than healthy controls (1.34±0.42 vs 1.89±0.39, p < 0.001). Segments downstream of unobstructed epicardial coronary arteries (FFR>0.8) had higher MPRI compared to obstructive-CAD, but significantly lower than controls (Control-MPRI 1.89±0.39, unobstructed-CAD 1.64±0.48, obstructed-CAD 1.34±0.42; all p < 0.001, *no LGE*). Segments with unobstructed epicardial coronary arteries and IMR < 20 had comparable MPRI to normal controls (1.89±0.48 vs 1.89±0.39, p=0.98). As IMR increased, there was progressive reduction in MPRI (IMR < 20: 1.89±0.48, IMR20-40: 1.56±0.42, IMR>40: 1.25±0.35; all p < 0.01, *no LGE*). Segments with high IMR>40 and unobstructed epicardial coronary arteries had equivalent MPRI to segments downstream of significant epicardial stenosis (1.24±0.35 vs 1.34±0.42, p=0.48, Fig 2). Downstream of unobstructed epicardial coronary arteries of CAD patients, an MPRI of ≤1.50 was optimal for detecting microvascular disease (as defined by IMR>40): sensitivity 82%, specificity 83%, and accuracy 83% on ROC analysis (AUC 0.87±0.06, Fig 3).

Conclusions: Microvascular ischaemia in CAD patients can be objectively diagnosed using CMR perfusion imaging. MPRI downstream of unobstructed epicardial coronary arteries is related to changes in microvascular resistance, as validated against invasive IMR. The novel MPRI threshold of ≤1.50, to detect high IMR>40, can confirm the diagnosis and potentially guide targeted therapies in patients with microvascular ischaemia.

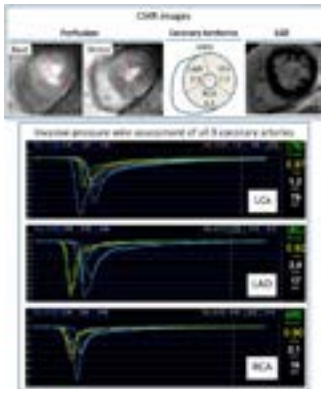

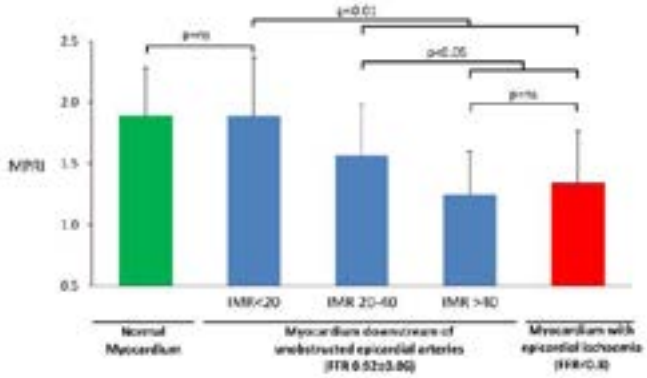

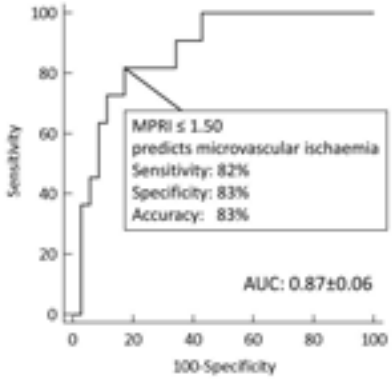

O060

Persistent Long-term Impairment of Cardiac Energetics after Tako-tsubo Cardiomyopathy

Caroline Scally, MBChB[1]Amelia Rudd, BSc[1], Trevor Ahearn, PhD[1], Beverly Maclennan, BSc[1], Heather M. Wilson, BSc (Hons) PhD[1], Paul Broadhurst, MD[2], Anke Henning, PhD[3], Dana Dawson, MD, PhD[1]

1. *University of Aberdeen, Aberdeen, Scotland, United Kingdom*
2. *Aberdeen Royal Infirmary, Aberdeen, Scotland, United Kingdom*
3. *Max Planck Institut for Biological Cybernetics, Tübingen, Baden-Wurttemberg, Germany*

Background: Tako-tsubo cardiomyopathy is an acute form of left ventricular (LV) systolic dysfunction triggered by intense emotional/physical stress. We have previously demonstrated that Tako-tsubo is characterized by profound cardiac energetic impairment with incomplete recovery at short term follow-up (4 months). Due to the persistence of symptoms in a majority of patients, we further hypothesised that impaired cardiac energetics continues during long-term follow-up (> 1 year).

Methods: Sixteen patients [all women, median age 68 years (range 44-81)] with a previously clearly demonstrated diagnosis of Tako-tsubo were invited from the Aberdeen Tako-tsubo registry and 10 healthy volunteers [(all women, median age 62 years (range 44-72)] were recruited from the Cardiology Healthy Volunteer Database. All subjects underwent ^{31}P-Cardiac Magnetic Resonance Spectroscopy (^{31}P-CMRS) and cardiac imaging on a 3T Philips scanner (Best, The Netherlands). ^{31}P-CMRS was analysed with JMRUi-3 (University of Lyon, France) to derive calculation of the Phosphocreatine/Gamma Adenosine Triphosphate (PCr/ATP) ratio as the gold-standard *in vivo* assessment of cardiac energetics. Standard cardiac analysis was performed using CMRTools (Cardiovascular Solutions, London, UK). All subjects underwent clinical interview [Minnesota Living with Heart Failure questionnaire (MLWHFQ)] to establish cardiac symptoms.

Results: All but one of the 16 patients complained of ongoing symptoms (chest pain, breathlessness, fatigue) since the acute Tako-tsubo event (mean MLWHFQ score 14.6). Median follow-up was 23 months (range 13-39 months).

There was no significant difference between the previous Tako-tsubo sufferers and the healthy volunteers with respect to their indexed LV volumes (end-systolic: 27.9± 9.9mls/m^2 vs 25.2±4.6mls/m^2, p=0.6, end-diastolic: 73.9±15.4 mls/m^2 vs 74.2±6.9mls, p=0.9) or LV mass (67±9.1g/m^2 vs 65±6.8g, p=0.7) or LV Ejection fraction 62±9.3 vs 65.9±4.3 p=0.2.

The resting cardiac energetic status (PCr/ATP ratio) was significantly decreased in Tako-tsubo patients compared with healthy volunteers: 1.3 ± 0.7 vs.1.9 ± 0.5, p=0.03.

Conclusions: The ongoing symptoms in patients who experienced an acute Tako-tsubo episode at least one year previously is accompanied by significant cardiac energetic impairment.

O061

Right ventricular function changes in Pectus Excavatum after vacuum bell correction: a CMR study

Orsola Montini, MD[1]Lorenzo Monti, MD[2], Marie Maagaard, MD[3], Sara Moscatelli, MD[1], Lucia Coppini, MD[1], Hans Pilegaard, MD[4], Emanuele Voulaz, MD[1], Barbara Nardi, MD[1], Luca Balzarini, MD[1], Maurizio Infante, MD[5]

1. *Humanitas Research Institute, Lombardia, Italy*
2. *Humanitas Research Institute, Rozzano, Lombardia, Italy*
3. *Aarhus University Hospital, Denmark, Aarhus N, Syddanmark, Denmark*
4. *Aarhus University Hospital, Denmark, N/A, Denmark*
5. *Azienda ospedaliera universitaria di Verona, Veneto, Italy*

Background: Evidence of cardiac dysfunction in patients with pectus excavatum (PEx) is controversial, and surgical correction is often regarded as a purely cosmetic intervention. However, patients report an increased exercise tolerance after surgery, which may be related to an improved cardiac performance. The Vacuum Bell (VB) is a medical device designed to gradually correct PEx thoracic deformity. The aim of this study was to understand whether and how cardiac function is affected by an immediate modification of the chest shape in PEx.

Methods: 20 male PEx patients (age: 22.6±6.5 years old; Haller index: 5.7±1.8), scheduled for the Nuss procedure, underwent cardiac magnetic resonance imagining (CMR) before and during VB application. 5 healthy individuals (2 females and 3 males, age: 28.6±5.8 years old, without chest deformity) underwent the same imaging protocol. Steady-state free precession (SSFP) and phase contrast sequences were acquired for quantification of right and left ventricular volumes and function, and the aortic and pulmonary output, before and during VB positioning.

Results: Baseline cardiac volumes and function of PEx patients were within the normal range. Following VB application, the cardiac performance improved with an immediate mean increase in stroke index of 8%, which could not be correlated to the baseline Haller index. This was mirrored by improvements in left ventricle end-diastolic volume index of 8%, and right ventricular ejection fraction (RV EF) of 7%. In the healthy group, VB application induced no changes in any of the analyzed cardiac volumes and functional parameters.

Conclusions: We saw an immediate improvement of stroke index after VB application in PEx patients, along with an increased RV EF. Similar improvements could not be seen in the healthy group. The concomitant increase in left ventricular volume may be regarded as a direct consequence of the improved RV EF. The immediate gain of RV contractility following VB application in PEx patients suggests that RV function may be affected by the mechanical compression caused by the sternum.

O062

Noninvasive Functional Evaluation of Coronary Stenosis Using MR Instantaneous wave-Free Ratio (MR-iFR): Initial Patient Study

Zixin Deng, MS[1]Sang-Eun Lee, MD[2], Zhaoyang Fan, PhD[1], Christopher Nguyen, PhD[1], Yibin Xie, PhD[1], Jianing Pang, PhD[3], Xiaoming Bi, PhD[4], Qi Yang, PhD[1], Byoung Wook Choi, MD, PhD[5], Jung-Sun Kim, MD[2], Daniel Berman, MD[6], Hyuk-Jae Chang, MD, PhD[2], Debiao Li, PhD[7]

1. *Cedars-Sinai Medical Center, CA*
2. *Severance Cardiovascular Hospital, Yonsei-Cedar Sinai Integrative Cardiovascular Imaging Research Center, Yeonsei University Health System, Seoul, South Korea, N/A, Republic of Korea*
3. *Siemens Healthcare, Chicago, IL*
4. *Siemens Healthcare, CA*
5. *Yonsei University, N/A, Republic of Korea*
6. *Cedars-Sinai Medical Center, Los Angeles, CA*
7. *Biomedical Imaging Research Institute, Cedars-Sinai Medical Center, Los Angeles, CA, CA*

Background: In patients with suspected coronary artery disease (CAD) undergoing invasive coronary angiography (ICA), approximately half results in nonsignificant stenoses, leading to unnecessary invasive procedures [1,2]. In this study, we evaluate the use of phase-contrast (PC)-MRI and Navier-Stokes analysis to derive pressure difference (ΔP) across a coronary stenosis, with the ultimate goal of estimating FFR. As FFR requires adenosine, which is technically challenging for PC-MRI due to high heart rates, the proposed technique mimics the instantaneous wave-free ratio (iFR), wherein measurements were obtained during diastole without adenosine, denoted as MR-iFR. We have previously shown the reproducibility of this technique in phantoms and healthy subjects. This work aims to evaluate its feasibility in patients using invasive measurements as the reference.

Methods: 28 patients with known/suspected CAD, scheduled for ICA were recruited. All patients had ≥1 coronary lesion (proximal and/or middle stenosis, 30-70%) detected by cCTA and/or ICA. Invasive P_a and pressure distal of the stenosis (P_d) during rest and stress, respectively, were measured in all patients and used for FFR and iFR [4] calculations. Cross-sectional 2D PC-MRI images were obtained at locations where invasive pressure measurements were obtained. 7.3±1.6 image slices were obtained across vessel segment of interest, specific imaging parameters were: in-plane spatial resolution = 0.5-0.6x0.5-0.6mm^2, slice thickness = 3.2mm, cardiac phase = 2 (~70ms/phase), and Venc = 30-50cm/s. MR-iFR was estimated based on ΔP_{MR} and invasive P_a measurements (MR-iFR = $P_d / P_a = (P_a - \Delta P_{MR}) / P_a$).

Results: Good quality PC-MRI data were acquired in 24 (86%) patients where poor quality data were due to cardiac/respiratory motion. Three (12.5%) of the 24 patients had a functionally significant stenosis (FFR≤0.80). Good correlation r=0.702/0.695 (*p=0.0001/0.0002)* and relatively small bias 0.082/0.0138mmHg, were observed between FFR/iFR and MR-iFR, respectively. Using FFR as gold standard and MR-iFR cut off of 0.89, the sensitivity, specificity, positive predictive value (PPV), and negative predictive value (NPV) were 67%, 95%, 67%, and 95%, respectively.

Conclusions: To the best of the authors' knowledge, the aforementioned patient study is the first demonstrating the feasibility of MR-iFR in diseased coronary arteries. High specificity and NPV were observed, demonstrating the potential of the proposed technique in identifying patients with functionally nonsignificant stenoses and eliminating unnecessary invasive procedures. More patient studies with positive invasive FFRs are needed to further investigate the sensitivity of the approach.

References: [1]Patel et al. AHJ, 2014;167 [2]Tonino et al. JACC, 2010;55 [3]Douglas et al. EHJ, 2015 [4]Sen et al. JACC, 2012;59

http://www.ConferenceAbstracts.com/uploads/cfp2/attachments/LDFAIBDN/LDFAIBDN--217709-1-ANY.pdf

http://www.ConferenceAbstracts.com/uploads/cfp2/attachments/LDFAIBDN/LDFAIBDN--217709-2-ANY.pdf

O063

Myocardial oedema in AL amyloidosis: new insight into pathogenesis

Tushar Kotecha, MRCP(UK) MBChB[1] Ana Martinez-Naharro, MD[2], Thomas Treibel, MBBS.MRCP(UK)[3], Sabrina Nordin, MBBS[3], Amna Abdel-Gadir, MBBS.MRCP(UK)[4], Daniel S. Knight, MBBS MRCP(UK)[5], Giulia Zumbo, MD[6], Stefania Rosmini, MD, PhD[3], Viviana Maestrini, MD[7], Heerajnarain Bulluck, MBBS[8], Roby Rakhit, MD, FRCP[9], Peter Kellman, PhD[10], Julian Gillmore, MD, PhD[6], James Moon, MBBS, MD, MRCP[11], Philip Hawkins, PhD[6], Marianna Fontana, MD, PhD[6]

1. *Royal Free London NHS Foundation Trust, Bushey, Hertfordshire, England, United Kingdom*
2. *National Amyloidosis Centre, University College London, London, England, United Kingdom*
3. *Barts Heart Centre, England, United Kingdom*
4. *University College London and Barts Heart Centre, London, England, United Kingdom*
5. *Royal Free London NHS Foundation Trust, London, England, United Kingdom*
6. *National Amyloidosis Centre, University College London, England, United Kingdom*
7. *Sapienza University of Rome, Lazio, Italy*
8. *University College London, England, United Kingdom*
9. *Royal Free Hospital, England, United Kingdom*
10. *Laboratory of Cardiac Energetics, National Institutes of Health/NHLBI, Bethesda, MD, United States., MD*
11. *Barts Heart Center, The Cardiovascular Magnetic Resonance Imaging Unit and The Center for Rare Cardiovascular Diseases Unit, St Bartholomew's Hospital, West Smithfield, London, UK, England, United Kingdom*

Background: The prognosis and treatment of the 2 main types of cardiac amyloidosis, immunoglobulin light chain (AL) and transthyretin (ATTR) amyloidosis are substantially influenced by cardiac involvement. ATTR amyloidosis has a better prognosis than AL amyloidosis despite a usually greater degree of amyloid infiltration. This paradox suggests an additional mechanism of damage in AL amyloidosis such as light-chain toxicity. The aim of this study was to assess the presence and prognostic significance of oedema in a large population of patients with cardiac amyloidosis and compare findings among those with TTR and AL types.

Methods: 288 patients (100 with AL, 188 with ATTR) and 30 healthy volunteers were recruited. All subjects underwent CMR with standard cine imaging, LGE and T1 and T2 mapping with Extracellular Volume (ECV) measurement.

Results: Left ventricular (LV) mass and ECV were higher in ATTR amyloidosis compared to AL (LV mass index: 135.7±33.7g/m^2 vs 98.6±31.5g/m^2, ECV: 0.63±0.10 vs 0.51±0.10, both $p < 0.001$) and LV ejection fraction (EF) was significantly lower (54.5±12.7% vs 63.3±13.1%, $p < 0.001$). T2 values were increased in cardiac amyloidosis compared to healthy volunteers, with the degree of T2 elevation being higher in AL than ATTR (T2: 56.3±5.2ms AL vs 54.7±4.0ms ATTR, vs 48.9±2.0ms controls, $p < 0.001$)(Figure 1a). During follow up (18.0±8.7 months), 28 (28%) deaths occurred in the AL group and 47 (25%) in the TTR group. Prognosis was better in ATTR compared to AL (median survival 14.6 months ATTR vs 7.1 months AL, $p < 0.001$). Using Cox regression models, T2 predicted death in AL amyloidosis (hazard ratio, HR, 1.48, 95% CI 1.20-1.82) and remained significant after adjusting for EF and ECV (HR 1.31, 95% CI 1.04-1.65)(Figure 1b).

Conclusions: Patients with AL amyloidosis have a worse prognosis compared to ATTR despite having less cardiac amyloid infiltration. However, T2 was significantly higher in AL amyloidosis compared to ATTR and was a predictor of prognosis in AL amyloidosis. This suggests the role of additional mechanisms causing increased mortality such as light chain toxicity and associated oedema in AL type, and highlights the unique role of CMR with multiparametric mapping in this patient population.

http://www.ConferenceAbstracts.com/uploads/cfp2/attachments/LDFAIBDN/LDFAIBDN--219497-1-ANY(1).pdf

O064

Chronic right ventricular remodeling in veteran endurance athletes: novel CMR insights into exercise-induced arrhythmogenic right ventricular cardiomyopathy

Abbas Zaidi, MBBS, MD[1] Ahmed Merghani, MBBS, MRCP[2], Viviana Maestrini, MD[3], Stefania Rosmini, MD, PhD[4], Rebecca Schofield, MBChB, MRCP[4], Charlotte Manisty, PhD MBBS[5], Sanjay Sharma, MBBS, MD[2], James C Moon, MD[4]

1. *Barts Heart Centre, London UK, Miskin, Wales, United Kingdom*
2. *St George's University of London, England, United Kingdom*
3. *Sapienza University of Rome, Lazio, Italy*
4. *Barts Heart Centre, England, United Kingdom*
5. *Barts Heart Centre and university college, London, England, United Kingdom*

Background: Regular exercise results in physiological cardiac adaptations including left ventricular (LV) dilatation and hypertrophy, designed to augment stroke volume during exertion. The concept has emerged that repetitive, intensive exercise might promote maladaptive remodeling, to which the thin-walled right ventricle (RV) may be particularly susceptible. Evidence for an exercise-induced form of arrhythmogenic right ventricular cardiomyopathy (ARVC) has to date however been derived from selected individuals presenting clinically with overt symptoms. The effects of chronic exercise on the RV have never been evaluated in a large cohort of asymptomatic veteran athletes.

Methods: 170 veteran endurance athletes (age >40yrs, multiple race participations over >10 years) were prospectively recruited and compared with 132 age-matched non-athletic controls. Investigations included electrocardiography, signal-averaged electrocardiography (SAECG), Holter monitoring, and CMR with free-breathing motion-corrected phase-sensitive inversion recovery late gadolinium enhancement (LGE). Results were compared against the 2010 Task Force Criteria for the diagnosis of ARVC.

Results: The mean age of the total cohort was 55yrs (68% male). Athletes exhibited greater RV dimensions than controls (RVEDV 164.1 *vs*. 137.2ml, $p < 0.001$), whilst systolic function and LV/RV ratio did not differ between groups (RVEF 65.3 vs. 64.5%, p=0.42; RVEDV/LVEDV 1.1 *vs*. 1.0, p=0.11). RV dilatation in the range compatible with diagnostic criteria for ARVC was >6-fold more prevalent in athletes than controls (28.5% *vs.* 4.5%, $p < 0.001$). However, CMR criteria for ARVC were not fulfilled, since none of the study participants exhibited RV regional wall motion abnormalities (RWMA). LGE was observed in 36.0% athletes vs. 6.2% controls ($p < 0.001$). Amongst athletes, 17.4% exhibited RV insertion point LGE and 3.1% RV trabecular LGE. Anterior T-wave inversion was present in 8.9% athletes vs. 3.8% controls (p=0.10), whilst non-sustained ventricular tachycardia (NSVT) was more common in athletes (11.0% *vs*. 1.8%, p=0.004). LV LGE (ischaemic and non-ischaemic patterns), but not RV LGE, predicted the occurrence of NSVT. Only 1 athlete (0.6%), who had completed 210 previous endurance events, fulfilled criteria for 'definite' ARVC (anterior T-wave inversion, NSVT and abnormal SAECG), although his CMR was normal.

Conclusions: RV dilatation is common in veteran endurance athletes, although the absence of RWMA supports physiological rather than pathological remodeling. Novel LGE sequences reveal a high prevalence of biventricular focal fibrosis which appears driven by chronic sports participation and not age alone. Whilst the mechanism and significance of this phenomenon is unclear, RV insertion point and RV trabecular LGE neither correlate with overt structural cardiac abnormalities nor predict adverse events in athletes. These findings raise significant doubts over the concept of exercise-induced ARVC.

O065

Derivation of reference ranges for cardiovascular magnetic resonance (CMR) imaging at 1.5 Tesla from 5,065 CMR examinations in the UK Biobank.

Steffen E. Petersen, MD DPhil MPH FRCP[1], Mihir M. Sanghvi, MB BS, BSc[2]Nay Aung, MD, MRCP[1], Filip Zemrak, MD MRCP[1], Kenneth Fung, MBBS BSc[3], Jose Miguel Paiva, MSc[1], Matthew D. Robson, PhD[4], Mohammed Y. Khanji, MBBCh, MRCP[5], Elena Lukaschuk, MSc[6], Aaron Lee, PhD, MBBS[1], Valentina Carapella, DPhil[7], Stefan K. Piechnik, PhD, MScEE[8], Stefan Neubauer, MD, FRCP[8], Young Jin Kim, MD, PhD[9]

1. *Barts Heart Center, The Cardiovascular Magnetic Resonance Imaging Unit and The Center for Rare Cardiovascular Diseases Unit, St Bartholomew's Hospital, West Smithfield, London, UK, England, United Kingdom*
2. *William Harvey Research Institute, NIHR Cardiovascular Biomedical Research Unit at Barts, Queen Mary University of London, Charterhouse Square, London EC1M 6BQ, UK, England, United Kingdom*
3. *Barts Heart Center, The Cardiovascular Magnetic Resonance Imaging Unit and The Center for Rare Cardiovascular Diseases Unit, St Bartholomew's Hospital, West Smithfield, London, UK, London, England, United Kingdom*
4. *OCMR, University of Oxford, England, United Kingdom*
5. *William Harvey Research Institute, London, England, United Kingdom*
6. *University of Oxford, Oxford, England, United Kingdom*
7. *University of Oxford, Oxford, United Kingdom, England, United Kingdom*
8. *University of Oxford, England, United Kingdom*
9. *Severance Hospital, Yonsei University College of Medicine, Seoul, N/A, Republic of Korea*

Background: Cardiovascular magnetic resonance (CMR) imaging is the gold standard method for the assessment of cardiac structure and function. Reference ranges permit differentiation between normal and pathological states. Reference ranges for left ventricular, right ventricular, left atrial and right atrial structure and function derived from healthy Caucasian adults aged 40-80 are presented here.

Methods: 5,065 UK Biobank participants underwent CMR examination using the steady-state free precession imaging technique at 1.5 Tesla. Manual analysis was performed for all four cardiac chambers. Participants with non-Caucasian ethnicity, known history of cardiovascular disease, respiratory disease, diabetes mellitus, hyperlipidaemia, haematological disease, renal disease, rheumatological disease, malignancy, symptoms of chest pain or dyspnoea, current- or ex-tobacco smokers, those taking medication for diabetes, hyperlipidaemia or hypertension and those with BMI < 18.5 or ≥25 kg/m^2 were excluded. Reference ranges were calculated using 95% prediction interval for absolute and body surface area-indexed values. Differences between genders were detected using t-test.

Results: Having excluded poor quality examinations and examinations with missing/incorrect identifier data, 4,974 participants were included in the analysis. Having applied the strict exclusion criteria, 431 (8.7%) participants were available for derivation of the validated-normal reference ranges. Left ventricular volumes are larger in males compared to females for absolute and indexed values. Left ventricular ejection fraction is significantly greater in females compared to males. Left ventricular mass is significantly greater in males compared to females. Right ventricular volumes are significantly larger in males compared to females for absolute and indexed values. Right ventricular ejection fraction is greater in females compared to males. Left atrial maximal volume and stroke volume, as determined by the biplane method, are significantly larger in males compared to females for absolute values but not for BSA-indexed values. Left atrial ejection fraction is similar for both sexes. Right atrial maximal volume is significantly larger in males for both absolute and indexed values.

Conclusions: Left ventricle, right ventricle, left atrium and right atrium sex-specific normal Caucasian reference ranges are presented here and have been derived in strictly-validated normal individuals in the largest from the largest population-based cohort of its kind. This will provide an important reference base in the analysis of CMR examinations in the clinical and research setting.

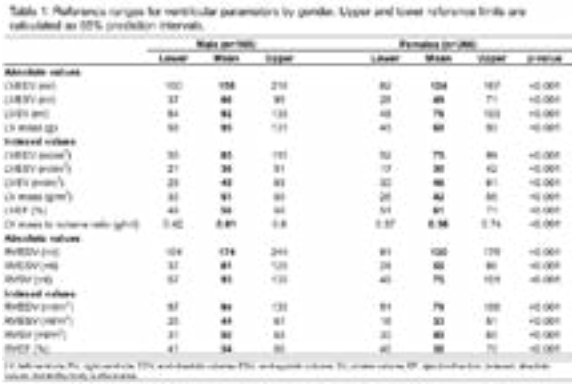

O066

Assessment of arterial stiffness in patients undergoing renal sympathetic denervation as predictor for blood pressure response

Karl Fengler, MD[1]Karl Rommel, MD[1], Stephan Blazek, MD[2], Maximilian von Roeder, MD[3], Christian Luecke, MD[4], Matthias Gutberlet, MD[5], Steeden Jennifer, MD[6], Vivek Muthurangu, MD[6], Gerhard Schuler, MD[5], Philipp Lurz, MD, PHD[3]

1. *Dept. of Internal Medicine / Cardiology University of Leipzig - Heart Center, Sachsen, Germany*
2. *Leipzig University Heart Center, Department of Cardiology, Leipzig, Sachsen, Germany*
3. *Leipzig University Heart Center, Department of Cardiology, Sachsen, Germany*
4. *Radiology, University Leipzig - Heart Center, Niedersachsen, Germany*
5. *University of Leipzig - Heart Center, Sachsen, Germany*
6. *Institute of Cardiovascular Science, University College London, England, United Kingdom*

Background: Most trials regarding catheter-based renal sympathetic denervation (RSD) describe a certain proportion of patients without blood pressure response following the procedure ("non-responders"). Recently, we were able to show that central arterial stiffness, measured by invasive pulse wave velocity (IPWV), seems to be an excellent predictor for this blood pressure response. However, given the invasiveness, IPWV is less suitable as a slelction criterion for patients undergoing RSD. Consequently, we aimed to investigate the value of cardiac magnetic resonance (CMR) based measures of arterial stiffness in predicting the outcome of RSD compared to IPWV as the considered reference-standard.

Methods: Patients underwent CMR prior to RDN to assess ascending aortic distensibility (AAD), volumetric and phase contrast flow derived total arterial compliance (TAC_{vol} and TAC_{flow}), total peripheral resistance (TPR) and Beta stiffness coefficient. In a second step, central aortic pressure and pulse wave velocity (cPWV) were estimated from ascending aortic area change and flow sequences and were used to re-calculate total arterial compliance (cTAC). Additionally, IPWV was acquired immediately before RSD.

Results: Thirty-two consecutive patients (24 responders and 8 non-responders) were available for this analysis. AAD, TAC_{flow}, TAC_{vol}, cAAD and cTAC were significantly higher among responders, IPWV was higher among nonresponders. Receiver operating characteristic (ROC) curves for IPWV, AAD, cPWV, cTAC, TAC_{vol}, revealed areas under the curve of 0.83, 0.83, 0.81, 0.78 and 0.75 (p = 0.006, 0.006, 0.009, 0.021 and 0.037 respectively). ROC curves for TAC_{flow} did not reach statistical significance.

Conclusions: Beyond IPWV, various CMR-derived markers of arterial stiffness appear as useful outcome predictors for RSD in patients with therapy resistant hypertension. CMR-derived markers of arterial stiffness might serve as noninvasive selection criteria for RSD.

O067

Left and right ventricular CMR strain changes in athletes after extreme mountain ultra-long exercise

Florian Espinosa, MD[1]Magalie Viallon, PhD Dr[2], Charles De Bourguignon, Master[3], Caroline Le Goff, PhD[4], Helene Feliciano, MSc[5], Ruud van Heeswijk, PhD[6], Gregoire P. Millet, PhD[7], Pierre Croisille, MD PhD[8]

1. *Uni Lyon, UJM-Saint-Etienne, CHU Saint-Etienne, L'Etrat, Rhone-Alpes, France*
2. *CREATIS UMR CNRS 5220 - INSERM U1206/ Hopital Universitaire de Saint-Etienne, Rhone-Alpes, France*
3. *Centre Hospitalier Universitaire de Saint-Étienne, Rhone-Alpes, France*
4. *University Hospital of Liege, Liege, Belgium*
5. *Lausanne University Hospital (CHUV), Vaud, Switzerland*
6. *Lausanne University Hospital (CHUV), N/A, Switzerland*
7. *ISSUL University of Lausanne, N/A, Switzerland*
8. *Univ Lyon, UJM-Saint-Etienne, INSA, CNRS UMR 5520, INSERM U1206, CREATIS, Saint-etienne, Rhone-Alpes, France*

Background: Endurance exercise races has grown in popularity in the last decades with a marked increase in the number of participants in marathons, triathlons, and long-distance races. Several recent reports have been suggesting that high volumes of aerobic exercise may be as bad for CVD outcomes as physical inactivity, and studies have reported unexpected, potentially adverse cardiovascular outcomes in athletes wtih the existence of functional and biochemical alterations in the myocardium after prolonged intense sport exercise, named exercise-induced cardiac fatigue. In this context, the effects and consequences of supra-physiological efforts of mountain ultramarathon (MUM) that combine extreme distance and elevation changes are still unclear and remain controversial.

Methods: We prospectively studied 50 ultra-trailers enrolled on the 2014 edition of the « Tor des géants », the most extreme ultra-long mountain marathon (330km in length, 24.000 m of climb) without clinical evidence of personal history of cardiac or pulmonary disease. Subjects were studied before and immediatly after the race. Imaging protocol combined a comprehensive protocol with cine SSFP for L4, L2 and LV base to apex, for global and regional functional assessement. Tissue Tracking algorithm (CVI42, Circle) was applied to measure LV and RV, systolic and diastolic strains (in radial, circumferential and longitudinal directions). Quantitative T1 and T2 maps were also acquired in addition to blood sampling to explore biomarkers of inflammation, myocardial stress and damage.

Results: 24 finishers (48%) completed the entire longitudinal study. There were no significant changes in LV volumes and EF after the race. Systolic circumferential peak strain was the only near significant LV strain change after the race ($p=0.056$) while radial and longitudinal strains were not different. RV strain changes were more pronounced involving both systolic and diastolic mechanics, with increased circumferential time-to-peak strain (p-0.01) and decreased longitudinal peak strain rate ($p < 0.03$). This was contrasting with the significant and diffuse increase of T1 and T2 ($p < 0.01$) as well as of (Gal3,ST2,NT-proBNP), plasmatic (CRP, CKs, hs-TNT) and cellular (WBC,lymphocytes, neutrophiles) biomarkers.

Conclusions: This is the first CMR study investigating the impact of MUM to myocardial strains together with T1 and T2 mapping. This study confirm the existence of only minor mechanical abnormalities of LV and RV strains, despite signs of myocardial inflammation. Such efforts are characterized by extreme distance and elevation changes but are performed at lower intensity that may explain their minimal impact compared to shorter but more intense exercise.

O068

Right and left atrial volume measured with cardiac magnetic resonance is associated with clinical outcome in patients with precapillary pulmonary hypertension

Anna Bredfelt[1] Roger Hesselstrand, M.D., Ph.D.[2], Göran Rådegran, M.D., Ph.D.[3], Ellen Ostenfeld, M.D., Ph.D.[4]

1. Lund University, Dept of Clinical Sciences, Clinical Physiology, Lund, Skane Lan, Sweden
2. Lund University, Dept of Clinical Sciences, Rheumatology, Lund, Skane Lan, Sweden
3. Lund University, Dept of Clinical Sciences, Cardiology, Lund, Skane Lan, Sweden
4. Lund University, Dept of Clinical Sciences, Clinical Physiology, Lund, and Skane University Hospital, Lund, Skane Lan, Sweden

Background: Precapillary pulmonary hypertension (PH) is a severe condition with a poor prognosis. Survival rates differ among subgroups of PH with the highest mortality in PH due to systemic sclerosis (SSC-PAH). There is limited knowledge on the prognostic value of atrial volumes with cardiac magnetic resonance (CMR) in PH. The objectives were to investigate 1) whether enlarged right and reduced left atrial maximal volumes, using CMR, is of importance for outcome with clinical event defined as lung transplantation or death 2) if atrial volumes differed among the four major PH subgroups, and specifically, between the two largest subgroups idiopathic/familial pulmonary arterial hypertension (IPAH/FPAH) and SSC-PAH when adjusting for invasive pressure.

Methods: Seventy-sixpatients with PH underwent CMR and invasive right heart catheterization (RHC), of which 33 IPAH/FPAH, 20 SSC-PAH, 14 PH associated to connective tissue diseases other than systemic sclerosis (CTD-PAH) and 9 chronic thromboembolic PH (CTEPH). PH is defined as mean pulmonary arterial pressure≥25mmHg with normal left atrial pressure≤15 mmHg from RHC. Short-axis stacks of cine images were analyzed and right and left atrial maximum (RAV_{max}, LAV_{max}) and minimum volume (RAV_{min}, LAV_{min}) were obtained **(Figure 1).** Enlarged (mean+2SD) and reduced (mean-2SD) volumes were predefined from previously reported normal values. Adjustment for invasive pressure between IPAH/FPAH and SSC-PAH was made by matching for pulmonary vascular resistance (PVR).

Results: Clinical characteristics are listed in **Table 1**. Patients with enlarged RAV_{max} had shorter median survival (3.1years) compared to patients with normal RAV_{max} (6.2years, p=0.02), with a hazard ratio for lung transplantation or death of 2.1 (**Figure 2A)**. Reduced LAV_{max} indicate shorter median survival (4.2years) than normal LAV_{max} (5.5 years) with hazard ratio for reduced LAV_{max} 1.9 (p=0.09). RAV_{max}, RAV_{min}, LAV_{max} and LAV_{min} showed no differences among groups (p=ns) **(Figure 2B).** When matched for PVR, SSC-PAH (n=19) and IPAH/FPAH (n=19) did not differ in right or left atrial volumes (p=ns).

Conclusions: Enlarged RAV_{max} is associated with worse clinical outcome in patients with precapillary pulmonary hypertension. The increased hazard ratio for small LAV_{max} was not found significant. There were no differences in atrial volumes among the four subgroups of PH or, when adjusting for invasive pressure, between IPAH/FPAH and SSC-PAH. This suggests that volume or pressure overload alone do not explain the differences in survival between precapillary pulmonary hypertension subgroups.

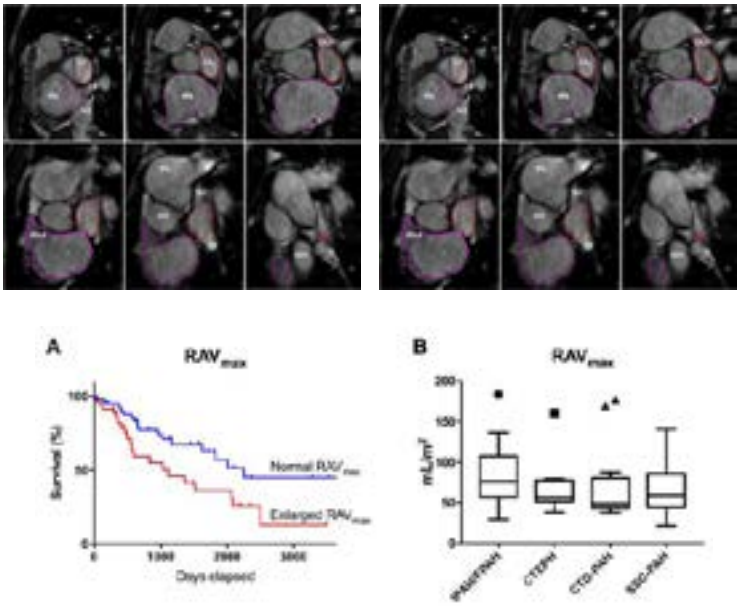

Table 1. Patient characteristics

All patients *(n=76)*	
57±19	Age (years)
22/29%	Males* (n/%)
1.84±0.24	BSA (m^2)
	CMR
76±37	RAV_{max}(mL/m²)
53±35	RAV_{min} (mL/m²)
41±19	LAV_{max}(mL/m²)
27±20	LAV_{min}(mL/m²)
(n=73)	*RHC*
74±18	sPAP (mmHg)
46±11	mPAP(mmHg)
8±4	PCWP(mmHg)
7±5	mRAP(mmHg)
10±8	PVR (WU)

Values expressed in mean ± SD. *expressed in absolute numbers and percent. Abbreviations in this table: BSA=body surface area, CMR = cardiac magnetic resonance, RAV_{max}=right atrial volume maximum indexed to BSA, RAV_{min}=right atrial volume minimum indexed to BSA, LAV_{max}=left atrial volume maximum indexed to BSA, LAV_{min}=left atrial volume minimum indexed to BSA, RHC=right heart catheterization, sPAP=systolic pulmonary arterial pressure, mPAP=mean pulmonary arterial pressure, PCWP=pulmonary capillary wedge pressure, mRAP=mean right atrial pressure, PVR=pulmonary vascular resistance.

O069

Genotype-phenotype correlations in ARVD/C: CMR reveals differences in LV function between PKP2 and non-PKP2 mutation carriers

Mounes Aliyari ghasabeh, MD[1] Anneline te Riele, MD phd[2], Cynthia James, phd[2], Crystal Tichnell, MD[2], Brittney Murray, MD[2], Bharath Ambale-Venkatesh, PhD[3], Ela Chamera, BSEE[4], Joao A.C. Lima, MD, MBA[5], David Bluemke, MD, Ph.D[6], Harikrishna Tandri, MD[2], Hugh Calkins, MD[7], Ihab Kame, MD phd[2], Stefan L. Zimmerman, MD[8]

1. *John Hopkins Hospital, MD*
2. *john hopkins hospital, baltimore, MD*
3. *Johns hopkins, MD*
4. *Johns hopkins, baltimore, MD*
5. *Johns Hopkins University, Baltimore, MD*
6. *National Institute of Health, MD*
7. *Johns Hopkins Medicine, MD*
8. *Johns Hopkins University School of Medicine, MD*

Background: Arrhythmogenic Right Ventricular Dysplasia/Cardiomyopathy (ARVD/C) is a hereditary disease characterized by fibrofatty replacement of cardiac muscle and lethal arrhythmias. Multiple disease-causing gene mutations have been discovered, the most frequentbeing in plakophilin-2 (*PKP2*). Mutations in *PKP2* have been associated with a right-ventricular (RV) predominant phenotype, whereas mutations in other genes, including desmoplakin (*DSP*), desmogelin-2 (*DSG2*), desmocollin-2 (*DSC2*), and phospholamban (*PLN*), more frequently present with left ventricular (LV) or biventricular disease. In this study we aimed to assess genotype-phenotype correlations with quantitative and qualitative cardiac MRI (CMR) findings in a group of mutation-positive ARVD/C and at-risk patients.

Methods: Retrospective international, multicenter, IRB-approved, HIPPA compliant study. We enrolled 397 individuals from a group of subjects referred to tertiary care centers in the United States and Holland for suspicion of ARVD/C. Genetic testing was performed in 116, of these, 87 (75%) had a known ARVD/C causing mutation. 52 gene-positive patients fulfilled ARVD/C diagnosis criteria based on 2010 Task Force Criteria, 35 gene-positive patients were considered at-risk for ARVD/C (phenotype-negative family members carrying the same pathogenic gene as proband). Global and regional longitudinal and circumferential strain analysis was performed on cine SSFP CMR images (Myocardial Tissue Tracking, Toshiba) for RV and LV. Images were reviewed for wall motion abnormalities, fatty infiltration and late gadolinium enhancement (LGE) by two experienced radiologists.

Results: Among gene-positive patients, 62 (71%) had mutations in *PKP2* and 25 (29%) had non-*PKP2* mutations, the most common of which were *PLN* (14) and *DSG2* (5). Patients were divided into two groups based on mutation: *PKP2* and non-*PKP2*. There were more LV wall motion abnormalities in non-*PKP2* patients (26% vs 0%, p=0.02), while the number of RV wall motion abnormalities were not different. Strain analysis showed worse global LV circumferential strain in the non-*PKP2* group (-12.8 vs -15.7, p= 0.02). No differences were seen in RV circumferential strain or for either RV or LV longitudinal strain. Global LV and RV ejection fractions were not different between groups (non-*PKP2* vs. *PKP2*: LVEF 56% vs. 60%, p=0.11; RVEF 58% vs. 63%, p=0.40) There were no differences in the number of patients with fat infiltration or LGE for either the RV or the LV.

Conclusions: Global circumferential LV strain is significantly reduced in non-*PKP2* mutation carriers compared to those with PKP2 mutations, despite similar LVEF. These findings support the concept of genotype-phenotype associations in ARVD/C, with non-*PKP2* mutation carriers showing greater intrinsic LV disease.

O070

Association of left atrial volumes and all-cause mortality in a large cohort of subjects with preserved ejection fraction.

Mohammad A. Khan, MBBS[1] Eric Y. Yang, MD PhD[2], Sherif F. Nagueh, MD[3], Faisal Nabi, MD[4], John Heitner, MD[5], Mohamad Ghosn, PHD[3], Robert M. Judd, PhD[6], Raymond J. Kim, MD[7], Igor Klem, MD[8], Dipan J. Shah, MD[3]

1. *Houston Methodist DeBakey Heart & Vascular Center, Sugar Land, TX*
2. *Houston Methodist Hospital, TX*
3. *Houston Methodist DeBakey Heart & Vascular Center, TX*
4. *Houston Methodist DeBakey Heart & Vascular Center, Houston, TX*
5. *New York Methodist Hospital, NY*
6. *Duke University Medical center, Durham, NC*
7. *Duke University School of Medicine, NC*
8. *Duke University Medical Center, Durham, NC*

Background: Left atrial volume indexed for body surface area (LAVI) determined by echocardiography is an established predictor of mortality. This can be attributed to presence of diastolic dysfunction. Reference values for left atrial (LA) sizes by cardiac magnetic resonance (CMR) have been published on presumably healthy individuals, but the association between degrees of LA dilatation and outcomes has not been established. We examined the relationship between LAVI and mortality in a large, unselected population with normal LVEF referred for routine CMR.

Methods: We identified 77 volunteers without known cardiovascular disease for calculation of reference LA volumes using biplane area-length method. Pulmonary veins, the LA appendage and the area below the mitral annulus were excluded when tracing LA areas from long-axis 4- and 2-chamber views. Normal reference ranges for LAVI from the reference population were mean 35.0 ± standard deviation 7.7 mL/m^2 for females and 36.4 ± 7.8 mL/m^2 for males (combined 36.0 ± 7.8 mL/m^2). Clinical reports of patients with LA volume measures available (n=8,329) were obtained from a cloud-based system that is currently receiving de-identified searchable data from electronically-signed clinical reports with full DICOM datasets for consecutive CMR exams performed at 3 geographically diverse U.S. medical centers from Jan 1, 2005 through Dec 31, 2015. All data fields were derived from CMR reports that had been electronically signed by board-certified physicians with Level 3 CMR training. We identified 3,634 cases with normal ejection fraction and no significant valvulopathies. Patients were categorized into 4 groups based on LAVI for each gender into "Normal" (< 52 ml/m^2), "Mild" (52 to 59 ml/m^2), "Moderate"(59 to 67 ml/m^2) and "Severe" (>67 ml/m^2). Mortality was ascertained for the group using Social Security Death Index (SSDI) on December, 2015.

Results: With a median duration of 36.5 (interquartile range 22.5–53.7) months from date of scan to SSDI check, there was an increase in the prevalence of mortality per group with increasing LAVI (Figure 1). Chi squared test for linear trend was significant for LAVI (p-value = 0.006). Enlarged LA volumes were associated with older age, atrial fibrillation, hypertension, use of renin-angiotensin-aldosterone system (RAAS) inhibitors and beta blockers; and ventricular dilatation. (Table 1). On univariate analysis age, heart rate, history of hypertension, history of diabetes, myocardial scar on CMR and severe LA enlargement [Odds Ratio (OR) = 2.29, Confidence Interval (CI) = 1.19 to 4.41] were significant predictors of death. After adjustment for these covariates, severe LA enlargement remained a significant predictor of death [OR = 2.13, CI = 1.03 to 4.11] (Table 2).

Conclusions: Left atrial enlargement determined on CMR is a strong predictor of all-cause mortality in patients with normal LVEF and no significant valve disease.

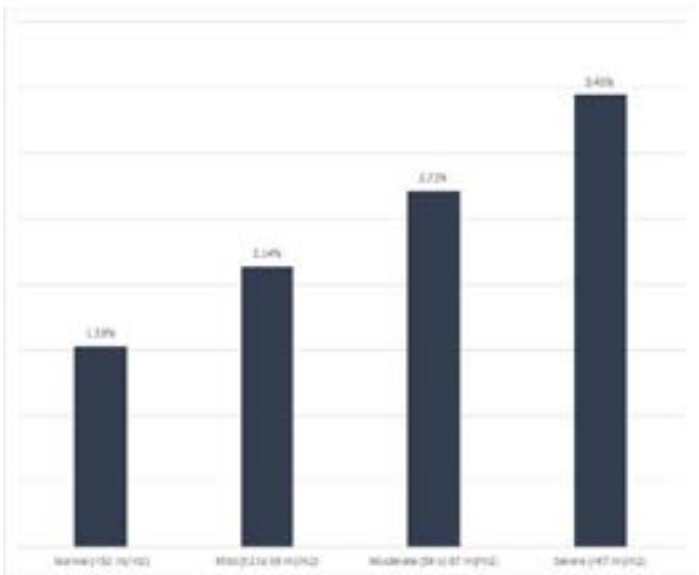

Table 1. Baseline characteristics, medications and CMR parameters.

p-value†	Severe (n = 348)	Moderate (n = 258)	Mild (n = 421)	Normal (n = 2607)	Variable*
0.0001	66 (59, 73)	65 (56, 72)	62 (51, 71)	58 (43, 68)	Age (years)
0.041	54.9%	57.4%	47.3%	51.2%	Male (%)
<0.0001	67%	68.2%	65.8%	63.2%	White (%)
<0.0001	14.1%	16.7%	12.8%	16%	Black (%)
<0.0001	1.7%	0.8%	2.6 %	3.5%	Asian (%)
<0.0001	17.2%	14.3%	18.8%	17.3%	Other (%)
0.003	33.5%	24.8%	22.7%	24.9%	Inpatient (%)
0.0096	170.2(162.6, 180.3)	172.7(165.1, 180.3)	167.6(160.02, 177.8)	170.2(162.6, 177.8)	Height (cm)
0.2317	82.6 (70.3, 97.3)	83.3 (70.8, 99.8)	83.5 (68, 97.5)	81.6 (68, 97.1)	Weight (kg)
0.1157	2 (1.8, 2.1)	2 (1.8, 2.2)	1.9 (1.73, 2.1)	1.9 (1.73, 2.1)	BSA (m^2)
0.0002	130 (118, 141)	127 (116, 142)	131 (118, 143)	127 (115, 139)	Systolic BP (mmHg)
0.6304	72 (65, 81)	73 (66, 82)	74 (65, 84)	73 (65, 82)	Diastolic BP (mmHg)
0.0001	68 (60, 80)	68 (60, 79)	69 (60, 79)	71 (63, 82)	Heart Rate (bpm)
<0.0001	23.56%	12.02%	9.98%	3.72%	Atrial fibrillation at time of scan (%)
<0.0001	70.9%	65%	62%	54.4%	Hypertension (%)
0.888	17.8%	17.9%	19.8%	18.8%	Diabetes mellitus (%)
Medication use					
<0.0001	42.2%	40.7%	33%	29.2%	RAAS inhibitors use (%)
<0.0001	60.9%	54.3%	51.4%	41.6%	Beta blocker use (%)
0.059	45.1%	42.5%	40.4%	38.4%	Statin use (%)
Cardiac magnetic resonance parameters					
0.0001	76.7 (70.9, 88.3)	62.5 (60.9, 64.6)	55 (52.9, 56.8)	36.8 (30, 43.2)	LA volume [Index]
0.0001	67.7 (56.4, 85.2)	64.7 (56.7, 76.4)	66 (57.4, 78.1)	58.3 (47.5, 68.8)	LVEDV [Index] (ml/m^2)
0.0001	22.7 (17.2, 29.7)	20.6 (15.5, 27.7)	20.5 (14.9, 27.8)	18.6 (13.7, 24.2)	LVESV [Index] (ml/m^2)
0.0001	46.8 (37.5, 55.6)	45.1 (36.5, 51.5)	45.9 (40.6, 51.1)	39.5 (32.8, 45.9)	LVSV [Index] (ml/m^2)
0.1111	67 (61, 72)	67 (61, 74)	68.9 (62, 74)	67 (61, 73)	LVEF (%)
0.0001	73.4 (59.5, 88.9)	69.5 (56, 84.2)	69.1 (56.7, 81.4)	61.1 (48.8, 73.9)	RVEDV [Index] (ml/m^2)
0.0001	32.3 (25.5, 42.3)	29.9 (23.2, 39.1)	28.9 (21.4, 37.9)	26.4 (20, 34)	RVESV [Index] (ml/m^2)
0.0001	39.6 (32, 48.7)	39 (32.8, 46.9)	39 (31.7, 47.2)	34.3 (26.7, 41.5)	RVSV [Index] (ml/m^2)
0.0001	54 (49, 60)	56 (50, 64)	58 (52, 63)	55.8 (50, 62)	RVEF (%)
<0.0001	0 (0, 2)	0 (0, 1)	0 (0, 0)	0 (0, 0)	Scar (%)

* All values are median (interquartile ranges) and proportions. BSA = body surface area; BP = blood pressure; RAAS = renin-angiotensin-aldosterone system; LA = left atrial; LV = left ventricular; RV = right ventricular; EDV = end diastolic volume; ESV = end systolic volume; SV = stroke volume; EF = ejection fraction.

† p-values are based on Kruskal Wallis test (continuous variables) and χ^2 test (categorical variables).

Table 2. Univariate and multivariate analysis for predictors of mortality.

Confidence Interval‡	p-value‡	Odds Ratio‡	Confidence Interval†	p-value†	Odds Ratio†	Variable
1.01 – 1.05	0.0001	1.05	1.02 – 1.06	0.0001	1.04	Age
-	-	-	0.83 – 2.2	0.225	1.35	Gender
1.77 – 4.97	0.0001	2.73	2.43 – 6.46	0.0001	3.96	Inpatient
-	-	-	0.99 – 1.02	0.622	1	Height
-	-	-	0.99 – 1.01	0.904	1	Weight
-	-	-	0.38 – 2.36	0.942	0.97	BSA
-	-	-	0.99 – 1	0.905	1	Systolic BP
-	-	-	0.98 – 1.02	0.873	1	Diastolic BP
1.02 – 1.05	0.0001	1.04	1.02 – 1.05	0.0001	1.03	Heart Rate
-	-	-	0.43 – 2.68	0.891	1.07	Atrial Fibrillation
0.49 – 1.62	0.34	0.74	1.01 – 2.91	0.047	1.7	History of Hypertension
1.04 – 3.1	0.045	1.83	1.52 – 4.2	0.0001	2.53	History of Diabetes
-	-	-	0.66 – 1.83	0.708	1.1	RAAS Inhibitors use
-	-	-	0.83 – 2.23	0.228	1.36	Beta Blocker use
-	-	-	0.65 – 1.78	0.789	1.07	Statin use
-	-	-	0.97 – 1.01	0.316	0.99	LVEDVi
-	-	-	0.97 – 1.04	0.842	1	LVESVi
-	-	-	0.95 – 1	0.089	0.98	LVSVi
-	-	-	0.98 – 1.05	0.48	1.01	LVEF
-	-	-	0.97 – 1.04	0.757	1.01	LVCOi
-	-	-	0.98 – 1.01	0.647	1	RVEDVi
-	-	-	0.98 – 1.03	0.811	1	RVESVi
-	-	-	0.96 – 1.01	0.311	0.98	RVSVi
-	-	-	0.97 – 1.04	0.757	1.01	RVEF
1 – 1.1	0.042	1.05	1.02 – 1.1	0.004	1.06	Scar
0.75 – 3.38	0.331	1.52	0.68 – 2.91	0.365	1.4	Mild LA Enlargement
0.78 – 4.2	0.272	1.66	0.79 – 4.04	0.161	1.8	Moderate LA Enlargement
1.05 – 4.11	0.041	2.13	1.19 – 4.41	0.013	2.29	Severe LA Enlargement

* BSA = body surface area; BP = blood pressure; RAAS = renin-angiotensin-aldosterone system; LA = left atrial; LV = left ventricular; RV = right ventricular; EDV = end diastolic volume; ESV = end systolic volume; SV = stroke volume; EF = ejection fraction.

† Univariate analysis for predictor of mortality.

‡ Multivariate analysis for predictor of mortality.

P001

Evaluation of Pulmonary Vein Scar Encirclement Patterns after Cryoballoon Ablation for Treatment of Atrial Fibrillation

John Oshinski, PhD[2] Adrian Lam, PhD[1], Michael S. Lloyd, MD[1]

1. *Emory University, Atlanta, GA*
2. *Emory Univeristy, Atlanta, GA*

Background: After pulmonary vein isolation therapy, gaps in the scar encircling the pulmonary veins (PV) have been linked to recurrence of atrial fibrillation (AF). Current MRI-based methods to assess the degree of scar encirclement of the PV are cumbersome to use, require subjective judgements by the user, and are difficult to visualize. We have developed a technique that uses a 3D, navigator-echo-gated, IR-prepared FLASH sequence acquired two times; first to acquire angiographic images of the left atrium during contrast infusion, followed by a second acquisition to acquire scar images of the atrial wall. Utilizing image processing and visualization techniques, atrial borders from the angiographic images are combined with enhancement patterns on the LGE images to visualize scar encirclement. The acquisition and processing methodology was applied in subjects undergoing cryoballoon ablation, and scar encirclement patterns between veins was assessed.

Methods: Ten patients who had undergone cryoballoon ablation 1-3 months prior to imaging were studied at 3T. Contrast was injected at 0.3 mL/sec (0.2 mmol/kg) and the 3D IR-FLASH sequence was acquired during contrast infusion for angiography images. Approximately 25 minutes after contrast injection, the same 3D, IR-FLASH sequence was run with a modified TI for LGE imaging. The inner atrial wall was segmented on the angiography images, and borders were dilated 3 pixels to create the outer atrial wall. Borders were then transferred to LGE images to determine the atrial wall. The LV myocardium was sampled, and pixels with intensity $> \mu + 7\sigma$ were defined as atrial wall scar (figure 1a-b). A 3D reconstruction of the atrial wall was done and locations 5 mm above and 5 mm below each pulmonary vein ostia were projected to a plane perpendicular to the pulmonary vein using a polar projection algorithm (figure 1c-d) to create four, 360° PV bullseyes for each patient. To assess gaps in scar encirclement and compare patterns over subjects, scar encirclement was projected into a circle, and quantified by determining the arc length of scar around the bullseye, expressed as a percent (figure 1,e-f).

Results: Bullseye plots were created for each pulmonary vein and the all patients. Encirclement was greatest in the left pulmonary veins compared to right pulmonary veins ($91.6 \pm 8.8\%$ vs $82.6 \pm 8.5\%$, $p < 0.05$). A 20° segment in the anteroinferior portion of the RSPV was successfully ablated in only 3 patients.

Conclusions: An acquisition method utilizing the same sequence repeated twice (once for angiography and one for LGE) combined with image processing and bullseye visualization enables more robust depiction of the atrial wall scar patterns and allows for visualization and quantification of scar encirclement. In the 10 subjects studied, encirclement was greater in the left pulmonary veins than the right pulmonary veins, specifically encirclement was greatest in the LIPV and lowest in the RIPV.

http://www.ConferenceAbstracts.com/uploads/cfp2/attachments/LDFAIBDN/LDFAIBDN--222905-1-ANY.pdf

P002

Using 4D Flow MRI to Evaluate Atrial Fibrillation Patients with Different Clinical Outcomes

Liliana E. Ma[1]Daniel C. Lee, MD, MSc[1], Jason Ng, PhD[1], Ozair Rahman, MD[1], James Carr, MD[2], Jeffrey Goldberger, MD, MBA[3], Michael Markl, PhD[4]

1. *Northwestern University, Feinberg School of Medicine, Chicago, IL*
2. *Northwestern Memorial Hospital, Chicago, IL*
3. *University of Miami, Miami, FL*
4. *Northwestern University, Chicago, IL*

Background: Atrial fibrillation (AF) is associated with an increased risk of ischemic stroke due to the development of thrombi in the left atrial appendage (LAA). Empirical risk scoring systems like the CHA_2DS_2-VASc are currently used to assess patients' thromboembolic risk but fail to reliably balance a patient's need for anticoagulation with bleeding risk. Transesophageal echocardiography (TEE) studies have found that decreased LAA peak emptying velocity and increased LAA stasis are associated with thrombus formation. However, TEE and other available diagnostic tools are limited as they are invasive and do not completely assess complex LAA/left atrial (LA) blood flow. This study aimed to evaluate the sensitivity of 4D flow MRI to detect LA/LAA hemodynamic differences among AF patients who had previously experienced thromboembolic events and AF patients who had not.

Methods: 4D flow MRI was used to measure in-vivo, time-resolved 3D blood flow velocities with full volumetric coverage of the left atrium (LA) in 24 subjects: 13 patients with a history of stroke/TIA (12 in AF at time of imaging, age 70.7 ± 6.6 years) and 11 with no thromboembolic history (9 in AF at time of imaging, age 73.2 ± 5.3 years). Data analysis (figure 1) included 3D segmentation of all LA and the LAA when visible (9 no stroke, 10 stroke). Absolute atrial velocities were calculated for all voxels and time frames inside the LA/LAA and used to quantify LA/LAA mean velocity, peak velocity, volume, and stasis (% voxels with velocities < 0.1 m/s) and to derive stasis maps (Fig 1 C).

Results: LAA mean stasis was significantly elevated for AF patients with prior stroke/TIA (76.2 ±11.0% vs 65.8 ± 7.2%, p=0.028). In addition, trends of decreased LAA mean velocity (p=0.11) and peak velocity (p=0.12) and increased LAA volume in the stroke group were noted in comparison to the no stroke group (figure 2). Differences in flow dynamics in the entire LA were less pronounced in this cohort of AF patients (figure 3).

Conclusions: The findings of this study demonstrate that flow and stasis measured in the LAA appear to be associated with the pathophysiology of thrombus formation in AF patients and indicate that 4D flow MRI can detect underlying differences in flow physiology between AF patient groups with different clinical outcomes (stroke vs. no stroke). This study thus indicates that individualized assessment of LAA stasis may be a potent identifier of thromboembolism risk in AF patients. However, studies with larger cohorts and further improvements of 4D flow methods are needed to confirm these preliminary findings.

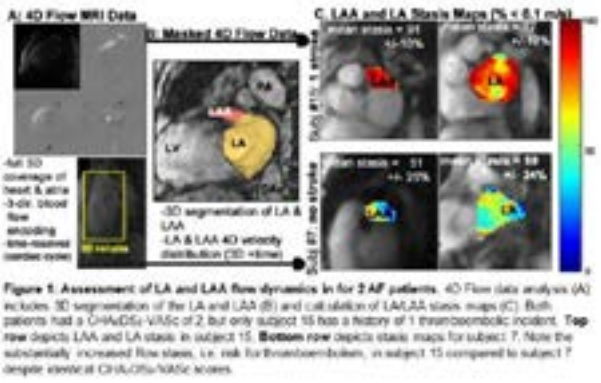

Figure 1. Assessment of LA and LAA flow dynamics in for 2 AF patients. 4D Flow data analysis (A) includes 3D segmentation of the LA and LAA (B) and calculation of LA/LAA stasis maps (C). Both patients had a CHA_2DS_2-VASc of 2, but only subject 15 has a history of 1 thromboembolic incident. **Top row** depicts LAA and LA stasis in subject 15. **Bottom row** depicts stasis maps for subject 7. Note the substantially increased flow stasis, i.e. risk for thromboembolism, in subject 15 compared to subject 7 despite identical CHA_2DS_2-VASc scores.

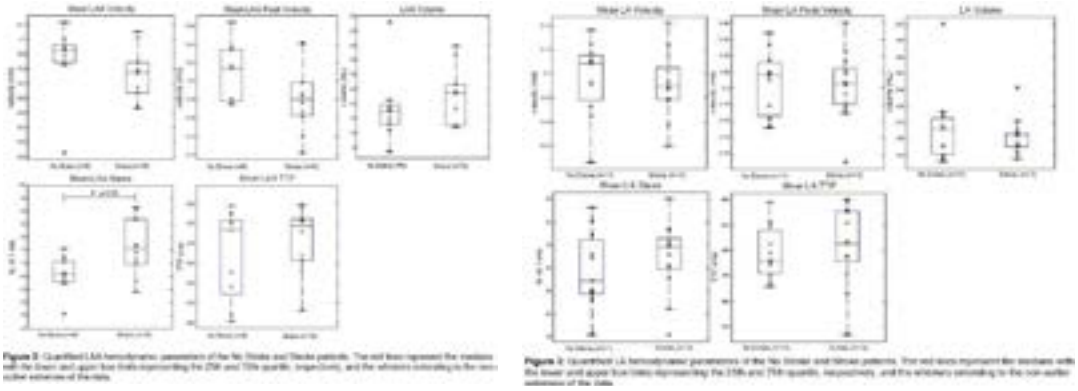

P003

Extracellular volume fraction in "lone" atrial fibrillation patients is similar to controls and unaffected by ablation: atrial fibrillation alone does not cause diffuse left ventricular fibrosis

Rohan S. Wijesurendra, MB BChir, MRCP[1] Alexander Liu, MBBS, MRCP[1], Christian Eichhorn[2], Theodoros Karamitsos, MD, PhD[3], Yaver Bashir, FRCP, MA, DM[4], Matthew Ginks, MD[4], Kim Rajappan, MD FRCP[4], Timothy Betts, MD FRCP[4], Stefan K. Piechnik, PhD, MScEE[5], Vanessa M. Ferreira, MD, DPhil[5], Barbara Casadei, MD DPhil FRCP FMedSci [2], Stefan Neubauer, MD, FRCP[5]

1. *University of Oxford, Oxford, England, United Kingdom*
2. *Division of Cardiovascular Medicine, University of Oxford, England, United Kingdom*
3. *NA, Thessaloniki, Greece*
4. *Oxford University Hospitals NHS Foundation Trust, England, United Kingdom*
5. *University of Oxford, England, United Kingdom*

Background: Atrial fibrillation (AF) is associated with subtle impairment of left ventricular (LV) function, even in the absence of underlying cardiovascular disease (so-called "lone" AF). One potential mechanism previously reported in AF patients is diffuse ventricular fibrosis; however, the precise nature of the relationships between AF, LV dysfunction and diffuse LV fibrosis remains incompletely understood. Here, we longitudinally studied "lone" AF patients before and after catheter ablation, to assess the effect of sinus rhythm restoration or reduction in AF burden on diffuse LV fibrosis and systolic function.

Methods: 59 subjects were included (Table 1): 41 pre-ablation AF patients and 18 sinus rhythm (SR) controls matched for age, gender and BMI. Patients (median AF duration 47 months [IQR 25-92]) had no valvular disease, significant coronary disease, diabetes, uncontrolled hypertension, inflammatory disease or inadequate ventricular rate-control. To determine extracellular volume fraction (ECV), systolic T1-mapping (ShMOLLI, 1.5T) was performed pre- and 15-minutes post-gadolinium contrast (0.16 mmol/kg) in a mid-ventricular slice; blood was drawn pre-scan for haematocrit. LV volumes, mass and function (ejection fraction [EF] and peak systolic circumferential strain [PSCS] by tissue tracking) were assessed by CMR short-axis cine stack; echocardiography determined LV diastolic function (E/E'). CMR images were analysed by an observer blinded to intra-scan rhythm and clinical status. CMR scans and 7-day Holters were repeated at 7±1 months post-ablation (in 34 of 41 patients).

Results: Compared to controls, patients had significantly reduced LV function (p=0.001 and p=0.006 for LVEF and PSCS, respectively), despite similar heart rates (p=ns; Table 1). However, in contrast to some previous reports, native/post-contrast myocardial T1, ECV and diastolic function were not significantly different between AF patients and controls (all p=ns, Table 1). There were minor differences in T1 times between paroxysmal and persistent AF patients (Table 2), but ECV was almost identical between these groups (p=ns). AF burden reduced significantly post-ablation (median 0% [IQR 0-0.05%] from pre-ablation median 24% [IQR 0-100%], p < 0.001). LVEF improved slightly (post-ablation LVEF 64±6% from 61±9%, n=34 paired analysis, p=0.045), but remained lower than in controls (p=0.02). However, there was no change in native/post-contrast T1 or ECV post-ablation (all p=ns; Fig 1).

Conclusions: Patients with "lone" AF do not demonstrate excess diffuse LV fibrosis compared with matched controls in SR, despite having lower LVEF and worse PSCS. ECV is also unchanged post-ablation despite a significant reduction in AF burden, and improvement in LVEF. These novel findings suggest that AF alone does not cause LV fibrosis or diastolic dysfunction, rather, alternative mechanisms independent of LV tissue characteristics may underlie LV systolic dysfunction in AF.

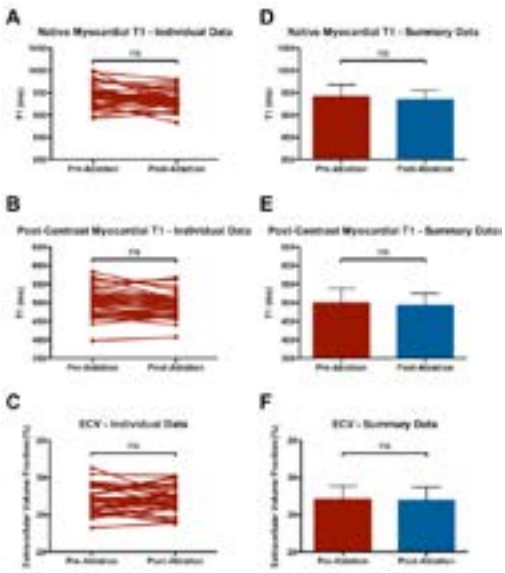

Table 1: Demographic, Haemodynamic, Cine, Diastolic Function and T1-Mapping Data from AF Patients Pre-Ablation and SR Controls.

p value	SR Controls (n=18)	AF Patients (n=41)	
			DEMOGRAPHICS
0.839	64 ± 6	63 ± 8	**Age, years**
1.000	78	76	**Male, %**
0.493	27 ±3	28 ± 6	**BMI, kg/m^2**
			HAEMODYNAMICS
0.603	66 ± 10	69 ± 22	**Heart rate, bpm**
0.102	144 ± 21	135 ± 18	**Systolic BP, mmHg**
0.639	81 ± 12	82 ± 12	**Diastolic BP, mmHg**
			CINE IMAGING
0.211	136 ± 29	149 ± 39	**LV EDV, ml**
0.001	69 ± 7	60 ± 10	**LV ejection fraction, %**
0.006	-23 ± 4	-20 ± 4	**Peak systolic circumferential strain, %**
0.151	113 ± 26	123 ± 24	**LV mass, g**
0.805	0.84 ± 0.1	0.86 ± 0.2	**LV mass/EDV, g/ml**
			DIASTOLIC FUNCTION
0.342	7.9 ± 2	7.2 ± 2	**E/E', ratio**
			T1-MAPPING
0.563	938 ± 26	943 ± 30	**Native myocardial T1, ms**
0.717	1514 ± 89	1522 ± 65	**Native blood T1, ms**
0.603	492 ± 26	498 ± 38	**Post-contrast myocardial T1, ms**
0.258	367 ± 34	381 ± 46	**Post-contrast blood T1, ms**
0.241	42 ± 4	43 ± 3	**Haematocrit, %**
0.747	27 ± 3	27 ± 2	**ECV, %**

BMI, body mass index; BP, blood pressure; E/E' ratio, ratio of peak early diastolic mitral inflow velocity to spectral tissue Doppler-derived peak early diastolic velocity at the mitral annulus (average of septal and lateral measurements); ECV, extracellular volume fraction; EDV, end diastolic volume; LV, left ventricular; T1, longitudinal relaxation time

Table 2: Pre-Ablation T1-Mapping Data, Split by AF Type.

p value	Paroxysmal AF (n=21)	Persistent AF (n=20)	
0.046	932 ± 20	954 ± 36	**Native myocardial T1, ms**
0.684	1531 ± 67	1513 ± 63	**Native blood T1, ms**
0.036	511 ± 36	484 ± 37	**Post-contrast myocardial T1, ms**
0.018	398 ± 43	363 ± 44	**Post-contrast blood T1, ms**
0.303	43 ± 3	44 ± 3	**Haematocrit, %**
0.882	27 ± 2	27 ± 2	**ECV, %**

ECV, extracellular volume fraction; T1, longitudinal relaxation time

P004

Assessment of RF Ablation Lesions with T1 Mapping

Daniel A. Herzka, PhD[1]Susumu Tao, MD, PhD[2], Sarah Fink, BA[3], Aravindan Kolandaivelu, MD[4], Michael A. Guttman, MS[5], Henry Halperin, MD, MA[6]

1. *Johns Hopkins University School of Medicine, Baltimore, MD*
2. *Johns Hopkins University, school of medicine, Baltimore, MD*
3. *Johns Hopkins University, MD*
4. *Johns Hopkins University School of Medicine, MD*
5. *The Johns Hopkins University, School of Medicine, MD*
6. *Johns Hopkins University, Baltimore, MD*

Background: The inability to visualize therapeutic effects of catheter-mediated radiofrequency ablation (RFA) during procedures using X-ray fluoroscopy guidance inhibits feedback to the electrophysiologist seeking to deliver sufficient and accurate therapy. Since RFA is known to induce changes in tissue native T1, post-procedural cardiac MRI presents a clear opportunity for the assessment of RFA therapy. However, the design of pulse sequences for visualization of RFA lesions requires knowledge of tissue native T1. This work aims to determine the native T1 of several tissues present after RFA including the lesion core exhibiting coagulation necrosis, and the lesion periphery which can include a variety of tissues including (hemorrhagic) contraction band necrosis, edema, and even surface thrombus.

Methods: Under IACUC-approved protocol, RFA lesions were created in the LV wall of N=5 swine using a 3.5 mm-tip irrigated catheter at 30 W for 60 sec. Imaging was performed at 1.5 T within 2 hr of ablation. Three different imaging sequences were acquired: 1) 2D motion-compensated breath-hold and free-breathing modified look locked imaging (MOLLI) [1], 2) 3D free-breathing navigator-gated T1W inversion recovery spoiled gradient echo (long-TI T1w SPGR) [2], and 3) 3D delayed contrast enhanced (DCE) imaging. An additional animal died prematurely after RFA, and the heart was imaged *ex vivo* using the same sequences (no DCE) to determine T1s without additional blurring due to motion. ROIs were draw on the MOLLI scans using long-TI T1w SPGR imaging and DCE as references. Native T1 of the RFA lesion core, lesion periphery, normal myocardium, and LV blood were measured. Partial volume averaging was avoided where possible.

Results: Figure 1A demonstrates the measured native T1 mean, minimum and maximum for the 4 tissues of interest. Figure 1B displays the same measurements performed *ex vivo*. Figures 2 displays native T1 maps and representative images of RFA lesions. There is clear correspondence between MOLLI and the Long-TI T1w SPGR sequence.

Conclusions: *In vivo* MOLLI measurements demonstrate the decreased T1 (~930) of the RFA lesion core (coagulation necrosis). *Ex vivo*T1 mapping indicates a lesion core T1 of ~ 815 ms indicating that motion and partial volume averaging may significantly affect T1 measurements of the small core structure. Heterogeneous lesion periphery demonstrates increased T1 though the multiplicity of tissues involved (hemorrhage vs. thrombus vs. edema) may confound results beyond partial volume averaging. References: [1] Kellman P. et al. MRM(2005). [2] Guttman M. et al. SCMR(2016).

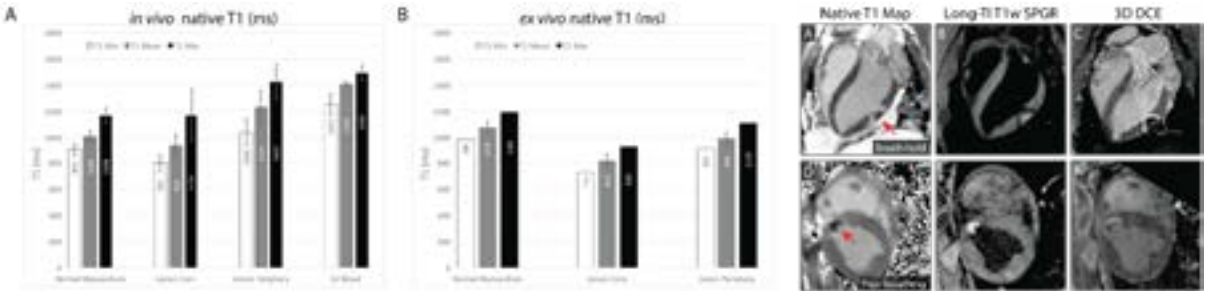

P005

Rotational Motion of the Left Ventricle: the Robust Normal Pattern

Abbas Nasiraei Moghaddam, PhD[2]Shahriar Shalikar, MSc[1], Vahid Ghodrati, MSc[1]

1. Amirkabir University of Technology, Tehran, Iran
2. Amirkabir University of Technology, Tehran, Tehran, Iran

Background: In order to decrease the rate of mortality related to cardiac disorders, it is essential to find easily accessible mechanical markers correlated to progression of failure [1-2]. LV twist is a sensitive index, which is affected before the emergence of defect [3]. It is essential, therefore, to investigate the robustness of the LV twist pattern in healthy subjects, so it can be used as a measure for prediction and control of the cardiac incompetency and arrhythmia.

Methods: For 12 healthy volunteers (43±13.6 y), radial tagged MRI images were acquired in short-axis view at Apex-, Mid- and base-level (14, 22 and 26 taglines around the LV for each level, respectively). A phase-based optical flow technique, called Monogenic signal method, was performed. It obtained local parameters of gray-valued image by a set of proper quadrature filters [4], and consequently the displacement field, relative to first image, was calculated at different levels. For each frame the average rotation, twist and torsion were subsequently calculated around the LV center. (According to [5], twist is defined as the difference between simultaneous rotations at two levels and torsion as normalized twist.)

Results: Peaks of LV rotation and twist/torsion as well as the corresponding peak-times are reported in table 1 and table 2 respectively. With given three imaging planes, namely, Apex, Base and Mid, located at the middling of apex and base in most cases, we can consider three attitudes for LV twist investigation: Apex2Base, Apex2Mid and Mid2Base. Although they evolve in different patterns, according to these results, the time to peak of them took place simultaneously (Figure 1 & Table 2). This coordination is stating the fact that there is a twist synchrony along the LV in healthy hearts. Apex2Mid is zero for first 12% of cardiac cycle and in general the Mid2Base have more contribution of twist motion than Apex2Mid in both twist and torsion peaks.`

Conclusions: The LV rotational motion was investigated in healthy subjects. The peak rotation at different levels were highly synchronized and the time to peak of twist/torsion was robustly located at around 41% of RR interval. This synchrony is hypothesized to serve as a complimentary parameters to predict cardiac disorders, especially at the onset of arrhythmia.

References: *[1] Bertini et al. JACC: Cardiovascular Imaging, vol. 2, pp. 1425-1435, 2009. [2] Phan et al. European Journal of Echocardiography, vol. 10, pp. 793-800, 2009. [3] Sengupta et al. JACC: Cardiovascular Imaging, vol. 1, pp. 366-376, 2008. [4]. Alessandrini et al., IEEE Trans on Image Processing, vol. 22, pp. 1084-1095, 2013. [5] Rüssel et al. JCMR, vol. 10 ,p. 26, 2008.*

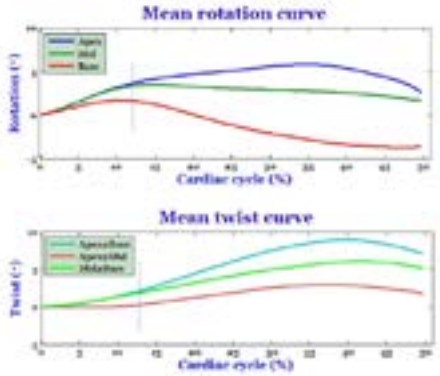

Table 1: LV rotation peak (Mean ± Standard Deviation).

Base (NP)	Base (PP)	**Mid**	**Apex**	
-4.1 ± 2.2	2.1 ± 1.1	4.6 ± 3.0	6.4 ± 2.4	Rotation peak (Degree)
50± 8	16± 1	20± 3	36 ± 2	Time to peak (%RR)

%RR, Percent of cardiac cycle (R-R interval) PP, Positive Peak - NP, Negative Peak

Table 2: LV twist/torsion peak (Mean ± Standard Deviation).

Mid2Base	Apex2Mid	Apex2Base	
6.5 ± 2.8	3.9 ± 3.2	9.7 ± 3.2	Twist peak (Degree)
8.0 ± 2.9	4.0 ± 2.3	5.6 ± 1.4	Torsion peak (Degree)
42± 5	41± 15	41 ± 5	Time to peak (%RR)

%RR, Percent of cardiac cycle (R-R interval)

P006

Altered mechanics of left ventricle in patients with atrial fibrillation and normal ejection fraction

Lei Zhao, M.D., Ph.D[1] Xiaohai Ma, M.D., Ph.D[1], Jing An, M.D., Ph.D[2], Marie-Pierre Jolly, Ph.D[3], Andreas Greiser, Ph.D[4]

1. Beijing Anzhen Hospital, Capital Medical University, Beijing, China (People's Republic)
2. MR Collaborations NE Asia, Siemens Healthcare, Beijing, China, Beijing, China (People's Republic)
3. Siemens Healthcare, Princeton, NJ
4. Siemens Healthcare GmbH, Erlangen, Germany, Erlangen, Bayern, Germany

Background: Atrial fibrillation (AF) and heart failure frequently coexist and both conditions affect patient prognosis. Early detection of ventricular dysfunction using cardiac magnetic resonance (CMR) feature tracking in patients with AF may provide information for therapeutic strategy. Therefore, the purpose of this study was to evaluate left-ventricular (LV) strain in patients with AF and normal controls.

Methods: 100 subjects underwent MRI using a clinical 3 T scanner (Magnetom Verio, Siemens Healthcare): 50 paroxysmal AF patients (12 female; mean age, 55 ± 13 years) and 50 controls (21 female; mean age, 55 ± 13 years). Left-atrial volume, LV functional indices and global circumferential strain parameters were evaluated from CMR cine imaging using a feature-tracking-based prototype software. Left-atrial volume and LV strain parameters were compared among AF patients with normal ejection fraction (EF), AF patients with decreased EF and controls.

Results: AF patients had larger left-atrial volume (125.0 ± 41.2 ml) than controls (100.0 ± 28.2 ml, P+ 13.9%; controls: 62.4 ± 6.4%, P>0.05). AF resulted in a significant impairment of LV global circumferential strain (AF patients: peak systolic circumferential strain: -16.1 ± 2.1%, systolic circumferential strain rate: -85.5 ± 17.2%, early diastolic circumferential strain rate: 91.7 ± 19.1%; controls: peak systolic circumferential strain: -18.1 ± 1.1%, systolic circumferential strain rate: -90.2 ± 8.1%, early diastolic circumferential strain rate: 107.0 ± 14.0%, all P 50% (68%, EF: 62.4% ± 6.8%), their LV globe circumferential strain was also reduced (peak systolic circumferential strain: -17.6 ± 1.4%, P>0.05; systolic circumferential strain rate: -88.9 ± 9.2%, P>0.05; early diastolic circumferential strain rate: 99.3±11.9%, P < 0.05).

Conclusions: Strain analysis by feature-tracking CMR helps to early and objectively detect global LV dysfunction in patients with AF and provides information for a better understanding of the association between AF and cardiac dysfunction.

P007

Detection of ablation related complications in patients with peristent atrial fibrillation using Cardiovascular Magnetic Resonance: Thoracoscopic surgical ablation versus catheter ablation

Evangelia Nyktari, MD[1] Rick Wage, DCR (R)[2], Shouvik Haldar, MD (Res), MRCP[3], Jenny Keegan, PhD,MSc[4], Tom Wong, MCCHB, MD, FRCP[4], Raad Hashem Mohiaddin, MD PhD[5]

1. *Royal Brompton Hospital, England, United Kingdom*
2. *NIHR Cardiovascular Biomedical Research Unit, Royal Brompton Hospital, England, United Kingdom*
3. *Royal Brompton & Harefield NHS Foundation Trust, England, United Kingdom*
4. *Royal Brompton Hospital , Imperial College, England, United Kingdom*
5. *Royal Brompton Hospital and Imperial; College London, London, England, United Kingdom*

Background: For atrial fibrillation (AF) refractory to medical treatment, catheter ablation (CA) and minimally invasive video-assisted thoracoscopic surgical ablation (SA) are two potential management options. The recent FAST randomized trial has shown better rhythm outcome for SA compared to CA, however with a higher complication rate. This is important for long standing peristent AF (LSPAF) as CA results are still suboptimal. We report the incidence of complications picked up on serial CMR follow-up studies in patients with LSPAF randomized to either SA or CA.

Methods: 48 consecutive patients (mean age 64.4±10.8 years, 30males) with LSPAF and a set of 3 CMR scans (pre-ablation, 3 and 9 months post ablation) were randomized to either CA or SA. Twenty-three (n=23) underwent SA and twenty-five (n=25) CA. In the SA group, ablation involved pulmonary vein isolation (PVI) using a bipolar RF clamp and a posterior wall box lesion. In the CA group, a stepwise lesion set was followed: 1) PVI; 2) linear ablation (LA roof and mitral isthmus); and 3) ablation of complex fractionated atrial electrograms in the LA. CMR was performed on a 1.5T Siemens MRI scanner (Avanto, 1.5T). PV diameter was measured at the ostial/proximal part of the vessels on both 3D Gadolinium-Enhanced MRA (Figure-1) and 3D SSFP MRA images. Moderate and significant PV stenosis was defined as 50-70% and > 70% reduction in diameter respectively compared to the pre-ablation scan.

Results: Baseline characteristics between the SA and CA group were non-significantly different: mean age 64±9 vs. 67±11; p=0.2, LA volume (indexed to BSA (ml/m2) 59±14 vs. 60±16; p=0.77, and LV ejection fraction 58±9 vs. 61±10; p=0.21. Out of 48 patients there were 6 with PVS >50% on follow-up CMR, 5 of them belonging to the SA group (21.7% vs 4%, RR 0.81; 95% CI 0.64 to 1.02; p 0.09) (diagram 1). 3 of them (2 in SA and 1 in CA group) had a significant PVS>70% (8.6% vs 4%, RR 0.95; 95% CI 0.81 to1.1; p 0.6) and only 1 (4% vs 0%, RR 0.94, 95% CI 0.84 to 1.05, p 0.41) was symptomatic requiring PV angioplasty. 2 patients had 2 PVs with stenosis and 4 patients had 1 PV with stenosis. Out of the 8 PVs with stenosis, only 1 was right sided. Both 3D GE-MRA and 3D SFFSP MRA identified the PVS correctly. All significant PVS on the CMR were confirmed by CT PV angiogram. There were more pleural effusions in the SA group (17% vs 12%). One patient in the SA group developed a large pleural lipoma and tight proximal right renal artery stenosis in addition to the significant LUPV and LLPV stenosis detected in the first post-ablation CMR (Image 1). CMR also detected pulmonary sarcoidosis in 2 patients and renal oncocytoma in one patient.

Conclusions: Thoracoscopic SA is associated with a higher incidence of significant PV stenosis compared to the percutaneous CA approach. Serial CMRs provide a radiation free alternative to CT for the detection and monitoring atrial ablation related complications.

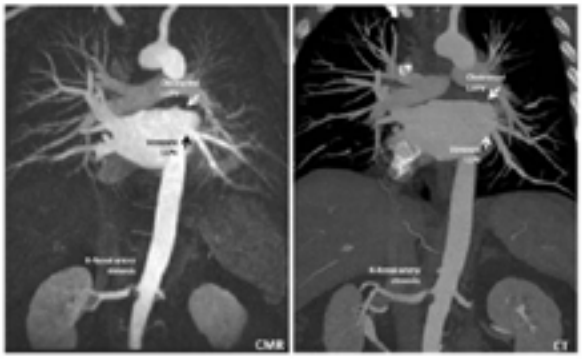

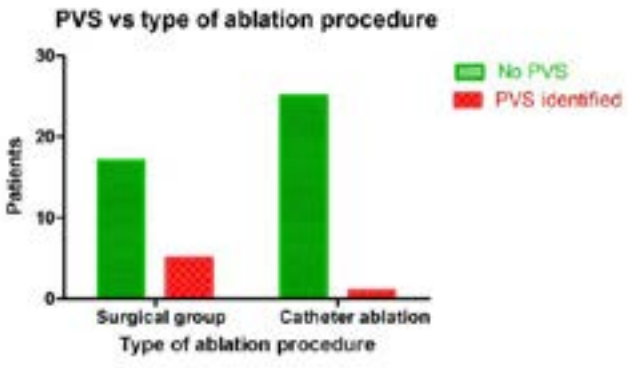

P008

Pulmonary Veins following Pulmonary Vein Isolation Procedure in Patients with Atrial Fibrillation: Remodeling and Prediction of outcome; a Cardiac MRI Study

Shimaa Sayed. Khidr, MD[1]Mark Doyle, Ph.D.[1], Sahadev Reddy, MD[1], Geetha Rayarao, MS[2], Moneal Shah, MD[3], William Belden, MD[1], Mohamed Abdel Ghany, MD[4], Hosam Ali, MD, PhD[4], Doaa Ahmed. Fouad, MD, PhD[4], Shimaa S. Khidr, MD[1]

1. Allegheny General Hospital, Pittsburgh, PA
2. Allegheny General Hospital, PIttsburgh, PA
3. Allegheny general hospital, pittsburgh, PA
4. Assiut University Hospital, N/A, Egypt

Background: After successful PVI for AF, the left atria undergo reverse remodeling from restoration of normal sinus rhythm (NSR). However, few studies have directly studied PV remodeling and none, to our knowledge, have identified any pre-PVI pulmonary vein conditions to predict outcome. We hypothesize that : 1) post-PVI, in addition to LA remodeling, the pulmonary veins undergo a parallel degree of remodeling and 2) that pulmonary vein characteristics pre-PVI can be used to identify patients more likely to achieve a long-term sustainable NSR following PVI.

Methods: Patients (101) scheduled to undergo PVI were evaluated with CMR imaging before and 6±2 months following PVI. At each time point, pulmonary vein cross sectional area measurements (CSA) triangulated to be within 1cm of the ostium as well as LA volumes were measured from the 3D MRA of the left atrium. Patients were categorized as responders (R) or non-responders (NR), based on being event-free on two separate 15-day Holter monitor evaluations.

Results: The population (71% male) had a 74% response rate. When pairing patients pre to post, the LA volume index decreased in both R (61±18 to 53±15 mlm^{-2} pre to post PVI and post vs post PVI (p 0.02 for both). This showed moderate correlation to the LA reverse remodeling (R 0.48, $p < 0.001$). Prior to PVI there was no significant difference between R vs. NR in LA volume index or PV CSA. However, pre-PVI, there was a weak trend for responders to have: a) lower average PV CSAs and b) a higher degree of heterogeneity. To define heterogeneity, we created a Heterogeneity Index as the relation of the pre-PVI ratio of average CSA to PVI standard deviation (CSA_{avg}/CSA_{SD}). Among the PV's, the Heterogeneity Index trended lower for R vs. NR (4.4±3.4 vs. 6.5±7.2, p=0.058). This physiologic parameter indicates that patients with a combination of lower average CSA but a greater anatomic range of PV area appear more likely to respond following PVI with long-term maintenence of NSR. This is consistent with a lower degree of adverse remodeling having occurred due to AFib.

Conclusions: Following PVI, favorable reverse remodeling occurs in pulmonary veins of all patients but is more pronounced in responders vs. non-responders. At baseline, responders tended to have lower PV CSA combined with higher Heterogeneity Index as compared to non-responders indicative of this easy metric to define liklihood for robust maintence of NSR following PVI.

P009

The ratio of left atrial volume/ left ventricular end systolic volume by CMR as a predictor of atrial fibrillation in patients with hypertrophic cardiomyopathy

Amardeep Ghosh Dastidar, MBBS(Hons), MRCP[1] Jonathan C. L. Rodrigues, MBChB (Hons), FRCR[2], Estefania De Garate, MD[1], Priyanka Singhal, MBChB[3], Anna Baritussio, MD[1], Alessandra Scatteia, MD[4], Tamas Erdei, PhD[5], Alan Graham Stuart, MBChB, FRCP[3], Angus K. Nightingale, MD FESC[6], Chiara Bucciarelli-Ducci, MD, PhD[1]

1. *NIHR Bristol Cardiovascular Biomedical Research Unit, Bristol, England, United Kingdom*
2. *Bristol Heart Institute, England, United Kingdom*
3. *NIHR Bristol CVBRU, England, United Kingdom*
4. *Division of Cardiology, Ospedale Medico-Chirurgico Accreditato Villa dei Fiori, Acerra, Naples, Italy. Cardiac Magnetic Resonance Unit, NIHR Bristol Cardiovascular Biomedical Research Unit, Bristol Heart Institute, Bristol UK, Naples, Campania, Italy*
5. *Cardiac MRI Unit, Bristol Heart Institute, Bristol, Bristol, England, United Kingdom*
6. *Bristol Heart Institute, Bristol, England, United Kingdom*

Background: Atrial fibrillation (AF) is the most common sustained arrhythmia in hypertrophic cardiomyopathy (HCM) and is associated with major adverse cardiovascular events. Cardiac magnetic resonance (CMR) with its superior tissue characterisation property is increasingly used in patients with HCM. **Aims:** To identify the structural predictors of AF in HCM using CMR.

Methods: 114 consecutive HCM patients were identified after reviewing approximately 3,100 CMR scans from our registry (Jan 2014 to Mar 2015). Comprehensive CMR protocol was used including cines, early and late gadolinium enhancement imaging. The diagnosis of HCM was based on left ventricular (LV) maximum wall thickness ≥15 mm (or 13-14 mm in the presence of familial history and/or ECG changes), in the absence of other cardiac/systemic disorders producing a similar degree of hypertrophy. Clinical notes were evaluated to identify a documented episode of AF. Univariate and multivariate logistic regression analyses were performed to determine the CMR imaging predictors of AF in HCM.

Results: The final study sample consisted of 104 patients with HCM with median age 60years (IQR = 54-70) and 70% male, (10 patients excluded due to uncertain/overlapping diagnosis). 70% had non-apical HCM; the remainder 30% apical HCM. 16% (n=17) had a documented episode of atrial fibrillation. The univariate predictors of AF included left atrial volume and the ratio of left atrial volume to LV end systolic volume whereas in the multivariate model the ratio of left atrial volume to LV end systolic volume remained the only significant predictor (p=0.034, OR=2.236, CI=1.063-4.702). Table 1

Conclusions: Our study suggests that the ratio of left atrial volume to LV end systolic volume is the best predictor of AF in HCM. The simple CMR derived ratio may have potential role for AF risk stratification in HCM.

http://www.ConferenceAbstracts.com/uploads/cfp2/attachments/LDFAIBDN/LDFAIBDN--219368-1-ANY.pdf

P010

Left Atrial Inflow and Vortex Imaging Using 4D flow MRI in Patients with Paroxysmal Atrial Fibrillation: Exploration for Novel Markers of Atrial Disease and Thrombo-embolic Risk

Julio Garcia, PhD[1]Michael Bristow, MD[2], Carmen P. Lydell, MD[2], Andrew G Howarth, MD[2], Bobby Heydari, MD, MPH[2], Frank S Prato, PhD[3], Maria Drangova, PhD[4], Rebecca E. Thornhill, PhD[5], Pablo Nery, MD[6], Stephen Wilton, MD[7], Allan Skanes, MD[8], James White, MD, FRCP(C) [9]

1. *Stephenson Cardiac Imaging Centre, Libin Cardiovascular Institute of Alberta, University of Calgary, Calgary, AB, Canada*
2. *Stephenson Cardiac Imaging Centre, Libin Cardiovascular Institute of Alberta, University of Calgary, AB, Canada*
3. *Medical BioPhysics and Physics, University of Western Ontario, ON, Canada*
4. *Department of Medical Imaging, Medical Biophysics and Physics, University of Western Ontario, ON, Canada*
5. *Medical Imaging, The Ottawa Hospital, ON, Canada*
6. *Electrophysiology, University of Ottawa, ON, Canada*
7. *Cardiac Sciences, Libin Cardiovascular Institute of Alberta, University of Calgary, AB, Canada*
8. *Department of Medicine, University of Western Ontario, ON, Canada*
9. *Stephenson Cardiovascular Imaging Center, University of Calgary, AB, Canada*

Background: Atrial fibrillation (AF) is associated with elevated morbidity and mortality, largely contributed by systemic thrombo-embolism and stroke. Previous studies using Doppler echocardiography have supported that thrombus formation is associated with alterations in left atrial flow. Recently, time-resolved three-dimensional phase-contrast (4D flow MRI) has been able to visualize and quantify markers of global LA flow in patients with AF versus healthy controls (HC). This study aims to explore LA inflow from the individual pulmonary veins and assess their relationship to LA vortex formation as a potential marker of atrial disease and thrombo-embolic risk.

Methods: 13 male subjects (9 with paroxysmal AF >2 years duration referred for pulmonary vein ablation and 4 HC) were enrolled in an IRB-approved study protocol. Patients were required to be in sinus rhythm and not have >mild mitral insufficiency. Imaging was performed using a 3T MRI scanner using a standardized protocol inclusive of 4D flow MRI with whole heart coverage. A time-averaged phase contrast MR angiogram was constructed from 4D flow MRI data (Fig. 1A) and used to perform 3D segmentation of the left sided chambers and proximal aorta (Fig. 1B-Top). Blood flow visualization was performed using 3D pathlines (Fig. 1B) initiated from specific plane locations (Fig. 1C-D). Blood flow analyses for each plane included: peak velocity (PV), net flow (NF), forward flow, retrograde flow, and regurgitant fraction.

Results: Median age was 54 years in AF subjects and 27 years in HC. At the top plane NF was significantly lower in subjects with AF versus HC (median= 39 ml/cycle vs. 48 ml/cycle, $p < 0.070$). Peak LA velocities were significantly lower in subjects with AF versus HC with median values of 0.5 m/s vs. 0.7 m/s ($p=0.076$) at the mid plane and 0.7 m/s vs. 0.9 m/s ($p=0.003$) at the bottom plane. No asymmetry in pulmonary vein inflow velocities were observed in HC, however patients with AF showed significant asymmetry in peak velocity of the left superior (LS) versus right superior (RS) pulmonary veins with median values of 0.57 m/s and 0.47 m/s ($p=0.001$), respectively (Fig. 2). While helical and vortical LA flow patterns were observed in both cohorts these patterns were broader, more complex, and fractionated in AF subjects (Fig 2). LA vortex rotation was clockwise (viewed from ventricular side) in all subjects.

Conclusions: This study demonstrates that: 1) 4D flow imaging of LA inflow and vortex formation is clinically feasible, 2) Significant differences in LA flow can be identified in patients with paroxysmal AF versus HC; 3) Asymmetry of pulmonary vein inflow may be contributory to alterations in LA vortical flow, and 4) Vortical flow is fractionated in patients with a history of paroxysmal AF. Collectively, these early observations seed interest for LA 4D flow as a marker of early or established left atrial disease and may provide value for the prediction of thrombo-embolic events.

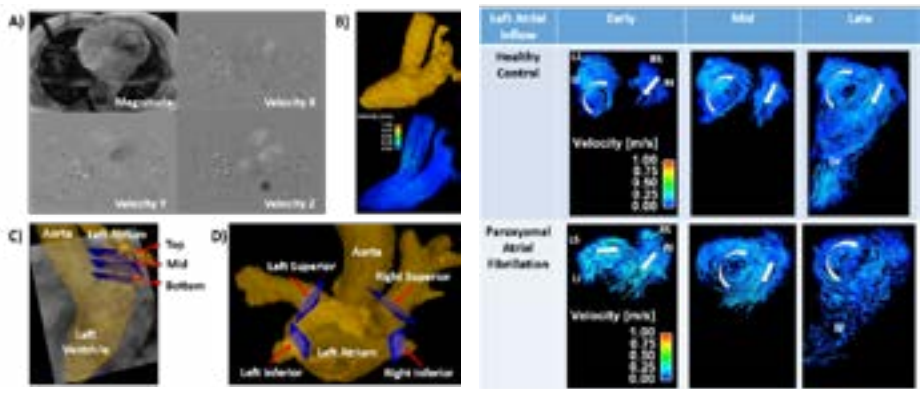

P011

Improved Reproducibility in Assessment of Left Atrial Late Gadolinium Enhancement with the Guidance of SPACE 3D T2 Sequence

Esra Gucuk Ipek, MD[1] Ashkan Malayeri, MD[2], Yuliya Mints, MD[3], Yoon Lee, BS[4], Muhammad Balouch, MD[5], Tarek Zghaib, M.D.[6], Adityo Prakosa, PhD[7], Qian Tao, Ph.D.[8], Rob J. van der Geest, PhD[9], Natalia Trayanova, PhD, FAHA[10], Saman Nazarian, MD, PhD[11], Stefan L. Zimmerman, MD[12], Sohail Zahid, BS[13]

1. Johns Hopkins Hospital, MD
2. NIH, MD
3. JOHNS HOPKINS HOSPITAL, MD
4. Johns Hopkins University School of Medicine, Baltimore, MD
5. Johns Hopkins Medicine, MD
6. Johns Hopkins University, Baltimore, MD
7. Johns Hopkins Unviersity, Biomedical Engineering, Baltimore, MD
8. Leiden University Medical Center, Leiden, Zuid-Holland, Netherlands
9. Department of Radiology, Leiden University Medical Center, The Netherlands, Leiden, Zuid-Holland, Netherlands
10. Johns Hopkins Unviersity, Biomedical Engineering and Medicine, Baltimore, MD
11. University of Pennsylvania Perelman School of Medicine, PA
12. Johns Hopkins University School of Medicine, MD
13. JOHNS HOPKINS UNIVERSITY, Baltimore, MD

Background: Left atrial (LA) imaging late gadolinium enhancement (LGE) cardiac magnetic resonance (CMR) has emerged as a method for non-invasive evaluation of tissue characteristics. However, LA LGE image segmentation is challenging due to the relatively low contrast of the LA myocardium against surrounding structures. In contrast, T2-weighted imaging offers improve resolution of the LA myocardium. In this study, we compared standard versus T2-SPACE (**S**ampling **P**erfection with **A**pplication optimized **C**ontrasts using different flip angle **E**volution) based LA-LGE segmentation.

Methods: A total of 10 patients that underwent CMR prior to atrial fibrillation ablation were included in the study. In all patients, 3D LGE images with a slice thickness of 2.0 mm and 3D T2-SPACE images with a slice thickness of 1.5 mm were acquired. Two novice readers performed: a) standard segmentation, where the endocardium and epicardium were contoured on LGE image planes, and b) T2-SPACE based segmentation, where semiautomatic contours were created on the T2-SPACE image planes and subsequently copied to LGE image planes (Figure). Readers performed segmentation twice by each method. The calculated extent of myocardial enhancement using standard and T2-SPACE based segmentation by the novice readers, and the standard segmentation by an expert reader (>100 study/year) were compared.

Results: Using standard segmentation, the intra-class correlation coefficient (ICC) for the percentage of enhanced LA on repeated measurement was 0.92 (CI 0.68-0.98) and 0.66 (CI -0.30-0.92) for novice readers 1 and 2, respectively. With T2-SPACE based segmentation, the intra-observer reproducibility was 0.99 (CI 0.97-0.99) and 0.96 (CI 0.83-0.99) for readers 1 and 2, respectively. Among the novice readers, inter-observer reproducibility was 0.44 (CI -0.34-0.83) with standard segmentation, whereas it was improved to 0.93 (CI 0.64-0.98) with T2-SPACE segmentation. Compared to expert contours, the ICC of novice measurements was 0.58 (CI -0.69-0.90) with standard segmentation, and 0.84 (CI 0.37-0.96) with T2-SPACE segmentation.

Conclusions: The inter-observer reproducibility of standard LA-LGE image segmentation is low when performed by inexperienced readers. T2-SPACE segmentation significantly improves the inter-observer reproducibility, allowing reliable segmentation even for novice readers.

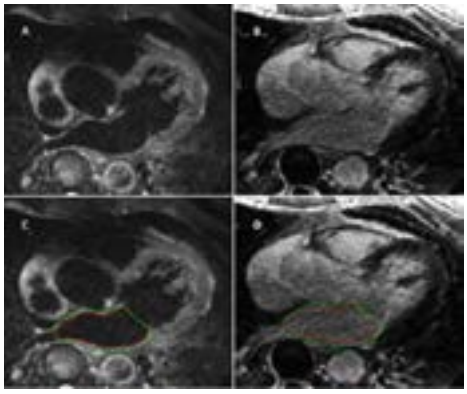

P012

Burden of Premature Ventricular Contractions and myocardial fibrosis as measured by Native Myocardial T1 Time: Is There An Association?

Amita Singh, MD[1] Keigo Kawaji, Ph.D.[2], Noreen Nazir, MD[3], Akhil Narang, MD[3], Karima Addetia, MD[4], Roderick Tung, MD[4], Erin E. Flatley, MSN, AGNP-BC[1], Roberto M. Lang, MD[3], Amit R. Patel, MD[3]

1. *University of Chicago Medical Center, Chicago, IL*
2. *University of Chicago, Chicago, IL*
3. *University of Chicago, IL*
4. *University of Chicago Medical Center, IL*

Background: A high burden of premature ventricular contractions (PVCs) are a known cause of cardiomyopathy (CM). The long-term effects of PVC on myocardial characteristics are not well-described. We hypothesized that the presence and extent of PVC burden would be associated with an increase in native myocardial T1 relaxation time, suggesting alterations in the underlying myocardial tissue characteristics.

Methods: Fifteen patients (48±18 years, 67% female) with a wide range of PVC burden (mean 11±10%, range 1-30%) demonstrated by Holter Monitor who were referred for CMR (1.5T, Achieva, Philips) were included for analysis. The protocol included Cine-CMR (steady state free precession (SSFP)), pre-contrast TI-mapping (MOdified Look Locker Inversion recovery (MOLLI) Imaging using a 5-3s-3 scheme), and late gadolinium enhancement ((LGE), phase sensitive inversion recovery (PSIR)) images were acquired in the 2-, 3-, and 4-chamber views and in consecutive short axis slices spanning the entire left ventricle (LV). Cine-CMR images were used to measure end-diastolic and end-systolic LV volumes (EDVi and ESVi) and ejection fraction (EF) using the method of discs. LGE was visually assessed as present or absent in each patient. The septal native myocardial T1 relaxation times were measured in the basal, mid and apical slices, as well as average T1 relaxation time for the entire basal, mid or apical slices using standard pixel-wise 3-parameter fitting. T1 gradient across segments was calculated using the difference between basal and apical T1 times. For comparison, patients were divided by PVC burden, and compared to 8 normal subjects who served as referent normal T1 relaxation times.

Results: Patients with PVC cardiomyopathy had enlarged LV volumes with lower left ventricular ejection fractions (Table 1). Frequency of LGE was 27% overall, remaining unchanged irrespective of PVC burden. In patients with PVC's, native T1 time was significantly longer in all segments when compared to normal subjects (p10%), native T1 time was non-significantly elevated in patients with a higher burden of PVC without a significant difference in LV volumes or EF.

Conclusions: These findings suggest that frequent PVCs are associated with increases in native myocardial T1 relaxation time, most pronounced in the basal segments, independently of LV size, function, and presence of LGE.

	All	PVC Burden<10%	PVC Burden>10%	Controls
Age (years)	48 ±18	48 ± 21	49 ± 19	
Female (%)	67	57	75	
PVC Burden (%)	10 ±10	1.1 ± 0.3	19 ± 8	
Subjects with LGE present	4	2	2	
Septal T1 relaxation time (ms)				
Basal	1118±61	1091 ± 61	1144 ± 50	1007 ± 46
Mid	1066 ±61	1042 ± 77	1091 ± 51	996 ± 32
Apical	1090 ± 62	1065 ± 66	1115 ± 51	1019 ± 61
Global T1 relaxation time (ms)				
Basal	1125 ±74	1110 ± 64	1139 ± 86	977 ± 44
Mid	1069 ± 68	1046 ±61	1093 ± 71	992 ± 42
Apical	1054 ± 57	1025 ± 56	1083 ± 45	1034 ± 67
T1 Gradient (ms)	54 ± 34	50 ± 30	58 ± 39	22 ± 17
LVEDVi	94 ± 14	96 ± 15	91 ± 14	
LVESVi	45 ± 12	43 ± 12	47 ± 13	
LV Ejection Fraction	52 ± 9	55 ± 6	49 ± 12	

P013

Impact of Left Ventricular Geometry in Predicting Ventricular Tachyarrhythmia in Patients with Left Ventricular Dysfunction: A Comprehensive Cardiovascular Magnetic Resonance Study

Shiro Nakamori, MD, PhD[1]Haisam Ismail, MD[1], Long Ngo, PhD[1], Alfred Buxton, MD[1], Warren J. Manning, MD[2], Reza Nezafat, PhD[3]

1. *Beth Israel Deaconess Medical Center, MA*
2. *Beth Israel Deaconess Medical Center, Boston, MA*
3. *Department of Medicine (Cardiovascular Division) Beth Israel Deaconess Medical Center, Harvard Medical School, Cardiology, East Campus, Room E/SH455, 330 Brookline Ave, Boston, MA, 02215, MA*

Background: The implantable cardioverter-defibrillator (ICD) therapy is an established therapy for reducing mortality in patients with a history of life-threating ventricular arrhythmia. However, only a minority of primary prevention ICD recipients under current guidelines actually receive appropriate ICD therapy. 2D transthoracic echocardiography (echo) evidence of adverse left ventricular (LV) remodeling is associated with appropriate ICD therapy [1,2]. We sought to determine whether volumetric cardiovascular magnetic resonance (CMR) LV geometry predicts future ventricular arrhythmias in primary ICD patients with reduced LV ejection fraction (EF).

Methods: Sixty-three consecutive patients with echo LVEF < 35% who underwent CMR prior to ICD implantation for primary implantation were studied. Sphericity index was measured as the ratio of LV end-diastolic volume (from short axis stack cine CMR) to the volume of a sphere with the diameter equal to LV end-diastolic 4-chamber length. The presence of late gadolinium-enhancement (LGE) was also assessed.

Results: During a median follow-up of 43 months (interquartile range, 27-76), 13 patients received appropriate ICD therapy (21%). Appropriate ICD therapies were delivered in 10/41 (24%) with conventional ICDs and 3/22 (14%) with biventricular ICDs (p=0.32). Patients with ischemic cardiomyopathy appeared more likely to receive appropriate ICD therapy (69% vs 40%, p=0.06). Multivariable Cox regression analyses revealed that CMR sphericity index is an independent predictor of ventricular arrhythmia requiring ICD therapy controlling for age and LVEF (hazard ratio: 1.10, 95% confidence interval: 1.02 to 1.19, p=0.01). Kaplan-Meier curves showed worse ICD therapy-free survival in patients with sphericity index value of 0.57 or greater, that was determined by the receiver operating characteristics curve analysis in predicting appropriate ICD therapy (Figure 1). Integration of sphericity index and LV mass index values to LVEF yielded 2 correct (up) reclassifications and 2 incorrect (down) reclassifications in the 13 patients receiving appropriate ICD therapy. Additionally, 18 correct (down) reclassifications and 6 incorrect (up) reclassifications occurred in the 50 patients without ICD therapy. When sphericity index, LVEF and LV mass index were used in combination, important incremental prognostic information was achieved (continuous net reclassification improvement; 0.78; 95% CI 0.22 to 1.35).

Conclusions: The combinational assessment of LV geometry, mass index and function provides incremental prognostic information for ventricular arrhythmia that requires appropriate ICD therapy in patients with reduced LVEF. Larger, multicenter prospective studies are needed to further confirm these observations.

Reference:

[1] Biton Y et al., JACC, 2016.

[2] Levine YC et al., Heart Rhythm, 2016.

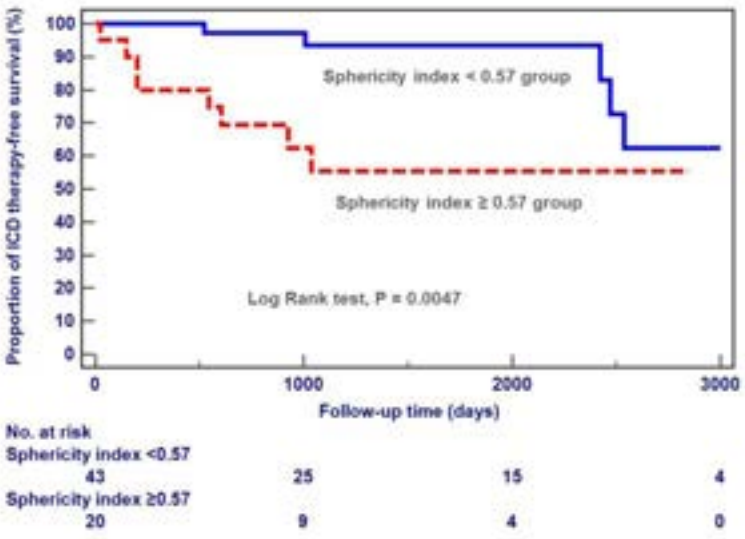

P014

Cardiovascular Magnetic Resonance Imaging in Acute Decompensated Heart Failure with Reduced Ejection Fraction

Christoph J. Jensen, MD[1]Roman Voss, MD[2], Ingmar Seifert, MD[1], Kai Nassenstein, MD[3], Thomas Schlosser, MD[3], Oliver Bruder, MD[2]

1. *Elisabeth Hospital, Department of Cardiology & Angiology, Essen, Germany, Essen, Nordrhein-Westfalen, Germany*
2. *Elisabeth Hospital, Department of Cardiology & Angiology, Essen, Germany, Nordrhein-Westfalen, Germany*
3. *University Hospital Essen, Department of Diagnostic and Interventional Radiology and Neuroradiology, Essen, Germany, Nordrhein-Westfalen, Germany*

Background: Heart failure is a complex clinical syndrome with growing prevalence and substantial impact on health care. Furthermore, mortality is enormous in these patients. Heart failure with reduced ejection fraction (HFrEF) may result from a variety of causes and delayed enhancement cardiovascular magnetic resonance imaging (DE-CMR) seems ideal to define the etiology thereof. A head to head real-world comparison of clinical parameters, biomarkers and DE-CMR in this population has not yet been performed.

AIm of this study was to evaluate the capability of DE-CMR to define the etiology of heart failure compared to clinical parameters and biomarkers in patients with acute decompensated HFrEF.

Methods: In this study consecutive patients hospitalized with acute decompensated heart failure and newly diagnosed reduced left ventricular function by echocardiography (EF≤45%) were included. Patients presenting with an acute coronary syndrome (ACS), preserved EF or contraindications to DE-CMR were excluded. All patients underwent DE-CMR within the index hospitalization.

Results: 339 consecutive patients were included (mean age 60±15 years, 62% male gender) in this study, whereof 241 patients (71%) experienced symptoms within 30 days prior to hospitalization. 166 (49%) patients presented with an EF between 30 and 45%, whereas 173 patients (51%) showed an EF of less than 30%. Despite excluding patients with an ACS a priori, DE-CMR detected silent myocardial infarction in 61 patients (18%). There was no statistical difference between ischemic and non-ischemic cardiomyopathies in EF, clinical parameters and biomarkers. Flu-like symptoms were more common in non-ischemic heart failure ($p < 0.05$).

Conclusions: In patients with acute decompensated heart failure and reduced ejection fraction, clinical parameters and biomarkers do not differentiate ischemic and non-ischemic causes of heart failure. Contrary, DE-CMR allows for accurate differentiation thereof and further refining the etiology of heart failure. Thus, DE-CMR facilitates patient management and impacts prognosis in the individual patient in a real-world setting.

P015

Characteristics of myocardial mechanics evaluated by feature-tracking MRI and its relationship with myocardial amyloid burden in AL amyloidosis

Ke Wan, MD[1]Hong Liu, MS[2], Dan Yang, msci[3], Jiayu Sun, MD[4], Wei Cheng, BS[5], Yucheng Chen, MD[6]

1. *Cardiology Division, West China Hospital, Sichuan University, Guoxue Xiang No. 37, Chengdu, Sichuan Province 610041, China, Sichuan, China (People's Republic)*
2. *Cardiology Department West China Hospital Sichuan University, Chengdu, Sichuan, China (People's Republic)*
3. *West China Hospital,Sichuan University, Sichuan, China (People's Republic)*
4. *west china hospital, Sichuan, China (People's Republic)*
5. *West China Hospital Sichuan University, Sichuan, China (People's Republic)*
6. *West China Hospital, CHENGDU, Sichuan, China (People's Republic)*

Background: Strain derived from FT-CMR has been demonstrated to be sensitive for the detection of myocardial impairment. However, myocardial deformation measured by FT-CMR in cardiac amyloidosis has not been investigated thoroughly.

Methods: Seventy-eight consecutive patients with biopsy-proven AL amyloidosis and 50 healthy subjects were recruited and received contrast-enhanced CMR. LV myocardial strains were measured using FT-CMR. Global and regional strains were analyzed and compared between different groups (controls, AL amyloidosis without/with cardiac involvement). Associations between myocardial strains and different extent of LGE (no LGE, sub-endocardial LGE, transmural LGE) or ECV were analyzed.

Results: Global longitudinal strain (GLS), global circumferential strain (GCS) and global radial strain (GRS) were reduced significantly in AL-amyloidosis patients with cardiac involvement, as were GLS and GCS in patients without cardiac involvement. Segmental strain analyses showed that circumferential strain was impaired in basal segments, but was normal in other segments in patients without cardiac involvement. GLS and circumferential strain in basal segments differed significantly and decreased gradually among patients with an incremental extent of LGE. In patients with AL amyloidosis, there were significant correlations between myocardial strains and ECV (GLS: $r=0.747$, $p < 0.001$; GCS: $r=0.783$, $p < 0.001$; GRS: $r=-0.633$ $p < 0.001$).

Conclusions: FT-CMR is a robust method to evaluate myocardial mechanics in AL amyloidosis that could be used to early detect and evaluate the different extent of cardiac amyloid infiltration.

P016

Differences in CMR global strain assessment in ischaemic and non-ischaemic cardiomyopathy: sub-group analysis of the VINDICATE trial.

James Foley, MBChB BSc (Hons)[1]Peter P. Swoboda, PhD[1], Graham J. Fent, MBChB, BSc (Hons)[1], Adam K. McDiarmid, MD[2], Pankaj Garg, MD[3], David Ripley, MBChB[2], Tarique Musa, MBBS[2], Sven Plein, MD PhD[4], Klaus Witte, MD[1], John P. Greenwood, PhD[2]

1. *University of Leeds, Leeds, England, United Kingdom*
2. *University of Leeds, England, United Kingdom*
3. *University of Leeds, UK, England, United Kingdom*
4. *St. Thomas' Hospital, London; King's College London; University of Leeds, England, United Kingdom*

Background: Prognosis and treatment of patients with chronic heart failure (CHF) differs according to whether it is ischaemic (ICM) or non-ischaemic cardiomyopathy (NICM). Multi-parametric cardiovascular magnetic resonance (CMR) can distinguish these aetiologies; strain imaging however may confer incremental diagnostic and prognostic information over left ventricular ejection fraction (LVEF). We hypothesised in a prospectively recruited random sample of CHF patients, ICM and NICM have different myocardial strain patterns.

Methods: The VINDICATE trial investigated efficacy of high dose vitamin D in patients with CHF. A subgroup of the trial underwent CMR, blood and cardiopulmonary exercise tests at baseline. 53 patients (31 ICM, 22 NICM) underwent identical 3.0T CMR protocols (Achievia, Philips Healthcare, The Netherlands). Tissue tagging by spatial modulation of magnetization (SPAMM) (spatial resolution 1.51x1.57x10mm^3, tag separation 7mm, ≥18 phases, typical TR/TE 5.8/3.5ms, flip angle 10^o, typical temporal resolution 55ms) was acquired in short axis slices acquired at the apex, mid-ventricle, and base. CMR data were analysed quantitatively using commercially available software (CVI42, Circle Cardiovascular Imaging Inc. Canada and inTag v1.0, CREATIS lab, France). Endocardial and epicardial contours were drawn on SPAMM sequences using a semi-automated process. Peak circumferential LV strain (E_{cc}) was measured at apex, mid-ventricle, and base. LV twist was calculated by subtracting basal from apical rotation. Torsion was determined: Torsion=Peak Twist×(Apical Radius+Basal Radius)/2×Apex to Base length. Late gadolinium enhancement (LGE) was performed 15 minutes following administration of 0.15 mmol/kg gadolinium DTPA.

Results: Both groups were comparable for baseline demographics (Table 1). The ICM group had significantly more prior revascularisation (CABG/PCI). There was no significant difference between the 2 groups in both LV dimensions and LVEF, however ICM had significantly more LGE (Table 2). There was no significant difference between the 2 groups in E_{cc}. NICM patients had significantly lower LV twist and torsion compared to the ICM group 6.0±3.68^o vs 8.8±4.32^o P=0.020 and 6.3±3.79 vs 8.8±4.69 P=0.048 respectively.

Conclusions: Despite having similar EF and E_{cc}, patients with NICM had significantly less LV torsion than with ICM. Myocyte dysfunction in ICM is more sub-endocardial due to the wave-front of ischaemia and more global in NICM. Increased torsion in ICM likely results due to an increased compensatory recruitment of sub-epicardial fibres.

Recognition of different torsion patterns of ICM and NICM may give insight into the aetiology of CHF, which may assist patient diagnosis and management, especially in those unable to have contrast agents.

Baseline demographics

P-value	NICM	ICM	
0.182	59.0±16.9	65.2±15.9	Age, years
0.582	36%	29%	Sex (female)
0.970	170.0±7.4	170.1±8.1	Height, cm
0.773	79.7±16.6	78.5±14.2	Weight, kg
0.654	27.6±5.6	26.9±3.9	BMI kg/m^2
0.399	115±18	119±21	SBP, mmHg
0.601	72±11	70±11	DBP, mmHg
0.195	4.5	19	Diabetes Mellitus, %
0.03	0	32	CABG, %
<0.001	0	55	PCI, %
0.949	64	65	AF, %
0.421	1118 ±1172	1084 ±1196	BNP pg/mL
0.162	19.7±7.7	16.8±5.0	VO2max, mlO_2/min/kg

BMI – Body mass index, SBP – systolic blood pressure, DBP – diastolic blood pressure, CABG – coronary artery bypass graft surgery, PCI – percutaneous coronary intervention, AF – atrial fibrillation, BNP - B-type natriuretic peptide, VO2max – maximal oxygen uptake, CMR and strain characteristics

P-value	NICM	ICM	
0.264	226±113.9	199.4±56.7	LVEDV, ml
0.343	115.3±48.5	104.9±30.5	LVEDVi, ml/m^2
0.767	36.0±11.7	35.1±10.6	LVEF, %
0.023	6.0±3.68	8.8±4.32	LV twist, ^{o}
0.048	6.3±3.79	8.8±4.69	LV torsion, ^{o}
0.689	-0.101±0.739	-0.101±0.646	E_{cc} Apex
0.828	-0.107±0.066	-0.103±0.068	E_{cc} Mid
0.064	-0.114±0.048	-0.082±0.068	E_{cc} Base
<0.001	0/22 (0%)	21/31 (68%)	LGE, infarct pattern n/ (%)
<0.001	3/22 (14%)	0/31 (0%)	LGE, mid wall pattern n/ (%)

LVEDV – left ventricular end diastolic volume, LVEDVi - left ventricular end diastolic volume index,
LVEF – left ventricular ejection fraction, E_{cc} – circumferential strain, LGE – late gadolinium enhancement

P017

Gender related differences in coronary endothelial function measured with MRI

Lena Matthews, MD[1]Micaela Iantorno, MD[1], Michael Schär, PhD[1], Gary Gerstenblith, MD[1], Matthias Stuber, PhD[2], Robert G. Weiss, MD[3], Allison G. Hays, MD[3]

1. *Johns Hopkins, MD*
2. *CHUV, University of Lausanne, Geneve, Switzerland*
3. *Johns Hopkins University School of Medicine, MD*

Background: Impaired coronary endothelial function (CEF) occurs at the earliest stage of atherosclerosis and predicts adverse cardiovascular (CV) outcomes. The risk of atherosclerotic cardiovascular (CV) events is lower in pre-menopausal, than it is in post-menopausal women and in men but CEF, a barometer of vascular health, has not been fully characterized in healthy individuals without traditional CV risk factors. Novel non-invasive MR methods can quantify CEF and can provide insight regarding the pathogenesis of gender-related differences in atherosclerotic development. We therefore used MR to quantify CEF as measured by changes in coronary area and flow in response to isometric handgrip exercise (IHE), an endothelial dependent stressor, to test the hypotheses that CEF is better in younger women than in age-matched men and that the gender difference is no longer present in older men and post-menopausal women.

Methods: Healthy women (n=23; age 44±8 yrs, all data shown:mean±SEM) and men (n=20; 42±8 yrs) with no history of CAD or traditional CV risk factors and Agatston coronary calcium score (on prior CT) < 10 for those ≥ 50 years, underwent CEF 3T MR measures of % change in coronary cross-sectional area (CSA) and coronary blood flow (CBF) from rest to IHE as previously described.[1] All women ≥50 yrs were post-menopausal and those under 50 yrs were premenopausal.

Results: The % changes in both CSA and CBF with IHE were significantly and nearly two-fold higher in young women than in young men (%CSA: 19.2±3.1% vs 9.3±2.3% p=0.01 and %CBF: 57.5±8.2% vs 33.5±4.2 p=0.01 respectively) (Fig 1a), but there were no gender differences in %CSA and %CBF changes in older men and women (Fig 1b).

Conclusions: Using noninvasive MR measures of CEF in healthy people, we observe that CEF is significantly better (nearly two-fold) in young premenopausal women (< 50 yrs) than in age-matched men; but there are no gender differences between older, post-menopausal women and older men. These results may contribute to our understanding of gender-specific differences in atherosclerotic development especially in the postmenopausal state and inform future trials designed to improve endothelial function for asymptomatic, but at-risk individuals.

References

1. Hays AG, Kelle S, Hirsch GA, et al. Regional coronary endothelial function is closely related to local early coronary atherosclerosis in patients with mild coronary artery disease: Pilot study. *Circulation. Cardiovascular imaging.* 2012;5:341-348

Figure 1

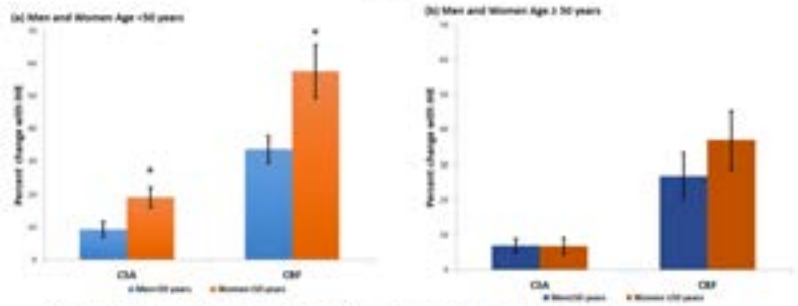

P018

Comparison of Cardiac Perfusion between Healthy Volunteers and Cardiac Transplant Patients with Various Degrees of Cardiac Allograft Vasculopathy

Travis B. DeSa, B.A. [1]Jeremy D. Collins, MD[2], James Carr, MD[2], Kai Lin, MD[3], Michael Markl, PhD[3]

1. *Northwestern Feinberg School of Medicine, Chicago, IL*
2. *Northwestern Memorial Hospital, Chicago, IL*
3. *Northwestern University, Chicago, IL*

Background: Cardiac Allograft Vasculopathy(CAV) is a significant cause of cardiac transplant(Tx) failure. Angiogram and intravascular ultrasound(IVUS) are primary and secondary methods of diagnosis, but both are invasive. Cardiac MRI(CMR) has become a promising noninvasive method to evaluate myocardial ischemia in CV disease. However, CMR has not been thoroughly studied in detecting CAV. We studied myocardial perfusion and CAV in 15 healthy volunteers and 25 Tx patients.

Methods: 15 volunteers without history of CVD and 25 Tx patients were recruited after IRB approval and written informed consent. MRI's were performed at 1.5 T systems(Magnetom Aera/Avanto, Siemens,Germany). Volunteers and patients underwent CMR enclosing first pass perfusion imaging after injection of Gd contrast and short axis CINE SSFP imaging for the assessment of global cardiac function. Perfusion images were acquired in left ventricular short axis orientation with three slices positioned at basal, middle, and apical locations after injection of gadopentetate dimeglumine(Magnevist,0.1 ml/Kg). Perfusion data reconstruction included inline and fully automated motion correction to compensate for cardiac and respiratory motion. Perfusion Imaging parameters were as follows: FOV=360x360 mm^2, Slice thickness=8mm, TR/TE/flip angle=168/1.14ms/12degree. CINE data were analyzed on a computer(Siemens Leonardo Syngo) using ARGUS software. A single reviewer semi-automatically drew the borders(endo and epi-cardial) of the LV at each slice and global cardiac function parameters were calculated. Perfusion data include LV contour segmentation, peak perfusion signal intensity, peak slope of the signal change, and time to peak perfusion(TTP). Data were evaluated in myocardial segments based on the AHA 16-segment model. In addition, the results of angiograms, IVUS, and echocardiograms from the date closest to each patient's CMR were collected. Differences in global perfusion parameters were assessed between 4 groups: volunteers, Tx without CAV(CAV-), Tx with CAV(CAV+), and Tx without CAV but with intimal medial thickening (IMT+ CAV-). CAV was defined as any sign of CAV measured by angiogram and IMT was defined as IMT$\geq$0.5 mm measured by IVUS. There were no CAV+IMT+ patients.

Results: 7 Tx had signs of CAV (5 w/ minimal, 2 w/ overt CAV). 8 Tx had IVUS records, 7 of whom had IMT. Significant differences were seen in perfusion between the IMT+CAV- and control groups (p=.025), the IMT+CAV- and CAV- groups (p=.005), and the IMT+CAV- and CAV+ groups (p=.011). Table 1 lists mean perfusion, slope, TTP, and EF of each group. No correlation was seen between perfusion parameters and echo.

Conclusions: The IMT+CAV- group showed significant differences compared to the other populations. This may reflect the fact that IVUS is a more sensitive method of CAV detection relative to angiogram. In addition, the lack of correlation between the perfusion parameters and echo may indicate that changes in perfusion precede global EF dysfunction.

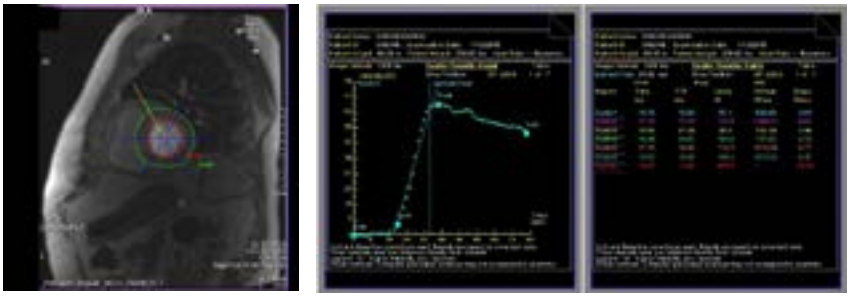

(Table 1) Comparison of Perfusion Parameters and Ejection Fraction for Transplant Subgroups and Controls

(4) IMT+CAV-	(3) CAV+	(2) CAV-	(1) Controls	Group
7	7	8	15	# subjects
48.4 $\pm$ 17.4	50.3 $\pm$ 17.3	48.7 $\pm$ 17.2	52 $\pm$ 17	Mean Age
6, 1	5, 2	12, 6	13, 2	Gender (m,f)
57.3 $\pm$ 6.32	56.1 $\pm$ 5.55	59.3 $\pm$ 5.11	not recorded	Mean EF
64.8 $\pm$ 19.2	105 $\pm$ 28.6	107 $\pm$ 47.8	86.1 $\pm$ 19.1	Mean Perfusion
2.24 $\pm$ 1.08	5.78 $\pm$ 3.77	4.74 $\pm$ 3.65	4.09 $\pm$ 1.87	Mean Slope
35.4 $\pm$ 11	28.9 $\pm$ 15.5	30.3 $\pm$ 11.4	26.8 $\pm$ 10.3	Mean TTP
(1) 0.025, (2) 0.005, (3) 0.011	(4) 0.011	(4) 0.005	(4) 0.025	significant differences in mean perfusion (associated group and p-value)

P019

Mechanisms of Abnormal Myocardial Perfusion In Post-Heart Transplant Patients

Akhil Narang, MD[1]John E. Blair, MD[2], Victor Mor-Avi, PhD[2], Keigo Kawaji, Ph.D.[1], Savitri E. Fedson, MD[3], Nir Uriel, MD[2], Roberto M. Lang, MD[2], Amit R. Patel, MD[2]

1. *University of Chicago, Chicago, IL*
2. *University of Chicago, IL*
3. *Baylor College of Medicine, TX*

Background: Previous studies have shown myocardial perfusion reserve (MPR) changes over time in post-heart transplant (HTx) patients compared to normal controls. The aim of this study was to investigate potential mechanisms (transplant rejection, coronary allograft vascuolpathy (CAV), presence of left ventricle (LV) dysfunction, or presence of underlying myocardial fibrosis) responsible for abnormal MPR late after HTx.

Methods: Twenty post-HTx patients and ten healthy controls underwent vasodilator cardiovascular magnetic resonance imaging (vCMR), including cine-CMR, myocardial perfusion imaging during hyperemia and recovery, and late gadolinium enhancement (LGE) using standard clinical pulse sequences. Cine-CMR images were used to calculate LV volumes and ejection fraction. Time-intensity curves generated from stress and recovery perfusion images were used to determine MPR index (MPRi), calculated as the up-slope ratio of stress to recovery (normalized to the LV cavity up-slope and rate-pressure-product). Quantitative LGE analysis (full-width, half maximum) was performed to determine the burden of LGE. The occurrence of HTx rejection was determined by review of tissue obtained during endomyocardial biopsy. The presence of CAV and its associated microvascular dysfunction was evaluated by review of coronary angiograms whereby severity was graded according to standardized classification and TIMI Frame Counts.

Results: The mean time from HTx to vCMR was 8.1 ± 4.1 years. MPRi in post-HTx patients was 0.50 (0.41, 0.54) was reduced compared to normal controls 0.74 (0.55, 0.88) (P=0.003). The majority of post-HTx patients (19/20) experienced one or more episodes of cellular or humoral rejection. There was no significant difference in MPRi when assessing total episodes or severity of rejection. Additionally, the correlation between LGE burden and MPRi was weak (R=0.36). When evaluating CAV, MPRi was noted to be lower in patients with more severe CAV (grade ≥2) compared to patients with none or mild CAV (grade 0 or 1) (0.34 ± 0.08 versus 0.51 ± 0.09, P=0.007) **(Figure A)**. Similarly, there was a correlation between MPRi and TIMI Frame Count (R=0.68, P=0.0009) **(Figure B)**. The mean LVEF by CMR was 60 ± 6%, and there was no association between LVEF and MPRi.

Conclusions: This study demonstrates that abnormally reduced MPRi late after HTx is related to CAV and specifically microvascular dysfunction. We found no relationship between abnormal MPRi and episodes of cellular or humoral rejection, the presence of myocardial scar/fibrosis (LGE), or LVEF. MPRi measured using vCMR is a potentially valuable tool to aid in the detection of CAV.

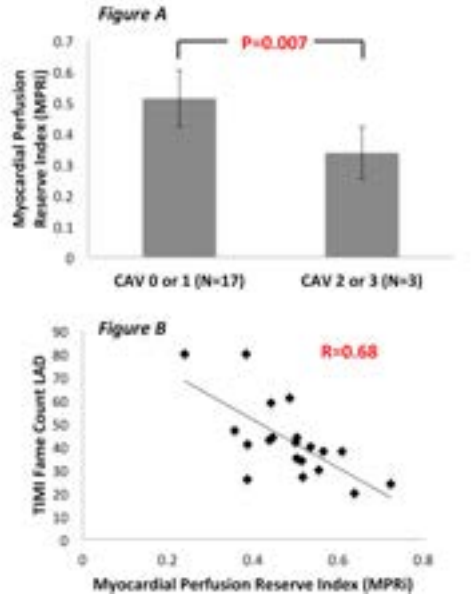

P020

Microvascular Obstruction following Acute Reperfused Myocardial Infarction characterized by multiparametric CMR

Enver Guner. Tahir, MD[1]Maxim Avanesov, MD[2], Martin Sinn, student[2], Dennis Saering, PhD[3], Sebastian Bohnen, MD[2], Ulf Radunski, MD[2], Kai Muellerleile, MD[2], Christian Stehning, PhD[4], Jitka Starekova, MD[2], Gerhard Adam, MD[2], Gunnar Lund, MD[2]

1. *University Medical Center Hamburg-Eppendorf, Hamburg, Hamburg, Germany*
2. *University Medical Center Hamburg-Eppendorg, Hamburg, Germany*
3. *FH Wedel Gemeinnützige Schulgesellschaft mbH, Hamburg, Germany*
4. *Philips Research Laboratories, Hamburg, Germany*

Background: Microvascular obstruction (MO) is a common result of reperfusion therapy after acute myocardial infarction (AMI) and a prognostic biomarker of subsequent adverse left ventricular remodeling. The aim of this study was to characterize MO following AMI using the novel quantitative techniques of T1 and T2 mapping in comparison to standard CMR.

Methods: In total sixty-seven patients with first-time reperfused AMI underwent CMR (1.5 Tesla Philips Achieva) at 7 ±3 days following AMI. MO had an incidence of 30% (20 patients). T1 Mapping was performed using the modified Look-Locker inversion recovery (MOLLI) sequence. A free-breathing, navigator-gated multi-echo sequence was used for short-axis T2 Mapping. T1 and T2 Maps were generated using a dedicated plug-in for the OsiriX software. Conventional CMR imaging was performed using black-blood T2-weighted (T2w) STIR and late gadolinium enhancement (LGE) sequences. Extracellular volume (ECV) calculations were done after post-processing. Two experienced observers independently evaluated the CMR data using the in-house developed HeAT-Software. MO area was manually identified and delineated using LGE images. Subsequently, the contours were used to determine lesion sizes and relaxation times (Figure 1). MO was defined using a threshold method as an area within LGE having a SI lower than 2SD compared to myocardium with LGE. Area of MO is given as a percentage of the left ventricle.

Results: MO sizes were determined as a percentage of the left ventricle and of the total infarct size was (Table 1). T1 and T2 relaxation times in the MO area were significantly lower than in the peripheral infarct zone and higher than in the remote myocardium (Table 2). ECV in the MO area was lower than in the infarct area and higher than in the remote myocardium (Table 2).

Conclusions: Multiparametric CMR assessment of the biomarker MO is promising in improving its extent and severity quantification, which may be useful in novel therapies to predict and reduce ischemic reperfusion injury.

http://www.ConferenceAbstracts.com/uploads/cfp2/attachments/LDFAIBDN/LDFAIBDN--219519-1-ANY.pdf

% MO of Infarct	MO	Infarct	Lesion size (%LV)
14	5 ±6	36 ±10	T2w
30	10 ±11	30 ±8	Native T1
30	10 ±9	33 ±9	T2
17	5 ±8	30 ±11	LGE
38	10 ±11	26 ±10	Post contrast T1
22	7 ±8	32 ±11	ECV

Post hoc	P value	Remote	MO	Infarct	Relaxation times (ms) or ECV (%)
<0.001 for all groups	<0.001	1044 ±40	1120 ±114	1309 ±119	Native T1
0.001 (Infarct vs. MO) <0.001 (Remote vs. Infarct and MO)	<0.001	54 ±3	68 ±8	85 ±11	T2
<0.001 (Infarct vs. Remote) 0.009 (Infarct vs. MO) ns (MO vs. Remote)	<0.001	552 ±59	515 ±144	402 ±57	Post contrast T1
<0.001 (Infarct vs. MO and Remote) 0.016 (MO vs. Remote)	<0.001	27 ±3	33±11	55 ±11	ECV

P021

Prognostic significance of combined native T1 mapping and tissue tracking analysis in the assessment of adverse LV remodeling following acute STEMI- an Oxford Acute Myocardial Infarction (OxAMI) study

Malgorzata Wamil, MD PhD[1] Alessandra Borlotti, PhD[2], Alessia Bracco, MD[3], Dan Liu, PhD[4], Mohammad Alkhalil, M.D, MRCP[4], Sam Dawkins, MRCP[5], Gregor Fahrni, MD[4], Giovanni Luigi De Maria, MD[6], Mathias Wolfrum, MD[7], Stefan K. Piechnik, PhD, MScEE[4], Vanessa M. Ferreira, MD, DPhil[4], Adrian Banning, MD[8], Rajesh K. Kharbanda, MBChB, PhD[9], Stefan Neubauer, MD, FRCP[4], Robin Choudhury, MD[2], Keith M. Channon, MD, FRCP[4], Erica Dall'Armellina, MD, PhD[10]

1. *University of Oxford, Horspath, England, United Kingdom*
2. *University of Oxford, Oxford, England, United Kingdom*
3. *University of Oxford, Veneto, Italy*
4. *University of Oxford, England, United Kingdom*
5. *University of Oxford, N/A, United Kingdom*
6. *Oxford University Hospitals, England, United Kingdom*
7. *Oxford University Hospitals, N/A, United Kingdom*
8. *Oxford heart center, England, United Kingdom*
9. *Oxford Heart Centre, England, United Kingdom*
10. *Oxford University, England, United Kingdom*

Background: Myocardial infarct (MI) size and left ventricular (LV) remodeling after ST-segment–elevation myocardial infarction (STEMI) are important determinants of clinical outcome, for which accurate early stratification would be of major clinical importance. Strain quantifies regional myocardial deformation and can demonstrate abnormal global and segmental myocardial function in acute ischemia. T1 mapping allows assessment of acute myocardial oedema and the severity of acute ischemic injury without use of gadolinium contrast agent. We aimed to explore relationship between T1 mapping and strain, to establish whether analysis of combined T1 mapping and strain could predict functional recovery after STEMI.

Methods: Patients with STEMI prospectively recruited to the OxAMI study underwent 3-T CMR acute scans (within 53 ± 32hours from PCI) and at 6 months (6M). Imaging protocol included: cine, pre-contrast native T1 mapping, T2-weighted images and late gadolinium enhancement (LGE). CMR imaging analysis was performed using CVI[42] (Circle Cardiovascular Imaging, Canada). Segments were grouped in the infarct and remote zones based on the presence of LGE% (mean± 5SD).

Results: Out of 96 patients (aged 60±11) with acute CMR scans, 66 underwent follow-up scans. Both peak radial and circumferential strain were significantly decreased in infarct (2.7±11.2%; $p < 0.01$ for radial strain and -2.2± 9.3%, $p < 0.01$ for circumferential strain) compared to remote myocardium (radial strain 44.3±20.4%; $p < 0.01$ circumferential strain -22.0±5.8%; $p < 0.01$). These changes were mirrored by changes in T1values (infarct 1363±108 msec and remote 1175±35 msec; $p < 0.01$). Peak strain correlated with segmental T1 values and segmental LGE (radial vs T1 r=-0.567, $p < 0.01$; radial vs LGE r=-0.484, $p < 0.01$; circumferential vs T1 r= 0.594, $p < 0.01$; circumferential vs LGE r=0.530, $p < 0.01$). Receiver operating characteristic (ROC) analysis of the T1 mapping and strain indicated the combined T1 mapping and strain analysis was superior in the identification of the infarct and remote zones (Fig.1, AUC 0.904 vs AUC 0.823 for strain and AUC 0.837 for T1 mapping analysis). Moreover, significant correlation was observed between the percentage of LV oedema (assessed by T2-weighted images) and native T1 mapping or strain (-0.518, $p < 0.01$ for radial strain and 0.485, $p < 0.01$ for circumferential strain, 0.482, $p < 0.01$ for T1 values analysis). Furthermore, the multiple regression analysis confirmed strain combined with segmental T1 mapping predicted LVEF (r^2 0.153, p=0.003) and the scar size (r^2 0.332, $p < 0.001$) on the follow-up scan at 6M.

Conclusions: Non-contrast CMR method using combined T1 mapping and tissue tracking analysis of acute CMR scans is a strong predictor of improvement in contractile function following myocardial infarction when compared to LGE.

http://www.ConferenceAbstracts.com/uploads/cfp2/attachments/LDFAIBDN/LDFAIBDN--219614-1-ANY.pdf

P022

Improvements in quantitative myocardial perfusion and carotid atheroma in patients with refractory angina and raised lipoprotein(a) treated with lipoprotein apheresis

Tina Z. Khan, MRCP, MBChB[1]Li-Yueh Hsu, DSc[2], Andrew E. Arai, MD[3], Rick Wage, DCR (R)[4], Peter D. Gatehouse, PhD[5], Shivraman Giri, PhD[6], Dudley J. Pennell, MD[7]

1. *Royal Brompton and Harefield NHS Foundation Trust, Imperial College London., London, England, United Kingdom*
2. *National Heart, Lung and Blood Institute, National Institutes of Health, Bethesda, MD*
3. *National Institues of Health, Bethesda, MD*
4. *NIHR Cardiovascular Biomedical Research Unit, Royal Brompton Hospital, England, United Kingdom*
5. *NIHR Cardiovascular Biomedical Research Unit, Royal Brompton Hospital, London, England, United Kingdom*
6. *Siemens Healthcare, IL*
7. *Royal Brompton Hospital and Imperial College, London, England, United Kingdom*

Background: Fully quantitative CMR perfusion can quantify absolute myocardial blood flow with high spatial resolution, providing a physiological clinical marker in coronary disease. In addition, assessment of carotid atheroma using fully quantitative CMR techniques provides more accurate information about carotid plaque burden than conventional methods such as carotid intima-media thickness (IMT) measured with ultra-sound. These fully quantitative methods have not previously been applied as end points to convey results in a randomised controlled trial. Previously, no randomised controlled trials have been conducted in patients with refractory angina with raised lipoprotein(a) [Lp(a)], a known cardiovascular risk factor; to determine the therapeutic role of lipoprotein apheresis.

Methods: We conducted a randomised controlled crossover study of patients with refractory angina and raised Lp(a), randomised to three months of weekly lipoprotein apheresis or sham apheresis. Patients then crossed over to the opposite study arm after a 1 month wash-out phase. The primary outcome measure was change in the Myocardial Perfusion Reserve (MPR) from baseline to after three months of lipoprotein apheresis. MPR was calculated as the ratio of quantitative average perfusion at adenosine induced stress to rest. We used a prototype saturation-recovery prepared balanced steady-state free precession (bSSFP) sequence including a low-resolution gradient echo (GRE) acquisition for estimation of arterial-input-function, a technique known as “dual-sequence acquisition”. Pixel-wise myocardial time-signal intensity curves were derived using a model-constrained deconvolution to estimate myocardial blood flow (MBF). Quantitative CMR carotid wall volume assessment was used as a secondary outcome measure.

Results: The primary endpoint, MPR increased following apheresis (0.47; 95% CI 0.31 to 0.63) compared with sham (-0.16; 95% CI -0.33 to 0.02) yielding a net treatment increase of 0.63 (95% CI 0.37 to 0.89; $p < 0.001$ between groups).The secondary endpoint median total carotid wall volume (mm^3) reduced during apheresis by -335 [IQR -423, -247] from 2482 [IQR 1910, 2836] before to 2251 [IQR 1719, 2437] after apheresis, but during sham increased from 2342 [IQR 1997, 2644] to 2455 [IQR 2166, 2831] ($p < 0.001$ between groups).

Conclusions: This is the first randomised controlled trial in which fully quantitative CMR perfusion and carotid wall volume measurement have been utilised as primary and secondary end points, representing a milestone towards advancing the application of quantitative CMR in cardiovascular research. These quantitative techniques have enabled us to demonstrate that lipoprotein apheresis is an effective novel treatment for patients with refractory angina and raised Lp(a), improving myocardial perfusion and atheroma burden.

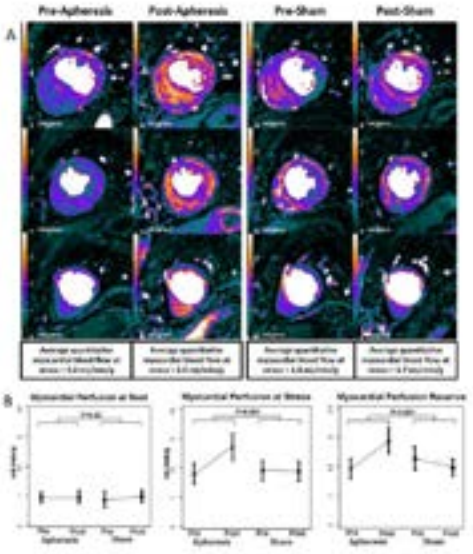

P023

Heart-Rate Independent T2 Mapping for Overcoming Loss of BOLD Sensitivity in Conventional T2 CMR Acquired Under Vasodilator Stress

Hsin-Jung Yang, PhD[1] Damini Dey, PhD[2], Jane Sykes, BS[3], John Butler, BSc MRT(MR)[4], Xiaoming Bi, PhD[5], Behzad Sharif, PhD[6], Ivan Cokic, MD[2], Sotirios Tsaftaris, PhD[7], Debiao Li, PhD[8], Piotr Slomka, PhD[2], Frank S Prato, PhD[9], Rohan Dharmakumar[10]

1. *Cedars Sinai Medical Center, Los Angeles, CA*
2. *Cedars Sinai Medical Center, CA*
3. *Lawson Health Research Institute, ON, Canada*
4. *Lawson Health Research Institute, London, ON, Canada*
5. *Siemens Healthcare, CA*
6. *Cedars-Sinai Medical Center, Los Angeles, Los Angeles, CA*
7. *The University of Edinburgh, Scotland, United Kingdom*
8. *Biomedical Imaging Research Institute, Cedars-Sinai Medical Center, Los Angeles, CA, CA*
9. *Lawson Health Research Institute, University of Western Ontario, ON, Canada*
10. *Cedars-Sinai Medical, CA*

Background: Myocardial blood-oxygen-level-dependent (BOLD) CMR is a non-contrast approach for examining myocardial perfusion. Despite the advances to date, BOLD CMR continues to be plagued by imaging confounders, which can limit its reliability. Unlike most applications that rely on T2 CMR, BOLD CMR is acquired at rest and under vasodilator stress, which is often associated with an increase in HR. We hypothesized that (a) the loss in BOLD sensitivity is directly dependent on the magnitude of the change in HR (DHR) between rest and vasodilator stress; and (b) HR-insensitive T2 maps can enable BOLD changes to be accurately captured. We tested our hypothesis by examining the BOLD response to a HR-insensitive T2 mapping approach and conventional T2 mapping. To assess whether DHR leads to a loss in myocardial BOLD sensitivity, we performed numerical simulations, ex-vivo imaging of dog hearts subjected to simulated DHR, and in-vivo imaging in healthy dogs during adenosine infusion.

Methods: A HR-insensitive (saturation-recovery (SR) prepared), free-breathing 3D T2 mapping sequence that is relatively insensitive to B0 and B1 variations at 3T with near perfect imaging efficiency was developed and studied in a hybrid clinical PET/MR system. Numerical simulations were performed using Bloch equations and ex-vivo images were acquired in freshly excised healthy dog hearts (n=3). In-vivo imaging was performed in healthy dogs (n=7) during adenosine infusion. Conventional 2D T2 mapping, and proposed sequence with and without SR preparation were prescribed under ex-vivo and in-vivo conditions. In-vivo studies were validated with simultaneously acquired ^{13}N-NH_3 PET perfusion. Myocardial BOLD Response (MBR) was computed as 100% x [T2(stress)–T2(rest)]/ T2(rest), where T2(rest) and T2(stress) are mean myocardial T2 pre- and post adenosine infusion.

Results: Numerical simulations and ex-vivo studies demonstrated that the proposed approach minimized the HR-dependent changes in T2 between rest and stress compared to the T2 maps acquired using conventional and proposed method without SR preparation (Fig. 1). T2 values acquired using the proposed sequence under adenosine stress was significantly greater than at rest (38.5±1.0 ms (rest) vs. 44.4±3.1 ms (stress), pprop – MBR_{conv})] was highly correlated (R=0.7, $p < 0.05$) as shown in Fig. 2C.

Conclusions: Conventional T2-based CMR is highly sensitive to DHR between rest and adenosine stress. These changes appear to decrease the expected BOLD response by counteracting the increase in T2 from vasodilator-induced hyperemia. The reliability of T2-based BOLD CMR would likely be improved through heart-rate-insensitive T2 acquisitions.

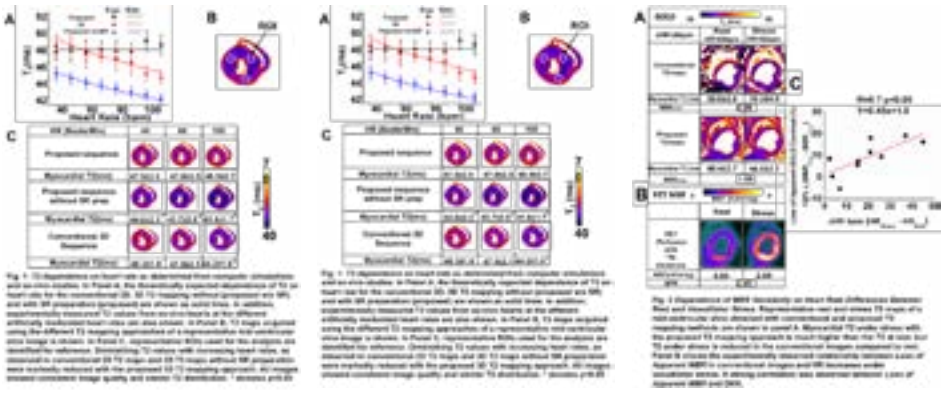

P024

Late gadolinium-enhanced Compressed sensing 3D IR FLASH sequence to assess focal myocardial fibrosis: comparison to standard breath-held and free-breathing methods

Matthieu Lepetit-Coiffe, PhD[1] Christoph Forman, MS[2], Michaela Schmidt[2], Bruno Quesson, PhD[3], Michel Montaudon, MD, PhD[4], Francois Laurent, MD,PhD[4], Hubert Cochet, MD, PhD[5]

1. *SIEMENS HEALTHCARE SAS, Bordeaux, Aquitaine, France*
2. *SIEMENS HEALTHCARE GmbH, Erlangen, Bayern, Germany*
3. *IHU Liryc, Université de Bordeaux, Pessac, Aquitaine, France*
4. *Unité d'imagerie cardio-thoracique, CHU Bordeaux, Pessac, Aquitaine, France*
5. *IHU LIRYC, Université de Bordeaux - Unité d'imagerie cardio-thoracique, CHU Bordeaux, Pessac, Aquitaine, France*

Background: Improving spatial resolution on LGE imaging is critical to accurately assess the structural remodeling of thin atrial walls, and the 3-dimensional architecture of ventricular scars.

Methods: MRI studies were performed on a 1.5 T system (MAGNETOM Avanto, Siemens Healthcare) in 22 patients (7 women, 54±19 years). Three 3D IR-FLASH sequences were performed to assess LGE: a conventional breath-held method (BH), a conventional free-breathing method using a cartesian and respiratory-navigated whole heart 3D IR FLASH sequence accelerated with GRAPPA factor 2 (FB, voxel size 1x1x2mm^3), and a highly accelerated free-breathing whole heart 3D IR FLASH prototype sequence with compressed sensing (FB-CS, 1mm^3 isotropic voxel size). For FB-CS, data acquisition was performed with incoherent Cartesian sub-sampling (acc. rate: 3.6) followed by compressed sensing reconstruction [1]. BH was performed 10 min after contrast, FB and FB-CS being sequentially performed afterwards in an alternating order from patient to patient. All images were acquired in axial orientation with a similar acquisition window. Image artifacts were assessed by summing 3 scores reflecting motion artifacts, inversion time inaccuracy, and fat suppression inaccuracy, respectively. Each score was graded on a 3-point scale, i.e. 0: none/mild, 1: moderate, 2: severe. Regions of interest were drawn within the remote ventricular myocardium and within the wall of descending aorta (fibrotic reference). Signal-to-noise and contrast-to-noise ratios (SNR and CNR) were computed between fibrosis and remote myocardium.

Results: The population was composed of 10 patients with ischemic ventricular scar, 4 with non-ischemic ventricular scar, 3 with post-ablation atrial scar, and 5 with no focal scar. Mean heart rate was 81±19 BPM. Acquisition time was 22±4s for BH, 14±10min for FB and 16±5min for FB-CS. It did not differ significantly between FB and FB-CS (P=0.59). Artifacts score was lower on BH as compared to the 2 other methods (P < 0.0001 for both), and also lower on FB-CS than on FB (2.2±1.1 vs. 2.8±1.2, P=0.02). Fibrosis SNR was similar between BH and FB-CS (15±8 and 16±9, P=0.61), while it was lower on FB images (11±2, P=0.006 vs. FB-CS and P=0.01 vs. BH). CNR between fibrosis and remote myocardium was also similar between BH and FB-CS methods (12±8 and 14±9, P=0.41), while it was also lower on FB images (8±2, P=0.005 vs. FB-CS and P=0.02 vs. BH).

Conclusions: As compared to a GRAPPA-accelerated but otherwise similar free-breathing LGE method, the prototype 3D IR-FLASH sequence featuring compressed sensing improves spatial resolution while preserving acquisition time. The method shows lower image artifacts and most importantly a higher contrast between fibrosis and remote myocardium, comparable to that obtained using conventional breath-held LGE at much lower spatial resolution.

References: *[1] Forman et al, Magn Reson Mater Phy 2014*

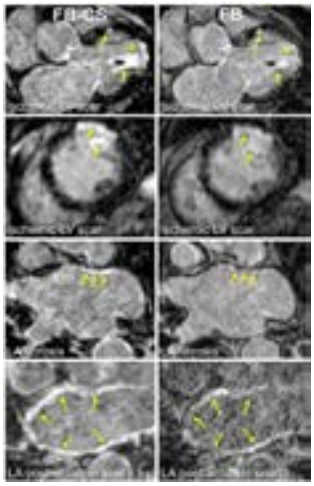

P025

Differential prognostic value of cardiac magnetic resonance tissue tracking after ST-segment elevation myocardial infarction

Yeonyee Elizabeth. Yoon, MD[1] Sang-Eun Lee, MD[2], In-Jeong Cho, MD[2], Sang Il Choi, MD[1], Goo-Yeong Cho, MD[1], Hyuk-Jae Chang, MD, PhD[2], Eun-Ju Chun, MD[1]

1. *Seoul National University Bundang Hospital, N/A, Republic of Korea*
2. *Severance Cardiovascular Hospital, Yonsei-Cedar Sinai Integrative Cardiovascular Imaging Research Center, Yeonsei University Health System, Seoul, South Korea, N/A, Republic of Korea*

Background: Although cardiac magnetic resonance (CMR) tissue tracking (TT) has technical advantages over traditional myocardial tagging to analyze left ventricle (LV) strain, its prognostic implication has not been tested so far. We sought to determine the prognostic value of CMR TT strain analysis in patients after ST-segment elevation myocardial infarction (STEMI).

Methods: We studied 247 consecutive patients (age, 58 ± 12 years; male, 81%) who underwent concurrent cine and late gadolinium ehnaced (LGE) CMR imaging after STEMI (range, 1 to 29 days). Global radial, circumferential, and longitudinal peak strains (GRS, GCS, GLS, respectively) were measured by CMR TT. Major adverse cardiac event (MACE) was defined as cardiac death and hospitalization due to heart failure.

Results: MACEs were observed in 20 patients (8.1%) during follow-up (median, 7.8 years; interquartile range, 6.0 to 9.1 years). In multivariate Cox regression analysis (adjusting for age, gender, hypertension, and diabetes), GRS, GCS, and GLS were independently assocaited with MACE (Table 1). Receiver operating characteristics curve anlaysis demonstrated the largest AUC in GLS for the prediction of MACE with optimal cut-off value of > -14.4% (Table 2). Interestingly, GLS > -14.4% was associated with worse event-free survival in both groups with and without extensive myocardial scar (LGE extent > 20%) (Figure 1).

Conclusions: CMR TT strain analysis provides further risk stratification in addition to LVEF and LGE in patients after STEMI.

Figure. Kaplan-Meier event-free survival

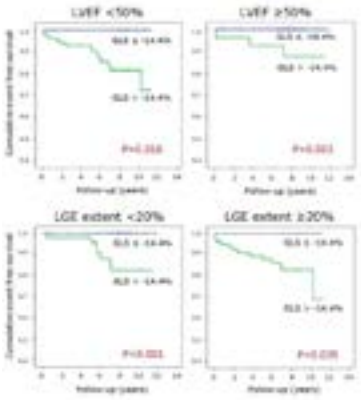

Multivariate Cox regression analysis adjusted to age, gender, hypertension, and diabetes

p-value	95% CI	HR	CMR variables
<0.001	1.019-1.054	1.036	LVEDV index, per ml/m^2
<0.001	1.026-1.062	1.044	LVESV index, per ml/m^2
<0.001	0.860-0.942	0.900	LVEF, per %
0.001	1.019-1.079	1.049	LV mass index, , per g/m^2
0.009	1.013-1.090	1.061	LGE extent, per %
0.002	0.859-0.966	0.911	GRS, per %
0.003	1.061-1.348	1.196	GCS, per %
<0.001	1.128-1.533	1.315	GLS, per %

optimal cut-off value	p-value	95% CI	AUC	
≤24.5	0.0001	0.668-0.782	0.728	GRS, %
>-9.9	0.0001	0.672-0.786	0.732	GCS, %
>-14.4	<0.0001	0.719-0.827	0.777	GLS, %

P026

3D High-Resolution LGE MRI using Shearlet-based Compressed-Sensing Image Reconstruction

Christoph Kolbitsch, PhD[7] Jackie Ma, PhD[1], Felix Schnabel[2], Zhong Chen, MD[3], Stephanie Funk, MD[4], Gitta Kutyniok, Prof. Dr.[5], Jeanette Schulz-Menger, MD[6], Tobias Schaeffter, PhD[2]

1. *Department of Mathematics, Technische Universitaet Berlin, Berlin, Germany, Berlin, Germany*
2. *Physikalisch-Technische Bundesanstalt (PTB), Braunschweig and Berlin, Germany, Berlin, Germany*
3. *Division of Imaging Science and Biomedical Engineering, Kings College London, London, United Kingdom, England, United Kingdom*
4. *Working Group on Cardiovascular Magnetic Resonance, Experimental and Clinical Research Center, a joint cooperation between the Charité Medical Faculty and the Max-Delbrueck Center for Molecular Medicine and HELIOS Hospital Berlin Buch, Berlin, Berlin, Germany*
5. *Technische Universität Berlin, Berlin, Berlin, Germany*
6. *Working Group on Cardiovascular Magnetic Resonance, Experimental and Clinical Research Center a joint cooperation between the Charité Medical Faculty and the Max-Delbrueck Center for Molecular Medicine HELIOS Klinikum Berlin Buch, Germany, Berlin, Germany*
7. *Physikalisch-Technische Bundesanstalt (PTB), Braunschweig and Berlin, Germany, Berlin, Berlin, Germany*

Background: Three dimensional (3D) high-resolution late gadolinium enhancement (LGE) MRI is a promising technique to assess fibrotic tissue in the myocardium. The increased resolution along the slice direction compared to a multi-slice 2D acquisition leads to an improved scar visualisation independent of the image orientation. Nevertheless, in order to acquire such high resolution in a clinically feasible scan time, high undersampling factors (i.e. SENSE factors) are required, which can lead to low signal-to-noise ratios. To overcome this problem, we propose a novel compressed sensing (CS) image reconstruction approach using shearlet-systems which are especially well-suited to describe curve-like structures, such as enhanced fibrotic tissue in 3D LGE MRI [1].

Methods: 3D LGE MRI was obtained in eight patients on a 1.5T MR scanner (Philips medical System, Best, The Netherlands), 25min post contrast (gadolinium-DTPA, 0.2mmol/kg) during mid-diastole with a FOV of 300x300x100mm, TR/TE 5.7/2.7ms, flip angle of 25° and an acquired voxel size of 1.3x1.3x2.6mm^3. SENSE undersampling of 2 and 1.3 was used along the phase and slice encoding direction, respectively. This led to a scan time of 3.8min assuming 100% respiratory navigator efficiency [2]. 3D LGE MR images were reconstructed using standard SENSE and the proposed Shearlet-CS approach from the same acquired raw data. Two clinical experts assessed if the images were diagnostic, if pathologies were visible and scored the image quality (0 non-diagnostic; 1 good; and 2 excellent) [3]. Contrast-to-noise ratios (CNR) were obtained between fibrosis and myocardium, fibrosis and blood and blood and myocardium.

Results: All images reconstructed with standard SENSE and Shearlet-CS were diagnostic and the observers found no difference in the visibility of pathologies between the two approaches. The observers scored the image quality of both methods as "good", with observer 2 scoring the Shearlet-CS approach higher than standard SENSE (1.4±0.5 vs 1.1±0.4). Shearlet-CS significantly improved CNR between scar and myocardium (+37%, $p < 0.05$).

Conclusions: Shearlet-CS can improve CNR and the diagnostic quality of 3D high-resolution LGE MR images, providing a better visualisation of fibrotic tissue. The proposed Shearlet-CS approach is a promising technique to translate 3D LGE MRI into clinical practise. [1] Ma, Appl. Comput. Harm. Anal. 2016. [2] Zhong et al., J. Cardiovasc. Magn. Reson. 2012. [3] Prothmann et al., Plos One. 2016.

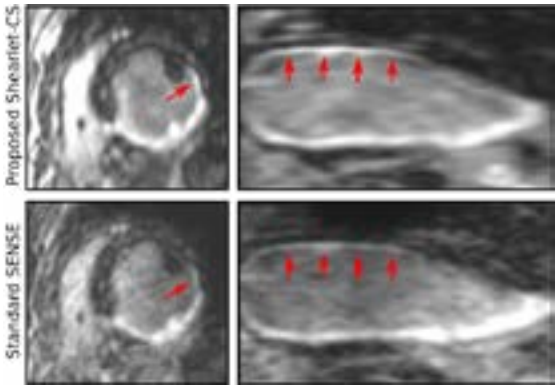

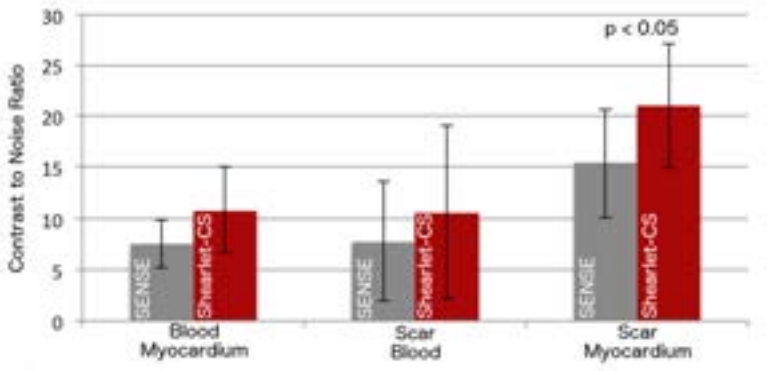

P027

Intramyocardial fat deposition in patients with previous myocardial infarction assessed using advanced CMR imaging – feature tracking, fat water separation and parametric mapping

Tomas Lapinskas, MD[1] Bernhard Schnackenburg, PhD[2], Rolf Gebker, MD, PhD[3], Remigijus Zaliunas, MD, PhD[1], Burkert Pieske, MD, PhD[3], Sebastian Kelle, MD, PhD[3]

1. *Lithuanian University of Health Sciences, Kaunas, Kauno Apskritis, Lithuania*
2. *Philips GmbH Marked DACH, Hamburg, Germany, Hamburg, Hamburg, Germany*
3. *German Heart Institute Berlin, Berlin, Berlin, Germany*

Background: Intramyocardial fat deposition predisposes an individual to ventricular arrhythmias and increased risk of sudden cardiac death. This study aimed to detect fat infiltration in patients with previous myocardial infarction (MI) using advanced cardiac magnetic resonance (CMR) imaging techniques – feature tracking, fat water separation and parametric mapping.

Methods: Twenty patients with chronic MI underwent advanced CMR imaging. The study protocol included conventional cine and late gadolinium enhancement (LGE) imaging. Additionally, fat water separation (2-point mDixon) and parametric mapping were performed in every patient. Left ventricular (LV) circumferential (Ecc_{LV}) and radial (Err_{LV}) strain were calculated using dedicated software (CMR^{42}, Circle Cardiovascular Imaging Inc., Calgary, Canada). The extent of global scar tissue was calculated in LGE and fat water separation images to compare advanced and conventional imaging techniques. The native and post-contrast T1 relaxation values of the remote myocardium, global LGE, intramyocardial fat, fibrosis and extracardiac adipose tissue were measured.

Results: The infarct size as derived from conventional LGE and fat water separation images was similar. However, detection of intramyocardial fat was only possible with fat water separation imaging. Subjects with intramyocardial fat deposition demonstrated significantly smaller percentage of fibrosis than those without fat deposition (10.68 ± 5.07 % vs. 13.83 ± 6.30 %; p = 0.005). There was no difference between the groups with respect of mean native T1 values. The mean post-contrast T1 values of global LGE in patients with intramyocardial fat were significantly higher than in patients without (372.26 ± 39.01 ms vs. 312.70 ± 33.02 ms; p = 0.017). There was no significant difference in LV circumferential (Ecc_{LV}) and radial (Err_{LV}) strain between myocardial segments containing fibrosis only and fibrosis with fat deposition (-11.94 ± 5.92 % vs. -12.63 ± 7.14 %; p = 0.668 for Ecc_{LV} and 20.85 ± 16.48 % vs. 17.89 ± 12.43 %; p = 0.607 for Err_{LV}).

Conclusions: Advanced CMR imaging enables more detailed tissue characterization in patients with previous MI without relevant increase in examination or post-processing time. Native T1 mapping and myocardial feature tracking technique is unable to detect intramyocardial fat deposition.

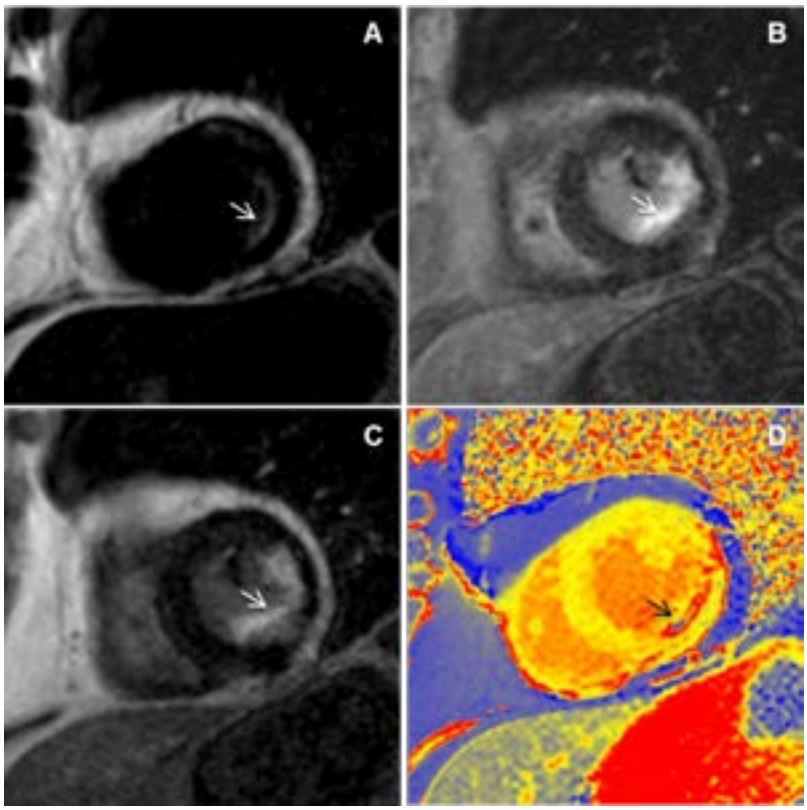

P028

Glasgow MRI Rotational Atherectomy Study: Semi-quantitative analysis of stress perfusion CMR reveals changes in myocardial perfusion following percutaneous coronary intervention with adjunctive HSRA

Thomas Athey[1] Guillaume Clerfond, MD[2], David Corcoran, BSc (Hons), MBChB, MRCP[3], Barry Hennigan, MB BCh BAO[4], David Carrick, PhD[4], Kenneth Mangion, MD[5], Paul Rocchiccioli, MD, FRCP[6], Mitchell Lindsay, MD[7], Hany Eteiba, MD[7], Colin Berry, PhD FRCP[5], Margaret McEntegart, MBChB PhD[4], Aleksandra Radjenovic, MSc PhD[8]

1. *University of Glasgow, PA*
2. *University Hospital of Clermont Ferrand, France, Clermont Ferrand, Auvergne, France*
3. *University of Glasgow, Scotland, United Kingdom*
4. *Golden Jubilee National Hospital, Glasgow, Scotland, United Kingdom*
5. *University of Glasgow, Glasgow, Scotland, United Kingdom*
6. *West of Scotland Regional Heart & Lung Centre - Golden Jubilee National Hospital, Clydebank, Scotland, United Kingdom*
7. *Golden Jubilee National Hospital, Scotland, United Kingdom*
8. *University of Glasgow, UK, Glasgow, Scotland, United Kingdom*

Background: Percutaneous coronary intervention (PCI) with adjunctive high-speed rotational atherectomy (HSRA) is commonly used to treat complex and calcified coronary artery stenoses. Theoretically, HSRA may have deleterious effects on the coronary microcirculation and hence myocardial perfusion. We studied the effects of HSRA PCI using serial multi-parametric cardiac magnetic resonance (CMR) imaging.

Methods: We prospectively enrolled 67 patients into this study (63 male, age range 41-83). Following baseline assessment, 58 patients underwent elective HSRA PCI. Multi-parametric CMR was performed at 3 time-points: before HSRA (baseline), 7 days, and 6 months post-HSRA. The CMR protocol comprised global and regional LV function assessment, rest and adenosine stress perfusion, and late gadolinium enhancement imaging (1.5 Tesla MAGNETOM Avanto, Siemens Healthcare, Germany). At each time-point, endocardial and epicardial borders were contoured using proprietary software (Medis QMass, Netherlands) on the stress perfusion slice with the most significant qualitatively assessed perfusion defect, and on the corresponding rest sequence. Regions of interest (ROIs) were drawn within the inducible perfusion defect. Motion correction, derivation of SI/time curves and computation of semi-quantitative perfusion parameters were performed using Matlab (MathWorks Inc., Natick, MA).

The following semi-quantitative metrics of myocardial perfusion were derived: Enhancement Ratio (ER) = maximal SI detected during first pass divided by baseline SI, expressed as a unit-free ratio; Initial Rate of Enhancement (IRE) = slope of the regression line fitted to the initial section of the SI/time curves, expressed in s^{-1}. The ER_{Index} and IRE_{Index} values represent the ratio between the ER and IRE values measured within the inducible perfusion defect (or a segment with a minimal ER value at baseline when no lesion could be identified qualitatively), divided by a contralateral myocardial segment. Results are expressed as means and standard deviations and are compared using Student's t-test for paired data.

Results: Summary of measured semi-quantitative perfusion parameters (mean±SD) is presented in Table 1. At rest, all parameters remained stable, with all paired t-test comparisons yielding $p>0.05$. There was a significant improvement in all 4 semi-quantitative perfusion metrics on stress perfusion acquisitions at 6 months follow-up post-HSRA PCI. Furthermore, ER and IRE indices showed a trend towards restoration of perfusion in the indexed lesion 7 days after HSRA ($p = 0.01$ and $p= 0.0018$, respectively).

Conclusions: This data demonstrates that semi-quantitative metrics of resting myocardial perfusion show no change post-HSRA PCI. At stress perfusion, however, all 4 metrics demonstrated significant increase consistent with improved myocardial perfusion. In particular, the ER_{Index} and IRE_{Index} demonstrated immediate improvement (7 days post-HSRA PCI) and this was maintained at 6 months follow-up.

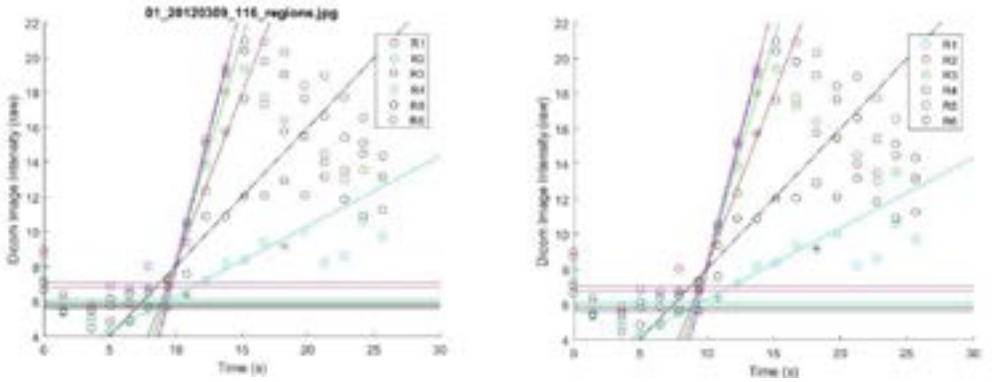

Semi-quantitative perfusion parameters at baseline, 7 days and at 6 months post-HSRA PCI

IRE Index	ER Index	IRE	ER	N	
0.97 ± 0.47	0.97 ± 0.14	2.54 ± 1.23	2.25 ± 0.28	49	REST at baseline
0.99 ± 0.50	0.96 ± 0.15	2.68 ± 1.44	2.24 ± 0.30	47	RESTat 7 days
1.00 ± 0.46	0.94 ± 0.12	2.78 ± 1.50	2.27 ± 0.31	47	REST at 6 months
0.76 ± 0.46	0.84 ± 0.22	3.79 ± 2.12	3.02 ± 0.47	51	STRESS at baseline
0.92 ± 0.52 ***	0.96 ± 0.22 *	4.23 ± 2.38	3.09 ± 0.66	47	STRESS at 7 days
0.95 ± 0.46 ***	0.97 ± 0.18 ***	4.69 ± 2.11	3.27 ± 0.59 **	46	STRESS at 6 months

ER = Enhancement Ratio, IRE = Initial Rate of Enhancement, ER and IRE indices are ratios of corresponding lesion/remote ER and IRE values. Significant changes with respect to baseline measurement are labelled as * ($p<0.05$), ** ($p<0.01$) and *** ($p<0.005$).

Semi-quantitative perfusion parameters at baseline, 7 days and at 6 months post-HSRA PCI.

IRE Index	ER Index	IRE	ER	N	
0.97 ± 0.47	0.97 ± 0.14	2.54 ± 1.23	2.25 ± 0.28	49	REST at baseline
0.99 ± 0.50	0.96 ± 0.15	2.68 ± 1.44	2.24 ± 0.30	47	REST at 7 days
1.00 ± 0.46	0.94 ± 0.12	2.78 ± 1.50	2.27 ± 0.31	47	REST at 6 months
0.76 ± 0.46	0.84 ± 0.22	3.79 ± 2.12	3.02 ± 0.47	51	STRESS at baseline
0.92 ± 0.52 ***	0.96 ± 0.22 *	4.24 ± 2.38	3.09 ± 0.66	47	STRESS at 7 days
0.95 ± 0.46 ***	0.97 ± 0.18 ***	4.69 ± 2.11 *	3.27 ± 0.59 **	46	STRESS at 6 months

ER = Enhancement Ratio, IRE = Initial Rate of Enhancement, ER and IRE indices are ratios of corresponding lesion/remote ER and IRE values. Significant changes with respect to baseline measurement are labelled as * ($p<0.05$), ** ($p<0.01$) and *** ($p<0.005$).

P029

Comparison of two-dimensional (2D) versus three-dimensional (3D) whole heart myocardial perfusion CMR in the diagnosis of CAD and in the estimation of myocardial ischaemic burden

Sven Plein, MD PhD[7] Joy Shome, MBBS, MRCP[1], Kerem C. Tezcan, MSc[2], Sohaib Nazir, MBBS MRCP[3], Pedro Pinto Teixeira, MD[3], Adriana Villa, MD[3], Antonis Pavlidis, MD PhD[4], Brian Clapp, PhD FRCP[4], Simon Redwood, MD FRCP[3], Kamran Baig, MD FRCS(C-Th)[4], Khaled Alfakih, MD MRCP[3], Reza Razavi, MD, PhD[5], Tevfik Ismail, PhD MRCP[3], Amedeo Chiribiri, MD, PhD[5], Divaka Perera, MD FRCP[3], Sebastian Kozerke, PhD[6]

1. *St. Thomas' Hospital, London; King's College London, Feltham, England, United Kingdom*
2. *Department of Information Technology and Electrical Engineering, ETH Zurich, Zurich, Switzerland*
3. *St. Thomas' Hospital, London; King's College London, England, United Kingdom*
4. *St. Thomas' Hospital, London, England, United Kingdom*
5. *King's College London, England, United Kingdom*
6. *ETH Zurich; King's College London, Zurich, Zurich, Switzerland*
7. *St. Thomas' Hospital, London; King's College London; University of Leeds, England, United Kingdom*

Background: Both 2D and 3D myocardial perfusion CMR are highly diagnostic for CAD. Ischemic burden is used to guide revascularization. 3D perfusion provides whole heart coverage, whereas high-resolution 2D perfusion can better detect sub-endocardial ischemia at the expense of limited coverage. We sought to investigate if novel 3D perfusion methods provide a more reliable estimation of myocardial ischemic burden (MIB) compared to 2D.

Methods: Patients with suspected angina referred for invasive coronary angiography as part of their routine clinical care were approached. One comprehensive CMR scan was performed for each patient prior to angiography or surgical revascularisation if so indicated, encompassing a high resolution 2D adenosine stress perfusion scan followed later by a 3D adenosine stress perfusion study. A 2D rest scan was performed at the end of the CMR exam. All other cine and late gadolinium images (LGE) were obtained as normal. The order of the stress scans was randomized with a minimum time interval of 30 min between the two. For 2D, three slices were reconstituted using kt-SENSE compared to 12 slices for 3D using TVSENSE-ktPCA reconstruction. Fractional Flow Reserve (FFR) measurements were performed for stenoses of 50-80% severity visually. An FFR $\leq$ 0.8 was considered to be haemodynamically significant. Using circleCVI software, after excluding areas of LGE, perfusion defects were contoured and MIB calculated for both 2D and 3D stress scans. From the invasive angiogram the Duke Jeopardy Score was calculated to estimate the myocardium at risk.

Results: 24 patients underwent 2D and 3D perfusion CMR and coronary angiography with FFR measurements. Patient characteristics have been summarized in Table 1. As referenced to FFR, the sensitivity, specificity for 2D perfusion in detecting ischaemia were 95%, 80% respectively. Corresponding values for 3D were 89%, 100%. 3D identified prognostically significant ischemic burden in 67% of patients, compared to 75% using 2D. There was no systematic bias between the two methods, however, the limits of agreement were wide (9%). (Refer Figure 1) However, both methods agreed well in identifying prognostically significant disease (Cohen's k-statistic = 0.865).

Conclusions: By using FFR and state of the art image reconstruction methods, and minimizing physiological variations by performing both 2D and 3D CMR perfusion in a single sitting, this study evaluates the measurement of ischemic burden in as ideal a setting as possible. Referenced to FFR, our study shows that both perfusion methods can reliably detect prognostically significant CAD.

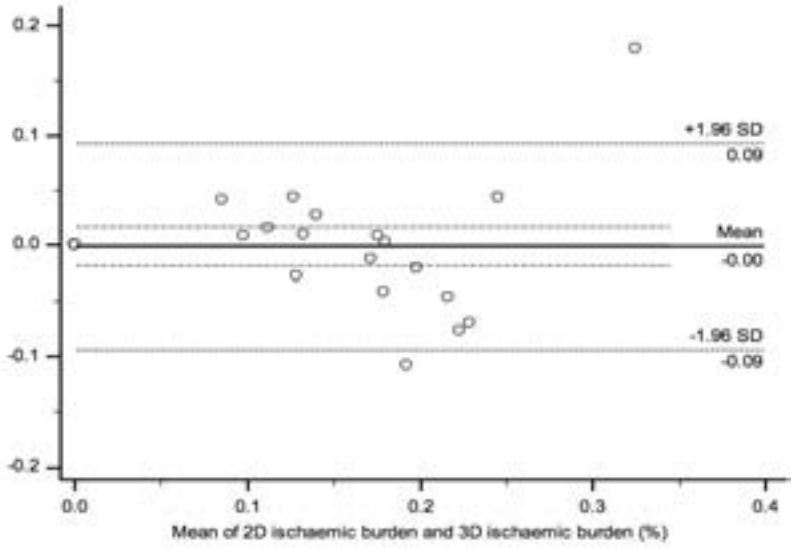

Table 1: Patient characteristics

Parameter	**n=24**	
Male, n, %	21	88%
Age, years	62.4 ± 5.8	
Age range, years	51 – 71	
BMI, kg/m^2	27.7 ± 2.7	
Cardiovascular Risk Factors, n, %		
Arterial hypertension	17	71%
Diabetes mellitus	3	13%
Hyperlipidemia	17	71%
Smoking	3	13%
Family history of CAD	13	54%
Peripheral Vascular Disease	4	17%
Medication, n, %		
β-Blocker	15	63%
ACE inhibitor/ ARBs	14	58%
Statin	21	88%
Nitrates	8	33%
Aspirin	20	83%
2nd Antiplatelet	5	21%
Coronary artery disease, n, %		
Single-vessel disease	8	33%
Multi-vessel disease	11	46%
Left ventricular function		
LVEF (%)	58.8 ± 7.2	
LVEDV (ml/m^2)	84.2 ± 11.1	
LVESV (ml/m^2)	34.9 ± 9.6	

P031

Identification of right ventricular infarction using dark-blood late gadolinium enhanced LGE-CMR in a swine ischemia-reperfusion model

John Whitaker, BM BCh[1]Cory Tschabrunn, PhD[2], Jihye Jang, M.Sc.[3], Shiro Nakamori, MD, PhD[4], Mark O'Neill, MD DPhil[5], Eran Leshem, MD[6], Elad Anter, MD[2], Warren J. Manning, MD[7], Reza Nezafat, PhD[8]

1. *King's College London/Beth Israel Deaconess Medical Centre, London, England, United Kingdom*
2. *Beth Israel Deaconess Medical Centre, MA*
3. *Beth Israel Deaconess Medical Center and Harvard Medical School, MA*
4. *Beth Israel Deaconess Medical Center, MA*
5. *King's College London, London, England, United Kingdom*
6. *Beth Israel Deaconess medical center, Boston, Brookline, MA*
7. *Beth Israel Deaconess Medical Center, Boston, MA*
8. *Department of Medicine (Cardiovascular Division) Beth Israel Deaconess Medical Center, Harvard Medical School, Cardiology, East Campus, Room E/SH455, 330 Brookline Ave, Boston, MA, 02215, MA*

Background: Right ventricular (RV) infarction is associated with morbidity and mortality and its identification identifies a subgroup of high-risk patients(1). RV infarction usually accompanies inferior myocardial infarction (MI) following right coronary artery occlusion. The identification of RV infarction with LGE is often challenging due to low blood-scar contrast of LGE sequence. We assessed the ability of dark-blood (DB) LGE to identify RV infarction in a swine ischemia-reperfusion model.

Methods: We utilized an optimized DB-LGE sequence that takes advantage of the high blood T_2 to suppress signal from both blood pool and normal myocardium (2). A T_2 magnetization preparation pulse is inserted between the inversion pulse and imaging readout of a conventional LGE sequence. 8 Yorkshire swine who had undergone three-hour occlusion of the mid left anterior descending artery and a control without MI were scanned at 15, 30 and 60 days post MI. A total of 18 pairs of LGE and DB-LGE scans of sufficient quality were acquired from this group of animals. 3D LGE and DB-LGE was acquired after 10–30 minutes following 0.2mmol/L gadopentetate dimeglumine (Multihance®) administration with the following parameters: TR/TE: 5.2/2.5ms; FOV: 320x335x90mm; flip angle: 25°. High resolution (0.4mm^3 isotropic) ex vivo T1 weighted imaging, acquired over 2.5 hours, was commenced within 1 hour of euthanasia with the following parameters: TR/TE: 17.2/8.0ms; FOV: 130x130x100mm; flip angle 25°. v Presence of RV enhancement on in vivo DB-LGE and LGE scans was determined by consensus of two cardiologists experienced in CMR. Ex vivo LGE imaging was taken as reference standard for identifying RV free wall infarction.

Results: 15 DB-LGE scans and 15 LGE scans were performed in animals with free wall RV scar demonstrated on ex vivo CMR. RV free wall enhancement was identified in 12 (sensitivity = 0.80) DB-LGE scans and 4 (sensitivity = 0.27) LGE scans in the same distribution as ex vivo imaging. No RV free wall enhancement was noted in DB-LGE or LGE scans from the control animal.

Conclusions: DB-LGE CMR demonstrated improved diagnostic sensitivity when compared with traditional LGE CMR in the detection of RV infarction. Further in vivo human studies are warranted to evaluate diagnostic accuracy of detecting RV infarct and evaluate its prognostic value.

References:

1. Kinch et al NEJM 1994
2. Basha et al JCMR 2015
3. Akcakaya et al. Radiology 2012

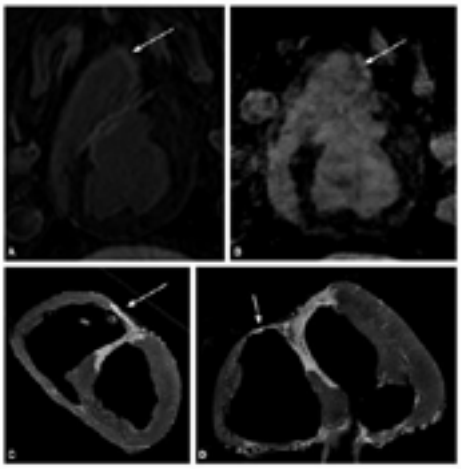

P032

The interplay between myocardial edema and hemorrhage after myocardial infarction reperfusion in rats, continuously evaluated by T2 mapping at 7.0T MR

Ziqian Xu[1] Wei Chen, Ph.D[2], Ruzhi Zhang[1], Bing Zhang[1], Jie Zheng, PhD[3], Fabao Gao, MD,PHD[4]

1. *Department of Radiology, West China Hospital, Sichuan University, Sichuan, China (People's Republic)*
2. *Department of Radiology, the 1st Affiliated Hospital of Kunming Medical University, Yunnan, China (People's Republic)*
3. *Mallinckrodt Institute of Radiology, Washington University School of Medicine, WA*
4. *China West Hospital, Sichuan, China (People's Republic)*

Background: Myocardial edema and hemorrhage were the common injuries in the early myocardial infarction reperfusion period. The purpose of this study was to continuously detect the interplay between edema and hemorrhage in rats by T2 mapping.

Methods: All of eight Sprague-Dawley rats (female, 200-250g) were underwent the ligation of the left anterior descending coronary artery for 60mins. After reperfusion for 24hours, 48hours, 72hours and 5days, all rats were underwent cardiac magnetic resonance at 7.0T MR (Bruker BioSpect70/30 Ettlingen, Germany). T2 mapping(TR/TE=1500ms/10,20,30ms, MTX=192×192 FOV=5cm×5cm, slice thickness=1.5mm), LGE (10min after Gd-DTPA injection, TR/TE=5.2ms/1.8ms, MTX=256×256, FOV=5cm×5cm) were performed to acquire T2 values of injured myocytes(edema and hemorrhage) and infarction size(LVEDV%). Images analysis was performed by the custom-made software written in Matlab 7.1.All rats were sacrificed after scanning at 5days reperfusion, myocardial tissue was used for hemaxylin-eosin staining. Data were expressed as mean ± SD. ANOVA analysis was used for the comparison of T2 values among edema, hemorrhage and remote myocardium.

Results: Infarct size (25.64±8.09%) was observed by LGE. All subjects were found intramyocardial hemorrhage by T2 mapping and HE staining, shown in Figure 1. T2 values of edema, hemorrhage and remote myocardium were significantly different, summarized in Table 1.

Conclusions: T2 value of hemorrhage was greater than remote myocardium, which indicates that area of hemorrhage is a blend of edema and hemorrhage. The decision for improper scanning time may cause false negative reaction and lower T2 value of edema.

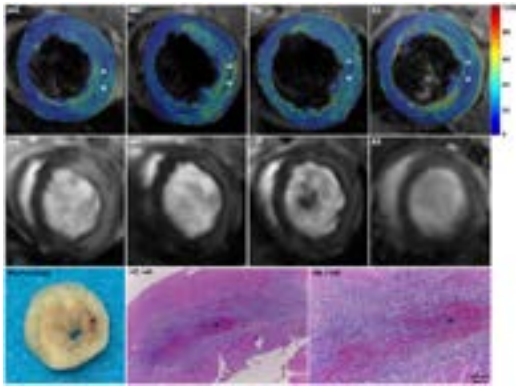

Table 1 T2 values of edema, hemorrhage and remote myocardium

5d	72h	48h	24h	T2 value(ms)
36.04±2.85	40.20±3.04	43.37±3.85	38.39±2.42	Edema
24.58±1.18	27.76±2.30	29.19±2.42	29.07±2.41	**Hemorrhage**
22.33±0.76	22.57±0.75	22.30±0.83	22.32±0.75	**Remote**

P033

Abnormalities In Myocardial Perfusion Are Associated With Subclinical Systolic Dysfunction in Post-Heart Transplant Patients

Akhil Narang, MD[1]John E. Blair, MD[2], Victor Mor-Avi, PhD[2], Savitri E. Fedson, MD[3], Nir Uriel, MD[2], Roberto M. Lang, MD[2], Amit R. Patel, MD[2]

1. *University of Chicago, Chicago, IL*
2. *University of Chicago, IL*
3. *Baylor College of Medicine, TX*

Background: Myocardial perfusion reserve (MPR) decreases over time in post-heart transplant (HTx) patients. Previous studies have suggested this may be related to coronary allograft vasculopathy (CAV) and microvascular dysfunction. The objective of this study was to characterize the consequences of reduced MPR on systolic function, as reflected by changes in myocardial strain.

Methods: We retrospectively studied 20 post-HTx patients who underwent vasodilator cardiovascular magnetic resonance imaging (vCMR), including cine-CMR, myocardial perfusion imaging during hyperemia and recovery, and late gadolinium enhancement (LGE), using standard clinical pulse sequences. Cine-CMR images were used to calculate left ventricular (LV) volumes and ejection fraction (EF). Time-intensity curves generated from stress and recovery perfusion images were used to determine MPR index (MPRi), calculated as the up-slope ratio of stress to recovery (normalized to the LV cavity up-slope and rate-pressure-product). Transthoracic echocardiography (TTE) was also performed to assess LV systolic function. LVEF was quantified using the biplane methods of discs (modified Simpson's rule). Strain analysis was performed using commercial automated speckle tracking software (QLAB 10). Global-longitudinal strain values were obtained from apical two-, three- and four-chamber views.

Results: The mean time from HTx to vCMR was 8.1 ± 4.1 years. The mean time between CMR and TTE was 240 ± 198 days. Median MPRi in post-HTx patients was 0.50 (range: 0.41-0.54). The mean LVEF measured by TTE and vCMR was 63 ± 6% and 60 ± 6%, respectively and there was no association between LVEF measured by either technique and MPRi. There were no visible regional LV wall motion abnormalities detected on either TTE or CMR. There was, however, a moderate correlation between MPRi and GLS (R=0.68, P=0.001) **(Figure A).**

Conclusions: This study demonstrates that reduced MPRi in late post-HTx patients is associated with subclinical systolic dysfunction. Our findings suggest that GLS measured using TTE may be a potential biomarker for detecting abnormalities in myocardial perfusion in patients following HTx.

Figure A

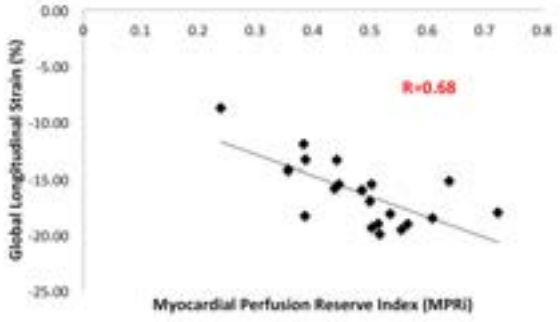

P034

Multiparametric cardiac MR imaging in the distinction of salvaged and infarcted myocardium within the ischemic area-at-risk.

Dongaolei An, M.D.[1] Jianrong Xu, Professor[2]

1. *Department of Radiology,Shanghai Renji Hospital, Liaoning, China (People's Republic)*
2. *Department of Radiology,Shanghai Renji Hospital, Shanghai, China (People's Republic)*

Background: To evaluate the diagnostic performance of cardiac magnetic resonance (CMR) imaging at 3.0 T in the distinction of salvaged and infarcted myocardium within the ischemic area-at-risk by using a multiparametric cardiac MR imaging approach including quantitative T2 mapping as an additional tool for tissue characterization.

Methods: Thirty-nine patients with established myocardial infarction and ten healthy volunteers were performed CMR at 3.0T,late gadolinium enhancement images were used to define the infarcted, salvaged, remote myocardium. Cardiac MR imaging approaches included T2 weighted image(T2WI) signal intensities(SI), early gadolinium enhancement ratio(EGE radio) and native T2 values. Receiver operating characteristic analysis was performed to compare diagnostic performance.

Results: There were no significant differences in mean T2WI-SI, EGE ratio and T2 relaxation times in the normal myocardium of healthy volunteers compared to the remote myocardium of acute MI patients ($p > 0.05$). T2 values were significantly longer in the infarcted myocardium than in the salvaged myocardium (67.8 ± 6.5 ms vs 58.6 ± 7.2 ms, respectively; $P < .001$). Areas under the curve of T2 values(0.89) were higher compared with those of other cardiac MR parameters (T2 intensity 0.76; EGE ratio, 0.71; $P = .38$ and $< .001$, respectively). Adopting a threshold value of 62.38 ms,T2 mapping resulted in 88.2% sensitivity, 78.3% specificity in the identification of salvaged and infarcted myocardium within the ischemic area-at-risk.

Conclusions: Diagnostic performance with T2 mapping was superior to that with T2WI-SI and EGE ratio, this study underlines the potential of T2 mapping to complement current cardiac MR approaches in the distinction of salvaged and infarcted myocardium within the ischemic area-at-risk.

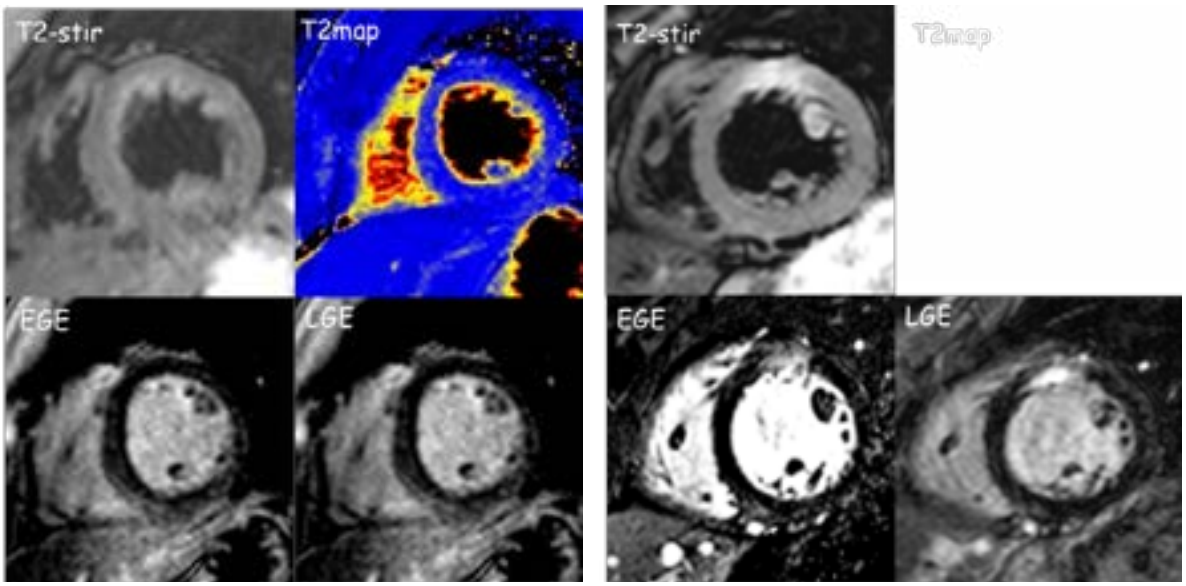

P035

Segmental Circumferential Strain and the Transmural Extent of Infarction are Closely Associated in Patients With a recent Non ST-Segment Elevation Myocardial Infarction

Nicole M M. Burke, B.Sc. (Med. Sci) Clinical Medicine[1], Kenneth Mangion, MD[1], Colin Berry, PhD FRCP[1]Samuli M. O. Rauhalammi, MSc, MSci, BA[2], Christie McComb, PhD[3], Hany Eteiba, MD[4], Mitchell Lindsay, MD[4], Margaret McEntegart, MBChB PhD[5], Stuart Hood, MD FRCP[6], Mark Petrie, MD[7], Stuart Watkins, MD, FRCP[5], Jamie Layland, MBChB PhD[8], Keith G. Oldroyd, MD (Hons); FRCP[4]

1. *University of Glasgow, Glasgow, Scotland, United Kingdom*
2. *University of Glasgow, Tonopah, AZ*
3. *NHS Greater Glasgow and Clyde / University of Glasgow, Glasgow, Scotland, United Kingdom*
4. *Golden Jubilee National Hospital, Scotland, United Kingdom*
5. *Golden Jubilee National Hospital, Glasgow, Scotland, United Kingdom*
6. *NHS Greater Glasgow and Clyde, Scotland, United Kingdom*
7. *Glasgow University, Scotland, United Kingdom*
8. *University of Glasgow, N/A, Australia*

Background: We investigated whether left ventricular (LV) segmental peak circumferential strain correlated with the transmural extent of infarction in myocardial segments in patients with recent non-ST elevation myocardial infarction (NSTEMI).

Methods: 103 patients underwent cardiac magnetic resonance imaging (CMR) at 3.0 Tesla 10 days post NSTEMI, along with healthy volunteers (HV, n=44). Mid LV peak circumferential strain was derived from cine images using feature-tracking software (TomTec, Germany). Segmental scar transmurality was derived from images acquired ~10 minutes after an intravenous injection of a gadolinium (Gd) contrast agent (Gadovist (0.1 mmol/kg) – Bayer Pharma, Berlin, Germany),and quantified using commercial software (QMass, Medis, Leiden, Netherlands). The segment with maximal scar transmurality and a remote segment (in a different coronary artery territory) were identified. Corresponding strain values were recorded for the scar and remote segment. Segments containing scar were allocated a score according to infarct transmurality - 0: 0 %, 1: 1–25 %, 2: 26–50 %, 3: 51–75 %, 4: 76–100 %. One-way ANOVA, with Dunnett's post-hoc analysis was used to assess correlations between the multiple groups. Receiver Operating Characteristic (ROC) analysis was used in order to asses specificity and sensitivity of segmental circumferential values as an indicator of segments with >50% scar transmurality. The study was publically registered https://clinicaltrials.gov/ct2/show/NCT02073422 and all of the subjects provided written informed consent.

Results: 103 patients with recent acute NSTEMI were prospectively enrolled (mean age of 56.9 (±9.9) and 81% were male). Mean mid LV circumferential strain was -22.9(± 5.8). 53 (51.5%) patients were identified as having significant scar in at least one segment. Of these patients, 24 had < 25% scar (45.28%), 15 had between 25% to < 50% (28.3%), 10 had between 50% and < 75% (18.9%), and 4 had between 75% to 100% (7.55%). Peak circumferential strain was associated with the transmural extent of myocardial scar on a per segment basis (-28.1%, p < 0.001). Segmental peak circumferential strain exhibited good accuracy at predicting the occurrence of >50% segmental scar transmurality (ΔAUC 0.79, SE 0.053, p=0.001, 95% CI 0.69 to 0.90), and this predictive accuracy was higher than for LV ejection fraction(ΔAUC 0.35, SE 0.095, p=0.091, 95% CI 0.16 to 0.53).

Conclusions: Circumferential strain and the transmural extent of infarction are closely associated in patients with recent NSTEMI. Circumferential strain is a potential new biomarker of the severity of MI, especially in patients with contra-indications to gadolinium-based contrast agents.

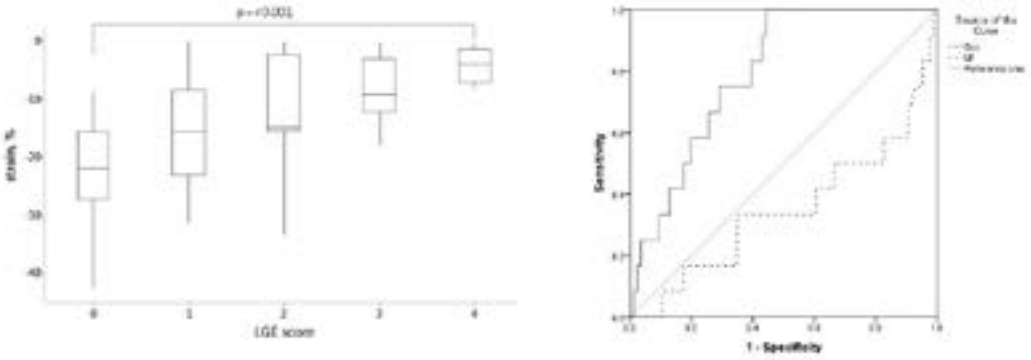

P036

Papillary Muscle Ischemia as Identified by Stress Perfusion CMR – A Novel Marker of Advanced Ischemic MR and Degenerative Mitral Apparatus Remodeling

Ashley Morgan, MD[1]Sophie Wells, MD[2], Jiwon Kim, MD[2], Samantha Goldburg, BA[2], Neil Mehta, MD[2], Pooja Maddula, BS (Anticipated)[2], Omar Khalique, MD[3], Antonino Di Franco, MD[2], Robert A. Levine, MD[4], Richard B. Devereux, MD[2], Thanh D. Nguyen, PhD[2], Mark B. Ratcliffe, MD[5], Jonathan W. Weinsaft, MD[2]

1. *University of California, San Francisco—East Bay Surgical Residency,, CA*
2. *Weill Cornell Medical Center, NY*
3. *Columbia University Medical Center, NY*
4. *Massachusetts General Hospital, MA*
5. *University of California San Francisco, San Francisco, CA*

Background: Papillary muscle ischemia (PMI) holds the potential to affect mitral valve function. PMI can be visualized via stress CMR, but its association with mitral apparatus remodeling and ischemic mitral regurgitation (iMR) severity is unknown.

Methods: The population comprised CAD patients with iMR prospectively enrolled in a multimodality imaging protocol concerning mitral apparatus remodeling. CMR was performed on a clinical (3 Tesla [GE]) scanner. Stress perfusion CMR (gradient echo) was used to identify PMI (defined as papillary hypo-enhancement during first pass regadenoson stress) as well as LV chamber wall ischemia. DE-CMR (IR-GRE) was used to identify infarction; LV ischemia and infarct size were both graded via a 17 segment model – regionality (anterior, inferior, lateral) was categorized using equidistant LV partitions. Global LV and regional mitral apparatus remodeling indices (tenting area, sphericity, interpapillary distance) were assessed via cine-CMR (SSFP). Transthoracic echocardiography (echo) provided an independent reference for MR (graded on a 5 point scale, concordant with consensus criteria). CMR and echo were performed within a 1-day interval; each was analyzed independently.

Results: 43 patients (68±10yo, 81% male) with iMR (58% [n=25] mild | 42% [n=18] ≥ moderate) were studied, among whom 72% had PMI identified via stress CMR. PMI was bilateral ($_b$PMI) in three-fourths (77% [24/31]) of affected patients (23% unilateral [5/31 posteromedial, 2/31 anterolateral). Advanced (≥moderate) MR was 3-fold more common among patients with, compared to those without, $_b$PMI (58% vs. 21%, p=0.03), corresponding to increased global LV ischemic burden ($p < 0.001$ [see **Table**]). Regarding regional LV ischemia and infarction, patients with $_b$PMI had larger perfusion deficits in the anterior and lateral walls (both $p \leq 0.01$), but similar global and regional infarct size. $_b$PMI was associated with increased global LV chamber size ($p < 0.001$), impaired LVEF (p=0.004), and adverse mitral apparatus remodeling - including larger tenting area, sphericity, and inter-papillary muscle distance (all $p \leq 0.05$), as well as a trend towards decreased papillary fractional shortening (p=0.11).

Conclusions: $_b$PMI identified by stress perfusion CMR is a novel marker of iMR severity. Patients with $_b$PMI have increased underlying LV chamber wall ischemic burden and greater adverse LV and mitral apparatus remodeling.

	$_b$PMI +	$_b$PMI -	p
Mitral Apparatus Remodeling			
Tenting area (3 chamber)	2.7±1.3	1.6±0.8	0.001
Tenting area (4 chamber)	1.9±0.9	1.2±0.7	0.008
Sphericity	0.5±0.1	0.4±0.1	0.001
Inter Papillary Muscle Distance (diastole)	2.8±0.6	2.5±0.5	0.04
Inter Papillary Muscle Distance (systole)	1.9±0.6	1.5±0.6	0.036
Papillary Muscle Shortening (%)	36±16	44±17	0.11
Cardiac Chamber Size and Function			
LV end-diastolic diameter (cm)	6.2±0.7	5.4±0.6	<0.001
LV end-diastolic volume (ml)	218±62	172±71	0.03
LV end-systolic volume (ml)	140±61	87±67	0.01
LV ejection fraction (%)	38±15	53±16	0.004
Left atrial diameter (cm)	4.3±0.5	4.1±0.5	0.17
Left atrial area (cm^2)	27.1±5.0	25.2±7.8	0.34
Left Ventricular Ischemia (# segments)			
Global Ischemia (# segments)	9.8±3.7	5.0±4.0	<0.001
Regional Ischemia			
Anterior	2.0±1.7	0.8±1.3	0.01
Inferior	3.8±1.2	2.7±2.2	0.06
Lateral	2.9±1.7	1.1±1.5	0.001
Left Ventricular Infarction			
Global Infarct Size (% LV myocardium)	11.5±8.7	7.3±9.1	0.14
Regional Infarction			
Anterior	2.0±3.2	1.2±3.0	0.41
Inferior	3.2±3.7	2.2±3.9	0.41
Lateral	4.3±5.4	3.0±6.6	0.47

P037

Early LGE may severely underestimate salvaged myocardium after acute myocardial infarction verified by MRI and histology

Yushu Chen, MD[1] Fabao Gao, MD,PHD[2]

1. Molecular Imaging Center,Department of Radiology, West China Hospital. Sichuan University, Sichuan, China (People's Republic)
2. China West Hospital, Sichuan, China (People's Republic)

Background: The enhanced myocardial areas in LGE images recede over time with corresponding recovery of function. Changes in the myocardium in acute ischemia are dynamic and complex, and the characteristics of myocardial tissue on cardiovascular magnetic resonance in the acute setting are not fully defined. The aim is to investigate the mechanism of the delayed enhancement of myocardium after myocardial ischemia, and re-understand the consensus that the area of high intensity at 10min to 30min in delayed enhancement means myocardial infarction with myocardium necrosis and apoptosis.

Methods: The left coronary artery was ligatured in 20 Sprague Dawley rats (250~300g, 12 weeks) for permanent ligation (Group 1, n=8) and 30min ligation followed by reperfusion (Group2, n=12). LGE scans were performed in Group 1 at 24h after rat model established by 7.0T MR, and performed in Group 2 at the rat analepsia after the operation by 7.0T MR. The short-axis LGE images were obtained from 5min to 75min with a 5min interval after Gd-DTPA injection (0.6 mmol/kg) by slice to slice and from apex to base. The intensity of enhanced myocardium area were defined by the $S_{ischemic}/S_{norm}$. The TTC stains and HE stains were used to evaluate the myocardium and intercellular substance alteration.

Results: 4 rats got the integrated data in each group. The hyperintensity distributed by the vascular domination of ischemia in Group 2 (4.92±1.05) after Gd-DTPA injection immediately was high greater than Group 1 (3.67±0.93). The area of ischemic were enhanced at 10~30min, and gradually wash-out during the scan experience in Group 2 but slowly wash-out in Group 1. But there were no significant differences among the different scan times in two groups. While the TTC stain found that there was high consistent between TTC infarct size and LGE size in Group 1, and a notable reduce from LGE size to TTC infarct size in Group 2. HE stains showed the obvious edema, inflammation, and slightly necrosis in the ischemic myocardium in Group 2. The vacuoles and necrosis with or without red blood cell were seen in the infarct area in Group 1.

Conclusions: The membrane integrity and the cardiocyte condition were diversity caused by different degree of ischemic. For myocardial ischemic, the hyperintensity of LGE-MRI might not represent the dead cardiocytes. LGE may severely underestimate salvaged myocardium.

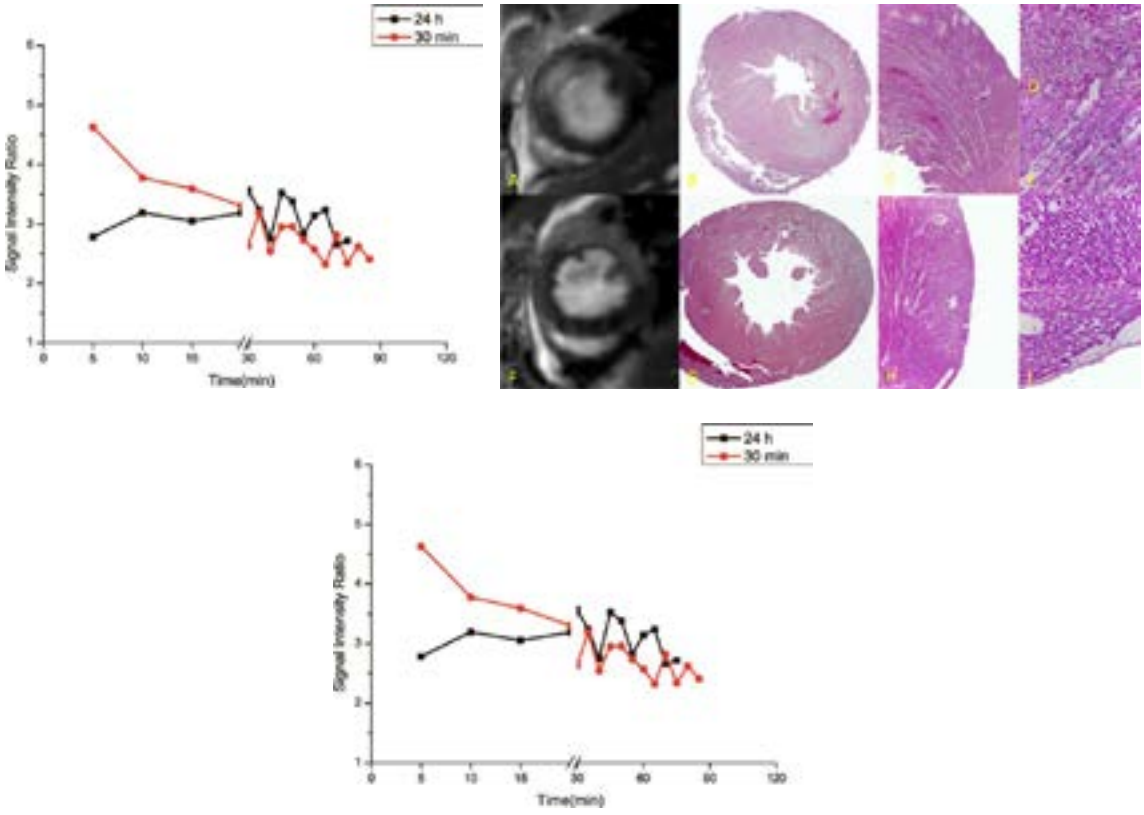

P038

Vasodilator-induced Myocardial Perfusion Gradients as a Surrogate Marker of Coronary Endothelial Function: Initial Results in Women with Suspected Microvascular Dysfunction

Behzad Sharif, PhD[1] Ahmed Albadri, MD[1], Janet Wei, MD[1], Debiao Li, PhD[2], Daniel Berman, MD[3], C. Noel Bairey Merz, MD[4]

1. *Cedars-Sinai Medical Center, Los Angeles, Los Angeles, CA*
2. *Biomedical Imaging Research Institute, Cedars-Sinai Medical Center, Los Angeles, CA, CA*
3. *Cedars-Sinai Medical Center, Los Angeles, CA*
4. *Cedars Sinai Medical Center, Los Angeles, CA*

Background: Nearly 50% of women with signs and symptoms of ischemic heart disease suffer from coronary microvascular dysfunction (CMD) in the absence of obstructive coronary artery disease. In this cohort, a common pathophysiologic mechanism involves dysfunction of coronary endothelium [1]. Despite several advancements and intense interest, accurate detection of *microvascular endothelial dysfunction* on the basis of stress perfusion CMR remains an ongoing challenge. Specifically, it is not known whether variables derived from perfusion CMR can be used as noninvasive surrogates for assessing coronary endothelial function. Inspired by a recent CMR study in a large animal model of CMD [2], we hypothesized that hyperemic myocardial perfusion gradients are correlated with the gold-standard invasive marker of coronary endothelial function in symptomatic subjects with angiographically-normal coronaries and normal *macrovascular* function.

Methods: Eight women with symptoms of ischemia and no angiographic disease (i.e., < 50% epicardial stenosis) underwent CMR and invasive coronary reactivity testing — the gold-standard measure of coronary endothelial-dependent and endothelial-independent function [3]. Microvascular endothelial function was assessed invasively by measuring the change in coronary blood flow (CBF) in response to intracoronary Acetylcholine (ACh) infusion, with >50% CBF increase considered normal [3]. The perfusion CMR study was performed using an improved free-breathing technique (in-plane resolution: 1.7 x 1.7 mm^2) that minimized the dark-rim artifact [4]. Myocardial blood flow (MBF) was quantified in the slice with the thickest myocardium (≥6 pixels transmurally) to ensure reliable assessment of perfusion gradients.

Results: Two patients were excluded from the analysis due to abnormal response to intracoronary Nitroglycerin, which indicates endothelial-independent *macrovascular* dysfunction. Fig. 1 shows representative results in two subjects with suspected CMD. In case (a), the subject had an abnormal ACh response and her CMR results demonstrated a visually detectable stress-induced perfusion gradient in the mid-basal slice (subendo/subepi MBF ratio = 0.72). The case in (b) had a normal ACh response and no detectable perfusion gradient (subendo/subepi MBF ratio = 0.98). Fig. 2 compares the intracoronary ACh response (% CBF change) versus the CMR-derived subendo/subepi MBF ratio in the 6 analyzed cases.

Conclusions: The aim of this study was to test whether high-resolution hyperemic myocardial blood flow maps obtained using vasodilator-stress perfusion CMR can be used to probe microvascular endothelial function in patients with suspected CMD. Our initial results are promising and suggest a potential role for CMR-derived hyperemic perfusion gradients as a noninvasive surrogate of the established invasive marker.

References:

[1] Camici P and Crea F. N Engl J Med 2007.

[2] Sharif B et al. SCMR 2016.

[3] von Mering G et al. Circ 2004.

[4] Zhou Z et al. JMRI 2016; In Press.

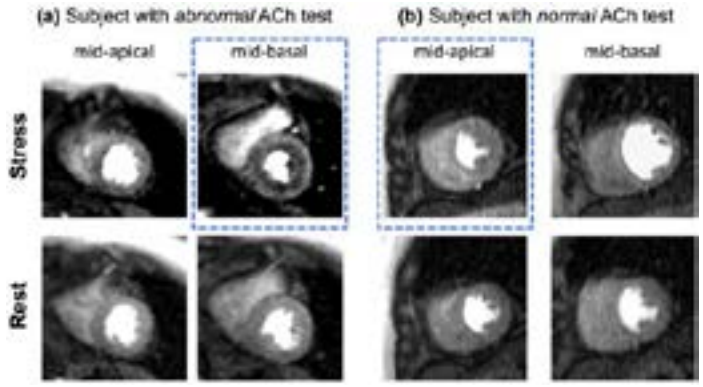

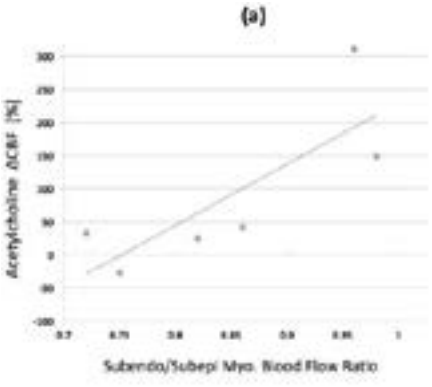

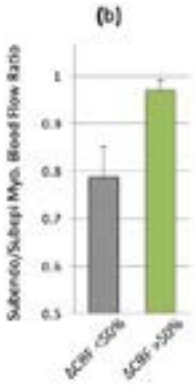

P039

The Glasgow MRI Rotational Atherectomy Study (GlaMoRoS): HSRA PCI is associated with a low rate of peri-procedural MI and a significant improvement in ischemic burden

David Corcoran, BSc (Hons), MBChB, MRCP[1] Colin Berry, PhD FRCP[2], Guillaume Clerfond, MD[3], David Carrick, PhD[4], Kenneth Mangion, MD[2], Barry Hennigan, MB BCh BAO[4], Paul Rocchiccioli, MD, FRCP[5], Aleksandra Radjenovic, MSc PhD[6], Mitchell Lindsay, MD[7], Hany Eteiba, MD[7], Keith G. Oldroyd, MD (Hons); FRCP[7], Margaret McEntegart, MBChB PhD[4]

1. *University of Glasgow, Scotland, United Kingdom*
2. *University of Glasgow, Glasgow, Scotland, United Kingdom*
3. *University Hospital of Clermont Ferrand, France, Clermont Ferrand, Auvergne, France*
4. *Golden Jubilee National Hospital, Glasgow, Scotland, United Kingdom*
5. *West of Scotland Regional Heart & Lung Centre - Golden Jubilee National Hospital, Clydebank, Scotland, United Kingdom*
6. *University of Glasgow, UK, Glasgow, Scotland, United Kingdom*
7. *Golden Jubilee National Hospital, Scotland, United Kingdom*

Background: Percutaneous coronary intervention (PCI) with adjunctive high speed rotational atherectomy (HSRA) is commonly used to treat complex and calcified coronary artery stenoses. Theoretically, HSRA may have deleterious effects on the coronary microcirculation and result in peri-procedural myocardial infarction (Type 4a MI). We studied the effects of HSRA PCI using serial multi-parametric cardiac magnetic resonance imaging (CMR).

Methods: We prospectively enrolled 58 patients undergoing elective HSRA PCI and performed multi-parametric CMR at 3 time-points: before HSRA (T1), < 7 days post-HSRA (T2), and 6 months post-HSRA (T3). The CMR protocol comprised global and regional LV function assessment, adenosine stress perfusion, and late gadolinium enhancement (LGE) (1.5 Tesla MAGNETOM Avanto, Siemens Healthcare, Germany). Myocardial perfusion abnormalities were assessed qualitatively. High-sensitivity cardiac troponin (hsTn) was measured post-HSRA. Results are expressed as means and standard deviations and are compared using Student's t-test for paired data with Bonferroni correction for multiple testing. A p value ≤0.0167 was considered significant.

Results: 46 participants had complete data for all 3 time-points (Table). There was no change in LV ejection fraction or volumes from baseline to < 7 days or 6 months post-HSRA. There was a reduction in ischemic burden from baseline to < 7 days and a further reduction at 6 months post-HSRA. 26 participants (57%) had a significant increase in hsTn (values > 5 × 99th percentile upper reference limit). Compared to baseline, 10 participants (22%) had evidence of new LGE in myocardium subtended by the target artery. Of these, 3 patients (30%) had a new regional wall motion abnormality on cine imaging at T2 which resolved by T3.

Conclusions: This data demonstrates that PCI with adjunctive HSRA can be performed with a low risk of significant peri-procedural MI assessed by CMR, and results in a significant improvement in ischemic burden both acutely and after longer term follow-up.

T1 vs. T3	T1 vs. T2	6 months post-HSRA (T3)	<7 days post-HSRA (T2)	Baseline pre-HSRA (T1)	
p = 0.210	p = 0.831	61.7 (10.1)	62.8 (9.9)	62.6 (11.0)	LV ejection fraction (%) (n = 46)
p = 0.833	p = 0.941	148.7 (33.5)	150.4 (34.6)	150.5 (37.6)	LV EDV (ml) (n = 46)
p = 0.871	p = 0.938	58.6 (31.6)	57.8 (27.2)	58.4 (31.6)	LV ESV (ml) (n = 46)
p <0.001	**p <0.001**	1.58 (2.6)	2.85 (3.1)	6.76 (4.5)	Number of ischemic segments (n = 46)

LV = left ventricular, EDV = end-diastolic volume, ESV = end-systolic volume.

P040

T1 mapping at rest and adenosine stress - comparison of T1 mapping sequences for feasibility and effect size

Valentina O. Puntmann, MD, PhD[6] Elif Peker, MD[1], Lea Winau[2], Robert Heinke[2], Katrin Schnoes, MD[2], Julian Lukas. Wichmann, MD[3], Thomas Vogl, MD[2], Andreas Zeiher, MD, PhD[2], Andreas Greiser, Ph.D[4], Eike Nagel, MD, PhD[5]

1. *Goethe University Hospital Frankfurt, Frankfurt, N/A, Germany*
2. *Goethe University Hospital Frankfurt, N/A, Germany*
3. *University Hospital Frankfurt, Frankfurt, Hessen, Germany*
4. *Siemens Healthcare GmbH, Erlangen, Germany, Erlangen, Bayern, Germany*
5. *University Hospital Frankfurt; Institute for Experimental and Translational Cardiovascular Imaging; DZHK Centre for Cardiovascular Imaging, Frankfurt, N/A, Germany*
6. *Institute of experimental and translational cardiovascular imaging, Frankfurt, N/A, Germany*

Background: Detection of myocardial ischemia supports targeted revascularization and improved clinical outcomes. T1 mapping at rest and during adenosine stress was proposed as a novel method for ischemia detection without the use of gadolinium contrast. The aim of this study was to evaluate the overall feasibility of T1 mapping sequences, as well as to compare their relative effect size.

Methods: Consecutive patients underwent T1 mapping with 3 MOLLI sequences (MOLLI5(3)3FA35; MOLLI 3(3)3(3)5FA50; MOLLI3(2)3(2)5FA50; 1.5T and 3.0T Siemens) in a single mid-ventricular slice prior to and 3 minutes into Adenosine infusion (140 mcg/kg/min; after a documented (>15%) heart rate response and onset of typical Adenosine-induced symptoms). All T1 maps were reconstructed inline with MOCO algorithm. T1 values were measured in septal segments in normal myocardium. Images were deemed diagnostic if free of artefacts (cardiac/respiratory motion, mistriggering, phase wrapping, less than 3-fold increase in SD of ROI). Obstructive coronary artery disease in these patients was excluded by means of contrast-enhanced MR-myocardial perfusion imaging and coronary angiography. Patients with LGE in septal segments were not included.

Results: A total of 55 patients were included (mean age 56±12; male n=16(67%). Of these stress-images were deemed diagnostic in 24(46%) subjects (1.5T; n=13; 3.0T n=11). A summary of observed technical issues in 31 excluded patients is provided in Table 1: respiratory motion at stress was the commonest cause of artefacts, where MOLLI3(3)3(3)5FA50 is particularly vulnerable due to a long breathhold. In the remaining 24 patients (Table 2), Figure 1), all 3 sequences were able to detect increase in blood flow, of these MOLLI3(2)3(2)FA50 showed the greatest effect size at both field strengths.

Conclusions: T1 mapping for detection of increased blood flow is only partially feasible in clinical routine, due to motion artefacts, which could not be overcome by the inline MOCO. In the remaining patients, all 3 sequences were able to detect increase in blood flow, of these MOLLI3(2)3(2)FA50 showed the greatest effect size at both field strengths. Further technical development is required to support such scans in clinical setting.

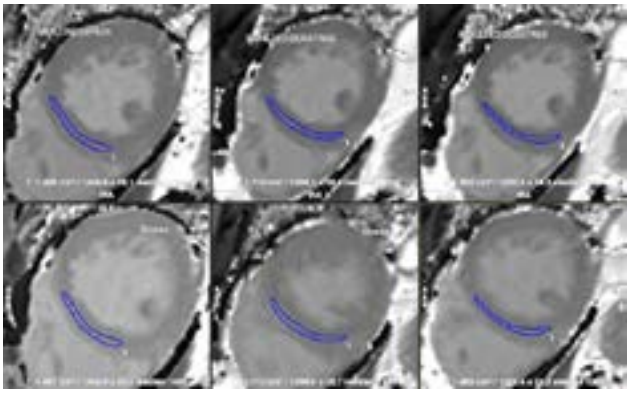

Table 1

Per sequence			Number(%)	Types of artefacts
MOLLI3(2)3(2)5FA50	MOLLI3(3)3(3)5FA50	MOLLI5(3)3FA35	All patients	
26(84)	31 (100)	25(81)	31 (100)	Respiratory motion
17(55)	22 (71)	16(52)	26 (84)	Cardiac mistriggering (scanner -> 2HB acquisition)
5(16)	6 (20)	6 (20)	6 (20)	Cardiac mistriggering (patient's arrhythmia)
5 (16)	5 (16)	5 (16)	5 (16)	Change of phase encoding direction at stress
16(52)	18 (58)	14(45)	18 (58)	3-fold increase in SD of the ROI

Table 2

Cohen-D	Sig.(p-value)	MD±SD	Stress	Rest	Native T1 (msec)
0.9	0.006	-12±8	75±23	59±11	Heart rate (bpm)
					1.5T (n=13)
0.6	0.001	-33±47	1034±55	1001±50	MOLLI5(3)3FA35
0.8	0.002	-45±47	1082±58	1036±56	MOLLI3(3)3(3)5FA50
0.9	<0.001	-47±38	1036±47	993±46	MOLLI3(2)3(2)5FA50
					3.0T (n=11)
0.6	0.039	-45±31	1217±95	1166±79	MOLLI5(3)3FA35
0.4	0.089	-40±45	1165±105	1130±75	MOLLI3(3)3(3)5FA50
0.7	0.013	-51±52	1153±89	1078±75	MOLLI3(2)3(2)5FA50

P041

Global Longitudinal Strain Predicts the Transmural Extent of Infarction Revealed by Late Gadolinium Enhancement in Patients with Recent Non ST-Segment Elevation Myocardial Infarction.

Nicole M M. Burke, B.Sc. (Med. Sci) Clinical Medicine[1], Kenneth Mangion, MD[1]Samuli M. O. Rauhalammi, MSc, MSci, BA[2], Christie McComb, PhD[3], Hany Eteiba, MD[4], Mitchell Lindsay, MD[4], Margaret McEntegart, MBChB PhD[5], Mark Petrie, MD[6], Stuart Hood, MD FRCP[7], Stuart Watkins, MD, FRCP[5], Jamie Layland, MBChB PhD[8], Keith G. Oldroyd, MD (Hons); FRCP[4], Colin Berry, PhD FRCP[1]

1. *University of Glasgow, Glasgow, Scotland, United Kingdom*
2. *University of Glasgow, Tonopah, AZ*
3. *NHS Greater Glasgow and Clyde / University of Glasgow, Glasgow, Scotland, United Kingdom*
4. *Golden Jubilee National Hospital, Scotland, United Kingdom*
5. *Golden Jubilee National Hospital, Glasgow, Scotland, United Kingdom*
6. *Glasgow University, Scotland, United Kingdom*
7. *NHS Greater Glasgow and Clyde, Scotland, United Kingdom*
8. *University of Glasgow, N/A, Australia*

Background: Patients diagnosed with a non-ST segment elevation myocardial infarction (NSTEMI) typically have a sub-acute presentation, associated with a limited infarct size and preserved LV ejection fraction (LVEF).We hypothesised that LV peak longitudinal strain is a stronger associate of segmental scar transmurality than LVEF in patients with recent NSTEMI. We also aimed to assess these associations for strain assessed in different LV planes.

Methods: Participants in the British Heart Foundation FAMOUS-NSTEMI CMR sub-study (ClinicalTrials.gov Identifier: NCT02073422) were invited to undergo cardiac magnetic resonance imaging (CMR) at 3.0 Tesla within 10 days post NSTEMI and age- and sex- matched healthy volunteers (HV, n=44) without any history of cardiovascular disease underwent CMR during the same time-frame. Longitudinal LV strain values were derived from horizontal (HLA), vertical long axis (VLA) and LV outflow tract (LVOT) cine images using feature-tracking software (TomTec, Germany). Strain values were averaged to provide a global longitudinal strain (GLS) value for each patient. LV mass and function was quantified using cine-SSFP imaging. Scar was quantified using late gadolinium enhancement imaging ~10 minutes after I.V.administration of a gadolinium (Gd) contrast agent (Gadovist (0.1 mmol/kg); Bayer Pharma, Berlin, Germany) and quantified using commercial software (QMass, Medis, Leiden, Netherlands). Receiver Operating Characteristic (ROC) analysis was used in order to asses specificity and sensitivity of GLS values as an indicator of a patient having a myocardial segment with >50% scar transmurality. All subjects provided written informed consent.

Results: 103 patients (mean age 56.90(±9.95) years; 81% male) with recent NSTEMI were enrolled. Overall, the mean±SD LVEF was 57.4±57.4 and infarct size was 2.3 (IQR 0% to 8.6%)of LV mass. The mean ±SD GLS was -17.96±4.2. 22 (21.36%) patients had ≥1segment with >50% scar transmurality. Averaged GLS had good predictive accuracy for >50% scar transmurality (ΔAUC 0.68, SE 0.07, p= 0.014 95% CI 0.54 to 0.80), unlike LVEF vs. >50% scar transmurality (ΔAUC 0.41, SE 0.08, p=.215, 95%CI 0.25 to 0.57). A GLS value of -15.93 had 0.71 specificity and 0.57 sensitivity at detecting >50% scar transmurality. GLS measured in the vertical long axis plane was the most accurate (ΔAUC 0.70, SE 0.06, p= 0.006, 95% CI 0.59 to 0.81).

Conclusions: In patients with recent NSTEMI, GLS was associated with the transmural extent of infarction on a per-segment basis, whereas LVEF was not. Our results support the clinical utility of GLS as a new biomarker of the severity of MI and its functional consequences in patients with recent NSTEMI.

P042

Global Longitudinal Strain is Independently Associated with Left Ventricular Infarct Characteristics in Patients with Recent Non ST-Segment Myocardial Infarction

Nicole M M. Burke, B.Sc. (Med. Sci) Clinical Medicine[1], Kenneth Mangion, MD[1]Samuli M. O. Rauhalammi, MSc, MSci, BA[2], Christie McComb, PhD[3], Hany Eteiba, MD[4], Hao Gao, PhD[5], Mitchell Lindsay, MD[4], Margaret McEntegart, MBChB PhD[6], Stuart Hood, MD FRCP[7], Mark Petrie, MD[8], Stuart Watkins, MD, FRCP[6], Jamie Layland, MBChB PhD[9], Keith G. Oldroyd, MD (Hons); FRCP[4], Colin Berry, PhD FRCP[1]

1. *University of Glasgow, Glasgow, Scotland, United Kingdom*
2. *University of Glasgow, Tonopah, AZ*
3. *NHS Greater Glasgow and Clyde / University of Glasgow, Glasgow, Scotland, United Kingdom*
4. *Golden Jubilee National Hospital, Scotland, United Kingdom*
5. *School of Mathematics and Statistics, University of Glasgow, Scotland, United Kingdom*
6. *Golden Jubilee National Hospital, Glasgow, Scotland, United Kingdom*
7. *NHS Greater Glasgow and Clyde, Scotland, United Kingdom*
8. *Glasgow University, Scotland, United Kingdom*
9. *University of Glasgow, N/A, Australia*

Background: Non-ST segment elevation myocardial infarction (NSTEMI) is typically associated with non-occlusive coronary thrombosis and non-transmural infarction, unlike STEMI. However, paradoxically, these conditions have a similar longer-term prognosis. We hypothesised that left ventricular (LV) circumferential strain (Ecc) and longitudinal strain (Ell) might provide novel insights into the functional consequences of infarct pathology in NSTEMI.

Methods: Patients underwent cardiac magnetic resonance imaging (CMR) at 3.0 Tesla within 10 days post NSTEMI, along with healthy volunteers (HV, n=44). LV ejection fraction (LVEF), and volumes were derived from cine-SSFP CMR images using dedicated software (Medis, NL). Longitudinal LV strain values were derived from vertical (VLA), horizontal long axis (HLA) and LV outflow tract (LVOT) cine scans, and averaged to derive global longitudinal strain (GLS). Mid LV Ecc was derived from the mid-LV short axis slice. Strain values were derived using feature-tracking software (TomTec, Germany). Oedema was quantified from T1 maps (ECG-gated single shot MOLLI) and T2 maps (T2 prepared TrueFISP pulse sequence), and the transmural extent of scar was assessed from late gadolinium enhancement imaging ((Gadovist (0.1 mmol/kg); Bayer, Germany),. The study was publically registered https://clinicaltrials.gov/ct2/show/NCT02073422 and all subjects provided written informed consent.

Results: 103 patients (mean age 56.9±9.9 years;81% male) and 44 healthy volunteers (mean age 56.6±11.2 years;52.3% male) were prospectively enrolled. The following CMR results were obtained in the NSTEMI patients:, the average infarct size (% LV mass) was 2.3 (IQR 0% to 8.6%), area-at-risk 15.0% (IQR 6.4% to 21.7%), LVEF 57.4 (±8.6), EDV 91.0ml/m^2 (±8.9) and ESV 39.4ml/m^2(±14.1). The mid LV Ecc were -22.9 (±5.8) and -29.9 (±3.6) for NSTEMI patients and healthy volunteers, respectively, ($p < 0.001$, 95%CI -7.5 to -4.4). Ecc correlated with total infarct size (r=0.20, p=0.045), and the extent of oedema (% LV mass) as revealed by T1 maps (r=0.31, p=0.002) and by T2 maps (0.32, p=0.002). Ecc was not correlated with either LVEF (p=0.31), LVEDV (p=0.20) or LVESV (p=0.80). Mean GLS values were -17.9±4.2 and -20.4±2.9 for NSTEMI patients and healthy volunteers, respectively ($p < 0.001$, 95%CI -3.9, -1.6). GLS was correlated with LVEF (r=-0.44, $p < 0.001$), ESV (r=0.41, $p < 0.001$), total infarct size (r=0.32, p=0.001) and extent of oedema (r=0.27, p=0.006). GLS did not correlate with EDV (r=0.18, p=0.076). LVEF correlated with infarct size (r-0.445, $p < 0.001$).

Conclusions: In invasively managed patients with recent NSTEMI, GLS was more closely associated with infarct characteristics and LVEF than Ecc. GLS potentially represents a new imaging biomarker in patients with recent NSTEMI.

P043

T1-based Synthetic Inversion Recovery Imaging for Quantitative Inversion Time Prescription for Late Gadolinium Enhancement – Eliminating the Subjective Estimation of Inversion Time

Akos Varga-Szemes, MD, PhD[1] Rob J. van der Geest, PhD[2], U. Joseph Schoepf, MD[1], Taylor M. Duguay, BS[1], Carlo N. De Cecco, MD, PhD[1], Christian Tesche, MD[1], Moritz Albrecht, MD[1], Domenico De Santis, MD[1], Pal Suranyi, MD, PhD[1]

1. *Medical University of South Carolina, SC*
2. *Department of Radiology, Leiden University Medical Center, Leiden, The Netherlands, Zuid-Holland, Netherlands*

Background: Conventional Look-Locker (LL)-based inversion time (TI) estimation ("TI-scout") is a requirement prior to late gadolinium enhancement (LGE) imaging to achieve the appropriate image contrast. The TI-scout sequence has multiple limitations, including: the long breath-hold necessary, the lack of cardiac gating, and the overly subjective and user-dependent TI estimation. In this study we aimed to develop a quantitative synthetic inversion recovery (IR)-based approach which allows the calculation of the most optimal TI for LGE imaging.

Methods: Twenty-one consecutive patients (53±18 years, 12 male) referred for myocardial viability evaluation underwent 1.5T MRI (MAGNETOM Avanto, Siemens AG, Erlangen, Germany). Twelve minutes after contrast (0.1mmol/kg gadobenate-dimeglumine) TI-scout (LL, 18 phases, TI range 90-600ms) and T1-mapping (modified LL IR, scheme 4(1)3(1)2) acquisitions were performed in the 4-chamber view in a random order. Based on the T1 maps, synthetic magnitude IR images were calculated in a TI range of 200-400 with 5ms increments. The most optimal TI was determined from both TI-scout and synthetic IR images, but randomly prescribed for the actual LGE acquisition. Image quality was subjectively rated by two observers and the nulling was objectively measured based on the myocardial/background signal ratio. The two groups were compared using the Kruskal-Wallis test.

Results: The optimal TI was estimated significantly lower by the TI-scout approach compared to the synthetic IR technique (251.6±43.9ms vs. 292.5±40.6ms, $P < 0.0001$). The acquisition order did not influence the value of optimal TI (P=0.4061). Using the synthetic IR-based TI for LGE acquisition (n=11) provided significantly higher image quality ratings (3 [2-3] vs. 2 [1.75-2], P=0.0078) and better myocardial signal nulling (1.2 [1.1-1.2] vs. 2.2 [1.6-3.1], P=0.0058) compared to the TI-scout-based group (n=10).

Conclusions: T1-based synthetic IR imaging provides objective, quantitative, and real-time prescription of the optimal TI for LGE imaging; eliminating the need for LL TI correction and the substantial operator dependence of the acquisition. In addition, given that all synthetic LGE images are in the same cardiac phase, the placement of the regions of interest to determine which image has the best timing is better optimized.

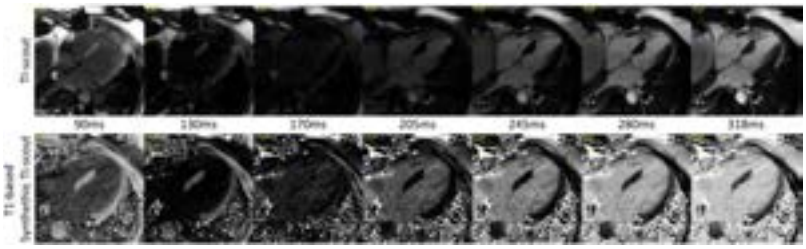

P044

Myocardial oxygenation changes during breathing maneuvers in patients with Syndrome-X.

Giulia Vinco, MD[1]Kady Fischer, BHSc[2], Dominik P. Guensch, MD[3], Matthias G. Friedrich, MD[1]

1. *McGill University Health Centre, PQ, Canada*
2. *McGill University Health Center, Montreal, PQ, Canada*
3. *Department of Anesthesiology and Pain Therapy / Institute for Diagnostic, Interventional and Pediatric Radiology, Bern University Hospital, Inselspital, University of Bern, Switzerland, Bern, Bern, Switzerland*

Background: The use of a breathing maneuver combining hyperventilation and a following breath-hold has been shown as an effective vasoactive stimulus, able to induce myocardial oxygenation changes which are detectable by Oxygenation-sensitive Cardiovascular Magnetic Resonance (OS-CMR). While hyperventilation leads to a reduction of blood flow, long breathholds result in coronary vasodilation. We applied this technique in a small cohort of patients with Syndrome X, which pathophysiologically remains controversial due to the association of angina and stress-induced ischemia despite angiographically normal coronary arteries. This is a sub-analysis of a currently ongoing multicenter trial applying OS-CMR on coronary artery disease (CAD) patients and healthy volunteers.

Methods: Six subjects presenting with Syndrome X (cardiac symptoms, positive stress test, normal coronary angiography), were studied using a clinical 3T MRI system. OS-CMR images were acquired in two short-axis slices (mid-basal and mid-apical) using an ECG-triggered balanced SSFP sequence. The subjects were instructed to perform a combined breathing maneuver by hyperventilating for 60s with a rate of 30 breaths/min paced by a metronome, followed by a maximal breath-hold at end-expiration (HVBH). OS-CMR images were obtained and analyzed for the global myocardial signal intensity (SI) at the beginning and at 30s timepoint of the HVBH, as well as prior to the maneuver. SI changes across hyperventilation (SI_{HV}) were calculated, as well as between the start of the breath-hold and the 30s time-point of the HVBH (SI_{30s}).

Results: The mean age of the patients was 56 ± 7 y, 4 patients were male and none of them was diabetic. The mean duration of the HVBH for the patients was 85 ± 42 s, and the the SI_{30s} was 3.2±4.9%. Compared with a previously published control group with a $SI_{30s}$of 11.7±6.4%, the response of myocardial oxygenation to the vasodilating apnea was blunted in Syndrome-X patients ($p < 0.05$, Eur Heart J Cardiovasc Imaging.2015;16:395-401). There was no significant difference between the two groups for the vasoconstricting hyperventilation stimulus (-8±13% vs -10.6±7.8%, p=ns).

Conclusions: Our preliminary data suggest that Syndrome-X patients have a blunted myocardial oxygenation response to the HVBH stimulus compared to healthy volunteers, which likely reflects an impaired coronary vascular function in terms of coronary vasodilation. In the controversial scenario of Syndrome-X, OS-CMR with breathing maneuvers could play a role in clarifying the pathogenesis of this disease and identifying patients with coronary vasomotion dysfunction.

Myocardial oxygenation changes during breathing maneuvers

SI CHANGE (%)	
- 8 ± 13	**SI_{HV} - global**
3.2 ± 4.9	**SI_{30s} - global**
- 9 ± 16.3	**SI_{HV} - midbasal**
3.8 ± 7.2	**SI_{30s} - midbasal**
- 6.1 ± 11.1	**SI_{HV} - midapical**
2.7± 5.3	**SI_{30s} - midapical**

P045

The Occurrence and Characteristics of Right Ventricular Dysfunction after Acute Anterior Myocardial Infarction by Cardiac Magnetic Resonance

Bo Jiang, M.D.[1] Yucheng Chen, MD[2], Yong He, M.D.[3]

1. *West China Hospital,Sichuan University, Liaoning, China (People's Republic)*
2. *West China Hospital, CHENGDU, Sichuan, China (People's Republic)*
3. *West China Hospital,Sichuan University, Sichuan, China (People's Republic)*

Background: Right ventricular (RV) dysfunction complicating acute myocardial infarction (AMI) have been proved as a predictor for adverse cardiac events. In patients with anterior wall AMI, RV function also could be affected. The occurrence and characteristics of RV dysfunction in acute phase of anterior AMI are still unclear. The aim of this study is to explore the occurrence and characteristics of RV dysfunction after acute anterior myocardial infarction by cardiac magnetic resonance (CMR).

Methods: 54 patients with acute anterior ST-segment elevated myocardial infarction (STEMI) were enrolled in this study after successful primary percutaneous coronary intervention (PCI). Cardiac magnetic resonance was performed within 7 days after STEMI. Evaluating biventricular function using SSFP sequences, T2 weighted turbo spin echo sequences and late gadolinium enhancement technique were used to characterize myocardial tissue. Patients were divided into two groups according to right ventricular function (RVEF $\geq$ 45% or RVEF < 45%). Comparison of clinical and CMR findings between two groups were undertaken. Correlation between RVEF and other factors were analyzed by univariate and multivariable linear regression. ROC curve was performed to evaluate predictive value to right ventricular dysfunction.

Results: 13 cases (24.1%) with RV dysfunction among the total of 54 patients were identified. LVEF was significantly less in patients with RV dysfunction than with normal RVEF (36.9±16.9%; 45.8±9.6%, $p < 0.05$); Interventricular septum infarct size (IS-IVS) was greater in the RV dysfunction group than RV normal group (72.9±7.5**%;** 62.7±14.3%, $p < 0.05$). RVEF was independently correlated with interventricular septal infarct size or LVEF respectively (β=-0.353, p=0.010; β=0.440, p=0.001). By ROC curve analysis, LVEF lower than 38.2% had a sensitivity of 69.2% and a specificity of 80.5% in predicting of RV dysfunction (AUC=0.75, 95%CI=0.587-0.914(p=0.007));IS-IVS greater than 66.88% had a sensitivity of 91.7% and a specificity of 65.9% (AUC=0.73, 95%CI=0.583-0.877 (p=0.016)).

Conclusions: Occurrence of right ventricular dysfunction in acute phase of anterior STEMI is not rare. Infarct size of interventricular septum or LVEF is the independent predictor of RV dysfunction in acute anterior STEMI.

P046

Evaluation of k-Space and Image-Space Motion Correction Schemes for CMR Perfusion.

Haris Jeelani[1] Yang Yang, PhD[2], Michael Salerno, MD, PhD[2], Daniel S. Weller, PhD[3]

1. *University of Virgnia, Charlottesville, VA*
2. *University of Virginia, VA*
3. *University of Virginia, Charlottesville, VA*

Background: First-pass stress perfusion CMR has high diagnostic and prognostic utility for CAD. Using spiral trajectories and advanced reconstruction techniques such as L1-SPIRIT that exploit temporal redundancy in the data, CMR perfusion images can be acquired with whole heart coverage and high spatial and temporal resolution. Such reconstruction techniques are limited by their sensitivity to heart motion during image acquisition, which is problematic clinically in the setting of poor breath-holding or free breathing acquisition. As respiratory motion is well approximated by rigid motion, this study compares the efficacy of k-space-domain versus image-domain rigid motion estimation techniques to improve reconstructed image quality.

Methods: This study utilized 10 clinical datasets, each containing fifty free-breathing perfusion images covering the whole heart obtained during 0.075 mmol/kg Magnevist injection at a rate of 4mL/s. Four proton-density images were acquired at the beginning for SPIRiT calibration. The remaining frames contain T1-weighted data acquired with SRT 80ms, TE 1.0ms, 5ms spiral and 3 spirals per slice, effective TR 14ms, FA 30o, FOV 340mm2, around 2mm in-plane resolution. The spiral trajectory is Fermi-shape dual density with 20% of the trajectory fully sampled, transitioning to an ending density of 0.13x Nyquist. For k-space motion-estimation, the data in the central $1/5^{th}$ of k-space was used to find the best linear phase shifts by minimizing the sum of squares error (SSE) between a reference frame and other linearly phase shifted k-space frames. For image-space estimation, gridding reconstruction is performed and the SSE is minimized between the reference image and translated individual frames. These translations are corrected via linear phase shifts in k-space. The images were visually inspected by a cardiologist on a five-point scale (1-poor to 5-excellent).

Results: Figure 1a shows similar temporal profiles (bottom two rows) for head-foot and left-right directions after applying the two motion compensation schemes. The blurring artifacts in top row of Figure 1b are significantly reduced (bottom row) after correcting motion. Figure 2a shows similar motion estimates found using k-space and image-space techniques for the dataset shown in Fig1. The images obtained using k-space estimation method received average rating of 3.8 whereas image-space method images got a score of 4.2. Images with no motion correction received a score of 3.2.

Conclusions: In this study, we implemented k-space and image-space motion correction techniques and found the latter performs better in the majority of cases.

http://www.ConferenceAbstracts.com/uploads/cfp2/attachments/LDFAIBDN/LDFAIBDN--218514-1-ANY(2).pdf

http://www.ConferenceAbstracts.com/uploads/cfp2/attachments/LDFAIBDN/LDFAIBDN--218514-2-ANY.pdf

P047

Impact of post-processing for motion correction on the evaluation of stress perfusion CMR

Stephanie Reiter, MD[1], Günter Pilz, MD, Professor[1] Anne Menini, PhD[2], Karl Ziegler, MD[1], Florian von Knobelsdorff-Brenkenhoff, MD[3], Berthold Höfling, MD[1]

1. *Cardiology at Clinic Agatharied, University of Munich, Bayern, Germany*
2. *General Electric Global Research Center, Bayern, Germany*
3. *Cardiology at Clinic Agatharied, University of Munich, Hausham, Bayern, Germany*

Background: Image analysis of stress perfusion CMR is predominantly done visually and naturally influenced by readers' experience and image quality, potentially leading to diagnostic uncertainty. Image post-processing has been developed to correct for inadequate cardiac and respiratory motion (MoCo) to improve image quality and facilitate image interpretation. Aim of this pilot study was to analyze the impact of MoCo on the evaluation of stress perfusion CMR.

Methods: Twenty-seven patients (mean age 61±10 years, 18 males) underwent CMR at 1.5T (GE Signa HDX 23) including a standard stress-rest-perfusion protocol: three short axes of the left ventricle, spatial resolution 2.0x3.1x8mm^3, adenosine as stressor and 2x0.1mmol/kg gadodiamid as contrast agent. Image reconstruction was done both conventionally, and with MoCo, which consists in: i) image intensity normalization, ii) group-wise motion extraction with iterative non-rigid registration using a cross-correlation similarity metric, and iii) motion warping of the native images with the combined displacement field. Two SCMR level III readers did the image evaluation by consensus. Each of the 16 AHA segments was evaluated regarding the presence of i) perfusion deficits, ii) dark rim artifacts, iii) uncertain signal loss, or iv) normal perfusion patterns. The general image quality (A=non-diagnostic, B=diagnostic, but imperfect, C=good, D=excellent) and the level of diagnostic confidence (A=not confident, B=confident, C=very confident) were assessed once for each dataset. Invasive coronary angiography ruled out coronary artery stenosis >50% in all subjects.

Results: Frequency and regional distribution of perfusion deficits, dark rim artifacts and uncertain signal loss were widely concordant on non-MoCo and MoCo images: 6 segments in 2 subjects (non-MoCo) and 5 segments in 2 subjects (MoCo) were classified as 'perfusion deficit'. Seven segments in 5 subjects (non-MoCo) and 5 segments in 4 subjects (MoCo) were classified as 'uncertain signal loss'. Dark rim artifacts were present in 22/27 subjects (non-MoCo and MoCo) and affected 57 (non-MoCo) and 55 (MoCo) segments, with predominance in the septum. Figure 1 illustrates the cardiac alignment of the CMR images with the use of MoCo. General image quality was rated superior for MoCo, and diagnosis based on MoCo images was rated more often as "very confident" compared to non-MoCo (p=0.008 and p=0.238, figure 2).

Conclusions: Motion correction of CMR perfusion images significantly improved the image quality leading more often to a 'very confident' assessment. To what extent this progress expedites CMR training and may influence clinical decision-making has to be determined in future studies.

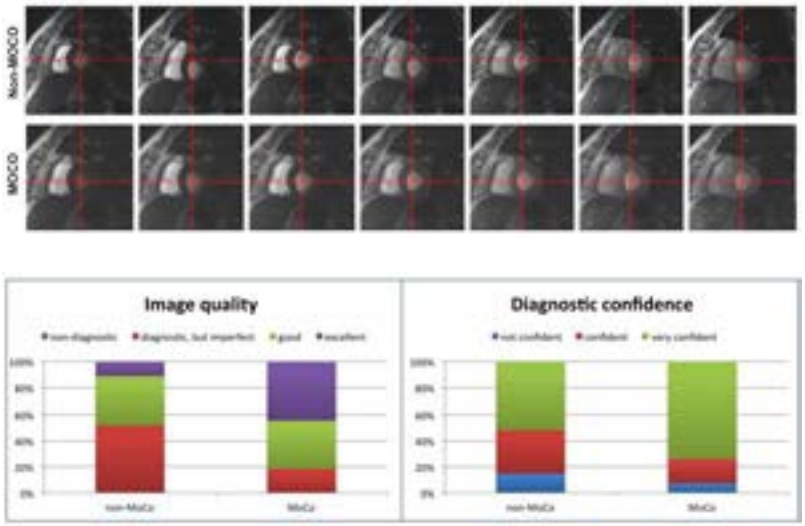

P048

Prognostic Utility of Delayed Enhancement CMR for Evaluation of Cardiac Masses among Patients with Advanced Systemic Cancer

Angel T. Chan, MD, PhD[1] Shawn Pun, MD[2], Andrew Plodkowski, MD[3], Yuliya Lakhman, MD[3], Darragh Halpenny, MD[3], Jiwon Kim, MD[4], Michelle Ginsberg, MD[3], Richard Steingart, MD[3], Jonathan W. Weinsaft, MD[4]

1. *Memorial Sloan Kettering Cancer Center, New York, NY*
2. *Massachusetts General Hospital, Boston, MA*
3. *Memorial Sloan Kettering Cancer Center, NY*
4. *Weill Cornell Medical Center, NY*

Background: CMR is well validated for cardiac mass (C_{MASS}) tissue characterization to differentiate between neoplasm (C_{NEO}) vs. thrombus (C_{THR}): Prognostic implications of C_{MASS} subtypes is unknown.

Methods: The population comprised C_{MASS+} adults and controls (C_{MASS-}) matched for cancer diagnosis and stage. A standardized CMR protocol was performed, including DE-CMR (IR-GRE) for tissue characterization and cine-CMR (SSFP) for cardiac structure/function. C_{NEO} and C_{THR} were defined via established DE-CMR criteria, based on presence or absence of enhancement; lesions were quantified for size and tissue properties [SNR, CNR]. Systemic cancer extent was assessed based on number of cancer-involved organs; follow-up was performed to evaluate prognosis in relation to C_{MASS} etiology.

Results: 118 cancer patients were studied, among whom 38 had C_{NEO} and 21 C_{THR} on CMR. Leading cancer etiology differed between C_{NEO} (sarcoma [21%], lung [16%]) and C_{THR} (lymphoma [29%], GI [24%]), but LVEF (63±9% vs 62±10%; p=0.70), RVEF (51±11% vs 55±8%; p=0.12), age (60±15 vs 54±16 yo; p=0.20) and gender (53% vs 57% male; p=0.74) were similar. C_{NEO} and C_{THR} markedly differed with respect to quantitative tissue properties (CNR: 12.3±10.9 vs 1.7±1.0; $p < 0.001$ | SNR: 27.7±20.9 vs 13.8±9.7; p=0.007). Regarding location, C_{THR} was 5-fold more likely to localize to the RA (81% vs. 16%, $p < 0.01$); 21% of C_{NEO} had multi-chamber involvement (0% C_{THR}). Lesion size (area: 16.0±21.8 vs 1.9±1.3 cm^2; $p < 0.001$ | length: 5.2±3.7 vs 2.3±1.7 cm, $p < 0.001$) was greater and pleural effusions more common (50% vs 19%, p=0.01) with C_{NEO} vs. C_{THR}, paralleling higher overall burden of systemic disease (# of cancer-involved organ systems: 3.6±2.1 vs 2.4±2.2; p=0.045). Both C_{NEO} and C_{THR} had similar burden of systemic disease vs. C_{MASS-} matched controls (C_{NEO}: 3.6±2.1 vs 2.9±2.1; p=0.13 | C_{THR}: 2.4±2.2 vs 1.8±1.3; p=0.25). All-cause mortality assessed 6 months (54% vs 21%, p=0.03) and 1 year (65% vs. 32%, p=0.03) post-CMR was 2-fold higher with C_{NEO} vs C_{THR}; C_{NEO} and C_{THR} patients each had similar 6 months mortality (C_{NEO}: 54% vs 38%; p=0.23 | C_{THR}: 21% vs. 25%; p=0.99) and 1 year mortality (C_{NEO}: 65% vs 59%; p=0.79 | C_{THR}: 32% vs. 32%; p=0.72) compared to C_{MASS-} controls matched for 1° cancer type and disease extent (see figure).

Conclusions: Among patients with systemic cancer, C_{NEO} and C_{THR} tissue properties parallel morphologic differences. Patients with C_{NEO} have poorer prognosis than those with C_{THR}; both are associated with similar prognosis compared to C_{MASS-} controls matched for 1° cancer type and disease extent.

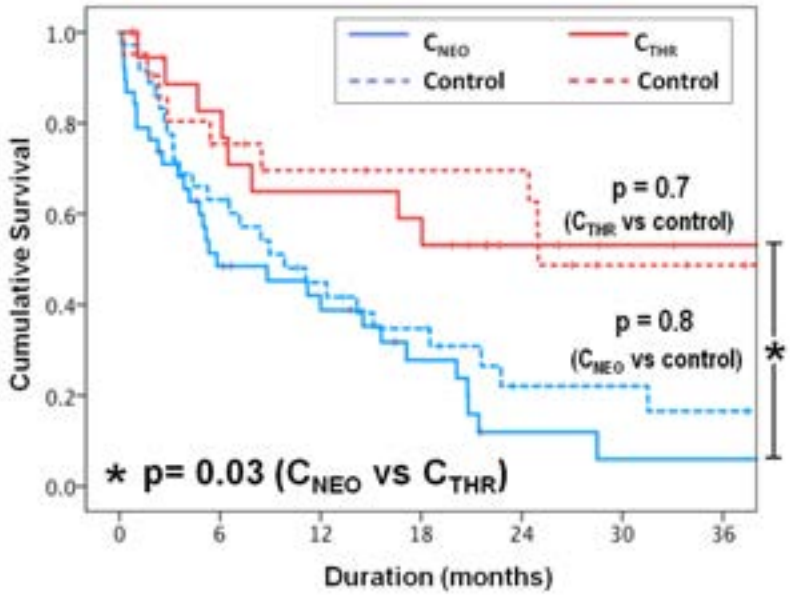

P049

Constrictive pericarditis mimicking left ventricular apical ballooning syndrome (Takotsubo cardiomyopathy)

Yue-Hin Loke, M.D.[1]Ashraf Harahsheh, M.D.[2], Laura Olivieri, M.D.[3]

1. *Children's National Medical Center, Washington Dc, DC*
2. *Children's National Medical Center, Washington, DC, DC*
3. *Children's National Medical Center, Washington, DC*

Description of Clinical Presentation: Patient is an athletic 17 year-old male who moved from Nepal 2 years ago. He presented to the ER with a 7 month history of shortness of breath and chest tightness with deep inspiration. He had difficulty keeping up with his teammates on the lacrosse team. His EKG demonstrated biatrial enlargement, and diffuse T wave inversion of the precordial leads concerning for ventricular strain. His echocardiogram demonstrated a moderate sized pericardial effusion, mildly reduced left ventricular ejection fraction, septal dyskinesis with abnormal septal motion on alternating beats. The concern was raised for constrictive pericarditis.

Diagnostic Techniques and Their Most Important Findings: Cardiac MRI was performed to evaluate for myopericarditis using a Siemens 1.5T scanner. Standard imaging, including functional assessment, T2-weighted and late gadolinium enhancement, were obtained. Cine steady-state free procession images demonstrated a moderate sized pericardial effusion localized to the midportion of the left ventricle with stranding. The pericardium was adherent to the myocardium in the region of the effusion and restricted motion of the myocardium, mimicking the appearance of left ventricular apical ballooning during systole. However, restricted ventricular relaxation was also demonstrated in the 4-chamber orientation as abnormal septal "bounce" and abrupt termination of diastolic filing. The pericardium was diffusely thickened and enhanced on late gadolinium enhancement imaging. There were no resting perfusion abnormalities detected, no areas of early gadolinium hyperenhancement to suggest myocarditis, nor areas of myocardial late gadolinium hyperenhancement to suggest fibrosis, infarction, or inflammatory process. The patient afterwards underwent pericardiectomy. Significant thickening of the pericardium was noted, along with multiple locules of hemorrhagic effusions. Tissue samples showed fibrosis with chronic inflammation. An infectious pathogen for the patient's constrictive pericarditis was not identified; cultures of the pericardial fluid were negative. The patient has since reported that he "feels like a new person," with significant improvement in his exercise tolerance. Follow-up echocardiograms have shown normal function and no effusion. His T wave abnormalities on EKG are also normalizing.

Learning Points from this Case: Hallmark features of constrictive pericarditis on MRI include pericardial thickening and/or enhancement, impaired diastolic filing (biatrial enlargement, distention of the inferior vena cava and hepatic veins), and abnormal diastolic septal "bounce" which can be demonstrated on cine SSFP. The conical deformity of the left ventricle mimicked left ventricular apical ballooning syndrome (Takotsubo cardiomyopathy) in this specific case, however the restricted motion and "apical ballooning" are wall motion abnormalities associated with focal restriction of left ventricular deformation. They resolved immediately with treatment of the pericardial effusion.

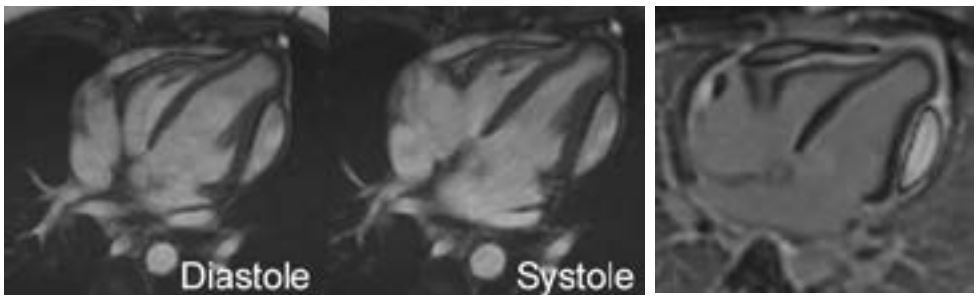

P050

Left Ventricular metastasis of Adenosquamous lung cancer

Clement C.H. Wu, MBBS, MRCP[1] Louis Loon-Yee Teo, MBBS, MRCP[2]

1. National Heart Centre Singapore, Singapore, N/A, Singapore
2. National Heart Centre Singapore, N/A, Singapore

Description of Clinical Presentation: A 66 year old Chinese man with a significant 50 pack-year smoking history presented with progressive left calf pain and numbness. Left lower limb pulses were absent. He was worked up to have acute left lower limb ischemia secondary to emboli in the left common femoral artery. Emergent left femoral endarterectomy and thrombectomy were performed. A post-operative Computed Tomography (CT) Aortogram showed a necrotic left lower lobe lung mass with left hilar lymphadenopathy, and a low density mass within the inferior wall of the left ventricle (LV). This was confirmed on transthoracic echocardiogram, which showed the large fixed, multilobular mass attached to the inferior, septal and posterior LV walls.

Diagnostic Techniques and Their Most Important Findings: Cardiac MRI was done for better delineation of the mass. A full thickness, lobulated elongated mass with post-contrast enhancement was located in the basal to mid LV, with a component protruding into the LV cavity. Importantly, MRI detected a mobile small bland thrombus along the superomedial aspect of the mass. Cardiac biopsy was therefore deemed unfeasible due to high risk of thrombus dislodgment and resultant vascular morbidity. A Transthoracic Needle Aspiration (TTNA) biopsy of the left lung lower lobe lesion was performed, which showed an adenosquamous carcinoma of the lung.

Learning Points from this Case: Our case highlights the utility of cardiac MRI in the further characterization of an intra-cardiac mass. The superior image resolution and classic enhancement in post-contrast phase discovered thrombus embedded within the intra-cardiac mass which was previously undetected on CT Aortogram and Transthoracic Echocardiogram. This guided subsequent decision for biopsy of the left lung lesion rather than a cardiac biopsy, which would have a high risk of vascular morbidity due to the thrombus within the LV mass.

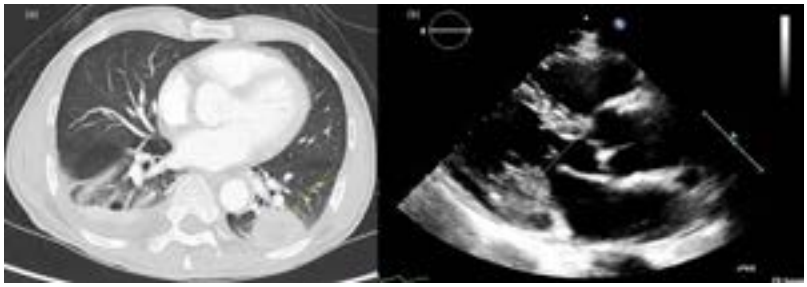

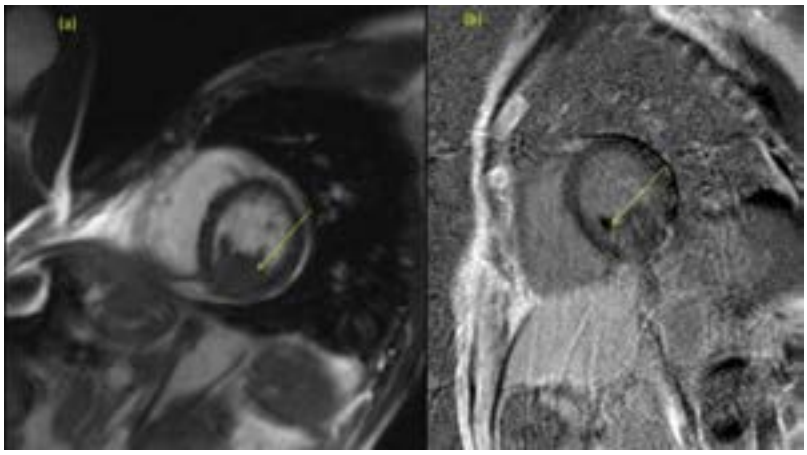

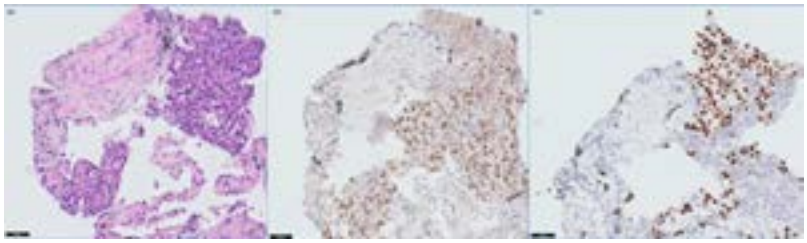

P051

Left Atrial Bronchogenic Cyst Diagnosed on Cardiac Magnetic Resonance Imaging

Alekhya Potluri, M.DSohaib Zahid, M.D, Sourabh Prabhakar, M.D, Robert W. Biederman, MD; FACC; FAHA

Allegheny Health Network, PA

Description of Clinical Presentation: 67 year-old caucasian female with history of paroxysmal atrial fibrillation and hypertension underwent a transthoracic echocardiogram (TTE) as a pre-operative evaluation for left hip fracture. TTE revealed a large cystic appearing mass measuring 3.4 x 2.9 cm in left atrium. Surprisingly, she had a TTE 8 months ago, but there was no evidence of mass during that time. Further testing with cardiac magnetic resonance imaging (CMRI) was consistent with bronchogenic cyst. Although surgery was offered, patient deferred the surgery. A month later, she presented with stroke symptoms and sub-therapeutic INR. She subsequently passed away from complications of IV tPA (tissue plasminogen activator) administration.

Diagnostic Techniques and Their Most Important Findings: CMRI was performed, which showed a 37 x 34 x 30 mm fluid filled cystic mass with air-fluid level. This mass was attached to the interatrial septum on left atrial side and was moderately mobile causing mild functional mitral stenosis. T1/ T2, SSFP (steady state free precision), black blood and triple inversion recovery sequences showed that the mass is proteinaceous and homogenous in nature. These findings were consistent with bronchogenic cyst.

Learning Points from this Case: Intra-cardiac bronchogenic cysts are extremely rare and very little is known about their natural progression, as they are surgically resected at the time of diagnosis. Based on our experience, they can grow rapidly attaining enormous sizes with increase in chamber size and thus leading to worsened atrial fibrillation and stroke as in our patient. We recommend prompt removal of the cyst when identified.

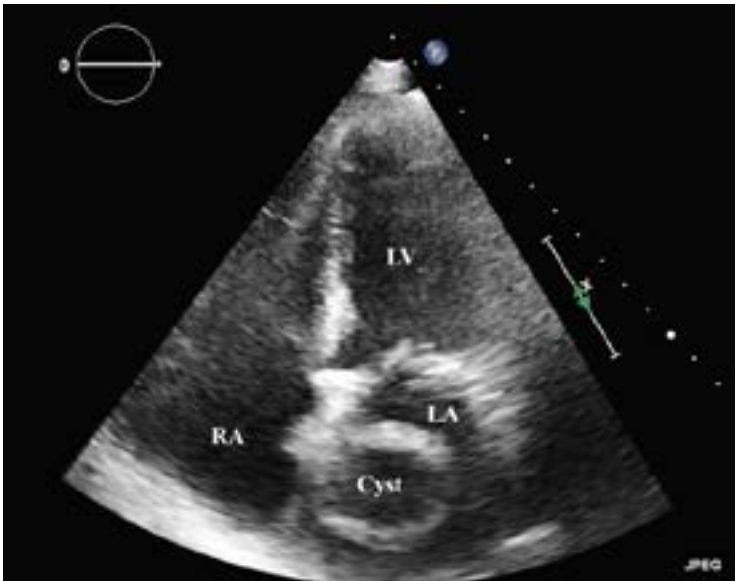

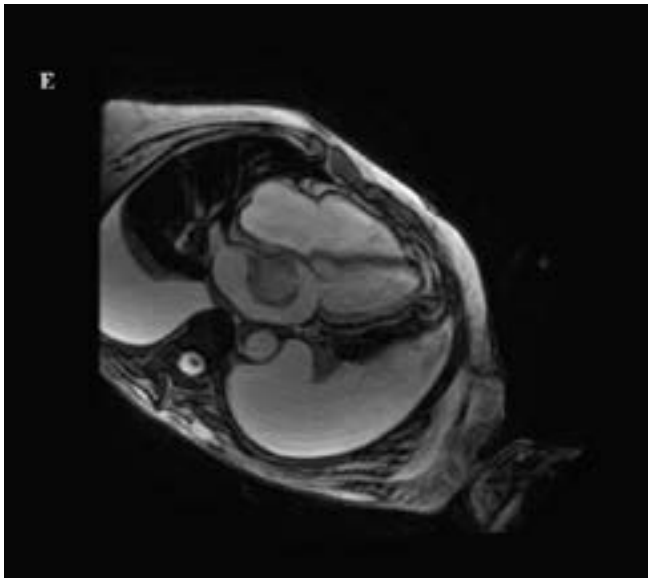

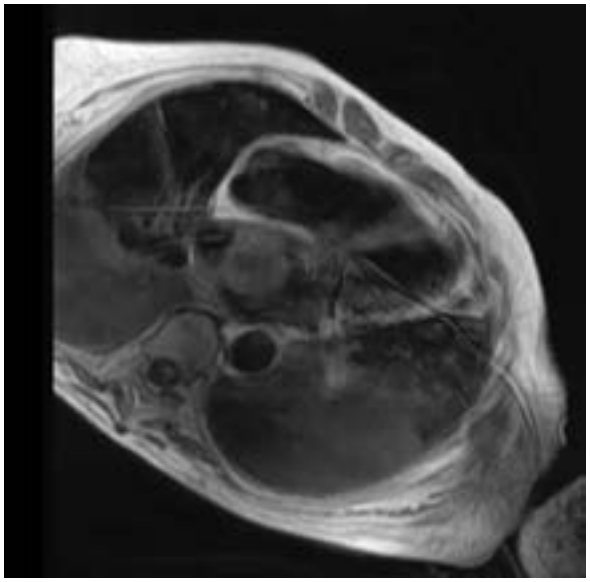

P052

Caseous calcification of the mitral annulus

Felipe Kazmirczak, MD[1] Prabhjot Nijjar, MD[2], Chetan Shenoy, M.D.[3]

1. *University of Minnesota, Minneapolis, MN*
2. *University of Minnesota, MN*
3. *Cardiovascular Division, Department of Medicine, University of Minnesota, Minneapolis, MN*

Description of Clinical Presentation: 61 year old female presented with an acute myocardial infarction, and coronary angiogram was suspicious for an embolic occlusion. Echocardiogram incidentally showed a left atrial mass measuring 2.1 x 2.0 cm in close proximity to the mitral annulus, that was suspicious for a myxoma. Cardiac MRI was ordered for better tissue characterization.

Diagnostic Techniques and Their Most Important Findings: SSFP cine imaging showed the mass straddling the posterior mitral valve annulus(figure1), extending into the left atrium and basal left ventricle. It protruded into the LV cavity, but with no independent motion. It appeared dark on first-pass perfusion(figure2) and long TI imaging, consistent with an avascular structure. On delayed enhancement imaging there was possibly a small rim of hyperenhancement with a large central area of non-enhancement. These features were felt to be consistent with caseous calcification of the mitral annulus (CCMA). This was confirmed with a non contrast CT scan showing a calcified mass(figure 3).
Patient underwent surgical excision of the mitral valve mass with mitral valve replacement; surgical report describes it as a liquefied mass, paste-like material from the sac. The pathology report showed fibrinous material with calcification.

Learning Points from this Case: Caseous calcification(CCMA) of the mitral annulus is seen in 0.63% of all cases of MAC.1 CCMA is usually a benign asymptomatic condition, in this case the stroke was attributed to the mitral valve mass so the patient underwent surgical excision of the mass.

References: *1. Harpaz D, Auerbach I, Vered Z, Motro M, Tobar A, Rosenblatt S J Am Soc Echocardiogr. 2001 Aug; 14(8):825-31.*

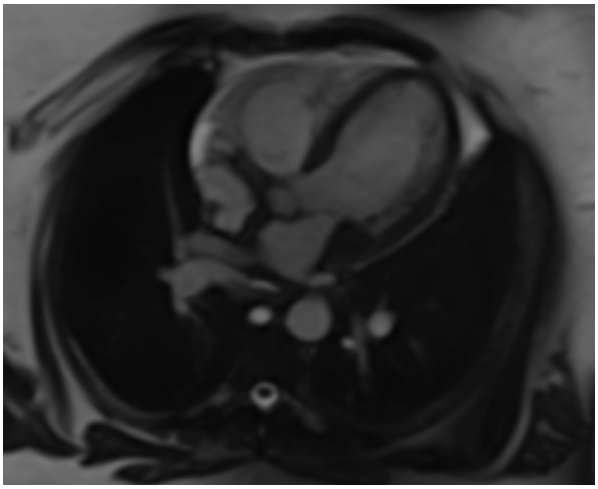

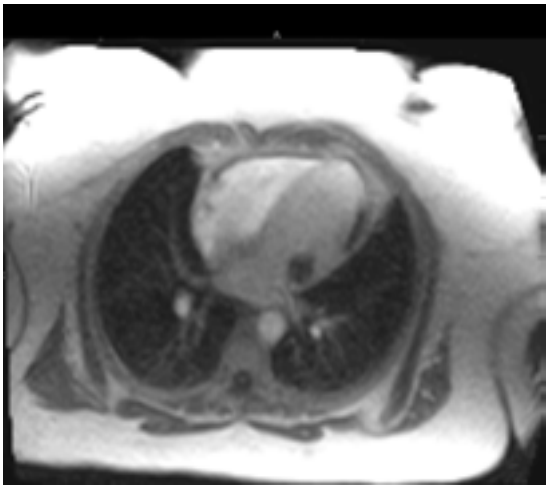

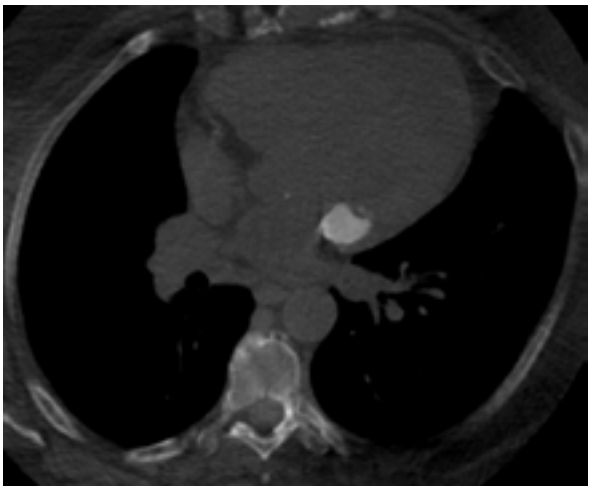

P053

Cardiac MRI with Tagging is a Key Imaging Modality for Guiding Successful Treatment of Pericardial Constriction with Totally Robotic Thoracosopic Pericardiectomy

Edward Passen, MD[1]Ryan Thompson, MS[2], Ina Zamfirova, MS[3], Amit R. Patel, MD[4], Husam Balkhy, MD[4]

1. *Advocate Lutheran General Hospital, Park Ridge, IL*
2. *Chicago Medical School, IL*
3. *Russell Institute for Research and Innovation at Advocate Health Care, IL*
4. *University of Chicago, IL*

Description of Clinical Presentation: A 68 year old male presented with worsening exertional dyspnea over several months. Vital signs and physical exam were normal. Workup for multiple cardiac and pulmonary etiologies was negative except for chest CT showing several areas of pericardial calcification and echocardiography suggesting mild pericardial constriction with constrictive hemodynamic parameters exacerbated with fluid loading. Cardiac MRI demonstrated cardiac anatomy, function and hemodynamic findings consistent with mild pericardial constriction. The patient underwent curative pericardiectomy by totally robotic thoracosopic pericardiectomy. The anterior and posterior pericardium were resected. The pericardium overlying the right ventricle and right atrium were not thickened. Follow-up after 1 year showed no recurrence of constrictive physiology.

Diagnostic Techniques and Their Most Important Findings: Cardiac MRI was performed with and without contrast. The pericardium was borderline thickened with areas of hypointense signal suggesting the presence of calcium. The left ventricle had normal systolic function without regional abnormalities. However there was a mild diastolic bounce of the interventricular septum and incomplete diastolic expansion of the basal anterior and anterolateral walls. These regions also had pericardial tethering to the myocardium based upon cine imaging and myocardial tagging. There was no late gadolinium enhancement. The left atrium, right ventricle, right atrium and IVC were normal.

Learning Points from this Case: Cardiac MRI, unlike other cardiac imaging modalities used for diagnosis of pericardial constriction, also has the ability to guide treatment. Cardiac MRI tagging used to identify where the pericardium is tethered is helpful in preoperative planning and the successful achievement of totally robotic thoracosopic pericardiectomy for pericardial constriction. Showing that the left ventricle is involved by cardiac MRI is important. This is because the robotic approach allows for a more complete pericardiectomy when performed from the left side, as well as allowing release of the left ventricle first, which is necessary in these cases. However, in cases where the constriction is located only on the right side of the pericardium, a right sided robotic approach maybe more efficacious. This case is one of few totally robotic thoracosopic pericardiectomies performed for pericardial constriction. Further study may establish the unique and important role of cardiac MRI for successful treatment of pericardial constrictions with minimally invasive totally robotic thoracosopic pericardiectomy.

http://www.ConferenceAbstracts.com/uploads/cfp2/attachments/LDFAIBDN/LDFAIBDN--222766-1-ANY(1).pdf

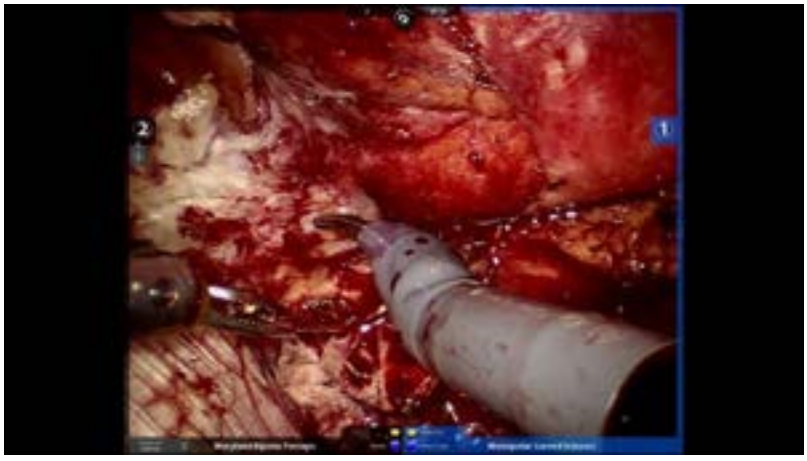

P054

Asymptomatic cardiac mass - thrombosed aneurysm of a coronary fistula

Felicity J. Lee, MBBS[1] Siang Ung, MBBS, FRACP[2], Joel Scadden, Diploma in Medical Imaging[3], Mark Preiato, Bachelor Degree in Medical Imaging Science[3], Arun Abraham, MBBS, FRACP[4]

1. *Fiona Stanley Hospital, Department of Cardiology, Perth, Western Australia, Australia*
2. *Royal Perth Hospital, Western Australia, Australia*
3. *Imaging Central Western Australia, Western Australia, Australia*
4. *Fiona Stanley Hospital, Royal Perth Hospital, Western Australia, Australia*

Description of Clinical Presentation: A 33 year-old female non-smoker, without cardiac symptoms or other medical history, was noted to have a systolic murmur during anaesthetic review prior to surgery for ectopic pregnancy. Heart rate was 85bpm. Examination was unremarkable except for an intermittent late systolic murmur over the 'pulmonic region'. Transthoracic echocardiogram (Figure 1) suggested an encapsulated relatively homogeneous immobile spherical right atrial mass (29 x 26 x 23 mm) attached to the membrane of the fossa ovalis by a small stalk. Focal irregular hypermobile elements suggestive of microvilli were noted. There was no evidence of flow obstruction of the superior and inferior vena cavae. Biventricular systolic function was normal. No definite cause for murmur was identified. A provisional diagnosis of myxoma was made. Low dose cardiac computed tomography (CT) revealed a large (57x23x26mm) mass in the epicardial tissue plane, with focal calcification, superoposterior to the right atrium, posterior to the aorta and superior vena cava, inferior to the right pulmonary artery, and anterior to the left atrium (Figure 2). The largest calibre branch of the dilated left main was a dilated proximal circumflex which supplied the mass, likely representing a thrombosed aneurysm of coronary fistula. No obvious connections to other vessels or cardiac chambers was identified. The coronary arteries were otherwise normal. CMR (Figure 3) performed concurrently confirmed the CT findings and further demonstrated low to intermediate signal intensity with some heterogeneity within the body of the mass on T1 and T2 imaging with no definite fat, and absence of first pass or delayed perfusion. There was no delayed enhancement within the body of the mass with high signal intensity along the edge of the mass. Previously noted mobile elements were identified as adjacent right atrial structures (likely displaced Chiari network). Diagnosis was changed to thrombosed aneurysm of a coronary fistula.

Given increased thromboembolic risk, coronary angiography to assess drainage of the mass was arranged.

Diagnostic Techniques and Their Most Important Findings: Transthoracic echocardiography: 2D, Doppler, colour Doppler. Low dose Cardiac CT (DLP 27mGy.cm): Prospective ECG-gating, 256-slice scanner, model based iterative reconstruction. CMR: SSFP cine, SSFP rest perfusion, T1 and T2 ± adiabatic fat saturation, SSFP single shot PSIR 'early enhancement' and delayed enhancement (2D PSIR SPGRE and navigated SPGRE 3D).

Learning Points from this Case:

1. Primacy of CMR in tissue characterisation of cardiac masses or thrombus.
2. Incremental value of cardiac CT and CMR over echocardiography in:
    1. Identifying cardiac masses and elucidating relationship to surrounding structures.
    2. Detecting coronary anomalies.
    3. Delineating anatomy prior to surgery.

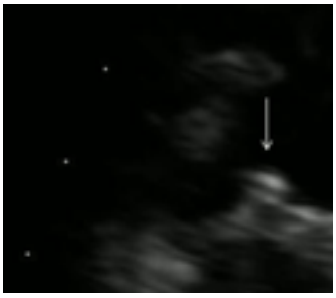

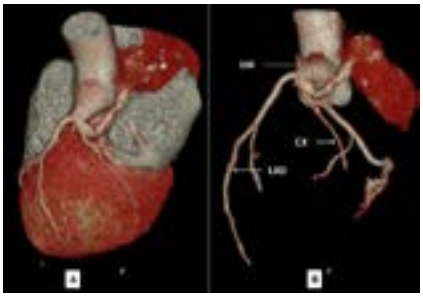

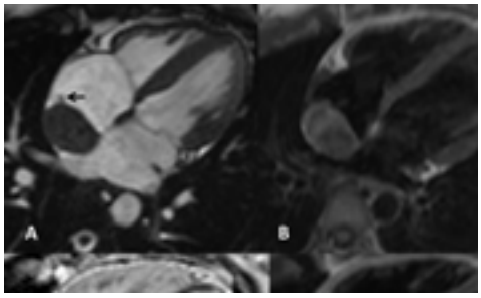

P055

Pericardial Constriction Secondary to an Unusual Presentation of a Post-operative Complication from Aortic Valve Surgery

Syed R. Latif, MD[1]Demetrius Dicks, MD[2], Tariq Ahmad, Md mph[3], Pramod Bonde, MD FACS[4], Steffen Huber, M.D.[5], Hamid Mojibian, M.D.[5], Judith L. Meadows, MD[4], Isabel Oliva, MD[6], David J. Hur, M.D.[7], Lauren A. Baldassarre, MD[5]

1. *Yale University, Hamden, CT*
2. *Yale University School of Medicine, NEW HAVEN, CT*
3. *Yale University, New Haven, CT*
4. *Yale School of Medicine, CT*
5. *Yale University, CT*
6. *YALE UNIVERSITY, MADISON, CT*
7. *Yale School of Medicine, New Haven, CT*

Description of Clinical Presentation: An 80 year old male with a past medical history of chronic obstructive pulmonary disease, atrial fibrillation, and a dilated aortic root underwent aortic aneurysm repair and bioprosthetic aortic valve replacement. He did well in the post-operative period and was asymptomatic for the succeeding three years. He then came to clinical attention again secondary to symptoms of heart failure and cardiogenic shock. An echocardiogram at that time suggested an extra-cardiac mass lateral to the left ventricular free wall with impingement on diastolic relaxation. At that time, he was sent for cardiac magnetic resonance (CMR) imaging which demonstrated a large intra-pericardial hematoma (10.5 x 7 x 4.7 cm, Image 1). The hematoma was subsequently surgically evacuated and he initially did well post operatively. Over the course of the next three years, he progressively developed worsening left and right sided heart failure symptoms with a preserved left ventricular ejection fraction. Serial echocardiography over this time demonstrated progressive tricuspid valve regurgitation, aortic insufficiency, and bi-atrial enlargement. He was then referred for another CMR which again demonstrated an intra-pericardial hematoma adjacent to the LV wall (6cm x 1cm, Image 3), thickened pericardium, tethering of the right atrium to the chest wall, and ventricular interdependence upon deep inspiratory maneuver (Image 2), consistent with constrictive cardiomyopathy. Invasive hemodynamic assessment in the cardiac catheterization laboratory also demonstrated equalization of intracardiac pressures and ventricular interdependence with respiration. He is currently planned for hematoma evacuation and pericardial stripping.

Diagnostic Techniques and Their Most Important Findings: The patient underwent serial CMR imaging (1.5 T, Aera, Siemens Healthcare, Erlangen, Germany). The initial CMR was performed for tissue characterization of the mass, including cine SSFP, T2-weighted, T1-weighted, perfusion, and delayed enhancement (DE) imaging. The mass did not demonstrate gadolinium uptake on perfusion or DE imaging, most consistent with a hematoma. Repeat CMR three years later was performed without contrast due to renal insufficiency and included cine SSFP, tagging, and real time cine imaging with inspiratory maneuvers which demonstrated residual hematoma, pericardial thickening with adhesions and ventricular septal flattening upon deep inspiration, consistent with ventricular interdependence and constrictive cardiomyopathy.

Learning Points from this Case: This case demonstrates the diagnostic importance of CMR in identifying pathology not easily characterized by echocardiography, it's additional role in tissue characterization of masses, and its ability to visualize fully the pericardium and adjacent structures without limitations of windows. In this case, both CMRs provided significant diagnostic utility that dictated clinical management and operative action.

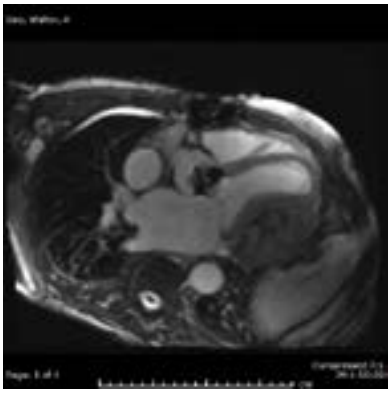
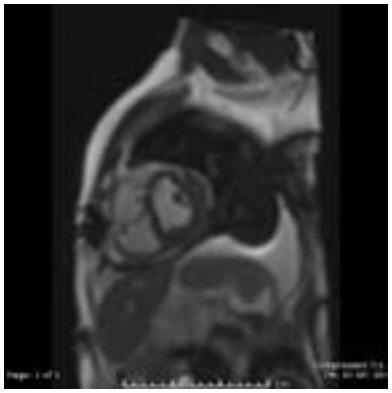
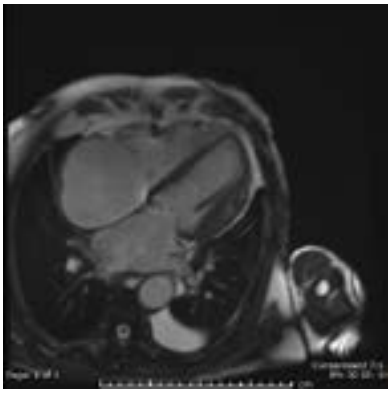

P056

An unusual right ventricular mass in a teenager diagnosed by cardiac magnetic resonance

Deepa Prasad, MBBS MD[1] Andrew J. Powell, M.D.[2]

1. Boston Children's Hospital, Boton, MA
2. Harvard Medical School and Boston Children's Hospital, Boston, MA

Description of Clinical Presentation: A previously healthy, 17-year-old female presented to cardiology clinic for evaluation of palpitations with exercise. There was no history of fatigue, syncope, or chest pain. She had no significant past medical or family history. Her physical exam was unremarkable except for a systolic click, which prompted an echocardiogram.

Diagnostic Techniques and Their Most Important Findings: Her echocardiogram showed a moderate-sized, echo-bright mass within the apex of the right ventricular cavity. Ventricular and valvular function was normal. Cardiac magnetic resonance (CMR) was performed to further characterize the mass. CMR showed a well-defined, spherical mass measuring 1.4 x 1.1 x 1.7 cm within the cavity of the right ventricle, near the apex. On cine SSFP imaging, the mass had a dark rim and bright center, and was not mobile (Figure A). The mass was bright on T1-weighted turbo spin echo (TSE) (Figure B), and became dark when fat saturation (Figure C) was applied suggesting that it was composed predominantly of fatty tissue. On first-pass perfusion imaging, it was poorly perfused; and on late gadolinium enhancement (LGE) imaging, it was hyperintense. When LGE imaging was repeated with a long inversion time (650 ms), the mass had a similar intensity to myocardium, making a thrombus unlikely. Based on these features, the mass was characterized as a lipoma.

Learning Points from this Case: Cardiac lipomas are uncommon, benign primary cardiac tumors composed of mature fat cells. They do not have a defined age or sex distribution and are usually found in the right atrium and left ventricle. The majority of the cardiac lipomas do not cause any symptoms but depending on the size and location, they may cause valvar dysfunction, outflow tract obstruction, or arrhythmias. This case illustrates the usefulness and accuracy of CMR in characterization of intracardiac masses, and specifically lipomas. The patient's palpitations resolved spontaneously and were not thought to be related to the lipoma. She underwent a repeat CMR in one year and the mass was unchanged. She has been scheduled for a follow-up CMR in 4 years.

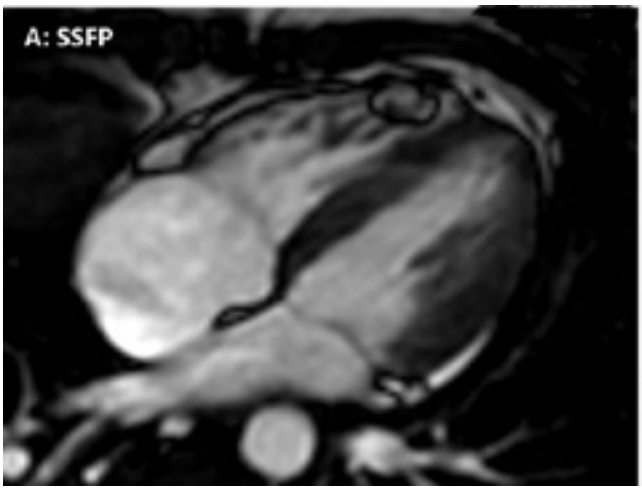

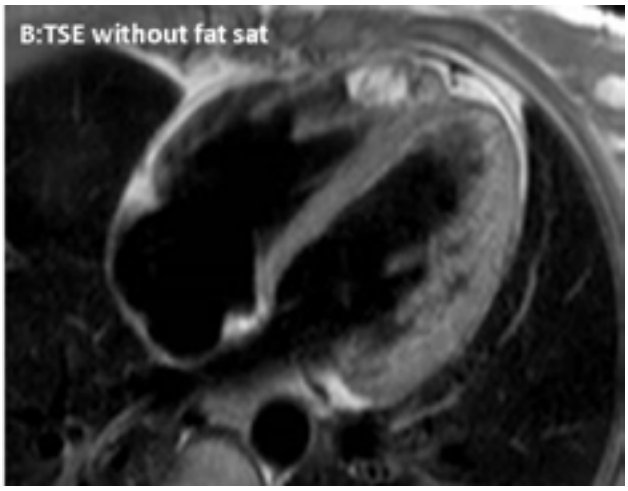

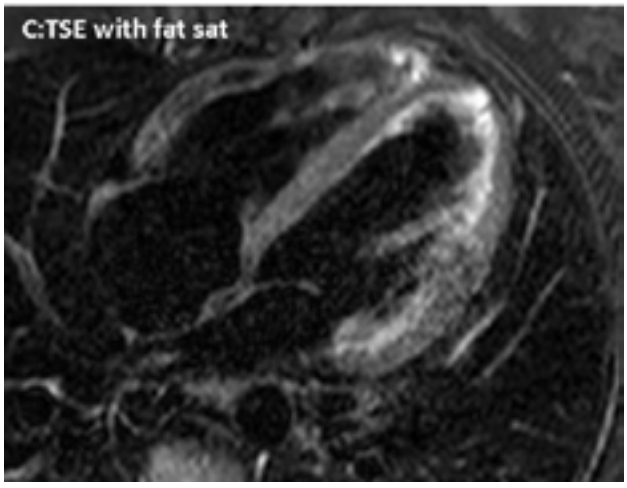

P057

Right Ventricular Tumor with Associated Thrombus: A Case Report

Neil G. Barry, IV, DO, MBA, RAJEEV Fernando, MD

University of Louisville, Louisville, KY

Description of Clinical Presentation: A 59 year old man with past medical history of metastatic oropharyngeal cancer on chemotherapy presented with acute onset dyspnea, tachypnea and cough. Chest computed tomography (CT) with IV contrast revealed pulmonary emboli in the right lower lobe branch, segmental and sub segmental branches and in the segmental branches of the left lower lobe. It showed a low attenuation lesion in the right ventricle that was poorly characterized. Given the prior history of cancer, there was concern for metastasis but right ventricular thrombus could not be excluded.

Diagnostic Techniques and Their Most Important Findings: A three dimensional survey was performed to locate the mass and exclude other intra-cardiac masses. Cine images focused on the right ventricle showed reduced regional systolic function along the insertion of the mass, numerous masses within the right ventricle attached to the free wall of the right ventricle, extending from the lateral tricuspid annulus to the insertion site of the moderator band. All of the masses had mobile components that extended into the right ventricular outflow tract. T-2 weighted imaging showed a heterogeneous mass with predominantly high signal intensity and areas of low signal intensity dispersed within the mass. T1 weighted imaging showed an isointense mass with areas of low signal intensity dispersed within the mass. The mass was not suppressed by a fat saturation pulse. On Dynamic contrast enhanced perfusion imaging, the region of the mass adjacent the right ventricular free wall was perfused but the endocardial surface was not perfused. Post contrast T1 weighted images showed increased signal intensity with areas of low signal intensity dispersed within the mass. Late gadolinium enhancement showed a hyper-intense mass with areas of low signal intensity. High Ti imaging showed the region of the mass adjacent the right ventricular free wall was hyperintense but the endocardial surface was hypointense. These findings are consistent with a tumor thrombus.

Learning Points from this Case: Our case study demonstrates that invaluable information can be provided by a comprehensive CMR exam of cardiac masses. Tissue characterization clearly demonstrated a right ventricular tumor with endocardial thrombus. Additional prognostic information was gathered into the embolic potential of these masses and co-existent pulmonary emboli. On the basis of CMR findings, the patient was placed on anticoagulation prior to endocardial biopsy to classify the tumor and offer definitive therapy. This case clearly illustrates that in patients in whom echocardiography and CT scan cannot conclusively confirm intra-cardiac thrombus, cardiac MRI can be a valuable tool to detect tumor.

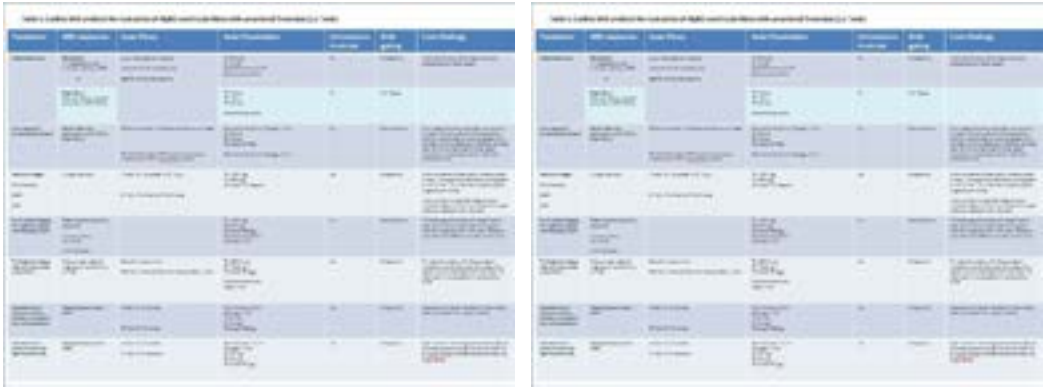

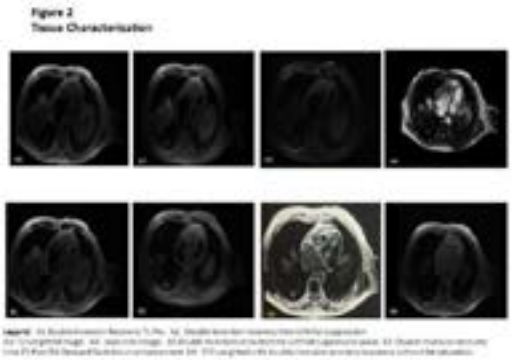

P058

Recurrent biatrial myxomas: Unusual case with underlying carneys complex

Supriya Gupta, MBBS MD[1] William Bates, MD[2], Jayanth H. Keshavamurthy, MD[3]

1. Medical college of georgia, Augusta, GA
2. Augusta University, GA
3. Medical College of Georgia at Augusta University, Augusta, GA

Description of Clinical Presentation: Although cardiac myxoma is the most commonly encountered benign cardiac tumor in cardiac surgery practice, recurrent cardiac myxoma is very rare, most commonly related to Carney complex, usually requiring multiple cardiac operations. Carney complex is a rare syndrome which includes cardiac myxoma, hyperactive endocrine neoplasm, spotty pigmented skin, and extra cardiac myxomatous tumors. We describe a patient who presented with fifth recurrence of his cardiac myxoma. A 38-year-old male with history of multiple recurrent bi-atrial myxomas, presents after 4 prior resections. His physician requests evaluation of Left Atrial Myxoma and vascular supply to myxoma in anticipation of a fifth resection.

Diagnostic Techniques and Their Most Important Findings: Patient underwent multiple echocardiograms, cardiac CT as well as cardiac MRI examinations (Figure 1), over a period of time. There was no evidence to suggest PV/mitral inflow obstruction. He is currently on apixaban. He has history of right atrial reconstruction as well as development of fistula between sinus of Valsalva and left atrium status post patch repair. Due to recurrent cardiac myxomas, dedicated physical examination was performed which showed skin lesions on the face and trunk (Figure 2). Diagnosis of Carneys complex was then made. Patient is being considered for a heart transplant versus fifth surgical resection.

Learning Points from this Case: Cardiac myxoma from Carney complex can occur in any cardiac chamber, presenting multiple times with postoperative recurrences, occurring at any age and without any predilection for gender, and is inherited in an autosomal-dominant manner. In patients with unusual recurrence of myxomas, it is important to consider underlying Carney's Complex, an autosomal dominant inherited syndrome normally characterized by recurrent myxomas, endocrine neoplasms, and skin nevi and lentigines. Treatment for cardiac myxoma from Carney complex is very important for patient mortality and morbidity and, despite its endocrine nature, cardiologists, cardiac imagers and cardiac surgeons play an important role

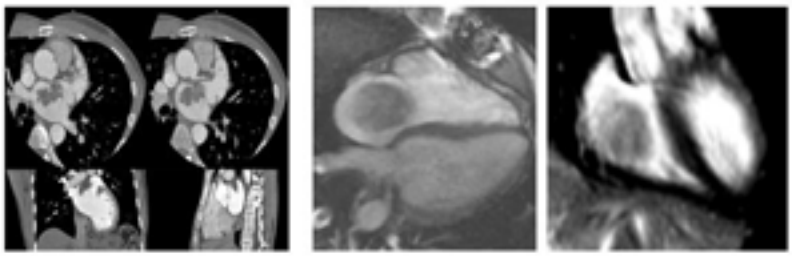

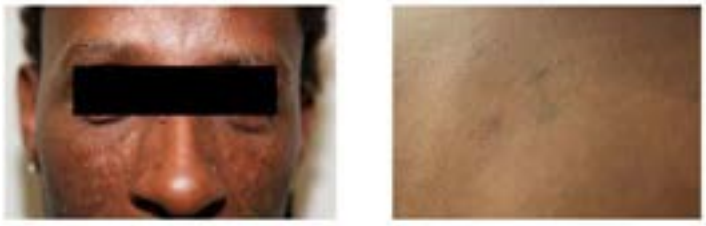

P059

Primary pericardial synovial sarcoma in a young child - A rare tumor

Madhusudan Ganigara, MD [1]James Starc, MD[2], Gina LaRocca, MD[3], James Nielsen, MD[4], Santosh Uppu, MD[5]

1. Icahn School of Medicine at Mount Sinai, NY
2. The Mount Sinai Hospital, New York, NY
3. Mount Sinai's Zena and Michael A. Wiener Cardiovascular Institute, NY
4. Stony Brook Medicine, New York, NY
5. The Mount Sinai Hospital, NY

Description of Clinical Presentation: An 8-year old boy with no significant past medical history presented with a 2 week history of cough, breathlessness with mild exertion and respiratory wheeze that did not respond to Albuterol. A chest x-ray revealed massive cardiomegaly. Echocardiogram showed a structurally normal heart with a large heterogeneous mass along the right ventricular free wall with large pericardial effusion and mildly depressed left ventricular systolic function.

Diagnostic Techniques and Their Most Important Findings: A CT angiogram confirmed the intrapericardial mass without additional mediastinal tumors. Cardiac MRI was then performed to tissue characterize this tumor (table 1); it measured about 10x8x4 cm. Differential diagnosis included intrapericardial teratoma, synovial sarcoma, paraganglioma or a metastatic tumor. Biopsy of the mass was performed, immunohistochemical staining revealed tumor cells positive for vimentin and BCL-2. Stains for smooth muscle actin, desmin, myogenin, S-100 protein, CD34 and MDM2 were negative. Interphase FISH showed 94% of cells positive for SS18 (18q11.2) gene rearrangement. These results were indicative of Synovial sarcoma (SS). The child was started on chemotherapy after a PET scan that showed no metastases. After 6 cycles of chemotherapy the tumor did not regress in size, he subsequently underwent an uncomplicated subtotal tumor resection 5 months after the initial presentation. He was continued on further chemotherapy and is being closely followed. Radiotherapy or complete excision was not performed in the patient due to concern for significant morbidity.

Learning Points from this Case: A CT angiogram confirmed the intrapericardial mass without additional mediastinal tumors. Cardiac MRI was then performed to tissue characterize this tumor (table 1); it measured about 10x8x4 cm. Differential diagnosis included intrapericardial teratoma, synovial sarcoma, paraganglioma or a metastatic tumor. Biopsy of the mass was performed, immunohistochemical staining revealed tumor cells positive for vimentin and BCL-2. Stains for smooth muscle actin, desmin, myogenin, S-100 protein, CD34 and MDM2 were negative. Interphase FISH showed 94% of cells positive for SS18 (18q11.2) gene rearrangement. These results were indicative of Synovial sarcoma (SS). The child was started on chemotherapy after a PET scan that showed no metastases. After 6 cycles of chemotherapy the tumor did not regress in size, he subsequently underwent an uncomplicated subtotal tumor resection 5 months after the initial presentation. He was continued on further chemotherapy and is being closely followed. Radiotherapy or complete excision was not performed in the patient due to concern for significant morbidity.

MRI tissue characteristics of the tumor

Interpretation	Finding	Cardiac Sequence
No Fat component	Isointense	T1w imaging without fat saturation
No Fat component	Isointense	T1w imaging with fat saturation
Fluid component	Heterogenous with >50% hyperintense regions	T2w imaging
Muscular component	Areas of isointensity	Steady state free precession imaging
Poorly vascular mass	Delayed entry of contrast to the center	First pass perfusion
Fibrous component	Areas of hyperintensity	Myocardial delayed enhancement imaging (Ti = 250 msec)
No Thrombi	Diffusely hyperintense	Myocardial delayed enhancement imaging (Ti = 600 msec)

P060

Right atrial myxoma in a patient with Budd Chiari syndrome

Fateh Ali Tipoo. Sultan, MBBS, FCPS

Aga Khan University Hospital, Karachi, Pakistan, Karachi, Sindh, Pakistan

Description of Clinical Presentation: A 29 year old female was referred for cardiac magnetic resonance (CMR) for evaluation of right atrial mass, found on CT and echocardiogram. She presented with right hypochondrial pain and abdominal distension and was diagnosed to have Budd Chiari syndrome. CT scan showed the evidence of thrombosis in the hepatic veins and hepatic and suprahepatic part of inferior vena cava. The scan revealed a filling defect in the right atrium and evidence of subsegmental pulmonary embolism. Echocardiogram showed the similar lesion in the right atrium with thrombus or tumor being the differentials. No evidence of hematological malignancy or polycythemia was found on routine blood tests.

Diagnostic Techniques and Their Most Important Findings: CMR with gadolinium enhancement was done on 1.5 Tesla, siemens avanto, which showed a large, mobile, irregular shape, pedunculated mass in the right atrium. It was measured upto 32mm X 21mm, attached to the interatrial septum at the site of fossa ovalis, obstructing the tricuspid valve. The mass was isointense on T1 weighted images and iso to hyperintense on T2 weighted images. The mass showed some perfusion on first pass perfusion images with gadolinium injection, ruling out the possibility of thrombus. No hyperenhancement was seen on late gadolinium images.

Learning Points from this Case: A diagnosis of right atrial myxoma was made on the basis of above findings on CMR. The patient underwent surgical removal of the mass and histopathology confirmed it to be a myxoma. The patient's clinical condition was improved after surgical removal of the mass.

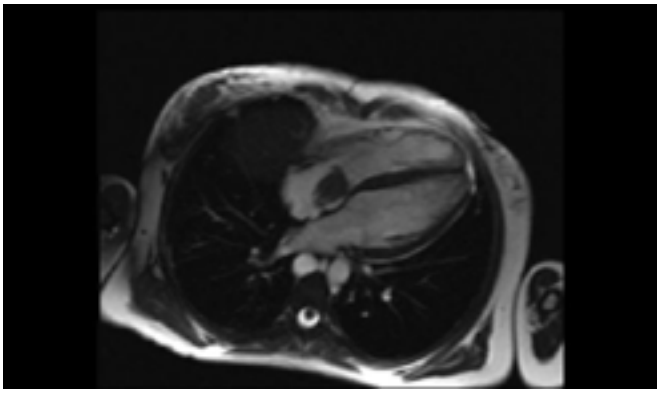

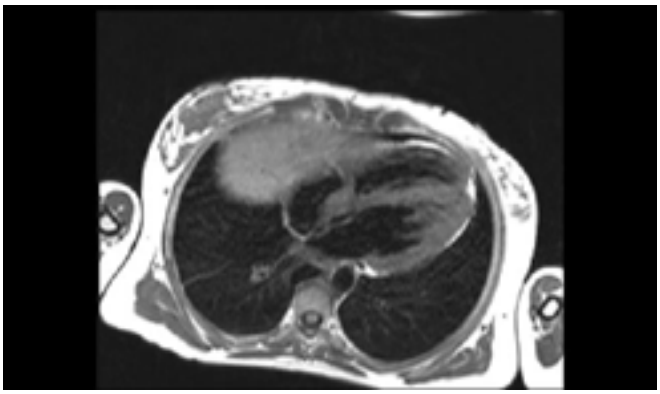

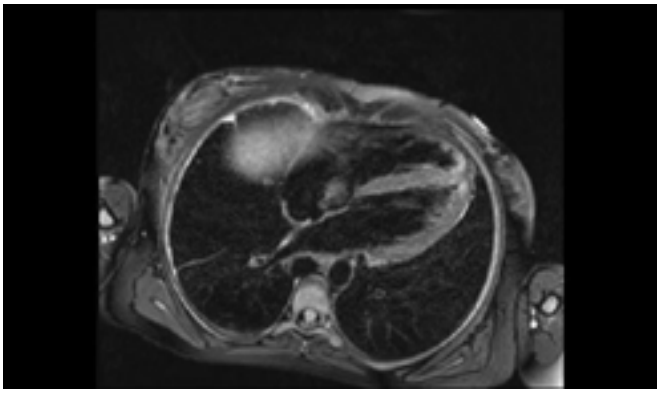

P061

Iatrogenic Right Atrial Compression & Collapse

Alexander S. Ross, MD[1], Auras R. Atreya, MD[2], Rita F. Pingree, MD[3], Joyce Schroeder, MD[3], Brent Wilson, MD, PhD[4] Leif Jensen, MD[3]

1. *University of Utah, Park City, UT*
2. *University of Massachusetts Medical School-Baystate, Springfield, MA*
3. *University of Utah, UT*
4. *University of Utah, Salt Lake City, UT*

Description of Clinical Presentation: A 27 year old woman with lupus nephritis presented to the hospital with acute on with chronic kidney disease and perinephric abscess. She underwent placement of a tunneled central venous catheter in the left internal jugular vein under fluoroscopic guidance for hemodialysis access. During dialysis, she experienced severe chest pain and the catheter was re-evaluated with fluoroscopy and contrast injection. The distal tip of the catheter was found to be in the azygous vein requiring catheter exchange over the wire. Post procedural CXR was unremarkable (figure 1a). A non-contrast CT scan of the abdomen and pelvis performed one week later for evaluation of perinephric abscess incidentally noted heterogeneity of the right atrium and right atrial appendage (figure 1b).

Diagnostic Techniques and Their Most Important Findings: Transthoracic echocardiography was performed which demonstrated significant external compression of the right atrium without evidence of atrial thrombus (figure 1c & 1d). A cardiac MRI was then performed with T1, T2 weighted static and cine steady state free precession images (figure 1e). Gadolinium was not used due to end-stage renal disease. A pericardial hematoma was demonstrated that originated at the cavo-atrial junction and caused significant compression of the right atrium. As the patient was hemodynamically stable, a watchful waiting approach was pursued. Repeat non-contrast chest CT scan 1 week later showed a slight decrease in the size of the pericardial hematoma (figure 1f).

Learning Points from this Case:

- An unremarkable CXR following line placement does not exclude significant cardiac pathology. Clinicians should have a low threshold for further imaging studies if warranted by patient symptoms.
- Clinically and hemodynamically significant cardiac abnormalities may be discovered as incidental findings on abdominal imaging studies.
- Even without use of gadolinium contrast, cardiac MRI may be helpful in cases where diagnosis remains unclear from CT and echocardiography.

http://www.ConferenceAbstracts.com/uploads/cfp2/attachments/LDFAIBDN/LDFAIBDN--219282-1-ANY(1).pdf

P062

Caseous Calcification of the Mitral Annulus

Pelbreton C. Balfour, Jr., MD, ScM[4]Jorge A. Gonzalez, M.D.[1], Peter W. Shaw, MD[2], Klaus Hagspiel, MD[3], Patrick Norton, MD[3], Michael Salerno, MD, PhD[4], Christopher M. Kramer, MD[5]

1. *Scripps Clinic Division of Cardiovascular Diseases, La Jolla, CA*
2. *Berkshire Medical Center, Lenox, MA*
3. *University of Virginia, VA*
4. *University of Virginia Health System, VA*
5. *University of Virginia Health System, Charlottesville, VA*

Description of Clinical Presentation: A 60 year old male with past medical history of non-obstructive coronary artery disease (CAD) and prior tobacco use presented to the ED with chest pain, dyspnea on exertion, and fatigue. Routine evaluation was negative for acute myocardial infarction and he was referred for a stress echo for further risk stratification. Baseline images on echocardiogram showed normal systolic function, but revealed a large atrial mass which appeared to be attached to the atrial septum (Figures 1 and 2), and thus stress imaging was not performed. He was subsequently referred to cardiothoracic surgery for possible resection of this mass. Computed tomography (CT) of the chest revealed a calcified lesion with central lucency along the anterior aspect of the left atrium (Figure 3). The patient underwent CMR, which demonstrated a mass located at the base of the anterior mitral valve leaflet in the mitral-aortic intervalvular fibrosa (Figures 4-6). The findings on CMR, along with initial echocardiogram and CT supported a diagnosis of caseous calcification of the mitral annulus (CCMA) rather than a tumor. Given these findings the patient did not undergo surgical resection of this mass.

Diagnostic Techniques and Their Most Important Findings: T1-weighted imaging revealed an immobile, hypointense, well-circumscribed mass measuring 24.1mm x 14.5mm located in the mitral-aortic inter valvular fibrosa, just adjacent to the base of the anterior mitral valve leaflet (Figure 4 and 5). There is focal internal T2 hyperintensity within the lesion suggesting necrosis (Figure 6). There was no apparent restriction of the anterior mitral valve leaflet, along with no mitral regurgitation. There was no enhancement of the mass on early or late gadolinium-enhancement images. The CT demonstrated that the mass was highly calcified with central lucency further supporting the diagnosis of caseous mitral annular calcification (Figure 3).

Learning Points from this Case: Caseous calcification of the mitral annulus is a rare variant of mitral annulus calcification (MAC) found in 0.06 to 0.07% of the population. This benign condition is known typically to be located on the posterior mitral leaflet. Resection of the mass reveals that the caseous contents have a toothpaste-like, milky material. Microscopic features are consistent with liquefaction necrosis showing a central region of amorphous eosinophilic acellular material surrounding by macrophages and lymphocytes. CCMA is most commonly an incidental finding with rare symptoms, and reportedly associated with CAD, aortic valve disease, hypertension, brady and tachyarrhythmias. Importantly, this uncommon lesion may often be misdiagnosed as a myocardial abscess, thrombus, or cardiac tumor, potentially leading to further unnecessary invasive testing and/or interventions. As in our case, comprehensive assessment with multimodality imaging including CMR, may be used to support the diagnosis of this rare condition, which in uncomplicated cases, can be conservatively managed.

http://www.ConferenceAbstracts.com/uploads/cfp2/attachments/LDFAIBDN/LDFAIBDN--222558-1-ANY.pdf

http://www.ConferenceAbstracts.com/uploads/cfp2/attachments/LDFAIBDN/LDFAIBDN--222558-2-ANY.pdf

http://www.ConferenceAbstracts.com/uploads/cfp2/attachments/LDFAIBDN/LDFAIBDN--222558-3-ANY.pdf

P063

Cardiac MRI for diagnosis of right hilar mass with cardiac invasion

Ross Roberts-Thomson, MBBS, BMedSci(Hons)[1]Michael B. Stokes, MBBS FRACP[2], Adam Nelson, BMedSc MBBS[3], Kurt Roberts-Thomson, MBBS, PhD[4], Karen S. Teo, MBBS, PhD[5]

1. *Royal Adelaide Hospital, Urrbrae, South Australia, Australia*
2. *Royal Adelaide Hospital, Wayville, South Australia, Australia*
3. *Royal Adelaide Hospital, South Australia, Australia*
4. *University of Adelaide, Adelaide, South Australia, Australia*
5. *Royal Adelaide Hospital, Adelaide, South Australia, Australia*

Description of Clinical Presentation: A 41-year-old man presented to our intitution with fatigue and 20kg weight loss in the past 6 months on a background of a significant smoking history and moderate-severe emphysema. Initial blood tests revealed and LDH of 455U/L but were otherwise unremarkable. A chest x-ray demonstrated a streaky opacity in the right lower lobe. A subsequent CT chest revealed a large hilar mass with invasion of the left atrium which was deemed to be most likely a malignancy but possibly an infective mass. Three bronchial biopsies were inconclusive however one of the bronchial specimens grew fungal hyphae. Several blood cultures were performed subsequently that were negative for fungaemia. Surgical or CT guided biopsy was considered too high risk for this cachetic individual with emphysematous lungs.

Diagnostic Techniques and Their Most Important Findings: A cardiac MRI (CMR) with multiplanar CINE SSFP, T1 TSE (Dark Blood), VENC (Mitral), contrast and post-contrast imaging were performed. The mass, measuring 13x9.7cm, was highly mobile and entered the left atrium posteriorly extending through the mitral valve. The mitral valve flow velocities did not indicate obstruction. The lesion demonstrated post-contrast enhancement which was heterogenous, possibly reflecting a combination of thrombus and neoplasm. Infective process was thought much less likely on the basis of the CMR.

Learning Points from this Case: CMR can provide useful additional information to aid the diagnosis of infiltrative cardiac masses, especially when obtaining definitive histology is considered too high risk. The addition of gadolinium in CMR provided useful diagnostic information for the differential diagnosis of the mass. CMR adds incremental value to CT when invasion into cardiac chambers is present to exclude significant obstruction from masses.

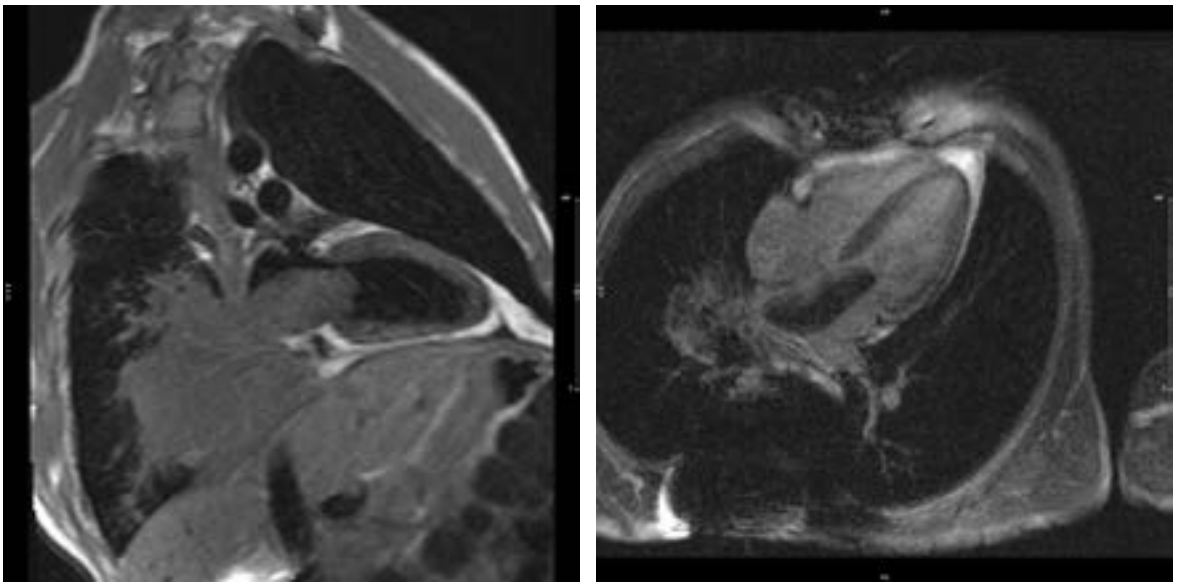

P064

The emblematic role of CMR in Constrictive Pericarditis; a 57 YO male with equivocal findings.

Richard Lombardi, RT(R)(MR), Shimaa S. Khidr, MDRonald Williams, RT(R)(MR), B.A.

Allegheny General Hospital, Pittsburgh, PA

Description of Clinical Presentation: History: 57 YOM with ASD repair 15 years ago presented with worsening dyspnea with exertion. CTA was negative for PE and a stress test was normal. Echocardiogram showed abnormal LV septal wall motion and thickened pericardium which recommended a MRI for constrictive pericarditis. The patient was referred for refractory symptoms and concern for constrictive pericarditis.

Diagnostic Techniques and Their Most Important Findings: Technique: SSFP in 2,3,4 chambers and SA, T1 morphology, T2, Tagging and LGE in 2,3,4 chambers and SA. The CMRI (SSFP) demonstrated prominent 'septal bounce' during early diastole, severely dilated left and right atrium, a thick calcified ring around almost the entire LV and RV myocardium extending into the atrium. T1 demonstrated a thickened pericardium. T2 (TIR) demonstrated increased water signal implying acute inflammation. Finally, LGE demonstrated pericardial enhancement confirming pericardial fibrosis. Radio-frequency Tissue-Tagging demonstrated lack of slippage of the visceral and parietal pericardium as well as adherence of the parietal pericardium to the diaphragm. Taken together, the above is pathognomonic for constrictive pericarditis. After discharge, colchicine and indomethacin, the patient returned 5 months later for a follow-up CMR using the same protocol. The septal bounce that existed during the first CMR was no longer evident. The increased signal pericardium remained but less. The left and right atria remained severely dilated. LGE imaging fibrosis was significantly less than prior study. RF Tagging demonstrated only mild residual adherence along the anterior and basal LV with corresponding marked improvement in constriction anatomy and physiology. Using Multiparametic CMR that intrinsically incorporates anatomy and physiology as well as 'Virtual Histology', the capability of CMR to uniquely define constrictive pericarditis non-invasively is highlighted. With this 'Great Masquerader', an often overlooked diagnosis, the role of CMR can be emblematic as it was in this patient as well as pointing towards pharmacologic, not surgical intervention as curative.

Learning Points from this Case:

References:

1) Power J A, Thompson D V, Rayarao G, Doyle M, Biederman R W. Cardiac magnetic resonance radiofrequency tissue tagging for diagnosis of constrictive pericarditis: A proof of concept study. *J Thorac Cardiovasc Surg*.2016;151(5):1348-1355.

2) Angheloiu GO, RayaraoG, Williams R, Yamrozik J, Doyle M, Biederman R W. Magnetic resonance characterization of septal bounce: findings of blood impact physiology. *Int J Cardiovasc Imaging*.2014;31(1):105-13.

3) Bogabathina H, Biederman R.Lack of "slippage" by Cardiovascular Magnetic Resonance Imaging is sine qua non for Constrictive Pericarditis. *Circulation*.2011.26;123(16):e418-9.

4) Power JA, Vido DA, Doyle M, Biederman RW. Can CMR be the new 'gold standard' for constrictive pericarditis? *Journal of Cardiovascular Magnetic Resonance*.2012;14(Suppl1):O33.

P065

Ockham's Razor put to the test

Paul Scully, MBBS MRes[1] Thomas Treibel, MBBS.MRCP(UK)[2], James C Moon, MD[2], Anna Herrey, MD PhD MRCP[2]

1. *Barts Heart Centre, London, England, United Kingdom*
2. *Barts Heart Centre, England, United Kingdom*

Description of Clinical Presentation: A 65-year-old Afro-Caribbean gentleman presented to his local Emergency Department with symptomatic atrial fibrillation and rapid ventricular response. His high-sensitivity troponin I level was elevated at 13,000 ng/L. He had attended hospital two months previously with an acute coronary syndrome, at which time he had undergone coronary angiography, which showed only mild atheroma. He gave a history over the last few years of mild shortness of breath on exertion. He was known to suffer with hypertension, diabetes mellitus and hypercholesterolaemia. His transthoracic echocardiogram performed during his previous admission had shown moderate biventricular hypertrophy (interventricular septal diameter 18mm), with preserved radial left ventricular systolic function (ejection fraction 55%) and impaired longitudinal function (S' 6cm/s). There was a pseudonormal filling pattern and a dilated left atrium (24.6cm^2).

Diagnostic Techniques and Their Most Important Findings: He was referred for a cardiovascular magnetic resonance (CMR) scan because of the elevated troponin in the context of the previously reassuring coronary angiogram and the echocardiogram appearances. The CMR showed evidence of basal-mid septal and apical hypertrophy (maximum wall thickness 22mm in the basal septum), with global hypokinesia and severely impaired radial left ventricular systolic function in the context of atrial fibrillation. There was mild-moderately impaired right ventricular systolic function. There was also diffuse late enhancement involving both ventricles, with enhancement of the atria also noted. There was evidence of microvascular obstruction apically in the inferolateral wall suggesting a small acute infarct, along with an apical thrombus. Native myocardial T1 was elevated at 1114-1157ms (MOLLI; normal 1024±39ms). Myocardial T2 values were normal (< 52ms). The diagnosis of cardiac amyloidosis and an acute apical infarct, with apical thrombus was made.

Learning Points from this Case: Ockham's razor would suggest that the simplest explanation is often the best, and is a principle often quoted in Medical practice. We present an interesting complex case that reminds us that patients do not always conform to this principle. Multiple pathologies are possible and do occur.

It reminds us that we should always consider the clinical context and presentation. In this case there was a preceding history of breathlessness giving a clue to the underlying cardiomyopathic process, but then a more acute presentation with a significant troponin rise in the context of cardiovascular risk factors making an acute coronary syndrome likely. The aetiology of the latter may have been a coronary embolism from the apical thrombus or potentially plaque rupture relating to the mild atheroma on the recent coronary angiogram.

This case nicely highlights the essential role that CMR has in these complex cardiac patients and in diagnosing previously under recognised conditions such as amyloid.

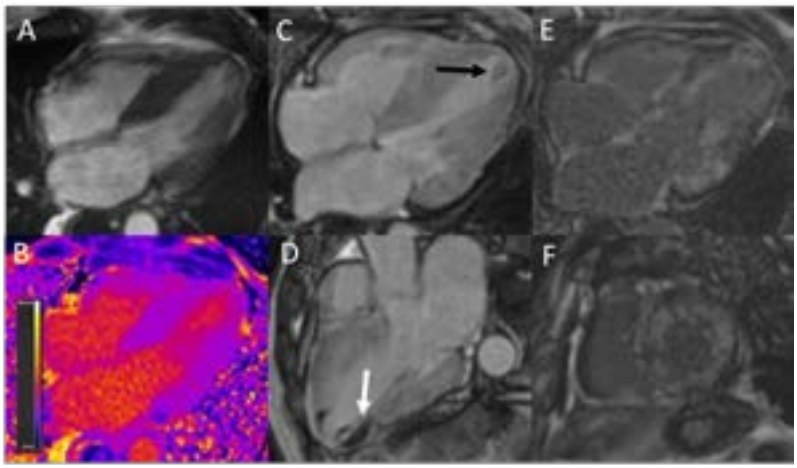

Figure 1: A: four-chamber SSFP cine image illustrating the degree of left ventricular hypertrophy; **B:** Modified Look-locker inversion recovery (MOLLI) T1 map showing an elevated T1 at 1114-1157ms (normal range 1024 ± 39ms); **C:** four-chamber early gadolinium image showing a small apical thrombus (see black arrow); **D:** three-chamber early gadolinium image showing microvascular obstruction at apex (see white arrow), with a small apical thrombus, **E:** four-chamber image showing extensive patchy late gadolinium enhancement effecting both ventricles, with some atrial enhancement also noted; **F:** short axis image at the mid-ventricle level showing patchy extensive transmural late gadolinium enhancement.

P066

Left Dominant Arrhythmogenic Right Ventricular Cardiomyopathy

Sainan Cheng, MD[3]Xinyu Wang, MD[1], Shihua Zhao, MD, FESC[2]

1. *Department of Cardiology, Beijing, Beijing, China (People's Republic)*
2. *Department of Radiology, Beijing, N/A, China (People's Republic)*
3. *National Center for Cardiovascular Diseases of China, Chinese Academy of Medical Sciences and Peking Union Medical College, Beijing, China (People's Republic)*

Description of Clinical Presentation: A 35-year-old man was admitted with 7-year history of exertional dyspnea and abdominal distention. His elder brother and male cousin, and his mother's younger brother died of cardiomegaly and heart failure when they were young.

Diagnostic Techniques and Their Most Important Findings: Electrocardiogram showed right ventricular high voltage. Holter monitoring revealed premature ventricular contractions (PVCs) originating the right ventricle (RV) and there were 2195 PVCs/24 hours. Coronary arterial disease was excluded with coronary CT. Cardiovascular magnetic resonance (CMR) demonstrated that the left ventricle (LV) severely dilated with severely reduced global systolic function, while the RV was mildly dilated with moderate systolic dysfunction (Figure 1A). LV lateral wall appeared thin and akinetic (Figure 1A, arrow). Transmural late gadolinium enhancement (LGE) occurred in the entire LV lateral wall and diffusely focal LGE was demonstrated in the interventricular septum (Figure 1B, arrow). The patient received cardiac transplantation. Histopathology examination showed myocardial fibro-fatty replacement in the entire lateral wall and focally in the subepicardium of other LV walls and RV free wall (Figure 2). The patient was on regular anti immune rejection treatment and lived well at the 3-year follow-up.

Learning Points from this Case: Traditionally arrhythmogenic right ventricular cardiomyopathy (ARVC) is one of the most arrhythmogenic forms of inherited cardiomyopathy and characterized pathologically by RV myocardial fibro-fatty replacement which predisposes patients to life-threatening ventricular arrhythmias. Although ARVC has low incidence, it is a frequent cause of sudden death in the young and in the athletes. This is a typical case of left dominant ARVC confirmed by pathology, which presented with predominant heart failure and LV impairments that leads to hard to distinguish from other dilated cardiomyopathy. As contrast-enhanced CMR is highly specific for evaluation of myocardial scar, left dominant ARVC should be differentiated in patients with cardiomegaly and unusual scar distribution.

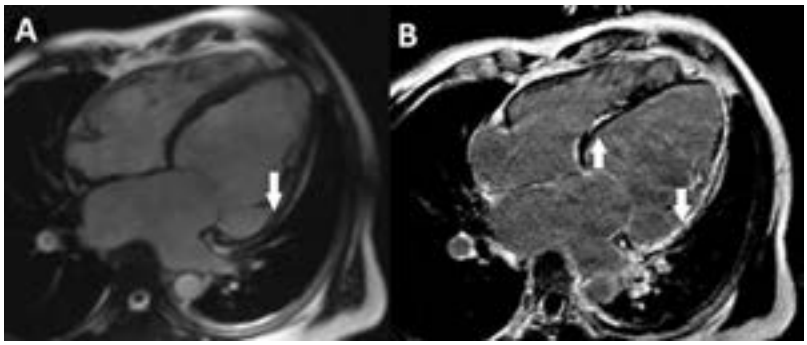

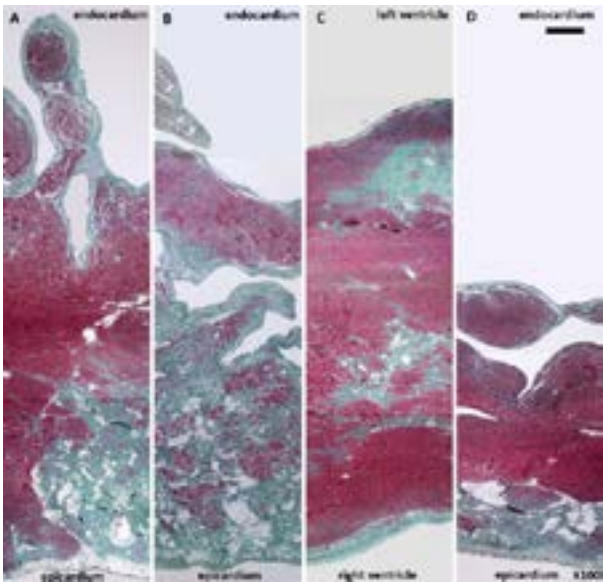

P067

A teenager with dry skin, wooly hair, and tachycardia.

Shivani G. Patel, MBBS[1], Andrew J. Powell, M.D.[2]

1. Boston Children's Hospital, Chicago, IL
2. Harvard Medical School and Boston Children's Hospital, Boston, MA

Description of Clinical Presentation: A 16-year-old girl presented with recent onset of emesis, shortness of breath, and chest pain. An ECG showed a wide complex tachycardia at 226 bpm. CBC, electrolytes, CRP, and ESR were normal. A troponin T level was elevated at 3.34 (normal < 0.09 ng/ml). Synchronized cardioversion converted her to sinus rhythm. Questioning revealed that she ran track and performed karate effortlessly. Her family history was unremarkable. On physical exam, she was noted to have very curly hair, and dry palms and soles, unlike anyone else in the family.

Diagnostic Techniques and Their Most Important Findings: An echocardiogram showed a severely dilated left ventricle (LV) with severe global systolic dysfunction (ejection fraction 30%) and regional variation. There was moderate mitral and tricuspid regurgitation. Cardiac MRI showed a severely dilated LV with severely depressed global systolic function (ejection fraction 24%). Mid and apical anterolateral and inferolateral segments were thin and akinetic (Fig A). Right ventricle (RV) was moderately dilated with moderately depressed global systolic function (ejection fraction 34%), and scalloping of multiple segments. Late gadolinium enhancement (LGE) was seen in the full thickness of the mid antero/inferolateral LV, epicardium of the remaining LV wall segments, LV papillary muscles, and the RV surface of the mid and apical ventricular septum (Fig B). A cardiac catheterization revealed an elevated LV end-diastolic pressure of 20 mm Hg, a normal cardiac index, and normal coronary anatomy. A biopsy from the RV septal wall showed a focal area of interstitial fibrosis suggestive of chronic ischemia. Two days later, she had a cardiac arrest and was placed on a LV assist device. A biopsy taken from the LV free wall showed extensive myocardial subepicardial fatty infiltration and fibrosis. The hypertrophic myocardium had multifocal interstitial lymphohistiocytic inflammation and myocyte damage. These findings were consistent with arrhythmogenic ventricular dysplasia (ARVD). The patient eventually underwent a heart transplant. The explanted heart pathology evaluation revealed marked myocyte hypertrophy, biventricular fibrosis/scar with partial fatty replacement, patchy granulation-type tissue, and patchy subendocardial fibromyxoid change. These findings were also diagnostic of ARVD. On genetic testing, she had two mutations in desmoplakin - a pathogenic truncating mutation Q625X and a missense variant of unknown significance A2148T.

Learning Points from this Case: Arrhythmogenic cardiomyopathy can be seen as part of a cardio-cutaneous syndrome with wooly hair and palmoplantarkeratoderma, and may be related to a pathogenic mutation in desmoplakin. This variant results in predominant LV involvement, early morbidity, and clinical features overlapping with dilated cardiomyopathy. The cardiac MRI in this patient showed areas of LGE which matched the distribution of fibrofatty tissue on histopathology. It was the first test to suggest ARVD rather than a general diagnosis of non-ischemic dilated cardiomyopathy.

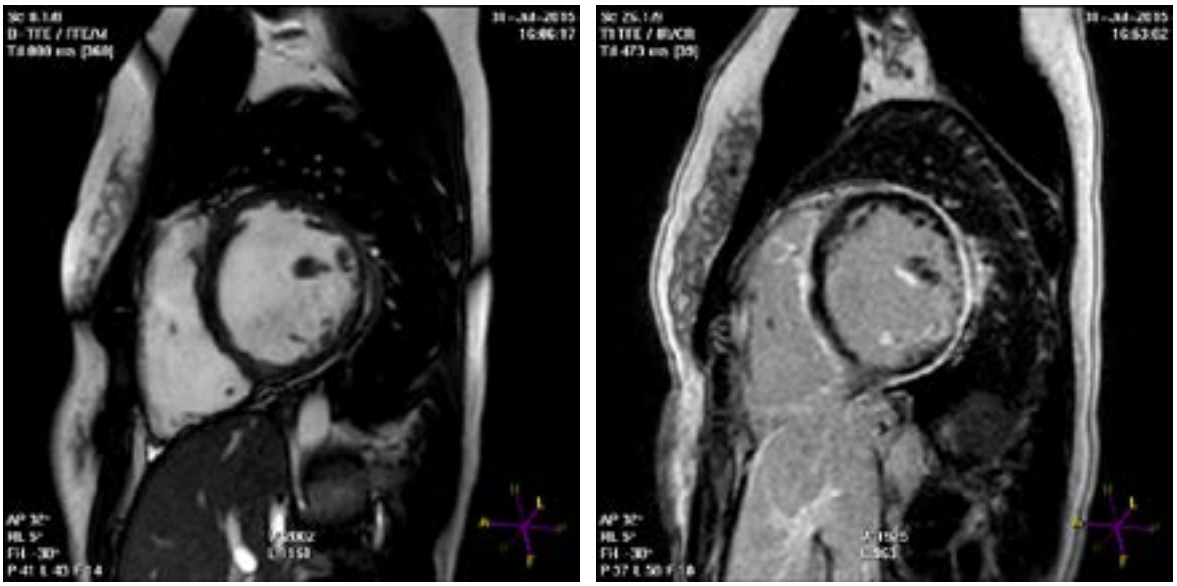

P068

Isolated right ventricular endomyocardial fibrosis in a young male with chronic myeloid leukemia

Fateh Ali Tipoo. Sultan, MBBS, FCPSYousuf Hasan, MBBS

Aga Khan University Hospital, Karachi, Pakistan, Karachi, Sindh, Pakistan

Description of Clinical Presentation: A 26 year old man was referred for cardiac magnetic resonance (CMR) for evaluation of suspected right ventricular mass, found on multiple serial echocardiograms. He was known to have chronic myeloid leukemia (CML) for the past three years, which was in a quiescent state on medical treatment. He presented with symptoms and signs of gradually worsening right heart failure. There was no eosinophilia with normal white blood cell counts. Echocardiogram which was done at some other hospital, revealed a suspicious right ventricular mass filling the entire right ventricle except the right ventricular outflow tract.

Diagnostic Techniques and Their Most Important Findings: CMR with gadolinium enhancement was done on 1.5 Tesla, Siemens avanto, which showed severely enlarged right atrium with some apical displacement of the septal leaflet of the tricuspid valve and significant tricuspid regurgitation. There was obliteration of the right ventricular apex with a mass like density which was isointense on turbo spin echo (TSE) T1 weighted images with and without fat suppression. It also appeared isointense on TSE T2 weighted images with mildly hyper-intense sub-endocardial rim. On first pass perfusion imaging after gadolinium injection, the obliterated apical region looked well perfused except a small superficial part which remained hypo-enhanced on early gadolinium images, suggestive of thrombus. On delayed enhanced imaging with gadolinium, a thin endomyocardial rim of hyper-enhancement was seen in the right ventricle, consistent with endomyocardial fibrosis. A diagnosis of isolated right ventricular endomyocardial fibrosis was made on the basis of typical findings on CMR.

Learning Points from this Case: It is a classic case of isolated right ventricular endomyocardial fibrosis in which the correct diagnosis would not have been made without CMR.

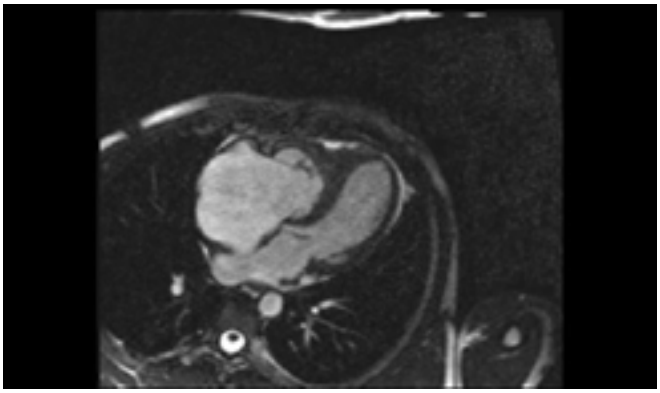

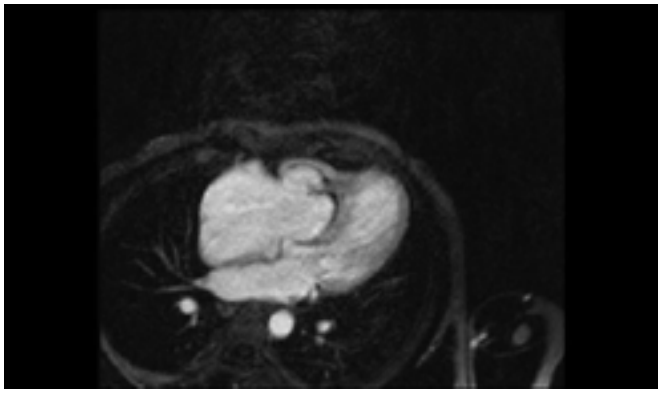

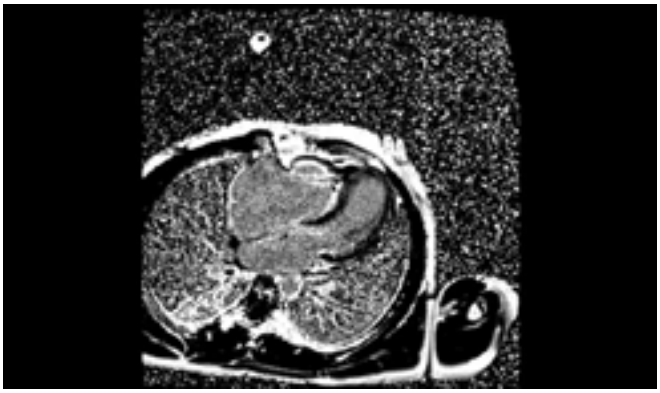

P070

Fatty RV…Thinking beyond ARVC

Vedant A. Gupta, MD[1]Steve W. Leung, MD[2], Michael Brooks, MD[1], Vincent Sorrell, MD[2]

1. University of Kentucky, Lexington, KY
2. University of Kentucky, KY

Description of Clinical Presentation: A 59 year-old Caucasian female with a history of chronic obstructive pulmonary disease presented for pre-operative risk assessment, prior to renal mass excision, due to an abnormal ECG, palpitations and shortness of breath. She denied history of syncope. She had no significant family history. Physical exam showed normal vitals and no evidence of right heart failure. The ECG showed sinus rhythm with possible right ventricular hypertrophy (RVH) and right atrial enlargement (Figure 1). Transthoracic echocardiogram showed severe RVH and a cardiovascular MRI (CMR) was recommended for possible arrhythmogenic right ventricular cardiomyopathy/dysplasia (ARVC/D) vs infiltrative cardiomyopathy.

Diagnostic Techniques and Their Most Important Findings: CMR with balanced steady state free precession sequences and T2 weighted images with and without fat saturation preparation showed a small RV cavity with fatty infiltration within the RV free wall (Figure 2). This was clearly demarcated from the epicardial fat. In addition, there was normal global RV function (RVEF of 62%) with no focal areas of RV dysfunction. There were no major or minor CMR criteria for ARVC/D, and findings were most consistent with adipositas cordis. Patient did well after her excision of the benign renal lesion (oncocytoma). Holter monitor showed rare PVCs (< 1%) with no sustained ventricular arrhythmias. Her palpitations resolved with beta-blockade.

Learning Points from this Case: ARVC/D is a rare inherited condition that is thought to affect the cell-to-cell binding proteins (desmosomes). This is associated with not only loss of integrity of gap junctions, leading to RV dysfunction from myocyte loss, but also an increased risk for sudden cardiac death. The hallmark of pathologic diagnosis is fibro-fatty replacement of the RV myocytes, and endomyocardial biopsy remains the gold standard. The major criteria and minor CMR criteria for ARVC/D emphasize the following 3 components: RV regional dysfunction, RV cavity dilation, and decreased RV global function. While pathological evidence of fibrofatty replacement of myocytes continues to remain a major diagnostic criteria, this does not extend to evidence of fibrofatty infiltrate in the RV on CMR. This patient does not have evidence of regional or global RV dysfunction, and meets no other Task Force Major criteria for ARVC/D.

This case is most consistent with adipositas cordis, a rare condition involving fatty infiltration of either ventricle with structurally normal myocytes and usually normal myocardial function. The association with sudden cardiac death or ventricular dysfunction has not been as clearly described. The natural history and prognosis is unknown for this condition. Accurate diagnosis of ARVC/D focusing on Task Force Criteria of validated imaging criteria is essential to guide clinical decision making. The identification of fatty infiltration of myocardium is not adequate for the diagnosis of ARVC/D.

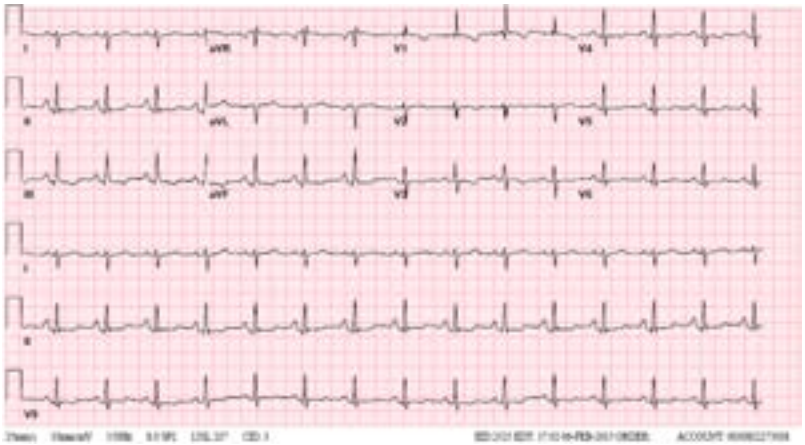

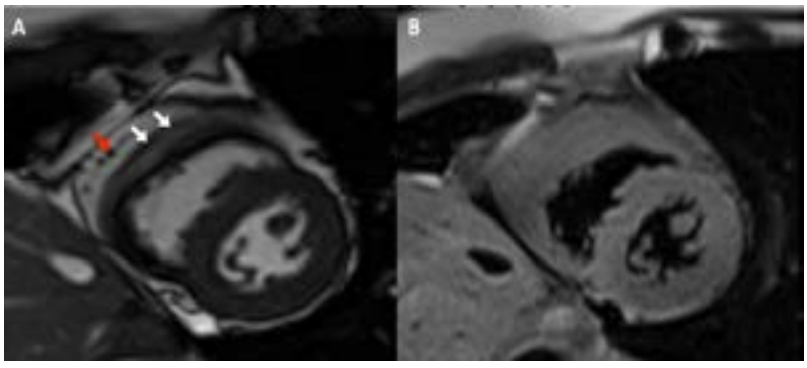

P071

Elevated troponin and ventricular tachycardia one year after coronary unroofing for anomalous aortic origin of the right coronary artery: Role of Cardiac MRI

Marc V. Lee, MD[1] Ranjit Philip, MD[2], Jean Ballweg, MD[2], Jason Johnson, MD, MHS[2]

1. University of Tennessee Health Science Center, Memphis, TN
2. Le Bonheur Children's Hospital, University of Tennessee Health Science Center, TN

Description of Clinical Presentation: An 8-year-old male had a history of anomalous aortic origin of the right coronary artery (AAORCA) from the left cusp diagnosed as a neonate. The orifice was slit like with intramural course so he had an elective unroofing procedure done one year prior to presentation. On the day of presentation he had left-sided chest pain and an 8 beat run of nonsustained ventricular tachycardia. He had a fever and general fatigue one week prior to presentation without cough, rhinorrhea, vomiting, or diarrhea. Except for mildly elevated blood pressures, his physical exam was normal. The chest x-ray showed mild cardiomegaly. ECG was concerning for deep Q-waves in II, III, AVF, and leads V4-V6 (Figure 1), with a troponin peak at 1.35 ng/mL.

Diagnostic Techniques and Their Most Important Findings: Transthoracic echocardiogram showed patent origin of the unroofed right coronary artery (RCA) as well as a normal left coronary artery (LCA), normal left ventricle (LV) and right ventricle (RV) size, and systolic function. A trivial pericardial effusion was also noted. Cardiac catheterization demonstrated that the RCA was widely patent at its ostium with no stenosis along the remainder of its course. The LCA, left anterior descending, and left circumflex coronary arteries were also widely patent. LV and RV end diastolic pressures were elevated at 19 mmHg and 17 mmHg, respectively. Cardiac index was normal at 3.5 L/min/m^2. Several endomyocardial biopsies were obtained. Contrast-enhanced cardiac MRI was performed without sedation with a free-breathing technique and showed normal LV chamber size (LV end diastolic volume indexed 83 ml/m2), normal wall thickness, and normal systolic function (ejection fraction 59%) with mild hypokinesia of the basal to mid lateral wall. There was patchy mid to epicardial late gadolinium enhancement (LGE) that spared the subendocardial region of the basal to apical LV lateral wall and apical LV anterior wall (Figure 2-3). The right ventricular septal myocardial biopsy showed mild myocardial hypertrophy, mild interstitial fibrosis, and a few interstitial lymphocytes. The Coxsackie B titers were elevated from 1:16-1:32.

Learning Points from this Case: The findings were consistent with acute myocarditis. Myocarditis in pediatric patients is most often due to an infectious etiology, with the majority of cases being viral. Although fulminant cases of heart failure occur, many children and adolescents present with chest pain, fatigue, or other nonspecific symptoms. There is a challenge in diagnostic workup especially in patients at risk for myocardial ischemia, such as coronary anomalies. The ability of the cardiac MRI to identify a LGE pattern that fit an inflammatory process versus an ischemic process proved to be an important diagnostic tool.

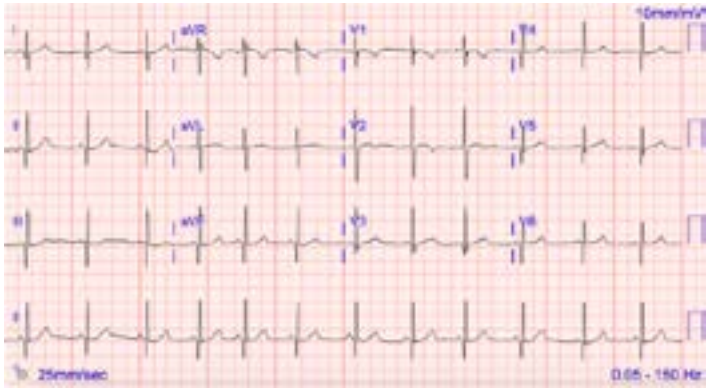

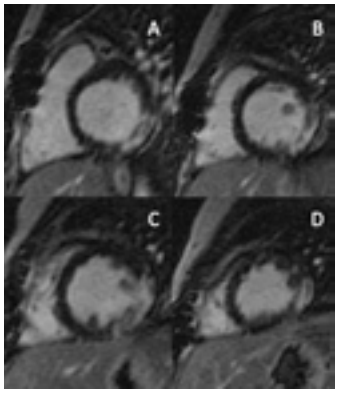

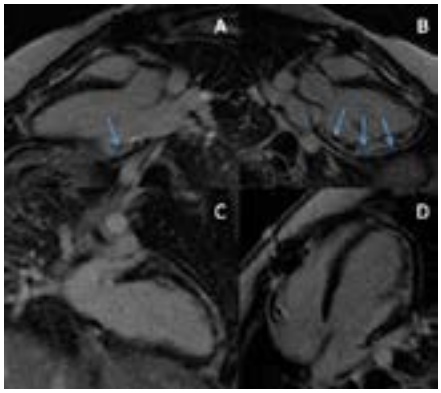

P072

A Late Phenotypic Debut of Hypertrophic Cardiomyopathy.

Alexander Ivanov, MD[1]Saadat A. Khan, MD[1], Jean Ho, BA[2], Noshin Khan[3], Stanislav Arkhipov[4], Jonathan M. Bae[5], Akash M. Thaker, B.A.[6], Bo Lu[7], Natalia Crenesse-Cozien, BA[1], Ethan Herrera[4], Michael Gerber[8], Alexandra Grossman[9], Zuhair Ali, M.D.[4], Mahmoud A. Mohamed, MD[10], Joshua Socolow, MD[1], John Heitner, MD[4]

1. *New York Methodist Hospital, Brooklyn, NY*
2. *New York Methodist Hospital, New York, NY*
3. *New York Methodist Hospital, Central Islip, NY*
4. *New York Methodist Hospital, NY*
5. *New York Methodist Hospital, Dix Hills, NY*
6. *New York Methodist Cardiology Research, Paramus, NJ*
7. *New York Methodist, New York, NY*
8. *City College of New York, New York, NY*
9. *New York Methodist Hospital, Charlotte, NC*
10. *New York Methodist Hospital, East Orange, NJ*

Description of Clinical Presentation: This is a 70-year-old African American female with obstructive sleep apnea, anxiety, depression, and gastro-esophageal reflux disease (GERD) who initially presented with atypical chest pain, exertional dyspnea and palpitations.

Diagnostic Techniques and Their Most Important Findings: The patient was noted to have ST-T wave abnormalities on her baseline ECG. Transthoracic echocardiogram (TTE) showed normal left ventricular systolic function with mild-to-moderate left ventricular hypertrophy (LVH) (maximal wall thickness 1.4 cm) and left ventricular ejection fraction (LVEF) of 75%. Coronary angiography revealed patent coronary arteries and elevated left ventricular end diastolic pressure. She was referred for CMR to rule out the presence of infiltrative cardiomyopathy. Initial CMR scan (1.5 T) revealed mildly enlarged left ventricle and LVEF of 74%. There was no evidence of infarct or fibrosis noted. The maximal wall thickness by CMR was only 0.8 cm with evidence of prominent trabeculation. The extent of trabeculation met all current criteria for left ventricular non-compaction (Petersen – end diastolic ratio of non compacted (NC) to compacted (C) myocardium >2.3, Stacey- end-systolic NC/C ratio>2, Jacquier – NC mass>20% of total mass and Captur- fractal dimensions maximum in mid-to-apical part of left ventricle >1.392). The chest pain was considered to be related to GERD and the patient was treated with a proton pump inhibitor. During the next seven years, the patient's course was relatively unremarkable with intermittent episodes of atypical chest pain. Subsequent TTE showed LVEF of 65%, with moderate end-diastolic dysfunction as well as a moderately enlarged left atrium and moderate mitral regurgitation (MR). The patient was referred for a follow-up CMR to assess for infiltrative cardiomyopathy due to LVH in the absence of hypertension. The CMR showed severe apical hypertrophy with a maximal wall thickness of 2.2 cm apical hypertrophic cardiomyopathy with no evidence of myocardial fibrosis. The left atrium was severely enlarged with moderate MR. The patient was referred for genetic consultation. The transgenomic genetic test was positive for a deleterious splice mutation in the MYBPC3 gene, consistent with the diagnosis of hypertrophic cardiomyopathy.

Learning Points from this Case: This case is the latest described phenotypic debut of hypertrophic cardiomyopathy in the seventh decade of patient's life. Our observation is in line with previous report that trabeculaton can be a preclinical abnormality in hypertrophic cardiomyopathy. Repeat CMR imaging may be helpful to follow up cases with unclear underlying pathology.

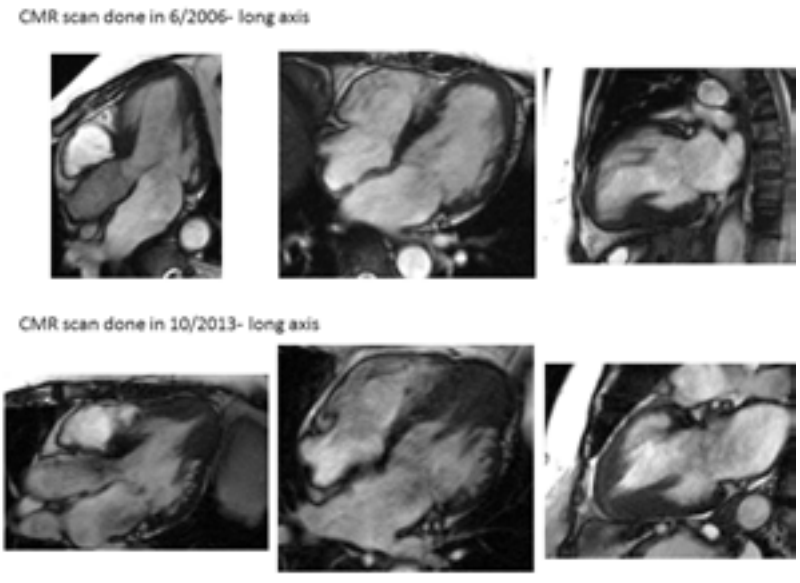

P073

Myocardial fibrosis in two siblings with limb-girdle muscular dystrophy type 2E

Tushar Acharya, MD[1]Meganne E. Leach, MSN[2], Daniel W. Groves, MD[3], A. Reghan Foley, MD[4], Sandra Donkervoort, MS, CGC[5], Carsten G. Bönnemann, MD[4], Andrew E. Arai, MD[6]

1. *National Heart, Lung and Blood Institute, National Institutes of Health, Bethesda, MD*
2. *National Institute of Neurological Disorders and Stroke, National Institute of Health, MD*
3. *National Heart, Lung and Blood Institute, National Institutes of Health, MD*
4. *National Institutes of Health, MD*
5. *National Institutes of Health, Neuromuscular and Neurogenetic Disorders of Childhood Section, Bethesda, MD*
6. *National Institues of Health, Bethesda, MD*

Description of Clinical Presentation: Cardiac Magnetic Resonance Imaging (CMR) findings of two siblings with limb-girdle muscular dystrophy type 2E (LGMD2E) due to homozygous mutations in the beta-sarcoglycan (*SGCB)* gene are reported. The siblings presented with mild motor delays, elevated creatine kinase levels (>10X upper limit of normal), and proximal muscle weakness affecting the lower > upper extremities around five years of age. Between 5-10 years of age, both developed exertional muscle pain and cramping, and the younger sibling, now a 10 year-old male, has had episodes of suspected rhabdomyolysis. He has been on daily prednisone for one year. Muscle weakness is progressive, and the elder sibling, a 13-year-old female, has developed mild distal weakness and cannot arise from the floor independently. She has been on weekend dosing of prednisone for 4 years. Both siblings have frequent falls, but neither complains of shortness of breath or chest discomfort.

Diagnostic Techniques and Their Most Important Findings: Both siblings have homozygous causative mutations in *SGCB*: c.355A>T; p.Ile119Phe. Electrocardiograms show sinus arrhythmia. Pulmonary function tests suggest respiratory muscle weakness in the sister (FVC 74% predicted in sitting) but not the brother (FVC 101% predicted in sitting), and muscle MRI show muscle atrophy and fatty infiltration of paraspinal, abdominal, gluteal and thigh muscles in both patients. Both siblings underwent non-contrast CMR imaging 3 years prior that showed normal ejection fraction and no other abnormalities. The repeat (current) CMR study showed a reduction in the sister's LV systolic function with a drop in ejection fraction over 3 years from 67% to 57%. Similarly, the brother's LV ejection fraction dropped from 70% but remained in the normal range at 64%. LV end diastolic volume and LV mass were within normal limits (z score < 2). No regional wall motion abnormalities were noted in either patient on steady state free precession cine imaging. Post-contrast images of the sister showed subepicardial late gadolinium enhancement (LGE) in the basal segment of the anterolateral and inferolateral walls. The brother's post-contrast images showed subepicardial and mid-myocardial LGE in the basal and mid segments of anterolateral and inferolateral walls. No lipomatous metaplasia was seen on fat-water separation imaging in either patient.

Learning Points from this Case: 1. Although cardiac dysfunction is known to occur in LGMD2E (beta-sarcoglycanopathy), no LGE pattern has been reported to date. We report for the first time, predominantly subepicardial but also mid-myocardial fibrosis in the basal segments of the anterolateral and inferolateral LV walls in two siblings with limb-girdle muscular dystrophy type 2E. 2. LGE in LGMD2E patients may be an early marker for LV dysfunction. 3. Screening CMR for LGMD2E patients should include LGE imaging to detect myocardial fibrosis which may be apparent prior to the development of overt LV systolic dysfunction.

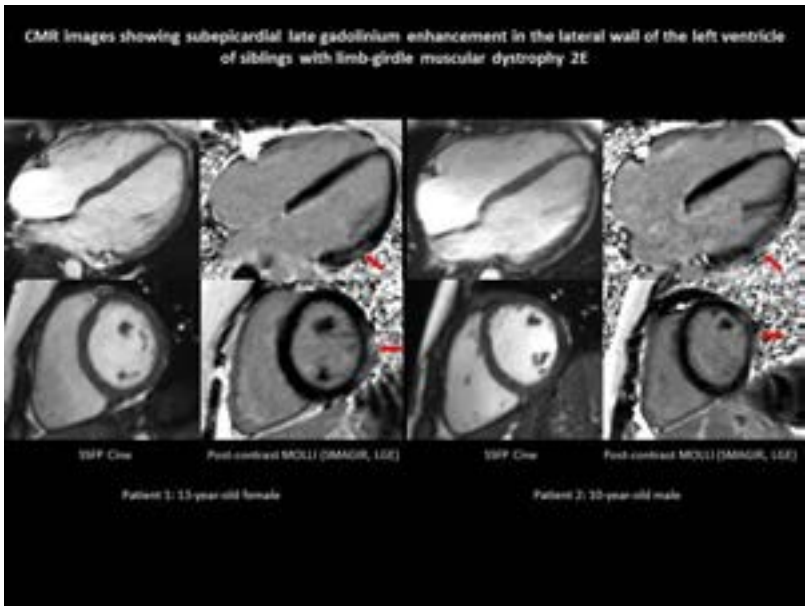

P074

Extensive Idiopathic Myocardial Calcification in an Octogenarian Female

Rajesh Janardhanan, MD, FACC[1] Nirmal Singh, MD[2], Gerald Wolff, MD[2]

1. Banner University Medical Center, Tucson, Tucson, AZ
2. Banner University Medical Center, Tucson, AZ

Description of Clinical Presentation: An 88-year-old Caucasian woman with past medical history of stable chronic kidney disease and hypothyroidism was incidentally noted to have cardiac calcifications on a chest CT scan. She was referred for cardiac MRI (CMR) for further evaluation of myocardial structure. Her past medical history was negative for coronary artery disease, myocardial infarction, pericarditis, myocarditis, tuberculosis, rheumatic heart disease, hypertension, diabetes mellitus, hyperlipidemia, cardiac surgery, malignancy or chest trauma. She did not have traditional cardiac risk factors. Social history was non-contributory. On physical examination, vitals were within normal limits. Patient appeared to be frail, but in no apparent distress. Physical examination was unremarkable. No significant skin changes, edema, ascites, or lymphadenopathy.

Diagnostic Techniques and Their Most Important Findings: EKG was normal. Lab work revealed normal values apart from an elevated of serum creatinine at 1.5 mg/dL. Calcium and phosphorus levels were normal. CT chest demonstrated extensive coarse calcification of the myocardium with no pericardial abnormalities. CMR revealed extensive scattered hypo-intense areas (suggesting diffuse calcifications) in the left ventricular myocardium in a non-coronary distribution with associated hypokinesis. The same segments were hypo-intense on T1 and T2 weighted **[Figure 1]** images with resting perfusion defects **[Figure 2].** Patchy gadolinium uptake on delayed enhancement imaging **[Figure 3]** was noted. The global left and right ventricular systolic function was preserved. No LV thrombus was seen.

Learning Points from this Case: Conventionally, pathological calcification is classified into dystrophic and metastatic calcification. Dystrophic calcification takes place in dying tissues despite normal calcium level and metabolism. Metastatic calcification takes place in normal tissue with underlying hypercalcemia due to deranged calcium metabolism, usually secondary to systemic disease. Myocardial calcification can manifest as rhythm disturbance, heart failure and sudden cardiac death.
Dystrophic myocardial calcification could be secondary to ischemic, traumatic, infectious, inflammatory or neoplastic causes. Metastatic calcification can be secondary to chronic renal failure, hyperparathyroidism, oxaluria, aluminum toxicity related to hemodialysis, dietary calcium deficiency, Vitamin D deficiency and sarcoidosis due to Vitamin D hyper-activation.
We present an unusual case of extensive myocardial calcification in an asymptomatic octogenarian female. Interestingly her overall LV systolic function was preserved. She has no prior history of myocardial infarction. Her chronic kidney disease was not significant enough to cause any derangement in calcium metabolism. Her calcium and phosphorus levels were normal. We do not have a definite etiology for the calcification. In the absence of a recognized etiology, we believe this is idiopathic calcification. Since patient is relatively asymptomatic, we opted to manage her conservatively.

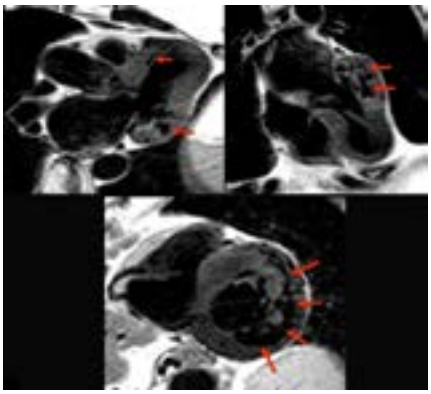

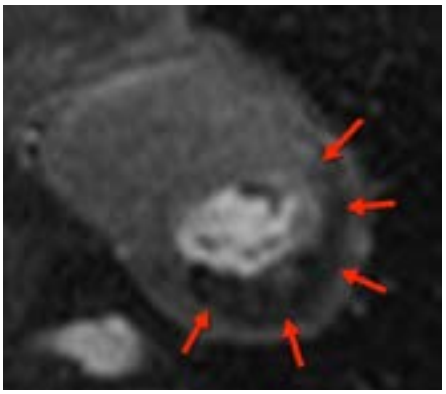

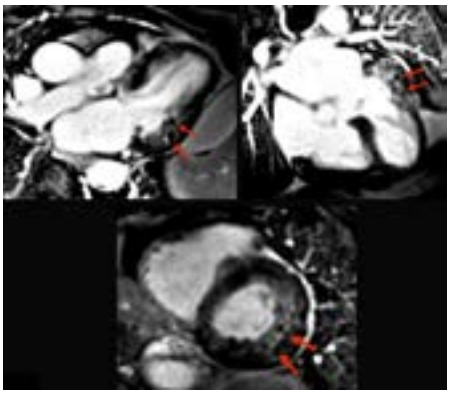

P075

2 cases with fibrofatty replacement of apical Left Ventricle in CMR findings diagnosed as Arrhtyhmogenic Right Ventricular Cardiomyopathy

Sony Hilal. Wicaksono, MD, FIHA

Rumah Sakit Pondok Indah, Kota Bekasi, Jawa Barat, Indonesia

Description of Clinical Presentation: 2 female patients, 55 and 73 years old, were referred to our imaging center in Pondok Indah Hospital Jakarta, Indonesia, to perform Cardiac Magnetic Resonance (CMR) examination to exclude arrhythmogenic right ventricular cardiomyopathy. Both patients have history of ventricular arrhythmia.

Diagnostic Techniques and Their Most Important Findings: We perform Cine, Edema, Blackblood with and without fat suppression, rest perfusion CMR and Late Gadolinium Enhancement in both patients, with Siemens Skyra 3 Tesla.

First patient findings: Cine CMR showed normal LV and RV wall motion, ejection fraction and volumes. Edema CMR showed spotty hypo-enhancement in apical septal segment of LV,, in blackblood CMR showed spotty hyperenhancement in apical septal, while blackblood CMR with fat suppression showed spotty hypo-enhancement. Perfusion CMR showed perfusion defect in apical septal. LGE-CMR showed spotty hyperenhancement in apical septal. We conclude that there are spotty fibrofatty replacement in apical septal.

Second patient findings: Cine CMR showed normal LV and RV wall motion, ejection fraction and volumes. Edema CMR showed large hypo-enhancement in apical septal segment of LV, in blackblood CMR showed large hyperenhancement in apical septal while blackblood CMR with fat supression showed large hypo-enhancement. Perfusion CMR showed perfusion defect in apical septal. LGE-CMR showed large hyperenhancement in apical septal. We conclude that there is a large fibrofatty replacement in apical septal of LV.

Both patients CMR results impression was ARVC

Learning Points from this Case:

1. From CMR examination, evidence of fibrofatty replacement in apical septal of LV in patients with cardiac electrical abnormality, without involvement of RV, can be diagnosed as ARVC.
2. Both patients are female.

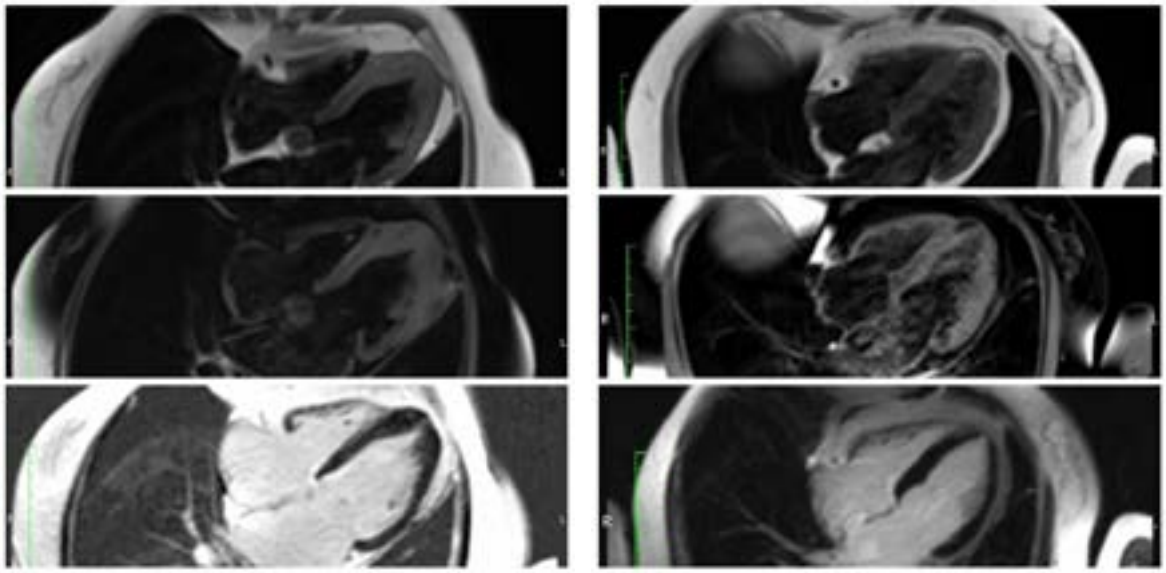

P076

Fabry disease

Sudip K. Saha, MD

Mid Atlantic Permanente Group, Mclean, VA

Description of Clinical Presentation: A forty-eight year old man presented to outpatient cardiology consultation with an abnormal ECG and hypertension. His other chronic symptoms and conditions included chronic kidney disease with proteinuria, history of strokes without residual deficits, unexplained nausea, and neuropathy with gait instability. He has had prior evaluations for his multiple conditions without an unifying diagosis. His ECG was remarkable for a right bundle branch block.

Diagnostic Techniques and Their Most Important Findings: Techniques: Cardiac MRI was performed on a Philips 1.5 T scanner with a commercial 5-element cardiac-surface coil. Cine images were acquired in a contiguous LV short-axis orientation with an ECG-gated, breath-hold, steady-state free-precession sequence with full LV coverage (8-mm slice thickness, 2-mm interslice gap, in-plane spatial resolution 2×2 mm, 30 ms temporal resolution). LGE-CMR was performed 15 minutes after the intravenous administration of 0.2 mmol/kg gadolinium-DTPA (Magnevist; Schering, Berlin, Germany) with a 2-dimensional breath-hold, segmented inversion-recovery sequence (inversion time optimized by the Look-Locker sequence [inversion time scout] to null normal myocardium) acquired in the same orientation (short-axis stack and four chamber view) as the cine images.

Most important findings: There was a symmetric increase in left ventricluar wall thickness throughout the myocardium with an increased left ventricular mass. There was LGE in the mid-distal lateral wall in a pattern consistent with Fabry disease given the clinical context. The patient underwent confirmatory enzyme assay testing which supported the diagnosis of Fabry disease and he is considering enzyme replacement therapy.

Learning Points from this Case: Cardiac MRI is a powerful tool to evaluate conditions that cause increased left ventricular wall thickness including infiltrative cardiomyopathies/storage disorders. As in this case, it can lead to confirmatory testing for rare conditions such as Fabry disease based on typical patterns such as distribution of late gadolinium enhancement in the lateral myocardial walls. It is important to maintain a wide differential and integrate non-cardiac findings in order to find a unifying diagosis.

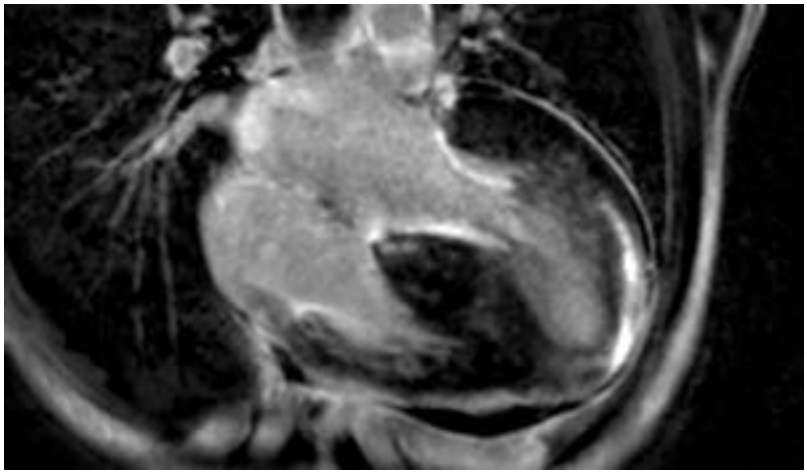

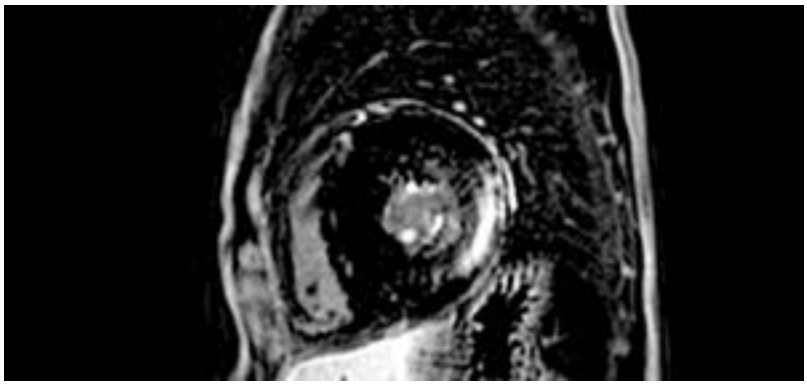

P077

A rare case of cardiac Amyloidosis presenting with new onset heart failure

Rujuta B. Katkar, MBBS[1] Andres Carmona Rubio, MD[1], James Yossef, MD[1], Umesh Sharma, MD[2]

1. University at Buffalo, Buffalo, NY
2. University at Buffalo, NY

Description of Clinical Presentation: Introduction- Amyloid cardiomyopathy is caused by infiltration of the heart by amyloidogenic proteins and there are multiple types: light-chain (AL) amyloidosis, familial ATTR amyloidosis and senile systemic amyloidosis. Cardiac amyloidosis should be considered in adults with unexplained heart failure and an echocardiogram showing increased wall thickness with a non-dilated left ventricular (LV) cavity, particularly in the absence of a history of hypertension or with a low or normal voltage on electrocardiography (EKG).

Case Report: Our case is of a 64 year-old Caucasian male with a history of coronary artery disease, ischemic stroke, hypothyroidism and laryngeal cancer treated with chemo-radiation who presented initially to an outside hospital with syncope. In the Emergency Department, an EKG revealed old Q-waves in the inferior leads, 1mm ST-elevation in I, V3 and V4 and T-wave inversions in V5-V6. His bloodwork showed an elevated troponin of 0.7. Furthermore, the patient underwent coronary angiography showing a distal right coronary artery (RCA) occlusion of 80% and a distal circumflex artery (LCx) occlusion of 60%, with the left ventriculogram estimating the ejection fraction (LVEF) at 20%. No intervention was done at that time, as the patient became unstable and urgently transferred to our tertiary center for further management. Upon arrival to the coronary care unit, the patient had an elevated jugular venous pressure and bilateral lower extremity edema, in addition to an elevated brain natriuretic peptide of 2932.

Diagnostic Techniques and Their Most Important Findings: His 2D transthoracic echocardiogram (TTE) demonstrated severe LV hypertrophy with grade-3 diastolic dysfunction, severe biatrial enlargement and moderate pericardial effusion that suggested an infiltrative cardiomyopathy. Once the patient was stable, he underwent repeat coronary angiography showing triple-vessel disease. Given the fact that ischemia was ruled out and there was a high suspicion of an infiltrative cardiomyopathy, a cardiac MRI was done that showed findings consistent with amyloidosis: diffuse thickening, global hypokinesis, LVEF of 27%. Further Right heart catheterization and right ventricle endomyocardial biopsy showed slight pulmonary hypertension and pathological diagnosis of amyloidosis, AL type. The patient was evaluated for a heart transplant in the following weeks after discharge, but unfortunately passed away while being medically optimized.

Learning Points from this Case: Conclusion- Timely diagnosis should be of vital importance in patients who present with new onset heart failure with unknown etiology with the help of advanced new non-invasive modalities such as cardiac MRI. This diagnostic tool can provide evidence strongly suggestive of infiltrative diseases, such as amyloid cardiomyopathy, particularly a distinctive pattern of global left ventricular late gadolinium enhancement rarely seen in other cardiomyopathies.

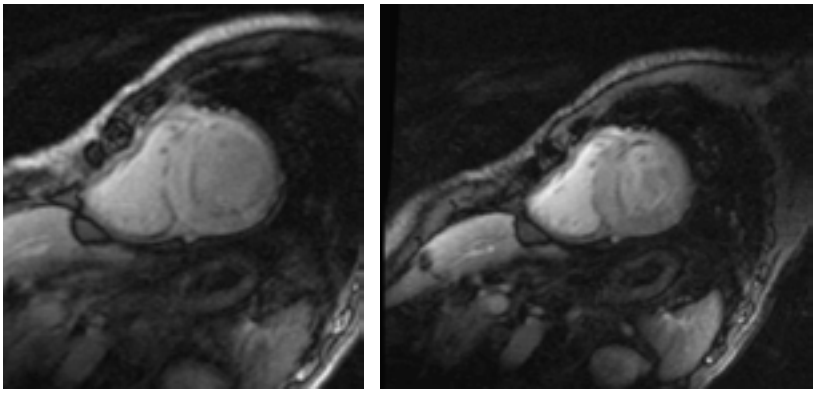

P078

Role of CMR in Cardiac Amyloidosis: How Far Have We Come?

Qurat-ul-ain Jelani, MD[1] Adam Schussheim, MD.[2]

1. Bridgeport Hospital- Yale New Haven Hospital, Bridgeport, CT
2. Bridgeport Hospital, Yale New Haven Health., Bridgeport, CT

Description of Clinical Presentation: A 60-year-old Caucasian male presents with syncope, hypotension, subsequent fall and bilateral periorbital ecchymosis. He endorsed recent onset exertional dyspnea and orthopnea, weight gain and generalised swelling. His past medical history was unremarkable. Blood pressure on presentation was 87/66. Pulmonary exam revealed dullness to percussion and decreased air entry bilaterally. Cardiac exam did not reveal any murmur or gallop.

Diagnostic Techniques and Their Most Important Findings: An electrocardiogram showed sinus rhythm with low voltage in the frontal and precordial leads. Chest xray showed bilateral pleural effusion and bilateral pulmonary vascular congestion. NT-proBNP levels were elevated at 17, 300 pg/ml (reference range: 0.0- 900.0 pg/ml). A transthoracic echocardiogram showed small left ventricular cavity, severe left ventricular hypertrophy with grade III diastolic dysfunction and biatrial enlargement. SPEP showed hypogammaglobinemia and immuonofixation revealed a monoclonal component with markedly elevated Ig lambda free light and borderline elevated Ig kappa free light chains. A cardiac MRI (1.5 T GE ESPREE) biventricular hypertrophy with an LV wall thickness of 15 mm, diffuse late gadolinium enhancement (LGE), predominantly subendocardial. There was near equilibration of the blood pool and myocardial gadolinium concentration, thus leading to similar blood pool and myocardial T1 . A bone marrow biopsy showed monoclonal lambda-restricted plasma cells constituting about 5-10 % of the total cell population. Given the lamba light chain preponderance, CMR and bone marrow biopsy findings, a diagnosis of plasma cell disorder with light chain monoclonal gammopathy with cardiac light chain (AL) amyloidosis was made was made.

Learning Points from this Case: This case highlights the role of CMR in the evaluation of possible cardiac amyloidosis- While endocardial biopsy was never performed, the clinical scenario and hematologic findings were highly suggestive. CMR showed 'classic' findings for cardiac amyloidosis including a) diffuse subendocardial LGE, not matching any specific coronary perfusion territory and b)similar T_1 values for the blood pool and myocardial suggestive of non-fibrotic extracellular expansion of the myocardium. These findings can help differentiate amyloidosis from other entities like ischemic cardiomyopathy, Sarcoidosis (patchy LGE; mostly midwall and subepicardial) and Myocarditis (LGE intra-mural/rim like pattern vs patchy epicardial distribution mostly in the lateral free wall) amongst others. When compared with the diagnostic test of choice of endomyocardial biopsy, cardiac MR imaging provides good sensitivity (80%) and high specificity (94%). Thus while not the gold standard for diagnosis of cardiac amyloidosis, CMR provides valuable diagnostic information when combined with other imaging (echo) and laboratory data. LGE has also been recently shown to provide incremental prognostic information over serum biomarkers in patients with AL cardiac amyloidosis.

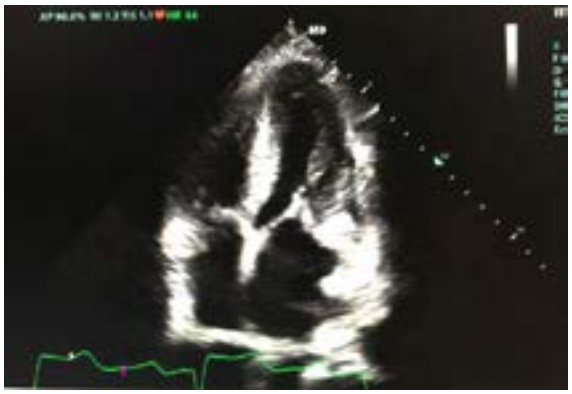

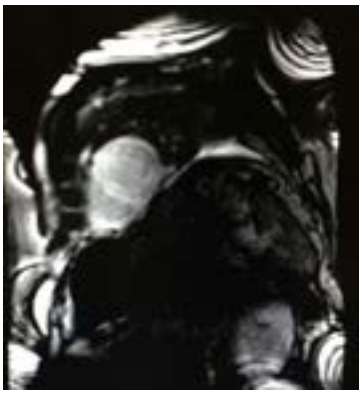

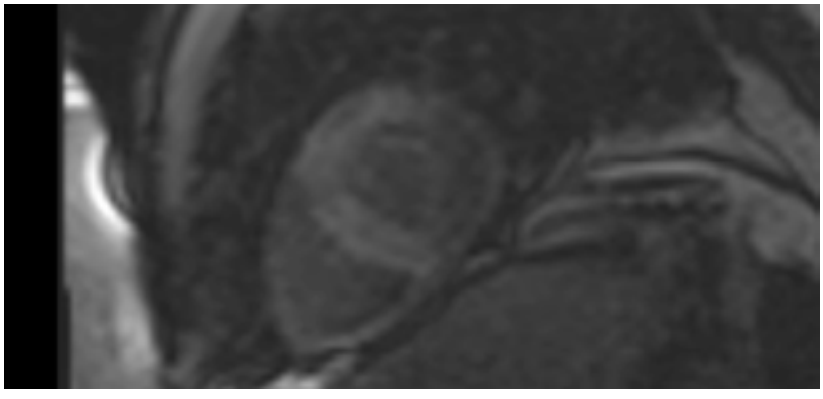

P079

Eosinophilic Granulomatosis with Polyangitis involving the Heart: Cardiac Magnetic Resonance Imaging

Rashid Saif. AL Umairi, MD, FRCR[1]Carole Dennie, MD[2], Joao Inacio, MD[2], Giselle Revah, MD[2], Girish Dwivedi, MD[3], Alexander Dick, MD[3], Elena Pena, MD[2]

1. *University of Toronto, Department of Medical Imaging, Toronto, ON, Canada*
2. *The Ottawa Hospital, ON, Canada*
3. *The Ottawa Heart Institute, ON, Canada*

Description of Clinical Presentation: A 45-year-old man with a two-year history of progressive cough and shortness of breath was admitted to hospital with hypoxic respiratory failure of unknown etiology. He had a history of severe steroid-dependent asthma, presumed allergic bronchopulmonary aspergillosis and supraventricular tachycardia (SVT).

Diagnostic Techniques and Their Most Important Findings: Initial laboratory tests revealed an elevated eosinophil count (7.3 x 109/L, normal 0.0-0.5x109/L) and negative anti-neutrophilic cytoplasmic antibodies. There was an elevated serum IgE (2,438 ug/L, normal - During admission, the patient developed an episode of SVT and the possibility of EGPA involving the heart was raised. Echocardiography was normal except for a small pericardial effusion. Subsequently, cardiac magnetic resonance (CMR) was performed. Steady state free precession CINE imaging demonstrated biventricular systolic dysfunction with associated mild global hypokinesis. On late gadolinium enhancement (LGE) images, diffuse left ventricular subendocardial and midmyocardial enhancement was noted. There was also a small pericardial effusion. In the patient's clinical scenario, the findings were most consistent with EGPA-related cardiomyopathy/myopericarditis.

Learning Points from this Case: Although the CMR findings are non-specific, in a patient with asthma, eosinophilia, lung infiltrates and arrythmia, the presence of a pericardial effusion combined with systolic dysfunction and diffuse subendocardial and midmyocardial hyperenhancement, should suggest the diagnosis of EGPA-related cardiomyopathy/myopericarditis. T2-weighted imaging together with LGE in patients with suspected cardiac-EGPA involvement may help differentiate areas of fibrosis from areas of inflammation, which may respond to immunosupressive therapy. Increased signal intensity on T2-weighted images would be compatible with inflammation. Both fibrosis and inflammation would demonstrate LGE. CMR can detect EGPA myopericardial involvement, guiding clinicians towards the use of appropriately aggressive therapy combining corticosteroids and immunosuprressive agents. CMR may be a valuable tool to monitor ventricular function and assess progression of the disease.

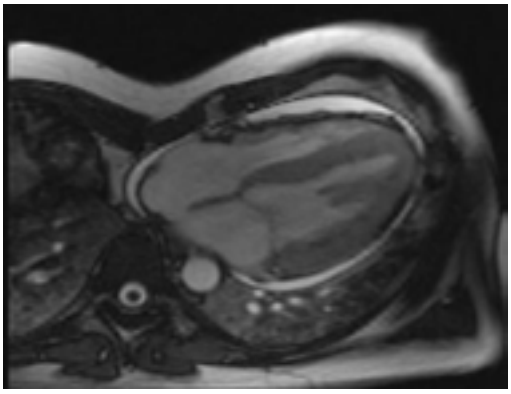
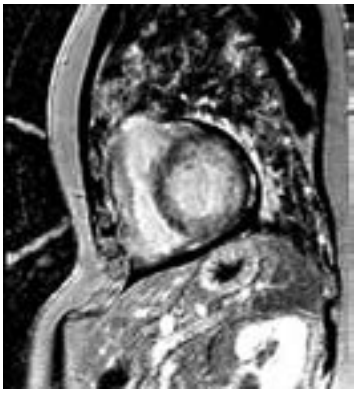
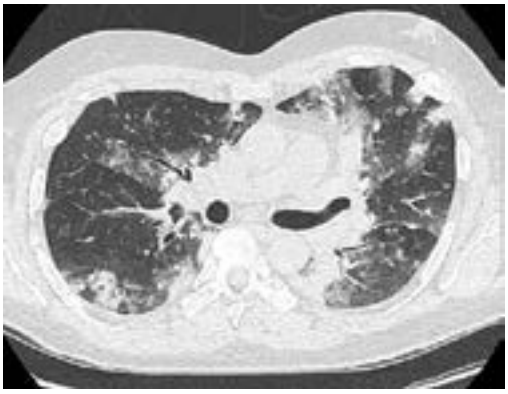

P080

Case session: MRI characterization of myocardial involvement in Duchenne muscular dystrophy (DMD)

Purvi Parwani, MBBS[1]Karen Ordovas, MD, MAS[2], Travis Henry, MD[2]

1. University of california, San Francisco, CA
2. University of California San Francisco, San Francisco, CA

Description of Clinical Presentation: 18-year-old man with biopsy-confirmed Duchenne's muscular dystrophy(DMD) secondary to an exon 2 duplication presented to the cardiologist office with chief complaint of fatigue. He was non ambulatory but denied any specific cardiac symptoms. Vitals and physical examination were within normal limits except generalized severe muscular weakness.

Diagnostic Techniques and Their Most Important Findings: An electrocardiogram showed sinus rhythm with a rate of 99 beats per minute and ST elevation suggestive of early re-polarization. The echocardiogram showed 4 valves, 4 chambers in the normal orientation and borderline right and left ventricular systolic function. Cardiac MRI was done. SSFP cine and late gadolinium enhanced(LGE) sequences were acquired in the short axis, horizontal and long axis planes. Cardiac MRI revealed regional hypokinesis of the lateral wall at the mid ventricular level with extensive area of delayed enhancement in the anterolateral and inferolateral segments with a sub-epicardial and mid wall distribution. Left ventricular and right ventricular ejection fraction was found reduced to 47%.

Learning Points from this Case: Myocardial fibrosis in DMD detected by LGE imaging may be observed even when findings by echocardiography are still normal. CMR can therefore serve as a more sensitive means to detect early cardiac involvement and help clinicians decide when cardioprotective treatment should be instituted.

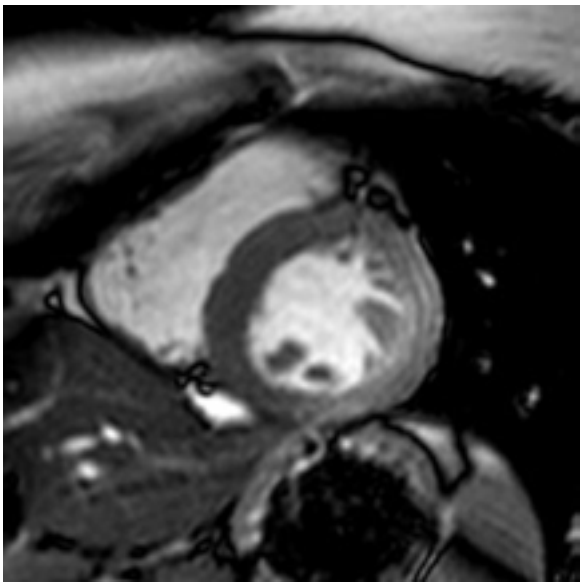

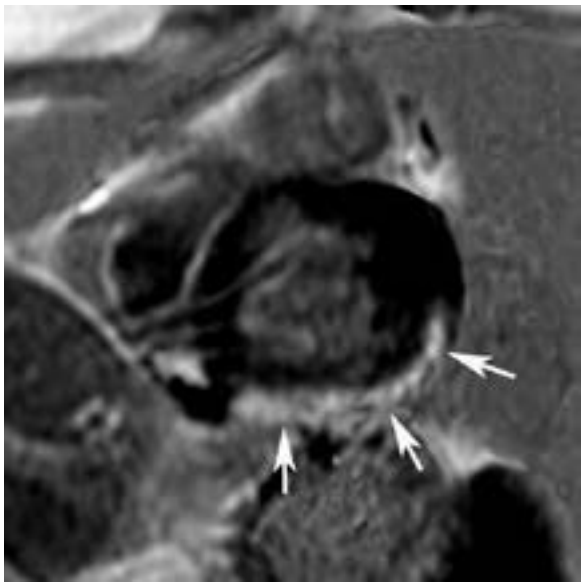

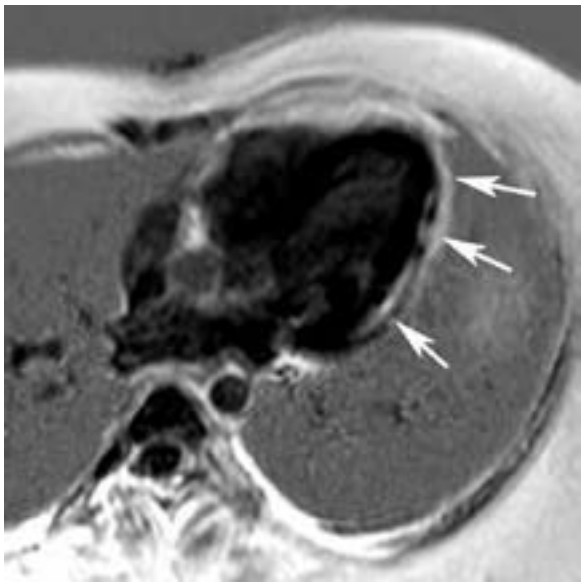

P081

Peripartum Cardiomyopathy: Comprehensive Evaluation by Cardiac MRI

Rajesh Janardhanan, MD, FACC[1] Mohit Pahuja, MD[2]

1. Banner University Medical Center, Tucson, Tucson, AZ
2. St. Joseph's Hospital and Medical Center, Phoenix, Arizona, AZ

Description of Clinical Presentation: A 22-year-old hispanic female with history of gestational diabetes mellitus, pre-eclampsia presented with shortness of breath for the prior 2 months. She had given birth to her third baby 3 months back. On admission she was short of breath and hypotensive.

Diagnostic Techniques and Their Most Important Findings: Her labs revealed coagulopathy with INR of 2.0 and pro BNP of 3000. EKG revealed sinus tachycardia with LBBB. A transthoracic echocardiogram revealed severe LV dysfunction with EF of 10-15%. No obvious LV thrombus was seen post contrast **[Figure 1].** She underwent a cardiac MRI (CMR), which revealed severe biventricular dysfunction with an LVEF of 16%. The perfusion images demonstrated a large mural thrombus **[Figure 2-Panel A]** within the left ventricle along the mid to distal anterior wall extending into the apex. Late gadolinium enhancement (LGE) images confirmed the mural LV thrombus along the anterior wall **[Figure 2-Panel B].** LGE images also revealed delayed enhancement suggesting myocardial fibrosis of the mid wall of the mid to distal anteroseptal wall with extension to the cardiac apex **[Figure 3].** CMR findings were thus consistent with peripartum cardiomyopathy associated with mural thrombus and mid-myocardial wall fibrosis. She was commenced on therapy for LV dysfunction and anticoagulation.

Learning Points from this Case: Peripartum cardiomyopathy (PPCM) is a rare cause of an idiopathic heart failure occurring in women in the last month of pregnancy or first five month after delivery. Some factors such as black race, multiparity, age >30 yrs, twin pregnancies, history of hypertension, pre-eclampsia and eclampsia are associated with high incidence of PPCM. Most of the cases occur in the first 4 months after delivery as seen in our case and less than 10% of them occur pre-partum. Some of the etiologies proposed to be associated with PPCM are stress related cytokines, myocarditis, and abnormal immune response to pregnancy. PPCM significantly increases the risk of thrombosis/thromboembolism due to a hypercoagulable state associated with pregnancy and secondary to increased stasis of blood from LV systolic dysfunction with EF.
CMR in PPCM can thus provide helpful diagnostic information regarding ventricular function and thrombi and prognostic information regarding presence and extent of fibrosis. Our patient is currently being monitored for recovery of LV function and resolution of thrombus. Our case demonstrates the value of CMR in the comprehensive evaluation of PPCM leading to accurate diagnosis and successful management.

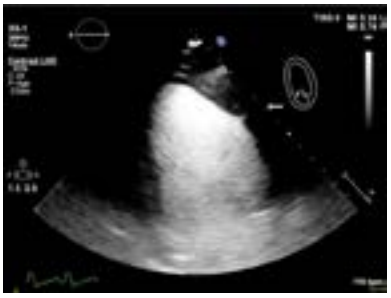

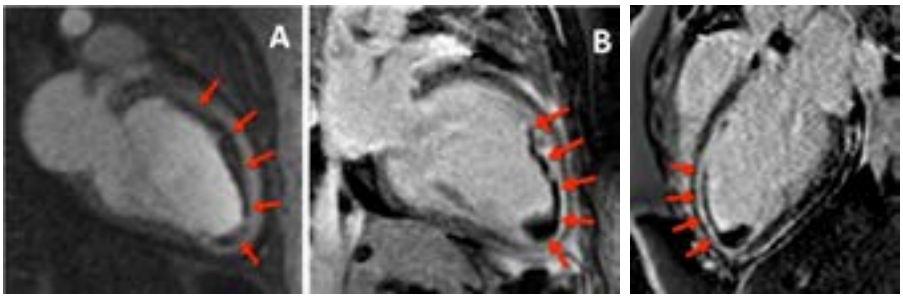

P082

Utility of Cardiac Magnetic Resonance Imaging in Diagnosing Hypertrophic Cardiomyopathy in Obese Patients

Dan F. Laney, IV, BA[1], Arun Nagabandi, MBBS[2]Jayanth H. Keshavamurthy, MD[1], Gyanendra Sharma, MD[2]

1. Medical College of Georgia at Augusta University, Augusta, GA
2. Medical College of Georgia at Augusta University, GA

Description of Clinical Presentation: A 45-year-old African American female with a medical history significant for obesity, hypertension, and OSA presented with recurrent, brief episodes of chest pain associated with shortness of breath following physical activity both at work and at home. Patient endorsed occasional lower extremity swelling and palpitations but denied any history of orthopnea, paroxysmal nocturnal dyspnea, or syncopal episodes. Patient denied any family history of sudden cardiac death or premature coronary artery disease. Echocardiogram showed LVEF of 74%, severe septal hypertrophy and mild left ventricular hypertrophy (LVH).

Diagnostic Techniques and Their Most Important Findings: Cardiac MRI showed a hyperdynamic LV with mildly increased myocardial mass index. MRI also showed mild mitral regurgitation, moderate LA enlargement, and systolic dephasing in the left ventricular outflow tract (LVOT) as well as patchy delayed myocardial enhancement in the mid-myocardium in a non-ischemic pattern involving the mid septum and anterior wall. These finding are phenotypically consistent with a diagnosis of hypertrophic cardiomyopathy.

Learning Points from this Case: Hypertrophic cardiomyopathy is a common, heritable cause of sudden cardiac death in young individuals that can be difficult to diagnose, especially in the obese, leading to grave consequences. As demonstrated by our patient, echocardiography is insufficient in screening for HCM in obese individuals because of image quality. Cardiac MRI provides superior resolution and reduced intra and inter-observer variations compared with other modalities. Post contrast delayed enhancement in a characteristic distribution is most helpful in establishing the diagnosis of HCM. This allows for more accurate assessment and subsequent diagnosis of HCM without radiation exposure making cardiac MRI the best modality for HCM in young, obese individuals with asymmetric LVH.

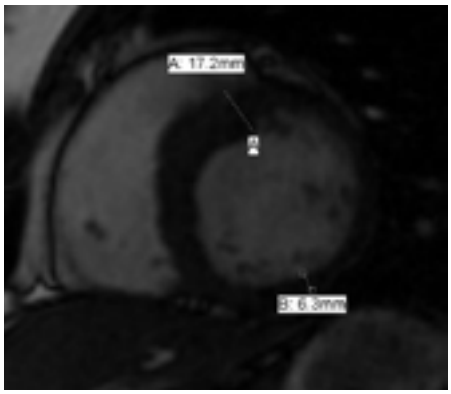

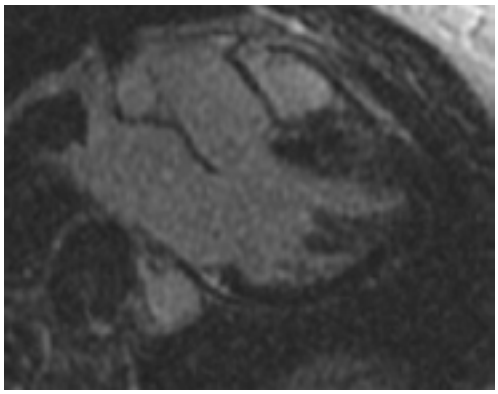

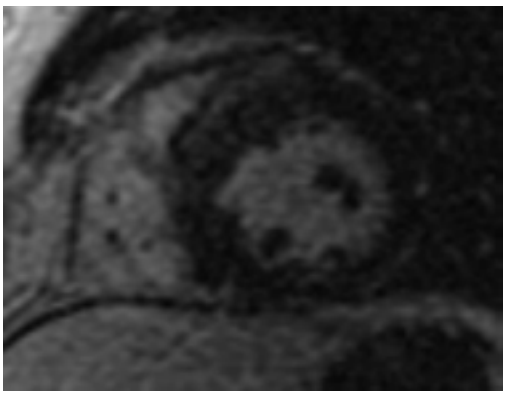

P084

Late Gadolinium Enhancement in Patients with Takotsubo Cardiomyopathy: Is that a Predictor for Ventricular Arrhythmias?

Rajesh Janardhanan, MD, FACC[1]Senthil Anand, MD[2], Kirk M. Gavlick, FACC, FSCAI[3]

1. *Banner University Medical Center, Tucson, Tucson, AZ*
2. *Banner University Medical Center, Tucson, AZ*
3. *Carondolet Heart and Vascular Institute, Tucson, AZ, AZ*

Description of Clinical Presentation: A 51-year-old female with no significant coronary risk factors presented to the emergency room with left sided chest pain radiating to the arm and shortness of breath. She had no prior history of coronary artery disease. Her initial EKG showed ST elevation in leads II, III, aVF. She developed ventricular fibrillation requiring debrillation and one round of chest compressions, before returning to normal sinus rhythm.

Diagnostic Techniques and Their Most Important Findings: She underwent emergent cardiac catheterization, which revealed angiographically normal coronary arteries and apical ballooning **[Figure 1]** consistent with classical Takotsubo cardiomyopathy. Upon further questioning, she endorsed significant recent stress related to her job loss. Her echocardiogram showed an LVEF of 55-60% with apical hypokinesis and basal segment hyperkinesis. She remained hemodynamically stable with no further arrhythmias and was discharged home. 2 months later, she had a cardiac MRI (CMR) as an outpatient. This confirmed good recovery of apical wall motion **[Figure 2]**. However, late gadolinium enhancement (LGE) sequences revealed focal, transmural delayed enhancement of the distal inferior septum and inferior apex **[Figure 3]** suggesting focal scar.

Learning Points from this Case: Takotsubo cardiomyopathy commonly presents similar to an acute coronary syndrome (ACS) with chest pain and ST elevations on EKG. While majority of patients recover, the in-hospital complication and mortality rate is similar to ACS. Malignant arrhythmias including ventricular tachycardia, torsades de pointes and ventricular fibrillation (as seen in our patient) occur in 5-8% of patients. The incidence of sudden cardiac death (SCD) has been reported at 1.1% on index episode and 0.5% in the weeks to months after. However, tools to risk stratify these patients have not been developed.

The traditional understanding has been that Takotsubo cardiomyopathy could cause myocardial edema on T2 imaging, but not residual LGE, suggestive of scar on CMR. However, a few studies have reported transmural LGE in patients with Takotsubo cardiomyopathy. Presence of LGE has also been associated with increased incidence of cardiogenic shock, increased disease severity and prolonged recovery in patients with Takotsubo cardiomyopathy. However, whether the presence of LGE in Takotsubo cardiomyopathy is associated with an increased risk of SCD is still unknown.

Our patient with a recent exposure to stress, presenting as ACS with angiographically normal coronary arteries, apical hypokinesis on admission and subsequent recovery of LV function is classical of Takotsubo cardiomyopathy. However, our patient had the very unusual presentation with ventricular fibrillation and subsequent demonstration of transmural LGE on CMR, which is exceedingly rare. This case highlights the need for risk stratification for SCD in Takotsubo cardiomyopathy patients, which merits further investigation with large studies involving CMR imaging.

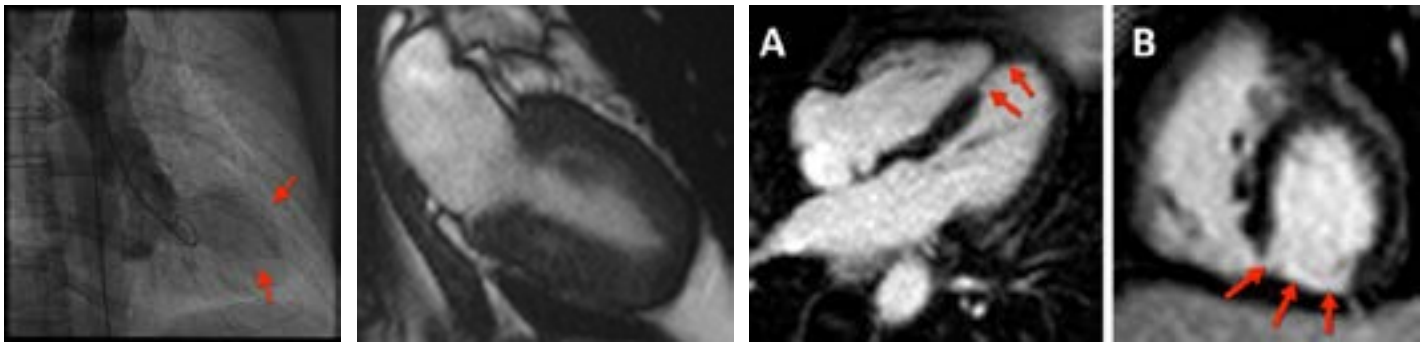

P085

Differential Diagnosis of Apical HCM Discovered with Cardiac Magnetic Resonance

Estefania De Garate, MD[1]Anna Baritussio, MD[1], Amardeep Ghosh Dastidar, MBBS(Hons), MRCP[1], Alessandra Scatteia, MD[2], Iwan Harries, MBBS, MRCP[3], Tamas Erdei, PhD[4], Giulia Pontecorboli, MD[3], Chris Lawton[5], Chiara Bucciarelli-Ducci, MD, PhD[1]

1. *NIHR Bristol Cardiovascular Biomedical Research Unit, Bristol, England, United Kingdom*
2. *Division of Cardiology, Ospedale Medico-Chirurgico Accreditato Villa dei Fiori, Acerra, Naples, Italy. Cardiac Magnetic Resonance Unit, NIHR Bristol Cardiovascular Biomedical Research Unit, Bristol Heart Institute, Bristol UK, Naples, Campania, Italy*
3. *NIHR Bristol CVBRU, England, United Kingdom*
4. *Cardiac MRI Unit, Bristol Heart Institute, Bristol, Bristol, England, United Kingdom*
5. *Bristol Heart Institute, Bristol, England, United Kingdom*

Description of Clinical Presentation: A 53 year old male, keen cyclist, was referred by a cardiologist after two echocardiograms indicating apical hypertrophic cardiomyopathy (Image 1). ECG showed only minor inferolateral ST changes (Image 2). No previous history of syncope or pre-syncope. No family history of sudden cardiac death. Patient was suggested to limit his usual rate of physical activity and cardiac magnetic resonance was indicated to confirm the diagnosis.

Diagnostic Techniques and Their Most Important Findings: CMR images were acquired with a 1.5 Tesla scanner. Protocol included HASTE localizer images, cine SSFP short axis and long axis images (2 chamber, 3 chamber and 4 chamber), and T1-weighted post contrast images. CMR found normal wall thickness in all segments, and good contractility. However, there was significant hypertrabeculation of all the apical segments, with non-compacted / compacted ratio >2.3 in the apical inferior wall (Image 3). There was also hypertrabeculation of the free wall of the right ventricle from mid-cavity to apex. Biventricular function was normal, with no evidence of regional wall motion abnormalities. There was no evidence of myocardial fibrosis on the late gadolinium enhancement images. The final diagnosis after cardiac magnetic resonance was Apical Left Ventricular Non-Compaction. Patient was followed up by the cardiology department.

Learning Points from this Case: Left ventricular non-compaction (LVNC) has been reported as a rare condition. However, recent studies describe an increase in prevalence. This growth in diagnostic rate is believed to be related to better myocardial definition with the current imaging modalities. Echocardiography is the first line tool for the diagnosis of LVNC, because it can identify the large broad trabeculae, characteristic of this condition, and Colour Doppler demonstrates the flow within the intertrabecular recesses. However, echocardiography cannot always provide good assessment of the apical segments, and sometimes the hypertrabeculation can mimic thickened myocardium. CMR is the method of choice to confirm or rule out LVNC, and in this case, it provided better definition of the apical segments, and changed the original diagnosis, which permitted the patient to continue with his usual physical activity and change his clinical management. Although LVNC is usually related to systolic dysfunction and wall motion abnormalities of the affected segments, the absence of these doesn't rule out the diagnosis Patients with normal left ventricular function usually undergo clinical monitoring, and family members are recommended echocardiographic screening.

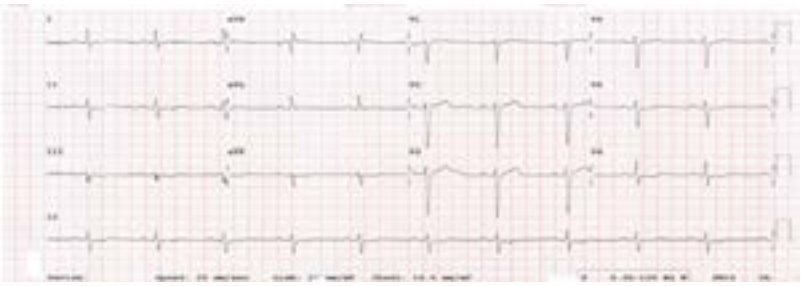

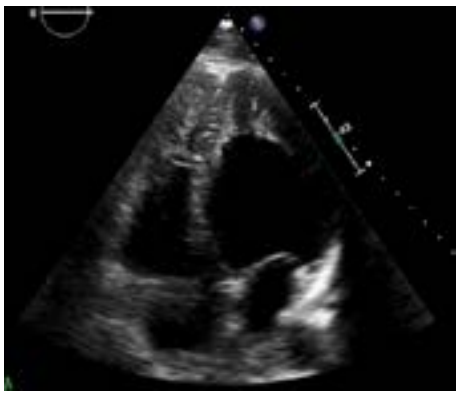

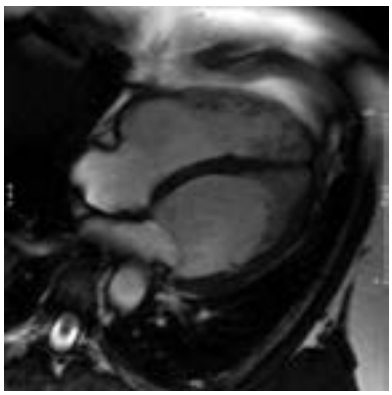

P086

A firefighter with sudden cardiac death: a case of ARVC

Mit Patel, M.D.[1]Auras R. Atreya, M.D.[2], Parthiv Mehta, M.D.[3], Tara Catanzano, M.D.[4]

1. *University of Massachusetts Medical School-Baystate, Broad Brook, CT*
2. *University of Massachusetts Medical School-Baystate, Springfield, MA*
3. *Baystate Medical Center, CT*
4. *Baystate Medical Center, MA*

Description of Clinical Presentation: A 52-year-old male with hypertension and dyslipidemia suffered a witnessed cardiac arrest while eating dinner and presented to the hospital after 25 minutes of BLS/ACLS including several defibrillations for ventricular fibrillation. Initial ECG on arrival did not show significant ST segment changes. He was taken to the critical care unit with targeted hypothermia management. After electrical stabilization with amiodarone and subsequent complete neurological recovery, he underwent several diagnostic tests as listed below.

Diagnostic Techniques and Their Most Important Findings: Cardiac Catheterization: Although initial ECG's failed to show dynamic ST changes concerning for ischemia, given his presentation, he underwent cardiac catheterization after hemodynamic stability was achieved 24 hours after initial presentation. He was noted to have angiographically normal coronary arteries without anomalies.

Echocardiogram: Normal left ventricular size and function was noted, however right ventricle was mildly dilated with mid-distal free wall hypokinesis. RVOT measurements could not be obtained due to inadequate parasternal short axis views.

For further structural evaluation and identification of pathology, a cardiac MRI was performed.

Cardiac MRI: Steady state free precession static and cine images were obtained. After gadolinium administration, delayed enhancement sequences were obtained. Mild reduction in right ventricular ejection fraction (38%), with abnormal mid wall enhancement and thinning of the right ventricular myocardium were noted. Although RV end diastolic volume to BSA ratio was < 110 ml/m^2, MRI criteria for ARVC by 2010 Task Force Criteria were met based on RV regional dyskinesia and reduced RVEF. Additionally, there was minimal delayed enhancement of the left ventricle (mid lateral and inferior wall) as well. Although no depolarization/ repolarization abnormalities were noted on 12 lead EKG, Hi Resolution Signal Average ECG was noted to be abnormal with evidence of late potentials.

Patient subsequently underwent MRI compatible single chamber ICD along with sotalol and was discharged with excellent neurologic recovery from this event.

Learning Points from this Case: Arrhythmogenic right ventricular cardiomyopathy is an under recognized clinical entity that is associated with ventricular arrhythmias due to fibro-fatty replacement of myocardium in the inflow or outflow tract, and/or apex of the right ventricle. It is a condition that should be suspected in a patient that presents with ventricular arrhythmias with subtle abnormalities on echocardiogram and with non obstructive coronary artery disease. For complete evaluation of structural abnormalities and infiltrative disorders, cardiac MRI is vital. Based on MRI findings, subsequent SAECG testing was performed and the patient was clinically diagnosed with ARVC, using the 2010 Task Force Criteria. Ultimately, secondary prevention with ICD along with antiarrhythmic therapy should be strongly considered along with genetic testing of family members.

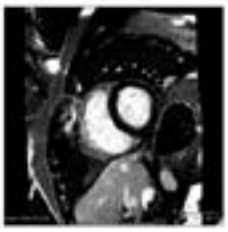

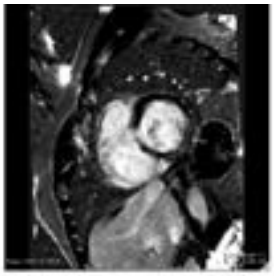

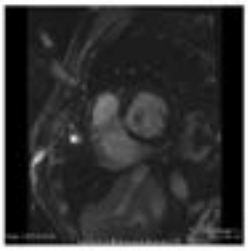

P087

CMR T2* analysis of myocardial iron deposition and mortality in liver transplant candidates

Kimberly Kallianos, MD[1]Ana Paula Santos Lima, MD[2], Gabriel Brooks, MD, MAS[1], Neil Mehta, MD[1], Atif Qasim, MD[1], Kanae Mukai, MD[3], Michael D. Hope, M.D.[1], Elyse Foster, MD[1], Teresa De Marco, MD, FACC[4], Karen Ordovas, MD, MAS[5]

1. *University of California, San Francisco, CA*
2. *UCSF, Mill Valley, CA*
3. *UCSF, Palo Alto, CA*
4. *Universtiy of California, San Francisco, CA*
5. *University of California San Francisco, San Francisco, CA*

Background: Despite the use of T2* CMR (cardiac magnetic resonance) technique to identify patients at risk of death and cardiac complications after orthotopic liver transplant (OLT), there is still limited data on the outcome of patients with various levels of myocardial iron deposition who are candidates for transplantation. We aimed to investigate the relationship between CMR T2* analysis of myocardial iron deposition and mortality in patients considered for liver transplantation, specifically in patients with abnormal T2* values (milliseconds, ms) who remained candidates for transplantation at our institution (T2*≥10ms but < 20ms) compared to those with normal T2* values (≥20ms)

Methods: We evaluated 178 patients (age 55.7±23.9 years, 73.0% male) who underwent CMR for T2* analysis as part of work up for potential OLT from 2008 – 2016. T2* values were obtained from the ventricular septum on short axis gradient echo CMR images. In patients where multiple T2* measurements were performed, the mean T2* value was used. Outcome data was obtained from medical records including date of OLT, date of death, and date of last follow-up visit. Follow-up-time was calculated as time between CMR and death or last follow-up visit. Statistical significance was set at $p < 0.05$.

Results: Mortality was 42/178 (23.6%) over a mean 2.2±2.1 years of follow-up, while 10/178 (5.6%) patients were lost to follow-up. Average T2* value was 27.3± 8.8ms. Of the 178 patients, T2* was < 10ms in 6 patients, ≥10ms but < 20ms in 31 patients, and ≥20ms in 141 patients. There was no significant difference in frequency of OLT between transplant candidates with abnormal and normal T2* values, 15/31 (48.4%) transplant rate in those with abnormal T2* (≥10ms but < 20ms) and 71/141 (50.4%) transplant rate in those with normal T2* (≥20ms), $p = 0.843$. Age and gender were also not significantly different between the groups. Mortality rate for transplant candidates with abnormal T2* values was 10/31 (32.3%) while morality rate was 29/141 (20.4%) in those with normal T2* values, p=0.130. Kaplan-Meier survival estimates were performed (Figure 1), and log-rank test for equality of survivor functions demonstrated a significant difference between these two groups $p = 0.0489$.

Conclusions: There is a significant difference in Kaplan-Meier survival curves between patients with abnormal (≥10ms but < 20ms) versus normal (≥20ms) T2* values who are candidates for liver transplantation at our institution, with increased early mortality in patients with abnormal T2* values. Knowledge of these results may be useful in determining prognosis of candidates for liver transplantation and may help to further establish the utility of CMR in the assessment of liver transplant candidates.

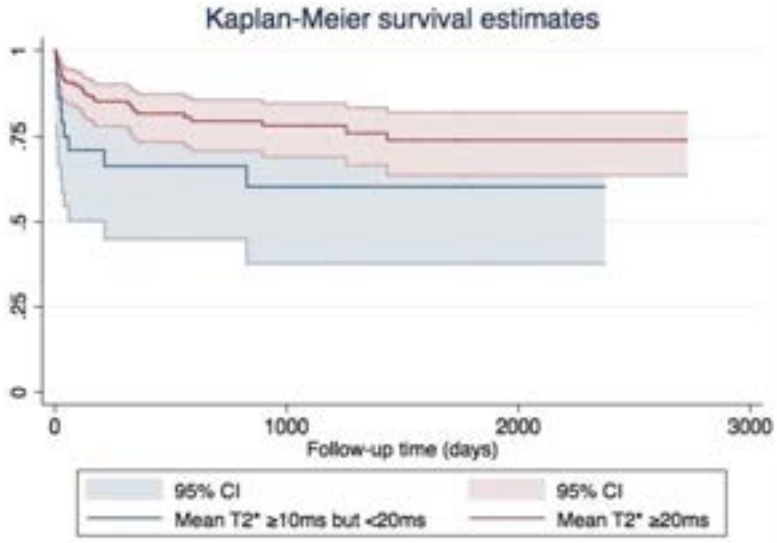

P088

Association between male sex and CMR abnormalities and cardiac complications in thalassemia major patients

Antonella Meloni, PhD[1]Silvia Maffei, MD[2], Laura Pistoia, MSc[2], Nicolò Schicchi, MD[3], Chiara Tudisca, MD[4], Massimiliano Missere, MD[5], Maurizio Mangione, MSc[2], Silvia Macchi, MD[6], Sabrina Armari, MD[7], Petra Keilberg, RT[2], Vincenzo Positano, MSc[2], Alessia Pepe, MD, PhD[2]

1. *Fondazione G. Monasterio CNR Regione Toscana, Pisa, Toscana, Italy*
2. *Fondazione G. Monasterio CNR Regione Toscana, Toscana, Italy*
3. *Azienda Ospedaliero-Universitaria Ospedali Riuniti, Marche, Italy*
4. *Policlinico "Paolo Giaccone", Sicilia, Italy*
5. *Fondazione di Ricerca e Cura "Giovanni Paolo II", Molise, Italy*
6. *Ospedale "Santa Maria delle Croci", Emilia-Romagna, Italy*
7. *Azienda Ospedaliera "Mater Salutis", Veneto, Italy*

Background: We aimed to prospectively assess if the male gender was associated with an higher risk of progressive cardiac iron accumulation, development of biventricular dysfunction and myocardial fibrosis assessed by CMR, and development of cardiac complications including heart failure (HF), arrhythmias and pulmonary hypertension (PH).

Methods: We considered 1711 TM patients (899 females, 31.09±9.08 years), consecutively enrolled in the Myocardial Iron Overload in Thalassemia (MIOT) Network. Myocardial iron overload was assessed by the multislice multiecho T2* technique. Biventricular function was quantified by cine images. Late gadolinium enhancement (LGE) images were acquired to detect myocardial fibrosis.

Results: Although having a similar risk of accumulating iron, males showed a significant higher risk of developing cardiac dysfunction, heart failure, arrhythmias and cardiac complications globally considered (Table 1). Figure 1 shows the Kaplan-Meier curves for the outcomes for which the male sex was a significant prognosticator. Until 20-30 years of follow-up the two lines (male and female sex) were almost overlapping while after they clearly diverged. So, patients were divided in two groups based on the follow-up duration. A significant gender-specific difference in the frequency of ventricular dysfunction and cardiac complications appeared for patients followed for at least 20 years. So, two subgroups of patients were identified: patients followed for less than 20 years and patients followed for more than 20 years. In the first subgroup males and females had a comparable risk of developing cardiac iron overload, ventricular dysfunction and cardiac complications. Conversely, if a follow-up longer than 20 years was considered, males exhibited a significant higher risk of having ventricular dysfunction, heart failure, arrhythmias, and cardiac complications.

Conclusions: Females seem to tolerate iron toxicity better, possibly as an effect of reduced sensitivity to chronic oxidative stress. According to the International Guidelines, TM patients should perform a complete cardiac evaluation every year. Our study suggested that in females older than 20 years the follow-up may be performed every 24 months, thus reducing health care costs.

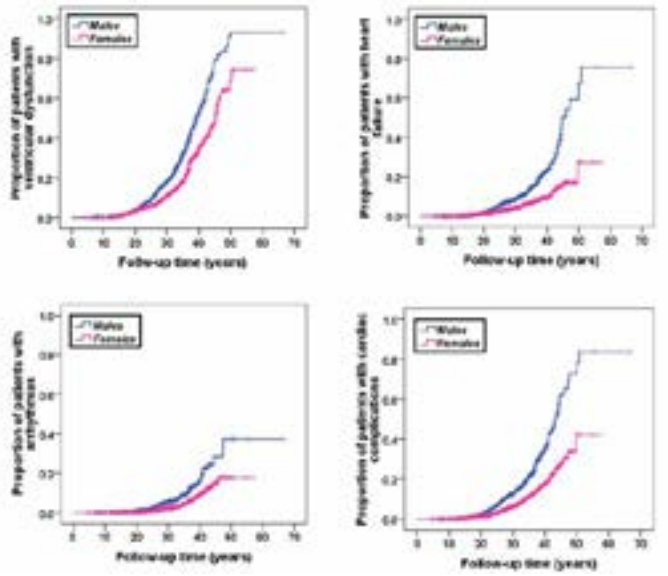

Cox Regression		N(%) with positive outcome	
P	HR (95%CI)		
0.470	Reference 0.93 (0.77-1.27)	253 (28.5) 191 (23.2)	Global heart T2* Female sex Male sex
<0.0001	Reference 1.84 (1.52-2.23)	179/771 (23.2) 262/721 (36.3)	Ventricular dysfunction: Female sex Male sex
0.247	Reference 1.17 (0.89-1.53)	113/611 (18.5) 106/585 (18.1)	Myocardial fibrosis: Female sex Male sex
<0.0001	Reference 2.57 (1.86-3.55)	56 (6.3) 109 (13.3)	Heart failure: Female sex Male sex
<0.0001	Reference 2.17 (1.46-3.23)	40 (4.5) 64 (7.8)	Arrhythmias: Female sex Male sex
0.446	Reference 1.51 (0.52-4.35)	7 (0.8) 7 (0.9)	Pulmonary Hyperthension: Female sex Male sex
<0.0001	Reference 2.31 (1.79-2.97)	96 (10.8) 166 (20.2)	Cardiac complications: Female sex Male sex

P089

The prognostic role of hypertrabeculation by cardiac magnetic resonance in thalassemia intermedia patients

Antonella Meloni, PhD[1]Francesca Macaione, MD[2], Pietro Giuliano, MD[3], Laura Pistoia, MSc[4], Andrea Barison, MD, PhD[4], Stefania Renne, MD[5], Riccardo Righi, MD[6], Vincenzo Positano, MSc[4], Angelo Peluso, MD[7], Mauro Caini, MD[8], Pasquale Assennato, MD[2], Alessia Pepe, MD, PhD[4]

1. *Fondazione G. Monasterio CNR Regione Toscana, Pisa, Toscana, Italy*
2. *Università degli Studi di Palermo, Policlinico "Paolo Giaccone", Sicilia, Italy*
3. *"ARNAS" Civico, Di Cristina Benfratelli, Sicilia, Italy*
4. *Fondazione G. Monasterio CNR Regione Toscana, Toscana, Italy*
5. *Presidio Ospedaliero "Giovanni Paolo II", Lamezia Terme, Calabria, Italy*
6. *Ospedale del Delta, Emilia-Romagna, Italy*
7. *Ospedale "SS. Annunziata" ASL Taranto, Puglia, Italy*
8. *Azienda Ospedaliero-Universitaria Senese Policlinico "S. Maria alle Scotte", Toscana, Italy*

Background: Differentiation of left ventricle non-compaction (LVNC) from hypertrabeculated LV due to a negative heart remodeling in thalassemia intermedia (TI) can depends on the selected CMR criterion. The recently proposed Piga's criterion (NC/C ratio threshold of >2.5, *Am J Haem 2012*) seems to have a low specificity to identify the true LVNC in TI. Anyway, the Piga's criterion could well detect easy a negative heart remodeling in TI patients.
Our aim was toassess prospectively whether the Piga's criterion has a prognostic role for adverse cardiovascular outcomes in TI patients.

Methods: We studied prospectively by CMR 168 TI patients (81 males, mean age 38.32 ±11.61 years) consecutively enrolled in the Myocardial Iron Overload in Thalassemia (MIOT) Network. Eight patients were excluded because a cardiac complication was present at the first CMR.
Using Piga's criterion the study population was divided into two groups: patients with Piga's positive criterion (n=18, 11.2%) and with Piga's negative criterion (n=143, 88.8%).

Results: Mean follow-up time was 57.50 ± 21.87 months. Sixteen cardiac new events were recorded: 1 heart failure (HF), 10 supraventricular arrhythmias and 5 pulmonary hypertension (PH).

The patients with Piga's positive criterion had a significant higher risk of developing arrhythmias (hazard ratio-HR= 5.35 ; 95%CI=1.51-18.98; P=0.009). The figure shows the Kaplan-Meier survival curve.

The positivity for the Piga's criterion was not predictive for PH or for cardiac complications globally considered.

Conclusions: Based on our data a NC/C ratio >2.5 provides prognostic information for patients with TI.

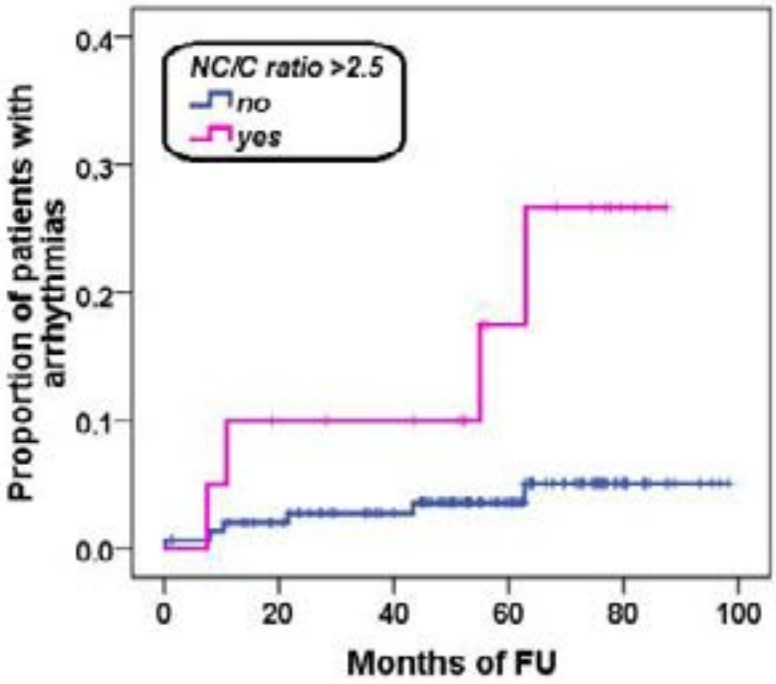

P090

Cardiac mechanics derived from three-dimensional feature tracking independently correlate with changes in ventricular size and function over time in patients with repaired tetralogy of Fallot

Linyuan Jing, PhD[1]Jonathan D. Suever, PhD[2], Richard J. Charnigo, PhD[3], Anne M. Valente, MD[4], Tal Geva, M.D.[5], Andrew J. Powell, M.D.[5], Brandon K. Fornwalt, MD, PhD[6]

1. *Geisinger Health System, State College, PA*
2. *Geisinger Health System, Bellefonte, PA*
3. *University of Kentucky, KY*
4. *Boston Children's Hospital; Brigham and Women's Hospital, Boston, MA*
5. *Harvard Medical School and Boston Children's Hospital, Boston, MA*
6. *Geisinger Health System, PA*

Background: Patients with repaired tetralogy of Fallot (rTOF) suffer from progressive ventricular dysfunction decades after their initial surgical repair. A recent study showed that cardiac mechanics (dyssynchrony and strain) derived from cine SSFP using two-dimensional (2D) feature tracking failed to predict changes in ventricular function in these patients. We developed a new method to perform feature tracking in three-dimensional (3D) space, which may be superior to 2D methods that ignore the effects of through-plane motion. We aimed to determine whether cardiac dyssynchrony and strain derived from 3D tracking could predict deterioration of ventricular function in patients with rTOF.

Methods: To perform 3D tracking, an endocardial surface for each ventricle was reconstructed from segmented 2D SSFP images (short-axis stack, 4-chamber and 2-chamber). 3D displacements were computed based on the 2D displacement fields derived from 2D feature tracking of the segmented 2D SSFP images. The 3D displacements were used to deform the endocardial surface through the cardiac cycle. Patients with rTOF who underwent cardiac magnetic resonance (CMR) at least twice, >6 months apart, were retrospectively identified from a single institution. Seven primary predictors were derived from the first CMR: left (LV), right (RV) and inter-ventricular dyssynchrony index (DI), and LV and RV circumferential (Ecc) and longitudinal (Ell) strains. Three outcomes were considered in assessing progressive development of ventricular dysfunction over time: indexed RV end-diastolic volume (RVEDVi), RV ejection fraction (RVEF), and LVEF. A multivariate model was fit which expressed mean levels of the outcomes as linear functions of time, with intercepts and slopes of these linear functions depending on various baseline predictors (see table and notes). Each baseline predictor's per-unit contribution to a slope is approximately related to that predictor's association with progression over time in the corresponding outcome; these contributions are then normalized to have magnitudes like correlations (labeled as β).

Results: 142 patients with rTOF (23±14 years, 51% male) were included, with an average follow-up duration of 2.9±1.3 years. Multivariate analysis revealed that, after adjusting for baseline confounders, LV DI (β=-0.05), RV Ecc (β=0.07) and RV Ell (β=0.05) were independently correlated with change in RVEF (ΔRVEF) over time, LV DI (β=-0.05) was correlated with ΔLVEF, and RV Ell was correlated with ΔRVEDVi (β=-0.04, Table). However, only 3–18% of the variability in the change over time in the outcome variables was explained by the multivariate model.

Conclusions: In patients with repaired TOF, LV dyssynchrony and RV strains derived from three-dimensional feature tracking performed on two-dimensional cine SSFP images independently correlate with changes in ventricular size and function over time.

Table: Summary of multivariate analysis.

ΔLVEF		ΔRVEF		ΔRVEDVi		Baseline Predictors
p	β	p	β	p	β	
0.02	-0.05	0.008	-0.05	0.82	-0.003	LV dyssynchrony
0.16	0.04	<0.001	0.07	0.32	0.02	RV circumferential strain
0.17	-0.04	0.03	0.05	0.01	-0.04	RV longitudinal strain
<0.001	-0.17	<0.001	-0.06	0.44	0.01	LV ejection fraction
0.25	0.03	<0.001	-0.16	0.37	0.01	RV ejection fraction

Note: all 7 primary predictors as well as 10 baseline confounders (indexed RV end-systolic volume, indexed RV end-diastolic volume, LV ejection fraction, RV ejection fraction, heart rate, gender, pulmonary regurgitant fraction, QRS duration, type of initial repair, age at initial repair) were entered in the multivariate model, but only 5 variables remained in the model after backward elimination.

P091

Cardiac Magnetic Resonance Imaging Characteristics and Clinical Outcomes in Adults with Repaired Truncus Arteriosus

Leena Robinson. Vimala, DMRD, MD(Radiology)[1]Kate Hanneman, MD[2], Ghadeera Almansoori, MD, FRCPC[1], Paaladinesh Thavendiranathan, MD, MS[3], Elsie T. Nguyen, MD, FRCPC[4], Candice Silversides, MD[5], Rachel Wald, MD[6]

1. *Toronto General Hospital, Toronto, ON, Canada*
2. *Department of Medical Imaging, University of Toronto, ON, Canada*
3. *Toronto General Hospital and University of Toronto, Toronto, ON, Canada*
4. *Department of Medical Imaging, University of Toronto, Toronto, ON, Canada*
5. *Toronto General Hospital, ON, Canada*
6. *Division of Cardiology, University of Toronto, ON, Canada*

Background: Truncus arteriosus (TA) is an uncommon form of cyanotic congenital heart disease. Cardiac magnetic resonance (CMR) is the imaging modality of choice for adults with complex congenital heart disease, however CMR findings post TA repair have not been well-defined. We sought to characterize CMR findings and clinical outcomes in adults with repaired TA.

Methods: Adults with a diagnosis of TA and a completed CMR were identified from an existing database. All available clinical data were reviewed. Subtypes of TA (1-4) were assigned according to the Collet and Edwards classification. A single observer completed CMR measurements of biventricular volumes/mass/ejection fraction, biatrial dimensions, semilunar valve dimensions, and aortic/pulmonary arterial dimensions and flows. Adverse clinical outcomes were recorded at last clinical follow-up (death, transplant, heart failure, arrhythmia requiring medical/device therapy, infective endocarditis and/or cardiac intervention). Total number of cardiac interventions (catheter/surgical) were recorded.

Results: A total of 26 patients were included (January 2010-June 2016). Demographics are shown in table 1 and CMR characteristics are demonstrated in table 2. At a median follow-up of 4 years between CMR and last clinical review (range 0.1-10), adverse outcomes included heart failure n=9 (35%), arrhythmia n=8 (31%) and infective endocarditis n=3 (12%). Maximum neo-aortic root dimension was found to be significantly different between the TA groups (p=0.0215, ANOVA); post hoc analysis demonstrated significantly lower neo-aortic root diameter in type 3 compared to type 1 (32.0±8.5 mm vs. 40.5±3.1 mm, p=0.023) and compared to type 2 (40.8±4.2 mm, p=0.025). Peak systolic velocity was significantly different among the TA subtypes (p=0.0354, ANOVA); post hoc analysis demonstrated significantly higher peak systolic velocity in main pulmonary artery in type 3 compared to type 2 (317.5±26.2 vs. 175.8±37.1 cm/sec, p=0.035). Median number of cardiac interventions for the entire population was 5 (range 1-13) and was not significantly different amongst the TA subtypes. Total number of cardiac interventions per patient correlated with left ventricular end diastolic volume (LVEDV) (r=0.65, $p < 0.001$) and a significant association between indexed LVEDV and heart failure was evident by logistic regression (OR 1.06, 95%CI [1.01, 1.12], p=0.025).

Conclusions: In this TA cohort, maximum neo-aortic root dimensions and peak pulmonary artery flow velocities on CMR were found to be significantly different between TA subtypes. LVEDV was associated with number of cardiac interventions and was the only CMR predictor of adverse clinical events, specifically heart failure. These preliminary findings require further validation in a larger TA population.

Demographics of patient cohort

Frequencies (%) or Median (range)	Characteristics
n=6 (23%)	Gender (male)
7 (1-72)	Age at surgical repair (months)
n=15 (58%) n=9 (35%) n=2 (7%) n=0 (0%)	Truncus arteriosus classification (Collet and Edwards) Type 1 Type 2 Type 3 Type 4
n=17 (66%) n=5 (19%) n=4 (15%	Aortic valve morphology Native valve Prosthetic valve Biologic Metallic
24 (18-40)	Age at first cardiac MRI at our institution (years)
4 (0.1-10)	Interval between cardiac MRI and last clinical follow-up

Characteristics of cardiac MR parameters

P value (*ANOVA comparison between types 1,2,3)	Type 3* (n=2) Mean ± SD	Type 2* (n=9) Mean ± SD	Type 1* (n=15) Mean ± SD	Entire Cohort (n=26) Median (Range)	Cardiac MRI Measurements
NS	174 ± 49	165 ± 43	177 ±58	161 (102-350)	LVEDV (mL)
NS	80 ±30	95 ± 25	96 ± 24	94 (58-158)	LVEDV indexed (mL/m2)
NS	61 ± 0	53 ± 7	55 ± 7	56 (42-64)	LVEF (%)
NS	202 ± 39	161 ± 40	180 ± 72	160 (118-413)	RVEDV (mL)
NS	109 ± 4	88 ± 19	99 ± 35	89 (61-201)	RVEDV indexed (mL/m2)
NS	46 ± 3	52±6	53± 12	52 (33-72)	RVEF (%)
NS	55 ± 18	47 ± 9	46 ± 10	45 (33-68)	RV mass (g)
NS	29 ± 6	26 ± 5	25 ± 5	25 (20-33)	RV mass (g/m2)
NS	22 ± 1	21 ± 4	23 ± 8	21(8-39)	Area of right atrium (cm2)
NS	8 ± 1	17 ± 6	17 ± 5	16 (7-29)	Area of left atrium (cm2)
0.021	32 ± 8	41 ± 4	41 ± 3	39 (26-50)	Maximum neo-aortic root diameter(mm)
NS	28 ± 3	32 ± 5	34 ± 3	35 (24-38)	Maximum ascending aorta diameter(mm)
NS	24 ± 1	24 ± 5	25 ± 4	25 (17-31)	Maximum aortic arch diameter(mm)
NS	21 ± 1	19 ± 3	21 ± 4	26 (17-29)	Maximum descending aorta diameter (mm)
NS	22 ± 1	18 ± 5	19 ± 6	20 (10-32)	Narrowest main pulmonary artery (MPA) dimension (mm)
NS	14 ± 1	13 ± 4	12 ± 4	12 (7-20)	Narrowest right pulmonary artery (RPA) dimension (mm))
NS	16 ± 1	14 ± 4	14 ± 5	14 (7-26)	Narrowest left pulmonary artery (LPA) dimension (mm)
NS	Not available	118 ± 27	131 ± 62	112 (88-2013)	Aorta peak systolic velocity (cm/s)
NS	Not available	78 ± 32	67 ± 8	72 (42-100)	Aorta forward flow (mL/beat)
NS	Not available	26 ± 20	18 ± 12	21 (0-40)	Aorta regurgitant fraction (%)
0.035	318 ± 26	176 ± 37	207± 68	190 (104-342)	MPA peak systolic velocity (cm/s)
NS	40 ± 7	9 ± 3	23 ± 63	15 (7-47)	MPA pressure gradient (mmHg)
NS	71 ± 13	67 ± 41	76 ± 21	67 (40-129)	MPA forward flow (mL/beat)
NS	5 ± 3	10 ± 15	15 ± 18	7 (0-50)	MPA regurgitant fraction (%)
NS	134 ± 33	148 ± 104	124 ± 63	115 (43-300)	RPA peak systolic velocity (cm/s)
NS	27 ± 7	32 ± 11	27 ± 12	29 (14-51)	RPA forward flow (mL/beat)
NS	0 ± 0	9 ± 17	13± 21	0 (0-48)	RPA regurgitant fraction (%)
0.071	179 ± 91	133 ± 13	180 ± 82	160 (114-312)	LPA peak systolic velocity (cm/s)
NS	38 ± 26	26 ± 10	46 ± 19	35 (19-91)	LPA forward flow (mL/beat)
NS	18 ± 5	12 ± 22	24 ± 17	18 (0-50)	LPA regurgitant fraction (%)
NS	56 ± 6	54 ± 17	42 ± 10	50 (18-60)	Differential flow right lung (%)
NS	44 ± 6	46 ± 17	58 ± 10	51 (40-82)	Differential flow left lung (%)

NS- not significant

P092

Myocardial T2 Mapping in Women with Early Stage Breast Cancer Receiving Anthracyclines

Mark T. Nolan, MBBS[1]Mustafa A. Altaha, MBBS[1], Eitan Amir, MD, PhD[2], Bernd J. Wintersperger, MD[3], Paaladinesh Thavendiranathan, MD, [4]

1. *University of Toronto, Toronto, ON, Canada*
2. *Princess Margaret Cancer Centre, ON, Canada*
3. *Department of Medical Imaging, University of Toronto, Toronto, ON, Canada*
4. *University of Toronto, ON, Canada*

Background: Anthracycline chemotherapy is associated with a risk of heart failure (HF). Animal studies have demonstrated that myocardial edema is an early marker of myocardial injury post anthracyclines. Therefore non-invasive identification of myocardial edema may provide an opportunity to institute cardio-protective strategies to prevent HF. Myocardial T2 mapping is a non-invasive method of identifying myocardial edema. The aim of our study was to examine whether quantitative T2 changes can be identified in women with breast cancer immediately post anthracycline therapy.

Methods: Thirty-four women (mean age 49.5 ± 10.1 years) with stage I-III human epidermal growth factor receptor positive (HER2+) breast cancer treated with 3 cycles of anthracycline prior to trastuzumab were prospectively recruited. Cardiac MR studies were performed pre and immediately post anthracycline therapy using a 1.5T Siemens (Avanto Fit) scanner. Short axis balanced steady state free precession (SSFP) cine images (8mm slice thickness with 2mm gap) covering the entire ventricle were obtained for LV function analysis. T2 maps were acquired in the basal, mid and apical SAX planes using T2-prepared single-shot SSFP sequence with breath hold. LV function analysis was performed as per SCMR recommendations, and T2 values were obtained for each of the 16 myocardial segments using a commercially available software (CMR42). Mean values were compared using a paired t-test, and correlations were determined using the Pearson correlation coefficient.

Results: Mean global LV T2 values (average of all 16 segments) increased by 2.4% (53.6 ± 2.2 msec to 54.9 ±2.3 msec, p=0.006) post anthracycline treatment. Nine patients (26.5%) had a >5% increase in the global T2 value. The most affected segments were the basal anteroseptum (+2.9msec) and mid-anteroseptum (+2.1 msec), with inferolateral segments being least affected. Mid and apical myocardial segments had larger T2 increases (respectively +1.5 msec and 1.3 msec) than basal segments (+1.1 msec). None of the patients developed cardiotoxicity based on established LVEF criteria. No significant correlation was seen between ΔT2 values and LVEF (r=-0.06, p=0.73), ΔLV end-diastolic volume (r=0.226, p=0.21) or ΔLV end-systolic volume (r=0.20, p=0.26).

Conclusions: A small but statistical significant increase in myocardial T2 value, potentially representing myocardial edema, was seen after exposure to anthracycline chemotherapy in women with HER2+ breast cancer. There appears to be regional differences in the increased T2 values .The change in T2 values was not associated with a change in LVEF suggesting that it may be an independent early marker of myocardial injury.

P093

Novel left ventricular segmentation for identifying myocardial histological changes by Cardiac Magnetic Resonance(CMR) in Pulmonary Hypertension

Geeshath Jayasekera, MBChB MRCP[1]Colin Church, MBChB PhD[1], Colin Berry, PhD FRCP[2], Aleksandra Radjenovic, MSc PhD[3], Andrew Peacock, MD[1]

1. *Scottish Pulmonary Vascular Unit, Glasgow, Scotland, United Kingdom*
2. *University of Glasgow, Glasgow, Scotland, United Kingdom*
3. *University of Glasgow, UK, Glasgow, Scotland, United Kingdom*

Background: Pulmonary hypertension, PH(mean pulmonary artery pressure>25mmHg) leads to right ventricular (RV) failure and death. CMR derived right and left ventricular(LV) functional variables have shown to be prognostic in PH. Late gadolinium enhancement which occurs at the RV insertion points is due to local fibrosis as a consequence of mechanical stress. Native T1 mapping is a technique of tissue characterisation without the need for contrast administration. Although identification of raised native T1 values has been used to identify myocardial histological changes this has been limited to visual assessment of the insertion points. The existing AHA segmentation of the LV fails to isolate RV insertion regions for analysis. We propose a new method of LV segmentation to aid in identifying changes in these regions in PH.

Methods: Seventy eight patients (age 61.3, ♀41, mPAP 40.7mmHg) suspected of PH underwent CMR and right heart catheterisation. T1 maps were acquired on a Siemens Avanto 1.5T scanner using a MOLLI sequence on a mid-ventricular short axis plane with a trigger delay to coincide with systole. The LV was segmented using a modified AHA segmentation carefully excluding blood pool, papillary muscles and trabeculae. S6 was drawn with the RV insertion point at its centre. S4 and S6 were defined as RV insertion regions. Global LV myocardial T1 times were calculated as means of segmental values. All measured myocardial T1 values were normalized to the mean blood T1 time of the study population assuming a common linear increase of T1 with T1 of blood (Coefficient k=0.257).

Results: Thirteen subjects did not have PH on cardiac catheterisation. Global myocardial T1 values (994.8 ± 38.84 vs 967.4 ± 28.74ms, $p < 0.05$) and insertion region T1 values(1018 ± 50.01 vs 968.8 ± 27.57ms, $p=0.001$) were higher in PH compared to patients without PH. Insertion region T1 values of patients with mpap>35mmHg were higher than in the 25-35 mmHg group($p < 0.001$). The S4 and S6 regional T1 values correlated with mPAP($P < 0.0001$) and pulmonary vascular resistance($P < 0.0001$) and to a lesser extent with cardiac index($p < 0.05$).

Conclusions: RV insertion regions are better characterised by a modified AHA model in PH. Insertion region T1 times are elevated in PH and are associated with pressure and resistance and to a lesser extent with markers of disease severity. The changes in the insertion regions may represent compensatory mechanisms of cardiac remodelling than changes associated with RV failure.

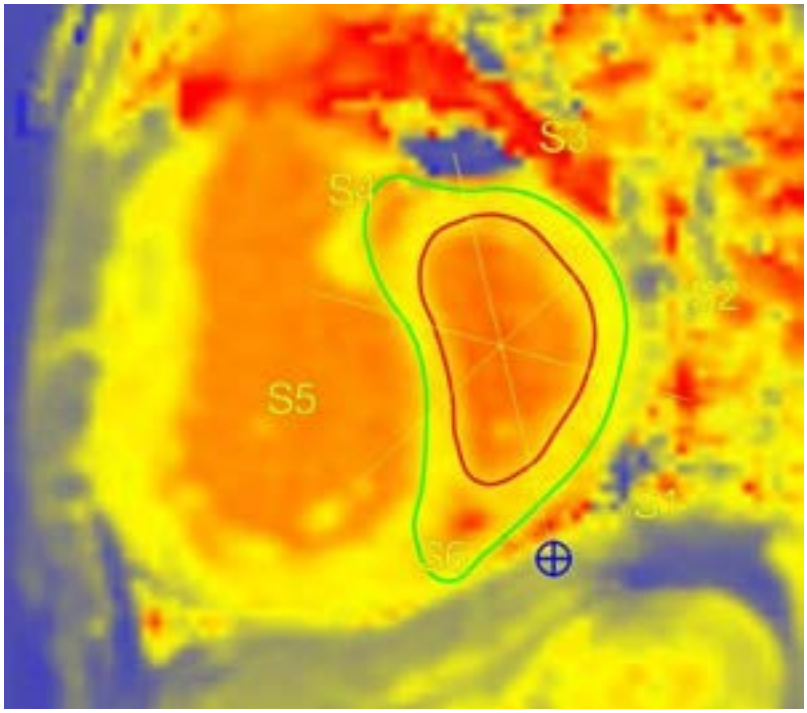

P094

Simple functional parameters by CMR are the most powerful prognostic predictors in the multimodality assessment of cardiac amyloidosis

Daniel S. Knight, MBBS MRCP(UK)[2]Giulia Zumbo, MD[1], William Barcella, BSc MSc[3], Martinez-Naharro Ana, MD[4], Thomas Treibel, MBBS.MRCP(UK)[5], Amna Abdel-Gadir, MBBS.MRCP(UK)[6], Heerajnarain Bulluck, MBBS[7], Tushar Kotecha, MBChB[1], Rohin Francis, MBBS[1], Tamer Rezk, BSc[1], Cristina Quarta, MD, PhD[1], David Hutt, BApSc[1], Julian Gillmore, MD, PhD[1], James Moon, MBBS, MD, MRCP[8], Philip Hawkins, PhD[1], Marianna Fontana, MD, PhD[1]

1. *National Amyloidosis Centre, University College London, England, United Kingdom*
2. *Royal Free London NHS Foundation Trust, London, England, United Kingdom*
3. *Department of Statistical Science, University College London, England, United Kingdom*
4. *UCL Department of Cardiac MRI, The National Amyloidosis Centre, England, United Kingdom*
5. *Barts Heart Centre, England, United Kingdom*
6. *University College London and Barts Heart Centre, London, England, United Kingdom*
7. *University College London, England, United Kingdom*
8. *Barts Heart Center, The Cardiovascular Magnetic Resonance Imaging Unit and The Center for Rare Cardiovascular Diseases Unit, St Bartholomew's Hospital, West Smithfield, London, UK, England, United Kingdom*

Background: Cardiac involvement in AL and ATTR amyloidosis is the main driver of prognosis and influences treatment strategies. Consequently, numerous measures of systolic and diastolic function are assessed by multiple imaging modalities in cardiac amyloidosis. However, the relative prognostic importance of these markers and how they develop in the natural history of cardiac infiltration has never been investigated. This study of the largest cohort of amyloidosis patients to date aims to: 1) describe the progression of functional and structural cardiac abnormalities associated with amyloid deposition, and 2) identify the most prognostic functional markers across cardiac magnetic resonance (CMR) and echocardiography techniques in cardiac amyloidosis.

Methods: Three-hundred and twenty-two patients with systemic amyloidosis were prospectively studied. All subjects underwent: 1) CMR with cine imaging, late gadolinium enhancement and T1 mapping with Extracellular Volume (ECV) measurement, and 2) transthoracic echocardiography. Structural and functional metrics by CMR (LV mass, LA area, RA area, LVEF, RVEF, stroke volume, MAPSE and TAPSE) and echocardiography (E/E' and global longitudinal strain) were studied. A multivariable model assessing the probability of functional indices becoming abnormal with increasing cardiac amyloid burden was evaluated. The prognostic capabilities of these parameters were assessed using a Cox proportional hazards model.

Results: Functional metrics can be divided into two groups based upon the probability of becoming abnormal either early or later in myocardial infiltration (Figure 1). LV mass and MAPSE by CMR together with strain and E/E' by echocardiography have a high probability of becoming abnormal early in the disease process. In contrast, bi-ventricular ejection fractions and bi-atrial areas become abnormal at later stages. The probability of indexed stroke volume and TAPSE becoming abnormal occurs more gradually over the spectrum of ECVs.

Ninety patients (28%) died during a median follow-up period of 22 months (IQR 10-38). Univariable analysis showed that all of the imaging markers studied were statistically significant predictors of outcome. However, multivariable analysis (adjusted for age) showed that TAPSE by CMR (hazard ratio, 0.90; 95% confidence interval, 0.84-0.96; $P < 0.001$) and indexed stroke volume (hazard ratio, 0.96; 95% confidence interval, 0.92-0.999; $P < 0.05$) were the only independent predictors of mortality.

Conclusions: Specific functional and structural abnormalities characterize different stages of amyloid deposition, highlighting the importance of simple functional indices in the evaluation of cardiac infiltration. In a comprehensive multi-modality imaging assessment of the largest cohort of cardiac amyloidosis patients studied, CMR-derived TAPSE and indexed stroke volume are the strongest functional markers of prognosis.

http://www.ConferenceAbstracts.com/uploads/cfp2/attachments/LDFAIBDN/LDFAIBDN--222672-1-ANY.pdf

P095

Pacemakers and AICD's in the Magnet; have we Turned the Corner?

Huma Samar, MD[1]Loretta Gevenosky, R.N.[2], Ronald Williams, RT(R)(MR), B.A.[2], Mark Doyle, PhD[3], Moneal Shah, MD[4], Christopher Bonnet, MD[2], Shimaa S. Khidr, MD[2]

1. Loma Linda University Medical Center, Pittsburgh, PA
2. Allegheny General Hospital, Pittsburgh, PA
3. Allegheny General Hospital, PA
4. Allegheny general hospital, pittsburgh, PA

Background: MR imaging is infrequently performed on patients with conventional pacemakers/ICD's. Multiple studies have documented the safety of MRI scans in patients with implanted devices, yet the diagnostic clinical value of this approach has not been established not even considered. We propose that MRI imaging patients with a pacemaker is crucial to the existing diagnosis and in many instances, substantially modifies diagnosis and patient management.

Methods: An evaluation of 276 consecutive patients with PM/AICD's who underwent MRI (GE CV/i, 1.5T, GE, Milwaukee,WI) over 10 years (90%< 5years) 1) Did the primary diagnosis change? 2) Did the MRI provide additional information to the existing diagnosis? 3) Was the pre-MRI (tentative) diagnosis confirmed? 4) Did patient management change? If 'Yes' was answered to any of the above questions, it was considered that MRI was of value to patient diagnosis and/or impending therapy.

Results: The average MRI scan time was 20±55minutes. Regarding the population, of the 276 patients imaged, 190(69%) were neurology/neurosurgery cases, 17 (6%) were musculoskeletal and 69 (25%) were cardiac/vascular cases.

After reviewing the 190 neurology/neurosurgery cases, 161 (85%) demonstrated MRI provided additional information of which 53 (28%) changed the original diagnosis and in turn, the course of medical treatment. Thus, for 238 (86%), MRI scan was of distinct value to the final diagnosis and management. In only 28 (10%) patients did MRI not provide further information but simply confirmed the original diagnosis. The 69 cardiac cases demonstrated that iin 60 patients (87%), the MRI provided additional information of which 25 (36%) changed the original diagnosis and 22 (32%) patient management changed while in 6(1%) the CMR was uninterpretable due to AICD artifact. In essence, 87% of the cardiac cases markedly benefited by CMR performance. Finally, in the 17 musculoskeletal cases, MRI provided additional information in15 (88%) of which 9(53%), changed patient management. Importantly, with careful attention to device reprogramming and scanner sequences, no safety issues were encountered and no adverse effects of undergoing the MRI scan were noted in any patient.

Conclusions: MR imaging in patients with implanted pacemakers and defibrillators added substantial clinical value to patient diagnosis and subsequent management justifying the risk of the procedure. To our knowledge, this large study is the first to focus *solely* on diagnostic value under the assumption that safety can be routinely accomplished. Perhaps,we have indeed turned the corner and we can now focus on the additive value of implanted devices in the MRI environment.

P096

Electrocardiographic left ventricular electrical remodeling - incremental prognostic value and relation to cardiovascular magnetic resonance measures of function and tissue characterization

Louise Niklasson, MS[1] Todd T. Schlegel, MD[2], Björn Wieslander, MD[3], Ljuba Bacharova, MD, DrS, MBA[4], Erik B. Schelbert, MD, MS[5], Martin Ugander, MD, PhD[1]

1. *Karolinska Institutet, Stockholms Lan, Sweden*
2. *Karolinska Institutet, Vaud, Switzerland*
3. *Department of Clinical Physiology, N2:01, Karolinska Institutet and Karolinska University Hospital, Stockholm, Stockholms Lan, Sweden*
4. *International Laser Center and Institute of Pathophysiology, Medical Faculty, Comenius University, Bratislava, Slovakia*
5. *University of Pittsburgh; Heart and Vascular Institute of UPMC, PA*

Background: Detection of left ventricular electrical remodeling (LVER) by the electrocardiogram (ECG) in those without severe coronary artery disease (CAD) or focal myocardial scar may provide prognostic value beyond cardiovascular magnetic resonance (CMR) measurements of tissue characterization, function and structure such as myocardial extracellular volume fraction (ECV) by T1 mapping, left ventricular ejection fraction (LVEF) and mass index (LVMI).

Methods: All adults undergoing CMR at University of Pittsburgh Medical Center who also had a 12-lead ECG within ±30 days were considered for inclusion. Exclusion criteria included non-sinus rhythm, bundle branch or fascicular block, any focal late gadolinium enhancement, or known or CMR-determined hypertrophic or dilated cardiomyopathy or coronary or severe valvular disease. The ECG raw data were used to calculate a previously validated advanced ECG (A-ECG) score for the likelihood of left ventricular systolic dysfunction (LVSD). The multivariate score is comprised of results from the 12-lead summed QRS voltage, the derived vectorcardiographic Z-lead integral and spatial mean QRS-T angle, and the singular value decomposition-based nondipolar QRS-wave and dipolar T-wave voltages. The prognostic value of the ECG and CMR measures were evaluated with respect to all-cause death and hospitalization for heart failure (HHF). The contribution of CMR measures to the A-ECG LVSD score was evaluated with multivariate linear regression.

Results: Of 1704 adults undergoing CMR, 472 (28%) (median age 51, range 18-83; 55% female) met the criteria for participation. During a median follow-up of 4 years, the combined endpoint of mortality or HHF was associated with the A-ECG LVSD score (chi^2 7.5, p=0.006), ECV (chi^2 5.8, p=0.02), LVEF (chi^2 5.5, p=0.02) and LVMI (chi^2 4.5, p=0.03). The A-ECG score was related to ECV, LVMI, LVEF, age and gender (global R^2=0.23, $p < 0.001$).

Conclusions: In a population without any focal myocardial scar or severe CAD, LVER by the A-ECG LVSD score provided prognostic information beyond CMR measurements of ECV, LVEF and LVMI. Age, gender and CMR measures together only explained less than a quarter of the A-ECG LVSD score, thus illustrating the unique and complementary prognostic information in the ECG.

P097

Prognostic Significance of Remote Myocardium Alterations Assessed by Quantitative Non-Contrast T1 Mapping Cardiac Magnetic Resonance in ST-Elevation Myocardial Infarction

Ingo Eitel, MD[1]Thomas Stiermaier, MD[1], Holger Thiele, MD[2]

1. *University Heart Center Lübeck, Lübeck, Schleswig-Holstein, Germany*
2. *University Heart Center Luebeck, Sachsen, Germany*

Background: The exact role and clinical relevance of remote myocardium native T1 mapping alterations assessed by cardiac magnetic resonance (CMR) after ST-elevation myocardial infarction (STEMI) remains to be defined. This study sought to assess the prognostic significance of remote zone native T1 alterations for the prediction of hard clinical events in a STEMI population treated by primary percutaneous coronary intervention (PPCI) and to compare it with conventional markers of infarct severity.

Methods: We included 255 consecutive STEMI patients reperfused by PPCI within 12 hours after symptom onset. CMR core laboratory analysis was performed to assess left ventricular (LV) function, standard infarct characteristics (infarct size, myocardial salvage, microvascular obstruction) and native T1 values of the remote, non-infarcted myocardium. The primary endpoint was a composite of death, reinfarction and new congestive heart failure within 6 months after index event (major adverse cardiac events, MACE).

Results: Patients with increased remote zone native T1 values (>1129 ms) had significantly larger infarcts (p=0.012), less myocardial salvage (p=0.002) and more pronounced LV dysfunction (p=0.011). In multivariable analysis, remote zone native T1 was independently associated with MACE after adjusting for clinical risk factors (p=0.001) or other CMR variables (p=0.007). Native T1 of remote myocardium provided incremental prognostic information above clinical risk factors, LV ejection fraction and other established markers of infarct severity including infarct size (all $p < 0.05$).

Conclusions: In STEMI patients treated by PPCI, evaluation of remote zone alterations by quantitative non-contrast T1 mapping provides independent and incremental prognostic information in addition to clinical risk factors and traditional CMR outcome markers. Remote zone alterations may therefore represent a novel therapeutic target as well as a useful parameter for optimized risk-stratification in STEMI patients.

P098

Comparative Effectiveness of CMR and 3D Echocardiography for Optimizing Left Ventricular Pacing Site Selection and Cardiac Resynchronization Therapy Response

Kenneth C. Bilchick, MD, MS[1]Daniel A. Auger, Ph.D[2], Wesley Anderson, BA[3], Xiaoying Cai, BS[2], Christopher M. Kramer, MD[4], Frederick H. Epstein, Ph.D.[4]

1. *UVA Health System, Charlottesville, VA*
2. *University of Virginia, Charlottesville, VA*
3. *University of Virginia Health System, Charlottesville, VA*
4. *University of Virginia, VA*

Background: Cardiac magnetic resonance (CMR) with cine DENSE (Displacement Encoding with Stimulated Echoes) provides high quality strain imaging for cardiac resynchronization therapy (CRT) response, but comparative effectiveness relative to 3D echocardiography (3DE) has not been assessed. We hypothesized that CMR with DENSE strain imaging and late gadolinium enhancement (LGE) would provide optimal strain and scar imaging for CRT patients, and that CMR strain parameters would be more strongly associated with clinical CRT response than 3DE strain parameters.

Methods: CMR with cine DENSE and LGE was performed prior to CRT on a 1.5T MRI system. DENSE images were acquired in standard short-axis planes at a temporal resolution of 17 ms, in-plane pixel size of 2.8 mm × 2.8 mm, and slice thickness of 8 mm. Displacement was encoded in two orthogonal directions, and a spiral k-space trajectory was used with 6 interleaves per image. Other parameters included: field of view = 350 × 350 mm2, displacement encoding frequency ke = 0.1 cycles/mm, flip angle = 15 degrees, and echo time = 1.9 ms. CRT response was assessed as the change in the left ventricular end-systolic volume (Delta-LVESV) by two-dimensional echocardiography 6 months after CRT. The standard deviation of time to peak (TTP) strain in 17 segments (SD17, as used in the 3DE literature) and the circumferential uniformity ratio estimate with singular value decomposition (CURE-SVD, as used in the CMR literature) were assessed. Different multivariable linear regression models were used to assess different combinations of CMR and 3DE parameters related to both dyssynchrony and mechanical activation for CRT response.

Results: 55 patients (age 63.8 +/- 10.1 years, 33.3% female) with pre-CRT MRIs were included in the analysis. 3DE CURE-SVD was correlated with CRT response based on the Delta-LVESV (R^2=0.120, p=0.04); however, neither the 3DE SD17 (P=0.64) nor the 3DE TTP strain at the LV pacing site (LVPS) (P=0.71) were significantly associated with the Delta-LVESV. Improved model performance was obtained by using 3DE strain data to determine a modified 3DE CURE-SVD and adding CMR DENSE mechanical activation at the LVPS (R^2=0.241, P=0.01) or both CMR mechanical activation at the LVPS and LGE-based scar at the LVPS (R^2=0.381, P=0.001). The best model for CRT response was obtained with CMR parameters exclusively. This optimal model included CMR-CURE-SVD, CMR LVPS Scar, and CMR DENSE activation timing (R^2=0.403, P < 0.0001). The R^2 values for these different multivariable linear regression models are shown in the Figure.

Conclusions: In summary, CMR parameters provided a better model for CRT response than 3DE parameters. In particular, CMR DENSE assessment of mechanical activation at the LVPS has a much stronger association with CRT response than 3DE-derived strain parameters for mechanical activation at the LVPS. Furthermore, the addition of CMR LGE findings to 3DE strain findings was critical for prediction of CRT response.

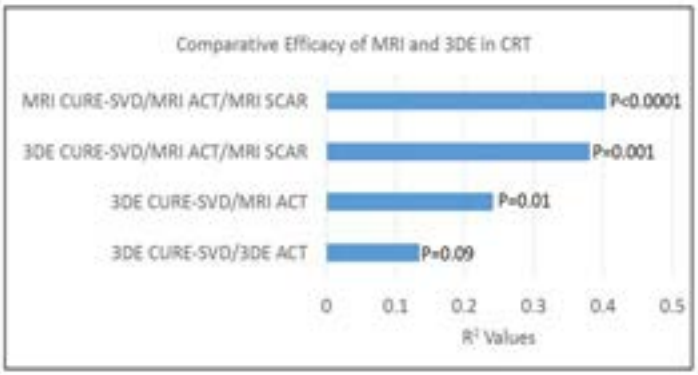

P099

Right Ventricular Remodeling Predicts Outcome in Patients with Symptomatic and Asymptomatic Heart Failure

Lingyu Xu, MD, MSc.[1] Harris Wang, Master student [2], Kelvin Chow, Ph.D[3], Joseph Pagano, MD[4], Anna Schmidt, MD, Ph.D[5], James White, MD, FRCP(C) [6], Mark Haykowsky, Ph.D[7], Evangelos Michelakis, MD[8], Justin Ezekowitz, MBBCh, MSc, FACC, FESC, FAHA[9], Jason Dyck, Ph.D[9], Gavin Oudit, MD, PhD, FRCPC[9], Richard Thompson, PhD[10], Ian Paterson, MD[2]

1. *Department of Cardiology, Faculty of Medicine, University of Alberta, Edmonton, AB, Canada*
2. *Faculty of Medicine, Department of Cardiology, University of Alberta, AB, Canada*
3. *Department of Medicine, University of Virginia Health System, USA, VA*
4. *Department of Biomedical Engineering, Faculty of Medicine and Dentistry, University of Alberta, AB, Canada*
5. *Stephenson Cardiovascular Magnetic Resonance Centre, University of Calgary, AB, Canada*
6. *Stephenson Cardiovascular Imaging Center, University of Calgary, AB, Canada*
7. *Faculty of Rehabilitation Medicine, University of Alberta, AB, Canada*
8. *Department of Medicine, University of Alberta, AB, Canada*
9. *Mazankowski Alberta Heart Institute, University of Alberta, AB, Canada*
10. *Department of Biomedical Engineering, University of Alberta, AB, Canada*

Background: Right ventricular (RV) structural and functional abnormalities are increasingly associated with poor clinical outcomes; however their utility of predicting adverse outcomes, among patients with heart failure (HF) and those at risk has not been well characterized. We hypothesize that cardiac magnetic resonance (CMR) derived RV measures provide additional prognostic information to patients with subclinical and clinical HF.

Methods: Healthy older controls and patients with ACC/AHA stage B or C HF underwent a standard CMR examination at 1.5T. Ventricular volumes and mass were traced from steady state free precession cine imaging. CMR measures from the healthy controls were used to define normal. Patient demographics, co-morbidities and clinical outcomes were obtained from administrative databases. The primary composite outcome was death, cardiovascular hospitalization or cardiovascular emergency room visit. A basic multivariable cox proportional regression model incorporating demographics and co-morbidities was constructed by using stepwise backward selection. Significant CMR parameters from univariate analysis ($P < 0.1$) were individually added into the basic model to identify the best predictors of outcome. Survival curves were plotted by Kaplan-Meier method.

Results: 89 healthy controls (male 53%, age 57±10 years) and 473 patients (male 64%, age 56±16 years), including 213 with stage B and 260 with stage C, were included (Table 1). Compared to stage B HF, patients with stage C HF were older and had a higher prevalence of cardiovascular risk factors, coronary artery disease, chronic obstructive pulmonary disease (COPD) and chronic renal failure, $p < 0.05$ for each. Additionally, patients with stage C HF had increased RV remodeling, and reduced RV function on CMR, $p < 0.05$ for each. 179 clinical events including 40 deaths occurred during a mean follow-up of 26±20 months. The basic multivariable model for predicting the primary outcome included age, diabetes mellitus, hypertension, COPD, and atrial fibrillation/flutter. Within this clinical model, CMR measures associated with the primary outcome on multivariate analysis included: RVESV/LVESV (adjusted HR 1.02 per 0.1, P=0.001), indexed RVESV (adjustedHR 1.08 per 10ml/m^2, P=0.01), and indexed RVEDV (adjusted HR 1.06 per 10ml/m^2, P=0.017). Patients with relative RV enlargement, defined from healthy controls as RVESV/LVESV > 1.51, had worse outcomes including among the subclinical and clinical HF subgroups, $p < 0.05$ (Figure 1).

Conclusions: Among patients with subclinical or clinical heart failure, only CMR measures of RV remodeling predicted cardiac events after adjusting for clinical characteristics. Therefore RV volumes should be routinely reported in HF patients and those at risk.

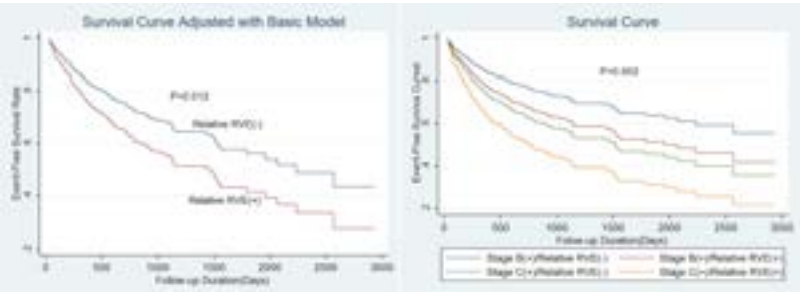

Table 1. Demographics, co-morbidities and CMR parameters of healthy controls and heart failure patients, including AHA/ ACC stage subgroups

P value†	ACC/AHA HF Stage C	ACC/AHA HF Stage B	P value*	All HF Patients	Healthy Controls	
0.72	260(169)	213(135)	0.05	473(304)	89(47)	Number (male)
0.003	58±16	54±17	0.57	56 ± 16	57 ± 10	Age (years)
0.09	2.04±0.29	2.00±0.27	<0.001	2.02±0.28	1.91±0.28	Body Surface Area
0.078	131(50%)	90(42%)	N/A	221(47%)	N/A	Hypertension
<0.001	88(34%)	33(15%)	N/A	121(26%)	N/A	Diabetes Mellitus
<0.001	88(34%)	33(15%)	N/A	121(26%)	N/A	Tobacco Use
<0.001	123(47%)	60(28%)	N/A	183(39%)	N/A	Coronary Heart Disease
<0.001	63(24%)	19(9%)	N/A	82(17%)	N/A	Chronic obstructive pulmonary disease
<0.001	98(38%)	29(14%)	N/A	127(27%)	N/A	Atrial fibrilation/flutter
<0.001	88(34%)	31(15%)	N/A	119(25%)	N/A	Chronic Renal Failure
0.18	17(7%)	8(4%)	N/A	25(5%)	N/A	Stroke
0.58	35(13%)	25(12%)	N/A	60(13%)	N/A	Cancer
<0.001	38±18	57±11	<0.001	47 ± 18	62 ± 4	LVEF (%)
<0.001	82±28	64±16	<0.001	74 ± 25	53 ± 9	Indexed LVmass(g/m^2)
<0.001	113±49	78±24	<0.001	97 ± 44	70 ± 10	Indexed LVEDV (mL/m^2)
<0.001	76±50	35±17	<0.001	58±44	27 ± 5	Indexed LVESV(mL/m^2)
<0.001	0.79±0.25	0.86±0.23	<0.001	0.83 ±0.24	0.76 ±0.11	LVmass/LVEDV (g/mL)
<0.001	42±13	54±9	<0.001	47 ± 13	60 ± 6	RVEF (%)
<0.001	91±33	77±23	<0.001	85 ± 30	67 ± 12	Indexed RVEDV(mL/m^2)
<0.001	55±30	36±15	<0.001	47±26	27 ± 7	Indexed RVESV(mL/m^2)
0.036	0.95±0.57	1.04±0.31	0.24	0.99±0.47	0.96 ±0.13	RVEDV/LVEDV
0.16	1.10±0.96	1.21±0.61	0.016	1.15 ±0.93	1.03±0.24	RVESV/LVESV

* P value for comparison between healthy control and patients.

† P value for comparison between ACC/AHA stage B and stage C heart failure patients.

Abbreviations: HF = heart failure, LVEF = left ventricular ejection fraction, LV mass = left ventricular mass, LVEDV = left ventricular end diastolic volume, LVESV = left ventricular end systolic volume, RVEDV = right ventricular end diastolic volume, RVESV = right ventricular end systolic volume, RVEF = right ventricular ejection fraction.

P100

Effects of environmental noise pollution on cardiac chamber size and function in UK Biobank participants

Nay Aung, MD, MRCP[1]Mihir M. Sanghvi, MB BS, BSc[2], Filip Zemrak, MD MRCP[1], Kenneth Fung, MBBS BSc[3], Jose Miguel Paiva, MSc[1], Aaron Lee, PhD, MBBS[1], Valentina Carapella, DPhil[4], Stefan K. Piechnik, PhD, MScEE[5], Stefan Neubauer, MD, FRCP[5], Steffen E. Petersen, MD DPhil MPH FRCP[1]

1. *Barts Heart Center, The Cardiovascular Magnetic Resonance Imaging Unit and The Center for Rare Cardiovascular Diseases Unit, St Bartholomew's Hospital, West Smithfield, London, UK, England, United Kingdom*
2. *William Harvey Research Institute, NIHR Cardiovascular Biomedical Research Unit at Barts, Queen Mary University of London, Charterhouse Square, London EC1M 6BQ, UK, England, United Kingdom*
3. *Barts Heart Center, The Cardiovascular Magnetic Resonance Imaging Unit and The Center for Rare Cardiovascular Diseases Unit, St Bartholomew's Hospital, West Smithfield, London, UK, London, England, United Kingdom*
4. *University of Oxford, Oxford, United Kingdom, England, United Kingdom*
5. *University of Oxford, England, United Kingdom*

Background: Noise pollution is associated with hypertension and increased incidence of myocardial infarction, stroke and mortality. Exposure to noise can lead to elevated heart rate, disturbed sleep and activation of stress and inflammatory pathways which are important in cardiovascular remodelling. Presently, there is no study on the effect of noise pollution on cardiovascular structures and function. The aim of this study was to investigate the impact of environmental noise on left and right atrial and ventricular structures and function.

Methods: We analysed 5,065 UK Biobank CMR studies to measure left and right atrial and ventricular volumes and ejection fraction using steady-state free precession sequences at 1.5T. The data on clinical characteristics and medical history were obtained from a standardised questionnaire. Noise exposure estimates were calculated from each participant's address using the Common Noise Assessment Methods (CNOSSOS-EU) and Land Use Regression (LUR) models. Noise variables categorized as average daytime [07:00 to 19:00], evening [19:00 to 23:00] and night-time [23:00 to 07:00] sound levels were expressed in decibels (dB). Due to highly-skewed distributions of noise variables, they were split at median into low and high exposure groups. The relationships between CMR parameters and noise metrics were assessed by multiple linear regression models adjusted for age, gender, ethnicity, Townsend deprivation index, education, job class, smoking and alcohol drinker status, systolic blood pressure, heart rate, medications for hypertension, diabetes and hyperlipidaemia, presence of diabetes, respiratory or cardiovascular diseases.

Results: After excluding CMR studies with poor quality or incorrect identifier data, 4,974 participants remained. Clinical characteristics of the cohort were presented in Table 1. In multivariate regression models, high exposure to daytime and evening noise were associated with a very minor but statistically significant reduction in both left atrial (LA) maximal volume (β coefficient -1.4, $p < 0.05$) and LA stroke volume (β coefficient -0.8, $p < 0.05$) (Table 2 and Figure 1). High exposure to night time noise was correlated with a small reduction in LA stroke volume only (β coefficient -0.7, $p < 0.05$) (Figure 1). Noise variables were not associated with ventricular or right atrial parameters. There was no interaction between noise and other significant covariates.

Conclusions: Higher exposure to residential noise was associated with trivial reduction in LA maximal volume and stroke volume. The minute effect sizes observed after robust adjustment for confounders suggest that typical ranges of noise in the community do not appear to have major influence on cardiac chamber size and function.

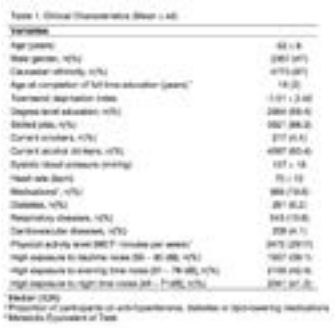

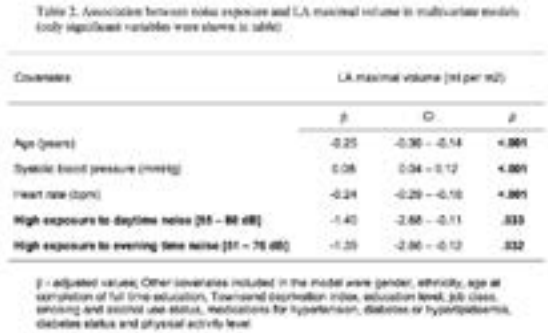

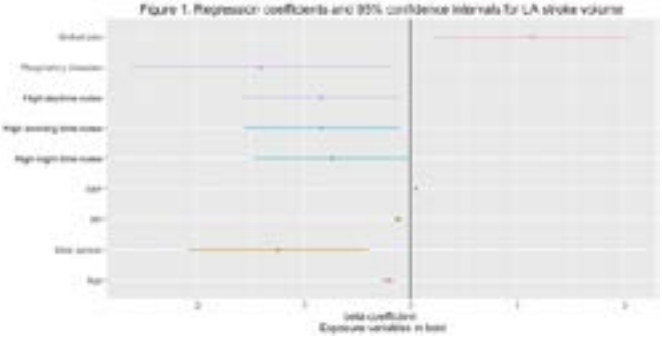

P101

Right and left atrioventricular plane displacement as a predictor of survival in precapillary pulmonary hypertension.

Anthony Lindholm[1] Felicia Seemann, MSc[2], Roger Hesselstrand, M.D., Ph.D.[3], Göran Rådegran, M.D., Ph.D.[4], Einar Heiberg, PhD[5], Ellen Ostenfeld, M.D., Ph.D.[6]

1. *Lund University, Dept of Clinical Sciences, Clinical Physiology, Lund, Lund, Skane Lan, Sweden*
2. *Lund University, Skane University Hospital, Dept of Clinical Physiology, Lund, Sweden; Lund University, Faculty of Engineering, Dept of Numerical Analysis, Lund, Sweden; Lund University, Faculty of Engineering, Dept of Biomedical Engineering, Lund, Skane Lan, Sweden*
3. *Lund University, Dept of Clinical Sciences, Rheumatology, Lund, Skane Lan, Sweden*
4. *Lund University, Dept. of clinical sciences, Cardiology, Lund and Skane University Hospital, Lund, Skane Lan, Sweden*
5. *Lund University, Department of Clinical Sciences Lund, Clinical Physiology, Skane University Hospital, Lund, Sweden; Lund University, Faculty of Engineering, Department of Biomedical Engineering, Lund, Sweden, Skane Lan, Sweden*
6. *Lund University, Dept of Clinical Sciences, Clinical Physiology, Lund, and Skane University Hospital, Lund, Skane Lan, Sweden*

Background: Precapillary pulmonary hypertension ($PH_{Pre\text{-}Cap}$) is a rare and complex vascular disease, with poor prognosis and high mortality due to right heart failure. Cardiac magnetic resonance imaging (CMR) can provide an accurate tool for diagnosis of impaired cardiac function. Right ventricular (RV) atrioventricular plane displacement (AVPD) is lower in patients with $PH_{Pre\text{-}Cap}$ compared to healthy controls. Likewise, left ventricular (LV) AVPD is lower in patients, despite preserved LV ejection fraction. Yet, AVPD as a predictor for major adverse cardiovascular events (MACE) is not investigated in $PH_{Pre\text{-}Cap}$ with CMR. The aim of this study was to evaluate if lower RVAVPD and LVAVPD, measured with CMR, are predictors for MACE in patients with $PH_{Pre\text{-}Cap}$.

Methods: Data was collected retrospectively from 86 $PH_{Pre\text{-}Cap}$ patients and 40 healthy controls. All subjects underwent CMR and patients had done right heart catheterization (RHC) on clinical indication. $PH_{Pre\text{-}Cap}$ was defined as mean pulmonary arterial pressure≥25mmHg with normal left atrial pressure≤15mmHg from RHC. Causes of $PH_{Pre\text{-}Cap}$ consisted of 8 with familial pulmonary arterial hypertension (FPAH), 24 PAH due to systemic sclerosis (SSc-PAH), 15 PAH associated with connective tissue disorders other than SSc (CTD-PAH), 11 chronic thromboembolic pulmonary hypertension (CTEPH) and 28 with idiopathic PAH (IPAH). For image acquisition, 1.5T MR scanner was used. LVAVPD and RVAVPD were calculated from 8 pre-specified points in three long-axis cine images from end diastole to end systole. MACE was defined as the combination of death, lung transplantation, or heart transplantation.

Results: Mean RVAVPD was 12.9±4.1 mm and LVAVPD 11.0±3.0 mm in patients. In controls, RVAVPD was 20.7±3.3 mm and LVAVPD 14.4±2.4 mm. Median follow up time was 2.7±3.0 years. Survival was lower in patients with RVAVPD lower than mean compared with patients with RVAVPD above mean (p=0.002) (Figure 1). Survival did not differ between patients with LVAVPD lower or above mean (p=0.1). However, RVAVPD and LVAVPD were lower in patients with MACE than patients without MACE (RV p=0.003, LV p=0.03) (Figure 2). There were no significant differences in RVAVPD (p=0.2) or LVAVPD (p=0.6) among the patient groups (Figure 3).

Conclusions: Reduced RVAVPD is associated with a higher risk for MACE in patients with precapillary pulmonary hypertension. Reduced LVAVPD did not show a significantly higher risk for MACE. However, patients with MACE have lower RVAVPD and LVAVPD than patients without MACE.

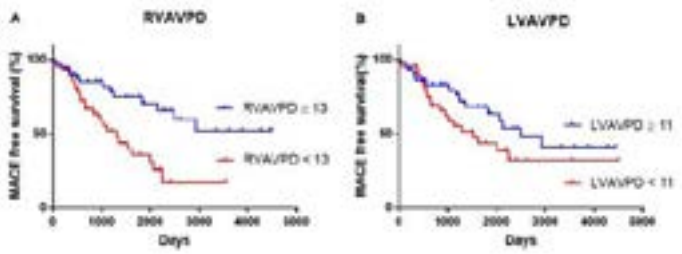

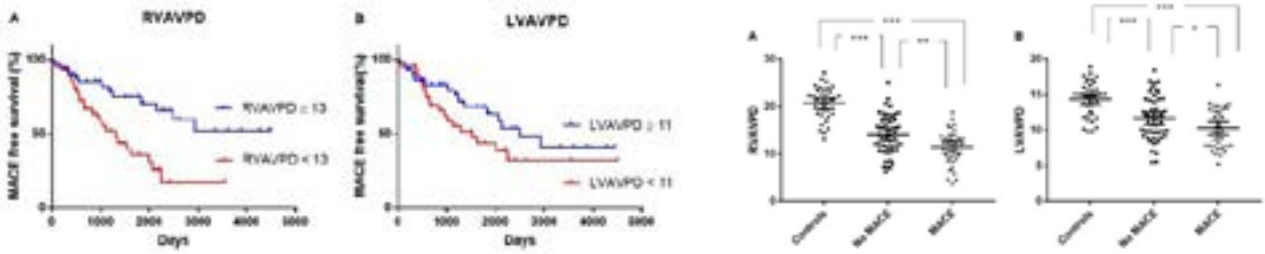

P102

Predictors of Success of PVI post-Atrial Fibrillation. Can their be a Pulmonary Vein Resonance Phenomenon; Insights from Cardiac Magnetic Resonance

Shimaa Sayed. Khidr, MD[1] Victor Farah, MD[1], Mark Doyle, Ph.D.[1], Geetha Rayarao, MS[2], Moneal Shah, MD[3], Mohamed Abdel Ghany, MD[4], Hosam Ali, MD, PhD[4], Doaa Ahmed. Fouad, MD, PhD[4], Shimaa S. Khidr, MD[1]

1. *Allegheny General Hospital, Pittsburgh, PA*
2. *Allegheny General Hospital, PIttsburgh, PA*
3. *Allegheny general hospital, pittsburgh, PA*
4. *Assiut University Hospital, N/A, Egypt*

Background: Atrial fibrillation recurrence after a single pulmonary vein isolation (PVI) procedure on paroxysmal AF ranges from 38% to 78%. In persistent AF PVI patients, the success rate of the initial procedure fails to reach 50%. Predictors of response are heavily studied, but currently are incomplete. Thus, a universal method, potentially devoid of tried classical metrics, may have far better predictabilty. If such were found, natural proclivity for its incorporation to aid in patient selection and optimization would follow.

Hypothesis: Pulmonary vein area at the ostium is characteristic of a resonance phenomena which relates to success or failure of the PVI procedure.

Methods: Patients (100) with AF who underwent PVI and who had CMR before and 6±2 months after the procedure were retrospectively analyzed. The cross sectional area (CSA) of each pulmonary vein was measured from the 3D MRA of the left atrium and pulmonary veins. Patient response was evaluated using Holter monitoring for 2x15 days post PVI and characterized as responders (R) if no or less than one minute of AF was experienced or non responders (NR) otherwise.

Statistical analysis: Topological cluster analysis was used to rank-order PVI patients. Patients were ordered on an organizing variable (average pre-PVI PV area) and the average failure rate was calculated. Clusters of size 12 pts were used with an overlap between clusters. Based on the organizing variable, the failure rate for each cluster was plotted, Fig 1. Similar analysis was conducted for data organized on average post-PVI PV area. In such analysis, if a resonance phenomena was present, it would be evident.

Results: The topological analysis for the average pre PVI PV area indicated that patients with average PV areas centered around 227 mm^2 and 270 mm^2 had a worse prognosis, Fig 1A. The topological analysis of the post PV area showed three sharp response regions for PVI failure at 155mm^2, 195mm^2 and 240mm^2, Fig 1B. A clear evidence for an unexpected resonance phenomenon is present.

Conclusions: Topological analysis reveals sharp resonance conditions that correspond to success or failure of PVI. These resonance states are assessed via average PV area, both pre and post PVI. Further work is needed to explore this unique phenomenon but topology analysis, recently shown to predict LV conditions, appears preserve in the pulminary veins characterizing a heretofore unexpected periodicity in Afib pts uniquely related to PVI success or failure.

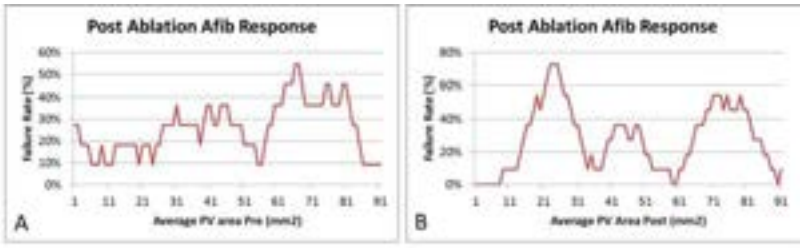

Figure 1 Periodic nature of PVI success rate ordered by A) average pulmonary vein area pre PVI and B) post PVI

P103

Presence of Late Gadolinium Enhancement Predicts All-cause Mortality and Cardiovascular Hospitalization in Patients with Known or Suspected Heart Failure

Masliza Mahmod, MBChB, DPhil[1]Michelle D'souza[1], Norliza Othman, MD(UKM), FRCR(UK)[2], Khaled Mahmoud-Tawfik, MBBS BSc[3], Francisco Alpendurada, MD PhD[4], Kanishka Bhatthacharya, PhD (Oxon)[5], Andrew Jabbour, MBBS, PhD[4], Cheuk F. Chan, MRCP MD [6], Isabelle Roussin, MD[7], Ankur Gulati, MD[4], Dudley J. Pennell, MD[8], Sanjay Prasad, MD[8]

1. *University of Oxford, England, United Kingdom*
2. *Hospital Sultanah Aminah, Johor Bahru, Johor, Malaysia*
3. *Royal Free London NHS Foundation Trust, England, United Kingdom*
4. *Royal Brompton Hospital, England, United Kingdom*
5. *Oxford University, London, England, United Kingdom*
6. *East Surrey Hospital, Surrey, England, United Kingdom*
7. *Lister Hospitsl Herts and North HERTFORDSHIRE trust, Stevenage, England, United Kingdom*
8. *Royal Brompton Hospital and Imperial College, London, England, United Kingdom*

Background: Late gadolinium enhancement cardiovascular magnetic resonance (LGE-CMR) can detect myocardial scar. The prognostic value of scar assessment by LGE-CMR in unselected patients presenting with known or suspected heart failure (HF) requires clarification. We investigated whether the detection of scar by LGE-CMR predicts adverse clinical outcomes in this cohort of patients.

Methods: We prospectively enrolled 550 consecutive patients with known or suspected HF referred for CMR from 2005 to 2012. HF etiology was due to coronary artery disease (CAD) in 274 (50%) patients, dilated cardiomyopathy (DCM) in 149 (27%) patients, and other causes such as hypertension, valvular heart disease or mixed-aetiologies in 127 (23%) patients. The predefined primary composite end point was all-cause mortality or cardiovascular (CV) hospitalization.

Results: Overall, 353 (64%) patients had LGE (LGE+) and 197 (36%) had no LGE (LGE-). LGE+ patients were more likely to be male, with increased left ventricular (LV) volumes and lower LV ejection fraction, compared with LGE- patients. After a median follow-up of 4.5 (2.9-6.4) years, 125 (35%) LGE+ patients and 39 (23%) LGE- patients experienced the primary end point. Kaplan-Meier analyses revealed that LGE+ was a significant predictor of all-cause mortality and cardiovascular hospitalisation for the whole cohort (p=0.001), as well as the sub-groups of patients with CAD (p=0.005) and DCM (p

Conclusions: In patients with known or suspected heart failure of different etiologies, the presence of LGE is an independent predictor of adverse outcome in unselected cohort as well as in DCM and CAD subgroups.

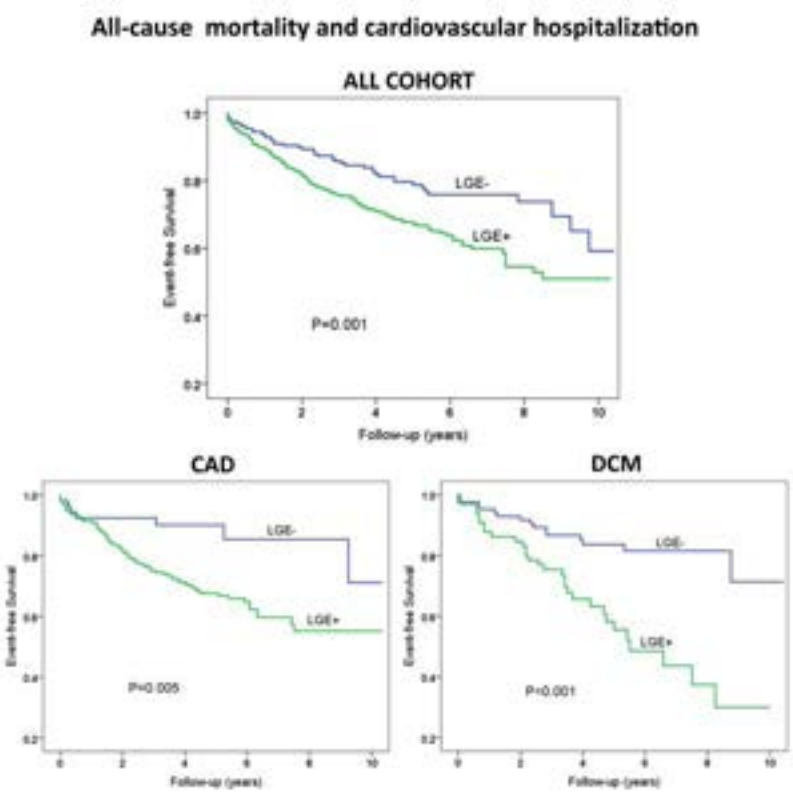

P104

Prevalence and prognostic significance of left atrial dilatation and right ventricular systolic dysfunction assessed by CMR in patients with suspected acute myocarditis

Amrit Lota, BMBCh BA[1] Adam Tsao[2], Rebecca Wassall, BN (Hons), MSc.[3], Rameen Shakur, BMBCh Mphil[4], Florence Mouy, BSc[4], Brian Halliday, BSc (Hons) MBChB (Hons)[5], Rick Wage, DCR (R)[6], Peter D. Gatehouse, PhD[7], Stuart Cook, PhD[8], John Cleland, MD PhD[8], Dudley J. Pennell, MD[9], Sanjay Prasad, MD[9]

1. *NIHR Royal Brompton Cardiovascular Biomedical Research Unit and National Heart and Lung Institute, Imperial College London, England, United Kingdom*
2. *Imperial College London, London, England, United Kingdom*
3. *Royal Brompton & Harefield NHS Foundation Trust, London, England, United Kingdom*
4. *Royal Brompton Hospital, England, United Kingdom*
5. *Royal Brompton Hospital and National Heart and Lung Institute, Imperial College London, London, England, United Kingdom*
6. *NIHR Cardiovascular Biomedical Research Unit, Royal Brompton Hospital, England, United Kingdom*
7. *NIHR Cardiovascular Biomedical Research Unit, Royal Brompton Hospital, London, England, United Kingdom*
8. *Imperial College, London, England, United Kingdom*
9. *Royal Brompton Hospital and Imperial College, London, England, United Kingdom*

Background: Spontaneous clinical recovery after acute myocarditis occurs in two thirds of patients but the reminder experience persistent or progressive left ventricular dysfunction. Risk stratification in the acute setting has focused on left ventricular ejection fraction and presence of late gadolinium enhancement. However, the prevalence and prognostic significance of right ventricular systolic dysfunction (RVSD) and left atrial (LA) dilatation has not been studied using CMR imaging, which is the methodological gold standard.

Methods: Consecutive patients referred to our centre for CMR with suspected acute myocarditis between 2005 and 2014 were retrospectively reviewed (n=1152). Acute myocarditis was diagnosed on clinical presentation and 2 out of 3 Lake Louise criteria. RVSD was assessed by two criteria; (i) RVEF < 45% on CMR, which is the definition used in the modified Task Force Criteria for arrhythmogenic right ventricular cardiomyopathy, (ii) RVEF indexed for age, gender and body surface area below the 95% confidence interval. LA dilatation was defined as an indexed 2D area of >15cm^2/m^2.

Results: Acute myocarditis was diagnosed in 170 patients (mean age 42±16 years, 84% men). Mean LVEF was 63±9% and mean RVEF was 60±8%. LVSD by indexed LVEF was present in 19% (n=32/170). Mean indexed LA area was 12±2cm^2/m^2 with LA dilatation present in 8% (14/170). RVSD by absolute RVEF < 45% was present in 4% (n=6/170), and by indexed RVEF in 7% (n= 12/170). LVEF was lower in patients with depressed compared to normal RVEF (46±15% v 64±7%, p < 0.001). LVEF was similar in patients with or without LA dilatation (63±7% vs 61±11%, p=0.4). Over a median follow-up of 4.0 years, 4 patients died resulting in cardiac mortality of 2.4%. Within this group, LVSD was present in 50% (mean LVEF 42±20%) and indexed RVSD and LA dilatation were also present in 50% (mean RVEF 50±17%, LA area 17±2cm^2/m^2).

Conclusions: Within this cohort, RVSD and LA dilatation were present in 7% and 8% of patients with acute myocarditis, respectively, compared to 19% with LVSD. However, amongst those that died, RVSD and LA dilatation were equally prevalent as LVSD. Whilst this may reflect LVSD severity by ventricular interdependence or in rare cases myocarditis of the RV free wall, data from a single echocardiographic study suggested that RVSD was the most powerful independent predictor of adverse outcomes. Recent CMR studies have omitted RVEF in baseline patient characteristics and any further analyses. There is unmet need for renewed focus on the right ventricle.

P105

Regional Myocardial Velocities and Dyssynchrony Influenced by Donor and Recipient Characteristics after Heart Transplantation

Ryan Dolan, MD[1] Amir Ali Rahsepar, MD[1], Julie Blaisdell[1], Allen Anderson, MD[2], Jane E. Wilcox, MD, MSc[3], Kambiz Ghafourian, MD, MPH[1], Jeremy D. Collins, MD[4], James Carr, MD[4], Michael Markl, PhD[1]

1. *Northwestern University, Chicago, IL*
2. *Northwestern Medicine, Chicago, IL*
3. *Northwestern University Feinberg School of Medicine, Chicago, IL*
4. *Northwestern Memorial Hospital, Chicago, IL*

Background: Heart transplant (Tx) recipients are closely monitored for potentially treatable complications, notably acute rejection and cardiac allograft vasculopathy. Because global ventricular function may not be affected until later stages, finding reliable imaging techniques to detect impairment in regional left ventricular (LV) performance is important for early diagnosis. Tissue phase mapping (TPM) has shown promise, as it allows for quantification of myocardial velocities and LV dyssynchony during systole and diastole (quantified by timing variability of regional peak velocities). The goal of this study was to determine if regional myocardial velocities and dyssynchrony were impacted by donor characteristics (age, difference in donor-recipient age, height and weight, cold ischemic time) and recipient characteristics (age, pre-Tx comorbidities) in a large cohort of Tx recipients.

Methods: Cardiac MRI (1.5T Aera, Siemens, Germany), including TPM in short-axis view (base,mid,apex) was performed in 50 patients (age 44.3±18.4,female 50%) prospectively recruited following Tx (6.5±6.4yrs after Tx, 9 < 1yr after transplant). Donor information (age 28.7±11.9,female 27%) was obtained from operative reports (table 1). Data analysis was based on the AHA 16-segment model and included quantification of radial and longitudinal systolic and diastolic peak LV velocities and time to peak (TTP). Global peak velocities were calculated as averages over all 16 segments. The standard deviations of TTP across all 16 LV segments were used to evaluate the extent of myocardial dyssynchrony. Study was approved by the Northwestern IRB.

Results: As summarized in table 2, recipient age at Tx and donor-recipient age difference showed a significant positive correlation with diastolic radial peak myocardial velocity (r=0.315,p=0.026; r=0.541,p=0.001) and dyssynchrony (r=0.425,p=0.002;r=0.459 ,p=0.008). Increased cold ischemic time demonstrated a significant inverse correlation with diastolic radial and longitudinal peak myocardial velocities (r=-0.371,p=0.024;r=-0.339,p=0.040). Prior significant rejection episodes (biopsies with ISHLT grade≥2) also showed a significant association with impaired diastolic radial and longitudinal peak myocardial velocities (r=-0.369,p=0.008;r=-0.362,p=0.010). Recipient hyperlipidemia was associated with lower systolic longitudinal dyssynchrony (p=0.017), and recipient CAD was associated with higher diastolic radial dyssynchrony (p=0.035).

Conclusions: These findings show an association between regional myocardial velocities and dyssynchrony and several donor and recipient characteristics: recipient age, recipient HLD, recipient CAD, donor age, donor-recipient age difference, donor weight, cold ischemic time, and past rejection episodes. The majority of the significant associations were in the radial LV motion direction during diastole, suggesting that diastolic dysfunction may be the most sensitive marker of regional motion changes in heart Tx patients.

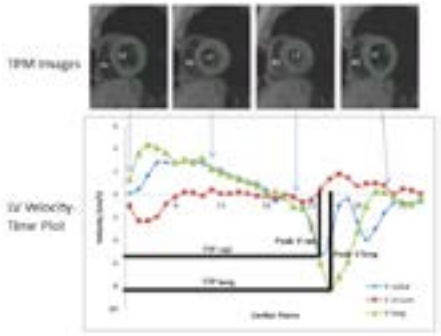

Age at Tx	44.3 ±18.4	Donor Age	28.7 ±11.9
Gender	25/50 (50%)	Donor-Recipient Age Diff	22.4 ±15.0
Race	Cauc 50%, AA 26%, Hisp 16%	Donor Gender (female)	10/37 (27%)
	Asian 2%, Other 6%	Donor Height (cm)	170.9 ±21.2
Recpt HTN	40/50 (80%)	Donor Weight (kg)	76.6 ±16.0
Recpt DM	15/50 (30%)	Cold Ischemic Time (min)	189.0 ±43.0
Recpt HLD	27/50 (54%)	Time from Tx to CMR (yrs)	6.5 ±6.4
Recpt CAD	11/50 (22%)	Prior Grade ≥2 Rejection (#)	10 tot | in 7 pts

Table 1: Recipient demographics and pre-Tx comorbidities (HTN, DM, HLD, CAD) are listed on the left. Donor demographics, cold ischemic time, and prior grade ≥2 rejection are listed on the right. Tx: cardiac transplant. Cauc: Caucasian. AA: African American. Hisp: Hispanic. Recpt: recipient. HTN: hypertension. DM: diabetes mellitus. HLD: hyperlipidemia. CAD: coronary arterial disease.

P106

Systemic vascular resistance is the main determinant of hypertension in pediatric chronic kidney disease

Mun H. Cheang, MBBS[1]Nathaniel Barber, MBBS[1], Grzegorz Kowalik, PhD[1], Steeden Jennifer, MD[1], Kjell Tullus, MBBS[2], Daljit Hothi, MBBS[3], Vivek Muthurangu, MD[1]

1. *Institute of Cardiovascular Science, University College London, England, United Kingdom*
2. *Great Ormond Street Hospital, England, United Kingdom*
3. *Great Ormond Street Hospital , England, United Kingdom*

Background: Cardiovascular (CV) risk is significantly elevated in children with chronic kidney disease (CKD) and one possible cause is hypertension (HTN). Unfortunately, the mechanism of HTN in pediatric CKD is poorly understood and this limits successful therapeutic intervention. Several mechanisms such as altered aortic stiffness, increased vascular resistance and high cardiac output are implicated. However, the relative significance of these mechanisms has previously been difficult to determine. Recent developments in cardiac magnetic resonance imaging (CMR) enable comprehensive assessment of all the components of afterload. The aim of this study is to determine the mechanism of HTN in pediatric CKD through comparison with healthy children and children with essential hypertension.

Methods: 70 children (40 with CKD, 10 with essential hypertension (eHTN) and 20 healthy volunteers (HV)) underwent a CMR study. Aortic flow and cardiac output (CO) was assessed using a high-resolution breath hold spiral phase contrast sequence. Non-invasive measurement of systolic, diastolic and mean blood pressure (SBP, DBP, MBP) was performed simultaneously. Left ventricular (LV) metrics (LV volumes, LV mass, LVEF, Mass Volume ratio (MVR)) were assessed using real-time radial SSFP sequence. Image analysis was performed using in-house plug-ins for OsiriX software. The aortic flow data was combined with blood pressure to calculate systemic vascular resistance (SVR) and total arterial compliance (TAC). Between group comparisons were performed with ANOVA with follow-up pairwise comparison using Duncans method.

Results: Both CKD and eHTN groups had higher SBP, DBP and MBP than HV (table 1). However, the mechanism of HTN was different. The CKD cohort had significantly elevated SVR with normal TAC and CO (table 1). Conversely, the eHTN cohort had a significantly reduced TAC with normal SVR and CO (table 1). There was no difference in LV volumes, EF, or CO between groups. However, there was evidence of LV remodelling with increased LV mass to volume ratio (table 1) in CKD children. On linear regression analysis, CKD and increasing SBP were both independent predictors of MVR (CKD P=0.014, SBP P=0.017). A diagnosis of CKD remained predictive when SBP was replaced with MBP or DBP (CKD P < 0.025).

Conclusions: Our data shows that elevated BP in pediatric CKD is mediated through increased resistance rather than reduced compliance in early renal disease. This novel finding goes against conventional thought and may enable better, more targeted antihypertensive therapy in these children.

Table 1: Comparison of demographics and cardiovascular metrics between groups

P-value	Hypertension patients (n=10)	CKD patients (n=40)	Healthy Volunteer (n=20)	
0.67	12±1.3	12±1.3	12±1.3	Age*(years)
0.97	50%	53%	55%	Sex¶ (% male)
<0.001	121±16§	120±15†	104±10	Systolic BP (mmhg)
<0.001	61±1§	68±1†	53±1	Diastolic BP* (mmhg)
<0.001	87±13§	90±11†	75±6.5	Mean BP (mmhg)
0.002	24±4.3	27±5.7†	21±4.2	SVR (WU.m^2)
0.08	0.48±0.11§	0.56±0.11	0.58±0.13	TAC (ml/mmHg. m^2)
0.53	3.7±1.3	3.4±1.2	3.6±1.2	CO* (ml/m^2)
0.21	52±1.2	55±1.3	49±1.2	LVMI*(g/m^2)
<0.001#	0.78±0.1	0.84±0.16†	0.69±0.11	MVR(g/ml)
0.09	68±7.5	67±10†	73±11	LVEDV (ml/m^2)
0.05	21±3.9	20±5.3†	24±5.3	LVESV (ml/m^2)
0.46#	69±3	70±6	68±4.2	EF (%)

*- Logarithmic transformation was applied (expressed as geometric mean ± geometric standard deviation). #- ANOVA Welch (W) test was used for non-homogenous variance. ¶-Chi-squared test was used. †- P-value <0.05 when CKD compared with HV. §- P-value <0.05 when eHTN compared to HV. Abbreviations: CKD=chronic kidney disease, BP=blood pressure, SBP=systolic BP, DBP=diastolic BP.

P107

Myocardial Fibrosis is Prevalent in Smokers and Associated with Hospitalization for Heart Failure or Death

Yaron Fridman, MD[1] Thomas Treibel, MBBS.MRCP(UK)[2], Peter Kellman, PhD[3], Timothy C. Wong, MD MS[1], Erik B. Schelbert, MD, MS[4]

1. *University of Pittsburgh Medical Center, Pittsburgh, PA*
2. *Barts Heart Centre, England, United Kingdom*
3. *Laboratory of Cardiac Energetics, National Institutes of Health/NHLBI, Bethesda, MD, United States., MD*
4. *University of Pittsburgh; Heart and Vascular Institute of UPMC, PA*

Background: Smoking, an exogenous pollutant, may promote myocardial fibrosis and increase vulnerability to hospitalization for heart failure (HHF) or death. Mechanistically, myocardial fibrosis mediates susceptibility to adverse outcomes by compromising cardiomyocyte energetics through microvascular dysfunction and limiting perfusion reserve (via capillary rarefaction, perivascular fibrosis), increased afterload with systolic and diastolic dysfunction (via myocardial stiffening), and electrical dysfunction (via reentry).

Methods: We quantified cardiovascular magnetic resonance (CMR) measures of extracellular volume fraction (ECV) in 1,674 consecutive enrolled patients referred for CMR without amyloidosis, congenital heart disease, stress cardiomyopathy, or hypertrophic cardiomyopathy, in non-infarcted myocardium, and tracked outcomes prospectively.

Results: Smoking remained associated with higher ECV in linear regression models adjusting for a total of 15 variables capturing demographic, comorbidity, and medication differences (p30) (n=115/233). Over a median of 2.6 years (IQR: 1.4-3.7), 54 smokers had 17 incident hospitalizations for heart failure and 43 deaths. In smokers, ECV was associated with events in multivariable Cox regression models adjusting for age, gender, myocardial infarction, ejection fraction, renal function, and history of CABG; HR: 1.55 (95% CI: 1.15–2.08 per 5% increase in ECV) (p=0.004).

Conclusions: Myocardial fibrosis is prevalent in smokers and associated with hospitalization for heart failure or death. These data further emphasize the potential for environmental pollutants to disrupt myocardial architecture and confer vulnerability to adverse outcomes.

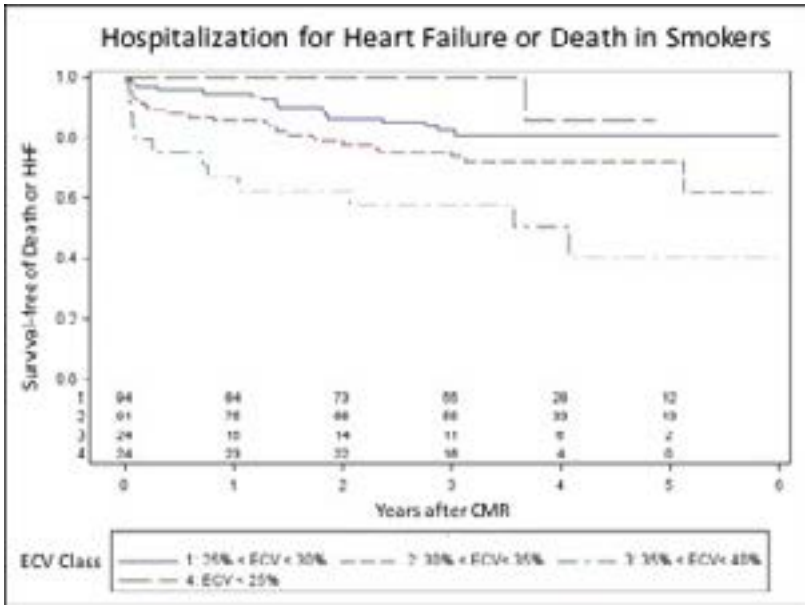

P108

Relationship between myocardial fibrosis and left ventricular functional impairment in diabetes mellitus type-II using T1-mapping technique.

Iacopo Carbone, Medicine[5]Federica Ciolina, Medicine[1], Nicola Galea, Medicine[2], Andrea Fiorelli, Medicine[3], Giulia Le Grazie, Medicine[4], Tiziana Feola, Medicine[3], Marco Francone, Medicine[5]

1. *Policlinico Umberto I, Sapienza University of Rome, Rome, Lazio, Italy*
2. *Policlinico Umberto I, Sapienza University of Rome, Calabria, Italy*
3. *SAPIENZA UNIVERSITA' DI ROMA-POLICLINICO UMBERTO I, Lazio, Italy*
4. *Sapienza University of Rome, Puglia, Italy*
5. *Policlinico Umberto I, Sapienza University of Rome, Lazio, Italy*

Background: Diabetic cardiomyopathy (DCM) can determine a progressive dysfunction of ventricular contraction with the evolution to heart failure, independently of ischaemic heart disease or hypertension. Early stages of DCM are asymptomatic and characterized by various degrees of myocardial fibrosis. Our aim was to detect non-invasively myocardial fibrotic infiltration in DM-II patients and to assess its relationship with ventricular function abnormalities.

Methods: Sixty diabetic patients (42 man and 18 women) with preserved ventricular function and no history of ischaemic disease and 20 matching controls underwent CMR. Imaging protocol included: modified Look-Locker sequence before and 20 minutes after 0.2 mmol/kg gadoterate meglumine injection; T2-mapping; ventricular function module; tagged-cineMR module; late gadolinium enhanced (LGE) imaging. Native myocardial T1 (nT1) and T2 values, extracellular volume fraction (ECV), ventricular torsion angle and myocardial strain values have been calculated and correlated to glycated haemoglobin (HbA1c) and duration of disease. Pearson Correlation, Mann-Whitney test and unpaired T-test were used for statistical analysis.

Results: Patient group had higher nT1 and ECV values compared to controls (1035±94 ms vs. 975±38 ms, 28.2±3.3% vs. 24.8±4.3% respectively, p<0.05 for both), whereas no significant differences occurred in T2 measurements (46.1±2.3ms vs. 47.0±2.8ms respectively, p=0.23). nT1 and ECV correlated with HbA1c (nT1:r2=0.98,ECV:r2=0.95,p<.001) and disease duration (nT1:r2=0.98; ECV:r2=0.55,p<.001) in diabetic patients. nT1 and ECV correlate positively with torsion (nT1:r2=0.98;ECV:r2=0.89;p<.001) and negatively with strain value in tagged-cineMR analysis (nT1:r2=-0.98;ECV:r2=0.92; p<.001). Ischaemic LGE areas were found in four patients as marker of silent infarction.

Conclusions: In diabetic patients with preserved ventricular function, HbA1c values and disease duration are correlated to myocardial nT1 and ECV increase, as reflection of diffuse fibrosis, and geometrical modification.

P109

Cardiac Magnetic Resonance Strain Imaging to Determine Disease Progression in Pulmonary Arterial Hypertension

Jordan C. Ray, MD[1] Elsayed Ibrahim, PhD[2], Brian Shapiro, MD[1]

1. Mayo Clinic, Jacksonville, FL
2. University of Michigan, MI

Background: Pulmonary arterial hypertension (PAH) is a disease of the pulmonary vasculature characterized by increased stiffness secondary to deleterious remodeling. Higher resistance and worsened pulmonary artery (PA) compliance causes disruptions in ventricular-arterial (VA) coupling, leading to excessive afterload and right ventricular (RV) dysfunction.

Methods: 90 patients were prospectively enrolled who received same day right heart catheterization and CMR. Patients with arrhythmia at time of CMR or those with non-group 1 PAH were excluded. Patients were grouped into quartiles based on increasing mean PA pressure (mPAP). CMR was used to calculate RV ejection fraction (EF), PA pulsatility, longitudinal RV strain, and VA coupling calculated as the end-systolic RV volume (ESV) divided by PA stroke volume (SV) obtained by CMR as previously described. Comparisons were made between quartiles and CMR parameters. Normal control subjects were enrolled for comparison.

Results: 78 were included in the study. The median mPAP for quartiles 1-4 were 21, 32, 47 and 61mmHg, respectively. Compared to controls, all patients with PAH had a progressive lower PA pulsatility (Control: 0.53, Q1: 0.46, Q2: 0.21, Q3: 0.15, Q4: 0.17; $p < 0.05$). Median VA coupling ratio progressively increased with quartiles 1-4 (Control: 0.65, Q1: 0.50, Q2: 0.63, Q3: 1.03, Q: 1.26). Significant differences were seen in VA coupling with quartile 3 and 4 but not with quartile 2 as compared to controls ($p < 0.005$). RV strain progressively decreased from quartiles 1 to 4 (Control: 18%, Q1: 18%, Q2: 17%, Q3: 14.5%, Q: 15.5%). Significant differences in RV strain were seen in quartiles 3 and 4 but not 1 and 2 as compared to controls ($p < 0.05$). Median RV ejection fraction was lowest in quartiles 3 and 4 (34% and 37%, respectively) and highest in controls (55%) with no difference in RV EF seen between quartile 1 and controls ($p = 0.38$).

Conclusions: PA pulsatility, or worsened compliance, is the earliest marker of PAH. However, with progression of adverse pulmonary vascular remodeling, worsened VA coupling, and increased RV strain occurred. This data reflects the progression of PAH from a disease of the pulmonary vasculature to poor VA coupling and ultimately RV dysfunction.

P110

Reference Values for Native Myocardial T1 Mapping: Insights from a 101-Chinese Healthy Volunteers Cohort

Jennifer Bryant, MSc, PhD[1]Heerajnarain Bulluck, MBBS[2], Yun Yun Go, MBBS[1], Thu-Thao Le, PhD[1], Ru San Tan, MBBS[3], Hak Chiaw Tang, MBBS, MRCP (UK)[1], Narayan Lath, MBBS, FRCR[4], Adrian Shoen Low, MBBS (Hons), FRCR[4], Calvin Woon-Loong Chin, MD, PhD[1], Stuart Alexander Cook, MBBS, PhD[1], Derek John Hausenloy, MD, PhD[5]

1. *National Heart Centre Singapore, N/A, Singapore*
2. *University College London, England, United Kingdom*
3. *National Heart Centre Singapore; Duke-NUS Medical School, Singapore, N/A, Singapore*
4. *Singapore General Hospital, N/A, Singapore*
5. *The Hatter Cardiovascular Institute, Institute of Cardiovascular Science, University College, N/A, Singapore*

Background: T1 mapping is emerging as a promising cardiovascular magnetic resonance (CMR) biomarker in various myocardial pathologies. However, there are conflicting reports on whether a gender difference exists, and whether adjusting for blood T1 could eliminate this difference. Furthermore, some groups have reported that myocardial T1 increased with age while others have shown a reduction in T1 with age. The aim was to obtain reference values for native myocardial T1 in a healthy cohort of Chinese Singaporeans and explore the interaction with age, gender, heart rate and blood T1.

Methods: 101 healthy volunteers underwent CMR (Siemens Aera 1.5T scanner). All participants were free of cardiovascular disease. A mid-ventricular short axis T1 map (5(3)3) Modified Look Locker Inversion recovery (MOLLI) was acquired. Images were analyzed on CVI42. Manual regions of interest were drawn in the inferior septum and in the blood pool (Figure 1).

Results: The mean age was 46±13 (range 21 to 68) years old and 51/101 (51%) were male. mean myocardial T1 and blood T1 were 1013±27ms and 1618±70ms respectively. Females had significantly higher myocardial T1 and blood T1 than males (1025±26ms versus 1001±23ms, $P < 0.001$; and 1659±60ms versus 1577±54ms, $P < 0.001$ respectively). There was no correlation between myocardial T1 and age. Factors significantly associated with myocardial T1 on univariable analysis (heart rate, gender and blood T1) were included in a multivariable analysis. Gender, blood T1 and heart rate remained significantly associated with myocardial T1 (Table 1). Myocardial T1 adjusted for blood T1 and heart rate was derived using the equation below: Adjusted myocardial T1 = measured myocardial T1 + slope (mean blood T1 – measured blood T1) + slope (mean heart rate – actual heart rate)

The mean adjusted myocardial T1 was 1013±24ms. The gender difference was still present despite adjusting for blood T1 and heart rate (females: 1018±23ms, males: 1008±23ms, $P < 0.0033$) but reduced from a mean difference of 23ms to a mean difference of 10ms after adjusting for blood T1 and heart rate. There was a 12% reduction in the standard deviation (SD) for myocardial T1 in the female cohort only.

Conclusions: Reference values for a Chinese Singaporean cohort of healthy volunteers are presented. Adjusting native myocardial T1 for heart rate and blood T1 only partially reduces the gender interaction, implying that a true biological difference likely exists and therefore reference ranges should be provided for each gender separately. Adjusting the myocardial T1 for heart rate and blood T1 in females reduced the SD of that cohort. This may be important when investigating small changes in the setting of early diffuse interstitial fibrosis.

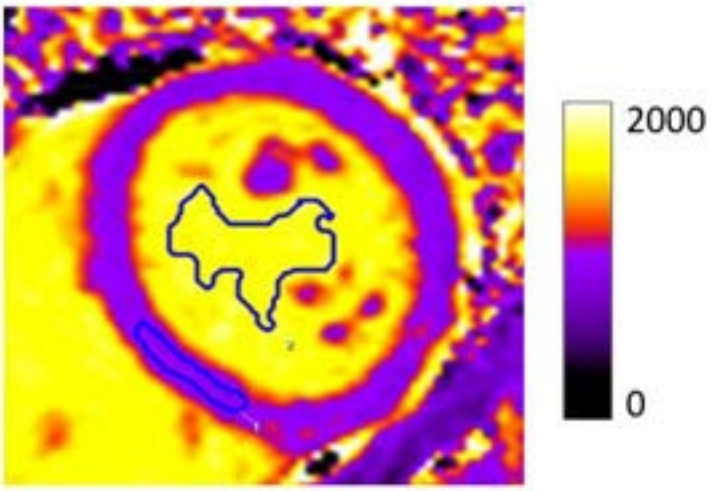

MOLLI T1 map

Multivariable Linear Regression Analysis of Factors Associated with Myocardial T1

Multivariable analysis	Univariable analysis	Correlation with myocardial T1	
P	P	R^2	
0.008	0.001	0.20	Gender
0.009	0.001	0.17	Blood T1
0.003	0.035	0.04	Heart rate
	0.28	0.01	Age

P111

Infarct size by CMR in STEMI patients in clinical cardioprotection studies : what lessons can we learn?

Heerajnarain Bulluck, MBBS[1]Matthew Hammond-Haley, MSc[2], Shane Weinmann, MBBS[2], Roberto Martinez-Macias, MSc[3], Derek Hausenloy, MD, PhD[4]

1. *University College London, England, United Kingdom*
2. *The Hatter Cardiovascular Institute, England, United Kingdom*
3. *The Hatter Cardiovascular Institute, N/A, Mexico*
4. *The Hatter Cardiovascular Institute, Institute of Cardiovascular Science, University College London; Cardiovascular and Metabolic Disorders Program, Duke-National University of Singapore, N/A, Singapore*

Background: CMR is increasingly being used to quantify myocardial infarct (MI) size in randomized controlled trials (RCTs). However, there is significant heterogeneity in trial design with no standardized approach to quantifying MI size. Here, we explore the published RCTs so far and investigate the lessons we can learn from them. Eventually, the aim is to provide guidance to help standardize the use of CMR to quantify MI size in studies investigating novel cardioprotective therapies for limiting MI size in ST-segment elevation myocardial infarction (STEMI) patients treated by primary percutaneous coronary intervention (PPCI).

Methods: We conducted an extensive literature search on Pubmed and Embase to identify all published RCTs using CMR. The inclusion criteria were RCTs that investigated the effects of novel cardioprotective therapies on MI size reduction either as a primary or secondary endpoint and including STEMI patients within 12 hours of symptom onset.

Results: 57 RCTs (9983 patients, published between January 2006 and June 2016) met the inclusion criteria for inclusion. Figure 1 shows the number of RCTs published per year since 2006. There was significant heterogeneity in trial design (Figure 2), but overall the major findings were as follows: The acute CMR scan was most commonly performed at 3 to 5 days, and the follow-up CMR scan at 6 months; the most frequently used gadolinium-based contrast agent (GBCA) were gadopentetate dimeglumine (Gd-DTPA, Magnevist®), gadobutrol (Gadovist®) and gadoterate meglumine (Gd- DOTA, Dorarem®), used in 90% of the RCTs, at a dose of 0.20 mmol/kg and late gadolinium enhancement acquisition starting at 10 minutes onwards; most studies quantified MI size manually, followed by the 5-standard deviation threshold and full-width-half-maximum techniques. Careful patient selection to include those most likely to benefit from a novel cardioprotective therapy for reducing MI size (ischemic time < 6 hours and pre-PPCI TIMI flow 0-1) reduced the sample size by 33-36%. Dropout rates were 9% for RCTs performing acute CMR only; 13% for RCTs performing follow-up CMR only; and 16% for RCTs performing paired acute and follow-up scans.

Conclusions: There is significant heterogeneity in trial design for RCTs using CMR to quantify MI size in STEMI patients. There is a need to standardize the selection of STEMI patients entering RCTs aiming to reduce MI size; the timing for performing CMR; the dose of GBCA and timing of LGE acquisition; and the technique for quantifying MI size in order to optimise the design of future cardioprotection studies.

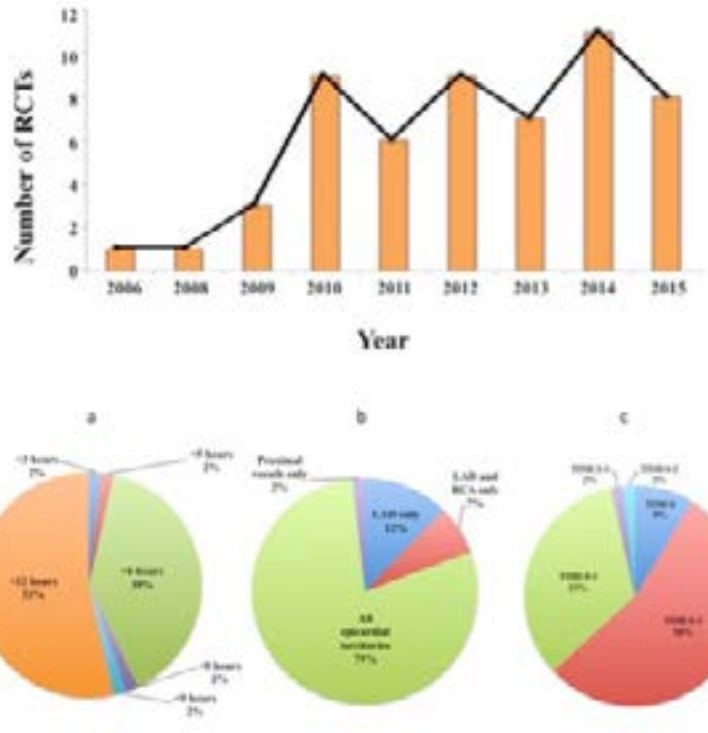

P112

Assessment of Cardiovascular Changes and Correlation with Lung Function in Patients with COPD using Cardiac Magnetic Resonance

Estefania De Garate, MD[1]Giovanni Biglino, MD, PhD[2], Amardeep Ghosh Dastidar, MBBS(Hons), MRCP[1], Anna Baritussio, MD[1], Tamas Erdei, PhD[3], Alessandra Scatteia, MD[4], Iwan Harries, MBBS, MRCP[5], James Dodd, MBCHB, MRCP, PhD[6], Chiara Bucciarelli-Ducci, MD, PhD[1], Amardeep Ghosh Dastidar, MD[7]

1. *NIHR Bristol Cardiovascular Biomedical Research Unit, Bristol, England, United Kingdom*
2. *Bristol Heart Institute, School of Clinical Sciences, University of Bristol, Bristol, England, United Kingdom*
3. *Cardiac MRI Unit, Bristol Heart Institute, Bristol, Bristol, England, United Kingdom*
4. *Division of Cardiology, Ospedale Medico-Chirurgico Accreditato Villa dei Fiori, Acerra, Naples, Italy. Cardiac Magnetic Resonance Unit, NIHR Bristol Cardiovascular Biomedical Research Unit, Bristol Heart Institute, Bristol UK, Naples, Campania, Italy*
5. *NIHR Bristol CVBRU, England, United Kingdom*
6. *University of Bristol, Bristol, England, United Kingdom*
7. *Cardiac Magnetic Resonance Unit, NIHR Bristol Cardiovascular Biomedical Research Unit, Bristol Heart Institute, Bristol UK, England, United Kingdom*

Background: COPD has been associated with increased cardiovascular risk, although the mechanisms for this are still unclear. Proposed theories include increased systemic inflammation and accelerated aging resulting in arterial stiffness and possible cardiac injury. However, there is no data establishing if the process is related to smoking habits or to the obstructive pathology itself.

We aimed to evaluate aortic distensibility, and biventricular functional parameters, using cardiac MRI in patients with COPD, compared to an age-matched non COPD, 'healthy' smoker control group.

Methods: We recruited 49 subjects, of which 27 had diagnosis of COPD and FEV1/FVC Biventricular functional analysis was performed using short axis and long axis SSFP cine images; and included assessment of biventricular volumes, ejection fraction and strain rate.

Aortic distensibility was measured using a validated method that takes in consideration aortic maximal and minimal areas from axial SSFP cine acquired perpendicular to the vessel, and blood pressure values.

Results: Aortic distensibility was reduced in the COPD patients compared to control (0.0022610 X10 -3mm Hg -1 vs 0.004337 X10 -3mm Hg-1, p=0.003). The distensibility of descending aorta was similar in both groups (p= 0.06).
Ejection fraction and biventricular volumes were also similar in the two groups. There was no difference in radial, longitudinal and circumferential strain rate.

Univariate analysis demonstrated a significant relationship between ascending aorta distensibility and FEV1/FVC ratio. There was no difference when comparing distensibility with smoking status or number of packs per year. Linear regression demonstrated that the degree of aortic distensibility was directly proportional to FEV1/FVC ratio

Conclusions: Patients with COPD have significantly increased aortic stiffness measured by cardiac magnetic resonance. This was observed in the presence of normal biventricular ejection fraction and volumes, and didn't affect regional myocardial deformation or left ventricular mass.

This difference was related to FEV1/FVC, and was independent of smoking. Preserved FEV1/FVC showed more elastic ascending aortas. Reduced aortic distensibility could represent the early phase changes in cardiovascular function but further research is needed.

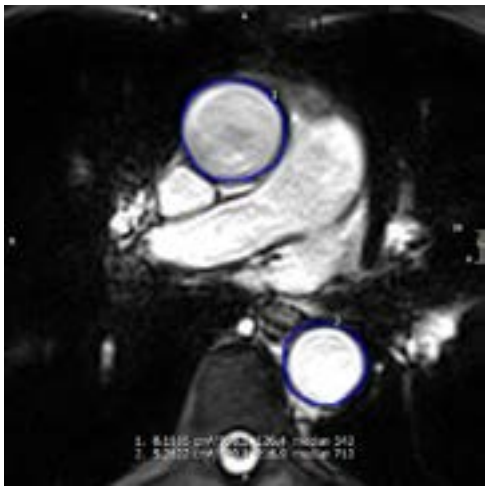

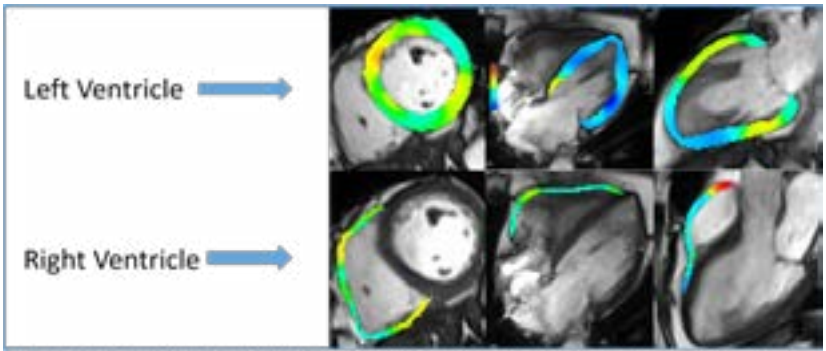

Longitudinal and radial strain of the left ventricle (top row) and right ventricle (bottom row)

P113

Prevalence of Late Gadolinium Enhancement in 53 Middle-Aged, Sub-Elite Athletes

Mustafa A. Altaha, MBBS[1]Jack Goodman, PhD[2], Paul Dorian, MD[2], Laura Jimenez-Juan, MD[3], Djeven P. Deva, MD[2], Vanessa Dizonno, BKin[2], Laura Banks, PhD, RKin[4], Andrew T. Yan, MD[5], Kim Connelly, MD, PhD[6]

1. *Institute of Medical Science, Faculty of Medicine, University of Toronto, Toronto, ON, Canada*
2. *University of Toronto, ON, Canada*
3. *Sunnybrook Health Sciences Centre, Toronto, ON, Canada*
4. *Faculty of Kinesiology and Physical Education, University of Toronto, ON, Canada*
5. *University of Toronto, Toronto, ON, Canada*
6. *St. Michaels Hospital and University of Toronto, Toronto, ON, Canada*

Background: It is not known if years of intensive endurance sports can cause cardiac fibrosis. Previous studies have reported wide variation in the prevalence of late gadolinium enhancement (LGE) in athletic cohorts. We sought to evaluate the presence of ventricular LGE in middle aged (45–65 years) sub-elite endurance-trained, and recreationally-active athletes.

Methods: Fifty-three asymptomatic athletes (males n=39, age: 55.4±5.5 years) were selected from a larger prospective athletic cohort study to undergo cardiac MRI (CMR). All participants had a>10-year history of vigorous exercise, which included: recreational athletes (RA; < 3 hours of exercise/week, n=14) and sub-elite endurance athletes (EA; running, cycling, and triathlon, n=39), with no previous cardiac history. Participants were evaluated for LGE using a standardized 3-Tesla CMR protocol. LGE was assessed using 2D phase-sensitive inversion recovery imaging performed on a short-axis stack from base to apex (~10 minutes) following the administration of 0.2mmol/kg gadolinium. The spatial resolution was ~1.4mmx1.7mmx8mm. CMR images were evaluated for presence of LGE by two experienced cardiologists blinded to clinical and CMR volumetric data (Table), and consensus was reached.

Results: No right ventricular (RV) LGE was noted. Twelve athletes had evidence of left ventricular (LV) LGE (9-EA and 3-RA). Of these, nine athlete had LV-LGE at the inferior RV hinge-point; one showed ischemic LV-LGE with < 25% high intensity at the anterolateral wall; and the remaining two demonstrated non-ischemic LGE (one lateral mid-wall LGE and the other mid-anteroseptal subendocardial LGE). The ventricular volumes of all 53 athletes were increased, consistent with an athletic heart. Further, EA had a significantly higher LV and RV volumes in comparison to RA; LV end-diastolic volume index (EDVi) for EA was 105.2 vs 87.3 for RA, and LV end-systolic volume index (ESVi) for EA was 44 vs 37.7 for RA. Similarly, RV-EDVi for EA was 111.6 vs 91.2 for RA and RV-ESVi for EA was 51.5 vs 42.3 for RA (Table). There were no significant differences between the LGE-positive and negative groups in terms of ventricular volumes and EF, VO2 max, blood pressure, age, or hours of weekly exercise (Table).

Conclusions: In this prospective study of a wide range of long-standing athletes with no known cardiovascular disease, 23% demonstrated LGE. In the majority, LGE was limited to the inferior RV hinge-point; three athletes (6%) had a clinically significant pattern of LV-LGE; yet everyone was asymptomatic. Larger and longitudinal studies are required to determine the true incidence and prognostic implications of LV-LGE in this population.

Table. Athletes' Demographics and Clinical Characteristics

	All Athletes (n=53)	LGE –ve (n=41)	LGE +ve (n=12)	Endurance (n=39)	Recreational (n=14)
Age (years)	55.4 ± 5.5	55.1 ± 5.6	56.5 ± 5.3	55 ± 5.7	56.6 ± 4.8
Sex (male)	74% (n=39)	73% (n=30)	75% (n=9)	77% (n=30)	64% (n=9)
Heart Rate (beats/min)	56.4 ± 8.2	57.3 ± 7.2	54.3 ± 10.4	53.5 ± 6.6	62.1 ± 8.5
Blood Pressure (mm/Hg)	115/74 ± 14/8	115/75 ± 13/8	114/71 ± 17/7	117/75 ± 14/8	112/72 ± 15/7
VO2max (ml/kg/min)	48.1 ± 10.9	48.9 ± 11.9	45.7 ± 6.7	52.6 ± 7.5	37.7 ± 9.2
Current Hours of Weekly Exercise	4.8 ± 3.1	5 ± 3.3	4.2 ± 2.2	5 ± 2.6	4.2 ± 4.4
Life Time Hours of Exercise	20832 ± 17705	20692 ± 19328	21191 ± 11844	19992 ± 11529	23421 ± 30803
Late Gadolinium Enhancement					
LV Ischemic	1.9% (n=1)	0%	8.3% (n=1)	2.6% (n=1)	0%
LV Non-Ischemic	3.8% (n=2)	0%	16.7% (n=2)	5.1% (n=2)	0%
Non-Specific RV hinge-point	17% (n=9)	0%	75% (n=9)	15.4% (n=6)	21% (n=3)
LGE Image Quality					
Good/Excellent	68%	66%	75%	69%	64%
Adequate	32%	34%	25%	31%	36%
Poor	0%	0%	0%	0%	0%
Left Ventricular measurements (indexed)					
End-Diastolic Volume (ml/m^2)	100.4 ± 14.5	100.6 ± 13.9	100.1 ± 17.1	105.2 ± 12.4	87.3 ± 11.7
End-Systolic Volume (ml/m^2)	42.3 ± 6.7	42.4 ± 6.2	42.1 ± 8.5	44 ± 6.3	37.7 ± 5.6
Ejection Fraction (%)	57.9 ± 3.4	57.8 ± 3.4	58 ± 3.6	58.2 ± 3.2	56.8 ± 3.9
Mass (g/m^2)	63.7 ± 11.5	63.9 ± 11.8	62.9 ± 10.7	66.6 ± 10.2	56.1 ± 11.5
Right Ventricular measurements (indexed)					
End-Diastolic Volume (ml/m^2)	106.2 ± 19.5	104.9 ± 17.5	100.4 ± 25.5	111.6 ± 18	91.2 ± 15.5
End-Systolic Volume (ml/m^2)	49.1 ± 11.2	48 ± 9.7	52.7 ± 15.2	51.5 ± 11.2	42.3 ± 8.2
Ejection Fraction (%)	54 ± 3.7	54.4 ± 3.6	55.7 ± 4.2	54.2 ± 3.8	53.7 ± 3.6

Data shown as mean ± SD

P114

CMR Strain Analysis using Feature-Tracking in Children with Transfusion Related Iron Overload

Deepa Prasad, MBBS MD[1]James Strainic, MD[2], Janine Arruda, MD[2], Jacqueline Stuber[3], Ravi Ashwath, MD[2]

1. Boston Children's Hospital, Boton, MA
2. Rainbow Babies and Children's Hospital, OH
3. Case Western School of Medicine, Cleveland Heights, OH

Background: Cardiac dysfunction secondary to iron-overload remains a concern in transfusion-dependent inherited or acquired anemias. Evaluation of T2 star (*) for the detection of myocardial siderosis in this patient population has shown to significantly reduce mortality from iron-overload by effectively using iron chelating agents. We sought to evaluate the utility of CMR-Feature tracking (FT) in the evaluation of ventricular function in transfusion dependent patients with risk of iron-overload cardiomyopathy.

Methods: Patients with transfusion related iron overload, who underwent CMR from 2011-2016 were included in the study. Patients referred for CMR for various reasons and had normal findings served as control group. CMR functional parameters and T2* were recorded. LV and RV global longitudinal, circumferential and radial strain analysis were done using TomTec Cardiac Performance Analysis 2D software , on 4 chamber and short axis images at the mid ventricular level. CMR functional parameters and strain values were also recorded for normal controls.

Results: A total of 58 iron overload patients and 20 controls were included in the study. Mean age was 13.5±4 vs 16±3.5 years in iron overload patients vs controls. Mean RVEF and LVEF in patients with iron overload patients and controls were 55±6.4% vs 56.2 ±4.7% (P=0.26) and 62 ±4 % vs 63 ±4% (P=0.31) respectively. Median T2* was 33 msec (10.7, 49.3). A total of 19% of the patients had T2* < 20 msec. Median RV global radial strain (9.8% vs 15%, P=0.01) and circumferential strain (-11.4% vs -14.3 %, P=0.0006) were significantly lower in iron overload patients when compared to controls. RV longitudinal strain was also lower but did not reach statistical significance. LV global longitudinal, radial and circumferential strain were not different between the 2 groups. T2* showed moderate negative correlation with RV global longitudinal strain (r=-0.4).

Conclusions: This is the first study evaluating the utility of CMR strain using FT in children with transfusion related iron overload. RV strain was lower in iron overload patients when compared to controls. There is limited data to show that RV dysfunction may occur in these patients, secondary to iron overload and possibly pulmonary hypertension. Myocardial strain analysis using CMR-FT can prove to be a sensitive tool for earlier detection of myocardial dysfunction, which allows appropriate management of these patients.

P115

Correlation of Early Markers in Childhood Cancer Survivors

Niti Dham, MD[1]Laura Olivieri, M.D.[1], Aerang Kim, MD, PhD[1], Deneen Heath, MD[2], Christopher Spurney, MD[3], Craig Sable, MD[4], Janet Scheel, MD[5]

1. *Children's National Medical Center, Washington, DC*
2. *Children's National Medical Center, DC*
3. *Children's National Health System, Washington, DC*
4. *Children's National Health Systen, Washington, DC*
5. *Childrens National Medical Center, Ellicott City, MD*

Background: Cardiac related mortality is 10-fold higher among childhood cancer survivors compared to age-matched controls and is the third leading cause of death in this population, after cancer recurrence and secondary malignancy. Higher cardiac MRI (CMR) extracellular volume (ECV), suggestive of early subclinical cardiac injury, including edema, inflammation and fibrosis, can be found early in patients that received anthracyclines, despite having no delayed enhancement on CMR and normal echocardiograms (echo). In this cross-sectional pilot study, we evaluated and correlated serum biomarkers with the echocardiograms and CMR to detect early signs of subclinical cardiac damage.

Methods: Subjects < 25 years old that completed an anthracycline based chemotherapy regimen within the last ten years were included. Each subject had serum biomarkers (myeloperoxidase, ST2, troponin I, and N-terminal brain natriuretic peptide (BNP)), an echo, and a CMR. Analyses for associations between the imaging and serum biomarkers were performed with the Pearson Correlation.

Results: There were 25 subjects, 16 males and 9 females, with a median age of 17 yrs (range 8-21)and median cumulative anthracyline dose of 351 mg/m2 (range 75-450). Subjects demonstrated normal systolic function (EF > 50%) and no evidence of late gadolinium enhancement on CMR. They had normal EF and SF on the echo. Median BNP was 47 (range 1 – 303) and ST2 was 25 (range 16-60). CMR ECV measure correlated with BNP in the apical 4 chamber ($r = 0.63$, $p = 0.003$) and short axis ($r = 0.59$, $p = 0.006$). CMR ECV also correlated with ST2 in the apical 4 chamber ($r = -0.57$, $p = 0.009$) and short axis ($r = -0.63$, $r = 0.003$). Echo derived wall stress correlated with CMR ECV in short axis ($r = -0.54$, $p = 0.01$). CMR ECV did not correlate with echo derived LV size, ejection fraction, shortening fraction, or diastolic function. CMR ECV measures demonstrated an upward trend with cumulative anthracycline dose: 4 chamber ($r = 0.39$, $p = 0.09$) and sagittal ($r = 0.39$, $p = 0.09$). BNP did not correlate with echo derived SF or EF, and there was no correlation between troponin I and myeloperoxidase and the imaging makers.

Conclusions: BNP and ST2 serum biomarkers have the potential to be used for detecting early signs of cardiac toxicity in cancer survivors as a precursor to changes seen in CMR and echo.

P116

Improved Depiction of Cardiac Anatomy Using 4D Flow MRI with k-t GRAPPA Accelerated 3D CINE bSSFP

Kelly Jarvis, MS[1] Bradley Allen, MD[1], Can Wu, PhD[2], Susanne Schnell, PhD[3], Shivraman Giri, PhD[4], Alex J. Barker, PhD[5], Michael Rose, B.S.E[6], James Carr, MD[7], Jeremy D. Collins, MD[3], Joshua D. Robinson, MD[5], Cynthia Rigsby, MD FACR[8], Michael Markl, PhD[3]

1. *Northwestern University, IL*
2. *Philips Healthcare, Bronx, NY*
3. *Northwestern University, Chicago, IL*
4. *Siemens Healthcare, IL*
5. *Northwestern University Feinberg School of Medicine, Chicago, IL*
6. *Ann & Robert H. Lurie Children's Hospital of Chicago, IL*
7. *Northwestern Memorial Hospital, Chicago, IL*
8. *Ann & Robert H Lurie Children's Hospital of Chicago, Chicago, IL*

Background: 4D flow MRI is a promising technique for the comprehensive assessment of cardiovascular anatomy and hemodynamics. However, anatomical 4D flow images (i.e. magnitude images), which are important for assessing cardiac function or as anatomical reference in flow assessment, suffer from the low blood-tissue contrast of 3D RF-spoiled gradient echo imaging. Spatio-temporal generalized autocalibrating partially parallel acquisitions 3D time-resolved balanced steady state free precession imaging (*k-t* GRAPPA accelerated 3D CINE bSSFP) offers improved contrast and can be combined with 4D flow. The aim of this study was to test the hypothesis that combining these techniques can provide a better depiction of cardiovascular anatomy and function with minimal scan time increase.

Methods: Free-breathing *k-t* GRAPPA 3D CINE bSSFP and 4D flow MRI were acquired in 7 patients (3 whole heart, 4 aorta; age=12±5[3-17] years, post-Gd-contrast) and 10 controls (aorta; age=44±18[21-68] years, non-contrast) at 1.5T (Area, Siemens, Germany) (Table 1). 3D CINE bSSFP was acquired with 3 averages to reduce respiratory artifacts and interpolated over time to match 4D flow. A phase contrast MR angiogram was calculated from 4D flow to segment the aorta and pulmonary artery. All data was visualized (Ensight, CEI, USA) in 3D showing standard magnitude images and 3D CINE bSSFP. Videos were prepared showing anatomy and blood flow visualization using pathlines emitted from segmented volumes over one cardiac cycle. A blinded radiologist performed semi-quantitative assessment of image quality. Quantitative assessment of blood-tissue contrast ratio (CR) was performed at one systolic time point and imaging slice.

Results: Visual grading showed improvements with 3D CINE bSSFP (e.g. image quality: patients p=0.048, controls p=0.004), and CR improved for all subjects (patients p=0.016, controls p=0.002) (Table 2, Fig. 1). Joint visualization of anatomy & flow was significantly improved in non-contrast control scans (p=0.018) but not in post-Gd-contrast patient scans (p=0.346). Also, 4D flow magnitude images showed enhanced blood-tissue contrast for post-Gd-contrast versus non-contrast scans ($p < 0.001$). Of note, one patient had a left pulmonary artery stent causing greater susceptibility artifact with 3D CINE bSSFP than 4D flow magnitude. Scan times for 3D CINE bSSFP ranged 1.8-2.6 min.

Conclusions: *k-t* GRAPPA 3D CINE bSSFP provides improved image quality and contrast compared to 4D flow magnitude images while adding only minimal scan time. This improvement is pronounced in non-contrast scans where 4D flow magnitude images have less blood-tissue contrast. Due to the nature of bSSFP imaging, 3D CINE bSSFP has limitations due to field inhomogeneity. This technique is useful for visualizing cardiovascular anatomy and flow. Future work will focus on utilizing this technique to improve vessel segmentation and cardiac functional analysis. ***Grant support by*** AHA 14PRE18620016, NIH R01 HL115828 & K25 HL119608

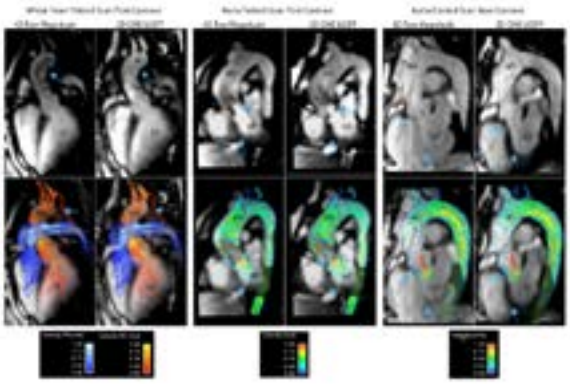

Table 1: Scan Parameters. *k-t 3D CINE bSSFP parameters were matched to 4D flow

Controls - Aorta *k-t* 3D CINE bSSFP MRI	Controls - Aorta 4D flow MRI magnitude	Patients - Aorta *k-t* 3D CINE bSSFP MRI	Patients - Aorta 4D flow MRI magnitude	Patients – Whole Heart *k-t* 3D CINE bSSFP MRI	Patients – Whole Heart 4D flow MRI magnitude	
360-400 x 270-300	360-400 x 270-300	250-400 x 188-275	250-400 x 188-275	250-320 x 125-240	250-320 x 125-240	Field of View [mm^2]*
72	72	54-80	54-80	106-140	106-140	Slab Thickness [mm]*
2.3-2.5 x 2.3-2.5 x 2.4	2.3-2.5 x 2.3-2.5 x 2.4	1.6-2.5 x 1.6-2.5 x 1.8-2.2	1.6-2.5 x 1.6-2.5 x 1.8-2.2	1.6-2.0 x 1.6-2.0 x 1.9-2.2	1.6-2.0 x 1.6-2.0 x 1.9-2.2	Spatial Resolution [mm^3]*
38.4	38.4-39.2	39.6-40.8	35.0-75.6	38.4-40.8	35.0-37.1	Temporal Resolution [ms]
1.6	2.4-2.5	1.6-1.7	2.5-2.8	1.6-1.7	2.5-2.8	Echo Time [ms]
3.2	4.8-4.9	3.3-3.4	5.0-5.4	3.2-3.4	5.0-5.3	Repetition Time [ms]
47-90	7	50-55	15	50	15	Flip Angle [deg]
5	2	5	5	5	5	Acceleration Factor, R
2.6	11.2	1.8	7.1	2.5	16.7	Average Scan Time [min]

Table 2: Results. *p<0.05. LV: left ventricle, VS: Ventricular septum.

Controls			Patients			
Wilcoxon Signed-Rank test P value	*k-t* 3D CINE bSSFP MRI	4D flow MRI magnitude	Wilcoxon Signed-Rank test P value	*k-t* 3D CINE bSSFP MRI	4D flow MRI magnitude	
0.004*	4.0±0.5 [3-5]	2.7±0.5 [2-3]	0.048*	3.9±0.4 [3-4]	3.0±0.6 [2-4]	**Overall image quality** scale: 1 (poor) to 5 (excellent)
0.005*	4.2±0.4 [4-5]	2.6±0.5 [2-3]	0.031*	4.4±0.5 [4-5]	3.3±0.8 [2-4]	**Presence of noise** scale: 1 (non-diagnostic secondary noise) to 5 (little to no appreciable noise)
0.424	3.6±0.5 [3-4]	3.4±0.7 [2-4]	0.345	3.9±0.7 [3-5]	3.4±0.8 [2-4]	**Severity of artifact** scale: 1 (non-diagnostic secondary to artifact) to 5 (no appreciable artifact)
0.018*	4.6±0.5[4-5]	3.7±0.7[3-5]	0.346	4.3±0.5 [4-5]	4.0±0.6 [3-5]	**Joint visualization of anatomy & flow** scale: 1 (poor) to 5 (excellent)
						Vessel wall depiction scale: 1 (poor) to 5 (excellent)
0.048*	3.6±0.7 [3-5]	2.9±0.7[2-4]	0.572	3.3±0.8 [2-4]	3.0±0.8 [2-4]	Sinuses of Valsalva
0.008*	4.0±0.9 [2-5]	2.3±0.7 [1-3]	0.086	3.9±1.1 [2-5]	2.9±1.1 [2-5]	Mid-ascending aorta
0.033*	4.6±0.8 [3-5]	3.5±0.8 [2-5]	0.048*	4.3±0.8 [3-5]	3.4±0.5 [3-4]	Distal arch
0.005*	3.9±0.7 [3-5]	1.5±0.7 [1-3]	0.054	3.4±1.0 [2-5]	2.3±0.8 [1-3]	Left Ventricle
-	-	-	-	3.3±0.6 [3-4]	3.3±0.6 [3-4]	Pulmonary Artery (whole heart only, n=3)
-	-	-	-	4.0±0.0 [4-4]	3.7±0.6 [3-4]	Caval Veins (whole heart only, n=3)
						Blood signal homogeneity scale: 1 (poor) to 5 (excellent)
0.057	3.4±0.5 [3-4]	2.5±0.8 [1-3]	0.120	3.3±0.8 [2-4]	2.6±0.8 [1-3]	Sinuses of Valsalva
0.031*	3.7±0.7 [3-5]	2.8±0.4 [2-3]	0.020*	3.9±0.7 [3-5]	3.0±0.6 [2-4]	Mid-ascending aorta
0.048*	3.4±0.5 [3-4]	2.8±0.8 [2-4]	0.011*	4.4±0.5 [4-5]	3.4±0.5 [3-4]	Distal arch
0.141	2.9±0.7 [2-4]	2.3±0.8 [1-3]	0.120	3.4±0.5 [3-4]	2.7±1.0 [1-4]	Left ventricle
-	-	-	-	2.7±0.6 [2-3]	3.0±1.0 [2-4]	Pulmonary Artery (whole heart only, n=3)
-	-	-	-	3.7±0.6 [3-4]	3.7±0.6 [3-4]	Caval Veins (whole heart only, n=3)
0.002*	0.6±0.1 [0.4,0.8]	-0.1±0.05 [-0.2,-0.1]	0.016*	0.7±0.1 [0.5,0.9]	0.3±0.1 [0.2,0.5]	**Contrast Ratio,** CR=signal_diff (LV-VS)/ signal_mean (LV,VS)

P117

Right Ventricular Strain from Displacement Encoding with Stimulated Echoes CMR is reduced in Overweight and Obese Children

Arichanah Pulenthiran, BS[1]Linyuan Jing, PhD[2], Jonathan D. Suever, PhD[3], Gregory J. Wehner, BS[4], Christopher Nevius, BT[5], Abba Mejia-Spiegeler, LLB[5], Christopher M. Haggerty, PhD[6], Brandon K. Fornwalt, MD, PhD[6]

1. *Geisinger Health System, Export, PA*
2. *Geisinger Health System, State College, PA*
3. *Geisinger Health System, Bellefonte, PA*
4. *University of Kentucky, KY*
5. *Geisinger Health System, Danville, PA*
6. *Geisinger Health System, PA*

Background: Pediatric obesity is a growing public health problem that is associated with increased risk of cardiovascular disease and premature death. Impaired cardiac strains, which are predictive of mortality in other disease states, have been documented in the left ventricle (LV) of obese children. Previous studies have also shown that obese adults generally have increased right ventricular (RV) mass and volumes. While a few studies have reported impaired RV strain in obese adults, no study has quantified RV strain in obese children. We hypothesized that RV strain is impaired in children with obesity, such that higher body mass index (BMI) is associated with lower RV strains.

Methods: Ninety children, ages 8–18 years, were prospectively enrolled. Exclusion criteria included diabetes, diagnosed hypertension, history of heart disease, contraindications for CMR, or a waist circumference greater than 125 cm (due to inability to fit safely within the bore). Subjects were divided into groups based on BMI percentiles, adjusted for age and sex: obese/overweight (BMI≥85th percentile) and healthy weight (5th–85th percentile). Children were also stratified by LV remodeling patterns (normal geometry, eccentric hypertrophy/concentric remodeling, or concentric hypertrophy) using cutoff values from a previous CMR study. All subjects underwent spiral cine displacement encoded (DENSE) CMR on a 3T Siemens Trio. RV free wall longitudinal strain was quantified from the four-chamber (horizontal) long-axis view using the open-source DENSEanalysis application (Fig. 1). Strain was quantified from the end-systolic frame, where the RV wall is thickest and most visible. Data analysis was performed in R, using Pearson correlation and one-way ANOVA with Dunnett post-hoc. Statistical significance was defined as $p < 0.05$.

Results: The RV was sufficiently visualized in 57 subjects (63.3%), comprising 27 healthy weight (13.5±2.5 years) and 30 obese/overweight (11.9±2.7 years) children. RV strain was impaired in obese/overweight children (16±5%) compared to healthy weight controls (18±5%; p=0.01, adjusted for age). BMI z-score was correlated with longitudinal RV strain (r=-0.31, p=0.02; Figure 2). Subjects were sub-divided by observed LV remodeling patterns: 6 (all obese/overweight) had concentric hypertrophy, 8 (5 obese/overweight) had either eccentric hypertrophy or concentric remodeling, and 42 (19 obese/overweight) had normal geometry. ANOVA showed a significant difference in RV strain among LV remodeling patterns (p=0.006). The concentric hypertrophy group had the most impaired strains compared to the group with normal geometry (Fig. 2), but this trend was not statistically significant via post-hoc testing.

Conclusions: Right ventricular longitudinal strain is impaired in overweight and obese children and may be particularly impaired in children with concentric hypertrophy of the LV. Future work is needed to determine the long term implications of these findings.

http://www.ConferenceAbstracts.com/uploads/cfp2/attachments/LDFAIBDN/LDFAIBDN--218611-1-ANY.pdf

http://www.ConferenceAbstracts.com/uploads/cfp2/attachments/LDFAIBDN/LDFAIBDN--218611-2-ANY.pdf

P119

Pulmonary blood volume variation is higher in patients with heart failure compared to healthy controls.

Mariam Al-Mashat, MSc[1]Mikael Kanski, MD, PhD[2], Jonas Jögi, MD, PhD[2], Håkan Arheden, MD, PhD[3]

1. *Lund University, Skåne University Hospital Lund, Lund, Skane Lan, Sweden*
2. *Lund University, Skåne University Hospital Lund, Skane Lan, Sweden*
3. *Lund University, Department of Clinical Sciences Lund, Clinical Physiology, Skane University Hospital, Lund, Sweden, Lund, Skane Lan, Sweden*

Background: The pulmonary venous flow pattern is known to be affected by the elevated left atrial pressure (LAP) in heart failure (HF). This can be seen as a decreased systolic venous flow, or decreased systolic fraction (SF) as measured by echocardiography [1]. Our group has suggested an alternative approach to study the effect of LAP on the pulmonary circulation in HF by quantifying how much the blood volume varies in the lungs (pulmonary blood volume variation, PBVV), using cardiovascular magnetic resonance (CMR) [2]. CMR is gold standard for quantifying blood flow non-invasively. To our knowledge, the SF and PBVV have never been investigated in patients with HF using CMR. Therefore, the aim of this study was to quantify the SF and PBVV in patients with HF and in healthy controls using CMR.

Methods: Twenty-six patients with HF (NYHA I-IV, 66±11 years, 6 women) and ten healthy controls (54±9 years, 7 women) were included. All subjects underwent CMR at 1.5T. The SF was calculated by dividing the systolic venous blood flow with the systolic + early diastolic pulmonary venous blood flow. PBVV was calculated using blood flow in the pulmonary trunk and in one pulmonary vein, and was defined as the maximum cumulative difference in pulmonary blood volume over one heartbeat. PBVV was normalized to stroke volume (SV) derived from the flow measurement in the pulmonary trunk.

Results: Patients with HF had higher PBVV/SV than healthy controls (0.62±0.19 vs 0.41±0.06 p=0.001, Figure 1). No statistically significant difference was seen in SF between patients with HF and healthy controls (0.51±0.24 vs 0.61±0.06, p=0.65, Figure 2).

Patients with NYHA class III-IV exhibited higher PBVV/SV compared to patients with NYHA class I-II (0.75±0.20 vs 0.53±0.15, p=0.01). Furthermore, there was a positive correlation between PBVV/SV and ejection fraction (EF) (p=0.006, R=0.59).

Conclusions: The PBVV/SV is higher in patients with HF compared to healthy controls. NYHA class III-IV, respectively low EF were associated with high PBVV/SV ratio. PBVV/SV, but not SF, could therefore be of value as a non-invasive tool in diagnosing HF severity.

References

1. Kuecherer HF, Muhiudeen IA, Kusumoto FM, Lee E, Moulinier LE, Cahalan MK, Schiller NB. Estimation of mean left atrial pressure from transesophageal pulsed doppler echocardiography of pulmonary venous flow. *Circulation*. 1990;82:1127-1139
2. Kanski M, Arheden H, Wuttge DM, Bozovic G, Hesselstrand R, Ugander M. Pulmonary blood volume indexed to lung volume is reduced in newly diagnosed systemic sclerosis compared to normals--a prospective clinical cardiovascular magnetic resonance study addressing pulmonary vascular changes. *Journal of cardiovascular magnetic resonance*. 2013;15:86

http://www.ConferenceAbstracts.com/uploads/cfp2/attachments/LDFAIBDN/LDFAIBDN--195061-1-ANY.pdf

http://www.ConferenceAbstracts.com/uploads/cfp2/attachments/LDFAIBDN/LDFAIBDN--195061-2-ANY.pdf

P120

CMR Endpoints Show their Merit in Trial of Exercise Therapy in PAD

Jorge A. Gonzalez, M.D.[1] Yan Li, PhD[2], Craig H. Meyer, PhD[3], Frederick H. Epstein, Ph.D.[3], Pelbreton C. Balfour, Jr., MD, ScM[4], Jennifer Kay, BSN[5], Joseph DiMaria, III, BA[3], Arthur Weltman, PhD[4], Brian Annex, MD[4], Christopher M. Kramer, MD[5]

1. *Scripps Clinic Division of Cardiovascular Diseases, La Jolla, CA*
2. *University of Virginia, Charlottesville, VA*
3. *University of Virginia, VA*
4. *University of Virginia Health System, VA*
5. *University of Virginia Health System, Charlottesville, VA*

Background: Exercise slows the progression and improves prognosis of peripheral arterial disease (PAD). Randomized controlled trials show that exercise therapy improves walking performance measures compared to usual care without a change in ankle brachial index (ABI). CMR may help understand mechanisms of this improvement by enabling measures of calf muscle perfusion and energetics.

Methods: Patients with mild-to-moderate PAD (ABI 0.4-0.9) and claudication were recruited to a blinded, randomized trial of home-based exercise therapy vs. usual care. Patients underwent a CMR on a Siemens Trio 3T. At peak exercise (plantar flexion on a MR-compatible ergometer), pulsed arterial spin labeling (ASL) was performed in the calf to measure peak perfusion. Seven control-tagged image pairs were acquired over 60 seconds with single-shot echo-planar imaging readouts (FOV 200x200 mm, matrix 64x64, TR 4000 ms, TE 32 ms, slice thickness 10 mm). Signal averaging and motion correction were performed and relative blood flow maps were calculated online using a single compartment ASL model. After 20 minute rest, exercise was repeated and ^{31}phosphorus spectroscopy (^{31}P MRS) was performed to measure phosphocreatine (PCr) recovery kinetics using a single-pulse, surface coil localized, 512ms free induction decay acquisition. 25 signal averages (TR 550ms) were acquired over 16s per spectrum and 18 spectra were acquired at end exercise. PCr recovery time constant was calculated by monoexponential fit of PCr vs. time. Patients also underwent a 6 minute walk (6MW) and a symptom limited treadmill test (TM) with V02 max measures. They were randomized to home-based exercise (3 d/wk walking to near maximal claudication pain) or usual care. After 12 weeks, all above tests were repeated.

Results: 21 patients were recruited but 5 did not follow-up and thus 16 patients (mean age 69±10, 10 M, ABI 0.67±0.11) completed all visits. Of these, 62% were diabetic, 87% hyperlipidemic, 69% had CAD, and 75% were smokers. The study blind remains unbroken as enrollment is not yet complete. Pre-and post-exercise ABI showed no change. Figure 1 shows ASL images from a patient at baseline and f/u with an increase in perfusion in the anterior tibialis from 23 to 44ml/min/100g. Table 1: Results of CMR data. *p < 0.07 vs. baseline. Table 2: Results of 6MW and TM.

Conclusions: Exercise is known to improve functional performance and outcomes in PAD. In this study of home-based exercise therapy that remains blinded to the investigators, the only change over 12 weeks of therapy was a strong trend towards an improvement in ASL. This is despite no change in ABI or any other objective measures of walking performance. With blinding, it is unclear if the ABI increase occurred in one of the 2 groups. However, ASL is able to detect a change in this size of a patient cohort before a change occurs in ABI or any other endpoint. Thus, exercise ASL measures of calf perfusion may be a useful endpoint in trials of other therapies in PAD.

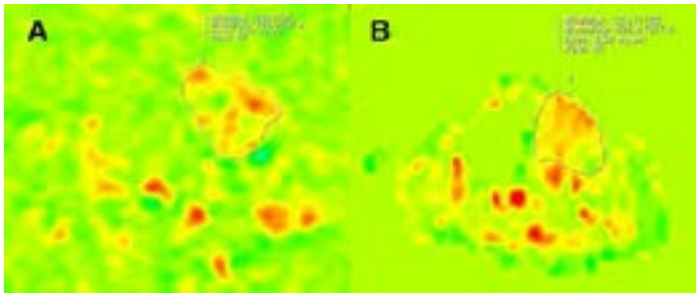

CMR Data

PCr recovery time constant (s)	^{31}P MRS exercise time (s)	ASL (ml/min/100g)	ASL exercise time (s)	
62±65	354±298	26±19	271±157	Baseline
61±48	304±211	38±24*	305±324	Follow-up

Exercise Laboratory Data

METS	$V0_2$ max (ml/min)	TM claudication time (s)	TM exercise time (s)	6MW claudication distance (ft)	6MW distance (ft)	
4.4±1.5	15.3±5.2	222±249	406±317	423±429	1058±408	Baseline
4.0±1.3	14.1±4.6	286±238	517±386	335±290	1107±366	Follow-up

P121

Quantification of Infarct Size in Acute and Chronic Ischemic and Non-Ischemic Heart Diseases: Reproducibility of Different Techniques

Gaetano Nucifora, MD, PhD[6]Jonan Chun Yin. Lee, MRCP(UK), FRCR(UK)[1], Ranjit Shah, MBBS, FRACP[2], Carl Gillebert, MD[3], Emma Smith[4], Joseph Selvanayagam, FRACP, DPhil[5]

1. *South Australian Health and Medical Research Institute, Adelaide, SA, Australia, South Australia, Australia*
2. *South Australian Health and Medical Research Institute, Adelaide, SA, Australia, Prospect, South Australia, Australia*
3. *Flinders Medical Centre, Adelaide, SA, Australia, South Australia, Australia*
4. *Flinders Medical Centre, Adelaide, Australia, South Australia, Australia*
5. *Flinders University, Adelaide, SA, Australia, South Australia, Australia*
6. *South Australian Health and Medical Research Institute, Adelaide, SA, Australia, Darlington, South Australia, Australia*

Background: Several techniques have been proposed for the quantification of late gadolinium enhancement (LGE), a surrogate of myocardial replacement fibrosis or necrosis, including: 1) manual planimetry; 2) manual thresholding; 3) the signal threshold versus reference myocardium technique (STRM) and 4) the full width at half maximum (FWHM) technique. However, uncertainty remains regarding the most reproducible method of LGE quantification in both ischemic and non ischemic heart disease. Intra- and inter-observer reproducibility of LV scar quantification is clinically important, for both prognostication and follow-up purposes. Hence, aim of the present study was to compare the intra- and inter-observer reproducibility of the aforementioned quantification techniques across different disease processes that give rise to LV scar/necrosis, i.e. acute myocardial infarction (AMI), acute myocarditis (AMy), chronic ischemic heart disease (CIHD), hypertrophic cardiomyopathy (HCM) and non-ischaemic dilated cardiomyopathy (NICM).

Methods: A total of100 patients (20 AMI patients, 20 AMy patients, 20 CIHD patients, 20 HCM patients and 20 NICM patients) referred to cardiac magnetic resonance (CMR) with LGE imaging and having visually detectable LGE were included in the study. LGE images were analysed offline (CVI[42], Circle Cardiovascular Imaging, Calgary, Canada) by two independent observers using the following techniques: manual thresholding; STRM-2SD, STRM-3SD, STRM-5SD; FWHM; manual planimetry (this last technique was used for AMI and CIHD patients only). Intra- and inter-observer agreement of each technique was reported using the intraclass correlation coefficient (ICC).

Results: Among AMI patients, all quantitative techniques had excellent intra- and inter-observer agreement (ICC values ≥0.95). Among AMy and CIHD patients, FWHM was the only method that performed well (intra- and inter-observer ICC were 0.96 and 0.92 among AMy patients and 0.95 and 0.93 among the CIHD patients). Among HCM and NICM patients, all quantitative techniques had good intra- and inter-observer agreement (ICC values ≥0.90), except manual thresholding, which had ICC values < 0.90; FWHM presented the highest intra- and inter-observer ICC (0.97 and 0.94, respectively).

Conclusions: The present study provides useful information regarding the reproducibility of quantification techniques across different disease processes that give rise to LV scar. FWHM technique performs well in all cardiac conditions; all STRM techniques represent a valid alternative in AMI, HCM and NICM.

P122

Optimal Dosing of USPIO to Detect Myocardial Inflammation

Caroline Scally, MBChB[1] Trevor Ahearn, PhD[1], Baljit Jagpal, BSc (Hons)[2], Heather M. Wilson, BSc (Hons) PhD[1], Paul Broadhurst, MD[3], Dana Dawson, MD, PhD[1]

1. *University of Aberdeen, Aberdeen, Scotland, United Kingdom*
2. *University of Aberdeen, Dundee, Scotland, United Kingdom*
3. *Aberdeen Royal Infirmary, Aberdeen, Scotland, United Kingdom*

Background: Inflammation is a well-recognized pathway in cardiovascular disease. Ultra-small paramagnetic iron oxide (USPIO) particles are engulfed by activated macrophages and have potential to detect and quantify vascular or myocardial inflammatory processes where macrophages are a prominent feature.

In the current study we explore the optimum dose of USPIO at 3T magnetic field for detecting regional inflammation in the myocardium.

Methods: Fourteen subjects [7 male and 8 female, median age 58.5 years(range 29-68)] were recruited from the Cardiology Healthy Volunteer database. All subjects underwent Cardiac MR imaging on a a 3T Philips scanner (Best, the Netherlands) with standard 2,3 and 4-chamber views and a short axis Cine stack to assess LV function and corresponding multi-gradient echo imaging [Turbo-Field Echo (mTFE)] at baseline and 24 hours following Infusion of Ferumoxytol (Rienso, Takeda, Italy). 10 subjects were infused at a dose of 4mg/kg and 4 subjects at a dose of 2mg/kg. Repeat mTFE was carried out exactly 24 hours after administration of USPIO. Images were analysed using CMRTools (Cardiovascular Solutions, London, UK). Regions of interest were drawn in each of the standard 16 myocardial segments and T2* was measured in each segment from the baseline scan and the post USPIO administration scan. The change in T2*was determined in 3 ways: The absolute difference in T2* values (change in T2*) The absolute difference in T2* divided by the pre-Infusion values (pre-post/pre) The ratio of pre-infusion T2* divided by post infusion T2* (pre/post)

Results: All results are shown as mean ± standard deviation. As seen from the table, there was a significant change in the mean pan-myocardial T2* at the 24 hour time point after administration of USPIO in healthy volunteers at both the 4mg and the 2 mg dose. A significantly higher magnitude of change in T2* was seen after administration of 4 mg compared to 2 mg Ferumoxytol regardless of the area of myocardium studied (apex, mid-cavity or base, $p < 0.05$ for all).

Conclusions: A significant change in T2* is seen 24 hours after USPIO administration in healthy subjects and this change in T2* is dose dependent. Careful dose-adjustment of USPIO is therefore necessary depending on the intensity of the myocardial inflammatory process that requires to be detected.

Table 1: T2* values following USPIO infusion.

Pre/post	Pre-post/pre	Change in T2*	Post Infusion T2*	Pre-infusion T2*	Myocardial Area	Dose of USPIO
1.3±0.1	0.2±0.1	5.4±2.5	19.1±1.8	24.5±2.4	Base	2mg/kg
1.3±0.04	0.2±0.04	4.9±1.3	19.9±1.2	24.8±1.1	Mid	
1.3±0.3	0.2±0.2	5.1±5.8	17.6±1.5	22.8±4.8	Apex	
1.3±0.4$^{\mu}$	0.2±0.2$^{\beta}$	5.2±5.7$^{\alpha}$	19.4±3.9	23.8±3.7	Pan-Myocardial	
1.8±0.3	0.4±0.1	10.5±2.3	13.8±2.6	24.3±2.6	Base	4mg/kg
1.8±0.3	0.4±0.1	11.0±3.7	13.7±2.3	24.7±2.6	Mid	
2.0±0.6	0.5±0.1	9.8±4.4	11.3±2.9	21.1±3.5	Apex	
1.9±0.6$^{\mu}$	0.4±0.2$^{\beta}$	10.4±5.5$^{\alpha}$	12.9±3.5	23.9±9.0	Pan-Myocardial	

α p= 0.00, β p=0.00, μ p+0.00

P123

Assessment of congenital vascular anomalies in people affected by Thalidomide using non-contrast MR-angiography.

Julius Matthias. Weinrich, M.D[1] Lennart Well, M.D[1], Beyer Rudolf, M.D[2], Gunnar Lund, MD[3]

1. Department of Diagnostic and Interventional Radiology, Hamburg, Hamburg, Germany
2. Schön Klinik Hamburg Eilbek, Hamburg, Germany
3. University Medical Center Hamburg-Eppendorg, Hamburg, Germany

Background: Thalidomide, a sedative drug first synthesized in 1953, caused a wide variety of birth defects which led to the death of about 40% of the affected children and multiple malformation in surviving children. Today, about 2,500 grown-up thalidomide receivers still live in Germany. Early post-mortem studies showed multiple cardiovascular birth defects caused by Thalidomide, but there are no current studies examining adult Thalidomide receivers for vascular malformations. The current study analyzed the presence of vascular malformations in adults receiving Thalidomide during embryonically development using non-contrast MR-angiography.

Methods: Non-contrast MR-angiography was performed in 29 Thalidomide receivers (54±0.7 years, 14 men) using a 3T scanner (Ingenia,Philips). Images were obtained by balanced turbo field echo sequences in coronal and sagittal planes. The scan range included the upper aortic branches, abdominal aorta and inguinal vessels. Two observers independently analyzed the MR-scans for vascular and non-vascular malformations.

Results: A total of 30 vascular variants and 5 non-vascular abnormalities were detected in 21 patients (65%). Most vascular variants included the renal system (n=17) and the supraaortic branches (11). These included one sided (n=9) and two sided double renal arteries (n=1), tripled renal arteries (n=1), retroaortic left renal veins (n=3), doubled renal veins (n=2) and bifurcated renal vein (n=1). Truncus bicaroticus (n=4) and left vertebral artery originating directly from the aortic arch (n=4) were the most common supraaortic variations. Two patients showed an elongation of the carotid vessels while one had an aberrant right subclavian artery. Two patients had a double inferior vena cava. Non-vascular abnormalities consisted of pelvic kidneys (n=2; left and right), double kidney (n=1), malrotated kidneys (n=2) gallbladder agenesis and Mayer-Rokitansky-Küster-Hauser syndrome.

Conclusions: We observed vascular abnormalities in 65% of the adult Thalidomide receivers, including some rare malformations. Knowledge about these vascular abnormalities may be important for future medical treatment such as elective operations or vascular interventions.

P124

Stress Cardiac MRI Strain Parameters in the Diagnosis of Perfusion Defects in Pediatrics

Edythe Tham, MBBS[2]Jiali Luan, Bachelor of Science[1], Michelle Noga, MD, FRCP(C)[1], Kumaradevan Punithakumar, PhD[1]

1. University of Alberta, Edmonton, AB, Canada
2. Stollery Children's Hospital, University of Alberta, AB, Canada

Background: Stress perfusion cardiac MRI (CMR) is a non-invasive method of assessing myocardial perfusion, but is largely qualitative. Myocardial strain imaging provides a reproducible method of quantifying myocardial deformation. The objective of this study was to evaluate the diagnostic value of CMR derived strain at rest and stress to detect perfusion defects.

Methods: Nineteen pediatric patients (11.9 ± 4.5 years) underwent CMR perfusion imaging during rest and adenosine stress for the following indications: 4 Kawasaki disease, 5 arterial switch for TGA, 3 heart transplant, 1 LV dysfunction after tetralogy of Fallot repair, 4 post repair of coronary artery anomalies and 2 chest pain. Four chamber cine images were obtained during rest and stress. Longitudinal strain and fractional area change (FAC) were calculated using a semi-automated MRI deformation software developed in-house. The presence of a stress perfusion defect was recorded by a single observer. Ratios (stress/rest) and differences (stress-rest) between stress and rest values were calculated for FAC and maximum strain. Receiver operating characteristic curves (ROC) were generated for each parameter, including the ratios and differences (Table 1). The area under the ROC curve quantifies the effectiveness of the parameter in separating patients with and without perfusion defects. We also determined the optimum threshold values for effective parameters in separating perfusion defect from perfusion normal patients.

Results: Six patients had perfusion abnormalities. The ratio and difference parameters for longitudinal strain separated patients with perfusion defects from those without more effectively than individual rest or stress parameters, showing high sensitivity and good diagnostic accuracy (Table 1). Patients with perfusion defects also had smaller maximum strain difference and ratio calculations compared to those with no perfusion defects. Likewise, FAC difference and ratio parameters were smaller for patients with perfusion defects compared to those without. The optimal threshold values for diagnosing patients with perfusion defects were: strain under stress of >-20.16%, strain ratio of < 1.19 and strain difference of >-2.81.

Conclusions: Ratio and difference parameters for longitudinal strain performed better than individual rest or stress parameters, and may be of discriminatory value in detecting children with perfusion defects. These findings suggests that there is reduced functional reserve in children with perfusion defects. The addition of CMR derived myocardial strain analysis may provide a serial method of quantifying myocardial defects in children with suspected coronary abnormalities.

ROC parameters corresponding to optimal threshold values in assessing left ventricular performance

Accuracy (%)	Specificity (%)	Sensitivity (%)	Area under the curve	
68	77	50	0.58	FAC rest
63	62	67	0.63	FAC stress
63	54	83	0.69	FAC ratio
63	54	83	0.71	FAC difference
58	46	83	0.53	Longitudinal strain at rest
68	69	67	0.69	Longitudinal strain at stress
74	62	100	0.73	Longitudinal strain ratio
68	62	83	0.73	Longitudinal strain difference

FAC=Fractional area change

P125

Quantification of left atrial volume and phasic function using cardiovascular magnetic resonance - Comparison of biplane area-length method and Simpson´s method in transversal slices

Background: Left atrial (LA) enlargement is a marker of chronic diastolic dysfunction and an important predictor of adverse cardiovascular and cerebrovascular outcomes. As a result accurate quantification of left atrial volume (LAV) is needed. In routine clinical cardiovascular magnetic resonance (CMR) the biplane area-length method (Bi-ALM) based on 2- and 4-chamber views (CV) is frequently applied due to timesaving image acquisition and analysis. However, given the various anatomy of the left atrium we hypothesised that results would be different from a precise volumetric assessment of transversal multi-slice cine images using Simpson´s method.

Methods: 31 patients (mean age 70.5 ± 6.2 years, 14 male), status post acute cerebral ischemia, with sinus rhythm during scan received cardiovascular imaging by 3 T CMR. The study protocol included cine SSFP sequences in standard 2- and 4 CV and a stack of contiguous slices in transversal orientation with full coverage of both atria and both ventricles (slice thickness 7 mm). Volumetric analysis was performed with commercially available software (QMass MR, Medis, Leiden, The Netherlands). Total, passive and active LA emptying fraction (LAEF Total, Passive, Active) were calculated from LA maximal volume (LAVmax), minimal volume (LAVmin) and volume prior to atrial contraction (LAVpre-ac) using Bi-ALM and Simpson´s method: LAEF Total= (LAVmax-LAVmin)x100/LAVmax, LAEF Passive= (LAVmax-LAVpre-ac)x100/LAVmax and LAEF Active = (LAVpre-LAVmin)x100%/LAVpre-ac. Results were compared using Bland-Altman-Plots, Wilcoxon signed-rank test and Student´s paired t-test as appropriate. Intra- and Inter-observer variability were assessed in 10 patients.

Results: Significant differences ($p < 0.05$) were found for LA volume and phasic function. The Bi-ALM significantly underestimated LA volume and overestimated LA function in comparison to Simpson´s method (Table 1). LA volumetric and functional parameters were reproducible on an intra- and inter-observer level for both methods. Intra-observer agreement for LA function was better for Simpson´s method (Bi-ALM vs. Simpson´s method; ICC LAEF Total: 0.84 vs. 0.96; ICC LAEF Passive: 0.74 vs. 0.92; ICC LAEF Active: 0.86 vs. 0.89).

Conclusions: The biplane area-length method significantly underestimates LA volume and significantly overestimates LA function in comparison to the evaluation of transversal slices using Simpson´s method. The Bi-ALM bases on geometric assumptions that do not reflect the complex individual LA geometry, which leads to an underestimation of LA volume. The assessment of transversal slices covering the left atrium with Simpson´s method might thus be more suitable for an accurate quantification of LA volume and phasic function.

Table 1: Comparison of biplane area-length and Simpson´s method for left atrial volume and phasic function. Values are given as mean ± standard deviation.

p value	Simpson´s method	Biplane area-length method	
< 0.001	98.8 ± 25.3	80.2 ± 22.9	LAVmax (ml)
< 0.001	50.7 ± 12.7	40.9 ± 10.7	LAVmax/BSA (ml/m²)
< 0.001	80.4 ± 24.0	61.1 ± 18.7	LAVpre-ac (ml)
< 0.001	41.2 ± 11.9	31.0 ± 8.4	LAVpre-ac/BSA (ml/m²)
< 0.001	52.7 ± 20.5	36.9 ± 15.1	LAVmin (ml)
< 0.001	26.9 ± 10.2	18.7 ± 7.4	LAVmin/BSA (ml/m²)
< 0.001	47.9 ± 7.8	55.2 ± 6.6	LAEF Total (%)
< 0.001	19.2 ± 6.1	24.0 ± 8.4	LAEF Passive (%)
< 0.001	35.6 ± 6.8	40.9 ± 7.4	LAEF Active (%)

LAVmax, left atrial maximal volume; LAVpre-ac, left atrial volume before atrial contraction; LAVmin, left atrial minimal volume; BSA, Body surface area; LAEF, left atrial emptying fraction; Italic p values indicate a significance level <0.05 as determined by Wilcoxon signed rank test or Students paired t-test

P126

Reference value of left and right atrial dimension, volume and phasic function by steady state free procession cardiac magnetic resonance imaging at 3.0T in a Chinese healthy adult population

Weihao Li, BMSci[1], Ke Wan, MD[2] Yuchi Han, MD[3], Hong Liu, MS[4], Wei Cheng, BS[5], Jiayu Sun, MD[6], Yong Luo[7], Dan Yang, msci[8], Yiu-Cho Chung, Ph.D.[9], Yucheng Chen, MD[10]

1. *West China Hospital / West China School of Medicine, Sichuan University, Chengdu, Sichuan, China (People's Republic)*
2. *Cardiology Division, West China Hospital, Sichuan University, Guoxue Xiang No. 37, Chengdu, Sichuan Province 610041, China, Sichuan, China (People's Republic)*
3. *University of Pennsylvania, Philadelphia, PA*
4. *Cardiology Department West China Hospital Sichuan University, Chengdu, Sichuan, China (People's Republic)*
5. *West China Hospital Sichuan University, Sichuan, China (People's Republic)*
6. *west china hospital, Sichuan, China (People's Republic)*
7. *Cardiology Department, The Affiliated Hospital of Southwest Medical University, TaiPing Street, NO.25, Luzhou, Sichuan province 646000 P.R.China, Sichuan, China (People's Republic)*
8. *West China Hospital,Sichuan University, Sichuan, China (People's Republic)*
9. *Shenzhen Institutes of Advanced Technology, Chinese Academy of Sciences, Guangdong, China (People's Republic)*
10. *West China Hospital, CHENGDU, Sichuan, China (People's Republic)*

Background: Size and function of left atrium (LA) and right atrium (RA) are closely related with the prognosis of cardiovascular diseases. However, their normal reference measured by cardiac magnetic resonance are still not well investigated, especially in Chinese population. Therefore, the present study sought to provide reference values of LA and RA size and function in a healthy adult Chinese population.

Methods: 135 Chinese healthy ambulatory subjects without cardiovascular disease or risk factors (male 66; female 69, age range 23-83 years) were recruited for this study. All subjects underwent a CMR examination at 3.0T scanner. We imaged the LA and RA using a stack of consecutive short axis slices and long axis (2, 3, 4 chamber and RV 2 chamber) by SSFP sequences. Size and function of LA and RA were measured at short axis or long axis slices. Age and gender difference in LA were further explored.

Results: Normal reference value of LA and RA dimensions, phasic volume and phasic empty fractions (EFs) were provided by short axis method (SAX method) or area length method. Volume and function parameters derived by area length method showed well correlations with the data derived by SAX method, however, area length method significantly underestimated volume either in LA or RA (all $P < 0.01$), whereas overestimated LA EF (all $P < 0.01$). LA and RA dimensions and volumes were significantly larger in male, while these parameters indexed by body surface area (BSA) weakened the gender difference. LA and RA conduit EF and booster EF showed an interesting gender difference ($P < 0.01$). Age was significantly correlated with LA dimensions and volume ($P < 0.01$), and negatively correlated with either LA or RA conduit EF and positively correlated with booster EF.

Conclusions: Normal reference values of left and eight atrial size, function were provided in this Chinese population with wide age range. SAX method is more accurate than area length method in calculation of atrial volume and function. Gender and age have significant impact on atrial size and phasic function.

P127

Inter-study reproducibility of traditional and novel cardiac MRI measures of structure, function and tissue characterization in hemodialysis patients

Matthew P M. Graham-Brown, MBChB (hons), MRCP (UK)[1], Gaurav S. Gulsin, MBChB(Hons) MRCP(UK)[2], Gerald P. McCann, MBChB, MD[3]Daniel Swarbrick, MBBS, BMedSci[3], Eylem Levelt, MBChB, DPhil[3], James O. Burton, MBChB, MD[3]

1. *University Hospitals Leicester, Leicester, England, United Kingdom*
2. *The University of Leicester, Nottingham, England, United Kingdom*
3. *University of Leicester, Leicester, England, United Kingdom*

Background: There is little data on the reproducibility of traditional and novel measures of left ventricular (LV) structure and function with cardiac MRI (CMR) in hemodialysis (HD) patients. HD patients are subject to fluctuations in volume status which affect measurement of LV dimensions and mass when measured with ECHO. We examined the inter-study reproducibility of traditional and novel measures of LV structure and function and the effect of changes in fluid status on peak systolic strain and early diastolic srain rates.

Methods: CMR was performed twice for 10 HD patients (80% male, mean age 57.8years±15, mean dialysis vintage 26±26.2 months) to assess reproducibility of LV mass, EF, LV volumes and global circumferential and longitudinal peak systolic and peak early diastolic strain and strain rates (GCS, GLS, GCSR, GLSR). Changes in LV end-diastolic volume (ΔLVEDV) and changes in weight (Δweight) between scans were used as surrogates of changes in intra-vascular fluid status and the associations between these and changes in strain measurements (ΔGCS, ΔGLS, ΔGCSR, ΔGLSR) between scans were assessed.

Results: Median interval between scans was 7 days. Inter-study reproducibility for all measures are shown in table 1. Bland-Altman analyses showed narrow limits of agreement with no systematic bias for all measures. LVEDV and patient weights were different between scans (mean change LVEDV 11.7ml±8.7, mean change weight 0.5kg±0.5), with a significant correlation between ΔLVEDV and Δweight (r=0.682, P=0.03). There were no associations between ΔGCS, ΔGLS, ΔGCSR, ΔGLSR and either ΔLVEDV or Δweight (r=-0.081, P=0.8, r=0.05, P=0.9, r=0.3, P=0.5, r=0.3, P=0.4 and r=0.2, P=0.7, r=0.05, P=0.9, r=0.3, P=0.3, r=0.3, P=0.6, respectively).

Conclusions: Traditional and novel CMR measures of cardiac structure and function show excellent inter-study reproducibility. Measurements of systolic strain and strain rate were unaffected by changes in markers of intravascular volume and loading status.

Table 1: Inter-study reproducibility of traditional measures of LV structure and function as well as global circumferential and longitudinal systolic strain and strain rates.

Coefficient of Variation	P-Value	Scan 2	Scan 1	Variable
1%	0.64	95.5g±22.7	95.2g±22	LV Mass
1.1%	0.8	54.4%±6.8	54.3%±7	LVEF
5.2%	0.9	138.5±27.8	139.3ml±21	LVEDV
6%	0.8	-21.4%±3.5	-21.7%±4.3	GCS
4.7%	0.34	-17.3%±2.3	-18.05%±3	GLS
7%	0.7	$-124.2\%^{-1}$±33.1	$-126.3\%^{-1}$±41.1	GCSR
10.9%	0.8	-95.7±15	$-94.2\%^{-1}$±23.8	GLSR

P128

Surgical Correction of Fontan using MR-based Computational Fluid Dynamics

Adam Dorfman, MD[1], Carlos Alberto Figueroa, PhD[3]Kevin D. Lau, Ph.D.[1], Jennifer Hirsch-Romano, M.D., MS[2]

1. *University of Michigan, MI*
2. *University of Michigan, Ann Arbor, MI*
3. *University of Michigan & King's College London, MI*

Background: Pulmonary arteriovenous malformations (PAVM) can complicate Fontan palliation. Although detailed mechanisms of PAVM development remain unknown, factors contained within hepatic venous flow (HVF) are involved. Restoring HVF to the pulmonary circulation induces PAVM regression . Successful Fontan revision relies in part on achieving even distribution of HVF between left and right pulmonary circulations. CMR data, with computational fluid dynamics (CFD) can predict HVF distribution in Fontan revision surgery.

Methods: An adolescent female Fontan subject presented with severe PAVM in the right lung. The patient had dextrocardia, interrupted inferior vena cava (IVC), a leftward hepatic vein (HV) to pulmonary artery conduit, and most of her systemic venous return through the azygous vein (AZV). The RPA:LPA flow ratio was 2.1:1, with suspicion that all HVF was directed to the LPA, leading to PAVM in the RPA. Surgical Fontan revision was proposed to achieve a balanced HVF distribution between both lungs. Two alternatives were considered: removing the Fontan conduit from the pulmonary artery and 1) anastomosing the hepatic veins to the distal part of the AZV (Fontan-to-Azygous); 2) extending the conduit to the innominate vein (INV) (Fontan-to-Innominate) (see Figure). Chest CTA and MRA data were used to create a computer model of the local anatomy. PC-MRI data were acquired at conduit, AZV, RPA, SVC and INV. Local pressures were obtained via cardiac catheterization. CFD simulations were run to match the pre-operative data and for each of the two surgical alternatives. Particle tracking techniques were used to examine the RPA:LPA HVF split for each case.

Results: The pre-operative model showed that 100% of the HVF was directed to the LPA. The Fontan-to-Azygous case produced a 80:20 RPA:LPA HVF split. The Fontan-to-Innominate case produced a 70:30 RPA:LPA HVF split. The Fontan-to-Innominate surgical option was subsequently performed. The post-operative angiogram shows a more balanced distribution between the RPA and LPA. At last follow-up, the patient's systemic oxygen saturation has increased from 82% to 91%, and symptoms have improved.

Conclusions: MRI and CFD were used to optimally plan a surgical Fontan revision. Post-operative imaging showed good qualitative agreement with the computer simulation. Early follow-up has shown clinical improvement fitting the predicted physiologic changes. This use of specific patient data with CFD modeling for surgical planning illustrates the potential benefit of clinician-engineer collaboration and the use of CFD to improve the care of individual patients with congenital heart disease.

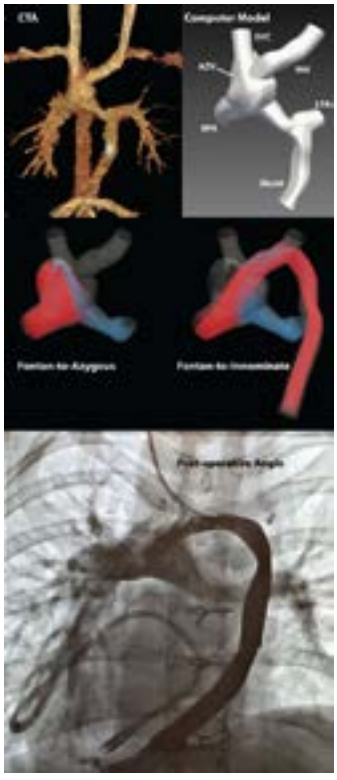

P129

Can Abbreviated CMR Adequately Support Clinical Decision Making After Repair of Tetralogy of Fallot?

Aswathy Vaikom House, MD[1] Vivek Muthurangu, MD[2], Alan Spanel, B.S[3], David Danford, MD[4], Valerie Shostrom, M.S[5], Bilal Mir[6], Andreas Schuster, MD, PhD[7], Howard Hsu, MD[8], Shelby Kutty, MD, PhD[4]

1. *Childrens Hospital and Medical Center, Omaha, University of Nebraska Medical Center, Creighton University, NE*
2. *Institute of Cardiovascular Science, University College London, England, United Kingdom*
3. *University of Nebraska Medical Center, NE*
4. *Childrens's Hospital and Medical Center, University of Nebraska Medical Center, Creighton University, NE*
5. *College of Public Health, University of Nebraska, Omaha, NE*
6. *Heart Imaging Technologies, Durham NC, NC*
7. *University Medical Center Göttingen, N/A, Germany*
8. *University of Nebraska Medical Center, Omaha, NE*

Background: Quantification of pulmonary regurgitation (PR), pulmonary flow distribution and right ventricular (RV) function are important for surveillance in repaired tetralogy of Fallot (TOF). Cardiovascular magnetic resonance (CMR) is the established reference for cardiac assessment, but cost, duration, data redundancy, and patient discomfort during examinations potentially limit serial use. We evaluated whether an abbreviated CMR protocol would impact clinical decisions in TOF.

Methods: All patients >7 years with repaired TOF and complete CMR images on file (1/08 to 1/15) were identified. CMR was performed according to SCMR complete TOF imaging protocol on 1.5T scanner (Philips), and post-processed using QMass-Qflow (Medis). CMRs were prepared in 2 ways (Full and Abbr) and submitted for review by 2 imaging specialists (Imagers) knowledgeable regarding guidelines for TOF care. "Full" included all cines (2, 3,4 chamber, outflow tracts, axial and short axis stacks), black bloods, MR angiogram, 3D isotropic whole heart, multiple Qflows and viability); "Abbr" included only 4 chamber, outflow tracts and short axis stack cines, main and branch pulmonary artery QFlows. Full and Abbr sets were anonymized and uploaded to a secure station (precessionsaas.com). A standardized clinical vignette accompanied each study. For half the cases, Imager 1 received Full and Imager 2 received Abbr sets along with identical case-specific quantitative CMR data (PR fraction, indexed biventricular volumes, ejection fraction, branch pulmonary artery flow) and clinical information (age, surgical and interventional history, symptoms, QRS duration, and results of echocardiogram, stress test, and catheterization hemodynamic data, if any). For the other half, Imager 1 received Abbr, and Imager 2 Full. Blinded to the other's choices, imagers provided clinical decisions (flow chart). Inter-rater agreement for each decision was measured using kappa statistic.

Results: In all, 124 CMR studies performed in 80 patients (53 males, 27 females, mean age 17.8 years) were analyzed. For 'intervention versus no intervention' analysis, the inter-rater agreement was strong (kappa 0.75, $p < 0.0001$, 95% CI (0.630, 0.869). Agreement regarding recommended 'follow-up imaging' was good (kappa 0.64, $p < 0.0001$, 95% CI (0.474, 0.811) in the 'no-intervention' group. Inter-rater agreement was modest for whether 'further imaging necessary' now (kappa 0.363 ($p < 0.0001$), 95% CI (0.038, 0.687).

Conclusions: Abbreviated CMR data yield decisions for clinical care similar to those made using the standard full protocol. These results suggest a potential enhancement of clinical practice in which efficiency and cost saving might be achieved using abbreviated CMR for routine surveillance of repaired TOF.

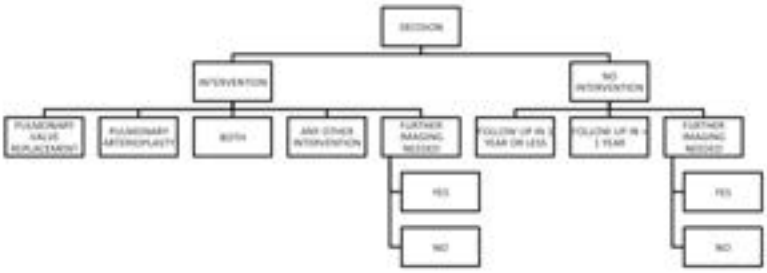

P130

Late gadolinium enhancement in Ebstein anomaly and its association with ventricular function and disease severity

Xiao Li, MD[1] Dan Yang, BMSci[2], Yucheng Chen, MD[3]

1. *Department of Cardiology, West China Hospital, Sichuan University, Chengdu, Sichuan, China (People's Republic)*
2. *Department of Cardiology, West China Hospital, Sichuan University, Sichuan, China (People's Republic)*
3. *West China Hospital, Sichuan University, Sichuan, China (People's Republic)*

Background: Ebstein anomaly is a rare congenital heart disease as well as a myopathy in the right ventricle (RV). Late gadolinium enhancement (LGE) in Ebstein anomaly was only sporadically reported. Its prevalence and clinical association with disease severity is still unclear.

Methods: In this prospective study, 63 patients with unrepaired Ebstein anomaly (age 5 to 70 years; 29 males. Excluding patients with associated lesions other than atrial septal defects) underwent cardiovascular magnetic resonance (CMR) comprising cine and LGE images. Biventricular volume and function was calculated with transverse stacks. Previously reported indices, severity index and total right/left volume index, were used to measure the anatomic severity of Ebstein anomaly. Other clinical data was also included in the analysis.

Results: LGE was found in the endocardium and subendocardium of RV basal septal wall in 14 of the 63 patients (22.2%) (Figure 1). Patients with positive LGE had worse NYHA functional classification, lower biventricular ejection fraction, larger atrialized RV and worse anatomic severity. Other differences between LGE negative and positive groups were shown in Table 1. Multivariate regression identified end-diastolic volume index of atrialized RV independently associated with LGE (P = 0.003; for every 50 ml/m^2, OR = 2.724, 95% confidence interval 1.399 to 5.306).

Conclusions: LGE in RV basal septal wall in patients with Ebstein anomaly is associated with poorer ventricular function and worse disease severity. LGE may play an important role in the natural history of Ebstein anomaly. Further validation is required to determine the mechanism and prognostic value of LGE in Ebstein anomaly.

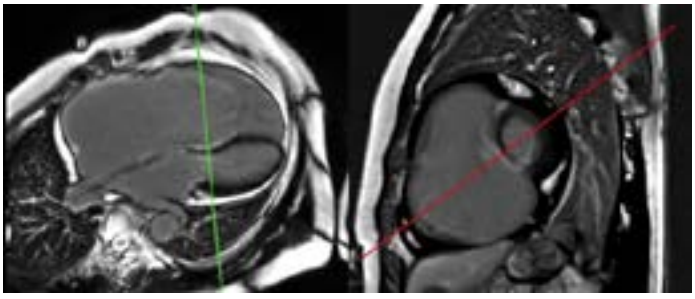

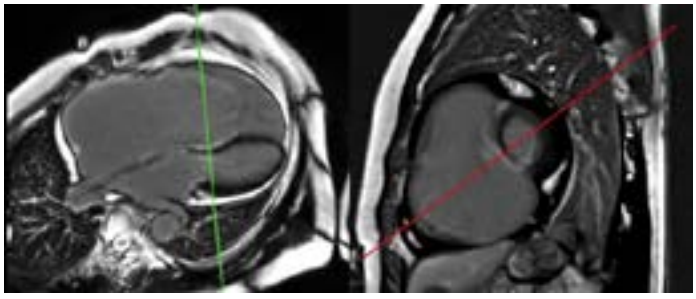

Differences between LGE-negative and LGE-positive groups

P value	LGE positive (N = 14)	LGE negative (N = 49)	
0.268	37.1 ± 15.6	31.2 ± 17.9	Age at study, yrs
0.120	9 (64.3)	20 (48.2)	Male
0.441	22.1 ± 4.5	21.1 ± 4.0	Body mass index, kg/m^2
0.009	2.29 ± 0.61	1.82 ± 0.57	NYHA functional class
0.199	77.9 ± 11.4	82.8 ± 12.5	Heart rate, bpm
0.117	118.6 ± 22.0	110.6 ± 14.7	QRS duration, ms
0.999	10 (71.4)	34 (69.4)	ASD or PFO, %
0.646	2 (14.3)	5 (10.2)	W-P-W, %
0.307	2 (14.3)	3 (6.1)	Atrial flutter/fibrillation
			Tricuspid regurgitation
0.314	2 (14.3)	16 (32.7)	Moderate
	12 (85.7)	33 (67.4)	Severe
0.065	169.4 ± 79.3	131.5 ± 62.8	fRV-EDV index, ml/m^2
0.005	107.6 ± 58.9	69.6 ± 37.2	fRV-ESV index, ml/m^2

0.022	38.9 ± 12.2	46.3 ± 9.8	fRV-EF, %
<0.001	113.5 ± 64.3	59.0 ± 32.9	aRV-EDV index, ml/m^2
0.775	69.3 ± 16.3	67.9 ± 16.4	LV-EDV index ml/m^2
0.220	34.3 ± 9.0	30.7 ± 10.0	LV-ESV index, ml/m^2
0.013	49.1 ± 9.9	54.9 ± 6.6	LV-EF, %
0.002	6.8 ± 5.2	3.6 ± 2.3	Total right/left volume index
0.022	1.1 ± 0.4	0.8 ± 0.3	Severity index

LGE, late gadolinium enhancement; NYHA, New York Heart association; ASD, atrial septal defect; PFO, patent foramen ovale; W-P-W, Wolff-Parkinson-White; fRV, functional RV; EDV, end-diastolic volume; ESV, end-systolic volume; EF, ejection fraction; aRV, atrialized right ventricle.

P value	LGE positive (N = 14)	LGE negative (N = 49)	
0.268	37.1 ± 15.6	31.2 ± 17.9	Age at study, yrs
0.120	9 (64.3)	20 (48.2)	Male
0.441	22.1 ± 4.5	21.1 ± 4.0	Body mass index, kg/m^2
0.009	2.29 ± 0.61	1.82 ± 0.57	NYHA functional class
0.199	77.9 ± 11.4	82.8 ± 12.5	Heart rate, bpm
0.117	118.6 ± 22.0	110.6 ± 14.7	QRS duration, ms
0.999	10 (71.4)	34 (69.4)	ASD or PFO, %
0.646	2 (14.3)	5 (10.2)	W-P-W, %
0.307	2 (14.3)	3 (6.1)	Atrial flutter/fibrillation
			Tricuspid regurgitation
0.314	2 (14.3)	16 (32.7)	Moderate
	12 (85.7)	33 (67.4)	Severe
0.065	169.4 ± 79.3	131.5 ± 62.8	fRV-EDVi, ml/m^2
0.005	107.6 ± 58.9	69.6 ± 37.2	fRV-ESVi, ml/m^2
0.022	38.9 ± 12.2	46.3 ± 9.8	fRV-EF, %
<0.001	113.5 ± 64.3	59.0 ± 32.9	aRV-EDVi, ml/m^2
0.775	69.3 ± 16.3	67.9 ± 16.4	LV-EDVi, ml/m^2
0.220	34.3 ± 9.0	30.7 ± 10.0	LV-ESVi, ml/m^2
0.013	49.1 ± 9.9	54.9 ± 6.6	LV-EF, %
0.002	6.8 ± 5.2	3.6 ± 2.3	Total right/left volume index
0.022	1.1 ± 0.4	0.8 ± 0.3	Severity index

NYHA, New York Heart Association; ASD, atrial septal defect; PFO, patent foramen ovale; W-P-W, Wolff-Parkinson-White symdrome; fRV, functional right ventrile; ESV, end-systolic volume, EDV, the endo-diastole symdrome.

P131

Accurate 3D Prints for RVOT Interventions: A Quantitative Study

Animesh Tandon, MD, MS[1] Rami Hallac, Ph.D[2], Nick Byrne, MPhys, MSc[3], Mari N. Velasco Forte, MD [4], Gerald F. Greil, MD, PhD[1], Tarique Hussain, MD, PhD[5]

1. *UT Southwestern/Children's Medical Center Dallas, Dallas, TX*
2. *Analytical Imaging and Modeling Center, Children's Health, TX*
3. *Guy's and St. Thomas' NHS Foundation Trust / King's College London, England, United Kingdom*
4. *King's College London, London, England, United Kingdom*
5. *Dept. of Pediatrics, UT Southwestern Medical Center, TX*

Background: Three-dimensional printed models (3DPMs) are increasingly used in congenital heart disease for pre-procedural planning, but quantitative data about printer and material accuracy is lacking. We investigated the accuracy of 3DPMs of right ventricular outflow tracts (RVOTs) derived from time-resolved cardiac magnetic resonance angiograms (TR-CMRAs) to better understand printer characteristics.

Methods: TR-CMRAs from 11 patients with RVOT lesions were collected. Images were segmented using Mimics (version 18.0, Materialise) and solid blood pool standard tessellation language (STL) files were created. Each RVOT STL was printed on 2 printers: a Z Corp 650Z (3D Systems) with ZP151 powder material (ZP151) and ZB63 binder; and a Projet 3510HD (3D Systems) with Visijet M3 Crystal (M3C) material. Standard post-processing was performed. The 3DPMs were then CT scanned at 0.5 mm resolution, and resulting DICOM files were resegmented to create derived STL files. The derived STLs were compared to the originals through overall size and geometric disagreement (1-Dice Similarity Coefficient) as a percent of volume. Comparisons were performed using Wilcoxon signed-rank and Kruskal-Wallis testing, with $p < 0.05$ considered significant.

Results: ZP151 models had a significantly larger volume (median 7.0%, IQR 6.3 to 8.3%, p=0.001) and M3C were significantly smaller (-8.8%, -12.5 to -8.4%, p=0.001), compared to the original STLs, and their sizes were significantly different than each other (p=0.001). There was statistically significant geometric disagreement for both models (ZP151 median 7.6%, 6.4 to 8.5%, p=0.001; M3C 9.6%, 9.4 to 12.8%, P=0.001), and was higher in M3C models compared to ZP151 (p=0.001).

Conclusions: 3DPMs may not always accurately represent the underlying patient anatomy, and differences exist as well between different printers. Care must be taken before using 3DPMs for pre-procedural planning in congenital heart disease. More studies to evaluate the consistency of printers, and the ideal method of printing, are required.

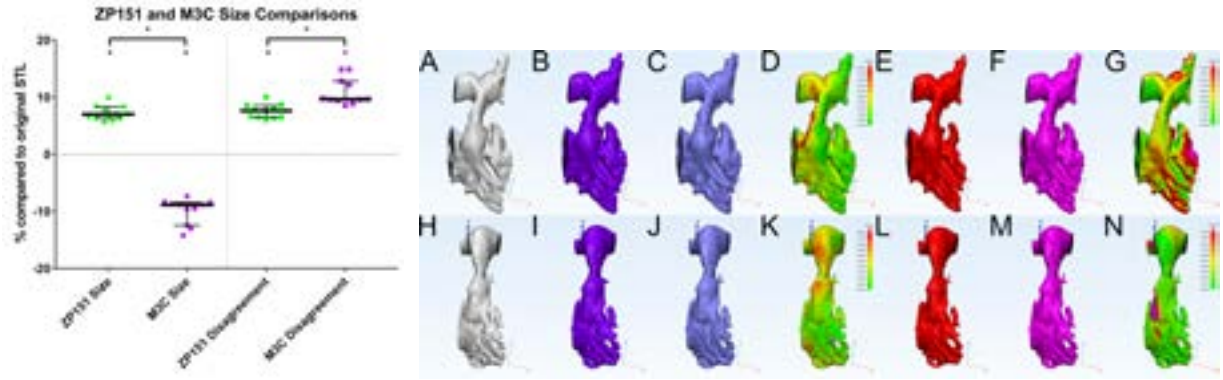

P132

Compressed Sensing real-time cine imaging: Right ventricle evaluation in congenital heart disease.

François Pontana, MD, PhD[1]Julien Pagniez, MD[1], Hedi Farah[1], Benjamin Longere, MD[1], Mathilde Vermersch[1], Valentina Silvestri, MD[1], Michaela Schmidt[2], Christoph Forman, MS[2]

1. Lille University Hospital, Nord-Pas-de-Calais, France
2. SIEMENS HEALTHCARE GmbH, Erlangen, Bayern, Germany

Background: As complex anatomy in congenital heart disease (CHD) often requires extensive CMR examinations, the use of compressed sensing (CS) could significantly reduce acquisition time. The purpose of this study was to evaluate the reliability of CS real-time single-breath-hold cine imaging (Sparse 2D cine, Siemens Healthcare) for quantification of right ventricular (RV) function and volumes in CHD patients in comparison with standard multi-breath-hold cine technique.

Methods: 61 consecutive CHD patients (29 males, 32 females; mean age = 22.2 ± 9.0 years) were evaluated for either initial work-up or following repair (tetralogy of Fallot: n=33, pulmonary atresia with ventricular septal defect: n=7, cardiac shunt: n=7, others: n=14). Single ventricle patients were excluded. For each patient, two series of cine images were systematically acquired: (a) a standard segmented multi-breath-hold steady-state free precession (bSSFP) sequence including short-axis stack, one four-chamber slice, one long-axis slice (Group 1) and (b) an additional real-time CS single-breath-hold prototype sequence (Group 2) providing the same slice number, position and thickness as the reference technique. Two radiologists independently assessed image quality and measured RV volumes and RV ejection fraction (RVEF) for both acquisition techniques.

Results: The mean acquisition time for the CS single-breath-hold sequence was 20.7 ± 4.2 seconds. The image quality of Group 2 was diagnostic in all examinations, mostly rated as good (n= 49/61). There was a high correlation between Group 1 and Group 2 images regarding (a) the RVEF measured 49.8 ± 7.8% vs 48.7 ± 8.6% respectively (r^2 = 0.8877); and (b) the RV end-diastolic volume measured 192.0 ± 61.1 ml vs 193.9 ± 63.3 ml respectively (r^2 = 0.9689).

Conclusions: Compressed sensing real-time cine imaging enables, in one breath-hold, an accurate assessment of RV function and volumes in patients with CHD in comparison with standard SSFP imaging, allowing an improvement in time efficiency and patient comfort.

P133

High prevalence of increased left ventricular myocardial extracellular volume fraction in adult women with coarctation of the aorta

Bengt Johansson, MD, PHD[1]Daniel Rinnström, MD[1], Peder Sörensson, MD, PhD[2], Martin Ugander, MD, PhD[3]

1. *Heart Centre and Department of Public Health and Clinical Medicine, Umeå University, Sweden, Vasterbottens Lan, Sweden*
2. *Karolinska University Hospital, Stockholms Lan, Sweden*
3. *Karolinska Institutet, Stockholms Lan, Sweden*

Background: Left ventricular hypertrophy (LVH) is common among patients with coarctation of the aorta (CoA). Cardiovascular magnetic resonance imaging (MRI) can be used to accurately measure left ventricular mass (LVM), but also the myocardial extracellular volume fraction (ECV), which reflects the degree of diffuse myocardial fibrosis. This study aimed to assess the prevalence of increased ECV and to identify related clinical features in a clinical CoA population.

Methods: Consecutive adult patients with CoA (n=21, age 37±17 years, all ≥ 18 years, 33% female, 86% with prior CoA repair) referred clinically for cardiac MRI were investigated with T1 and ECV mapping. Clinical and echocardiographic data were retrieved from medical records.

Results: Mean ECV was 29.1±3.5% (27.7±2.9% for men versus 31.7±3.1% for women, $p = 0.009$). Mean LVM indexed to body surface area (BSA) was 73±15ml/m^2, and LVM/BSA did not correlate with ECV (r = -0.233, $p = 0.337$). An increased myocardial ECV exceeding the upper normal limit (30.6%) was found in 6/21 (29%) of the patients. Of the patients with increased ECV, 5/6 (83%) were female ($p = 0.002$). Patients with increased ECV did not differ from the rest of the study population in terms of age, age at intervention, blood pressure, or functional parameters such as left ventricular volumes or ejection fraction ($p > 0.05$ for all).

Conclusions: In a consecutive clinical population of adults with CoA, increased myocardial ECV was common, and associated with v female sex, but not with LVM.

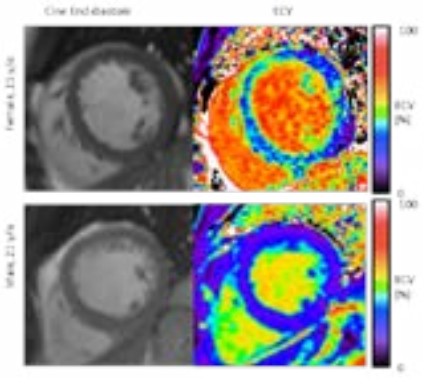

Patient characteristics grouped by extracellular volume (ECV) fraction expressed in percent

t-test for continuous variables, or Chi2-test for nominal variables	ECV > 30.6 %		ECV ≤ 30.6 %		All patients		Variable
p	**% or mean ± SD**	**n**	**% or mean ± SD**	**n**	**% or mean ± SD**	**n**	
General medical demographics							
0.002*	83.3 %	5/6	13.3 %	2/15	33.3 %	7/21	Sex (female)
0.216	29.6 ± 16.5	6	39.4 ± 15.4	15	36.6 ± 16.0	21	Age (years) [1]
0.844	83.3 %	5/6	86.7 %	13/15	85.7 %	18/21	Repaired CoA
0.937	9.1 ± 11.2	5	8.7 ± 9.9	13	8.8 ± 10.0	18	Age at repair (years)
-	-	-	-	-	-	-	Type of repair
0.844	20.0 %	1/5	15.4 %	2/13	16.7 %	3/18	Subclavian flap
0.890	60.0 %	3/5	53.8 %	7/13	55.6 %	10/18	End-to-end anastomosis
0.347	0.0 %	0/5	15.4 %	2/13	11.1 %	2/18	Graft
0.844	20.0 %	1/5	15.4 %	2/13	16.7 %	3/18	Balloon angioplasty with stent implantation

0.861	20.0 %	1/5	23.1 %	3/13	22.2 %	4/18	Reintervention
0.424	3.2	1	26.6 ± 20.4	3	20.7 ± 20.3	4	Age at reintervention (years)
0.255	169.5 ± 9.8	6	175.7 ± 11.4	15	174.0 ± 11.1	21	Height (cm)
0.611	77.5 ± 22.7	6	73.3 ± 14.3	15	74.5 ± 16.6	21	Weight (kg)
0.152	26.6 ± 5.5	6	23.6 ± 3.5	15	24.5 ± 4.3	21	BMI (kg/m^2) [2]
0.098	121.8 ± 30.2	5	145.6 ± 24.7	14	139-3 ± 27.5	19	Systolic BP, arm (mmHg) [3]
0.193	73.8 ± 17.1	5	83.7 ± 12.9	14	81.1 ± 14.4	19	Diastolic BP, arm (mmHg) [3]
0.915	14.6 ± 16.3	6	15.3 ± 13.7	15	15.1 ± 14.1	21	Systolic arm-leg BP gradient (mmHg) [3]
0.477	50.0 %	3/6	66.7 %	10/15	61.9 %	13/21	Arterial hypertension
0.844	16.7 %	1/6	13.3 %	2/15	14.3 %	3/21	Signs of LVH on ECG
0.481	16.7 %	1/6	6.7 %	1/15	9.5 %	2/21	Smoking [4]
Echocardiography							
0.517	0.0 %	0/6	6.7 %	1/15	4.8 %	1/21	Decreased left ventricular function [5]
0.347	0.0 %	0/6	13.3 %	2/15	9.5 %	2/21	Mechanical aortic valve prosthesis [6]
0.890	50.0 %	3/6	46.7 %	7/15	47.6 %	10/21	Bicuspid aortic valve
0.580	2.8 ± 0.6	5	2.6 ± 0.7	13	2.6 ± 0.7	18	Vmax in aorta descendens (m/s)
0.589	31.4 ± 11.9	5	27.6 ± 13.4	13	28.7 ± 12.8	18	Peak gradient over the aortic valve (mmHg)
0.306	50.0 %	3/6	26.7 %	4/15	33.3 %	7/21	Aortic regurgitation [7]
MRI examination							
0.687	181.8 ± 48.2	5	173.6 ± 35.5	15	175.7 ± 37.9	20	LVEDV (ml) [8]
0.662	68.4 ± 16.1	5	72.7 ± 19.6	15	71.6 ± 18.5	20	LVESV[9] (ml) [9]
0.196	61.8 ± 5.4	5	58.5 ± 4.6	15	59.3 ± 4.9	20	EF (%) [10]
0.735	133.2 ± 58.5	5	140.9 ± 36.6	15	138.8 ± 41.7	19	LVM (g) [11]
0.577	70.1 ± 17.5	5	74.5 ± 14.2	14	73.3 ± 14.7	19	LVM/BSA (g/m^2) [12]
0.234	0.7 ± 0.1	5	0.8 ± 0.1	14	0.8 ± 0.1	19	LVMVI (g/ml) [13]

[1]Age denotes age at MRI examination. [2]BMI denotes body mass index. [3]BP denotes blood pressure. [4]No previous smokers were present in the study population. [5]The term decreased left ventricular function only describes mild disease, as no moderate or severe cases were present in the study population. [6]No biological aortic valve prostheses were present in the study population. [7]The term aortic regurgitation includes mild (6 patients) and moderate (1 patient) cases, but no severe. [8]LVEDV denotes left ventricular end-diastolic volume. [9]LVESV denotes left ventricular end systolic volume. [10]EF denotes ejection fraction. [11]LVM denotes left ventricular mass. [12]BSA denotes body surface area. [13]LVMVI denotes left ventricular mass volume index. * denotes $p < 0.05$.

P134

Similar Patterns of Brain Growth and Prevalence of Pre- and Post-Operative Brain Injury in infants with Single Ventricle Physiology and Transposition of Great Arteries

Davide Marini, MD, PhD[1] Jessie Mei Lim, BSc[1], Prashob Porayette, MD[2], Brahmdeep Saini[1], Susan Blaser, MD[3], Lara Leijser, MD[1], Lars Grosse-Wortmann, MD[4], Vann Chau, MD[5], Shi-Joon Yoo, MD[6], Steven Miller, MDCM, MAS[7], Mike Seed, MBBS[8]

1. *The Hospital of Sick Children, ON, Canada*
2. *The Sick Kids Hospital, ON, Canada*
3. *The Hospital of Sick Children, Toronto, ON, Canada*
4. *The Hospital for Sick Children, ON, Canada*
5. *The Hospital for Sick Children and University of Toronto, Toronto, ON, Canada*
6. *Hospital for Sick Children, Toronto, ON, Canada*
7. *The Hospital for Sick Children and the University of Toronto, ON, Canada*
8. *SickKids, Toronto, ON, Canada*

Background: Reduced brain volumes and ischemic injuries are common magnetic resonance imaging (MRI) findings in infants with congenital heart disease (CHD) both before and after surgery. The aim of this study was to investigate the pattern of brain growth and the prevalence of brain injuries in a large cohort of newborns with single ventricle physiology (SVP) and transposition of the great arteries (TGA).

Methods: Between July 2015 and July 2016, 95 consecutive patients with TGA and SVP underwent pre- and/or post-operative brain MRI at the Hospital for Sick Children.

Results: 70% of subjects had both pre- and post-operative imaging. Five patients died following surgery. Pre- and post-operative scans were performed at an age of 6.9 ± 14 days and 7.6 ± 8.7 weeks respectively. At pre-operative MRI there was no difference in term of gestational or postnatal age, birthweight, or APGAR score between the TGA and SVP groups ($p < 0.05$). At pre-operative MRI, brain volume Z-score was smaller in patients with SVP than in patients with TGA ($p=0.014$). There was no difference in the prevalence of stroke, hemorrhage, white matter injury (WMI) or diffuse excessive high signal intensity (DEHSI) between the TGA and SVP groups (Table 1). Between pre- and post-operative MRI mean brain volume Z-score decreased from 0.02 to -0.55 in the TGA group and -0.23 to -0.91 in the SVP group ($p < 0.0005$). The percentage of patients with increased extra-axial cerebro-spinal fluid (CSF) spaces increased significantly at post-operative MRI in the total group and in the SVP group ($p=0.005$ and $p=0.03$ respectively). The prevalence of WMI and punctate hemorrhages increased ($p=0.019$ and $p < 0.0001$) and prevalence of DEHSI decreased ($p=0.013$) between the pre- and post-operative scans in both groups.

Conclusions: In this MRI study of peri-operative brain development and injury in newborns with CHD, the prevalence of pre- and post-operative brain injury was similar in subjects with SVP and TGA. In both groups, the prevalence of WMI and hemorrhage increased between the pre- and post-operative scan, while normalized brain volume decreased, in keeping with a pattern of incremental injury and impaired growth and/or volume loss.

P135

Preserved Myocardial Deformation after Coarctation Repair, a CMR Feature Tracking Study.

Elles J. Dijkema, Bsc[1] Tim Leiner, MD, PhD[2], Heynric Grotenhuis, MD, PhD[3]

1. *UMC Utrecht, Utrecht, Utrecht, Netherlands*
2. *Utrecht University Medical Center, Utrecht, Utrecht, Netherlands*
3. *Wilhelmina Children's Hospital, Bilthoven, Utrecht, Netherlands*

Background: Patients with coarctation of the aorta (CoA) have a reduced life expectancy and increased risk for cardiovascular complications later in life, despite adequate and timely repair. Frequently described arterial vasculopathy and hypertension in CoA-patients are associated with increased left ventricular (LV) afterload, which may lead to coronary disease and LV dysfunction related to adverse ventriculo-arterial coupling. Quantification of myocardial deformation with CMR feature-tracking (FT) provides insight in global and regional LV function, and is correlated to cardiovascular outcome. This study aimed to investigate potential differences in LV myocardial deformation between well-repaired CoA-patients and healthy controls.

Methods: Twenty-two well-repaired (no signs of obstruction, arm-leg blood pressure gradient < 20mmHg) CoA patients (age 30±10.6 years) after surgical repair(12) or balloon angioplasty(10) (at 0.3-16 years) with >10 years of follow-up were compared to 22 healthy matched controls (age 30±3.8 years). Five CoA patients had been treated for re-CoA. LV longitudinal-, circumferential-, radial- and rotational deformation indices were derived using CMR-FT.

Results: Global systolic LV function was preserved (LV ejection fraction 58±4.8 vs 60±6.8%, p=0.56) in CoA patients with normal indexed LV end-diastolic volume (81±16.7 vs 77±14.7ml/m^2, p=0.50), LV end-systolic volume (26±7.0 vs 31±7.3ml/m^2, p=0.05) and LV mass (69±8.6 vs 65±9.2g/m^2, p=0.23). Twelve CoA patients (55%) were hypertensive. LV global longitudinal strain was preserved in the horizontal (-18±4.4 vs -16±4.7%, p=0.06) and vertical (-22±5.1 vs -20±6.0%, p=0.22) long axis in CoA patients compared to controls. Global circumferential strain was preserved at basal (-29±4.1 vs -28±4.8%, p=0.43), mid-ventricular (-27±4.2 vs -25±3.0%, p=0.09) and apical levels (-35±7.8 vs -32±34.9%, p=0.32). Basal radial strain was preserved (34±12.8 vs 32±11.6 %, p=0.59), whereas mid-ventricular and apical radial strain were increased (42±10.2 vs 35±8.0%, p=0.04, and 35±12.4 vs 28±11.6%, p=0.04). Segmental increase of circumferential strain was seen in the basal anterior (-28±10.1 vs -21±9.6%, p=0.03) and the mid posterior (-23±6.3 vs -27±7.3%, p=0.04) segments when compared to controls. No significant differences were found in global torsion (2.4±1.3 vs 2.0±1.4°/cm, p=0.28), twist (14±5.8 vs 12±6.3°, p=0.34) and recoil rate (-17±9.7 vs -17±7.1°/cm/s, p=0.97). Analysis of intra-observer variability demonstrated good reproducibility for all deformation indices.

Conclusions: Global and regional myocardial deformation indices are preserved in well-repaired CoA patients long-term after repair, and do not explain the impaired cardiovascular outcome in CoA patients.

P136

Patient-specific Modeling of Cardiac Biomechanics in Repaired Tetralogy of Fallot

Sanjeet R. Hegde, MD, PhD[5]Nickolas Forsch, B.S.[1], Cherilyn Go, M.S.[2], Alistair Young, PhD[3], Andrew D. McCulloch, PhD[4], Jeff Omens, PhD[4], James C. Perry, MD[5]

1. *UC San Diego, San Diego, CA*
2. *UC San Diego, Hayward, CA*
3. *The University of Auckland, New Zealand, GRAFTON, Auckland, New Zealand*
4. *UC San Diego, La Jolla, CA*
5. *UC San Diego/Rady Children's Hospital, San Diego, CA*

Background: Tetralogy of Fallot (TOF) is the most common cyanotic congenital heart disease in children and accounts for about 10% of all congenital cardiac malformations. Surgical advancements in the management of TOF have allowed individuals to survive into adulthood, however, most of them develop pulmonary regurgitation (PR), causing right ventricular (RV) volume overload, dilatation, and possible dysfunction. The strategy for preserving RV function often relies on surgical or transcatheter pulmonary valve replacement (PVR), the timing of which is guided by indicators such as RV end-diastolic volume index (RVEDVI) greater than 150 mL/m^2. Although PVR is an unavoidable operation for most repaired TOF patients, it is not always effective in normalizing RV size and function. The goal of this preliminary study is to find quantitative measures in addition to RV volume that correlate with the degree of reverse remodeling in response to PVR.

Methods: Bi-ventricular image-based computational models were developed using cardiac magnetic resonance images (cMRI) and clinical data of a single patient with repaired TOF who had a surgical PVR due to severe pulmonary regurgitation and right ventricular dilatation. Full beat simulations of two different models, one with a high RVEDVI (170 mL/m^2) and one with a low RVEDVI (115 mL/m^2) at time of PVR, were run under conditions representing before and after PVR. Mean values of end-diastolic fiber strains, indicating muscle fiber lengthening due to diastolic loading, were calculated in the right ventricular free wall (RVFW) for all simulations.

Results: Table 1 shows a summary of steady-state cardiac measurements from the patient data and the two models with different RVEDVI. Both models were able to produce a decrease in RVEDV, decrease in RV cardiac output, increase in LV preload, and observation of isovolumic contraction and relaxation in response to virtual PVR. Figure 1 shows the difference in the post-PVR magnitudes of the regional diastolic fiber strain. The relative comparison of the post-PVR regional diastolic fiber strain in the two models suggests that post-PVR fiber strain in the model with lower RVEDVI at time of PVR is greater in RVFW regions closest to the septum.

Conclusions: A preliminary study of two computational models of biomechanics in a repaired TOF patient shows regional RVFW diastolic fiber strain generally decreases after PVR, and the magnitudes of post-PVR diastolicfiber strain in RVFW regions near the septal wall were relatively lower in the model with a higher RVEDVI at time of PVR. This result suggests that RV reverse remodeling may be more likely to occur in regions of the RVFW near the septal wall, and that the degree of reverse remodeling may be greater in patients with greater RVEDVIs at the time of PVR. Patient-specific modeling of the RV has the potential to improve outcomes in children with TOF by predicting optimal volumes to pursue PVR and identifying other biomarkers that associate with clinical endpoints.

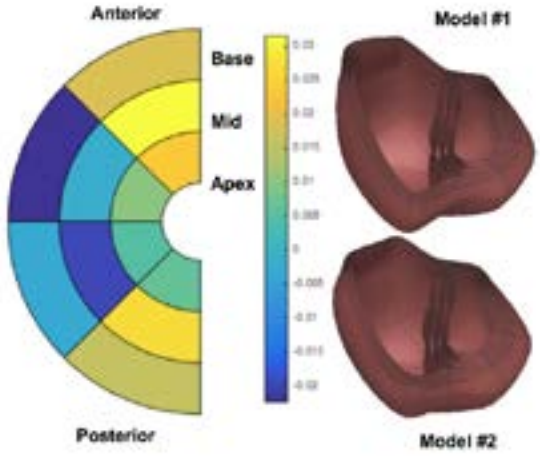

Table 1: Summary Table of Steady-State Cardiac Measurements

Model #2		Model#1		Patient	
Post-PVR	Pre-PVR	Post-PVR	Pre-PVR	Pre-PVR	
120	111	126	120	109	LVEDV (mL)
61	61	58	58	37.7	LVESV (mL)
6.0	5.1	6.9	6.3	7.3	LV CO (L/min)
82 / 17	82 / 15	86 / 25	86 / 22	108* / 15*	LVESP / LVEDP (mmHg)
204	223	263	306	316.6	RVEDV (mL)
118	118	182	181	130.6	RVESV (mL)
8.8	10.7	8.2	12.8	19	RV CO (L/min)
17 / 6	17 / 13	25 / 6	25 / 12	32* / 10*	RVESP / RVEDP (mmHg)
0%	58%	0%	50%	58%	PR fraction
-	115	-	170	174.9	RVEDVI (mL/m^2)
0.060	0.063	0.047	0.056	-	Mean (+) RVFW fiber strain

*Data estimated from another repaired TOF patient

P137

Degree of agreement between aortic root measurements by cardiac MRI and 2D-echocardiogram in patients with repaired tetralogy of Fallot

Sushitha Surendran, MD[1] Ronak Naik, MD[1], Mehmet Kocak, PhD[2], Jason N. Johnson, MD MHS[1]

1. LeBonheur Children's Hospital, University of Tennessee Health Sciences Center, Memphis, TN
2. University of Tennessee Health Sciences Center, Memphis, TN

Background: Echocardiogram (2DE) has been traditionally used in evaluating the aortic root in patients with tetralogy of Fallot (TOF). Cardiac magnetic resonance (CMR) is being used more often to collect 3D data and reliably measure ventricular volumes. Both modalities have multiple methods to measure the aortic root. We designed a study to evaluate an agreement between 2DE and CMR, and between the different modalities in CMR in order to find a consistent method of measurement.

Methods: A retrospective review was performed on 2DE and CMR obtained 6 months apart from 2009-2015 on patients with repaired TOF. On 2DE the aortic root was measured at sinus of Valsalva (SOV) in peak systole from inner-inner edge (IIE), leading-leading edge (LLE) and outer-outer edge (OOE). CMR measurements were made at the level of SOV from angiogram (bolus triggered, breath held, and non-ECG gated), 3D steady state free precession (SSFP) (cusp to commisure smallest, middle, and largest) and cine SSFP (IIE, LLE, OOE). A pairwise comparison from sets of measurements from 2DE and CMR was performed. Pairs were tested for non-zero difference with Bland Altman plot. Linear modelling and ANOVA were used to test linear association and correlation between the pairs.

Results: A total of 67 patients were included in the study, 45 (67%) male and 22 (33%) females. The mean age at CMR and 2DE was 13.7±6.9 years. The best agreement was obtained between 2DE SOV IIE (mean 29.7±6.3mm) and cine SSFP SOV IIE (mean 29.5±6.1mm) with a mean difference of 0mm (p=0.99), slope estimate of 1.0 (p=0.4) and high correlation (R^2 0.89). The 2DE SOV IIE measurement also had good correlation with the CMR SOV angio largest measurement (mean 29.7±6.2mm) with a mean difference of 0.35mm (p=0.23), slope estimate of 1 (p=0.06) and high correlation (R^2 0.86). Among the CMR only measurements, the best agreement was obtained between cine SSFP SOV IIE and 3D SSFP largest (mean 30.1±5mm) with a mean difference of 0.02mm (p=0.93), slope estimate of 1.0 (p=0.97) and high correlation (R^2 0.9). Indexing to body surface area did not change the degree of agreement.

Conclusions: IIE aortic root measurement on 2DE has good agreement with CMR IIE cine SSFP and SOV angiogram measurements in patients with repaired TOF. Aortic root measurement by 2DE and CMR cine SSFP and SOV angiogram may be utilized as a universal method of measurement and reporting in repaired TOF.

P138

4D flow CMR in assessment of neo-aortic root dilatation after the arterial switch operation

Milou P.M. van Poppel, MD[1] Sebastiaan W.H. van Wijk, MD[2], Jos J.M. Westenberg, PhD[3], Rob J. van der Geest, PhD[4], Hans M.P.J. Breur, MD, PhD[2], Tim Leiner, MD, PhD[5], Heynric Grotenhuis, MD, PhD[6]

1. *Wilhelmina Children's Hospital, Utrecht, the Netherlands, Utrecht, Utrecht, Netherlands*
2. *Wilhelmina Children's Hospital, Utrecht, the Netherlands, Utrecht, Netherlands*
3. *Department of Radiology, Leiden University Medical Center, Leiden, The Netherlands, Leiden, Zuid-Holland, Netherlands*
4. *Department of Radiology, Leiden University Medical Center, The Netherlands, Leiden, Zuid-Holland, Netherlands*
5. *Utrecht University Medical Center, Utrecht, Utrecht, Netherlands*
6. *Wilhelmina Children's Hospital, Bilthoven, Utrecht, Netherlands*

Background: Neo-aortic root dilatation, a common complication after the arterial switch operation (ASO) for transposition of the great arteries (TGA), could theoretically be related to the changed geometric and hemodynamic characteristics of the reconstructed left ventricular outflow tract (LVOT) after ASO. The aim of this study was to determine if geometric characteristics of the LVOT and related blood flow patterns are associated with neo-aortic root dilatation by using four-dimensional (4D) flow cardiovascular magnetic resonance (CMR) and cardiovascular computed tomography (CCT).

Methods: The study cohort consisted of 59 TGA patients who underwent ASO between 1978 and 2001. The following neo-aortic root measurements were performed using CCT: (1) surface area of aortic valve annulus indexed by *Z-score*, (2) surface area at level of aortic root sinuses indexed by *Z-score* and (3) spatial relationship between aortic root and pulmonary trunk in the transverse plane. (4D flow) CMR was used to assess (4) the geometric relationship between LV and ascending aorta, expressed by 4 angles between the LV and LVOT as seen in Figure 1 and (5) degree of flow eccentricity by measuring the angle between peak systolic flow direction and aortic valve annulus (Figure 2). Correlations were determined using Pearson's correlation coefficient.

Results: Neo-aortic root dimensions were increased in TGA patients (mean±SD for *Z-score* annulus: 2.98±1.60, *Z-score* sinus of Valsalva: 2.43±1.41). Neo-aortic root dimensions were not correlated with any of the four angles as described (4) ($r < 0.06$, $p>0.05$), nor to the spatial relationship between aortic root and pulmonary trunk (3) ($r=-0.20$, $p=0.14$) or flow eccentricity (5) ($r=0.04$, $p=0.79$). Patients with pre-operative ventricular septal defect (VSD) (n=16, 27%) had similar aortic root dimensions as patients without, and the presence of pre-operative VSD was not correlated with aortic root dilatation. ASO patients demonstrated good ventricular systolic function (mean LVEF 56.8% (95% CI[55.3, 58.3])).

Conclusions: Frequent neo-aortic root dilatation in TGA patients is not related to the geometric characteristics of the LVOT after ASO, nor to the pre-operative presence of a VSD. Neo-aortic root dilatation is likely to be explained by other factors like abnormal aorticopulmonary septation and surgical manipulations.

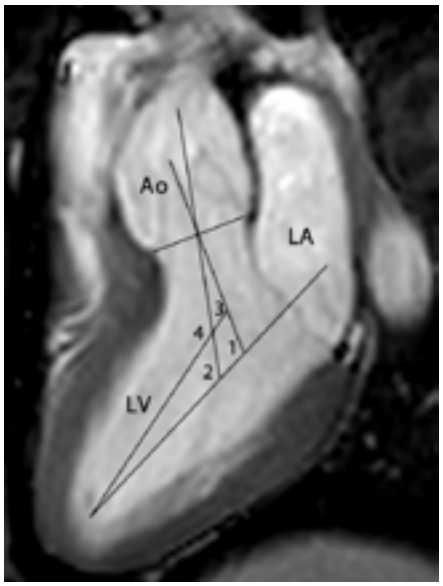

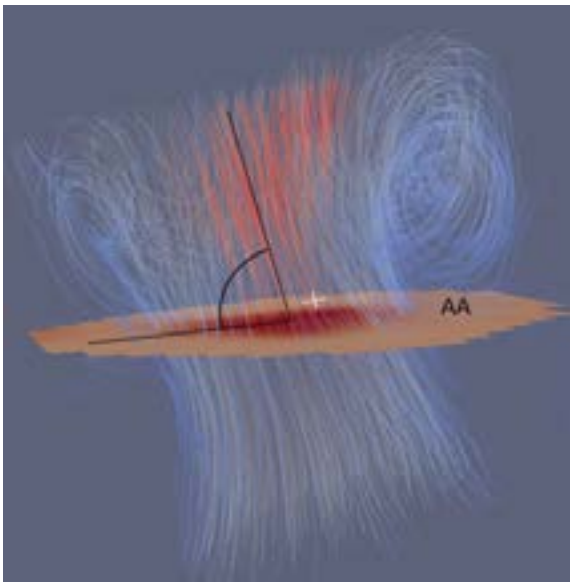

P139

Ventricular volume assessment in Congenital Heart Disease using k-t BLAST Cine SSFP

Srinivas Ananth Narayan, MD, MRCPCH[1] Tiina Ojala, MD, PhD[2], Saravanan Durairaj, MRCPCH[3], Mari Nieves Velasco Forte, MD[4], Sujeev Mathur, MD[5], Israel Valverde, MD PhD[6], Aaron Bell, MB.ChB[7], Kuberan Pushparajah, MD [8], Markus Henningsson, PhD[1]

1. *King's College London, England, United Kingdom*
2. *Helsinki University Central Hospital, N/A, Finland*
3. *Glenfield Hospital, Leicester, England, United Kingdom*
4. *Kings College London, England, United Kingdom*
5. *Guy's & St Thomas' Hospital NHS Foundation Trust, England, United Kingdom*
6. *Hospital Universitario Virgen del Rocío Sevilla, Spain, England, United Kingdom*
7. *Guy's & St Thomas' Hospital NHS Foundation Trust, London, England, United Kingdom*
8. *Guy's & St Thomas' Hospital NHS Foundation Trust, Evelina London Children's Hospital, England, United Kingdom*

Background: Cardiac MRI is currently the most accurate practical tool for assessment of ventricular volumes and function in Congenital Cardiology. However, low spatiotemporal resolution hampers acquisition at fast heart rates, respiratory motion and inability to breath-hold consistently, in children with congenital heart disease. Since the last few years, techniques like k-t BLAST (broad-use linear acquisition speed-up technique), which permit acquisition of a reduced amount of data and recovery of the missing part of the data by well-defined algorithms, has been used and reported to be useful in many clinical studies. Most of these studies relate to assessment of cardiac function in the non-congenital heart disease. The purpose of this study was to compare ventricular volumes in patients with congenital heart disease obtained by k-t BLAST accelerated single breath-hold three-dimensional cine b-SSFP (balanced steady-state free precession gradient echo) with current standard multiple-breath-hold M2D cine b-SSFP (2D-cine) stack (Parameters in Table 1).

Methods: Patients with congenital heart disease who were undergoing cardiac MRI for clinical indications were included in the study, after obtaining informed consent. Immediately after the standard 2D-cine sequence, a k-t BLAST sequence was performed with the same geometry, slice thickness and at least half the phases of the 2-D cine sequence, with a single maximum breath-hold of around 20 seconds. Ventricular volumes were then calculated by manual contouring of endocardial borders in visually identified end-systolic and end-diastolic phases. Use of general anaesthesia, gadolinium based contrast were recorded. Comparisons were made between times taken for the sequence and reporting, quality of images and ventricular volumes obtained using appropriate statistical tests.

Results: 21 patients (Median weight 23 kg, range 3.2–62, Median age 9y, range 24 days to 17 y) were included. Diagnosis in Table 2. 86% of studies were under general anaesthesia and Gadolinium based contrast was administered in 67%. Scan time was significantly shorter with k-t BLAST sequence (19 ± 0.84 s) compared to 2-D cine stack (300+156 s). However, image quality was inferior and in two cases images were non-diagnostic with k-t BLAST sequence due to motion and reconstruction artefact. All images were of good quality in M2D cine stack (image 1). Bland-Altman analysis (Image 2) revealed that there were no statistically significant differences in values of ventricular volumes obtained by either method. Reporting time for k-t blast sequence (12.5 ± 1) was significantly lesser than M2D cine stack (17.6 ± 7 min).

Conclusions: k-t BLAST 3D sequence allows for accurate assessment of ventricular volumes in congenital heart disease, comparable to 2D cine SSFP in selected cases. It can reduce scan time and can help avoid misregistration of ventricular cine slices due to inability to breath-hold consistently at the same point in the respiratory cycle.

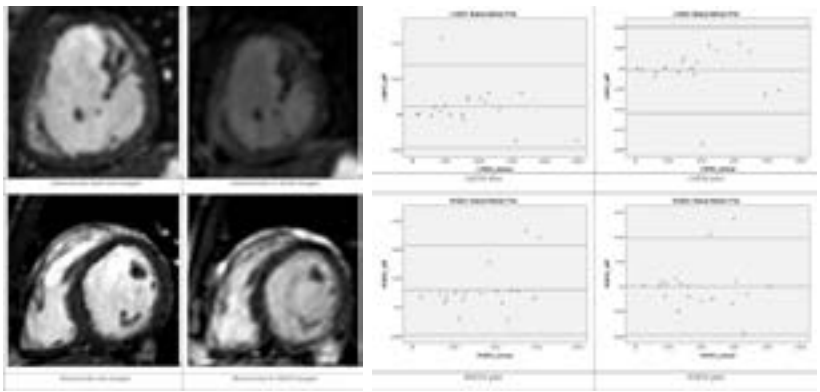

Table 1: Image Protocol Parameters

M2D Cine stack	k-t BLAST sequence	Parameter
320-360	320-360	Field of view (mm)
288	256	Recon Matrix
10 – 13	10 – 13	Number of 'sections'
300 (in 8 - 14s periods)	16 – 21	Breath hold duration (s)
30 -40	16 - 24	Number of profiles per cardiac phase
1.5 x 1.5 x 7 - 10	2.3 x 2.3 x 7 - 10	Acq Voxel (mm)
1.125	1.25	Recon Voxel (mm)
3 - 4	3 - 4	Repetition time (ms)
1.6 - 2	1.5 - 2	Echo time (ms)
60	50	Flip angle
-	4	Acceleration factor

Table 2: Diagnosis in patients recruited

%	N	Main Diagnosis
10	2	Aortic Valve disease (Post Repair)
10	2	Congenitally Corrected Transposition of Great Arteries
10	2	Coarctation of Aorta (Post Repair)
14	3	DILV, TGA - Post Fontan
14	3	DORV
10	2	HLHS - Post Hemi Fontan
5	1	Mitral Valve Disease
10	2	PA, VSD (Repaired)
10	2	Ventricular Septal Defect
10	2	TGA - Post Arterial Switch Operation
100	21	**Total**

P140

High afterload supports ventricular synchrony in discordant ventriculo-arterial connections and in normal subjects

Barbara E. U. Burkhardt, M.D.[1]Christian J. Kellenberger, M.D.[2], Emanuela R. Valsangiacomo Büchel, M.D.[1]

1. Pediatric Heart Center, University Children's Hospital Zurich, Switzerland, Zürich, Zurich, Switzerland
2. Diagnostic Imaging, University Children's Hospital Zurich, Switzerland, Zürich, Zurich, Switzerland

Background: The atrial switch operation (Senning) used to be the repair technique of choice for d-transposition of the great arteries and results in a subsystemic morphologic right ventricle (RV) and a subpulmonary morphologic left ventricle (LV). These chronically altered loading conditions might result in intraventricular contraction delays and in interventricular dyssynchrony between RV and LV.

Methods: 29 patients after Senning repair (age 29± 7y) and 23 normal controls (age 22± 10y; p=n.s.) underwent cardiac magnetic resonance (CMR) imaging for assessment of RV function. 2D SSFP cine images with high temporal resolution (26±11 ms) were acquired in four-chamber and short-axis views covering both ventricles. A feature tracking software (TomTec 2D CPA) was used for analysis of myocardial deformation. Times to peak strain (TTP) for each ventricle were measured in longitudinal and in circumferential directions. Intraventricular dyssynchrony was expressed as systolic dyssynchrony index (SDI) = SD of TTP of all segments divided by cardiac cycle length. Interventricular delay was calculated as the difference between RV versus LV mean TTP per cycle length.

Results: When comparing the RV in either position, circumferential SDI was lower in subsystemic (Senning) than in subpulmonary position (controls) (6.2± 3% vs. 9.3± 6.3%; $p < 0.05$), while longitudinal SDI was similar (10.9± 7.9% vs. 10.9± 6.7%; p=n.s.). In contrast, LV circumferential (8.6± 6.7% vs. 3.5± 1.4%; $p < 0.001$) and longitudinal (15.4± 7.2% vs. 9.2± 5.6%; $p = 0.001$) SDI were higher in subpulmonary (Senning) than in subsystemic position (controls).

In Senning patients, circumferential SDI of the subsystemic ventricle was still higher than in controls (6.2± 3% vs. 3.5± 1.4%; $p < 0.001$); longitudinal SDI was similar in both groups (10.9± 7.9% vs. 9.2± 5.6%; p=n.s.). On the other hand, Senning subpulmonary longitudinal SDI was higher than in controls (15.4± 7.2% vs. 10.9± 6.7%; $p < 0.05$), while Senning subpulmonary circumferential SDI was similar to controls (8.6± 6.7% vs. 9.3± 6.3%; p=n.s.).

Interventricular delay was not significantly different between Senning and controls (longitudinal 4.8± 4.1% vs. 4.8± 4.7%; circumferential 5± 4.2% vs. 4.7± 2.8%).

Conclusions: Elevated RV afterload leads to a more synchronous circumferential contraction, albeit not like in a normal LV, whereas longitudinal synchrony is unchanged. Similarly, the LV presents more intraventricular dyssynchrony when it is unloaded than under normal loading conditions, and synchrony is highest in subsystemic LVs circumferentially. Thus, high afterload in general favors synchronous contraction in both ventricles. In Senning patients, synchrony between the ventricles is not impaired.

P142

Predictors of missed appointments in patients referred for congenital cardiac magnetic resonance

Jimmy Lu, MD[1] Ray Lowery, BS[2], Sunkyung Yu, MS[2], Maryam Ghadimi-Mahani, MD[2], Prachi Agarwal, MD[2], Adam Dorfman, MD[2]

1. *University of Michigan, Dexter, MI*
2. *University of Michigan, MI*

Background: Congenital cardiac magnetic resonance (CMR) is a limited resource due to availability of both scanner time and physicians for real time monitoring. Missed appointments decrease scheduling efficiency, have financial implications, and represent missed care opportunities. This study aimed to identify predictors of missed appointments.

Methods: This retrospective study included all patients with outpatient congenital CMR appointments at the University of Michigan from 1/1/2014-12/31/2015. Missed appointments (no-shows or same-day cancellations) were identified from the electronic medical record. Predictors included on univariate analysis were: age, gender, socioeconomic status (SES), distance from hospital, completion of prior CMR, indication for CMR, referring physician, CMR site, requirement for sedation, and referral for a research study. SES data included household income and parent education based on census block data by patient zip code. Statistically significant variables ($p < 0.05$) were included into a multivariable analysis.

Results: During the study period, 795 outpatients (median 18.5 years old, interquartile range [IQR] 13.4-27.1 years) were referred for congenital CMR; 772 (97.1%) were referred by a cardiologist, and 31 (3.9%) were referred for a research study. A total of 91 patients (11.4%) missed appointments; 28 (3.5%) missed multiple appointments, and 53 (58.2%) completed an eventual CMR a median of 60 days (IQR 29-107) later. Reason for missed appointment could be identified in only 38 patients (41.8%); illness (n=6, 6.6%) and appointment conflict (n=6, 6.6%) were the most common reasons. On univariate analysis, having public insurance, lower median household income, referral for a research study and referral by a non-cardiologist or adult cardiologist were associated with missed appointments. Single ventricle patients were more likely to miss appointments; tetralogy of Fallot patients were less likely to miss appointments. In multivariable analysis, independent predictors of missed appointments were referral by a non-cardiologist (adjusted odds ratio [AOR] 5.8, p=0.0002), referral for research (AOR 3.6, p=0.01), and public insurance (AOR 2.1, p=0.005). Independent predictors of having multiple missed appointments were referral by a non-cardiologist (AOR 21.3, $p < 0.0001$) and referral for research (AOR 9.4, p=0.0005). Compared to patients with a single missed appointment, patients with multiple missed appointments were older (median 23.4 vs. 18.2 years, p=0.01), more commonly referred by non-cardiologists (35.7% vs. 3.2%, $p < 0.0001$) or for research (21.4% vs. 4.8%, p=0.02), and more likely to be scheduled for CMR at the hospital (89.3% vs. 69.8%, p=0.046).

Conclusions: Sociodemographic factors can identify patients at higher risk for missing appointments. These data may inform initiatives to limit missed appointments, such as targeted education of referring providers and patients. Further data are needed to evaluate the efficacy of interventions.

P143

Use of a novel data warehouse tool to compare left ventricular size between Echocardiography and MRI in children with mitral and aortic regurgitation: Echocardiography underestimates LV size

Yue-Hin Loke, M.D.[1]Justin Wiggs, B.S.[2], Qianxi Li, M.S.[3], Roel Truyen, mSc[4], Merlijn Sevenster, PhD[5], Craig Sable, MD[6], Laura Olivieri, M.D.[7]

1. *Children's National Medical Center, Washington Dc, DC*
2. *Children's National Medical Center, DC*
3. *Philips Research North America, MA*
4. *Philips Research, Eindhoven, Noord-Brabant, Netherlands*
5. *Philips Research North America, Cambridge, MA*
6. *Children's National Health Systen, Washington, DC*
7. *Children's National Medical Center, Washington, DC*

Background: Two-dimensional echocardiography is the primary modality used to evaluate LV size in children, including those with mitral and aortic regurgitation. There are notable differences in echocardiography-derived measurements of LV diastolic dimension and MRI-derived measurements of LV end diastolic volume (LVEDV). This study aims to utilize a novel data warehouse tool that combines echocardiography and MRI databases to compare differences in LV measurements between the two modalities in children with and without left-sided valvar regurgitation. We hypothesize that the differences are more divergent in patients with AR or MR compared to normal patients.

Methods: A local SQL Server 2012 based data warehouse was created that incorporated all patients from a single institution with both cardiac MRI (Digisonics) and echocardiography (xCelera) databases (from January 2014 to present). Customized queries via data visualization software (Tableau, Seattle, USA) were performed to identify a patient cohort who had undergone both CMR and echo within 3 months of each other, and had left ventricular enlargement secondary to moderate to severe AR/MR. A second query of both databases identified another patient cohort with no AR/MR and normal LV volumes. The MRI-derived LVEDV was compared against the echocardiogram LVEDV (calculated from Simpson's rule from the apical view) by t-test. MRI-derived LVEDV z-score was compared to the echo-derived left ventricular internal diameter (LVIDd) z-score. Pearson's correlation coefficients from both the AR/MR group and the non-AR/MR group were calculated.

Results: Twenty-eight patients (average age 14) with at least moderate AR (n=18) or MR (n=10) were compared with 28 patients (average age 13) with normal LV volume and systolic function. MRI-derived LVEDVs were consistently higher than echo-derived LVEDV for both the AR/MR group (LVEDV 171+/-101 ml vs. 132+/-59 for CMR and echo respectively, $p < 0.05$) and normal group (LVEDV 111+/-23mL vs. 65+/-36 mL, $p < 0.05$). In the AR/MR group, the LVIDd z-score derived by echo was poorly correlated with LVEDV z-score derived by MRI ($R2 = 0.11$, $p < 0.05$). In the non-AR/MR group the LVIDd z-score derived by echo had a stronger correlation with LVEDV z-score derived by MRI ($R2 = 0.68$, $p < 0.05$).

Conclusions: We used a unique data warehouse tool aggregated multiple cardiology databases to show that LV measurements of pediatric patients with AR/MR are underestimated in echocardiography compared to MRI. A single LVIDd measurement is poorly correlated with LV size as measured by CMR in LV volume-loaded lesions, such as AR or MR.

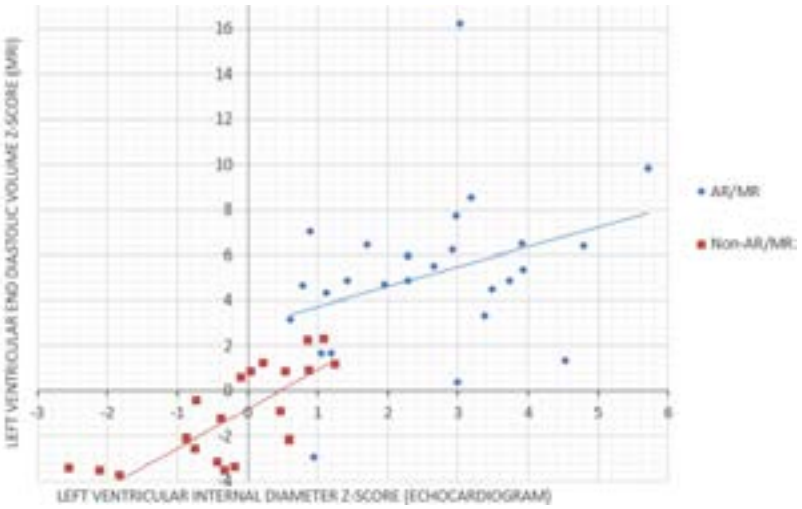

P144

Postoperative pulmonary stenosis assessment in transposition of the great arteries repaired by arterial switch.A 4D flow resonance study

Zahra zb. Belhadjer[1], Gilles Soulat, MD[2]Laurence Iserin, MD[3], Magalie Ladouceur, MD[2], Damien Bonnet, MD,PHD[4], Elie Mousseaux, MD, PhD[2]

1. *European Hospital Georges Pompidou APHP; INSERM U970 PARCC Paris descartes University, Neuilly Sur Marne, Ile-de-France, France*
2. *European Hospital Georges Pompidou APHP; INSERM U970 PARCC Paris descartes University, Ile-de-France, France*
3. *European Hospital Georges Pompidou APHP, Ile-de-France, France*
4. *European Hospital Georges Pompidou APHP; Paris descartes University, Ile-de-France, France*

Background: Patients operated for transposition of the great arteries by arterial switch defines a new population coming to adulthood with unknown long term prognosis. The main complication in adulthood is pulmonary stenosis, occurring in 17% of patients and leading to re-intervention in 15% of cases. Repair of this right ventricle outflow is recommended in symptomatic patients when systolic pressure of the right ventricle is greater than 60 mmHg (velocity of tricuspid regurgitation (IT)> 3.5 m./ s^{-1}). However pulmonary flow measurement cannot be always measured with transthoracic echocardiography Doppler (TTE) due to vessels anatomy features. 4D flow in magnetic resonance is a new imaging method, allowing analysis of blood velocity and flow in an entire volume, permitting detection, quantification and location of vascular stenosis. The objective of this study was to compare this 4D flow imaging to TTE for the diagnosis of pulmonary stenosis in adult with transposition of the great arteries corrected by arterial switch.

Methods: MR Acquisitions were performed on a 3 Tesla scanner (GEHC, 750w) with a 10 minutes 4D flow acquisition (Venc ranging from 300 to 450 cm/s) . Segmentation and velocity estimates of the 4D flow acquisition were done by using cloud computing (Arterys sofware). TTE and MRI were done the same day

Results: 33 patients (19 men, 14 women, mean age 25.5 years old) were prospectively included .In 16 of them (48.5%), right ventricle out flow was not correctly evaluated by TTE against 0(0%) in 4D flow. TTE detected 11 (33.3%) patients with an upper speed over 2m/s and 2 (6%) patients with a higher speed over 3.5m/s against 14 (42%) and 4 (12.1%) respectively with 4D flow. The peak flow velocities measurements in Doppler and 4D flow were highly correlated (r=0.79; p Moreover, even when Doppler was contributory, there was an higher correlation between the pulmonary peak velocity and the right ventricle mass index to BSA in 4D flow than TTE (r=0.74; p 4D flow was able to precise the location of the peak velocity: on the distal pulmonary trunk for 19 (54.5%) patients and on the pulmonary arteries for the other 14 (40.5%).

Conclusions: In Patients with transposition of the great arteries treated by arterial switch, 4D flow CMR provide an accurate pulmonary stenosis assessment, with peak flow velocities measurement correlated to TTE, and detect more stenosis with the ability to specify their location.

P145

High-resolution 3D black-blood turbo spin echo sequence with variable flip angles (SPACE) for the evaluation of cardio-thoracic anatomy in infants with congenital heart disease

Aurelio Secinaro, MD[1] Giuseppe Muscogiuri, MD[2], Teresa Pia Santangelo, MD[1], Paolo Ciliberti, MD[1], Benedetta Leonardi, MD[1], Carmela Napolitano, MD[1], Paolo Tomà, MD[1]

1. *Bambino Gesù Children's Hospital and Research Institute, Rome. Italy, Lazio, Italy*
2. *Bambino Gesù Children's Hospital and Research Institute, Rome, Italy, Lazio, Italy*

Background: In literature the role of 3 dimensional SSFP Navigator is a well established technique for the evaluation of cardio-vascular anatomy in pediatric patients. Recent pubblication described the role of high-resolution systolic 3D black-blood turbo spin echo sequence with variable flip angles (3D-SPACE) for the evaluation of cardio-thoracic anatomy in adult patients with congenital heart disease. We investigate the potential benefit of the 3D-SPACE in infants with congenital heart disease.

Methods: From February 2015 to July 2016, 10 infants (6.3±3.0 months; 6.4±3.5 Kg) with congenital heart disease underwent cardiac MR (1.5 T Aera, Siemens, Erlangen, Germany) under general anesthesia. All examinations were performed for clinical purpose in order to assess the complex cardiac anatomy, ventricular function and flow quantification. MR protocol included a volumetric T1 TSE (TR: 550ms, TE:22ms, voxel size:0.9 mm^3, acquisition matrix 256x192) with respiratory navigator and ECG triggering in the systolic phase. Subsequently the possibility to evaluate intracardiac findings (yes=1, 0=non diagnostic) and the image quality of great vessels and airways was evaluated using the following score (0=non diagnostic, 1= poor quality, 2= good quality, 3= excellent quality).

Results: In all patients (100%), the identification of complex anatomy was possible. Three patients had aortic coarctation, two patients had hypoplastic left heart complex, two patient showed pulmonary atresia with intact interventricular septum, one patient had tetralogy of Fallot, one patient showed a complex case of transposition of great arteries and finally one patient had double outflow right ventricle. In the whole population was possible to depict the presence of atrial and ventricular septal defect. The image quality for visualization of great vessel was 2.9±0.3, while for the airways was 2.6±0.7.

Conclusions: The high-resolution systolic 3D black-blood turbo spin echo sequence with variable flip angles (3D-SPACE) is a robust volumetric acquisition which can provide detailed information of static intra and extra-cardiac anatomy of infants with congenital heart disease. The 3D-SPACE sequence allows additional morphological assessment of the airways.

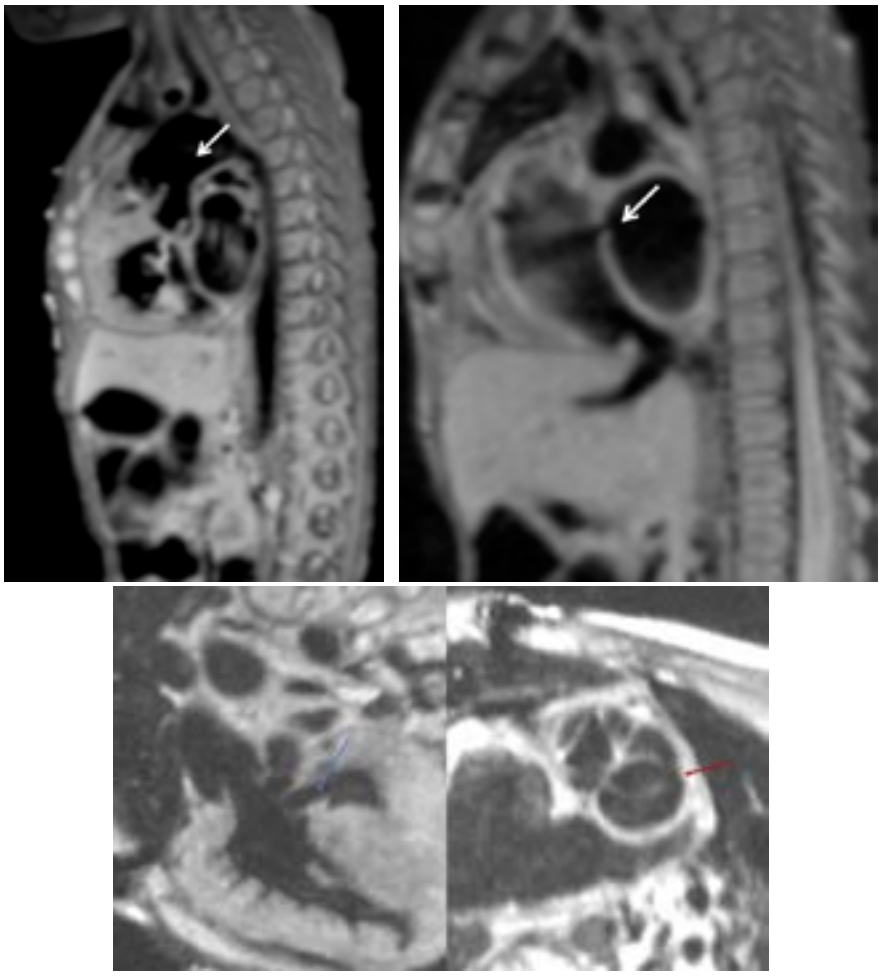

P146

3D localization technique for congenital heart disease with double console machine: reduction in examination time but preserve validity

Keisuke Sato, MD

Shizuoka Children's Hospital, Shizuoka City, Shizuoka, Japan

Background: In the patients with congenital heart disease, evaluation of blood flow and ventricular volume with CMR brings useful information. To obtain the images for evaluating the flow and the volume, it is important to set appropriate cross sections. But it is sometimes difficult to localize them because of the structural complexity. And it takes long time to complete the examination. We assumed that 3D images would be useful to localize them and using two consoles –main console for operation of the machine and sub console for localization- would reduce the examination time. Therefore, the aim of this study was to propose new localization technique with 3D images using double console machine as "3D localization technique" and to compare usual technique and 3D localization technique in the aspect of examination time and validity.

Methods: All CMR examination was performed with MAGNETOM Symphony 1.5T (Siemens). Volume analysis was performed with SA stacked images of white-blood cine. And flow analysis was performed with phase contrast images. For performing 3D localization technique, there are three steps below. 1) 3D images are obtained by main console and are sent to sub console, 2) localization images of suitable cross section are made with 3D images on sub console and are sent to main console, 3) Expected images are obtained with positional information from localization images. 64 consecutive patients with tetralogy of Fallot who underwent CMR from January 2009 to December 2015 were eligible for this retrospective study. All study patients were divided into two groups. Group 1 (Usual Group): Patients to whom usual localization technique was applied. Group2 (3D Group): Patients to whom 3D localization technique was applied. Two groups were compared in some aspects below. 1) Time and amount of the examination, 2) Difference between RV stroke volume and PA forward flow volume.

Results: The usual group consisted 17 patients and the 3D group consisted 47 patients. More PC images were obtained in the 3D group. Total examination time was shorter in the 3D group (80.1±19.5 min for usual group and 67.2±24.2 min for 3D group). The time to obtain SA stack images, AAO-PC images and MPA-PC images was also shorter in the 3D group (57.9±17.4 min for usual group and 35.6±10.2 min for 3D group, $p < 0.001$). PA forward flow and RV stroke volume were almost same value between two groups in the patient with trivial TR.

Conclusions: 3D localization technique reduces examination time but preserves validity.

P147

Pulmonary Insufficiency after isolated pulmonic stenosis repair. Can Cardiac MRI help predict how long we can wait? A pilot study.

Jennifer G. Co-Vu, MD[1]Kimberley Jacobs, BS[2], Dalia Lopez-Colon, PhD[2], Arwa Saidi, MBBCh[2], Murat Tatari, MD[2], Arun Chandran, MD[2], Diego Moguillansky, MD[2]

1. *University of Florida, Gainesville, FL*
2. *University of Florida, FL*

Background: Isolated severe pulmonary valve stenosis (PS) often needs either balloon valvuloplasty or surgical valvotomy leading to significant pulmonary insufficiency (PI), which may warrant pulmonary valve replacement (PVR). The indications and timing for PVR for patients with isolated PS are often extrapolated using data from Tetralogy of Fallot studies. We sought to determine whether thresholds from cardiac magnetic resonance imaging (CMR) can be used to predict timing for PVR in patients with isolated PS.

Methods: Retrospective review of all patients with isolated pulmonary stenosis who underwent CMR from 2003-2015. Pre and post-PVR CMR data included ventricular volumes, ejection fraction (EF) and valvar regurgitation. Post-op evaluation included CMR when available (7 patients) and echocardiograms in the remaining patients (9 patients). We defined PVR success as normalization of right ventricular volume and EF based on CMR and echocardiogram data. Data was analyzed using non-parametric statistics. Results are presented as median [IQR].

Results: Fifty-four patients underwent CMR for evaluation of significant PI following intervention for isolated PS, with 87.5% success rate. Pre PVR CMR RV end-diastolic volume, RV EF, and pulmonary regurgitation were all significantly associated with normalization of RV volumes and EF after PVR (Table 1).

Conclusions: Pre PVR CMR parameters such as RV end-diastolic volume, RV EF and pulmonary regurgitation appear associated with normalization of RV volumes and EF after PVR. This study was limited due to small sample size; larger studies will be required to confirm these preliminary findings.

Table 1: Comparison of pre-PVR CMR variables

p-Value	Success	Failure	Variable
0.025	221 [186-344]	266 [215-317]	RV end-diastolic volume, mL (median[IQR]
0.025	47.5 [42.2-49.9]	39 [32.2-46.1]	RV EF, % (median [IQR])
0.025	36 [31-46]	38 [29-47]	Pulmonary regurgitation, % (median [IQR])

P148

Unusual case of syncope

Sudip K. Saha, MD

Mid Atlantic Permanente Group, Mclean, VA

Description of Clinical Presentation: A twenty-eight year old man presented with sudden onset syncope while jogging. Initial cardiac evaluation including ECG, echocardiogram, and holter monitor were unrevealing. A cardiac MRI was ordered to evaluate for any other structural abnormalities that could have led to his syncope.

Diagnostic Techniques and Their Most Important Findings: Technique: Cardiac MRI was performed on a Philips 1.5 T scanner with a commercial 5-element cardiac-surface coil. Cine images were acquired in a contiguous LV short-axis orientation with an ECG-gated, breath-hold, steady-state free-precession sequence with full LV coverage (8-mm slice thickness, 2-mm interslice gap, in-plane spatial resolution 2×2 mm, 30 ms temporal resolution). LGE-CMR was performed 15 minutes after the intravenous administration of 0.2 mmol/kg gadolinium-DTPA (Magnevist; Schering, Berlin, Germany) with a 2-dimensional breath-hold, segmented inversion-recovery sequence (inversion time optimized by the Look-Locker sequence [inversion time scout] to null normal myocardium) acquired in the same orientation (short-axis stack) as the cine images.

Most important finding: An anomalous left anterior descending artery was discovered that was originating from the right coronary cusp. The patient was referred to cardiac surgery for further intervention.

Learning Points from this Case: This case highlights the utility of cardiac MRI to define coronary anatomy without the use of ionizing radiation. A systematic approach, including confirming origins or the coronary arteries, is important to fully evaluate symptoms such as syncope.

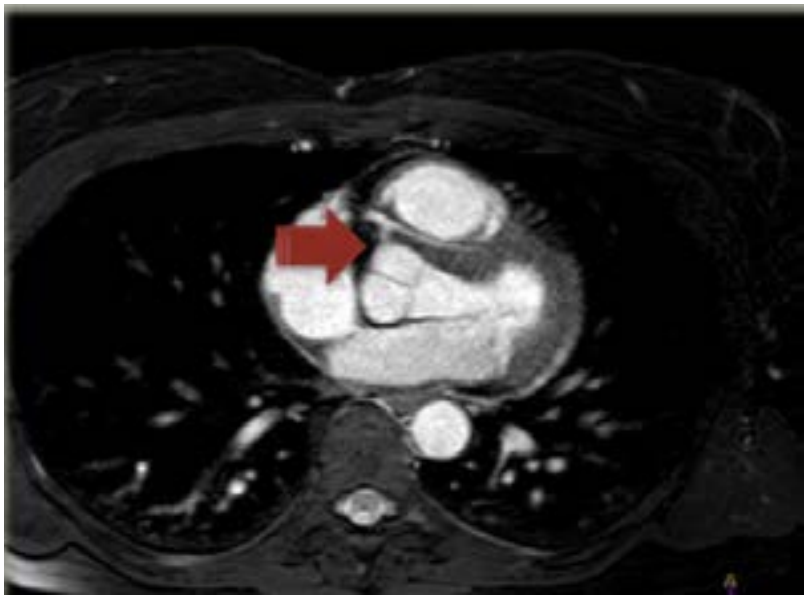

P149

Takotsubo Cardiomyopathy in an Asymptomatic Adult Woman With Repaired Tetralogy of Fallot.

Manish B. Malkar, MD, MPH, Wilson King, MDSaar Danon, MD, Lisa Alderson, MD, Nadeem Parkar, MD

Saint Louis University, St Louis, MO

Description of Clinical Presentation: Takotsubo cardiomyopathy is a syndrome characterized by a reversible hypokinesis of the apical and midcavitary segments and hyperkinesis of the basal segments of the ventricle. It is rarely reported in the adult patients with congenital heart disease which represent a growing population. We describe a case of a 45-year-old woman with repaired tetralogy of Fallot with Takotsubo cardiomyopathy. She previously underwent initial palliation with a classic right Blalock–Taussig shunt in infancy followed by complete repair with ventricular septal defect closure and a transannular right ventricular outflow tract patch at six years of age. She was asymptomatic and lost to follow up for about 25 years.

Diagnostic Techniques and Their Most Important Findings: On re-establishing medical care, cardiovascular magnetic resonance (CMR) demonstrated severe pulmonary valve insufficiency (regurgitant fraction 58%) with severe right ventricular enlargement (RVEDVi 210 mL/m2) but normal biventricular function (RVEF 62%, LVEF 75%). She underwent cardiac catheterization about 3 months after the initial CMR to evaluate candidacy for transcatheter pulmonary valve placement. Cardiac catheterization demonstrated globally depressed left ventricular systolic function and normal coronary angiography. Repeat CMR showed severely depressed left ventricular systolic function (LVEF: 26%) with hypokinesis of midcavitary and apical wall of the left ventricle and hyperkinesis of the base of left ventricle(figure 1) but no myocardial edema (figure 2) or myocardial fibrosis (figure 3), which are characteristics of Takotsubo cardiomyopathy. CMR also demonstrated new onset of moderately depressed right ventricular systolic function in addition to persistent severe pulmonary regurgitation (regurgitant fraction 70%) and severe right ventricular dilation (RVEDVi 246 mL/m2, RVEF 31%). A 12-lead electrocardiogram revealed new diffuse anterolateral T-wave inversion and ST segment depression on anterior leads in addition to a persistent right bundle branch block.

Learning Points from this Case: Takotsubo cardiomyopathy can present in adults with congenital heart disease, and must be considered in the differential diagnosis.

CMR is an important diagnostic tool in the evaluation of cardiomyopathies in adults with congenital heart disease.
This is the first case of Takotsubo cardiomyopathy with biventricular involvement in adults with congenital heart disease.

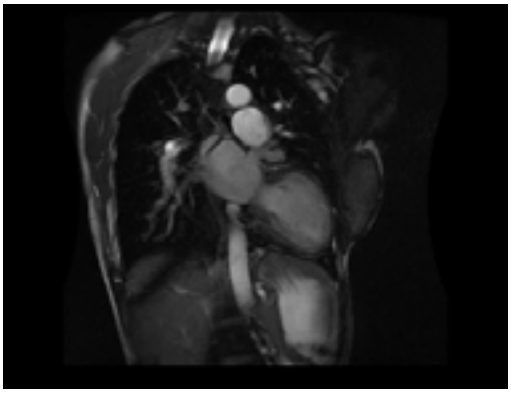

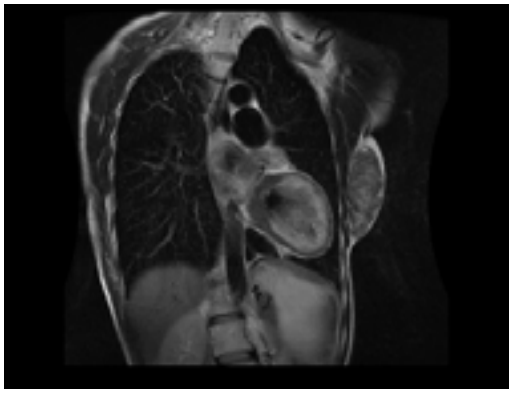

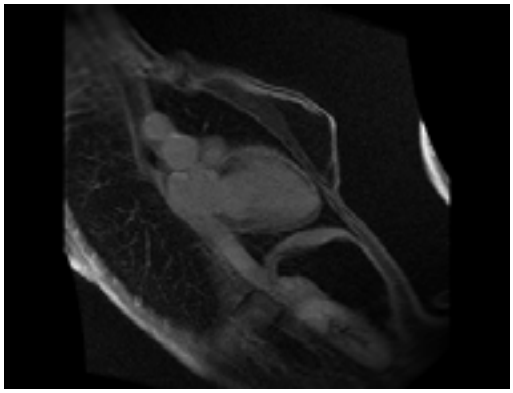

P150

Cardiac MRI Aids Diagnosis for Cardiac Arrest in a Previously Healthy Child

Nikki Singh, MD[1]Joshua Kovach, MD[1], Todd Gudausky, MD[1], Peter Kouretas, MD[1], Ronald Woods, MD PhD[1], Margaret M. Samyn, MD[2]

1. Medical College of Wisconsin/ Children's Hospital of Wisconsin, WI
2. Medical College of Wisconsin/ Children's Hospital of Wisconsin, Milwaukee, WI

Description of Clinical Presentation: A previously healthy 12 year old girl suffered an out of hospital (unwitnessed) cardiac arrest with ventricular tachycardia noted by Emergency Medical Services (EMS); she had successful resuscitation.

Diagnostic Techniques and Their Most Important Findings: While initially her cardiac arrest was thought to be due to a primary arrhythmia, echocardiogram showed a sinus venosus (SV) defect with possible partial anomalous pulmonary venous return (PAPVR). Cardiac magnetic resonance imaging (CMR) was undertaken to further understand her anatomy. CMR confirmed SV defect with anomalous drainage of the right sided pulmonary veins to the superior vena cava-right atrial junction with dilated right atrium and right ventricle. It also showed a small area of delayed enhancement (DE) for the apical, inferior left ventricular free wall. Because brain imaging showed embolic phenomena, this CMR scan supported the diagnosis of paradoxical embolus causing myocardial infarction and leading to her cardiac arrest. Coronary angiogram confirmed an abnormality in the distal left anterior descending coronary artery.

Learning Points from this Case:

1. CMR can be a helpful diagnostic tool in pediatric patients with unclear etiology for cardiac arrest.
2. Paradoxical emboli can lead to myocardial ischemia/ infarct in pediatric patients with congenital heart disease.

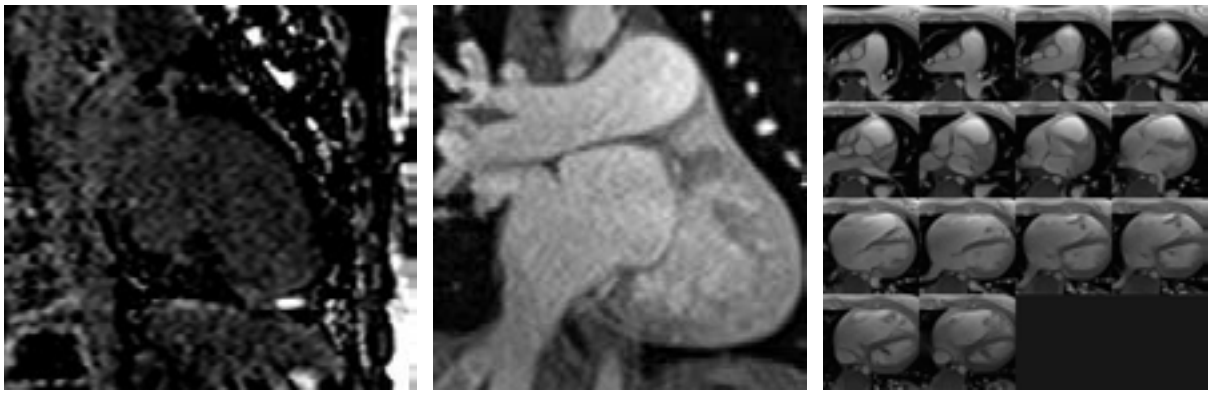

P151

First Report of Congenital Right Ventricular Aneurysm with Transmural Late Gadolinium Enhancement

Pankaj Gupta, MD(Pediatrics) and fellowship in Pediatric cardiology[1] Sunil Ghelani, MD, MBBS[2], Puja Banka, MD[3]

1. *University of Sydney, Westmead, New South Wales, Australia*
2. *Boston Children's Hospital, Boston, MA*
3. *Boston Children's Hospital, MA*

Description of Clinical Presentation: A 42-year-old woman in her third trimester of an otherwise uncomplicated pregnancy was referred with suspected fetal right ventricular (RV) structural abnormality. A fetal echocardiogram found a moderate-sized, broad-based outpouching from the RV anterior wall. Infant was born at 40 weeks gestation (birth weight 3.7 kg) and was asymptomatic with a normal electrocardiogram. Echocardiography demonstrated a poorly contracting, thin-walled aneurysm of the basal, anterior RV free wall with qualitatively moderately depressed global RV dysfunction. Cardiac magnetic resonance (CMR) examination was requested to better characterize the lesion and quantify ventricular size and function.

Diagnostic Techniques and Their Most Important Findings: As seen in the figure 1, CMR revealed a large, broad-based aneurysm (12 mm x 25 mm) at the base of the right ventricle, under the anterior aspect of the tricuspid valve annulus. The aneurysm was thin-walled with paradoxical motion and transmural late gadolinium enhancement (LGE). Global right ventricular systolic function was moderately depressed with an ejection fraction of 31%. Left ventricular size and ejection fraction were normal. No thrombi were seen. The infant remained asymptomatic and was managed conservatively, with discharge at 6 days of age on aspirin to reduce thrombotic risk. He remains asymptomatic at 2 months.

Learning Points from this Case: Congenital RV aneurysm is a rare congenital heart disease and the published literature is limited to a few case reports. To our knowledge, there are no reports of LGE imaging in this lesion. This case shows the utility of CMR in: 1) estimating the size and shape of the aneurysm including the defining its communication with the ventricle which may be helpful in estimating risk of thrombosis, 2) tissue characterization of the aneurysm wall, 3) estimation of right ventricular size and function including regional wall motion abnormalities, 4) and excluding other possible diagnoses. The presence of transmural LGE may also provide insight into the pathophysiology of this lesion which is, as yet, not well understood.

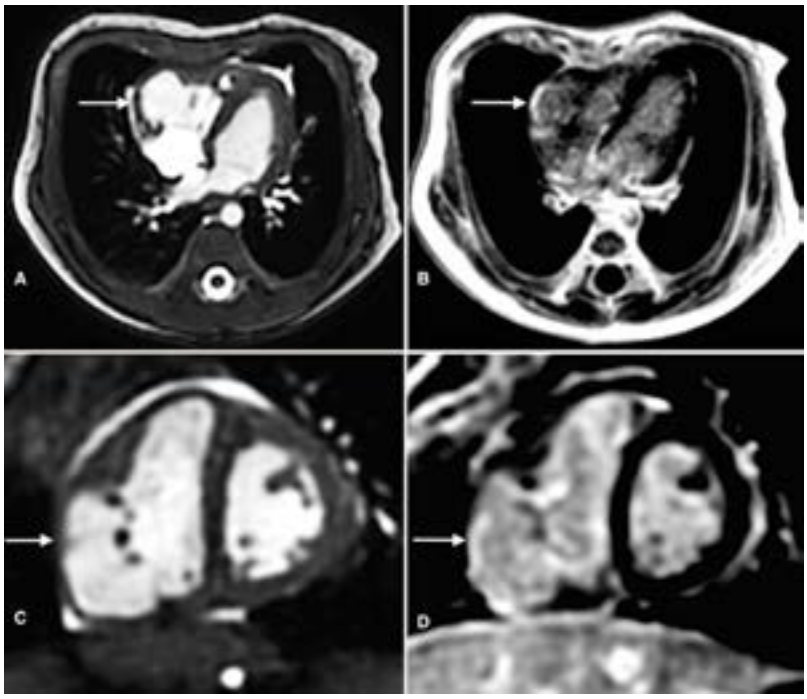

P152

Free-breathing, swaddled, non-contrast-enhanced CMR in 1-day old with cervical circumflex right aortic arch

Christopher J. Francois, MD[1] Shardha Srinivasan, MBBS[2], Alejandro Roldan, PhD[3]

1. *University of Wisconsin - Madison, Madison, WI*
2. *University of Wisconsin, Madison, Madison, WI*
3. *University of Wisconsin - Madison, WI*

Description of Clinical Presentation: A one-day old male infant born at 37W4D was referred for cardiovascular magnetic resonance (CMR) to further delineate details of complex aortic arch anatomy to supplement initial post-natal trans-thoracic echocardiography (TTE). With respect to the aortic arch, the initial TTE suggested the patient had (A) a high right cervical arch with a hypoplastic and elongated transverse arch measuring 2.6-3mm in diameter, (B) an aberrant left subclavian artery, and (C) a left descending aorta with sinusoidal shape to the transverse arch. In addition, the patient had a large membranous ventricular septal defect with extension to the outlet septum, conal hypoplasia, and a patient ductus arteriosus (PDA).

Diagnostic Techniques and Their Most Important Findings: Due to the patient's young age and complex congenital heart disease, CMR was performed with the patient swaddled without the use of any sedation or anesthesia. CMR consisted of free-breathing, black-blood, cine balanced steady-state free precession, and four-dimensional flow-sensitive (4D flow) sequences. Intravenous contrast was not given.

CMR confirmed the presence of (A) a circumflex cervical right aortic arch with the distal arch coursing posterior to the esophagus with a diffusely hypoplastic aortic arch, (B) aberrant left subclavian artery, and (C) a left descending thoracic aorta. The membranous VSD was clearly delineated and at the time of the CMR, the PDA was in the process of closing, measuring only 1mm in diameter.

Learning Points from this Case: There are two main teaching points that will be addressed with this case.

First, this case of one of the rare vascular rings will be compared to other types of aortic arch anomalies to illustrate how vascular rings develop.

Second, this case will be used to discuss how CMR can be successfully performed in neonates with complex congenital heart disease without anesthesia, sedation or intravenous contrast.

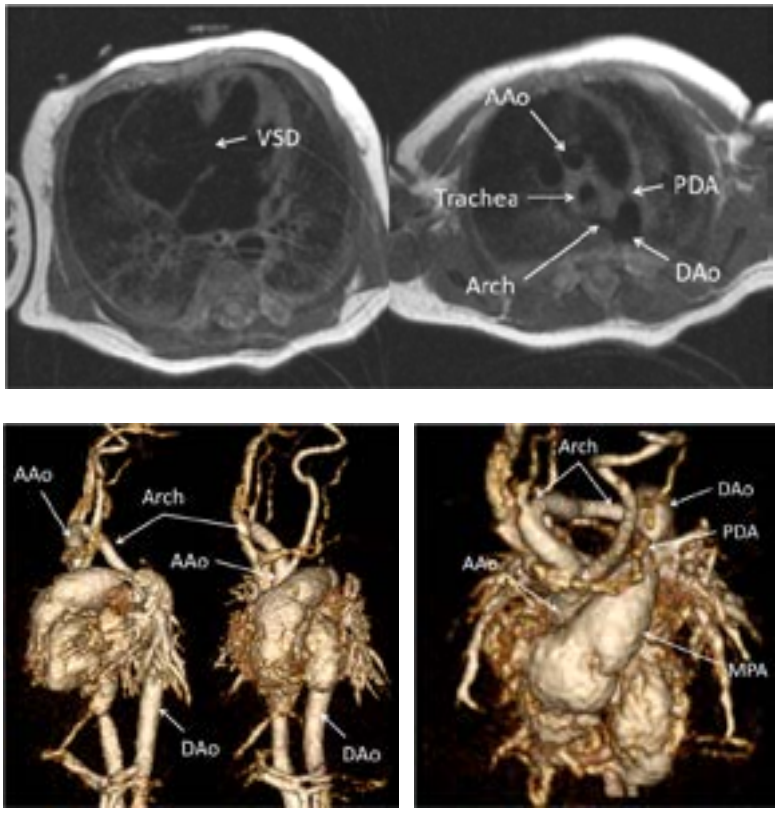

P153

Case-based approach to demonstrate utility of cardiac MRI for planning biventricular repair with inconclusive echo results

Supriya Gupta, MBBS MD[1] Alison Ulbrandt, D.O.[2], Supriya Gupta, MBBS[3], Jayanth H. Keshavamurthy, MD[4]

1. Medical college of georgia, Augusta, GA
2. Medical College of Georgia, Augusta, GA
3. Medical college of georgia, GA
4. Medical College of Georgia at Augusta University, Augusta, GA

Description of Clinical Presentation: Complex congenital heart defects that present earlier in life are sometimes channelled towards single-ventricle repair, because of anatomical or logistic challenges. Given long-term functional and survival advantage, exploring feasibility of biventricular repair is essential for improving prognosis. We describe 2 cases from our practice where MRI was used to steer cardiac surgeon's decision towards biventricular repair when cardiac echocardiogram was inconclusive. The first case describes a 7 month old baby who initially presented with hypoplastic left heart syndrome from coarctation as seen on fetal echocardiogram, and second case of a 6 week old female with Trisomy 21, complete AV canal defect and small RV.

Diagnostic Techniques and Their Most Important Findings: In first case, echocardiogram demonstrated hypoplastic mitral and aortic valve with a small left ventricle. Single ventricle repair (Fontan) was planned; Cardiac MRI demonstrated normal size and function of LV (Figure 1). Biventricular repair was performed based on MR results with favorable outcome. For second case, initial echo showed complete AV canal defect with small right ventricle (Figure 2). Initial MRI showed LV stroke volume and index as 5.3 mL and 23 mL/sqm while for RV these were 4.4 mL and 19.2 mL/sqm respectively, which improved after 2 months. Biventricular repair is being considered based on these findings (Figure 3).

Learning Points from this Case: Cardiac MRI was specifically used in these 2 patients in whom echocardiography provided insufficient information due to complexity of intracardiac anatomy, poor transthoracic ultrasound signals and/or inability to accurately assess the adequacy of ventricular volumes and functions. Electrocardiography-gated 2D SSFP with breath-hold sequences in multiple planes (orthogonal, four-chamber, two-chamber, ventricular short axis and oblique outflow planes) provided excellent dynamic visualization of the ventricular septal anatomy and the LV-to-aorta pathway. Thus, cardiac MRI provided clear understanding of intracardiac and extracardiac anatomy, allowing accurate assessment of ventricular volumes and provided excellent non-invasive haemodynamic assessment of function, aiding planning towards biventricular repair.

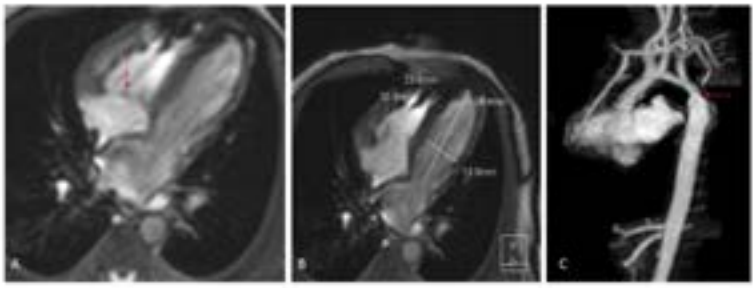

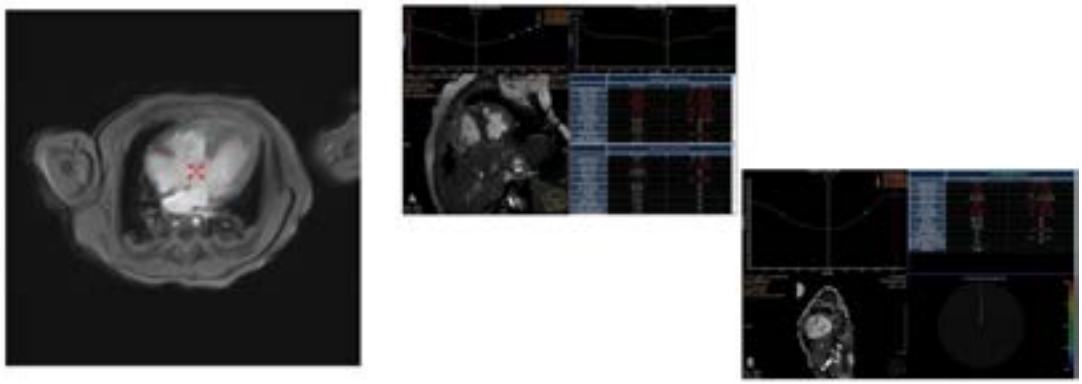

P154

Real World Comparison of 2D-Biplane Echocardiography Based Left Ventricular Ejection Fraction and Volumes to Cardiac Magnetic Resonance Imaging: Results from a Tertiary Care Community Hospital

Robi Goswami, MD[1]Myles Lefkovitz, BS[1], Michael Lunney, MPH, NRP[1], Ashish Kabra, MD[2], Naveen Rajpurohit, MD[3], Venkateshwar Polsani, MD[4]

1. *Piedmont Heart Institute, Atlanta, GA*
2. *Piedmont Heart, Atlanta, GA*
3. *Sanford Cardiovascular Institute, Sioux Falls, SD*
4. *Piedmont Heart Institute, Atlanta, GA., Atlanta, GA*

Background: Cardiac Magnetic Resonance (CMR) is considered the gold standard for assessment of left ventricular (LV) ejection fraction (EF) and LV volumes. The American Society of Echocardiography recommends biplane assessment for LV EF and LV volume by transthoracic echocardiography (TTE). Clinically significant decisions are routinely made based on echo-based LV EF and LV volume assessment. There may be a need to use CMR LV EF and LV volumes more routinely in clinical decision making.

Methods: We completed a retrospective analysis on 368 consecutive patients who had TTE and CMR within 60 days of each other from May 2015 to July 2016. The protocol was approved by the local IRB as part of a Piedmont Heart Institute CMR registry. Eighteen patients were excluded due to poor biplane data quality on TTE. LV EF and LV volumes were compared between TTE and CMR.

Results: A total of 350 patients were included in the study. There were 198 men (57%), 148 patients with body surface area (BSA) < 1.9, and 230 patients with body-mass index (BMI) < 30. 125 TTEs (35.7%) showed an LVEF difference > 10% from that obtained by CMR ($p < 0.001$). Of patients with LVEF 25-40% by TTE, 33.8% had an LVEF difference of >10% by CMR ($p< 0.001$). When divided by gender, females had a higher proportion of >10% LVEF difference between TTE and CMR than males (44.7% vs 28.8%, $p < 0.01$). A BSA > 1.9 or BMI > 30 were not more likely to result in >10% difference in LVEF between TTE and CMR than smaller subjects. Scatterplots for LVEF and volume comparison between TTE and CMR are included below ($p < 0.0001$ for all plots). Diastolic volumes were less correlated than systolic volumes between echo and CMR. This difference in diastolic volume correlation is more exaggerated in women (r^2 0.53) vs men (r^2 0.71).

Conclusions: Despite advances in echocardiography, this data suggests that significant differences persist in volumetric analysis between 2D biplane echo volumes and CMR volumes. This difference is particularly clinically important in patients with intermediate range LV EF (25-40%). Notably, there is a significant gender difference in volumetric assessment as well. These data suggest that inaccurate assessment of diastolic volumes is the main determinant of differences in LVEF measurements by 2D-Biplane TTE and CMR. It is important to reassess LV volumes and LV EF in targeted populations using CMR in contemporary imaging.

http://www.ConferenceAbstracts.com/uploads/cfp2/attachments/LDFAIBDN/LDFAIBDN--222494-1-ANY.pdf

P155

Clinical Operating Points for Non-Invasive Cardiac Imaging Modalities Lead to Low Detection of Coronary Artery Disease

Michelle Wu, BS[1] Mark Doyle, PhD[2], Geetha Rayarao, MS[3], Shimaa S. Khidr, MD[4]

1. *Carnegie Mellon University, PA*
2. *Allegheny General Hospital, PA*
3. *Allegheny General Hospital, PIttsburgh, PA*
4. *Allegheny General Hospital, Pittsburgh, PA*

Background: Interpretation of non-invasive cardiac images depicting MPI, including CMR and SPECT rely on physician training and lab culture. In part, lab culture includes interactions with the cath lab, and in particular, a tolerance for the high number of false positive patients presenting to the cath lab. Modalities can be characterized by a receiver operator characteristic (ROC) curve with the operating point on that curve representing a compromise between sensitivity and specificity (Sens/Spec). We note that as sensitivity increases, specificity decreases with a resulting linear increasing rate of false positive patients. We hypothesize that under clinical conditions, the operating points on the ROC curve are shifted from an equalization of Sens/Spec towards higher specificity but lower sensitivity.

Methods: Modality-based studies used to evaluate myocardial ischemia and CAD were selected from peer-reviewed literature published after 2009. Studies were categorized as either 1) modalities applied in routine clinical fashion or 2) comparison of modalities under controlled conditions. The Sens/Spec was calculated for each study and plotted on an ROC graph.

Results: We evaluated data from 10 modality testing studies and 7 clinical usage studies repesenting >4000 pts. Average Sens/Spec values for clinical studies were 24±23/92±7% for SPECT, 31±22/ 92±6% for CTA and 17/ 93% for PET. For modality comparison studies, Sens/Spec values were 70±7/ 73±9% for SPECT, 88±10/ 90±1% for PET, 95±5/81±14% for CTA and 75±27/88±9% for CMRI. The sensitivities for SPECT and CTA clinical studies were lower than modality studies ($p=.07$ and $p < 0.001$, respectively).

Conclusions: Clinical studies, not modality-base studies, operate at low sensitivity and high specificity. As specificity increases, false positive rates for CAD decrease. This feature is observable in the cath lab and may well be the metric that forces the clinical operating point to high specificity. This is in contrast to modality comparison studies where the operating point on the ROC curve is generally chosen to be closest to the ideal test point (top left of ROC curve, Figure 2). For a given modality, the spread of operating points are consistent with a single ROC curve and thus there are no fundamental differences between performance under modality testing or clinical usage. Recognition of this crucial difference is critical as we aim to place current CMR Trials into their proper context with other image modalities.

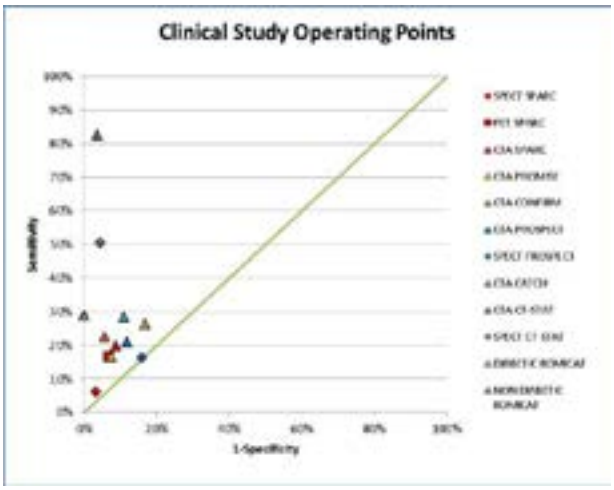

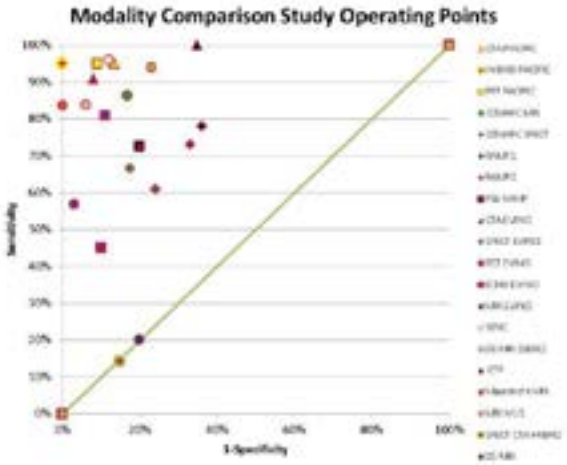

P156

The ability of the electrocardiogram in left bundle branch block to detect myocardial scar determined by cardiovascular magnetic resonance

Björn Wieslander, MD[1] Xiaojuan Xia, Master of Science[2], Robert Jablonowski, MD, PhD[3], Jimmy Axelsson[4], Igor Klem, MD[5], Robin Nijveldt, MD, PhD[6], Charles Maynard, PhD[7], Erik B. Schelbert, MD, MS[8], Peder Sörensson, MD, PhD[9], Andreas Sigfridsson, PhD[10], Uzma Chaudhry, MBBS[11], Pyotr Platonov, MD, PhD[11], Rasmus Borgqvist, MD PhD[12], Henrik Engblom, MD, PhD[3], Jean-Philippe Couderc, PhD, MBA[13], David Strauss, MD, PhD[14], Brett D. Atwater, MD[15], Martin Ugander, MD, PhD[16]

1. *Department of Clinical Physiology, N2:01, Karolinska Institutet and Karolinska University Hospital, Stockholm, Stockholms Lan, Sweden*
2. *University of Rochester, Rochester, NY*
3. *Lund University, Skane Lan, Sweden*
4. *Department of Clinical Physiology, Karolinska Institutet, and Karolinska University Hospital, Stockholms Lan, Sweden*
5. *Duke University Medical Center, Durham, NC*
6. *VU University Medical Center, Amsterdam, Noord-Holland, Netherlands*
7. *University of Washiington, WA*
8. *University of Pittsburgh; Heart and Vascular Institute of UPMC, PA*
9. *Karolinska University Hospital, Stockholms Lan, Sweden*
10. *Karolinska Institute, Stockholm, Stockholms Lan, Sweden*
11. *Department of Cardiology, Clinical Sciences, Lund University, Skane Lan, Sweden*
12. *Lund University, Dept of Clinical Sciences, Lund, Cardiology, and Skane University Hospital, Lund, Skane Lan, Sweden*
13. *Heart Research Follow-Up Program, University of Rochester, NY, USA, Rochester, NY*
14. *FDA, Silver Spring, MD*
15. *Duke University School of Medicine, NC*
16. *Karolinska Institutet, Stockholms Lan, Sweden*

Background: A prognostically useful method for electrocardiographic (ECG) left ventricular (LV) scar quantification using the left bundle branch block (LBBB) Selvester QRS Score was published in 2009 (2009 LBSS). Subsequent evaluation of the 2009 LBSS demonstrates limited diagnostic performance for identification and quantification of LV scar compared to cardiovascular magnetic resonance imaging (CMR). We aimed to revise the 2009 LBSS to develop an improved method for LV scar screening by ECG using a large and broadly selected dataset.

Methods: We retrospectively identified LBBB patients (n=325, 142/325 [44%] with LV scar by CMR) with ECG and late gadolinium enhancement (LGE) CMR exams from four centers. ECG metrics were measured digitally and semi-automatically, and were compared to semi-automatically CMR-determined scar presence and extent.

Results: The 2009 LBSS had a limited correlation with, and diagnostic performance compared to CMR (R^2=0.04, $p < 0.001$, area under the curve to detect any scar [AUC] 0.60, 95%CI 0.54-0.66, sensitivity 54%, specificity 60%, for cutoff = 6 points). Performance was improved using a forward selection stepwise logistic regression model that yielded six ECG predictor variables associated with CMR identified LV scar (AUC 0.72, 95%CI 0.66-0.77, p=0.006 vs 2009 LBSS, sensitivity 54%, p=1.0 vs 2009 LBSS, specificity 84%, $p < 0.001$ vs 2009 LBSS).

Conclusions: Exploration of a wide range of ECG predictor variables in a large training set yielded a logistic model with an improved accuracy for detecting myocardial scar by ECG in LBBB compared to the 2009 LBSS.

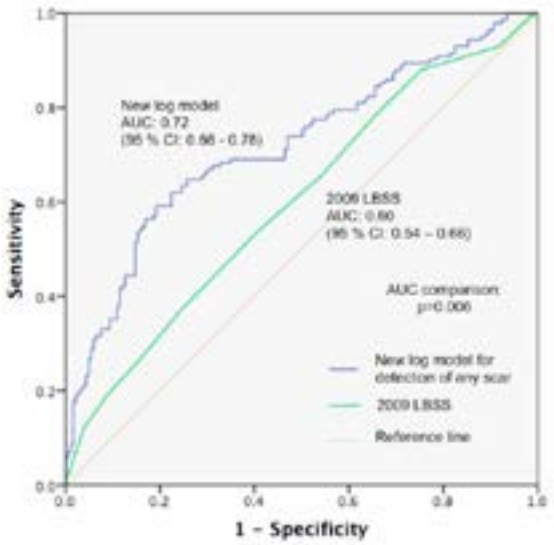

P157

Safety of Cardiovascular Magnetic Resonance Regadenoson Stress Imaging without Pre- and Post-Test 12-Lead Electrocardiography

Michael E. Hall, MD, MS[3]Mark Rushing[1], Daisuke Kamimura, MD, PhD[1], Candace Howard, MD, PhD[2], Kristen Miller, MD[1], Michael McMullan, MD[1], William Campbell, MD[2], Cameron Guild, MD[1], Michael Winniford, MD[1]

1. *University of Mississippi Medical Center, MS*
2. *University of Mississippi Medical Center, Ridgeland, MS*
3. *University of Mississippi Medical Center, Jackson, MS*

Background: Cardiovascular magnetic resonance (CMR) stress imaging often utilizes regadenoson stress similar to nuclear imaging regadenoson stress testing (NRST). However, electrocardiographic (ECG) monitoring is challenging in the MR environment and for interpreting radiologists. It is unclear if CMR regadenoson stress testing (CMRRST) is safe without pre-and post-test ECG monitoring; therefore we compared safety of CMRRST without 12-lead ECG monitoring to NRST with continuous 12-lead ECG monitoring.

Methods: A single center, retrospective comparison of outpatient CMRRST without 12-lead ECG testing versus outpatient NRST with continuous 12-lead ECG testing was performed after matching for age and sex (n=100 for CMR and 98 for nuclear stress). Events included arrhythmias noted on telemetry (CMRRST) or arrhythmias or diagnostic ST-T changes noted on 12-lead ECG (NRST), need for aminophylline and coronary angiography or acute coronary syndromes (ACS) within 30 days of stress testing. All nuclear stress tests were interpreted by board certified cardiologists and all CMR stress tests were interpreted by an advanced imaging cardiologist or radiologist.

Results: There were no significant differences in age, sex, race, BMI, prevalent hypertension or diabetes between those undergoing CMRRST versus NRST (all p-values >0.05). Patients undergoing CMRRST had lower systolic blood pressure (130 vs 141mmHg, $p < 0.001$), more prevalent coronary disease (52% vs 31%, p=0.004) and lower left ventricular ejection fractions (54% vs 63%, $p < 0.001$) compared to those undergoing NRST. Patients undergoing NRST received more aminophylline (18% vs 1%, $p < 0.001$) compared with the CMRRSTgroup. There were no reported significant arrhythmias noted on telemetry (CMRRST) or diagnostic regadenoson-induced ECG changes (NRST) in any patients. There were no significant differences in the number of patients who underwent subsequent coronary angiography (n=7 for both groups) or had ACS (n=3 for CMRRST and n=1 for NRST) within 30 days after stress testing.

Conclusions: Regadenoson stress imaging is associated with a low rate of significant adverse events and appears to be safe regardless of environment. Based on our findings, regadenoson stress without 12-lead ECG testing before and after stress imaging appears to be as safe as a strategy utilizing continuous 12-lead ECG monitoring. In our center, aminophylline was more frequently administered during NRST which may reflect practice differences between cardiologists and radiologists. Overall, these findings suggest that pre- and post-regadenoson stress 12-lead ECG testing may not be necessary which would preclude some logistic challenges particularly for radiology-based CMR practices.

P158

MRI-guided cardiac catheterisation using a partial saturation (pSAT) approach in patients with congenital heart disease

Mari N. Velasco Forte, MD [1]Sébastien Roujol, PhD[1], Kuberan Pushparajah, MD [2], Nick Byrne, MPhys, MSc[3], Bram Ruijsink, MD[4], Israel Valverde, MD PhD[5], Tobias Schaeffter, PhD[6], Reza Razavi, MD, PhD[4]

1. *King's College London, London, England, United Kingdom*
2. *Guy's & St Thomas' Hospital NHS Foundation Trust, Evelina London Children's Hospital, England, United Kingdom*
3. *Guy's and St. Thomas' NHS Foundation Trust / King's College London, England, United Kingdom*
4. *King's College London, England, United Kingdom*
5. *Hospital Universitario Virgen del Rocío Sevilla, Spain, England, United Kingdom*
6. *Physikalisch-Technische Bundesanstalt (PTB), Braunschweig and Berlin, Germany, Berlin, Germany*

Background: Cardiac catheterisation is a common diagnostic and interventional procedure in patients with congenital heart disease (CHD). This procedure is commonly performed under X-ray guidance, which is associated with ionizing radiation and increased risks for cancer. MRI represents a promising alternative approach for the guidance of these procedures. However, simultaneous high contrast visualization of catheter, soft tissue and blood remains challenging using MRI. In this study, we sought to evaluate the benefit of a novel passive tracking sequence based on partial pre-saturation (pSAT) for MR-guided catheterization in patients with CHD.

Methods: Two patients aged 12 and 39 years in whom an XMR was clinically indicated for pulmonary vascular resistance assessment were recruited for this study. Underlying diagnosis were severe right pulmonary stenosis and atrioventricular septal defects (child and adult, respectively). MR-guided catheterization was performed using a real-time single shot acquisition with bSSFP readout (TR/TE=2.6ms/1.3ms, flip angle=60°, FOV=370×370mm^2, voxel size=2.2×2.5mm^2, bandwidth=1190Hz, SENSE factor=2.5, partial Fourier=0.65, acquisition time=145ms, linear ordering). Each image was acquired immediately after an optimized partial saturation prepulse (saturation pulse with modified angle to 30°). The sequence was run in interactive mode and the imaging plane location was modified in real time by the interventional cardiologist using a set of pre-programmed pedals located inside the scanner room. 1% gadolinium (DotaremÒ) was used to fill the balloon of the wedge catheter (Arrow Ò) for positive contrast visualization of the catheter tip. The entire setup was initially tested, optimized and validated using a 3D printed heart phantom (Figure 1).

Results: The balloon of the wedge catheter was clearly depicted during navigation in the phantom with the pSAT sequence. In both patients the catheter was inserted via the femoral vein and directed through the inferior vena cava to the right atrium, right ventricle, pulmonary artery and its branches (Figure 2). Pulmonary artery wedge measurements were also performed. The pSAT sequence was found successful to passively track the catheter and simultaneously visualize soft tissue and blood. However, in the first patient, the catheter lacked the stiffness required to cross the pulmonary valve. In this patient, the procedure was completed with X-ray support using a braided non MRI compatible catheter over a wire with higher stiffness. The procedure was completed solely under MRI guidance in the second patient. Total procedure time was 172 and 170 minutes, cardiac catheterisation time was 55 and 25 min in child and adult, respectively.

Conclusions: The proposed pSAT sequence provides real-time simultaneous high contrast visualization of the catheter balloon, soft tissues and blood. This technique provides excellent passive tracking capabilities during MR-guided catheterization in patients.

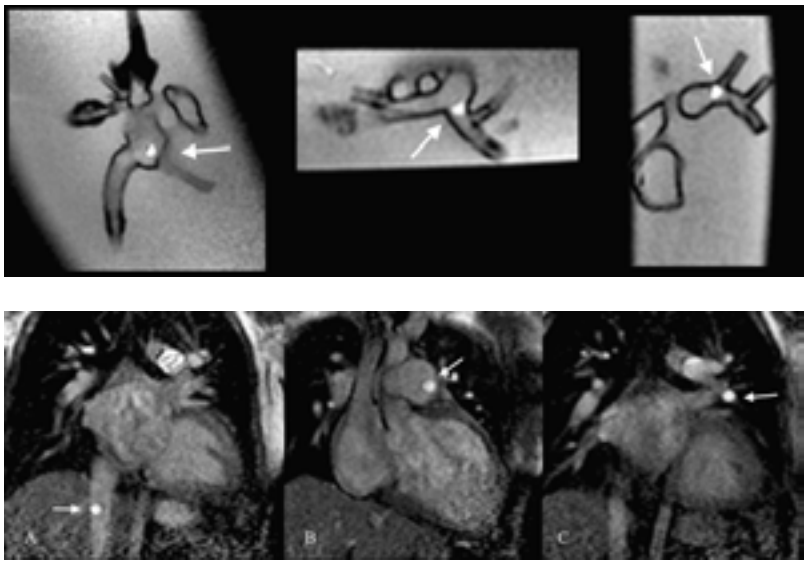

P159

Passive Catheter Tracking with Positive Contrast using Partial Saturation (pSAT) for MR-guided Cardiac Catheterisation

Mari N. Velasco Forte, MD [1], Reza Razavi, MD, PhD[4]Kuberan Pushparajah, MD [2], Nick Byrne, MPhys, MSc[3], Bram Ruijsink, MD[4], Israel Valverde, MD PhD[5], Tobias Schaeffter, PhD[6], Sébastien Roujol, PhD[1]

1. *King's College London, London, England, United Kingdom*
2. *Guy's & St Thomas' Hospital NHS Foundation Trust, Evelina London Children's Hospital, England, United Kingdom*
3. *Guy's and St. Thomas' NHS Foundation Trust / King's College London, England, United Kingdom*
4. *King's College London, England, United Kingdom*
5. *Hospital Universitario Virgen del Rocío Sevilla, Spain, England, United Kingdom*
6. *Physikalisch-Technische Bundesanstalt (PTB), Braunschweig and Berlin, Germany, Berlin, Germany*

Background: X-ray guided cardiac catheterisation is an essential procedure for both diagnosis and treatment of congenital heart disease. MRI-guided cardiac catheterization has been proposed to provide better soft tissue contrast and avoid ionising radiation. Current approaches include positive and negative contrast techniques using Gadolinium and CO2 filled balloon catheters, respectively. Gadolinium-based techniques were found superior to CO2-based techniques. However, gadolinium-based techniques rely on real-time bSSFP images acquired without saturation (non-SAT) prepulse which leads to poor catheter balloon/blood contrast or with saturation (SAT) prepulse which suppresses soft tissue/blood signal. In this study, we developed and optimized a novel Gadolinium-based positive contrast sequence to provide simultaneous high contrast visualization of soft tissue, blood and catheter balloon using a partial saturation (pSAT) pre-pulse.

Methods: The proposed sequence uses a real-time single shot acquisition with bSSFP readout (TR/TE=2.6ms/1.3ms, flip angle=60°, FOV=370×370mm^2, voxel size=2.2×2.5mm^2, bandwidth=1190Hz, SENSE factor=2.5, partial Fourier=0.65, acquisition time=145ms, linear ordering). Each image was acquired immediately after a saturation pre-pulse with a reduced saturation angle to only achieve partial saturation. Optimization of the pSAT angle was first performed using Bloch equation simulations and for different level of intra-voxel partial voluming of the catheter balloon. In-vivo optimization of the sequence was then performed in one patient undergoing MRI-guided cardiac catheterization with a balloon catheter filled with 1% gadolinium (DotaremÒ). The proposed sequence was run several times to study the influence of the pSAT angle. Catheter balloon/blood CNR, catheter balloon SNR, blood SNR, and overall subjective assessment (by a cardiologist blinded from the simulation findings) of contrast quality were measured in the 20th image of each acquisition.

Results: Numerical simulations shows a 20-40° pSAT angle provides a good compromise between high catheter balloon/blood contrast, high SNR and reduced sensitivity to intra-voxel partial voluming of the catheter balloon(Figure 1). The proposed pSAT approach also provides better contrast than conventional non-SAT sequences (pSAT angle=0°) and better SNR than SAT sequences (pSAT angle=90°). The proposed sequence with a 20-40° pSAT angle provided a good in-vivo compromise between catheter balloon/blood CNR and blood SNR (Figure 2). This sequence successfully enabled simultaneous visualization of both catheter balloon and soft tissue/blood signal. Subjective in-vivo assessment of contrast quality resulted in the selection of a pSAT angle of 30°.

Conclusions: The proposed pSAT approach provides positive contrast and simultaneous high contrast visualization of soft tissues, blood and catheter balloon. This sequence shows promising capabilities for MRI-guided cardiac catheterization.

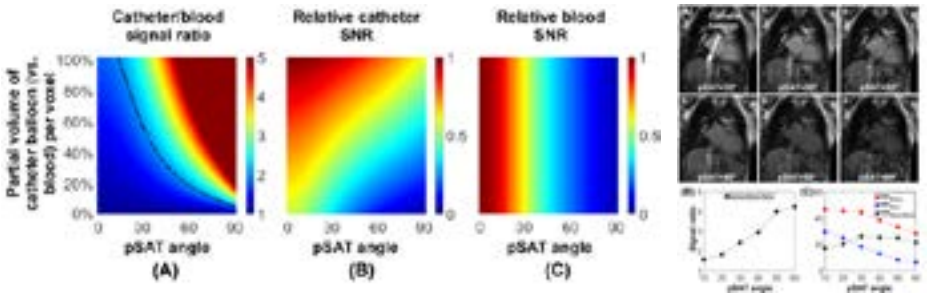

P160

Estimation of Circulating Blood Volume using Ferumoxytol

Rajiv Ramasawmy, PhD[1] Miguel A. Alcantar[2], Jaffar M. Khan, BM BCh[3], Robert J. Lederman, MD[4], Anthony Z. Faranesh, PhD[4]

1. National Institutes of Health, Bethesda, MD
2. National Heart,Lung, and Blood Institute, National Institutes of Health, CA
3. NHLBI, NIH, Washington, DC
4. National Heart, Lung, and Blood Institute, National Institutes of Health, MD

Background: Cardiovascular MRI can be used to measure parameters such as cardiac function and flow, while minimizing potential exposure to ionizing radiation commonly used for such procedures. However there is not presently a robust method using MRI to measure circulating blood volume, which would inform treatment based on a patient's volume status. This initial study investigates measuring total blood volume using Ferumoxytol (Feraheme, AMAG, Cambridge, MA, USA), an FDA approved iron-nanoparticle typically used for iron replacement, which has also been investigated as an MR contrast agent due to its long intravascular half-life (~14 hrs) [1-3].

Methods: Animal studies were approved by the NHLBI institutional Animal Care and Use Committee. Scanning was performed on a 1.5T Siemens scanner (Siemens Healthcare, Erlangen, Germany), with phased array coils (*Body 18*) on the anterior and posterior chest. *In vitro*: Longitudinal relaxavity (r_1) of Ferumoxytol was characterized in 7 linearly spaced dilutions between 0.1-1.72 mM in blood and T_1 measurements were acquired at 37 °C using SASHA [4]. *In vivo*: SASHA estimations of T_1 were acquired breath-held, in a mid-ventricle, short-axis image prior and post administration of 0.6 mg/kg Fe in three pigs (average weight 52 kg). At twenty minutes, a post-administration T_1 map was acquired. Total blood volume was estimated using the following relation: $TBV = n_{Fe} \cdot r_1 / \Delta R_1$, where n_{Fe} is the molar mass of administered contrast agent, r_1 is the relaxivity of Ferumoxytol and ΔR_1 is the change (post – pre) in the longitudinal relaxation rate in the blood [5].

Results: SASHA-derived estimation of Ferumoxtyol relaxivity (r_1) was 18.0 $mM^{-1} \cdot sec^{-1} \pm 0.4$ $mM^{-1} \cdot sec^{-1}$, in good agreement to previous literature [2]. Blood T1 measurements taken within the LV were measured to be 1.46 ± 0.07 s at baseline, which shortened to 0.33 ± 0.01 s at twenty minutes post administration of Ferumoxytol. This yielded an estimated blood volume of 81.6 ± 1.1 mL/kg.

Conclusions: Reported circulating blood volume ranges within 56-69 ml/kg [6], which is 69 – 85% of what was measured in vivo using Ferumoxytol. These animals were on intravenous fluid, which may contribute to the higher observed values. The technique used here is promising as a MR-derived estimation of circulating blood volume. Future experiments will use a gold-standard carbon monoxide tracer method to validate these measurements.

Funding: This work was supported by the NHLBI DIR (Z01-HL006039, Z01-HL005062).

References [1] S. Reeder, *et al***.** *Magn Reson Med***, 2016; 75(4):** 1556-1564. [2] C. Corot, *et al*. *Advanced Drug Delivery Reviews*, 2006; 58: 1471-1504. [3] M. Bashir, *et al*. *JMRI*, 2015; 41:884-898. [4] K. Chow, *et al*. *Magn Reson Med*, 2014; 71: 2082–2095 [5] K. Pannek, *et al*. *Magn Reson Mater Phy*, 2012; 25: 215-222. [6] https://www.nc3rs.org.uk/blood-sample-volumes

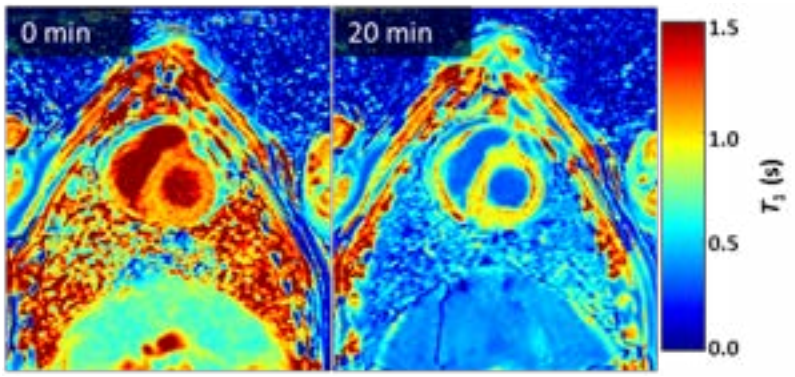

P161

Interventional Planning through 3D printing techniques

Mari N. Velasco Forte, MD [1]Nick Byrne, MPhys, MSc[2], Israel Valverde, MD[3], Kuberan Pushparajah, MD [4], Eric Rosenthal, MD FRCP[5], Shakeel Qureshi, MD [6], Reza Razavi, MD, PhD[7], Tarique Hussain, MD, PhD[8]

1. *King's College London, London, England, United Kingdom*
2. *Guy's and St. Thomas' NHS Foundation Trust / King's College London, England, United Kingdom*
3. *King's College London, Andalucia, Spain*
4. *Guy's & St Thomas' Hospital NHS Foundation Trust, Evelina London Children's Hospital, England, United Kingdom*
5. *Evelina London Children's Hospital, England, United Kingdom*
6. *Guy's & St Thomas' Hospital NHS Foundation Trust, England, United Kingdom*
7. *King's College London, England, United Kingdom*
8. *Dept. of Pediatrics, UT Southwestern Medical Center, TX*

Background: The spatial relationships of anatomical structures in patients with complex congenital heart disease (CHD) can represent a challenge for interventional and surgical planning. In these cases, cardiac magnetic resonance (CMR) and multi-detector computed tomography (MDCT) are diagnostic tools commonly employed when considering a further management in patient care. Both techniques provide information that can be reproduced in a 3D printed model to assess the feasibility of interventional treatment in complex patients.

Methods: For cases in whom cardiac catheterisation was controvertible, we fabricated a patient-specific 3D printed model of their heart to assess feasibility of interventional approach. Segmentation was performed from previous imaging acquired dataset using Mimics software v.18. Models were fabricated by polyjet technology or fused deposition modelling. Cardiac catheterisation was performed in the model before proceeding in the patient.

Results: Fifteen patients were referred for cardiac 3D printing (60% females, 40% males; mean age 41 years, range: 1.5 – 65, 87% adults). Four patients had partial anomalous pulmonary venous drainage, three had transposition of the great arteries (TGA), four had coronary artery fistula, one had an aortic aneurysm post aortic valve replacement, one had tetralogy of Fallot (TOF) and one had multiple ventricular septal defects (VSD). 67% of the patients underwent cardiac catheterisation after procedure planning with 3D printing techniques (figures 1 and 2), 1 case with coronary fistula and one TGA (13%) were considered unsuitable after reviewing the model and 20% are awaiting further management. Consideration of LPA stenosis motivated printing for 2/3 of the patients with TGA and the TOF case. 3D models provided interventionalists with the opportunity to select stent length and size beforehand for all these cases. The remaining TGA had an atrial switch operation (Senning) during childhood, developing a baffle leak that was considered unsuitable for stent closure. All 3 coronary fistulas have successfully been closed after device sizing and landing point were established by in vitro simulation (figure 3). Occlusion of the aortic aneurysm was achieved using an AVP II device and a large VSD was closed with an 8 mm occlutecth device in the case with multiple VSDs. All patients in which cardiac catheterisation was planned and implemented using 3D printing techniques had a successful result.

Conclusions: 3D models provide the opportunity to select materials and plan access routes for specific patients before cardiac catheter intervention. This is beneficial where spatial complexity obstructs expert led treatment and interventional planning. This can provide the interventional cardiologist with the confidence necessary to address conditions that might otherwise be resolved with open heart surgery.

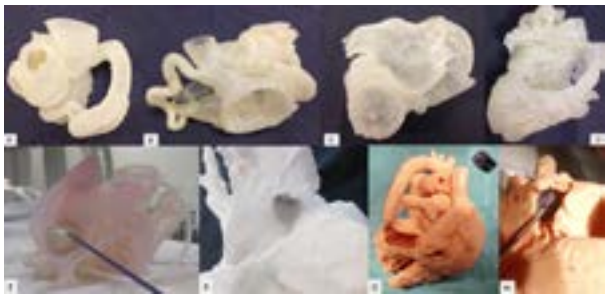

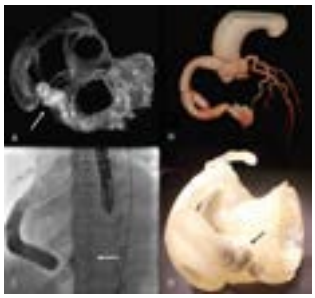

P162

High frame rate multislice golden angle radial imaging with GIRF distortion correction

Adrienne E. Campbell-Washburn, PhD[1]Robert J. Lederman, MD[1], Anthony Z. Faranesh, PhD[1], Michael Hansen, PhD[2]

1. National Heart, Lung, and Blood Institute, National Institutes of Health, MD
2. National Heart, Lung, and Blood Institute, Bathesda, MD

Background: MRI–guidance of cardiovascular interventions depends on high frame rate multi-plane imaging [1]. Typically, real-time bSSFP sequences generate frame rates of ~5-10 frames/s and up to 3 slices are interleaved in rapid succession. Golden angle radial acquisitions (Figure 1A) provide rotationally symmetric k-space sampling for any arbitrary number of radial spokes and therefore are robust to undersampling and ideal for variable rate sliding window reconstruction [2]. However, these acquisitions are susceptible to image artifacts caused by inaccurate gradient waveforms. In this work, we use golden angle radial image acquisitions for very high apparent frame rate imaging in multiple slice planes with real-time distortion correction using calibration of the gradient system impulse function (GIRF).

Methods: Golden angle radial acquisition with 2 slice planes interleaved on a spoke-by-spoke basis (Figure 1B) was implemented on a 1.5T scanner (Aera, Siemens, Erlangen) (gradient echo acquisition, TE/TR = 1.75/3.88 ms, flip angle = 20°, FOV = 300 mm, matrix = 128x128, radial arms = 201). Sliding window reconstruction was applied such that imaging frames were updated every 4 spokes (31ms for 2 slices). The GIRF was calculated as previously described [3] and convolved with gradient waveforms in order to predict the true k-space trajectories. Images generated with GIRF-predicted k-space trajectories were compared to images with distortion correction by calculated gradient delays [4] in a phantom.

Results: Each slice was updated at a rate of 33 frames/s using this golden angle radial imaging method. Streaking artifacts and signal shading were apparent in the images reconstructed using nominal k-space trajectories (Figure 2A). Signal shading was improved in images generated with the GIRF-predicted k-space trajectories and gradient delay compensation (Figure 2B,C), and additional streak improvement was produced using GIRF-predicted trajectories. Figure 3 illustrates the application of this method for high frame rate imaging in two oblique slice planes enabling procedural monitoring in multiple views.

Conclusions: Using the GIRF to predict k-space trajectories enabled the correction of gradient waveform inaccuracies and gradient delays simultaneously. Furthermore, this one-time calibration step can be used in real-time for effective distortion correction at an arbitrary imaging orientations [3]. The golden angle radial acquisition presented here is appealing for interventional MRI when device navigation is monitored in multiple planes simultaneously and high frame rate imaging is essential.

Funding: NHLBI DIR (Z01-HL006039, Z01-HL005062).

References: [1] Campbell-Washburn AE et al, Magnetic Resonance Imaging Clinics of North America 23(4):669-679 (2015), [2] Winkelmann S et al, IEEE Trans Med Imaging 26:68–76 (2007), [3] Campbell-Washburn A et al, MRM 75(6):2278-85 (2016), [4] Moussavi A et al, MRM 71(1):308-12 (2014).

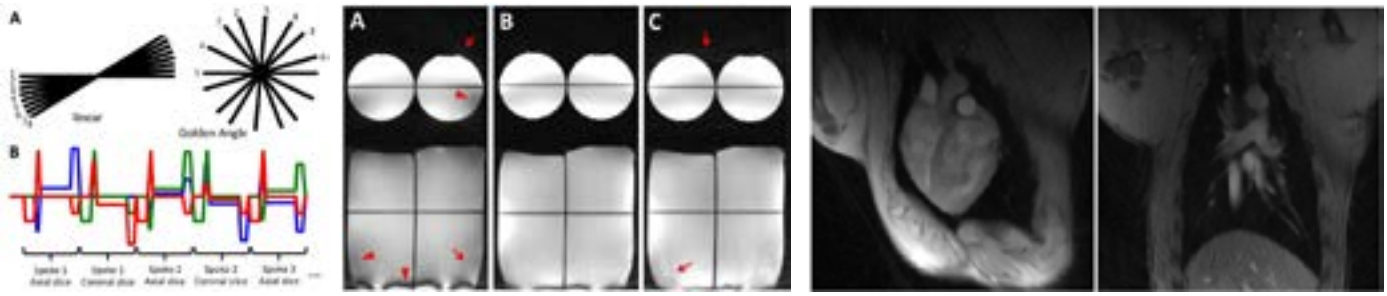

P163

53 year-old female with recurrent chest pain and a coronary CT angiogram three years earlier which showed mild, non-obstructive coronary artery disease.

Arlene Sirajuddin, MD[1]Marcus Y. Chen, MD[2], Gina LaRocca, MD[2], Andrew E. Arai, MD[2]

1. National Institutes of Health, Bethesda, MD
2. National Institues of Health, Bethesda, MD

Description of Clinical Presentation: This 53 year-old female has had chest pain on exertion as well as chest pain at rest dating back to 2006. The chest pain typically lasts for 30 to 60 minutes. Rest, aspirin, and deep breathing have relieved the chest pain. The chest pain became significantly worse in 2012. In 2013, the patient had a coronary CT angiogram study, which showed only mild, non-obstructive coronary artery disease. Since that time, the chest pain has continued. She continues to smoke cigarettes. She also has a history of hypertension and hyperlipidemia.

Diagnostic Techniques and Their Most Important Findings: The coronary CT angiogram from 2013 showed non-obstructive coronary artery disease. There was a mild (30-49%) stenosis of the proximal first diagonal branch as well as minimal (< 30%) stenoses of the left main coronary artery, left anterior descending coronary artery, and distal right coronary artery. The calcium score was 269.

SPECT myocardial perfusion imaging was obtained in 2016 and was equivocal. An adenosine stress CMR about one month later showed severe subendocardial stress perfusion defects involving all myocardial segments. There was normal global and regional left ventricular systolic function (ejection fraction 61%). Late gadolinium enhancement showed subsegmental foci of enhancement in 4 of the 5 apical segments, compatible with patchy subendocardial infarctions. Additionally, there was some enhancement of the left ventricular myocardium near the right ventricular insertion points. The differential diagnosis included microvascular disease and three vessel coronary artery disease. Invasive quantitative coronary angiography showed a 72% stenosis of the distal left main coronary artery, a 68% proximal RCA and 68% distal RCA stenosis as well as moderate LAD stenoses.

Learning Points from this Case:

1. Stress perfusion CMR can be useful when SPECT myocardial perfusion imaging is equivocal but this is an uncertain indication by current US guidelines.
2. A coronary artery CT angiogram 3 years prior showing mild, non-obstructive coronary artery disease does not exclude development of significant coronary artery disease, especially if there are risk factors present.
3. Stress perfusion CMR showed diffuse, severe perfusion defects which could have represented microvascular disease or 3-vessel coronary artery disease although this seemed less likely since the chest pain syndrome was relatively stable.

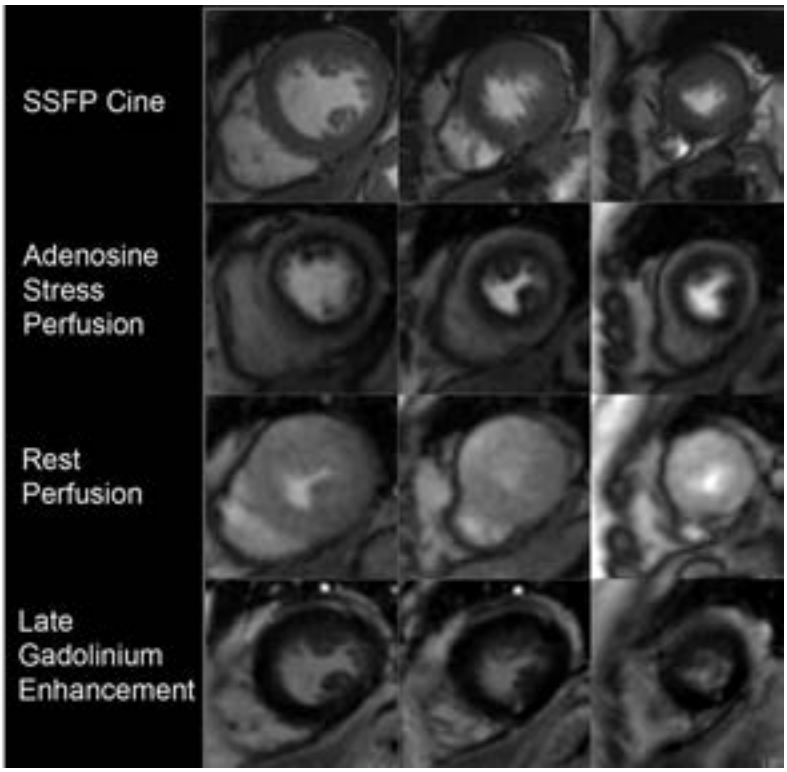

P164

Myocardial edema assessed by CMRI in non-culprit artery bed in STEMI setting?

Asmaa M. N. Elsayed Ahmed, MD, MSc.[1]Ahmed Samir, MD, MSc[2], Mohammed Hosny, MD, MSc, PhD[2], Wesam E. El Mozy, MD, MSc[2], Megahed El-Bayoumy, MD, MSc, MRCP [2], Ahmed Kharabish, MD, MSc, PhD[2]

1. Aswan Heart Centre - Magdi Yacoub Heart Foundation, Aswan, Egypt
2. Magdi Yacoub Foundation - Aswan Heart Centre, Aswan, Egypt

Description of Clinical Presentation: 63y/o♂patient presented with typical chest pain. BP: 200/90 mmHg, ECG: inferior STEMI (Fig.1), Echo: LVEF of 52%, akinesia of the inferior wall. Labs: Peak troponin-I level: 5.4 ng/ml. 1ry PCI was performed, followed on next day by CMRI to calculate the myocardial salvage index.

Diagnostic Techniques and Their Most Important Findings: 1ry PCI:
Coronary angiography revealed abrupt occlusion in the co-dominant left circumflex (LCx) artery (culprit artery) (Fig.1), proximal ulcerative lesion in the left anterior descending (LAD) coronary artery and severe mid segment right coronary artery (RCA) lesion.

Cardiac MRI: Standard cine cardiac chamber views and short axis (SAX) steady state free precession [SSFP] sequence were performed in order to measure the ventricular volumes and functions [1,2]. Also the standard 2D phase contrast (2D PC) blood flow was measured in the aorta as previously described [3]. ***Delayed enhancement (DE):*** was performed 10 minutes after contrast injection. Slice location was copied from the cine SAX covering the entire LV. ***Turbo Inversion Recovery Magnitude (TIRM):*** Myocardial edema of the acute myocardial injury was assessed using the TIRM [4,5]. Slices' location was copied from SAX slices. Areas of myocardial edema was considered in case of culprit artery segments' signals exceeded the remote myocardium's signals in addition to twice its standard deviation. Also, other methods used were:

1. Ratio of myocardium's signals to the nearest skeletal muscles' signals >1.9 was considered edema.
2. T2 mapping of slices acquired in the same position and covering the entire left ventricle as in T2-TIRM images [4,5]. A signal above 60msec was considered abnormal.

The TIRM in the culprit artery territory showed myocardial edema signals only when compared to the nearest skeletal muscles (Fig.2). Surprisingly; a high edema signals were found along the LAD territory using the T2 mapping as well as when the myocardial signals were compared to the skeletal muscles. Yet; no evidence of LGE is seen along the LAD territory as well as no abnormal wall motion (Fig.2). After 48 hours during the PCI to RCA and due to the CMRI findings (edema along the LAD territory), fractional flow reserve (FFR) was measured in mid LAD and was 0.82 denoting that the proximal LAD ulcerative lesion was functionally non-significant lesion (Fig.3).

Discussion: Mural thrombi at complex non-culprit coronary lesions with subsequent micro-infarctions in the corresponding myocardial territories were frequently encountered in autopsy studies of fatal MI cases [6]. Subsequently, the myocardial edema using CMRI in LAD territory could speak of resultant micro-embolization of minute thrombotic material and/or platelets aggregates disintegrating from the ulcerative LAD lesion during the episode of pan-coronary inflammation accompanying the inferior STEMI.

Learning Points from this Case: Ulcerative coronary artery lesions may cause micro-embolization, a phenomenon to be studied, and if proved; CMRI is a modality to be used for assessment.

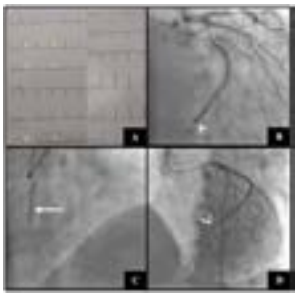

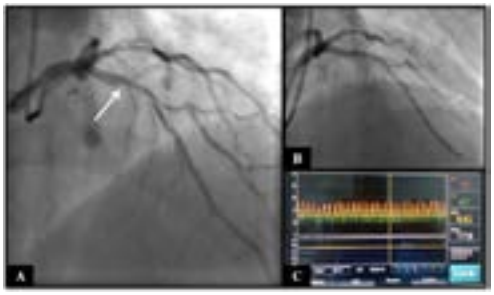

P165

Clinical Dilemma In A Subset Of ST Elevation Myocardial Infarction: "Door To Balloon Or Door To Magnet"?

Arun Nagabandi, MBBS[1] Supriya Gupta, MBBS MD[2], Jayanth H. Keshavamurthy, MD[3]

1. Augusta University/Medical College of Georgia, Augusta, GA
2. Medical college of georgia, Augusta, GA
3. Medical College of Georgia at Augusta University, Augusta, GA

Description of Clinical Presentation: This is a 16 year old male presented to our children's hospital with chief complaints of left arm pain that progressed to left sided pressure like chest pain, ongoing for 10-12 hours prior to presentation. He never experienced similar symptoms in past. His physical exam including vital signs were unremarkable. His laboratory tests were significant only for elevated cardiac troponin I at 17.5 and total CK at 601. Initial electrocardiogram (EKG) showed focal 1mm ST segment elevation in inferior (II, III and aVF) and lateral leads (V5, V6). He did not have any reciprocal ST segment depressions and his chest pain was not relieved by Nitroglycerin (NTG). He had no risk factors for Coronary Artery Disease (CAD), nor had any history of connective tissue disorders or autoimmune diseases. CODE STEMI was activated and coronary angiogram was pursued, which revealed normal epicardial coronary arteries

Diagnostic Techniques and Their Most Important Findings: He then underwent Cardiac MRI (CMR) which showed evidence of myocarditis with patchy myocardial enhancement in mid inferolateral wall and no subendocardial involvement in any specific vascular territory to suggest Acute Myocardial Infarction (AMI). His nasopharyngeal respiratory pathogen panel was negative for common viral infections and vasculitis workup was negative as well. Serum inflammatory markers (ESR and CRP) are within normal limits. He had uncomplicated hospital course and discharged eventually. His troponins very quickly downtrended and it was concluded Myocarditis was responsible for his clinical presentation.

Learning Points from this Case: Review of literature shows numerous case series of Myocarditis masquerading AMI, especially in patients < 30 years. All of them have similar clinical presentation of chest pain, elevated cardiac biomarkers, EKG changes and most of them that are ultimately diagnosed with myocarditis have low pretest probability of CAD and normal coronary angiogram like our case. Nowadays the wide and quick availability of CMR and its ability in accurately diagnosing myocarditis, raises the question whether CMR should be the initial diagnostic test in a subset of patients (young individuals with low pretest probability of CAD, hemodynamic stability, no reciprocal ST changes on EKG, history of viral infection etc), potentially obviating the need for coronary angiogram. Implementation of this strategy needs further understanding of focal EKG changes and validation of its safety in larger clinical trials.

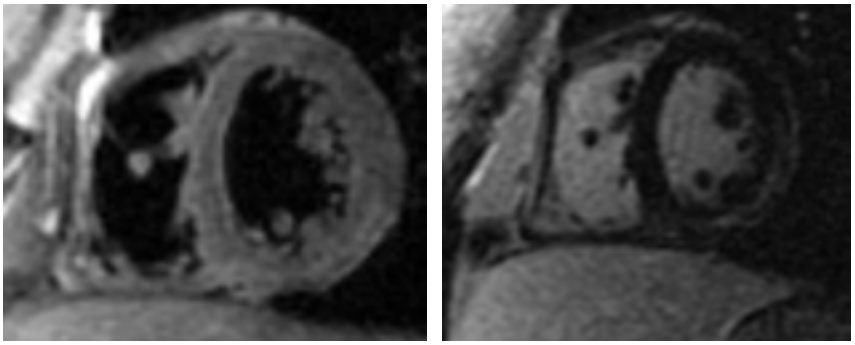

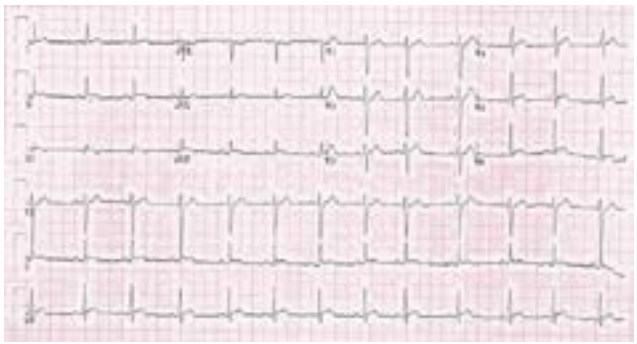

P166

Utility Of Cardiovascular MRI In Sudden Cardiac Death Survivors

Noreen Nazir, MD[1] Amita Singh, MD[2], Gaurav Upadhyay, MD[1], Amit R. Patel, MD[1], Karima Addetia, MD[3]

1. *University of Chicago, IL*
2. *University of Chicago Medical Center, Chicago, IL*
3. *University of Chicago Medical Center, IL*

Description of Clinical Presentation: A 38 year-old male with schizophrenia well controlled on haloperidol presented with a 1-week history of left arm pain and 4 hours of new chest discomfort with radiation to the neck. Initial EKG was suggestive of acute myocardial infarction (AMI) (Figure 1A). Soon after presentation, the patient sustained an episode of polymorphic ventricular tachycardia (VT) which degenerated into ventricular fibrillation that was successfully defibrillated. Coronary angiography revealed thrombus in the second obtuse marginal artery which was revascularized. Same-day echocardiogram showed a left ventricular (LV) ejection fraction of 50-55%, normal right ventricle and no valvulopathy. As the amount of coronary disease and the echocardiographic findings did not explain the etiology of the polymorphic VT arrest and along with a prolonged QT noted in the rhythm strip prior to arrest, a cardiac magnetic resonance (CMR) scan was ordered to evaluate for any underlying disease prior to defibrillator placement.

Diagnostic Techniques and Their Most Important Findings: Steady-state free precession cine images revealed mild hypokinesis of the basal inferior and inferolateral walls. LV size and systolic function was normal (65%) with mild LV hypertrophy. T2-weighted short tau inversion-recovery (STIR) images showed high-signal-intensity transmural edema in the basal inferior and inferolateral walls (Figure 1B). T2-Weighted MRI revealed myocardial edema and allowed identification of acutely ischemic myocardium. There was also subendocardial late gadolinium enhancement (LGE) in the basal inferior and inferolateral walls which was transmural at the base (Figure 1C).

Learning Points from this Case: In this case, the patient had a prolonged QT, likely due to haloperidol use, which degenerated into polymorphic VT in the setting of an AMI. The area of ischemic myocardium outlined by the T2-STIR images appeared much larger than what was thought to be the area supplied by the middle-sized obtuse marginal vessel seen on coronary angiogram, thus the CMR also aided in understanding the impact of the AMI. Subtracting the area of myocardial edema on T2-STIR images with the infarct size on LGE equates to the myocardial area of risk, from which an estimation of salvageable myocardium can be made. In this case the edema on T2-STIR covers a larger area than the LGE, which suggests that some degree of myocardial recovery should take place.

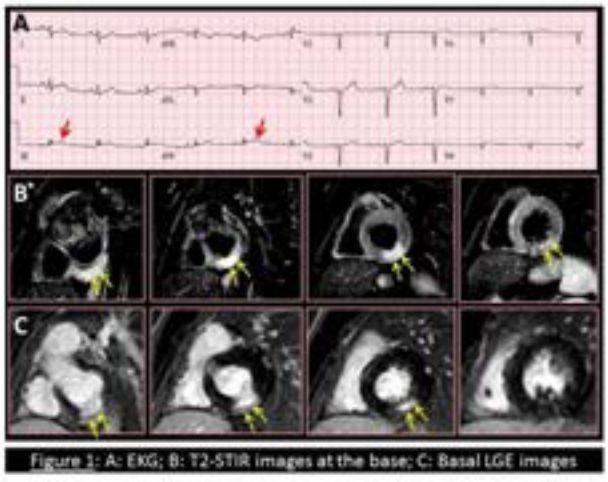

Figure 1: A: EKG; B: T2-STIR images at the base; C: Basal LGE images

P167

Improved Assessment of Ischemia: A comparison of Intermediate Dose Dobutamine Strain Encoded Cardiac Magnetic Resonance Against Single Photon Emission Computed Tomography

Noreen Nazir, MD[1] John E. Blair, MD[1], Keigo Kawaji, Ph.D.[2], Donel Tani, MS[3], Nael Osman, Ph.D.[3], Amit R. Patel, MD[1]

1. *University of Chicago, IL*
2. *University of Chicago, Chicago, IL*
3. *Myocardial Solutions, Inc., Morrisville, NC*

Description of Clinical Presentation: Recent studies have suggested that intermediate dose dobutamine Strain ENCoded (SENC) cardiac magnetic resonance (CMR) may have a similar diagnostic performance to single photon emission computed tomography (SPECT) for detecting coronary artery disease (CAD). We present two cases selected from an ongoing multicenter trial evaluating the diagnostic performance of SENC-CMR using intermediate dose dobutamine for the detection of CAD.

Diagnostic Techniques and Their Most Important Findings: CMR imaging was performed on a 1.5T scanner (Achieva, Philips). Two-chamber, 3-chamber, 4-chamber, and 3 short axis slices were acquired using both cine CMR and SENC CMR during resting conditions and three minutes after dobutamine 20 µg/kg/min infusion. SENC employed the following parameters: TR=13ms; TE=0.7ms; FA=30; 256x256mm^2; slice thickness=10mm; with a 24ms SENC magnetization preparation prior to continuous acquisition of 40ms (3 spiral interleaves) per temporal frame over 1R-R cycle. Late gadolinium enhancement (LGE) imaging was also performed. SPECT was performed using standard clinical practices. Case 1 is an 83 year old male with a history of 4-vessel coronary artery bypass graft presenting with atypical angina. Regadenoson SPECT revealed fixed perfusion defects in the left circumflex artery (LCx) and right coronary artery (RCA) territories. CMR showed transmural LGE in a pattern consistent with myocardial infarction (MI) in the RCA territory and longitudinal and circumferential regional strain values that were unchanged between rest and stress conditions suggesting the absence of ischemia (figure) and correlating with ICA findings. Case 2 is a 76 year old male with coronary artery disease (CAD) status post MI with chronic stable angina. Exercise SPECT showed fixed perfusion defects in the LCx and RCA. On CMR, LGE imaging demonstrated a non-transmural infarction in the basal inferolateral wall, consistent with LCx territory. On SENC-CMR, longitudinal and circumferential regional strain worsened following dobutamine infusion (figure), correlating with ICA findings.

Learning Points from this Case: We present two patients undergoing SPECT stress, intermediate dose dobutamine SENC-CMR, and ICA. These findings suggest that intermediate dose dobutamine SENC-CMR may potentially detect ischemia that is not otherwise evident by non-invasive testing. Further investigation is needed to determine the role of intermediate-dose dobutamine SENC-CMR to the assessment of CAD.

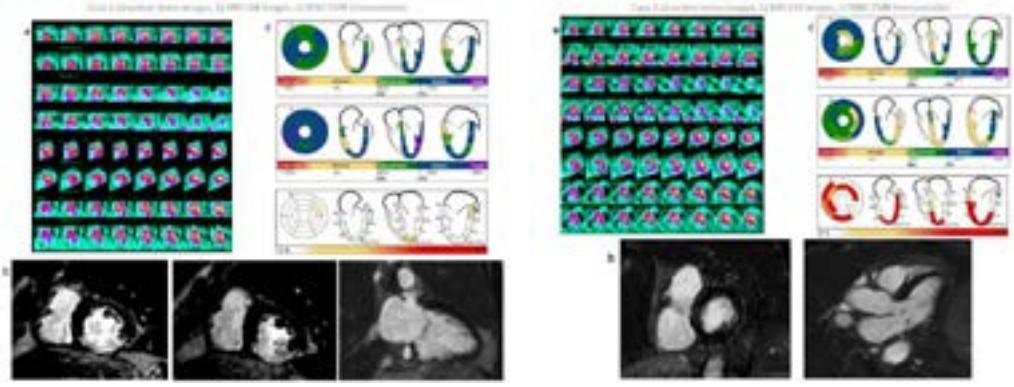

P168

Utility of CMR in detecting clinically and angiographically missed acute myocardial infarction

Mayil S. Krishnam, MD, MBA[1]Edgar Karanjah, MD[2], Eduardo Hernandez-Rangel, MD[2], Teferi Mitiku, MD[2], Pranav Patel, MD[2]

1. University of California, Irvine, Irvine, CA
2. University of California, Irvine, CA

Description of Clinical Presentation: A 55 year-old Caucasian man presented to the Emergency Department with a 4 hour history of sub-sternal, non-radiating, and non-exertional chest pain and pressure. Clinical examination was unremarkable with stable vital signs, sinus rhythm,negative initial troponin but baseline ECG showed borderline ST depressions in V4 and V5.Repeat troponins were abnormal and repeat EKG showed a new RBBB. Patient was reviewed by cardiology team and started on heparin infusion, aspirin and high dose statin and transferred to the CCU. Emergent echocardiogram demonstrated dyskinetic basal and mid septum.Catheter coronary angiography was performed and interpreted as mild non-obstructive coronary artery disease and thus medical management was maximized. Subsequently patient developed palpitations, nausea and vomiting; repeat ECG showed type 1 Mobitz heart block with intermittent 3rd degree heart block and troponins were increasing CMR was ordered to look for a non-ischemic etiology including acute myocarditis given the negative catheterization, AV Block and the rising troponins

Diagnostic Techniques and Their Most Important Findings: Emergent CMR was obtained and Cine SSFP showed normal thickness with akinesis of the basal anterior, anteroseptal and septal walls and associated T2 darkblood hyperintensity and delayed post contrast PSIR images showed subendocardial pattern of very dark signal with near transmural extent and a thin peripheral rim of late hyperenhancement, Overall CMR findings were compatable with acute transmural myocardial infarction and associated extensive microvascular obstruction(MVO) (no reflow phenomenon). Corresponding magnitude IR images showed high signal of MVO due to long T1 effect. Findings of AMI and MVO were immediately discussed with cardiology team by an experienced cardiac radiologist and recatheterization was strongly recommended to identify a culprit vessel. Coronary catheter angiography was repeated and this time a total occlusion of a large first obtuse marginal branch, had a very early take off of the circumflex coronary artery, was identified and successful stenting was placed.Patient's post procedure course was unremarkable and he was discharged two days later following a permanent pacemaker.

Learning Points from this Case: Power of CMR in depicting acute myocardial infarction, which was missed clinically and also on the gold standard catheter angiography in our patient.

T2 hyperintensity(edema), MVO, late hyperenhancement with normal wall thickness and systolic wall motion abnormality indicate AMI on CMR

MVO is a poor prognostic predictor due to the risk of future CV events such as fatal arrhythmia

MVO on TI dependent magnitude IR images may have patchy high signals due to long TI effect of an acute thrombus, but will depict dark signal on non TI dependent PSIR sequence.

It is important for cardiac imagers to recognize findings of acute myocardial infarction on CMR in patients presenting with chest pain as clinical indication and traditional cardiac tests including catheter angiography can be misleading.

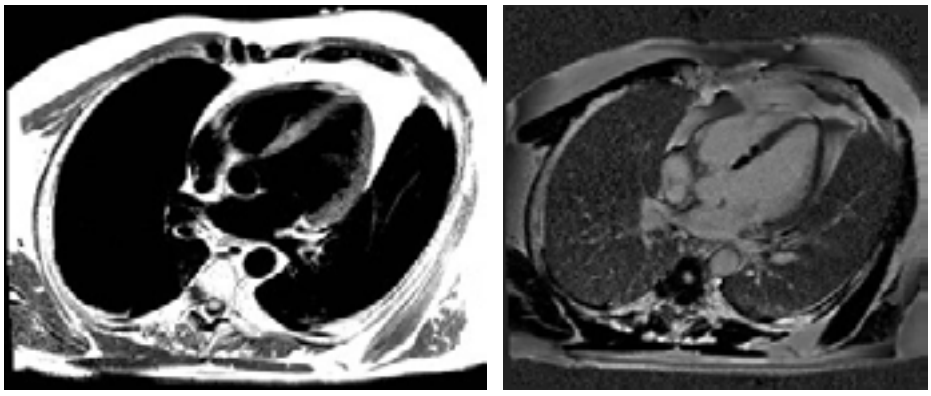

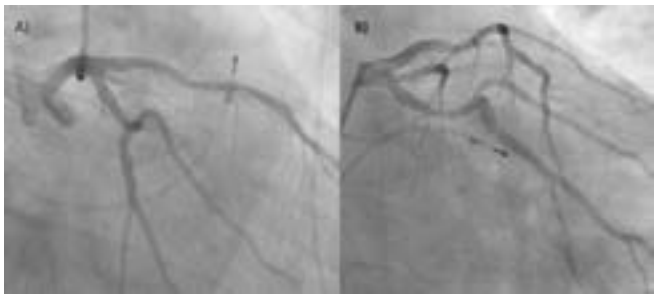

P169

Delayed myocardial infarction complicated by massive left ventricular aneurysm and thrombus.

Felicity J. Lee, MBBS[1] Eric Slimani, MBBS, FRACS[2], Leonie Maddren, Diploma in Applied Science [3], Scott O'Connor, Diploma in Medical Ultrasound[2], John Nolan, Diploma in Medical Ultrasound[2], Arun Abraham, MBBS, FRACP[4]

1. *Fiona Stanley Hospital, Department of Cardiology, Perth, Western Australia, Australia*
2. *Fiona Stanley Hospital, Western Australia, Australia*
3. *Royal Perth Hospital, Western Australia, Australia*
4. *Fiona Stanley Hospital, Royal Perth Hospital, Western Australia, Australia*

Description of Clinical Presentation: Sixty-seven year old male smoker presented to the emergency department with a prolonged episode of chest pain a month after onset of pain. ECG showed deep Q waves anteriorly with ST elevation in the inferior leads. Troponin was elevated (603; normal < 26ng/L). Coronary angiography revealed proximal left anterior descending artery (LAD) thrombus, which was treated with aspiration and stenting. Echocardiography revealed severe overall left ventricular (LV) systolic dysfunction (EF 28%) and a pedunculated mobile mass attached to the apical inferior wall consistent with thrombus. The patient was anticoagulated with warfarin while also on dual antiplatelet therapy.

He was readmitted two months later with dyspnoea. Echocardiogram showed a large apical aneurysm and laminated thrombus involving the inferior aspect of the aneurysm. The patient was commenced on diuretics and prognostic heart failure medications. His INR target was revised to up to 3.

Fourteen months later, while asymptomatic, echocardiography (Figure 1A) performed to assess role for ongoing anticoagulation, suggested increase in size of the left ventricular aneurysm with stasis and thrombus including new mobile elements. Cardiac MRI (Figures 1B and 2E) demonstrated severe LV dilation (end-diastolic volume 660ml), moderately severe LV systolic dysfunction (EF 31.3%) excluding the aneurysm and severe LV systolic dysfunction (EF 12.6%) including the aneurysm. Transmural infarction involving all of the apical segments with a massive thin walled LV aneurysm (95x93x80mm, 330ml), significant stasis and minimal residual thrombus was noted (Figures 1C and 2E). He was changed from warfarin to subcutaneous enoxaparin.

An implantable cardiac defibrillator was inserted for primary prevention. Due to the risks of LV decompensation, anticoagulation and progressive heart failure, aneurysmectomy was performed five months later (Figure 3). Intraoperative transoesophageal echocardiogram (Figure 2F) revealed a laminated thrombus (5x5cm, when excised) within the aneurysm. He was discharged on warfarin and aspirin.

Diagnostic Techniques and Their Most Important Findings: Transthoracic Echocardiography (including 3D and contrast) and transoesophageal echocardiogaphy: Elucidation of cardiac structure and function with diagnosis of LV stasis and thrombus.

Cardiac MRI (SSFP cine, SSFP rest perfusion, SSFP single shot PSIR 'early enhancement' and delayed enhancement (2D PSIR SPGRE): More accurate and comprehensive evaluation of the above with ability to accurately characterise the aneurysm, thrombus and stasis.

Findings as above.

Learning Points from this Case:

1) Role for imaging in informing treatment decisions in patients with LV aneurysms and thrombus.
2) Benefits of CMR over echocardiography in:
   - Diagnosis and characterisation of LV thrombus.
   - Evaluating LV systolic function and volume assessment particularly in the setting of a large LV aneurysm.

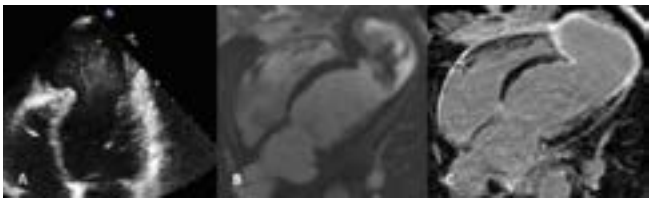

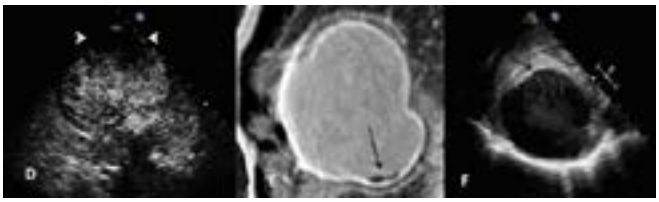

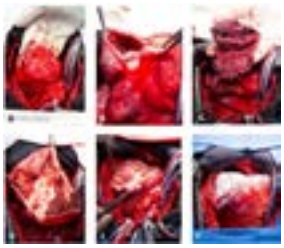

P170

LV pseudoaneurysm

Manoj Joseph[1]Samavia Raza[2], Sacha Bull[3], Oliver Rider[4], Andrew Elkington[3]

1. *Royal Brompton & Harefield NHS Foundation Trust, England, United Kingdom*
2. *Royal Brompton & harefield NHS Foundation Trust, Oxford, England, United Kingdom*
3. *Royal Berkshire Hospital, Reading, Reading, England, United Kingdom*
4. *University of Oxford Centre for Clinical Magnetic Resonance, Oxford, England, United Kingdom*

Description of Clinical Presentation: Left ventricular pseudoaneurysm represent contained myocardial rupture. They are covered by adherent pericardium or scar tissue.

A 75 year old male with history of myocardial infarction and known subsequent formation of LV pseudoaneurysm who was deemed unfit for surgery at the time of presentation came for his follow up scan as planned. Cardiac MR for function and viability was performed.

Diagnostic Techniques and Their Most Important Findings: Cardiac MRI with administration of 0.1mmol/kg body weight of Gadovist was performed that revealed further progression of the previously known LV pseudoaneurysm that now had an appearance of another focal aneurysmal dilatation within the sac. Dyskinetic wall motion was noted. Special cuts through the aneurysm confirmed absence of any endo or myocardium. After clinical team was informed, patient was still deemed too unfit for surgery and continues to be managed conservativel.

Learning Points from this Case: It is generally thought that pseudoaneurysm of the left ventricle are rapidly fatal and all chronic aneurysm represent true aneurysm made of scarred endo and myocardium. As demonstrated here, that is not always the case and pseudoaneurysm can on rare occasion present as stable aneurysms with a hemodynamically stable patient.

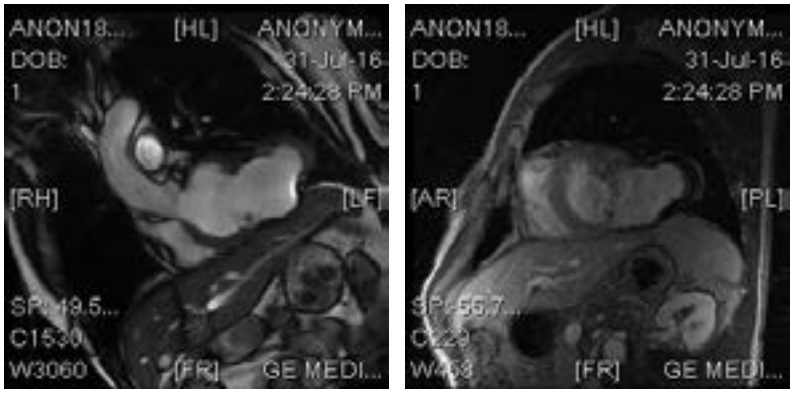

P171

Single-shot T2STIR Preparation bSSFP for Myocardial Edema Imaging

Yanjie Zhu, Ph.D.[1]Dan Yang, msci[2], Yucheng Chen, MD[3], Xin Liu, M.D.[4], Yiu-Cho Chung, Ph.D.[5]

1. *Shenzhen Institutes of Advanced Technology, Chinese Academy of Sciences, Shenzhen, Guangdong, China (People's Republic)*
2. *West China Hospital,Sichuan University, Sichuan, China (People's Republic)*
3. *West China Hospital, CHENGDU, Sichuan, China (People's Republic)*
4. *Lauterbur Research Center for Biomedical Imaging, Shenzhen Institutes of Advanced Technology, Chinese Academy of Sciences, Shenzhen, China, Guangdong, China (People's Republic)*
5. *Shenzhen Institutes of Advanced Technology, Chinese Academy of Sciences, Guangdong, China (People's Republic)*

Background: Myocardial edema in acute myocardial infarction (MI) or myocarditis is commonly imaged using dark-blood STIR TSE (STIR-TSE) [1]. However, STIR-TSE is sensitivity to cardiac motion, resulting in myocardial signal inhomogeneity. Single-shot T2-prepared bSSFP (T2p-bSSFP) overcomes this issue [2], but averaging is commonly used to improve its contrast. We propose a novel single-shot imaging technique that improves contrast between edema and normal myocardium compared to T2p-bSSFP in one heartbeat.

Methods: Both T1 and T2 are elevated in edema [3]. Introducing T1 weighting to T2 preparation would increase its sensitivity to edema detection. The proposed sequence, T2STIR-bSSFP, has two parts. First, a preparation module called "T2STIR" is used to generate "STIR-like contrast" using a series of adiabatic pulses that tip the magnetization down to –z axis after T2 preparation. After a time TI selected to null fat signal, single-shot bSSFP is used for image acquisition. Optionally, proton density weighted image is acquired in another heart beat for image normalization (Figure 1(a)). The proposed sequence was implemented on a 3T scanner (TIM Trio, Siemens) and tested on a phantom (Resonance Health). It was then evaluated in an IRB approved patient study. Five patients (informed consent given) with confirmed acute MI were recruited. At the edematous region, T2STIR-bSSFP and T2p-bSSFP images were acquired and compared. Imaging parameters for both sequences were: TR=2.6ms, flip angle=60^{o}, base resolution=192, GRAPPA rate 2, TE_{prep}=60ms, linear reordering, TI=125ms for T2STIR-bSSFP. To better characterize edema, STIR-TSE, T1 and T2 maps and LGE images at identical locations were acquired.

Results: Figure 1(c)-1(h) show the images from one patient with myocardial edema. T2STIR-bSSFP and T2p-bSSFP images were windowed the same to facilitate comparison. Signal for remote myocardium is lower in T2STIR-bSSFP compared to T2p-bSSFP while the reverse is true for edema. Fat suppression in T2STIR-bSSFP eliminates the dark rim at the fat-water interface (yellow arrow), and helps distinguish between pericardial fluid and fat. Table 1 shows the T1 and T2 values of myocardium and edema, and the CNR between them in all the patients. The CNR between edema and normal myocardium in T2STIR-bSSFP is about 1.3~3 times higher than that of T2p-bSSFP.

Conclusions: Single-shot T2STIR-bSSFP has improved contrast compared to T2p-bSSFP in myocardial edema imaging. The technique would help improve the detection of myocardial edema.

Funding: National Natural Science Foundation of China (61401449)

Reference:

1. Simonetti OP, et al., Radiology, 199:49, 1996.
2. Kellman P, et al., MRM 57:891, 2007.
3. Ugander M, et al. JACC, 5(6):596, 2012.

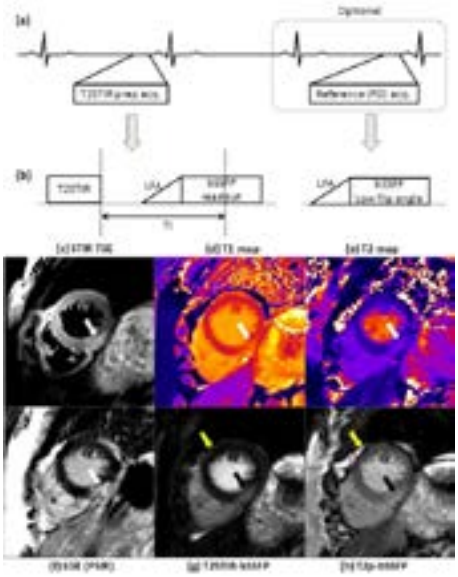

Table 1. The T1 and T2 values of myocardium and edematous region and the CNR between them from the two single-shot imaging sequences in the five patients.

CNR		Edema		Remote myocardium		Patient
T2STIR	T2p	T2	T1	T2	T1	
36.1	26.1	62.4±4.6	1571.8±47.8	40.3±2.0	1251.3±26.0	1
42.0	29.3	62.0±2.4	1543.7±35.9	45.6±0.7	1305.6±39.2	2
42.8	32.6	61.2±2.6	1556.1±53.3	40.8±1.4	1318.4±33.8	3
59.8	24.3	58.3±1.9	1509.2±45.7	44.6±3.2	1223.3±23.5	4
34.6	11.3	61.0±4.3	1516.4±112.3	39.8±1.9	1272.6±34.1	5

Table 1. The T1 and T2 values of myocardium and edematous region and the CNR between them from the two single-shot imaging sequences in the five patients.

CNR		Edema		Remote myocardium		Patient
T2STIR	T2p	T2	T1	T2	T1	
36.1	26.1	62.4±4.6	1571.8±47.8	40.3±2.0	1251.3±26.0	1
42.0	29.3	62.0±2.4	1543.7±35.9	45.6±0.7	1305.6±39.2	2
42.8	32.6	61.2±2.6	1556.1±53.3	40.8±1.4	1318.4±33.8	3
59.8	24.3	58.3±1.9	1509.2±45.7	44.6±3.2	1223.3±23.5	4
34.6	11.3	61.0±4.3	1516.4±112.3	39.8±1.9	1272.6±34.1	5

P172

Cine T1 Mapping: B1 corrected Look-Locker inversion recovery for phase resolved T1-Mapping At 3T

Sebastian Weingärtner, Ph.D.[1]Chetan Shenoy, M.D.[2], Mehmet Akçakaya, Ph.D.[3]

1. *Electrical and Computer Engineering, University of Minnesota; Center for Magnetic Resonance Research, University of Minnesota; Computer Assisted Clinical Medicine, University Medical Center Mannheim, Heidelberg University, Mannheim, Baden-Wurttemberg, Germany*
2. *Cardiovascular Division, Department of Medicine, University of Minnesota, Minneapolis, MN*
3. *Electrical and Computer Engineering, University of Minnesota; Center for Magnetic Resonance Research, University of Minnesota, Minneapolis, MN*

Background: Myocardial T_1 mapping allows assessment of a large variety of diffuse pathologies in the myocardium [A.-Venkatesh NatureRevCard2015]. It is commonly acquired with single-shot imaging, typically during diastolic quiescence, giving one snapshot of the cardiac cycle. Recently, systolic T1 mapping has shown promise, providing supplementary information [Ferreira JCMR2015]. Cardiac phase-resolved T1 mapping would provide information through the cardiac cycle, which may improve depiction of subtle lesions and reveal information about myocardium in the presence of abnormal contractility, e.g. in restrictive cardiomyopathy or restrictive pericarditis [Hamlin Radiographics2014]. In this study, we sought to develop a steady-state Look-Locker imaging sequence for phase-resolved myocardial T1 mapping in a single breath-hold.

Methods:

Sequence: Fig. 1 depicts the sequence: 1) Magnetization is driven to steady-state with FLASH excitations, 2) Inversion pulse is applied, 3) k-space segments are acquired for each cardiac phase until steady-state is reached again. Since steady-state after the inversion is reached over a number of R-R intervals, multiple T1-weighted images are acquired for each cardiac phase. After re-reaching steady state, steps 2 and 3 are repeated to get more segments for the cardiac phases, until the k-space is filled. To mitigate R-R variability, dummy pulses with no ADC are played after the last cardiac imaging phase until R-wave is detected.

Reconstruction: T1* can be extracted from a three parameter inversion-recovery model-fit (Eq. 1). The knowledge of TR and the excitation flip angle (FA) allows to calculate T1 (Eq. 2). The efficiency of the rectangular inversion pulse (B in Eq. 1), allows correction of B1+ inhomogeneities in the FA.

Imaging Parameters: Field strength=3T, TR/TE/FA=5/2.5ms/3°, FOV=300x300mm^2, resolution=1.9x1.9mm^2, slice thickness=10mm, temp. resolution=40-60ms, breath-hold duration=19-23s. T1 mapping was compared to SAPPHIRE [Weingärtner MRM2014] in phantom scans. In vivo imaging of a single short-axis slice was performed on 4 healthy adults.

Results: The phantom results show good agreement for short T1 time (difference: -0.5±0.8%), and underestimation of long T1 times (-5.1±2.1%) (Figure 2a). The coefficient of variation among the T1 times at different cardiac phases, as depicted in Figure 2, was: 0.8%-2.4% (phantom), 2.0% (in vivo). Decreased precision for end-diastolic phases is observed due to the lack of short inversion times.

After correction, homogeneous T1 maps in the 3T T1 value range (diastole: 1328±53ms, mid diastole: 1383±65ms) are reconstructed. Without B1+ correction, the values are severely underestimated. The B1+ maps generated in this process are also homogeneous and largely T1 insensitive.

Conclusions: The proposed cine T1 mapping sequence allows for cardiac phase-resolved T1 mapping with high temporal and spatial resolution in a single breath-hold.

Funding: NIH R00HL111410, P41EB015894

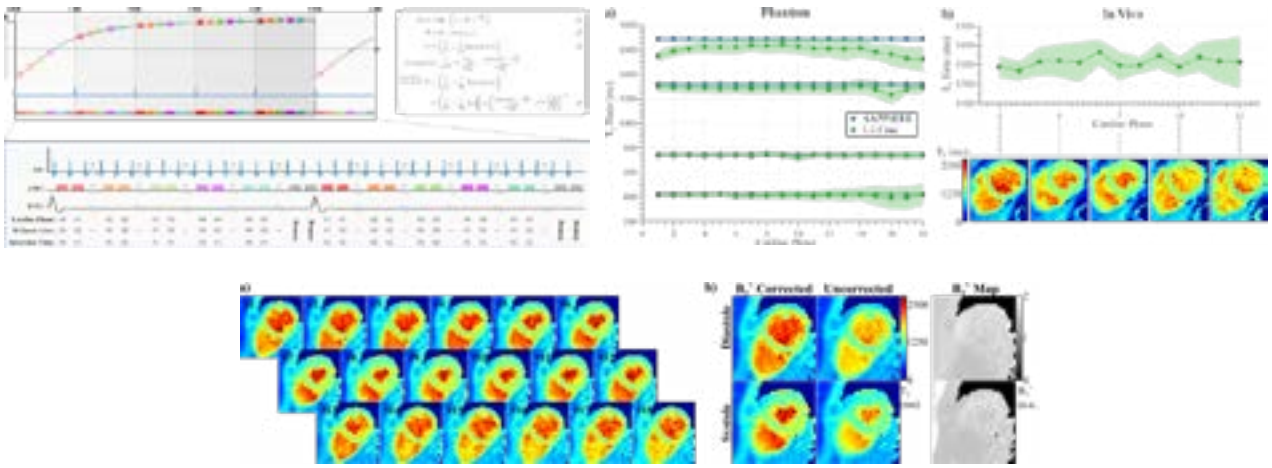

P173

Low Power Wideband Dark-Blood Delayed-Enhancement Imaging

Elizabeth Jenista, Ph.D.[1]David Wendell, PhD[2], Enn-Ling Chen, PhD[2], Wolfgang Rehwald, PhD[3], Stephen Darty, RT-N,MR; BSRS[2], Han Kim, MD[1], Michele Parker, MS[4], Raymond j. Kim, MD[2]

1. *Duke University, Durham, NC*
2. *Duke University Medical Center, NC*
3. *Siemens Healthcare, NC*
4. *Duke Cardiovascular MR Center, Durham, NC*

Background: We recently introduced a flow-independent dark-blood delayed-enhancement technique (FIDDLE, 1), which provides superior diagnostic performance than conventional delayed-enhancement (DE-MRI) for the diagnosis of MI. Imperfections in the inversion (IR) pulse can reduce FIDDLE and DE-MRI image quality, especially in the presence of metal. Recently, a wideband IR pulse based on a standard adiabatic hyperbolic secant (HS) waveform, has improved DE-MRI image quality in patients with implanted cardiac devices (2). However, the HS waveform has inefficient distribution of RF power requiring high peak amplitudes (3). Since this limitation is of particular importance at 3T we implemented a low power, wideband IR pulse for use at 3T which is based on a constant amplitude linear sweep for the central region which can be "stretched" to fit the desired effective inversion bandwidth (3). This stretched adiabatic (SA) pulse has its origins in spectroscopy, and has never been used for proton imaging. In this study, we compared the SA to the conventional HS pulse for wideband FIDDLE at 3T.

Methods: IR pulses were evaluated in Bloch equation simulations, phantoms, and in 13 patients (n = 9 with implanted metal, 4 without). In patients, the two sets of FIDDLE images were acquired in an interleaved fashion 10-20 mins after gadolinium administration (0.2 mmol/kg) using identical parameters. Images were visually graded for image quality, overall, and immediately adjacent to metal, and for quality of blood pool suppression (0=poor, 3=excellent). Blood pool homogeneity was quantitatively assessed by placing ROIs in the LV and RV blood pools and over the entire heart (blood pool and myocardium in all chambers), and reported as the percent variation in blood pool signal normalized to the standard deviation of the signal from the entire heart.

Results: Simulations showed both had similar inversion bandwidths, but SA required 34% less B1. Example images from patients with implanted metal are shown in **Figure 1.** Assessment of the images (**Table 1)** showed that while both pulses performed well near metal, SA inversion provided better blood pool homogeneity and improved overall image quality. Similarly, in the quantitative assessment of blood pool homogeneity (**Figure 2**), there was a significant improvement with SA inversion.

Conclusions: We have implemented a novel wideband inversion pulse with lower RF power requirements for clinical imaging. This pulse provides improved image quality in the presence of metal for dark blood delayed enhancement imaging at 3T.

References:

1. Kim, H et al, JCMR 2016 18(supp1):O55
2. Rashid, S et al, Radiology 270(1), 269-274 (2014)
3. Kupce, E; Freeman, R; JMR 117, 246-256 (1996)

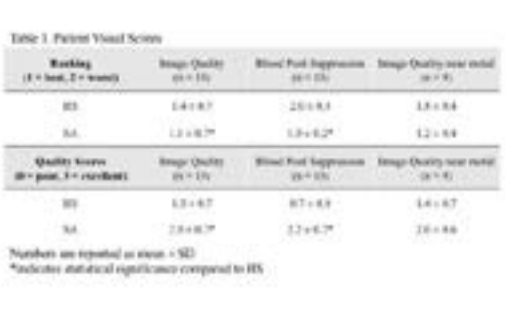

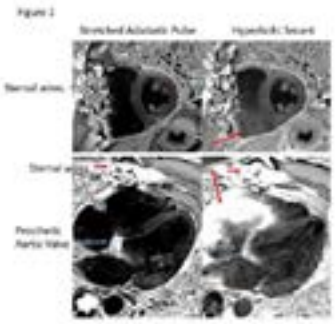

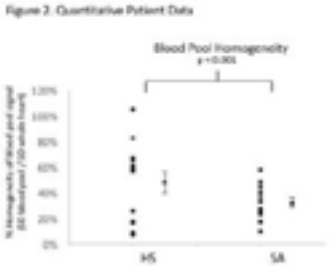

P174

Cardiac MRI with Spatially Resolved MR-Compatible Ultrasound Doppler Triggering for Function and Flow Quantification at 3T.

Lindsey A. Crowe, PhD[1] Gibran Manasseh, MD[1], Aneta Chmielewski, PhD[2], Anne-Lise Hachulla, MD[1], Daniel Speicher, MSc[3], Andreas Greiser, Ph.D[4], Hajo Muller, MD[1], Thomas de Perrot, MD[1], Jean-Paul Vallée, MD PhD[1], Rares Salomir, PhD[1]

1. *Geneva University Hospital, Geneve, Switzerland*
2. *The Hospital for Sick Children, Toronto, ON, Canada*
3. *Fraunhofer Institute for Biomedical Engineering, Saarland, Germany*
4. *Siemens Healthcare GmbH, Erlangen, Germany, Erlangen, Bayern, Germany*

Background: We demonstrate a Magnetic-Resonance-compatible ultrasound (US) imaging probe using spatially resolved Doppler as an alternative to standard ECG triggering. We assess feasibility of triggering to carotid ultrasound for potential cases where the ECG signal is compromised by pathology or interference at higher magnetic fields, or where direct ECG is impossible.

Methods: A dedicated MR-compatible phased array ultrasound probe was designed for this study. Pulsed-Doppler images, exported from a clinical console to an external computer providing an output trigger signal to a 3T MR scanner. Conventional MR cardiac protocol cine and flow phase contrast images were acquired in 10 healthy volunteers with gold standard ECG triggering and the proposed spatially resolved Doppler triggering from common carotid blood flow.

Image quality was scored (blinded, scale 0-3, two experienced radiologists) on randomized 4-chamber, 2-chamber and short-axis cines. Quantitatively, images were analyzed for sharpness. Ejection fractions (EF) were calculated, and flow was compared in the ascending and descending aorta.

Retrospective processing from a synthetic 'false trigger', using Metric Optimized Gating (MOG), was included for comparison, and the preprocessed false-trigger images were an example of failed triggering.

As a final step, 4D flow acquisitions using a prototype sequence with US Doppler triggering and ECG triggering showed feasibility of Doppler triggering over a long acquisition time.

Results: Imaging modalities were compatible with no significant artifacts from the other modality that could compromise triggering signal or acquired images. Image quality scored a mean of 2.6 for Doppler and 2.7 for ECG (out of 3 for all subjects). Doppler-triggered EF was equivalent to ECG-triggered and MOG ($p=1$), with false-triggered EF much more variable and significantly lower ($p < 0.0005$). Mean EF (%) were Doppler trigger 64.5±3.1, ECG 64.7±5.3, MOG 62.2±5.3 and false 38.9 ± 14.9. Inter-observer agreement for EF was excellent ($p=0.89$ for Doppler and 0.52 for ECG). Doppler triggering showed no difference in flow quantification in the ascending and descending aorta to both ECG-triggered and MOG. 4D Flow quantification gave consistent results between the two triggering methods on visually comparable images.

Conclusions: Doppler-triggered cine and phase contrast images were successfully obtained in healthy volunteers. Image quality is highly comparable to ECG triggering, and accurate functional parameters accessible. Quantitative images are obtained without an ECG signal, with Doppler fast enough to trigger functional images. The hardware platform is designed to further enable advanced cardiac imaging in complex cases and under free breathing, and has the potential for robust fetal cardiac imaging.

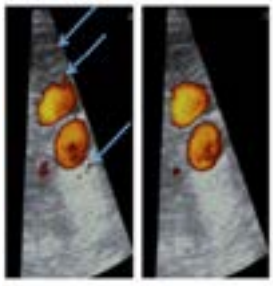

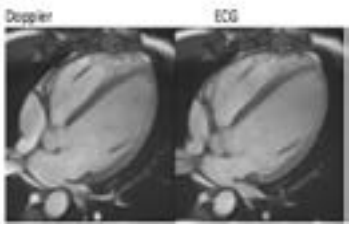

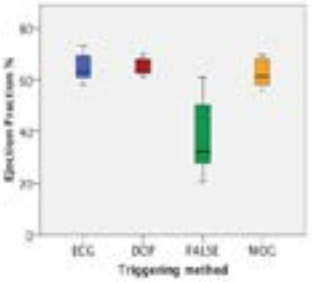

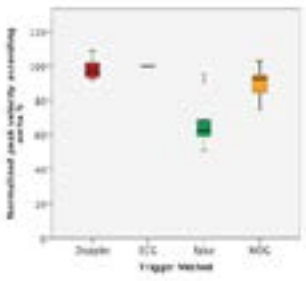

P175

Metal Artifact Reduction for Accurate Myocardial Scar Assessment in Patients with Cardiac Implanted Electronic Devices Using Cardiovascular Magnetic Resonance

El-Sayed H. Ibrahim, PhD[1]Jadranka Stojanovska, MD[2], Prachi Agarwal, MD[2], Maryam Ghadimi-Mahani, MD[2], Anil Attili, MD[2], Chiel den Harder, PhD[3], Mariska Damen, MSc[3], Frank Bogun, MD[2]

1. *University of Michigan, Ann Arbor, MI*
2. *University of Michigan, MI*
3. *Leiden University, Zuid-Holland, Netherlands*

Background: Late gadolinium enhancement (LGE) CMR is the gold standard for imaging myocardial viability. An important application of LGE CMR is the assessment of myocardial scar in patients with ventricular tachycardia (VT) before ablation procedure. Nevertheless, in patients with cardiac implanted electronic devices (CIEDs), LGE imaging is challenging due to device-generated metal hyperintensity artifacts that compromise the effect of the inversion recovery (IR) pulse used in the LGE sequence and obscure the region of interest. In this study, we propose a modified IR technique to alleviate these artifacts and improve diagnostic image quality.

Methods: The modified pulse sequence includes a wideband IR RF pulse with adjustable frequency offset and bandwidth, which allows for optimal myocardial signal nulling even in the presence of off-resonance effects. A phantom experiment was conducted on a 1.5T Philips scanner, where a CIED was placed one-inch away from a water bottle. A cross-sectional image of the bottle was acquired using conventional and wideband IR sequences with different frequency offset and bandwidth (BW) values. Twelve patients (10 males, age=60±18 y.o.) with CIEDs (5 Boston Scientific, 5 Medtronic, and 2 St Jude; 7 Bi-Ventricular, 4 Dual-Chamber, and 1 Single-Chamber) were then imaged on the same scanner using the conventional and optimized wideband LGE techniques for assessment of myocardial scar prior to ablation procedure to treat VT. The imaging parameters were optimized for each patient to improve myocardial nulling while minimizing metal artifacts.

Results: Conventional IR sequence resulted in severe hyperintensity artifacts that obscured ventricular segments, making the images non-diagnostic for scar evaluation. The wideband IR sequence significantly minimized the artifacts, such that anatomical details could be seen and scar assessment could be confidently performed (Figure-1). Increasing the IR frequency BW results in better artifact reduction, although this comes at the cost of incomplete myocardial nulling (Figure-2). So, BW should be set to the minimum value that eliminates the artifact, which is affected by the device type and location. Similarly, the frequency offset of the IR pulse affects the artifact appearance (Figure-3), so proper setting of the frequency offset could allow for removing the artifact without the need to increase the frequency BW. Based on the studied cases, optimal BW was in the range of 2000-3000Hz with optimal frequency shift up to 1000Hz.

Conclusions: The developed wideband IR technique minimizes the CIED-generated hyperintensity artifacts without increasing scan time, and allows for accurate identification of arrhythmogenic substrate and ablation target in VT patients.

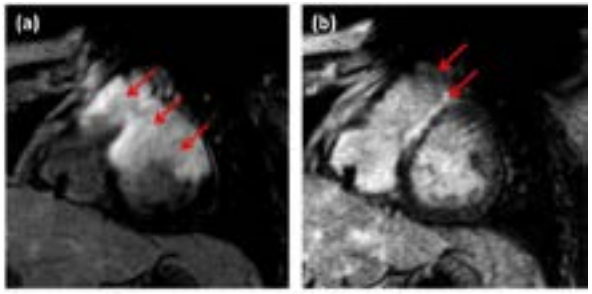

Fig 1. (a) Conventional LGE image showing metal hyperintensity artifact (arrows) from the ICD. (b) The same image in (a) acquired with optimized wideband-IR sequence, which eliminates the artifact and reveals underlying scar (arrows).

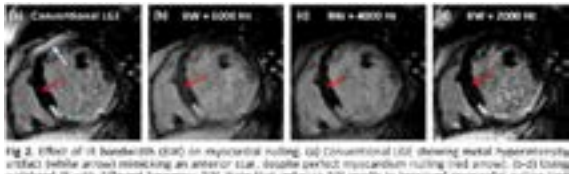

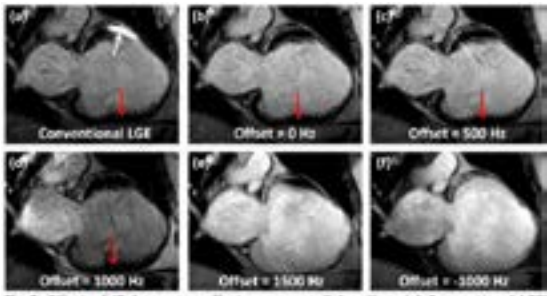

P175

Changes in Myocardial Native T1 and T2 After Physical Exercise: A Feasibility Study

Shiro Nakamori, MD, PhD[1]Javid Alakbarli, MD[1], Gifty Addae, BS[1], Jihye Jang, M.Sc.[2], Sophie Berg, RN[1], Kraig Kissinger, RT[1], Beth Goddu, RT[1], Warren J. Manning, MD[3], Reza Nezafat, PhD[4]

1. *Beth Israel Deaconess Medical Center, MA*
2. *Beth Israel Deaconess Medical Center and Harvard Medical School, MA*
3. *Beth Israel Deaconess Medical Center, Boston, MA*
4. *Department of Medicine (Cardiovascular Division) Beth Israel Deaconess Medical Center, Harvard Medical School, Cardiology, East Campus, Room E/SH455, 330 Brookline Ave, Boston, MA, 02215, MA*

Background: Cardiovascular magnetic resonance (CMR) T_1 and T_2 techniques are highly sensitive to myocardial water content and allow for the quantification of myocardial tissue characterization. However, the feasibility of native T_1 and T_2 for the assessment of changes in myocardial blood flow (MBF) due to exercise remains to be clarified. Therefore, this study sought to assess changes in measured myocardial T_1 or T_2 after physiological stress.

Methods: A total of 15 young healthy adult subjects (3 men, mean age: 26 years) were prospectively enrolled. Whole heart T_1 and T_2 mapping were performed using free-breathing slice-interleaved T_1 and T_2 mapping sequence [1,2] at 1.5 T Philips scanner. The exercise test was performed with a supine cycle ergometer (Lode B.V., Groningen, NL) secured on CMR sliding table such that the subject could exercise without leaving the table. Ergometer exercise was begun at 50W and workload was increased in increments of 25W until a strenuous workload was reached. Fig. 1 shows the study protocol. After image localization, the subjects underwent cine CMR and rest T_1/T_2 mapping, followed by repeated T_1/T_2 mapping scans: (a) 1,3,5 minutes after cessation of 1st maximal exercise, (b) 1,3 minutes after 2nd exercise. Heart rate and ECG data were recorded by using the three-lead ECG device and blood pressure was monitored every two minutes during exercise. Maximum heart rate-blood pressure product was calculated as the index of external cardiac work.

Results: Fig. 2 shows the mean ± SD of changes in T_1 and T_2. Native T_1 value was significantly elevated in all subjects immediately after exercise and had trends to decrease 3 minutes after exercise and return to baseline 5 minutes later. This trend was observed in native T_1 value after 2nd exercise. On the other hand, the increase in T_2 value was gradual and significantly more pronounced 5 minutes after 1st exercise (baseline: 40 ± 4 ms, 5min: 46 ± 5 ms, $P < 0.05$ after Bonferroni correction). Native T_1 immediately after exercise had moderate correlation with maximal cardiac workload, indicating MBF during exercise ($r=0.55$, $p < 0.05$) while T_2 value 5min after exercise was correlated with it ($r=0.61$, $p < 0.05$).

Conclusions: Native T_1 as well as T_2 mapping protocol can detect changes in MBF after physical exercise. Further studies in patients are warranted to investigate if native T_1 and T_2 can detect abnormal MBF in patients.

Reference:

[1] Weingartner S et al., MRM, 2014.

[2] Basha TA et al. MRM, 2015.

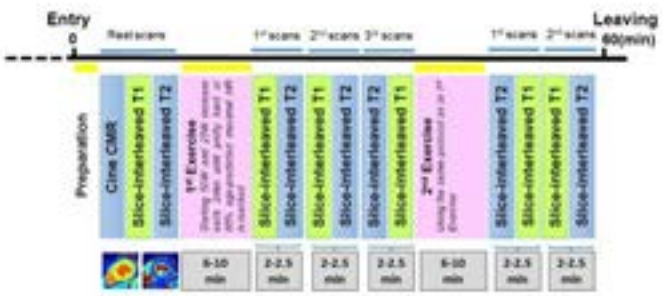

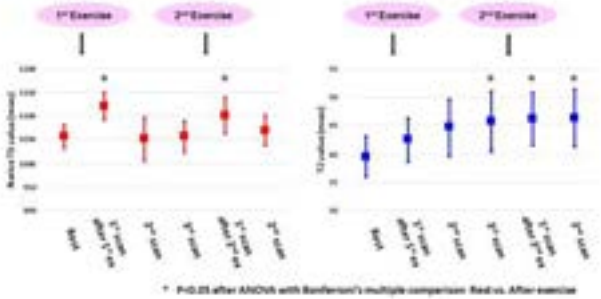

P176

A Novel Single-Cardiac-Cycle Phase Sensitive Inversion Recovery (PSIR) Method Improves Free Breathing Single Shot Flow Independent Dark Blood Delayed Enhancement (FIDDLE)

Wolfgang G. Rehwald, Ph.D.[1]David Wendell, PhD[2], Louis A. Klem[3], Dina Labib, MD[2], Denise Garman, BSRT (MR)[4], Nestor Mena, B.A., A.S.[5], George Gamoneda, AS[6], Stephen Darty, RT-N,MR; BSRS[2], Michele Parker, MS[7], Han Kim, MD[8], Elizabeth Jenista, Ph.D.[8], Raymond j. Kim, MD[2]

1. *Siemens Medical Solutions USA, Inc., Chapel Hill, NC*
2. *Duke University Medical Center, NC*
3. *Duke University, Chapel Hill, NC*
4. *Duke University, NC*
5. *Duke University Hospital, Clayton, NC*
6. *Duke University Hospital, NC*
7. *Duke Cardiovascular MR Center, Durham, NC*
8. *Duke University, Durham, NC*

Background: PSIR can be challenging in patients with poor breath holding capability since it requires matched acquisition of two data sets, a magnetically prepared (MP) and a reference (REF) set, in separate heart beats (HB), which increases the chance for misregistration artifacts. Likewise, PSIR combined with 3D and respiratory navigation is problematic, as registration of MP and REF by navigator more than doubles acquisition time compared to MP alone. Single shot (SSH) imaging can reduce respiratory motion artifacts for MP data, but SSH PSIR may still be susceptible to respiratory motion as MP and REF are typically acquired two HBs apart. We hypothesized that acquiring REF and MP in one (SINGLE) instead of separate HBs (SEPARATE), would reduce motion artifacts in SSH PSIR images acquired during free-breathing. To obtain single-cardiac-cycle PSIR, we moved REF to the beginning of the R-wave (i.e. prior to systole) and limited its acquisition to 90 ms to provide spatial registration with MP acquired later in mid-diastole. We applied the new SINGLE PSIR scheme to FIDDLE as FIDDLE requires PSIR reconstruction, and compared it to the standard SEPARATE scheme.

Methods: To fit REF within the first 90 ms of the RR we reduced its phase encoding and temporal resolution to 50% ($\Delta t/2$=90ms) of MP, see figure 1. We acquired 27 short or long axis steady state free precession FIDDLE images with SEPARATE and SINGLE, using matched parameters. Typical parameters were fov 340 x240 mm, resolution 1.6 x 1.9 x 8 mm, TR 2.7 ms, TE 1.5 ms, parallel acquisition factor 2, partial Fourier factor 7/8, and temporal solution 180 ms. Three blinded readers scored both image types for presence of misregistration artifacts and image quality (IQ) as excellent-good (score=2), moderate (1), and poor (0). We measured myocardium and blood signal in the PSIR images. Scores and signal values were compared by paired t-tests.

Results: Out of 27 images, misregistration artifacts were present in 14 SEPARATE, but only 2 SINGLE images ($p < 0.001$), see figure 2. SEPARATE and SINGLE images received 10 and 24 excellent-good scores, 11 and 3 moderate scores, 6 and 0 poor IQ scores, respectively. Mean IQ (± sem) score was 1.18 ± 0.009 for SEPARATE and 1.88 ± 0.003 for SINGLE, which was significantly better ($p < 0.005$, mean across readers). Blood signal of SEPARATE and SINGLE was identical ($p > 0.05$); so was myocardium ($p > 0.05$). The SEPARATE image in figure 3 demonstrates an artefactual thick RV freewall and bright artefactual signal across the LV (red arrows). No artifacts are observed in the corresponding SINGLE image.

Conclusions: Misregistration artifacts are common in free breathing SSH PSIR. The SINGLE method significantly reduces these artifacts and improves IQ, likely because MP and REF have better spatial registration during free breathing. Acquiring a short REF scan at the R-wave ensures good registration to MP despite different time within the RR. Placing this short REF before MP causes no significant signal saturation.

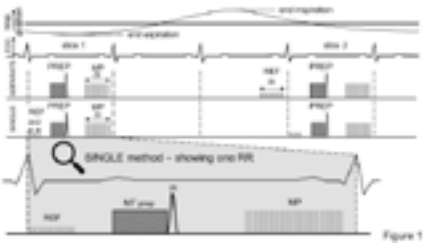

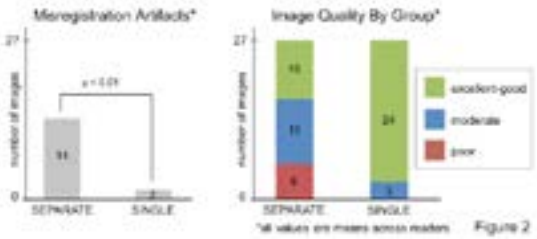

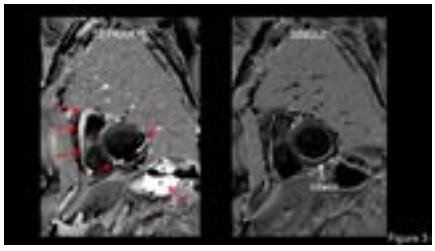

P177

T1-refBlochi: High resolution 3D cardiac T1 mapping methods based on 3D late gadolinium enhancement, Bloch equations, and a reference T1.

Dana C. Peters, PhD[1]Chenxi Hu, PhD[1], Albert J. Sinusas, M.D.[2], Steffen Huber, M.D.[1], Stephanie Thorn, PhD[1], Mitchel R. Stacy, PhD[1], Hamid Mojibian, M.D.[1]

1. *Yale University, CT*
2. *Yale University, New Haven, CT*

Background: High resolution T1-mapping for applications such as left atrial fibrosis assessment is important. T1-refBlochi uses a single high-resolution 3D late gadolinium enhancement (LGE) volume to generate a T1-map, based on the Bloch equations to generate a signal vs. T1 curve, and a single calibration measurement, using a reference T1 and its mean signal within the image.

Methods: The T1-refBlochi method (Figure 1) recognizes that the LGE signal is a product of weightings due to coil, proton density (PD), T2*, and T1. Coil-sensitivity is removed by measuring and removing the 3D trend observed in the blood pool. We hypothesize that weightings of PD and T2* are small or can be minimized, and this weighting is assumed to be a scalar. Using the exact Bloch equations, the steady state signal (proportional to image intensity) vs. T1 function is modeled. Since it is monotonic for T1s greater than the nulled T1, the signal can be transformed into T1 directly, using a reference T1 and signal (e.g. blood—measured previously) to calibrate the signal vs. T1 relationship. **Phantom studies** were performed with known T1s ranging from 200-560ms. The base LGE protocol modeled was: TR/TE/Θ/TI/RR/vps = 3.8ms/2ms/15◦/TI=300ms/800ms/37, with multiple variations (including RR) studied. **In vivo imaging** in 8 pigs (4 with infarction) was performed, comparing refBlochi with T1-mapping using multiple-TIs. The T1s (in myocardium, scar and blood) were measured and compared in identical ROIs. Using multiple-TI approach, the non-T1 related weightings were also mapped (combined PD and T2*), to assess our hypothesis that T2* and PD are minor weightings.

Results: In phantoms, over all protocols, RR intervals, and T1s, T1-refBlochi was validated vs. true T1s (R^2=0.99, mean bias ± 2SDs = -3ms±11ms). The T1-maps with refBlochi agreed well with multiple-TI T1-mapping (Figure 2C, D). Comparing T1s in matched ROIs in myocardium and scar, the quantitative in vivo agreement was good (R^2=0.94, slope=0.99) between T1s measured by T1-refBlochi and the multi-TI method (bias ±2Ds of -10 ±42ms). The maps of combined weightings of T2* and PD (Figure 2B) were analyzed, yielding a mean scar/blood ratio of 0.94±0.01 and myocardium/blood ratio of 1.03±0.02 (p=0.02) (Figure 2B), indicating minor T2*/PD weighting.

Conclusions: RefBlochi is a high resolution T1-mapping method, with estimate only limited by effects of PD and T2* weighting. T2* weighting can be minimized using shorter TEs, and is likely the predominant confounder. This is a powerful new tool for T1-mapping of the left atrium.

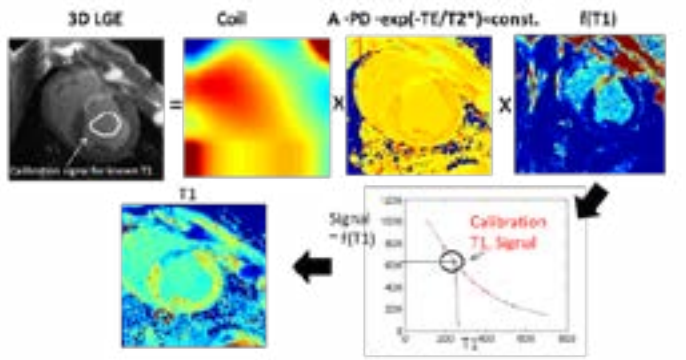

Figure 1: The 3D LGE image is composed of weightings due to the coil, proton density (PD), and T2*, in addition to the predominant T1 weighting, f(T1). The T1-refBlochi method removes coil-sensitivity with image processing, and assumes that T2* and PD weightings are minor. Then the underlying T1-weighting can be modeled using Bloch equations, and a T1 map can be extracted with a single calibration point on the T1 vs. signal curve.

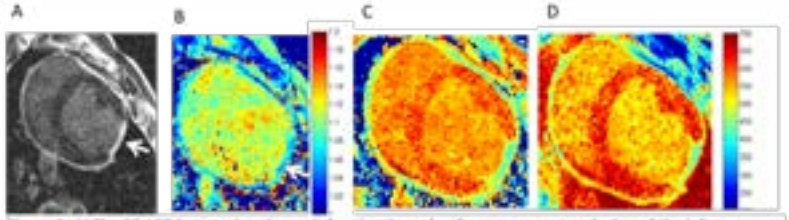

Figure 2: A) The 3D LGE image, showing an infarction 2 weeks after permanent occlusion of the left circumflex (arrow). B) The combined T2* and PD weighting map. The mean ratio of blood to myocardium was 1.03±0.02, blood to scar 0.94±0.01. C) The T1 map using multi-TIs. D) T1-mapping with refBlochi. Overall T1 agreement was good compared to multi-TI methods, with bias ±2SDs of -10 ±42ms.

P178

Initial Experience with the New Dark Blood LGE Images for Detecting Left Ventricular Fibrosis- A Comparison of the Novel TRAMINER Sequence to Gold-Standard Delayed Enhancement Images.

Nayla Chaptini, MD FACC[1] Firas Dabbous, PhD[2], Darach O H Ici, MD[3], Wolfgang G. Rehwald, Ph.D.[4]

1. *Advocate Lutheran General Hospital, Chicago, IL*
2. *Russell Institute of Research and Innovation, Park Ridge, IL*
3. *Deutsches Herzzentrum Berlin, Berlin, Berlin, Germany*
4. *Siemens Medical Solutions USA, Inc., Chapel Hill, NC*

Background: Cardiac MRI (CMR) is known for its ability to assess myocardial fibrosis, inflammation and infiltration. The late Gadolinium enhancement (LGE) sequences are a mainstay in detecting different patterns of fibrosis. However, because in these images, both the LV cavity and the LV scar appear bright, it is more difficult to discern smaller scars, especially subendocardial, due to their closeness to the LV cavity. The TRAMINER sequence is a novel developed single-shot post-Gd sequence designed to detect myocardial fibrosis (Fig 2). Like other LGE sequences, it shows myocardial scarring, inflammation or fibrosis as hyperintense signals. However, it displays the LV cavity as dark. Therefore, it should give better contrast, and hence better visualization of subendocardial scarring (Fig 1).
Moreover, TRAMINER is a fast -to-run free-breathing sequence, posing less inconvenience to patients. This pilot study aims to show that the TRAMINER sequence is effective in detecting myocardial fibrosis, and is as sensitive as the traditional segmented delayed Inversion Recovery (IR) Turbo Flash sequence.

Methods: We prospectively enrolled 25 adult clinical patients (52% male) ordered a CMR with contrast. TRAMINER was run in addition to the standard clinically-indicated CMR protocol, which includes the gold-standard IR Turbo Flash sequence. Two blinded readers then separately read the TRAMINER and the IR Turbo Flash sequences as 50 sets of de-identified images. The areas of delayed enhancement (DE) are then graded based on segment location (AHA 17-segment model), on wall thickness involvement (0 no fibrosis,1 1-25%, 2 26-50%, 3 51-75%, 4 76-100%), and on presence of image artifact (Y/N). To determine if the use of the TRAMINER sequence resulted in an equal frequency of detecting fibrosis, we used kappa statistic to examine the interobserver and intraobserver agreement.

Results: We found substantial intraobserver reader agreement between the TRAMINER and gold standard (GS) images in Reader 1 and moderate reader agreement in Reader 2. There was moderate interobserver agreement for both (Table). Artifact detection yielded different interpretations. However, both readers found that there was artifact in 11 of 25 patients in the GS sequences, and no artifact in 18 of 25 patients with TRAMINER.

Conclusions: TRAMINER is a sensitive and convenient free-breathing sequence allowing for quantifying LV fibrosis, whether subendocardial (Fig1), midmyocardial or epicardial (Fig 3).
Variations in interpretetation in this pilot study can be attributed to image artifacts (more common in GS sequences), to reader variability in a sensitive fibrosis quantification scale, and to a learning curve for interpreting novel image appearance.
As further data is acquired, this study has the strength of using correlation with a more sensitive fibrosis quantification scale.
Also, TRAMINER is potentially a reasonable alternative to the more cumbersome breath-held IR Turbo Flash sequence in more challenging clinical cases.

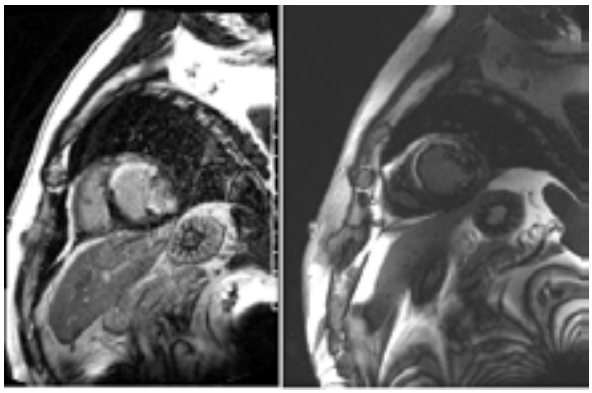

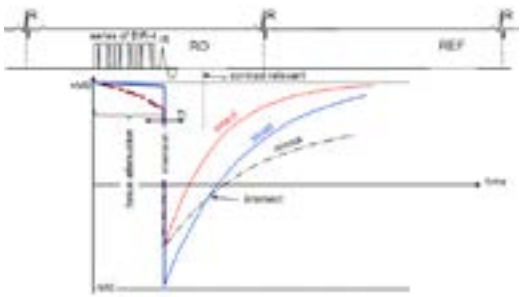

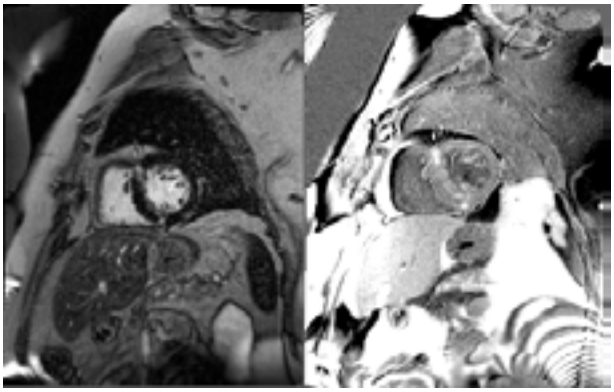

Intraobserver and Interobserver Agreement

Kappa	Lower CI	Upper CI	
Intra observer Reader 1	0.64	0.29	0.92
Intra observer Reader 2	0.43	0.16	0.68
Gold Standard—Inter Observer	0.55	0.25	0.83
Traminer—Inter Observer	0.46	0.11	0.78

CI = Confidence Interval
Gold Standard= InversionRecovery Turbo Flash segmented LGE images.
Kappa Agreement
< 0 Less than chance agreement
0.01–0.20 Slight agreement
0.21– 0.40 Fair agreement
0.41–0.60 Moderate agreement
0.61–0.80 Substantial agreement
0.81–0.99 Almost perfect agreement

P179

Normal Ranges Of Myocardial Strains By 4 Different Cardiac Magnetic Resonance Methods: Systematic Reviews And Meta-analyses From 1254 Healthy Subjects

Ha Quang. Vo, MSc[1] Kazuaki Negishi, MD, PhD[2]

1. Menzies Institution for medical research, Hobart, Tasmania, Australia
2. Menzies Research Institute Tasmania, Hobart, Tasmania, Australia

Background: Cardiac wall motion analysis is a crucial component for cardiac functional assessment. In literature, there are four different myocardial strain methods with cardiovascular magnetic resonance (CMR) existing: myocardial tagging (MT), displacement-encoding with stimulated echoes (DENSE), strain-encoded (SENC), and feature tracking (FT). However, relationship among these has not been fully elucidated yet. We performed systematic reviews and meta-analyses to identify normal strain values and identify sources of variation, if exists.

Methods: Four databases (EMBASE, SCOPUS, PUBMED, Web of Science) were systematically searched for normal strain values of left (LV) and right ventricles (RV) by above four methods. Randomeffects models were used to pool LV global longitudinal (GLS), circumferential (GCS), radial (GRS), RV GLS, and RV GCS.

Results: 1254 healthy subjects were included from 41 articles (MT 10 articles; DENSE 7; SENC 10; and FT 18). Normal ranges are summarized in Table. In general, FT yielded equal or higher values than the other methods. Normal ranges of LV GLS by FT and SENC were similar to those reported in speckle tracking echo (STE), and seem higher than those by MT. LV GCS by FT was analogous to that by STE, and seems higher than those by other methods. There were discrepancies in LV GRS, RV GLS, and RV GCS among methods. Meta-regression revealed that 1) the differences in field strength (1.5T/3T) among studies contributed for the heterogeneity of LV GLS by FT; 2) the variability in LV GCS by MT was associated with heart rate; 3) the variability in RV GLS by SENC was related to age and gender; and 4) the heterogeneity in LV GLS and GCS by MT seemed to be explained by the difference in MRI vendors.

Conclusions: FT yields equal or higher strain values than the other CMR strain methods. Normal ranges of LV GLS and GCS were quite similar among the four different CMR strain methods. However, there were considerable discrepancies in LV GRS and RV GLS.

Comparison between DENSE, SENC, Myocardial Tagging, STE and MRI-FT in normal strain values

Speckle tracking*	Feature tracking	Tagging	DENSE	SENC	
-19.7 [-20.4, -18.9]	-20.1 [-20.9, -19.3]	-14.6 [-16.2, -12.9]	-	-20 [-22.5, -17.4]	LV GLS
-23.3 [-24.6, -22.1]	-23 [-24.3, -21.7]	-19.9 [-21.1, -17.7]	-19.0 [-19.7, -18.3]	-20.9 [-22.4, -19.3]	LV GCS
47.3 [43.6, 51]	34.1 [28.5, 39.7]	-	24.3 [16.2, 32.3]	-	LV GRS
-27 [-29, -24]	-21.8 [-23.3, -20.2]	-	-	-18.7 [-19.5, -17.9]	RV GLS
-	-	-	-	-19.3 [-21.2, -17.4]	RV GCS

*Yingchoncharoen T, JASE, 2013;26:185-191.

P180

Clinical Validation of Free Breathing CArdioREspiratory Synchronized (CARESynch) Balanced Steady-State Free Precession (bSSFP) Cine Imaging

Amol Pednekar, PhD[1] Benjamin Cheong, MD[2], Melissa Andrews, RN[2], Debra Dees, RN[2], Raja Muthupillai, PhD[3]

1. *Philips Healthcare, TX*
2. *CHI St.Luke's Health, TX*
3. *Diagnostic and Interventional Radiology, CHI St Luke's Health, TX*

Background: Notwithstanding all the advantages of breath-hold cine bSSFP imaging, respiratory suspension – as essential mechanism for acquiring bSSFP cine images in the steady state – is not suitable for many patients, such as sedated patients and patients with impaired breath-holding capacity and/or cardiac arrhythmias. Any respiratory motion due to unsteady breath-hold during data acquisition causes motion artifacts, sacrificing endocardial border definition. In this prospective study we evaluated the performance of a CArdioREspiratory Synchronized (CARESync) sequence for free breathing acquisition of bSSFP cardiac cine images.

Methods: All imaging for this prospective, IRB approved, study in 14(54(32-80)yrs,70(58-104)hbm,19(18-22)rpm) consecutive patients undergoing clinically indicated cardiac MR, was performed on 1.5T(9)/3T(5) commercial MR scanners (Achieva/Ingenia , Philips Healthcare). A real-time adaptive CARESync-bSSFP sequence that performs a) respiratory synchronized drive to steady state, b) prospective cardiorespiratory synchronized cine data acquisition with arrhythmia rejection, and c) retrospective cardiac gating was implemented (Fig 1). The performance of CARESync was validated prospectively against breath-hold (BH–SSFP) acquisition with identical acquisition parameters (TR/TE/flip angle = 2.5-3.2ms/1.25-1.6ms/ 65°(40°,3T); acqd voxel size = 1.7-2.0×1.6-2.0×8mm^3; SENSE factor = 1.3-1.9; temp resolution 40-50ms; imaging time : 6-8 RR intervals/slice) for LV function evaluation. The image quality (IQ) was scored by blinded reviewer for blood to myocardial contrast, endocardial edge definition, and motion artifacts (Table 1). Bland-Altman analysis was performed on clinical scores assigned to both the techniques.

Results: The CARESync sequence ran successfully in all 14 patients. Total image acquisition time for CARESync (7.4±1.8 min) was significantly longer than conventional BH-SSFP (5.6±1.7 min). Combined clinical score was Excellent (11) to Good (3) for BH-SSFP and Excellent (9) to Good (5) for CARESync (Fig. 2). In all categories all data sets were scored 4 or more. The bias and limits of agreement for clinical scores were 0.29 and ±0.68.

Conclusions: IQ scores were equivalent for CARESync compared to BH-SSFP with identical spatio-temporal resolution and were consistently rated as Excellent or Good. Previous studies have shown good agreement of global LV functional indices between FB and BH. Thus, CARESync is a robust alternative for evaluating global LV function in patients with impaired breath-holding capacity. Inclusion of more difficult clinical cases may reveal the added value of FB cine SSFP alternative. The strength of the CARESync cine bSSFP approach is that the RF duty cycle typically remains at about 50-60%, allowing the bSSFP sequence to be acquired over several minutes without specific energy deposition constraints, even at high field strengths allowing higher spatio-temporal resolutions.

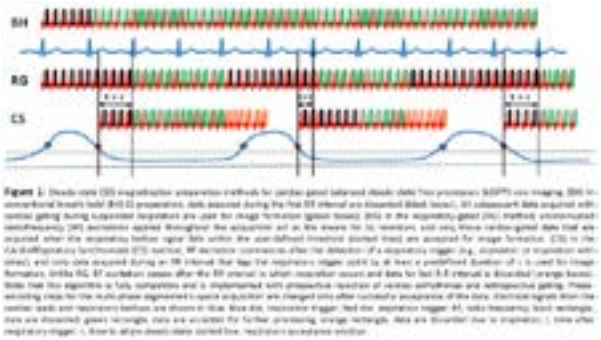

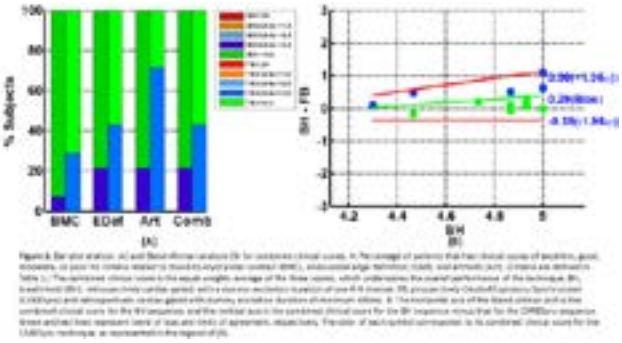

Art	Edef	BMC	Score
Excellent: Image is nearly artifact free.	Excellent: Papillary and endocardial trabeculae are clearly visible in the bright backdrop of the blood pool.	Excellent: Blood pool is hyperintense with excellent contrast against the myocardium; myocardium is uniformly bright throughout the cardiac cycle with little evidence of flashing.	5
Good: Some motion artifact is present but does not affect overall image quality.	Good: Papillary and endocardial trabeculae are visible but somewhat blurred during the cardiac cycle.	Good: Blood pool is significantly brighter than the myocardium, or myocardial signal intensity is fairly uniform throughout the cardiac cycle.	4
Moderate: Motion artifacts are visible, but image is still of diagnostic quality.	Moderate: Myocardial walls are barely distinguishable from endocardial trabeculae.	Moderate: Image is of diagnostic quality but features significant loss of blood to myocardial contrast or noticeable variation in myocardial signal throughout the cardiac cycle.	3
Poor: Images are nearly nondiagnostic with significant artifacts.	Poor: Myocardial walls and endocardial trabeculae are significantly blurred.	Poor: Blood-to-myocardial contrast is poor, but the image is still of diagnostic quality.	2
Image is of nondiagnostic quality.	Nondiagnostic: Blood-to-myocardial edge definition is poor; image was deemed nondiagnostic.	Nondiagnostic: Blood-to-myocardial contrast is poor; image was deemed nondiagnostic.	1

P181

Retrospectively gated 2D CINE and phase contrast flow imaging for accurate assessment of cardiac volumes, wall motion and blood flow during strenuous exercise.

Bram Ruijsink, MD[1]Muhammad Usman, PhD[1], Mari Nieves Velasco Forte, MD[1], Torben Schneider, PhD[2], Esther Puyol Anton[1], Claudia Prieto, PhD[1], Kuberan Pushparajah, MD[1], Alessandra Frigiola, MD, PhD[3], David Nordsletten, PhD[1], Reza Razavi, MD, PhD[1]

1. *King's College London, England, United Kingdom*
2. *Health Systems, Philips, Guildford, England, United Kingdom*
3. *Guys and St Thomas Hospital NHS Foundation Trust, England, United Kingdom*

Background: Bodily motion, unreliable ECG signals and the inability to breath hold severely limits the use cardiac MRI during exercise. Real time imaging during exercise has been proposed but often lacks temporal resolution at high heart rates. We propose a method to acquire high temporal resolution cardiac and respiratory gated 2D CINE and high temporal resolution blood flow profiles that allow accurate assessment of the heart and blood flow during strenuous exercise.

Methods: Exercise was performed on an MRI compatible supine bicycle. Highly accelerated real time multislice 2D CINE acquisitions (FOV 300 x 250, matrix 128 x 128, Sense-factor 2, half-Fourier imaging, flip angle 50°, TR 1.8ms,TE 0.9ms) were acquired. Contrast based automated manifold learning was used to estimate timing of end-diastole and respiratory motion directly from the images. After respiratory gating, images were ranked for position in cardiac cycle and binned in 20 cardiac phases. An averaged image was reconstructed for each bin resulting in a cardiac and respiratory gated 20-phase 2D CINE dicom image stack of the heart. We compared our proposed method to conventional breath held CINE at rest and during exercise with the only available validated real time imaging and analysis method for exercise MRI so far (RightVol, KU Leuven; La Gerche, Circulation 2013). Real time 2D phase contrast flow was acquired in the aorta (FOV 300 x 240, matrix 128, flip angle 40°, TR 18, TE 5.2). Upslopes of each individual beats from the undersampled multiple beat flow profile (typical 8-10 points/beat) was automatically detection and aligned in time. From the resulting dense point-cloud we reconstructed one averaged flow curve. To compute beat to beat flow we rescaled the average 'master' curve to optimally match acquired data of each individuals heartbeat, hereby reconstructing the flow curve from sparse data. From the resulting flowprofiles we calculated mean flow and standard deviation of flow between cycles. Flow imaging was validated using a flow phantom with variable heart rates and compared with conventional flow imaging during dobutamine stress cardiac MRI.

Results: Validation was performed in 15 healthy volunteers and 6 patients at rest and during exercise / dobutamine stress cardiac MRI. Cardiac volumes measured with our proposed method had good agreement with conventional breath held short axis CINE imaging at rest (mean difference 2±2,4%, R = .97). During moderate (HR~120 bpm) and high (HR~160 bpm) exercise, our method agreed well (+6.1±6%, R =.94) with the previously proposed real time imaging method. For flow imaging there was good agreement with conventional 2D PC flow imaging during flow phantom tests (-2±2.5%, R=.98, p=.26) and in vivo during dobutamine stress testing (-2±2.1%, R = .97).

Conclusions: Retrospective cardiac and respiratoiry gated 2D CINE and phase contrast flow imaging allows for accurate assesment of heart and blood flow during strenuous exercise.

http://www.ConferenceAbstracts.com/uploads/cfp2/attachments/LDFAIBDN/LDFAIBDN--217985-1-ANY.pdf

http://www.ConferenceAbstracts.com/uploads/cfp2/attachments/LDFAIBDN/LDFAIBDN--217985-2-ANY.pdf

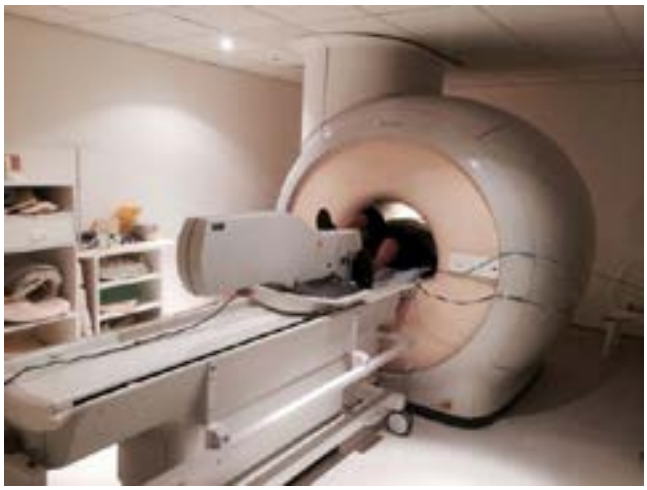

P182

CMR Feature Tracking: a Useful Surrogate of Myocardial Fibro-Fatty Tissue Replacement in Left Atrial Cardiomyopathy?

Adrian Huber, MD[1]Jérôme Lamy, MSc[2], Amer Rahhal, -MD[3], Morgane Evin, PhD[4], Fabrice Atassi, -[3], Carine Defrance, -[3], Guillaume Lebreton, -[3], Karine Clément, -[3], Pascal Leprince, -[3], Philippe Cluzel, -[3], Nadjia Kachenoura, PhD[5], Stéphane Hatem, -[3], Alban Redheuil, MD, PhD[2]

1. *Sorbonne Universités, UPMC Univ Paris 06, INSERM, CNRS, UMR 7371, UMRS 1146, Laboratoire d'Imagerie Biomédicale, 75013, Paris, France, Paris, Ile-de-France, France*
2. *Sorbonne Universités, UPMC Univ Paris 06, INSERM, CNRS, UMR 7371, UMRS 1146, Laboratoire d'Imagerie Biomédicale, 75013, Paris, France, Ile-de-France, France*
3. *-, Ile-de-France, France*
4. *Sorbonne Université, Université Pierre et Marie Curie, Laboratoire d'Imagerie Biomédicale, UMRS 1146 INSERM-CNRS, Paris, France, Ile-de-France, France*
5. *Sorbonne Universités, UPMC , INSERM UMRS 1146, Laboratoire d'Imagerie Biomédicale, Ile-de-France, France*

Background: Left atrial (LA) cardiomyopathy is a final consequence of aging and several intricated disease processes. Its key morphologic substrate is LA fibro-fatty replacement, a histological diagnosis, which acts as a potential trigger for AF and adverse clinical outcome. Non-Invasive characterization of LA cardiomyopathy in an early, reversible stage could thus serve as a useful biomarker to guide clinical decisions. The objective of this study was to characterize left atrial (LA) cardiomyopathy by analyzing left atrial deformation using cardiac magnetic resonance imaging (CMR) feature tracking in relation to fibrosis and adipose tissue infiltration in histology.

Methods: LA strain was prospectively evaluated with CMR feature tracking in 26 individuals: 13 patients with mitral regurgitation (MR) scanned in the 24 hours before mitral valve surgery and 13 age and sex matched healthy controls (LIB INSERM software). High quality histological correlation from per-operative biopsies was available in 10 patients. LA volumes as well as LA ejection fraction have been calculated. The areas of myocytes, intra-myocardial fat and fibrosis have been semi-automatically segmented in histology and correlated to several LA strain parameters.

Results: We found a significant association between altered LA strain and increased interstitial LA remodeling in histology, with the strongest association between decreased peak longitudinal atrial strain (PLAS) and increased degree of fibro-fatty myocardial replacement in histology ($r^2 = 0.62$, $p = 0.007$). A significantly lower PLAS in MR patients was found compared to healthy controls ($p < 0.001$). PLAS was also significantly lower in MR patients with atrial fibrillation compared to patients in sinus rhythm ($p = 0.011$) as well as in patients with chronic MR compared to acute onset MR (mitral valve prolapse due to chordae tendinae rupture in the 4 weeks prior to surgery) ($p = 0.028$). Of note, LA end-diastolic volume discriminated MR patients and healthy volunteers (ROC area under the curve: 0.98, $p < 0.0001$) but did not correlate with the degree of LA fibro-fatty replacement in histology ($r^2 = 0.002$).

Conclusions: LA strain, especially PLAS correlates well with the degree of fibro-fatty replacement in histology and is a promising and highly reproducible functional imaging biomarker to characterize LA cardiomyopathy. Since myocardial fibro-fatty replacement is a key LA arrhythmogenic morphologic substrate such non-invasive imaging biomarker in combination with LA volumetry could help to guide early clinical management in AF and MR.

P183

Assessment of Myocardial Blood Flow with Fully Automated CMR Perfusion Pixel Maps in Patients with Coronary Artery Disease

Li-Yueh Hsu, DSc[1]Matthew J. Jacobs, MSc[2], Mitchel Benovoy, PhD[3], Allison Ta, MD[4], Hannah Conn, BSc[5], W. Patricia Bandettini, MD[6], Andrew E. Arai, MD[7]

1. *National Institutes of Health, Bethesda, MD*
2. *The Catholic University of America, Riverdale, MD*
3. *NIH/NHLBI, PQ, Canada*
4. *NIH/NHLBI, Bethesda, MD*
5. *National Heart Lung and Blood Institute, National Institutes of Health, Bethesda, MD*
6. *National Heart, Lung and Blood Institute, National Institutes of Health, MD*
7. *National Institues of Health, Bethesda, MD*

Background: Myocardial blood flow (MBF) quantification from first-pass CMR perfusion imaging is useful for assessing the severity of coronary artery disease (CAD). However, the current method of MBF quantification requires manual processing that creates barriers for routine clinical usage. We developed a fully automated image processing method to generate MBF pixel maps and compared MBF in ischemic and remote sectors in patients with known CAD.

Methods: Rest and regadenoson stress perfusion imaging was performed on 34 patients with ≥ 70% stenosis in at least one major vessel as confirmed by quantitative coronary angiography. An additional 17 healthy volunteers were included for comparisons. A saturation recovery SSFP dual-sequence technique was used to acquire both myocardial and arterial input function image series. Raw perfusion images were processed by the automated method, including non-rigid motion correction, intensity bias correction, myocardial signal and contrast timing detection, and model constrained deconvolution. The automatically generated MBF pixel maps were analyzed in 6 sectors per slice. MBF as well as myocardial perfusion reserve (MPR) in a remote sector and an ischemic sector in the CAD cohort was compared with the results from healthy volunteers.

Results: Computation time for processing automated perfusion pixel map averaged 78.0±6.5 second per slice on an Intel Core i7 processor. Table-1 summarizes the MBF for the CAD patients and healthy volunteers. In patients with CAD, MBF in the ischemic sector is significantly lower than the remote for both stress and rest perfusion ($p < 0.01$). Furthermore, MBF ratio between ischemic vs. remote sectors in stress is significantly lower than in rest (0.54±0.22 vs. 0.80±0.21, $p < 0.01$). Both stress MBF and MPR in the remote sector of CAD patients are significantly lower than in healthy volunteers ($p < 0.01$). However, rest MBF was not significantly different between the remote sector in CAD patients and healthy volunteers (p=NS).

Conclusions: Fully automated MBF pixel maps can be generated from first-pass CMR perfusion images within a timeframe that is practical for routine clinical use. Our results demonstrate the automated perfusion maps reliably differentiate ischemic vs. remote MBF in patients with CAD. Further studies are warranted to evaluate this automated method in large clinical trials.

Table-1: Comparison of automated estimated MBF between CAD patients vs. healthy volunteer.

MPR		Rest		Stress		MFB (ml/g/min)
Ischemic	Remote	Ischemic	Remote	Ischemic	Remote	
1.59±0.68	2.34±0.66	0.90±0.36	1.15±0.34	1.37±0.68	2.57±0.63	CAD Patients
NA	3.15±0.92	NA	1.22±0.33	NA	3.67±0.79	Healthy Volunteers

P184

Cardiac motion-insensitive black-blood TSE based on reverse double inversion and diastolic preparation

Chenxi Hu, PhDHamid Mojibian, M.D., Dana C. Peters, PhD

Yale University, CT

Background: The commonly used double inversion recovery (DIR) black-blood turbo spin echo (TSE) method[1] is susceptible to motion of heart when used for cardiac magnetic resonance (CMR). This is due to slice misregistration between the double-inversion preparation slice and the excited slice, which leads to inhomogeneous signal or dropout in right ventricular (RV)[2] and left ventricular (LV) myocardium[3]. In this work, we propose a novel reverse double-inversion (RDIR) preparation that eliminates the slice misregistration. We employed RDIR to investigate the causes of signal loss in black blood TSE.

Methods: Figure 1 shows the sequence timing. The two inversion pulses are swapped in time in RDIR TSE and the slice-selective IR (IRsel) is moved to mid-diastole in the prior RR. This change minimizes slice misregistration by timing the preparation and acquisition identically within the RR interval. The blood nulling is not influenced by these changes since the non-selective IR (IRns) is not moved. Signal-to-noise ratio (SNR) is lower in RDIR TSE due to a delay between IRsel and IRns (Figure 1); however, the impact should be minimal due to inherent high SNR of the TSE sequence.

Seven healthy subjects were imaged on a 3.0 T scanner (Siemens Trio), after providing written informed consent. Imaging was performed in the highly mobile basal short-axis slice. For the IRsel, two preparation slice thicknesses: 110% (almost no increase) and 200% (standard thickness) were used. Other parameters: FOV/slice thickness/resolution/echo train length/bandwidth: 360x270mm/5 mm/192 x 114/19/789 Hz/pixel. SNR/myocardium-to-blood CNR/LV wall homogeneity/RV wall visibility were evaluated for all seven subjects.

Results: Table 1 and Figure 2 show the results. There were significant improvements in LV wall homogeneity and RV wall visibility, comparing DIR and RDIR with 110% preparation slice thickness. The main signal loss area for DIR TSE matches previous findings[2,3]. Image quality/SNR/CNR were improved for DIR TSE with 200% vs. 110% preparation thickness; however, RV wall visibility was still significantly lower than that in RDIR TSE even with the 200% preparation. SNR/CNR were similar for RDIR between 110% and 200%, indicating that a global myocardial signal loss exists in DIR TSE but not RDIR.

Conclusions: Double thickness preparation is critical to DIR TSE, but not RDIR TSE, because the latter minimizes slice misregistration. RDIR is promising to improve clinical robustness of black-blood TSE in both LV and RV edema identification.

References: 1. Simonetti, Radiology 1996 2. Berkowitz, MRM 2009 3. Keegan, JMRI 2006

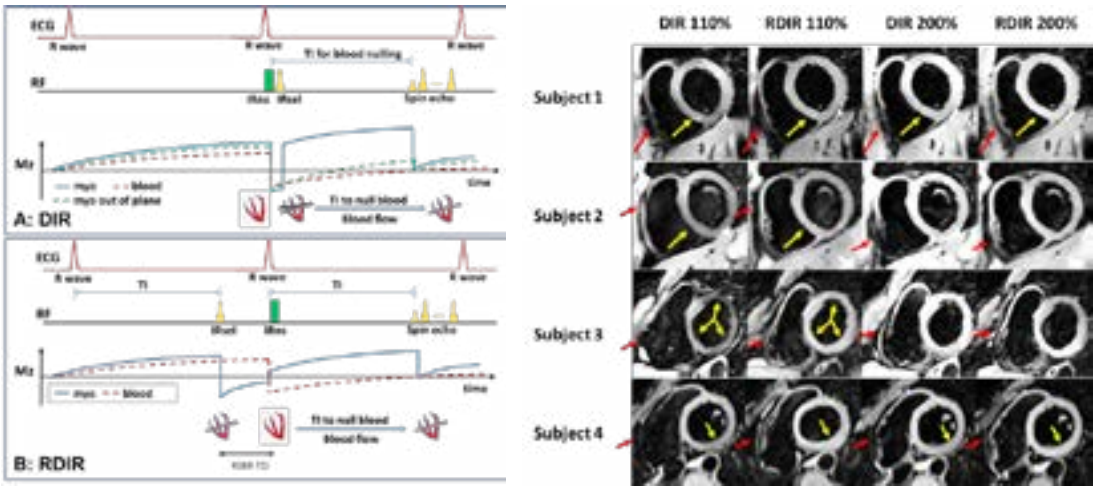

Table 1. Comparison between DIR and RDIR under different preparation slice thickness (110% & 200%)

P value	RDIR 200%	DIR 200%	P value	RDIR 110%	DIR 110%	
0.88	13%±7%	14%±6%	0.02	13%±6%	23%±11%	LV wall homogeneity*
0.02	122±62	150±75	0.30	121±59	115±60	SNR
0.01	92±27	121±43	0.10	99±46	90±42	CNR
0.006	75%±21%	57%±15%	0.002	76%±11%	31%±15%	Ratio of visible RV wall to total RV wall length (%)

*LV wall homogeneity was defined by standard deviation of LV wall divided by mean intensity of LV wall.

P185

3T Cardiac Magnetic Resonance Quantification of Myocardial Extracellular Volume and Left Ventricular Strain in Amyloidosis Patients without Late Gadolinium Enhancement

Lu Lin, M.D.[1] Yining Wang, M.D.[2], Xiao Li, M.D.[2], Shu Jiang[2], Jian Cao, M.D.[2], Jing An, M.D., Ph.D[3], Andreas Greiser, Ph.D[4]

1. *Peking Union Medical Collge Hospital, Beijing, Beijing, China (People's Republic)*
2. *Peking Union Medical College Hospital, Beijing, China (People's Republic)*
3. *MR Collaborations NE Asia, Siemens Healthcare, Beijing, China, Beijing, China (People's Republic)*
4. *Siemens Healthcare GmbH, Erlangen, Germany, Erlangen, Bayern, Germany*

Background: Cardiac involvement in systemic light-chain (AL) amyloidosis generally associates with a worse outcome. Cardiac magnetic resonance (CMR) myocardial extracellular volume (ECV) and strain quantification may have advantages over traditional late gadolinium enhancement (LGE) for early diagnosis of cardiac amyloidosis. This study aims to assess left ventricular (LV) myocardial ECV and strain changes in AL amyloidosis patients without identifiable LGE on 3T CMR.

Methods: This IRB-approved retrospective case-control study included 13 clinically and histologically diagnosed AL amyloidosis patients (age, 55.0±10.8 years; male/female=5/8; LVEF=63.8±12.0%) without identifiable myocardial LGE on CMR (3T, Magnetom Skyra, Siemens Healthcare, Erlangen, Germany) as well as 16 healthy control subjects (age, 40.5±11.2 years; male/female=6/10; LVEF=72.4±18.8%). Myocardial ECV was measured based on the basal, mid and apex LV short-axis inline motion-corrected TI images using a prototype MOLLI sequence. Left ventricular strain was measured by the average total peak systolic strain in longitudinal, radial and circumferential direction on cine images using cvi42 software (version 5.3, Circle Cardiovascular Imaging, Canada). Mann-Whitney U test was used to compare ECV and strain results between amyloidosis and control groups.

Results: In amyloidosis patients without LGE, LV myocardial ECV significantly elevated in basal segments (33.2±3.8 vs. 27.8±5.6, p=0.010) and global (31.3±4.1 vs. 27.7±3.6, p=0.036) compared with control subjects. There were no significant differences of the LV longitudinal, radial or circumferential strain values between the amyloidosis and control groups.

Conclusions: ECV quantification on CMR may identify cardiac involvement of AL amyloidosis before LGE and LV strain analysis.

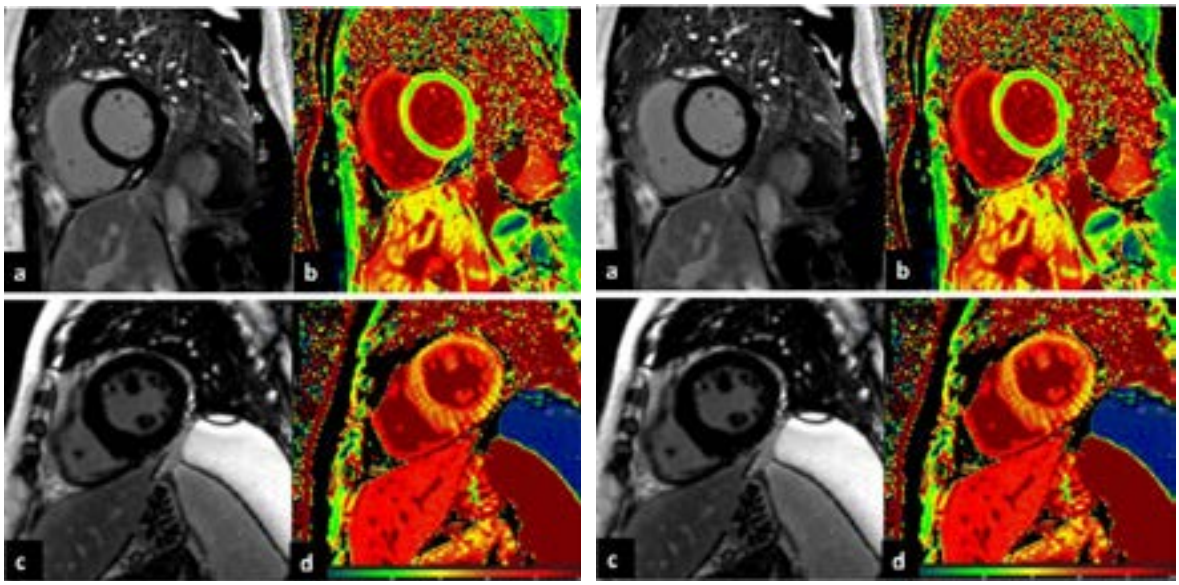

P186

T2 mapping by cardiac magnetic resonance imaging: from theoretical validation to clinical implication

Mary R. Mahrous, MD, MSc[1] Wesam E. El Mozy, MD, MSc[2], Asmaa M. N. Elsayed Ahmed, MD, MSc.[3], Asmaa R. Abd El-Naby, MD, MSc[4], Nahla D. Ali, MD, MSc[5], Ahmed Kharabish, MD, MSc, PhD[2]

1. *Magdi Yacoub foundation-Aswan Heart Center, Aswan, Egypt*
2. *Magdi Yacoub Foundation - Aswan Heart Centre, Aswan, Egypt*
3. *Aswan Heart Centre - Magdi Yacoub Heart Foundation, Aswan, Egypt*
4. *Cardiology department- Tanta university, Aswan, Egypt*
5. *Radiology department-Faculty of medicine- Cairo university, Al Qahirah, Egypt*

Background: The known limitations of the turbo inversion recovery magnitude (TIRM) sequence in detection of myocardial edema in patients presenting with acute myocardial injury inspired us to evaluate the clinical implication of the T2 mapping sequence.

Methods: Thirty patients presented with acute myocardial injury (inflammatory and ischemic) were sent to cardiac magnetic resonance (CMRI) within 24 hour after conventional coronary angiography in patient with acute ischemic insults in order to assess myocardial edema. All CMRI studies were scanned using the routine protocol of cine, TIRM and late gadolinium enhancement (LGE) in short axis (SAX) views covering the entire left ventricle (LV). SAX-T2 mapping slices were added. Thickness and slice location of the T2 mapping slices were copied from the TIRM. The LV was divided into apical, mid and basal segments according to visualization of the papillary muscles. Edema mass was assessed separately in each segment using both the TIRM and T2 mapping; i.e. 16 segments in all subjects in both sequences (16x30= 480 segments per sequence i.e. 480x2=960). Total amount of edema from both sequences was compared as well as the agreement of the amount of edema per segment.

Results: Two cases diagnosed with acute myocarditis (6.6%). Twenty-eight cases with acute ischemic insults (93.4%). Three of acute ischemic cases (10%) had multi- vessel disease (two cases with LCx and RCA MI and one case with three vessel disease). No statistically significance difference between the total amount of edema, basal segments' edema, mid segments' edema, and apical segments' edema (p value 0.49, 0.48, 0.09, and 0.69 respectively) measured by both sequences.

Conclusions: Edema detection using TIRM was confusing due to multi segmental edema affection in cases of myocarditis and multi coronary involvement which hinders the known methods of CMRI edema assessment (myocardial signals: skeletal muscle signal > 1.9, affected territory signals > remote myocardial signals+ 2SD). It may therefore be clinically important to perform T2 mapping as a supplementary tool in routine clinical CMRI to the current edema sequences.

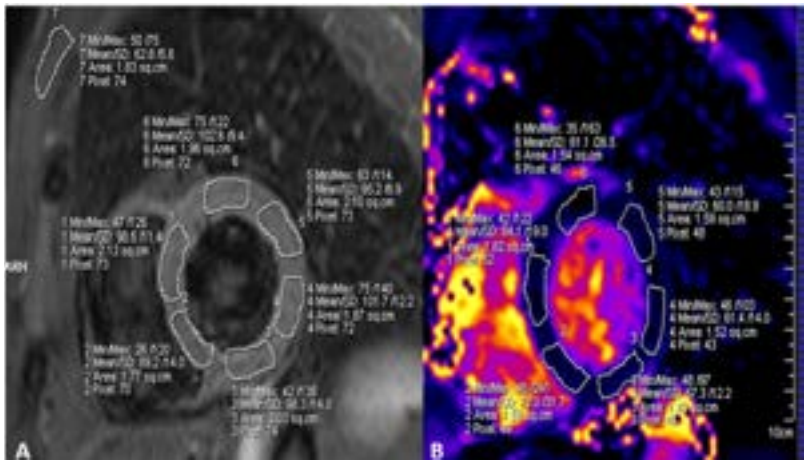

P187

Radial and circumferential strain of the thoracic aorta measured by cardiovascular magnetic resonance feature tracking: a novel marker of aortic stiffness

Graham J. Fent, MBChB, BSc (Hons)[1]Peter P. Swoboda, PhD[1], James Foley, MBChB BSc (Hons)[1], Pankaj Garg, MD[2], Bara Erhayiem, BMBS[3], John P. Greenwood, PhD[3], Sven Plein, MD PhD[4]

1. *University of Leeds, Leeds, England, United Kingdom*
2. *University of Leeds, UK, England, United Kingdom*
3. *University of Leeds, England, United Kingdom*
4. *St. Thomas' Hospital, London; King's College London; University of Leeds, England, United Kingdom*

Background: Aortic stiffness has been proposed as a surrogate marker of generalised atherosclerosis with the potential to identify patients at increased risk of cardiovascular disease (CVD). Aortic strain analysis has emerged as a promising technique which appears more sensitive than traditional methods in detecting age-related changes in vascular performance. Studies using echocardiographic speckle tracking have measured circumferential and radial strain in vivo, providing normal values and demonstration of lower values in atherosclerotic disease. No study to date has demonstrated aortic strain analysis using cardiovascular magnetic resonance imaging (CMR). We sought to assess the feasibility and reproducibility of measuring aortic strain by CMR feature tracking and compare values in healthy controls with a cohort of rheumatoid arthritis (RA) patients at high risk of CVD.

Methods: The study population included 10 healthy controls (HC) and 10 RA patients with no history of CVD or diabetes. All CMR studies were performed at 3.0T (Philips Achieva TX). For each patient, a 50-phase axial bSSFP cine acquisition was acquired of the ascending and descending thoracic aorta at the level of the main pulmonary artery. Radial and circumferential strain values were obtained by feature tracking of the ascending and descending aortic walls using dedicated post-processing software (CVI 42, Circle Cardiovascular Imaging Calgary, Canada). Interobserver and intraobserver reproducibility for HCs was assessed. For interstudy reproducibility, separate CMR studies were carried out on the same healthy controls 7 days apart.

Results: Demographics of all study participants and results of strain analysis are in table 1.

Radial strain of the ascending and descending aorta showed excellent interstudy, intraobserver and interobserver reproducibility with a coefficient of variability of less than 10% for each of these measures. Circumferential strain of the ascending aorta also showed a coefficient of variability of less than 10% for all measures of reproducibility but were slightly less reproducible in the descending aorta. Descending aorta radial strain was significantly lower in HCs versus RA patients (-10.1 ± 2.8 vs -6.7 ± 3.0, p= 0.019) as was circumferential strain (13.1 ± 3.7 vs. 8.1 ± 4.1, p =0.020). Radial and circumferential strain were also lower in the ascending aorta, though this did not reach statistical significance.

Conclusions: Aortic strain analysis using CMR feature tracking is feasible and demonstrates excellent reproducibility. Aortic strain measured in the descending aorta is reduced in RA versus HCs. Studies are needed to validate this technique against established measures of aortic vascular performance.

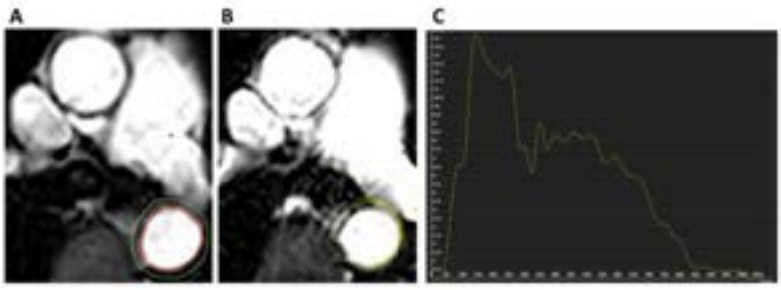

Baseline characteristics and results of strain analysis

			Baseline Characteristics
p Value	Rheumatoid Arthritis	Healthy Controls	
	10 (6)	10 (6)	Number (men)
0.523	43 ± 10	40 ± 10	Age
0.739	121 ± 14	119 ± 11	Systolic blood pressure
0.250	68 ± 11	63 ± 7	Diastolic blood pressure
			Reproducibility Measurements
Interstudy Coefficient of Variability (%)	Interobserver Coefficient of Variability (%)	Intraobserver Coefficient of Variability (%)	
			Ascending aorta
8.3	8.0	4.8	Radial strain
8.3	9.4	6.5	Circumferential strain
			Descending aorta
9.5	8.6	7.1	Radial strain
12.3	10.7	8.5	Circumferential strain
			Strain in RA vs Controls
p value	Rheumatoid Arthritis Mean (%)	Healthy Controls Mean (%)	
			Ascending aorta
0.302	-11.4 ± 3.1	-13.0 ± 3.7	Radial strain
0.260	15.4 ± 5.3	18.8 ± 7.4	Circumferential strain
			Descending aorta
0.019	-6.7 ± 3.0	-10.1 ± 2.8	Radial strain
0.02	8.1 ± 4.1	13.1 ± 3.7	Circumferential strain

P188

Segmental variation of native myocardial T1 in healthy volunteers and hypertrophic cardiomyopathy at 3T using ShMOLLI.

Betty Raman, MBBS, FRACP[1]Rina Ariga, MBBS, MRCP[2], Masliza Mahmod, MBChB, DPhil[2], Vanessa M. Ferreira, MD, DPhil[2], Jane M. Francis, DCR(R) DNM[3], Hugh Watkins, MD PhD FRCP FMedSci[4], Stefan Neubauer, MD, FRCP[2], Stefan K. Piechnik, PhD, MScEE[2]

1. *University of Oxford, Division of Cardiovascular Medicine, Oxfordshire, England, United Kingdom*
2. *University of Oxford, England, United Kingdom*
3. *University of Oxford, OX39DU, England, United Kingdom*
4. *Radcliffe Department of Medicine, England, United Kingdom*

Background: Native T1-mapping is increasingly being used to quantify myocardial fibrosis in hypertrophic cardiomyopathy (HCM). Segmental assessment of T1 relaxation time in HCM may be important due to disease heterogeneity. Segmental variation in native T1 in healthy subjects has already been described by Piechnik et al (2010) and von Knobelsorff-Brenkenhoff et al (2013).To further understand the impact of this, we sought to assess this variation of T1 values in HCM to improve discrimination between health and disease.

Methods: 32 controls (46 ± 16 years) and 55 patients with HCM (47 ± 14 years) underwent cine imaging and native T1-mapping (using Shortened MOdified Look-Locker Inversion recovery, ShMOLLI) at 3T. Mean myocardial T1 relaxation times were calculated for six AHA mid ventricular segments. HCM was defined as left ventricular hypertrophy ≥12mm with a pathogenic mutation or ≥15mm in the absence of mutation. Comparison between segment and group was performed by analysis of variance with post hoc t-tests using Bonferroni correction for multiple testing.

Results: In controls, we observed segmental variation of T1, consistent with prior reports (Figure 1). The anterior segment had the lowest T1 (1140±39ms) compared to all segments except the anterolateral segment ($p < 0.01$). The inferoseptal segment had the highest T1 (1198±31ms), which was significantly higher than the anterolateral segment ($p=0.04$).

A similar pattern of segmental T1 variation existed in HCM (Figure 1) with low T1 in anterior segment and the lowest in anterolateral (1178±38ms) segment compared to septal and inferior segments ($p < 0.01$). The inferoseptal segment had the highest T1 (1233±49ms) and was significantly higher than the lateral segments ($p < 0.001$).

Despite the segmental variation, HCM had consistently higher T1 compared to controls, albeit only anterior and septal segments showed significant differences ($p < 0.001$). This was in keeping with the location of hypertrophy: maximal wall thickness per segment only correlated significantly with T1 in anterior and septal segments ($p < 0.01$).

Conclusions: There is a concurrent significant spatial variation of native T1 in both controls and HCM at 3T: lowest T1 in the anterior and anterolateral segments and highest T1 in the inferoseptal segment. Segment-matched comparisons show that T1 abnormalities in HCM are seen in anterior and septal segments, in keeping with the location of hypertrophy but T1 in other segments fall within normal limits. Given that inter-segmental variation appears to be prominent at high field systems, the use of focal reference values may be useful when assessing pathological impact on T1-mapping at 3T.

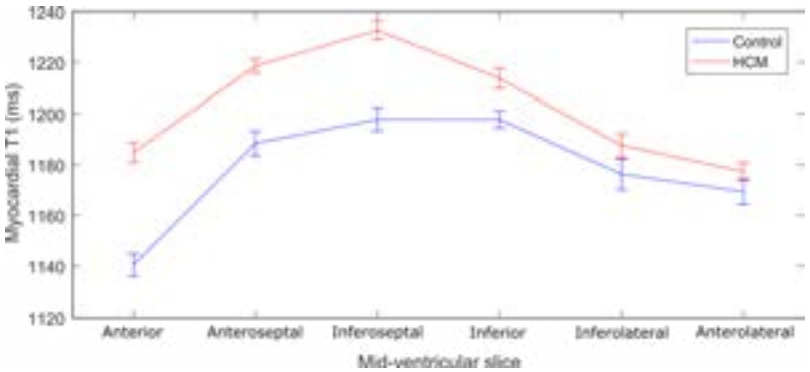

P189

Fast assessment of left atrial function by novel CMR feature tracking derived long-axis strain

Liang Zhong, Ph.D.[2]Shuang Leng, Ph.D.[1], Xiaodan Zhao, Ph.D.[1], Ru San Tan, M.D.[2]

1. National Heart Centre Singapore, N/A, Singapore
2. National Heart Centre Singapore; Duke-NUS Medical School, Singapore, N/A, Singapore

Background: Left atrial (LA) function has been increasingly recognized as a significant indicator of clinical outcome in adults with various cardiovascular diseases. LA functional assessment is conventionally conducted through volume quantification, tissue Doppler and more recently, myocardial deformation analysis. Lack of standardization in strain imaging, however, affect the reproducibility of the LA strain and strain rate (SR) measurements. Accordingly, the objective of this study was to 1) develop a novel and fast assessable long-axis strain with standard cardiovascular magnetic resonance (CMR) imaging; 2) test its utility to differentiate hypertrophic cardiomyopathy (HCM).

Methods: The study population consisted of 20 patients (51±13 yr) with HCM and 20 age- and gender-matched healthy volunteers. All subjects underwent CMR scan (Siemens Avanto) using steady-state free precession (SSFP) cine gradient echo sequences. SSFP end-expiratory breath hold cine images were acquired in multi-planar short- and long-axis views. An in-house developed program [1, 2] was applied to semi-automatically track the atrioventricular junction (AVJ) points and the LA apex in 2- and 4-chamber views. The long-axis LA longitudinal strain was calculated as $LS(t) = (L(t) - L_0)/L_0$, with LS the longitudinal strain, L_0 the initial length, and L(t) the length at cardiac time t (**Fig. 1(A-B)**). Six clinically useful LA data were extracted: reservoir strain $\mathbf{LS_s}$ and SR $\mathbf{LSR_s}$, conduit strain $\mathbf{LS_e}$ and SR $\mathbf{LSR_e}$, and contraction strain $\mathbf{LS_a}$ and SR $\mathbf{LSR_a}$. **Fig. 1(C-D)** showed the strain and SR curves for a 48-yr-old female healthy volunteer and 52-yr-old female patient with HCM.

Results: The LA strain and SR parameters were successfully derived from standard CMR in all subjects. Intra- and inter-observer reproducibility was excellent for all strain and SR measurements (All Pearson's correlation coefficients more than 0.92, and coefficient of variation less than 5.4%). All strain and SR parameters were significantly reduced in the HCM patient group as compared to normal control (**Table 1**). As demonstrated in **Table 2**, the LA strain and SR parameters achieved superior performance compared to volumetric measurements in characterizing HCM patients.

Conclusions: The current study presented highly reproducible and fast assessable LA longitudinal strain and SR measurements for the assessment of LA deformation and functionality. The LA strain and SR outperformed conventional LA volumetric measurements to differentiate HCM.

References:

1. Leng S, et al. Am J Physiol Heart Circ Physiol 2015.
2. Leng S, et al. Ann Biomed Eng 2016.

http://www.ConferenceAbstracts.com/uploads/cfp2/attachments/LDFAIBDN/LDFAIBDN--222206-1-ANY.pdf

Table 1: Comparison of LA strain and strain rate parameters between study groups

P value	HCM patients (n = 20)	Normal subjects (n = 20)	Variables	LA function
			LA longitudinal strain (%)	
< 0.0001	21.34 ± 8.16	42.00 ± 6.92	$LA\text{-}LS_s$	Reservoir
< 0.0001	10.05 ± 4.77	22.37 ± 6.15	$LA\text{-}LS_e$	Conduit
< 0.0001	10.40 ± 4.60	18.53 ± 4.07	$LA\text{-}LS_a$	Booster pump
			LA longitudinal strain rate (1/s)	
< 0.0001	0.99 ± 0.32	2.14 ± 0.67	$LA\text{-}LSR_s$	Reservoir
< 0.0001	-0.90 ± 0.40	-2.44 ± 0.70	$LA\text{-}LSR_e$	Conduit
< 0.0001	-1.18 ± 0.52	-2.68 ± 0.65	$LA\text{-}LSR_a$	Booster pump

Data are represented as mean ± SD. LA: left atrial; LS: longitudinal strain; LSR: longitudinal strain rate; HCM: hypertrophic cardiomyopathy.

Table 2: Utility of LA volumetric, strain and strain rate parameters to differentiate HCM patients from controls

Cut-off value	Specificity	Sensitivity	AUC	Variables
				LA volumes and EF
47.9	0.73	0.80	0.798	LA EDV index (ml/m^2)
23.4	0.82	0.85	0.864	LA ESV index (ml/m^2)
50.0	1.00	0.70	0.873	LA EF (%)
				LA longitudinal strain (%)
33.3	0.91	0.95	0.984	$LA\text{-}LS_s$
16.3	0.82	0.95	0.948	$LA\text{-}LS_e$
13.9	0.96	0.80	0.932	$LA\text{-}LS_a$
				LA longitudinal strain rate (1/s)
1.57	0.91	1.00	0.977	$LA\text{-}LSR_s$
-1.24	1.00	0.90	0.982	$LA\text{-}LSR_e$
-1.77	1.00	0.95	0.986	$LA\text{-}LSR_a$

Results of the receiver operating characteristic (ROC) analysis with area under the curve (AUC), sensitivity, specificity and cut-off values. LA: left atrial; EDV: end-diastolic volume; ESV: end-systolic volume; EF: ejection fraction; LS: longitudinal strain; LSR: longitudinal strain rate.

P190

Right atrial function assessed with novel CMR feature tracking based long-axis strain in patients with pulmonary hypertension

Liang Zhong, Ph.D.[1]Shuang Leng, Ph.D.[2], Xiaodan Zhao, Ph.D.[2], Ju Le Tan, M.D.[1], Ru San Tan, M.D.[1]

1. National Heart Centre Singapore; Duke-NUS Medical School, Singapore, N/A, Singapore
2. National Heart Centre Singapore, N/A, Singapore

Background: Pulmonary hypertension (PH) can lead to the development of right-sided heart enlargement and eventually right heart failure (RHF). Studies have suggested that right atrial (RA) dysfunction has significant implications for assessing the severity of RHF in patients with PH. Despite its prognostic importance, the right atrium is still less investigated. Hence, the aim of this study was to evaluate the RA dysfunction in PH patients using a novel long-axis strain parameter derived from cine cardiovascular magnetic resonance (CMR) imaging feature tracking.

Methods: A group of 20 patients with PH (48±13 yr) and 20 normal controls (48±15 yr) were enrolled and underwent CMR scan on 3T systems (Ingenia, Philips Healthcare) using balanced turbo field echo sequence (BTFE). An in-house developed program [1, 2] was used to perform the semi-automatic tracking of the right atrioventricular junction (RAVJ) points and the RA apex in 4-chamber cine long-axis view. The RA longitudinal strain (LS) was mathematically expressed as $LS(t) = (L(t) - L_0)/L_0$, where L_0 is the initial length and $L(t)$ is the length at time instance t (**Fig. 1(A-B)**). Time derivative of LS resulted in longitudinal strain rate (LSR). Six RA strain parameters were extracted from strain and strain rate curves (**Fig. 1(C-D)**): total strain during reservoir phase (**LS_s**), passive strain during conduit phase (**LS_e**), active strain during atrial contraction phase (**LS_a**), and the corresponding strain rate parameters (**LSR_s**, **LSR_e**, **LSR_a**) in each phase of the atrial deformation.

Results: The RA LS and LSR parameters were successfully derived from standard cine CMR in all subjects. **Figure 1(C-D)** showed the LS and LSR curves for a 41-yr-old female healthy volunteer and 44-yr-old female PH patient. The average values of LS_s, LS_e, LS_a, LSR_s, LSR_e, and LSR_a were 46.5% vs. 23.6%, 26.1% vs. 11.3%, 19.7% vs. 11.1%, 2.7 s^{-1} vs. 1.2 s^{-1}, -2.3 s^{-1} vs. -1.1 s^{-1} and -2.3 s^{-1} vs. -1.4 s^{-1}, respectively. The patients with PH had significantly impaired RA strains and strain rates relative to the group of normal controls of similar age (**Table 1**). Analysis also showed that the RA LS and LSR measurements demonstrated superior performance compared with RA volumetric measurements and ejection fraction (EF) in differentiating between normal and diseased states (**Table 2**).

Conclusions: The novel CMR feature tracking based long-axis strain parameters could become clinically valuable markers for detecting abnormalities in RA deformation and allow evaluation of clinical changes in RA function of patients with PH.

References:

1. Leng S, et al. Am J Physiol Heart Circ Physiol 2015.
2. Leng S, et al. Ann Biomed Eng 2016.

http://www.ConferenceAbstracts.com/uploads/cfp2/attachments/LDFAIBDN/LDFAIBDN--222207-1-ANY.pdf

Table 1: Comparison of RA strain and strain rate parameters between study groups.

P value	PH patients (n = 20)	Normal subjects (n = 20)	Variables	RA function
			RA longitudinal strain (%)	
< 0.0001	22.14 ± 12.34	51.19 ± 8.31	RA-LS_s	Reservoir
< 0.0001	7.89 ± 5.15	25.80 ± 7.98	RA-LS_e	Conduit
< 0.0001	12.30 ± 7.72	22.85 ± 3.90	RA-LS_a	Booster pump
			RA longitudinal strain rate (1/s)	
< 0.0001	1.31 ± 0.80	2.51 ± 0.47	RA-LSR_s	Reservoir
< 0.0001	-0.90 ± 0.49	-2.22 ± 0.55	RA-LSR_e	Conduit
< 0.0001	-1.62 ± 1.04	-3.09 ± 0.71	RA-LSR_a	Booster pump

Data are represented as mean ± SD. RA: right atrial; LS: longitudinal strain; LSR: longitudinal strain rate; PH: pulmonary hypertension.

Table 2: Utility of RA volumetric, strain and strain rate parameters to differentiate PH patients from controls.

Cut-off value	Specificity	Sensitivity	AUC	Variables
				RA volumes and EF
52.6	0.90	0.70	0.743	RA EDV index (ml/m^2)
32.0	1.00	0.70	0.803	RA ESV index (ml/m^2)
40.0	0.75	0.90	0.905	RA EF (%)
				RA longitudinal strain (%)
39.2	1.00	0.95	0.993	RA-LS_s
15.1	0.90	0.90	0.973	RA-LS_e
17.7	1.00	0.75	0.905	RA-LS_a
				RA longitudinal strain rate (1/s)
1.90	0.95	0.90	0.930	RA-LSR_s
-1.56	0.90	0.90	0.973	RA-LSR_e
-2.43	0.85	0.75	0.857	RA-LSR_a

Results of the receiver operating characteristic (ROC) analysis with area under the curve (AUC), sensitivity, specificity and cut-off values. RA: right atrial; EDV: end-diastolic volume; ESV: end-systolic volume; EF: ejection fraction; LS: longitudinal strain; LSR: longitudinal strain rate.

P191

Right ventricular turbulent kinetic energy: a potential marker for risk stratification of adults with repaired Tetralogy of Fallot

Alexandru G. Fredriksson, MD[1] Aleksandra Trzebiatowska-Krzynska[2], Petter Dyverfeldt, PhD[1], Jan Engvall, MD, PhD[3], Tino Ebbers, PhD[3], Carl-Johan G. Carlhäll, MD, PhD[4]

1. *Linköping University, Linköping, Ostergotlands Lan, Sweden*
2. *Department of Cardiology and Department of Medicine and Health Sciences, Linkoping University, Sweden, Linkoping, Ostergotlands Lan, Sweden*
3. *Linkoping University, Linkoping, Ostergotlands Lan, Sweden*
4. *Linköping university, Ostergotlands Lan, Sweden*

Background: The number of adult patients with long-term complications after early repair Tetralogy of Fallot (ToF) is increasing. In these patients, development of pulmonary regurgitation (PR) leads to progressive right ventricular (RV) remodeling and dysfunction (Apitz et al. Lancet 2009). Pulmonary valve replacement (PVR) has shown beneficial effects, but the timing of PVR is discussed (Cheung et al. Am J Cardiol, 2010). PR causes disturbed or turbulent flow within the RV, which is known to be harmful to cardiovascular tissues and may contribute to RV remodeling. 4D flow CMR permits quantification of intracardiac turbulent kinetic energy (TKE). We hypothesized that adult early repair ToF patients with PR will present increased levels of TKE compared to healthy controls, that further will relate to the RV remodeling.

Methods: Seventeen early repair ToF patients and 5 healthy controls were included. The patients were divided into two groups for comparison based on their respective PR-fraction, one lower PR-fraction group (< 15%) and one higher PR-fraction group (>15%). 4D flow, conventional 2D flow data and morphological images were acquired using a 1.5 T MRI scanner (Philips Achieva). The RV volume was segmented in the morphologic short-axis images for all diastolic timeframes and resampled to the 4D flow data. TKE was computed inside the segmented RV volume throughout diastole (Dyverfeldt et al. JMRI, 2008). TKE-specific markers were calculated: the integrated TKE over diastole divided by the number of timeframes, *Average TKE*; the total TKE in the RV volume at the timeframe with highest TKE, *Peak Total TKE*; the maximal TKE intensity inside any given 4D flow voxel over diastole, *Peak TKE*. PR-fractions and PR-volumes were derived from 2D flow data.

Results: The patient sub-groups and the healthy controls presented no intergroup differences in any basic clinical parameter (Table 1). The higher PR-fraction group had more remodeled RVs, more severe PR and higher TKE values compared to the other two groups (Table 1). The TKE developed around the regurgitant jet within the RV outflow tract (Figure 1). Regression analysis between RVEDVI and the different 4D/2D flow parameters showed that *Peak Total TKE* best predicted RVEDVI (R^2=0.506, P < 0.001), followed by *Average TKE* (R^2=0.464, P < 0.001) (Table 2).

Conclusions: 4D flow CMR was utilized to successfully quantify and visualize turbulence intensity in the RV of early repair ToF. The 4D flow specific TKE markers *Peak Total TKE* and *Average TKE* predicted RV remodeling better than conventional 2D flow PR-parameters. These results propose novel hemodynamic aspects of pathophysiologic mechanisms of PR in the development of late complications after early ToF repair that may serve as potential markers for risk stratification.

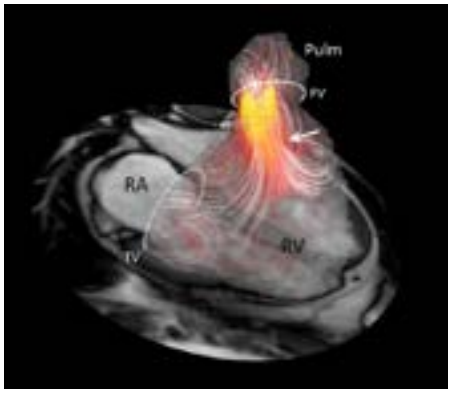

Table 1. ANOVA of basic clinical, conventional 2D flow and 4D flow parameters of the healthy control group and the two patient sub-groups.

ToF with higher PR-fraction (>15%) N=8	ToF with lower PR-fraction (<15%) N=9	Healthy control group N=5	
Clinical parameters			
36 ± 14	30 ± 8	30 ± 8	Age (y)
1.85 ± 0.27	1.94 ± 0.21	1.95 ± 0.30	Body Surface Area (m^2)
70 ± 13	76 ± 12	72 ± 8	HR at rest (bpm)
119 ± 13	119 ± 16	124 ± 7	Systolic blood pressure (mmHg)
73 ± 13	75 ± 12	75 ± 5	Diastolic blood pressure (mmHg)
140 ± 25**†	107 ± 22	96 ± 9	RVEDVI (ml/m^2)
82 ± 15***††	58 ± 12	44 ± 4	RVESVI (ml/m^2)
42 ± 4***	46 ± 5*	54 ± 5	RVEF (%)
32 ± 9	25 ± 9	-	Time from ToF repair (y)
2D flow parameters			
37 ± 20***†††	3.9 ± 3.7	1.9 ± 1.0	PR Volume (ml)
32 ± 11***†††	4 ± 4	2 ± 0.8	PR Fraction (%)
4D flow parameters			
3.22 ± 1.58*††	1.44 ± 0.49	1.37 ± 0.45	Average TKE (mJ)
5.95 ± 3.15**††	2.23 ± 0,81	2.01 ± 0.87	Peak Total TKE (mJ)
343 ± 71.5***†††	130 ± 70.6	86.3 ± 22.2	Peak TKE (mJ/m^3)

*P<0.05 vs Healthy control group, **P<0.01 vs Healthy control group, ***P<0.001 vs Healthy control group.
†P<0.05 vs ToF with lower PR-fraction (<15%), ††P<0.01 vs ToF with lower PR-fraction (<15%), †††P<0.001 vs ToF with lower PR-fraction (<15%).
HR = heart rate, PR = pulmonary regurgitation, RVEDV = right ventricular end diastolic volume, RVEF = right ventricular ejection fraction,
RVESV = right ventricular end systolic volume, TKE = turbulent kinetic energy, ToF = tetralogy of Fallot.

Table 2. Simple linear regression analysis between RVEDVI and clinical, conventional 2D flow and 4D flow parameters (n=22).

P	R^2	
*Clinical parameter*s		
0.750	0.052	Age (y)
0.665	0.096	Body Surface Area (m^2)
0.913	0.083	Time from ToF repair (y)
2D flow parameters		
<0.001*	0.442	PR Volume (ml)
<0.001*	0.431	PR Fraction (%)
4D flow parameters		
<0.001*	0.464	Average TKE (mJ/ml)
<0.001*	0.506	Peak Total TKE (mJ/ml)
0.003*	0.358	Peak TKE (mJ/m^3)

PR = pulmonary regurgitation, ToF = tetralogy of Fallot, TKE = turbulent kinetic energy.

P192

Simultaneous Myocardial and Fat Signal Suppression for Late Gadolinium Enhancement

Mehdi Hedjazi Moghari, Ph.D.Andrew J. Powell, M.D.

Harvard Medical School and Boston Children's Hospital, Boston, MA

Background: With late gadolinium enhancement (LGE), the signal from normal myocardium is nulled by an inversion pulse and abnormal regions appear bright. When myocardial hyperenhancement has an epicardial location, it may be difficult to differentiate it from epicardial/pericardial fat which also appears bright. Previously, this challenge has been addressed by nulling the fat signal using 2 fat-selective inversion pulses (1-3). However, with that approach, beat-to-beat variability in the R-R interval leads to poor fat suppression. Therefore, we developed and examined a more robust fat-suppression technique for phase sensitive inversion recovery (PSIR) LGE.

Methods: A diagram of the proposed fat-suppressed PSIR LGE sequence and longitudinal magnetization is shown in Fig. 1A. The standard non-selective inversion pulse is performed to null the signal of normal myocardium. Following this, the longitudinal magnetization of fat signal will regrow above the transverse plane. Immediately before the data acquisition, a fat-selective inversion pulse is applied to bring the longitudinal signal of fat below the transverse plane. Data acquisition is then performed with a low-to-high k-space profile ordering. Under the typical circumstances (heart rate ‹120 bpm, shot duration ‹80 ms, and inversion time for myocardium ›280 ms [4]), the longitudinal fat signal will be below the transverse plane during the data acquisition. Hence, the signal of fat and myocardium will be dark in the phase-corrected images while the signal of blood and scar will be bright. To assess the efficacy of this technique, 12 patients (5 females; age 24 ± 10 years) underwent both conventional PSIR and fat-suppressed PSIR LGE acquisitions in a horizontal long-axis plane. This was performed on a 1.5T scanner, 15 min after receiving 0.15mmol/kg gadobutrol contrast. For both acquisitions, imaging parameters were FOV 300×300 mm^2, in-plane spatial resolution 2.0 mm^2, slice thickness 7 mm, α 25°, TE/TR 3/6 ms, bandwidth 247 Hz, shot duration 80 ms, and inversion time 290-360 ms. The normalized contrast-to-noise ratio (CNR) between blood and myocardium, and blood and fat were measured.

Results: All acquisitions were successfully completed. PSIR LGE images without and with fat-suppression are shown in Fig. 1B. Fat was successfully suppressed in all PSIR images without affecting the CNR between blood and myocardium (Table 1).

Conclusions: We developed and examined a fat-suppressed PSIR LGE technique that successfully nulls the signal of fat without affecting the CNR between blood and myocardium. Our approach may be less sensitive to the field inhomogeneity and beat-to-beat variability than the previously reported 2 fat-selective inversion pulse approach.

References: [1] Foo TKF, JMRI 2007; [2] Janich MA, ISMRM 2014; [3] Janich MA, JCMR 2016; [4] Huber AM, Radiology 2005.

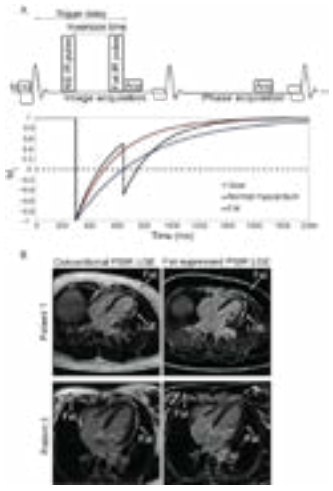

Table 1: Normalized contrast-to-noise ratio between blood and myocardium, and blood and fat for PSIR LGE without and with fat suppression (n=12). Values are mean ± standard deviation. Normalized CNR: 0-minimum to 1-maximum.

Normalized CNR		
Blood and Fat	Blood and Myocardium	
0.06 ± 0.18	0.83 ± 0.19	Conventional PSIR LGE
1.00 ± 0.00	0.85 ± 0.15	Fat-suppressed PSIR LGE
‹0.001	0.54	P-value

P193

Joint Estimates of Myocardial T2 and Apparent Diffusion Coefficient Using Motion Compensated Spin Echo Diffusion Weighted Imaging

Eric Aliotta, M.S.[1]Kévin Moulin, PhD[2], Zhaohuan Zhang, B.S.[1], Daniel B. Ennis, PhD[3]

1. UCLA, CA
2. UCLA, Los Angeles, CA
3. Department of Radiological Sciences, University of California, Los Angeles, CA, USA., CA

Background: Diffusion weighted imaging (DWI) is an emerging non-contrast tool for characterizing myocardial infarcts (MI) wherein an increase in apparent diffusion coefficient (ADC) indicates the presence of fibrosis. Quantitative T_2 mapping can further characterize MI by detecting edema, a hallmark of acute MI, via an increase in T_2. Co-registered ADC and T_2 maps can thus provide significant value in MI diagnosis and management. Herein, we describe a free-breathing technique for the joint estimate of myocardial T_2 and ADC maps (T_2+ADC) that are perfectly co-registered and cardiac phase matched. T_2+ADC requires only minor modification to a spin-echo (SE) DWI acquisition and no increase in scan time as shown *ex vivo* (*Aliotta et al*, JCMR 2015) and in the brain (*Aliotta et al*, ISMRM 2015). The ***objective*** of this work was to demonstrate myocardial T_2+ADC in healthy volunteers and in a phantom and to compare with conventional T_2 and ADC mapping.

Methods: Free-breathing, diastolic T_2+ADC mapping was performed at 3T (Siemens Prisma) in a single mid-ventricular short-axis slice in healthy volunteers (N=8) using SE-EPI DWI with motion compensated (M_1=M_2=0) convex optimized diffusion encoding (CODE-M_1M_2) (*Aliotta et al,* MRM 2016) with b=350s/mm^2 and 3 directions (2.0x2.0x5.0mm, TE=65ms, TR≥4s). Ten signal averages were acquired (scan time ~5min) with TE varied between b=0 repetitions: TE_1=25ms (x3 averages), TE_2=65ms (x7 averages) (Fig 1). T_2 and ADC maps were then jointly reconstructed using a least squares fit to the signal model: $S(b,D) = S_0 e^{-bD} e^{-TE/T2}$. For comparison, independent T_2 and ADC mapping was performed using breath-held T_2-prepared bSSFP (TE_{prep}=0,25,55ms) and a conventional DWI reconstruction (b=350s/mm^2, TE=65ms). Validation data was acquired in a phantom containing varying concentrations of $CuSO_4$ and agar with a range of T_1 and T_2 values (T_1=400-2000ms, T_2=30-75ms) using the *in vivo* protocols. A single-echo SE T_2 map was also acquired as a reference (TE=12,25,55,85,100ms, TR=12s).

Results: There were no significant differences in ADC values between techniques *in vivo* (T_2+ADC: ADC=1.38±0.27mm^2/ms, DWI: ADC=1.38±0.28mm^2/ms, p=N.S.), but T_2+ADC measured significantly shorter myocardial T_2 values than bSSFP (T_2+ADC: T_2=38.5±4.5ms, bSSFP: T_2=46.3±3.1ms, P=0.002) (Fig 3).

Excellent agreement was observed in the phantom between ADC values measured by T_2+ADC and DWI (Fig 2A). Compared with SE, T_2+ADC slightly underestimated T_2 while bSSFP overestimated T_2 (Fig 2B).

Conclusions: T_2+ADC can simultaneously map T_2 and ADC in the heart during free breathing. This method generates perfectly registered T_2 and ADC maps, which can aid the clinical evaluation of MI. While myocardial T_2 values from T_2+ADC were shorter than T_2-prepared bSSFP, they were closer to reference SE T_2 maps in a phantom and are in line with previous reports of normal myocardial T_2 (*Guo et al*, JMRI 2009).

http://www.ConferenceAbstracts.com/uploads/cfp2/attachments/LDFAIBDN/LDFAIBDN--212859-1-ANY.pdf

http://www.ConferenceAbstracts.com/uploads/cfp2/attachments/LDFAIBDN/LDFAIBDN--212859-2-ANY(1).pdf

http://www.ConferenceAbstracts.com/uploads/cfp2/attachments/LDFAIBDN/LDFAIBDN--212859-3-ANY.pdf

P194

Accuracy and precision of four T1 estimation algorithms for the MOLLI sequence

Jiaxin Shao, PhD[1] Kim-Lien Nguyen, M.D.[2], Peng Hu, PhD[1]

1. university of california los angeles, CA
2. Division of Cardiology, David Geffen School of Medicine at UCLA and VA Greater Los Angeles Healthcare System, CA

Background: Myocardial T1 mapping plays a vital role in diagnosis of various myocardial diseases. The Modified Look-Locker Inversion Recovery (MOLLI) sequence is most widely used for myocardial T1 mapping, but has several limitations. The original MOLLI uses a 3-parameter exponential fitting algorithm to calculate the T1 value, which is known to underestimate T1 values and be sensitive to factors such as heart rate and flip angle. Recently, several novel T1 calculation algorithms were proposed for the MOLLI sequence including instantaneous signal loss simulation (InSiL) T1 estimation, inversion group (IG) fit, and Bloch equation simulation with slice profile correction (BLESSPC) T1 estimation. These algorithms have added value, but no comparison has been performed across these recently developed T1 estimation algorithms. The goal of this work was to compare the accuracy and precision of the four T1 estimation for the MOLLI sequence.

Methods: Four MOLLI T1 estimation algorithms, including the original fit, IG fit, InSiL and BLESSPC were studied. The inversion factor (δ) correction algorithm was applied for original fit and IG fit. The original BLESSPC T1 estimation algorithm was proposed for the FLASH-MOLLI sequence. In this work, we extended the BLESSPC algorithm to calculate T1 values for the standard bSSFP-based MOLLI sequence wherein the signal evolution of bSSFP readouts are simulated using the Bloch equation. T1 estimation accuracy, precision and sensitivity to heart rate (HR), flip angle (FA) and acquisition scheme (AcS) variations of the four algorithms were compared using phantom studies and eight healthy volunteers. The average inversion factors for phantoms and in vivo were preliminary measured using the "MOLLI+M0" sequence (JMRI 2015; 41:721–9) with BLESSPC 4-parameters fit.

Results: In phantom studies, T1 estimation accuracy was lower with IG and original fit than with BLESSPC and InSiL for the MOLLI 5(3)3 sequence. Compared with the other three methods, BLESSPC generated the most consistent T1 values for the MOLLI sequence at different HR, FA and AcS (Figure 1a-1d). Compared to the original fit with a FA =35°, using a FA = 50° and BLESSPC T1 estimation resulted in better accuracy (7.6±13.0 ms vs. -30.8±27.7 ms) and precision (0.59%±0.07% vs. 0.67%±0.15%) (Figure 1e-1f). In vivo results confirmed that BLESSPC is least sensitive to FA and AcS variations (Table 1). One example is shown in Figure 2. There were no statistically significant differences in reproducibility among the four algorithms for MOLLI 5(3)3 acquisition with FA = 35° ($p>0.3$) (Figure 3). When using FA=50°, the reproducibility was significantly improved only when using BLESSPC (1.6%±0.9 vs. 2.6%±1.9%, $p < 0.05$).

Conclusions: BLESSPC has superior accuracy and is the least sensitive to FA, HR and AcS variations. T1 estimation using BLESSPC and FA=50° appears to be superior than conventional MOLLI with FA=35°.

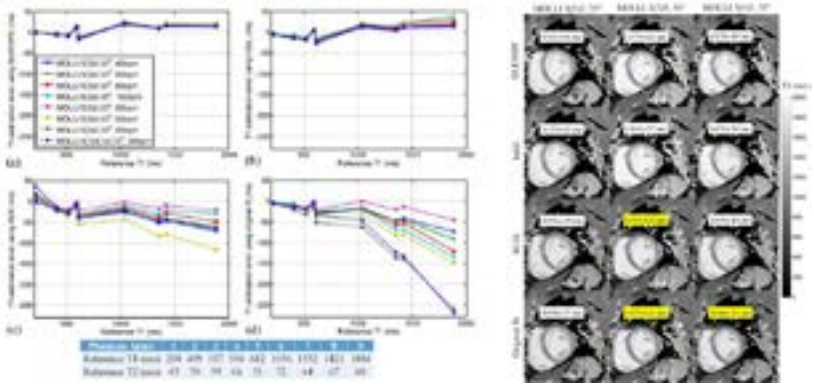

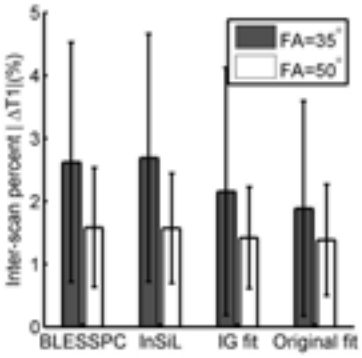

P196

T1 mapping in healthy subjects using SMART1Map at 3T: a comparison with MOLLI.

Pauline Ferry, Ph.D.[1]Andrei Codreanu, MD[2], Shufang Liu, Ph.D. student[3], Aurélien Bustin, Ph.D. student[3], Anja CS Brau, Ph.D.[4], Marine Beaumont, Ph.D.[5], Martin A Janich, Ph.D.[6], Glenn Slavin, Ph.D.[7]

1. *U947, INSERM, Nancy, France, N/A, France*
2. *Centre Hospitalier de Luxembourg, Luxembourg, N/A, Luxembourg*
3. *Technology University of Munich/ GE Global Research, N/A, Germany*
4. *GE healthcare, CA*
5. *6CIC-IT 1433, INSERM, Nancy, France, N/A, France*
6. *GE Global Research, N/A, Germany*
7. *GE Healthcare, MD*

Background: The saturation method using adaptive recovery times for cardiac T1 mapping (SMART1Map) is a single-point, multi heart-beat technique for cardiac T1 mapping, aimed at reducing the systematic biases related to breath-hold inversion-recovery methods. The SMART1Map scan consists of a first image without magnetization preparation and several post saturation-recovery images over 7 to 9 heart beats (depending on heart rate), with actual recovery times ensured by measuring true R-R intervals in real time. Its accuracy and robustness to imaging parameters, T2, B1 variation and heart rate have been previously demonstrated in phantom.

Methods: Twenty healthy volunteers (14 men, age 38±8 y.) were scanned on a 3.0T (GE, Signa HDxt) scanner, using both SMART1Map and MOLLI (5/3/3 protocol). Robust saturation is achieved by a train of 4 HS8 RF pulses. Pre- and post-contrast myocardial and blood T1 values were measured on a mid ventricular short axis view. After non rigid registration and image denoising according to techniques previously described, pixel wiseT1 maps were generated using a 3 parameter Levenberg–Marquardt fit. Manual contouring of myocardial borders and 6 AHA-defined segments were used. Segmental myocardial T1 values and blood T1 values were used for extracellular volume (ECV) calculation according to consecrated method. Pixel wise ECV maps were further generated by merging the original SMART1Map data.

Results: Acquisition was completed in all patients, with comparable breath-hold times (p = ns, table). Visual quality analysis led to discard 6%of segments with either technique.

Global pre contrast T1 values showed comparable inter patient variability with the two techniques (p = ns.). Segmental T1 values were significantly correlated betweenSMART1Map and MOLLI for all but the anterior and lateral segments ($r = 0.53$ to 0.72, $p < 0.05$). ECV values correlated between the two techniques for the global slice ($r = 0.63$, $p = 0.01$), and for the septum ($r > 0.71\%$, $p < 0.01$), but less for the free walls. Both pre contrast T1 and ECV values showed significantly less intersegmental variation with SMART1Map compared to MOLLI (* $p < 0.01$ MOLLI vs. SMART1Map).

Pixel wise ECV maps based on SMART1Mapshowedexcellent correlation with the calculated ECV values for all segments ($r > 0.84$, $p < 0.01$), confirming the robustness of the map generation.

Conclusions: SMART1Map provided similar image efficiency and patient acceptability as compared to MOLLI. The two techniques showed comparable precision, under reserve of the number of subjects, lack of pathology and the 3T field. SMART1Map measures showed lower intersegmental variation, and by consequence no significant difference between septum and non-septal regions. This was different from MOLLI data and the data published so far, and might reflect a lower dependence on scanning conditions, which is a requisite for objective quantitative results. The clinical relevance of these findings needs further investigation.

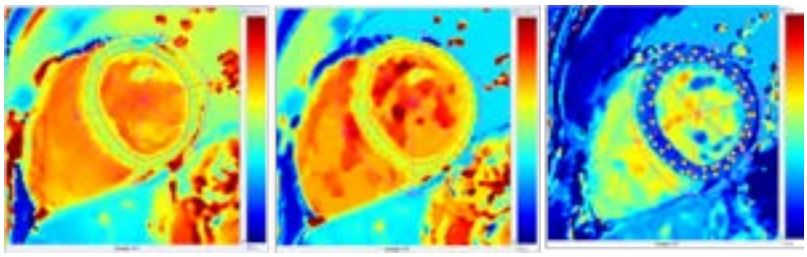

MOLLI	SMART1Map	
1177 ± 42	1447 ± 45	Pre contrast myocardial T1 (msec)
4 ± 1,3 *	2 ± 0.8	Intersegmental T1 variation (%)
0.29 ± 0.05	0.22 ± 0.03	ECV
9 ± 6 *	4.5 ± 4	Intersegmental ECV variation (%)
0.31 ± 0.06 vs. 0.29 ± 0.05 (p = 0.01)	0.22 ± 0.03 vs. 0.21 ± 0.03 (p = ns)	ECV septum vs. non septal ECV
15 ± 2.4	14 ± 2 sec	Breath-hold time

* ($p<0.01$ vs, SMART1Map)

P197

Comparisons of Myocardial Mechanical Properties of the Right Ventricle and Atrium in Patients With Left Ventricular Systolic And Diastolic Dysfunction With And Without Clinical Heart Failure

Qizhi Chen, MD, PHD[1] Lynette Duncanson[1], Javed Butler, MD, MPH[2], Jie jane. Cao, MD, MPH[3]

1. St Francis Hospital, The DeMatteis Center for Cardiac Research & Education, Greenvale, NY
2. Division of Cardiology, Deparment of Medicine, Stony Brook University, Stony Brook, NY
3. St Francis Hospital, The DeMatteis Center for Cardiac Research & Education, roslyn, NY

Background: Reduced right ventricular (RV) function is associated with adverse clinical outcome in patients with left heart failure (HF). We sought to examine the RV strain and RA function in patients with LV systolic dysfunction without HF (LVSD), HF with reduced EF (HFrEF), LV diastolic dysfunction without HF (LVDD) and HF with preserved ejection fraction (HFpEF).

Methods: Participants were enrolled prospectively undergoing cardiac MRI.HF was diagnosed with clinical manifestations and elevated BNP or NT-BNP. LVSD was defined as having LVEF < 50%. LVDD was determined by echocardiographic criteria or by elevated LV filling pressure assessed during the same day catheterization. RV and RA strain were assessed using dedicated right heartfeature tracking software analyzing MRI cine images. The RV circumferential strain (CS) was assessed including all consecutive short axis planes. The RV longitudinal strain (LS) was analyzed in 4-chamber view. The RA volume and RAejection fraction(RAEF) were assessed using Tomtec software.

Results: Mean RVEF was reduced in HFrEF (35±5%) (N=16) and LVSD (45±9%) (N=14) compared to normal control (56±5%) (N=11), HFpEF (59±8%) (N=9) and LVDD (57±6%) (N=14). The global RV CS was lowest in HFrEF (-8±3%) followed by LVSD (-11±3%) compared to normal (-13±3%, $p < 0.05$). In contrast, global RV CS was largely unaltered in HFpEF and in LVDD. Reduced LS was only present in HF groups, HFrEF (-13±5%) and HFpEF (-15±11%) compared to normal (21±4%). LS was preserved in LVSD and LVDD. Mean RAEF was reduced in HFrEF (31±16%) and HFpEF (35±15%) compared to normal control (49±10%, $p < 0.05$). RA volume at ventricular end diastole was increased significantly in HFrEF (79±45ml) and HFpEF (56±39ml) compared to normal control (24±13ml, $p < 0.05$). In contrast, RA volume at ventricular end systole was increased only in HFrEF (91±52ml)compared to normal control (59±33ml $p < 0.05$).

Conclusions: Reduced RV longitudinal strain, is only seen in subjects with HF including HFrEF and HFpEF whereas reduced RV circumferential strain is present in individuals with reduced RVEF including HFrEF and LVSD. In patients with HF, there is also increased RA volume and reduced RAEF. Our findings suggest that the assessment of RV and RA properties can be critical in the understanding stages of LV dysfunction and HF.

P198

Synthetic magnitude and phase sensitive inversion recovery images derived from MOLLI acquisitions accurately determine size of myocardial infarction compared to conventional CMR methods in patients.

Arlene Sirajuddin, MD[1] Sophia Hammer-Hansen, MD[2], Li-Yueh Hsu, DSc[3], W. Patricia Bandettini, MD[4], Sujata M. Shanbhag, MD, MPH[5], Christine Mancini, RT[6], Andrew E. Arai, MD[7]

1. *National Institutes of Health, Bethesda, MD*
2. *National Institutes of Health, Hovedstaden, Denmark*
3. *National Heart, Lung and Blood Institute, National Institutes of Health, Bethesda, MD*
4. *National Heart, Lung and Blood Institute, National Institutes of Health, MD*
5. *NIH/NHLBI, Bethesda, MD*
6. *Suburban Hospital, MD*
7. *National Institues of Health, Bethesda, MD*

Background: Conventional segmented magnitude and phase sensitive inversion recovery gradient recalled echo (IR-GRE) late gadolinium enhancement images can evaluate myocardial infarction (MI) size and viability. However, these images are sensitive to patient motion, and magnitude inversion recovery methods depend on selecting the correct inversion time. If one accurately quantified post-contrast myocardial T1, these measurements could be used to generate synthetic magnitude and phase sensitive inversion recovery images that appear similar to the traditional IR-GRE images. The synthetic magnitude and phase sensitive inversion recovery images can be retrospectively created at any inversion time despite the limited number of inversion times sampled by MOLLI. The aim of this study was to determine how accurately the synthetic inversion recovery images measured the size of MI compared to segmented IR-GRE and to measure T1 and extracellular volume fraction (ECV).

Methods: In this institutional review board-approved, prospective study, a research CMR scan was performed at 1.5T within 7 days of acute MI. The MOLLI acquisition followed a 4s(1s)3s(1s)2s protocol with a field of view of 360 x 270 mm, slice thickness of 6 mm, and 256 x 144 matrix. MOLLI images were obtained pre-contrast administration and about 15 minutes after injection of gadopentetate dimeglumine. MI was defined using a 50% threshold between enhanced and remote myocardium using research software.

Results: Out of 37 consecutive patients, 34 had both MOLLI and conventional IR-GRE images at the same slice location. The synthetic inversion recovery image quality was good to excellent in 25 of 34 patients and generally looked the same as conventional images except for the random phase speckle in regions of low signal intensity like the lungs. All images were quantifiable. An example of each image type is shown in the figure. Infarct size on conventional magnitude inversion recovery images correlated well with synthetic magnitude inversion recovery (r2=0.98, y=1.04x+0.00). Infarct size on conventional phase sensitive IR-GRE also correlated well with synthetic phase sensitive inversion recovery (r2=0.98, y=1.02x-0.00). The ECV of infarcted myocardium was 53 ± 7 which was significantly greater than the ECV of remote myocardium 26 ± 4 ($p < 0.001$).

Conclusions: Synthetic magnitude and phase sensitive inversion recovery images can accurately measure the size of MI. This method has good image resolution, includes motion correction to minimize artifacts from respiratory motion, does not require selection of an inversion time, and also can quantify myocardial T1 and ECV.

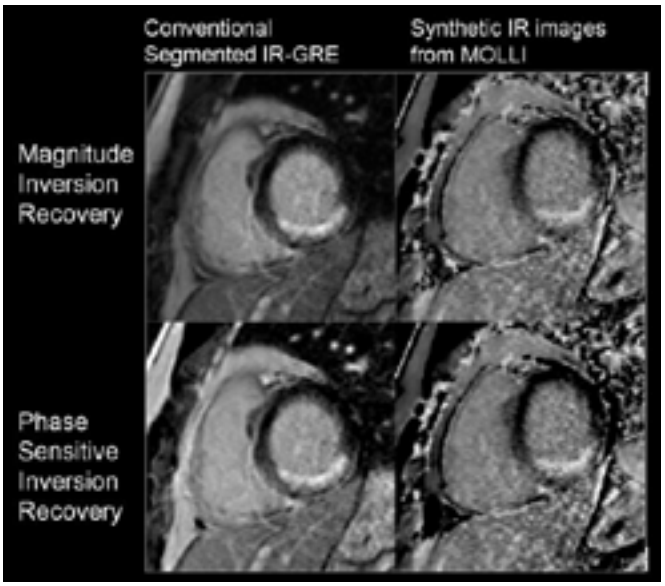

P199

Community delivery of the first semi-automated fractal analysis tool in CMR

Dina Radenkovic, BSc; MD Candidate [1]Gabriella Captur, MD, PhD, MRCP, MSct[2], Chunming Li, PhD[3], Yu Liu, PhD[4], Nay Aung, MD, MRCP[5], Filip Zemrak, MD MRCP[5], Catalina Tobon-Gomez, PhD[6], Xuexin Gao[7], Steffen E. Petersen, MD DPhil MPH FRCP[5], Matthias Friedrich, MD[8], James Moon, MBBS, MD, MRCP[5]

1. *UCL Medical School, London, UK, London, England, United Kingdom*
2. *UCL Biological Mass Spectrometry Laboratory, Institute of Child Health and Great Ormond Street Hospital, 30 Guilford Street, London, UK';, England, United Kingdom*
3. *Department of Radiology, University of Pennsylvania, Philadelphia, PA, PA*
4. *College of Electronic Science and Engineering, Jilin University, Changchun, P.R.China, Chongqing, China (People's Republic)*
5. *Barts Heart Center, The Cardiovascular Magnetic Resonance Imaging Unit and The Center for Rare Cardiovascular Diseases Unit, St Bartholomew's Hospital, West Smithfield, London, UK, England, United Kingdom*
6. *Division of Imaging Sciences, King's College, London, UK, England, United Kingdom*
7. *Circle Cardiovascular Imaging Inc, Panarctic Plaza, Calgary, Canada, PQ, Canada*
8. *Philippa & Marvin Carsley CMR Centre at the Montreal Heart Institute, Montreal, QC, Canada, PQ, Canada*

Background: A variety of trabecular patterns are being identified in the left ventricle (LV) by cardiovascular magnetic resonance (CMR) in healthy subjects and across the spectrum of cardiac disease. Fractal analysis can reliably quantify LV trabeculation. Promising cardiovascular research tools based on fractal analysis have been reported in the literature, but their open delivery to the CMR community is still missing. We present the development and validation of the first community-accessible semi-automated fractal tools for measuring endocardial complexity in the LV as a fractal dimension (FD).

Methods: The LV endocardium inclusive of trabeculae was segmented using a region-based level-set segmentation algorithm applied to the LV short axis cine stack. Extracted contours subsequently underwent standard mono-fractal box-counting analysis to derive the FD per slice. The original MATLAB implementation was recoded in the Objective-C programming language and deployed on two independent platforms, each with its own graphical user interface (OsiriX and the commercial MR reporting software cvi[42]; **Fig.1**). A total of 30 CMR cine stacks at 1.5 Tesla (15 healthy volunteers and 15 patients with LV noncompaction) were analysed using each of the three platforms and the repeatability of FD values per slice across platforms was determined.

All cine slices were manually contoured by an expert reader (R1) using OsiriX providing ground truth contours for validation of segmentation accuracy by point-to-curve (P2C) estimates. P2C analysis compared semi-automated segmentation results from OsiriX and cvi[42] against the ground truths. Manual contouring was repeated by R1 and by a second independent reader (R2) on 15 randomly selected stacks to measure intra- and inter-observer variability of manual contouring by P2C.

Results: Fractal outputs by the OsiriX or cvi[42] platforms are highly correlated with MATLAB-derived values (correlation coefficients: 0.966 [95% CI: 0.957-0.974] and 0.969 [0.962-0.976] respectively). The semi-automated level-set segmentation results by OsiriX|cvi[42] were highly correlated with ground truth contours as evidenced by low P2C errors: P2C, 0.88 ± 0.39 mm and 0.61 ± 0.23 mm respectively. Validity of the ground truth contours was inferred from the favourably low P2C errors between readers (R1-R1: 0.89 ± 0.92 mm; R1-R2: 0.71 ± 0.33 mm).

Conclusions: The first set of accessible fractal tools have been validated and are now being released to the CMR community to facilitate further experimentation with, and novel clinical applications of fractals in the cardiac imaging domain. Online links to downloadable plugins and training manuals will be advertised during the poster presentation.

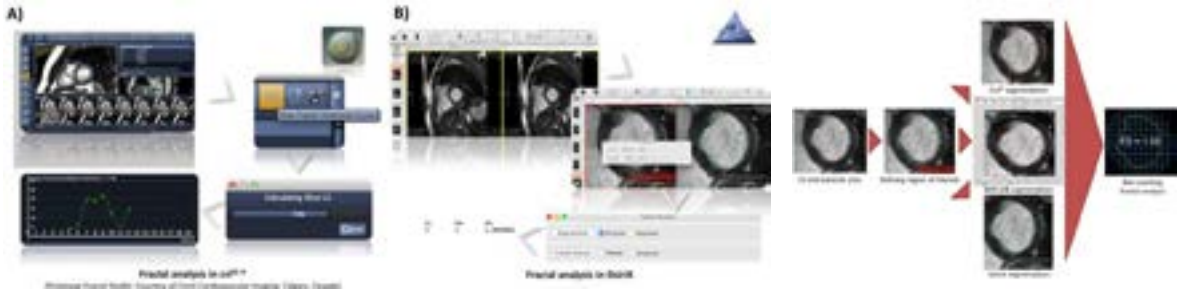

P200

Inter- and intra-observer reproducibility of cardiac magnetic resonance feature tracking and sample size calculation in small animals

Tomas Lapinskas, MD[1] Seyedeh Mahsa Zamani, MD[2], Sarah Jeuthe, MD[3], Daniel R. Messroghli, MD[4], Rolf Gebker, MD, PhD[2], Heike Meyborg, MD[2], Ulrich Kintscher, MD, PhD[3], Remigijus Zaliunas, MD, PhD[1], Burkert Pieske, MD, PhD[2], Philipp Stawowy, MD, PhD[2], Sebastian Kelle, MD, PhD[2]

1. *Lithuanian University of Health Sciences, Kaunas, Kauno Apskritis, Lithuania*
2. *German Heart Institute Berlin, Berlin, Berlin, Germany*
3. *Charité-Universitätsmedizin Berlin, Berlin, Berlin, Germany*
4. *Charité Universitätsmedizin and Deutsches Herzzentrum Berlin, Berlin, Berlin, Germany*

Background: Cardiovascular magnetic resonance feature tracking (CMR-FT) is a novel tissue tracking technique developed for noninvasive assessment of myocardial function. This study aimed to assess the inter- and intra-observer reproducibility of CMR-FT in a small animal (mouse) model and define sample size calculation for future trials.

Methods: Six C57BL/6J mice were selected and underwent CMR with a 3 Tesla small animal MRI scanner (MRS 3017, MR Solutions, Guildford, UK). Myocardial deformation was analyzed using dedicated software (TomTec Imaging Systems, 2D CPA, MR, Cardiac Performance Analysis, Unterschleissheim, Germany) by two observers. Left ventricular (LV) longitudinal strain (Ell_{LAX}) was calculated from two long-axis cine images, and circumferential and radial strain (Ecc_{SAX}, Err_{SAX}) were derived from one mid-ventricular short-axis cine image. To assess intra-observer agreement, all data analysis was repeated 4 weeks after the initial assessment. The sample size required to detect a relative change in strain was calculated.

Results: Myocardial deformation parameters were successfully derived in all animals. Ecc_{SAX} and Ell_{LAX} demonstrated highest inter-observer reproducibility (ICC 0.79 (0.46-0.91) and 0.73 (0.56-0.83) for Ecc_{SAX} and Ell_{LAX} respectively). In contrast, at the intra-observer level Ell_{LAX} was more reproducible than Ecc_{SAX} (ICC 0.83 (0.73-0.90) and 0.74 (0.49-0.87) for Ell_{LAX} and Ecc_{SAX} respectively). The reproducibility of Err_{SAX} was weak at both observer levels. Sample size calculation revealed that detection of a relative 10% change in Ecc_{SAX} in mice would require ten animals (not measures). In contrast, 85 mice are required to detect a 5% relative change in Err_{SAX} with CMR-FT (power of 90% and α error of 0.05).

Conclusions: Cardiac mechanics parameters derived from conventional cine images using CMR-FT technique in small animal models are highly reproducible. The most reproducible measures are global circumferential and global longitudinal strain, whereas reproducibility of radial strain is weak. Sample size calculation demonstrates that a small number of animals is sufficient detect changes in wall motion using CMR-FT-derived target parameters in preclinical trials.

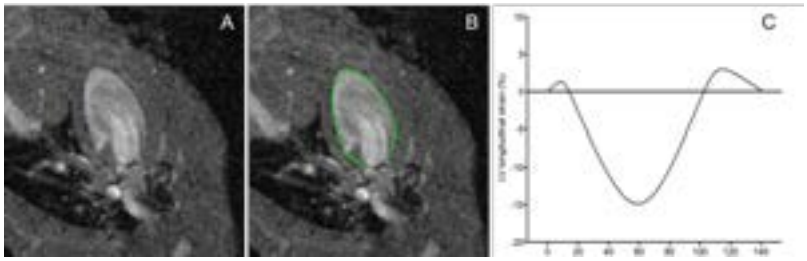

P201

T1 mapping as a new technique in detection of Fractional flow reserve and developing ischemia

Nahla D. Ali, MD, MSc[1], Mary R. Mahrous, MD, MSc[2], Asmaa M. N. Elsayed Ahmed, MD, MSc.[3]Wesam E. El Mozy, MD, MSc[4], Megahed El-Bayoumy, MD, MSc, MRCP [4], Asmaa R. Abd El-Naby, MD, MSc[5], Sameh Abdel Latif, MD, MSc[6], Mohammad Gibreel, MD, MSc[7], Soha Romeih, MD, MSc, PhD[2], Ahmed Kharabish, MD, MSc, PhD[4]

1. *Radiology department-Faculty of medicine- Cairo university, Al Qahirah, Egypt*
2. *Magdi Yacoub foundation-Aswan Heart Center, Aswan, Egypt*
3. *Aswan Heart Centre - Magdi Yacoub Heart Foundation, Aswan, Egypt*
4. *Magdi Yacoub Foundation - Aswan Heart Centre, Aswan, Egypt*
5. *Cardiology department- Tanta university, Aswan, Egypt*
6. *Facullty of medicine Cairo university, Al Qahirah, Egypt*
7. *Magdi Yacoub foundation- Aswan heart center, Aswan, Egypt*

Background: Computed tomography was introduced as an alternative tool to measure the fractional flow reserve (FFR) non-invasively. However, cardiac magnetic resonance imaging (CMRI) through its new techniques namely the T1 mapping may provide an alternative as well. Therefore we aimed to assess the T1 mapping technique in that field.

Methods: Sixteen patients presenting with multi-vessel coronary artery disease were sent to CMRI to assess myocardial viability. All patients were scanned using routine protocol of cine images, late gadolinium enhancement (LGE) and T1 mapping (MOLLI technique). Three cuts short axis (SAX) T1 mapping sequence were taken pre and post contrast in basal, mid and apical levels. Extracellular volume (ECV) was measured in all scanned segments. ECV above 29% was considered expanded. Results were compared to LGE images and conventional coronary angiography (CCA) as well as the FFR when available.

Results: Segments that showed LGE also showed evidence of ECV expansion. Seventy eight segments showed expanded ECV along the non culprit artery without evident enhancement on LGE images. T1 mapping results were correlated to CCA. It discovered that ECV expansion along the non culprit artery was along territorial supply of other moderately stenotic lesions on CCA. FFR was done for five patients. It discovered a great match to T1 mapping results showing that insignificant lesions by FFR had no evidence of ECV expansion despite being moderately stenotic by CCA. As well it showed expanded ECV along FFR significant lesions.

Conclusions: T1 mapping is a developing tool for assessment of myocardial fibrosis before being detected by LGE sequences. It may then detect ischemia before developing to infarction. It also shows potential comparable results to FFR in detecting the significance of coronary artery lesions.

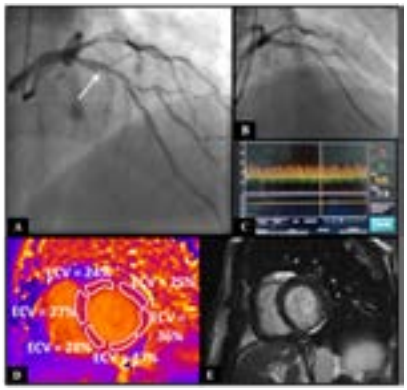

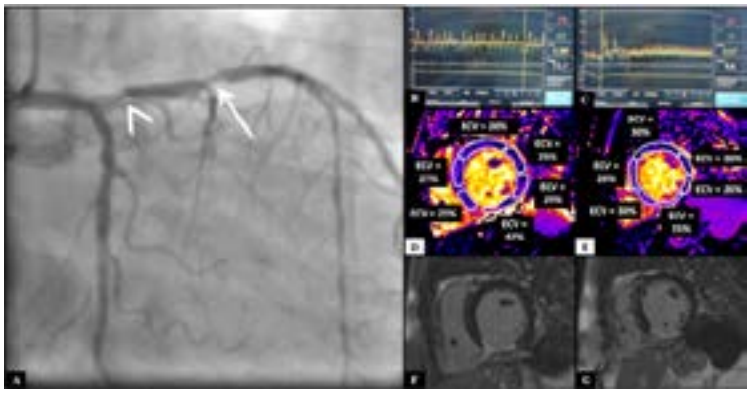

P202

Myocardial T1 mapping using free breathing MOLLI with Real-time Slice Tracking

Céline Smekens, MSc[1], Sébastien Roujol, PhD[1]Radhouene Neji, PhD[2], Reza Razavi, MD, PhD[3], Rene Michael. Botnar, PhD[1]

1. *King's College London, London, England, United Kingdom*
2. *Siemens Healthcare Limited, Frimley, England, United Kingdom*
3. *King's College London, England, United Kingdom*

Background: Quantitative myocardial T1 time has been shown to be altered in the presence of a variety of cardiomyopathies. The modified Look Locker (MOLLI) technique is the most widely used myocardial T1 mapping approach. In this 2D sequence, several T1-weighted images are acquired within a breath-hold and fit to a model of the T1 recovery. However, some patients are unable to sustain stable breath-holds which results in important in-plane and through-plane motion. While in-plane motion can potentially be corrected using image registration algorithms, through-plane motion cannot be corrected retrospectively in 2D acquisition and may introduce bias in T1 estimates. In this study, we sought to develop a free breathing MOLLI sequence with real-time slice tracking to reduce through-plane motion.

Methods: The MOLLI sequence was modified to add a navigator echo before each imaging acquisition for real-time slice tracking (tracking factor=0.6), as well as a navigator restore pulse immediately after each inversion pulse. N=6 volunteers were recruited for a cardiac MRI study on a 1.5T Aera SIEMENS scanner. Each volunteer was imaged twice using the conventional breath-hold (BH) MOLLI sequence and the proposed free breathing (FB) MOLLI sequence. Both sequences used a balanced SSFP readout (TR/TE=2.5ms/1.2ms, flip angle=35°, FOV=360×306mm^2, voxel size=2.2×2.5mm^2, slice thickness=8mm, bandwidth=1085Hz, GRAPPA acceleration factor=2, partial Fourier=0.87, MOLLI scheme: 5-(3)-3). Native T1 measurements and reproducibility (absolute difference between the two scan repetitions) were evaluated. Both metrics were calculated for each of the 16 AHA myocardial segments as well as over all myocardial segments. The feasibility of FB MOLLI was demonstrated in 3 patients referred to CMR for assessment of cardiomyopathy.

Results: Figure 1 shows example native T1 maps acquired in one healthy volunteer using both techniques. Overall subjects, native T1 times were 995±24ms using FB MOLLI and 974±16ms using BH MOLLI (p=0.01). T1 reproducibility over all myocardium was 8±8ms (FB MOLLI) vs. 8±7ms (BH MOLLI), p=0.46. T1 reproducibility per myocardial segment was 23±8ms (FB MOLLI) 18±6ms (BH MOLLI), p=0.22. Example native T1 maps obtained in one patient are shown in Figure 3. Both techniques provided similar image quality.

Conclusions: The proposed FB MOLLI sequence provides similar reproducibility to the conventional BH MOLLI sequence and may represent a valuable alternative in patients unable to hold their breath.

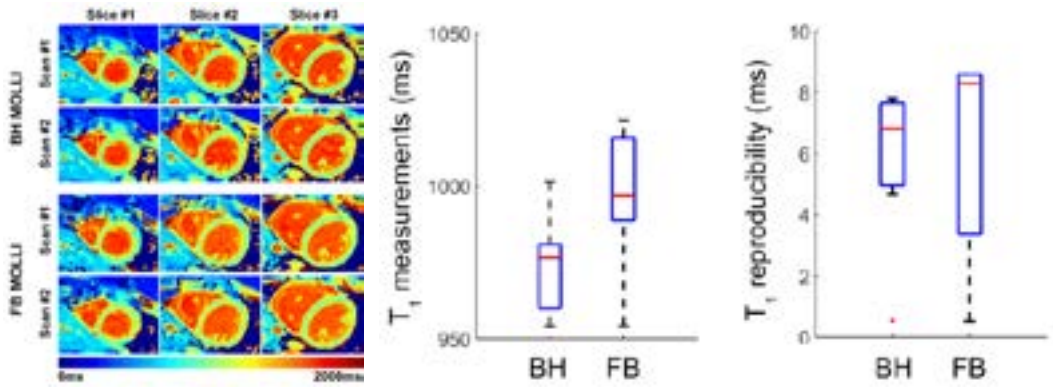

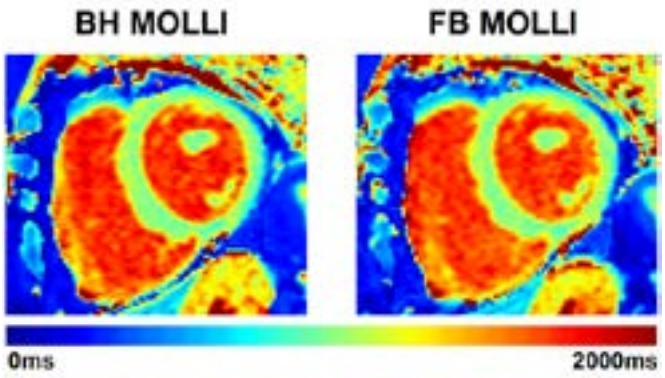

P203

Single Point Technique SMART1Map on 1.5T CMR: Initial Single Centre Experience of Normative Reference Values and Measurement Technique

Jeanette Soon, MBBS (Hons) FRANZCR[1]Shaw Hua (Anthony) Kueh, MBChB, FRACP[2], Chesnal Dey Arepalli, MD[2], Chaitu Cheruvu, MBBS FRACP[3], Christopher Naoum, MBBS PhD[4], Nada Sulaiman, M.D.[5], Rominder S. Grover, MBBS (Hons) FRACP[6], John Mooney, MBBS[6], Stephanie Sellers[7], Cameron Hague, MD[2], Jen Ellis, MD[6], Philipp Blanke, MD[8], Jonathon Leipsic, MD[6], Darra T. Murphy, MD[6]

1. *St Paul's Hospital, Vancouver, ON, Canada*
2. *St Paul's Hospital, Vancouver, BC, Canada*
3. *St Paul's Hospital, Botany, New South Wales, Australia*
4. *Concord Hospital, The University of Sydney, Sydney, Concord, Sydney, New South Wales, Australia*
5. *St.. Paul's Hospital, Al Madinah, Saudi Arabia*
6. *St Paul's Hospital, BC, Canada*
7. *University of British Columbia, BC, Canada*
8. *St. Paul's Hospital & University of British Columbia, Vancouver, BC, Canada*

Background: Non-invasive detection of diffuse myocardial fibrotic or infiltrative conditions by T1 mapping has implications for diagnosis, treatment, and prognostication of non-ischemic cardiomyopathies. SMART$_1$Map (Saturation Method using Adaptive Recovery Times for cardiac T1 Mapping) is a new method of measuring true T1 relaxation values. We determine native T1 values in healthy myocardium and compare two measurement methods in order to determine that which is least susceptible to measurement variation.

Methods: Twenty-four healthy volunteers consented to undergo non-contrast, single shot equatorial short axis slice T1 mapping at 1.5 Tesla (T) MRI (Signa Twin Speed, GE Healthcare). Five were excluded due to motion artefact. For each control, T1 values were measured twice on a short axis oblique map; firstly with 7 independent regions of interest (ROI's), minimum area 0. 5cm^2 in the mid LV myocardium in the mesomyocardial anterior, anteroseptal, mid septal, inferoseptal, inferior, inferolateral and anterolateral segments; secondly, with a single continuous circumference entailing all mesomyocardial segments (Figure 1). To confirm normative values, standard left and right ventricular volumetric measurements were performed. Baseline characteristics were recorded immediately prior to scanning.

Results: Nineteen healthy volunteers (11 male, 36.9 years ± 10.7) with BMI 21.7 ± 8.0kg/m2 had imaging quality suitable for evaluation. Mean heart rate and blood pressure (SBP/DBP) were 65 ± 9bpm and 120/69 ± 10/8 mmHg. LVEDVI and RVEDVI were 73.3 ± 13.9 ml/m2 and 75.1 ± 14.2 ml/m2 respectively, LV ejection fraction 59 ± 6 %. Mean native T1 values (ms) at 1.5T were as follows: anterior segment 1158.9 ± 159.6, anteroseptum 1208.5 ± 94.3, mid septum 1225.2 ± 95.5, inferoseptum 1223.2 ± 113.6, inferior 1270.7 ± 159.5, inferolateral 1254.8 ± 123.6, and anterolateral 1178.4 ± 123. Measurements in the anteroseptum and the single continuous measurement (1222.82 ± 88.2ms) yielded the least variation as determined by SD. Other segments yielded increasing T1 variance (mid septum < inferoseptum < anterolateral < inferolateral < inferior < anterior) (Figure 2).

Conclusions: We provide T1 values acquired in a healthy population using a novel method of measuring true T1 (SMART$_1$Map), which uses a single point approach as opposed to an estimated T1* deduced from curve fitting. Using this method, anteroseptal ROI and continuous mesomyocardial all segment measurement showed the least variation. Values may help to serve as reference for the future evaluation of suspected diffuse myocardial fibrosis in undifferentiated non-ischemic cardiomyopathy.

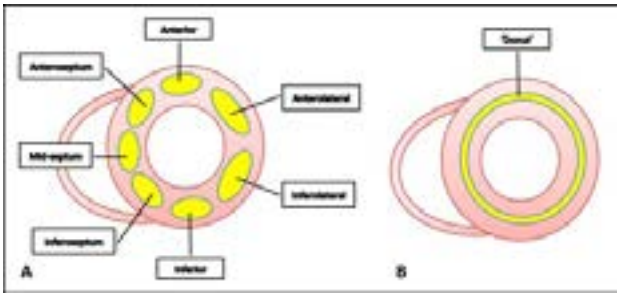

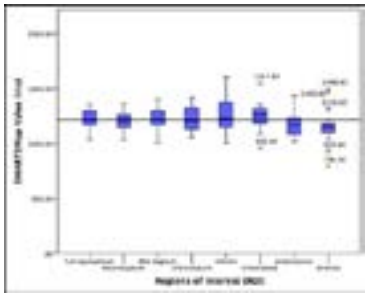

P204

Cardiovascular Magnetic Resonance Myocardial Feature Tracking using a Novel Non-Rigid, Elastic Image Registration Algorithm. Assessment of Reproducibility in a Real Clinical Setting.

Jan Bogaert, MD, PhD[4] Alberto Marchi, MD[1], Pedro Morais, MSc[2], Tom Dresselaers, PhD[3], Brecht Heyde, PhD[1], Jan D'hooge, PhD[1]

1. *UZ Leuven - KU Leuven, Vlaams-Brabant, Belgium*
2. *Lab on Cardiovascular Imaging & Dynamics, Department of Cardiovascular Sciences, KULeuven - University of Leuven, Leuven, Belgium, Vlaams-Brabant, Belgium*
3. *Radiology, Dept. of Imaging and Pathology, University Hospitals Leuven, Belgium, Vlaams-Brabant, Belgium*
4. *UZ Leuven - KU Leuven, Leuven, Vlaams-Brabant, Belgium*

Background: Cardiovascular magnetic resonance myocardial feature tracking imaging (CMR-FTI) is a promising technique for quantification of myocardial strain from routinely acquired cine steady-state free precession (SSFP) images. We sought to determine the reproducibility of CMR-FTI of a novel non-rigid, elastic registration algorithm (Segment, Medviso) in a real clinical setting.

Methods: Firstly, we studied the reproducibility in one healthy volunteer who underwent 10 CMR studies over a period of five consecutive days. Secondly, we selected from our database 10 patients yielding normal CMR findings (normal group). Finally, we prospectively studied 10 patients with known or suspected ischemic and non-ischemic myocardial pathology referred for further investigation to CMR (patient group). In the patient group a second study was performed respecting an interval of 30 minutes between studies. In all subjects left ventricular (LV) circumferential and radial strain were calculated in short-axis direction (Ecc_{SAX} and $Err_{SAX,}$ respectively) and longitudinal strain in long-axis direction (Ell_{LAX}). The level of CMR experience of the observers was 6 months and >20 years.

Results: Mean contouring time was 7±1 min, mean FTI calculation time 13±2 min. Manual contour correction was needed in less than 5% of subjects. Overall, moderate to excellent reproducibility was obtained for radial, circumferential and longitudinal strains, largely independent whether subjects presented myocardial pathology or not at CMR. Reproducibility was better for global strain than segmental strain assessment. Inter-study variability contributed the most to the overall variability. Conversely, intra-observer variability was excellent with a coefficient of variation (CV) ranging 3.7% to 6.3%, and an intraclass correlation coefficient (ICC) ranging 0.885 (0.733-0.953) for Ell_{LAX} (healthy volunteer) to 0.998 (0.996-0.999) for Err_{SAX} (patient group) for global strain calculation. The level of CMR experience did not impact inter-observer nor inter-study variability. In short-axis direction, Ecc_{SAX} and Err_{SAX} variability was higher in the basal and apical segments compared to the mid segments. Myocardial strain correlated well with global LVEF ranging R=0.70 for Ell_{LAX} to R=0.86 for Err_{SAX}.

Conclusions: CMR-FTI using a novel non-rigid, elastic registration algorithm is a robust approach for myocardial strain analysis in patients routinely scheduled for CMR, and is not influenced by the level of training (basic training versus expert reader). In contrast to CMR-FTI algorithms using optical flow technology, reproducibility of radial strain seems superior with an elastic algorithm. However, similar to previous reports, further improvement is needed to reliably assess segmental strain in particular for repeated studies, and regionally towards the base and apex in short-axis direction.

Reproducibility in the patient group

inter-study	**inter-observer**	**intra-observer**	patient group
			Bias
-2.25	0.26	-0.23	ErrSAX
-0.31	0.51	-0.16	EccSAX
0.04	0.71	0.34	EllLAX
			CV (%)
23.68	8.57	4.08	ErrSAX
27.11	3.02	4.74	EccSAX
12.31	7.93	6.27	EllLAX
			ICC(95%)
0.911(0.850-0.945)	0.973(0.979-0.985)	0.998(0.996-0.999)	ErrSAX
0.832(0.753-0.887)	0.988(0.963-0.994)	0.994(0.991-0.996)	EccSAX
0.949(0.868-0980)	0.965(0.854-0.989)	0.982(0.951-0.993)	EllLAX

P205

Push-Button Solution for Fully Self-Gated Functional and Anatomical 3D Assessment of the Heart: Preliminary Results

Matthias Stuber, PhD[5] Jerome Yerly, PhD[1], Davide Piccini, PhD[2], Lorenzo Di Sopra, MSc[3], Jessica A.M. Bastiaansen, PhD[4]

1. *CIBM / CHUV / UNIL, Fribourg, Switzerland*
2. *Advanced Clinical Imaging Technology, Siemens Healthcare, Vaud, Switzerland*
3. *CIBM / CHUV / UNIL, Lausanne, Vaud, Switzerland*
4. *Department of Radiology, University Hospital (CHUV) and University of Lausanne (UNIL), Lausanne, Vaud, Switzerland*
5. *CHUV, University of Lausanne, Geneve, Switzerland*

Background: Recent advances in cardiac MR imaging, which make use of modern acquisition [1] and reconstruction schemes [2,3], have the potential to challenge existing paradigms by enabling simultaneous functional and anatomical 3D assessment of the whole-heart in one scan. However, current solutions still mandate the use of contrast agents for image contrast [4], ECG to synchronize the acquisition [2], or the use of sub-optimal fat suppression which interrupts steady-state magnetization and results in extended scan time [1,2] and inefficiency of data collection. To address these limitations, we present a "push-button" solution, which synergistically combines advanced acquisition and reconstruction techniques.

Methods: This preliminary study was performed on a 1.5T clinical MRI scanner (MAGNETOM Aera, Siemens Healthcare) using a prototype free-running non-ECG-triggered 3D golden angle radial bSSFP sequence (Fig 1a) in N=3 healthy volunteers. Data were continuously acquired during free breathing over a large number of cardiac cycles. To fully preserve the steady-state magnetization and minimize eddy currents, the sequence combined a novel 3D radial Rosetta sampling pattern (Fig 1b) with a 1-1 180 binomial water excitation radiofrequency (RF) pulse for fat suppression. The sequence parameters are shown in Table 1. Self-gated cardiac and respiratory signals were extracted from the modulations of the k-space center amplitude (Fig 1c) by selecting frequency ranges of 0.7-1.5Hz and 0.1-0.5Hz, respectively (Fig 1d). The signals were then used to sort the readouts into 6 different respiratory states and cardiac phases of 50 ms window width (Fig 1e). The resulting 5D (x-y-z-cardiac-respiratory dimensions) undersampled datasets were reconstructed using a sparse SENSE algorithm (2), which exploited sparsity along both cardiac and respiratory dimensions, and standard gridding. The temporal accuracy of the self-gated cardiac signal was assessed by comparing the self-gated trigger intervals with the RR intervals of the ECG.

Results: Cardiac and respiratory self-gating signals were automatically extracted in all volunteers and successfully used to reconstruct cardiac and respiratory motion-resolved whole heart 3D images. The durations of each cardiac cycle measured from the self-gated cardiac signals were very accurate with respect to the reference ECG signals (recorded for reference) and only deviated by 30.2±14.1ms. The fully self-gated framework yielded good depiction of the coronary arteries (Fig 2) despite a significant dilution of the data consistent with 6 respiratory and 28 cardiac phases.

Conclusions: The proposed framework enables a fully self-gated free-breathing functional and anatomical 3D assessment of the heart with minimal operator-interaction. Only one single acquisition is needed. Neither contrast enhancement nor external synchronization devices are required. Validation of this framework on a larger volunteer and patient population is currently ongoing.

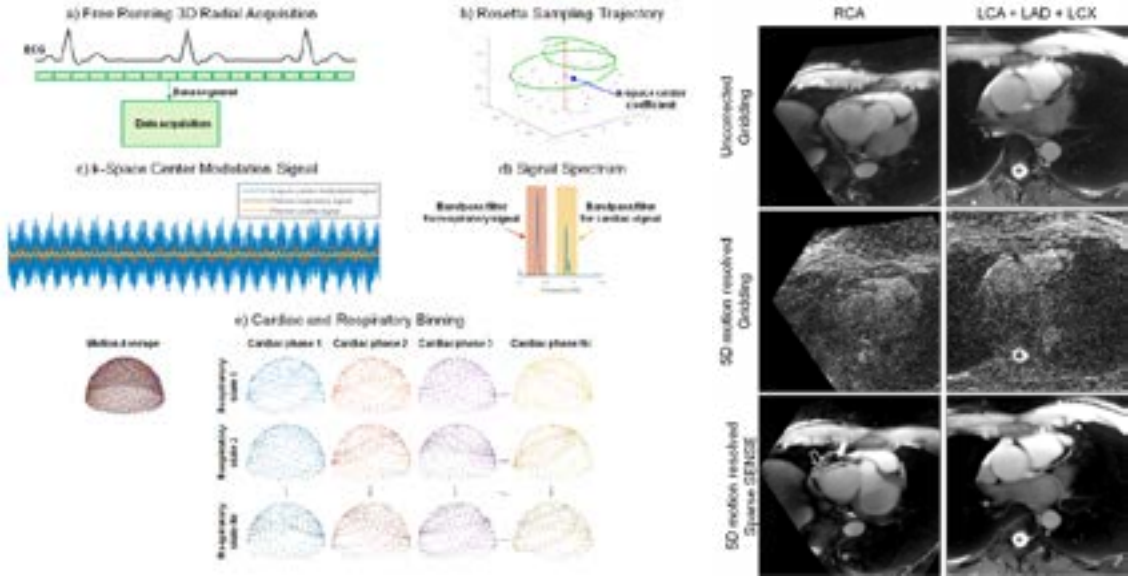

ACKNOWLEDGEMENTS: The authors would like to acknowledge Dr. Florian Knoll from NYU School of Medicine for support with the GPU implementation of the 3D NUFFT. This work was supported by the Swiss National Science Foundation grants 320030_143923 and 326030_150828.

Table 1: MR sequence parameters

Value	Parameter
2.7/5.5 ms	TE/TR
220 mm^3	FOV
192x192x192	Matrix
1.15 mm^3	Voxel size
126582	Radial views
60°	RF angle
11.5 min	scan time
1130 Hz/Px	Pixel BW

P206

Can quantitative tissue-tracking cardiac magnetic resonance (CMR) of left-ventricular deformation be used to diagnose cardiac amyloidosis?

Lu Lin, M.D.[1] Yining Wang, M.D.[2], Shu Jiang[2], Jian Cao, M.D.[2], Xiao Li, M.D.[2], Jing An, M.D., Ph.D[3], Andreas Greiser, Ph.D[4]

1. *Peking Union Medical Collge Hospital, Beijing, Beijing, China (People's Republic)*
2. *Peking Union Medical College Hospital, Beijing, China (People's Republic)*
3. *MR Collaborations NE Asia, Siemens Healthcare, Beijing, China, Beijing, China (People's Republic)*
4. *Siemens Healthcare GmbH, Erlangen, Germany, Erlangen, Bayern, Germany*

Background: Tissue-tracking (TT) technique has recently emerged as a method to quantify myocardial strain by analyzing standard cine MR images. The purpose of this study was to assess the feasibility of using myocardial TT to diagnose cardiac amyloidosis (AL).

Methods: In this IRB-approved retrospective case-control study, 39 patients with AL and 16 healthy controls were included. Patients with AL were confirmed histologically and had clinical symptoms of cardiac involvement. Healthy controls had neither clinical evidence of infiltrative cardiomyopathy nor CMR myocardial LGE. All participants underwent a 3T (Magnetom Skyra, Siemens Healthcare, Erlangen, Germany) CMR examination. Feature-tracking analysis was applied to the cine CMR images to assess peak global strain in longitudinal, circumferential and radial direction of the left ventricle (LV) by using CVI42 software (version 5.3, Circle Cardiovascular Imaging, Canada). Differences in strain were compared between AL and healthy controls. Receiver-operating characteristic (ROC) analysis was performed, and the area under the ROC curve (AUC) was calculated. Sensitivity (Se), specificity (Sp), positive predictive value (PPV), negative predictive value (NPV) and accuracy were calculated by using the cut-off value corresponding to the highest AUC.

Results: There were significant differences in global longitudinal (GLS) and radial strain (GRS), while there was no difference in global circumferential strain between AL and healthy controls. Compared to healthy controls AL had decreased GLS (-0.11±0.08 vs -0.18±0.04, *P*) and GRS (0.19±0.13 vs 0.33±0.10 , *P* (Se=65.1%, Sp=81.2%, PPV=90.3%, NPV=46.4%, Accuracy=73%).

Conclusions: TT measurement of global longitudinal strain could be used to identify AL from the healthy controls although diagnosis performance was slightly compromised.

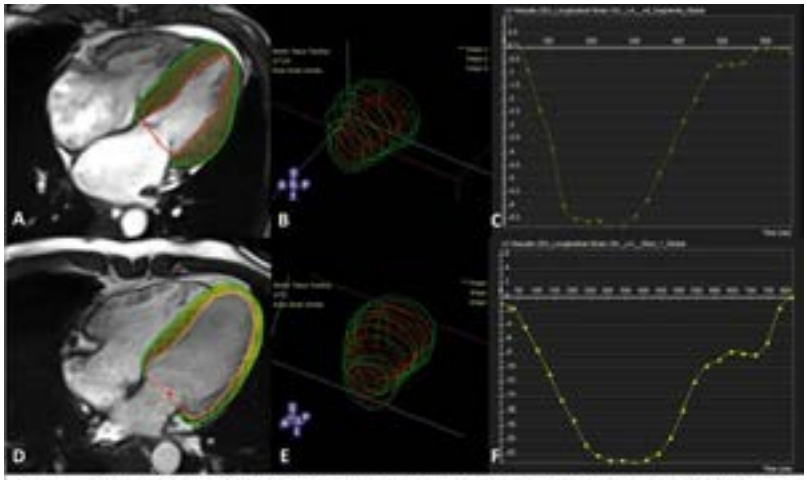

Figure. Demonstrating CMR end diastolic cine, tissue tracking imaging and longitudinal strain curve of AL (A-C) and healthy control (D-F) respectively.

P207

The impact of age and gender on right ventricle myocardial systolic strain evaluated by Tissue-Tracking cardiac magnetic resonance

Alessandra Scatteia, MD[1]Anna Baritussio, MD[2], Estefania De Garate, MD[2], Amardeep Ghosh Dastidar, MBBS(Hons), MRCP[2], Alicia Maceira, MD,PhD[3], Dudley J. Pennell, MD[4], Chiara Bucciarelli-Ducci, MD, PhD[2]

1. *Division of Cardiology, Ospedale Medico-Chirurgico Accreditato Villa dei Fiori, Acerra, Naples, Italy. Cardiac Magnetic Resonance Unit, NIHR Bristol Cardiovascular Biomedical Research Unit, Bristol Heart Institute, Bristol UK, Naples, Campania, Italy*
2. *NIHR Bristol Cardiovascular Biomedical Research Unit, Bristol, England, United Kingdom*
3. *Coordinadora, Unidad de Imagen Cardíaca - ERESA Centro Médico Unidad de Resonancia Magnética. Hospital Arnau de Vilanova, Comunidad Valenciana, Spain*
4. *Royal Brompton Hospital and Imperial College, London, England, United Kingdom*

Background: The assessment of right ventricular (RV) systolic function carries implications for patient diagnosis, prognosis, and treatment; however, the complex geometry of the RV makes this task difficult in daily clinical practice. Cardiac magnetic resonance (CMR) is the gold standard for the volumetric and functional assessment of the RV, and the recently developed RV-Tissue-tracking software estimates RV myocardial strain in the 3 deformational directions using cine CMR images, allowing early detection of RV dysfunction. However, before the technique can be used clinically, it is important to provide normal RV strain values. Therefore, aim of the study was to define normal RV myocardial strain values in a cohort of healthy volunteers using RV-Tissue-tracking CMR.

Methods: 94 healthy volunteers were recruited (20-80 years, 51 men). CMR at 1.5T was performed. Tissue-tracking software (CVI42, Circle Cardiovascular Imaging Inc.) estimated RV global longitudinal strain from two long-axis steady-state free precession (SSFP) cines and mid-circumferential and radial strain from short-axis SSFP cines (Fig.1). The entire cohort was analyzed by two independent observers. Inter-observer variability was determined by intra-class correlation coefficient (ICC). Statistical analysis was made using independent sample T test, one-way ANOVA, Pearson's correlation and multiple linear regression, as appropriate (p

Results: In gender subgroup analysis, there were no significant gender differences for all the right ventricular strain parameters: longitudinal (-23.4±5% vs -21.9±4%, P=0.731) circumferential (-9.89±4% vs -10.8±3%, P=0.924) and radial (18.2±7% vs 20.3±7%, P=0.81) strain. However, a trend toward greater radial and circumferential strain values in men was observed. Age correlated positively with radial (R=0.266, P=0.015) and longitudinal (R=-0.214, P=0.040) but not circumferential strain (R=0.193, P=0.07) **(Table 1)**. RV EF correlated positively with radial (R=0.463, P < 0.0001) and circumferential (R=-0.401 P < 0.001) strains. However, in multiple linear regression, with all strain parameters as covariates, only radial strain demonstrated a significant relationship with RV EF. Each percentage-point increase in radial strain resulted in a 0.6 percentage-point increase in EF (standardized β-coefficient: 0.645, P=0.020). Reproducibility analyses showed a poor reproducibility (ICC < 0.7) for all three right ventricular strain parameters.

Conclusions: We showed that RV myocardial strain in the three directions does not differ between genders. Age regresses positively with radial and longitudinal deformation while radial strain is the largest determinant of RV EF. Our gender- and age- specific normal values will help the use of RV tissue-tracking in daily clinical practice; however, the poor reproducibility underlines the need for semi-automated software which can help the assessment of the RV strain.

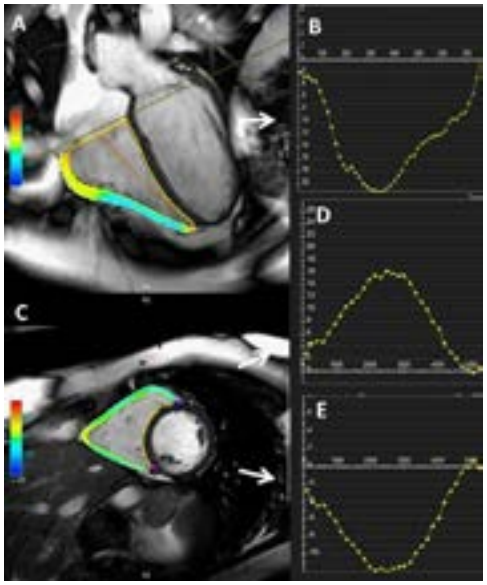

	All subject N= 94	Male N=51	Female N=43	Age 20-39 N= 28	Age 40-59 N=35	Age 60-80 N=31
Systolic BP (mmHg)	122 ± 12	126 ± 9	119 ± 14	124 ± 8	118 ± 11	127 ± 13
Diastolic BP (mmHg)	73 ± 7	70 ± 8	75 ± 6	75 ± 6	71 ± 8	75 ± 7
Heart rate (beats / min)	66 ± 8	65 ± 9	66 ± 8	67 ± 9	65 ± 8	65 ± 8
BMI (kg/m²)	24 ± 4	24 ± 4	24 ± 4	23 ± 3	25 ± 4	24 ±4
RV Ejection fraction (%)	58 ± 5	59 ± 5	58 ± 5	56 ± 6	57 ± 5	61 ± 4
RV longitudinal strain (%)	-22 ± 4	-21 ± 4	-23 ± 5	-21 ± 4	-22 ± 5	-23 ± 5
RV radial strain (%)	19 ± 7	20 ± 7	18 ± 7	17 ± 6	18 ± 6	21 ± 9
RV circumferential strain (%)	-10 ± 4	-10 ± 4	-9 ± 4	-9 ± 3	-10 ± 3	-10 ± 4

P208

Comparison of cardiovascular magnetic resonance feature tracking with harmonic phase for the assessment of left ventricular strain in patients post myocardial infarction

Henrique T. Moreira, MD, PhD[1] Gustavo J. Volpe, MD, PhD[2], Bharath Ambale-Venkatesh, PhD[3], Giovani L. De Santi, MD, PhD[4], Lourenço Gallo, Jr., MD, PhD[2], Joao A.C. Lima, MD, MBA[5], André Schmidt, MD, PhD[2]

1. University of São Paulo, Ribeirao Preto, Sp, N/A, Brazil

2. University of São Paulo, Medical School of Ribeirão Preto, N/A, Brazil

3. Johns Hopkins University, MD

4. University of São Paulo, Medical School of Ribeirão Preto, Sao Paulo, Brazil

5. Johns Hopkins University, Baltimore, MD

Background: Myocardial strain is a sensible measure of regional ventricular function. Harmonic phase method has been widely used to quantify myocardial deformation using cardiovascular magnetic resonance (CMR) tagged images. Recently, a novel technique based on feature tracking CMR has allowed the assessment of myocardial strain from cine CMR non-tagged images. However, agreement between both techniques is not well established, especially in specific clinical settings. So, we aimed to compare feature tracking and harmonic phase methods for the assessment of left ventricular circumferential strain in individuals post myocardial infarction.

Methods: This cross-sectional study consecutively enrolled 15 patients post ST-segment elevation myocardial infarction of the anterior wall. All participants underwent CMR imaging acquired with a 1.5T commercial scanner (Magnetom Vision, Siemens, Germany), with 25 mT/m maximum gradient strength, circular polarized coil, and EKG-triggered. Harmonic phase method was applied to balanced fast gradient echo sequence with spatial modulation of magnetization (SPAMM) superimposed as grid images (tagging), using HARP software (commercial v.3.0, Diagnosoft, CA). Feature tracking was applied to cines obtained by steady state free precession pulse sequence, using Multimodality Tissue Tracking software (MTT v.6, Toshiba, Japan). Left ventricular deformation was evaluated by circumferential strain, defined as the average of peak systolic strain measured at basal, mid and apical short-axis slices. Continuous data are presented as mean ± standard deviation. Agreement between measurements of circumferential strain obtained from feature tracking and harmonic phase techniques was evaluated by concordance correlation coefficient and Bland-Altman plot.

Results: Mean age of the participants was 56 ± 7 years, 80% males. All patients underwent cardiac catheterization, with normal flow (TIMI III) after reperfusion therapy. Mean left ventricular ejection fraction was 46 ± 11%. Mean circumferential strain measured by MTT and HARP were -13.4% and -12.6% respectively. Concordance correlation coefficient for circumferential strain measured by MTT and HARP was 0.76. According to Bland-Altman analysis, mean difference of circumferential strain obtained by MTT and HARP was -0.8%, with 95% limits of agreement of -5.3% and 3.7% (figure 1).

Conclusions: In patients post anterior wall myocardial infarction,left ventricular circumferential strain measured by CMR feature tracking presented a good concordance with measurements obtained with harmonic phase, demonstrating a small trend towards more negative circumferential strain values, but a narrow and clinically acceptable limits of agreement.

http://www.ConferenceAbstracts.com/uploads/cfp2/attachments/LDFAIBDN/LDFAIBDN--219777-1-ANY.pdf

P209

Assessment of right atrioventricular junction (RAVJ) motion using radially rotational long-axis CMR

Liang Zhong, Ph.D.[3]Shuang Leng, Ph.D.[1], Shuo Zhang, Ph.D.[2], Xiaodan Zhao, Ph.D.[1], Yi-Hui Hung, BSc[1], Alicia Ting Er, BSc[1], Elizabeth Pee Chong Goh, BSc[1], Ru San Tan, M.D.[3]

1. *National Heart Centre Singapore, N/A, Singapore*
2. *Philips Healthcare, Singapore, N/A, Singapore*
3. *National Heart Centre Singapore; Duke-NUS Medical School, Singapore, N/A, Singapore*

Background: Atrioventricular valves are complex anatomical structures, which play an important role in the cardiac function and indicate underlying mechanism of different pathophysiological conditions. However, its 3D morphology and dynamics, particularly in the right heart including the tricuspid valve annulus (TVA), has been less extensively studied. Here, we developed a semi-automatic feature-tracking technique and applied it to 18 radially rotational long-axis cine cardiovascular magnetic resonance (CMR) planes for dynamic assessment of right atrioventricular junction (RAVJ) deformation.

Methods: Six healthy subjects (46±22 yr) underwent CMR scan on a 3T system (Philips Ingenia). Based on the standard survey images, 18 radial slices were acquired with 10° angular equidistance in the right ventricular (RV) long axis, defined from the apex to the centre of the TVA orifice (**Fig. 1(a)**). Typical imaging parameters were: field of view 300 x 300 mm^2, voxel size 1.04 x 1.04 x 8.00 mm^3, 40 frames/cardiac cycle, SENSE factor 2, breath-hold time 7s. An in-house developed program [1, 2] was applied to semi-automatically track the RAVJ motion throughout the cardiac cycle in each of the 18 planes (**Fig. 1(b)**). Four clinically useful data were extracted: Sm, peak systolic velocity; Em, peak early diastolic velocity; Am, peak late diastolic velocity; and TAPSE, tricuspid annular plane systolic excursion. The CMR-based motion parameters were averaged over all, and every two, three and four RAVJ points. In addition, RV 2-, 3-, and 4-chamber CMR long-axis views (**Fig. 2(a)**) were used to generate results based on an average of 6 RAVJ points.

Results: Figure 1(c-d) showed the RAVJ velocity and displacement distribution map with respect to cardiac cycle time and TVA region for a 53-yr-old male healthy volunteer. **Figure 2(b-c)** showed the velocity and displacement curves in RV 2-, 3-, and 4-chamber CMR views. The extracted 6-point mean Sm, Em, Am and TAPSE were 7.8, 8.2, 9.6 cm/s and 14.9 mm, respectively. **Table 1** compared the mean motion parameters based on different number of RAVJ points. It was well demonstrated that, first, RAVJ motion parameters derived from all radially rotational CMR reflected the regional function of TVA. Second, averaged result from RV 2-, 3-, and 4-chamber views was in good agreement to the global values from all 36 RAVJ points.

Conclusions: Regional RAVJ motion parameters were derived by post-processing multiple radially rotational long-axis CMR. RV 2-, 3-, and 4-chamber views were reliable enough for global assessment of RAVJ deformation.

References:

1. Leng S, et al. Am J Physiol Heart Circ Physiol 2015.
2. Leng S, et al. Ann Biomed Eng 2016.

http://www.ConferenceAbstracts.com/uploads/cfp2/attachments/LDFAIBDN/LDFAIBDN--220870-1-ANY(1).pdf

http://www.ConferenceAbstracts.com/uploads/cfp2/attachments/LDFAIBDN/LDFAIBDN--220870-2-ANY(1).pdf

Table 1: Averaged peak RAVJ motion parameters over all subjects with different number of radial long-axis cine CMR planes.

P Value**	RV 2-, 3-, and 4-chambers* (6 Points)	Every 4 (9 Points)	Every 3 (12 Points)	Every 2 (18 Points)	All (36 Points)	CMR-derived RAVJ motion parameters
0.905	9.8 ± 2.8	9.9 ± 2.7	9.8 ± 2.8	9.8 ± 2.8	9.9 ± 2.9	Sm, cm/s
0.740	9.8 ± 3.9	9.8 ± 3.8	9.9 ± 3.8	10.0 ± 3.8	10.0 ± 3.9	Em, cm/s
0.967	11.5 ± 4.9	11.7 ± 4.7	11.5 ± 4.8	11.7 ± 4.8	11.5 ± 4.8	Am, cm/s
0.846	19.1 ± 6.4	19.3 ± 6.4	19.2 ± 6.1	19.3 ± 6.4	19.3 ± 6.3	TAPSE, mm
0.998	96.4 ± 52.7	95.4 ± 50.0	96.7 ± 51.1	97.6 ± 51.7	96.4 ± 51.4	Time to Sm, ms
0.909	457.9 ± 29.8	458.1 ± 29.0	455.6 ± 30.8	456.7 ± 32.3	458.5 ± 32.0	Time to Em, ms
0.906	737.5 ± 67.7	737.9 ± 66.1	737.3 ± 64.9	738.1 ± 65.3	738.9 ± 65.4	Time to Am, ms
1.000	361.4 ± 33.3	360.2 ± 33.7	363.6 ± 34.3	363.3 ± 35.7	361.4 ± 35.3	Time to TAPSE, ms

*6 RAVJ points were selected from RV two-, three-, and four-chamber long-axis CMR planes. **between 6-point and 36-point based results. Sm: peak systolic velocity; Em: peak early diastolic velocity; Am: peak late diastolic velocity; TAPSE: tricuspid annular plane systolic excursion.

P210

A Novel MRI Technique to Quantify Diffuse Interstitial Fibrosis in the Right Ventricle

Stanley Swat, MD[1] Brandon C. Benefield, MS[2], Emily J. Li, BA[3], Daniel C. Lee, MD, MSc[4], Jeremy Collins, MD[5], Benjamin H. Freed, MD[2]

1. *Northwestern Memorial Hospital, Northwestern University Feinberg School of Medicine, IL*
2. *Northwestern University Feinberg School of Medicine, Chicago, IL*
3. *Northwestern University, IL*
4. *Northwestern University, Feinberg School of Medicine, Chicago, IL*
5. *Northwestern University, Chicago, IL*

Background: Cardiovascular magnetic resonance-derived T1-mapping enables non-invasive quantification of myocardial fibrosis in the left ventricle (LV) but attempts to quantify right ventricular (RV) fibrosis have been challenging due to spatial resolution limitations of the thin-walled RV. The objective of this study is to histologically validate a novel MR technique, high resolution modified look-locker inversion recovery (HR-MOLLI), for quantification of fibrosis in the right ventricle.

Methods: Two dogs underwent rapid RV pacing for 4 weeks to produce congestive heart failure (CHF) and RV diffuse interstitial fibrosis. Two sham-operated dogs served as controls. T1 mapping was performed 1 day after pacing on 1.5T (MAGENTOM Aera) using an investigational HR-MOLLI technique with a 1x1 mm2 in-plane resolution that applies motion correction with synthetic image estimation (Figure 1). Motion corrected images were used to generate parametric maps with (T1) and without (T1*) the MOLLI correction. The MOLLI sequence uses a 5 heart-beat (HB) acquisition, 3 HB recovery, 3 HB acquisition scheme with a single shot bSSFP diastolic readout. Images were acquired pre- and 10-25 minutes post- 0.2 mmol/kg gadobenate dimeglumine bolus infusion (Multihance, Bracco Diagnostics, Monroe, NJ). T1 and T1* parametric maps were used to quantify the T1 of tissue and blood, respectively. A reviewer blinded to pathologic data quantified basal and mid RV free wall, interventricular septal, and lateral LV wall T1 values on T1 parametric maps. Extracellular volume (ECV) was calculated as originally described by Jerosch-Harold. Tissue samples from corresponding regions of the LV and RV were stained with Masson's Trichome and the collagen volume fraction (CVF) was calculated by reviewer blinded to MRI data. Multilevel linear regression was used to evaluate the relationship between ECV and CVF. Student's t-test was used to compare RV and LV ECV.

Results: Multilevel linear regression analysis showed a significant relationship between HR-MOLLI derived ECV and CVF with a likelihood ratio of 3.86 (p=0.02) (Figure 2). RV ECV was significantly increased in CHF dogs compared to control dogs (28.2% vs. 23.6%, p=0.05). LV ECV did not significantly increase (23.5% vs. 23.3%, p=0.92). There was a significant difference between RV and LV ECV in CHF dogs (28.2% vs. 23.5%, p= 0.02).

Conclusions: HR-MOLLI is able to accurately detect diffuse LV and RV interstitial fibrosis in dogs with and without heart failure. The heart failure model used in this study induces significantly more RV fibrosis than LV fibrosis compared to controls. Based on these initial results, HR-MOLLI may be a novel non-invasive technique for evaluating the degree of RV diffuse interstitial fibrosis in patients with pulmonary hypertension or CHF.

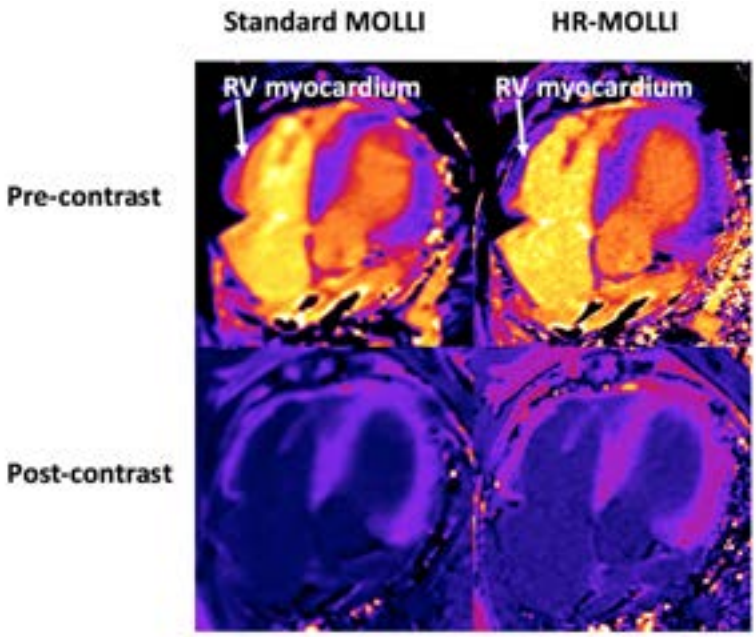

http://www.ConferenceAbstracts.com/uploads/cfp2/attachments/LDFAIBDN/LDFAIBDN--222418-2-ANY.pdf

P211

Fully automated online compressive recovery for real-time, free-breathing cine

Yingmin Liu, Ph.D.[1], Rizwan Ahmad, PhD[4], Samuel T. Ting, Ph.D.[2], Ning Jin, Ph.D.[3], Orlando Simonetti, PhD[4]

1. The Ohio State University, Columbus, OH
2. Genetesis, LLC., OH
3. Siemens Medical Solutions USA, Inc., OH
4. The Ohio State University, OH

Background: Compressive sensing-inspired recovery methods enable imaging from highly undersampled data, leading to improved spatial and temporal resolutions. However, such methods are computationally intensive and require selecting parameter values, e.g., regularization weights, which impact the image quality. We recently proposed a method called sparsity adaptive compressive recovery (SCoRe) that employs multiple sparse representations to expose and utilize rich data structure that is not fully exploited by a single orthogonal sparsifying transform [1]. More importantly, SCoRe provides a data driven tuning of regularization weights for each sparse representation. In this study, we apply SCoRe to real-time, free-breathing cine.

Methods: Eight healthy volunteers were imaged on a 1.5T scanner. A short-axis stack was acquired twice: once using segmented acquisition under breath-held conditions and once using real-time (RT) acquisition under free-breathing conditions. For RT, the data were collected with prospective downsampling using VISTA (R = 8-10) [2] and processed with SCoRe. The reconstruction was performed online using Gadgetron-based GPU computation with bFISTA, an optimization routine that we recently proposed [3]. For SCoRe, sub-bands of redundant wavelet transform were used as independent sparsifying transforms. All RT images possessed a spatial resolution of 2.5 mm or better and a temporal resolution of 45 ms or better. The overall quality of RT images was evaluated by an expert on the scale of 1 to 5 (1: non-diagnostic, 2: poor, 3: acceptable, 4: good, 5: excellent). The EDV, ESV and SV computed from RT images were compared to that of standard segmented acquisition.

Results: Figure 1 shows an example where SCoRe reconstruction is compared against standard segmented acquisition. All RT images reconstructed with SCoRe received a score of 3 or higher for all eight volunteers. For EDV, ESV and SV, a strong agreement was found between the standard and proposed imaging protocols; see Figure 2. The average reconstruction time for SCoRe was 8.4 s per slice.

Conclusions: There are two major limitations associated with compressive sensing-based image recovery methods: long computation times and a need to manually tune parameters. The proposed method, SCoRe, and its GPU-based implementation overcome these limitations, enabling highly accelerated imaging that is both data adaptive and computationally fast. The results of this preliminary study show that SCoRe provides a viable avenue to promote free-breathing cine in clinical settings. Future validation studies will include a larger sample size and multiple CMR applications.

References:

[1] Ahmad et al. TCI IEEE (2015), 1(4) p220-235.

[2] Ahmad et al. MRM (2015), 74(5) p1266-1278.

[3] Ting et al. MRM (2016), in press.

http://www.ConferenceAbstracts.com/uploads/cfp2/attachments/LDFAIBDN/LDFAIBDN--222761-1-ANY(2).pdf

http://www.ConferenceAbstracts.com/uploads/cfp2/attachments/LDFAIBDN/LDFAIBDN--222761-2-ANY(2).pdf

P212

In vivo Cardiac Diffusion Imaging with High-speed Single-shot TSE

Masoud Edalati[1] Gregory Lee, Ph.D.[2], Hui Wang, Ph.D.[3], Michael Taylor, MD, PhD[4], Jie Zheng, Ph.D.[5], Yu Li, Ph.D.[2]

1. *Mallinckrodt Institute of Radiology, Washington University in St. Louis, Saint Louis, MO*
2. *Cincinnati Children's Hospital Medical Center, Imaging Research Center, OH*
3. *Philips Healthcare, OH*
4. *Cincinnati Children's Hospital Medical Center, Cincinnati, OH*
5. *Mallinckrodt Institute of Radiology, Washington University School of Medicine in St. Louis, MO*

Background: Magnetic resonance (MR) diffusion tensor imaging (DTI) offers the potential to noninvasively visualize the microstructure of myocardial fiber tissues by measuring diffusion activities of water molecules. Cardiac DTI is challenging because of physiological motion, short T2 relaxation, and low SNR. The aim of this work is to explore the feasibility of free-breathing in vivo cardiac DTI using turbo spin echo (TSE). A novel high-speed imaging technique, "correlation imaging" is used to enable single-shot TSE for the collection of a whole k-space during the quiescent phase of a single cardiac cycle. The potential of single shot TSE with correlation imaging for cardiac DTI is investigated in this study.

Methods: Correlation imaging is a recently-developed high-speed imaging technique. In comparison to conventional parallel imaging that relies only on coil sensitivity encoding, this technique can use both coil sensitivity encoding and tissue boundary sparsity in image reconstruction from undersampled data, thereby providing a higher imaging speed. Correlation imaging accelerates TSE data acquisitionuses with non-uniform undersampling (Figure 1). This allows the entire diffusion imaging sequence to be squeezed into the quiescent phase of a cardiac cycle, making it possible to collect a full cardiac diffusion image with single-shot TSE in a single cardiac cycle.

In vivo cardiac DTI was performed with the IRB approval. Three healthy volunteers (2 females, 1 male) with a heart rate of 65 ± 8 and an age of 33 ± 7 were scanned. The DTI datasets were obtained at diastolic quiescent phase under free-breathing condition with the imaging parameters: TR = 1 R-R (1 s for heartbeat of 60 bpm), TE = 30 ms, matrix size = 108 × 80, spatial resolution 2.96 × 2.96 mm^2 interpolated to 1.48 × 1.48 mm^2, slice thickness 8 mm, 24 dynamic scans, 6 diffusion directions for the following b-values: 10, 20, 30, 40, and 50 s/mm^2 plus a non-diffusion (b_0) image. TSE readout was shortened from 290 to 72 ms by correlation imaging.

Results: Figure 2 shows the DTI results for the left ventricle myocardium, excluding the papillary muscles. TSE diffusion metrics such as fractional anistropy (FA), mean diffusivity (MD), and color-coded eigenvector map associated with the myocardium fiber orientation were obtained by a bi-exponential diffusion tensor estimation. The mean myocardium FA value of the subjects was 0.55 ± 0.05, and mean MD was 2.03 ± 0.21 × 10^{-3} mm^2/s. The color-coded eigenvector map supports the circumferential myofibers arrangment at the mid-level of human heart as previously illustrated in the literature.

Conclusions: The mean diffusion quantitative values (FA, MD) and the circumferential structure of the myocardium in color-coded map acquired with the accelerated TSE were consistent with those reported in several studies. The presented results demonstrate the potential of single-shot TSE with correlation imaging for in vivo cardiac DTI.

http://www.ConferenceAbstracts.com/uploads/cfp2/attachments/LDFAIBDN/LDFAIBDN--207501-1-ANY(3).pdf

http://www.ConferenceAbstracts.com/uploads/cfp2/attachments/LDFAIBDN/LDFAIBDN--207501-2-ANY.pdf

P213

Risk Stratification for Ventricular Arrhythmia in Patients with Hypertrophic Cardiomyopathy (HCM) via MRI-Based Computational Simulations: A Pilot Study

Mark J. Cartoski, MD, FAAP[1] Maximilian P. Reymann, BS[2], Plamen P. Nikolov, MS[3], Adityo Prakosa, PhD[3], Patrick M. Boyle, PhD[3], Philip J. Spevak, MD, MPH[4], Natalia Trayanova, PhD, FAHA[5]

1. *Johns Hopkins University, Baltimore, MD*
2. *Johns Hopkins University, MD*
3. *Johns Hopkins Unviersity, Biomedical Engineering, Baltimore, MD*
4. *Johns Hopkins University, Pediatric Cardiology, Baltimore, MD*
5. *Johns Hopkins Unviersity, Biomedical Engineering and Medicine, Baltimore, MD*

Background: HCM is a disease of progressive myocardial thickening, fibrosis, and scar formation. It remains the most common cause of sudden cardiac death (SCD) in the young. Patients with HCM have a high ventricular arrhythmia burden which contributes to their risk of SCD. Using late gadolinium enhancement MRI (LGE-MRI), our recently validated Virtual-heart Arrhythmia Risk Prediction (VARP) protocol has been able to assess the risk of arrhythmia in patients with ischemic cardiomyopathy. Because of the known scar and fibrosis in patients with HCM, we hypothesized that patient specific models reconstructed from LGE-MRI scans could similarly assess the risk of arrhythmia in patients with HCM.

Methods: As a proof-of-concept retrospective study, we developed personalized 3D computational models of pediatric HCM hearts from short-axis LGE-MRI scans performed at 1.5T (Siemens Aera). Each model included patient specific distribution of fibrotic tissue and normal myocardium (Fig 1). Five phenotypically positive patients were included. Patient 1 (P1) had clinical episodes of ventricular tachycardia (VT) and required defibrillator implantation while the remaining four patients (P2-P5) had no known episodes of ventricular arrhythmia. Clinical history and arrhythmia status were documented from the time of MRI acquisition. Blinded researchers then applied our VARP protocol to assess the inducibility of reentrant arrhythmia from 26 pacing sites distributed throughout the right and left ventricles.

Results: VARP outcomes correlated with clinical observations in all five patients. In the P1 model, sustained VT was induced in the anterior-medial wall of the hypertrophied left ventricle from multiple pacing locations (Fig 2). The locations of organizing centers of reentrant arrhythmia correlated with an extensive area of fibrotic tissue extending through nearly the entire length of the anterior-medial wall of the left ventricle (Fig 2). No sustained arrhythmias were induced in the remaining four patient models with our rapid pacing protocol despite similar degrees of fibrosis and myocardial hypertrophy as that seen in P1.

Conclusions: Our study demonstrates that application of the VARP approach using clinically available cardiac LGE-MRI scans is feasible in patients with HCM. This methodology has the potential to correctly identify patients with a high risk of developing arrhythmia with a degree of precision beyond traditional risk assessment measures. With additional validation, this non-invasive technique could serve as an effective and powerful tool for assessing longitudinal risk.

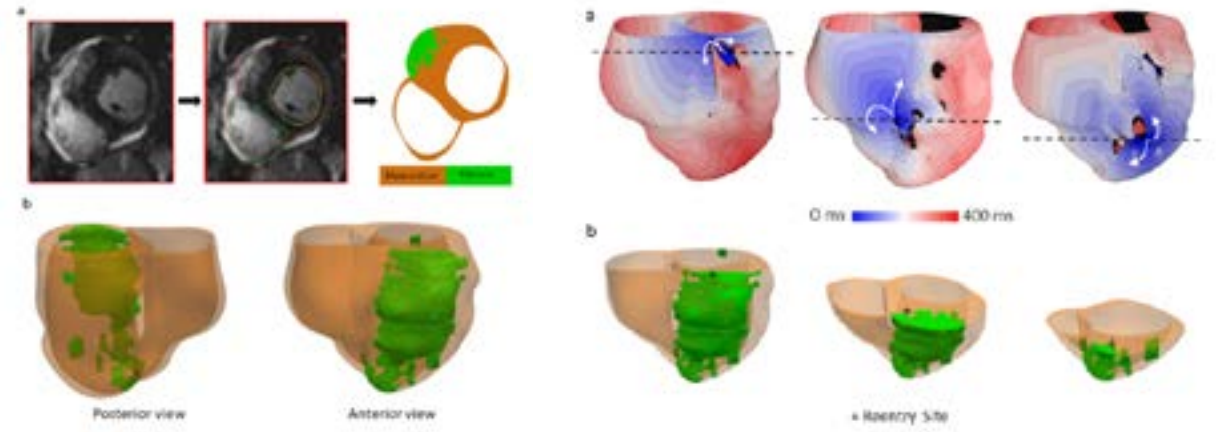

P214

Detailed Left Atrial Assessment in Left Ventricular Hypertrophy

Anna Reid, MBChB(Hons) MRCP[1] Wendy Gamlin, BSE[2], Jakub Lagan, LEKARZ MRCP[3], Christopher A. Miller, MBChB PhD[1], Matthias Schmitt, MD PhD[1]

1. *University Hospital of South Manchester, England, United Kingdom*
2. *University Hospital of South Manchester, Manchester, England, United Kingdom*
3. *University Hospital of South Manchester, Liverpool, England, United Kingdom*

Background: The cardiac manifestations of Anderson- Fabry disease (AFD) are important phenotypic mimics for hypertrophic cardiomyopathy (HCM). Histological LA abnormalities are identifiable post-mortem in both HCM and Fabry disease. Left atrial (LA) size and function are important prognostic markers in multiple cardiac pathologies. The aim of this study was to compare LA size and function in a cohort of patients with AFD and HCM.

Methods: 20 patients with non-obstructive, asymmetrical septal hypertrophy- type HCM, 20 patients with AFD (matched for age, gender and left ventricular mass), and 10 healthy volunteers underwent CMR at 1.5T (Avanto, Siemens AG, Erlangen, Germany). Left ventricular mass (LVM) was determined from the left ventricular short axis stack (CMR Tools). Biplane LA volumes were obtained from 4- and 2-chamber SSFP cine images (cmr42, Circle Cardiovascular Imaging Inc., Calgary, Canada). Mean atrial strain and strain-rate parameters were also derived from these sequences using dedicated CMR feature tracking software (Diogenes® TomTec, Germany).

Results: Results are shown in table 1. Compared to healthy volunteers, those with HCM had significantly larger LA volumes, and worse volumetric and strain indices of LA function. Those with AFD had significantly worse total ejection fraction, reservoir expansion index, and passive ejection fraction, reflecting impaired reservoir and conduit function. Despite similar cardiac phenotypes and LVM, patients with AFD had significantly smaller left atrial volumes, and higher active ejection fraction and reservoir expansion index, reflecting relatively better reservoir and active function. Total atrial strain was significantly higher in AFD, reflecting better atrial compliance. Atrial booster function, previously thought to be increased in HCM, was also worse in HCM than AFD.

Conclusions: LA function, is reduced in HCM and AFD. Despite similar LV morphology and mass, LA function in HCM appears to be significantly worse, particularly in those reflecting LA compliance and contraction. This may imply inherently different LA myopathies, with disturbances in LA function not solely reflective of altered LV compliance, relaxation, or systolic function. This is may be important for risk stratification and disease staging.

Detailed Left Atrial Assessment in Left Ventricular Hypertrophy

p-Value (HCM vs. AFD)	AFD (n=20)	HCM (n=20)	Healthy Volunteers (n=	
	16	16	8	**Male**
0.09	49.5 ± 9.9	55.1 ± 8.4	47.0 ± 7.0	**Age (years)**
0.43	74.1 ± 20.6	73.1 ± 17*	46.7 ± 4.2	**Left Ventricular Mass (g/m²)**
0.003	23.1 ± 9.7	36.9 ± 18.9*	19.9 ± 7.5	**LA Minimum Volume (ml/m²)**
0.005	45.0 ± 12.8	60.6 ± 22.5*	38.0 ± 9.9	**LA Maximum Volume (ml/m²)**
0.003	35.4 ± 10.8‡	49.9 ± 19.7*	28.7 ± 4.8	**LA Pre-Atrial 0.003Contraction Volu0.006me (ml/m²)**
0.006	49.6 ± 9.7‡	41.3 ± 10.3*	55.8 ± 4.1	**Total Ejection Fraction (%)**
0.004	1.05 ± 0.39‡	0.75 ± 0.28*	1.3 ± 0.19	**LA expansion index (%)**
0.03	26.5 ± 7.5‡	21.9 ± 0.8*	33.7 ± 7.0	**Total strain (%)0.03**
0.005	1.08 ± 0.27‡	0.87 ± 0.48*	1.3 ± 0.34	**Peak systolic strain rate (-1)**
0.08	21.2 ± 7.9‡	18.2 ± 5.2*	28.4 ± 38	**Passive Ejection Fraction (%)**
0.09	12.8 ± 5.3‡	10.6 ± 5.4*	17.8 ± 5.7	**Passive Strain (%)**
0.28	0.63 ± 0.26‡	-0.57 ± 0.39*	-0.9 ± 0.34	**Peak early negative strain rate (-1)0.**
0.006	36.3 ± 8.3	28.3 ± 10.5*	38.3 ± 4.0	**Active Ejection Fraction**
0.07	13.7 ± 5.8	11.2 ± 4.4*	15.9 ± 2.3	**Active Strain (%)**
0.03	-1.01 ± 0.41	-0.76 ± 0.4*	-1.21 ± 0.36	**Peak late negative strain rate (-1)**

* $p<0.01$ Healthy Volunteers vs. HCM
‡ $p<0.05$ Healthy Volunteers vs. AFD

P215

Right atrial booster pump function compensates for impaired diastolic right ventricular filling in heart failure with preserved ejection fraction

Maximilian von Roeder, MD[1]Karl Rommel, MD[2], Johannes T. Kowallick, MD[3], Christian Besler, MD[1], Stephan Blazek, MD[4], Andreas Schuster, MD PhD MBA FESC[5], Philipp Lurz, MD, PHD[1]

1. *Leipzig University Heart Center, Department of Cardiology, Sachsen, Germany*
2. *Dept. of Internal Medicine / Cardiology University of Leipzig - Heart Center, Sachsen, Germany*
3. *Institute for Diagnostic and Interventional Radiology, University Medical Center Göttingen, Germany, Niedersachsen, Germany*
4. *Leipzig University Heart Center, Department of Cardiology, Leipzig, Sachsen, Germany*
5. *Department of Cardiology and Pneumology, University Medical Center Göttingen, Germany, Niedersachsen, Germany*

Background: Right heart dysfunction is an important and independent contributor in heart failure with preserved ejection fraction (HFpEF). Little is known about the diastolic properties of the right ventricle and the influence of RA function. Cardiovascular magnetic resonance (CMR) is regarded the gold standard for imaging of the right ventricle. CMR feature tracking (CMR-FT) is a novel tool measuring myocardial strain from routine cine CMR images using standard steady-state free precession sequences (SSFP). Aim of the current study was to elucidate diastolic RV properties using CMR-FT and invasive pressure-volume-loops (PVL).

Methods: We performed CMR-FT in 21 patients with HFpEF and 8 patients without heart failure symptoms. All patients were compensated outpatients without prior history of heart failure hospitalisation. Full cardiac cycle time-volume curves of the right ventricle were obtained from short axis stacks and early and late diastolic filling as relative to RV stroke volume was analyzed. RV function was analyzed using 4-chamber views (4Ch) for assessment of systolic RV strain (RVs), early diastolic strain (RVe) and RV diastolic strain during atrial contraction (RVa). Right atrial function and stroke volume was analyzed measuring RA volume at maximal RA filling, RA volume before atrial contraction and minimal RA volume. Invasive pressure-volume-loops were obtained with a conductance catheter during basal conditions, transient preload reduction and handgrip exercise. Diastolic stiffness constant Beta was extrapolated during transient preload reduction and isovolumetric relaxation time Tau was measured during maximal handgrip exercise.

Results: Pulmonary artery pressure was higher and isovolumetric relaxation time Tau was longer in HFpEF (PA mean 24±6 vs 16±4 mmHg, p=0.02, Tau 36±8 vs. 29±7 ms, p=0.04). RV-EF (69±9 vs. 60±11%, p=0.04) and systolic RV strain (-24±4 vs. -20±3, P=0.03) were increased in HFpEF with similar stroke volumes in HFpEF and controls (43±7 vs. 41±8 ml/m², p=0.54). Early RV filling was lower in HFpEF (21±11 vs. 31±11 % of RV stroke volume, p=0.03) and late filling was higher (80±10 vs. 69±11 % of RV stroke volume, p=0.04). Correspondingly RV diastolic strain during atrial contraction was higher in HFpEF (12±5 vs. 8±3 %, p=0.04) while early diastolic RV strain was similar in both groups (13±6 vs. 13±2 %, p=0.96). Right atrial active stroke volume was higher in HFpEF (14±5 vs. 10±49 ml/m², p=0.02).

Conclusions: In stable HFpEF patients without prior HF hospitalisation RV diastology is characterized by impaired relaxation with impaired early filling. Impaired RV filling is compensated by higher atrial stroke volume to maintain RV filling and stroke volume.

http://www.ConferenceAbstracts.com/uploads/cfp2/attachments/LDFAIBDN/LDFAIBDN--222484-1-ANY.pdf

P216

The impact of diabetes on left and right ventricular structure and function: insights from the UK Biobank

Mihir M. Sanghvi, MB BS, BSc[1]Nay Aung, MD, MRCP[2], Jose Miguel Paiva, MSc[2], Filip Zemrak, MD MRCP[2], Kenneth Fung, MBBS BSc[3], Aaron Lee[4], Valentina Carapella, DPhil[5], Stefan K. Piechnik, PhD, MScEE[6], Stefan Neubauer, MD, FRCP[6], Steffen E. Petersen, MD DPhil MPH FRCP[2], Elena Lukaschuk, MSc[7]

1. *William Harvey Research Institute, NIHR Cardiovascular Biomedical Research Unit at Barts, Queen Mary University of London, Charterhouse Square, London EC1M 6BQ, UK, England, United Kingdom*
2. *Barts Heart Center, The Cardiovascular Magnetic Resonance Imaging Unit and The Center for Rare Cardiovascular Diseases Unit, St Bartholomew's Hospital, West Smithfield, London, UK, England, United Kingdom*
3. *Barts Heart Center, The Cardiovascular Magnetic Resonance Imaging Unit and The Center for Rare Cardiovascular Diseases Unit, St Bartholomew's Hospital, West Smithfield, London, UK, London, England, United Kingdom*
4. *William Harvey Research Institute, NIHR Cardiovascular Biomedical Research Unit at Barts, Queen Mary University of London, Charterhouse Square, London EC1M 6BQ, UK, N/A, United Kingdom*
5. *University of Oxford, Oxford, United Kingdom, England, United Kingdom*
6. *University of Oxford, England, United Kingdom*
7. *University of Oxford, Oxford, England, United Kingdom*

Background: There is growing evidence for the presence of a distinct clinical entity known as diabetic cardiomyopathy – myocardial dysfunction in the absence of coronary disease or hypertension. This study explores the relationship between diabetic status and left and right ventricular structure and function as assessed by cardiovascular magnetic resonance (CMR) imaging in the large scale UK Biobank population-based cohort.

Methods: A total of 5,065 UK Biobank participants underwent CMR examination using the steady-state free precession imaging technique at 1.5 Tesla. Manual analysis was performed for the left and right ventricle. Participants with cardiovascular disease, including stroke and peripheral vascular disease were excluded from the analysis. Diabetic status was determined using self-reported responses in the UK Biobank "health and medical history" questionnaire. Differences between left and right ventricular parameters in diabetic vs. non-diabetic participants were initially examined using t-test. The influence of diabetic status on ventricular measures was further assessed using multivariate linear regression with adjustment for age, sex, body mass index, systolic blood pressure, smoking status, amount of physical activity and ethnicity.

Results: On exclusion of poor quality examinations and examinations with missing/incorrect identifier data, 4,974 participants remained. Having applied exclusion criteria, 4,768 (95.8%) participants were available for analysis; of these, 219 (4.6%) had a self-reported diagnosis of diabetes. Baseline characteristics are presented in *Table 1* and values for direct (end-diastolic volume, end-systolic volume, stroke volume) and derived (ejection fraction) volumetric measures for both the left and right ventricle (RV) demonstrated no significant difference between the two cohorts in univariate analysis (*Table 2).* In multivariate regression (*Table 3)* LV (β = -5.4ml, pLV (β = -5.4ml, $p < 0.01$) and RV (β = -7.0ml, $p < 0.01$) end-diastolic volumes are marginally lower with presence of diabetic disease. LV end-diastolic volume:mass ratio increases slightly with presence of diabetes. Left ventricular ejection fraction is marginally lower in participants with diabetes (β = -0.95%, $p < 0.01$).

Conclusions: In a large cohort free of cardiac, cerebrovascular or peripheral vascular disease, we demonstrate that diabetic disease appears to hahas evident negative impacts on myocardial function in both the left and right ventricle as well as on left ventricular remodelling, but . Even though the effect sizes are very small, the cumulative heath impacts in the individuals with diabetes can be large given the long-term aspect of the condition.

Table 1: Baseline Characteristics

	Diabetics (n=219)	Non-diabetics (n=4768)	p-value
Age (years)	63.8±7.1	61.5±7.6	<0.001
Female (%)	96 (44%)	2451 (54%)	<0.001
BMI (kg/m2)	29.9±5.4	26.0±4.2	<0.001
BSA	1.39±0.49	1.24±0.43	<0.001
Caucasian (%)	94.1	95.8	<0.001
Systolic blood pressure (mmHg)	140.2±17.1	136.4±18.1	<0.001
Diastolic blood pressure (mmHg)	78.8±9.8	78.9±10.0	NS
Current smokers (%)	3.2	4.4	<0.001
Ex-smokers (%)	44.3	30.7	<0.001

Table 2: Characteristics of left and right ventricular structure and function by diabetic status in UK Biobank participants

	Diabetics	Non-diabetics	p-value
LV end-diastolic volume (ml)	144±32	142±33	NS
LV end-systolic volume (ml)	61±21	59±20	NS
LV stroke volume (ml)	84±19	83±19	NS
LV ejection fraction (%)	59±7	60±6	NS
LV mass (g)	97±24	89±24	<0.001
LV mass volume ratio	0.66±0.13	0.62±0.12	<0.001
RV end-diastolic volume (ml)	152±35	151±37	NS
RV end-systolic volume (ml)	68±24	67±23	NS
RV stroke volume (ml)	84±19	83±19	NS
RV ejection fraction (%)	56±7	57±7	NS

Table 3: Differences in left and right ventricular structure and function between diabetics and non-diabetics after multivariable linear regression among UK Biobank participants.

	Diabetics (β coefficient)	p-value
LV end-diastolic volume (ml)	-5.408	<0.01
LV end-systolic volume (ml)	-2.431	NS
LV stroke volume (ml)	-4.15	<0.01
LV ejection fraction (%)	-0.943	<0.05
LV mass (g)	5.434	NS
LV mass volume ratio	0.026	<0.01
RV end-diastolic volume (ml)	-7.004	<0.01
RV end-systolic volume (ml)	-2.37	NS
RV stroke volume (ml)	-4.488	<0.01
RV ejection fraction (%)	-0.142	NS

P217

Does stress perfusion imaging improve the diagnostic accuracy of late gadolinium enhanced cardiac magnetic resonance for establishing the etiology of heart failure?

Gaurav S. Gulsin, MBChB(Hons) MRCP(UK)[1]Jayanth Arnold, MBBS[2], Jeffrey Khoo, FRCP DPhil[3], Abishek Shetye[2], Daniel Swarbrick[2], Eylem Levelt, DPhil[4], Florence Lai[2], Iain B. Squire[2], Gerry P. McCann, MBChB, MD[5]

1. *The University of Leicester, Nottingham, England, United Kingdom*
2. *The University of Leicester, England, United Kingdom*
3. *University Hospitals of Leicester NHS Trust, Leicester, England, United Kingdom*
4. *University of Oxford, England, United Kingdom*
5. *The University of Leicester, Leicester, United Kingdom, Leicester, England, United Kingdom*

Background: Identifying the aetiology of heart failure has important management and prognostic implications. Late gadolinium enhanced cardiovascular magnetic resonance (LGE-CMR) has been shown to be non-inferior (and indeed may be superior) to coronary angiography in differentiating heart failure due to coronary artery disease (CAD) from non-ischaemic dilated cardiomyopathy (NICM). CMR first-pass myocardial perfusion imaging (perfusion-CMR) has been shown in several large studies to have excellent sensitivity and specificity for detection of CAD and may thus play a role in distinguishing heart failure of ischaemic and non-ischaemic origins. However, the added value of adenosine stress perfusion-CMR in subjects with severe left ventricular systolic dysfunction (LVSD) has not been investigated previously. Given that LGE-CMR alone has excellent specificity, sensitivity and diagnostic accuracy for differentiating between ischaemic cardiomyopathy (ICM) and NICM, the utility of additional of stress perfusion imaging in such patients is questionable.

The aim of this retropsective study was to assess whether the addition of adenosine stress perfusion imaging to LGE-CMR is of incremental value for differentiating ICM and NICM in patients with severe LVSD of uncertain aetiology.

Methods: We retrospectively identified one hundred consecutive adult patients (median age 69 years (IQR 59-73)) with severe LVSD (mean left ventricular ejection fraction 26.6±7.0%) referred for perfusion-CMR to establish the underlying aetiology of heart failure. The cause of heart failure was first determined on examination of CMR cine and LGE images in isolation. Subsequent examination of complete adenosine stress perfusion-CMR studies (cine, LGE and perfusion images) was performed to identify whether this altered the initial diagnosis. CMR diagnoses were compared with findings from invasive coronary angiography, where available.

Results: On LGE-CMR, 38 patients were diagnosed with ICM, 46 with NICM and 16 with dual pathology. With perfusion-CMR, there were 39 ICM, 44 NICM and 17 dual pathology diagnoses. There was excellent agreement in diagnoses between LGE-CMR and perfusion-CMR (κ 0.968, $p < 0.001$). The addition of adenosine stress perfusion images to LGE-CMR altered the diagnosis in only two of the 100 patients.

Conclusions: The addition of adenosine stress perfusion-CMR to cine and LGE-CMR provides minimal incremental diagnostic yield for determining the aetiology of heart failure in patients with severe LVSD.

Cause of LVSD diagnosed by LGE-CMR and perfusion-CMR

	Perfusion-CMR	LGE-CMR	Cause of LVSD (%)
Kappa=0.968, p<0.001	39	38	Ischemic
	44	46	Non-ischemic
	17	16	Dual pathology

P218

A simplified left ventricular end-diastolic mean wall thickness-to-volume ratio estimated from left ventricular mass and end-diastolic volume distinguishes physiological from pathological hypertrophy

Magnus Lundin, MD[1] Einar Heiberg, PhD[2], David Nordlund, MD[3], Tom Gyllenhammar, MD[4], Katarina Steding-Ehrenborg, PhD[5], Henrik Engblom, MD, PhD[6], Marcus Carlsson, MD, PhD[7], Dan Atar, MD, PhD[8], Jesper van der Pals, MD, PhD[9], David Erlinge, MD, PhD[10], Rasmus Borgquist, MD, PhD [11], Ardavan Khoshnood, MD[12], Ulf Ekelund, MD, PhD[13], Jannike Nickander, MD[14], Raquel Themudo, MD, PhD[15], Peder Sörensson, MD, PhD[16], Håkan Arheden, MD, PhD[17], Martin Ugander, MD, PhD[18]

1. *Karolinska institutet, Stockholms Lan, Sweden*
2. *Lund University, Department of Clinical Sciences Lund, Clinical Physiology, Skane University Hospital, Lund, Sweden; Lund University, Faculty of Engineering, Department of Biomedical Engineering, Lund, Sweden, Skane Lan, Sweden*
3. *Lund University, Lund, Skane Lan, Sweden*
4. *Cardiac MR group, Dept of Clinical Physiology Lund University Hospital, Lund University, Skane Lan, Sweden*
5. *Lund University, Skane University Hospital, Department of Clinical Physiology, Lund, Sweden; Lund University, Department of Health Sciences, Physiotherapy, Lund, Sweden, Skane Lan, Sweden*
6. *Lund University, Skane Lan, Sweden*
7. *Lund University, Department of Clinical Sciences Lund, Clinical Physiology, Skane University Hospital, Lund, Sweden, Skane Lan, Sweden*
8. *Department of Cardiology B, Oslo University Hospital Ullevål and Faculty of Medicine, University of Oslo, Oslo, Norway, N/A, Norway*
9. *Dept of Cardiology, Skane University Hospital, Skane Lan, Sweden*
10. *Lund University, Department of Cardiology, Clinical Sciences, Lund, Sweden, Lund, Skane Lan, Sweden*
11. *Lund University, Dept of Clinical Sciences, Lund, Cardiology, and Skane University Hospital, Lund, Lund, Skane Lan, Sweden*
12. *Department of Emergency Medicine, Lund University, Skane University Hospital Lund, Sweden, Skane Lan, Sweden*
13. *Dept of Clinical Sciences, Lund University, Lund, Skane Lan, Sweden*
14. *Karolinska Institute, Stockholm, Stockholms Lan, Sweden*
15. *Department of Clinical Physiology, Karolinska Institutet and Karolinska University Hospital, Stockholms Lan, Sweden*
16. *Karolinska University Hospital, Stockholms Lan, Sweden*
17. *Lund University, Department of Clinical Sciences Lund, Clinical Physiology, Skane University Hospital, Lund, Sweden, Lund, Skane Lan, Sweden*
18. *Karolinska Institutet, Stockholms Lan, Sweden*

Background: Cardiovascular magnetic resonance (CMR) accurately measures left ventricular (LV) end-diastolic (ED) volume (EDV) and LV mass (LVM), but LVED mean wall thickness (LVEDMWT) is not routinely measured clinically. We sought to (1) derive and validate a simplified measure of LVEDMWT estimated from LVEDV and LVM by CMR, and (2) evaluate the ability of a thickness-to-volume ratio (TVR) to distinguish pathological from physiological hypertrophy.

Methods: Patients underwent LV cine CMR imaging at 1.5T. LV epicardial and endocardial borders were manually delineated in all slices in a full coverage LV short-axis cine stack in end diastole and end systole. An in-house developed algorithm measured the LVED wall thickness at 24 equally circumferentially distributed positions per slice, excluding regions with thickness < 2 mm, and averaged over the whole LV with weighting according to slice circumference. Based on geometrical assumptions of the relationship mass and volume upon wall thickness, the formula LVEDMWT[mm]=a+b*LVM[g]^x*LVEDV[ml]^y was optimized iteratively compared to measured LVEDMWT. TVR was calculated as TVR[dimensionless]=LVEDMWT[mm]/LVEDV indexed to body surface area [ml/m^2]*1000.

Results: A validation-derivation cohort (n=537) was comprised of volunteers, endurance athletes and patients with varying pathologies. In a derivation subset (n=269/537), the best fit formula was: estimated LVEDMWT[mm]=0.050+1.60*LVM[g]^0.837*EDV[ml]^-0.487. In a separate validation subset (n=268/537), estimated LVEDMWT agreed with measured LVEDMWT (R2=0.95, p < 0.001, mean±SD bias 0.01±0.23 mm), Figure 1. In a largely overlapping cohort enriched with healthy volunteers and hypertrophic cardiomyopathy (HCM), healthy volunteers (n=56) yielded 95% confidence intervals for LVEDMWT: 5.63-8.67 mm (men) and 4.47-7.42 mm (women), and for TVR: 58.4-104.4 (men) and 51.9-97.8 (women). Compared to healthy volunteers, gender-specific estimated LVEDMWT was higher in both athletes (n=86) and in patient groups including cardiac resynchronization therapy candidates (CRT, n=35), acute myocardial infarction (AMI, n=300), cardiac syndrome X (CSX, n=39), and HCM (n=26), p < 0.05 for all groups, Figure 2. In contrast, gender-specific TVR was lower in athletes (all athletes had TVR < 95) and CRT, and higher in CSX and HCM compared to normals, p < 0.05 for all groups. For AMI, women had higher TVR than normals (p=0.002) whereas there was no difference for men (p=0.24), Figure 3.

Conclusions: LVEDMWT can be simply estimated from LVM and LVEDV with high accuracy and precision. Estimated LVEDMWT can in turn be used to calculate TVR as a new index of relative wall thickness. The maximum TVR found in endurance athletes was lower than the upper limit for healthy normals. Therefore, increased TVR effectively rules out athlete's heart as an alternative diagnosis in patients with increased wall thickness.

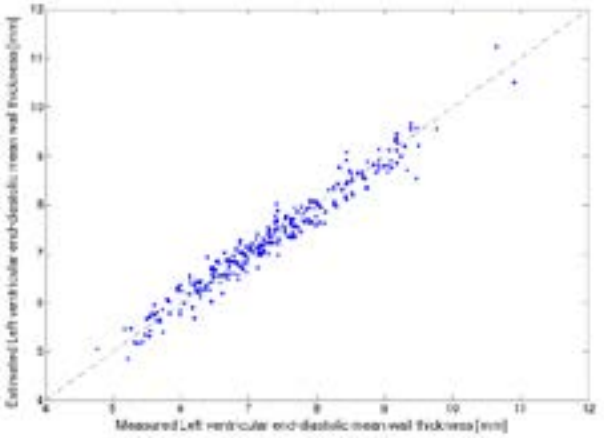

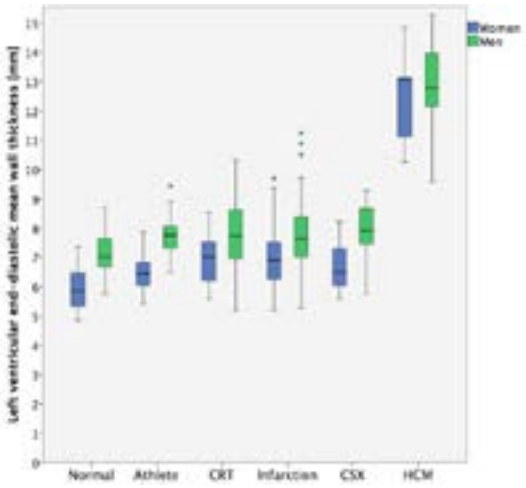
Left ventricular end-diastolic mean wall thickness [mm]
Normal
Athlete
CRT
Infarction
CSX
HCM

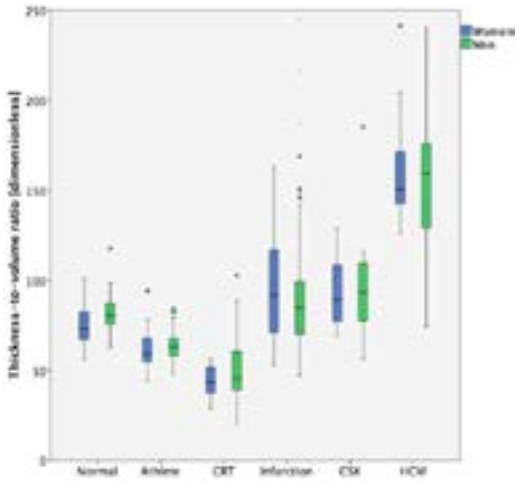
Thickness-to-volume ratio [dimensionless]
Normal
Athlete
CRT
Infarction
CSX
HCM

P219

Gender Difference in Dilated Cardiomyopathy Phenotype as determined by Cardiovascular Magnetic Resonance

Brian Halliday, BSc (Hons) MBChB (Hons)[1] Aamir Ali, MBBS[2], Ankur Gulati, MD[2], Simon Newsome, MA MSc[3], Amrit Lota, BMBCh BA[4], Vassilis Vassiliou, MBBS[2], Upasana Tayal, BMBCh[2], Kayla Chiew[5], Rick Wage, DCR (R)[6], Stuart Cook, PhD[5], Dudley J. Pennell, MD[7], John Cleland, MD PhD[5], Sanjay Prasad, MD[7]

1. *Royal Brompton Hospital and National Heart and Lung Institute, Imperial College London, London, England, United Kingdom*
2. *Royal Brompton Hospital, England, United Kingdom*
3. *London School of Hygiene and Tropical Medicine, England, United Kingdom*
4. *NIHR Royal Brompton Cardiovascular Biomedical Research Unit and National Heart and Lung Institute, Imperial College London, England, United Kingdom*
5. *Imperial College, London, England, United Kingdom*
6. *NIHR Cardiovascular Biomedical Research Unit, Royal Brompton Hospital, England, United Kingdom*
7. *Royal Brompton Hospital and Imperial College, London, England, United Kingdom*

Background: Gender differences in the presentation and outcome of coronary artery disease are well described. Gender-dependent differences in dilated cardiomyopathy (DCM) are less-well understood. Understanding of gender-related variation of a disease provides insight into disease mechanisms and identifies groups of patients at highest risk of adverse outcomes.

Methods: We prospectively investigated all patients with DCM referred for cardiovascular magnetic resonance imaging between 2000 and 2011. The diagnosis of DCM was confirmed by independent operators using clinical, angiographic and CMR data. Baseline clinical and CMR data were compared between males and females using unpaired t-tests for continuous data or Fisher's exact test for categorical data.

Results: 800 patients were included, of whom 530 were male, with a mean left ventricular ejection fraction (LVEF) of 39%. CMR demonstrated that males had significantly higher indexed left ventricular end diastolic volume (LVEDVi: 133.0ml/m^2 vs 124.8ml/m^2; p=0.006), higher indexed left ventricular mass (100.2g/m^2 vs 87.9g/m^2; p < 0.001), higher indexed right ventricular end-diastolic volume (RVEDVi: 94.2ml/m^2 vs 79.4ml/m^2; p < 0.001), lower right ventricular ejection fraction (RVEF: 49.0% vs 55.0%; p < 0.001) and higher indexed left atrial volume (LAVi: 68.2ml/m^2 vs 61.3ml/m^2; p < 0.001) (Table 1). There was also a significantly higher incidence of mid-wall fibrosis in males (37.7% vs 25.0%; p < 0.001). There was, however, no significant difference in left ventricular ejection fraction (38.5% vs 40.3%; p=0.052) between genders. At presentation, males had a higher incidence of atrial arrhythmia (25.3% vs 10.4%; p < 0.001), were more likely to have a history of excess alcohol consumption (16.8% vs 2.2%; p < 0.001) and less likely to have a family history of DCM (8.3% vs 13.0%; p=0.04). Males also reported a significantly lower New York Heart Association symptom class (Class 1 45.4% vs 32.6%, Class 2 39.2% vs 41.9%, Class 3 14.4% vs 22.5%, Class 4 1.0% vs 3.0%; p < 0.001). There were no significant differences in the prescription of loop diuretics or neurohormonal medical therapy between the groups.

Conclusions: Males with DCM have a more severe disease phenotype as determined by CMR compared to females. Despite this worse phenotype, self-reported heart failure symptoms were milder in males. Later presentation to medical services, poorer compliance with medication and differences in disease aetiology may help to explain the more severe disease demonstrated in males.

		Sex		
	All Patients (n=800)	Female (n=270)	Male (n=530)	P
Age (years)	52.2 (14.9)	53.3 (15.2)	51.7 (14.8)	0.1
Atrial Fibrillation / Flutter	162 (20.3)	28 (10.4)	134 (25.3)	<0.0
Hypertension	177 (22.1)	65 (24.1)	112 (21.1)	0.3
Diabetes	65 (8.1)	23 (8.5)	42 (7.9)	0.7
Excess Alcohol	95 (11.9)	6 (2.2)	89 (16.8)	<0.0
Family History of DCM	79 (9.9)	35 (13.0)	44 (8.3)	0.04
Midwall Fibrosis	266 (33.4)	67 (25.0)	199 (37.7)	<0.0
LBBB	230 (28.9)	115 (42.8)	115 (21.8)	<0.0
Medications				
Beta Blocker	575 (72.1)	191 (71.0)	384 (72.6)	0.6
ACE Inhibitor	577 (72.3)	183 (68.0)	394 (74.5)	0.0
Loop Diuretic	349 (43.7)	116 (43.1)	233 (44.0)	0.8
Aldosterone Inhibitor	268 (33.7)	100 (37.3)	168 (31.8)	0.1
NYHA				
I	326 (41.1)	87 (32.6)	239 (45.4)	
II	318 (40.1)	112 (41.9)	206 (39.2)	<0.0
III	136 (17.2)	60 (22.5)	76 (14.4)	
IV	13 (1.6)	8 (3.0)	5 (1.0)	
Cardiovacular Measurements				
LVEDVi	130.3 (39.8)	124.8 (35.2)	133.0 (41.7)	0.00
LVEF (%)	39.1 (12.6)	40.3 (12.0)	38.5 (12.9)	0.05
LV Mass Index (g/m2)	96.1 (28.2)	87.9 (25.0)	100.2 (28.8)	<0.0
RVEDVi	89.3 (26.1)	79.4 (21.4)	94.2 (26.9)	<0.0
RVEF (%)	51.2 (14.3)	55.5 (14.7)	49.0 (13.6)	<0.0
LAVi	65.9 (26.5)	61.3 (24.5)	68.2 (27.1)	<0.0

P220

Right ventricular strain in acute thromboembolic pulmonary hypertension: A CMR study in a pre-clinical model

Christopher J. Francois, MD[1]Naomi C. Chesler, PhD[2], Alejandro Roldan, PhD[2]

1. *University of Wisconsin - Madison, Madison, WI*
2. *University of Wisconsin - Madison, WI*

Background: Acute pulmonary embolism (PE) is a common problem that can severely impact right ventricle (RV) function. In patients without pre-existing pulmonary hypertension (PH) the effects of an acute increase in pulmonary vascular resistance on the RV can be more severe due to the absence of compensatory RV hypertrophy. The prognosis after acute PE is related to the degree of RV dysfunction. Although signs of adverse outcomes in acute PE include dilated RV, bowing of the interventricular septum and decreased RV systolic function (as measured by tricuspid valve annulus displacement or RV ejection fraction(EF)), these may not be the earliest signs of RV dysfunction. The purpose of this study was to determine if RV radial and longitudinal strain and strain rate were impaired earlier than decreases in RV EF in a pre-clinical model of acute thromboembolic pulmonary hypertension.

Methods: After IACUC approval, six adult female beagles were induced with propofol and maintained under anesthesia with isoflurane. Right heart catheterization (RHC) and cardiac magnetic resonance (CMR) measurements were performed prior to and following induction of acute PH by injection of embolizing micro-beads (150-500µm) into the right atrium and ventricle. RV function was assessed at CMR with axial cine balanced steady state free precession covering the entire RV. RV end-diastolic (EDV), end-systolic (ESV) and stroke (SV) volumes and ejection fraction (EF) were calculated using ReportCard (GE Healthcare, Waukesha, WI). Tissue tracking was used to calculate RV radial and longitudinal strain and strain rate (cmr42, Circle Cardiovascular Imaging, Inc., Calgary, Canada) (Figure 1). For strain measurements, three slices in the mid RV were analyzed. The RV free wall was divided into three regions of interest (ROI) covering the base (ROI1), mid (ROI2) and apical (ROI3) segments of the RV free wall. The differences in peak systolic strains and strain rates pre- and post-embolization were compared using a paired t-test.

Results: At RHC, mPAP, PCWP, and PVR were 25.5±3.3mmHg, 17.3±4.0 mmHg, and 2.45±0.8mmHg-min/L pre-embolization and 46.2±5.2mmHg, 22.6±4.3mmHg, and 8.23±4.4mmHg-min/L post-embolization, respectively (all p0.05). Representative RV radial and longitudinal strain and strain rate plots are shown in figure 2. The results are summarized in the Table. The effects of acute PE on RV strain varied from base to apex and from inferior to superior. The greatest changes were observed in radial strain rate, especially in the apical region.

Conclusions: This pre-clinical CMR study demonstrated that the effects of acute PE on RV function are heterogeneous, with significant decreases in RV radial strain rate in the apex occurring prior to any detectable significant changes in RV EF. Future longitudinal studies are needed to determine the evolution of these changes after resolution of PE and in the setting of chronic thromboembolic pulmonary hypertension.

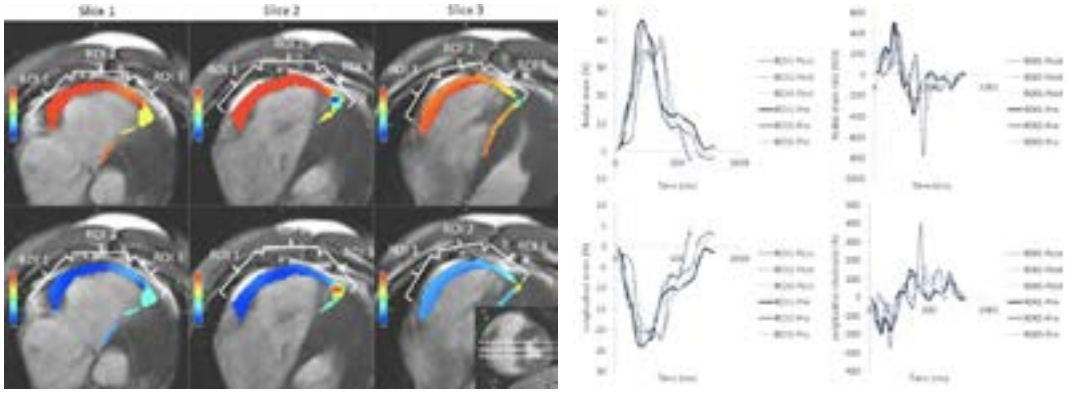

P221

Non-contrast multi-parametric myocardial mapping in patients with pulmonary artery hypertension

Hang Zhao, MD[1], Yuchi Han, MD[2]Jing Wang, MD[1], Patricia O'Donnell, RT[2], Jacqueline Meeks, MBA, RT(R)(MR)[1], Walter R. Witschey, PhD[2]

1. *University of Pennsylvania, PA*
2. *University of Pennsylvania, Philadelphia, PA*

Background: Detection of altered myocardial composition may be possible using advanced cardiovascular magnetic resonance (CMR) multiparametric mapping techniques. Quantified myocardial T1, T2, and T1 rho values may provide characterization of underlying composition of the myocardium without the use of contrast agents. The aims of this study were to observe whether CMR could characterize native myocardial T1 values, T2 values as well as T1 rho values in patients with PAH in comparison to healthy volunteers and to evaluate the association of T1, T2, and T1 rho values with clinical, functional, and hemodynamic parameters.

Methods: CMR was performed for in 22 patients with PAH (61±11 years, 14 female), and 5 volunteers (37±13 years, 2 female) on a 1.5T MRI scanner (Avanto, Siemens, Germany). T1 (5/3/3 MOLLI), T2 (3 point T2-preped SSFP) and T1 rho (single shot SSFP with 8 spin lock times) mapping in addition to ventricular volumes and function of the left and right ventricle (LV and RV) were performed, BNP, PVR, mPAP were collected and the values were compared using Student t tests and Pearson's correlation.

Results: Compared with healthy volunteers, patients with PAH had elevated T1 at RV insertion points (1129.7±61.7 ms vs 1036.1±63.8 ms, p=0.007), and RV free wall (1035.9±78.6 ms vs 947.9±59.9 ms, p=0.031). They also have higher T2 values at the same locations, RV insertion points (53±4.6 ms vs 42.5±3.3 ms, p=0.00) and RV free wall (47.6±3.5 ms vs 41.0±2.9 ms, p=0.001). There was no significant difference of T1 rho value between PAH group and healthy groups. At RV insertion point, T2 showed a significant correlation with RVEDVI, RV mass index and BNP (r=0.608, p=0.016; r=0.573, p=0.026; r=0.557, p=0.031, respectively). No correlation was found between RV insertion point T1 or RV free wall T1 and RV volume, or ejection fraction. No correlation was found between T1 or T2 and PVR or mPAP.

Conclusions: T1 and T2 values are both elevated in the RV insertion points and the RV free wall of patients with PAH, but T1 rho values didn't show significant difference. T2 values at RV insertion showed a significant correlation with RVEDVI, RV mass index and BNP. The combination of CMR mapping techniques maybe helpful to follow patients without the need of contrast agents.

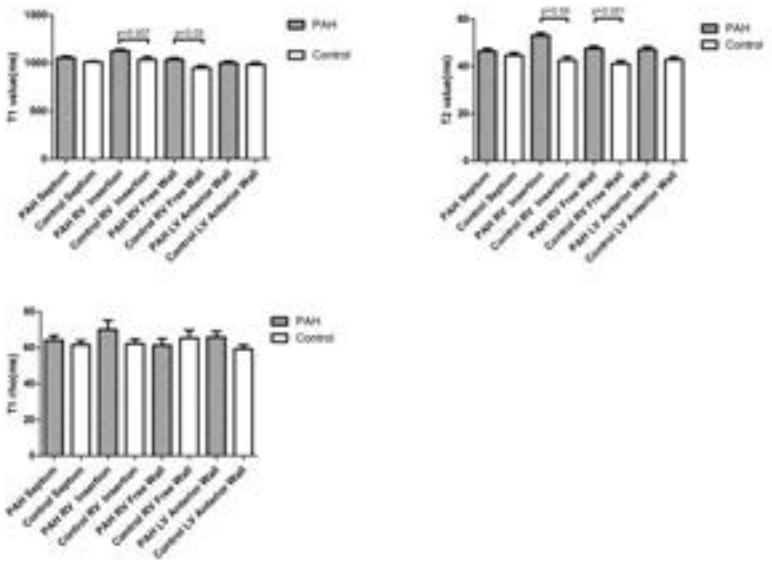

P222

Native T1 Mapping for Detection of Cardiac Iron Overload in Patients with Thalassemia

Shuo Zhang, Ph.D.[3]Rungroj Krittayaphong, MD[1], Pairash Saiviroonporn, PhD[2], Vip Viprakasit, MD[2], Prajak Tanapibunpon, MSc[2]

1. Siriraj Hospital, Mahidol University, Bangkok, Krung Thep, Thailand
2. Siriraj Hospital, Mahidol University, Krung Thep, Thailand
3. Philips Healthcare, Singapore, N/A, Singapore

Background: Survival of patients with thalassemia has much improved after the introduction of cardiac magnetic resonance (CMR) for the assessment of iron overload in patients with thalassemia. While cardiac T2star is the conventional method, T1 mapping has become an emerging technique that may be useful to evaluate iron overload. In this study, we aimed to study the diagnostic value of T1 map for assessment of cardiac iron overload (CIO) in thalassemia patients who were referred for CMR.

Methods: All patients underwent CMR on a 1.5T system (Philips Achieva), on which native T1 and conventional T2star mapping were performed. Native T1 maps were acquired in the mid-cavity short-axis level with a 5(3)3 MOLLI scheme and balanced steady-state free precession (bSSFP) contrast. Global T1 values were reported as mean ± standard deviation (SD). CIO was defined by a T2star of less than 20 ms. Severe CIO was considered if T2star less than 10 ms.

Results: A total of 200 patients were enrolled. There were 102 male (51%) with the mean age of 23.9 ± 14.6 years. Average T2star was 37.8 ± 7.0 ms and average T1 was 1002 ± 79.8 ms. 8 patients (4.0%) had CIO. Receiver operating characteristic (ROC) curve showed that the best cut off of T1 for detection of CIO was below 887 ms which yielded sensitivity, specificity and area under the curve (AUC) of 100%, 98% and 0.997. For the detection of severe CIO, the best cut off of T1 was below 634 ms which yielded sensitivity, specificity and AUC of 100%, 100% and 1.0 respectively. Figure 1 and 2 demonstrated a high T2star and T1 in a patient without CIO and a low T2star and T1 in another patients who had CIO. Figure 3 showed bar graph of T1 levels with 95% CI of patients with severe CIO, mild to moderate CIO and without CIO.

Conclusions: T1 map seems to be promising for the detection of CIO in patients with thalassemia. Further studies are warranted to investigate its values in clinical practice.

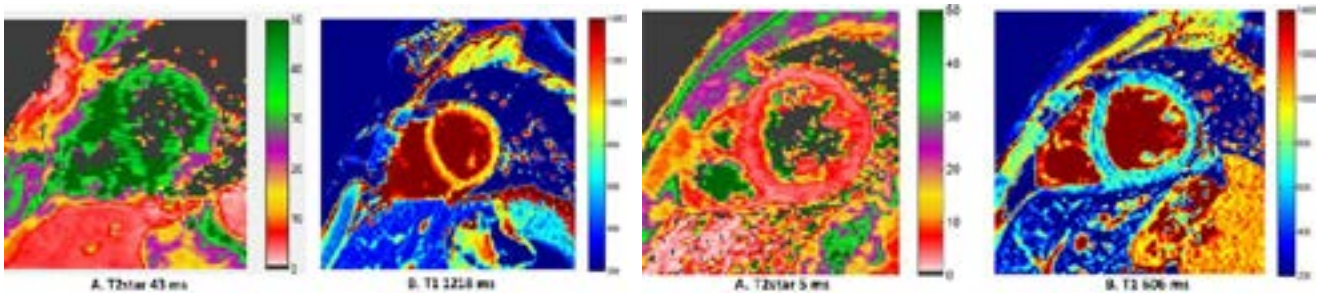

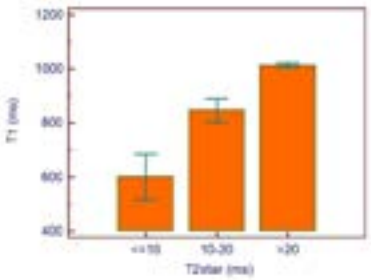

P223

Myocardial Strain, Not Native T1 Mapping, Corresponds with Presence and Severity of Late Gadolinium Enhancement in Patients with Duchenne Muscular Dystrophy

Jonathan H. Soslow, M.D., M.S.C.I.[1]Larry W. Markham, M.D.[2], Kimberly Crum, RN[3], Meng Xu, M.S.[4], James C. Slaughter, Dr.PH.[4], Bruce Damon, PhD[5], David A. Parra, M.D.[2]

1. *Vanderbilt University Medical Center, Nashville, TN*
2. *Vanderbilt University Medical Center, Division of Pediatric Cardiology, Nashville, TN*
3. *Vanderbilt University Medical Center, TN*
4. *Vanderbilt University Medical Center, Department of Biostatistics, Nashville, TN*
5. *Vanderbilt Unicersity, TN*

Background: Duchenne muscular dystrophy (DMD) leads to progressive cardiomyopathy. Late gadolinium enhancement (LGE) by cardiac MRI (CMR) plays an integral role in clinical management. There are growing concerns about gadolinium safety, especially in children. We hypothesized that data obtained from CMRs without contrast, specifically T1 mapping and strain, correlates with presence, severity, and progression of LGE in DMD.

Methods: CMRs included tagging, modified Look-Locker inversion recovery (MOLLI), and late gadolinium enhancement (LGE). Native T1 maps were contoured in the 6 mid-LV segments in the short axis; strain was calculated using harmonic phase (HARP) technique. LGE was evaluated as: 1) presence or absence in the mid-LV; 2) mid-LV severity (average severity of individual mid-LV segments, with 0=none, 1=mild, 2=moderate, 3=severe). Ordinal logistic regression estimated odds ratios (OR) for the association of age, native T1, and strain with presence and severity of LGE accounting for repeated measures (using the Huber-White estimator). Linear regression estimated the association of change in LGE severity with change in strain and native T1 from first to last CMR.

Results: Forty-two patients with DMD underwent 66 CMRs. The mean age at most recent CMR was 14.5 ± 4.7 years and mean LV ejection fraction (LVEF) was 55% ± 10 (range 27-74). Twenty-nine patients (69%) had LGE at most recent CMR with a median severity score of 2. Eighteen patients had serial CMRs. Evaluating all CMRs performed, 45 of 66 CMRs (68%) had LGE. The mean global strain was -15.1% ± 3.1 and the mean native T1 was 1059ms ± 48. Age and strain were associated with presence of LGE (both $p < 0.05$, OR 9.1 for 9-year increase in age and 3.5 point worsening of strain). Age and strain were also correlated with LGE severity (both $p < 0.001$, OR 5.4 and 4.3, respectively) while native T1 was not significant ($p=0.13$). Change in LGE severity correlated with T1 ($p=0.01$) but not with strain ($p=0.27$, Figure 1).

Conclusions: Strain may help distinguish presence or absence of LGE and LGE severity. Native T1 does not correlate with either, likely due to the presence of underlying diffuse fibrosis. However, change in native T1 may help detect a progression of disease from baseline. Further validation of these models is necessary to evaluate whether frequency of contrast administration can be decreased in this patient population.

http://www.ConferenceAbstracts.com/uploads/cfp2/attachments/LDFAIBDN/LDFAIBDN--222240-1-ANY.pdf

P224

Early and Serial Cardiac Magnetic Resonance Studies in Duchenne Muscular Dystrophy Patients Allows Early Detection of Myocardial Fibrosis and Global Ventricular Dysfunction

Kan Hor, MD[1] Thomas P. Johnston, M.D.[1], D. Woodrow Benson, MD, PhD[2], Linda Cripe, MD[1]

1. Nationwide Children's Hospital, Columbus, OH
2. Children's Hospital of Wisconsin, Milwaukee, WI

Background: Cardiovascular complications are a leading cause of disease-related morbidity and mortality among Duchenne muscular dystrophy (DMD) patients. Use of cardiac magnetic resonance (CMR) has become more common but timing of first CMR study and follow-up evaluation remains unclear. We hypothesized that late gadolinium enhancement (LGE) indicative of myocardial fibrosis and abnormal ejection fraction (EF < 55%) is common and progress over a short time.

Methods: We reviewed our CMR database for patients with known DMD who underwent at least 1 CMR study. Age, LGE and LVEF findings were collected as well as time to LGE positive findings. Statistical analysis was performed using Student's t-test.

Results: 418 patients had complete CMR assessment. 345 (82.5%) were LGE negative and 73 (17.5%) were LGE positive on the first study. The LGE negative group was younger ($p < 0.00001$), average age 10.5±3 years compared to 15.7±5 years. 5/345 (1.4%) LGE negative patients compared to 25/73 (34%) LGE positive patients had abnormal EF. 85/345 (24.6%) became positive over an average time of 18.4±8.9. Age at first CMR study in those who became LGE positive was not significant ($p=0.83$).

Conclusions: In conclusion, CMR study with LGE should be performed when sedation is no longer indicated and should be performed at minimal every 1-2 years. This finding has been important in determine initiation and escalation of therapy as well as follow-up plans at our institution and can be used to better understand the natural history of DMD-associated cardiomyopathy.

P225

Ejection fraction in left bundle branch block is disproportionately reduced by small amounts of myocardial scar

Jimmy Axelsson[1] Björn Wieslander, MD[2], Robert Jablonowski, MD, PhD[3], Igor Klem, MD[4], Robin Nijveldt, MD, PhD[5], Erik B. Schelbert, MD, MS[6], Peder Sörensson, MD, PhD[7], Andreas Sigfridsson, PhD[8], Uzma Chaudhry, MBBS[9], Pyotr Platonov, MD, PhD[9], Rasmus Borgqvist, MD PhD[10], Henrik Engblom, MD, PhD[3], David Strauss, MD, PhD[11], Håkan Arheden, MD, PhD[12], Brett D. Atwater, MD[13], Martin Ugander, MD, PhD[14]

1. *Department of Clinical Physiology, Karolinska Institutet, and Karolinska University Hospital, Stockholms Lan, Sweden*
2. *Department of Clinical Physiology, N2:01, Karolinska Institutet and Karolinska University Hospital, Stockholm, Stockholms Lan, Sweden*
3. *Lund University, Skane Lan, Sweden*
4. *Duke University Medical Center, Durham, NC*
5. *VU University Medical Center, Amsterdam, Noord-Holland, Netherlands*
6. *University of Pittsburgh; Heart and Vascular Institute of UPMC, PA*
7. *Karolinska University Hospital, Stockholms Lan, Sweden*
8. *Karolinska Institute, Stockholm, Stockholms Lan, Sweden*
9. *Department of Cardiology, Clinical Sciences, Lund University, Skane Lan, Sweden*
10. *Lund University, Dept of Clinical Sciences, Lund, Cardiology, and Skane University Hospital, Lund, Skane Lan, Sweden*
11. *FDA, Silver Spring, MD*
12. *Lund University, Department of Clinical Sciences Lund, Clinical Physiology, Skane University Hospital, Lund, Sweden, Lund, Skane Lan, Sweden*
13. *Duke University School of Medicine, NC*
14. *Karolinska Institutet, Stockholms Lan, Sweden*

Background: The relationship between maximum possible left ventricular (LV) ejection fraction (EF) (LVEFmax) and LV myocardial scar has been studied without considering electrocardiographic (ECG) conduction abnormalities. Left bundle branch block (LBBB) alters the electrical and mechanical activation of the LV. We hypothesized that the relationship between LVEF and scar is different in LBBB compared to patients without LBBB.

Methods: A four center multicenter retrospective study identified patients with LBBB who had undergone cardiovascular magnetic resonance (CMR) imaging. LBBB was defined according to strict ECG criteria (Strauss DG, 2011, Am J Cardiol). LVEF (%) was measured by cine imaging and scar by late gadolinium enhancement (LGE) quantified as %LV mass (%LVM). LVEFmax was defined as the function describing the hypotenuse in the LVEF versus myocardial scar extent scatter plot with the smallest possible integral while still covering ≥95% of all data points with >0% scar extent. Scar sensitivity ratio (SSR) was defined as LVEF[%]/scar[%LVM].

Results: LBBB patients with no scar (n=153) had higher LVEF than LBBB with scar (n=135, median [interquartile range] LVEF 44 [32-54] vs 27 [19-38] %, $p < 0.001$). Compared to a control group with ischemic heart disease, scar, and no LBBB (n=91), LBBB with scar had a lower LVEF (27 [19-38] vs 36 [25-50] %, $p < 0.001$), smaller scar (4 [1-9] vs 11 [6-20] %LVM, $p < 0.001$] and greater SSR (7.6 [2.7-18.3] vs 3.2 [1.5-7.1], $p < 0.001$). The figure shows the linear relationship between the LVEFmax and scar in patients with LBBB as well as no LBBB.

Conclusions: In patients with LBBB, there is a linear relationship between maximum possible LVEF and myocardial scar extent, and it differs considerably compared to patients with no LBBB. Large scar is exceedingly uncommon in LBBB. LBBB patients experience a greater reduction in LVEF for each percentage of LV scar compared to non-LBBB controls.

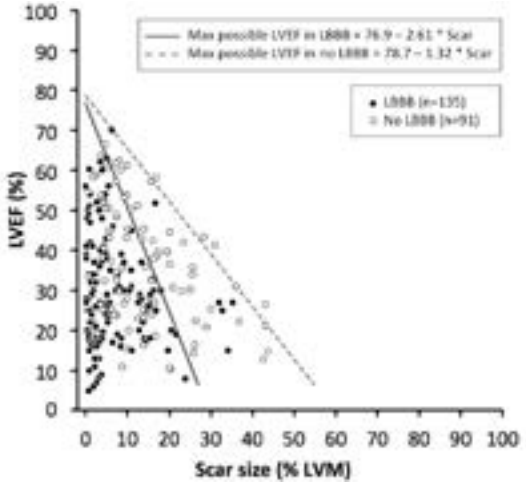

P226

Hypertrophic cardiomyopathy is characterized by both increased native T1 and absolute reduction in myocardial blood flow.

Betty Raman, MBBS, FRACP[1] Rina Ariga, MBBS, MRCP[2], Masliza Mahmod, MBChB, DPhil[2], Stefan K. Piechnik, PhD, MScEE[2], Alessandra Borlotti, PhD[3], Michael Jerosch-Herold, PhD[4], Jane M. Francis, DCR(R) DNM[5], Vanessa M. Ferreira, MD, DPhil[2], Erica Dall'Armellina, MD, PhD[6], Hugh Watkins, MD PhD FRCP FMedSci[7], Stefan Neubauer, MD, FRCP[2]

1. *University of Oxford, Division of Cardiovascular Medicine, Oxfordshire, England, United Kingdom*
2. *University of Oxford, England, United Kingdom*
3. *University of Oxford, Oxford, England, United Kingdom*
4. *Department of Radiology, Brigham & Women`s Hospital & Harvard Medical School, Boston, United States., MA*
5. *University of Oxford, OX39DU, England, United Kingdom*
6. *Oxford University, England, United Kingdom*
7. *Radcliffe Department of Medicine, England, United Kingdom*

Background: Native T1 is widely recognized as a quantitative marker of diffuse fibrosis in hypertrophic cardiomyopathy (HCM). T1 relaxation time is, however, also influenced by intra- and extracellular water content. The intravascular space (component of extracellular water content) has been proposed to significantly influence T1 due to capillary recruitment and microvascular dilation in other pathologies such as coronary disease and aortic stenosis respectively. To clarify the mechanisms of increased T1 in HCM, we therefore sought to investigate the relationship between native T1 and myocardial blood flow in HCM.

Methods: 62 age- and gender- matched subjects (31 HCM and 31 controls) underwent cardiovascular magnetic resonance at 3 T for assessment of function (cine), native T1 mapping (Shortened modified look locker inversion recovery), myocardial blood flow-MBF (adenosine stress first pass perfusion imaging) and replacement fibrosis (late gadolinium enhancement-LGE imaging).T1 values were derived from 6 AHA segments of a mid-ventricular short axis (SAX) slice. Absolute resting MBF was calculated by using Fermi function deconvolution model on matched slice.

Results: HCM patients had higher left ventricular ejection fraction, mass index and mean wall thickness compared to controls. Mean segmental native T1 was significantly higher in HCM compared to controls (Mean±SD, 1204±40 ms vs. 1177±40 ms, $P < 0.01$) and rose with increasing quartiles of wall thickness (P=0.01) (Figure 1). Native T1 was highest in segments with LGE (1218±53 ms) but also increased in those without LGE compared with controls (1197±37 vs. 1177±45, P=0.03). Conversely, both resting and hyperemic blood flow (corrected by rate pressure product) were lower in HCM versus controls with a difference of -0.33±0.14 [SE] ml/min/gram (P=0.04) (Figure 2) and -0.65±0.14 [SE] ml/min/gram (P=0.02) respectively. As with native T1, reduction in resting MBF and hyperemic MBF was greater in hypertrophied segments versus segments with normal wall thickness ($P < 0.05$).

Conclusions:

1. In HCM, native T1 increases and absolute MBF decreases in the myocardium with increasing wall thickness in HCM compared to controls. 2. These findings highlight a complex relationship between native T1 and MBF and provide further support that the HCM phenotype extends beyond conventional measures such as wall thickness and LGE, and may be detected using advanced CMR techniques such as native T1 mapping and absolute myocardial blood flow.

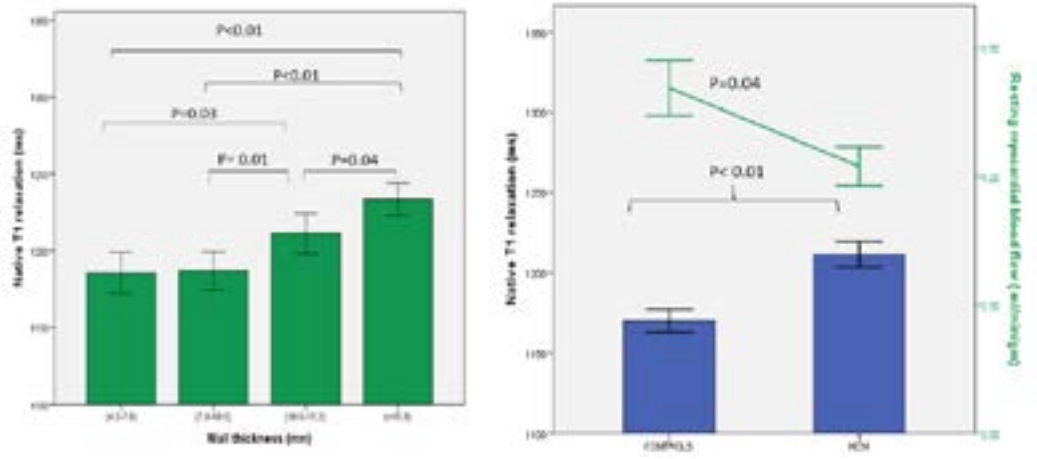

P227

Regional Structure-Function Cardiac MRI to Assess Cardiotoxicity in Breast Cancer Patients

Nivedita K. Naresh, Ph.D.[1]Amir Ali Rahsepar, MD[1], Ahmadreza Ghasemiesfe, M.D[2], Kai Lin, MD[1], Julie Blaisdell[1], Bradley Allen, MD[3], Nausheen Akhter, MD[4], Michael Markl, PhD[1], Jeremy D. Collins, MD[5], James Carr, MD[5]

1. *Northwestern University, Chicago, IL*
2. *Yale affiliated Bridgeport Hospital, Milford, CT*
3. *Northwestern University, IL*
4. *Northwestern Memorial Hospital, IL*
5. *Northwestern Memorial Hospital, Chicago, IL*

Background: Cardiotoxicity following chemotherapy is commonly observed in cancer patients treated with anthracyclines. Current echocardiography methods, aim at measuring global reductions in left-ventricular ejection fraction (LVEF) and strain, however they do not provide insight into regional structural and functional changes. Recent advances in MRI such as T1-mapping to assess regional extracellular volume (ECV) and CMR-based myocardial strain analysis allow to probe regional myocardial tissue structure and function. The purpose of this study was to evaluate changes in regional ECV and strain in cancer patients to test the hypothesis that treatment with chemotherapy results in regional abnormalities in cardiac ECV and function.

Methods: Ten healthy subjects (43±18 years) and nine breast cancer patients (56±12 years) who underwent chemotherapy and presented with more than a 5% drop in LVEF from initial echocardiography were prospectively recruited. Cardiac MRI was performed at 1.5T (Magnetom Avanto or Aera, Siemens, Erlangen, Germany). 2D CINE SSFP CMR data and tissue tracking software (Circle 5.3, Canada) was used to calculate peak radial (Err), peak circumferential (Ecc), and peak longitudinal strains (Ell) as well as systolic radial strain rate (SR), systolic circumferential strain rate (SC) and systolic longitudinal strain rates (SL) using the standard AHA 16-segment model. MOLLI T1 mapping was performed pre-contrast and at 12-25 minutes post-gadobutrol (0.2 mmol/kg) in basal, mid-ventricular and apical slices. Using the pre- and post-contrast T1 mapping data, ECV was calculated using the 16-segment AHA model. Regional strains and ECV measurements were determined by averaging over all LV segments in the basal, mid-ventricular and apical slices. ECV could not be calculated in the healthy volunteers due to the inability to obtain Hct.

Results: The breast cancer patients demonstrated an average LVEF of 33±15%. Err and Ecc were significantly reduced in patients at all slice locations compared with controls ($p < 0.05$). Compared to controls, patients had higher T1 values ($p < 0.05$). In patients, there was a significant association between regional ECV and reduced peak strains and systolic strain rates predominantly at the basal location ($p < 0.05$) (Table and Figure).

Conclusions: The results from this ongoing study looking at long-term outcomes in patients who underwent chemotherapy with anthracyclines may indicate that strain is reduced in these patients. There was a significant association between regional ECV and decreased regional strain values in the basal myocardium suggesting that chemotherapy mediated cardiotoxicity may initiate from the basal chamber. These preliminary results suggest a regional structure-function relationship between altered ECV and reduced myocardial function in chemotherapy-induced cardiotoxicity. While these initial results are promising, longitudinal studies are required to evaluate the effect of chemotherapy on cardiac function.

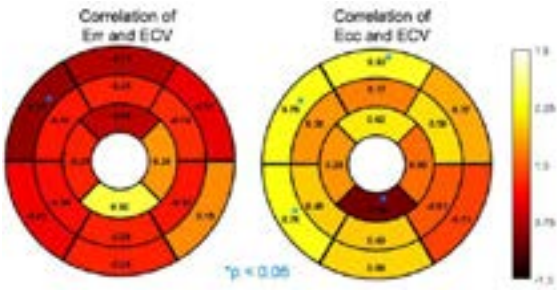

Correlations Between ECV and Strain and Strain Rate in Breast Cancer Patients after Chemotherapy at Basal, Mid-ventricular and Apical Slice Locations

Apex	Mid	Base	Correlations
-0.14	-0.55	-0.72*	ECV and Err
0.16	0.42	0.86*	ECV and Ecc
0.19	0.42	0.78*	ECV and Ell
-0.23	-0.39	-0.79*	ECV and SR
0.31	0.09	0.74*	ECV and SC
0.31	0.06	0.78*	ECV and SL

*$p < 0.05$

P228

Systolic vortices in the pulmonary artery: energy conservation or wasting?

Joyce Han, BA[1], Yuchi Han, MD[5]Jelena Bock, PhD[2], Per M. Arvidsson, MD[3], Einar Heiberg, PhD[4]

1. *university of pennsylvania, NH*
2. *Lund University, Department of Clinical Sciences Lund, Clinical Physiology, Skane University Hospital, Lund, Sweden, Skane Lan, Sweden*
3. *Lund University, Department of Clinical Sciences Lund, Clinical Physiology, Skane University Hospital, Lund, Sweden, Luns, Skane Lan, Sweden*
4. *Lund University, Department of Clinical Sciences Lund, Clinical Physiology, Skane University Hospital, Lund, Sweden; Lund University, Faculty of Engineering, Department of Biomedical Engineering, Lund, Sweden, Skane Lan, Sweden*
5. *University of Pennsylvania, Philadelphia, PA*

Background: Diastolic filling pattern of the left ventricle (LV) suggests that healthy hearts accommodate LV diastolic filling vortices and utilizing the energy in the vortex to maximize pumping efficiency and to conserve energy. Vortices are also observed inside dilated pulmonary arteries (PA) during systolic ejection, but their significance has not been investigated. We used two readily established methods: Lagrangian coherent structures (LCS), which defines boundary layers present in a mixture of fluids of different origins, and vortex core detection to study the formation and development of vortices in the PA of patients with pulmonary arterial hypertension (PAH).

Methods: Seven PAH patients underwent *cine* and four-dimensional phase-contrast MRI of the right ventricle (RV) and PA on a 1.5T scanner (Avanto, Siemens, Germany). Analyses were performed in Segment (Medviso, Lund, Sweden) with special plug-in functions and MatLab scripts (MatWorks, Natick, MA). Visualization was done in FourFlow (Lund, Sweden). When applied to PA flow, LCS outlines the borders of vortices formed by the blood newly ejected into the PA and residual blood from the preceding diastole. We traced the borders and calculated the total kinetic energy (KE) associated the vortex/ces inside the PA during systole. LCS was calculated in PA cross-sections at 8mm increments spanning the entire PA, from the pulmonic valve (PV) to the first PA bifurcation. Vortex boundaries were then traced manually throughout systole, defined from PV opening to closing. The minimum threshold for a vortex core was set at radius of 125% voxel size (2.75mm) and sigma value of 1000. KE of the vortex was calculated inside the traced vortex volume, and the viscous energy loss was derived from Navier-Stokes equations applied to the entire PA as previously described.

Results: Vortex cores were observed in all PAH patients, and Figure 1 features a typical progression of the formation and dissipation of vortices inside the PA throughout systole. Note that in phases D-F, the "upward" vortex core may explain the characteristic hump seen on the PA flow curves of PAH patients. Viscous energy loss increased as the KE of the vortex increased (Figure 2).

Conclusions: We found proportional viscous energy loss as the vortex dissipated. We suspect that recurrent vortices exacerbates PA dilation by exerting shear forces on the wall. The magnitude of energy loss was not correlated with the RV ejection fraction in these patients. The quantitative nature of the vortex analysis may provide explanation on PA dilation in patients with PAH.

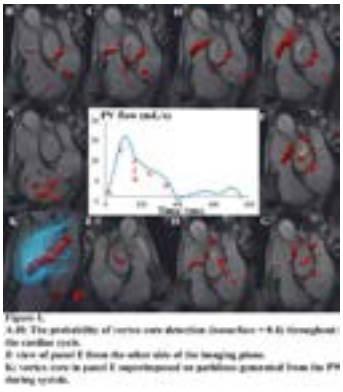

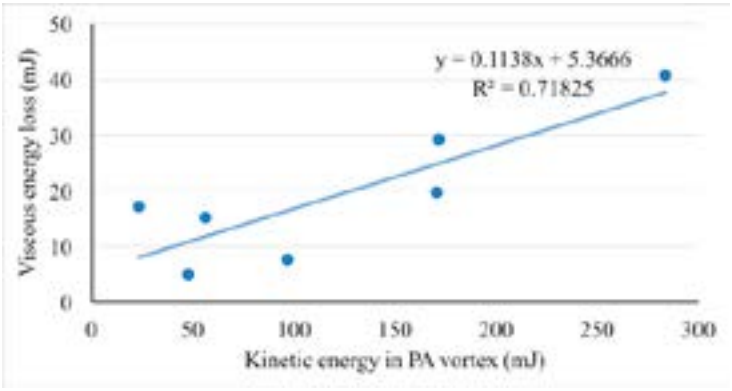

P229

Relationship between electrical and myocardial abnormalities in patients with myotonic dystrophy type 1

Anca R. Florian[1], Ali Yilmaz, Prof. Dr.[3]Alexandru Patrascu[2], Lukas Chmielewski[3], Michael Bietenbeck[3], Sabine Roesch[2], Udo Sechtem, Prof. Dr.[2]

1. *University Hospital Muenster, Muenster, Nordrhein-Westfalen, Germany*
2. *Robert-Bosch Hospital Stuttgart, Baden-Wurttemberg, Germany*
3. *University Hospital Muenster, Nordrhein-Westfalen, Germany*

Background: Myotonic dystrophy type 1 (MD1) is an autosomal dominant disorder characterized by skeletal muscle symptoms, cardiac abnormalities, and other systemic manifestations. Cardiac involvement in MD1 is characterized by fibro-fatty infiltration leading mostly to conduction disturbances and arrhythmias as well as to an increased risk of sudden cardiac death (SCD). Additionally, cardiomyopathy with LV dilatation and/or systolic dysfunction as well as non-specific late gadolinium enhancement (LGE) patterns are described in up to 40% of cases. However, the relationship between myocardial and electrical abnormalities is still unclear.

Methods: Fifty-five MD1 patients (43±13 yrs, 46% male) prospectively underwent multi-parametric CMR studies comprising cine- and LGE-CMR as well as ECG monitoring. A pathologic CMR was defined by either of: LV end-diastolic volume index (LV-EDVi) >100ml/m2, LV-EF 12 mm in males and >11 mm in females. An abnormal ECG included: rhythm other than sinus and any conduction abnormality.

Results: Abnormal ECGs were recorded in 29% (n=16) of the study patients whereas a pathologic CMR was found in 40% (n=22): 16% (n=9) had an impaired LV-EF (all mild or moderate), 33% (n=18) showed non-ischemic LGE with an intramural and/or subepicardial pattern and one patient had LV hypertrophy. In contrast to patients without ECG abnormalities, patients presenting with arrhythmia and/or conduction disturbances were older (48±9yrs vs. 41±14yrs, p=0.047) and showed more frequently presence of LGE (56% vs. 23%, p=0.027) and a pathologic CMR result (69% vs. 33%, p=0.038). However, there were no significant differences in LV-EF (58±6% vs. 60±7%, p=NS) or LV-EDVi (66±16ml/m² vs. 70±11ml/m², p=NS).

Conclusions: In this cross-sectional study, MD1 patients with conduction disturbances and/or arrhythmias were older and showed more frequently structural cardiac abnormalities as shown by LGE-CMR.

P230

Segmental Analysis of T2 and T1 Mapping in Patients with Clinical Acute Myocarditis: Evidence of Diffuse Myocardial Process

Emmanuelle Vermes, MD[1] Helena Daurel[2], Julien Pucheux, MD[3]

1. *CHU trousseau, Tours, Centre, France*
2. *CHU trousseau Tours, Centre, France*
3. *CHU Trousseau, Tours, Centre, France*

Background: Cardiac magnetic resonance (CMR) is an important diagnostic tool to establish the diagnosis of myocarditis. The detection of focal myocardial injury on T2 weighted images and late gadolinium enhancement (LGE) are criteria for the diagnosis. More recently, T2 and T1 mapping have emerged as promising techniques to detect injury by measuring global T1 and T2 indexes of the myocardium. However, no study has evaluated the ability of segmental measurement of T2 and T1 indexes to detect myocardial injury. The purpose of the study was to assess the ability of segmental analysis of T2 and T1 mapping for detecting myocardial injury in patients with clinical acute myocarditis .

Methods: CMR was prospectively performed in 47 patients referred for acute myocarditis within 5 days of the onset of symptoms and after 3 –month follow up. We also included 34 healthy controls. Images were acquired on a 1.5 Tesla scanner including T2 mapping (T2 prepared-SSFP) and T1 mapping using a modified look locker inversion recovery sequence (MOLLI) at, mid level in short axis view. Segmental analysis was performed by tracing a ROI in 6 segments of the myocardium according to the AHA segmentation. T2 and T1 values were measured before and 15 minutes (for T1 mapping) after contrast administration. LGE images were acquired in short and long axis view. The results are expressed by the median and the 5th and the 95th percentiles.

Results: Compared with control subjects, T2, native T1 and ECV values were significantly higher in all segments except the anteroseptal region (cf Table). Post contrast T1 indexes were not significantly different between the 2 groups. Out of 47 patients, LGE was absent in 6 patients. However, T2, native T1 and ECV indexes were significantly higher in these 6 patients compared to the control group. At 3 month-follow up, T2, native T1 and ECV indexes were significantly lower compared to the acute phase and were not significantly different from the control group

Conclusions: Segmental analysis of T2, T1 and ECV indexes demonstrated that myocarditis is a diffuse process involving all segments of the myocardium (except the antero septal region) either LGE is present or absent. Further studies are required to confirm these data.

p	Control group n=34	Myocarditis group n=47	
			T2 indexes by segment (ms)
0,046	50 [48-52]	52 [49-56]	anterieur
0.028	51 [49-53]	52 [49-58]	antero-lateral
0.011	51 [49-54]	54 [50-58]	infero-lateral
0.026	51 [50-54]	54 [50-57]	inferieur
0.04	51 [47-54]	53 [51-56]	infero-septal
0.407	52 [50-55]	52 [49-58]	antero-septal
			Native T1 indexes by segment (ms)
0.010	946 [924-989]	980 [950-1037]	anterieur
0.02	943 [911-978]	973 [933-1026]	antero-lateral
0.044	986 [944-1009]	1000 [974-1064]	infero-lateral
0.046	977 [952-1006]	1029 [995-1074]	inferieur
0.044	950 [926-962]	966 [926-998]	infero-septal
0.878	949 [928-977]	935 [912-992]	antero-septal
			ECV by segment (%)
0.013	0.22 [0.21-0.25]	0.26 [0.22-0.29]	anterieur
0.02	0.22 [0.206-0.24]	0.26 [0.21-0.28]	antero-lateral
0.01	0.22 [0.20-0.24]	0.25 [0.23-0.31]	infero-lateral
0.01	0.22 [0.20-0.24]	0.26 [0.22-0.29]	inferieur
0.03	0.22 [0.21-0.23]	0.24 [0.22-0.27]	infero-septal
0.171	0.23[0.21-0.25]	0.24 [0.22-0.26]	antero-septal

P231

Harmonic Phase versus Feature Tracking for Evaluating Regional Myocardial Function in Hypertrophic Cardiomyopathy

El-Sayed H. Ibrahim, PhD[1] Eric Kersjes[2], Sara Saberi, MD[2], Sharlene Day, MD[2], Prachi Agarwal, MD[2]

1. *University of Michigan, Ann Arbor, MI*
2. *University of Michigan, MI*

Background: CMR Imaging is often used in hypertrophic cardiomyopathy (HCM) for assessing morphology and function. However, global function measures, e.g. ejection-fraction (EF), do not provide information about abnormal myocardial contractility patterns due to the compensatory effects of different myocardial regions. Regional function analysis by CMR tagging provides valuable information about myocardial deformation, which may allow for early intervention and improved outcome. CMR feature tracking (CMR-FT) is a recently developed technique for measuring myocardial deformation. In this study, we evaluate CMR-FT for measuring myocardial strain in HCM and compare the results to harmonic-phase (HARP) tagging analysis.

Methods: Fifteen HCM patients (8 males; ages=48±14y.o.; HR=67±8.6bpm; BP=119±13/73±10mmHg) underwent 1-2 CMR scans over a period of 4 years, which resulted in total of 20 different scans. Each CMR scan included cine (short-axis slices covering the heart) and tagged (basal, mid-ventricle, and apical short-axis slices) imaging. The tagged images were analyzed using HARP (Myocardial Solutions) to measure circumferential (Ecc) and radial (Err) strain, while the cine images were analyzed by QStrain (Medis) to measure Ecc and Err, as well as EF. Statistical paired *t*-test and correlation analysis were conducted between the measurements by the two techniques.

Results: Both HARP and QStrain successfully analyzed all acquired images (Figures 1 and 2). EF=63±8.2. Global Ecc was -17.3±1.9% (range=-11.7 – -20.0%) by HARP and -19.1±4.4% (range=-12.4 – -26.1%) by QStrain. Global Err was 35.1±12.4% (range=12–56%) by HARP and 57.5±11.1% (range=39.4–80.3%) by QStrain. Basal, mid-ventricle, and apical Ecc (Err) by HARP were -17.9±2.6% (30.5±15.6%), -18.2±2.0% (32.4±18.4%), and -18.0±1.7% (44.7±21.4%), respectively. Ecc and Err measurements were different (P=0.07) and significantly different (P < 0.001), respectively, by QStrain compared to HARP. Ecc measurements showed moderate correlation between the two techniques (R=0.41; Figure-3), while Err measurements were uncorrelated (R < 0.1). Both global Ecc and Err by HARP as well as global Err by QStrain showed moderate correlation with EF (R=0.37-0.4), while only global Ecc by QStrain showed high correlation with EF (R=0.83).

Conclusions: Global Ecc can be used to evaluate myocardial contractility by either tagging or CMR-FT; however, the measurements by the two techniques are not interchangeable in the HCM population. The lack of correlation between Err measurements by the two techniques could be attributed to the large tag spacing compared to wall thickness, which affects Err measurement by tagging. The high correlation between EF and Ecc by QStrain reflects the averaging nature of CMR-FT, which makes it more suitable for evaluating global, rather than regional, cardiac function.

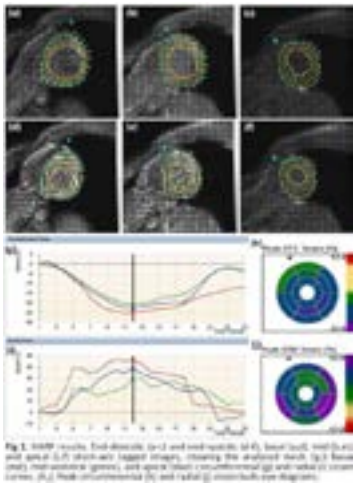

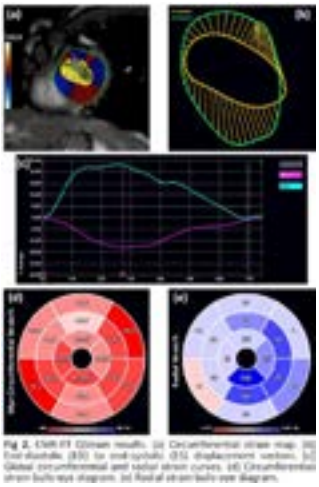

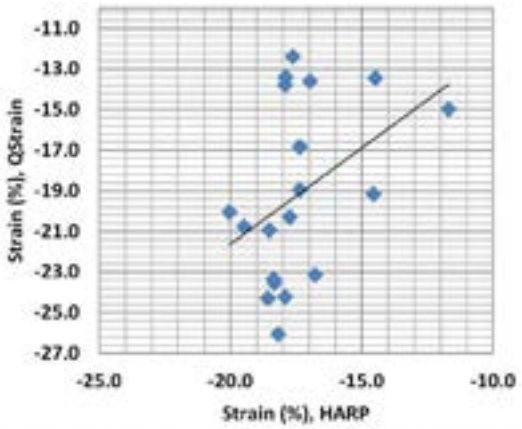

Fig 3. Correlation analysis of circumferential strain measured by HARP and QStrain (R = 0.41).

P232

Regional Travel Award Application: Adolescence with Duchenne and Becker Muscular Dystrophy: A Cardiac Magnetic Resonance Comparison Study

Thomas P. Johnston, M.D.Linda Cripe, MD, Kan Hor, MD
Nationwide Children's Hospital, Columbus, OH

Background: Duchenne muscular dystrophy (DMD) is the most common neuromuscular disease with high prevalence of DMD-associated heart disease as defined by late gadolinium enhancement (LGE) indicative of myocardial fibrosis and progressive ventricular dysfunction by ejection fraction (EF). The use of cardiac magnetic resonance imaging (CMR) is standard at our institution for DMD patients when sedation is no longer required. LGE by CMR occurs early in DMD patients and is an established marker of myocardial fibrosis which precedes systolic dysfunction. In contrast, patients with Becker muscular dystrophy (BMD) are assumed to have a milder cardiac phenotype and thus have later and less frequent CMR evaluation. As such, it is less well characterized with reports of LGE and dysfunction in the third decade of life. We hypothesize that BMD patients will demonstrate high prevalence of LGE and EF abnormality (EF < 55%) in late adolescence similar to DMD patients.

Methods: We reviewed our CMR database for BMD and age-matched DMD patients with complete CMR studies blinded to the patients CMR findings. Statistical analysis was performed using a two-sided unpaired Student's t-test for continuous data. The presence of LGE was dichotomized.

Results: Of the DMD patients, 23/30(77%) were LGE positive compared to 10/22(45%) of BMD patients with no difference in age. The mean age for LGE positive versus negative BMD patients was 22.7 ± 6.4 and 15.7 ± 4.8 years respectively. The mean age for LGE positive versus negative DMD patients was 19.9 ± 2.6 and 17.9 ± 2.0 years. The youngest LGE positive BMD patient was 15.7 years of age. Of those with positive LGE, 12/23 (52%) of DMD had abnormal LVEF while 6/10 (60%) of BMD had abnormal LVEF. LGE positive DMD patients had a significantly lower LVEF of 50.5 ± 12.1% compared with 61.3 ±5.1% for LGE negative patients. LGE positive BMD patients also trended toward a lower LVEF of 50.3 ± 8.4% versus 59.9 ± 4.6% for LGE negative patients, although this did not achieve statistical significance (Table 1).

Conclusions: This study demonstrates a higher prevalence of LGE and ventricular dysfunction in BMD patients by late adolescence approaching that of age-matched DMD patients. Although BMD patients have been reported to have milder cardiac disease a substantial percentage of these adolescent BMD patients have LGE and ventricular dysfunction than previously reported. Larger studies will be needed to confirm this finding.

DMD verus BMD CMR Results

p value	BMD (n= 22)	DMD (n=30)	
0.722	19.4(6.5)	18.9(2.6)	Age
0.922	59.1(4.8)	59.2(6.1)	RVEF(%)
0.591	55.5(11.6)	52.6(8.1)	LVEF(%)
.001	145.4(25.9)	107.7(29.3)	RVEDV(ml/m^2)
.007	158.8(36.7)	126.2(47.6)	LVEDV(ml/m^2)
	10(45)	23(77)	LGE + (%)
0.204	22.7(6.4)	19.9(2.6)	Age
0.972	50.3(8.4)	50.5(12.1)	LVEF
	6(60)	12(52)	Total Abn LVEF*(%)

*Defined as LVEF <55%

P233

The association between coronary flow reserve, extracellular volume fraction and left ventricular function in patients with non-ischemic dilated cardiomyopathy

Yoshitaka Goto, MD[1]Masaki Ishida, MD[2], Akimasa Yamada, MD[3], Mio Uno, MD[2], Wakana Makino, MD[1], Motonori Nagata, MD[1], Yasutaka Ichikawa, MD[2], Kakuya Kitagawa, MD[2], Hajime Sakuma, MD[4]

1. *Department of Radiology, Mie University Hospital, Tsu, Mie, Japan*
2. *Radiology, Mie, Japan*
3. *Radiology, Tsu, Mie, Japan*
4. *Department of Radiology, Mie University Hospital, Mie, Japan*

Background: Myocardial fibrosis and left ventricular (LV) dysfunction are the known clinical predictors for the adverse events in patients with non-ischemic dilated cardiomyopathy (DCM). In addition, several studies reported that coronary flow reserve (CFR) was impaired in patients with DCM and associated with an increased risk of adverse events. However, it has not fully understood that whether reduced CFR was associated with myocardial fibrosis and cardiac function in the patients with DCM. The aim of this study was to investigate the association between CFR measured in the coronary sinus, global extracellular volume fraction (ECV) and LV volumetric and functional parameters in patients with DCM.

Methods: Twenty patients (17 male, mean age 58 ± 13 yr.) with DCM who underwent CMR at 3.0T including MR flow measurements in the coronary sinus during ATP stress and in the resting state, cine CMR, pre- and post-contrast T1 mapping and LGE CMR were studied. CFR was calculated as the ratio of stress blood flow divided by rest blood flow in the coronary sinus. T1 mappings were performed with a modified Look-Locker inversion recovery sequence on 3 LV short-axis slices (basal, mid, and apical). ECV was determined from pre- and post-contrast T1 maps with correction of hematocrit measure. Global ECV was determined as a mean value of three short-axis slices. LV volumetric and functional parameters were measured in cine CMR. LV global longitudinal peak strain was measured by feature tracking analysis of cine CMR.

Results: Baseline data are summarized in Table 1. The CFR and global ECV were 3.04±0.78 and 30.0±3.0%, respectively. LGE was observed in 6 of the 20 patients on LGE CMR. There was no significant difference between CFR in patients with LGE and those without LGE (3.12±0.79 vs. 3.00±0.83, p=0.980). Linear regression analysis demonstrated that CFR had only weak association with global ECV (β = -0.991, R2 = 0.142, p = 0.101), LV volumetric and functional parameters, while global ECV was significantly associated with LV volumes, LV mass and LV longitudinal strain (β = 0.449, R2 = 0.262, p = 0.021) (Figure 1 and Table 2).

Conclusions: CFR showed weak association with ECV and LV volumetric and functional parameters, generating the hypothesis that CFR might be an independent predictor among known clinical parameters including myocardial fibrosis and LV dysfunction for the adverse outcome in patients with DCM.

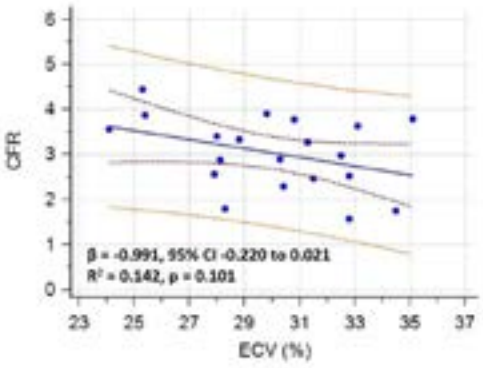

Table 1. Baseline data in 20 patients with DCM

58±13	Age (yr.)
17 / 3	male/female
1.75±0.2	BSA (m^2)
130.2±36.9	EDV index (ml/m^2)
87.6±34.6	ESV index (ml/m^2)
71.1±16.4	LV mass index (g/m^2)
34.6±9.2	LVEF (%)
-11.2±3.4	Longitudinal strain (%)
6 (30%)	LGE positive
3.0±0.8	CFR
30.0±3.0	ECV (%)

BSA; body surface area, EDV; end diastolic volume, ESV end systolic volume, LV; left ventricular, EF; ejection fraction, LGE; late gadolinium enhancement, CFR; coronary flow reserve, ECV; extra cellular volume fraction

Table 2. Linear regression analysis of CFR, ECV and LV parameters

ECV			CFR			
R^2	p value	β	R^2	p value	β	
—	—	—	0.142	0.101	-0.099	ECV
0.257	0.023	0.041	0.031	0.455	-0.004	EDV index
0.220	0.037	0.040	0.010	0.700	-0.002	ESV index
0.209	0.043	0.083	0.113	0.148	-0.016	LV mass index
0.030	0.469	0.425	0.046	0.364	-0.138	Cardiac index
0.139	0.106	0.120	0.001	0.903	-0.002	LVEF
0.262	0.021	0.449	0.005	0.774	-0.016	Longitudinal peak strain

P234

Diffuse myocardial pathology determined by extracellular volume cardiovascular magnetic resonance imaging is clinically common and independent of focal myocardial scar

Magnus Lundin, MD[1] Peder Sörensson, MD, PhD[2], Peter Kellman, PhD[3], Andreas Sigfridsson, PhD[4], Martin Ugander, MD, PhD[5]

1. *Karolinska institutet, Stockholms Lan, Sweden*
2. *Karolinska University Hospital, Stockholms Lan, Sweden*
3. *Laboratory of Cardiac Energetics, National Institutes of Health/NHLBI, Bethesda, MD, United States., MD*
4. *Karolinska Institute, Stockholm, Stockholms Lan, Sweden*
5. *Karolinska Institutet, Stockholms Lan, Sweden*

Background: Myocardial extracellular volume fraction (ECV) cardiovascular magnetic resonance (CMR) enables quantitative myocardial tissue characterization to identify diffuse pathology not detected using late gadolinium enhancement (LGE) images, and these findings have prognostic significance. The aim of the study was to better understand the clinical utility of ECV CMR by determining the prevalence of increased myocardial ECV and relate this to cardiac systolic function, left ventricular (LV) size and LGE findings.

Methods: Consecutive patients (n=666, median age 54 years, 63% male) referred for clinical CMR of known or suspected heart disease were prospectively enrolled. CMR was undertaken at 1.5T using LGE and Modified Look-Locker Inversion recovery (MOLLI) sequences. ECV images were generated using MOLLI T1 mapping before and 15-30 minutes after intravenous contrast (gadoteric acid, 0.2 mmol/kg), and calibrated to hematocrit. LGE images were examined for focal lesions, and diffuse changes by ECV were defined as ECV>30% in regions without LGE abnormalities. Increased LV end-diastolic volume index and decreased ejection fraction (EF) were determined as >3 standard deviations from the gender-specific normal mean.

Results: Out of 666 patients, 11.6% had diffusely increased ECV, and 7.5% of all patients had diffusely increased ECV without any focal LGE findings, see Figure. Diffusely increased ECV was found in 16.5% of patients with a dilated LV, and in 9.5% of patients without dilatation (p=0.01). Focal LGE was found in 53% of patients with decreased EF and in 30% of patients with normal EF (p < 0.001).

Conclusions: One in nine patients had diffusely increased ECV and 1 in 13 had diffusely increased ECV without any focal LGE findings in this consecutive clinical population. Increased ECV was more common in patients with a dilated LV, whereas focal LGE findings were much more common in patients with decreased systolic function. This study demonstrates that it is clinically common that ECV CMR provides additional diagnostic information beyond LGE and imaging of LV size and systolic function.

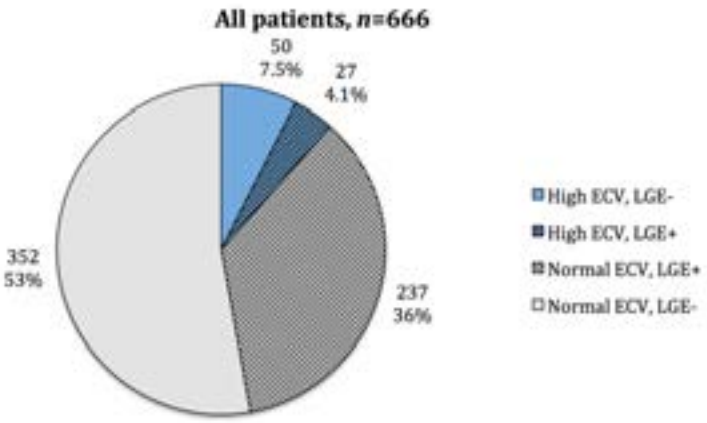

P235

Biopsy-based calibration of T2* magnetic resonance for estimation of cardiac iron concentration

Antonella Meloni, PhD[1]Aurelio Maggio, MD[2], Filippo Leto, MSc[2], Daniele De Marchi, RT[3], Vincenzo Positano, MSc[3], Laura Pistoia, MSc[3], Lorella Pitrolo, MD[4], Alessia Pepe, MD, PhD[3]

1. *Fondazione G. Monasterio CNR Regione Toscana, Pisa, Toscana, Italy*
2. *Ospedale "V. Cervello", Sicilia, Italy*
3. *Fondazione G. Monasterio CNR Regione Toscana, Toscana, Italy*
4. *Ospedale "V. Cervello", Toscana, Italy*

Background: The measurement of myocardial iron by T2* CMR has been established as fundamental to the best practice management of thalassemia. However, iron calibration data in humans is limited and CMR calibration varies according to instrumentation and technique.
The aim of this study was to calibrate the T2*-CMR technique for noninvasive cardiac iron assessment, by considering a segmental approach.

Methods: Four human hearts were studied from transfusion-dependent patients after their death within the MIOT network (Myocardial Iron Overload in Thalassemia). A multislice multiecho T2* approach was adopted. After CMR, used as guidance, the heart was cut in three short-axis slice and each slice was cut into different equiangular segments, the same ones in which the T2* was assessed. Tissue iron concentration in the segments was measured with inductively coupled plasma atomic emission spectroscopy.

Results: T2* and iron concentration were overall assessed in 36 myocardial segments: 6 in the first heart (year 2004), 6 in the second one (year 2004), 8 in the third one (year 2005), and 16 in the fourth one (year 2010),
Figure 1A shows the segmental iron concentration (in milligrams per gram dry weight) plotted versus the correspondent segmental T2* value (in milliseconds). As expected, the relationship was not linear. In Figure 1B the R2* values (R2*=1000/T2*, in s^{-1}) were considered. Regression analysis yielded a linear calibration of the following form: $[Fe]_{R2*}$ =0 .0079 × R2* - 0.1262 (R-square=0.999).

Conclusions: As in the only previously proposed calibration curve by Carpenter et al Circulation 2011, we did not collected hearts with an intermediate iron burden. We found an excellent linear agreement between R2* and cardiac iron with a model similar to the calibration curve in the gerbil showed by Wood J et al Circulation 2005. The results further validate the current clinical practice of monitoring cardiac iron in vivo by CMR.

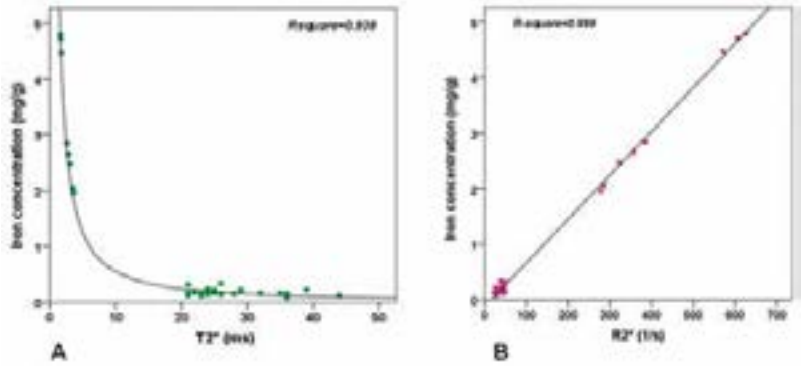

P236

Evolution of late gadolinium enhancement burden in the early phase of acute myocarditis

Patrizia Pedrotti, MD[8]Enrico Ammirati, MD[1], Francesco Moroni, MD[2], Angelica Peritore, MD[3], Paola Sormani, MD[4], Angela Milazzo, MD[5], Giuseppina Quattrocchi, MD[5], Manlio Cipriani, MD[3], Fabrizio Oliva, MD[3], Cristina Giannattasio, MD[6], Maria Frigerio, MD[3], Alberto Roghi, MD[5], Paolo Camici, FACC FESC[7]

1. *Department of Cardiology and Cardiac Surgery ASST Grande Ospedale Metropolitano Niguarda Milano, Italy, Milano, N/A, Italy*
2. *Università Vita e Salute - Milano - Italy, N/A, Italy*
3. *Departmente of Cardiology and Cardiac Surgery ASST Grande Ospedale Metropolitano Niguarda Milano, Italy, N/A, Italy*
4. *Health Science Department - Bicocca Univeristy - Milano - Italy, N/A, Italy*
5. *Department of Cardiology and Cardiac Surgery ASST Grande Ospedale Metropolitano Niguarda Milano, Italy, Lombardia, Italy*
6. *Department of Cardiology and Cardiac Surgery, ASST Grande Ospedale Metropolitano Niguarda, Milano, Italy, Milano, Lombardia, Italy*
7. *Vita Salute University San Raffaele, N/A, Italy*
8. *Department of Cardiology and Cardiac Surgery ASST Grande Ospedale Metropolitano Niguarda, Milano, Italy, Milano, Lombardia, Italy*

Background: Acute myocarditis (AM) is an inflammatory disease of the heart muscle. Clinical presentation and outcome are variable, ranging from asymptomatic to fulminant myocarditis (FM). Cardiac magnetic resonance (CMR) is increasingly employed in the diagnosis and follow-up (f.u.) of AM.

Methods: We retrospectively analyzed 75 consecutive pts (68 M;median age 33 yrs) with AM who underwent CMR within 30 days (median 6 days) from clinical presentation;17 (23%) pts had FM. Cine, STIR T2-w and late-enhancement (LE) images were acquired on matching planes (1.5 T, Siemens Avanto, Germany; gadobutrol, Gadovist, Bayer-Schering, 0.15 mmol/kg). CMR diagnosis of AM was based on Lake Louise Criteria. Biventricular indexed end-diastolic and end-systolic volumes and ejection fraction were calculated (Argus Software, Siemens, Germany).The volume of LE (LE%) was calculated using a single threashold vs reference myocardium technique, with a threashold ≥ 5DS (Medis,The Neatherlands). 47 follow-up (f.u.) scans were available and were similarly analyzed.

Results: Median baseline left ventricular ejection fraction (LVEF) was 64% (IQR:56-67%) and LE% 9.4% (IQR:7.4-13.1%). LE% was correlated with LV end-systolic volume index (LV-ESVi, r=+0.32; p=0.005) and LVEF (r=-0.29; p=0.01). Baseline LE% was inversely correlated with time between admission and CMR scan (r=-0.28; p=0.015). A similar pattern was present in the 58 hemodynamically stable patients in whom CMR was performed after a median of 5 days. Baseline LE% was higher in patients with LVEF < 55% (13.9% [10.3-19.0%]) compared with those with LVEF ≥55% (8.8% [6.8-10.7%]; p=0.004),Figure 1A. Patients with FM performed CMR later (median time 14 days, IQR:7-22;p=0.0005) and had LE% comparable to non-fulminant AM. The latter could be partly explained by the delayed time to CMR in the FM group.In the 47 patients that repeated CMR at f.u., a significant decrease of LE% was observed (Figure 1B). No correlation was found between baseline LE% and LVEF at f.u. (r=-0.19; p=0.19) nor between LE% at f.u. and LVEF at f.u. (r= -0.15; p=0.31).Similar results were obtained correlating baseline and f.u. LE% with LV-ESVi at f.u. The median clinical f.u. for the 75 patients was 4.2 years (2.6-5.9), and neither cardiac deaths nor heart transplantations were reported.

Conclusions: In the acute phase of AM the extent of LE is a dynamic process that reflects impairment of LV function (significant correlation with increased LV-ESVi and decreased LV-EF). Furthermore, LE% is time dependent (inverse correlation with time to first CMR, and significant decrease of 35%, at 4 months from the first exam). It is likely that in the acute phase the extent of LE is highly compounded by tissue oedema, while at f.u. LE will mainly reflect permanent myocardial scarring. Repeat CMR and quantitative LE% assessment could help tracking the evolution of myocardial oedema, complementing standard T2-w and newer mapping techniques, to monitor pts early after AM and possibly to guide treatment.

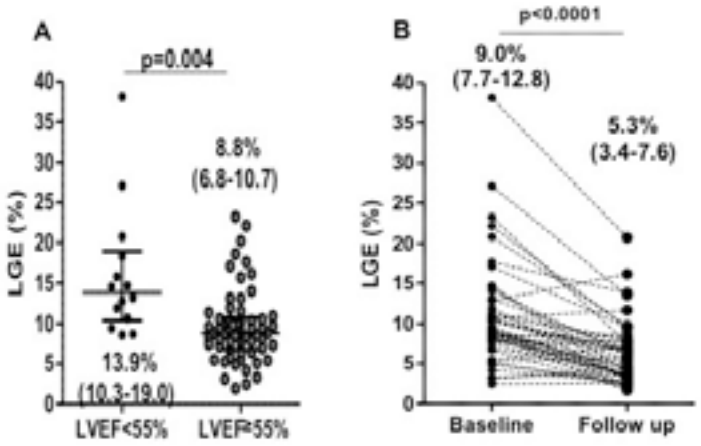

P237

Regadenoson-induced microvascular dysfunction in children with hypertrophic cardiomyopathy.

Lazaro E. Hernandez, M.D.

Joe DiMaggio Children's Hospital, Hollywood, FL

Background: Microvascular dysfunction in hypertrophic cardiomyopathy (HCM) has been associated with poor clinical outcome. Several studies have demonstrated a reduced perfusion reserve particularly in the endocardium proportional to the magnitude of the hypertrophy. To the best of our knowledge no data have been published about the use of regadenoson to detect microvascular dysfunction in children with HCM.

Methods: ***Patient population***: We reviewed our initial clinical experience with regadenoson stress CMR in 10 subjects (mean 16.8 years) with clinical and echocardiographic diagnosis of HCM as part of our ongoing analysis. ***Acquisition protocol***: CMR images were acquired using a 1.5-T Siemens Aera (18-elements phased array cardiac coil). Retrospective gated cine images were acquired using a steady-state free precession (SSFP) sequence. Coronary vasodilatory stress was achieved by injecting 0.4 mg of regadenoson. Aminophylline was administered to reverse effect of regadenoson. The dynamic perfusion during stress and at rest was obtained by administering 0.05 mml/kg IV of gadolinium. Native T1 using a modified look-locker (MOLLI) sequence was performed in three SAX slices of the left ventricle before and after the administration of regadenoson. Myocardial viability images were obtained. ECG and blood pressure were monitored during the entire exam as protocol. Patients were observed for about 90 minutes after the exam. ***Data analysis:*** Myocardial perfusion and delayed enhancement images were reviewed by a pediatric cardiologist.

Results: Exams were completed as planned with no serious adverse events. Chest discomfort and palpitations were the most common side effects (n=4). Patients with wall thickness ≥ 20 mm (n=4) developed subendocardial and transmural ischemia 60 seconds after the administration of regadenoson (peak stress). Premature ventricular contractions were recorded in these 4 patients. Native T1 values pre and post regadenoson were unchanged in those segments of ischemia and significantly higher post regadenoson in the normally perfused myocardium. Gadolinium delayed (10 min) enhancement was found in the ischemic areas. Rest myocardial perfusion was unremarkable in all the patients. 2 of the 4 patients with positive stress-CMR have undergone implantable cardioverter defibrillator (ICD) placement. Two patients were discontinued from competitive sport.

Conclusions: Despite the small number of patients, regadenoson stress CMR has proven to be very effective to induce myocardial ischemia during peak exercise in pediatric patients with HCM and microvascular dysfunction and therefore it has become in our practice an important imaging modality for the comprehensive evaluation and stratification of this patient population.

P238

Left Ventricular Trabeculation Extent is Associated with Reduced Myocardial Strain in Healthy Individuals

Jiashen Cai, B.Eng (Hons)[1], Jennifer A. Bryant, PhD[2]Calvin Woon-Loong Chin, MD, PhD[2], Antonio de Marvao, MB ChB, PhD[3], Declan O'Regan, MBBS, PhD[4], Stuart Alexander Cook, MBBS, PhD[2]

1. *Duke-NUS Medical School, N/A, Singapore*
2. *National Heart Centre Singapore, N/A, Singapore*
3. *MRC Clinical Sciences Centre, London, England, United Kingdom*
4. *MRC Clinical Sciences Centre, England, United Kingdom*

Background: Left Ventricular non-compaction (LVNC) can cause cardiomyopathy and is associated with heart failure and adverse cardiovascular events. Variable degrees of LV trabeculation are observed in healthy individuals, but their physiological consequence is unknown. Here we examined the relationship between myocardial morphology and function, and LV trabeculations in healthy individuals. We hypothesized that, as an extension of the LVNC cardiomyopathy phenotype, the degree of LV trabeculation in healthy individuals is associated with reduced myocardial function.

Methods: Cardiovascular magnetic resonance (CMR) was performed in 180 healthy Chinese (age 21 – 70 years; males, n = 91), using steady state free precession cine imaging at 3T (Ingenia, Philips). The degree of LV trabeculation was assessed by fractal dimension (FD, a dimensionless robust measure of trabeculation complexity) from LV short axis (LVSA) cine images using a semi-automated technique (MATLAB, Mathworks Inc). Myocardial deformation was evaluated using cvi42 (Circle Cardiovascular Imaging Inc.), with measurement of circumferential and radial strain from LVSA cine images and longitudinal strain from long axis cine images.

Results: LV trabeculation extent (assessed by global FD; mean 1.205 ± 0.031) was independently associated with increased indexed LV end-diastolic volume and indexed LV end-systolic volume (per % increase in global FD: LV EDVi, ß = 0.21 ml/m^2, $p < 0.001$; LV ESVi, ß = 0.08 ml/m^2, $p = 0.002$), after adjusting for other parameters (age, gender, BMI). Increased LV trabeculation was negatively associated with myocardial deformation across all three measures of global strain (circumferential, $r = -0.29$, $p < 0.001$; radial, $r = -0.20$, $p = 0.008$; and longitudinal, $r = -0.24$, $p = 0.001$; absolute values). In multivariable regression analysis, global circumferential strain alone remained independently associated with LV trabeculation extent (per % increase in global FD: ß = -0.024%, $p = 0.013$; absolute values).

Conclusions: Increased myocardial trabeculation is independently associated with reduced LV circumferential strain and increased LV volumes, which are features of cardiomyopathy. The functional effects of non-compaction and trabeculation may not confined to patients with LVNC, demonstrating a continuum of effect in health and disease.

http://www.ConferenceAbstracts.com/uploads/cfp2/attachments/LDFAIBDN/LDFAIBDN--217363-1-ANY(3).pdf

http://www.ConferenceAbstracts.com/uploads/cfp2/attachments/LDFAIBDN/LDFAIBDN--217363-2-ANY.pdf

P239

Detection of myocardial fibrosis and geometrical dysfunction in hypertrophic cardiomyopathy: Assessment by 3T high temporal tagged CMR

Eri Watanabe, MD, PhD[1]Michinobu Nagao, MD, PhD[1], Kenji Fukushima, MD, PhD[1], Akiko Sakai, MD, PhD[1], Tsuyoshi Shiga, MD, PhD[2], Shuji Sakai, MD, PhD[2], Nobuhisa Hagiwara, MD, PhD[2]

1. *Tokyo Women's Medical University, Shinjuku-ku, Tokyo, Japan*
2. *Tokyo Women's Medical University, Tokyo, Japan*

Background: Left ventricular (LV) circumferential strain (Ecc) measured by CMR tagging is a sensitive index of regional myocardial function and considered as the gold standard noninvasive method of assessment of LV deformation. However, the value of Ecc in patients with cardiac diseases has not been fully explored. The purpose of this study was to investigate the characteristics of geometrical dysfunction and the relation to late gadolinium enhancement (LGE) in hypertrophic cardiomyopathy (HCM) using the Ecc derived from tagged CMR.

Methods: 3-Tesla (Ingenia, Philips) CMR study including cine, tagging imaging, and LGE was performed for 17 patients who consisted of 5 patients with HCM, 6 patients with dilated cardiomyopathy (DCM), and 6 normal controls. Short-axis tagging imaging at basal, mid, and apical LV walls was scanned using TFEPI sequence with a resting grid pulse and had 50 phases per beat. According to the AHA segment model, myocardial segments were divided into 16 segments. Time-curve of Ecc strains for each segment was automatically drawn by available software (Ziostation2, Ziosoft). Ecc at end-systole was measured as peak Ecc, and was used as a functional parameter. Ecc-global, Ecc-basal, Ecc-mid and Ecc-apical were calculated and compared them among three patients groups. In addition, the Ecc between LGE positive and negative segments was compared.

Results: In patients with HCM, the peak Ecc was significantly lower for LGE positive segments (-9.1 ± 2.5%) than LGE negative segments (-14.2 ± 3.1%, $p < 0.0001$). Use of cutoff thresholds (-11.6%) for Ecc differentiated LGE positive segments from LGE negative segments with 84% sensitivity, 80% specificity, and areas under the curve of 0.89. In patients with DCM, there was no difference in the Ecc between LGE positive and negative segments (-6.9 ± 3.2% vs. -9.1 ± 4.4%, $p=0.058$). In addition, the Ecc-grobal, Ecc-basal, Ecc-mid, and Ecc-apical were significantly lower for patients with DCM than controls (-8.6 ± 3.2% vs. -15.8 ± 1.9%, $p=0.004$, -7.8 ± 2.3% vs. -14.8 ± 2.2%, $p=0.002$, -8.7 ± 3.4% vs. -15.9 ± 1.9%, $p=0.002$, -9.8 ± 4.5 vs. -17.3 ± 2.8%, $p=0.017$, respectively). Ecc-basal was significantly lower for patients with DCM than HCM (-7.8 ± 2.3% vs. -12.5 ± 1.6%, $p=0.009$). Ecc-grobal was significantly lower for patients with HCM than control (-12.6 ± 2.3% vs. -15.8 ± 1.9%, $p=0.03$).

Conclusions: Analysis of tagged CMR can non-invasively demonstrate the impairment of strain in the segments with fibrosis in patients with HCM.

P240

Left Ventricular Strain in Hypertrophic Cardiomyopathy: A Cardiac MRI Tissue Tracking Study

Stephanie Ambach[1] Vien Truong, MD[1], Michael Taylor, MD, PhD[2], John Jefferies, MD[2], Wojciech Mazur, MD[3]

1. *The Christ Hospital Health Network, Cincinnati, OH*
2. *Cincinnati Children's Hospital Medical Center, Cincinnati, OH*
3. *The Christ Hospital Health Network, Mason, OH*

Background: Hypertrophic cardiomyopathy (HCM) is associated with increased risk of sudden cardiac death, diastolic and systolic heart failure. The purpose of this study was to investigate left ventricular (LV) strain pattern in patients with hypertrophic cardiomyopathy using cardiac magnetic resonance tissue tracking (CMR TT).

Methods: Thirty patients with hypertrophic cardiomyopathy, mean age 50 ± 14 (years) underwent cardiac magnetic resonance imaging (CMR). All patients have preserved left ventricular ejection fraction defined as LVEF over 50%. Myocardial late gadolinium enhancement was present in all patients. LV longitudinal and circumferential strain was assessed by dedicated LV tissue tracking software. (Circle Cardiovascular Imaging Inc.)

Results: Thirty patients with images of sufficient quality were included in the analysis. There was no significant difference in age, gender, circumferential strain at base, mid-cavity, apex between patients and controls (P > 0.05 for each). However, there was significant decrease in longitudinal strain magnitude in hypertrophic cardiomyopathy patients compared with controls ($P < 0.01$) (Table).

Conclusions: Longitudinal but not circumferential strain is reduced in hypertrophic cardiomyopathy patients with normal LVEF but evidence of septal fibrosis. This finding is in contrast to previously published studies demonstrating reduction in circumferential strain in HCM population using echocardiographic or CMR derived harmonic phase imaging (HARP) techniques. Possible explanation of this discrepancy is a different stage of disease versus unique tissue tracking algorithm of CMR TT. Further studies directly comparing CMR TT to HARP derived circumferential strain in HCM population to validate this finding.

Left Ventricular Strain

P	Hypertrophic Cardiomyopathy (N=30)	Normal (N=28)	
0.79	50 ± 14	51 ± 16	Age (years)
0.07	9	15	Sex (female)
		-	LV Longitudinal strain (%)
<0.001	-14.60 ± 3.55	-18.28 ± 2.31	Global
<0.001	-14.24 ± 4.48	-18.58 ± 2.60	2-chamber
<0.001	-14.92 ± 4.66	-19.10 ± 2.62	3-chamber
0.012	-14.73 ± 3.92	-17.12 ± 2.97	4-chamber
			LV Circumferential strain (%)
0.82	-19.38 ± 3.39	-19.20 ± 2.40	Global
0.08	-16.72 ± 3.93	-18.52 ± 3.61	Basal
0.62	-18.89 ± 4.75	-18.38 ± 2.66	Mid-cavity
0.06	-22.54 ± 4.10	-20.70 ± 2.97	Apex

Continuous variable are expressed as mean ± standard deviation.
Categorical variables are presented as n.

P241

T1 mapping reproducibility in HFpEF: is native T1 or ECV more reproducible and comparison with healthy controls.

Vass Vassiliou, MA, MD[1]Hitesh Patel, MBBS PhD[2], Amrit Lota, BMBCh BA[3], Tamir Malley, MBChB[2], Hasan Mohiaddin, BSc[4], Brian Halliday, BSc (Hons) MBChB (Hons)[5], Shivraman Giri, PhD[6], Dominique Auger, MD, PhD[7], David N. Firmin, PhD[8], Dudley J. Pennell, MD[9], Peter D. Gatehouse, PhD[10], Sanjay Prasad, MD[9]

1. *Royal Brompton, London, England, United Kingdom*
2. *Royal Brompton Hospital, England, United Kingdom*
3. *NIHR Royal Brompton Cardiovascular Biomedical Research Unit and National Heart and Lung Institute, Imperial College London, England, United Kingdom*
4. *Royal Brompton, England, United Kingdom*
5. *Royal Brompton Hospital and National Heart and Lung Institute, Imperial College London, London, England, United Kingdom*
6. *Siemens Healthcare, IL*
7. *RBH, England, United Kingdom*
8. *NIHR Cardiovascular Biomedical Research Unit, Royal Brompton Hospital, England, United Kingdom*
9. *Royal Brompton Hospital and Imperial College, London, England, United Kingdom*
10. *NIHR Cardiovascular Biomedical Research Unit, Royal Brompton Hospital, London, England, United Kingdom*

Background: Diffuse fibrosis is an important predictor of outcome in all cardiomyopathies and likely to be a key determinant in the development of heart failure with preserved ejection fraction (HFpEF). T1 mapping allows a non-invasive estimation of diffuse fibrosis providing prognostic information but also a platform for serial measurements to assess increase or decrease of this type of fibrosis in response to pharmacotherapy. Atrial fibrillation (AF) occurs in ~50% of patients with HFpEF decreasing potentially the quality and precision of CMR.

Methods: A single centre pilot study to establish intrastudy reproducibility of native T1 maps and ECV using an 11 heart beat MOLLI T1 mapping (figure 1) as a measure of diffuse fibrosis in patients fulfilling ESC criteria for HFpEF, and compare native T1 maps and ECV with healthy controls. Ten HFpEF patients (age 72 age± 8 years. 5 male, 4 in sinus rhythm, 6 in AF) underwent CMR on an 1.5T Siemens Avanto with a MOLLI Siemens 448B sequence. Haematocrit was sampled on the day of the CMR before the scan and analysed in our biochemistry laboratory to enable calculation of ECV. Two repeats of the MOLLI sequence at the same location were undertaken to allow intrastudy reproducibility as a means of testing precision. The results were compared to 15 healthy volunteers (age 31±5 years, 8 male, all in sinus rhythm) using intraclass correlation coefficient (ICC).

Results: Overall, MOLLI had good intrastudy reproducibility in HFpEF patients both when sinus rhythm (SR) and AF as shown in figure 2. ICC for native T1 for the whole cohort= 0.853, whilst ICC for AF=0.903 and SR=0.771. ICC for ECV=0.903 for the whole cohort, for AF=0.835 and for SR=0.935. This compared satisfactorily to healthy controls who had ICC native T1 of 0.925 and ICC ECV of 0.924 (all in SR). Interestingly there was no evidence to suggest that HFpEF patients and controls had different native T1; 1036±32 vs 1017±27 respectively p= 0.14; however there was a significant difference in ECV; HFpEF 28.5%±2.6% vs 25.6%±2.6% in controls $p < 0.001$. This appeared to be driven primarily by different haematocrit 0.39±0.05 vs 0.44±0.06, for HFpEF and controls respectively, $p = 0.03$.

Conclusions: Our findings confirm a very good intrastudy reproducibility for the assessment of native T1 and excellent reproducibility for the assessment of ECV in patients with HFpEF, even in the presence of AF. As the reproducibility of HFpEF even in AF is high such patients should not be excluded from research with T1 mapping endpoints. Although both native T1 and ECV showed good reproducibility, the difference in haematocrit would explain similar native T1 between HFpEF and controls and also suggest that ECV might be a better (and more accurate) measure of diffuse fibrosis in the HFpEF population. T1 mapping with ECV might also enable a distinct cohort of HFpEF patients to be identified who are more likely to benefit from antifibrotic therapy.

http://www.ConferenceAbstracts.com/uploads/cfp2/attachments/LDFAIBDN/LDFAIBDN--222321-1-ANY(1).pdf

http://www.ConferenceAbstracts.com/uploads/cfp2/attachments/LDFAIBDN/LDFAIBDN--222321-2-ANY.pdf

P242

CMR in the Detection of Potential Causes of Sudden Cardiac Death in Professional Soccer Players

Erasmo De La Pena-Almaguer, MD[1], Alejandro R. Trevino, MD[2]Tania Vargas, MD[1], Francisco Garcia, MD[2], Emilio Frech, MD[2]

1. *Tecnologico de Monterrey, Monterrey, Nuevo Leon, Mexico*
2. *Tecnologico de Monterrey, Nuevo Leon, Mexico*

Background: Yearly, a high number of Sudden Cardiac Deaths (SCD) occur in professional sport players in which, SCD´s, are mainly caused by pre-existent heart disease. The International Football Association Federation (FIFA) has created a comprehensive Pre-Competition Medical Assesment (FIFA-PCMA) for determination of risks of SCD and to determine wether a prospective player is able to compete proffesionally, however, FIFA-PCMA is based mainly on questionnaire, ECG and ECHO, which may remain inconclusive in many cases. The main causes of SCD are HCM, ARVD and Anomalous origins of the Coronaries, all of which have shown a high diagnostic sensitivity and specificity by CMR.
We hypothetized that these 3 causes may be identified or ruled out by CMR alone.

Methods: We prospectively studied 20 professional Elite Soccer players who underwent a routine FIFA-PCMA and CMR on a 1.5 Tesla MR (Aera, Siemens Medical Solutions, Erlangen, Germany) scanner. Using SSFP Cines and Coronary Localizers, Left and Right ventricular EF, ventricular mass index, end-diastolic, end-systolic and stroke volume index, diastolic wall thickness, wall thickness ratio and diastolic and systolic wall-to-volume ratios were determined. Main origins of the of major coronary arteries were identified, and Hypertrophic cardiomyopathy as well as the revised ARVD CMR Diagnostic criteria were studied.

Results: Results for left and right ventricular function, wall thickness, mass and volumes are shown in table 1.
No evidence of diagnostic criteria for HCM, or ARVD were found in this population. In all athletes, the right and left coronary arteries and their proximal trayectory were visualized, with no cases of anomalous origins. All of the subjects had mild LV dilatation with preserved ventricular function, with diagnostic criteria for Athlete`s heart.

Conclusions: CMR was able to analyse and rule out the main causes of SCD in all the athletes studied, thus, suggesting that it could complement the current requirements established by FIFA in the assesment of the main causes of SCD. Further studies are warranted.

Table 1.

	LV*	RV*
Internal Dimension Diastole (mm)	60.42 ± 3.3	63.6 ± 11.3
Internal Dimension Systole (mm)	42.36 ± 4.2	-
EDV (ml)	197.3 ± 30.9	172.1 ± 32.8
EDV Index (ml/m2)	101.7 ± 14.8	88.9 ± 17.4
ESV (ml)	76.7 ± 15.1	85.3 ± 17.7
ESV Index (ml/m2)	39.5 ± 7.3	51.5 ± 33.8
LVPW (mm)	8.4 ± 1.9	-
IVSd (mm)	8.8 ± 1.7	-
LV Mass/Volume Ratio	0.09 ± 0.03	-
SV (ml)	120.6 ± 20.6	87.6 ± 20.4
SV Index (ml/m2)	62.4 ± 9.8	54 ± 33.6
CO (lt/min)	6.4 ± 1.4	4.6 ± 1.0
CI (lt/m2/min)	3.3 ± 0.6	2.4 ± 0.5
EF (%)	61.1 ± 4.5	50.9 ± 5.3
Mass (gr)	142.5 ± 26.1	-
Mass Index (gr/m2)	73.4 ± 12.6	-

* Values represent mean and standard deviation. LV: Left Ventricle; RV: Right Ventricle; LVPW: Left Ventricle Posterior Wall; IVSd: Interventricular Septum Diastole; EDV: End Diastolic Volume; ESV: End Systolic Volume; SV: Stroke Volume; CO: Cardiac Output; CI: Cardiac Index; EF: Ejection Fraction

P243

Age and Gender influences T2 mapping in Healthy Volunteers

Stefania Rosmini, MD, PhD[1] Heerajnarain Bulluck, MBBS[2], Giulia Benedetti, MD[3], Thomas Treibel, MBBS.MRCP(UK)[1], Amna Abdel-Gadir, MBBS.MRCP(UK)[4], Anish Bhuva, MRCP MBBS[1], Veronica Culotta, MD[5], Viviana Maestrini, MD[6], Marianna Fontana, MD, PhD[7], Anna Herrey, MD PhD MRCP[1], Charlotte Manisty, PhD MBBS[8], James Moon, MBBS, MD, MRCP[9]

1. *Barts Heart Centre, England, United Kingdom*
2. *University College London, England, United Kingdom*
3. *Barts Heart Centre, London, England, United Kingdom*
4. *University College London and Barts Heart Centre, London, England, United Kingdom*
5. *Barts Heart Centre, St Bartholomew's Hospital, England, United Kingdom*
6. *Sapienza University of Rome, Lazio, Italy*
7. *National Amyloidosis Centre, University College London, England, United Kingdom*
8. *Barts Heart Centre and university college, London, England, United Kingdom*
9. *Barts Heart Center, The Cardiovascular Magnetic Resonance Imaging Unit and The Center for Rare Cardiovascular Diseases Unit, St Bartholomew's Hospital, West Smithfield, London, UK, England, United Kingdom*

Background: T2 mapping can detect myocardial oedema (acute myocarditis, myocardial infarction) and is recently being investigated for prognostic significance in cardiomyopathies like amyloidosis, Fabry disease and sarcoid. However, normal reference ranges are not well defined. We investigated the influence of age, gender and heart rate (HR) on T2 values in a large healthy cohort of subjects.

Methods: 88 healthy volunteers with no known cardiovascular disease underwent CMR at 1.5 T (Siemens, Avanto). Basal-ventricular short axis native T2 maps consisting in 3 single-shot images at different T2 preparation times (0ms, 24ms, 55ms) were acquired (WIP 448B, Siemens Healthcare). The color maps (with MOCO) had manual epi-and endocardial contours drawn using cvi[42] (Calgary, Canada) and a 10% border erosion applied (Rosmini S, JCMR 2016;18:1-2) to reduce partial volume effects from blood pool. The mean T2 value was analysed globally the basal slice (Figure 1A) and for each of the 6 basal segments (Figure 1B).

Results: Mean age was 50±14 years, range 20-76 years, male 55%, with no age difference between genders (males 51±13 years; females 48±14 years, p=0.415). Median global T2 was 50(49-51)ms. T2 was heart rate independent (R^2=0.024, p= 0.397, global, same for regional). Global T2 increased with age (p= 0.004, R^2= 0.106 - Figure 2, by 2ms between 3rd and 4th decade and by 1 ms between 5th and 6thdecade). On a segmental basis, T2 values increased with age for the antero-septal and infero-septal, inferior and infero-lateral segments (p=0.004, p < 0.001, p=0.002 and p= 0.015, respectively) while there were no changes in T2 for the anterior and antero-lateral segments (p=0.439 and p=0.127, respectively). Women had slightly higher basal global T2 values compared to men [51 (49-52)ms vs 50(49-51)ms, p= 0.046). There was no gender difference for the anterior [52(49=54)ms; 50(49-52)ms, p=0.074), inferior [50(49-52)ms; 50(48-52)ms, p=0.393) and infero-lateral [49(47-50)ms,49(47-51)ms, p=0.886) segments, while T2 was higher in women in the antero-septal [51(49-53)ms vs 50(48-51)ms, p= 0.003), infero-septal 51(49-52)ms vs 49(48-51)ms, p=0.005) and antero-lateral 51(48-52)ms vs 49(48-51)ms, p=0.014) segments. Multivariate analysis showed age to be a stronger influence than gender on global T2 (Age: p= 0.001, Gender: p=0.007, cumulative R^2=0.181)

Conclusions: In health, T2 is not affected by HR. Global basal myocardial T2 increases slightly with age and is slightly higher in women than in men. Although statistically significant, in health variations of T2 with age and gender are subtle suggesting no need for specific reference ranges.

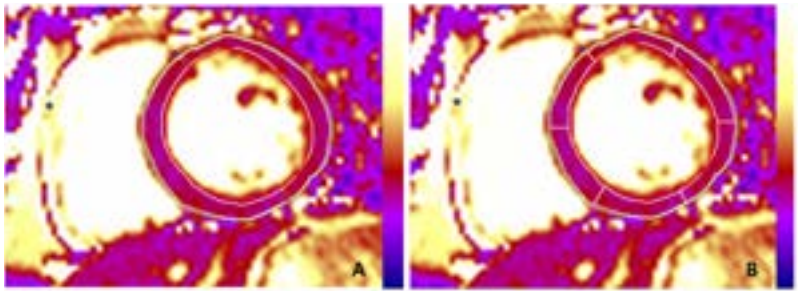

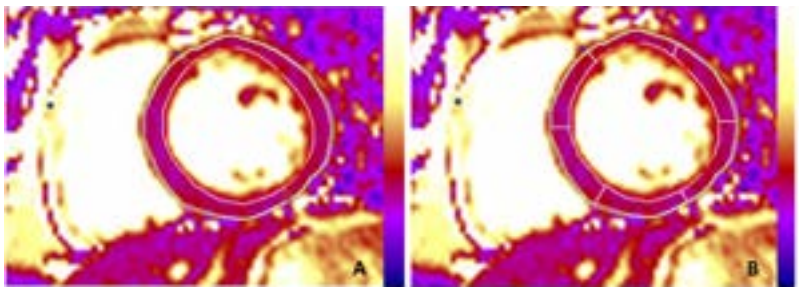

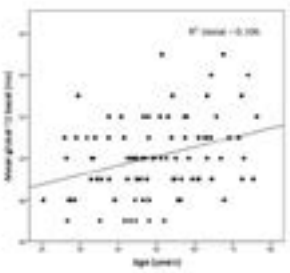

P244

Non-invasive quantification of right ventricular diffuse interstitial fibrosis in heart failure with preserved ejection fraction

Emily J. Li, BA[1] Jeremy Collins, MD[1], Brandon C. Benefield, MS[2], Stanley Swat, MD[3], Caitlin Brady, MS[4], Rebecca A. Ditch, BS[5], Rachel Davids[4], Benjamin H. Freed, MD[2]

1. *Northwestern University, Chicago, IL*
2. *Northwestern University Feinberg School of Medicine, Chicago, IL*
3. *Northwestern Memorial Hospital, Northwestern University Feinberg School of Medicine, IL*
4. *Northwestern University, IL*
5. *NORTHWESTERN UNIVERSITY, CHICAGO, IL*

Background: Right ventricular (RV) dysfunction is a powerful predictor of adverse outcomes in heart failure with preserved ejection fraction (HFpEF). RV diffuse interstitial fibrosis likely plays a significant role in the pathology of this disease but data on non-invasive methods to detect and quantify this type of fibrosis are lacking.

Hypothesis: HFpEF patients with pulmonary hypertension (PH) have significantly more RV than left ventricular (LV) diffuse interstitial fibrosis and a greater degree of RV fibrosis compared to controls.

Methods: Fourteen HFpEF patients with PH identified by right heart catheterization (RHC) (57% female, 70±6.1yrs) underwent cardiovascular MRI scanning (1.5T MAGENTOM Aera) within 30 days of the RHC (Table 1). Thirteen healthy volunteers (31% female, 48.8±12.4 years) were also included. T1 mapping was performed in the axial orientation using an investigational high-resolution modified look-locker inversion recovery (HR-MOLLI) technique with a 1x1 mm^2 in-plane resolution that applies motion correction with synthetic image estimation. Motion corrected images were used to generate parametric maps with (T1) and without (T1*) the MOLLI correction. The MOLLI sequence uses a 5 heart-beat (HB) acquisition, 3 HB recovery, 3 HB acquisition scheme with a single shot bSSFP diastolic readout. Images were acquired pre- and 10-25 minutes post- 0.2 mmol/kg gadobenate dimeglumine bolus infusion (Multihance, Bracco Diagnostics, Monroe, NJ). T1 and T1* parametric maps were used to quantify the T1 of tissue and blood, respectively. A reviewer quantified basal and mid RV free wall, interventricular septal, and lateral LV wall T1 values on T1 parametric maps. Extracellular volume (ECV) was calculated as originally described by Jerosch-Harold. Student's t-test was used to compare ECV values between HFpEF and controls as well as between LV and RV ECV. Pearson's correlation was used to compare RV ECV with RHC hemodynamics and MRI measures for RV size and function.

Results: RV ECV was significantly higher in HFpEF patients compared to controls, whereas there was no significant difference in LV ECV between HFpEF patients and controls (Figure 1). Furthermore, there was significantly more RV than LV diffuse interstitial fibrosis in the HFpEF patients (37±11% vs. 30±7%, p=0.002). There was no significant correlation between RV ECV and invasive hemodynamics or MRI parameters of size and function.

Conclusions: Patients with HFpEF have a significantly higher degree of RV diffuse interstitial fibrosis compared to controls and may be present despite significant PH or adverse RV remodeling. Although biventricular diffuse fibrosis is present, the RV appears to be particularly vulnerable. Non-invasive identification and quantification of RV diffuse interstitial fibrosis may provide mechanistic insight and a target for future therapies.

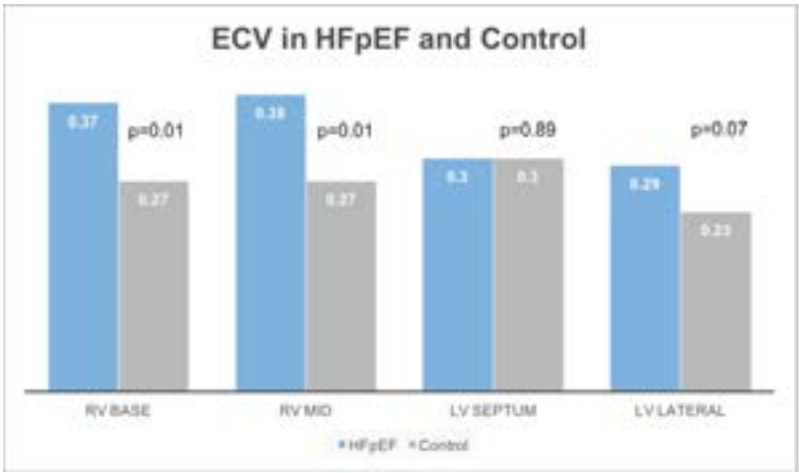

Summary of Demographics, Invasive Hemodynamics, and MRI Characteristics of the Study Cohort

Total Cohort (n=14)	Parameters
	Demographics
70±6.1	Age, y
8 (57)	Women, n (%)
2.1±0.4	BSA, m^2
	Invasive Hemodynamics
11.4±5.7	Right atrial pressure, mm Hg
6.7±3.6	RV diastolic pressure, mm Hg
52.6±18.0	PA systolic pressure, mm Hg
22.4±5.2	PA diastolic pressure, mm Hg
35.2±8.4	Mean PA pressure, mm Hg
18.2±5.4	PCWP, mm Hg
3.4±3.0	Pulmonary vascular resistance, WU
2.8±0.8	Cardiac index, $L/min/m^2$
	MRI
91.7±46.2	RV end-diastolic volume index, ml/m^2
50.3±31.9	RV end-systolic volume index, ml/m^2
47.7±8.3	RV ejection fraction, %

P245

Geometrical characterization of left ventricular hypertrophy in Fabry Cardiomyopathy: insight into pathogenesis

Antonia Camporeale, MD[1]Maurizio Pieroni, MD, PhD[2], Federico Pieruzzi, MD[3], Paola Lusardi, MD[4], Marco Spada, MD[5], Ilaria Tanini, MD[6], Silvia Pradella, MD[6], Federico Ambrogi, MS[7], Iacopo Olivotto, MD[6], Franco Cecchi, MD[6], Massimo Lombardi, MD[8]

1. *IRCCS Policlinico San DOnato, Milano, N/A, Italy*
2. *ASL8 Arezzo San Donato Hospital Via Pietro Nenni, 20, Toscana, Italy*
3. *ASST Monza - San Gerardo Hospital, Lombardia, Italy*
4. *San Giovanni Bosco Hospital, Torino, Piemonte, Italy*
5. *Department of Pediatrics, University of Torino, Piemonte, Italy*
6. *Careggi Hospital, Florence, Toscana, Italy*
7. *Department of Clinical sciences and Community Health, University of Milan, Lombardia, Italy*
8. *IRCCS Policlinico San Donato, Milan, Italy, Lombardia, Italy*

Background: Heart involvement in Anderson-Fabry disease (AFD) is characterized by left ventricular hypertrophy (LVH), often mimicking sarcomeric hypertrophic cardiomyopathy (HCM). Widespread application of cardiac magnetic resonance (CMR) in the evaluation of HCM allowed to describe a wide variety of hypertrophy patterns in both sarcomeric HCM and Fabry Cardiomyopathy (FC). More recently a longitudinal distribution of LVH with a spiral pattern has been identified in patients with asymmetrical septal HCM but has never been assessed in FC. We aim to characterize by CMR the geometrical distribution of LVH in a cohort of patients with genetic diagnosis of AFD.

Methods: From April 2009 to June 2016, 21 patients with genetic diagnosis of AFD (mean age 50 ± 14 years, 9 males) were referred for CMR at San Donato Hospital (Milan) or Careggi Hospital (Florence). The CMR protocol included cine sequences and post-contrast sequences for late gadolinium enhancement (LGE). Maximum end-diastolic wall thickness (mEDWT) was measured from cardiac short axis cine images according to a 16-segment model. LVH was defined as mEDWT ≥13 mm in male patients and mEDWT ≥ 12 mm in female patients without history of arterial hypertension.

Results: LVH was reported in 14 patients (67%, mean age 57 ± 11 years, 8 males) and septal to lateral wall ratio resulted > 1.3 (asymmetric LVH) in 9 patients. In all patients with LVH, a spiral distribution in a counterclockwise direction from basal antero-septal segment to mid ventricular infero-septal segment was observed, irrespective from the degree and the symmetry of LVH. Indeed basal antero-septal segment and mid-ventricular infero-septal segment presented the highest values of mEDWT in all the hypertrophic cases (correlation between segments 0,76; 95% CI: 0,38-0,92). Excluding the apical segments, mid ventricular anterior wall was found to be on average the thinnest segment, spared from LVH in all but one patient. LVH extended at the apical level in 4 patients. LGE was present in 9 patients (5 male), all of them with LVH, involving on average 2,7 (± 2.5) segments. Infero-lateral wall was the prevalent location for LGE in all but one patients, who showed LGE at apical anterior level.

Conclusions: LVH in AFD presents a spiral distribution in a counterclockwise direction, always involving basal and mid-ventricular septum and sparing the anterior wall. The presence of a common spiral pattern of LVH in sarcomeric HCM and FC supports the notion that in AFD cardiac wall thickening is due not only to Gb3 storage but also to myocyte hypertrophy resulting from activation of non-specific cellular hypertrophy pathways.

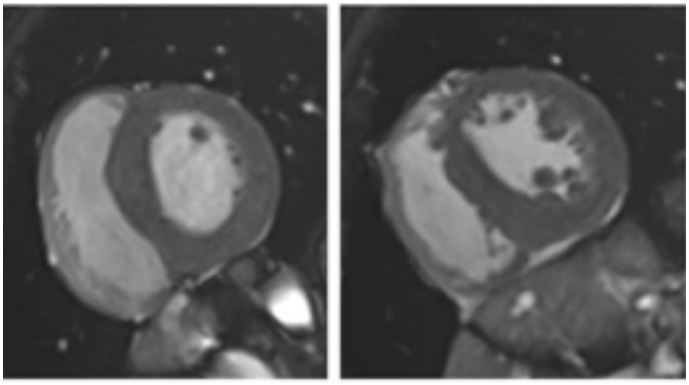

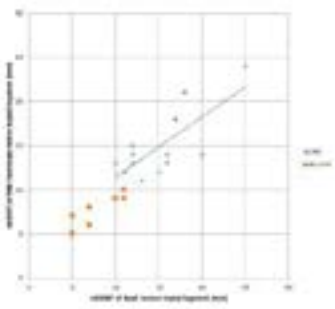

P246

Variations in late gadolinium enhancement in the interventricular septum in asymptomatic subjects

Hae jin Kim, Dr.[1], Yeon Hyeon Choe, MD, PhD[2]

1. Samsung Medical Center, N/A, Republic of Korea
2. Samsung Medical Center, Sungkyunkwan University School of Medicine, N/A, Republic of Korea

Background: The purpose of this study was to identify variations in the late gadolinium enhancement (LGE) in the left ventricular (LV) myocardium.

Methods: Among 1105 consecutive asymptomatic subjects (948 males and 157 females) who underwent stress perfusion CMR and LGE, 101 patients (91 males [mean age, 55 years; age range, 45-78 years], 10 females [mean age, 56 years; age range, 45-70 years]) exhibited areas of high signal intensity (thickness ≥ 4 mm) on LGE images and were included in this study. All the included subjects had normal LV ejection fraction (≥ 55%) and no stress-induced myocardial ischemia/infarction. Areas of high signal intensity were visually evaluated on LGE images 10 minutes after injection of 0.2 mmol/kg gadobutrol. The maximal thickness of plate-like LGE in the interventricular septum was measured on a workstation.

Results: There were areas of high signal intensity in a plate-like shape in basal and mid-anteroseptal interventricular septum and mid-to-basal inferoseptal trigone of right ventricle-LV junction in a triangular or focal round appearance in all the included subjects. The mean thickness of the high signal intensity plate was 5.7 mm (range, 4.4-8.0 mm) in the basal anteroseptal interventricular septum.

Conclusions: The fibrous portion of the interventricular septum (FIVS) may exhibit plate-like areas of high signal intensity of ≥ 4 mm in the middle myocardium of mid-to-basal interventricular septum in the asymptomatic subjects with normal LV function. One should be familiar with normal LGE variations and FIVS should not be misdiagnosed as a pathological condition such as cardiomyopathy.

P247

Native T1 and T2 mapping in left and right pressure overloaded hearts

Yuchi Han, MD[2]Jing Wang, MD[1], Hang Zhao, MD[1], Doris Cain, RT[2], jacqueline Meeks, RT[1], Howard Herrmann, MD[1], Walter R. Witschey, PhD[2]

1. *University of Pennsylvania, PA*
2. *University of Pennsylvania, Philadelphia, PA*

Background: Aortic stenosis (AS) is a disease where the left ventricle (LV) is under pressure overload and pulmonary arterial hypertension (PAH) is a disease where the right ventricle (RV) is under pressure overload. For patients with PAH, is the left heart also involved? For patients with AS, is the right side involved? How does the left versus right-sided pressure overload affect the septum? Our study aims to compare T1 and T2 relaxation times in left versus right-sided pressure overload.

Methods: We prospectively imaged 22 patients with PAH, 21 patients with severe AS, and 5 healthy volunteers on the same 1.5T MRI scanner (Avanto, Siemens, Germany). Cine cardiac function, native T1 (5/3/3/ MOLLI) and T2 (3 point T2-preped SSFP) images were obtained. Assessment of T1 and T2 relaxation time was obtained at the RV free wall (FW), superior RV insertion, inferior RV insertion, septum, and LV anterior wall on the mid-ventricular slice. T1 and T2 comparisons were carried out using Student t test between the groups. A p value < 0.017 was considered statistically significant.

Results: T1 values in PAH group were higher at septum, RV insertion and RV FW than AS group and control group, but only RV FW and RV insertion T1 value showed statistical significance($p=0.000$, $p=0.007$ respectively) between PAH group and control group . T1 value of the septum, RV insertion and RVFW in AS patients were greater than the control group, but lower than PAH group, however not statistically significant. In AS group, T2 value of septum, RV insertion and RV FW were greater than control group, but lower than PAH group. In the AS group, RV insertion and anterior wall T2 value were higher than controls ($p=0.000$, 0.017 respectively). PAH RV insertion T2 was significantly higher ($p=0.001$) than AS group. RV insertion T2 value was significantly correlated with both RV EDVI ($r = 0.608$, $P= 0.016$) and RV mass index ($r =0.57$, $P=0.026$) in PAH group. LV anterior wall and RV insertion T2 value was significantly correlated with aortic valve mean gradients in AS group ($r = 0.56$, $P= 0.02$; $r = 0.58$, $P= 0.01$, respectively). There were no significant correlations between T1 values and cardiac function parameters.

Conclusions: T1 and T2 relaxation time are markers of myocardial structure changes. T2 values may be more sensitive than T1 in detecting changes in the septum. In RV pressure overload, the impact on the septum may be greater than in LV pressure overload.

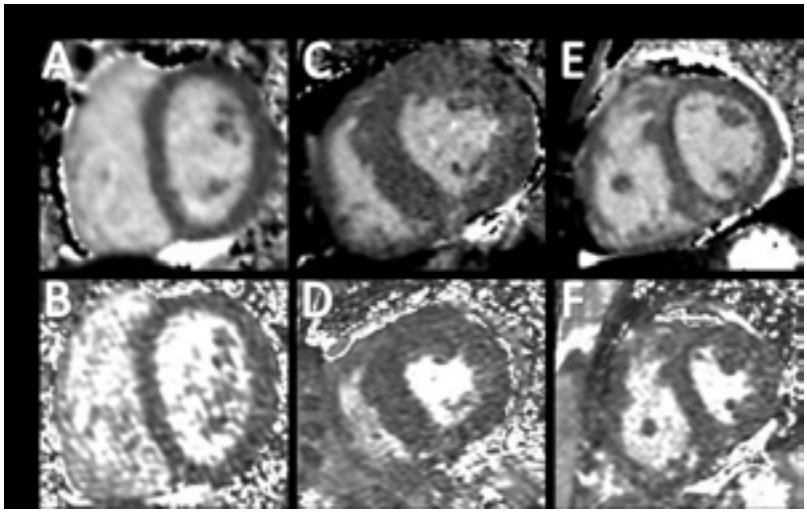

P248

Circumferential RV strain is reduced in patients with pectus excavatum

Stephanie Ambach[1] Vien Truong, MD[1], John Jefferies, MD[2], Wojciech Mazur, MD[3], Eric Crotty, MD[2], Candace Li, MD[2], Victor Garcia, MD[2], Michael Taylor, MD, PhD[2]

1. *The Christ Hospital Health Network, Cincinnati, OH*
2. *Cincinnati Children's Hospital Medical Center, Cincinnati, OH*
3. *The Christ Hospital Health Network, Mason, OH*

Background: Depression of the sternum in pectus excavatum patients distorts the RV geometry. Reduced RV systolic function in this patient population has been reported previously suggesting that these geometric changes may influence myocardial performance. However, the mechanism is not well understood. The purpose of the study was to investigate right ventricular (RV) strain patterns in pectus excavatum patients using cardiac magnetic resonance tissue tracking (CMR TT).

Methods: Fifty pectus excavatum patients, 10 to 32 years of age, underwent cardiac magnetic resonance imaging (CMR). Standard planimetric variables were measured for all studies. Dedicated RV tissue tracking software was used to calculate RV longitudinal and circumferential strain. (Circle Cardiovascular Imaging Inc.). The pectus patient strains were compared to those of a normal control group.

Results: Fifty patients with images of sufficient quality were included in the analysis. There was no statistically significant difference in age, right ventricular or left ventricular ejection fraction compared with normal controls ($P > 0.05$ for each). However, there was significant decrease in mid-cavity circumferential strain magnitude in pectus patients compared with controls ($P < 0.001$) (Table). There was no significant difference in RV global longitudinal between patients and controls ($P = 0.93$).

Conclusions: In the current study, extrinsic RV compression in patients with pectus excavatum did not result in reduction of RVEF, but there was significant reduction in RV circumferential strain. It appears the RV has some ability to compensate for limited circumferential contraction to preserve RV performance. Further studies are needed to establish clinical significance of this decreased strain.

Right ventricular strain

P	Pectus patient (n=50)	Normal (n=20)	
0.27	16 ± 4	17 ± 5	Age
0.12	55.06 ± 4.94	57.05 ± 4.44	RVEF
0.46	58.97 ± 4.07	58.20 ± 3.47	LVEF
0.93	-21.88 ± 4.63	-21.99 ± 3.58	RV longitudinal strain
<0.001	-11.31 ± 2.79	-16.19 ± 2.86	RV circumferential strain (mid-cavity)

Continuous variable are expressed as mean ± standard deviation.

P249

Assessing the myocardial structure-function relationship by Cardiac Magnetic Resonance Imaging: Relationship of Extracellular volume and myocardial strain in normal and in patients with cardiomyopathy

Naveen Rajpurohit, MD[1] Allison L. Drew, RT MR CT R[2], Zhen Qian, PhD[3], Robi Goswami, MD[4], Ashish Kabra, MD[2], Venkateshwar Polsani, MD[5], Karen Nelson, BMSc[6]

1. *Sanford Cardiovascular Institute, Sioux Falls, SD*
2. *Piedmont Heart, Atlanta, GA*
3. *Piedmont Heart Institute, GA*
4. *Piedmont Heart Institute, Atlanta, GA*
5. *Piedmont Heart Institute, Atlanta, GA., Atlanta, GA*
6. *Piedmont Heart, atlanta, GA*

Background: Global extracellular volume (ECV) is a measure of total left ventricular fibrosis burden and could provide a quantitative method for assessing cardiomyopathies with focal or diffuse myocardial fibrosis. Left ventricular peak systolic global circumferential strain (GCS) using myocardial tagging is a sensitive marker of left ventricular systolic function (LV) and can be helpful in assessing LV systolic function in different cardiomyopathies. The purpose of this study was to assess the relationship of global ECV with global GCS using myocardial tagging in patients with three different types of cardiomyopathies (ischemic cardiomyopathy, non-ischemic cardiomyopathy and hypertrophic cardiomyopathy) and compare them with control.

Methods: 86 patients with cardiomyopathy (n=55) and 21 normal patients (n=21) underwent a comprehensive CMR including cine imaging, mid ventricular short axis tagging and LGE. ECV was measured from pre and post contrast T1 of mid-myocardium and blood using modified Look-locker inversion recovery (MOLLI) pulse sequences. Peak systolic global circumferential LV strain was generated from tagging sequences using CS-PAMM.

Results: The mean ECV and GCS values for normal patients were 27%±2% and -20%±4% respectively (figures 1 and 2). HCM subjects had mean ECV values of 31%±4% ($p>0.05$, HCM vs normal) and mean GCS values of -15%±4% ($p>0.05$, HCM vs normal). The mean ECV values for ICM patients were 36%±7% ($p < 0.05$, ICM vs normal) and mean GCS values were -10%±5%, ($p < 0.05$, ICM vs normal). Subjects with NICM had mean ECV values of 33%±5% ($p < 0.05$, NICM vs normal) and mean GCS values of 9%±5%, ($p < 0.05$, NICM vs normal). ECV and GCS correlated moderately but significantly ($R2=0.23, P < 0.05$) for the cohort as a whole (figure 3).

Conclusions: Our study concluded that ECV fraction correlated with GCS across three different types of cardiomyopathies and normal subjects, thus validating the hypothesis that cardiomyopathies result in altered structure (increased ECV) and thus altered function (decreased GCS). In contrast to ICM and NICM, ECV and GCS values of subjects with HCM were not statistically different from normal subjects.

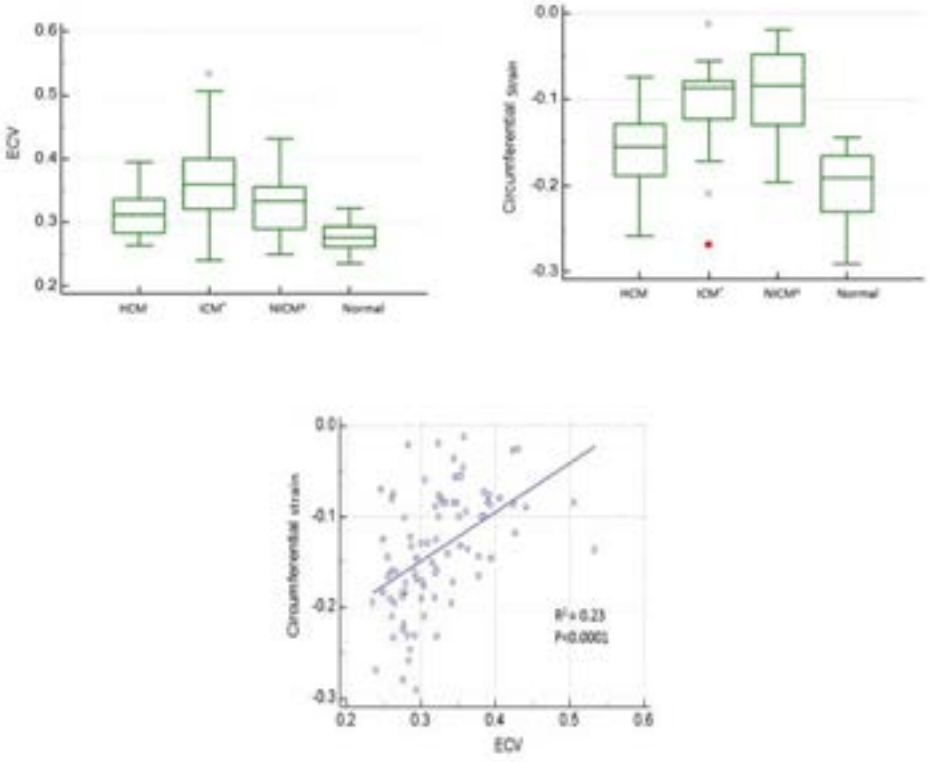

P250

Assessment of Right Ventricular Myocardial Deformation in Takotsubo Syndrome Using Cardiovascular Magnetic Resonance Myocardial Feature Tracking

Thomas Stiermaier, MD[1] Torben Lange[2], Uwe Raaz, MD[3], Johannes T. Kowallick, MD[4], Joachim Lotz, MD[5], Gerd Hasenfuß, MD[6], Holger Thiele, MD[7], Andreas Schuster, MD PhD MBA FESC[6], Ingo Eitel, MD[8]

1. *University Heart Center Lübeck, Lübeck, Schleswig-Holstein, Germany*
2. *DZHK (German Centre for Cardiovascular Research) partner site Göttingen, Niedersachsen, Germany*
3. *University Medical Center Göttingen, Niedersachsen, Germany*
4. *Institute for Diagnostic and Interventional Radiology, University Medical Center Göttingen, Germany, Niedersachsen, Germany*
5. *Institute for Diagnostic and Interventional Radiology, University Medical Center Göttingen, Germany, Goettingen, Niedersachsen, Germany*
6. *Department of Cardiology and Pneumology, University Medical Center Göttingen, Germany, Niedersachsen, Germany*
7. *University Heart Center Luebeck, Sachsen, Germany*
8. *University Heart Center Lübeck, Schleswig-Holstein, Germany*

Background: Takotsubo syndrome (TTS) is characterized by a distinctive pattern of completely reversible left ventricular (LV) contraction abnormalities. However, right ventricular (RV) involvement can be observed in about one-third of patients and has a major prognostic impact. The aim of the present study was to assess RV myocardial strain using cardiovascular magnetic resonance myocardial feature-tracking (CMR-FT) in a large cohort of patients with acute TTS as well as after recovery of LV function.

Methods: CMR imaging was performed in 125 patients with acute TTS in median 2 days (IQR 2-3 days) after initial presentation. Furthermore, a subgroup of 20 patients underwent follow-up CMR imaging 3.3 months (IQR 3-5 months) after the acute event. The CMR protocol included balanced steady state–free precession sequences in 4-chamber long-axis views to assess longitudinal RV strain with dedicated evaluation software (TomTec Imaging Systems, Munich, Germany).

Results: The study population comprised a typical TTS collective of postmenopausal females (92% women, median age 72 years) with a predominance of typical apical LV ballooning (66%) while midventricular (32%) and basal ballooning (2%) patterns were less frequent. The peak global average RV longitudinal strain could be assessed in 119 patients (95%) and yielded in a median of -15% (IQR -10% to -20%) whereby the apical (-11%) and basal (-16%) segments of the free RV wall were more severely affected than the midventricular parts (-24%). RV myocardial deformation was similar among TTS patients with different LV ballooning patterns ($p=0.12$). However, patients with visually impaired RV function (n=37) demonstrated a significantly lower peak global average RV longitudinal strain compared to patients with visually normal RV function (n=80; -14% versus -20%; $p < 0.01$). Among the 20 TTS patients with serial CMR data, there was a trend to an improvement of RV strain from -13% (IQR -10% to -18%) at the acute stage to -20% (IQR -17% to -25%) at follow-up ($p=0.08$).

Conclusions: RV myocardial deformational impairments can be assessed with CMR-FT in patients with TTS. Quantitative RV functional analysis might help to identify patients with RV involvement who are at increased risk of complications.

P251

74 Year Old Male with Chest Pain after Recent Percutaneous Coronary Intervention

Evan A. Nelson, MD[1] W. Patricia Bandettini, MD[2], Sujata M. Shanbhag, MD, MPH[3], Christine Mancini, RT[4], Andrew E. Arai, MD[1]

1. National Heart, Lung and Blood Institute, National Institutes of Health, Bethesda, MD
2. National Heart, Lung and Blood Institute, National Institutes of Health, MD
3. NIH/NHLBI, Bethesda, MD
4. Suburban Hospital, MD

Description of Clinical Presentation: A previously healthy 74-year-old male presented with acute inferior ST elevation MI (STEMI) treated with emergency percutaneous coronary intervention (PCI) of the right coronary artery (RCA) with a peak troponin-I 1.93 ng/ml. Significant left anterior descending artery (LAD) disease was also discovered which was treated with a DES 4 days after his initial infarct. He had a research CMR between his acute PCI and his staged PCI and was subsequently discharged without complications. The patient again presented with acute anterior STEMI and was found to have acute stent thrombosis of both his LAD and RCA stents (peak troponin-I 6.34 ng/mL). After successful intervention on both the LAD and RCA stents, cardiac MRI was repeated. His in-stent thrombosis was secondary to medication non-compliance.

Diagnostic Techniques and Their Most Important Findings: Initial CMR documented a small inferior and inferoseptal MI on late gadolinium enhancement imaging (LGE) which involved 6.2 grams of myocardium. There was no microvascular obstruction (MVO) on early gadolinium enhancement (EGE) imaging. Myocardial T1, T2, and EGE were consistent with acute inferior myocardial infarction, all with similar area at risk that was more extensive than the delayed enhancement on LGE. There was hypokinesis of the infarcted regions and the ejection fraction was 53%. The second cardiac MRI showed a new, anterior and anteroseptal MI as well as a larger infarction in the inferior and inferoseptal segments (19.6 g). Total infarct size was now 34.3g. The EGE images showed MVO in the septal wall. Beyond the MVO, the EGE as well as T1 and T2 all showed more extensive regions of abnormalities in the involved segments. Cine MRI showed new and more extensive regional wall motion abnormalities and the ejection fraction decreased to 40%.

Learning Points from this Case: 1. In acute MI, cine MRI, T1, T2, early gadolinium enhancement, and late gadolinium enhancment provide clinically relevant insight into the pathophysiology and coronary artery distributions involved. 2. On the first CMR, T1, T2, and early gadolinium enhancment clearly showed a larger area at risk compared to the relatively small amount of late gadolinium enhancment. 3. The second CMR clearly demonstrated progressive LV dysfunction, more extensive T1 and T2 abnormalities, new MVO, and a marked increase in infarct size after the second MI. Myocardial T1 and T2 in the peri-infarction time period post-MI can be potentially ambiguous; however the second CMR clearly shows a larger area at risk. Additionally, early gadolinium enhancment showed new MVO and late gadolinium enhancment showed a marked increase in infarct size in the two coronary distributions.

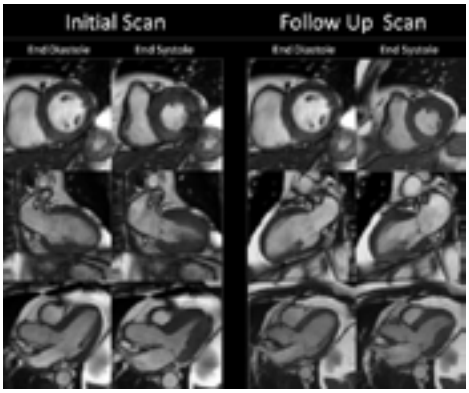

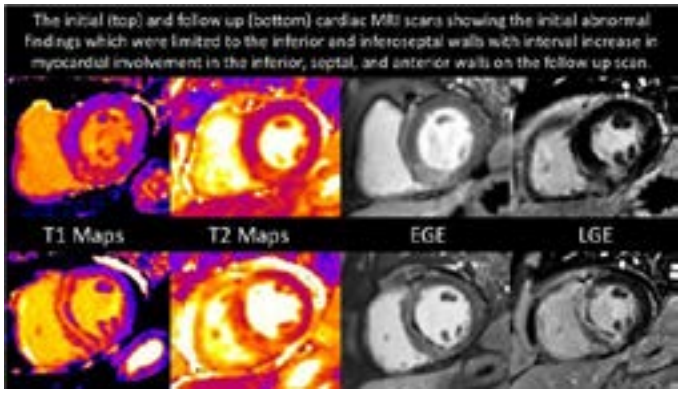

P252

A novel case of Occult Spontaneous coronary Artery Dissection, identified by CMR

Abtehale Al-hussaini, MBBS,BSC, MRCP.[1]David Adlam, BM DPhil[2], Gerry McCann[3], Joanne Wormleighton, DCR(R)[4]

1. *Cardiovascular Sciences, Glenfield Hospital, University Hospitals of Leicester NHS Trust, Leicester United Kingdom, Leicester, England, United Kingdom*
2. *University of Leicester, Leicester, England, United Kingdom*
3. *university of Leicester, England, United Kingdom*
4. *Glenfield Hospital, University Hospitals of Leicester NHS Trust, Leicester, England, United Kingdom*

Description of Clinical Presentation: 38-year-old Scottish head teacher had presented with ST elevation MI recently. Angiogram demonstrates Spontaneous Coronary Artery dissection (SCAD) of the mid LAD, which was conservatively managed. She had been experiencing ongoing episodes of chest pain most pronounced around the peri-menstrual phase. All ECG's and Troponin tests have been found to be within normal limits.

Diagnostic Techniques and Their Most Important Findings:
This lady is a participant in the SCAD UK research study. At baseline and part of the deep phenotyping of this study, she had a cardiac MRI (3T CMR) for assessment of LV function and Late Gadolinium enhancement. In addition, she also underwent an MRA of head and neck vessels, aorta extending to the femoral arteries screening for aortopathy including Fibromuscular dysplasia. Initial results of cardiac MRI demonstrated small focal apical infarct and preserved LV function. A follow up MRI 6 months later as she had been experiencing ongoing chest pain, demonstrated a further mid anterolateral infarct suggestive of a likely missed recurrent SCAD.

Learning Points from this Case: This is the first case in the literature that highlights a case of missed recurrent occult SCAD diagnosed with Cardiac MRI. This demonstrates the clinical value in follow up MRI scans in this population of young women with no cardiac risk factors who may be at increased risk of recurrence of SCAD, leading to myocardial infarction. Cardiac MRI assessment of LV function and infarct with LGE may be of particular value in women who present with normal ECG and recurrent episodes of chest pain.

P253

Acute Myocardial Infarction with Angiographically Normal Coronary Arteries: Accurate Diagnosis by Cardiac MRI

Rajesh Janardhanan, MD, FACC[1]J.R.Exequiel T. Pineda, MD[2], Ranjith Shetty, MD[2]

1. Banner University Medical Center, Tucson, Tucson, AZ
2. Banner University Medical Center, Tucson, AZ

Description of Clinical Presentation: A 76 year-old female with chronic atrial fibrillation (AF) [CHADS2-VASc score = 4] and hypertension was admitted with chest pain. She had no other significant risk factors for coronary disease. EKG revealed AF with non-specific ST-T changes, and her troponin levels were elevated. She was diagnosed to have an acute coronary syndrome and commenced on aspirin, heparin and loaded with Clopidogrel. She admitted non-compliance to Coumadin for the prior three weeks while she was on vacation. Her INR on admission was sub therapeutic at 1.2

Diagnostic Techniques and Their Most Important Findings: Her echocardiogram revealed an ejection fraction of 54% with akinesia of the basal antero-septum and normal valves. She underwent cardiac catheterization, which revealed angiographically normal coronary arteries and normal left and right side filling pressures. She underwent a cardiac MRI. This demonstrated basal antero-septal akinesia **[Figure 1]** with a very prominent resting perfusion defect **[Figure 2]**. Late Gadolinium enhancement imaging confirmed transmural, delayed enhancement with microvascular obstruction **[Figure 3].** The cardiac MRI findings were consistent with a very focal, acute basal antero-septal myocardial infarction. Testing for a hypercoagulable state was negative. Since she had angiographically normal coronaries, the infarction was presumed to be from a cardio-embolic source most likely atrial fibrillation in this patient with sub-therapeutic INR.

Learning Points from this Case: In our patient presenting with chest pain, no significant multiple coronary risk factors, wall motion abnormalities on echocardiography and angiographically normal coronary arteries, acute myocarditis was considered as a strong possibility. Interestingly, the cardiac MRI revealed a focal area of transmural infarction. With the history of chronic AF with subtherapeutic anticoagulation on initial presentation, it was concluded that the clinical picture was most consistent with a cardioembolic infarct. The coronary arteries appeared normal, most likely due to recanalization of the occluded territory.
In an autopsy study by Prizel et al. in patients with cardio-embolic infarction, 35% of the subjects were female. Valvular abnormality was the source of emboli in 40%, cardiomyopathy in 29%, AF in 24%, coronary artery disease in 16%, 4% related to cardiac catheterization and the remaining cases had collagen vascular disease. The LAD was the site of occlusion in 72% of all emboli. 75% of the infarcts were transmural. Clinically evident myocardial infarction was documented in 27% of patients. A coronary embolic event was implicated in the death of 20% of patients.
In patients with AF, there is an uncertainty whether anticoagulants are superior to antiplatelets in preventing myocardial infarction. In a very recent study by Wandell et al in a primary healthcare setting, warfarin seems to prevent myocardial infarction among patients with AF, which emphasizes the importance of persistent anticoagulant treatment in these patients.

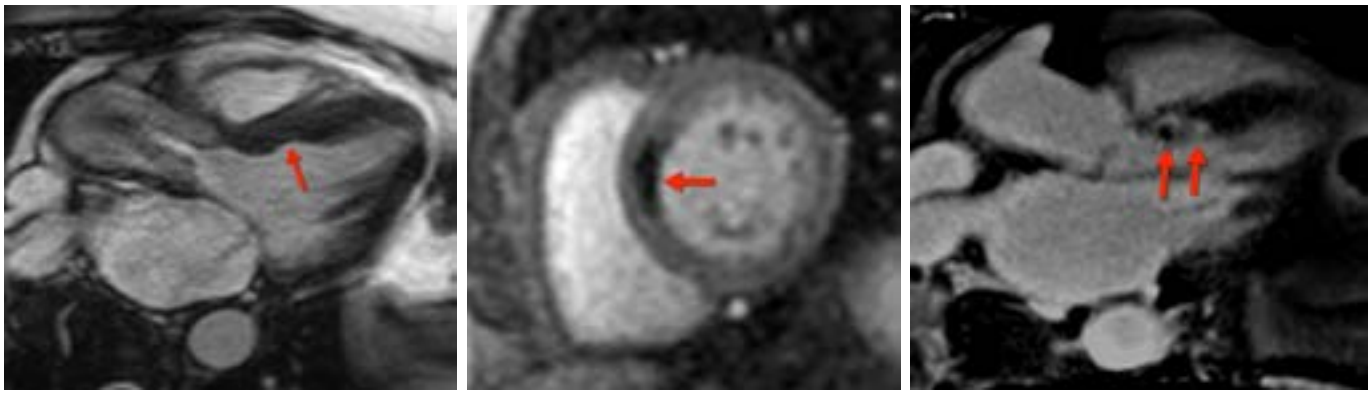

P254

Use of Cardiac MRI to recognize Myocardial Infarction with normal Coronary Angiogram

Harjot Singh, M.D.[1]Jered Cook, MD[2], Madhavi Kadiyala, M.D.[3]

1. St. Francis Hospital, Long Island City, NY
2. University of Toledo, Toledo, OH
3. St. Francis Hospital, NY

Description of Clinical Presentation: 79 year old female with history of chronic atrial fibrillation, type 2 diabetes mellitus, hyperthyroidism, hyperlipidemia who came to hospital after she had developed acute substernal chest pain last night that radiated to her neck and shoulder. Her symptoms lasted for an hour and prompted a visit to the emergency room. She also complained of recent onset of dyspnea of exertion, dizziness and fatigue over the past few days.

Her vitals and physical exam were unremarkable in the ER except for irregularly irregular heart rhythm with low normal heart rate. The troponin levels peaked at 14.34 with BNP of 320. EKG showed q waves in V1 and V2 leads along with t-wave inversions. She was immediately taken for a coronary angiogram which was completely normal but showed ejection fraction of 35-40% on ventriculography. Transthoracic echocardiography was ordered that showed some wall motion abnormality with reduced ejection fraction. MRI was ordered to evaluate newly diagnosed cardiomyopathy.

Diagnostic Techniques and Their Most Important Findings: Left ventricle was normal in size with severely reduced global systolic function (EF - 31%). There was akinesis of the basal to mid septal wall along with hypokinesis of both anteiror and inferior wall but the apical segments are spared.

On delayed gadolinium enhancement images, there was a transmural infarct of the basal to mid anteroseptum extending to the portion of the inferoseptum and anterior wall with evidence of mild microvascular obstruction, suggesting prolonged ischemic duration. On T2-weighted dark blood images, there was evidence of extensive myocardial edema in basal to mid anteroseptal and inferoseptal wall extending to both anterior and inferior wall, suggesting a much larger territory of area-at-risk than area of infarct.

Learning Points from this Case: Upto 9% of myocardial infarction goes unrecognized with coronary angiogram in patient with acute coronary syndrome and elevated troponins. The work up for these patients shouldn't stop at normal angiogram and requires further investigation such as cardiac CT angiogram or cardiac MRI.

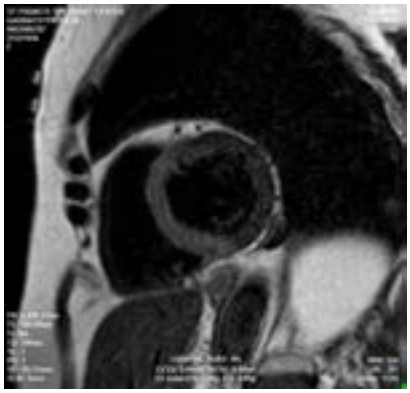
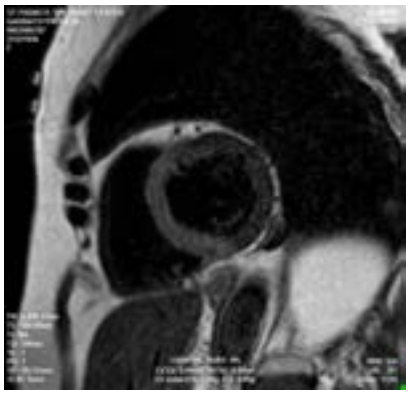
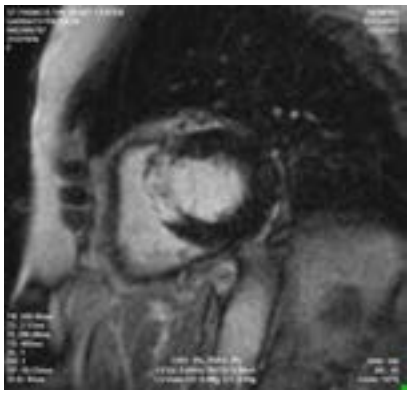

P255

Manganese-Enhanced T1 mapping: novel infarct quantification and detection of calcium-handling dysfunction in cardiomyopathy

Nick B. Spath, BSc MD[1], Marc R. Dweck, MD PhD[1] Gillian A. Gray, BSc PhD[2], Lydia M. Le Page, MChem PhD[2], David ML. Lilburn, BSc PhD[3], Maurits A. Jansen, MSc PhD[2], David E. Newby, MD PhD[2], Phillip Yang, MD[4], Scott I. Semple, BSc PhD[2]

1. *University of Edinburgh, Edinburgh, Scotland, United Kingdom*
2. *University of Edinburgh, Scotland, United Kingdom*
3. *Clinical Research Imaging Centre, University of Edinburgh, Scotland, United Kingdom*
4. *Stanford University School of Medicine, CA*

Background: Gadolinium delayed-enhancement magnetic resonance imaging (DEMRI) is a valuable tool in myocardial viability assessment but is relatively non-selective given its passive extracellular distribution and inability to characterise viable myocardium directly. Manganese, a paramagnetic calcium analogue, avidly enters active cardiomyocytes via voltage-gated Ca^{2+}-channels, increasing MRI-detectable T1 relaxativity. Manganese-enhanced MRI (MEMRI) therefore has potential to characterise functional viable myocardium directly, and quantify calcium influx and handling. In a rodent myocardial infarction (MI) model, we aimed to determine if MEMRI with T1 mapping can more accurately assess infarct size and detect alterations in the remote myocardium secondary to left ventricular remodelling.

Methods: Male Sprague-Dawley rats (180-300g) underwent permanent coronary artery ligation to induce anterior MI, or sham surgery. Animals (n=13 MI, n=4 sham) underwent dual assessment with DEMRI followed by MEMRI 48 hours later, under isoflurane (0.5-4%) anaesthesia, at both 3 and 10 weeks post-MI using a 7T horizontal bore NMR spectrometer (Agilent Technologies, UK), equipped with a high-performance gradient insert, maximum gradient strength 400mT/m. Pulse, respiration, and temperature (maintained at 37°C) were monitored. MEMRI was achieved using SeeMore (Eagle Vision Pharmaceuticals, Downingtown, USA; n=8) and Teslascan (Mangafodipir, IC Targets AS, Norway; n=9) at doses of 22 and 44µmol/kg respectively, administered intravenously over 1-2 minutes. Standard anatomical and functional imaging was acquired, followed by gradient-echo, cardiac-gated Modified Look-Locker Inversion recovery (MoLLI) sequences before and 20 mins post-contrast at the maximal infarct short-axis slice. T1 colour maps were created using commercially available software (CVI4.2®, Circle Cardiovascular Imaging, Canada) by defining ROIs±2xSD for infarct and remote, with an intermediate averaged value defined as borderzone, allowing ROI contouring.

Results: At 3 weeks post-MI, infarct size assessed by MEMRI was smaller than by DEMRI ($P < 0.05$). This reduction appeared to persist at 10 weeks, but failed to reach significance (P=0.067; Figure 1). In a subgroup of highest myocardial insult, remote myocardium showed a reduction T1 with MEMRI between early and late imaging time points. Remote myocardium in sham animals with preserved left ventricular function demonstrated a small increase in T1 (Figure.2).

Conclusions: MEMRI identified a smaller infarct size than DEMRI consistent with oedema-related overestimation of infarct size by DEMRI. MEMRI combined with T1 mapping identifies functional changes in the remodelling remote myocardium following acute infarction. This technique represents a unique imaging approach with the potential to track and quantify myocardial viability and function. This has potential applications for the assessment of myocardial infarction, cardiomyopathies and regenerative therapies.

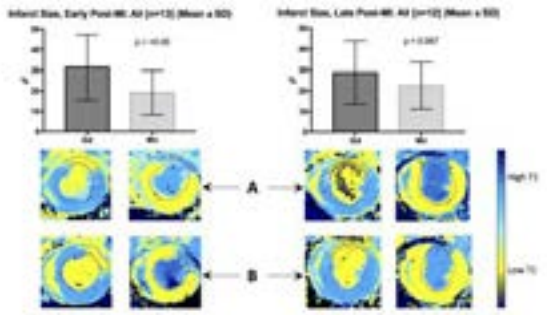

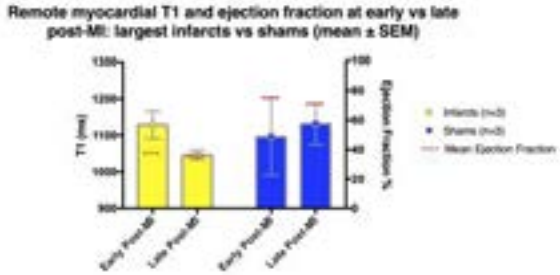

P256

Aortic Wall Inflammation Occurs Independently of Anatomic Dilation in Marfan Syndrome: A Multimodality Study via Integrated MRI-PET Imaging

Parmanand Singh, MD[1] Zaid Almarzooq, MD[2], John Babich, PhD[2], Shankar Vallabhajosula, PhD[2], Yi Wang, PhD[2], Mary J. Roman, MD[2], Richard B. Devereux, MD[3], Jonathan W. Weinsaft, MD[3]

1. *Weill Cornell Medical College, New York, NY*
2. *Weill Cornell Medical College, NY*
3. *Weill Cornell Medical Center, NY*

Background: Aortic size is widely used to stratify risk among patients with Marfan Syndrome (MFS). However, size imperfectly predicts outcomes, as many MFS patients develop dissection despite aortic dimensions below the threshold for prophylactic surgery. Hybrid MRI-PET technology provides a new means of concomitantly assessing aortic size and vessel wall inflammation. This study tested whether MFS patients manifest vessel wall inflammation (via MRI-PET) independent of aortic dilation.

Methods: Hybrid MRI-PET (Siemens Biograph mMR [3.0T]) was performed among MFS patients without prior dissection via a prospective protocol for aortic remodeling. For MRI, aortic size was assessed via contrast-enhanced MRA (GRE, typical TR 3.0 msec, TE 1.13 msec, flip angle 16^{o}, gadolinium 0.2mmol/kg); dimensions were measured in double oblique orientation at pre-specified locations (root, ascending, arch, mid and distal descending aorta). For PET, 18F-flourodeoxyglucose (10 mCi given post carbohydrate deprivation) was used to assess aortic inflammation via standardized aortic wall ROIs (target 0.5cm^2) placed in native (non-grafted) segments co-localized to MRI landmarks. Increased FDG uptake was defined via standard threshold (>2 SUV) concordant with prior validated work. MFS measurements were referenced to a normative control dataset (imaged for QA purposes). MRI and PET data was acquired simultaneously - analysis performed by independent readers, blinded to results of the other modality.

Results: MRI-PET was successfully completed (mean exam time 60±10 minutes) in 4 MFS patients (41.75±17.91, 75% male); all exams yielded fully interpretive PET datasets (18 evaluable segments) with discriminative SUVs between MRI-verified aortic lumen except for 2 patients with root grafts (prior aneurysm). Only one MSF patient had aortic dilation within any native aortic segments (aortic root: 4.5cm) – 94% of remaining segments (17/18) were within normative size-based limits based on established MRI reference cutoffs. All MFS patients (4/4) had increased (>2 SUV) PET uptake involving more than one aortic segment (67% of segments; root 1/2 | ascending 3/4 | arch 4/4 | mid descending 3/4 | distal descending 1/4). Aggregate MFS aortic wall inflammation (18 segments from 4 participants) was 70% higher than that derived from normative (MFS-) control data (2.17±0.28 vs. 1.28±0.25, p=0.001). Among MFS patients, FDG uptake was highest in the aortic arch (2.24±0.20) and lowest in the aortic root (1.81±0.30). MRI-quantified aortic size was non-significantly correlated with vessel wall inflammation as measured via PET (r=-0.06, p=0.81; see **Figure**).

Conclusions: Aortic wall inflammation can occur independently of anatomic dilation among patients with MFS. MRI-PET hybrid imaging enables integrated assessment of aortic physiology, demonstrating increased inflammatory activity even in regions of normal aortic caliber as assessed by conventional MRA anatomic assessment.

http://www.ConferenceAbstracts.com/uploads/cfp2/attachments/LDFAIBDN/LDFAIBDN--222703-1-ANY(1).pdf

P257

Detection of Myocardial Scar by Late Gadolinium Enhancement Cardiac MR using Gadoterate Meglumine

Amir Ali Rahsepar, MD[1]Ahmadreza Ghasemiesfe, M.D[2], Monica Korell, MPH[3], Ann Ragin, PhD[1], Jeremy D. Collins, MD[4], James Carr, MD[4]

1. *Northwestern University, Chicago, IL*
2. *Yale affiliated Bridgeport Hospital, Milford, CT*
3. *Northwestern University, IL*
4. *Northwestern Memorial Hospital, Chicago, IL*

Background: Recent reports have demonstrated that serial application of linear gadolinium based contrast agents (GBCA) increases the risk of gadolinium retention, an effect not seen with macrocyclic GBCA. Here, we aimed to evaluate myocardial scar evaluation at Late gadolinium enhancement cardiac MR (LGE-CMR) using a macrocyclic GBCA (gadoterate meglumine, Dotarem, Guerbet, France) compared with a reference standard linear GBCA (gadopentetate dimeglumine, Magnevist, Bayer, Germany).

Methods: Sixteen subjects (54.1±15.7 years, 8 men) with suspected myocardial scar on LGE-CMR performed using 0.2mmol/kg gadopentetate dimeglumine were recruited for a research CMR scan using 0.2mmol/kg gadoterate meglumine. Quantitative assessment of myocardial scar was performed on LGE-CMR data on short-axis images using a conventional segmented gradient recalled echo phase-sensitive inversion recovery pulse sequence by QMass MR 7.2 software (Medis, Netherlands). Qualitative scar analysis was performed by scoring hyperenhanced myocardial scar on the 16-segment AHA model at LGE-CMR based on the area of scar per segment and summed across all 16 segments to derive a global scar score. Reader confidence in visualizing the scar tissue for each agent was recorded on a 5-point scale.

Results: Percentage myocardial scar mass averaged 6.32±4.62 and 6.55±4.89 for gadopentetate dimeglumine and gadoterate meglumine, respectively. Intraclass correlation (ICC) showed excellent reliability (ICC=96.7%) between the two GBCAs in quantifying LGE. Global qualitative segmental LGE scores showed a trend of larger scar detection using gadoterate meglumine vs. gadopentetate dimeglumine (3.00±4.04 vs. 5.18±4.99, p=0.01). Reader confidence in scar visualization was similar between gadopentetate dimeglumine and gadoterate meglumine (4.2 vs 3.6, p=0.11).

Conclusions: We found that gadoterate meglumine has equivalent diagnostic accuracy to gadopentetate dimeglumine in identifying myocardial scar at LGE-CMR qualitatively and quantitatively and can detect the scar with a similar degree of confidence as gadopentetate dimeglumine. Based on current results, macrocyclic agents like gadoterate dimeglumine may be an accurate alternative to linear GBCA for LGE-CMR.

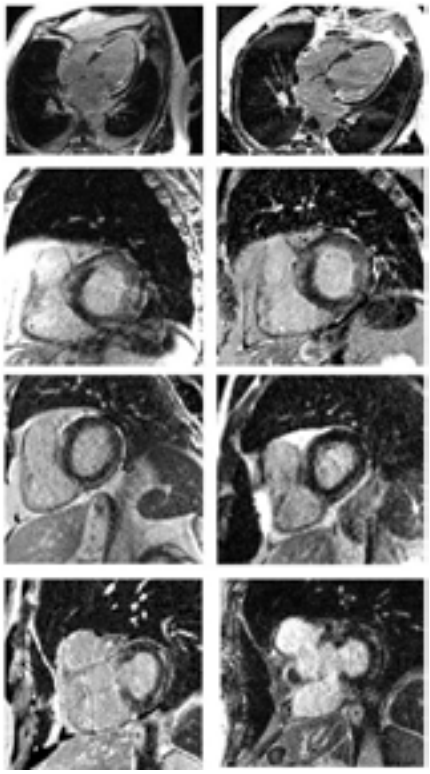

P258

Effects of intravenous contrast administration on ventricular quantification.

Jonathan Weir-McCall, MBChB, FRCR[1] Amir Fathi, MSc, BSc[2], Allan Struthers, FRCP, MD[1], Brian Lipworth, MD, FRCP[3], Graeme Houston, MD, FRCR[1]

1. *University of Dundee, Scotland, United Kingdom*
2. *University of Dundee, London, England, United Kingdom*
3. *university of Dundee, Scotland, United Kingdom*

Background: Gadolinium contrast agents are extensively used within cardiac MRI (CMR) due to their usefulness for angiography and myocardial scar assessment. To improve workflow efficiency these agents are frequently administered close to the start of the examination before the short axis stack is acquired for volumetric analysis and quantification. However normal values have without exception been published for non-contrast CMR, and the effects of contrast on quantification of right (RV) and left (LV) volumetric analysis has been poorly studied. Thus the aim of the current study was to determine the effects of contrast on volumetric quantification.

Methods: 50 study participants free from known cardiovascular disease were recruited. CMR was performed on a 3T scanner (Prisma, Seimens, Gr). A short axis stack was performed of the ventricles from the atrioventricular ring to the apex using balanced steady state free precession cine imaging pre- and post the administration of 10mls 0.5mmol/ml gadoterate meglumine (Guerbet, Fr). The image sequences were analysed by a single observer experienced in CMR analysis using Circle CVI42(Calgary, Ca). The studies primary end-points are differences between pre and post contrast measurements of: LV mass, LV and RV end-diastolic (EDV) and end-systolic volumes (ESV), LV and RV ejection fractions (EF) and stroke volume (SV) compared using a paired-sample t-test using SPSS v22 (IBM, NY).

Results: 45 completed the study protocol with analyzable images. The administration of contrast resulted in a significant increase in signal to noise ratio (pre:830±398 vs. post 1028±540, p=0.003) with no significant change in CNR (pre:583±302 vs. post:559±346, p=0.54). On left ventricular analysis, post contrast analysis yielded significantly higher LVESV (54±20 vs. 57±18 ml, p=0.04), and lower LVEF (59±9 vs. 57±8 %, p=0.023. But with with no significant difference in LVEDV (131±31 vs. 132±30 ml, p=0.54) or LVM (105±29 vs. 107±26 g, p=0.38). On right ventricular analysis, contrast resulted in no significant change in RVEDV (129.5±35.3 vs. 130.5±36.2, p=0.66), RVESV (54.3±22.8 vs. 54.7±23.3, p=0.87) RVEF (58.7±8.5 vs 59.3±10.4,p=0.60) or RVM (37±9 vs 35±11 g, p=0.13). Contrast improved the agreement between RV and LV stroke volumes (mean±SD difference pre= 1.42±7.0ml vs post=-0.9±5.6).

Conclusions: Post contrast left ventricular analysis yields significantly lower ejection fraction without significantly changing right ventricular analysis. This has clinical implications when comparing values with normal reference values, and when comparing follow-up studies with baseline studies when the contrast has differed either in timing in relation to the left ventricular short axis acquisition or in administration.

P259

Characterization of a recurrent sub-aortic membrane utilizing cardiovascular magnetic resonance imaging

Bharath Sathya, MD[1] Andrew E. Arai, MD[2]

1. National Institutes of Health, Bethesda, MD
2. National Heart, Lung and Blood Institute, National Institutes of Health, Bethesda, MD

Description of Clinical Presentation: A 59 year old female with history of a previously resected sub-aortic membrane and basal septal hypertrophy was evaluated for new onset dyspnea on exertion. Physical examination at the time of exam revealed normal vital signs, and a mid-peaking systolic murmur with a preserved S2 auscultated loudest at the right upper sternal border. During her prior uncomplicated resection, a sub-aortic membrane was described in the left ventricular outflow tract (LVOT), which spanned 270 degrees circumferentially and did not extend to the level of the basal septum near the anterior mitral valve leaflet.

Diagnostic Techniques and Their Most Important Findings: A transthoracic echocardiogram revealed the presence of flow acceleration within the left ventricular outflow tract with Doppler spectral waveforms demonstrating a peak velocity of 3.7 m/s and mild aortic regurgitation. The patient was referred for a cardiac MRI to investigate the cause of the increased velocity in the LVOT. On cardiac MRI, a 3-chamber steady state free precession (SSFP) sequence revealed the presence of a high velocity jet emanating approximately ~20 mm below the aortic valve in the LVOT. Multiple SSFP images adjacent to the 3-chamber were obtained, which also revealed prominent basal septal hypertrophy measured maximally at 15 mm with systolic anterior motion of the mitral valve. There was also a small protrusion from the basal antero-septum into the LVOT near the origin of the flow acceleration thought to represent sub-aortic membrane. Subsequent velocity encoded phase contrast imaging in a 3chamber orientation with velocity encoding (VENC) defined as 300 cm/s demonstrated aliasing in the left ventricular outflow tract at the level where the sub-aortic membrane was detected. Late gadolinium enhancement utilizing phase sensitive inversion recovery demonstrated no evidence of fibrosis or infarct in the septum.

Learning Points from this Case: 1) This study demonstrated significant left ventricular outflow obstruction utilizing velocity encoded phase contrast imaging as a result of a recurrent sub-aortic membrane in the presence of basal septal hypertrophy and systolic anterior motion of the mitral valve. 2) Per the 2008 ACA/AHA guidelines, it is recommended that patients with sub-valvular obstruction resulting in a peak instantaneous velocity greater than 50 mm Hg have surgical resection (Class Ic). A surgical case series demonstrated that in patients with simple sub-aortic membrane, 37% of studied population also required myomectomy with initial operative intervention. 3) A surgical series following patients post enucleation of sub-aortic membrane has shown that 27% of patients experience recurrence with 8% of patients requiring re-operation. According to a study conducted by Takkenberg et al, women and the elderly are more likely to experience recurrence and require intensive surveillance.

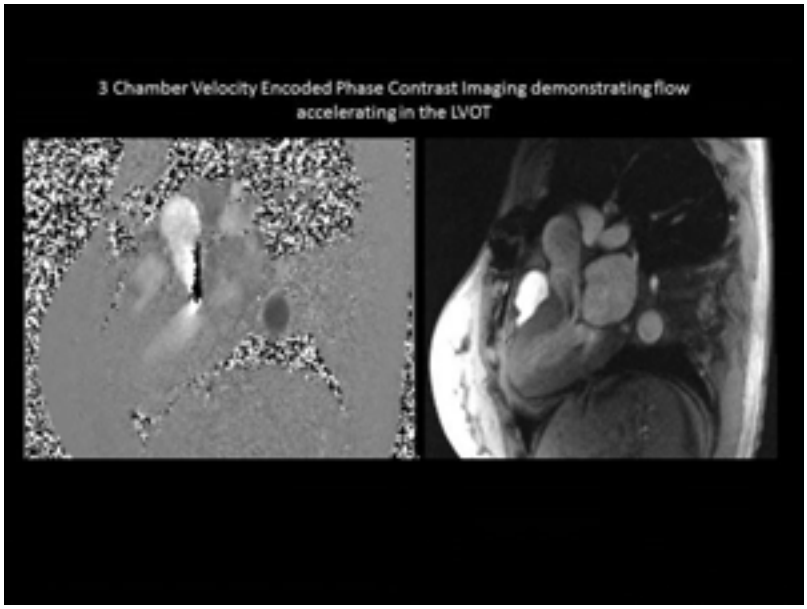

P260

Unusual cardiac sarcoidosis; the benefits of a multi-modality approach

Zohya Khalique, MBBS[1]John Baksi, MBBS PhD[2], Kshama Wechalekar, MBBS DNB (Nuclear Medicine)[3], Athol Wells, MD[4], Rakesh Sharma, MBBS PhD[4], Francisco Alpendurada, MD PhD[4], Cemil Izgi, MD[5]

1. *NIHR Cardiovascular Biomedical Research Unit, Royal Brompton Hospital, London, England, United Kingdom*
2. *NIHR Cardiovascular Biomedical Research Unit, Royal Brompton Hospital, England, United Kingdom*
3. *Royal Brompton Hospital, London, England, United Kingdom*
4. *Royal Brompton Hospital, England, United Kingdom*
5. *Cardiovascular Magnetic Resonance Unit, Royal Brompton Hospital, London, UK, England, United Kingdom*

Description of Clinical Presentation: A 68 year old man with sarcoidosis was referred for consideration of infliximab therapy. He was highly symptomatic with fatigue, dyspnea, painful lower body sensory disturbance, bilateral leg oedema and visual disturbance. He originally presented in 2004 with worsening lower body weakness and sensory disturbance and was diagnosed with neurosarcoidosis after a sural nerve biopsy. Since then he has developed multi-organ involvement of his skin, parotid glands, eyes and lungs. His medical history includes primary biliary cirrhosis, hypertension, atrial fibrillation, type II diabetes mellitus and an atrophic left kidney. The patient has multiple drug intolerances and has been unable to take steroids, immunoglobulins or disease modifying drugs including hydroxychloroquine and mycophenolate. Azathioprine and methotrexate were contra-indicated due to the primary biliary cirrhosis. Hence he was referred for systemic review including cardiac evaluation, prior to potential infliximab therapy.

Diagnostic Techniques and Their Most Important Findings: The patient had CMR imaging including volumetric assessment, STIR and gadolinium imaging. He had normal left ventricle (LV) size with a low-normal ejection fraction of 59%. No obvious areas of increased signal intensity on STIR imaging or late gadolinium enhancement were reported, suggesting no cardiac involvement (Figure 1). However, his FDG PET-CT scan showed uptake in the free wall of the right atrium with a maximum standardised uptake value (SUV_{max}) of 3.7 (Figure 2). There was also a small focus of mildly avid uptake in the LV papillary muscle (SUV_{max} of 3.1). Bilateral basal lung uptake was seen as well as right apical scarring. On re-evaluation of the CMR images, it is possible to retrospectively appreciate a subtle area of thickening of the free wall of the right atrium with suggestion of increased signal intensity. After 3 pulses of iv methylprednisolone (but no oral prednisolone maintenance due to intolerance) he was re-imaged with CMR. STIR imaging was tricky to interpret due to fast AF and difficulty in breath-holding, but no convincing areas of active inflammation were identified. FDG PET-CT some months later showed a slight increase in the right atrial wall uptake (SUV_{max} 4.0) as well as further LV involvement in the basal septal and basal-mid lateral regions (SUV_{max} 5.7). Same day SPECT showed normal myocardial perfusion at rest, but a deterioration in LV function with an EF of 40%. These findings point towards worsening cardiac sarcoid despite iv steroid therapy.

Learning Points from this Case: This unusual case of cardiac sarcoidosis of the right atrium reinforces the need for careful evaluation of CMR images, particular in the atria where interpretation of STIR images can be challenging and potentially insensitive. A multi-modality approach is particularly beneficial in this instance. In addition, the case raises the question of how to manage progressive cardiac sarcoidosis when usual treatment strategies fail.

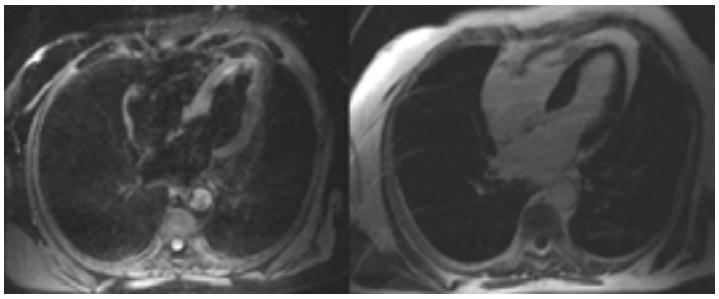

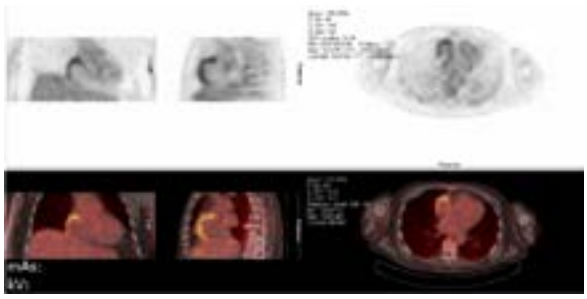

P261

Idiopathic left ventricular outflow tract pseudoaneurysm

Rashid Saif. AL Umairi, MD, FRCR[1]Idan Roifman, MD[2], Lan Chau Kha, MD[2], Anastasia Oikonomou, MD[2], Gideon Cohen, MD[2], Laura Jimenez-Juan, MD[3]

1. University of Toronto, Department of Medical Imaging, Toronto, ON, Canada
2. Sunnybrook Health Sciences Centre, ON, Canada
3. Sunnybrook Health Sciences Centre, Toronto, ON, Canada

Description of Clinical Presentation: 28-year-old male presented to Emergency Department with a 3-week history of worsening dry cough and epigastric pain. The past medical history was unremarkable. On physical examination, the patient was tachycardic at 115 bpm and afebrile. He had mild-moderate bilateral pedal edema and an elevated jugular venous pressure. The patient was started on diuresis with impression of heart failure.

Diagnostic Techniques and Their Most Important Findings: Blood work revealed mildly raised troponin (166 ng/L) and D-dimer (1206 ng/mL), otherwise normal. CT pulmonary angiography was performed to rule out pulmonary embolism and it was negative, however, an incidental mass was seen adjacent to the left ventricle (LV) which followed LV blood pool enhancement. Evaluation with transesophageal echo showed a pseudoaneurysm arising from the left ventricular outflow tract (LVOT), in communication with the left atrium. Flow was noted from the (LVOT) pseudoaneurysm to the left atrium during systole. No valvular vegetations identified. Further evaluation with cardiac CT or MRI was recommended. The patient was admitted and a cardiac MRI was performed. Steady state free precession CINE imaging and MR angiography demonstrated two aneurysms arising from the LVOT. The larger was arising from the lateral wall of the LVOT whereas the smaller was arising from the posterior wall and communicating with the left atrium. The left atrium was severely dilated. The masses were considered to be causing reflux symptoms and right-sided heart failure. The primary differential diagnosis proposed was extra-pulmonary TB. Results returned negative as did those for Brucellosis, Q- fever, Bartonellosis, Whipple disease and syphilis. During admission, the patient developed severe chest pain with global ischemic changes on his ECG. He underwent coronary angiography which showed severe extrinsic compression of the left main, left anterior descending and circumflex arteries. The patient was taken urgently to the OR with repair of LV outflow tract pseudoaneurysm and coronary bypass with saphenous vein graft to obtuse marginal. Surgical specimens were sent to the lab and results came negative for infection.

Learning Points from this Case: Left ventricular outflow tract (LVOT) pseudoaneurysm is a rare condition which usually associated with a predisposing factors such as history of infective endocarditis, prosthetic aortic valve replacement or chest trauma. In our case no cause has been identified. Patients with LVOT pseudoaneurysm usually present with vague symptoms secondary to obstruction produced by the aneurysmal sac on surrounding structures. In the present case, the patient presented with severe chest pain during admission due to coronary artery compression. Cardiac MRI is a very useful modality which allows a good delineation of the anatomy of the pseudoaneurysm, localization of the neck and detection of complications such as rupture or compression of adjacent structures. Understanding LVOT pseudoaneurysm anatomy is essential for surgical planning.

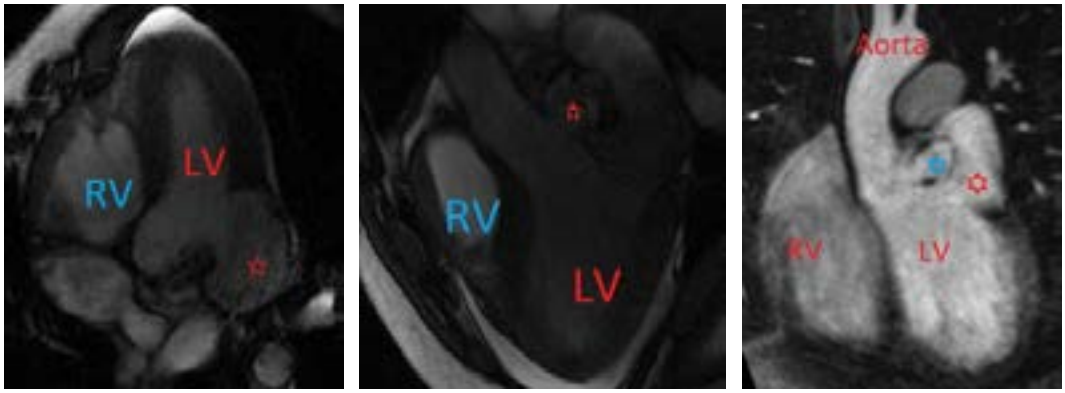

P262

Multimodality Imaging of Paravalvular Pseudoaneurysms Associated with Prosthetic Mitral Valvular Replacement

Harold Goerne[1], Sachin Saboo[2]Tomoyuki Kido[2], Prabhakar Rajiah[2], Nagina Malguria[2], Ronald Peshock[2], Suhny Abbara[2]

1. UT Southwestern Medical Center, Dallas, TX
2. UT Southwestern Medical Center, TX

Description of Clinical Presentation:

- 53-year-old woman with history of mitral valve replacement 10-years ago complicated by paravalvular pseudoaneurysms and patch repair.
- History of tricuspid annuloplasty.

Diagnostic Techniques and Their Most Important Findings:

- Transthoracic Echocardiogram (TTE) demonstrated linear and nodular hyperechogenicity in the basal lateral and inferolateral LV segments consistent with post-surgical changes from pseudoaneurysm repair. Pseudoaneurysm is noted as large anechoic outpouching from the basal lateral wall (difficult to completely visualize). Small bidirectional flow between the repaired pseudoaneurysm and the LV cavity is noted.
- Retrospective ECG-gated Cardiac Computed Tomography Angiography (CTA) revealed mechanical replaced mitral valve and patch repair of two paravalvular pseudoaneurysms. Small leaks adjacent to the prosthetic mitral annulus ring were identified across the patch repair site communicating with three discrete pseudoaneurysms with largest being lateral and two small in the inferior basal regions. The larger pseudoaneurysm did not opacify on the arterial phase however delayed phase proved to be useful to demonstrate it's near complete opacification and small laminar thrombus. Relatively smaller pseudoaneurysms opacified on the early phase thereby excluding thrombus. Prosthetic mitral valve with slight asymmetry of the valve leaflets during opening was noted.
- Cardiac Magnetic Resonance Imaging (MRI) confirmed two paravalvular pseudoaneurysms with evidence of leak across the patched pseudoaneurysm. Linear delayed enhancement of the patch was related to prior patch repair. Small non-enhancing thrombus was confirmed within the larger pseudoaneurysm. The third smaller pseudoaneurysm was not seen due to its size and lesser spatial resolution of MRI compared to CT. Normal LVEF of 58% was present.
- Patient did not undergo surgical repair due to multiple comorbidities and prior sternotomy. Patient is now regularly followed up in clinic and with imaging to assess the status and size of the pseudoaneurysm which remained unchanged.

Learning Points from this Case:

- TTE, Cardiac CT and MRI are complementary studies in above scenario.
- TTE was helpful in identify the patent pseudoaneurysm in the lateral wall, but was unable to identify the two small pseudoaneurysm in the inferior wall.
- Cardiac CT was superior to demonstrate the site of leak around the patch and one smallest pseudoaneurysm that was not visualized on MRI due to its better spatial resolution while the delayed phase was helpful to demonstrate patency of the larger pseudoaneurysm and delineate the small thrombus within. The MPR and 3D capabilities of CT helped in the precise measurement of the size and volume of the pseudoaneurysm.
- MRI is superior in assessment of ventricular functions, wall motion abnormalities, and detection of delayed enhancement related to fibrosis.

http://www.ConferenceAbstracts.com/uploads/cfp2/attachments/LDFAIBDN/LDFAIBDN--222398-1-ANY.pdf

http://www.ConferenceAbstracts.com/uploads/cfp2/attachments/LDFAIBDN/LDFAIBDN--222398-2-ANY.pdf

http://www.ConferenceAbstracts.com/uploads/cfp2/attachments/LDFAIBDN/LDFAIBDN--222398-3-ANY.pdf

P263

The effects of intravenous contrast administration on automated and semi-automated left ventricular quantification

Amir Fathi, MSc, BSc[1] Jonathan Weir-McCall, MBChB, FRCR[2], Allan Struthers, FRCP, MD[2], Brian Lipworth, MD, FRCP[3], Graeme Houston, MD, FRCR[2]

1. *University of Dundee, London, England, United Kingdom*
2. *University of Dundee, Scotland, United Kingdom*
3. *university of Dundee, Scotland, United Kingdom*

Background: Gadolinium contrast agents are extensively used within cardiac MRI (CMR) due to their usefulness for angiography and myocardial scar assessment. To improve workflow efficiency contrast is frequently administered close to the start of examination before the short axis cine stack is acquired for volumetric analysis and quantification. Current routinely used software analysis relies on signal differences and thresholds to aid in the detection of endo- and epicardial borders for ventricular quantification. Contrast agents are known to alter T1 relaxation of tissues, thereby altering the inherent blood-myocardial signal and contrast. The aim of this study is thus to ascertain the effects of contrast agents on left ventricular analysis using semi-automated and fully automated analysis.

Methods: 50 study participants free from known cardiovascular disease were recruited. CMR was performed on a 3T scanner (Prisma, Seimens, Gr). A short axis stack was performed of the ventricles from the atrioventricular ring to the apex using balanced steady state free precessional cine imaging pre- and post administration of 10mls 0.5mmol/ml gadoteric acid (Guerbet, Fr). The image sequences were analysed using a semi-automated technique whereby the centre of the ventricle on each slice was selected and a ROI grown outward from this using a signal threshold technique. A fully automated technique was also preformed whereby the mitral valve and apex were manually identified after which the software automatically generated left ventricular contours. Both techniques were performed using Circle CVI42(Calgary, Ca).

Results: 45 completed the study protocol with analyzable images. The administration of contrast resulted in a significant increase in signal to noise ratio (pre:830±398 vs. post 1028±540, p=0.003) with no significant change in CNR (pre:583±302 vs. post:559±346, p=0.54). Using the semi-automated technique, post contrast analysis yielded significantly higher LVESV (48±20 vs. 53±21 ml, $p < 0.001$), and lower LVEF (62±10 vs. 60±9 %, $p < 0.001$), with no significant difference in LVEDV (126±31 vs. 129±31 ml, p=0.058) or LVM (109±27 vs. 109±26 g, p=0.69). On fully automated analysis, post contrast analysis yielded significantly higher LVEDV (117±32 vs. 127±31 ml, $p < 0.001$) and LVESV (62±22 vs. 70±26 ml, $p < 0.001$), and lower LVM (111±24 vs. 105±25 g, p=0.03), but with no significant difference in LVEF (47±11 vs. 46±12 %, p=0.49).

Conclusions: Contrast administration significantly alters endo- and epicardial contour detection using both automatic and semi-automatic analysis techniques resulting in significant differences in left ventricular quantification. Care must be taken when comparing values obtained before or after contrast administration.

P264

Determining left and right ventricular cardiac magnetic resonance parameters using threshold-based trabecula quantification method by three independent observers

Ibolya Csecs, MD[1]Csilla Czimbalmos, MD[2], Ferenc I Suhai, MD[3], Róbert Mikle, MD[1], Beata Horvath[3], Zsofia Dohy[3], Attila Toth, MD[3], Bela Merkely, MD, PhD, DSc[3], Hajnalka Vago, MD, PhD[3]

1. Heart and Vascular Center, Semmelweis University, Budapest, Hungary
2. Heart and Vascular Center, Semmelweis University, Budapest, Budapest, Hungary
3. Semmelweis University Heart and Vascular Center, N/A, Hungary

Background: While cardiovascular magnetic resonance (CMR) is the gold standard method to evaluate left and right ventricular functions, volumes and masses, there is no widely accepted method for the quantitative analysis of trabeculae (TrM) and papillary muscles (PM). During the past few years besides conventional segmentation algorithms, threshold-based (TB) quantification options also became available.

Our aims were 1) to evaluate left (LV) and right ventricular (RV) CMR parameters by conventional and threshold-based quantification methods 2) measure the papillary and trabecular masses in both ventricles 3) compare CMR parameters determining by three independent observers with both methods.

Methods: At our Clinic 60 healthy volunteer (mean age 30±5 years, 30 male) underwent CMR scan performed on a 1.5T Philips Achieva MR machine. On short-axis cine images endo- and epicardial contours were detected by three independent observers with different level of experience (Level1=75, Level2 >800, Level3 >5000 original CMR cases). Using conventional and threshold-based methods (Medis 7.6 QMass) we measured LV and RV ejection fractions, volumes and masses which enables threshold-based quantification of PM and TrM in ventricles. Using the same contours we compared the impact of threshold-based option at all readers. Expert observer also contoured the papillary muscles manually in end-systolic (ES) and end-diastolic (ED) phases. (Figure1)

Results: Comparing conventional and threshold-based quantification methods significant difference were detected for each investigated parameters regardless of experience level (L1, L2 and L3 $P < 0.0001$) . Taking into account the effect of PM's quantification resulted significant changes in LV volumetric and mass parameters (LVMi $P < 0.0001$). TrM was higher than PM (31.4% vs 5.5% of LVM $P < 0.0001$). Interobserver agreement was excellent for volumetric parameters with both methods (intraclass correlation coefficient (ICC) of LVEDVi 0.978 and 0.969, RVEDVi 0.947 and 0.959), measuring LV and RV masses threshold-based quantification seems to be more reliable (ICC of LVEDMi 0.867 and 0.936, RVMi 0.754 and 0.920).

Conclusions: The quantitative analysis of papillary muscles and myocardial trabeculation could fundamentally alter the normal LV and RV parameters. Threshold-based algorithm could be a consistent method to assess the trabeculae quantitatively.

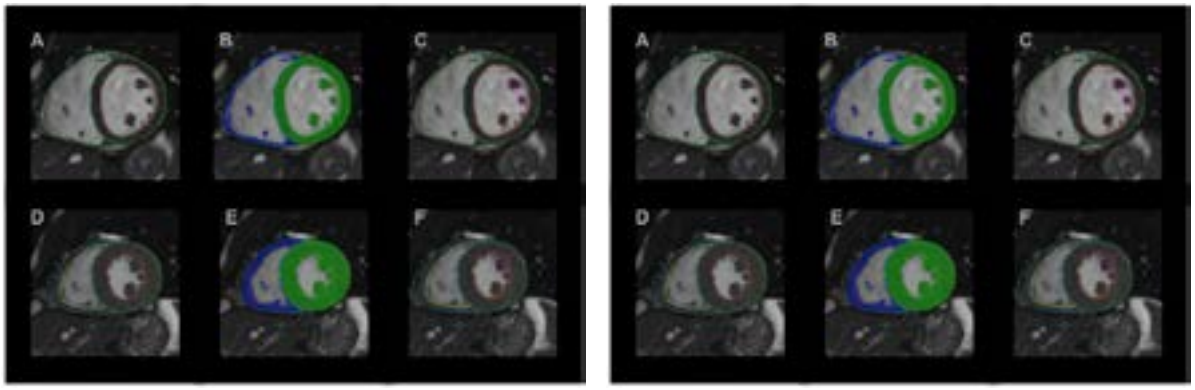

P265

The effect of magnetization transfer on myocardial native T1 in health and disease – implications for phantom calibration of T1 results

Rebecca Kozor, MBBS[1] Gabriella Captur, MD PhD MRCP MSc[2], Sabrina Nordin, MBBS[3], Thomas Treibel, MBBS.MRCP(UK)[3], Stefania Rosmini, MD, PhD[3], Amna Abdel-Gadir, MBBS.MRCP(UK)[4], Peter Kellman, PhD[5], James C Moon, MD[3]

1. *Royal North Shore Hospital, Sydney, New South Wales, Australia*
2. *Barts Heart Centre and NIHR University College London Hospitals Biomedical Research Centre, London, England, United Kingdom*
3. *Barts Heart Centre, England, United Kingdom*
4. *University College London and Barts Heart Centre, London, England, United Kingdom*
5. *Laboratory of Cardiac Energetics, National Institutes of Health/NHLBI, Bethesda, MD, United States., MD*

Background: T1 mapping has potential as a biomarker because T1 changes reflect key myocardial disease processes. However, measured T1 has confounders so standardization is needed. One solution is normalization – the correction of invivo measured T1 using phantom calibration. Complicating this is that human tissue exhibits Magnetization transfer (MT) not present in phantoms. MT reduces measured T1 in MOLLI (modified Look-Locker inversion recovery) and ShMOLLI (shortened MOLLI) but not SASHA, SAturation-recovery single-SHot Acquisition, so SASHA measures T1 higher. If MT varies by disease then firstly, a phantom approach might not work and secondly, MT could be an important biomarker itself. **Aim:** to establish if there is a fixed MT effect on T1 values in human myocardium using examples across health and (diffuse) disease.

Methods: Native T1 mapping (1.5 T Avanto, single UK centre) was performed using 3 different sequences: ShMOLLI (with iterative/conditional reconstruction), MOLLI (with 5s(3s)3s sampling and motion correction) and SASHA (2 parameter fit) in 148 subjects. A single mid ventricular short axis slice was analysed with identical piloting in 4 different cohorts: Fabry disease (n=58), thalassaemia with varying cardiac iron deposition (n=5), severe symptomatic aortic stenosis (AS, n=3), and healthy controls (n=75).

Results: Subject characteristics are shown in Table 1. As expected, iron had the lowest T1, then Fabry, then controls, with AS having T1 elevation. ShMOLLI, MOLLI and SASHA results are plotted against the mean of measured T1, Figure 1. Across the range of T1 values, the average MOLLI T1 measured 64ms higher than ShMOLLI, and SASHA 111ms higher than MOLLI (reflecting sequence design and MT). However, this offset was greater with higher T1s. The better description is of a fixed % bias: with MOLLI higher than ShMOLLI by 7% and SASHA higher than MOLLI by 11% (and SASHA higher than ShMOLLI by 19%). This appears disease independent. Figure 2 demonstrates that the 3 methods are in close agreement after scaling by their respective slopes from least squares fit to the average.

Conclusions: MT does not appear to play a disease specific role in iron, Fabry and diffuse fibrosis although may have a greater affect in other diseases where edema is higher. This implies that a normalized T1 biomarker may be established that can reliably detect disease by the presence of abnormal T1. The ability to use this normalized value to accurately quantify the change in T1 due to disease may be influenced to some degree and requires further study.

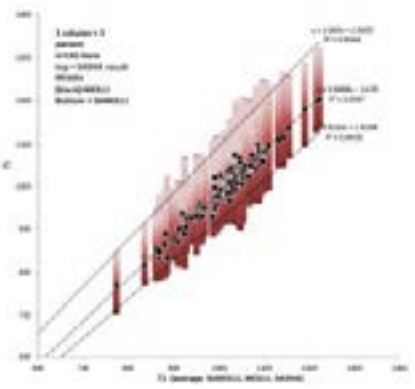

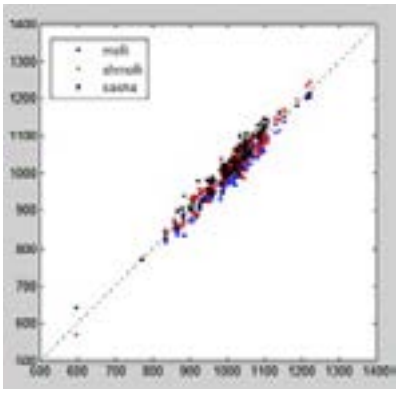

Subject characteristics and T1 results

SASHA T1 (ms)	MOLLI T1 (ms)	ShMOLLI T1 (ms)	Males (%)	Age (years)	
1047±65	946±63	888±57	41	44±14	Fabry
1227±29	1089±22	1019±29	100	74±13	Aortic stenosis
898±172	824±167	772±169	20	39±7	Iron
1144±47	1017±37	958±31	59	48±14	Controls

P266

Motion-Insensitive Reconstruction of Parametric Map: Application to Myocardial T1 mapping

Sébastien Roujol, PhD[1] Céline Smekens, MSc[1], Radhouene Neji, PhD[2], Reza Razavi, MD, PhD[3], Rene Michael. Botnar, PhD[1]

1. King's College London, London, England, United Kingdom
2. Siemens Healthcare Limited, Frimley, England, United Kingdom
3. King's College London, England, United Kingdom

Background: Quantitative myocardial T1 mapping has potential for non-invasive assessment of cardiomyopathies. Although most available myocardial T1 mapping sequences are acquired in a breath-hold acquisition, motion can be observed between T1-weighted images in ~50% of acquisitions. Image registration algorithms can be used for motion correction but they can occasionally fail and remain challenging for saturation or inversion-based T1 mapping techniques. In this study we sought to develop and evaluate a novel motion-insensitive T1 mapping reconstruction approach which automatically discards misaligned/artefact T1-weighted images.

Methods: T1-weighted image selection is achieved by performing several T1 map reconstruction using all images and different image subsets (all images excluding one). Each reconstruction performs an exhaustive search (using a graphic processing unit (GPU)-based implementation) of the minimal error between the normalized measured signal and a dictionary of a normalized 1-parameter model (S(t)=1–2*e(-t/T1). The mean error of each reconstruction (ME) is computed over the myocardium/blood area (obtained by manual delineation of the epicardial contour on the first image, which serves as reference). An image is discarded when its associated subset (where this image was excluded) leads to substantial ME reduction (ME < Median - 6*median absolute deviation (MAD) of all ME). This process is then iterated. Final T1 maps are reconstructed using conventional 3-parameter model fitting with the preselected T1-weighted images. The proposed reconstruction was evaluated in 5 healthy volunteers using a breath-hold MOLLI sequence with bSSFP readout acquired on a 1.5T Siemens Aera scanner (TR/TE=2.5ms/1.2ms, flip angle=35°, FOV=360×306mm^2, voxel size=2.2×2.5mm^2, slice thickness=8mm, bandwidth=1085Hz, GRAPPA acceleration factor=2, partial Fourier=0.87, MOLLI scheme: 5-(3)-3). Reference MOLLI T1 maps were reconstructed for each volunteer using conventional 3-parameter model fitting. Multiple datasets were then created from each MOLLI acquisition with a simulated motion (1D foot-head translation of one T1-weighted image, amplitude={2,4,6,8,10} pixels) and reconstructed using the proposed approach. Correct discard rate and T1 bias over the entire myocardium (with respect to reference MOLLI T1 map) were evaluated. The benefit of the proposed approach was demonstrated in one healthy volunteer who underwent a free breathing MOLLI acquisition.

Results: One misaligned image in the MOLLI series can lead to important T1 bias (up to 100ms). The proposed approach provided reduced T1 bias (< 10ms in all tested cases, see Figure 1) and improved the quality of native T1 maps in the presence of simulated motion (Figure 2) and physiological motion with incorrect image registration (Figure 3).

Conclusions: The proposed reconstruction approach enables identification of misaligned images and reduces motion-related T1 reconstruction artefacts.

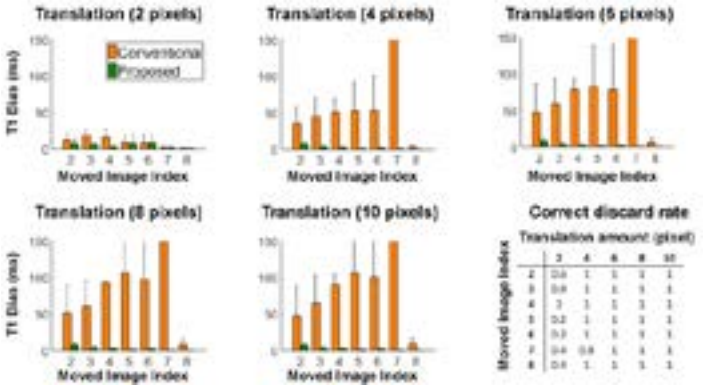

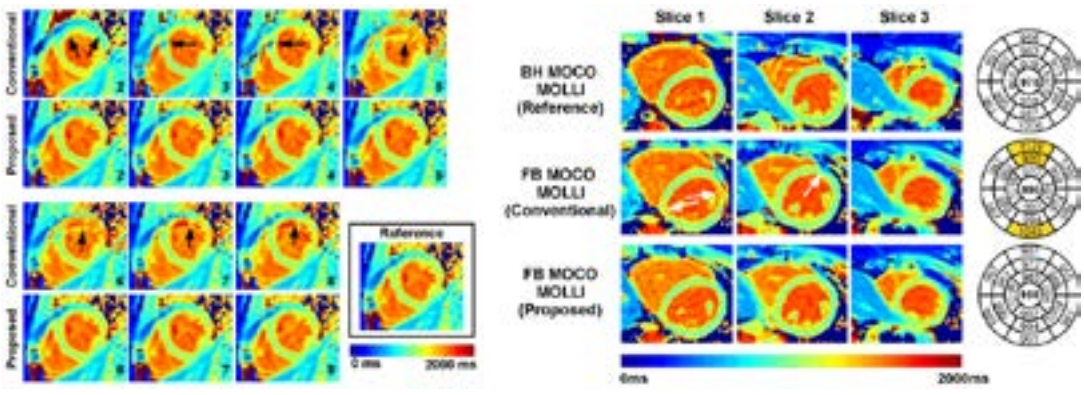

P267

Improved Quantitative evaluation of Cardiac perfusion using bayesian estimation: accuracy and reproducibility against conventional post-processing techniques on digital and clinical data.

Clement Daviller, engineer[1], Magalie Viallon, PhD Dr[2]Timothé Boutelier, PhD[3], Pierre Croisille, PhD[2]

1. *Univ Lyon, UCBL, INSA, CNRS UMR 5520, INSERM U1206, CREATIS, Rhone-Alpes, France*
2. *CREATIS UMR CNRS 5220 - INSERM U1206/ Hopital Universitaire de Saint-Etienne, Rhone-Alpes, France*
3. *Olea Medical, Provence-Alpes-Cote d'Azur, France*

Background: Magnetic Resonance (MR) contrast enhanced Myocardial Perfusion Imaging (ceMPI) is a promising non-invasive non-irradiant technique for providing insight into microcirculation in the myocardial tissue, myocardial angiogenesis, and how reduced coronary flow affects the myocardial tissue[1]. Bayesian based frameworks have received attention from the ce dynamic MR-community due to its flexibility in dealing with rapid changes in the response function[2,3], and in ceMPI due to their capacity to model the AIF to free it from bias resulting from the non-linear relationship between signal intensity (SI) and contrast concentration[4].

Methods: In this work, we evaluate Bayesian deconvolution, a probabilistic method that performs a non-parametric deconvolution of the tissue curve by the arterial input function (AIF) [5] against standard Fermi modelling of myocadial perfusion tissue curves and oscillating singular value decomposition (oSVD) [6]. All 3 methods to derive the quantitative perfusion indexes of interest were evaluated on the same digitally simulated dataset. Digital data were obtained using an arterial input fonction (Ca(t)) (obtained in a patient without CAD using a dual-imaging approach [7]) to generate the myocardial tissue curves (Ct(t)) using the Fermi model. The whole simulation and post-processing pipeline is illustrated in figure 1: Myocardial Blood Flow (MBF), Blood Volume (MBV), MTT parametric maps are calculated, as well as SSE error maps.

Statistics were performed on the results to compare with the reference simulated indexes. All calculations were done in Matlab : parametric maps, error maps in statistics.

Results: Bayesian processing resulted in reduced errors across the phantom when compared to the Fermi or oSVD results (Figure1). The r^2 coefficient (SSE) for Bayesian were 0.988(0.06), 0.981(0.09) and 0.974(0.1) for Bayesian, Fermi and oSVD respectively (Figure1) and mean bias (RPC) for all methods were: 0.004 (0.029(6.5%)), 0.004 (0.029(6.5%)), and 0.0008 (0.019(4.2%)).

Conclusions: Bayesian perfusion fitting/modelling is considered as a promising approach to map myocardial blood flow. Further work will consider studying local perfusion changes during both rest and pharmacologically induced stress in ischemic patients, true clinical data and PET comparison.

References:

1. M. Jerosch-Herold et al. J Magn Reson Imaging, 19, 6, 758–70, 2004.
2. V. Schmid. et al. IEEE TMI 2008.
3. V. Schmid , et al. IEEE TMI 2009.
4. V. J. Schmidet al., MICCAI 2007, 10, 2007, 393–400.
5. K. Kudo, et al. IEEE Trans. Med. Imaging. 2012. 31(7) 1381-1395.
6. Wu, et al. MRM 2003, 50:164-174
7. P. Gatehouse et al. J Magn Reson Imaging, 20, 39–45, 2004.

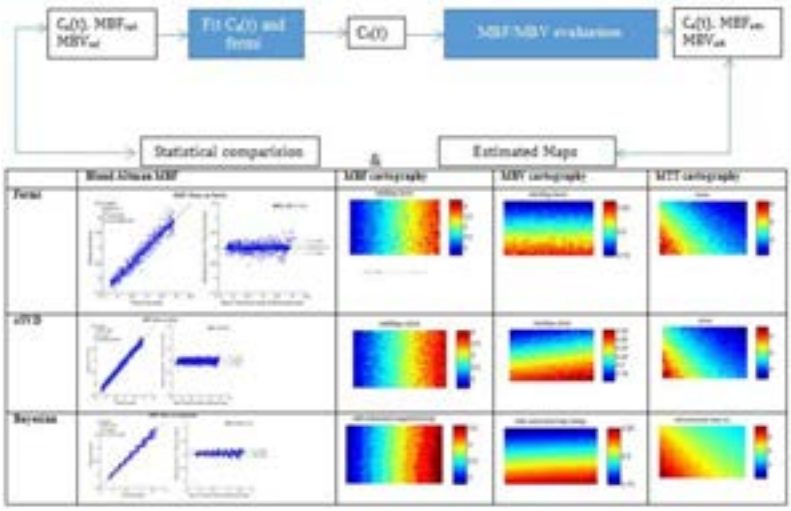

P268

Blood correction reduces variability in native myocardial T1 values at 1.5T cardiac magnetic resonance

Jannike Nickander, MD[1]Magnus Lundin, MD, MSc[2], Goran Abdula, MD[2], Peder Sörensson, MD, PhD[3], James Moon, MBBS, MD, MRCP[4], Peter Kellman, PhD[5], Andreas Sigfridsson, PhD[1], Martin Ugander, MD, PhD[6]

1. *Karolinska Institute, Stockholm, Stockholms Lan, Sweden*
2. *Karolinska Institute, Stockholms Lan, Sweden*
3. *Karolinska University Hospital, Stockholms Lan, Sweden*
4. *Barts Heart Center, The Cardiovascular Magnetic Resonance Imaging Unit and The Center for Rare Cardiovascular Diseases Unit, St Bartholomew's Hospital, West Smithfield, London, UK, England, United Kingdom*
5. *Laboratory of Cardiac Energetics, National Institutes of Health/NHLBI, Bethesda, MD, United States., MD*
6. *Karolinska Institutet, Stockholms Lan, Sweden*

Background: Native T1 measurements in myocardium are likely contaminated by myocardial capillary blood. Since blood has a longer and more variable T1 compared to myocardium, this will degrade the precision of myocardial T1 measurements. Precision could be improved by correction, but both the amount of correction and the optimal blood T1 variable to correct with (left ventricular blood (LV), right ventricular blood (RV), T1 or T1*) are unknown, and no reference standard is obvious. We hypothesized that an appropriate correction would reduce the standard deviation (SD) of native myocardial T1 in a population. We used this to explore T1 blood correction.

Methods: Consecutive patients (n=400) without focal septal abnormalities were split into a derivation cohort for model construction (n=200, age 51±18years, 50% male) and a validation cohortfor assessing model performance (n=200, age 48±17, 50% male). A modified Look-Locker inversion recovery sequence (MOLLI, 1.5T Siemens Aera) was used to acquire T1 and T1* maps. A region of interest was placed in the septum on a midventricular short-axis T1 or T1* map to measure native myocardial T1, and RV and LV blood T1 and T1* (figure 1). Hematocrit was measured by venous sampling. The correction model used the formula T1corrected = T1uncorrected + constant (mean(X)-X), where X is the blood measurement of R1 (1/T1), R1* (1/T1*) or hematocrit, and the constants calculated as the slope of multiple linear regression in the derivation cohort. The correction model from the derivation cohort was applied to the validation cohort, and assessed for reduction in variability with the F-test.

Results: Blood mean R1, mean R1* and hematocrit correlated with myocardial T1 (Pearson's *r*, range 0.37 to 0.45, $p < 0.05$ for all) in both the derivation and validation cohort, respectively, supporting the notion that myocardial T1 measurements are influenced by intramyocardial blood. Mean myocardial native T1 did not differ in the derivation and validation cohorts (1030±42.6ms and 1023±45.2ms respectively, p=0.07). In the derivation cohort, correction using LV and RV mean R1 and mean R1* yielded a decrease in myocardial T1 SD (45.2ms to 36.6ms, p=0.03). Correction for hematocrit did not provide an incremental reduction in SD. When the model from the derivation cohort was applied to the validation cohort, the SD reduction was maintained (39.3ms, p=0.049, figure 2).

Conclusions: Correcting native myocardial T1 for R1 and R1* of blood improves the precision of myocardial T1 measurement by ~13% and could consequently improve disease detection.

http://www.ConferenceAbstracts.com/uploads/cfp2/attachments/LDFAIBDN/LDFAIBDN--219959-1-ANY(5).pdf

http://www.ConferenceAbstracts.com/uploads/cfp2/attachments/LDFAIBDN/LDFAIBDN--219959-2-ANY(1).pdf

P269

Non-binary Technique Accounting for Partial Volume Averaging for the Quantification of Myocardial Late Gadolinium Enhancement

Akos Varga-Szemes, MD, PhD[1]Pal Suranyi, MD, PhD[1], U. Joseph Schoepf, MD[1], Rob J. van der Geest, PhD[2], Carlo N. De Cecco, MD, PhD[1], Taylor M. Duguay, BS[1], Moritz Albrecht, MD[1], Domenico De Santis, MD[1], Gabriel A. Elgavish, PhD[3], Balazs Ruzsics, MD, PhD[4]

1. *Medical University of South Carolina, SC*
2. *Department of Radiology, Leiden University Medical Center, Leiden, The Netherlands, Zuid-Holland, Netherlands*
3. *University of Alabama at Birmingham, AL*
4. *Royal Liverpool and Broadgreen University Hospitals, England, United Kingdom*

Background: Binary myocardial infarct (MI) quantification techniques ignore the heterogeneous distribution of MI and do not take partial volume averaging into consideration, resulting in an overestimation in MI size. Non-binary approaches, such as Percent Infarct Mapping (PIM), are able to address these shortcomings. The aim of this study was to investigate the influence of true MI content determined by PIM on segmental myocardial contraction.

Methods: One-hundred-nine patients (54±14 years, 58 males) with suspected prior MI underwent 1.5T MRI (MAGNETOM Avanto, Siemens AG, Erlangen, Germany). Short-axis balanced steady-state free-precession (bSSFP) cine imaging, post-contrast (0.1mmol/kg gadobenate-dimeglumine) T1-mapping (modified Look-Locker inversion recovery (IR), scheme 4(1)3(1)2), and late gadolinium enhancement (LGE) imaging (bSSFP with IR pulse) were performed. Myocardial contraction was quantified as radial wall thickening (RWT) using the centerline method (including 100 chords per slice) according to the 17-segment model. Segmental MI content was calculated based on both T1 and LGE images applying the previously described PIM algorithm (PIM_{T1} and PIM_{LGE}, respectively) using an in-house developed application integrated into the Research Mass Software. MI was also quantified based on LGE images using a binary approach (full-width at half-maximum, FWHM). Relationship between MI percentage (MI%) and RWT was tested using a linear regression.

Results: A total of 1632 segments in 96 patients were analyzed, from which LGE was detected in 259 (15.8%) segments in 47 (48.9%) patients. In these 47 patients, 42 segments were excluded due to image artifacts or inadequate coverage. LGE was consistent with MI in all 47 patients. The FWHM method measured significantly higher global MI% compared to PIM_{T1} and PIM_{LGE} (12.9±2.8%, 8.1±3.2%, and 8.4±3.4%, respectively, PT1 (r=-0.618, P=0.0008) and PIM_{LGE} (r=-0.602, P=0.0011) methods, while the correlation was weaker using the binary FWHM threshold (r=-0.345, P=0.0247).

Conclusions: Both PIM_{T1} and PIM_{LGE} showed good correlation with segmental myocardial contraction. The PIM-based methods measured lower MI% due to their ability to account for partial volume averaging. Non-binary approaches may become preferred techniques for quantitative LGE evaluation as they are able to account for partial volume averaging thus provide more reliable MI measurement and better prediction of segmental myocardial contraction.

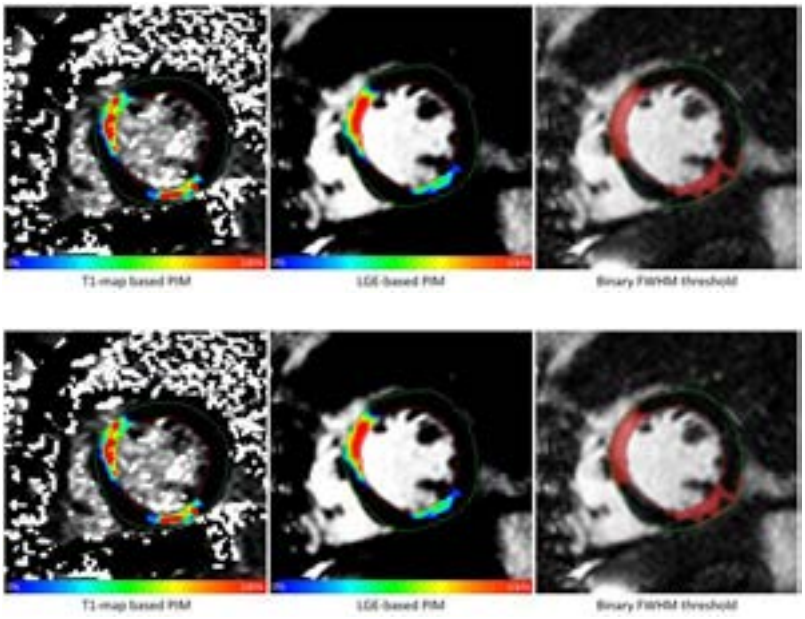

P270

A fast semi-quantitative assessment of atrial fibrosis strongly correlates to fully quantitative segmentation

Dana C. Peters, PhDLauren A. Baldassarre, MD, Steffen Huber, M.D., Hamid Mojibian, M.D., Mark Marieb, M.D., Karl Grunseich, M.D.

Yale University, CT

Background: Several studies have demonstrated the ability of left atrial (LA) fibrosis, quantified by 3D late gadolinium enhancement (LGE) (1) to predict response to therapies for atrial fibrillation (2,3). However, fully-quantitative assessment of LGE requires tedious segmentation of enhanced myocardium, and left atrial volume, in order to obtain "percent enhancement." Work is underway to automate this process (4). We compared semi-quantitative and fully-quantitative assessments of left atrial fibrosis in a large cohort.

Methods: The cohort included 135 patients with no prior ablation, with a diagnostic 3D LGE sequence, imaged between 2012-2014. The semi-quantitative method relied on visual scoring of 18 segments as either enhanced (1) or unenhanced (0). Segments included 4 segments around each vein, and a posterior wall and septal wall segment (Figure 1A). The total score was normalized by 18. The fully-quantitative method manually segmented fibrosis in the entire left atrium, using a contrast to noise ratio of 3.5. The enhanced volume was normalized by the atrial wall volume. Atrial wall volume was approximated as the surface area of a scalene ellipsoid, with radii estimated using 4-chamber area, 2-chamber area, and the long-axis dimension. The surface area was multiplied by 2 mm (LA wall thickness). Indexed minimum LA volumes (LAVI) and LA ejection fraction (LAEF) were measured and recorded.

Results: The semi-quantitative LGE score was highly correlated with the fully quantitative method, R=0.69, $p < 0.001$ (Figure 1B). The semi-quantitative measurements had an intra-observer correlation of R=0.85 with a slope of 0.94. Table 1 compares the correlations between atrial fibrosis, measured with both fully-quantitative and semi-quantitative methods, to expected correlates of LAVI, LAEF, and age. The correlations are similar although weaker using the semi-quantitative method, and remain highly significant. Processing time for semi-quantitative analysis was four times faster. For assessments using quartiles of LGE enhancement extent, the classification discordance was one quartile or less in 90% of patients, with complete agreement in 47% of subjects.

Conclusions: There was a strong correlation between semi-quantitative and fully-quantitative assessments of atrial fibrosis. Importantly, the semi-quantitative method is four times faster and clinically feasible, and does not require specialized software. These findings indicate that a semi-quantitative analysis may be sufficient for assessment of scar burden.

1. Peters DC et al. Radiology 2007.
2. Marrouche NF, et al. JAMA 2014.
3. Malcolme-Lawes LC et al., Heart rhythm, 2013.
4. Tao Q et al. JMRI 2016.

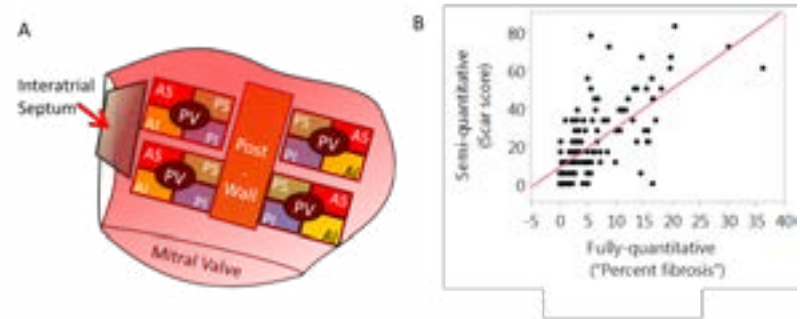

A) The semi-quantitative analysis graded 18 segments for presence of LGE enhancement. The total LA LGE score was then normalized and expressed as %. AS=anterior superior. AI=anterior inferior. PS=posterior superior. PI=posterior inferior. B) The semi-quantitative score was well correlated with the fully quantitative measure of left atrial "percent fibrosis" (R=0.69,p<0.001).

Table 1: Comparison of fully and semi-quantitative measurements of atrial fibrosis.

Analysis time	vs. Age	vs. LAEF	vs. LAVI	
9 ±3 minutes	R=0.36, p<0.001	R=0.42, p<0.001	R=0.41, p<0.001	LA LGE % fibrosis
1.7±0.7minutes	R=0.22, p<0.01	R=0.34, p<0.001	R=0.35, p<0.001	LA LGE scar score

P271

Visualization Methods to Reduce the Opportunities in the Clinic for User Error with Cardiac T1 Mapping

Matthew D. Robson, PhD[2] Isobel C. Gordon[1], Vanessa M. Ferreira, MD, DPhil[3]

1. *University of Oxford, Oxford, England, United Kingdom*
2. *OCMR, University of Oxford, England, United Kingdom*
3. *University of Oxford, England, United Kingdom*

Background: T1 mapping is becoming ever more widespread in clinical practice and as such it is used by an increasing number of clinicians and radiographers who have limited T1 training. This may result in erroneous interpretation of artefactual data. Parametric mapping methods do enable data quality evaluation via the fit error, (R^2 maps) but this can be easily overlooked. This work compares visualisation methods that incorporate R^2 data directly into the map as movie loops to make the error information unavoidable to the radiographer and interpreting physician. These methods should minimise the consequences of incorrect acquisition whilst not influencing the results of quantitative ROI measurements.

Methods: Seven novel methods were built in MATLAB to form movie loops. These included the Twinkling-'A' method where the amplitude of the pixel intensity fluctuation is proportional to ($1-R^2$) of each pixel. Binary matrices were superimposed over the T1 map proportionally to ($1-R^2$) in the Checkerboard-'A' method. Static images were formed in the Blackout method, a masking technique that blacks out pixels which have $R^2 < 0.95$ - an arbitrary cut-off selected for illustration. A preliminary qualitative survey was conducted amongst OCMR physicists – the Checkerboard-'A', Twinkle-'A' and Blackout methods were agreed as preferential to continue development with. It was found that masking methods are preferred to proportionality techniques which require a level of experience to interpret, as is needed in practice today, and hence the Twinkle-'B' and Checkerboard-'B' methods were built - these only introduce intensity fluctuation for pixels with $R^2 < 0.95$. A final survey was conducted amongst 7 trained CMR cardiologists. A quantitative analysis was conducted by considering the mean T1 value in 8 ROIs drawn in original T1 maps and in the altered frames. Examples of the visualisation methods are shown here https://docs.google.com/document/d/1dVp4SKbzZv-ZARNp3uA_bctoapI5uF9uLtlJVjAOnLI/edit?usp=sharing.

Results: The novel visualisation methods rated best for potential translation into clinical trialling were Checkerboard-'B' and Blackout. It was deemed that an automated error message which would appear if the R^2 inside a ROI were less than a user-defined value would also be a useful addition.

Conclusions: This pilot study found that incorporating error information directly into T1 maps is a useful practice. The Checkerboard-'B' approach was highly rated by clinicians and does not bias ROI measurements - this method will be evaluated in more detailed assessments, including real-time generation of movies on the scanner. Clinically-validated thresholds for acceptable R^2 will also be explored.

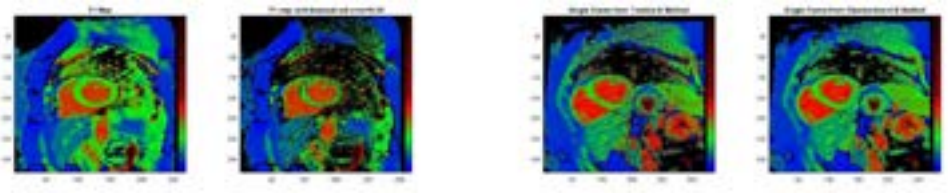

Quantitative Results of Final Survey and of ROI Analysis

Mean Percentage Bias	Mean Percentage Error	Mean Ranking Score for how Well Each Method would Translate into Clinical Trialling (/5, with 5 as best)	
+0.03	0.26	2.00	Twinkle 'A'
-1.20	1.20	2.71	Checkerboard 'A'
+1.09	1.63	2.86	Twinkle 'B'
-0.53	0.88	3.71	Checkerboard 'B'
-3.67	3.67	3.71	Blackout

Table 1: 8 ROIs were taken on 8 different frames for each method over 4 data sets - one set with 'good' R^2, one with poor R^2, one in which the patient had been breathing and one in which mistriggering had occurred. The mean T1 value in the ROI in the T1 map was compared to that in the altered frame to obtain the percentage error and bias above. Since eliminating the Checkerboard 'A' method, the format of the checkerboard pixel fluctuations were altered to eliminate the strong bias, explaining why the error and bias do not take the same value in Checkerboard 'B'. The ROIs were drawn in positions where it would be unwise for the clinician to take a reading but where they could potentially be drawn, so in general practise the percentage error will be lower than the values above.

P272

Comparing myocardial T1 relaxometry post-processing techniques for pediatric and congenital heart disease: interchangeability and reproducibility.

Christopher Z. Lam, MD[1], Lars Grosse-Wortmann, MD[2]Joseph J. Pagano, MD[2], Deane Yim, MBchB[3], Shi-Joon Yoo, MD[4], Mike Seed, MBBS[5]

1. *The Hospital for Sick Children, University of Toronto, Toronto, ON, Canada*
2. *The Hospital for Sick Children, ON, Canada*
3. *The Hospital for Sick Children, Toronto, ON, Canada*
4. *Hospital for Sick Children, Toronto, ON, Canada*
5. *SickKids, Toronto, ON, Canada*

Background: Quantification of myocardial T1 relaxometry can be performed by individually contouring corresponding regions of interest on each of the source images ('Source method'), followed by a curve-fitting algorithm, or, by contouring a single region of interest on a composite parametric T1 map where each pixel encodes for a specific T1 value ('Mapping method'). This study assesses whether these two methods are interchangeable in the pediatric population.

Methods: Two groups of pediatric patients that had clinically indicated cardiac magnetic resonance imaging (CMR) with extracellular volume (ECV) quantification were included in this single institution retrospective study. Group A comprised of 20 consecutive asymptomatic subjects with normal CMR exams referred for screening. Group B included 20 consecutive tetralogy of Fallot (TOF) patients status post primary repair. T1 relaxometry was performed in a midventricular short axis slice on a 1.5 Tesla scanner using the Modified Look-Locker Inversion Recovery (MOLLI) sequence with inline motion correction. Two independent observers quantified native T1 and ECV% for the entire left ventricle (LV) using both the Source and integrated Mapping approaches. The LV contour was subdivided into 6 equiangular segments. A correction factor of 1.0365 for nonideal inversion was applied to the T1 values. Bland-Altman analyses and paired student t-tests were used to compare the Source and Mapping methods for intermethod agreement. Intraclass correlation coefficients and Bland-Altman analyses were used to assess reproducibility between two independent observers.

Results: Table 1 is a summary of the analysis comparing Source and Mapping methods. In Group A with normal anatomy, the Source and Mapping methods produced different results for the entire LV native T1 (mean difference 11 +/- 17 ms, P=0.01), interventricular septum (IVS) native T1 (mean difference 10 +/- 14 ms, P=0.01), and entire LV ECV% (mean difference 0.8% +/- 1.6%, P=0.04). In Group B with TOF, the Source and Mapping methods produced different results for the IVS native T1 (mean difference 9 ms +/- 20 ms, P=0.05). The Bland-Altman scatter plot for the differences in IVS native T1 in TOF subjects is shown in Figure 1. Intraclass correlation coefficients were greater for the Mapping method compared to the Source method (Table 2). There was less interobserver variability in patients with TOF compared with subjects with normal anatomy.

Conclusions: The Source and Mapping methods produce different values and may not be interchangeable. The Mapping method is more reproducible in normal subjects, while both Source and Mapping methods are equally highly reproducible in TOF patients.

http://www.ConferenceAbstracts.com/uploads/cfp2/attachments/LDFAIBDN/LDFAIBDN--219076-1-ANY.pdf

Comparison of Native T1 and ECV values between Source and Mapping methods

P-Value	SD 95% CI	SD	Mean Difference (Mapping - Source)	
				Normal CMR Subjects
0.01	-22 to 44 ms	17 ms	11 ms	*Entire LV T1*
0.01	-37 to 18 ms	14 ms	-10 ms	LV Septum T1
0.40	-72 to 59 ms	34 ms	- 6 ms	LV Free Wall T1
0.04	-2.3 to 3.8%	1.6%	0.8%	Entire LV ECV%
				TOF Subjects
0.66	-36 to 40 ms	19 ms	2 ms	Entire LV T1
0.05	-48 to 30 ms	20 ms	-9 ms	LV Septum T1
0.12	-107 to 73 ms	46 ms	-17 ms	LV Free Wall T1
0.28	-1.6 to 2.1%	0.9%	-0.2%	Entire LV ECV%

SD: Standard Deviation of difference. CI: Confidence Interval.
P-values derived from paired student T-tests.

Intraclass Correlation Coefficients between two independent observers

ICC for Mapping Method	ICC for Source Method	
		Normal CMR Subjects
0.87	0.58	*Entire LV*
0.87	0.75	LV Septum
0.67	0.62	LV Free Wall
0.97	0.87	Entire LV ECV%
		TOF Subjects
0.95	0.94	Entire LV
0.98	0.96	LV Septum
0.90	0.92	LV Free Wall
0.97	0.97	Entire LV ECV%

ICC: Intraclass Correlation Coefficient.

P273

Quantitative Evaluation of Myocardial Fibrosis by CMR in Non-Ischemic Heart Disease Using a Semi-Quantitative Visual Analysis Technique: Comparison with Standard Semi-Automated Thresholding Techniques

Livia M. Castro, MD[1], Filipe P. Carvalho, MD[2]Ronaldo S. L. Lima, MD PhD[3], Andréa A. Brandão, MD PhD[4], Denilson C. Albuquerque, MD PhD[4], Carlos E. Rochitte, MD PhD[5], Clerio F. Azevedo, MD PhD[3]

1. *CDPI-DASA, Rio de Janeiro, Rio de Janeiro, Brazil*
2. *CDPI-DASA, Rio De Janeiro, Rio de Janeiro, Brazil*
3. *CDPI-DASA, Rio de Janeiro, Brazil*
4. *Universidade Estadual do Rio de Janeiro - UERJ, Rio de Janeiro, Brazil*
5. *Heart Institute - InCor, N/A, Brazil*

Background: The assessment of myocardial fibrosis (MF) by cardiac magnetic resonance (CMR) using late gadolinium enhancement (LGE) has been shown to provide valuable prognostic information in patients with non-ischemic heart diseases (NIHD).

Currently, quantitative assessment of MF requires time-consuming analyses using commercially available dedicated software.

We describe a new method of MF quantification using a semi-quantitative visual analysis of LGE images and evaluate its agreement with frequently used thresholding techniques.

Methods: Contrast-enhanced CMR was performed in 90 patients with NIHD (hypertrophic cardiomyopathy [n=30]; non-ischemic dilated cardiomyopathy [n=30]; and acute myocarditis [n=30]). Only patients with identifiable regions of LGE were included.
In order to quantify MF by the semi-quantitative visual analysis technique (Visual), LGE slices were segmented into 44 segments (2 apical slices with 4 segments each, 3 mid-ventricular slices with 6 segments each and 3 basal slices with 6 segments each). The amount of LGE in each segment was scored using a 6-point scale: 0-no LGE; 1->0% and ≤5%; 2->5% and ≤25%; 3->25% and ≤50%; 4->50% and ≤75%; and 5->75%. The total amount of LGE was calculated as the sum of the scores of all 8 slices divided by 220 (maximum possible score: 5*44=220) and was reported as a percent of LV mass.
MF quantification was also performed using 4 different semiautomated thresholding techniques: 2SD of remote (2SD); 6SD of remote (6SD); manual threshold (Manual); and full width at half maximum (FWHM).

Results: The amount of MF quantified by Visual (15.8±9.7%) was similar to that quantified by Manual (15.8±10.5%, p=0.85) and FWHM (16.2±10.1%, p=0.27), was slightly higher than 6SD (14.4±10.5%, p=0.002) and was significantly lower than 2SD (39.6±14.5%, p < 0.001).

The results of Bland-Altman and concordance correlation coefficient analyses are summarized in Table 1. There was good agreement between Visual and all thresholding techniques, except 2SD, which significantly overestimated the amount of LGE. When we evaluated the agreement within each disease subgroup the pattern was similar to that observed for the entire population (Table 1). Inter- and intra-observer variabilities were small for all measurements (Table 2). Importantly, the average time per patient for the Visual technique (1'21'') was significantly shorter than Manual (9'7'', p < 0.001), FWHM (9'12'', p < 0.001) and 2SD/6SD (9'33'', p < 0.001).

Conclusions: Quantification of MF by the novel semi-quantitative visual technique demonstrated good agreement with standard thresholding methods. Our results indicate that it could represent a faster and more practical alternative for the post-processing analyses of LGE images in patients with NIHD.

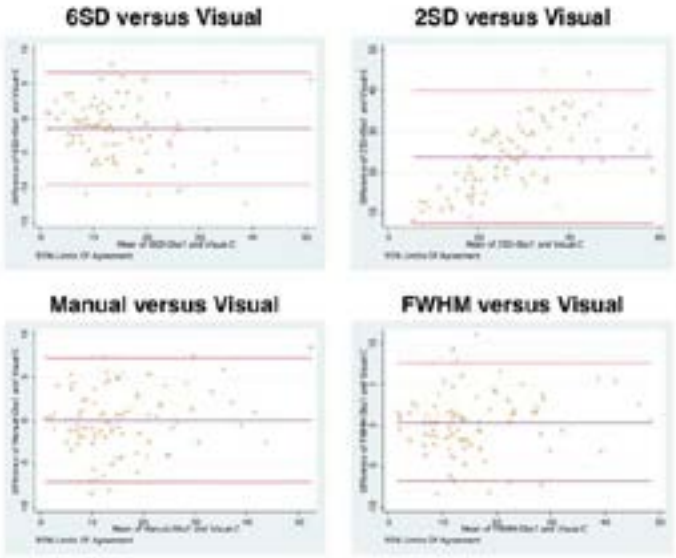

Agreement Between the Visual Technique and Standard Threshold Methods

r	CCC	95% LoA	Mean diff.	Method
All patients (n = 90)				
0.93	0.93	-7.1 — 7.2%	0.1 ± 3.6%	Manual vs Visual
0.93	0.92	-6.8 — 7.7%	0.4 ± 3.7%	FWHM vs Visual
0.90	0.89	-9.4 — 6.6%	-1.4 ± 4.1%	6SD vs Visual
0.84	0.27	7.6 — 39.9%	23.7 ± 8.2%	2SD vs Visual
Hypertrophic cardiomyopathy (n = 30)				
0.95	0.94	-8.2 — 7.9%	-0.2 ± 4.1%	Manual vs Visual
0.95	0.95	-7.0 — 6.3%	-0.3 ± 3.4%	FWHM vs Visual
0.95	0.93	-8.8 — 5.5%	-1.6 ± 3.6%	6SD vs Visual
0.86	0.28	10.2 — 38.3%	24.3 ± 7.1%	2SD vs Visual
Non-ischemic dilated cardiomyopathy (n = 30)				
0.93	0.93	-7.1 — 7.4%	0.1 ± 3.7%	Manual vs Visual
0.93	0.91	-5.8 — 9.3%	1.7 ± 3.8%	FWHM vs Visual
0.89	0.86	-10.6 — 6.5%	-2.0 ± 4.3%	6SD vs Visual
0.84	0.27	5.6 — 43.3%	24.4 ± 9.6%	2SD vs Visual
Acute myocarditis (n = 30)				
0.88	0.88	-6.0 — 6.4%	0.2 ± 3.1%	Manual vs Visual
0.84	0.84	-7.1 — 7.0%	-0.1 ± 3.6%	FWHM vs Visual
0.78	0.78	-8.8 — 7.9%	-0.4 ± 4.2%	6SD vs Visual
0.78	0.17	7.2 — 37.9%	22.5 ± 7.8%	2SD vs Visual

P<0.001 for all CCC and Pearson Correllation Coefficients; Mean diff. = Mean difference, 95% LoA = 95% Limits of Agreement, CCC = Concordance Correlation Coefficient, r = Pearson correlation coefficient

Inter-observer and Intra-observer Variability of LGE Quantification Using the Different Techniques

r	CCC	95% LoA	Mean diff.	Method
Inter-observer - All patients (n = 90)				
0.92	0.90	-9.2 — 9.5%	0.1 ± 4.7%	Visual
0.96	0.95	-5.8 — 6.5%	0.3 ± 3.1%	Manual
0.95	0.94	-6.0 — 7.4%	0.7 ± 3.4%	FWHM
0.91	0.90	-8.9 — 7.3%	-0.8 ± 4.1%	6SD
0.86	0.85	-13.0 — 15.9%	1.4 ± 7.3%	2SD
Intra-observer - All patients (n = 90)				
0.98	0.97	-4.8 — 4.6%	-0.1 ± 2.4%	Visual
0.97	0.97	-5.0 — 4.9%	-0.1 ± 2.5%	Manual
0.96	0.96	-6.9 — 4.9%	-1.0 ± 3.0%	FWHM
0.91	0.89	-10.3 — 6.9%	-1.6 ± 4.4%	6SD
0.89	0.87	-15.4 — 10.0%	-2.7 ± 6.4%	2SD

P<0.001 for all CCC and Pearson Correllation Coefficients; Mean diff. = Mean difference, 95% LoA = 95% Limits of Agreement, CCC = Concordance Correlation Coefficient, r = Pearson correlation coefficient

P274

Automated Detection of Myocardial Pixels in First-Pass CMR Perfusion Maps

Matthew J. Jacobs, MSc[1] Mitchel Benovoy, PhD[2], Lin-Ching Chang, DSc[3], Andrew E. Arai, MD[4], Li-Yueh Hsu, DSc[5]

1. *The Catholic University of America, Riverdale, MD*
2. *NIH/NHLBI, PQ, Canada*
3. *The Catholic University of America, Washington, DC*
4. *National Institues of Health, Bethesda, MD*
5. *National Institutes of Health, Bethesda, MD*

Background: Fully quantitative myocardial blood flow (MBF) pixel maps of Cardiac Magnetic Resonance (CMR) first-pass perfusion imaging may be useful for assessing coronary artery disease (CAD). However, segmental analysis of the myocardium requires manual identification of the myocardial pixels within each MBF pixel map. We aim to develop a fully automated method to detect the myocardial region of interest (ROI) within the MBF pixel maps.

Methods: Rest and regadenoson stress gadolinium-enhanced CMR perfusion images were acquired from 17 healthy volunteers with a saturation recovery steady-state free precession dual sequence technique. A fully automated method was first used to compute MBF maps covering the entire image. Next, an automated method is developed to detect the myocardial pixels from the perfusion images and the MBF maps. This method starts with motion correction, intensity bias correction, and left ventricular (LV) detection for image preprocessing. The myocardial pixels are then detected using morphological processing, active contours modeling, and MBF thresholding. The automatically detected myocardial pixels were compared with manually traced myocardial ROI in the pixel maps using both Dice and Cohen Kappa statistics to measure agreement within the myocardial area. After converting myocardial pixels to myocardial ROI, the Euclidean distance was evaluated to assess the similarity of the epicardial and endocardial borders between the two methods.

Results: Figure 1 shows an example of the automatically and manually segmented myocardial pixels. The automated myocardial regions match well with the manual results except the papillary muscles within the myocardial region. For the myocardial area assessment, both Dice and Kappa statistics show good agreement between the automated and the manual ROI with an average of 0.80±0.07 and 0.79±0.07 respectively. The Euclidean distance metrics for comparing the myocardial border between the automated and the manual segmentations also show good similarity. The epicardial borders were separated by an average distance of 2.05±1.21mm while the endocardial borders' distance were on average 1.95±0.70mm.

Conclusions: Myocardial pixels in MBF maps from first-pass CMR perfusion images can be automatically detected by a fully automated process. The proposed method demonstrated good agreement with the manual reference, while removing the need for manual processing. The results warrant further investigation in a larger dataset to validate the applicability of the proposed method in CAD patients.

http://www.ConferenceAbstracts.com/uploads/cfp2/attachments/LDFAIBDN/LDFAIBDN--221065-1-ANY(1).pdf

P275

SinMod method for quantification of LV rotational motion

Abbas Nasiraei Moghaddam, PhD[2]Fatemeh Rastegar, BSc[1], Elham Mohammadi, MSc[1]

1. Amirkabir University of Technology, Tehran, Iran
2. Amirkabir University of Technology, Tehran, Tehran, Iran

Background: Assessment of left ventricle (LV) rotational motion is hypothesized to help in early diagnosis of heart failure [1]. Cardiac MR tagging facilitates the measurement of LV rotational motions. Due to angular geometry of LV, Radial tagging is the method of choice to capture this motion [2]. In this study Sine wave modeling (SinMod), previously developed to extract cardiac deformation from tagged images [3], was applied on radially tagged images to directly measure the rotational motion.

Methods: The SinMod method fits a sine wave to tagging intensity, perpendicular to taglines [3]. In polar system the intensity was formulated as , based on magnitude, phase and frequency of changes. Therefore, SinMod is able to estimate the local rotation, , in azimuth direction. Short-axis radial tagging was performed on Mid level of human LV for 8 healthy subjects and 7 patients with Duchene muscular dystrophy (DMD). Number of radial taglines was set to 22 per circle while the images had a matrix size of 192x156, resulting in a pixel size of 1.45x1.45 mm. The myocardium region was manually masked and images were converted to polar coordinate based on center of gravity of epicardium. The local circumferential displacement field was then estimated in successive images by implementation of SinMod method (Figure 1). Finally, the global rotation was obtained and compared to another method.

Results: Figure 2-top shows the average of global rotation for healthy subjects based on the proposed method (polar SinMod) and one calculated from decomposition of deformation gradient tensor [4]. The patterns of global rotation are concordant with those reported in literature with 1.13% difference in global rotation peak. Figure 2-bottom shows the average global rotation for volunteers and DMD patients separately. As expected, the LV counterclockwise rotation peak for DMD patients (2.7±1.38 degrees) was significantly lower than healthy volunteers (4.48±1.29 degrees) ($p=0.032$). Also there was a significantly higher clockwise rotation peak in patients with DMD (-8.17±2.37) compared to volunteers (-2.35±0.97) ($p=0.0013$). (Figure 3)

Conclusions: We have shown that SinMod method can be applied on radial tagged images to obtain the rotation of myocardium both locally and globally. As an example, Results showed that LV peak rotation in DMD patients is significantly higher in the clockwise direction. The measurement of rotational motion as a cardiac index can be further accelerated when combined with a recently developed PFT method [5] in which the entire process of acquisition/reconstruction takes place in the polar coordinates.

References: [1] Kaveh, et al., *JCMR* 16(Suppl 1):P24 (2014). [2] Nasiraei-Moghaddam, et al., MRM, 71:1750–1759 (2014). [3] Arts, et al., TMI, 29.5: 1114-1123 (2010). [4] Kaveh, et al., *JCMR* 15(Suppl 1): p. E48 (2013). [5] Golshani, et al., MRM, DOI: 10.1002/mrm.26219 (2016).

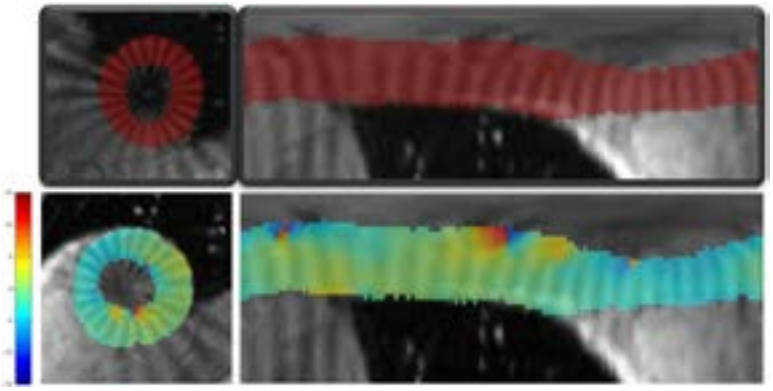

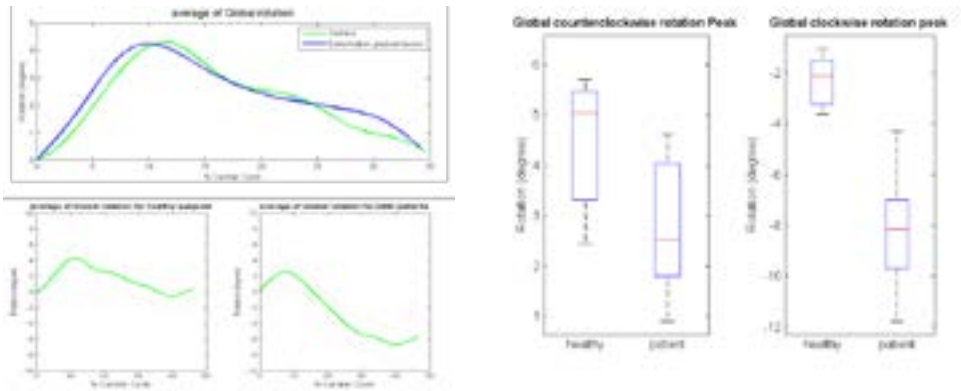

P276

Same sequence – different software provider: different results? A post-processing comparison of flow, T1 and T2 mapping.

Leonora Zange, MD[1] Fabian Muehlberg, MD[2], Stephanie Funk, MD[2], Edyta Blaszczyk, MD[2], Julius Traber, MD[2], Johannes Schueler, MD[3], Luisa Schmacht[2], Jeanette Schulz-Menger, MD[3]

1. *Working Group on Cardiovascular Magnetic Resonance, Experimental and Clinical Research Center, a joint cooperation between the Charité Medical Faculty and the Max-Delbrueck Center for Molecular Medicine and HELIOS Hospital Berlin Buch, Berlin, Berlin, Berlin, Germany*
2. *Working Group on Cardiovascular Magnetic Resonance, Experimental and Clinical Research Center, a joint cooperation between the Charité Medical Faculty and the Max-Delbrueck Center for Molecular Medicine and HELIOS Hospital Berlin Buch, Berlin, Berlin, Germany*
3. *Working Group on Cardiovascular Magnetic Resonance, Experimental and Clinical Research Center a joint cooperation between the Charité Medical Faculty and the Max-Delbrueck Center for Molecular Medicine HELIOS Klinikum Berlin Buch, Germany, Berlin, Germany*

Background: Technical aspects and patient-related factors during image acquisition influence CMR. There is a big effort towards standardization [1]. Little is known about the impact of post-processing software on image analysis. The aim of this study was to investigate the agreement of different post-processing software packages (SW).

Methods: 30 data sets of consecutive patients who underwent CMR at 1.5T (Siemens) were analyzed using 3 different SW. We compared conventional phase contrast measurements (TR 33.36 ms, TE 2.3 ms, voxel size 1.8 x 1.8 x 6 m^3, 30 phases) acquired perpendicular in ascending aorta at sinotubular junction, native T1 map (MOLLI 5s(3s)3s, motion corrected) and T2 map (SSFP, motion corrected) in one midventricular short axis.

All data sets were analyzed by one reader blinded to former results using Syngo/Argus version VE53A, Siemens; CVI42®, Circle CVI version 5.3.2 and Qmass/Qflow version 8.1., Medis. Peak velocity (Vmax) was measured by contouring the border of ascending aorta in the magnitude image with the sharpest blood/tissue contrast, transmitted automatically in all temporal phases and corrected manually. Slice-based T1 and T2 times were obtained by contouring endo- and epicardial borders of compact myocardium in raw images, copied into scanner generated maps and manually corrected or directly drawn into the map, depending on software configuration.

Results: All images could be analyzed with all SW (figure 1 for means). SW names were anonymized.
Vmax: Best agreement was detected between SW A-B (r^2=0.995). In contrast, A-C (r^2=0.569) and B-C (r^2=0.572) had a weaker concordance (figure 2). T1-time: Smallest bias was found between SW B-C (r^2= 0.924), (table1). Agreement was less between A-C (r^2=0.790) and A-B (r^2=0.808). T2-time: All SW had a negligible bias and presented a close agreement (table 1). Strongest correlation was found between B-C (r^2=0.867), followed by A-C (r^2=0.832) and A-B (r^2=0.805).

Conclusions: The best agreement between SW was found in quantification of T2 time. A noticeable bias was revealed in T1 time and Vmax. This could be due to different software algorithm in flow analysis and software distinct pixel-definition and needs to be further investigated. A change of post-processing software may influence results.

References: 1. Schulz-Menger et al., J Cardiovasc Magn Reson 2013.

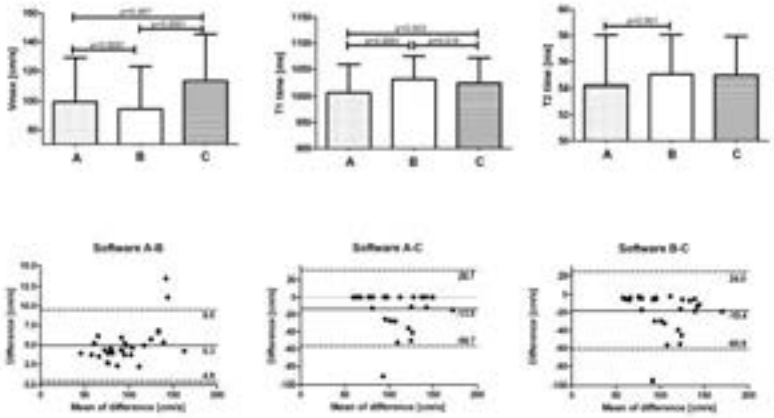

Table 1: Mean difference ± SD and limits of agreement (95% confidence interval) between Software.

B-C	A-C	A-B	
7.6 ± 13.6 (-19.2 – 34.3)	-16.3 ± 24.0 (- 63.3 – 30.8)	-23.8 ± 23.0 (-68.9 – 21.2)	T1 time [ms]
0.1 ± 1.1 (-2.1 – 2.3)	-0.8 ± 1.7 (-4.0 – 2.5)	-0.8 ± 1.8 (-4.3 – 2.6)	T2 time [ms]

P277

Advancing quantitative 4D flow MRI: Assessment of manual versus automatic boundary definition in the aorta

Judith Zimmermann, MS[1] Lennart Tautz, MS[2], Naira Mkrtchyan, Dr.[3], Heiko Stern, Prof. Dr.[3], Christian Meierhofer, Dr. Dr.[4], Anja Hennemuth, Dr.[2]

1. *Pediatric Cardiology and Congenital Heart Disease, German Heart Center Munich, München, Bayern, Germany*
2. *Fraunhofer MEVIS, Bremen, Germany*
3. *Pediatric Cardiology and Congenital Heart Disease, German Heart Center Munich, Bayern, Germany*
4. *Pediatric Cardiology and Congenital Heart Disease, German Heart Center Munich, Munich, Bayern, Germany*

Background: 4D flow MRI enables the assessment of various quantitative hemodynamic parameters (e.g. velocity profiles) in the heart and surrounding vessel (Dyverfeldt et al., 2015). However, calculation of these parameters relies on a pre-computed lumen boundary, which should be defined individually at all cardiac phases (Köhler et al., 2016). In contrast, if vessel movement throughout the cardiac cycle is not taken into account, velocities originating from outside the vessel of interest will contribute (Fig. 1). Our objective was to study the performance of automatic contour propagation in the aorta based on an image registration approach using quadrature filters (*Morphon*).

Methods: Six subjects underwent a 4D flow MRI exam (1.5T Siemens Avanto) to acquire a parasagittal slab of the aorta. Acquisition parameters were: TE/TR [ms] = 2.6/40; FOV [mm] = 400x300x60; Voxel resolution [mm] = 2.3x2.3x2.3; VENC [cm/s] = 150. Prospective ECG-triggering and navigator gating was employed. All data processing was performed using application tailored software implemented with the MevisLab framework (Ritter et al., 2011). 3D+t magnitude image data was reformatted to obtain image planes (MPR) orthogonal to the aortic centerline at three locations: ascending aorta (aAo), arch, and descending aorta (dAo). Manual vessel contours were obtained from two independent experts for all datasets, for all defined MPRs and for all given cardiac phases. Accordingly, automatic contour propagation of a single manually defined contour at systole and diastole throughout the cardiac cycle was performed based on the suggested image registration approach (Forsberg, 2013). Dice indices and Hausdorff distance (HD, in mm) were computed to evaluate inter-expert variability as well as algorithm performance given the corresponding manual contours as ground truth.

Results: Inter-observer variability resulted in acceptable scores for Dice (median = 0.88) and HD (median = 5.23), with max/min outliers of 0.99/0.72 and 12.6/1.27 for Dice and HD, respectively (Fig. 2C). Similarly, performance of the automatic propagation was consistently decent when compared to the manual contours: 0.92/0.98/0.72 and 4.86/13.8/1.46 (median/max/min) for Dice and HD, respectively (Fig. 2B) Different initializations (i.e. manual starting contours) did not impact propagation results, showing acceptable agreement in overall Dice (median = 0.91) and HD (median = 4.97) with small deviations (Fig. 2C).

Conclusions: Automatic propagation is feasible and shows consistent results when compared to manual contours. Inter-observer median similarity scores are acceptable, however, outliers are present and would negatively influence subsequent quantitative flow data analysis. Here, propagation offers results with increased reproducibility. In addition, automation will speed up the workflow where a time-variant volumetric surface mesh is required for quantitative 4D flow analysis.

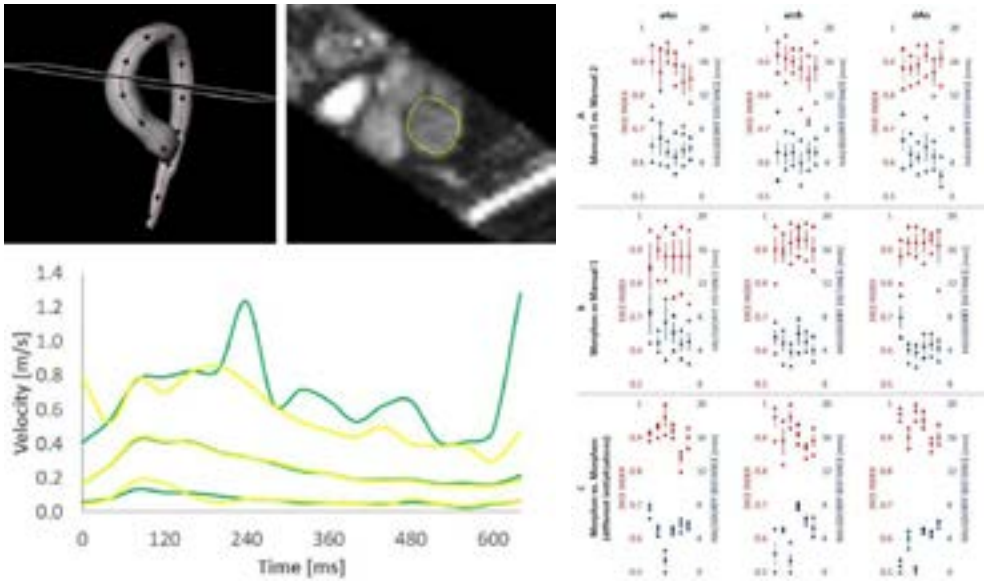

P278

Comparison of Myocardial Fibrosis Quantification Using Magnitude and Phase-Sensitive Inversion Recovery Late Gadolinium Enhancement Images in Patients with Non-Ischemic Heart Disease

Filipe P. Carvalho, MD[1], Livia M. Castro, MD[2]Fabio P. R. Siqueira, MD[3], Anna X. Alvim, MD[4], Diogo B. Peixoto, MD[3], Mariá C. Coeli, MD[5], Ronaldo S. L. Lima, MD PhD[3], Clerio F. Azevedo, MD PhD[3]

1. *CDPI-DASA, Rio De Janeiro, Rio de Janeiro, Brazil*
2. *CDPI-DASA, Rio de Janeiro, Rio de Janeiro, Brazil*
3. *CDPI-DASA, Rio de Janeiro, Brazil*
4. *CDPI - DASA, Rio de Janeiro, Brazil*
5. *CDPI- DASA, Rio de Janeiro, Rio de Janeiro, Brazil*

Background: The assessment of myocardial fibrosis (MF) by cardiac magnetic resonance (CMR) using late gadolinium enhancement (LGE), either with magnitude-reconstructed inversion recovery (MIR) or phase sensitive inversion recovery (PSIR) images, has been shown to provide valuable prognostic information in patients with non-ischemic heart diseases (NIHD). Quantitative assessment of MF using on MIR images has been extensively validated in the literature. Recently, however, it has been demosntrated that systematic bias may exaggerate MF quantification when PSIR images are used, especially in the setting of NIHD. In the present study we sought to evaluate the agreement and reproducibility of LGE quantification using MIR and PSIR images in a cohort of NIHD patients.

Methods: Contrast-enhanced CMR was performed in 90 patients with NIHD (hypertrophic cardiomyopathy [HCM, n=30]; non-ischemic dilated cardiomyopathy [DCM, n=30]; and acute myocarditis [n=30]). Only patients with identifiable regions of LGE were included.

MF quantification was performed using both MIR and PSIR datasets by 2 independent observers using 3 different thresholding techniques: 2SD of remote (2SD); 6SD of remote (6SD); and manual threshold (Manual).

The agreement between each threshold technique was evaluated by Bland-Altman and concordance correlation coefficient (CCC) analyses.

Results: The amount of MF quantified by MIR and PSIR demonstrated good correlation for all 3 threshold techniques evaluated (Table 1). MF was slightly underestimated on PSIR when compared to MIR for all techniques (6SD: 11.3±9.2% vs 13.6±10.0%, p 0.001; 2SD 39.3±13.2% vs 41.0±13.6%, p=0.04; Manual: 15.7±11.3% vs 16.2±11.2%, p=0.009). Remarkably, Manual threshold yielded the best agreement between PSIR and MIR (mean difference = 0.5±1.9%, 95%LoA = -3.2−4.2%, CCC=0.98, r=0.99). When the agreement within each disease subgroup was evaluated, 6SD PSIR underestimated MF on HCM (17.2±13.5% vs. 13.8±12.7%, $p < 0.001$) and DCM (12.0±7.3% vs. 9.0±6.4%, $p < 0.001$) populations, but not on the myocarditis subgroup (mean difference = 0.5±3.3%, 95%LoA = -6.0−7.0%, CCC=0.89, r=0.89). Manual threshold yielded the best agreement between PSIR and MIR on all subgroups. Bland-Altman and CCC analyses are summarized on Table 1. Inter- and intra-observer variabilities were small for all measurements (Table 2).

Conclusions: Quantification of MF using LGE PSIR images demonstrated good agreement with conventional assessment using standard MIR images. Among the 3 different signal intensity threshold techniques, Manual has been shown to provide the highest degree of agreement and to be the most reproducible. Our findings indicate that both PSIR and MIR image datasets can be used for the quantitative assessment of MF in patients with NIHD with comparable results.

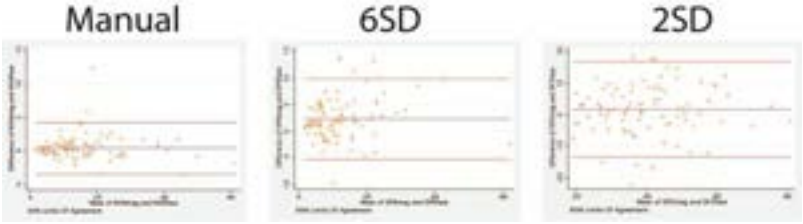

Agreement Between MIR and PSIR Images LGE Quantification Using Standard Threshold Methods.

r	CCC	95% LoA	Mean diff.	Method
All patients (n = 90)				
0.99	0.98	-3.2% – 4.2%	0.5 ± 1.9 %	Manual
0.92	0.89	-5.3% – 9.9%	2.3 ± 3.9 %	6SD
0.83	0.82	-13.4% – 17.0%	-1.8 ± 7.8 %	2SD
HCM (n = 30)				
0.99	0.99	-2.7% – 2.3%	-0.2 ± 1.3%	Manual
0.95	0.91	-5.0 – 11.8%	3.4 ± 4.3%	6SD
0.85	0.85	-16.0 – 18.0%	0.8 ± 8.8%	2SD
DCM (n = 30)				
0.97	0.96	-3.7 – 6.1%	1.2 ± 2.5%	Manual
0.87	0.79	-4.1 – 9.9%	2.9 ± 3.6%	6SD
0.83	0.76	-8.5 – 18.1%	4.8 ± 6.8%	2SD
Myocarditis (n = 30)				
0.97	0.96	-2.5 – 3.7%	0.6 ± 1.6%	Manual
0.89	0.89	-5.9 – 6.9%	0.5 ± 3.3%	6SD
0.82	0.82	-4.0 – 13.4%	-0.3 ± 7.0%	2SD

P<0.001 for all CCC and Pearson correlation coefficients. Mean diff = mean difference, 95% LoA = 95% Limits of Agreement, CCC = Concordance Correlation Coefficient, r = Pearson Correlation coefficient

Inter-Observer and Intra-Observer Variability on PSIR Image LGE Quantification

r	CCC	95% LoA	Mean Diff	Method
Inter-Observer - All patients (n=90)				
0.96	0.96	-5.2 − 4.2%	-0.2 ± 2.6%	Manual
0.94	0.93	-8.7 − 5.7%	-1.5 ± 3.7%	6SD
0.92	0.90	-11.6 − 11.4%	-0.1 ± 5.9%	2SD
Intra-observer - All patients (n=90)				
0.99	0.98	-3.9 − 4.3%	0.2 ± 2.1%	Manual
0.91	0.88	-7.9 − 10.5%	1.3 ± 4.7%	6SD
0.90	0.89	-13.8 − 10.0%	-1.9 ± 6.1%	2SD

P<0.001 for all CCC and Pearson correlation coefficients. Mean diff = mean difference, 95% LoA = 95% Limits of Agreement, CCC = Concordance Correlation Coefficient, r = Pearson Correlation coefficient

P279

Fully automated myocardial segmentation of cardiac BOLD MRI

Ilkay Oksuz, M.sc.[1]Rohan Dharmakumar[2], Sotirios A. Tsaftaris[3]

1. *IMT Institute for Advanced Studies Lucca, Lucca, Toscana, Italy*
2. *Cedars-Sinai Medical, CA*
3. *The University of Edinburgh, Scotland, United Kingdom*

Background: Cardiac Phase-resolved Blood Oxygen-Level-Dependent (CP-BOLD) MRI is an emerging modality for detect an ongoing myocardial ischemia at stress or rest. It relies on the observation that myocardial signal intensity varies as a function of cardiac phase and disease. Myocardial segmentation is an indispensable step to detect these changes. Automated analysis approaches, which can obtain accurate segmental delineation are desirable since they can lead to improved and repeatable accuracy in detection of the disease. Unfortunately, at present due to BOLD contrast variations, classical approaches to segmentation are unable to reach desirable accuracy of segmentation and consequently to accurately determine signal variations across the regions. Here, we propose an algorithm that relies on sparse features coupled with cardiac motion to ensure high accuracy of segmentation.

Methods: Imaging studies were performed on a 1.5T Espree (Siemens Healthcare). TR/TE 6.2/3.1ms; spatial resolution=1.2x1.2x8 mm3, flip-angle=70°, ~25 frames per cardiac cycle Flow- and motion-compensated 2D short-axis CP-BOLD was acquired along the mid ventricle in 10 canines at baseline and under severe LAD stenosis. The main principle of our method (Fig. 1) is to first use a rough myocardial segmentation estimate to learn sparse features (dictionaries for myocardium and background) to classify the pixels according to the residuals (relying on classification when projecting on discriminatory dictionaries) of an input CP-BOLD subject exam. Then a Markov Random Fields (MRF) scheme applied on the residuals favors similar labels in local neighborhoods and creates a smoother outcome. Sparse information is learnt directly from the images in the cardiac cycle (cine acquisition) without any supervision and manual interaction and this information is used to classify the pixels of the myocardium for segmentation. The precision of the segmentation is reflected with the accuracy of regional intensity curves generated using segmentations from our method.

Results: Dice coefficient is used as a metric for the evaluation with the expert annotated ground truth segmentations. As seen in Table 1, experiments with different groups of data sets show that the proposed approach obtains accurate regional segmentations. In an example from a canine the proposed approach delineates myocardial region accurately (Fig. 2a), which leads to high timeseries match (Fig. 2b) compared to other automated methods with cosine similarity.

Conclusions: The experiments clearly underline the need for a new representation in image segmentation. Using the information from the same subject to train the dictionaries generates a compact representation of the information and improves the accuracy of segmentation. Even tough, coupling this method with registration should lead to better results, our is method opens the road to repeatable, truly non-invasive diagnosis of ischemic heart disease from CP-BOLD.

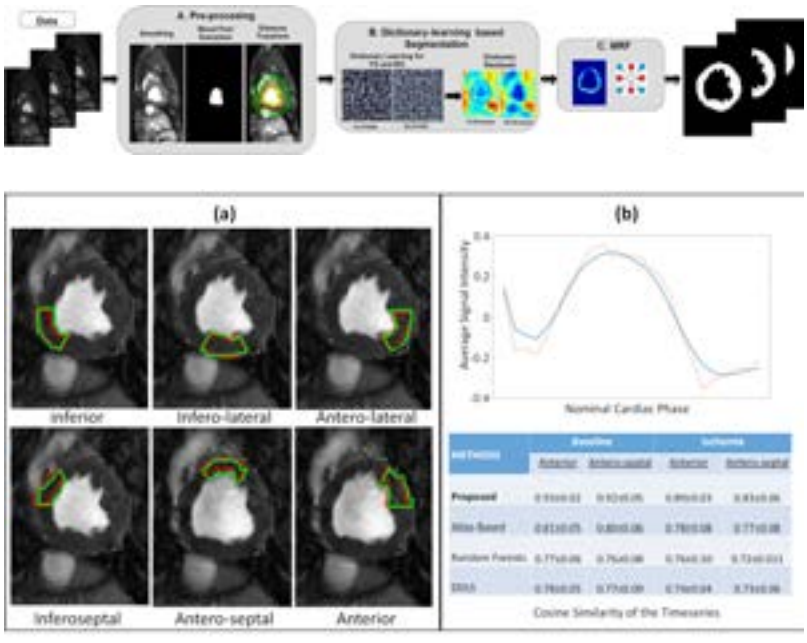

	Baseline		Ischemia	
Regions	Standard Cine	CP-BOLD	Standard Cine	CP-BOLD
Anterior	81±13	83±10	78±10	79±8
Antero-septal	79±10	82±9	75±10	75±9
Infero-septal	75±12	72±16	75±12	75±9
Inferior	72±11	70±12	69±11	71±8
Infero-lateral	73±11	72±12	71±13	71±11
Antero-lateral	82±7	81±9	76±11	74±9

Regional Segmentation accuracy with Dice coefficients (MEAN±STD) for the 6-mid ventricular cavity regions. Our algorithm is robust to regional complexities inside myocardium region. The results clearly show that ischemia conditions slightly influence the performance especially in the regions that are under influence of LAD stenosis (Antero-septal and Anterior). The inferior and infero-lateral regions show lower performance due to the presence of liver.

Ischemia		Baseline		
CP-BOLD	Standard Cine	CP-BOLD	Standard Cine	Methods
79±8	78±10	83±10	81±13	Anterior
75±9	75±10	82±9	79±10	Antero-septal
75±9	75±12	72±16	75±12	Infero-septal
71±8	69±11	70±12	72±11	Inferior
71±11	71±13	72±12	73±11	Infero-lateral
74±9	76±11	81±9	82±7	Antero-lateral

P280

Ferumoxytol MRA and Non-Contrast CT Fusion in TAVR Patients with Implantable Cardiac Device

Takegawa Yoshida, M.D.[1]Kim-Lien Nguyen, M.D.[2], Fei Han, Ph.D.[3], Ziwu Zhou, B.S.[1], Peng Hu, PhD[4], J. Paul Finn, M.D.[1]

1. *Department of Radiology, David Geffen School of Medicine at UCLA, CA*
2. *Division of Cardiology, David Geffen School of Medicine at UCLA and VA Greater Los Angeles Healthcare System, CA*
3. *UCLA, LOS ANGELES, CA*
4. *university of california los angeles, CA*

Background: Whereas MRA provides excellent intraluminal contrast, it is insensitive to vascular calcification and fails to image indwelling metal devices due artifact. CT is exquisitely sensitive to calcium and can image a variety of indwelling hardware devices. However, in many patients, including some TAVR candidates, renal impairment makes iodinated contrast media and many gadolinium agents undesirable or contraindicated. We hypothesize that in patients where ferumoxytol is a suitable alternative to CTA, calcification and hardware devices may be accurately displayed over luminal anatomy by fusing non-contrast CT and ferumoxytol enhanced MRA (FEMRA) images. In a proof-of-concept study, we aim to demonstrate the accuracy of fusing both modalities.

Methods: Seven patients who were TAVR candidates and two patients with implantable device underwent FEMRA and also had non-contrast CT. CT and MR DICOM data were processed using Mimics software V18.0 (Materialize, Leuven, Belgium). Regions of interest (ROIs) on CT, which represent vascular calcification and implanted leads and devices, were isolated and registered to the FEMRA data. The ROI coordinates were registered in 3-dimensions on a Cartesian grid (x, y and z). Calcification voxels, pacing coil voxels and pacing box voxels were registered to the original FEMRA images and the fused images were marked as point ROIs using a DICOM viewing software (OsiriX®, Geneva, Switzerland). The location of each ROI from both sets of images were compared and evaluated.

Results: All patients had vascular calcification to varying degrees. One pacemaker patient (67 years, F) was evaluated pre-TAVR and another (78 years, F) was evaluated post-TAVR (Figure 1). Of the device patients, fifty-four ROIs were defined in case 1 and 30 ROIs in case 2. No significant offset errors were noted between the original FEMRA and fused
FEMRA for case 1 (x= 0.75 (0.28 – 2.50) mm, y= 0.13 (0.00 – 0.23) mm, z= 1.58 (0.00 – 2.56) mm) and case 2 (x= 0.66 (0.00 – 1.40) mm, y= 0.05 (0.00 – 0.13) mm, z= 0.56 (0.00 – 1.50) mm). In all cases, the vascular calcification and implantable devices were fused successfully with the 3D FEMRA data. Volume rendered images clearly demonstrate the pacemaker lead and generator along with its positional relationship to vascular and intracardiac structures.

Conclusions: By fusing non-contrast CT and FEMRA, the locations of luminal anatomy, vascular calcification, and implantable devices can be accurately defined, thereby addressing the respective limitations of MR and CT for vascular and cardiac imaging.

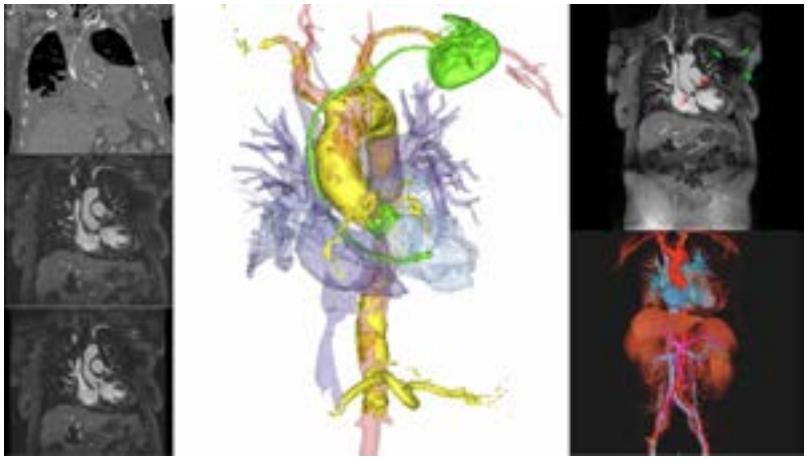

P281

Multiple-2D Dual Active Shape Model Framework for Right-Ventricle Segmentation in CMR Images

El-Sayed H. Ibrahim, PhD[2], Ahmed Fahmy, PhD[1]Hossam El-Rewaidy, MSc[1]

1. Harvard University, MA
2. University of Michigan, Ann Arbor, MI

Background: We propose a modified active-shape-model (ASM) for efficiently measuring shape variation of right-ventricle (RV) surfaces. The proposed method includes three modifications (Figure-1) compared to conventional ASM: 1)RV shape is split into two surfaces: free-wall and septal-wall; 2)3D RV surface is presented by multiple parallel 2D contours, where anatomical correlation among these contours is taken into consideration; and 3) contours of each model are aligned using Bookstein transformation.

Methods: Two datasets were used for training and testing the proposed framework: York-database (908 images from 29 subjects) and Local-database (255 images from 27 subjects), where images are acquired at basal, mid-ventricle, and apical short-axis locations. For each subject, the images are segmented, and landmarks are extracted to form a 3D mesh representing RV surface at end-diastole and end-systole. Seventy-nine different RV shapes were used for training and 197 RV surfaces were used for testing. For each contour, two RV-septal wall insertion points are used to form baseline of the Bookstein transformation. After constructing the shape model, principal-component-analysis is applied to estimate the RV surfaces' mean-shape and variance. Finally, the constructed mean-shape is transformed from Bookstein-coordinates back to image-coordinates. The mean-shape then iteratively evolves under guidance of the appearance model. The final extracted contours were evaluated against ground-truth manually extracted contours using mean-absolute-distance (MAD), Hausdorff-distance, and Dice-index measures. In order to clinically evaluate the proposed method, we calculated RV EF by both techniques and quantified its error.

Results: The proposed ASM framework converges after almost 5 iterations, compared to 20 iterations in the conventional method, and provides accurate segmentation (Figure-2). The multiple-2D ASM framework outperforms conventional ASM, as evidenced by lower MAD and Hausdorff measures and higher Dice-index (Table-1). The error of conventional ASM is higher at the apical slices compared to the basal and mid-ventricle slices. This is not the case in multiple-2D ASM due to higher influence of the cross-sectional levels with larger certainty, e.g. basal and mid-ventricle slices, on the developed ASM. Error in RV EF measurement was 9.2% and 14.2% for the proposed and conventional ASM models, respectively. The average computation times for segmenting 8 slices using personal-computer were 1.2s and 5.3s for the conventional and proposed ASM models, respectively. However, the parallel nature of the developed techniques makes this time difference less relevant.

Conclusions: The multiple-2D ASM framework significantly outperformed conventional ASM for segmenting RV surfaces with more robust performance and accurate results that are reached in less number of iterations.

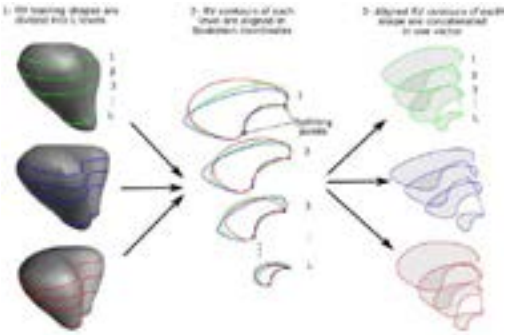

Fig 1. Training of the multiple-2D ASM framework includes: 1) dividing the RV shapes into L levels from base to apex; 2) aligning the RV contour in the Bookstein's coordinates; and 3) stacking the aligned contours of each RV shape in one vector.

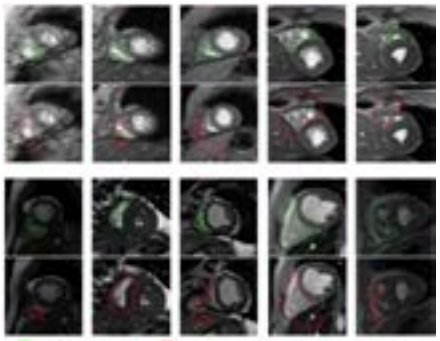

Fig 2. RV segmentation results using the multiple-2D ASM (green) and conventional ASM (red) techniques for some apical slices.

Table 1. Mean ± Standard deviation of the MAD, Hausdorff, and Dice Index measures of the segmented contours at basal, mid-ventricle, and apical levels using the proposed and conventional ASM methods with respect to the ground truth. *Top*: York database, *Bottom*: Local database.

	MAD			Hausdorff			Dice Index		
	Basal	Mid	Apical	Basal	Mid	Apical	Basal	Mid	Apical
Multiple-2D ASM	2.2±1.4	2.8±1.6	2.7±2.1	7.8±6.7	10.1±5.1	8.8±7.2	90.8±6.5	86.4±7.2	85.2±8.2
Conventional ASM	3.5±2.3	3.6±2.1	4.7±3.4	16.9±16.3	14.8±8.9	18.6±12.2	86.4±9.4	83.4±9.7	76.5±15.9
	MAD			Hausdorff			Dice Index		
	Basal	Mid	Apical	Basal	Mid	Apical	Basal	Mid	Apical
Multiple-2D ASM	3.1±1.7	2.8±1.6	3.0±1.8	9.7±8.9	7.9±3.8	8.1±5.1	86.9±6.8	84.9±10	81.6±16.3
Conventional ASM	5.9±3.9	6.2±3.8	8.5±5.6	18.2±12.5	19.5±11.8	27.2±15.7	72.2±23	72.9±17	57.8±28.4

P282

A new approach to manage the absence of full recovery of the longitudinal magnetization between the Look-Locker blocs in MOLLI sequence: temporal registration

Habib Rebbah[1] Thierry Galas[2], Gilles Soulat, MD[3], Anne Menini, PhD[4], Nadjia Kachenoura, PhD[5], Charles A. Cuenod, MD, PhD[6], Elie Mousseaux, MD, PhD[3]

1. *PARCC, INSERM, Paris, France / GE Healthcare, Buc, France, Paris, Ile-de-France, France*
2. *GE Healthcare, Buc, France, Buc, Ile-de-France, France*
3. *European Hospital Georges Pompidou APHP; INSERM U970 PARCC Paris descartes University, Ile-de-France, France*
4. *General Electric Global Research Center, Bayern, Germany*
5. *Laboratoire d'Imagerie Fonctionnelle - U678 Faculté de Médecine Pierre et Marie Curie - Pitié Salpétrière, Paris, Ile-de-France, France*
6. *Radiology Department, European Hospital Georges Pompidou, PARCC, INSERM, Paris, France, Ile-de-France, France*

Background: The Modified Look-Locker Inversion recovery (MOLLI) is a well-established sequence for T1 mapping. However, the absence of full recovery of the longitudinal magnetization before a new inversion pulse leads to discrepancies between signals of each Look-Locker (LL) and consequently to a lower accuracy of T1 estimates. This point is particularly met for long T1. Two main solutions were proposed to limit this issue of the MOLLI sequence. A first technique, The ShMOLLI assumes that for long T1, the signal of the first LL is enough for T1 estimation and a second technique uses the dynamic of the first LL's signal for all the LL blocs, so the non-recovery of the signal of first LL doesn't impact the estimation.

Methods: The signals of each LL are used independently while assuming that they should have the same parameters, with a simple time shift of the affected LL's signal defined by: $S_i(t) = A_i - B_i \exp(-(t+t_{0i})/T1_i^*)$, where t_{0i} is the shift of the i^{th} LL. To estimate t_{0i} we used the variation of the signal between the previous LL's equation and the observations of the current one and then we applied a temporal registration to the signal. Tubes with growing concentration of Gadolinium based agent were scanned on a 3T GE system, with different MOLLI schemes at different heartrate, see table 1. T1 values obtained with the widely used basic fit (Levenberg-Marquardt) without (BF) and with the aforementioned temporal registration (BFR) were compared with reference IR-Spin-Echo (IR) based on the mean value of the ROIs and the relative mean error.

Results: As compared to BF, BFR resulted in a significant decrease of error (around 10%) overall the schemes in regards to the IR (subfigure b). They also show a decrease of variation between schemes (SD in subfigure a). In case of no-rest period (subfigure c), our fitting approach allows us to recover the results that we should have had with a scheme involving a rest period.

Conclusions: To handle the absence of full recovery between LLs (long T1, high heartrate and short acquisition time) we used a time registration before fitting all data set of the MOLLI sequence. The proposed technique resulted in a higher accuracy of T1 estimates and a better reproducibility than the basic fitting of all the data as performed usually.

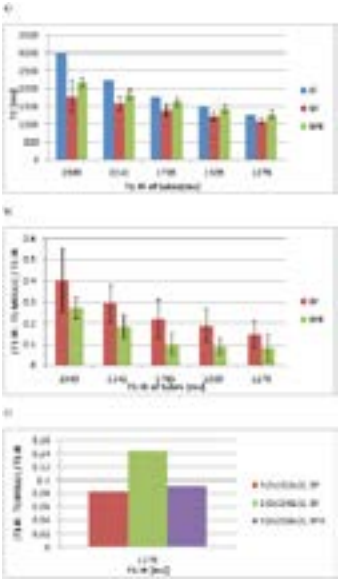

List of experiments

Number of acquisitions	Heartrate (bpm)	Flip Angle (°)	Rest period (s)	Scheme
10	60	35	3	533
10	60	35	0	533
10	100	35	3	533
10	120	35	3	533
10	40	35	3	533
10	60	35	1	511
10	100	35	1	511
10	120	35	1	511
10	60	35	1	432

P283

Polar Processing of Cine Displacement Encoding with Stimulated Echoes (DENSE) Data Provides More Accurate Quantification of Cardiac Mechanics than Traditional Cartesian Analysis

Jonathan D. Suever, PhD[1] Gregory J. Wehner, BS[2], Linyuan Jing, PhD[3], Sean M. Hamlet, MS[2], Christopher M. Haggerty, PhD[4], Brandon K. Fornwalt, MD, PhD[4]

1. *Geisinger Health System, Bellefonte, PA*
2. *University of Kentucky, KY*
3. *Geisinger Health System, State College, PA*
4. *Geisinger Health System, PA*

Background: Cardiac strains derived from displacement-encoded CMR (DENSE) are important in a variety of disease states. In 2D DENSE, X and Y displacements are directly encoded into phase images. Because strain calculations are sensitive to displacement noise, the Cartesian displacements are typically smoothed to minimize noise prior to deriving strains. However, Cartesian displacements are inherently discontinuous and change signs across the blood pool cavity due to the left ventricular (LV) geometry and inward myocardial motion (Figure 1). Standard Cartesian smoothing cannot reconcile this discontinuity while preserving the integrity of the underlying displacement data (Figure 1B).

We propose combining the X and Y displacements into radial and circumferential components to yield more continuous displacement fields prior to smoothing (Figure 1C). Compared to Cartesian processing, we hypothesized that polar processing would yield more accurate strains regardless of the amount of smoothing or phase noise.

Methods: Displacement-encoded images were simulated with prescribed strains and corrupted with a range of Gaussian noise (0.0–0.5 mm). Cartesian and polar post-processing were performed with a range of smoothing factors (0.2–0.9) via *DENSEanalysis*, an open-source application.

For polar processing, the LV centroid was used as the origin to decompose X and Y displacements into radial and circumferential components. After smoothing, a myocardial mesh was deformed using the smoothed polar displacements to obtain circumferential (Ecc) and radial (Err) strains.

Finally, we compared mid-ventricular strains using Cartesian and polar processing in 8 healthy individuals.

Results: In the simulations, polar processing provided accurate measures of strains across a wide range of displacement noise and smoothing. While the improvement relative to Cartesian was modest for global Ecc (Figure 2, left), it was significant for global Err (Figure 2, right) with the largest differences occurring at large smoothing factors and high displacement noise. Large differences were also seen for subendocardial strains for both Err and Ecc (data not shown).

Compared to polar, Cartesian processing underestimated Err in humans even at low smoothing (Figure 3). The severity of underestimation worsened with increased smoothing, which was consistent with the simulation results.

Conclusions: Polar processing yields more accurate measures of cardiac strains than traditionally used Cartesian processing, and is less sensitive to phase noise and the degree of smoothing used. Polar processing is particularly more accurate for assessing left ventricular radial strain.

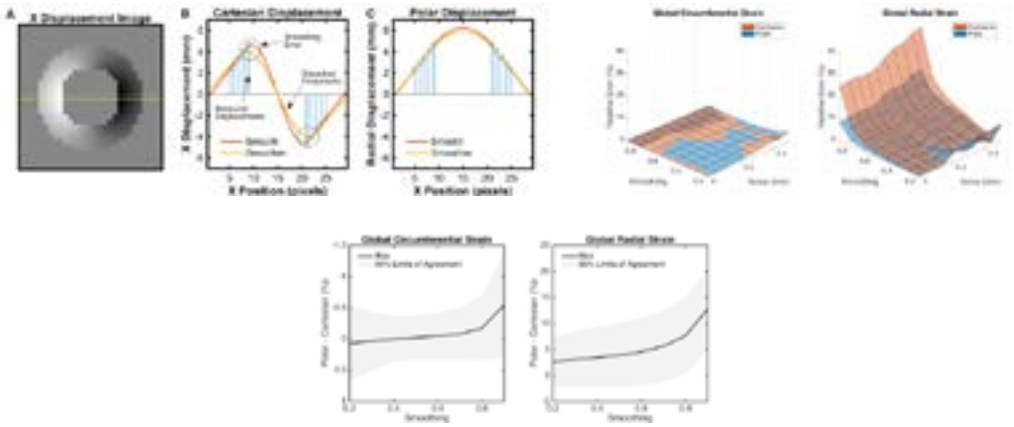

P284

Optimisation of post processing analysis of circumferential strain and strain rate using novel cine-based tissue tracking at different field strengths

Daniel Swarbrick, MBBS, BMedSci[1] Anvesha Singh, MBChB[2], Chris Steadman, MB ChB, MD[3], Matthew Graham-Brown, MBBS[2], Gerry P. McCann, MBChB, MD[4]

1. *University of Leicester, Leicester, England, United Kingdom*
2. *University of Leicester, England, United Kingdom*
3. *University of Leicester, Poole, England, United Kingdom*
4. *The University of Leicester, Leicester, United Kingdom, Leicester, England, United Kingdom*

Background: There are several methods for assessing myocardial strain with magnetic resonance imaging. At present, most of these however are hampered by the need for additional sequences, and often time consuming post processing. Recently, the technique of tissue tracking, that can utilise standard SSFP cine images of the left ventricle to assess strain, has been developed. The optimal post processing method for performing tissue tracking is unknown. In addition, it is unclear if the technique is more robust at 1.5T or 3T.

We sought to assess a variety of methods of post processing of SSFP cine images, from a spectrum of different clinical settings at both 1.5T and 3T, using tissue tracking to assess circumferential peak systolic strain and diastolic strain rates, and compared their inter and intra variability, as well as test-retest reproducibility.

Methods: 25 patients in total were included, including 18 with aortic stenosis (AS) with 10 at 3T and 8 at 1.5T, and 7 with type 2 diabetes who underwent testing at both field strengths. Standard short axis SSFP cine images were acquired, then repeated on a different day 7-18 days later. Peak circumferential systolic strain (PSS) and peak early diastolic strain rates (PEDSR) were then assessed using tissue tracking, using a variety of methods. Intra- and inter-observer variability and test-retest reproduciblity were compared for each technique.

Results: In patients with aortic stenosis (mean age 67 +/-8), test-retest reproducibility of circumferential peak systolic strain was marginally better at 1.5T versus 3T (CoV 11.6 vs 8.5). In contrast, test-retest reproducibility of circumferential peak early diastolic strain rate was markedly worse at 1.5T than 3T (20.9 vs 14.3).

In the cohort of patients with type 2 diabetes (mean age 34+/-5), test retest reproducibility at both field strengths was superior to the group with AS. Similar values were obtained at both field strengths for measurement of PSS (CoV 9.1 and 9.8 at 1.5T and 3T) and PEDSR (CoV 11.0 and 8.9).

Optimal intraobserver variability was seen when 5 contiguous slices from the base of the left ventricle were included, compared to only using slices around the mid ventricule (CoV 20.9 vs 27.1 for PEDSR at 1.5T). In addition, intraobserver variabilty was lower when using rounded endocardial and epicardial contours compared to smoothed contours (CoV 6.1 vs 8.3 for PEDSR at 3T).

Conclusions: Test-retest reproducibility using tissue tracking is similar at both 1.5T and 3T for the assessment of circumferential PSS. In patients with aortic stenosis, measurement of PEDSR with tissue tracking has superior test-retest reproducibility at 3T versus 1.5T. In contrast, in a younger cohort with type two diabetes, reproducibility at both field strengths was excellent.

Intraobserver variability was imporved by using 5 contiguous basal slices, and by using rounded contours as compared to smoothed contours.

P285

Physiological variation and correction of myocardial extracellular volume fraction (ECV) - calculation and preliminary application of expected ECV value

Shi-Jun Zhang, MD, PhD

Zhongda Hospital, Southeast University, Nanjing, Jiangsu, China (People's Republic)

Background: The physiological variation of the extracellular volume fraction (ECV) increases overlap between normal and abnormal values, thus limiting the use of individual ECV values to determine a diseased state or progression. Additionally, it is difficult to determine diagnostic cutoff values with desired sensitivity and specificity. The accuracy of using ECV to assess diffuse myocardial fibrosis, especially early myocardial micro-lesions, may be improved by elucidating the source of physiological variation for individual correction, and small ECV changes may be detectable from physiological variations. Sex, age, physical activity or exercise may be the source of individual ECV variations. Previous animal experiments (unpublished) have shown that the breadth of myocardial cells under a physiological state was associated with ECV, which provided clues for individual ECV correction.

Methods: The variables of a multivariable linear regression model for ECV are screened statistically based on data of 49 heathy volunteers. Candidate variables include demographic indicators, body size measures, geometric measures of the heart and background of high-strength exercise. The established model is used for calculation of individual expected values of ECV (ECV_0). The ECV expansion index (EEI) is defined as ECV - ECV_0. The EEI of the healthy volunteers is compared with a group of patients with hypertension (n = 39) and a group of patients with diabetes (n = 22). Data from 10 different published studies are subjected to calculation of the mean EEI values in different cardiac diseases.

Results: Left ventricular mass (LVM), sex and body mass index (BMI) enter the model. The EEI calculated using this model trends higher in the hypertension and diabetes groups than in the control group. The EEI in the normal controls and in hypertensives without and with left ventricular hypertrophy exhibited a progressively increasing trend. According to published data, the EEI is generally higher in disease groups than in normal control groups. In a study of aortic stenosis, the EEI of the 6-month follow-up group decreases after surgery.

Conclusions: LVM, sex and BMI are associated with physiological variations in ECV. The adjustment of the physiological variation of ECV improves the evaluation of diseases involving the myocardium.

P286

Quantification of ventricular function with MRI, CT and Echocardiography: Regional Travel Award Application

Asik Ali Mohamed Ali, MD[1] Tony Sedlic, MD, FRCPC[2], Ana-Maria Bilawich, MD, FRCPC[3], John Mayo, MD, FRCPC[3]

1. *Vancouver General Hospital - University of British Columbia, Vancouver, BC, Canada*
2. *Vancouver General Hospital, BC, Canada*
3. *Vancouver General Hospital - University of British Columbia, BC, Canada*

Background: Cardiac function plays a vital role in in terms of patient management, outcome, and long-term survival of patients with cardiac disease. This study was designed to calculate the correlation of functional CT in comparison with cardiac MR and echocardiography in quantification of ventricular function.

Methods: A single center study reviewing functional cardiac imaging performed. 15 patients, underwent retrospective functional cardiac CTA, echocardiography and cardiac MRI within 12 months. Retrospectively gated functional CT was performed with 64 slice (Siemens Force, Erlangen, Germany) or 128 slice (Toshiba Aquilion scanner, Japan) scanners. Functional data was processed with Siemens syngo.via automated cardiac analysis software. MRI was performed on a 1.5-T scanner (Magnetom Avanto, Siemens AG, Erlangen, Germany) with CINE sequences acquired in short axis and 4-chamber (horizontal long axis) planes. Functional data was manually processed with the Siemens syngo.via cardiac application. The ejection fraction was calculated by cardiothoracic radiologist blinded to each modality. Statistical analysis was conducted using SPSS software (SPSS, Inc., Chicago, Illinois).

Results: Functional cardiac CT in detecting left ventricular systolic dysfunction (LVEF < 60%) demonstrated significantly higher correlation with MR (0.748, $p < 0.001$) than ECHO with MR (0.016, $p < 0.016$). However, functional cardiac CT and ECHO showed weak correlation with MR (0.398, $p < 0.142$ and 0.087, $p < 0.758$, respectively) in detecting right ventricular systolic dysfunction (RVEF < 55%). CT also demonstrated significantly higher correlation with MR in calculating left ventricular end systolic volume (0.766, $p < 0.001$), end diastolic volume (0.587, $p < 0.021$) and right ventricular end systolic volume (0.555, $p < 0032$).

Conclusions: Functional cardiac CT is superior to echocardiography for assessment of LV dysfunction and showed higher correlation with MR. Manual processing of right ventricle in MRI, which has complex geometry and anatomy, makes MRI more accurate and reliable in assessing right ventricular dysfunction as compared to automated software analysis in cardiac CT and echocardiography.

P287

Automated Beat to Beat Cardiac Function Assessment from Real-time Cardiac MRI

Rahil Shahzad, PhD[1] Bas van den Berg, Master of Science[1], Martin Fasshauer[2], Joachim Lotz, MD[3], Rob J. van der Geest, PhD[1]

1. *Department of Radiology, Leiden University Medical Center, Leiden, The Netherlands, Zuid-Holland, Netherlands*
2. *Institute for Diagnostic and Interventional Radiology University Medical Center Goettingen, N/A, Germany*
3. *Institute for Diagnostic and Interventional Radiology, University Medical Center Göttingen, Germany, Goettingen, Niedersachsen, Germany*

Background: In conventional cine cardiac MRI data is collected over multiple cardiac cycles and combined to reconstruct multiple phases over an average cardiac cycle. This assumes the heart stays in place and beats regularly. Real-time cardiac MRI can be used to acquire images at high frame rate resulting in image data over multiple cycles at fixed time intervals. This enables imaging of patients with cardiac arrhythmia, or those who have trouble holding their breath. From the collected data beat to beat variations in cardiac function and cycle length can be derived. An automated method was developed that can propagate contours drawn in any phase to all other phases and also detect all end-diastolic (ED) and end-systolic (ES) phases.

Methods: In patients with cardiac arrhythmia real time MR imaging was performed in short-axis orientation at a frame rate of 25 fps over a duration of 10 seconds per slice. The developed automated method was evaluated in a mid-basal slice. A deformable registration method was developed, which minimizes the variance over the time dimension[1]. User interaction was limited to manually drawing the endocardial contours in four phases (two ED phases and two ES phases). These are transformed according to the acquired registration and combined using majority voting. Variation in contours area was computed and the peaks and valleys were detected using a multi-scale peak detection method[2]. Automated results were compared to manually derived contours in ED and ES phases of multiple cardiac cycles.

[1]Medical-Image-Analysis 2011-Apr;15(2):238-49

[2]Algorithms 2012,5,588-603

Results: Table 1 shows the deviation of the calculated contours from the reference data. Figure 1 shows the correspondence of the ED and ES volumes between the results and the reference for the analysed cycles detected in all patients. Figure 2 shows the automatically derived temporal variation in endocardial area of one patient together with the reference results. The detected ED areas were more accurate than the ES areas as the ES contours were usually too large. The ED and ES phases were correctly detected most of the time, but also here the detected ES phases had a larger error.

Conclusions: Our results show that the registration method and ED and ES phase detection correspond well to the expert contours. This suggests that our method can be used to quickly generate contours for a whole slice, and consequently for all recorded slices. This enables detailed quantitative analysis of cardiac function in arrhythmia patients.

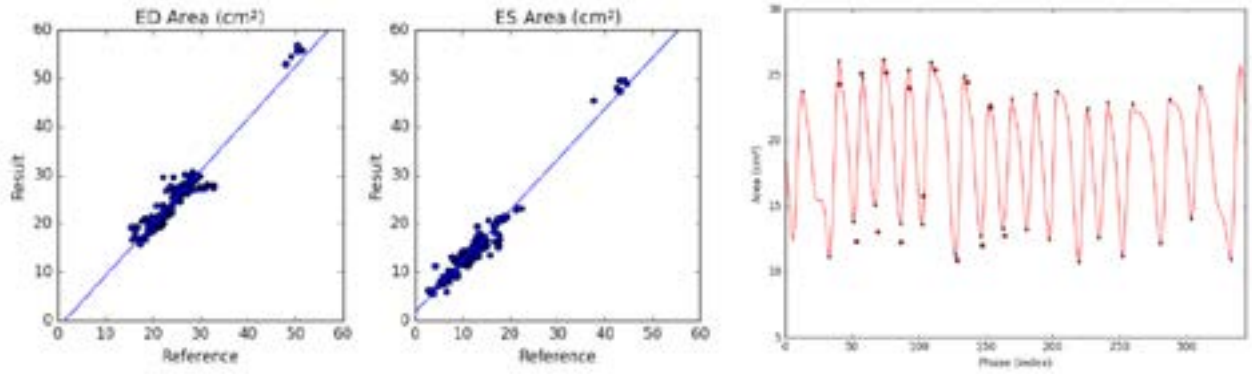

Average and Error Statistics

Average error	Average value	
-8.36±7.26	49.00	Area Ejection (%)
0.95±11.70	75.45	Heart Rate (cycles/min)
-1.93±2.30	11.68	Stroke Surface (cm²)
0.39±2.15	24.77	ED Area (cm²)
2.32±1.66	13.09	ES Area (cm²)
0.58±7.36		ED Phase (#)
-1.45±8.66		ES Phase (#)

The statistics are calculated over all detected cycles. The differences are calculated by subtracting the values of the automated analysis from the manual reference, so positive average values indicate overestimation of the automated method.

P288

Factors Influencing the Reproducibility of Right Ventricular Volume Measurement

Agnieszka Töpper, MD[1] Edyta Blaszczyk, MD[2], Susanne Schwenke, Dipl-Stat[3], Jeanette Schulz-Menger, MD[4]

1. *Working Group on Cardiovascular Magnetic Resonance, Experimental and Clinical Research Center a joint cooperation between the Charité Medical Faculty and the Max-Delbrueck Center for Molecular Medicine HELIOS Klinikum Berlin Buch, Department of Cardiology and Nephrology, Berlin, Germany., Berlin, Berlin, Germany*
2. *Working Group on Cardiovascular Magnetic Resonance, Experimental and Clinical Research Center, a joint cooperation between the Charité Medical Faculty and the Max-Delbrueck Center for Molecular Medicine and HELIOS Hospital Berlin Buch, Berlin, Berlin, Germany*
3. *SCO:SSiS, Berlin, Berlin, Germany*
4. *Working Group on Cardiovascular Magnetic Resonance, Experimental and Clinical Research Center a joint cooperation between the Charité Medical Faculty and the Max-Delbrueck Center for Molecular Medicine HELIOS Klinikum Berlin Buch, Germany, Berlin, Germany*

Background: Despite an established prognostic value of right ventricular (RV) function in numerous cardiovascular entities and published post-processing recommendations(1), there is no agreement, whether to use the transaxial (TA) or short axis (SAX) acquisition for RV quantification. Aim of this study was to analyse the reader influence on RV quantification in different entities.

Methods: We screened 91 consecutive patients referred for RV evaluation at 1.5 Tesla scanner (Siemens). TA and SAX full coverage of the RV was performed using cine SSFP. First observer quantified all TA and SAX scans. Differences between TA and SAX were investigated based on a t-test. Interobserver analysis was performed in 27 randomly chosen individuals by two experienced observers. Furthermore, each reader performed an intraobserver analysis in both orientations in this subgroup. Reproducibility was assessed using Bland-Altman plots. Linear models were used with patients as a repeated factor to be able to account for the correlatedness between measurements of the same patients.

Results: 70 datasets were eligible for the analysis (normal RV=24, thoracic deformities=22, RV pathologies=24). Excluded: 16 due to arrhythmia, 5 due to technical issues. Analysis of the whole group: No significant difference detected in the mean RVEF (SAX 47.4%; TA 47.7% p=0.5) and mean right ventricular endsystolic volume RVESV (SAX 102ml; TA 104ml p =0.12) but in the right ventricular enddiastolic volume RVEDV (SAX 191ml; TA 195ml p=0.02). Reproducibility results are shown in table1,2 and figure1. Model for subgroup analysis:

Interobserver: the observer was found to constitute a statistically significant factor in both orientations for RVEDV (estimated mean difference (EMD) in ml SAX 10.5 p=0.0002, TA 11.8 p < 0.0001), RVESV (EMD SAX 8.9 p < 0.0001 and TA 4.6 p=0.0029). For the RVEF there was statistically significant observer influence in the SAX orientation (EMD -1.4 p=0.0343) but not in TA (EMD -0.4 p=0.4259)

Intraobserver: the read was found to be a statistically significant factor in the models for RVEDV and RVESV in both orientations. RVEDV (EMD SAX 4.6 p=0.0204; TA 4.4 p=0.0015), RVESV (EMD SAX 3.8 p=0.0020; TA 3.3 p=0.0020). No significant difference between the reads was found for RVEF in SAX and TA.

Conclusions: Our results show that RV quantification is challenging in both orientations. There is a statistically significant influence of the observers. Not all statistically significant values reach clinical relevance. Our findings underline the need for standardization and an identification of the underlying cause.

1. Schulz-Menger J, Nagel E, et al; JCMR2013;15:35.

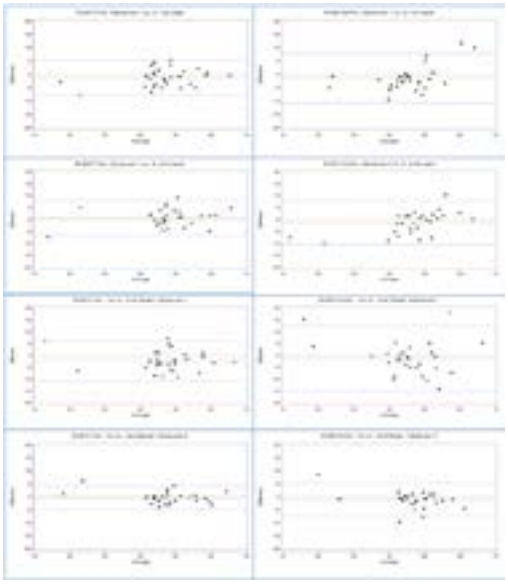

Mean differences and 95% limits of agreement for RVEDV (SAX, TA).

TA		SAX		RVEDV
95% Limits of Agreement	Mean Difference	95% Limits of Agreement	Mean Difference	Comparison
-17.5; 36.2	9.4	-40.9; 50.3	4.7	Observer I, 1st vs. 2nd read
-10.0; 17.4	3.7	-19.8; 28.9	4.6	Observer II, 1st vs. 2nd read
-13.7; 42.9	14.6	-24.9; 46.1	10.6	1st read, observer I vs. II
-19.4; 37.3	9.0	-30.6; 51.6	10.5	2nd read, observer I vs. II

RVEDV - right ventricular enddiastolic volume
SAX - short axis
TA - transaxial

Mean differences and 95% limits of agreement for RVESV (SAX, TA).

TA		SAX		RVESV
95% Limits of Agreement	Mean Difference	95% Limits of Agreement	Mean Difference	Comparison
-11.7; 31.2	9.8	-26.9; 36.4	4.7	Observer I, 1st vs. 2nd read
-9.1; 12.9	1.9	-11.1; 18.2	3.6	Observer II, 1st vs. 2nd read
-13.4; 36.1	11.4	-18.8; 37.8	9.5	1st read, observer I vs. II
-11.7; 18.7	3.5	-18.2; 35.0	8.4	2nd read, observer I vs. II

RVESV - right ventricular endsystolic volume
SAX - short axis
TA - transaxial

P289

The Effects of Interventricular Uncoupling In Pulmonary Arterial Hypertension 0n MRI-Derived Metrics 0f Right and Left Ventricular Volumes And Function: Comparison With Invasive Hemodynamics

Aiden Abidov, MD, PHD[1]Mohit Pahuja, MD[2], Petimat Dudurkaeva[3], Ankit A. Desai, MD[3], Roberto Bernardo, MD[3], Franz Rischard, MD[3]

1. Wayne State University, MI
2. St. Joseph's Hospital and Medical Center, Phoenix, AZ
3. University of Arizona, AZ

Background: In patients with primary pulmonary arterial hypertension (PAH), interventricular septal (IVS) uncoupling from increased pulmonary arterial afterload results in dyssynchrony and electromechanical delay between the right and left ventricles (RV, LV). This uncoupling has been largely ignored in the assessment of ventricular function by MRI. Thus, we sought: 1) to assess the impact of the RV-LV uncoupling on estimates of cardiac volumes and function derived from cardiac MRI (CMR) and 2) to compare the CMR data obtained with and without consideration of the RV-LV uncoupling, to the invasive volume-based measurements.

Methods: We identified 20 patients with Group I PAH (85% female; age 53±10 years) who underwent CMR and right heart catheterization within 24 hours. Bi-ventricular volumes at end-diastole (ED) and end-systole (ES) were measured from the short axis cine images of the ventricles, based on the following methods:
1) ED and ES estimates for the LV and the RV, based on evaluation of the LV cavity size changes; 2) Separate ED and ES estimates for the LV and the RV, based on separate evaluation of the LV and RV cavity size changes; 3) Seperate ES and ED estimates for the LV and the RV, based on opening and closure of the aortic and the pulmonary valves. We compared ventricular stroke volumes (SV) derived from these three CMR methods with results from the right heart catheterization. We defined SV from the invasive data as Cardiac Output/Heart Rate. Rho- and T- statistics were utilized for the variable comparisons.

Results: Correlative analysis revealed that CMR calculations of the RV SV by method 2 demonstrated the best agreement (*) with the invasively calculated SV (Table 1). Method 3, in contrast, demonstrated lower values than the RV SV compared to all other methods.

Conclusions: CMR-derived RV SV assessment taking into a consideration the LV-RV uncoupling in patients with PAH, demonstrates excellent agreement with invasive assessments of SV in PAH. Clinical significance of this methodology requires further investigation.

Variable	MRI Assessment of the Volumes (n=120 datasets/20 pts)			Invasive Assessment
	Method 1	Method 2	Method 3	
LV Stroke volume, ml	48.3 ± 18.6	43.1 ± 19.5	40.7 ± 19.5	47.8 ± 19.1 *
RV Stroke Volume, ml	40.3 ± 19.5	47.7 ± 19.5 *	35.3 ± 19.5	
LVEF, %	62.3 ± 19.5	57.7 ± 19.5	62.2 ± 19.5	n/a
RVEF, %	23.1 ± 10.9	24.4 ± 10.8	18.7 ± 8.5	n/a

P290

Semi-Automated Segmentation of the Right Ventricular Short Axis Derived from Identification of Four Anatomic Landmarks in Long Axis

Ryan Avery, MD[1]Jose A. Rosado-Toro, PhD[1], Rajesh Janardhanan, MD, FACC[2], Maria Altbach, phD[3]

1. *University of Arizona, Tucson, AZ*
2. *Banner University Medical Center, Tucson, Tucson, AZ*
3. *University of Arizona, AZ*

Background: Reference standard quantitative analysis of ventricular function utilizing manual contouring is time-consuming, even when performed by an experienced post-processor. To improve efficiency, both semi-automated and automatic segmentation algorithms have been developed. Commercially available algorithms are promising for left ventricle segmentation, but due to the anatomic complexity of the right ventricle (RV) a reliable algorithm is not currently available. Presented is a novel algorithm that uses landmarks selected in the 4-chamber long axis view to segment the complete RV short-axis (SAX) series.

Methods: This novel algorithm uses a single 4-chamber and complete SAX cine series of the ventricles, and incorporates 7 anatomic landmarks in the 4-chamber view (blood pool in ED; RV apex, lateral and medial tricuspid valve margins in ED and ES) selected by an experienced physician. Using these landmarks, the algorithm segments the 4-chamber view of the RV and LV throughout the cardiac cycle using a novel variation of the polar dynamic programming (PDP) algorithm. With these segmentations, the algorithm identifies representative basal, mid, and apical RV slices in the SAX cine series, and an RV model is generated by segmenting the basal-most mid RV slice in ED. Subsquently, a temporal and spatial propagation is performed using the relationship between the 4-chamber and SAX views.

Results: Cine images of 10 SAX slices from a single patient were evaluated using the novel PDP algorithm. Two cardiac imaging-trained physicians identified the ED and ES frames, and then proceeded to outline the RV in the slices they deemed appropriate. Correlation coefficents (R^2) of the mean Dice metric between manual samples provided by the physicians was 0.8208 for ED, and 0.7285 for ES. A similiar R^2 for endocardial contours peformed by the PDP algorithm in ED was generated with an R^2 of 0.8502 compared to Physician 1, and 0.8099 compared to Physician 2; the R^2 for the PDP algorithm was also similiar in ES compared to manual traces by Physician 1 with R^2 of 0.6534, and by Physician 2 with 0.6815.

Conclusions: Presented is a robust semi-automated algorithm that segments a complete RV SAX cine series, while reducing user input to identification of 4 anatomic landmarks in ED and 3 landmarks in ES. While this study focused on segmentation of the RV endocardium in ED and ES, further stuides of this novel algorithm will evaluate segmentation of the entire cardiac cycle utilizing both the endocardial and epicardial RV borders.

P291

The Value of Feature/Contour-based Registration in Quantification of Myocardial Extracellular Volume Fraction Based on T1 Mapping Technique

Ling Lin, Master of Medicine[1] Xu-Hui Zhou, MD, PhD[1], Mei Zheng, Master of Medicine[2], Qiu-Xia Xie, Bachelar of Medicine[1]

1. *The First Affiliated Hospital of Sun Yat-Sen University, Guangdong, China (People's Republic)*
2. *The Third Affiliated Hospital of Sun Yat-Sen University, Guangdong, China (People's Republic)*

Background: T1 mapping images of different inversion time might not be completely identical in cardiac features, which might impact on the quality of T1 maps as well as quantification of extracellular volume fraction (ECV). Motion correction and rigid co-registration of the source images can help to reduce this impact, but have limited effect on images with inconsistent ventricular shape. Feature/Contour-based Registration is a non-linear transformations using predefined myocardial contours to align multiple images before T1 map generation. We evaluated the role of feature/contour-based registration in quantification of ECV with healthy adult volunteers.

Methods: T1 mapping images of the mid-ventricular short axis slice (SAX) of 25 healthy volunteers (16 males, 9 females, age 24 to 65 years old) were obtained before and 15 minute after administration of contrast agent using ECG triggered modified Look-Locker Inversion Recovery (MOLLI) on a 3.0T Magnetic Resonance Imaging system (Magnetom Verio, Siemens). ECV was calculated using a software (cvi42 v5.3, Circle Cardiovascular Imaging) by two methods: routine ECV by T1 maps automatically generated by the scanner, and registered ECV by T1 maps generated after feature/Contour-based registration. 10 cases with inconsistent left ventricular shape among source images were picked out as the deformation group, and the rest 15 cases formed the control group. ECVs of all the subjects as well as each group were analyzed with pared comparison. The registered ECVs of the 6 segments of mid-ventricular SAX, as well as the 50% epi-layer, 50% endo-layer, middle layer and the whole myocardium were also compared.

Results: There was statistical difference (P=0.025) between routine ECV (25.30±3.16%) and registered ECV (24.17±2.41%) of all the volunteers. In deformation group, routine ECV (26.76±3.47%) and registered ECV (24.03±2.10%) were statistically different (P=0.021). While in control group, there was no difference (P=0.707) between routine ECV (24.32±2.61%) and registered ECV (24.26±2.66%). 6 cases presented artifacts in routine ECV maps, which were eliminated or mitigated in registered ECV maps (Figure 1). There was no statistical difference among registered ECVs of the 6 segments (F=1.166 P=0.329). Neither did those of different layers and the whole myocardium of mid-ventricular SAX (F=0.393 P=0.758).

Conclusions: Feature/Contour-based registration can improve the quality of T1 maps in cases with inconsistent ventricular shape among T1 mapping images, thus leads to higher accuracy of ECV quantification. Different segments and layers of mid-ventricular SAX myocardium have even ECVs, indicating the feasibility of preciser analysis in specific clinical scenarios.

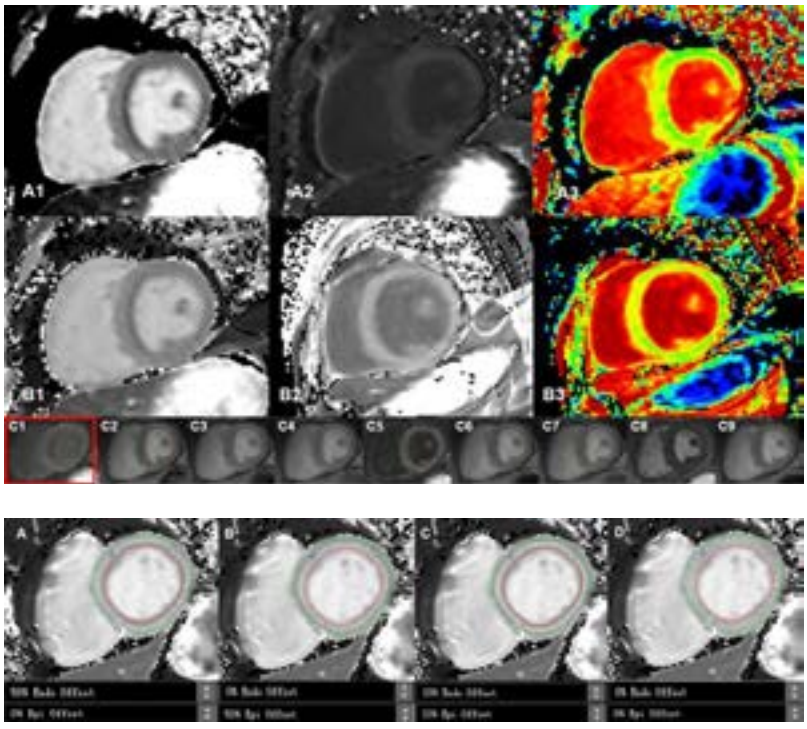

P292

Saturation-based myocardial T1 mapping with denoising: initial comparative study with MOLLI

Aurelien Bustin, MSc[1] Anne Menini, PhD[2], Shufang Liu, MSc[3], Darius Burschka, PhD[4], Andrei Codreanu, MD[5], Mouaz H Al-Mallah, MD Ms[6], Martin A Janich, Ph.D.[7], Anja CS Brau, Ph.D.[8], Freddy Odille, PhD[9]

1. *Technische Universität München, Munich, Bayern, Germany*
2. *General Electric Global Research Center, Bayern, Germany*
3. *Technology University of Munich, München, Bayern, Germany*
4. *Technische Universitaet Muenchen, Garching, Bayern, Germany*
5. *Centre Hospitalier de Luxembourg, Luxembourg, N/A, Luxembourg*
6. *King Saud bin Abdulaziz University for Health Sciences, King Abdullah International Medical Research Center, King ABdulAziz Cardiac Center, Ministry of National Guard, Health Affairs, Saudia Arabia, N/A, Saudi Arabia*
7. *GE Global Research, N/A, Germany*
8. *GE healthcare, CA*
9. *Inserm, Vandoeuvre-lès-Nancy, Lorraine, France*

Background: Quantitative myocardial T_1 mapping is a valuable tool that intrinsically studies tissue properties in the human body. Among all cardiac mapping sequences, inversion-recovery (IR) techniques for T_1 assessment, such as MOLLI (Messroghli et al., MRM 2004), have received most clinical interest due to their high precision and satisfactory SNR, but suffer from the underestimation of myocardial T_1 values. On the other hand, saturation-recovery (SR) based myocardial T_1 mapping techniques, such as SMART$_1$Map (Slavin et al., JCMR 2013), have shown better accuracy but are more sensitive to acquisition noise and are therefore limited by low precision of T_1 values. We propose to further improve the precision of SR-based techniques by employing a novel denoising method which exploits the spatio-temporal correlations in the T_1-weighted images.

Methods: 16 healthy volunteers (12 males, 39±8 years) were included in the study. Both SMART$_1$Map and MOLLI sequences were scanned on a 3T MRI scanner (HDxt signa, GE Healthcare, Milwaukee, WI). Imaging parameters for SMART$_1$Map were: FOV=220x220 mm^2, slice thickness=8mm, TR/TE=3.74/1.63ms, FA=45°. T_1-weighted images were acquired in short-axis views before and 15 min after gadolinium injection. Our proposed denoising technique uses a coupling between the T_1-weighted images by employing a Beltrami constraint along the T_1-weighted images (Bustin et al., ISMRM 2016). T_1 maps were then reconstructed using a 3-parameter-fitting. Regions of interest in the left ventricular septum were drawn by an expert observer and statistical analysis was performed to compare accuracy and precision of T_1 values.

Results: The average time to complete denoising was ~1.4 sec for one map. Precision of T_1 values was significantly improved using the proposed technique (Figure 1), with a decrease in standard deviation (pre-contrast: 33%, post-contrast: 27%, $p < 0.05$). Precision tends to be closer to MOLLI after correction in pre-contrast (SMART$_{uncorr}$:182ms / SMART$_{corr}$:122ms / MOLLI:55ms, $p < 0.05$) and post-contrast (153/111/37ms, $p < 0.05$). Accuracy was preserved as no difference in mean T_1 values was observed in the myocardium (pre-contrast: 1411/1407ms, post-contrast: 767/760ms, $p>0.05$). Noise observed in the original SMART$_1$Map was considerably reduced by the denoising, with sharp edges, better visualization of cardiac features and homogeneous maps, as observed in MOLLI maps (Figure 2 and 3).

Conclusions: We demonstrated the feasibility of denoised SR-based myocardial T_1 mapping to perform accurate and precise T_1 analysis even in the setting of significant noise. Therefore, this approach could be beneficial to accurately detect and quantify myocardial fibrosis at no additional cost.

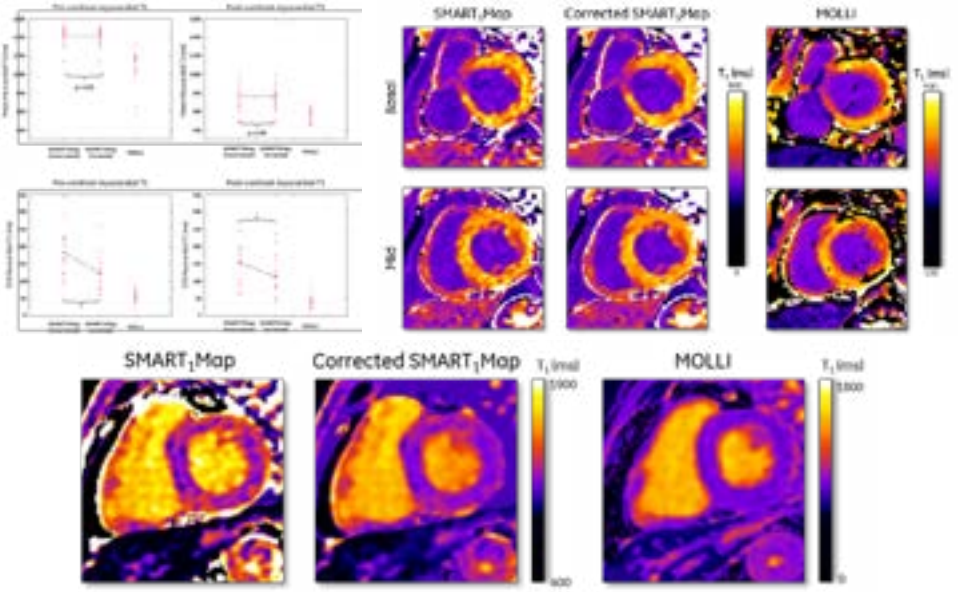

P293

Influence of breathing on septum motion from multi-dimensional cardiac MRI

Teodora Chitiboi, PhD[1] Rebecca Ramb, PhD[2], Eve Piekarski, MD[3], Lennart Tautz, MS[4], Li Feng, PhD[5], Anja Hennemuth, Dr.[4], Leon Axel, PhD, MD[1]

1. *NYU School of Medicine, New York, NY*
2. *NYU School of medicine, Brooklyn, NY*
3. *Center for Biomedical Imaging, NYU School of Medicine, Paris, Ile-de-France, France*
4. *Fraunhofer MEVIS, Bremen, Germany*
5. *NYU School of Medicine, NY*

Background: Multi-dimensional cardiac MRI enables the study of the effects of breathing on cardiac function, through varying preload. XD-GRASP (eXtra-Dimension-Golden-Angle-Radial-Sparse-Parallel) [1] combines self-navigated radial imaging with accelerated compressed sensing. This imaging technique parameterizes physiological motion (breathing and cardiac) as extra dimensions in a multi-dimensional image space to be reconstructed. In this space, we analyze the left ventricle (LV) and right ventricle interaction by tracking the septum displacement over the cardiac and respiratory cycles. End-diastolic distance between LV center and septum can be considered a 1D measure of LV preload, with systolic shortening as a measure of ejection. We measured the modulation of septum position during the respiratory cycle for normal subjects and patients with reduced ejection fraction (EF).

Methods: For 15 subjects: 8 normal (N) and 6 with reduced EF, without left bundle branch block, hypertrophic cardiomyopathy, or infarction (reducedEF) we acquired a self-gated free-breathing 2D single-slice short-axis XD-GRASP dataset, with a 1.5T scanner (Avanto-Siemens) , using a 2D radial golden-angle SSFP sequence (TR/TE=2.8/1.4ms, spatial resolution=2×2×8mm, acquisition time=23s). The breathing and cardiac signals were separately extracted from the image data post-acquisition, in order to reconstruct the physiologic dimensions. The LV myocardium was automatically segmented [2] and manually corrected. The images were transformed into polar coordinates, using the LV center at end-systole as origin, and the septum was automatically detected (Figure1). The average distance between the LV center and the endocardial septum border $d_{c,r}$ was computed for each cardiac c and respiratory r frame. The normalized relative change in septum distance during the cardiac cycle $cd_r=(d_{end\text{-}diastole,r}-d_{end\text{-}systole,r})/d_{end\text{-}diastole,r}$ was computed for each respiratory phase.

Results: The relative septum displacement during the cardiac and respiratory cycles differs between N and reducedEF (Figure2). The septum position during end-diastole varies with respiration for N, due to the changing intrathoracic pressures, but less so for reducedEF, while the septum position during end-systole remains relatively constant with breathing (Figure3a). The relative septal displacement cd_r decreases during inspiration and increases during expiration for N, but this mechanism is partially disrupted for reducedEF (Figure3b). The degree of septum position modulation between end-expiration and end-inspiration phases was significantly lower in reducedEF compared to N (0.043±0.024 vs. 0.0969±0.025, p=0.0009).

Conclusions: The septum position and motion is modulated by the varying preload due to breathing for N, but this is altered for patients with reduced EF.

[1]MRM 2016, *75*(2), pp.775-788

[2]ISBI 2014, pp.943-946

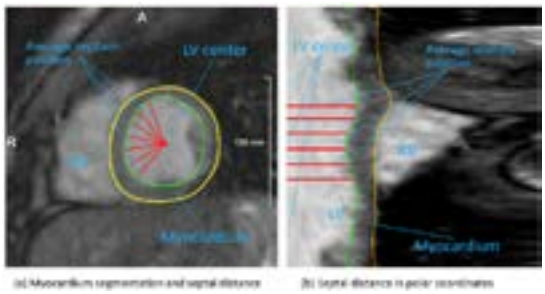

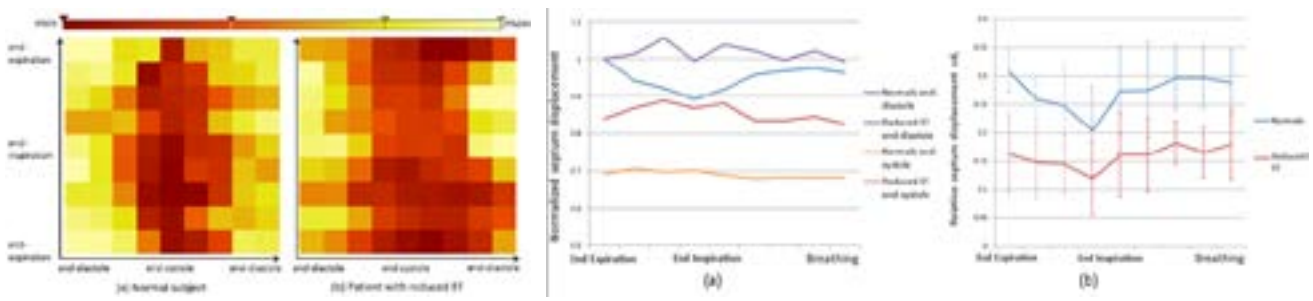

P294

Validation of multiple T1 Mapping algorithms

Markus Huellebrand, M.Sc.[1]Michael Markl, PhD[2], Anja Hennemuth, Dr.[1]

1. *Fraunhofer MEVIS, Bremen, Germany*
2. *Northwestern University, Chicago, IL*

Background: The model fit for the calculation of the T1 maps can be done with optimization algorithms such as the Levenberg-Marquardt method. Goal of this work is to test how the influence of the algorithmic approach and the noise level on the robustness of the quantitative analysis.

Methods: Data of 20 healthy subjects (age: 51+-14 years) were acquired on Siemens 1.5T Aera scanner (Siemens Medical Solutions, Erlangen,Germany). Pre- and post-contrast T1 MOLLI MRI images were acquired in basal, mid-ventricular and apical slices in two spatial resolutions. For pre-contrast T1 images 8 images were acquired in 11 heart cycles, using a 5(3)3 scheme, with 35° flip-angle, FoV: 285*380, 8mm slice thickness. In addition to images with a conventional voxel size of 1.5x1.5x8mm^3, images with a spatial resolution of 1.0x1.0x8.0mm were acquired. Post-contrast images were acquired by a 4(1)3(1)2 scheme with same resolution. In this work we integrated two derivative-based algorithms, Levenberg-Marquardt in two implementations, and the Quasi Newton. Furthermore the direct search algorithms Simplex, and Hooke were applied. We set the initial parameters for all algorithms as suggested in [1]. For a statistical analysis, we calculated the T1 maps by the different fitting algorithms and compared the results by a Bland Altman analysis. To further test the influence of noise on the different algorithms, we added different levels of Gaussian noise (2,4,6 times the estimated myocardial noise level [EN]) as well as the high resolution images to the original data. We also analyzed the performance of the algorithms, at all noise levels.

Results: Mean T1 values per segment of the complete population is shown in figure 1. Except for the Quasi-Newton method, all algorithms were able to fit the myocardial voxels successfully. For the Quasi-Newton method, a number of voxels failed in all segment for pre- and post-contrast T1 maps. These voxels were removed from the following analyses. Bland-Altman analysis comparing the algorithms shows an acceptable agreement over all algorithms and noise levels figure 2. Figure 3 shows the Bland-Altman analysis comparing different noise levels.

Conclusions: Except for the Quasi-Newton method, the tested algorithms showed a good agreement and are robust against simulated Gaussian noise. The unsuccessfull fits of the Quasi-Newton algorithm might result from a higher requirement for good initial parameters. The increased limit of agreement between the low- and high-resolution images might result from the different ROIs defined on the different images.

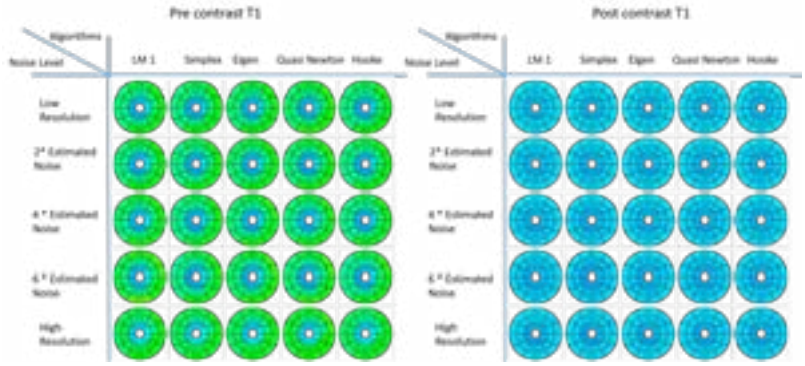

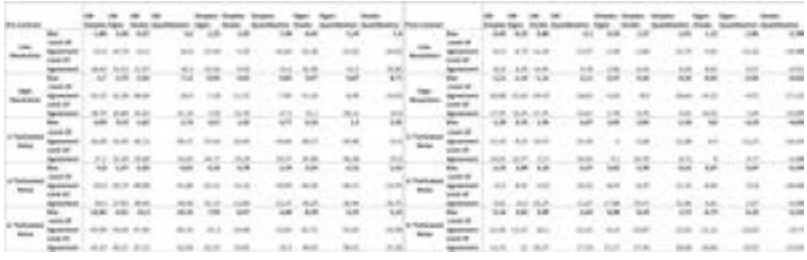

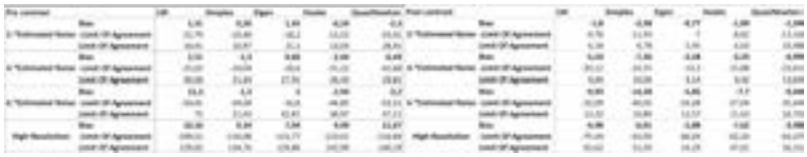

P295

Visualization and Quantification of Right Ventricular Wall Velocities and Blood Flow by 3T 4D PC-MRI

Stig F. Samnøy, MSc[1] Terje H. Larsen, Dr, PhD[2], Gottfried Greve, Prof. Dr. Med[3]

1. *Bergen University College, Bergen, Hordaland, Norway*
2. *Departement of Heart Disease, Haukeland University Hospital, Bergen, Norway, Bergen, Hordaland, Norway*
3. *Department of Clinical Science, University of Bergen, Norway, Bergen, Hordaland, Norway*

Background: Assessment of ventricular morphology and function by the use of cardiac magnetic resonance is gaining popularity in the cardiac imaging field. While the left ventricle has been studied extensively due to its major role in the cardiovascular system, analyses of right ventricular function and blood flow pattern has been restrained mainly because of its complex shape. Nevertheless, knowledge of the right ventricular function and blood flow is of great importance in cardiac disorders such as pulmonary hypertension, coronary heart disease, and in patients with congenital heart disease. We sought to assess and characterize the three-directional right ventricular wall motion as well as the intra-cavity blood flow by using a retrospective 4D PC-MRI technique.

Methods: Velocity measurements were acquired by applying a retrospective 4D PC-MRI, ECG gated, CINE imaging technique during breath hold. Velocity components in all three orthogonal directions were obtained from consecutive 2D short-axis slices covering the entire right ventricle throughout the cardiac cycle. Data were acquired with a 3.0T GE Signa Excite scanner (Milwaukee, WI, USA). Sequence parameters were: TR=11 ms, TE=4 ms, Flip Angle=20°, Matrix=256x256, Slice Thickness=8 mm, Slice Resolution=1.25 mm per pixel, VENC=150 cm/s, and Field of View=320x320 mm. The ventricular wall was segmented from the images in all slices throughout the cardiac cycle. The coordinates of the wall segments were used to construct a time-varying surface model that was colored according to the ventricular motion. The velocity pattern of the blood flow was displayed as three-directional vectors at each pixel position according to its velocity.

Results: Using data from controls, this method was able to present the intra-cavity blood flow pattern as well as the motion of the ventricular wall. Figure 1 illustrates right ventricular blood flow during systole (left) and diastole (right).

Conclusions: This 4D PC-MRI technique show the possibility to study the three-directional movement of the myocardium and the intra-cavity blood flow. The visualization technique reveals the blood flow pattern and the contraction pattern of the wall throughout the cardiac cycle and may reveal right ventricular dysfunction and abnormal blood flow pattern.

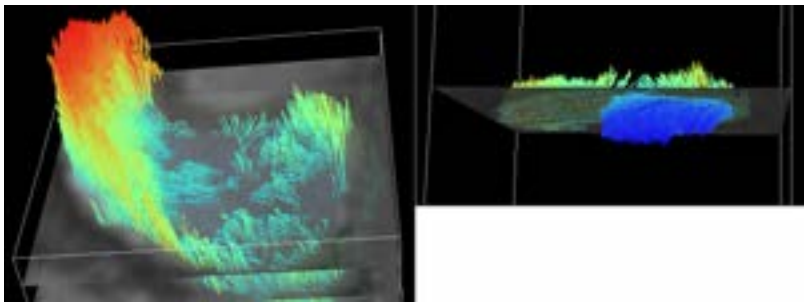

P296

Shape-based Segmentation on 3D Cardiac Cine MRI for Cardiac Functional Measurements

Yan Wang, Ph.D.[1]Evan Kao, B.S.[2], Liang Ge, Ph.D.[3], Yue Zhang, Ph.D.[3], Li Feng, PhD[4], Kanae Mukai, MD[5], David Saloner, Ph.D.[1], Jing Liu, Ph.D.[1]

1. *University of California, San Francisco, CA*
2. *University of California San Francisco, CA*
3. *Northern California Institute for Research and Education, CA*
4. *NYU School of Medicine, NY*
5. *UCSF, Palo Alto, CA*

Background: Automatic segmentation provides essential and efficient tools for accurate functional measurements, especially because manual segmentation is impractical for analysing massive and complex 3D/4D data sets. We here propose an automatic segmentation based on the level set method to efficiently segment left ventricle (LV) and right ventricle (RV) on a 3D cardiac CINE data.

Methods: 1) Data acquisition: We have proposed a highly accelerated free-breathing self-gated 3D CINE MRI to image the heart through the entire cardiac cycle. The sequence was applied on 8 healthy volunteers (4 female, age 29.9±5.7 years, heart rate 62.0±8.5 bpm) on a 3.0T MR scanner (GE Medical Systems, Milwaukee, WI) with an 8-channel cardiac coil, 3D bSSFP sequence with a golden-ratio-based variable-density pseudo-random sampling strategy, Circular Cartesian UnderSampling (CIRCUS), was applied, with FOV=34.0×25.5cm2, TR/TE=4.1/1.7ms, FA=60°, BW=±125kHz, slice thickness of 4mm, image matrix=256×144, temporal resolution of 41 ms, and scan time of 2.5±0.3 minutes. Cardiac phases were reconstructed using a combined compressed sensing and parallel imaging method, k-t SPARSE-SENSE. 2) Image segmentation: Automatic segmentation in 3D or 4D (3D+t) MRI data is difficult given the inherent noise associated with MRI data from inconsistent cardiac motion and inhomogeneous image gradient. The proposed method consists of detecting the circular structures using the Hough transform, and segmenting both the LV and RV using the circular structure in the proposed elliptically refined level set.

Results: We have successfully acquired and segmented 3D CINE images from all 8 subjects. Figure 1 (left) shows the LV and RV segmentation results in short-axis view along multiple slices, using our proposed automatic segmentation algorithm on 3D cardiac CINE images. Figure 1 (right) gives the measurements of LV and RV volume and myocardial mass during the entire cardiac cycle. Table 1 shows parameters for LV and RV measurement including end-diastolic volume (EDV), end-systolic volume (ESV), stroke volume (SV), ejection fraction (EF) and cardiac output (CO). In our study, the RVEF is a little smaller than the real one, since the delineation from the proposed method of RV is the epicardium.

Conclusions: In summary, we have developed an automatic cardiac segmentation algorithm for improving cardiac function measurements applied on an accelerated free-breathing self-gated non-contrast-enhanced 3D CINE imaging.

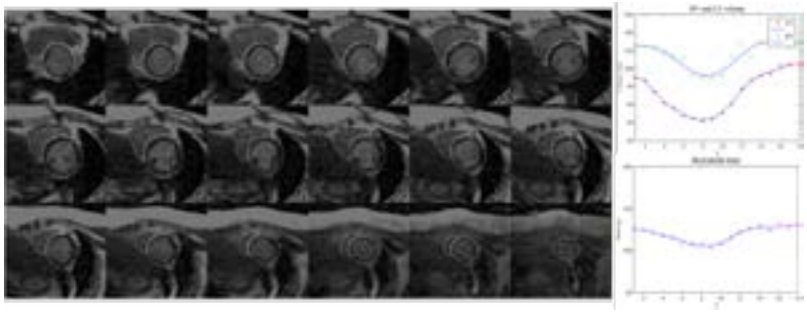

LV and RV functional measurements.

LVCO (L/m^2/min)	LVEF	LVSV (ml)	LVESV (ml)	LVEDV (ml)
4.34	0.58	61.12	43.92	105.05
RVCO (L/m^2/min)	RVEF	RVSV (ml)	RVESV (ml)	RVEDV (ml)
2.82	0.30	39.83	88.89	128.73

P297

Optimization of LV Flow Component Quantification from 4D Flow MRI - Parameter Sensitivity Analysis

Inês C. Bagulho[1] Mohammed S.M. Elbaz, PhD[2], Pankaj Garg, MD[3], Sven Plein, MD PhD[4], Rob J. van der Geest, PhD[2]

1. *(1) Department of Radiology, Leiden University Medical Center, The Netherlands; (2) Faculty of Science, University of Lisbon, Portugal, Leiden, Zuid-Holland, Netherlands*
2. *Department of Radiology, Leiden University Medical Center, The Netherlands, Leiden, Zuid-Holland, Netherlands*
3. *University of Leeds, UK, England, United Kingdom*
4. *St. Thomas' Hospital, London; King's College London; University of Leeds, England, United Kingdom*

Background: Particle tracing from 4D-Flow CMR, as proposed by Bolger et al [JCMR-2007], allows quantitative classification of left ventricular (LV) flow into Direct flow, Retained inflow, Delayed ejection flow and Residual volume. As particle tracing is based on integration, it can be sensitive to errors in the MR-derived velocity data, especially velocity offset errors. The aims of this study were to 1) investigate the sensitivity of flow component quantification to such velocity errors 2) investigate approaches to minimize quantification errors.

Methods: In 9 post-myocardial infarct patients and 9 healthy volunteers, whole-heart 4D-Flow MRI was performed on a 1.5T Philips system (spatial resolution 3x3x3 mm³, temporal resolution ~40ms, full cardiac cycle coverage). Concomitant gradient correction and local phase-offset correction was performed using the scanner software. Short-axis cine-MR was performed for LV volume assessment at end-diastole (ED) and end-systole (ES).
Virtual particles were placed inside the LV at a predefined spacing (between 2 and 10 mm) in the ED phase and their paths were assessed forward and backward in time. The particle classification was done, according to previously described by Bolger et al, using a plane defining both entrance and exit of blood from the LV. Particles below this plane were labeled as invalid if the distance to the LV cavity was more than a predefined acceptance distance.

In addition to the phase-offset error correction provided by the scanner software, LV-specific offset correction was tested based on subtracting the median velocity of the LV myocardium or the whole LV region at either the ED or ES phase. The optimal offset method for each subject was based on visual analysis by selecting the approach with minimal amount of global particle drift.
Flow component classification reliability was quantified using the error metrics in Table 1.

Results: Using the best offset correction approach (Graph 1) the number of invalid particles reduced significantly ($P < 0.005$) while the ejection fraction and delayed-retained errors reduced marginally (Graph 2).
The effect of the acceptance distance in the error is presented in Graph 3.
A particle spacing denser than the acquired voxel size did not improve the errors. A particle spacing > 6 mm resulted in significantly increased errors.

Conclusions: The results demonstrate that velocity offset correction is required to minimize errors in flow component quantification. In more than 50% of the cases (Graph 1) the proposed correction improved the results. Further research is needed to investigate automated ways to identify the optimal offset correction method for each specific case.

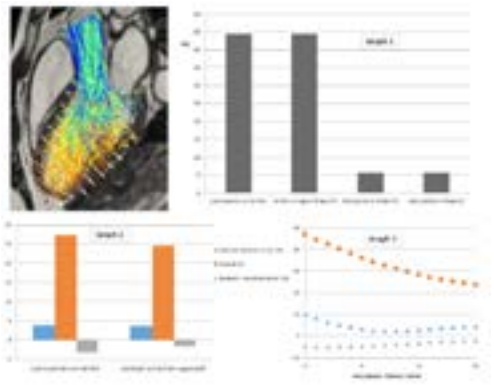

Definition of the three different error types

Definition	
Difference between the ejection fraction, obtained through cine short-axis MRI, and the sum of direct and delayed flow components	***Ejection Fraction***
Percentage of invalid particles	***Invalid Particles***
Difference between the percentages of the delayed and retained flow components.	***Delayed - Retained***

P298

Validation of fully automated quantitative myocardial perfusion by cardiovascular magnetic resonance compared to coronary sinus flow

Raquel Themudo, MD, PhD[1]Jannike Nickander, MD[2], Peter Kellman, PhD[3], Hui Xue, PhD[4], Andreas Sigfridsson, PhD[2], Martin Ugander, MD, PhD[5]

1. *Department of Clinical Physiology, Karolinska Institutet and Karolinska University Hospital, Stockholms Lan, Sweden*
2. *Karolinska Institute, Stockholm, Stockholms Lan, Sweden*
3. *Laboratory of Cardiac Energetics, National Institutes of Health/NHLBI, Bethesda, MD, United States., MD*
4. *National Heart, Lung, and Blood Institute, Bethesda, MD*
5. *Karolinska Institutet, Stockholms Lan, Sweden*

Background: Coronary artery disease and several non-ischemic heart diseases lead to changes in myocardial blood flow (MBF). Quantitative stress first-pass perfusion CMR has been possible to perform, but it has entailed unreasonably cumbersome manual post-processing that has made it impossible to use clinically. A new automated method to generate perfusion color maps in absolute units [mL/min/g] has been developed and integrated within the clinical workflow on the scanner. The aim of this study was to validate quantification of MBF by quantitative perfusion color maps compared to an independent method of quantifying MBF by phase contrast coronary sinus (CS) flow imaging.

Methods: Healthy subjects (n=24, age 26±6 years, 38% females) underwent CMR imaging (1.5T, Siemens Aera) including velocity encoded phase contrast imaging of the CS and first first-pass perfusion in 3 short-axis slices, prior to and during adenosine stress (140 microgram/kg/min). During first past perfusion an intravenous bolus of gadolinium contrast agent (0.05 mmol/kg gadobutrol, Gadovist®) was used. Cine imaging of the entire left ventricle in short-axis slices was performed to obtain the left ventricular mass in grams. First-pass perfusion images were analyzed by drawing regions of interest (ROIs) over the whole myocardium in the 3 short-axis slices. Average myocardial perfusion was obtained in ml/min/g. CS flow was determined by drawing an ROI in the coronary sinus over the 30 phases in the velocity-encoded phase contrast images. Coronary sinus flow was divided by the LV mass to obtain myocardial blood flow in mL/min/g. An example of quantitative perfusion color maps and image analysis of CS flow is illustrated in figure 1. Linear regression analysis was performed to compare MBF from the quantitative perfusion maps with the MBF calculated from the CS phase contrast images.

Results: Quantitative myocardial perfusion from color maps at rest (n=16; 0.7±0.8, mean±SD) and stress (n=20; 3,6±0.2, mean±SD) correlated with myocardial blood flow quantified in the coronary sinus (n=36, R^2=0.77, $p < 0.001$) (Figure 2).

Conclusions: Automatic quantification of myocardial perfusion is feasible in clinical workflow and shows a good correlation compared to the independent measure of myocardial blood flow by coronary sinus flow measurement.

http://www.ConferenceAbstracts.com/uploads/cfp2/attachments/LDFAIBDN/LDFAIBDN--222865-1-ANY(1).pdf

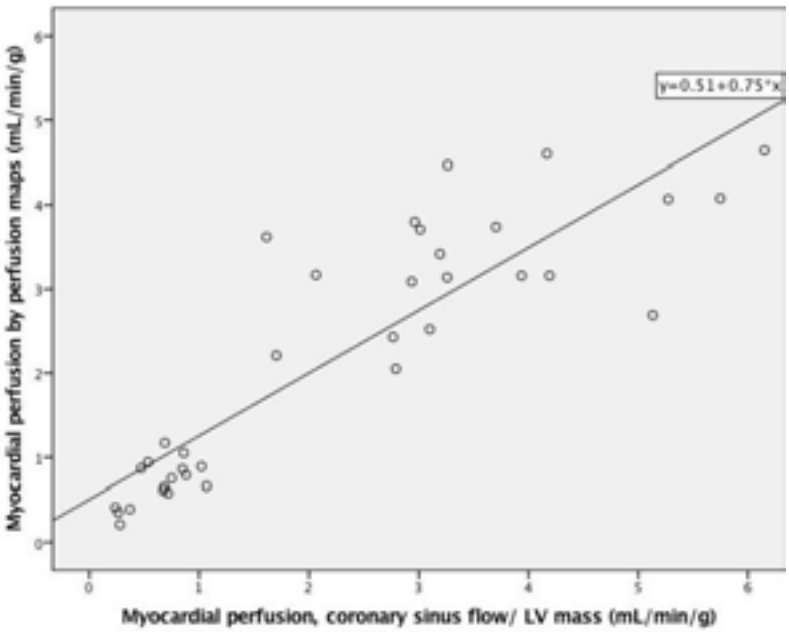

P299

T1 mapping and extracellular volume in patients with healed myocarditis

Amrit Lota, BMBCh BA[1]Rebecca Wassall, BN (Hons), MSc.[2], Vassilis Vassiliou, MBBS[3], Rick Wage, DCR (R)[4], Andrew D. Scott, PhD[5], Adam Tsao[6], Brian Halliday, BSc (Hons) MBChB (Hons)[7], Rameen Shakur, BMBCh Mphil[3], Shivraman Giri, PhD[8], Peter D. Gatehouse, PhD[9], David N. Firmin, PhD[4], John Cleland, MD PhD[10], Stuart Cook, PhD[10], Dudley J. Pennell, MD[11], Sanjay Prasad, MD[11]

1. *NIHR Royal Brompton Cardiovascular Biomedical Research Unit and National Heart and Lung Institute, Imperial College London, England, United Kingdom*
2. *Royal Brompton & Harefield NHS Foundation Trust, London, England, United Kingdom*
3. *Royal Brompton Hospital, England, United Kingdom*
4. *NIHR Cardiovascular Biomedical Research Unit, Royal Brompton Hospital, England, United Kingdom*
5. *NIHR Cardiovascular Biomedical Research Unit, The Royal Brompton Hospital, Sydney Street, London, SW3 6NP, UK, England, United Kingdom*
6. *Imperial College London, London, England, United Kingdom*
7. *Royal Brompton Hospital and National Heart and Lung Institute, Imperial College London, London, England, United Kingdom*
8. *Siemens Healthcare, IL*
9. *NIHR Cardiovascular Biomedical Research Unit, Royal Brompton Hospital, London, England, United Kingdom*
10. *Imperial College, London, England, United Kingdom*
11. *Royal Brompton Hospital and Imperial College, London, England, United Kingdom*

Background: Acute myocarditis remains a challenging diagnosis with poorly defined markers of risk and adverse remodelling. CMR based tissue characterisation using T1 mapping sequences can accurately and non-invasively quantify extracellular space expansion. Recent studies have suggested that T1 mapping may identify low-level myocardial injury remote from the primary site of inflammation.[1] Furthermore, T1 mapping may also distinguish acute and convalescent forms of myocarditis.[2] This study aimed to investigate the value of native T1 times and extracellular volume fraction (ECV) in the remote myocardium of patients with so-called 'healed' myocarditis with preserved LV function.

Methods: Seventeen patients (average age 35±13 years, 94% male) with a history of acute myocarditis defined by clinical presentation (chest pain, troponin rise, unobstructed coronary arteries) and 2 out of 3 CMR Lake Louise Criteria underwent repeat CMR on a 3T system (MAGNETOM Skyra, Siemens Healthineers, Erlangen, Germany) to assess T1 and ECV using native 5(3)3 and post-gadolinium 4(1)3(1)2 T1 maps. Twenty healthy volunteers (average age 36±9 years, 65% male) also underwent a 3T CMR scan for native T1. Diastolic native T1 maps were taken after manually identifying diastasis from the short-axis cine and calculating the diastolic trigger delay for each individual. Gadolinium (Gadobutrol) 0.1 mmol/kg was administered and post-gadolinium T1 maps were taken 14 minutes later. The hematocrit was measured in the biochemistry laboratory on the same day. The MOLLI sequence was acquired twice at the basal short-axis left ventricular level and twice at the mid-ventricular level to obtain an average basal and mid-level T1 value, as well as an overall average of all four values. Regions of interest were drawn in the septum to acquire T1 values and derive ECV as ECV=(1-hematocrit)* [(1/T1myocardium post contrast-1/T1 myocardium native)]/[(1/T1 blood post contrast-1/T1 blood native)].

Results: In patients with healed myocarditis, the interval from baseline presentation to follow-up CMR was 5.7+/-3.9 years. Using averages from all 4 MOLLI sequences, the mean native T1 value was 1263±33msec in healed myocarditis compared to 1285±37 msec in healthy volunteers (p=0.063). The average ECV in patients with healed myocarditis was estimated at 24.4±1.9%.

Conclusions: Our findings suggest that remote measurement of normal appearing myocardium remains robust as native T1 values did not differ significantly from healthy volunteers and ECV was not elevated. Whilst patients with residual late gadolinium enhancement from a previous episode of myocarditis may have increased arrhythmic risk, the evaluation of diffuse interstitial fibrosis appears in this cohort of limited value in further risk stratification.

References: 1. Radunski et al. Clin Res Cardiol. 2016. **2.** Hinojar et al. JACC Cardiovasc Imaging 2015

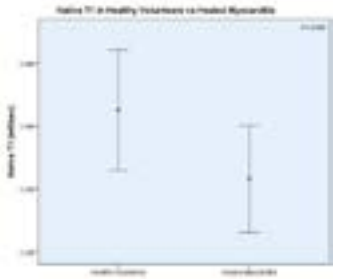

P30

The effect of myocardial infarct size and location on longitudinal and radial left ventricular function in STEMI patients.

Ulrika Pahlm, MD[1] Tom Gyllenhammar, MD[2], Dan Atar, MD, PhD[3], Sigrun Halvorsen, MD, PhD[4], David Erlinge, MD, PhD[5], Marcus Carlsson, MD, PhD[1], Einar Heiberg, PhD[6], Håkan Arheden, MD, PhD[1], Henrik Engblom, MD, PhD[1]

1. *Lund University, Department of Clinical Sciences Lund, Clinical Physiology, Skane University Hospital, Lund, Sweden, Skane Lan, Sweden*
2. *Cardiac MR group, Dept of Clinical Physiology Lund University Hospital, Lund University, Skane Lan, Sweden*
3. *Department of Cardiology B, Oslo University Hospital Ullevål and Faculty of Medicine, University of Oslo, Oslo, Norway, N/A, Norway*
4. *Department of Cardiology, Oslo University Hospital, Ullevaal, Norway, Oslo, Norway*
5. *Lund University, Department of Clinical Sciences Lund, Cardiology, Skane University Hospital, Lund, Sweden, Skane Lan, Sweden*
6. *Lund University, Department of Clinical Sciences Lund, Clinical Physiology, Skane University Hospital, Lund, Sweden; Lund University, Faculty of Engineering, Department of Biomedical Engineering, Lund, Sweden, Skane Lan, Sweden*

Background: Background: In the healthy heart, the majority (60%) of left ventricular (LV) stroke volume (SV) is generated by longitudinal shortening caused by atrioventricular plane displacement (AVPD) from diastole to systole. The remaining SV (40%) is caused by radial inward motion of the epicardium both in the septal and the lateral wall. How the size and location of an ST-elevation myocardial infarction (STEMI) affects the different contributors of LV function in the sub-acute setting is not completely understood. The purpose of this study was to determine how the longitudinal and radial components of LV function are affected by STEMI, and to study the impact of infarct location and infarct size (IS) on these contributors to LV function.

Methods: Methods:Patients from two recent international multicenter cardioprotection studies, CHILL-MI and MitoCare, with CMR 2-7 days after reperfused STEMI were included. Endo- and epicardium was traced in SSFP short-axis cine images and septal insertion points of the right ventricle were placed. AVPD was traced in three long-axis cine images. Longitudinal function was calculated as the AVPD multiplied with the short-axis epicardial area. Radial function was obtained from short-axis cine images and subdivided into septal and lateral contributions. Late gadolinium enhanced (LGE) images were acquired to determine infarct size 15 - 20 min after injection of 0.2 mmol/kg gadolinium contrast. Results are presented as mean±SD.

Results: Results: A total of 177 patients (59 ± 11 years, 87% males) and 23 healthy controls (61 ± 11 years, 52% males) were included. Infarct size in patients was 17±10% and ejection fraction 48±8%. Ejection fraction in healthy volunteers was 62±6%. There was a negative correlation between infarct size and EF (R^2=0.33, y=0.49x+57 pThe longitudinal AV-plane contribution to SV was 58±9%, septal contribution 10±5% and lateral contribution 31±10% in patients (Figure 1) and did not differ from healthy controls (p>0.05 for all). There was no correlation between infarct size and longitudinal or radial contribution to stroke volume and no differences in contributions to stroke volume between patients with infarction in the LAD, RCA or LCx territories.

Conclusions: Conclusion: Reperfused STEMI have significantly decreased absolute AVPD but the proportional contribution of longitudinal and radial shortening to SV is similar to that in healthy controls, despite a significantly lower EF. Interestingly, longitudinal shortening remains the major part of left ventricular function after STEMI despite significantly decreased AVPD.

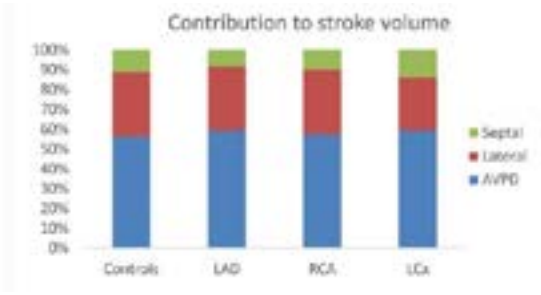

Mean AVPD	anterolateral	Inferolateral	Inferior	Inferoseptal	Anteroseptal	Anterior	
11.2±2.3	12.5±2.7	12.7±3.4	13.0±3.0	10.7±2.8	8.0±2.5	9.5±2.8	LAD
11.6±2.3	13.9±2.7	13.5±3.0	12.1±3.1	10.4±2.2	8.9±2.7	10.7±2.9	RCA
11.9±2.1	13.1±3.0	12.4±2.7	13.9±3.4	11.7±2.3	9.3±2.3	10.9±2.1	LCx
15.5±1.5	16.9±2.3	17.6±2.3	18.4±2.4	15.0±1.7	12.1±1.9	13.4±2.2	Controls

Table 1. AVPD (mean±SD in mm) in the left ventricular walls for patients and healthy controls.

P300

Bringing the T1 mapping sequences together: A study of the T2 effects in ex vivo pig hearts

Tarik Hafyane, MSC[1] Catherine Duquette[2], François-Pierre Mongeon, MD[1], Julien Cohen-Adad, PhD[3], Nikola Stikov, PhD[1]

1. *Montreal Heart Institute, PQ, Canada*
2. *École Polytechnique de Montréal, Montréal, PQ, Canada*
3. *École Polytechnique de Montréal, PQ, Canada*

Background: Different sequences have been proposed to compute T1 values either using inversion recovery (MOLLI, ShMOLLI and IR TSE) or saturation recovery (SASHA) techniques. Previous work based on the Bloch- McConnell equations simulation has demonstrated that T1 measured by saturation-recovery single-shot acquisition is insensitive to T2 effect. In this work, we used ex-vivo pig hearts to demonstrate that T2 effects can account for the difference in T1 values between inversion recovery and saturation recovery sequences.

Methods: Four explanted pig hearts kept in formaline solution were imaged right after explantation and weekly thereafter using inversion recovery sequences MOLLI, SHMOLLI, IR TSE, and a saturation recovery SASHA sequence. The experiments were performed on a 3T system with an 18-channel phased-array cardiac coil. A simulated heart rate of 60 bpm was used. IR-SE T1 maps were generated offline using a custom program (Matlab, The MathWorks, Inc., Natick, MA, USA) and were based on five images collected using slice selective IR with TI=33, 100, 300, 900, 2700 ms; TR/TE=5s/12ms, turbo factor=7. The MOLLI 5(3)3 sequence was used with TE/TR = 1.07/275 ms. SHMOLLI was used with 7 SSFP readouts; TE/TR = 1.07/275 ms. SASHA used 11 SSFP readouts; TE/TR = 1.07/912 ms. The same FOV (360x270mm), acquisition matrix (192x144) and 8mm slice thickness were used for all sequences. T1 quantification from a basal slice was performed by manually delineating the endocardial and epicardial contours of the LV myocardium on the parametric map provided by the scanner using validated software (CMR42, Circle CVI Inc., Calgary, AB, Canada), and computed using freely available software for IR T1 mapping. For each time point, we calculated four T1 maps and observed how the computed T1 values changed over time compared to T2 values. The error was computed as the difference between each of the inversion recovery sequences and the saturation recovery sequence. The T2 correlation equation was used to heuristically eliminate the T2 effect from the calculated T1 values.

Results: All four sequences demonstrated a decrease in T1 over time, which is expected given that fixation results in lower T1 values (Figure 1). All inversion recovery sequences showed a significant correlation between the error and T2 values,with MOLLI ($r=0.89$, $p < 0.001$), SHMOLLI ($r=0.63$, $p=0.009$) and IR-TSE ($r=0.70$, $p=0.003$) (Figure 2). After correcting T1 values from inversion recovery sequences using the correlation equations we found that T2 values account for all the difference between inversion recovery and saturation recovery sequences (Figure 3).

Conclusions: We confirmed simulation results demonstrating that inversion recovery sequences are sensitive to changes in T2. Doing an inline correction by using T2 values will close the gap between inversion recovery and saturation recovery sequences. This result helps understand the difference between the two main techniques of quantitative myocardium T1 mapping.

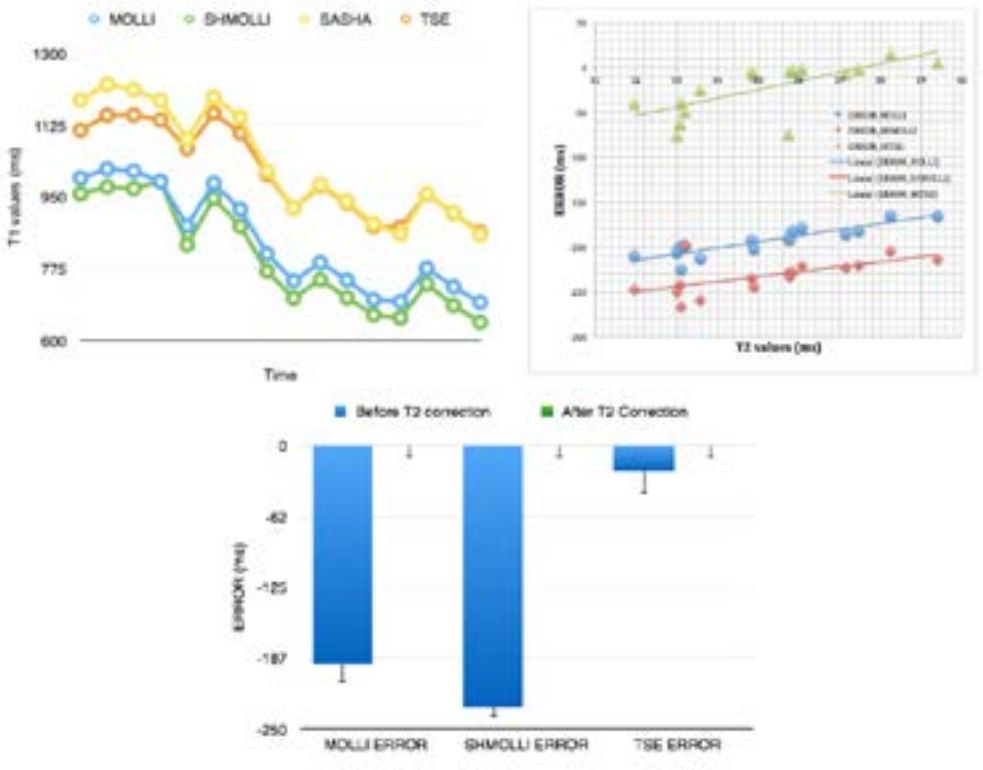

P301

Non-contrast T1 Mapping at 3 Tesla Identifies Regional Replacement Fibrosis in Ischemic, Dilated and Hypertrophic Cardiomyopathy: Comparison of Quantitative Analyses Versus Late Gadolinium Enhancement

Yoko Mikami, MD, Ph.D[1] Aidan Cornhill, BMSc, HBA[2], Michael Bristow, MD[2], Naeem Merchant, MD[2], Bobby Heydari, MD, MPH[2], Andrew Howarth, MD[2], Carmen P. Lydell, MD[2], James White, MD, FRCP(C) [3]

1. *Stephenson Cardiac Imaging Centre, Libin Cardiovascular Institute of Alberta, University of Calgary, Calgary, AB, Canada*
2. *Stephenson Cardiac Imaging Centre, Libin Cardiovascular Institute of Alberta, University of Calgary, AB, Canada*
3. *Stephenson Cardiovascular Imaging Center, University of Calgary, AB, Canada*

Background: The clinical role of non-contrast (i.e. native) T1 mapping for the characterization of replacement fibrosis is poorly explored. We aimed to compare signal characteristics and thresholds for native T1 mapping versus late gadolinium enhancement (LGE) imaging at 3T for the detection of chronic replacement fibrosis in ischemic (ICM), non-ischemic dilated (NIDCM) and hypertrophic (HCM) cardiomyopathy.

Methods: Sixty patients (20 ICM, 20 NIDCM and 20 HCM) with definite fibrosis seen on LGE imaging had non-contrast T1 mapping performed (shMOLLI-based) at 3T (Skyra or Prisma, Siemens). Slice matched LGE images were analyzed using >2, >3 and >5SD thresholds above the mean signal intensity (SI) of reference myocardium. The mean signal and SD of regional fibrosis and reference tissue were recorded using manual regions of interest. Identical contours were applied to spatially matched T1 maps and the same measurements performed. Manual adjustment of the signal threshold was incrementally performed on LGE images to define regional fibrosis according to expert visual segmentation. Signal characteristics of reference tissue and fibrosis, as well as fibrosis extent, were compared between LGE and T1 map analyses using a slice-based approach.

Results: The mean LGE fibrosis burden for ICM, DCM and HCM patients was 3.8g, 2.3g and 3.8g per slice, respectively, when measured using expert adjusted signal threshold. The mean signal values of reference tissue and fibrosis are shown in Figure 1 for LGE and native T1 mapping, consistently providing elevation in T1 values within fibrosis across all 3 cohorts. The mean T1 signal elevation was 128ms, 103ms and 91ms, respectively above reference tissues (corresponding to 2.2, 1.9 and 2.1 times reference tissue SD). Application of a >2SD threshold on T1 maps provided good agreement for fibrosis mass compared with expert manual LGE segmentation for all cohorts (Bland-Altman analysis: mean difference and 95% limits of agreement: ICM 0.8 ± 3.1g, NIDCM 0.06 ± 3.9g, HCM 0.05 ± 4.8g). However, spatial agreement of segmented tissue was unreliable in some patients with NIDCM.

Conclusions: Non-contrast T1 mapping at 3T consistently demonstrates elevated T1 values in regions of LGE-confirmed replacement fibrosis across various cardiomyopathy etiologies. A >2SD threshold provides good approximations of LGE-based fibrosis burden. However, spatial agreement may be impaired in NIDCM. Native T1 mapping may provide value for the measurement of chronic replacement fibrosis where contrast administration is not desired or is contra-indicated.

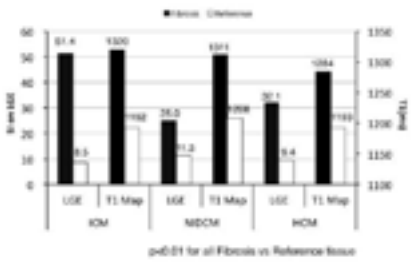

Figure 1. The mean signal for fibrosis and reference tissue for LGE and T1 maps for ischemic (ICM), non-ischemic dilated (NIDCM) and hypertrophic (HCM) cardiomyopathy. Signal intensity (SI) on LGE in fibrosis area were significantly increased compared to those in reference tissue for all across the 3 cohorts. T1 values in fibrosis area were also significantly higher compared to those in reference tissue.

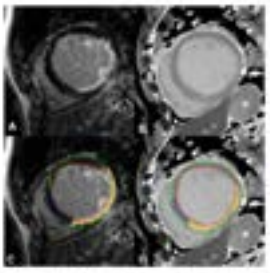

Figure 2. Images for a patient with ischemic cardiomyopathy (ICM). (A) LGE image, (B) T1 map, (C) LGE segmentation with threshold of >5SD above reference myocardium and (D) T1 map segmentation with the threshold of >2SD above reference myocardium. On T1 maps, a threshold of >2SD most closely approximated the identification of replacement fibrosis by LGE imaging.

P302

T1 mapping sequence comparison - normal ranges and reproducibility in healthy human myocardium

Valentina O. Puntmann, MD, PhD[8] Elif Peker, MD[1], Lea Winau[2], Martin Gerster, B.Sc.[3], Robert Heinke[2], Julian Lukas. Wichmann, MD[4], Simon S. Martin, MD[5], Katrin Schnoes, MD[2], Andreas Zeiher, MD, PhD[2], Thomas Vogl, MD[2], Andreas Greiser, Ph.D[6], Eike Nagel, MD, PhD[7]

1. *Goethe University Hospital Frankfurt, Frankfurt, N/A, Germany*
2. *Goethe University Hospital Frankfurt, N/A, Germany*
3. *Institute for Experimental and Translational Cardiovascular Imaging, DZHK Centre for Cardiovascular Imaging, Goethe University Hospital Frankfurt, Frankfurt am Main, Germany;, Hessen, Germany*
4. *University Hospital Frankfurt, Frankfurt, Hessen, Germany*
5. *University Hospital Frankfurt, Department of Diagnostic and Interventional Radiology, Frankfurt, Hessen, Germany*
6. *Siemens Healthcare GmbH, Erlangen, Germany, Erlangen, Bayern, Germany*
7. *University Hospital Frankfurt; Institute for Experimental and Translational Cardiovascular Imaging; DZHK Centre for Cardiovascular Imaging, Frankfurt, N/A, Germany*
8. *Institute of experimental and translational cardiovascular imaging, Frankfurt, N/A, Germany*

Background: T1 mapping is a promising tool for characterization of diffuse myocardial disease and risk stratification in non-ischaemic cardiomyopathies (NICMs). The body of evidence supporting its role is based on a number of different sequences (sequence scheme, flip angle (FA)), mode of acquisition (single slice vs. multiple slices), or postprocessing approach (septal vs SAX). This aim of this study was to undertake intra-subject sequence comparison of precontrast and postcontrast acquisitions using 3 most prominent modified Look-Locker (MOLLI) sequences in myocardial tissue characterization in health and disease.

Methods: Three different T1 mapping MOLLI sequence schemes (MOLLI 5(3)3(3) T1 Long), MOLLI 3(3)3(3)5FA50), and MOLLI 3(2)3(2)5FA50) were acquired in normotensive healthy subjects with no medical history or regular medication served as controls (n=19). Images were acquired in 3 short axis (SAX) slices prior to and after the application of gadolinium contrast agent at 1.5 Siemens scanner using an inline MOCO algorithm. Analysis was performed with regions of interest (ROI) placed within the septum or to include the whole myocardium of a SAX slice. Lateral ROIs were obtained to examine regional variations. Intraobserver and interobserver reproducibility was assessed using Bland Altman methods.

Results: Table 1 provides normal values per slice/sequence/postprocessing approach, relevaing sequence specific-normal ranges. Generally, for native T1, MOLLI3(3)3(3)5FA50 showed higher values; sampling in apical slice showed considerable dispersion. All sequences showed regional variation, by significantly lower lateral T1 values ($p < 0.01$). Intraobserver and interobserver reproducibility of septal measurements was superior to SAX approach in all groups for native and postcontrast T1 measurements (**Table 2**). All 3 sequences showed respectable reproducibility and coefficient of variation; whereby MOLLI 3(2)3(2)5FA50 septal sampling showed the highest agreement and tightest MD(SD) and CoVs.

Conclusions: We demonstrate that the 3 MOLLI sequences prvide sequence-specific normal ranges. Measurements with all 3 sequences are highly reproducible. Septal sampling in midventricular SAX slice is the least prone to partial volume errors. On the contrary, apical (and less so basal) slice suffers with greater dispersion. Of teh 3 sequences, MOLLI 3(2)3(2)5FA50 septal sampling showed the highest agreement and tightest MD(SD) and CoVs.

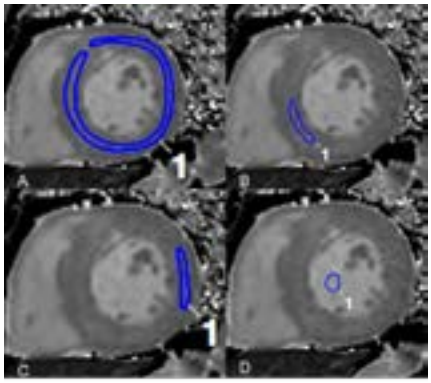

Table 1

Sig.(p-value)	Apical	Midventricular	Basal	Native T1
				SAX-ROI
0.34	983±72	964±24	987±35	MOLLI 5(3)3(3)FA35
0.88	996±64	993±31	1001±36	MOLLI 3(3)3(3)5FA50
0.53	960±59	946±30	961±37	MOLLI 3(2)3(2)5FA50
	0.34	<0.001	0.008	Sig. (p-value)
				Septal ROI
0.048	958±49	975±25	990±32	MOLLI 5(3)3(3)FA35
0.364	1019±71	1003±31	995±37	MOLLI 3(3)3(3)5FA50
0.347	972±61	963±27	951±28	MOLLI 3(2)3(2)5FA50
	0.014	<0.001	<0.001	
				Postcontrast T1
				SAX-ROI
0.322	478±30	491±26	478±30	MOLLI 4(1)3(1)FA35
0.194	500±30	515±26	515±27	MOLLI 3(3)3(3)5FA50
0.486	508±25	516±29	519±28	MOLLI 3(2)3(2)5FA50
	0.010	0.013	<0.001	Sig (p-value)
				Septal ROI
0.503	485±23	493±25	484±25	MOLLI 4(1)3(1)FA35
0.310	507±25	521±28	519±32	MOLLI 3(3)3(3)5FA50
0.435	512±22	521±30	524±31	MOLLI 3(2)3(2)5FA50
	0.003	<0.001	<0.001	

SAX - short axis slice, ROI - region of interest.

Table 2

		Blood-ROI			Lateral-ROI			Septal-ROI			SAX-ROI	Native T1
Pearson(r)	CoV (%)	MD+/-SD	Pearson(r)	CoV (%)	MD+/-SD	Pearson(r)	CoV (%)	MD+/-SD	Pearson(r)	CoV (%)	MD±SD	
												Basal slice
0.87	4.4	13.8±36.5	0.97	4.1	0.72±10.10	0.98	3.3	0.31±7.4	0.98	3.7	0.24±5.7	MOLLI 5(3)3(3) FA 35
0.93	4.4	22.6±33.7	0.93	3.4	1.4±13.1	0.97	3.9	-1.1±8.4	0.97	3.6	1.2±8.5	MOLLI 3(3)3(3)5 FA50
0.94	6.5	5.9±35	0.96	4.1	-4.37±10.9	0.97	3.3	0.92±8.52	0.97	3.8	0.95±8.2	MOLLI 3(2)3(2)5 FA 50
												Midventricular slice
0.94	4.9	5.1±25.8	0.96	4.1	3.4±10.9	0.97	2.5	0.6±7.8	0.95	2.6	1.2±8.1	MOLLI 5(3)3(3) FA 35
0.95	5.1	-9.7±24	0.89	3.4	2.9±15.5	0.97	3.3	0.8±12.5	0.97	3.4	-0.4±8.4	MOLLI 3(3)3(3)5 FA50
0.92	5.9	-5.8±33.7	0.93	3.5	3.5±10.9	0.98	1.8	-0.4±9.1	0.98	2.3	-0.5±5.7	MOLLI 3(2)3(2)5 FA 50
												Apical slice
0.88	15.5	-5.5±36	0.94	12.2	-5.2±36	0.99	5.1	-0.9±6.3	0.98	7.7	0.8±12	MOLLI 5(3)3(3) FA35
0.92	5.4	-1.18±33	0.98	10.7	-4.9±15.9	0.99	6.5	1.4±7.3	0.98	6.8	2.6±14.4	MOLLI 3(3)3(3)5 FA50
0.91	6.4	11.8±39	0.98	10.1	3.8±17.1	0.99	5.0	-0.6±5.09	0.99	6.1	0.75±8.9	MOLLI 3(2)3(2)5 FA 50

		Blood-ROI			Lateral-ROI			Septal-ROI			SAX-ROI	Post-contrast T1
Pearson(r)	CoV (%)	MD+/-SD	Pearson'r(p)	CoV	MD+/-SD	Pearson'r(p)	CoV	MD+/-SD	Pearson'r(p)	CoV	MD±SD	
												Basal slice
0.96	8.8	1.9±7.9	0.97	5.8	-1.4±6.6	0.99	5.2	-0.1±4.4	0.99	5.2	0.4±3.8	MOLLI 4(1)3(1) FA35
0.94	8.3	1.7±7.9	0.96	6.3	2.9±7.2	0.98	4.7	-0.6±4.8	0.99	5.2	-1.0±3.3	MOLLI 3(3)3(3)5 FA50
0.95	8.6	1.1±4.9	0.92	6.4	-3.3±2.0	0.99	4.7	-0.8±4.4	0.98	5.4	-1.7±4.4	MOLLI 3(2)3(2)5 FA 50
												Midventricular slice
0.96	8.1	2.1±7.2	0.96	5.8	-1.3±6.9	0.98	5.1	-0.3±6.9	0.99	5.2	0.6±3.2	MOLLI 4(1)3(1) FA35
0.97	7.2	-1.8±6.9	0.98	6.1	1.9±5.6	0.99	4.8	0.2±3.9	0.99	5.2	0.5±3.8	MOLLI 3(3)3(3)5 FA50
0.98	6.4	-2.4±5.9	0.96	6.8	-0.6±10	0.99	4.3	0.5±2.0	0.99	4.9	-0.4±2.9	MOLLI 3(2)3(2)5 FA 50
												Apical slice
0.97	10.1	-2.4±7.6	0.97	6.8	-1.8±9.1	0.97	4.9	-0.5±1.5	0.96	4.7	0.7±4.4	MOLLI 4(1)3(1) FA35
0.97	8.9	-2.8±9.6	0.96	7.2	0.6±7.7	0.99	4.8	0.3±3.1	0.99	5.7	-1.0±2.4	MOLLI 3(3)3(3)5 FA50
0.96	9.5	1.2±5.2	0.94	5.9	-0.4±11.1	0.97	4.8	0.4±5.3	0.94	5.3	0.4±7.6	MOLLI 3(2)3(2)5 FA 50

P303

Study on the impact of strain correction on the secondary eigenvector of diffusion with in vivo and ex vivo porcine hearts

Pedro F. Ferreira, PhD[1]Sonia Nielles-Vallespin, PhD, MSc[2], Ranil de Silva, FRCP PhD[3], Andrew D. Scott, PhD[4], Daniel B. Ennis, PhD[5], Daniel A. Auger, Ph.D[6], Jonathan D. Suever, PhD[7], Xiaodong Zhong, PhD[8], Bruce Spottiswoode, PhD[9], Dudley J. Pennell, MD[10], Andrew E. Arai, MD[11], David N. Firmin, PhD[12]

1. *Cardiovascular Biomedical Research Unit, The Royal Brompton Hospital, Sydney Street, London, SW3 6NP, UK, England, United Kingdom*
2. *NIH, MD*
3. *National Heart and Lung Institute, Imperial College London, London, England, United Kingdom*
4. *NIHR Cardiovascular Biomedical Research Unit, The Royal Brompton Hospital, Sydney Street, London, SW3 6NP, UK, England, United Kingdom*
5. *Department of Radiological Sciences, University of California, Los Angeles, CA, USA., CA*
6. *University of Virginia, Charlottesville, VA*
7. *Geisinger Health System, Bellefonte, PA*
8. *Siemens Healthcare, GA*
9. *Siemens Medical Solutions USA, Inc., Knoxville, TN*
10. *Royal Brompton Hospital and Imperial College, London, England, United Kingdom*
11. *NIH/NHLBI, MD*
12. *NIHR Cardiovascular Biomedical Research Unit, Royal Brompton Hospital, England, United Kingdom*

Background: Myocytes have a laminar organization, where sheets of myocytes are surrounded by collagen-lined shear layers. These myolaminae, also named sheetlets, play a major role in explaining wall thickening during the heart cycle. It has been shown that cardiac diffusion tensor imaging (DTI) with a STEAM sequence is capable of probing sheetlet orientation with the secondary eigenvector of diffusion, although questions remain about the possible confounding effects of tissue strain throughout the cardiac cycle [1,2]. Recent work has shown that strain correction greatly affects the secondary diffusion eigenvector, but no validation of the correction was possible [3]. In this work we try to provide more insights into this topic by directly comparing in-vivo diffusion tensors with ex-vivo strain-free diffusion imaging of the same porcine hearts.

Methods: All imaging was done at 3T. 11 pigs were successfully scanned with a multi-slice 3D encoded spiral cine DENSE (2.5x2.5x8 mm^3), and with a STEAM-EPI DTI sequence (6 directions, b=500smm^{-2}, 2.8x2.8x8 mm^3) at the diastolic pause, systolic pause, and strain sweet-spots in a mid-ventricular slice. The same DTI sequence was repeated in the hearts after the hearts were excised with arrest induced in either a diastolic-like (KCl) or systolic-like ($BaCl_2$) state. The multi-slice DENSE data was used to strain correct the in-vivo DTI data in systole and diastole on a pixelwise basis. The orientation of the primary (helix-angle HA) and secondary (E2A) eigenvectors was compared between diastole (without/with strain correction), systole (without/with strain correction), the two strain sweet-spots where strain effects are minimized, and the strain-free ex-vivo data.

Results: The measured mean (std) peak radial, circumferential and longitudinal strains were: Err=0.21 (0.06), Ecc=-0.14 (0.02), Ell=-0.11 (0.01) (figure 1). The sweet-spots given by the Ecc curves are located at 24% (7%) and 74% (12%) of the RR interval time. The intersubject median [IQR] histograms for HA and E2A are shown in figure 2. The diastolic and systolic in-vivo mean E2A frequency count difference to ex-vivo is 0.021/0.031 (without/with strain correction). The median absolute E2A for each pig is shown in figure 3.

Conclusions: In-vivo HA distribution remains relatively unchanged throughout the cardiac cycle, with little impact from strain-correction. The ex-vivo distribution is slightly broader, but with little difference between the diastolic and the systolic arrests. In contrast large changes are seen in E2A throughout the cardiac cycle and between without/with strain correction. E2A differences between diastole and systole are greatly reduced with strain correction. However, ex-vivo arrested strain-free E2A conformation is closer to in-vivo values before strain correction, which raises questions about the validity of the current correction.

References: 1-Reese et al. J Magn Reson B 1996 112, 253 2-Axel et al. JCMR 2014 16, 89 3-Stoeck et al. PLoS One 2014 9, e107159

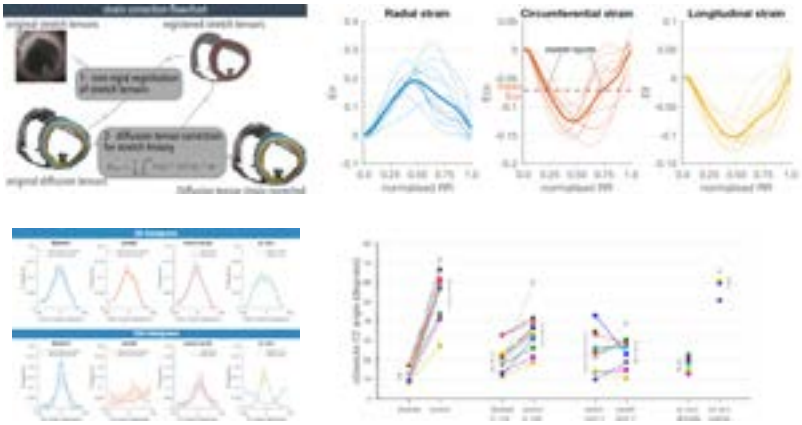

P304

Myocardial Extracellular Volume Fraction of the Left Ventricle in Healthy Adults Based on MOLLI T1 Mapping: Segmental Quantification And Influence Factors

Ling Lin, Master of Medicine[1] Mei Zheng, Master of Medicine[2], Qiu-Xia Xie, Bachelar of Medicine[1], Xu-Hui Zhou, MD, PhD[1]

1. *The First Affiliated Hospital of Sun Yat-Sen University, Guangdong, China (People's Republic)*
2. *The Third Affiliated Hospital of Sun Yat-Sen University, Guangdong, China (People's Republic)*

Background: Extracellular volume fraction (ECV) of myocardium based on T1 mapping techniques is a promising index in early diagnosis and prognosis of various diseases. However, the ranges of normal myocardial ECV varied and overlapped with those in pathologic situations in previous studies. And the influences of individual factors on the myocardial ECV remains controversial. We intended to investigate into the normal range of myocardial ECV and its influence factors.

Methods: 25 healthy volunteers (16 males, 9 females, age 24 to 65 years old) underwent cardiovascular magnetic resonance imaging on a 3.0T system (Magnetom Verio, Siemens). T1 mapping images were obtained in basal, mid-ventricular and apical short axis (SAX) slices before and 15 minute after administration of contrast agent using Modified Look-Locker Inversion Recovery (MOLLI, 5(3)3 and 4(1)3(1)2 for pre-contrast and post-contrast, respectively). T1 maps and ECV maps were generated by Motion-corrected T1 mapping images after feature/contour based registration using a software (cvi42 v5.3, Circle Cardiovascular Imaging). Total left ventricular myocardial ECV, as well as ECV of each slice and segment were calculated and compared. We compared total ECVs in different genders and age groups (divided by 45 years old). Correlation between total ECV and heart rate, BMI, EF, EDV, ESV and LV-Mass were evaluated. Influences of the above factors on total ECV were evaluated by multiple linear regression analysis.

Results: Total left ventricular myocardial ECV of the 25 volunteers was 25.66±2.40%. Myocardial ECV of the basal (25.63±2.70%), mid-ventricular (24.17±2.41%) and apical (27.03±3.31%) SAX were not all equal ($F=6.364$, $P=0.003$), with apical ECV higher than the other two slices. ECVs of the 16 AHA segments were not all equal ($P < 0.001$), with ECVs of segment 2, 3 (basal SAX) and segment 13, 14, 16 (apical SAX) higher than the other segments. Total myocardial ECVs of females were slightly higher than those of males ($P=0.003$). ECVs of subjects elder than 45 (n=13) were higher than those younger than 45 (n=12) ($P=0.047$). There was no correlation between ECV and heart rate, BMI, EF, EDV, ESV and LV-Mass ($P>0.05$). ECV was not affected by these factors ($P>0.05$).

Conclusions: Myocardial ECVs of the 16 segments of left ventricle were not all equal, which probably due to partial volume effect and cardiac motion artifacts. ECV might increases with age and varies between genders, which calls for further large scale analysis. Heart rate, BMI, EF, EDV, ESV and LV-Mass were not correlated with myocardial ECV.

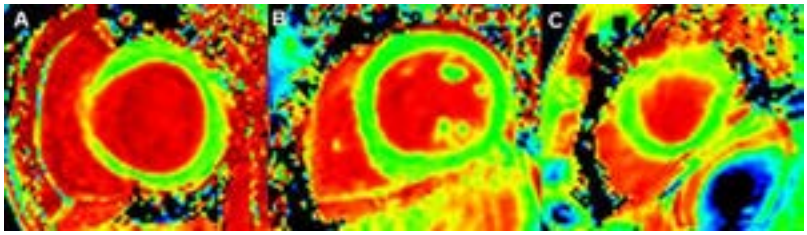

P305

SMART1Map in Hypertrophic Cardiomyopathy (HCM): Initial Experience

Shaw Hua (Anthony) Kueh, MBChB, FRACP[1]Jeanette Soon, MBBS (Hons) FRANZCR[2], Chesnal Dey Arepalli, MD[1], Nada Sulaiman, M.D.[3], Chaitu Cheruvu, MBBS FRACP[4], Christopher Naoum, MBBS PhD[5], Philipp Blanke, MD[6], Rominder S. Grover, MBBS (Hons) FRACP[7], John Mooney, MBBS[7], Stephanie Sellers[8], Jen Ellis, MD[7], Cameron Hague, MD[1], Jonathon Leipsic, MD[7], Darra T. Murphy, MD[7]

1. *St Paul's Hospital, Vancouver, BC, Canada*
2. *St Paul's Hospital, Vancouver, ON, Canada*
3. *St.. Paul's Hospital, Al Madinah, Saudi Arabia*
4. *St Paul's Hospital, Botany, New South Wales, Australia*
5. *Concord Hospital, The University of Sydney, Sydney, Concord, Sydney, New South Wales, Australia*
6. *St. Paul's Hospital & University of British Columbia, Vancouver, BC, Canada*
7. *St Paul's Hospital, BC, Canada*
8. *University of British Columbia, BC, Canada*

Background: Cardiac MRI with T1 mapping has been shown to be useful in the detection of diffuse myocardial pathological processes, such as hypertrophic cardiomyopathy (HCM). SMART1Map (Saturation Method using Adaptive Recovery Times for cardiac T1 Mapping) is a novel technique that allows direct measurement of true T1 relaxation(Slavin and Stainsby 2013). We provide our first real-world single-center experience of SMART1Map in evaluating patients referred with HCM.

Methods: Between November 2014 and August 2016, total of 300 patients undergoing cardiac MRI were consented to undergo additional SMART1Map evaluation. SMART1Map was performed using a series of single-point saturation-recovery method and balanced SSFP readout to generate a T1Map. Cardiac MRI were performed on GE Signa Infinity 1.5 Tesla(T) TwinSpeed MRI. Native T1 measurements were made on the generated SMART1map by drawing the circumference of the myocardium as the region of interest (ROI). Those referred for HCM evaluation were included in this study cohort. Patients were separated into 2 categories according to their MRI findings: those with normal cardiac examination (normal) and those with abnormal cardiac findings with or without abnormal Late Gadolinium Enhancement (LGE) (abnormal). Nineteen healthy volunteers served as control. Parametric variables were compared using one-way analysis of variance (ANOVA). Non-parametric variables were compared using Mann-Whitney U for 2 group comparison and Kruskal-Wallis test for multiple group comparison. P-value of value of < 0.05 was considered statistically significant.

Results: Forty-four patients were referred for HCM evaluation. Five patients were excluded due to poor image quality. The baseline characteristics of the remaining 39 patients are shown in table 1. Patients referred for HCM evaluation were generally older compared to the control group (54.6±15.2 vs 36.9±10.7 years, $p < 0.01$). The medians and interquartile ranges (IQR) derived from the measured mean native T1 values were as follow: control – 1217.7ms (1167.2–1303.6ms); normal – 1229.3ms (1178–1391.6ms); abnormal – 1289.4ms (1224.0–1375.1ms), $p = 0.04$. The T1 values were significantly higher in the abnormal group compared to the control (p=0.11). No difference was seen in the mean T1 value between control and normal group (p=0.74) or between normal and abnormal group (p=0.24).

Conclusions: Using SMART1Map, the native T1 value was significantly higher amongst patients referred with HCM with abnormal cardiac MRI compared to healthy controls.

http://www.ConferenceAbstracts.com/uploads/cfp2/attachments/LDFAIBDN/LDFAIBDN--222336-1-ANY.pdf

Table 1. Baseline characteristics. The mean and standard deviation (SD) of each variable were compared between the 4 groups using one-way analysis of variance (ANOVA). * denotes $\chi 2$ test for categorical variable

P-value	Abnormal (n=21)	Normal (n=8)	Control (n=19)	
<0.01	57.4±13.0	43.9±19.0	36.9±10.7	Age, mean ± SD
0.31*	23 (74)	4 (50)	11 (58)	Male, n(%)
0.13	25.5±7.0	27.5±8.7	21.8±8.1	Body mass index (kg/m^2), mean ± SD
0.18	55±17	64±5	59±6	LVEF (%), mean ± SD
0.26	85.6±31.0	83.0±22.8	73.3±13.9	LVEDVI (ml/m^2), mean ± SD
0.07	45.1±33.6	29.7±7.4	29.2±6.9	LVESVI (ml/m^2), mean ± SD
0.09	52±11	57±8	58±6	RVEF (%), mean ± SD
0.59	70.0±19.9	74.5±21.1	75.1±14.2	RVEDVI (ml/m^2), mean ± SD
0.67	34.5±14.8	36.6±14.1	32.0±8.0	RVESVI (ml/m^2), mean ± SD

P306

Reproducibility of aortic wall shear stress as assessed by multiphase segmentation with 4D flow CMR in healthy volunteers

Roel L.F. van der Palen, M.D.[1]Arno A.W. Roest, MD, PhD[2], Pieter J. van den Boogaard, BSc[3], Nico A. Blom, MD, PhD[2], Albert de Roos, MD, PhD[3], Jos J.M. Westenberg, PhD[4]

1. *Division of Pediatric Cardiology, Department of Pediatrics, Leiden University Medical Center, Leiden, The Netherlands, Leiden, Zuid-Holland, Netherlands*
2. *Division of Pediatric Cardiology, Department of Pediatrics, Leiden University Medical Center, Leiden, The Netherlands and Netherlands Heart Institute, Utrecht, The Netherlands, Zuid-Holland, Netherlands*
3. *Department of Radiology, Leiden University Medical Center, Leiden, The Netherlands, Zuid-Holland, Netherlands*
4. *Department of Radiology, Leiden University Medical Center, Leiden, The Netherlands, Leiden, Zuid-Holland, Netherlands*

Background: Alterations in wall shear stress (WSS) within the aorta have been associated with vascular wall remodelling and is of interest in patients with aortopathy. Accurate measurement of WSS is essential and most studies use an aortic segmentation from one single systolic cardiac phase to assess WSS over the complete cardiac cycle. However, peak systolic time differs along the thoracic aorta for different aortic segments, thus calculations from a static single phase aorta segmentation could lead to an incorrect assessment of peak WSS. We evaluated the reproducibility of 4D flow WSS assessment with a semi-automatic time-resolved 3D vessel segmentation model over 5 systolic cardiac phases by a scan-rescan analysis.

Methods: Eight healthy volunteers (age 27.3±1.6 yrs) underwent an aortic 4D flow CMR scan and subsequently a rescan after a 10-minute break at a 3.0T scanner (Philips Healthcare; retrospective ECG and respiratory navigator gating; spatial resolution 2.5x2.5x2.5 mm^3, temporal resolution 34 ms, FOV 350x250x75 mm, VENC 200 cm/s, segmentation factor 2, SENSE 2.5 in anterior-posterior direction). From 3D phase contrast MR images, a 3D aorta segmentation was automatically performed using CAAS MR 4Dflow v1.0 software (Pie Medical Imaging) for 5 systolic cardiac phases after manually defining start and endpoint and automated centerline detection of the thoracic aorta. The 3D aortic segmentation was manually checked and adapted. Five aortic regions-of-interest were manually determined by placing six planes on anatomic landmarks along the aorta (Figure 1). Maximum WSS (WSSmax) and mean WSS (WSSmean) for different aortic regions over 5 systolic cardiac cycles were determined and a reproducibility analysis (Bland-Altman) was performed.

Results: Heart rate (HR) was similar for the scan (60.9±6.2 bpm) and rescan (62.7±6.9 bpm) in the volunteers (p=0.55). Phase 1 or 2 represented peak systolic flow in the ascending aorta and phase 3-4 peak systolic flow in the arch, proximal and distal descending aorta (Figure 1D and Figure 3). Scan-rescan data showed overall good reproducibility for WSSmean (≤12.5% variation compared with average values) with moderate to good intraclass correlation. The variability in the magnitude of WSSmax was high (ranging from 9.5%-28.5%), with moderate ICC (Figure 2, Figure 3).

Conclusions: Reproducibility of WSSmean in this scan-rescan study in healthy volunteers was good for all aortic regions along the cardiac cycle. However, the variability of WSSmax measures was high and out of clinically acceptable margins. Factors that potentially contribute to this lower WSSmax reproducibility: 1. Operator dependent factors: plane placement for determination of aortic segments; manual defined markers for automatic vessel segmentation 2. Patient factors: although averaged HR was similar, individual variations could have contributed. Assessment of the observer variability needs to be done to evaluate an observer-dependent contribution.

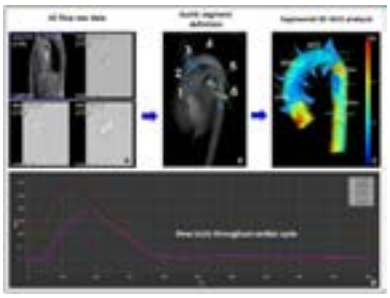

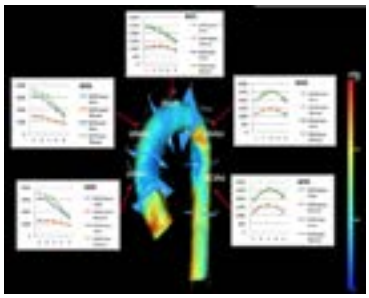

Table 1. Average time of the 5 systolic phases (ms) throughout the cardiac cycle.

P-value	Rescan	Scan	
0.906	103.4±19.0	104.1±19.2	**Phase 1 (ms)**
0.864	135.4±18.1	136.8±18.4	**Phase 2 (ms)**
0.847	167.5±17.6	169.0±17.5	**Phase 3 (ms**
0.834	199.9±17.2	201.5±17.6	**Phase 4 (ms)**
0.832	232.0±17.1	233.6±17.6	**Phase 5 (ms)**

Statistics: Paired sample-t-test.

P307

Histopathololgic validation of synthetic inversion recovery CMR in canine acute myocardial infarction.

Arlene Sirajuddin, MD[1] Sophia Hammer-Hansen, MD[2], Li-Yueh Hsu, DSc[3], Joni L. Taylor, BS[3], Shawn Kozlov, BS[3], Andrew E. Arai, MD[4]

1. *National Institutes of Health, Bethesda, MD*
2. *National Institutes of Health, Hovedstaden, Denmark*
3. *National Heart, Lung and Blood Institute, National Institutes of Health, Bethesda, MD*
4. *National Institues of Health, Bethesda, MD*

Background: Conventional segmented magnitude and phase sensitive inversion recovery gradient recalled echo (IR-GRE) late gadolinium enhancement images can evaluate myocardial infarction (MI) size and viability. However, these images are sensitive to patient motion, and magnitude inversion recovery methods depend on selecting the correct inversion time. If one accurately quantified post-contrast myocardial T1, these measurements could be used to generate synthetic magnitude and phase sensitive inversion recovery images that appear similar to the traditional IR-GRE images. The synthetic magnitude and phase sensitive inversion recovery images can be retrospectively created at any inversion time despite the limited number of inversion times sampled by MOLLI. The aim of this study was to validate how accurately the synthetic inversion recovery images measured the size of MI in a preclinical canine model.

Methods: This study was approved by the Animal Care and Use Committee at our institution. Coronary artery occlusion was maintained for 2 hours in 11 mongrel dogs, who then underwent 48 hours of reperfusion before being scanned on a 1.5T scanner. MOLLI images were taken at one slice location (5s(3s)3s protocol, field of view of 280 x 154mm^2, slice thickness of 6 mm, 192 x 80 matrix, parallel imaging factor of 2) pre-contrast and at approximately 15 minutes after contrast injection. Late gadolinium enhancement images were obtained between 10-15 minutes after contrast injection. MI was defined using a 50% threshold between enhanced and remote myocardium using research software for all MR images. The animals were euthanized after the MRI scan and the explanted hearts were stained with triphenyltetrazolium chloride (TTC) to determine the size of the myocardial infarction via manual planimetry on research software.

Results: For each of the 11 dogs, synthetic inversion recovery images from MOLLI and matched conventional IR-GRE images and TTC images at the same slice location were analyzed. An example of each image is shown in figure 1. Infarct size on synthetic magnitude inversion recovery images correlated well with the TTC images (r2=0.99, y=0.91x+0.01). The infarct size on synthetic phase sensitive inversion recovery images also correlated well with TTC (r2=0.99, y=0.94x+0.01). Infarct size on conventional IR-GRE images also correlated well with TTC.

Conclusions: Synthetic magnitude and phase sensitive inversion recovery images from MOLLI can accurately measure MI size. MOLLI also provides high quality T1 maps for tissue characterization (data not shown). This method has good image resolution, includes motion correction to minimize artifacts from respiratory motion, and does not require selection of an inversion time.

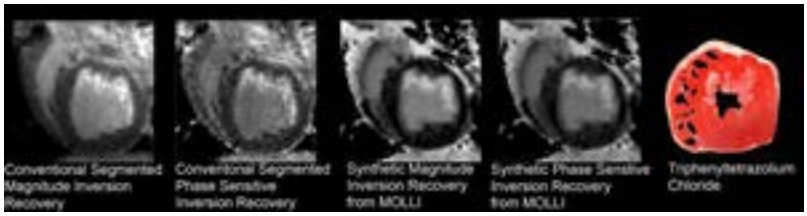

P308

Repeatability of Myocardial Tissue Phase Mapping in Mice

Nivedita K. Naresh, Ph.D.[1]Cynthia Yang, BS[2], Sol Misener, AAS, RVT[2], Bradley Allen, MD[2], Michael Markl, PhD[1], James Carr, MD[3], Daniele Procissi, Ph.D.[2]

1. *Northwestern University, Chicago, IL*
2. *Northwestern University, IL*
3. *Northwestern Memorial Hospital, Chicago, IL*

Background: Mouse models can help investigate the molecular mechanisms underlying complex cardiovascular diseases. Assessment of myocardial regional wall motion plays a very important role in the diagnosis and management of several cardiovascular diseases and can be linked to many underlying biological processes. Our purpose was to study the repeatability of myocardial tissue phase mapping (TPM) method and to quantify the variability in TPM-derived global and regional velocities.

Methods: 10 week old female C57Bl/6 mice (n=6) were imaged at 7T. Mice were maintained at 1.25% isoflurane and 36±1^{0}C during MRI. 2D cine black-blood phase-contrast MRI with prospective ECG and respiratory triggering of the mouse heart was performed at basal, mid-ventricular, and apical locations. Imaging parameters included: TE/TR =3.4/5.2 ms, FOV=30x30 mm^2, phase resolution=50%, image resolution =117x117 µm^2, flip angle=15^0, slice thickness=1 mm, averages=3, in-plane VENC= 4 cm/s and through-plane VENC= 4cm/s. A segmented acquisition (1 line per heartbeat) was used and the velocity–encoded scans were acquired in consecutive heartbeats to perform imaging at a high temporal resolution. The scan time was 7-8 min per slice depending on the ECG and respiratory rates. All mice were scanned on two separate days to test for reproducibility of the TPM method. For all mice, radial and longitudinal mean velocity-time curves were measured at base, mid, and apex. Global peak and time-to-peak (TTP) radial and longitudinal velocities were also quantified for all mice. For regional analysis, all velocity data were mapped on the standard American Heart Association 16 segment LV model. Regional peak radial and longitudinal velocities were calculated by averaging over all LV segments in the basal, mid-ventricular and apical slices.

Results: Example magnitude and phase difference images obtained in a mouse using the TPM method are shown in Figure (A-B, E-F). Also shown are mean radial and longitudinal velocity-time curves obtained from a mid-ventricular slice (Figure, C and G) showing good agreement between the two scans. Bland-Altman plots shows the repeatability of peak radial (D) and longitudinal velocities (H). Table 1 compares the global and regional systolic and diastolic peak radial and longitudinal velocities for the basal, mid-ventricular and apical slice locations obtained from the two scans. No significant differences were observed between the two scans globally and for all slice locations.

Conclusions: In conclusion, myocardial TPM can be performed with good repeatability in mice to reliably quantify both global and regional myocardial velocities.

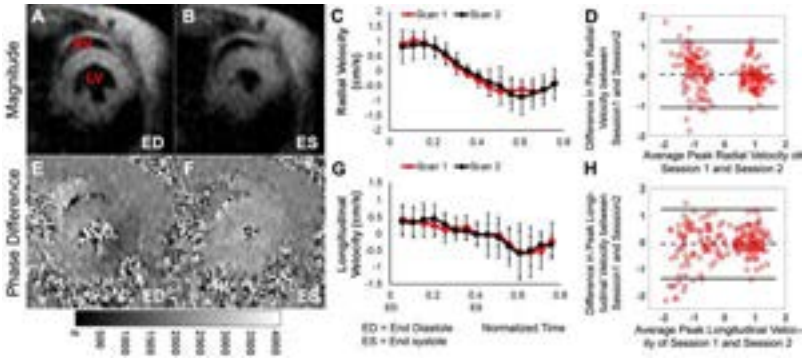

Scan-rescan of Systolic and Diastolic Peak Radial and Long-axis Velocities for Scan1 and Scan2

Peak long-axis vel. (cm/s)		Peak radial vel. (cm/s)		
Diastole	Systole	Diastole	Systole	
				Global
-0.97 ± 0.52	0.88 ± 0.23	-0.92 ± 0.21	0.94 ± 0.12	Scan 1
-0.85 ± 0.34	0.87 ± 0.26	-1.04 ± 0.33	0.96 ± 0.27	Scan 2
0.70	0.96	0.56	0.89	p value
				Base
-1.50 ± 0.49	1.12 ± 0.24	-0.77 ± 0.14	0.77 ± 0.18	Scan 1
-1.17 ± 0.43	1.02 ± 0.21	-0.87 ± 0.25	0.87 ± 0.23	Scan 2
0.38	0.44	0.46	0.40	p value
				Mid
-0.92 ± 0.75	0.68 ± 0.31	-1.06 ± 0.26	1.09 ± 0.14	Scan 1
-0.92 ± 0.43	0.79 ± 0.38	-1.22 ± 0.42	1.06 ± 0.30	Scan 2
0.99	0.50	0.56	0.79	p value
				Apex
-0.26 ± 0.33	0.80 ± 0.24	-0.93 ± 0.31	0.99 ± 0.22	Scan 1
-0.25 ± 0.21	0.76 ± 0.42	-1.04 ± 0.40	0.95 ± 0.33	Scan 2
0.99	0.88	0.72	0.85	p value

P309

Feasibility Study of Free-breathing in vivo Cardiac Quantitative Susceptibility Mapping

Yan Wen[1] Thanh D. Nguyen, PhD[2], Pascal Spincemaille, PhD[3], Jiwon Kim, MD[2], Jonathan W. Weinsaft, MD[2], Yi Wang, PhD[4]

1. *Cornell University, New York, NY*
2. *Weill Cornell Medical Center, NY*
3. *Weill Cornell Medicine, New York, NY*
4. *Weill Cornell Medical College, NY*

Background: Mixed-venous oxygen saturation (SvO2) is an important measure of cardiopulmonary function that is widely used to manage critically ill patients. Quantitative Susceptibility Mapping (QSM) can be used to non-invasively quantify SvO2. The feasibility of *in vivo* Cardiac QSM has recently been demonstrated using a conventional ECG-gated 2D GRE sequence which acquires one slice per breath-hold (1). Although this approach can provide high quality QSM in cooperative subjects, it has relatively low SNR and is highly susceptible to slice misregistration in subjects with inconsistent breath-holding. To address these challenges, we studied the feasibility of free-breathing 3D sequence in healthy volunteers.

Methods: We developed an ECG-triggered navigator gated multi-echo 3D GRE sequence for cardiac QSM on a 1.5T scanner (GE Healthcare). A pencil beam navigator echo was used to detect the respiratory motion of the right diaphragm, and a 3-bin PAWS gating algorithm (2) was used to control the data acquisition in real time. The typical scan parameters were: 5 echoes, first TE≈2.8ms, DTE≈3.5ms, TR≈23ms, voxel size≈1.25x1.25x5mm^3, 8 views per heartbeat, 16 slices. A graph cut based phase unwrapping and fat-water separation method (3) combined with a chemical shift update method (4) was used to compute the susceptibility field. A Total Field Inversion method (5) was used to obtain the final susceptibility map.

Results: The average susceptibility difference between right ventricular and left ventricular blood pool on two volunteers were measured to be 251 ppb, which translates to an 80.8% SvO2. Figure 1 shows the T2* weighted magnitude image and the QSM from one volunteer, demonstrating high quality source images with minimal motion artifacts and the expected high contrast between RV and LV in QSM. The average SNR of the eight cases reported in the previous 2D breath-hold study (1) was 26.7±5.7, and the average SNR of the two cases from this study was 38.5±.8.

Conclusions: The proposed navigator 3D approach improves SNR and eliminates the need for breath-hold, significantly enhancing clinical applicability of cardiac QSM. Future work will focus on incorporating parallel imaging for acceleration, and investigating utility in patients.

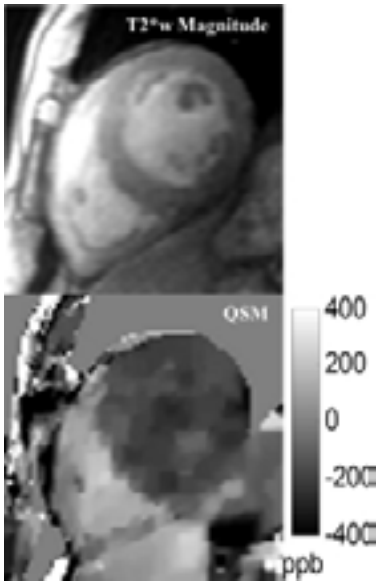

P310

Accurate and reliable 2D and 4D flow measurements in pulmonary branch pulsatile phantom

Ana Beatriz Solana, Dr.[1], Martin A Janich, Ph.D.[4], Anja CS Brau, Ph.D.[5], Christian Meierhofer, Dr. Dr.[6]Fatih Hafalir[2], Peng Lai, Ph.D.[3]

1. *GE Global Research, Garching B München, Bayern, Germany*
2. *Technical University Munich, Bayern, Germany*
3. *GE Healthcare, CA*
4. *GE Global Research, N/A, Germany*
5. *GE healthcare, CA*
6. *Pediatric Cardiology and Congenital Heart Disease, German Heart Center Munich, Munich, Bayern, Germany*

Background: 4D Flow is an emerging technique which provides rich information about flow hemodynamics. It has great potential to replace 2D phase contrast (PC). However, the accuracy and reproducibility in 4DFlow need to be thoroughly validated for multiple flow conditions [1]. Previously, we obtained reliable and accurate results using a phantom with 2 parallel tubes [2]. Here, we used a Y-shaped pulsatile flow phantom that simulates pulmonary branching. This configuration allows internal flow quantification accuracy validation for tubes at different velocities and flow volumes.

Methods: Acquisition: We used a closed-circuit pulsatile flow phantom; composed by an industrial membrane flow pump, an agar box containing three silicone tubes in Y-shaped (Figure 1, middle, branch left and branch right tubes) and a Coriolis flow meter (PROMASS 80F, Endress+Häuser), to measure a ground-truth net flow value with a precision of about ±1ml/s. The agar box was placed in the scanner in a double-oblique position. The gating signal was obtained by attaching the MR scanner pulsioxymeter to the inflow tube.
Flow phantom scans were performed on a GE 3T MR750w MR scanner (Waukesha, WI). Retrospectively gated PC; "breathhold" and "free-breathing" (3 averages) 2D through-plane FastCINE and kat ARC 4D Flow [3] were scanned at two different pump rates (Figure 2).
Analysis: PC net flow measurements were evaluated using CVI42 software (Calgary, Canada) for 2D and Arterys (San Francisco, CA) for 4DFlow. For both, background phase correction (BPC) using static phantom correction and image-based correction was applied. The Bland-Altman plot was used to compare the obtained net flow from the middle tube as measured by MR to the ground-truth value measured by the flow meter (*percentage difference middle tube = 100 x* $((flow_{MiddleTube}-flow_{meter})/flow_{meter})$) and to compare the net flow from the middle tube to the sum of the right and left branch tubes (*percentage difference branch tubes = 100 x* $((flow_{MiddleTube}-(flow_{rightTube}+flow_{leftTube})/flow_{middleTube})$), as measures of accuracy.

Results: Figure 3 shows that the errors for all measurements were below 6%, theoretical threshold of acceptability [4], apart from one outlier in the right tube for 4DFlow for pump rate 60 (peak velocity was 50 cm/s). We hypothesized that the low velocity to noise ratio (VNR) may cause the wrong flow measurement. Background phase error for all 2D data was less than 1ml/beat while we observed more than 10ml/beat in some 4Dflow calculations which was compensate by BPC.

Conclusions: Reliable and accurate results have been shown for 2D PC and 4DFlow using a pulmonary artery branch pulsatile flow phantom. Quantitative net flow in low velocity vessels may be affected by low VNR in single-VENC 4DFlow compromising accuracy. This issue may be solved by the use of dual-VENC approach.

References:[1] Dyverfeldt, JCMR 2015, [2] Solana, EuroSCMR 2016, [3] Lai, ISMRM 2015, [4] Gatehouse, JCMR 2010.

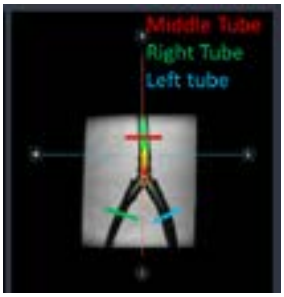

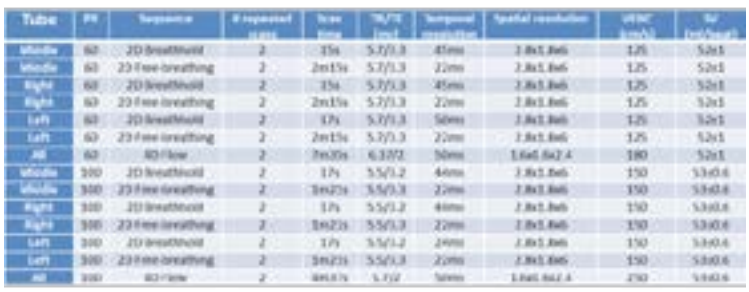

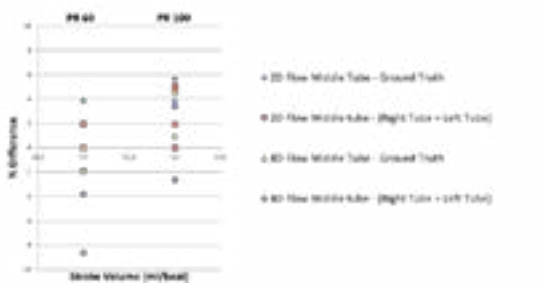

P311

Visualization of coronary arteries in patients with congenital heart disease using whole-heart image navigated coronary MR angiography

Mari N. Velasco Forte, MD [1]Kuberan Pushparajah, MD [2], Srinivas Ananth Narayan, MD, MRCPCH[3], Sujeev Mathur, MD[4], Israel Valverde, MD[5], Aaron Bell, MB.ChB[6], Hannah Bellsham-Revell, MD[4], Markus Henningsson, PhD[3]

1. *King's College London, London, England, United Kingdom*
2. *Guy's & St Thomas' Hospital NHS Foundation Trust, Evelina London Children's Hospital, England, United Kingdom*
3. *King's College London, England, United Kingdom*
4. *Guy's & St Thomas' Hospital NHS Foundation Trust, England, United Kingdom*
5. *King's College London, Andalucia, Spain*
6. *Guy's & St Thomas' Hospital NHS Foundation Trust, London, England, United Kingdom*

Background: Whole-heart MR angiography (CMRA) is commonly used in patients with congenital heart disease (CHD) to assess cardiac morphology and structural disease. However, respiratory motion remains an impediment in a substantial amount of patients undergoing CMR. Studies in healthy subjects and cardiac patients have shown that image-based navigation (iNAV) improves respiratory motion compensation compared to the conventional method. Here, we investigated the use of iNAV with advanced respiratory gating in patients with CHD

Methods: The iNAV allowed for direct tracking of the respiratory heart motion and was generated using the bSSFP startup echoes. Gating was achieved using the diminishing variance gating (DVG) algorithm with a 50% gating efficiency. Whole-heart CMRA was acquired with 1.3mm isotropic resolution and a SENSE=2. For comparison, CMRA with identical imaging parameters were acquired using the conventional diaphragmatic navigator with a window of 3 - 5 mm and 0.6 tracking factor. Use of contrast agent (Dotarem® or Gadovist®) before whole-heart imaging acquisition and need for general anaesthesia (GA) was recorded. Scan time, visualization of coronary artery origins and distal course and imaging quality was compared between the two sequences. Image quality was scored 1-5 for each dataset

Results: A total of 27 patients (19 males, 8 females; median weight: 49 kg; range:6.5–70; mean age:13, range:5 months–18 years) were recruited. Diagnosis are summarised in table 1 and representative images from 4 patients are shown in Figure 1. 66% scans were performed in awake patients and 33% under GA. A contrast agent was used in 51%. Scan time was significantly shorter using iNAV (mean:6:59 ±1:23) compared to conventional (9:17±2:34) ($p < 0.05$). Difference in visual score, using Wilcoxon sign-rank, was improved using iNAV and the difference was statistically significant ($p < 0.001$). The coronary arteries origin was depicted in all patients using iNav and 96% using conventional techniques. Distal course of all coronary arteries was more often visualized when using iNav compared to respiratory acquisition (85% vs 57%). In 3.5% none of the coronary arteries could be visualized distally using respiratory navigation and in 35% they were depicted only partially

Conclusions: iNav allows for a higher success-rate and clearer depiction of the distal course of the coronary arteries in patients with CHD. Its acquisition time is shorter and image quality score was found to be equal or superior to the conventional method in all cases

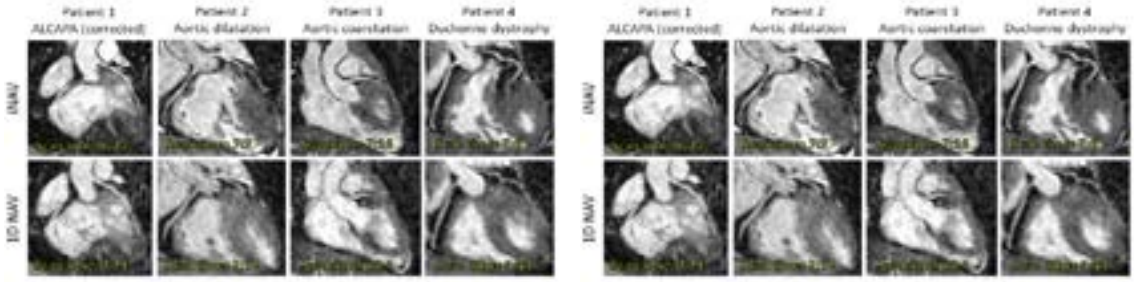

Diagnosis in patients recruited in the study

%	N	**Main diagnosis**
18	5	**Structurally normal hearts (arrhythmia/cardiomyopathy screening)**
22 (7)	6 (2 dextrocardia)	**AV valve disease**
14	4	**TGA**
25	7	**Aortic valve and arch abnormalities**
7	2	**ALCAPA**
11	3	**Tetralogy of Fallot**

P312

How to obtain accurate MOLLI measurements by means of advanced MR simulations (SQUAREMR)

Christos Xanthis, PhD[1] Sebastian Bidhult, MSc[2], Frederik Testud, Dr. rer. nat.[3], Andreas Greiser, Ph.D[4], Kelvin Chow, PhD[5], Bruce Spottiswoode, PhD[6], Richard Thompson, PhD[7], Henrik Engblom, MD, PhD[1], Håkan Arheden, MD, PhD[8], Anthony H. Aletras, PhD[9]

1. *Lund University, Skane Lan, Sweden*
2. *Lund University, Department of Clinical Sciences Lund, Clinical Physiology, Skane University Hospital, Lund, Sweden; Faculty of Engineering, Lund University, Department of Biomedical Engineering, Lund, Sweden, Skane Lan, Sweden*
3. *Siemens Healthcare AB, Skane Lan, Sweden*
4. *Siemens Healthcare GmbH, Erlangen, Germany, Erlangen, Bayern, Germany*
5. *Siemens Medical Solutions, Chicago, IL*
6. *Siemens Medical Solutions USA, Inc., Knoxville, TN*
7. *Department of Biomedical Engineering, University of Alberta, AB, Canada*
8. *Lund University, Department of Clinical Sciences Lund, Clinical Physiology, Skane University Hospital, Lund, Sweden, Lund, Skane Lan, Sweden*
9. *Aristotle University of Thessaloniki/Lund University, Thessaloniki, Thessaloniki, Greece*

Background: Recently, SQUAREMR, a method for improving measurements from clinical pulse sequences in CMR, was presented [1]. SQUAREMR is based on massively parallel realistic simulations of pulse sequences on tissue models of T1 and T2 values and has already demonstrated improvement in the T1 estimates obtained with clinical MOLLI protocols. However, the clinical pulse sequence MOLLI has been designed so as to reduce the T2-sensitivity of the T1 estimates. This may limit the performance of SQUAREMR, which searches through a {T1, T2} parameter space. The aim of this study was to obtain accurate MOLLI T1 maps by means of advanced MR simulations. We hypothesized that this could be accomplished via SQUAREMR by increasing the T2-sensitivity of MOLLI.

Methods: A clinical 5sec(3sec)3sec MOLLI protocol [2] was modified so as to increase its T2-sensitivity. In the modified MOLLI, the inversion pulse was modified from a 2.56msec tangent/hyperbolic tangent adiabatic pulse to a 10.24msec hyperbolic secant adiabatic pulse and the excitation flip angle of the 480μsec sinc-shaped RF pulse of the bSSFP-readout was increased from 35° to 70°. Six phantoms were used with T1s and T2s of four pre-contrast tissue types (normal myocardium, blood, infarcted myocardium and edematous myocardium) and two post-contrast tissue types (normal myocardium at 2-3min and 13-15min after contrast administration). T1 and T2 reference values were measured with Saturation Recovery (Tsat=0.01-15sec) and T2rep-bSSFP (T2-prep =0-0.5sec), respectively (TR>10msec). Data with both clinical and modified-MOLLI sequences were acquired. For the two post-Gd tissue types phantoms, the 4sec(1sec)3sec(1sec)2sec MOLLI acquisition scheme was used [2]. Six healthy volunteers (5 men, 1 woman, age 26±4 years) were also studied. The MOLLI T1 values obtained in healthy volunteers were compared against SASHA T1-mapping values [3]. All experiments were performed on a Magnetom Aera 1.5T scanner (Siemens Healthcare, Erlangen, Germany).

Results: Figure 1 demonstrates the increased T1 accuracy in phantom studies of the modified-MOLLI protocol using SQUAREMR against the clinical MOLLI protocol. Figure 2 shows the mean T1 values of a short-axis, mid-ventricular septal ROI for clinical MOLLI, SASHA and modified-MOLLI with SQUAREMR for the healthy volunteers. The latter yielded T1 values closer to SASHA (difference about 2.5%) compared to the clinical MOLLI (about 12.7%).

Conclusions: In this study, an accurate MOLLI T1-mapping technique was presented through the utilization of SQUAREMR. This work suggests that the accuracy and design of future quantitative MR methods may benefit from incorporating advanced simulations that take into account pulse sequence imperfections.

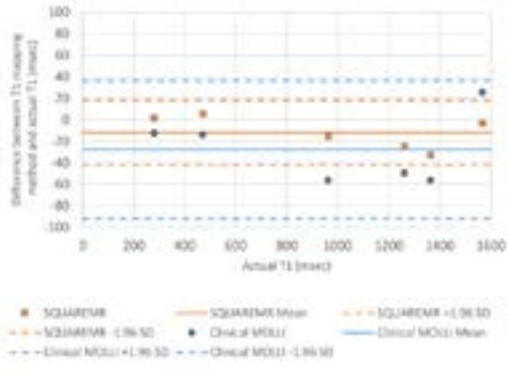

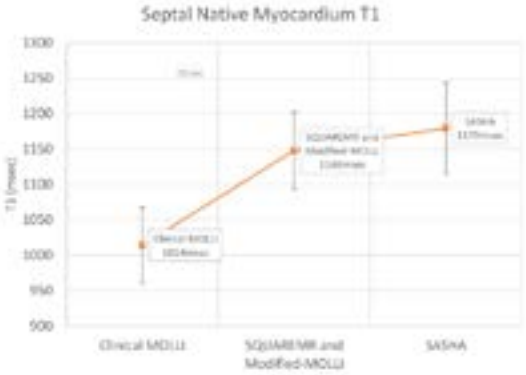

P313

Chemotherapy effect on the myocardial interstitium: CMR T1 mapping in a preclinical model

Chia-Ying Liu, Ph.D[1]Cynthia Davies-Venn, PhD[1], Comfort Elumogo, BS[2], Victoria Hoffmann, VMD[1], Kelly Rice, VMD[1], Veit Sandfort, MD[1], Stefan L. Zimmerman, MD[3], David Bluemke, MD, Ph.D[1]

1. *National Institute of Health, MD*
2. *National Institute of Health, OH*
3. *Johns Hopkins University School of Medicine, MD*

Background: Myocardial infarction is associated with LV remodeling and alterations of the extracellular matrix even in regions remote from the myocardial infarction territory. Chemotherapy is associated with acute (hypotension, arrhythmias) and chronic (congestive heart failure) cardiotoxic effects. The purpose of current study is to compare changes in the myocardial interstitium induced in the remote myocardium by both myocardial infarction and chemotherapy with cardiac MRI.

Methods: Adult male mongrel dogs (weighted 26-30 kg) were used in the chronic myocardial infarction (MI) model and chemotherapy (ChT) model. Induction of MI was performed by vascular clamp occlusion of the left anterior descending (LAD) artery for 90 minutes followed by reperfusion. CMR were performed 6-8 weeks after the surgical procedure. In the chemotherapy model, once weekly infusions of 7.5-15mg of doxorubicin via intracoronary was infused for four weeks. CMR was performed 8-12 weeks after the first infusion. Dogs were anesthetized, intubated and ventilated in preparation for imaging studies. Cardiac function, late gadolinium enhancement (LGE), and T1 mapping were acquired with a 3T scanner. Mean myocardial segmental ECV values were calculated using pre- and post-contrast T1 imaging and hematocrit obtained at the time of CMR. Segmental native T1 values were also recorded. Only segments that were completely free from LGE (defined as remote segments) were included in the analysis. Mann-Whitney test was used to compare remote myocardial ECV and native T1 between groups.

Results: There were three control dogs. Ten MI (LGE>5%) and six ChT dogs were included in the final analysis. In the territory of the subendocardial infarction as well as the intracoronary doxorubicin infusion, areas of LGE were clearly identified. Figure 1 demonstrates representative LGE images and ECV maps from each group. ChT dogs had significantly higher LV volumes and LGE than the other two groups (Fig 2). In the remote myocardial segments, ECV in the ChT group was elevated by 23% compared to the MI group (remote MI ECV 26.7 ± 3.7; ChT ECV 32.9 ± 6.3%, p<0.001). Native T1 was also higher in the ChT dogs than the other two groups. (Fig3).

Conclusions: Doxorubicin-induced cardiomyopathy by intracoronary chemotherapy infusion in myocardium remote from the infusion territory results in expansion of the extracellular volume in the subacute setting (8-12 weeks). These changes were more prominent than corresponding changes related to subendocardial myocardial infarction. Masson's Trichrome and Hematoxylin and Eosin (H&E) stained slides have been collected for further pathological evaluations.

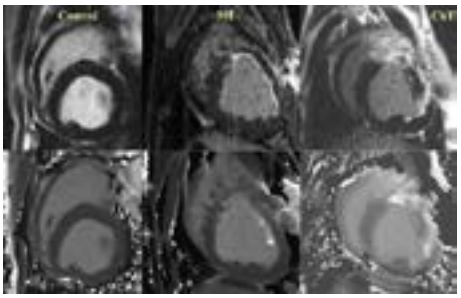

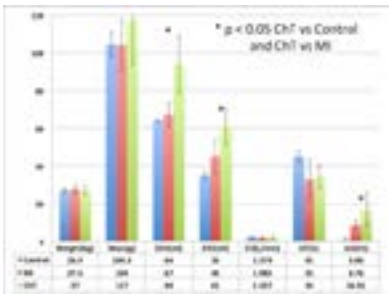

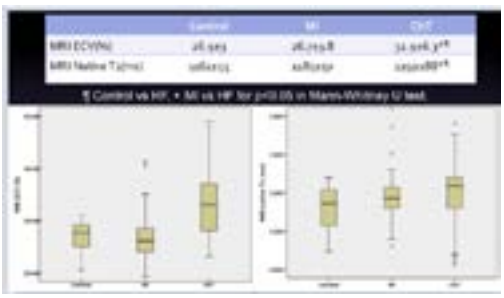

P314

Assessment of Myocardial Contractility Using Strain Imaging

Tazim Merchant[1] Nathaniel Reichek, MD[2]

1. Northwestern University, Roslyn, NY
2. St. Francis Hospital-The Heart Center, Roslyn, NY 11576, Fort Salonga, NY

Background: Reduced systolic strain(ST) can be caused by afterload(A) excess, reduced contractility(C), inadequate preload or combinations of the three. But physiologic determinants of myocardial strain(St) abnormalities are often ignored and optimal analytic methods are lacking. We developed a nongeometric left ventricular(LV) end-systolic afterload index(PV/M, P= pressure, V= volume, M= LV mass) more effective than wall stress(WS) indices and showed that ratios of ST/A and ST rate(StR)/A depict C differences. We found that A excess causes 80% of ST reduction in dilated cardiomyopathy but A remains normal in aortic stenosis with LVH, while C is reduced. We now seek to determine the optimal method for evaluation of C .

Methods: Global circumferential and longitudinal ST (CST, LST) and mean STRs were determined using feature tracking(FT), DENSE and tagged imaging in 8 normals (7 male, mean age 47.9 ± 6.6 yrs) at rest and during low dose DOB infusion (1.25-2.4 mcg/kg/min), titrated to avoid altered HR and BP. Pre and post contrast T1 mapping for ECV were also obtained. Rest and DOB FT and DENSE CST, LST, ST rates, CWS,meridional (M)WS and PV/M ((cuff systolic BP)*(end-systolic volume at rest)/(LV mass)) were determined.

Results: (See Tables 1 & 2) Gradient echo cine SPAMM image quality during DOB was inadequate for analysis. There were no significant changes in HR, BP or A indices during DOB thus the data were not normalized for afterload differences. DENSE LST and all ST rates increased significantly but FT CST, LST and DENSE CST did not. All S/A ratios increased significantly with DOB except FTCST/(PV/M). Finally, strong inverse correlations between ECV and FT LST, LST/A as well as DENSE CST and LST indices and ratios were found during DOB (r=0.68-0.88),

Conclusions: Of the 3 strain evaluation methods tested, DENSE data were the most sensitive to changes in C while gradient echo SPAMM tagging was unable to reliably capture quantifiable data when strain rate increased. Of the strain based parameters evaluated, global longitudinal strain and strain rate were the most consistent in demonstrating the positive inotropic effect of low dose dobutamine. Of the contractility indices evaluated the ratios of strain rate to afterload indices were the most consistent indices of increased contractility. The inverse relationships found between ECV and dobutamine response in these clinically normal individuals suggests that the interstitium plays an important role as a determinant of myocyte deformation.

Feature Tracking Strains, Strain Rates, Afterload and Contractility Indices

p value	%change	Mean DOB ± SD	Mean Rest ± SD	Variable
ns	-10.8%	225.4 ± 129.8	252.6 ± 107.6	CWS
ns	-16.8%	86.4 ± 59.2	103.76 ± 48.8	MWS
ns	-13.3%	76.9 ± 15.3	88.66 ± 19.0	SA PV/M
ns	-12,3%	78.6 ± 25.7	89.6 ± 20.3	LA PV/M
ns	=1.9%	-16.0 ± 2.4	-15.7 ± 2.2	C Str
ns	+7.0%	-15.2 ± 1.0	-14.2 ± 1.4	L Str
0.015	**+23.8%**	**-0.52 ± 0.1**	**-0.45 ± 0.1**	**C Str R x10^{-1}**
0.014	**+21.2%**	**-0.497 ± 0.1**	**-0.41 ± 0.1**	**L Str R x10^{-1}**
ns	+23.9%	-0.88 ± 0.4	-0.71 ± 0.27	C Str/CWS x10^{-1}
0.018	**+50.0%**	**-0.24 ± 0.1**	**-0.16 ± 0.1**	**L Str/MWS**
0.03	**+50.0%**	**-0.30 ± 0.2**	**-0.20 ± 7.3**	**C Str R/CWS x10^{-3}**
0.017	**+82.6%**	**-0.84 ± 0.5**	**-0.46 ± 0.2**	**L Str R/MWS x10^{-2}**
ns	+15.8%	-0.22 ± 0.1	-0.19 ± 0.1	C Str/PV/M
0.03	+23.5%	-0.21 ± 0.05	**-0.17 ± 0.05**	**Global L Str/PV/M**
0.01	+35.8%	-0.72± 0.3	-0.53 ± 0.2	C Str R/PV/M x10^{-3}
<0.02	+36.4%	3.97 ± 1.4	2.91 ± 0.95	L Str R/PV/M x10^{-5}

DENSE Strain, Strain Rates, and S/A Ratios

p value	%change	Mean DOB ± SD	Mean Rest ± SD	Variable
ns	-10.9%	223.9 ± 121.4	251.3 ± 103.6	CWS
ns	-14.7%	88.4 ± 57.6	103.6 ± 49.9	MWS
ns	-5.9%	83.0 ± 31.5	88.2 ± 17.3	SA PV/M
ns	-6.5%	83.31 ± 34.1	89.1 ± 19.5	LA PV/M
ns	+5.4%	-15.5 ± 2.6	-14.7 ± 1.8	C Str
0.02	**+32%**	**-10.3 ± 1.3**	**-7.8 ± 2.3**	**L Str**
0.01	**+20.8%**	**-0.506 ± 0.068**	**-0.419 ± 0.059X10^{-1}**	**C Str Rate**
0.013	**+54.5%**	**-0.340 ± 0.0584**	**-0.222 ± 0.0069 X10^{-1}**	**L Str Rate**
p<0.01	+27.3%	-0.822 ± 0.0315	**-0.646 ± 0.0195 X10^{-1}**	**C Str/CWS**
0.02	+81.4%	-0.1571 ± 0.0792	-0.0866 ± 0.0435 X10^{-1}	L Str/MWS
p<0.01	+43.2%	-0.279 ± 0.133	-0.183 ± 0.06 X10^{-3}	C Str Rate/CWS
0.017	+122%	-0.546 ± 0.332	-0.246 ± 0.124 X10^{-3}	L Str R/MWS
0.035	+16.7%	-0.2005 ± 0.0552	-0.1718 ± 0.0413	C Str/PV/M
0.025	+48.9%	-1.376 ± 0.0416	-0.924 ± 0.0380 X10^{-1}	L Str/PV/M
p<0.01	+39.8%	-0.668 ± 0.225	-0.492 ± 0.132 X10^{-3}	C Str Rate/PV/M
0.015	+74.5%	-0.4625 ± 0.169	-0.265 ± 0.115 X10^{-3}	L Str Rate/PV/M

P315

The Reproducibility of T1 and T2 Measurements Varies in Different Sites of the Heart and Correlates with Wall Thickness

Hang Zhao, MD[1], Yuchi Han, MD[2]Jing Wang, MD[1]

1. *University of Pennsylvania, PA*
2. *University of Pennsylvania, Philadelphia, PA*

Background: T1 and T2 relaxing time are important parameters for evaluating tissue properties. However, whether the measurements of these two indexes at different sites of the heart have different reproducibility has not been studied. We aim to explore the inter-observer variability of T1 and T2 measured at different sites of the heart, and study the relationship with wall thickness.

Methods: We retrospectively studied 10 patients (5 with severe aortic stenosis, 5 with pulmonary hypertension) performed in our institution from July - Oct 2015 on the same scanner (1.5 T Avanto, Siemens, Germany). T1 scans were performed using the standard (5/3/3) MOLLI method during late diastole and T2 scans were performed with 3 point fit T2-prepared SSFP sequence during end-systole. The relaxing times were measured at 6 sites of the heart including the mid septum, the left ventricular (LV) anterior wall, the upper and lower right ventricular (RV) insertion, the RV free wall, and the blood pool. Two different readers blind to each other's results performed the measurements. Intraclass correlation coefficients (ICC) were calculated in a two-way mixed model with 95% confidence intervals (CIs). We also assessed the thickness of the sites where T1 and T2 were measured.

Results: CMR measurement for T1 and T2 yield good inter-observer reproducibility (ICC 0.993(CI: 0.987-0.996), ICC 0.997 (CI: 0.995-0.998), respectively). The average thicknesses of the ventricular walls were higher on T2 images due to the acquisition timing difference. There is a corresponding difference in T1 and T2 reproducibility at different sites of the heart. The ICC of the RV free wall was lower compared with the left heart and the septum (T1 ICC 0.80 (CI:0.12-0.96); T2 ICC 0.851 (CI 0.340-0.966), respectively). For the LV, the measurements of the septum, LV anterior wall, and the upper RV insertion (T1 ICC 0.95 (CI:0.79-0.99), ICC 0.89 (CI:0.50-0.96), ICC 0.96 (CI: 0.79-0.99); T2 ICC 0.96 (CI 0.82-0.99), ICC 0.97 (CI:0.85-0.99), ICC 0.975 (CI:0.89-0.994) respectively) had better reproducibility than the lower RV insertion (T1 ICC 0.86 (CI:0.396-0.97); T2 ICC 0.90 (CI 0.56-0.98), respectively). Pearson correlation analyses reveal that the ICC improves as the wall thickness increases (r-=0.701, p=0.011).

Conclusions: The reproducibility of T1 and T2 measurements differs with the site of measurement. The measurement of T2 has better reproducibility than T1 likely due to increased thickness of the ventricular wall as T2 images were acquired at end-systole.

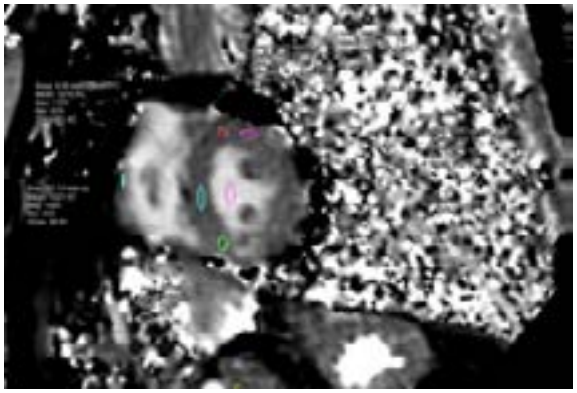

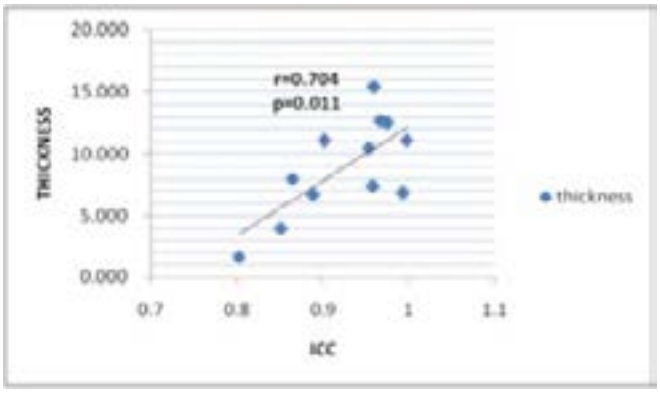

P316

SMART1Map in Non-ischaemic Cardiomyopathy: Initial Single-Centre Experience

Rominder S. Grover, MBBS (Hons) FRACP[1]Shaw Hua (Anthony) Kueh, MBChB, FRACP[2], Jeanette Soon, MBBS (Hons) FRANZCR[3], Chesnal Dey Arepalli, MD[2], Chaitu Cheruvu, MBBS FRACP[4], Christopher Naoum, MBBS PhD[5], Nada Sulaiman, M.D.[6], John Mooney, MBBS[1], Cameron Hague, MD[2], Jen Ellis, MD[1], Philipp Blanke, MD[7], Stephanie Sellers[8], Jonathon Leipsic, MD[1], Darra T. Murphy, MD[1]

1. *St Paul's Hospital, BC, Canada*
2. *St Paul's Hospital, Vancouver, BC, Canada*
3. *St Paul's Hospital, Vancouver, ON, Canada*
4. *St Paul's Hospital, Botany, New South Wales, Australia*
5. *Concord Hospital, The University of Sydney, Sydney, Concord, Sydney, New South Wales, Australia*
6. *St.. Paul's Hospital, Al Madinah, Saudi Arabia*
7. *St. Paul's Hospital & University of British Columbia, Vancouver, BC, Canada*
8. *University of British Columbia, BC, Canada*

Background: Cardiac MRI with T1 mapping has been shown to be useful in the detection of diffuse myocardial pathological processes such as non-ischaemic cardiomyopathy (NICM). SMART1Map (Saturation Method using Adaptive Recovery Times for cardiac T1 Mapping) is a novel technique that allows direct measurement of true T1 relaxation (Slavin and Stainsby 2013). We provide our first real-world single-centre experience in evaluating whether SMART1Map is able to detect a significant difference in T1 value between structurally normal and abnormal myocardium.

Methods: 64 consecutive patients undergoing evaluation for NICM with adequate image quality were consented to undergo additional SMART1Map evaluation. Patients were separated into 2 categories according to their MRI findings: those with no cardiac abnormalities including no derangement in ventricular volumes or systolic function (normal n = 21) and those with abnormal cardiac findings defined as deranged ventricular volumes and/or systolic function, with or without abnormal Late Gadolinium Enhancement (LGE) (abnormal n = 43). Nineteen healthy volunteers served as control. SMART1Map was performed using a series of single-point saturation-recovery methods to generate a T1Map, which consists of a saturation pulse, a delay time during which free T1 relaxation occurs and balanced SSFP readout. SMART1Maps were performed using a GE 1.5 Tesla Signa Twin-Speed magnet. Native T1 measurements were obtained by drawing a circumferential region of interest (ROI) to encompass the maximum volume of myocardium possible. Parametric variables were compared using one-way analysis of variance (ANOVA). Non-parametric variables were compared using Mann-Whitney U for 2 group comparison and Kruskal-Wallis test for multiple group comparison. A p-value of < 0.05 was considered statistically significant.

Results: Baseline characteristics between the study cohorts are as shown in table 1. The medians and interquartile ranges (IQR) derived from the measured mean native T1 values (ms) were as follows: control 1217.7 (1167.2 –1303.6); normal 1171.1 (1141.0 – 1210.6); and abnormal 1243.7000 (1184.9 – 1291.7) ($p = 0.04$). The T1 values were significantly higher in the abnormal group when compared to the normal group ($p = 0.01$) but not when compared to the control group ($p = 0.73$).

Conclusions: Using SMART1Map, the native T1 value was significantly higher amongst patients referred for evaluation of NICM with abnormal as compared to normal myocardial findings.

http://www.ConferenceAbstracts.com/uploads/cfp2/attachments/LDFAIBDN/LDFAIBDN--222595-1-ANY.pdf

Table 1. Baseline Characteristics: The mean and standard deviation (SD) of each variable was compared between the 3 groups using one-way analysis of variance (ANOVA). * denotes $\chi 2$ test for categorical variables

P-value	Abnormal (n = 43)	Normal (n = 21)	Control (n = 19)	
<0.01	53.9±17.9	51.5±16.1	36.9±10.7	Age, mean ± SD
0.12*	28 (65)	8 (38)	11 (58)	Male, n(%)
<0.01	23.9±2.9	26.8±4.6	24.3±8.7	Body mass index (kg/m^2), mean ± SD
0.07	55±13	57±10	59±6	LVEF (%), mean ± SD
<0.01	97.5±36.4	82.1±23.7	73.3±13.9	LVEDVI (ml/m^2), mean ± SD
<0.01	50.0±27.2	35.5±15.0	29.2±6.9	LVESVI (ml/m^2), mean ± SD
0.03	54±9	50±8	58±6	RVEF (%), mean ± SD
0.57	82.7±28.4	81.2±28.1	75.1±14.2	RVEDVI (ml/m^2), mean ± SD
0.15	38.1±14.1	40.0±15.9	32.0±8.0	RVESVI (ml/m^2), mean ± SD

P317

Improved Black Blood Imaging of the Heart using Radial Balanced Steady-State Free Precession

Robert R. Edelman, MD[1]Marcos Botelho, MD[2], Amit Pursnani, MD[3], Shivraman Giri, PhD[4], Ioannis Koktzoglou, PhD[2]

1. NorthShore University HealthSystem, Evanston, IL
2. NorthShore University HealthSystem, IL
3. 8475702000, IL
4. Siemens Healthcare, IL

Background: Breath-hold, dual-inversion Cartesian fast spin-echo (FSE) is the standard-of-care (SOC) technique for black blood cardiac imaging at most institutions. However, this technique has the drawbacks of being relatively inefficient and motion-sensitive. Our aim was to develop a faster, more flexible approach that would be less motion-sensitive and provide improved image quality. For this purpose, we implemented a prototype black blood radial balanced steady-state free precession (bSSFP) pulse sequence.

Methods: The study was approved by the institutional IRB. Six healthy volunteers were evaluated using the following black blood techniques: (1) SOC FSE (BW 305 Hz/px, echo spacing 5.8 ms, ipat 2), high-bandwidth FSE (BW 977 Hz/px, echo spacing 3.0 ms, ipat 2), 4-shot radial bSSFP (1002 Hz/px, echo spacing 2.8 ms, 140 views), and single shot radial bSSFP (1002 Hz/px, echo spacing 2.8 ms, 35 and 72 views). Fat suppression was used for all sequences, which were each acquired using both breath-holding and free breathing. In addition, 27 subjects undergoing clinically-indicated cardiac MRI had black blood imaging using SOC FSE and 4-shot radial bSSFP. Image quality was assessed by two observers. Overall image quality, fat suppression and blood nulling were scored in a 5-point Likert scale. The quality of visualization of the ventricular walls were individually scored. Streaking, signal dropout, and ghosting artifacts were noted.

Results: Radial bSSFP matched or outperformed both high- and low-bandwidth Cartesian FSE. Preference for radial bSSFP over Cartesian FSE was highly significant for overall image quality (3.9±0.59 vs. 3.4±0.74, $P < 0.001$), fat suppression (4.2±0.4 vs. 3.5±0.53, $P < 0.001$), RV free wall visibility (3.8±0.75 vs.2.8±0.88, $P < 0.001$), LV free wall visibility (4.3±0.67 vs. 3.6±0.88, $P < 0.001$) and septum visibility (4.5±0.6 vs. 4.0±0.74, $P < 0.001$). Radial bSSFP images showed fewer motion artifacts and were judged to provide better myocardial visibility (Fig. 1). In addition, radial bSSFP allowed the use of higher undersampling factors and fewer shots than FSE, so that substantially more slices could be acquired in each breath-hold.

Conclusions: In conclusion, our data indicate that radial bSSFP should be considered as an efficient alternative to Cartesian FSE for improved black blood imaging of the heart. Fig. 1. Comparison of black blood radial bSSFP (left) with black blood Cartesian FSE (right) in a patient. The right and left ventricular myocardium is better demonstrated with radial bSSFP. With Cartesian fast spin-echo, motion artifacts obscure the inferior wall (arrows) of the left ventricle and free wall of the right ventricle (arrowheads).

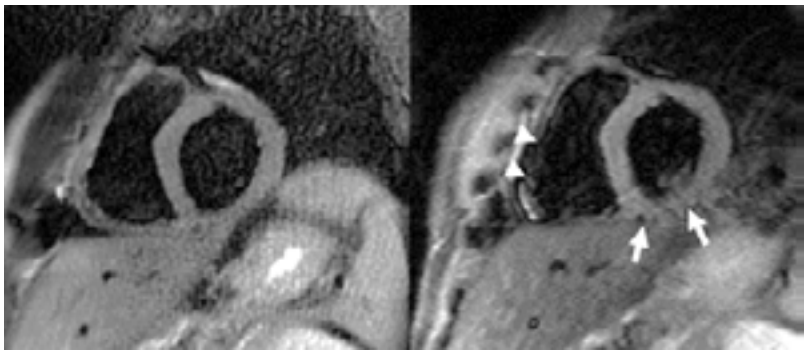

P318

Comparison of PSIR Motion Correction Late Gadolinium Enhancement Sequence with TurboFLASH and TrueFISP Late Gadolinium Enhancement Sequences

Ming-Yen Ng, BMBS, FRCR[2] Yan Chen, MD[1], Xiao-Wan Tong, MD[2], Jian-Long He, MD[1], Lin Luo, MD[1], Kai-Hang Yiu, MD[2], Xin-Ping Shen, MD[1]

1. HKU-Shenzhen Hospital, Guangdong, China (People's Republic)
2. The University of Hong Kong, N/A, Hong Kong

Background: TurboFLASH/ segmented late gadolinium enhancement (LGE) sequences are routinely employed for tissue characterisation but are highly susceptible to arrhythmmias, breathing and patient motion as well as being time consuming. TrueFISP/ single-shot LGE sequences can be employed for these difficult cases but it has reduced spatial resolution and is still susceptible to motion artefact. A phase sensitive inversion recovery with motion correction sequence (PSIR MoCo) has been developed (Ledesma-Carbayo et al, JMRI 2007) which provides improved spatial resolution (1.87mmx1.87mm) and eliminated motion artifact compared to TrueFISP (2.13mmx2.13mm). Acquisition is rapid due to its single-shot acquisition. The objectives were:

1. Determine the amount of time saved using PSIR MoCo compared to TurboFLASH and TrueFISP acquisitions
2. Determine if PSIR MoCo results in higher image quality than TurboFLASH and TrueFISP

Methods: Inclusion criteria was patients/ normal volunteers undergoing cardiac MR. Exclusion criteria were patients who did not have LGE images. Data was acquired on a 1.5T MR System (MAGNETOM Avanto, Siemens Healthcare, Germany) using a prototype PSIR MoCo sequence. Time was measured based on the timings from the MRI times stated on the images. Image quality was based on a 4-point Likert scale (1 = worst; 4= best). Patients were recruited consecutively for a 3 month period. MRI TurboFLASH images were acquired first starting at 8 minutes post contrast injection followed by the PSIRMoCo sequence and the TrueFISP PSIR. Images with poor contrast differentiation between the myocardium and blood pool were excluded from the analysis. For statistical analysis a p-value < 0.05 was regarded as statistically significant. ANOVA was used for comparing the three groups.

Results: 37 subjects (4 healthy volunteers) were recruited (mean age 48.5 ± 15.2 years, 59% male). Time taken for the acquisition of the PSIR MoCo, TurboFLASH and TrueFISP LGE images are shown in Table 1. Overall, PSIR MoCo was significantly faster than the TurboFLASH LGE sequence . There was no statistically significant difference in time between PSIR MoCo and TrueFISP sequences. Overall, average time saving was 444 seconds (>7mins) between PSIR MoCo and TurboFLASH. Image quality scores are listed in Table 2. PSIR MoCo showed statistically significant difference in the total score as well as the 3 and 4 chamber LGE sequences compared to TurboFLASH.

Conclusions: PSIR MoCo shows statistically significant time saving and improvement in image quality compared to TurboFLASH. There is a trend of improvement in image quality compared to TrueFISP LGE. Further study is warranted to confirm these findings.

Average time taken with standard deviation to acquire the LGE sequences

p-value	TrueFISP	PSIR Moco	TurboFLASH	
<0.001	46 ± 16sec*	59 ± 26sec*	500 ± 145sec	**Short Axis Stack**
0.01	33 ± 11sec♯	41 ± 19sec	44 ± 9sec♯	**2 Chamber**
0.04	36 ± 19sec♯	42 ± 17sec	47 ± 13sec♯	**3 Chamber**
0.47	50 ± 23sec	56 ± 24sec	56 ± 21sec	**4 Chamber**
<0.001	165 ± 44sec*	197 ± 49sec*	641 ± 148sec	**Total**

* = no statistically significant difference between PSIR MoCo and TrueFISP LGE
♯= statistically significant difference between TurboFLASH and TrueFISP LGE

Average image quality scores with standard deviations. Image score was based on a Likert scale from 1-4

p-value	TrueFISP	PSIR Moco	TurboFLASH	
0.2	3.3 ± 0.77	3.6 ± 0.55	3.5 ± 0.35	Short Axis Stack
0.10	3.5 ± 0.72	3.6 ± 0.57	3.2 ± 0.65	**2 Chamber**
0.0004	3.3 ± 0.58	3.7 ± 0.45*	3.1 ± 0.74*	**3 Chamber**
0.001	3.4 ± 0.58♯	3.8 ± 0.39♯	3.3 ± 0.58♯	**4 Chamber**
0.0001	3.5 ± 0.37	3.8 ± 0.26*	3.3 ± 0.47*	**Total**

* = Statistically significant difference between TurboFLASH and PSIR MoCo only
♯ = Statistically significant difference between TurboFLASH and PSIR MoCo as well as PSIR MoCo and TrueFISP

P319

Compressed Sensing real-time cine imaging: Can it accurately assess ventricular and valvular function in clinical routine?

François Pontana, MD, PhD[1]Benjamin Longere, MD[1], Mathilde Vermersch[1], Julien Pagniez, MD[1], Hedi Farah[1], Valentina Silvestri, MD[1], Michaela Schmidt[2], Christoph Forman, MS[2]

1. Lille University Hospital, Nord-Pas-de-Calais, France
2. SIEMENS HEALTHCARE GmbH, Erlangen, Bayern, Germany

Background: In patients with cardiac condition that may prevent from iterative breath-holds, Compressed Sensing (CS) real-time cine imaging could improve CMR scan time efficiency. The purpose of this study was to evaluate the accuracy of a CS real time prototype cine sequence (SPARSE 2D cine, Siemens Healthcare) for quantification ventricular function and volumes including contractility disorder and valvulopathy visualization in clinical pratice.

Methods: 100 consecutive patients (66 males, 34 females, 53.07 ± 18.1 years) refered for cardiac magnetic resonnance (CMR) examination were prospectively enrolled. CMR were performed for ischemic heart disease (n=24), infiltrative cardiomyopathy (n=17), valvular disease (n=16), heart rythm disorder (n=14), dilated cardiomyopathy (n=13), hypertrophic cardiomypathy (n=8), myocarditis (n=8). Grown up congenital heart disease patients were excluded. The CMR protocol included short axis stack, one four chamber slice and one long axis slice using (a) a conventionnal segmented multi-breath-hold steady state free precession acquisition (b-SSFP) as a reference (Group 1) and (b) a CS real time single-breath-hold sequence (Group 2) providing the same slice number, position and thickness. Two radiologists independently assessed left ventricle (LV) and right ventricle (RV) ejection fraction (LVEF & RVEF), end diastolic volumes (LVEDV and RVEDV), LV mass (LVM) as well as LV contractility disorder and atrioventricular valvulopathy in both Groups.

Results: The CS sequence mean scan time was 23.16 ±6.42 seconds and for the multi-breath-hold b-SSFP sequence it was 510 ±109 seconds ($p < 0.001$). There was a high correlation between Group 1 and 2 regarding LVEF (49.025 ±16.785 % vs 48.715 ±16.63 % ; $r^2=0.99$), mean LVEDV (191.53 ±80 ml vs 188.01 ±78.72 ml ; $r^2=0.99$), and mean LVM (149.725 ±49.85 g vs 152.175 ±49.72 g ; $r^2=0.96$). There was also strong correlation between Group 1 and 2 for RV assessment: mean RVEF (53.02 ±11.79 % vs 52.765 ±11.49ml; $r^2=0.96$) and RVEDV (157.44 ±45.17 ml vs 155.12 ±42.79 ml; $r^2=0.97$). There was also a good correlation for the detection of mitral (AUC=0.85) and tricuspid valvulopathy (AUC=0.81) and contractility disorders (AUC>0.97).

Conclusions: Compressed sensing single-breath-hold cine imaging provides LV function, volumes and mass as well as RV function and volumes, which are comparable to the conventional SSFP multi-breath-hold imaging without significant loss of information regarding the detection of contractility disorder or valvulopathy.

P320

Accelerated Whole-heart 3D T2 Mapping: Comparison of Reconstruction Strategies

Dan Zhu, PhD student[1] Haiyan Ding, PhD[2], Henry Halperin, MD, MA[3], Daniel A. Herzka, PhD[4]

1. *Department of Biomedical Engineering, Johns Hopkins University School of Medicine, Baltimore, MD*
2. *Center for Biomedical Imaging Research, Department of Biomedical Engineering, Tsinghua University, Beijing, N/A, China (People's Republic)*
3. *Johns Hopkins University, Baltimore, MD*
4. *Johns Hopkins University School of Medicine, Baltimore, MD*

Background: Myocardial T2 relaxometry can detect changes associated with many cardiac pathologies. To generate T2 maps, multiple fully-sampled volumes with varying amounts of T2-weighting are needed. Those volumes differ in image contrast but share significantly structural similarity that can be exploited to improve the quality of undersampled reconstruction with parallel imaging. Here, we compare the performance of traditional SENSE[1] in which each volume is subsampled similarly and reconstructed independently to: standard SENSE which reconstructs all volumes jointly, Joint-Sparsity SENSE (JS-SENSE) which uses a sparsity transform to exploit the structural similarities[2], and Model-Based SENSE (MB-SENSE) which drives optimization with an exponential decay model[3].

Methods: *Imaging:* N=3 normal swine were imaged using a 3D T2 mapping method with whole-heart coverage[4]. Four fully-sampled volumes with different T2-weighting were acquired with partial Fourier sampling in the readout direction, no parallel imaging and a resolution of 1.25x1.25x5.0 mm^3. Data were retrospectively undersampled (R=2-8) in two ways: Caipirinha[5] and variable density random (VDR)[6] sampling (Fig. 1). calibration lines were used for sensitivity map estimation, and homodyne detection was applied[7]. As an additional gold-standard, regularly (equally-spaced, ES) undersampled data were restored using a traditional volume-by-volume SENSE. For standard SENSE and JS-SENSE, a conjugate-gradient method was used, while for MB-SENSE, projection onto convex sets was used[4]. *Image Analysis*: T2 was determined as in [4] and the mean and standard deviation (SD) over the whole heart were calculated. Voxels with T2>100ms or T26. The number of pixels rejected due to poor fits was recorded as a metric of reconstruction quality. Image-based and T2-Map based errors were calculated.

Results: Figure 2 shows images and T2 maps reconstructed using the various methods for R=3, with corresponding error maps. Figure 3 illustrates RMSE of images and T2 maps, the bias in mean T2, and the SD of T2 values vs. net reduction factor in the LV myocardium.

Conclusions: Figure 1 demonstrates accelerated T2 mapping is feasible. Image quality is maintained for high reduction factors. However, the RMSE of T2 maps increases at a faster rate, acting as the limiting factor on maximum acceptable acceleration rate. Joint reconstructions incorporating all data outperformed traditional volume-by-volume SENSE. MB-SENSE with VDR generally outperformed other iterative approaches.

References: [1]Pruessmann K. MRM 42(1999). [2]Majumdar A. JMR 210(2011). [3]Samsonov A. ISMRM (2015). [4]Ding H. MRM 74(2015). [5]Tsao J MRM 53(2005). [6]Lustig MRM 58(2007). [7]Noll IEEE-TMI 10(1991).

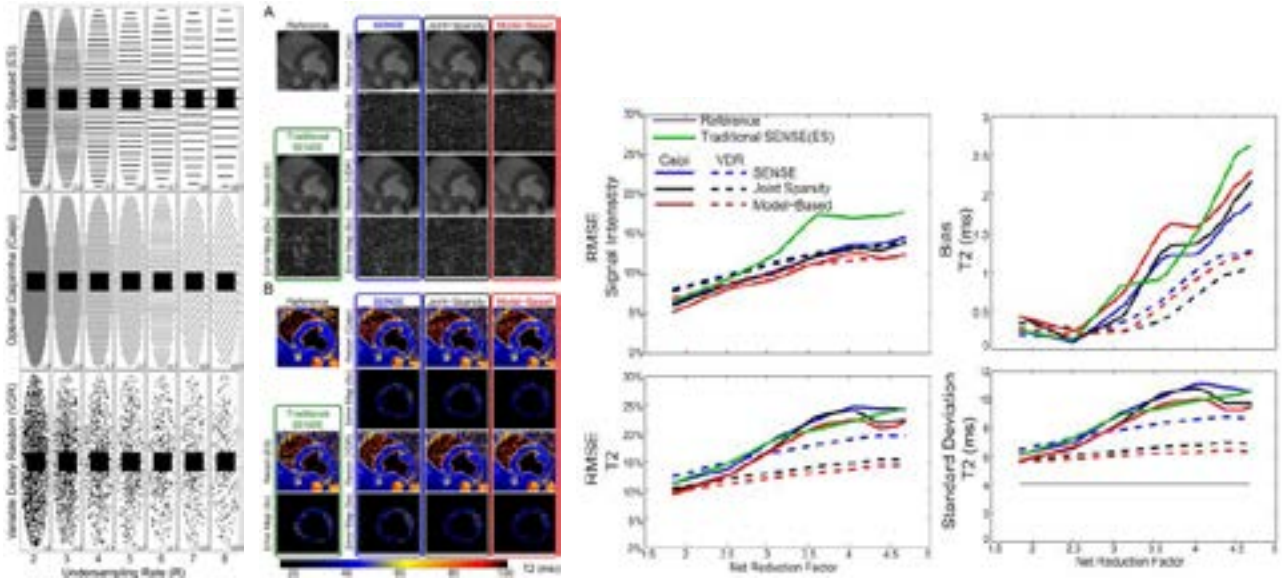

P321

Golden-Angle Spiral Sparse Parallel-Imaging for Coronary Lumen Area Measurements in Short Breath-Holds

Michael Schär, PhD[1] Gabriele Bonanno, PhD[2], Allison G. Hays, MD[2], Dinghui Wang, PhD[3], Zhiqiang Li, PhD[3], James G. Pipe, PhD[3], Robert G. Weiss, MD[2]

1. Johns Hopkins University, MD
2. Johns Hopkins University School of Medicine, MD
3. Barrow Neurological Institute, AZ

Background: Endothelial cell release of nitric oxide (NO) in response to some stressors results in arterial dilatation and is a defining characteristic of healthy vascular tissue. Endothelial dysfunction manifests as impaired dilatation and is a marker for sub-clinical disease, an independent predictor of atherosclerotic progression and adverse cardiac events, and a potential target for medical interventions.[1-6] Coronary artery endothelial function (CEF) could historically only be measured with invasive catheterization-based testing.[1,7] Recently, a noninvasive, NO-dependent, reproducible MRI means to quantify CEF was developed that uses spiral cine MRI.[8-10]

The current MRI acquisitions to measure lumen area are performed during 20-25s breath-holds, which are sometimes too long for patients leading to degraded image quality. Here we propose and test the combination of a golden-angle rotated spiral acquisition with a sparse parallel-imaging reconstruction to *shorten* the breath-hold duration to make the technique more robust and tolerable for more patients.

Methods: Acquisition: Data were acquired perpendicular to linear segments of the right coronary artery in 4 healthy subjects on a 3T scanner (Philips). Spiral interleaves were acquired for ~20s while rotating consecutive interleaves by the golden-angle (137.508°). ECG-signal was recorded and used for retrospective data binning to 40 cardiac phases.
Reconstruction: The same data were reconstructed in GPI[11] with 4 different approaches: 1) For reference, data from each phase was reconstructed with a standard conjugate gradient SENSE reconstruction (**CG-SENSE**).[12] 2) We adapted the GRASP[13] reconstruction, originally for radial trajectories to spiral trajectories, minimizing the combination of parallel-imaging data consistency and temporal total-variation based sparsity constraints; and named it Golden-Angle Spiral Sparse Parallel-imaging (GASSP). First using all data (**GASSP 20s**). Then only data from 3) the first 10s (**GASSP 10s**) and 4) the first 5s (**GASSP 5s**). In each approach data during the transition to steady-state (first heart-beat) was rejected.

Vessel sharpness[14] and cross-sectional lumen area (by FWHM) were determined in both systole and diastole.

Results: Figure 1 shows images from all approaches and volunteers. Because the total-variation reconstruction-constraint leads to temporal blurring, Figure 2 shows images from 5 different cardiac phases to visually assess temporal resolution. Vessel sharpness was not significantly different with CG-SENSE: 65±2; GASSP-20s: 66±3; GASSP-10s: 67±4; GASSP-5s: 65±5. GASSP lumen areas were compared to CG-SENSE with Pearson's correlation and Bland-Altman analysis (Figure 3).

Conclusions: GASSP promises coronary lumen area measurements with equivalent vessel sharpness in breath-holds as short as 5s.

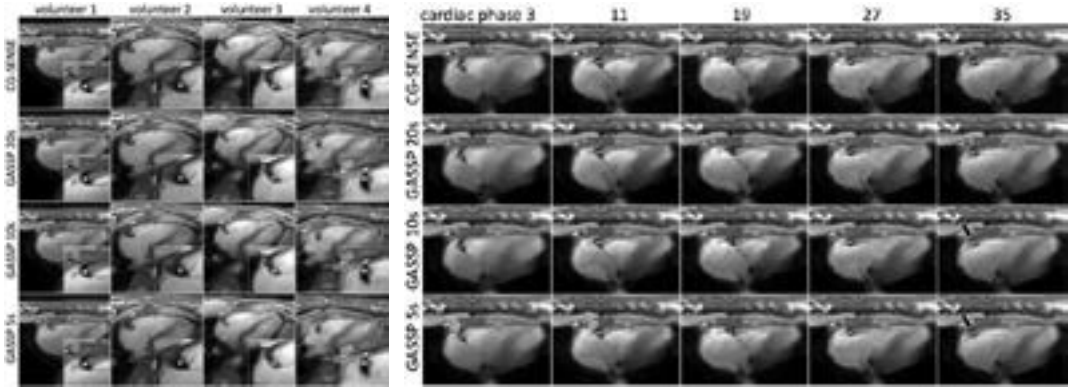

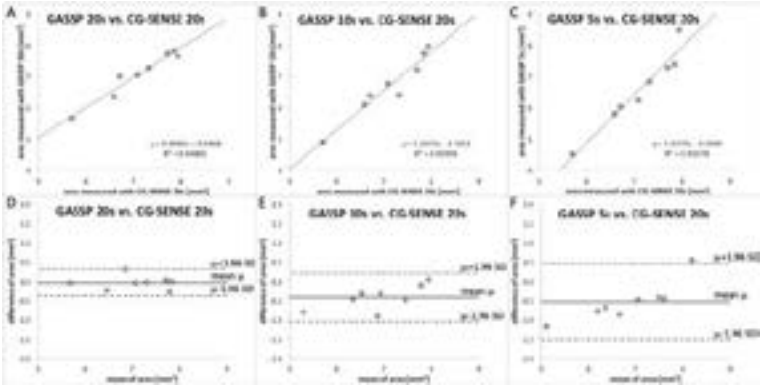

References

1. Ludmer PL, Selwyn AP, Shook TL, Wayne RR, Mudge GH, Alexander RW, et al. Paradoxical Vasoconstriction Induced by Acetylcholine in Atherosclerotic Coronary Arteries. N. Engl. J. Med. 1986;315:1046–51.
2. Suwaidi JA, Hamasaki S, Higano ST, Nishimura RA, Holmes DR, Lerman A. Long-term follow-up of patients with mild coronary artery disease and endothelial dysfunction. Circulation. 2000;101:948–54.
3. Schächinger V, Britten MB, Zeiher AM. Prognostic impact of coronary vasodilator dysfunction on adverse long-term outcome of coronary heart disease. Circulation. 2000;101:1899–906.
4. Halcox JPJ, Schenke WH, Zalos G, Mincemoyer R, Prasad A, Waclawiw MA, et al. Prognostic Value of Coronary Vascular Endothelial Dysfunction. Circulation. 2002;106:653–8.
5. Treasure CB, Klein JL, Weintraub WS, Talley JD, Stillabower ME, Kosinski AS, et al. Beneficial Effects of Cholesterol-Lowering Therapy on the Coronary Endothelium in Patients with Coronary Artery Disease. N. Engl. J. Med. 1995;332:481–7.
6. Pugh CJA, Spring VS, Kemp GJ, Richardson P, Shojaee-Moradie F, Umpleby AM, et al. Exercise training reverses endothelial dysfunction in nonalcoholic fatty liver disease. Am. J. Physiol. Heart Circ. Physiol. 2014;307:H1298–306.
7. Veerasamy M, Bagnall A, Neely D, Allen J, Sinclair H, Kunadian V. Endothelial Dysfunction and Coronary Artery Disease: A State of the Art Review. Cardiol. Rev. 2014;1.
8. Hays AG, Hirsch GA, Kelle S, Gerstenblith G, Weiss RG, Stuber M. Noninvasive visualization of coronary artery endothelial function in healthy subjects and in patients with coronary artery disease. J. Am. Coll. Cardiol. 2010;56:1657–65.
9. Hays AG, Iantorno M, Soleimanifard S, Steinberg A, Schär M, Gerstenblith G, et al. Coronary vasomotor responses to isometric handgrip exercise are primarily mediated by nitric oxide: a noninvasive MRI test of coronary endothelial function. Am. J. Physiol. Heart Circ. Physiol. 2015;308:H1343–50.
10. Hays AG, Stuber M, Hirsch GA, Yu J, Schär M, Weiss RG, et al. Non-Invasive Detection of Coronary Endothelial Response to Sequential Handgrip Exercise in Coronary Artery Disease Patients and Healthy Adults. Pasterkamp G, editor. PLoS ONE. 2013;8:e58047.
11. Zwart NR, Pipe JG. Graphical programming interface: A development environment for MRI methods. Magn. Reson. Med. 2015;74:1449–60.
12. Pruessmann KP, Weiger M, Börnert P, Boesiger P. Advances in sensitivity encoding with arbitrary k-space trajectories. Magn. Reson. Med. 2001;46:638–51.
13. Feng L, Grimm R, Block KT, Chandarana H, Kim S, Xu J, et al. Golden-angle radial sparse parallel MRI: combination of compressed sensing, parallel imaging, and golden-angle radial sampling for fast and flexible dynamic volumetric MRI. Magn. Reson. Med. 2014;72:707–17.
14. Botnar RM, Stuber M, Danias PG, Kissinger KV, Manning WJ. Improved Coronary Artery Definition With T2-Weighted, Free-Breathing, Three-Dimensional Coronary MRA. Circulation. 1999;99:3139–48.

P322

Developing an analysis pipeline for global T1 mapping quality control in the T1 Mapping and ECV Standardization in CMR (T1MES) Program

Richard J. Eames[1]Gabriella Captur, MD, PhD, MRCP, MSct[2], Peter D. Gatehouse, PhD[3], Redha Boubertakh, PhD[4], Camilla Torlasco, MD[5], Giulia Benedetti, MD[6], Friso G. Heslinga, MSc[7], Ruediger Bruehl, PhD[8], Martin J. Graves, PhD[9], Kathryn Keenan, PhD[10], Bernd Ittermann, PhD[11], Wenjie Pang, PhD, MSc[12], Reza Nezafat, PhD[13], Michael Salerno, MD, PhD[14], James Moon, MBBS, MD, MRCP[15]

1. *Imperial College London, London, England, United Kingdom*
2. *UCL Biological Mass Spectrometry Laboratory, Institute of Child Health and Great Ormond Street Hospital, 30 Guilford Street, London, UK';, England, United Kingdom*
3. *NIHR Cardiovascular Biomedical Research Unit, Royal Brompton Hospital, London, England, United Kingdom*
4. *Cardiovascular Biomedical Research Unit, Barts and the London School of Medicine and Dentistry, Queen Mary University of London, London, UK, London, England, United Kingdom*
5. *Barts Heart Center. St Bartholomew's Hospital, West Smithfield, London, EC1A 7BE, England, United Kingdom*
6. *Barts Heart Centre, London, England, United Kingdom*
7. *NeuroImaging group, MIRA Institute for Biomedical Technology and Technical Medicine, University of Twente, Enschede, Netherlands, Overijssel, Netherlands*
8. *PTB, Berlin, Berlin, Germany*
9. *Cambridge University Hospitals NHS Foundation Trust, Cambridge, UK, Cambridge, England, United Kingdom*
10. *NIST Headquarters, 100 Bureau Drive Gaithersburg, MD 20899, MD*
11. *Physikalisch-Technische Bundesanstalt (PTB), Abbestr. 2 – 12, D-10587 Berlin, Germany, Berlin, Germany*
12. *Resonance Health, 278 Stirling Highway, Claremont WA 6010, Australia, Western Australia, Australia*
13. *Department of Medicine (Cardiovascular Division) Beth Israel Deaconess Medical Center, Harvard Medical School, Cardiology, East Campus, Room E/SH455, 330 Brookline Ave, Boston, MA, 02215, MA*
14. *University of Virginia, VA*
15. *Barts Heart Center, The Cardiovascular Magnetic Resonance Imaging Unit and The Center for Rare Cardiovascular Diseases Unit, St Bartholomew's Hospital, West Smithfield, London, UK, England, United Kingdom*

Background: We created T1MES: the T1 Mapping and ECV Standardization Program to deliver T_1 mapping to global clinical care using phantoms that have received regulatory clearance by the Food and Drug Administration and Conformité Européene marking. 69 Phantoms were distributed with a multi-vendor user manual for fortnightly scanning in centers worldwide. To verify measurement stability over time at individual sites, with further aims of generalization across sites using different systems, software and sequences we developed a semi-automated analysis pipeline for processing incoming multi-center data.

Methods: The T1MES quality assurance (QA) program generates three main types of multicenter data: 1) raw data from long reference scans for T1 (IRSE) and T2 (SE); 2) raw T1 mapping data from some centers without the ability to reconstruct their own maps locally; 3) reconstructed T1|T2 maps (majority of sites). A comprehensive set of MATLAB utilities developed at the US National Institutes of Health were customized to serve as the image data analysis platform to support T1MES. The pipeline was integrated with a large-capacity remote server for image data exchange using a secure file transfer protocol and a web-based electronic data capture infrastructure (based on REDCap) to host and curate the 27,164 metadata elements. For each T1 map irrespective of sequence type or vendor, the pipeline is designed to automatically extracts the following DICOM metadata elements: 9 T1 values from the regions of interest (**Fig 1.A**); flip angle; repetition time, echo time; image object position; image orientation position; nominal interval; all acquisition times and inversion recovery times.

Results: The contribution to T1MES consists of conventional CMR scans: A) the initial localizers; and B) at least any one T1 mapping sequence with simulated electrocardiogram set at 67bpm (inter-beat [RR] interval 900ms). Analysis of a typical dataset and data upload into REDCap using this pipeline is achievable in < 3 minutes (example results **Fig.1B**). Long term stability of the agarose gel used in the tubes is being investigated and at study end (Dec 2016) results are expected to inform the stability of T1 measurements over time at each scanner, including a potential temperature correction model for T1.The project intends to curate phantom data long-term in the open access repository and datasets will be made available to the wider CMR community after publication of study results.

Conclusions: The T1MES program provides an opportunity for inter-sequence and inter-site analyses and comparisons. The T1MES data analysis pipeline we have created is the first large-scale effort within academia, aimed at supporting T1 mapping QA with the capacity to semi-automatically analyse large volumes of datasets. This pipeline is efficient and is now being used for the academic exploration of T1 mapping sequences, platform performance, stability and the potential for standardization in line with the research goals of T1MES.

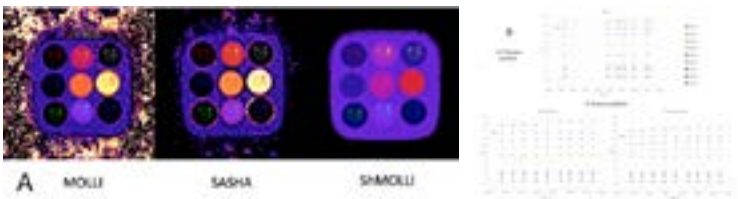

P323

Validation of Rapid Real-Time Cine MRI with Radial k-space Sampling and Compressed Sensing in Children and Young Adults

Simon Lee, M.D.[1]Joshua D. Robinson, MD[2], Daniel Kim, PhD[3], Hassan Haji-Valizadeh, Masters[4], Cynthia Rigsby, MD FACR[5]

1. *Ann & Robert H. Lurie Children's Hospital of Chicago, IL*
2. *Northwestern University Feinberg School of Medicine, Chicago, IL*
3. *Northwestern University Feinberg School of Medicine, IL*
4. *Northwestern University, IL*
5. *Ann & Robert H Lurie Children's Hospital of Chicago, Chicago, IL*

Background: Rapid real-time (RT) cine imaging using compressed sensing (CS) and radial k-space undersampling has been shown to yield relatively high spatio-temporal resolution images (spatial resolution = 1.3 mm x 1.3 mm; temporal resolution = 38 ms). Despite the growing interest in accelerated cardiovascular MRI with CS, there have been few evaluations in a truly clinical setting, particularly in children. The purpose of this study was to evaluate the accuracy of rapid RT cine MRI compared to traditional breath-held cine SSFP (BH-SSFP) in children and young adults, including those with congenital heart disease (CHD).

Methods: In this prospective, IRB-approved study, informed consent was obtained on consecutive patients undergoing clinically-indicated cardiac MRI, which included BH-SSFP and RT cine sequences. Both sets of images were post-processed by a single observer using QMass® MR to calculate EDV, ESV, and EF for the right (RV) and left ventricles (LV), as well as LV mass. Measurements between the two techniques were compared using linear regression analyses and Bland-Altman plots.

Results: Data from twenty patients were analyzed, with a median age of 16.9 (range 1.7-36 years) and 80% of patients with CHD. Figure 1 shows representative image quality of BH-SSFP and RT images. There was a very strong linear relationship ($R^2 >$ 0.94) between BH-SSFP and RT for LV and RV volumes and LV mass. There was also a very strong linear relationship for LVEF (R^2 = 0.83) and RVEF (R^2 = 0.92). Bland-Altman analysis showed good agreement with minimal mean bias for all measurements (Figure 2). The LVEF (mean bias -2.4 ± 5.1%) and RVEF (mean bias -1.8 ± 3.6%) showed excellent agreement.

Conclusions: This study demonstrates that rapid RT cine MRI produces relatively accurate measurements for ventricular quantification in children and young adults as compared with standard BH-SSFP cine MRI.

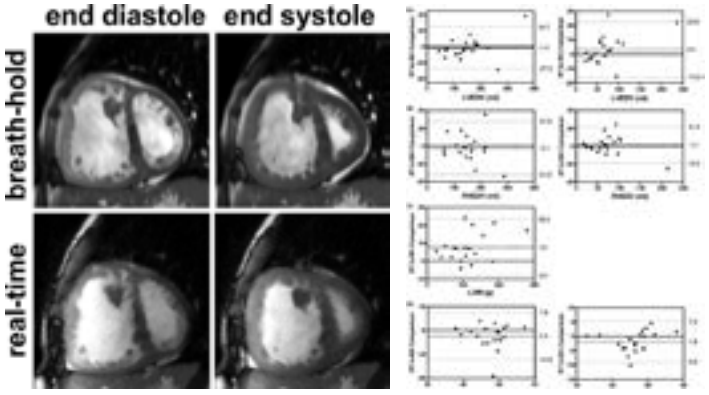

P324

Automatic Isocenter Positioning with Deep Learning

Xiaoguang Lu, Ph.D.[1], Carmel Hayes, Ph.D.[2]

1. Siemens Healthineers, Princeton, NJ
2. Siemens Healthineers, Bayern, Germany

Background: One of the first steps in cardiac MRI is to ensure that the heart is at the isocenter of the magnet. This requires the technician to identify the heart in a few localizer images. Automatically localizing the heart from these images remains an open challenge. We propose a data-driven deep learning-based approach to localizing the heart, with the aim to fully automate heart view planning.

Methods: The deep learning (DL)-based scheme learns task-specific image features and models based on the annotation of large representative datasets. We adopt convolutional neural network [1] architectures specialized for image analytics, containing 5 convolution layers and 3 fully connected layers. We propose a slab-based scanning and detection scheme within each localizer image as shown in Fig. 1. Each slab is evaluated by the DL model to determine whether the slab contains the heart. We calculate the scores/likelihood of each slab along row/column directions using DL models, then jointly analyze the clusters in the score curves along row, m, and column, n, to determine the heart location. The total slab/model evaluations in our method is of the order of O (m+n).

Results: We collected 98 patient cases for training the deep neural networks and another 20 patient cases acquired at a different clinical site for performance evaluation. All datasets were acquired using 1.5T Siemens MR scanners. In total, 10785 column slabs and 10227 row slabs were generated for training. The DL prototype was applied to predict the heart center from three coronal localizer images for each of the 20 test cases. Visual inspection (examples in Fig. 2) showed that all predicted locations were within the heart region. Retrospectively, the operator-chosen table offset position, recorded in the DICOM fields, was retrieved for ground truth comparisons. For the 20 test cases, the [mean, std, median, min, max] of the absolute difference between model prediction and ground truth are [6.93, 5.22, 5.25, 0, 19.00] in mm, respectively. The heart localization process took less than 1 second per case.

Conclusions: We demonstrate the feasibility of an automated method for heart localization from a few localizer images. Together with automated view planning [2,3], it offers a promising means to achieve fully automated heart view planning, thus warranting larger-scale investigations.

References:

[1] Krizhevsky et al., NIPS, pp. 1106-1114, 2012.

[2] Lu et al., MICCAI, pp. 479-486, 2011.

[3] Nitta et al., Magn Reson Mater Phy 26, pp. 451–461, 2013.

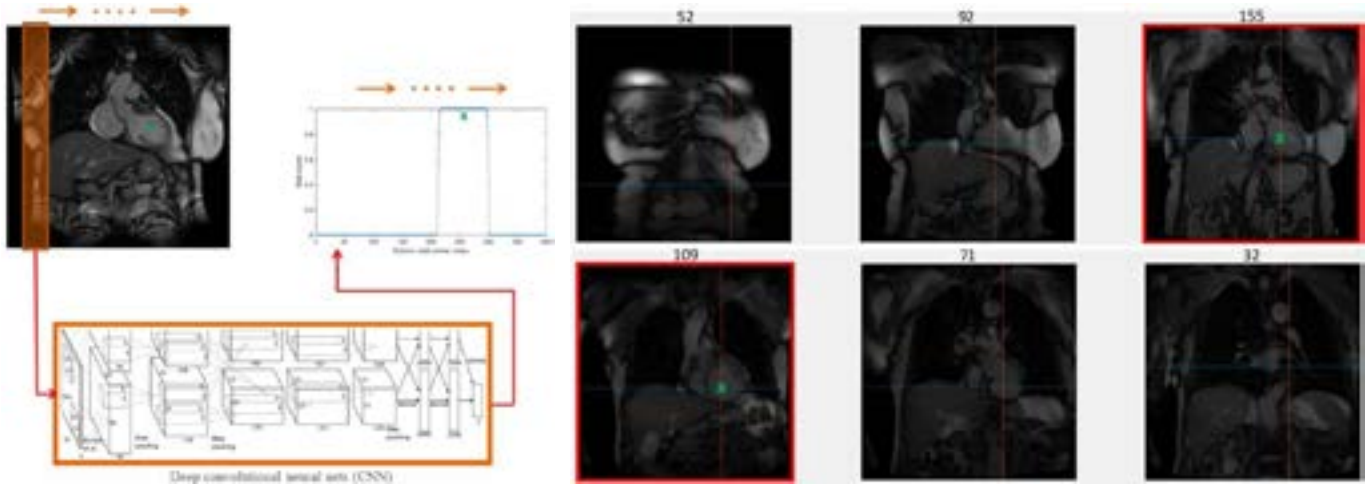

P325

Evaluation of Regional Right-Ventricular Function in Patients with Tetralogy of Fallot Using Real-Time Strain-Encoding CMR

El-Sayed H. Ibrahim, PhD[1] Prachi Agarwal, MD[2], Maryam Ghadimi-Mahani, MD[2], Jimmy Lu, MD[3], Adam Dorfman, MD[2]

1. *University of Michigan, Ann Arbor, MI*
2. *University of Michigan, MI*
3. *University of Michigan, Dexter, MI*

Background: Tetralogy of Fallot (TOF) is the most common form of cyanotic congenital heart disease. Surgical repair of ToF is associated with good long-term survival, leading to a growing adult population of survivors. Assessment of right-ventricular (RV) function plays an important role in clinical decision making for these patients. However, global measures of RV function, e.g. ejection fraction (EF), are not sensitive for identifying early ventricular dysfunction. In this study, we evaluate fast strain-encoding (fast-SENC) for measuring regional RV strain in post-repair TOF and compare the results to global RV function.

Methods: Ten post-repair TOF patients (4 males; age=42±22 y.o.) were imaged on a 1.5 Tesla scanner using cine, velocity-encoding, and SENC CMR to measure EF, flow in large arteries and atrioventricular valves, and myocardial strain, respectively. Fast-SENC images were acquired at basal, mid-ventricle, and apical short-axis slices and a 4-chamber slice to measure longitudinal (Ell) and circumferential strain (Ecc) strain, respectively. Fast-SENC allows for acquiring strain maps in a one-heartbeat free-breathing scan, compared to ~14-second breath-hold scan in conventional SENC (Figure-1), which makes it more suitable for imaging patients with congenital heart disease, and it has been previously validated against conventional SENC (MRM; 55:386). Strain maps were used to characterize RV and LV myocardial contractility, and correlation analysis was conducted between strain and EF.

Results: Two patients showed residual ventricular septal defects (Qp/Qs=1.6 and 1.2), six patients showed mild RV hypertrophy (mass-to-volume ratio=0.2-0.25), six patients showed RV dilation (indexed end-diastolic volume=138±20mL/m2), and nine patients showed both tricuspid regurgitation (12.4±6.4%) and pulmonary regurgitation (26.1±16%). RVEF=46±6.4% and LVEF=55±8.5%. RV-Ecc = 15.7±6.4%, RV-Ell = 20.2±2.9%, LV-Ecc = 18.3±4.7%, and LV-Ell = 21.7±3.7%. There existed moderate and weak correlations for RV-Ecc (R=0.41) and RV-Ell (R=0.16), respectively, against RVEF. There existed moderate correlations between LV-Ecc (R=0.54) and LV-Ell (R=0.30) against LVEF. Compared to LV strain, RV strain showed regional heterogeneity with a trend for strain depression from inferior to anterior regions (Figure-2). Further, Ell was the dominant strain component in the RV in most patients (Figure-3).

Conclusions: Fast-SENC allows for detecting subclinical regional RV dysfunction in TOF in real-time without breath-holding. RV strain in post-repair TOF is depressed, has weaker correlation with EF (than does LV strain), and is heterogeneous among different RV regions and strain components. This could be attributed to RV dilation and geometrical shape remodeling in TOF, which affects the orientation of the RV myofiber tracts and corresponding strain components.

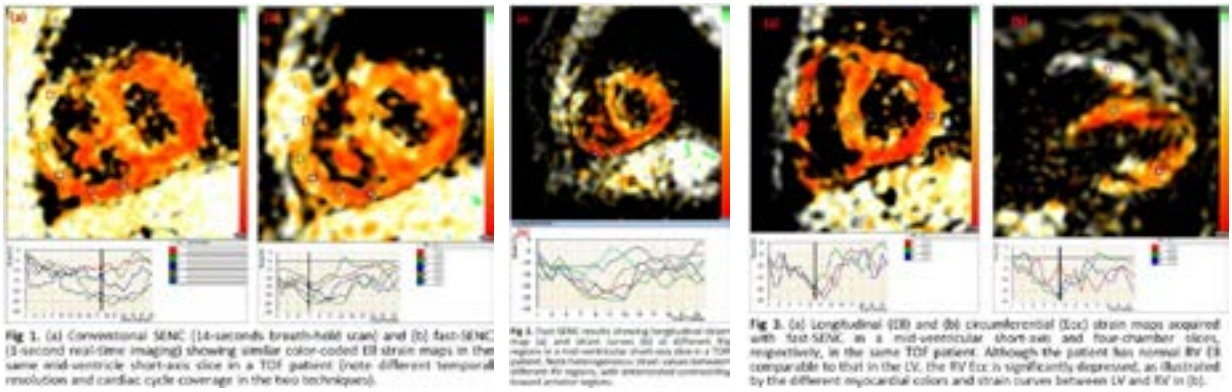

P326

The one minute short-axis stack: cardiac assessment with ultra-fast real time imaging compared to cine at 1.5 T.

Betty Raman, MBBS, FRACP[1] Adam J. Lewandowski, DPhil[2], Joana Leal, Bsc[3], Jane M. Francis, DCR(R) DNM[4], Masliza Mahmod, MBChB, DPhil[5], Dirk Voit, Dr. rer. nat.[6], Markus Untenberger, Dr. rer. nat.[7], Jens Frahm, Prof. Dr.[8], Stefan Neubauer, MD, FRCP[5], Matthew D. Robson, PhD[9], Aaron T. Hess, PhD[9]

1. *University of Oxford, Division of Cardiovascular Medicine, Oxfordshire, England, United Kingdom*
2. *University of Oxford, OXFORD, England, United Kingdom*
3. *University Of Oxford Centre for Clinical Magnetic Resonance Research, England, United Kingdom*
4. *University of Oxford, OX39DU, England, United Kingdom*
5. *University of Oxford, England, United Kingdom*
6. *Biomedizinische NMR Forschungs GmbH, Göttingen, Niedersachsen, Germany*
7. *Biomedizinische NMR Froschungs. GmbH am MPI for biophysical Chemistry, Göttingen, Niedersachsen, Germany*
8. *MPI for biophysical Chemistry, Goettingen, Niedersachsen, Germany*
9. *OCMR, University of Oxford, England, United Kingdom*

Background: ECG gated balanced steady state free precession (bSSFP) breath-hold (BH) cine is currently the mainstay in cardiac assessment of biventricular function. Image quality is often compromised by patient's cardiac rhythm and capacity to breath-hold. Recent advances in methodology have made real time (RT) cardiovascular magnetic resonance (CMR) imaging possible which does not require ECG synchronization or breath-holding. Inter -observer variability and systematic differences between these two methods have not previously been studied. We therefore sought to investigate the level of agreement between an ultra-fast real time free breathing 1 min short-axis (SA) sequence and BH retro gated ECG bSSFP cine.

Methods: 10 healthy volunteers were scanned on a 1.5 T Avanto-Fit Siemens MR scanner equipped with a radial RT pulse sequence and a high performance online image reconstruction computer (GPU server) supplied by the Max-Planck-Institut für biophysikalische Chemie, Göttingen, Germany. Whole heart short axis stack was acquired with (1) standard BH cine and (2) free breathing ECG-free RT with a duration of 1 min for 15 slices (4s per slice). Scan parameters included slice thickness of 8mm with no gap, nominal temporal resolution of 33 ms for RT and 40 ms for cine, resolution of 1.6x1.6mm^2 for RT and 1.4x1.4 mm^2 for cine. Two blinded, experienced CMR observers independently analyzed cardiac mass, chamber volumes and ejection fraction (EF) on bSSFP cine and RT imaging using a standard software package (cvi42 version 5.3.4, Circle Cardiovascular Imaging Inc). The real-time analyses of EF, volumes and chamber size mirrored routine echocardiographic assessment of cardiac function and therefore restricted to 1 heart beat with no discrimination of respiratory phase.

Results: Images were of good quality for both acquisition schemes (Figure 1). The inter-observer variability was similar for both RT and cine for all volume and mass parameters with a marginal increase for RT of < 1.6% in the coefficient of variation (Figure 2). The limits of agreement were within 10% for all measures with no significant differences (paired t-test) except those relating to systolic volume (Table 1) which was marginally higher resulting in lower EF. Despite this, the limits of agreement for EF were still within acceptable limits (2.5% to 6.2%).

Conclusions: With comparable diagnostic image quality to BH cine, RT imaging offers the potential for fast, reliable, ECG-free, non-breath hold cardiac assessment of left ventricular volumes, mass and EF over several heart beats in just 1 minute.

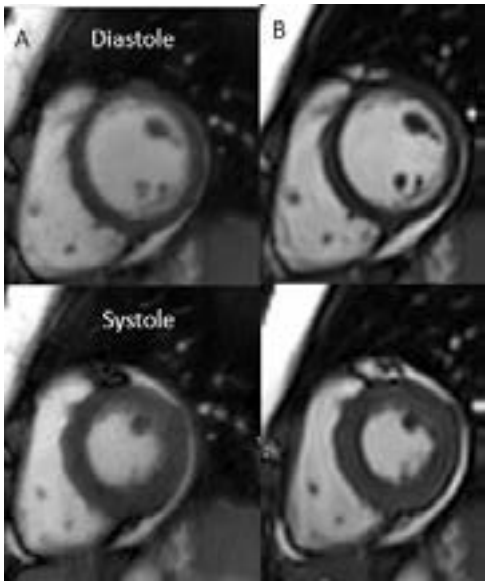

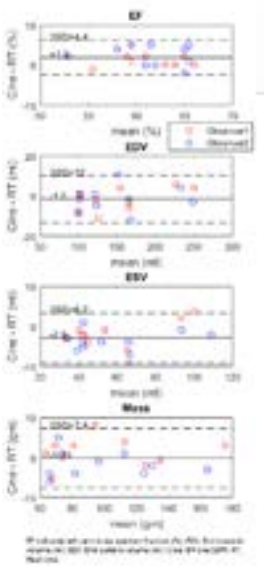

Table 1. Comparing ultra-fast real time sequence to cine for cardiac volumes and mass assessment.

RT Inter-observer variability Coefficient of variation	Cine Inter-observer variability Coefficient of variation	Limits of agreement (cine – RT)	Mean difference cine - RT	Mean±SD cine	
2 %	2 %	-2.5 : 6.2	1.9*	63 ± 4	EF (%)
3 %	3 %	-7.6 : 7.3	-0.2	99 ± 34	Mass (gm)
2 %	1 %	-13.3 : 10.3	-1.5	150 ± 53	EDV (ml)
5 %	4 %	-9.0 : 3.3	-2.9*	57 ± 24	ESV (ml)
3 %	2 %	-9.8 : 12.7	1.5	93 ± 30	SV (ml)
2 %	1 %	-7.5 : 5.2	-1.1	82 ± 19	EDVBSA (ml/m^2)
4 %	3 %	-5.7 : 2.0	-1.9	31 ± 9	ESVBSA (ml/m^2)
3 %	2 %	-5.7 : 6.8	0.6	51 ± 11	SVBSA (ml/m^2)
3 %	3 %	-4.8 : 4.3	-0.3	54 ± 13	MassBSA (gm/m^2)

EF indicates left ventricular ejection fraction; EDV, End diastolic volume; ESV, End systolic volume; SV, Stroke Volume; BSA, Body Surface Area.*P <0.001

P327

Multi-vendor whole-heart 4D flow validation study with and without respiratory gating

Marcus Carlsson, MD, PhD[1]Jelena Bock, PhD[1], Sebastian Bidhult, MSc[2], Karin Markenroth Bloch, PhD[3], Per M. Arvidsson, MD[4], Mikael Kanski, MD, PhD[1], Håkan Arheden, MD, PhD[5], Frederik Testud, Dr. rer. nat.[6], Andreas Greiser, Ph.D[7], Einar Heiberg, PhD[8]

1. *Lund University, Department of Clinical Sciences Lund, Clinical Physiology, Skane University Hospital, Lund, Sweden, Skane Lan, Sweden*
2. *Lund University, Department of Clinical Sciences Lund, Clinical Physiology, Skane University Hospital, Lund, Sweden; Faculty of Engineering, Lund University, Department of Biomedical Engineering, Lund, Sweden, Skane Lan, Sweden*
3. *Lund University Bioimaging Center, Lund University, Lund, Sweden, Skane Lan, Sweden*
4. *Lund University, Department of Clinical Sciences Lund, Clinical Physiology, Skane University Hospital, Lund, Sweden, Luns, Skane Lan, Sweden*
5. *Lund University, Department of Clinical Sciences Lund, Clinical Physiology, Skane University Hospital, Lund, Sweden, Lund, Skane Lan, Sweden*
6. *Siemens Healthcare AB, Skane Lan, Sweden*
7. *Siemens Healthcare GmbH, Erlangen, Germany, Erlangen, Bayern, Germany*
8. *Lund University, Department of Clinical Sciences Lund, Clinical Physiology, Skane University Hospital, Lund, Sweden; Lund University, Faculty of Engineering, Department of Biomedical Engineering, Lund, Sweden, Skane Lan, Sweden*

Background: Today's scanner hardware allows for acceleration factors higher than 2 and therefore reduced scan times. The aim of this study was to validate higher accelerated 4D-flow sequences with and without respiratory gating with scanners from two different vendors and to compare them quantitatively.

Methods: Eight healthy subjects (2 female, age 33±9 years) underwent back-to-back CMR, on the same date on two 1.5T scanners (scanner A: Magnetom Aera, Siemens Healthcare, Erlangen, Germany; scanner B: Achieva dStream, Philips, Best, Netherlands). Acquisition protocols included 2D-flow and whole-heart 4D-flow with retrospective ECG triggering and 2x2 parallel imaging acceleration, with a prototype sequence on Scanner A. Sequence and image reconstruction parameters are summarized in Table 1. 4D-flow scans were acquired with (nav+) and without (nav-) respiratory gating. Stroke volumes (SV) were calculated and Bland-Altman analysis was performed for 2D vs. 4D-flow. Left-ventricular kinetic energy (KE) was calculated from 4D-flow data. SV and KE were calculated using Segment (Software version 2.0 R5080).

Results: Compared to standard 2D-flow, 4D-flow generally underestimated the stroke volume (Figure 1A). The 4D-flow scans with respiratory gating on scanner A showed the lowest bias (Figure 1B). Average 4D-flow scan duration for scanner A was 9±3 (nav+) and 6±2 (nav-) minutes, and for scanner B 17±3 (nav+) and 10±1 (nav-) minutes. The reason for differences in 4D-flow acqusition time between scanners is due to default phase encode oversampling of 1.4 in slice direction on Scanner B. The kinetic energy time course showed similarity in shape for different scanners (Figure 2A), but systolic and diastolic peak values were lower on scanner A (Figure 2B).

Conclusions: Our findings show that even higher accelerated 4D-flow data can be acquired with reasonable quality. Even without gating 4D-flow data show acceptable parameter estimation with acqisition duration within a clinically feasible time window. Kinetic energy comparison shows the expected time-course of this parameter for the investigated scanners. Higher peak KE values on Scanner B are probably due to the use of squared velocities for KE calculation, making this parameter sensitive to artifacts that were more present on scanner B.

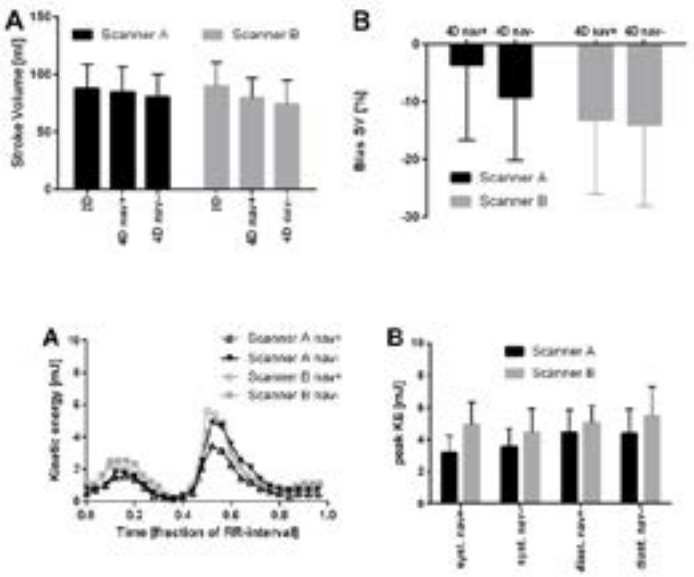

Table 1: Typical acquisition and reconstruciton parameters for 2D- and 4D-flow on investigated scanners.

4D flow		2D flow		
B	A	B	A	Scanner
2.5/4.2	3.5/5.7	5.3/8.6	2.3/9.8	TE/TR [ms]
3x3x3 mm^3	3x3x3 mm^3	1.3x1.3 mm^2	1.5x1.5 mm^2	Spatial resolution
240-288x240-288x168-216 mm^3	240-288x240-288x168-216 mm^3	256x256 mm^2	208x168 mm^2	FOV
45.3	45.6	29.3	28.9	Temporal resolution [ms]
100	100	200	200	Venc [cm/s]
SENSE	GRAPPA			Parallel imaging method
1.4	1.0			Oversampling factor (slice dimension)

P328

Combined heart lung MRI protocol for simultaneous interrogation of heart and lung structure and function

Jakub Lagan, LEKARZ MRCP[1]Josephine Naish, PhD[2], David Clark, BSc(Hons)[3], Anna Reid, MBChB(Hons) MRCP[3], Gavin Lewis, MBChB[3], Robert M. Niven, MBChB MD[3], Rowland Bright-Thomas, MBChB MD[3], Matthias Schmitt, MD PhD[3], Christopher A. Miller, MBChB PhD[3]

1. *University Hospital of South Manchester, Liverpool, England, United Kingdom*
2. *University of Manchester, England, United Kingdom*
3. *University Hospital of South Manchester, England, United Kingdom*

Background: Many conditions considered to be primary lung diseases are independently associated with cardiovascular disease and adverse cardiovascular outcome. Systemic inflammation and subsequent fibrosis are hypothesised mechanisms. However, beyond the mechanical impact on right heart structure and function, characterization of myocardial involvement in lung disease remains limited. We present a combined heart-lung MRI protocol which allows simultaneous interrogation of heart and lung structure and function.

Methods: We developed a protocol at 1.5T (Siemens Avanto), which includes steady state free precession (SSFP) cine imaging of the heart (standard long and short axis views), followed by inspiration and expiration cine lung imaging (sagittal planes). T2 prepared SFFP and Modified Look Locker Inversion Recovery images are acquired to allows T2 and T1 mapping in standard cardiac planes and left and right lungs. Dynamic contrast enhanced MRI (DCE-MRI) sequences are performed using free breathing 2D saturation-recovery FLASH dynamic acquisitions in four planes (two LV short axis slices, left and right lung sagittal slices) with temporal resolution equal to 50% of patient's heart rate. Three boluses of gadolinium contrast (dotarem) are administered: 0.005 mmol/kg, followed by 2 minutes of dynamic acquisitions; 0.05 mmol/kg followed by 6 minutes of dynamics; final dose of 0.1 mmol/kg. Finally, late enhancement imaging (LGE) using standard inversion recovery gradient echo sequences and post-contrast T1 mapping are performed. Overall each scan protocol lasted for approximately 60 minutes.

Results: Parametric mapping and LGE imaging providee direct tissue characterization. Myocardial and lung contrast agent kinetics are modeled from the DCE images in matlab to determine heart and lung capillary permeability (Ktrans), extracellular volume (ECV) or plasma volume fraction (vp). Regions of interest are drawn in the LV and RV cavities to obtain myocardial and lung arterial input functions (AIF). The low dose AIF is multiplied by a factor of ten and the first pass peak combined with the high dose AIF curve in order to correct for saturation effects, as shown in figure 1. Contrast agent kinetics are assessed using the extended Kety model providing values and maps for Ktrans, ECV and vp in myocardium and lungs. Examples shown in figure 2 and 3.

Conclusions: This combined heart lung protocol is an efficient and comprehensive imaging tool for simultaneous myocardial and pulmonary assessment. It has a potential to help ellucidate complex links between pulmonary and myocardial pathologies, and is a model for other dual organ parametertric MR imaging

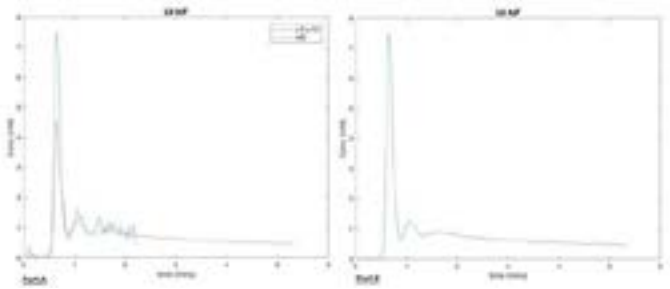

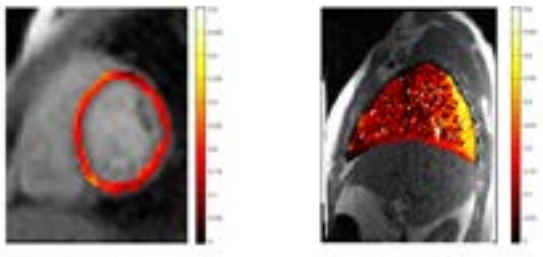

P329

A Single Breath-Hold Simultaneous Acquisition Approach of both Cine-CMR and Strain-Encoded CMR for a Combined Assessment of Myocardial Wall Motion

Keigo Kawaji, Ph.D.[1]Noreen Nazir, MD[2], Akhil Narang, MD[2], Donel Tani, MS[3], Hui Wang, Ph.D.[4], Jouke Smink, MSc[5], Nael Osman, Ph.D.[3], Amit R. Patel, MD[2]

1. University of Chicago, Chicago, IL

2. University of Chicago, IL

3. Myocardial Solutions, Inc., Morrisville, NC

4. Philips Healthcare, OH

5. Philips Healthcare, Noord-Brabant, Netherlands

Background: Steady-State Free Precession (SSFP) Cine-CMR is the standard method for assessing regional wall motion; however, subtle wall motion abnormalities may still be difficult to appreciate. Strain-ENCoded (SENC) has been shown as an alternative method to improve assessment regional wall motion both qualitatively and quantitatively. In this study, we propose a simultaneous, single breath-hold (BH) Cine-SENC acquisition that eliminates the need to have these scans acquired separately; thereby overcomes limiations of intra-BH scans such as cross-registration steps, and improves scanner throughput.

Methods: The combined acquisition protocol was achieved by customizing a dedicated MR system architecture that enables "Multiple Instantaneous Switching between Scans" (or MISS), which then allows for interleaved SENC+Cine acquisitions within the same BH (Fig 1).

Eight healthy volunteers were imaged on a 1.5T system (Philips Achieva) using a 5-channel cardiac array. For the cine-CMR approach, the scan parameters were as follows: TR=2.2-2.4ms; TE=1.1-1.2ms; FA=60°; 300-340x300-340mm^2, resolution 1.1-1.3x1.1-1.3mm^2, slice thickness=6mm; sensitivity encoding (R=2). SENC employed the following parameters: TR=13ms; TE=0.7ms; FA=30°; 256x256mm^2; thickness=10mm; with 24ms SENC magnetization preparation prior to continuous acquisition of 40ms (3 spiral interleaves) per temporal frame over 1R-R.

In all subjects, the protocol consisted of acquiring 2-chamber, 4-chamber, and 3-chamber long-axis slices, and basal, mid, and apical short-axis slices (n=6 slices per case; SENC=1R-R; Cine(long-axis)=4R-R; Cine(short-axis)=3R-R per slice). Total hardware preparation and acquisition times were measured. The extent of required cross-registration steps was also evaluated.

Results: All combined Cine+SENC approaches were acquired successfully, resulting in half as many BHs from n=8 (4xCine+4xSENC) to n=4 combined BHs. The prep times per BH doubled due to the simultaneous mounting of both Cine and SENC scans. Each pair of Cine+SENC long-axis planes were acquired in a fixed, single 5-6R-R breath-hold; The 3-slice short-axis Cine+SENC scan was acquired in a single 12-15R-R breath-hold. Fig 2 shows the Cine+SENC post-processing pipeline. Conventional cross-registration sub-steps were eliminated by the single-BH scheme. In all 48 acquired planes (n=8 per 2, 4, 3ch, and SA-base/mid/apex), no extensive registration beyond in-plane resolution and cardiac phase adjustments were required. All 48/48 BH-derived reconstructions (Cine+SENC-strain colormaps) were successful; (0% failure rate).

Conclusions: We demonstrate the feasibility of a combined single-BH acquisition of two CMR sequences that eliminated intra-BH motion and complex post-processing sub-steps that were prevalent in previous clinical evaluations. This acquisition approach provides a clinically translatable myocardial wall motion assessment that inherently compensates for intra-scan motion, and requires fewer breath-holds per exam.

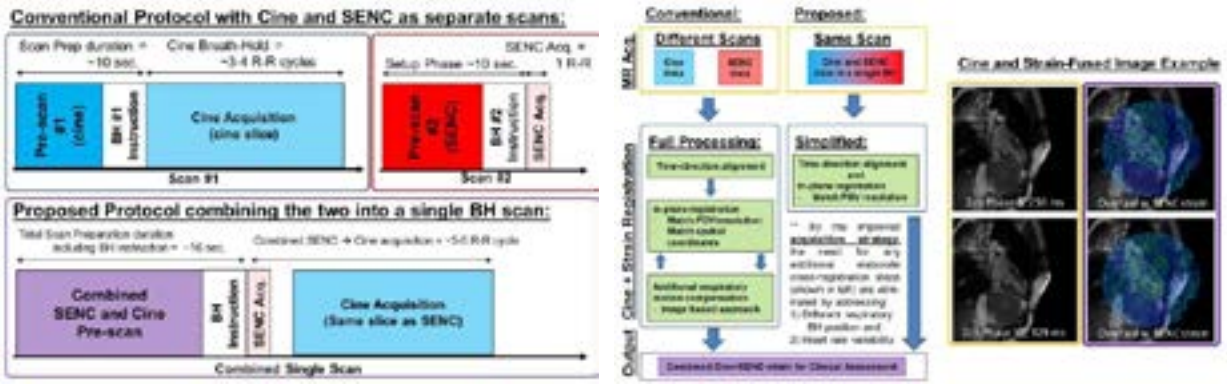

P330

Should we correct MAPSE for LV length when evaluating LV long axis function with CMR?

Stuart Moir, FRACP PhD[1] Thomas Treibel, MBBS.MRCP(UK)[2], Stefania Rosmini, MD, PhD[2], James Moon, MBBS, MD, MRCP[3]

1. *Monash Heart, Melbourne, Victoria, Australia*
2. *Barts Heart Centre, England, United Kingdom*
3. *Barts Heart Center, The Cardiovascular Magnetic Resonance Imaging Unit and The Center for Rare Cardiovascular Diseases Unit, St Bartholomew's Hospital, West Smithfield, London, UK, England, United Kingdom*

Background: CMR is the gold standard technique for evaluating left ventricular (LV) volume and ejection fraction (EF). Nevertheless significant myocardial dysfunction can be present in patients with normal EF. Echocardiographic studies evaluating mitral annular motion in a variety of cardiac pathologies have demonstrated abnormalities of LV long axis myocardial contraction before detectable changes in LV size or EF. Mitral annular plane systolic excursion (MAPSE) has been used with CMR to evaluate long axis function, but it reduces with age, as does myocardial length. We sought to identify whether correcting MAPSE for LV end diastolic length would therefore provide a more robust diagnostic measure.

Methods: 100 control subjects (aged 20-80) and 100 patients with cardiac pathology were studied including 30 with hypertrophic cardiomyopathy (HCM), 20 with cardiac amyloid and 50 with severe aortic stenosis (AS). MAPSE and LV end diastolic length (EDL) were measured in all subjects (see figure 1), and a corrected MAPSE was calculated (MAPSE/EDL). Parameters were evaluated in each decade for the controls. ROC curves were created to evauate MAPSE Vs corrected MAPSE for prediction of cardiac pathology.

Results: In normal controls there was a statistically significant reduction in both the MAPSE and the LV length with increasing age (by 17% AND 11% respectively between the third and 8th decades - see table 1). The MAPSE/EDL reduced by 7% between the third and 8th decades p=0.26. Both MAPSE and MAPSE/EDL were highly significantly reduced in cardiac pathology ($p < 0.001$ for all versus controls), with amyloid patients most profoundly affected (table 2) with no significant difference in MAPSE/EDL between AS and HCM patients (table 2). Compared with MAPSE alone, MAPSE/EDL led to a better differentiation between cardiac pathology and normality as evidenced by area under ROC curve of 0.94 Vs 0.90 (see figure 2).

Conclusions: Corrected MAPSE reduces with age in the normal population, but significantly less than MAPSE alone. Corrected MAPSE is markedly reduced in HCM, severe AS and amyloid patients and is a better discrinminator of cardiac pathology than MAPSE alone.

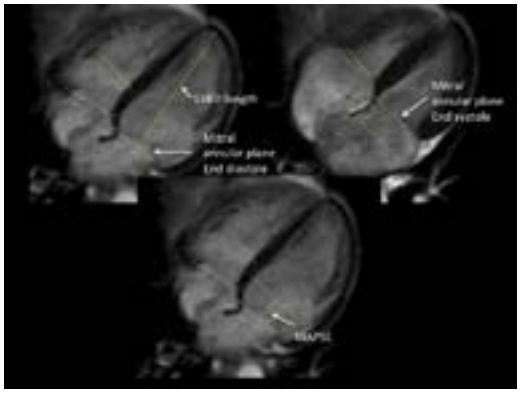

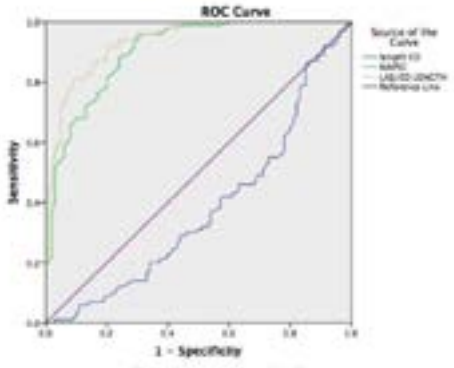

EDL, MAPSE and corrected MAPSE in normal controls with age

71-80	61-70	51-60	41-50	31-40	21-30	age
5	11	19	19	26	20	Number
87	88	89	91	93	98	EDL mm
12.3	12.8	13.0	13.6	14.7	14.8	MAPSE mm
14.1	14.6	14.7	15.0	15.8	15.2	cMAPSE %

cMAPSE %	MAPSE mm	EDL mm	
15.1 +- 2.1	13.9 +- 2.1	91.9 +- 8.4	controls
10.9 +- 2.5	10.8 +- 2.2	100.3 +- 11.7	HCM
10.5 +- 2.3	9.9 +- 2.1	94.9 +- 10.4	severe AS
6.8 +- 2.2	6.3 +- 1.9	93.9 +- 9.7	Amyloid

P331

Free-Breathing Whole-Heart T2* Cine Mapping at 3T

Jing Liu, Ph.D.[3]Li Feng, PhD[1], Yan Wang, PhD[2], David Saloner, Ph.D.[3], Karen Ordovas, MD, MAS[4]

1. *NYU School of Medicine, NY*
2. *University of California San Francisco, CA*
3. *University of California, San Francisco, CA*
4. *University of California San Francisco, San Francisco, CA*

Background: T2* mapping has been used for detecting iron overload in the myocardium. Given the difficulties of quantitative mapping in addition to those of cardiac MRI itself, T2* mapping of the whole heart, particularly 3D evaluation throughout the entire cardiac cycle, is very challenging and has rarely been reported. CIRcular Cartesian UnderSampling (CIRCUS) is a novel data acquisition strategy featuring variable-density randomization with flexible interleaving trajectories on a 3D Cartesian grid [1]. Combination of CIRCUS and multi-coil sparse reconstruction has been tested for highly-accelerated 3D cardiac cine imaging [2], DCE-MRI [3] and 4D flow [4]. In this study, we further extended the sequence to multi-echo data acquisition and investigated this in application to whole-heart cardiac T2* mapping throughout the entire cardiac cycle.

Methods: Free-breathing 3D multi-echo cardiac imaging was performed in a healthy volunteer on a 3T scanner (GE Medical Systems, Milwaukee, WI). Data acquisition took ~6 minute in a short-axis orientation with 10 echoes. Relevant imaging parameters included: TR/TE1/echo spacing=26/2.05/2.37ms, voxel size=1.3x1.8x5mm, matrix size=256x144x20, and the temporal resolution=78ms (3xTR). Retrospective cardiac and respiratory gating was performed based on synchronized ECG triggers and bellow gating signals. With 50% respiratory gating efficiency, the data were subsequently sorted into 13 cardiac phases, each with 10 echoes, resulting in an acceleration rate of R=8. Undersampled dataset was reconstructed using k-t SPARSE-SENSE [5,6], which exploits joint temporal sparsity constraint using a total variation (TV) along the cardiac dimension. In the current study, the same sampling pattern was applied through all echo times. 3D T2* mapping of the myocardium was derived by fitting the voxel-wise signals acquired at different echo times to the T2* decay curve. Averaged T2* values at end-systolic and end-diastolic phases were measured over selected ROIs on the ventricular spectrum at three center slices.

Results: Figure 1a&b show the reconstructed 3D cardiac images in three orthogonal views at the 1st and 10th echo times respectively, and Figure 1c shows the corresponding voxel-wise T2* maps derived by fitting data at different echo times. Averaged T2* values over ventricular spectrum were measured as 30.4 ± 4.6 ms at end-systolic phase and 32.2 ± 8.0 ms at end-diastolic phase, which are within the range of the normal myocardium T2* values that have been previously reported at 3T [7,8].

Conclusions: We have demonstrated the feasibility of whole-heart cardiac T2* cine mapping, which could be used to simultaneously assess cardiac function and myocardial diseases related to T2* changes.

References: 1. Liu J, et al. QIMS, 2014. **2.** Liu J, el al, ISMRM 2014, p429. **3**. Liu J, el al. NMR Biomed, 2016. **4.** Liu J, et al. ISMRM 2016, p458. **5.** Otazo R et al. MRM, 2010. **6**. Feng L et al, MRM, 2013. **7.** Storey P, et al. JMRI, 2007. **8.** Guo H el al. JMRI, 2009.

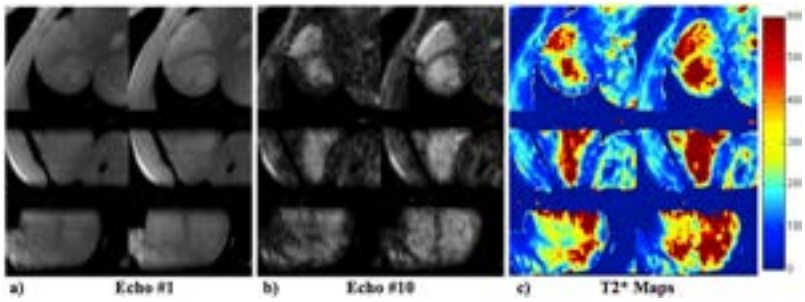

P332

Scan-Time Reduction by Improved Utilization of Idle Times by Permuting Pre-Scan Ordering: Feasibility Demonstration of a Single Breath-Hold Strain-Encoded CMR

Keigo Kawaji, Ph.D.[2]Noreen Nazir, MD[1], Amit R. Patel, MD[1], Akhil Narang, MD[1], Kohei Matsumoto, MA[2], Donel Tani, MS[3], Hui Wang, Ph.D.[4], Jouke Smink, MSc[5], Nael Osman, Ph.D.[3]

1. *University of Chicago, IL*
2. *University of Chicago, Chicago, IL*
3. *Myocardial Solutions, Inc., Morrisville, NC*
4. *Philips Healthcare, OH*
5. *Philips Healthcare, Noord-Brabant, Netherlands*

Background: In time-critical cardiac magnetic resonance (CMR) protocols such as stress-CMR, consecutive acquisition of successive long-axis and short-axis geometric planes without interruption from pre-scan preparations would be desirable. In this study, we propose an approach that permutes all the conventional pre-scan calibrations for all geometry-specific MR preparations into a single step, and allows for a single breath-held multi-planar acquisition of these planes in succession without interruption. This approach was incorporated into a single-shot Strain-ENCoded (SENC) CMR protocol to enable a single-breath-hold (BH) acquisition of 3x short- and 3x long-axis planes.

Methods: The proposed approach permuted the conventional ordering of pre-scan and scan phases for each singular geometric acquisition using a dedicated MR system architecture on the Philips MRI system; "Multiple Instantaneous Switching between Scans", or MISS. Figure 1 shows the schematics of the proposed approach. The SENC-stress CMR protocol employed following parameters: TR=13ms; TE=0.7ms; FA=30°; 256x256mm^2; slice thickness=10mm; 24ms SENC magnetization prep prior to continuous 40ms (3 spiral interleaves) temporal phase over 1R-R interval. This sequence was typically acquired in 3x long-axis (n=3BHs), and a 3-slice short axis views (n=1BH), and was combined into a single-BH scan. Seven healthy volunteers were imaged on a 1.5T system (Philips Achieva) using a 5-channel cardiac array with the proposed SENC protocol, which consisted of acquiring 6x slices that typically required 4 separate breath-holds. Both hardware preparation and acquisition time benchmarks were measured. These benchmarks were compared against the times from five clinical SENC-rest/stress protocols, each undergo 4x sets of 4-BH SENC-acquisitions per exam.

Results: All scans completed successfully. The combined SENC acquisition was successfully completed each within a single-BH duration of 8±1 seconds for subject heart beats 55-100 BPM. For high heart beat cases, 2R-R acquisition scheme was used to eliminate both cross-talk artifacts and previous SENC tag memory. The reference patient cohort from the 5 patients at 4x yielded an average time of 83±31 seconds (n=17 sets), which excluded three sets that required patient interaction/intervention that further prolonged these scan durations to 4, 4, and 7 minutes, respectively. Figure 2 summarizes the measured timing benchmarks.

Conclusions: We demonstrate the feasibility of reducing the total acquisition time from multiple scans by employing a new MR system architecture that allowed for simultaneous mounting of multiple sequences, and permuting these pre-scan ordering to all up front. This approach enabled an uninterrupted multi-planar acquisition that bypassed conventional pre-scan pauses, and was incorporated into a single-breath-hold SENC-strain CMR approach.

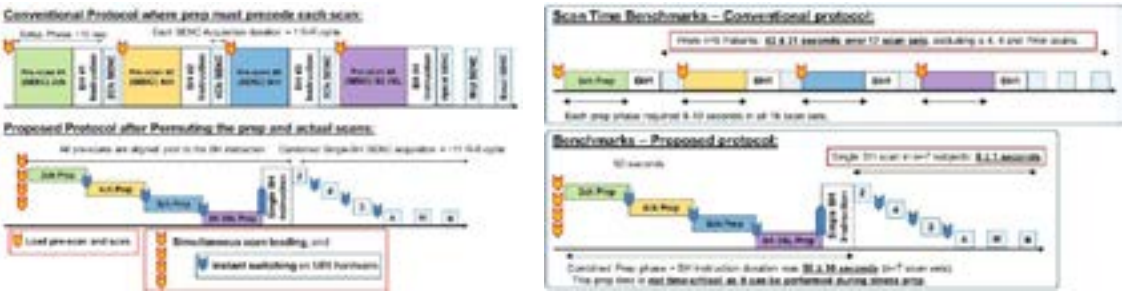

P333

Assessment of reverse remodeling predicted by myocardial deformation on feature tracking as new technique in the patients with severe aortic stenosis: Cardiac magnetic resonance imaging study

Hae jin Kim, Dr.[2]Sung Mok Kim[1], Ji-won Hwang[2], Sung-Ji Park[2], Sung-A Chang[2], Sang-Chol Lee[2], Yeon Hyeon Choe[2], Seung Woo Park[2]

1. Sa, N/A, Republic of Korea
2. Samsung Medical Center, N/A, Republic of Korea

Background: In severe aortic stenosis (AS), diffuse fibrosis in the myocardium is linked to clinical outcome and reverse remodeling. Myocardial deformation analysis as left ventricular strain has been used for analysis of myocardial viability and myocardial fibrosis. Recently, the novel technique of feature tracking (FT) with balanced steady-state free precession cine sequences was introduced, with which myocardial strain can be derived directly, and had advantages over traditional myocardial tagging. The aim of this study was that we could evaluate the correlation between reverse remodeling as outcome and left ventricular strain by cardiac magnetic resonance imaging (CMR) FT, and prediction of reverse remodeling by myocardial deformation in the patients with severe AS.

Methods: We enrolled 63 patients with severe AS, who performed both CMR and 2D echocardiography (ECHO) before surgical aortic valve replacement (AVR). CMR at 1.5T, including non-contrast T1 mapping, was carried out to define the amount of myocardial fibrosis. Cardiac Performance Analysis software was used to derive myocardial deformation as strain parameters from three short-axis cine view (balsa, mid and apical levels) and apical 2, 3, 4 chamber views. The primary outcome was the reverse remodeling, as the regression of left ventricular mass index (LVMI).

Results: Median follow-up was 28.77 months (interquartile range 11.27-38.33 months). The left ventricular ejection fraction by Simpson's method in ECHO was 60.8±7.3% (mean±SD) as normal range in all patients. There was a positive correlation between the amount of myocardial fibrosis determined by non-contrast T1 value and longitudinal strain ($r=0.460$, $p < 0.001$) and 3D longitudinal strain ($r=0.411$, $p < 0.001$) by CMR FT.As compared with LVMI between baseline and follow-up, the mass regression was significantly improved after AVR (baseline 145.09±42.46[g/m2] vs. follow-up 99.19±23.75[g/m2], $p < 0.001$). For correlation of reverse remodeling, good correlation by Pearson's correlation analysis was observed for the longitudinal strain ($r=0.413$, $p= < 0.001$), axial radial strain ($r=-0.371$, p=003), longitudinal radial strain ($r=-0.477$, $p < 0.001$), and circumferential strain ($r=0.336$, $p=0.007$). The value of area under the curves (AUC) for longitudinal strain by ECHO and CMR was compared to 0.604 and 0.736, therefore the longitudinal strain by CMR indicated more predicting reverse remodeling.

Conclusions: The longitudinal strain measured by CMR FT as new technique was correlated with reverse remodeling as the regression of LVMI. In the point of feasibility and simplicity as advantages, FT could be a promising method to assess strain and predict reverse remodeling in severe AS, especially in patients with suboptimal ECHO image quality.

http://www.ConferenceAbstracts.com/uploads/cfp2/attachments/LDFAIBDN/LDFAIBDN--219499-1-ANY.pdf

http://www.ConferenceAbstracts.com/uploads/cfp2/attachments/LDFAIBDN/LDFAIBDN--219499-2-ANY.pdf

http://www.ConferenceAbstracts.com/uploads/cfp2/attachments/LDFAIBDN/LDFAIBDN--219499-3-ANY.pdf

P334

Ventricular-arterial coupling in Patients with Bicuspid Aortic Valve

Julia Geiger, MD[1] Amir Ali Rahsepar, MD[2], Kenichiro Suwa, MD[3], Ahmadreza Ghasemiesfe, M.D[4], Alex Powell, MS[5], Alex J. Barker, PhD[5], Jeremy D. Collins, MD[6], James Carr, MD[6], Michael Markl, PhD[2]

1. *Department of Radiology, Northwestern University, Chicago, IL*
2. *Northwestern University, Chicago, IL*
3. *Northwestern University Feinberg School of Medicine Department of Radiology, IL*
4. *Yale affiliated Bridgeport Hospital, Milford, CT*
5. *Northwestern University Feinberg School of Medicine, Chicago, IL*
6. *Northwestern Memorial Hospital, Chicago, IL*

Background: Bicuspid aortic valve (BAV) affects 1-2% of the population and can result in severe complications such as aneurysms. Studies have shown that BAV morphology is associated with altered aortic hemodynamics (peak velocities, wall shear stress (WSS)). However, the impact of these changes on left ventricular (LV) loading and subsequent risk for LV remodeling (i.e. ventricular-arterial coupling) is poorly understood. Advances in CMR allow for the simultaneous assessment of cardiac function and vascular hemodynamics by cine-imaging and 4D flow MRI. In addition, T1 mapping techniques for calculation of the Gadolinium extracellular volume fraction (ECV) help to identify structural myocardial changes such as myocardial fibrosis. The aim of this study was to apply comprehensive cardiac and aortic MRI to test the hypothesis that BAV mediated changes in aortic hemodynamics are associated with parameters of LV remodeling.

Methods: With institutional IRB approval, 24 patients with BAV (age 50.6±13 years, table 1) underwent CMR including conventional SSFP-cine-imaging in the short axis for the assessment of volumetric data and myocardial mass (Circle 5.3, Canada) as well as pre- and post-contrast T1 mapping (Modified Look-Locker inversion recovery sequence (MOLLI), double dose Gadobutrol (Gadavist)) for assessment of ECV in the 16 segment AHA model in basal, mid-ventricular and apical short axis slices. In addition, 4D flow CMR (venc 250cm/s, resolution 2.2-2.8mm^3, temporal resolution 35-45ms) covering the thoracic aorta was acquired. The retrospective data analysis included 3D segmentation of the aorta (Mimics, Materialise, Leuven, Belgium) and quantification of peak systolic velocities and 3D WSS in the ascending aorta (AAo), arch, and descending aorta (DAo) (fig.).

Results: Ventricular-aortic analysis revealed significant relationships between increased myocardial mass and ECV (r=0.56, p=0.006), elevated peak systolic velocity (r=0.70, p=0.001) and WSS in the AAo (r=0.81, p=0.001). Global ECV(26.0±3.3%) and left ventricular function (EF=62±7%) were within the normal ranges. We observed a significant association between increased WSS in the AAo and elevated ECV (r=0.46, p=0.02). There was a trend towards an association between ECV and AAo peak systolic velocity (r=0.3, p=0.15) which, however, was not significant. In addition, we detected a relationship between ECV and aortic regurgitation (r=0.58, p=0.004).

Conclusions: The results of our study show that there is evidence for ventricular-arterial coupling in BAV patients with regard to relationships between increased myocardial mass, ECV, and alterations in WSS and peak systolic velocities in the AAo. A larger patient cohort could improve our understanding of the complex correlations between multiple factors in ventricular remodeling and the role of ECV in BAV patients with abnormal aortic hemodynamics but preserved ventricular function.

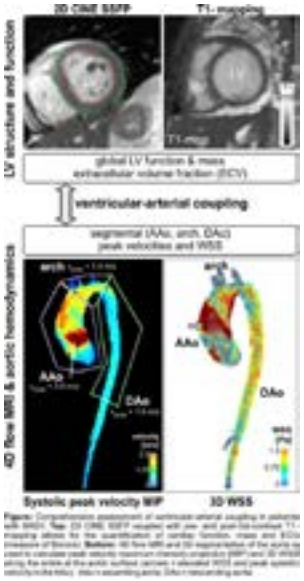

patient demographics

	Patient Characteristics
17 RL, 4 RN, 2 true, 1 type 2	BAV type (Sievers)
50.6 ± 13	age (years)
17male/7 female	gender
	Aorta & Valve Parameters
mild 2, moderate-severe 8	Aortic valve stenosis
3.58 ± 1.82	Aortic valve area (cm^2)
mild 7, moderate-severe 7	Aortic regurgitation
4.0 ± 0.7	Diameter in mid ascending aorta (cm)
	Peak systolic velocity (m/s)
2.65 ± 1.21	AAo
1.37 ± 0.45	arch
1.29 ± 0.28	DAo
	Peak systolic WSS (N/m^2)
0.76 ± 0.23	AAo
0.67 ± 0.16	arch
0.72 ± 0.16	DAo
	Cardiac Function and ECV
26.03 ± 3.3	ECV (%)
89.4 ± 34.1	EDVI (ml/m^2)
36.4 ± 20.5	ESVI (ml/m^2)
52.9 ± 16.7	SVI (ml/m^2)
56.5 ± 16.6	Myocardial mass (g/m^2)
62 ± 7	EF (%)
7.0 ± 2.1	CO (L/min)

Table 1: Patient demographics, aorta and valve parameters, cardiac function and ECV for all n=24 BAV patients. AAo = ascending aorta, DAo = descending aorta, EDVI = end-diastolic volume indexed to BSA, EDVI = end-systolic volume indexed to BSA, SVI = stroke volume indexed to BSA, EF = ejection fraction, CO = cardiac output.

patient demographics

	Patient Characteristics
17 RL, 4 RN, 2 true, 1 type 2	BAV type (Sievers)
50.6 ± 13	age (years)
17male/7 female	gender
	Aorta & Valve Parameters
mild 2, moderate-severe 8	Aortic valve stenosis
3.58 ± 1.82	Aortic valve area (cm^2)
mild 7, moderate-severe 7	Aortic regurgitation
4.0 ± 0.7	Diameter in mid ascending aorta (cm)
	Peak systolic velocity (m/s)
2.65 ± 1.21	AAo
1.37 ± 0.45	arch
1.29 ± 0.28	DAo
	Peak systolic WSS (N/m^2)
0.76 ± 0.23	AAo
0.67 ± 0.16	arch
0.72 ± 0.16	DAo
	Cardiac Function and ECV
26.03 ± 3.3	ECV (%)
89.4 ± 34.1	EDVI (ml/m^2)
36.4 ± 20.5	ESVI (ml/m^2)
52.9 ± 16.7	SVI (ml/m^2)
56.5 ± 16.6	Myocardial mass (g/m^2)
62 ± 7	EF (%)
7.0 ± 2.1	CO (L/min)

P335

Myocardial Deformation Properties in Patients with Isolated Bicuspid Aortic Valve Disease: a Tissue-Tracking Magnetic Resonance Study

Gaetano Nucifora, MD, PhD[1]Jamie Miller, BMs[2], Carl Gillebert, MD[3], Ranjit Shah, MBBS, FRACP[4], Cherie Raven, MRS[3], Majo Joseph, MBBS[3], Joseph Selvanayagam, FRACP, DPhil[2]

1. *South Australian Health and Medical Research Institute, Adelaide, SA, Australia, Darlington, South Australia, Australia*
2. *Flinders University, Adelaide, SA, Australia, South Australia, Australia*
3. *Flinders Medical Centre, Adelaide, SA, Australia, South Australia, Australia*
4. *South Australian Health and Medical Research Institute, Adelaide, SA, Australia, Prospect, South Australia, Australia*

Background: Patients with bicuspid aortic valve (BAV) disease are known to have associated ascending aorta remodelling abnormalities; whether this abnormal remodelling process also extends to the left ventricle (LV) in such patients is controversial. The aim of this study is to assess the LV systolic and diastolic myocardial mechanics in isolated BAV patients with normal ejection fractions (EF) using tissue-tracking cardiac magnetic resonance (CMR) imaging, which allows LV strain to be measured directly from cine images with good accuracy and reproducibility.

Methods: A total of22 consecutive patients (mean age 38±14, 9 males) with normofunctional BAV (i.e. without stenosis or regurgitation), and normal LV ejection fraction (i.e. >55%) and without coarctation of the aorta and ascending aorta dilatation at trans-thoracic echocardiography were recruited for CMR imaging. 17 age and gender matched control subjects (i.e. without structural heart disease and no history of hypertension, diabetes mellitus, or any other systemic disease were also included in the study. CMR imaging was performed to evaluate LV function and LV mass index. Tissue-tracking analysis (CVI^{42}, Circle Cardiovascular Imaging, Calgary, Canada) was applied to LV long-axis and LV short-axis images to assess global LV systolic longitudinal (GLS) and circumferential (GCS) strain and global LV diastolic longitudinal (GLSr) and circumferential (GCSr) strain rate.

Results: No significant difference was observed between BAV and control patients in terms of LV end-diastolic volume index (75±18 ml/m^2 vs. 78±11 ml/m^2, p = 0.54), LV ejection fraction (71±6% vs. 71±6%, p = 0.96), and LV mass index (46±12 g/m^2 vs. 42±7 g/m^2, p = 0.22). Tissue-tracking analysis however demonstrated that BAV patients had significant lower global LV systolic GLS (-19±2% vs. -21±2%, p = 0.019) and GCS (-21±3% vs. -23±3%, p = 0.010). Diastolic mechanical properties were significantly lower among BAV patients as well (GLSr: 0.93±0.21%/sec vs. 1.24±0.22%/sec, p < 0.001; GCSr: 1.26±0.38%/sec vs. 1.60±0.38%/sec, p = 0.010).

Conclusions: Systolic and diastolic LV myocardial deformation properties are significantly impaired among BAV patients, even if the aortic valve is normofunctional, the LV ejection fraction is normal and the ascending aorta is not dilated. Further studies with long-term clinical follow-up are required to determine whether these mild abnormalities in LV strain parameters also confer prognostic information in this patient population.

P336

Off-resonance error following aortic valve replacement: the effect on myocardial T1.

Paul Scully, MBBS MRes[1] Thomas Treibel, MBBS.MRCP(UK)[2], Anish Bhuva, MRCP MBBS[2], Camilla Torlasco, MD[3], Andrew D'Silva, MRCP[4], Charlotte Manisty, PhD MBBS[5], Peter Kellman, PhD[6], James C Moon, MD[2]

1. *Barts Heart Centre, London, England, United Kingdom*
2. *Barts Heart Centre, England, United Kingdom*
3. *Barts Heart Center. St Bartholomew's Hospital, West Smithfield, London, EC1A 7BE, England, United Kingdom*
4. *Cardiovascular Sciences Research Centre, St. George's, University of London, London, United Kingdom, London, England, United Kingdom*
5. *Barts Heart Centre and university college, London, England, United Kingdom*
6. *Laboratory of Cardiac Energetics, National Institutes of Health/NHLBI, Bethesda, MD, United States., MD*

Background: T1 mapping is an emerging imaging biomarker of myocardial fibrosis. Implantation of sternal wires and valve prostheses may introduce error into measured T1 due to significant off-resonance. The off-resonance effecting T1 can be quantified using field maps and T1 error extrapolated in turn (the T1 error at 1000ms with an off-resonance of 50Hz is 10ms, whereas at 100Hz this rises to 50ms). We used field maps to assess whether there is a clinically significant impact on T1 values in the presence of an aortic valve replacement (AVR).

Methods: Shimmed native T1 maps (MOLLI) and paired single breath-hold ECG-gated field maps were acquired at 1.5T in 30 healthy volunteers (age 30±3 years), and 31 patients with aortic valve replacements (age 69±8 years; 14 metallic; 17 tissue). T1 values and frequency shifts were measured segmentally in the basal, mid and apical myocardial short axis in patients after AVR, and in the mid myocardial short axis in the healthy volunteers.

Results: There was no difference in maximum segmental off-resonance in patients post AVR versus healthy volunteers (48±16Hz vs 43±17Hz respectively, p=0.6). There was no gradient from basal to apical short axis slice off-resonance (38±16Hz vs 42±17Hz vs 42±15Hz, p>0.1). Furthermore, there was no subgroup difference between mechanical or tissue AVR and controls (p=0.7 and 0.6 respectively). Applying a simulated error correction for T1 to this cohort, this equated overall to an average maximum change in T1 of 9±8ms in the patients post-AVR and 8±7ms in healthy volunteers (p=0.6).

Conclusions: Aortic valve prostheses and sternal wires do not cause significant off-resonance artefact in T1 mapping.

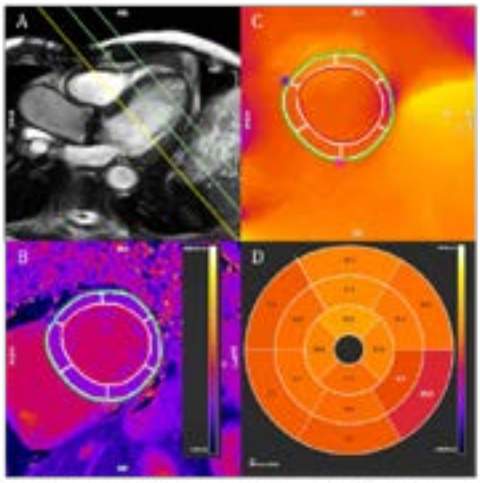

P337

Use of novel, SSFP cine-based tissue-tracking to assess myocardial strain in aortic stenosis

Daniel Swarbrick, MBBS, BMedSci[1], Aaron Long, BSc Science[5]Abtehale Al-hussaini, MBBS,BSC, MRCP.[2], Jayanth Arnold, MBBS[3], Gaurav S. Gulsin, MBChB(Hons) MRCP(UK)[4], Gerry P. McCann, MBChB, MD[6]

1. *University of Leicester, Leicester, England, United Kingdom*
2. *Cardiovascular Sciences, Glenfield Hospital, University Hospitals of Leicester NHS Trust, Leicester United Kingdom, Leicester, England, United Kingdom*
3. *The University of Leicester, England, United Kingdom*
4. *The University of Leicester, Nottingham, England, United Kingdom*
5. *University of Coventry and Warwickshire, Oxford, England, United Kingdom*
6. *The University of Leicester, Leicester, United Kingdom, Leicester, England, United Kingdom*

Background: In aortic stenosis, abnormalities in strain parameters manifest early in the disease process, and also have prognostic value. There are several methods for assessing myocardial strain with magnetic resonance imaging, Most of these however need the acquisition of additional sequences, and often time consuming post processing, which have limited the uptake of these methods outside of a research setting.

Recently, the novel post-processing technique of tissue tracking has been developed, that can utilise standard balanced steady state free precession (SSFP) cine images of the left ventricle to measure strain. We sought to assess firstly, if tissue tracking could reliably detect changes in circumferential and longitudinal strain in patients with severe aortic stenosis, with or without symptoms, compared to both young and age matched controls. Secondly, we evaluated whether these changes resolved following aortic valve surgery.

Methods: A total of 74 patients, with a spectrum of LV pressure overload including young healthy controls, older controls and both asymptomatic and symptomatic severe aortic stenosis (AS), underwent cardiac MRI scanning, including steady state free precession (SSFP) cine imaging. Tissue tracking analysis was performed on the cine images, and circumferential and longitudinal systolic and diastolic strain parameters were derived. In addition, the same measurements were performed in the studies with symptomatic aortic stenosis 6 months following aortic valve replacement (AVR).

Results: Tissue tracking was able to demonstrate a reduction in both longitudinal and circumferential systolic strain in symptomatic AS compared to asymptomatic AS (-19.1 ± 3.7% vs -14.1 ± 5.7, $p < 0.001$ and -23.5 ± 3.8 vs -19.7 ± 4.3, $p < 0.005$). In contrast, circumferential strain in asymptomatic AS was signficantly higher than young controls (- 23.5 ± 3.8 vs -18.96 ± 2.8%, $p < 0.05$).

Tissue tracking also demonstrated significant improvement in circumferential peak systolic strain (-19.7 ± 4.3 vs -21.6 ± 2.9, $p < 0.05$) and peak early diastolic strain rate (0.97 ± 0.38 vs 1.14 ± 0.35, $p < 0.05$) following AVR.

Conclusions: Tissue tracking can successfully demonstrate differences in both systolic and diastolic strain rate parameters between different a spectrum of left ventricular pressure overload, as well as reveal changes in the same population before and after AVR. This suggests it may have utility as an easily performed and accessible tool for the assessment of myocardial strain

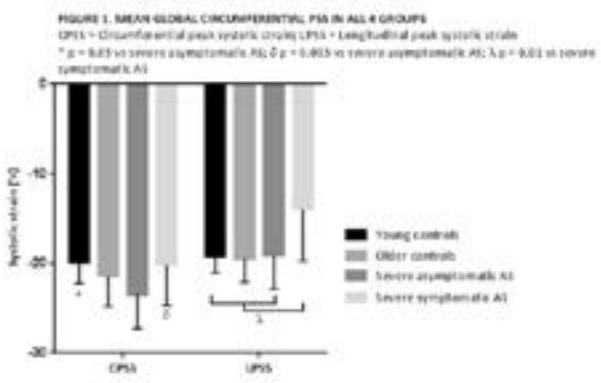

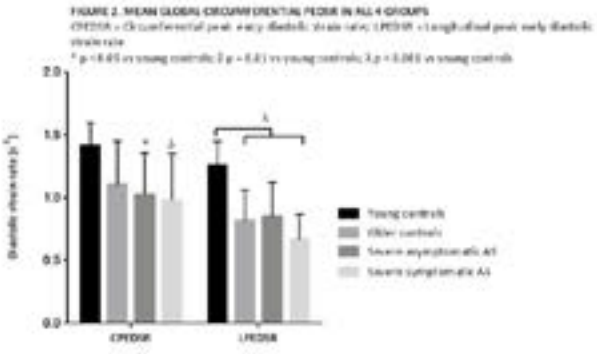

P338

Evolution of myocardial relaxation times with 3D-QALAS in aortic stenosis patients: before, 3- and 12- months after aortic valve replacement

Sofia Kvernby, MSc[1]Mattias Rönnerfalk, MD[1], Marcel Warntjes, PhD[2], Carl-Johan G. Carlhäll, MD, PhD[3], Éva Tamás, MD, PhD[4], Jan E. Engvall, MD, PhD[5], Tino Ebbers, PhD[5]

1. *Linköping University, Ostergotlands Lan, Sweden*
2. *IMH, Linköping University Hospital, Linköping, Ostergotlands Lan, Sweden*
3. *Linköping university, Ostergotlands Lan, Sweden*
4. *Linköping University, N/A, Sweden*
5. *Linkoping University, Linkoping, Ostergotlands Lan, Sweden*

Background: Severe aortic valve stenosis is associated with increased diffuse myocardial fibrosis (DMF). Previous studies have demonstrated correlations between DMF and elevated native T1 relaxation time (Dass et al, Circ Cardiovasc Imag, 2012) together with shortened contrast enhanced T1 relaxation time (Iles et al, J Am Coll Cardiol, 2008). Furthermore, myocardial fibrosis has been correlated to shortened T2 relaxation times in animal studies (Bun et al, Invest Radiol, 2012). To our knowledge, the relative change in T1 and T2 has not been investigated for human myocardial tissue post aortic valve replacement. The purpose of this study was to investigate whether myocardial relaxation times (T1 and T2), which might be an indicator of DMF, in patients with severe aortic valve stenosis alter over time, from pre-surgery to 12 months after aortic valve replacement.

Methods: Eighteen patients with severe aortic stenosis referred for surgical aortic valve replacement were included in this pilot study. Quantitative CMR scans were performed at baseline (prior to), 3 months and 12 months post surgery. The CMR scans included one 3D-QALAS acquisition pre contrast and one 3D-QALAS acquisition post injection of Gd-based contrast agents. The 3D-QALAS method [Kvernby et al, JCMR 2014] provides full coverage of the LV myocardium with simultaneous three-dimensional quantification of T1- and T2 relaxation times in one breath hold. Data from each patient were analyzed in 16 segments. Pairwise comparisons of segmental relaxation times between the three different time points were made to characterize tissue changes with respect to T1 and T2 over time after surgery.

Results: For native data, the T1 relaxation times were significantly shorter at 12 months post surgery than at baseline (figure 1). The T2 relaxation times were significantly longer at 3 and 12 months post surgery than at baseline. These native results might be interpreted as a recovery of myocardial tissue over time. T1 relaxation times in contrast enhanced tissue were significantly shorter at 3 months compared to baseline and significantly longer at 12 months compared to 3 months. No difference was found between baseline and 12 months follow up. This greater enhancement of contrast at 3 months after surgery might reflect the initial reversal of myocyte hypertrophy, subsequently leading to increased relative concentrations of DMF at this point.

Conclusions: Myocardial relaxation times with 3D-QALAS, native T1 and T2 together with contrast enhanced T1, in patients with severe aortic valve stenosis alter over time, from pre-surgery to 12 months post aortic valve replacement.

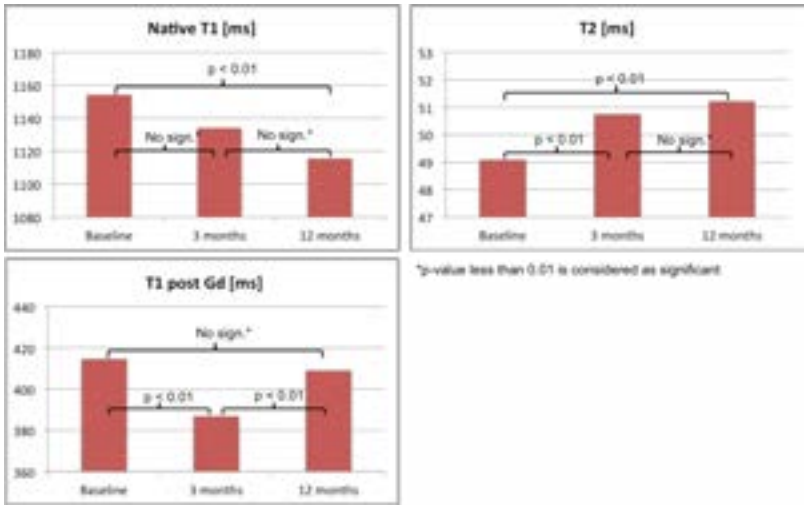

P339

Microscopic myocardial scarring is present in patients with Bicuspid Aortic Valves with preserved systolic function

Amir Ali Rahsepar, MD[1]Kenichiro Suwa, MD[2], Ahmadreza Ghasemiesfe, M.D[3], Julia Geiger, MD[4], Alex J. Barker, PhD[5], Jeremy D. Collins, MD[6], Michael Markl, PhD[1], James Carr, MD[6]

1. *Northwestern University, Chicago, IL*
2. *Northwestern University Feinberg School of Medicine Department of Radiology, IL*
3. *Yale affiliated Bridgeport Hospital, Milford, CT*
4. *Department of Radiology, Northwestern University, Chicago, IL*
5. *Northwestern University Feinberg School of Medicine, Chicago, IL*
6. *Northwestern Memorial Hospital, Chicago, IL*

Background: Cardiac magnetic resonance imaging (CMR) is commonly performed in patients with bicuspid aortic valve (BAV) for evaluation of aortic dimensions and valvular function. Several echocardiographic studies have reported evidence of subclinical systolic and diastolic dysfunction in patients with congenital BAV. Recent advances in myocardial MR imaging has enabled us to measure pre- and post-contrast T1 mapping to calculate the Gadolinium extracellular volume fraction (ECV) as a measure of myocardial fibrosis. We aimed to investigate if there is any increase in ECV values in BAV patients with normal ejection fraction (EF) compared to patients with trileaflet aortic valve (TAV).

Methods: IRB-approved retrospective evaluation of 162 patients with LVEF≥40%, including 108 BAV (70% male, 51.3±15.6 years) and 54 TAV patients with aortic aneurysm (80% male, 56.8±15.7, $p < 0.05$) who were referred for evaluation of aortic dimensions and valvular function were retrospectively studied. The LV size, mass, and ejection fraction were measured on commercially available software (Circle 5.3, Canada). T1 mapping was performed pre-contrast and at 12-20 minutes post-injection of Gadobutrol (0.2 mmol/kg body weight) using a modified Look-Locker inversion recovery (MOLLI) sequence in three short axis slices at basal, mid-ventricular and apical levels at either 1.5 or 3T (Avanto or Skyra, Siemens Medical Systems, Erlangen, Germany). The ECV was calculated using the 16-segment AHA model using a laboratory hematocrit obtained before the exam.

Results: BAV patients had significantly higher native T1 and ECV values compared to TAV patients (ECV: 26.1±4.7 vs. 24.3±2.3, $p=0.02$) (Table). When only those patients without any aortic stenosis or regurgitation were included, no significant differences were found for myocardial mass, LVESV, or LVEDV between groups ($p>0.05$); however, the statistically significant differences in ECV remained (ECV: 26.3±5.6 vs. 24.3±2.4, $p=0.04$). In addition, ECV was significantly associated with an increase in ESV and EDV ($p=0.03$), while this association were not observed in TAV patients. No differences in ECV were observed by severity of aortic stenosis, regurgitation or BAV morphology ($p>0.05$). Although TAV patients were older, multiple linear regression did not show any significant association between age and ECV values ($p>0.05$).

Conclusions: Our results indicate that BAV patients with preserved systolic function have an increased ECV, a measure of myocardial fibrosis, compared with TAV patients. Elevated ECV values were independent of severity of aortic stenosis, regurgitation and type of BAV. The association between ECV and increased volumes in these patients may indicate initiation of changes in cardiac structure in these patients.

Extracellular volume fraction and native T1 values between different groups of patients.

TAV	BAV		
24.3±2.3	26.1±4.7*	ECV %	
962.6 ± 87	1010.7 ± 47.5*	1.5-T	Native T1 (ms)
1247.8 ± 9.6	1249.9 ± 44.8*	3-T	
1 (2%)	8 (7%)	Mild	AS
0 (0%)	9 (8%)	Moderate	
0 (0%)	8 (7%)	Severe	
19 (35%)	32 (30%)	Mild	AR
1 (2%)	19 (17.6%)	Moderate	
0 (0%)	3 (2.7%)	Severe	
ECV: Extracellular volume fraction, AS: Aortic Stenosis, AR: Aortic regurgitation.			

Correlation between ECV and Left Ventricular Volumes in different groups of patients.

TAV		BAV		
r= -0.036	69 ± 9.4	r=0.380	77.1 ± 26	EDVI (ml/m^2)
p= 0.872		p=0.007**		
r= -0.025	27.8 ± 5.8	r=0.373	28.7 ± 12.1	ESVI (ml/m^2)
p= 0.913		p=0.008**		
r= -0.069	41.2 ± 7.1	r=0.346	48.35 ± 15.4	SVI (ml/m^2)
p= 0.760		p=0.014*		
r= -0.058	60 ± 7	r= -0.062	63 ± 7	EF %
p=0.798		p=0.668		
r=-0.552	5.5 ± 1.2	r= 0.165	6.1 ± 2	CO (L/min)
p=0.004**		p=0.252		

There was no significant difference between volumes in BAV patients vs. TAV patients. BAV: bicuspid aortic valve, TAV: Trileaflet Aortic valve, EDVI: End-diastolic volume index, ESVI: End-systolic volume index, SVI: Stroke volume index, EF: Ejection fraction, CO: Cardiac output. *, and ** mean $p<0.05$, and $p<0.01$.

P340

Assessment of left ventricular shape and remodelling pattern in severe aortic stenosis before and after aortic valve replacement

Masliza Mahmod, MBChB, DPhil[1] Ernesto Zacur, PhD[2], Michelle D'souza[1], Jane M. Francis, DCR(R) DNM[3], Rina Ariga, MBBS, MRCP[1], Betty Raman, MBBS, FRACP[4], Sairia Dass, MRCP, DPhil[1], Saul Myerson, MD, FRCP[5], Theodoros Karamitsos, MD, PhD[6], Stefan Neubauer, MD, FRCP[1], Pablo Lamata, PhD, MSc[7]

1. *University of Oxford, England, United Kingdom*
2. *University of Oxford, Oxford, England, United Kingdom*
3. *University of Oxford, OX39DU, England, United Kingdom*
4. *University of Oxford, Division of Cardiovascular Medicine, Oxfordshire, England, United Kingdom*
5. *NA, Oxford, England, United Kingdom*
6. *NA, Thessaloniki, Greece*
7. *King's College of London, England, United Kingdom*

Background: In aortic valve stenosis (AS), left ventricular (LV) remodelling serves to normalise LV wall stress and maintain oxygen demand. However, LV remodelling carries significant adverse cardiovascular risks and reversal of this process is accompanied by improvement in outcome. While both the extent and regression of LV hypertrophy (LVH) can be measured by cardiovascular magnetic resonance imaging (CMR), the comprehensive 3D pattern of LV remodelling in severe AS has never been examined previously. We aimed to determine the detailed morphology of LV in severe AS before and after aortic replacement (AVR) using advanced computational anatomy tools.

Methods: 30 patients with severe AS, normal LV systolic function and no obstructive coronaries, and 27 age, gender and body mass index matched controls underwent cine CMR imaging. 18 AS patients had a repeat CMR eight months post AVR. Assessments included LV mass index (LVMI), wall thickness, systolic function, and the shape coefficients obtained from a statistical shape model built from the 75 anatomies. This model was obtained with a principal component analysis of the reconstructed 3D meshes from the myocardial contours of the images.

Results: Compared to controls, patients with severe AS had significantly increased LV wall thickness (16±3mm vs 9±1mm, $p < 0.05$) and LVMI (98±33kg/m^2 vs 53±13 kg/m^2, $p < 0.05$). LV systolic function was similar in both groups. Shape analysis confirmed that severe AS was associated with thicker and larger LV, and further revealed a shift in the LV orientation (Figure 1A-B). Post AVR, there was partial LVMI & wall thickening reduction. However there was also significant differences ($p < 0.01$) in the shape coefficients that revealed more spherical LV shape and irreversible shift in the LV orientation (Figure 1A-B). Furthermore there was focal dilatation seen in the postero-septal wall near the valve region which is most likely related to surgery (Figure 1C).

Conclusions: This study provides novel insight into characteristics of LV remodelling in AS and the effect of AVR. The novel shape metrics that comprehensively quantify the morphology of the LV may be a potential marker for risk stratification in the management of AS.

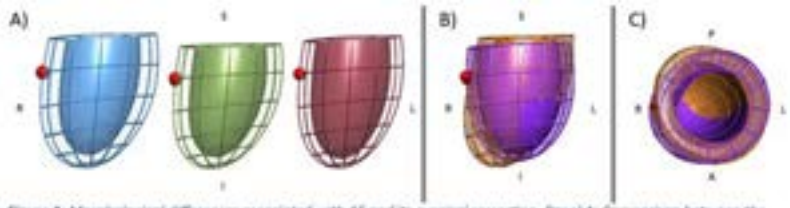

Figure 1. Morphological differences associated with AS and its surgical correction. Panel A: Comparison between the average anatomy of severe AS before AVR (blue), 8 months after AVR (green) and controls (red). The red sphere indicates the location of the right ventricle. Panel B: Overlay of two shapes illustrating the change of axis of inertia caused by AS (orange represents an AS patient before AVR, and purple represents a healthy control). Panel C: Overlay of two shapes illustrating focal dilatation in the postero-septal region post AVR (orange represents an AS patient after AVR and purple represents a healthy control).

P341

Novel ways to characterize systolic and diastolic function in severe aortic stenosis using left atrial CMR feature tracking

Bettina Baeßler, M.D.[1]Ana Fehrmann[1], Melanie Treutlein[1], Daniel Giese, PhD[1], Alexander Bunck, M.D.[1], Kilian Weiss, PhD[2], Tanja Rudolph, M.D.[3], Volker Rudolph, M.D.[3], David Maintz, M.D.[1]

1. *University Hospital of Cologne, Department of Radiology, Nordrhein-Westfalen, Germany*
2. *Philips GmbH, Nordrhein-Westfalen, Germany*
3. *University Hospital of Cologne, Department III of Internal Medicine, Heart Center, Nordrhein-Westfalen, Germany*

Background: Severe aortic stenosis (AS) leads to the development of left ventricular (LV) hypertrophy and to consecutive alterations of passive elastic properties, which are known to be a predisposing factor for diastolic dysfunction. In the present study, we aimed at characterizing LV systolic and diastolic function in patients with severe AS using LA CMR feature tracking (FT) in order to evaluate the potential of LA strain analysis for a more sensitive detection of altered myocardial function.

Methods: 20 patients with severe AS and 15 age-matched healthy controls underwent a CMR examination on a clinical 3T scanner. The CMR protocol included cine images in a short-axis stack covering the LV and in two long axes (2- and 4-chamber views). Standard functional analysis was performed using a dedicated post-processing platform. Analysis of longitudinal strain and strain rate (SR) of the left atrium (LA) was performed on the 2- and 4-chamber views using a dedicated FT-software (TOMTEC). LA performance was analyzed including reservoir function (total strain [ε_s], peak positive SR [SR_s]), conduit function (passive strain [ε_e], peak early negative SR [SR_e]) and booster pump function (active strain [ε_a], late peak negative SR [SR_a]).

Results: LV ejection fraction (LV-EF) reflecting LV systolic function was not significantly different between AS patients and controls (67 ± 18 vs. 73 ± 5 %, p=.323; Figure 1), and only two AS patients demonstrated a reduced LV-EF < 50 %. In contrast, LA reservoir function was significantly impaired in AS patients (ε_s: 27.7 ± 10.8 vs. 47.3 ± 10.9 %; ps: 1.1 ± 0.4 vs. 1.6 ± 0.4 s^{-1}, p < .001), showing a moderate correlation to LV-EF (r=0.49). LV peak filling rate (LV-PFR) reflecting LV diastolic function was significantly impaired in AS patients when compared to controls (0.12 ± 0.05 vs. 0.17 ± 0.04 ml/ms*m², p=.021). In addition, LA strain parameters reflecting atrial conduit function were significantly impaired in AS patients (ε_e: 12.2 ± 5.7 vs. 25.7 ± 6.3 %, pe: -0.6 ± 0.2 vs. -1.3 ± 0.3 s^{-1}, p< .001) and were highly correlated to LV-PFR (r=0.69). In multiple logistic regression analysis, SR_e proved to be the best parameter in order to differentiate between the two groups, and 14 out of 15 patients demonstrated an $SR_e \geq 0.9$ s^{-1} (none of the controls; sensitivity 93%, specificity 100%). In contrast, LV-PFR did not allow such a clear separation of the two groups on a per-patient level (sensitivity 67%, specificity 85%).

Conclusions: LA strain parameters reflect LV systolic and diastolic properties and might be more sensitive parameters for the evaluation of LV systolic and diastolic function when compared to LV-EF or LV-PFR. Especially LA SR_e might represent a surrogate parameter for LV diastolic function and should be further evaluated in future studies.

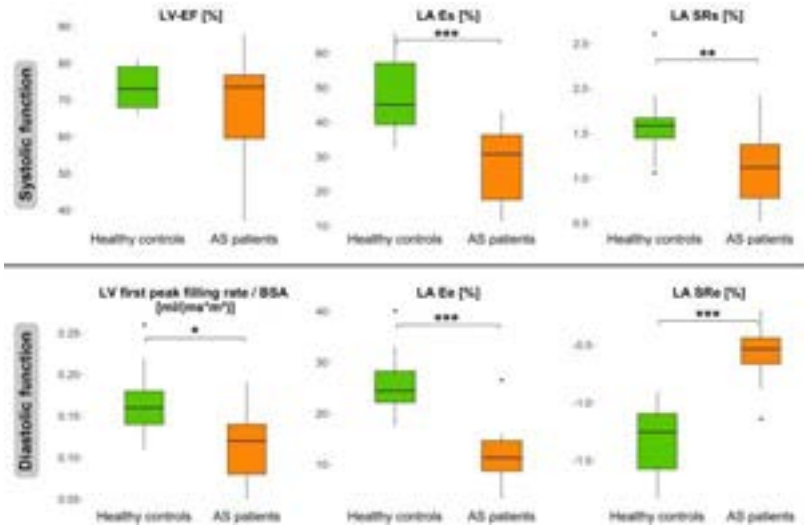

P342

Can blood biomarkers substitude ECV for estimation of diffuse fibrosis?

Vass Vassiliou, MA, MD[1]Katharina Wassilew, MD DScmed[2], Peter D. Gatehouse, PhD[3], Shivraman Giri, PhD[4], Ololade Adeyemi, BSc[5], Claire E. Raphael, PhD[6], Dudley J. Pennell, MD[7], Sanjay Prasad, MD[7]

1. *Royal Brompton, London, England, United Kingdom*
2. *Blegdamsvej 9 2100 Copenhagen Denmark, Copenhagen, Hovedstaden, Denmark*
3. *NIHR Cardiovascular Biomedical Research Unit, Royal Brompton Hospital, London, England, United Kingdom*
4. *Siemens Healthcare, IL*
5. *Royal Brompton & Harefield NHS Foundation Trust, Kent, England, United Kingdom*
6. *Royal Brompton Hospital, England, United Kingdom*
7. *Royal Brompton Hospital and Imperial College, London, England, United Kingdom*

Background: Cardiovascular magnetic resonance (CMR) can provide an accurate estimation of diffuse ventricular fibrosis using T1 mapping sequences. This however, requires availability of cardiac enabled MRI scanners which might not be widely available. We investigated 15 blood biomarkers and their ability to correlate with histologically identified fibrosis.

Methods: An initial pilot study of ten patients with aortic stenosis had analysis of 15 blood biomarkers, imaging CMR parameters including ECV quantification using an 11 heart beat MOLLI on a 1.5T Siemens Avanto and intraoperative biopsy for quantification of diffuse fibrosis. All had undergone the CMR and 15 biomarker analysis prior to the surgery. The intraclass correlation (ICC) was calculated between the histological fibrosis, all the biomarkers and ECV.

Results: Multiple candidate blood biomarkers including highly sensitive troponin, NT Pro-BNP, ST2, Galectin 3, MMP9, MMP 12 and TIMP4 failed to show a correlation with histological fibrosis, table 1. Only osteoprotegerin showed a trend towards good correlation with histological fibrosis (ICC=0.477, p=0.174) but this did not reach significance. ECV showed excellent correlation with diffuse fibrosis (ICC=0.874, p=0.002). No other imaging biomarker (ejection fraction, left atrial volume, left ventricular function correlated with diffuse fibrosis).

Conclusions: ECV shows excellent correlation with histological fibrosis and can provide an accurate non-invasive method for quantification of fibrosis. No other clinical, imaging or blood biomarker showed good correlation. A larger study is required to confirm these findings. At present however, this work would suggest that a single blood biomarker is unlikely to correlate with histological fibrosis and ECV appears to be the only accurate non-invasive method for estimating diffuse fibrosis.

Funding: Rosetrees Trust and NIHR BRU Royal Brompton and Harefield NHS Trust and Imperial College London

http://www.ConferenceAbstracts.com/uploads/cfp2/attachments/LDFAIBDN/LDFAIBDN--222318-1-ANY(2).pdf

P343

Aortic Valve Stenosis and Regurgitation Does not Change Extra Cellular Volume Fraction in Bicuspid Aortic Valve

Kenichiro Suwa, MD[1]Amir Ali Rahsepar, MD[2], Ahmadreza Ghasemiesfe, M.D[3], Julia Geiger, MD[4], Alex J. Barker, PhD[5], Jeremy D. Collins, MD[6], Michael Markl, PhD[2], James Carr, MD[6]

1. *Northwestern University Feinberg School of Medicine Department of Radiology, IL*
2. *Northwestern University, Chicago, IL*
3. *Yale affiliated Bridgeport Hospital, Milford, CT*
4. *Department of Radiology, Northwestern University, Chicago, IL*
5. *Northwestern University Feinberg School of Medicine, Chicago, IL*
6. *Northwestern Memorial Hospital, Chicago, IL*

Background: Bicuspid aortic valve (BAV) often develops aortic valve stenosis (AS) and/or regurgitation (AR), which might cause left ventricular (LV) injury. However, the impact of BAV on ECG characteristics, LV mass and gadolinium extracellular volume fraction (ECV) in patients remains unclear. We hypothesized that Sokolow-Lyon voltage by ECG (an index of LVH and LV enlargement if greater than 3.5 mV), LV volume, LV mass and ECV can detect LV remodeling in BAV patients with AS or AR.The purpose of this study is to compare Sokolow-Lyon voltage, LV volume, LV mass and ECV between AS and AR and without AS/AR in BAV patients.

Methods: With institutional IRB approval, a total of 123 patients with BAV were retrospectively divided into those with moderate or severe AS without AR (n=13, 62±8 years, 77% men), those with moderate or severe AR without AS (n=15, 44±13 years, 84% men), and those with mild or less in AS and AR (no AS/AR) (n=95, 53±15 years, 69% men). All patients underwent cardiac magnetic resonance (CMR) including cine CMR and T1 mapping using 1.5 or 3T scanner (Avanto or Skyra, Siemens, Germany). Moderate or severe AS was defined when the systolic peak velocity by 2D phase contrast MRI (2D-PCMRI) exceeded 3.0 m/s. Moderate or severe AR was defined when regurgitation fraction by 2D-PCMRI exceeded 30% or was qualitatively defined using cine image when 2D-PCMRI underestimated the regurgitation flow. As summarized in Fig. 1, Modified Look-Locker inversion recovery (MOLLI) was performed for T1 mapping in basal, mid-ventricular and apical short axis orientation. Regional native T1 and post-contrast T1 were measured in AHA 16 segment model. Global ECVs were calculated with patient specific hematocrit, native T1 values and post-contrast T1 values using a clinical workstation (Circle 5.3, Canada). LV end-diastolic volume index (LVEDVI), end-systolic volume index (LVESVI) and LV mass index (LVMI) were measured from short axis cine CMR. ECG was performed within 1 year of CMR. Sokolow-Lyon voltages were calculated using the following equation: SV1+RV5 (Fig. 2).

Results: Sokolow-Lyon voltage exceeded 3.5 mV in 5 patients with AS and 3 patients with AR and was significantly elevated in the patients with AS and those with AR compared to those with no AS/AR ($p < 0.05$ and < 0.001). LVEDVI and LVESVI expressed significant enlargement in the patients with AR compared to those with AS and no AS/AR ($p < 0.05$). LVMI increased significantly in the patients with AS and those with AR compared to those with no AS/AR ($p < 0.01$ and < 0.001). ECV was similar between the three patient groups.

Conclusions: Elevation in Sokolow-Lyon voltage and LVMI suggested LV remodeling in AS and AR. However, ECV was not associated with LV remodeling secondary to aortic valve disease. Our results suggests that LV fibrosis in BAV patients may develop independent of aLV remodeling secondary to aortic valve disease.

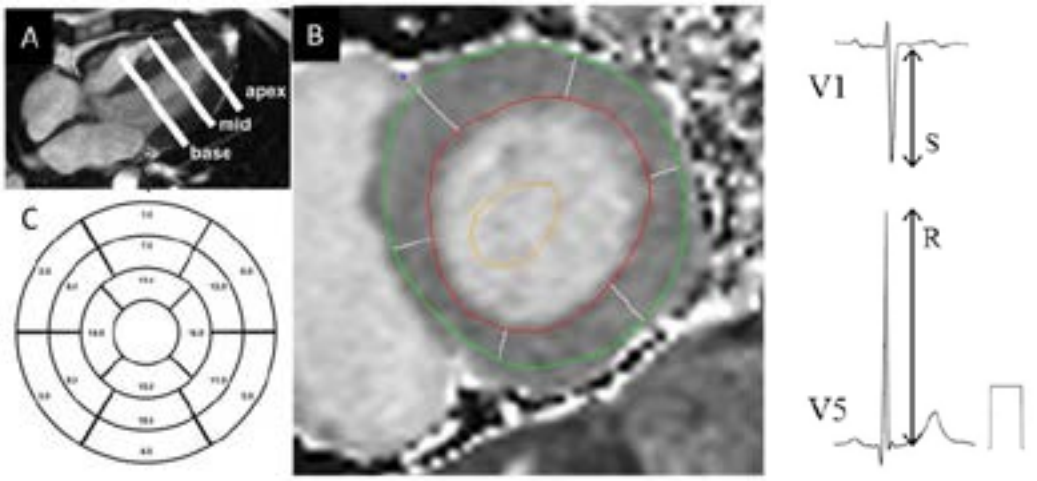

Table 1. LV characteristics in BAV with AS (without AR), AR (without AS), and no AS/AR (neither AS nor AR).

No AS/AR (n=95)	AR (n=13)	AS (n=15)	
1.9 ± 7.2	2.7 ± 1.2*	2.5 ± 1.2*	Sokolow-Lyon voltage (mV)
71 ± 20	107 ± 36*†	69 ± 17	LVEDVI (ml/m^2)
28 ± 10	39 ± 17*†	22 ± 8	LVESVI (ml/m^2)
50 ± 10	65 ± 12*	63 ± 16*	LVMI (g/m^2)
25.4 ± 4.6	25.6 ± 2.5	25.8 ± 2.1	ECV (%)
LVEDVI: left ventricular end-diastolic volume, LVESVI: left ventricular end-systolic volume, LVMI: left ventricular mass index, ECV: gadolinium extracellular volume fraction, * means significant difference compared to those with no AS/AR ($p<0.05$). † means significant difference compared to those with AS ($p<0.05$).			

P344

T2 mapping CMR for the assessment of myocardial remodelling after TAVI

Mareike Gastl, MD[1] Verena Veulemanns, MD[2], Patrick Behm, MD[1], Sebastian Haberkorn, MD[2], Christoph Jacoby, PhD[2], Bernhard Schnackenburg, PhD[3], Tobias Zeus, MD[2], Malte Kelm, MD[4], Florian Bönner, MD[5]

1. *Division of Cardiology, Pulmonology and Vascular Medicine, Heinrich Heine University, Düsseldorf, Medical Faculty, Germany, Düsseldorf, Nordrhein-Westfalen, Germany*
2. *Dept. Cardiology, Pneumology and Angiology, Heinrich Heine University, Düsseldorf, Germany, Nordrhein-Westfalen, Germany*
3. *Philips GmbH Marked DACH, Hamburg, Germany, Hamburg, Hamburg, Germany*
4. *Division of Cardiology, Pulmonology and Vascular Medicine, Heinrich Heine University, Düsseldorf, Medical Faculty, Germany; Cardiovascular Research Institute Düsseldorf (CARID), Heinrich Heine University Düsseldorf, Medical Faculty, Germany, Nordrhein-Westfalen, Germany*
5. *Division of Cardiology, Pulmonology and Vascular Medicine, Heinrich Heine University, Düsseldorf, Medical Faculty, Germany, Nordrhein-Westfalen, Germany*

Background: Hypertrophic cardiomyopathy (HCM) is a common appearance in patients with severe aortic stenosis (AS) leading to increased morbidity and mortality. As has been shown by cardiovascular magnetic resonance (CMR), beneficial left-ventricular remodelling with an improvement in prognosis can be achieved by transcatheter aortic valve implantation (TAVI). Besides myocardial function, CMR is able to provide information on magnetic relaxation parameters (i.e. T2 time). In fact, increased T2 times are common in patients with pathologic biopsy proven myocarditis or HCM. It is unknown if T2 times respond to TAVI procedure.

Methods: CMR was conducted with a 1.5 Tesla MRI-System (Achieva, Philips, Best, Netherlands) using a 32-channel coil pre and 6 months after TAVI. T2 mapping was achieved using a respiration navigator gated Gradient-And Spin-Echo sequence (GRASE, 15 T2 echoes separated by 10ms, res: 1x1x10mm², 3 short axis slices). Afterwards images were post-processed for T2 value generation with software based on the LabView environment. A cohort of age and gender matched volunteers served as controls. Analysis parameters included ejection fraction (EF), left ventricular mass per body surface area (LVM/BSA), interventricular septum thickness (IVS), peak diastolic strain rate (SR) and T2-mapping.

Results: 43 patients with severe AS (19 males, 82.1±4.5 years) received CMR pre and post TAVI. Baseline characteristics showed an HCM compared to controls (IVS 15.2±3.2 vs. 8.7±1.6mm, LVM/BSA 818±22.6 vs. 56.5±9.5g/m$^{2)}$. Alongside HCM, average myocardial T2 time was significantly increased (67.8±3.5 vs. 62.6±2.8ms, $p< 0.01$) and peak diastolic SR was reduced (1.1±0.5 vs.1.9±0.6s^{-1}, $p< 0.01$). After TAVI, HCM significantly improved (LVM/BSA to 62.9±15.4g/m^2; IVS to 13.3±2.6mm, $p < 0.01$) coincident with a signficiant reduction of average T2 time (67.8±3.5 to 63.2±4.2ms, $p < 0.01$). Patients with EF < 55% benefited most in terms of EF- and SR improvement (EF:40.6±9.3 to 57.1±10.0%, $p < 0.01$; SR:0.7±0.3 to 1.1±0.4s^{-1}, $p < 0.05$) as well as mass- and T2 time reduction (mass:100.1±21.7 to 74.7±15.4g/m^2; T2 time:68.7±3.5 to 60.2±3.6ms, $p < 0.01$). Odds ratio analysis revealed baseline IVS >15mm, LVM/BSA > 95g/m^2 and T2 time > 70ms as predictors for an EF improvement of 10% after TAVI ($p < 0.05$)

Conclusions: Patients with severe AS were characterized by HCM predominantly in septal segments, impaired global diastolic compliance and increased myocardial T2 time. 6 months after TAVI, HCM decreased accompanied by a reduction in myocardial T2 time. Patients with reduced EF at baseline showed the most prominent HCM reduction alongside improvement of myocardial compliance and a return to control T2 values. Besides mass and septum thickness, initial T2 time identifies patients who benefit the most from TAVI.

P345

Cardiac Magnetic Resonance Imaging Improves Assessment of Paradoxical Low Flow-Low Gradient Aortic Stenosis

Matthew D. Roby, DO[1]Timothy R. Larsen, DO[1], Nabil Jarmukli, MD[2], Amitabh Parashar, MD[2]

1. Carilion Clinic-Virginia Tech Carilion School of Medicine, VA
2. Salem VA Medical Center, VA

Background: Transthoracic Echocardiography (TTE) is the mainstay for aortic valve stenosis (AS) evaluation. Accurate assessment is dependent on quality imaging data. This issuebecomes especially important in patients with paradoxical low flow-low gradient (PLFLG), normal left ventricular systolic function (LVSF), severe AS which, is designated "D3" in the American College of Cardiology valve guidelines. Obtaining the specific structural and hemodynamic measurements outlined in the guidelines for the diagnosis of PLFLG AS can represent a challenge in patients who have clinically significant AS and suboptimal echocardiographic images. Cardiac magnetic resonance (CMR) can provide valuable data in such cases.

Methods: We had a total of 10 patients from 2015-16 with clinically severe AS, normal LVSF and suboptimal echocardiographic data not meeting standard criteria for high gradient severe AS and were therefore referred for CMR aortic valve assessment. A Siemans Aera 1.5 Tesla CMR machine with a 2-2.5 millisecond echo time was used.

Results: Table 1 details TTE and CMR findings. Peak aortic valve velocity, mean gradient, and valve area (AVA) suggested moderate to severe AS or PLFLG AS. Suboptimal echocardiographic data limited confidence in calculating the continuity equation-derived AVA and stroke volume index. CMR aided in the evaluation for PLFLG AS by allowing direct planimetery of the AVA using dedicated aortic valve steady-state free precession sequencing and accurate, reproducible stroke volume index (SI) calculation. TTE data had misclassified 3 patients with PLFLG AS as having a SI >35 ml/m2. CMRs superior volumetric assessment identified that low SI was in fact present in these patients, therefore reclassifying the degree of obstruction to severe PLFLG AS.

Conclusions: Paradoxical Low Flow Low Gradient Normal LVEF AS is a diagnostic challenge. In combination with TTE, CMR enables cardiologists to confidently diagnose this condition via accurate AVA and SI evaluation. This is accomplished without radiation or contrast and is largely unaffected by body habitus. Additionally CMR, as opposed to transesophageal echocardiography, does not require sedating medications, which can impact hemodynamic measurements. Our case series highlights that while in some subjects echocardiogram-derived data can identify PLFLG AS, CMR reclassified 3/10 (30%) patients as severe PLFLG AS. When faced with suboptimal or conflicting echocardiographic and clinical data, CMR can be used as a safe and valuable tool to complement TTE and help guide treatment decisions in a timely fashion.

Table 1: Patient demographics, echocardiographic and cardiac MRI data

CMR Data			Echocardiographic Data					Demographics		
Vmax (m/sec)	SI (ml/m^2)	AVA (cm^2)	AVA (cm^2)	SI (ml/m^2)	DI	Vmax (m/sec)	Mean PG (mmHg)	BSA (m^2)	Age (Years)	Patient
2.9	23	0.8	0.8	22	0.19	3.7	34	2.1	72	1
2.9	26	1	1.1	38	0.4	3.9	41	2.1	77	2
2.4	24	1	0.9	26	0.3	3	24	2.3	64	3
2.9	30	1	0.9	36	0.3	2.9	17	2	69	4
3.5	30	0.7	1.5 Plan 0.9 Dop	21	0.18	4.9	58	2.1	68	5
2.9	27	0.8	0.7	29	0.3	3.1	22	2	89	6
2	27	0.7	0.9	50	0.3	3.7	38	2	83	7
1.7	25	1	1	31	0.3	2.8	18	1.8	83	8
2.7	35	1	0.9	29	0.3	3.3	25	2	81	9
2.9	27	0.9	0.8	28	0.3	2.9	19	2	68	10

Abbreviations: BSA: Body surface area, PG: Aortic valve pressure gradient, Vmax: Maximum velocity across the aortic valve, DI: Dimensionless index, SI: Stroke index, AVA: Aortic valve area, Plan: Planimetry measurement, Dop: Doppler continuity equation derived measurement

P346

Early hemodynamic effects of transcatheter tricuspid valve therapy - Insights from cardiac magnetic resonance

Karl Rommel, MD[1] Christian Besler, MD[2], Jörg Ender, MD[3], Thilo Noack, MD[4], Joerg Seeburger, MD[4], Maximilian von Roeder, MD[2], Stephan Blazek, MD[5], Matthias Gutberlet, MD[6], Gerhard Schuler, MD[2], Friedrich-W. Mohr, MD[4], Axel Linke, MD[2], Philipp Lurz, MD, PHD[2]

1. *Dept. of Internal Medicine / Cardiology University of Leipzig - Heart Center, Sachsen, Germany*
2. *Leipzig University Heart Center, Department of Cardiology, Sachsen, Germany*
3. *Leipzig University Heart Center, Department of Anesthesiology, Sachsen, Germany*
4. *Leipzig University Heart Center, Department of Surgery, Sachsen, Germany*
5. *Leipzig University Heart Center, Department of Cardiology, Leipzig, Sachsen, Germany*
6. *Leipzig University Heart Center, Department of Radiology, Sachsen, Germany*

Background: Functional tricuspid regurgitation (TR) is a major determinant of functional status and prognosis in advanced heart failure patients. Recently, transcatheter therapies have been proposed as a novel promising treatment option in these patients. So far, data on functional consequences of tricuspid valve intervention are scarce, partly due to the difficulty of imaging the right ventricle. Cardiac magnetic resonance (CMR) is the reference method for assessment of right ventricular (RV) volumes and function. We therefore sought to characterize effects of interventional tricuspid valve repair by repeated CMR scans before and early after the intervention.

Methods: Eight patients (age 78.1 ± 2.3 years) with severe functional TR, right heart failure and prohibitive surgical risk underwent interventional tricuspid valve repair using the MitraClip (n=7) or the Trialign system (n=1) and CMR imaging with volumetric and flow studies one the day before and on median 4 days (confidence intervall 1-4) after the intervention. Concomitant clipping of the mitral valve was realized in four patients.

Results: After the intervention TR fraction was significantly reduced (47.1 ± 11.6 vs. 22.7 ± 11.9 %, $p < 0.01$) and mitral regurgitant fraction (35.8 ± 6.0 vs. 16.9 ± 5.5 %, p=0.04) improved in patients with mitral intervention, while no change was observed for patients with isolated tricuspid intervention (23.1 ± 3.8 vs. 20.9 ± 3.0%, p=0.50).
Overall, RV endsystolic volume (109.4 ± 3.4 vs. 90.1 ± 24.4 ml/m², p=0.055), RV stroke volume (86.7 ± 24.8 vs. 47.0 ± 18.3 ml/², $p < 0.01$) and RV ejection fraction (40.3 ± 9.2 vs. 34.1 ± 7.7 %, p=0.056) decreased, while pulmonary forward flow significantly increased (56.2 ± 19.6 vs. 68.7 ± 30.1ml, p=0.03). LV enddiastolic volumes (80.1 ± 3.4 vs. 90.0 ± 25.6, p=0.29) increased numerically with no changes in endsystolic volumes (p=0.86) and heart rate (p=0.60). Transcatheter tricuspid valve repair resulted in improved Cardiac index (2.16 ± 0.4 vs. 2.43 ± 0.55 l/m², p=0.04) four days after the procedure.

Conclusions: The present study is the first to characterize acute functional effects of transcatheter treatment of functional TR by CMR. Our findings suggest that interventional treatment of functional TR has the capacity to significantly reduce TR and augment cardiac output in advanced heart failure patients early after the intervention. Cardiac magnetic resonance is well suited to assess procedural success of this novel transcatheter valve intervention.

P347

4D Flow Tracking Improves Assessment of Mitral Regurgitation Severity

Kanae Mukai, MD[1]Nicholas Burris, MD[2], Karen Ordovas, MD, MAS[3], Michael D. Hope, M.D.[4]

1. *UCSF, Palo Alto, CA*
2. *University of Michigan, Ann Arbor, MI*
3. *University of California San Francisco, San Francisco, CA*
4. *University of California, San Francisco, CA*

Background: Quantification of mitral regurgitation (MR) can guide the optimal timing of valve replacement, but is challenging to accurately perform with imaging. Standardization is needed for MR assessment with 4D Flow, an investigational cardiac magnetic resonance (CMR) sequence. We hypothesized that mitral annulus and flow jet tracking with 4D Flow correlate better with the CMR reference for mitral regurgitant fraction than conventional 2D flow assessment.

Methods: Adult patients referred for clinically indicated CMR (n=13) were prospectively and consecutively recruited for 4D Flow imaging. CINE steady-state free precession (SSFP) and ascending aortic phase contrast sequences were also performed. Image quality was assessed with a 5-point Likert scale (1=no visualization of mitral annular ring; 2=partial visualization; 3=visible for most of the cardiac cycle with color flow; 4=visible in systole and diastole; 5=excellent definition of the annulus and leaflets). Likert score > 2 was considered acceptable image quality. CMR reference mitral valve regurgitant fraction (RF) was derived from left ventricular stroke volume (LVSV) and forward flow in the ascending aorta (AoFF) using the standard equation: (LVSV-AoFF)/LVSV.

Six approaches for 4D Flow RF calculation were compared against the CMR reference: 1) fixed plane at the mitral annulus at end diastole; 2) fixed plane 1cm towards the atria; 3) fixed plane 1cm towards the ventricle; 4) 3D annulus tracking using anatomy; 5) 3D annulus tracking using flow and anatomy; and 6) 3D flow jet tracking.

Results: All patients had acceptable image quality (average Likert score of 4), and demonstrated mild (n=10), moderate (n=1) and severe (n=2) mitral regurgitation. The strongest correlation between the 4D Flow approaches and the CMR reference was seen with 3D annulus tracking using flow and anatomy (r=0.89, p=0.00) and 3D flow jet tracking (r=0.85, p=0.00). 3D annulus tracking using anatomy alone had a moderate correlation (0.61, p=0.03). None of the fixed plane methods had a significant correlation: method 1 (0.30, p=0.32); method 2 (-0.15, p=0.63); and method 3 (0.25, p=0.41).

Conclusions: 3D mitral annulus and flow jet tracking are the preferred 4D Flow approaches for determining mitral regurgitation fraction, exhibiting strong correlation with the CMR reference measurement.

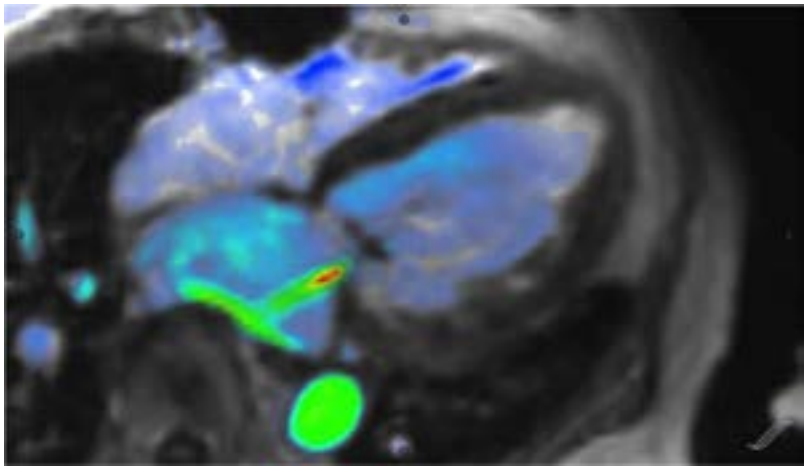

P348

A Rare Case of Progressive Pulmonary Valve Disease Post Radiation Therapy

Rajesh Janardhanan, MD, FACC[1] Nirmal Singh, MD[2]

1. Banner University Medical Center, Tucson, Tucson, AZ
2. Banner University Medical Center, Tucson, AZ

Description of Clinical Presentation: A 41-year-old obese woman presented with gradually progressing exertional shortness of breath and fatigue. She had a past medical history of multiple relapses of Hodgkin Lymphoma [HL] and had undergone several cycles of mediastinal radiation and anthracycline-based chemotherapy 8 years ago. Her past medical history was negative for any congenital cardiac or valvular disease. She had no prior history of any heart murmurs. Physical examination was unremarkable except for a harsh systolic murmur in the 2nd left intercostal space.

Diagnostic Techniques and Their Most Important Findings: EKG and labwork were unremarkable. Transthoracic echo was abnormal with increased color flow across the pulmonary valve, later confirmed on transesophageal echo **[Figure 1].** Doppler evaluation confirmed moderate pulmonary stenosis and an eccentric jet of moderate pulmonary regurgitation. Patient had a cardiac MRI (CMR), which confirmed mixed pulmonary valve disease [moderate pulmonary valvular stenosis and moderate pulmonary regurgitation] **[Figure 2]**. The right ventricle was mildly dilated with mildly reduced bi-ventricular function. Chest MRA **[Figure 3]** revealed narrowing in the region of the pulmonary valve and a dilated main pulmonary artery.

Learning Points from this Case: The incidence and prevalence of acquired pulmonary valve disease is very low. Radiation and anthracycline-based chemotherapy used in HL are major risk factors for acquired valvular heart disease. These factors affect endothelial surface producing oxidative stress and activates fibrinogenic growth factors such as tissue growth factor beta-1 and myofibroblasts leading to increased collagen and extracellular matrix deposition culminating in fibrosis. The clinical manifestations also include myocardial ischemia and heart failure. The proposed surveillance interval recommended is about 10 years after exposure.

We present an exceedingly rare case of acquired cancer therapy induced mixed pulmonary valve disease with valvular stenosis/ regurgitation and progressive worsening of right sided systolic function. Typically, clinical manifestations become evident 10-20 years post-exposure. Interestingly, our patient manifested with clinical features 8 years post cancer therapy. Although left sided valvular heart disease (commonly involving the aortic valve) is more common post cancer therapy, our patient had acquired pulmonary valve disease. She had 2 relapses of HL requiring anthracycline-based chemotherapy regimen and mediastinal irradiation. We believe the cumulative chemo-toxicity and radiation toxicity potentially caused accelerated damage to the pulmonary valve. Our patient is currently being discussed by the heart team meeting to decide on appropriate intervention.

This case highlights the need for close imaging surveillance for valvular heart disease post cancer therapy. This should not be limited to left sided valves and left ventricular function, but should also extend to include the right-sided valves and right ventricular function.

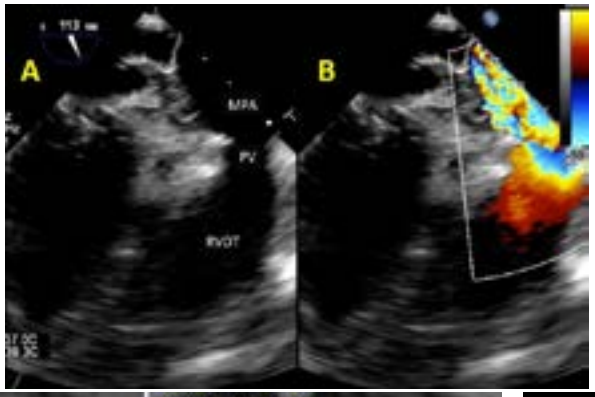

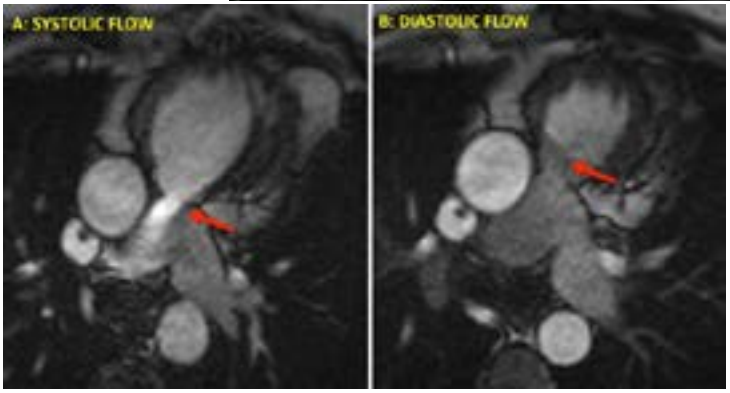

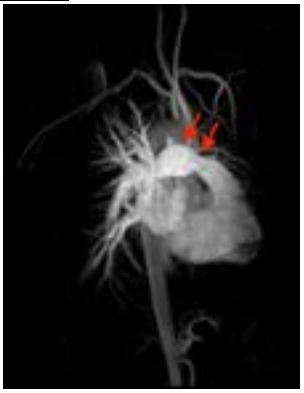

P349

Bad Childhood Memories: traumatic tricuspid regurgitation revealed by cardiovascular magnetic resonance.

Alessandra Scatteia, MD[1], Santo Dellegrottaglie, MD; PhD[3]Pasquale Guarini, MD[2], Carmine Pascale, RT[2]

1. *Division of Cardiology, Ospedale Medico-Chirurgico Accreditato Villa dei Fiori, Acerra, Naples, Italy. Cardiac Magnetic Resonance Unit, NIHR Bristol Cardiovascular Biomedical Research Unit, Bristol Heart Institute, Bristol UK, Naples, Campania, Italy*
2. *Clinica Villa dei Fiori Acerra, Naples, Campania, Italy*
3. *Clinica Villa dei Fiori, Acerra (Naples,), Italy, Campania, Italy*

Description of Clinical Presentation: A 31-year-old man, asymptomatic and involved in amateur sport activities, has been on echocardiographic follow up for ten years since the incidental diagnosis of tricuspid regurgitation (TR) during a sport qualifying physical examination. The only relevant anamnestic note was a blunt chest trauma following a car accident at age of 2 years. He was not on regular medications and with negative personal and family history for congenital heart disease.

Diagnostic Techniques and Their Most Important Findings: Transthoracic echocardiography showed right heart chambers dilatation with normal ventricular function, and severe TR, but the precise mechanism for the valve dysfunction was not clearly identified. The left ventricle (LV) and the remaining valves were normal. Therefore, to better assess right ventricle (RV) dimension and function, as well as to understand the etiology of the severe TR, the patient underwent a cardiac magnetic resonance (CMR) examination. CMR images were acquired using a 1.5T whole body scanner (Achieva, Philips) and a 16-channel torso coil. The cardiac imaging protocol included the acquisition of a series of cine SSFP images, FSE and post-contrast T1-weighted inversion recovery images, in short-axis planes as well as in the standard long axis planes for the LV and the RV. In addition, phase-contrast images of the aortic and pulmonary valves were acquired to better characterize the TR. CMR showed normal LV dimensions and global systolic function, with an ejection fraction of 64%. The right chambers were severely dilated with preserved RV ejection fraction. Severe eccentric TR was detected (**Figure 1 A**: RVOT from cine image (systolic frame) showing a wide jet of tricuspid regurgitation (arrowheads); regurgitant fraction = 45%). In addition, a flail structure was noted attached to the anterior tricuspid valve leaflet, with rapid systolic movement in the right atrium, consistent with tricuspid chordal rupture (**Figure 1 B-C:** 4-chamber and RVOT cine images (systolic frame) showing a flail structure (white arrow) attached to the anterior tricuspid valve leaflet.). There were no areas of increased signal intensity on FSE T1-weighted images and no late gadolinium enhancement was noted on post-contrast images (Figure 1 D). Based on these findings, the mechanism of the TR was considered to be the rupture of a chorda tendinea attached to the anterior leaflet of the tricuspid valve, secondary to blunt chest trauma. The patient was then referred to the cardio-thoracic surgery department to define the most appropriate treatment.

Learning Points from this Case: Cardiac injury secondary to blunt chest trauma has been seen more frequently during the last 10 years. Traumatic TR is rare, but the real incidence is probably underestimated because of its commonly asymptomatic nature and the typical coexistence with more life-threatening lesions. The valve injury is usually caused by an abrupt deceleration coupled with an increase in right-side cardiac pressures due to antero-posterior compression from the adjacent sternum. The mean interval to diagnosis may vary and severe TR may lead to RV dilatation and, eventually, progressive right heart failure. Chordal rupture is the most frequently reported injury, but papillary muscle rupture and leaflet tear may also occur. CMR is considered the gold standard imaging technique for the volumetric assessment of the RV, while its ability to detect small, highly mobile intracardiac structure is generally poor. However, in this case CMR was able to identify an uncommon etiology of TR, proving to be a potenatial alternative to transesophageal echocardiography and providing the opportunity for an effective surgical treatment. Physicians should always consider this potential complication of non-penetrating chest trauma in order to plan an appropriate initial and follow up evaluation with non-invasive cardiovascular imaging, keeping in mind that in some cases the responsible trauma may be very distant in time.

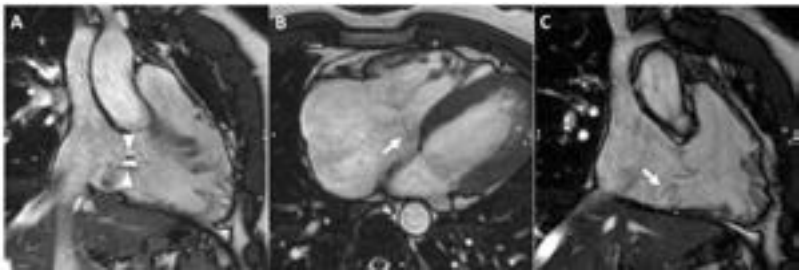

P350

An unusual cause of aortic regurgitation: Incremental value of CMR in diagnostic workup

Rahul Dhawan, M.B.B.S.[1] Adnan Sultan, MD[2], Rajeev R. Fernando, MD[2]

1. *University of Louisville, KY*
2. *University of Louisville, Louisville, KY*

Description of Clinical Presentation: A 57 year old man with hypertension presented with sudden onset retrosternal chest pain. Initial workup revealed non-diagnostic electrocardiogram and negative cardiac enzymes. Bedside transthoracic echocardiography showed an intimal flap in the proximal ascending aorta with aortic regurgitation. He was rushed to the operating room. Intraoperative findings included tricuspid aortic valve and aortic dissection extending into the arch vessels. He underwent emergent ascending aorta and hemi-arch replacement. He was discharged to rehabilitation and was lost to follow up. A year later he presented with progressive exertional dyspnea. Transthoracic echocardiography showed *bicuspid aortic valve* with fusion of the left and right coronary cusps, systolic doming and diastolic retraction and severe eccentric aortic regurgitation and an intact proximal ascending aortic graft. Transesophageal echocardiography confirmed these findings by both 2D and 3D methods. No communications were identified between the true and false lumen. However, on review of the intraoperative TEE, the aortic valve was clearly tricuspid prior to surgery. Cardiac MRI was performed to clarify the diagnosis for the aortic valve, exclude additional communications between the true and false lumen in the setting of a dilated descending thoracic aorta and evaluate the ascending aortic graft. Gated FIESTA cine images confirmed the TEE findings of systolic doming and diastolic retraction of the aortic valve, severity and mechanism of aortic regurgitation, presence of intimal tear and dilated dissected descending thoracic and abdominal aorta. In addition, thin aortic valve stack images excluded fusion of the commissures but documented fusion of the tip of the right and left coronary valve leaflets; likely from surgical aortic valve repair. Time resolved magnetic resonance angiography excluded contrast extravasation from the aorta, showed the site of an uncorrected communication to the false lumen and delineated the true and false lumen. Due to his high operative risk, he underwent successful trans-catheter aortic valve replacement for management of severe aortic regurgitation.

Diagnostic Techniques and Their Most Important Findings: Please see table 1

Learning Points from this Case: This case illustrates the incremental value of CMR in the workup of postoperative aortic regurgitation, assessment of the ascending aortic graft, quantifying the extent of dissection and identifying the presence of communication between the true and false lumens of the dissected aorta. It was also helpful in clarifying the mechanism of aortic regurgitation. Furthermore, it emphasizes the importance of a detailed intraoperative and postoperative imaging in diagnosis of valve regurgitation and verification of successful correction

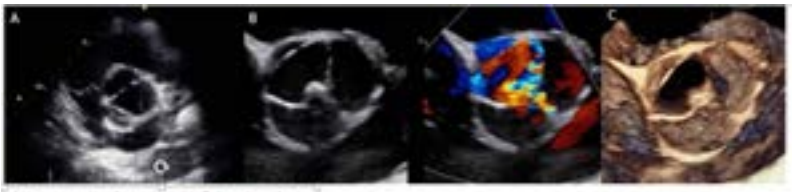

A: Pre-operative TTE with trileaflet aortic valve
B: Post-operative TEE with fusion of right and left cusps
C: 3D TEE better showing the fusion of the right and left cusps

P351

Unicuspid aortic valve

Sudip K. Saha, MD

Mid Atlantic Permanente Group, Mclean, VA

Description of Clinical Presentation: A forty-three year old woman presented to her primary care physician with worsening dyspnea and orthopnea. She had a long history of a murmur since her childhood and was given reassurance by her prior physicians. Prior transthoracic echocardiograms noted a difficult to visualize aortic valve. Given her new symptoms, another transthoracic echocardiogram was obtained and her aortic valve was once again noted to be difficult to visualize. There was concern for thoracic aortic dilation and a cardiac MRi was obtained to further characterize her aortic valve and thoracic aorta.

Diagnostic Techniques and Their Most Important Findings: Techniques: Cardiac MRI was performed on a Philips 1.5 T scanner with a commercial 5-element cardiac-surface coil. Cine images were acquired in a contiguous LV short-axis orientation with an ECG-gated, breath-hold, steady-state free-precession sequence with full LV coverage (8-mm slice thickness, 2-mm interslice gap, in-plane spatial resolution 2×2 mm, 30 ms temporal resolution). Contrast enhanced MRA of the aorta was performed.

Most notable findings: On a short axis view through the aortic valve, the patient was found to have an unicuspid aortic valve. Other findings on her cardiac MRI included a dilated ascending aorta (maximal diameter of 4.9 cm), moderate aortic regurgitation, and mild left ventricular cavity enlargement indexed to body surface area. Given her symptoms, she was referred to cardiac surgery for the evaluation of aortic valve replacement and possible root replacement.

Learning Points from this Case: Cardiac MRI is a powerful tool to define anatomy such as aortic valve leaflet morphology when other non-invasive techniques are inadequate. Associated findings such as thoracic aortic dilation, aortic coarctation, and valvular regurgitation/stenosis should prompt further investigation for less common entities such as unicuspid, bicuspid, or quadricuspid aortic valves.

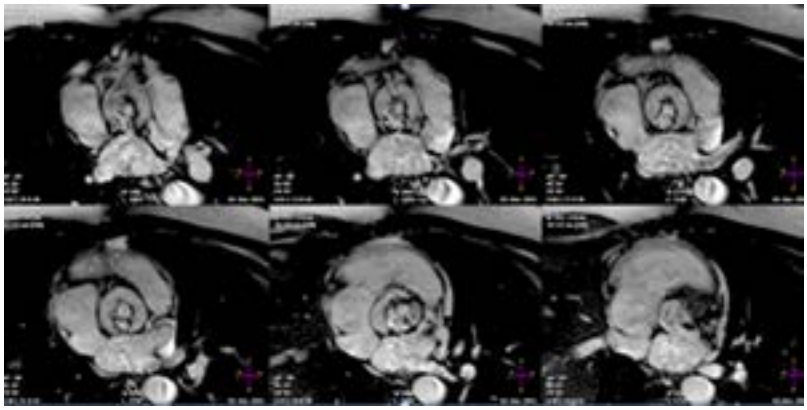

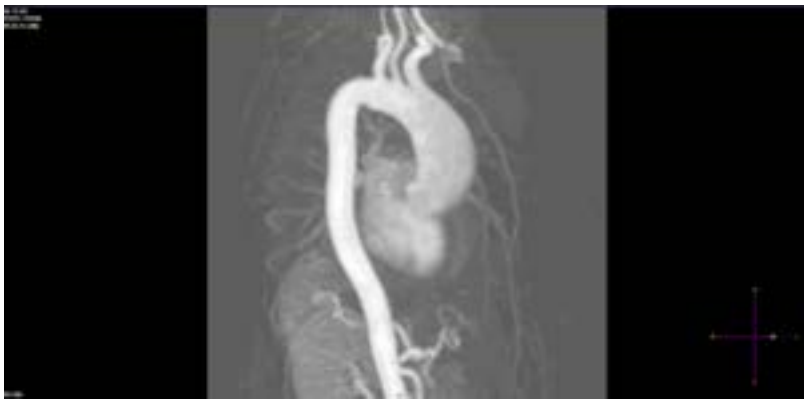

P352

Unusual case of infundibular pulmonic stenosis- Cardiac MRI findings

Supriya Gupta, MBBS MD[1], Christopher Scelsi, DO[2]Arun Nagabandi, MBBS[3], Ankur Sharma, MD[4], Jayanth H. Keshavamurthy, MD[5]

1. *Medical college of georgia, Augusta, GA*
2. *Augusta University, augusta, GA*
3. *Medical College of Georgia at Augusta University, GA*
4. *Presence St. Joseph Medical Center, IL*
5. *Medical College of Georgia at Augusta University, Augusta, GA*

Description of Clinical Presentation: Isolated primary infundibular pulmonic stenosis with an intact ventricular septum is an uncommon cardiac abnormality, with a reported incidence of about 0.4% of patients with congenital heart disease. Right ventricle gets divided into a proximal “high-pressure” chamber and a distal “low-pressure” chamber. The condition can be misdiagnosed as ventricular septal defect or valvular pulmonic stenosis and the disease severity underestimated. This case describes a 34 year old man who was misdiagnosed at an outside hospital with ventricular septal defect in infancy. Patient presented with tightness in chest and mild shortness of breath. No signs of cardiac failure are present on initial presentation.

Diagnostic Techniques and Their Most Important Findings: Patient underwent transesophageal echocardiography demonstrating sub pulmonic/infundibular pulmonic stenosis with peak velocity 3.31m/s, equalling a gradient of 44mm of mercury. No VSD identified. There was mild aortic, tricuspid and mitral regurgitation. Cardiac MRI performed using SSFP in standard cardiac projections demonstrated severe asymmetric hypertrophy of RV free wall near RVOT measuring up to 1.5 cm. (Figure 1). RVOT narrowed to about half a centimeter below pulmonic valve. Proximal RVOT distal to sub pulmonic stenosis measured 2.4 cm. Dephasing was seen across RVOT from sub-pulmonic stenosis. Patient is currently being referred for surgical evaluation and correction. (Table 1).

Learning Points from this Case: Primary infundibular stenosis is a rare anomaly. The views used in a standard TEE examination may not provide detailed morphologic and hemodynamic assessment of the RVOT and PA, thus underestimating or misdiagnosing this entity. Cardiac MRI using SSFP sequences provides a definitive diagnostic study if clinical concern arises, can measure the RVH, RV muscle mass more accurately than echocardiogram. Knowledge of the anatomy of the obstructing lesion could influence options for corrective interventions. Accurate determination of the severity of the stenosis and the anatomy of the obstructing lesion are important in devising a treatment strategy.

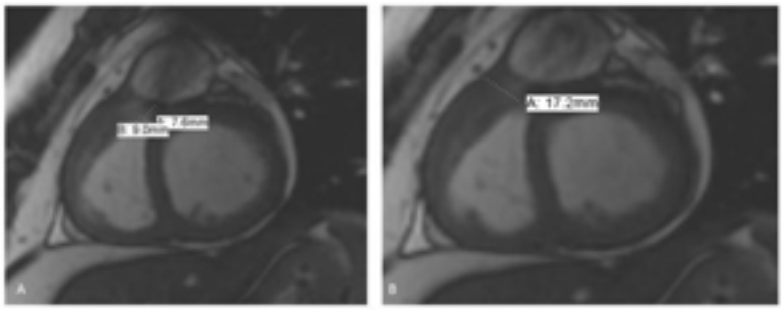

Transesophageal Echocardiography Measurements across Pulmonary artery

2.1 cm	Left ventricular outlet tract diameter
2.3 cm	Main pulmonary artery diameter
4.2 cm2	Main pulmonary artery area
314.9 cm/sec	PA Velocity max
39.8 mmHg	PA max Pressure gradient
195.4 cm/sec	PA velocity mean
19.1 mmHg	PA mean Pressure graient
77.2 cm	PA velocity VTI

P353

Massive pulmonary arterial dilatation visualized on Cardiac MRI in a patient with long term Idiopathic Pulmonary Arterial Hypertension.

Michael B. Stokes, MBBS FRACP[1] Ross Roberts-Thomson, MBBS, BMedSci(Hons)[2], Adam Nelson, BMedSc MBBS[3], Karen S. Teo, MBBS, PhD[4]

1. *Royal Adelaide Hospital, Wayville, South Australia, Australia*
2. *Royal Adelaide Hospital, Urrbrae, South Australia, Australia*
3. *Royal Adelaide Hospital, South Australia, Australia*
4. *Royal Adelaide Hospital, Adelaide, South Australia, Australia*

Description of Clinical Presentation: A 53-year-old female with a 10 year history of Idiopathic Pulmonary Arterial Hypertension (IPAH) presented for a Cardiac MRI (CMR) to investigate echocardiographic findings of a severely dilated pulmonary trunk and moderate to severe pulmonary regurgitation. The patient was stable symptomatically at NYHA Class II and managed on combination therapy with Macitentan 10mg Daily, Sildenafil 25mg TDS and Selexipag.

Diagnostic Techniques and Their Most Important Findings: SSFP images (including short-axis stack, trans-axial stack, RVOT, RV-VLA as well as piloted pulmonary trunk and pulmonary branch images) enabled accurate quantification of a dilated pulmonary annulus (45mm diameter), a grossly dilated main pulmonary artery (7.4cm diameter) and dilated left and right main pulmonary artery branches (both 3.6cm diameter). Right ventricular volume was mildly increased (RVEDVI = 90ml/m2) and ejection fraction was mildly reduced (RVEF 48%). VENC sequence of the pulmonary valve quantified severe pulmonary regurgitation (47% regurgitant fraction). Pulmonary-MRA enabled visualisation of the dilated pulmonary arterial branches and excluded arteriovenous malformation and any shunts.

Learning Points from this Case: Long term IPAH may result in development of pulmonary arterial aneurysms and dilatation of the pulmonary arterial tree which can progress to dissection and rupture. CMR enables accurate measurement and visualization of the pulmonary arterial tree and exclusion of AVMs. CMR also accurately meaures right ventricular function and quantifies pulmonary regurgitation.

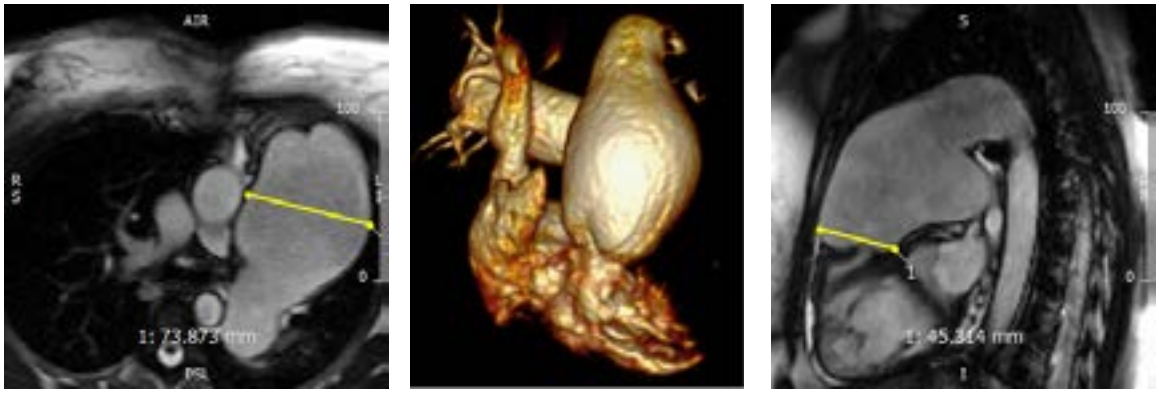

P354

Recognizing Arrhythmic Mitral Valve Prolapse Syndrome on Cardiac MRI

Madhur Roberts, MD[1] Ashish Kabra, MD[2], Robi Goswami, MD[3], Venkateshwar Polsani, MD[1]

1. Piedmont Heart Institute, Atlanta, GA., Atlanta, GA
2. Piedmont Heart, Atlanta, GA
3. Piedmont Heart Institute, Atlanta, GA

Description of Clinical Presentation: A 48-year-old male presented with premature ventricular contractions (PVCs) as noted incidentally on his electrocardiogram (ECG). He denied any symptoms including chest pain, palpitations, dyspnea or syncope. He had no prior history of cardiovascular disease.

His prior echocardiogram showed normal left ventricular size and function with an LVEF of 55-60% and a prior coronary artery calcium score was zero.

His EKG showed frequent PVCs and the morphology had two different morphologies. One of the PVC morphology suggested right ventricular outflow tract and the origin of other morphology PVCs was unclear. A holter monitor was done that showed 8.3% of ventricular ectopic activity.

Diagnostic Techniques and Their Most Important Findings: A contrast-enhanced cardiac MRI was performed to further investigate the etiology of PVCs. The cardiac MRI showed normal ventricular sizes and function. There was bileaflet mitral valve prolapse (**image 1**) associated with mild mitral regurgitation (MR). A significant Mitral annular disjunction (MAD, **image 1**) was noted. On delayed hyperenhacement imaging (**image 2**), there was focal subendocardial scar in the inferolateral wall of the left ventricle, at the site of papillary muscle insertion. There was macroscopic scar noted in the postero-medial papillary muscle.

Learning Points from this Case: Mitral valve prolapse is a common disorder effecting 2-3% of the general population. Although usually thought to be benign, it can be associated with significant atrial and ventricular arrhythmias and sudden cardiac death in some patients. The risk factors for patients with MVP prone to arrhythmias and possible sudden cardiac death is still uncertain and can be subclinical (i.e. only found on diagnostic imaging). Several such factors that have been highlighted as potential predictors of arrhythmias and sudden cardiac death in MVP are mitral annulus disjunction (MAD), posterior systolic curling, mitral annular dilatation and left ventricular fibrosis. Although, no specific MAD threshold has been set, one study showed that a disjunction >8.5 mm predicted non-sustained ventricular arrhythmias with a sensitivity of 67% and a specificity of 83%. LV fibrosis in these patients was mostly detected close to the annulus in the basal LV wall (papillary muscles and inferior-basal free wall). Patients with MVP in conjunction with these above mentioned findings have been correlated to have higher frequency of ventricular arrhythmia and sudden cardiac death. However, at present, risk stratification for these subsets of patients is uncertain. Our case highlights the serious consequences associated with MVP and the use of cardiac MRI to help assess the concealed myocardial substrates.

REFERENCE:

Circ Cardiovasc Imaging. 2016 Aug;9(8):e005248

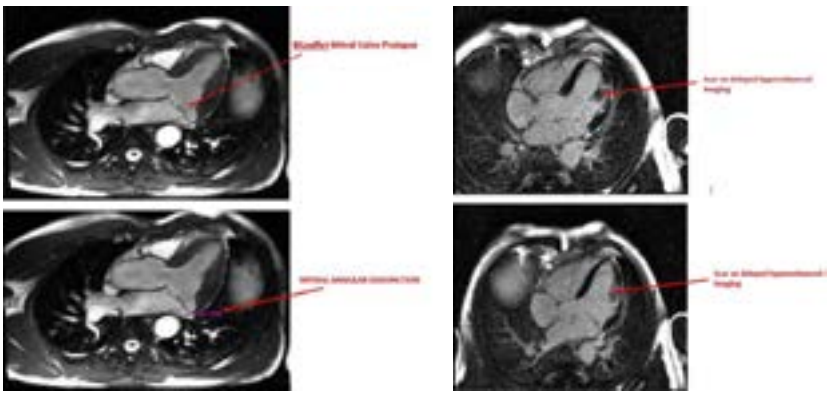

P355

Getting rid of the grind: automated analysis of large quantity data and intraindividual stability on MRI aortic blood flow measurements for vascular age assessment.

Alexander Knorr, MD[1] Thomas Re, MD[2], Bram Stieltjes, MD[2], Denise Yates, Ph.D.[3], Roland Schmieder, MD[4], Jens Bremerich, MD[2], Tobias Heye, MD[2]

1. *University Hospital Basel, Basel, Basel-Stadt, Switzerland*
2. *University Hospital Basel, Basel-Stadt, Switzerland*
3. *Novartis Institutes for Biomedical Research, MD*
4. *University Hospital Erlangen, Bayern, Germany*

Background: Aortic blood flow (ABF) characteristics are useful indicators for structural and functional vascular changes. In this study we assessed the capabilities of an in-house developed software tool to automatically analyze ABF curves obtained from magnetic resonance imaging (MRI) and to evaluate the intraindividual curve stability over time.

Methods: The MRI data was acquired in an IRB approved, HIPAA compliant prospective study. A subset of 101 adult patients (70 male, age 60±11 yrs.) with essential arterial hypertension were included from a multicenter trial (3 sites, 140 patients total) on antihypertensive treatment. All patients underwent standardized cardiovascular 3T MRI at 3 time points (0, 12, 52 wks.). ABF in ascending and descending aorta was measured by one observer using semi-automatic analysis software (Syngo.via Siemens Healthcare, Erlangen, Germany) on axial phase-contrast scans (100 frames/RR-interval). The flow measurements were then evaluated for all 303 examinations simultaneously for 40 curve-defining characteristics using a sophisticated Python (Python 2.7.11, Python Software Foundation) algorithm. Intraindividual ABF variability over time was characterized by per patient full width half maximum (FWHM), peak acceleration and systolic area under the curve (AUC) coefficient of variation (COV). Observer-results-dependence was assessed by five observers for a subset of 45 patients.

Results: The automated analysis tool was able to process ascending and descending ABF curves for 303 examinations with speed and accuracy. Calculation time of the entire data set was 2.6 s for 40 curve parameters in each data set including various time periods, functional ratios and AUCs. Median FWHM, peak acceleration and systolic AUC COV in the ascending aorta were 8.44%, 7.13% and 7.57% (range 0-31.96%, 0-24.80% and 0.63-28.06%). Median intra- and inter-observer COV was 0.67% (range 0.48-1.20%) and 1.54%.

Conclusions: Fully automated curve analysis facilitates evaluation of ABF data, allowing for scalable and fast analysis thus shifting the radiologist time and focus from time-intensive manual evaluation to data interpretation. ABF characteristics show a clear stability over time independent of the observer.

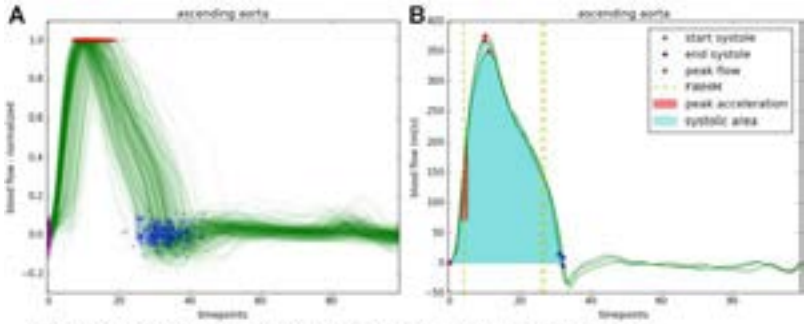

A: overlay of normalized flow over time curves for each individual with key points highlighted **B**: superimposed flow over time curves of one individual showing key points, peak acceleration (red slope), systolic AUC (cyan area) and FWHM (yellow broken lines)

P356

Is there more to aortic flow curves than meets the eye? MRI blood flow analysis of large quantity data as a substitute marker for vascular age assessment.

Alexander Knorr, MD[1] Thomas Re, MD[2], Bram Stieltjes, MD[2], Denise Yates, Ph.D.[3], Roland Schmieder, MD[4], Jens Bremerich, MD[2], Tobias Heye, MD[2]

1. *University Hospital Basel, Basel, Basel-Stadt, Switzerland*
2. *University Hospital Basel, Basel-Stadt, Switzerland*
3. *Novartis Institutes for Biomedical Research, MD*
4. *University Hospital Erlangen, Bayern, Germany*

Background: Aortic blood flow (ABF) characteristics are useful indicators for structural and functional vascular changes. In this study we assessed ABF curve parameters of a large number of magnetic resonance imaging (MRI) measurements to assess their potential as substitute markers for aortic stiffness.

Methods: The MRI data was acquired in an IRB approved, HIPAA compliant prospective study. A subset of 101 adult patients (70 male, age 60±11 yrs.) with essential arterial hypertension were included from a multicenter trial (3 sites, 140 patients total) on antihypertensive treatment. All patients underwent cardiovascular 3T MRI with a standardized imaging protocol at 3 different time points (0 wks., 12 wks., 52 wks.). ABF in the ascending and descending aorta was measured by one reader using semi-automatic analysis software (Syngo.via Siemens Healthcare, Erlangen, Germany) on axial phase-contrast scans (100 frames/RR-interval). Aortic stiffness was estimated via aortic strain calculations on maximum/minimum area measurements on cine gradient-echo scans. The flow measurements were then evaluated for all 303 examinations simultaneously for several curve-defining characteristics using a sophisticated Python (Python 2.7.11, Python Software Foundation) algorithm. Pearson's product moment correlations and clustering between variables was done in RStudio (RStudio, Inc., Boston, MA).

Results: Peak acceleration, systolic, acceleration and deceleration time, as well as areas under the curve before and after peak flow of the ascending aorta emerged as significantly correlated to strain in the proximal descending aorta (r = 0.44, -0.40, -0.37, -0.19, -0.27 and -0.23; p-value

Conclusions: ABF measurements are a simple, reproducible and fast technique compared with other approaches to obtain aortic strain or stiffness and shows promise as a substitute marker for vascular age/aortic stiffness thus facilitating long-term prediction of vascular health.

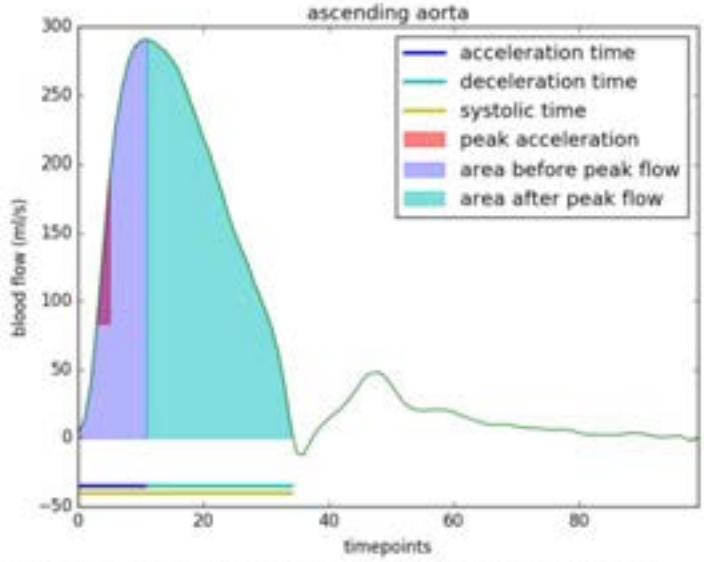

Figure: flow over time curve demonstrating extracted parameters: acceleration (blue line), deceleration (cyan line) and systolic (yellow line) time, peak acceleration (red slope) and areas before/after peak flow (blue/cyan area).

P357

Non-invasive Assessment of Pulmonary Artery Vasoreactivity at Rest in Healthy Subjects Using 3T MRI

Monica Mukherjee, MD, MPH[1]Michael Schär, PhD[2], Gabriele Bonanno, PhD[3], Gary Gerstenblith, MD[2], Robert G. Weiss, MD[3], Allison G. Hays, MD[3]

1. *Johns Hopkins University School of Medicine, Baltimore, MD*
2. *Johns Hopkins, MD*
3. *Johns Hopkins University School of Medicine, MD*

Background: Pulmonary arterial vasoreactivity is typically measured by catheter-based invasive assessment of changes in pulmonary artery cross-sectional area (CSA) and blood flow (BF) in response to an endothelial-dependent stress and is predictive of cardiovascular outcomes in patients with pulmonary hypertension.[1] The invasive requirement, however, significantly limits the clinical utility of this technique, and therefore, a non-invasive, safe means to measure pulmonary arterial vasoreactivity would be a potent clinical and research tool.[2,3] Here we demonstrate reactive changes in pulmonary artery CSA and BF during isometric handgrip exercise (IHE), a proven endothelial-dependent stressor, in healthy subjects as detected by 3T MRI.

Methods: We studied nine healthy subjects (6 women, age 45±1.4 years (mean±SEM for all data) placed prone in a 3T MRI scanner (Philips). Scout scans were obtained to determine the 3D course and orientation of the pulmonary arterial tree. VCG-triggered breath-hold cine MRI perpendicular to the descending branch of the left and/or right pulmonary artery (PA) was performed to measure CSA (TFE-factor=5, SENSE factor=2) and velocity (TFE factor=4,SENSE=2,VENC=100cm/s, Fig 1), with a temporal resolution of 34ms, and in plane resolution of 0.8x0.8mm. After baseline imaging, each subject performed IHE for 6 min at 30% of their maximum grip strength on a non-magnetic, handgrip dynamometer, during which repeat PA imaging was performed. Blood pressure, heart rate and rate pressure product (RPP) were recorded at rest and during IHE. The images were analyzed for PA CSA and integrated volume flow (in mL/mm, over cardiac cycle using QFlow software) for each PA segment at baseline and during IHE.

Results: Image quality at baseline and during IHE was sufficient for analysis in all volunteers. The mean percent increase in rate pressure product with stress was 26±2.2% (p=0.001 vs. baseline). IHE induced significant increases in PA cross sectional area (baseline 109.2±20.7mm^2 vs. stress 116.2±12.1mm^2, p=0.001). The mean increase in PA CSA with stress was 6.4±2.6%. Similarly, there was a significant increase in PA volume flow with IHE (baseline 948±177 mL/min vs. stress 1087±188 mL/min, p=0.0003, relative change Fig 2).

Conclusions: 3T MRI with IHE enables the quantification of PA area and flow volume changes in response to an endothelial-dependent stress with both high temporal and spatial resolutions. In healthy adults, isometric handgrip causes significant increases in PA area and volume flow. The present findings warrant further studies using this technique in patients at risk for pulmonary artery disease and those with suspected endothelial dysfunction.

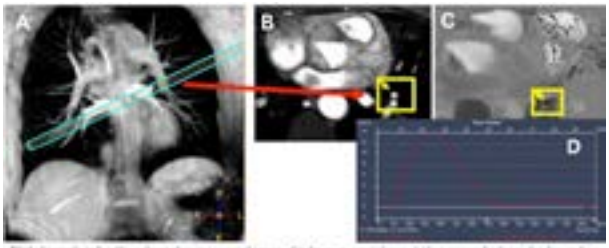

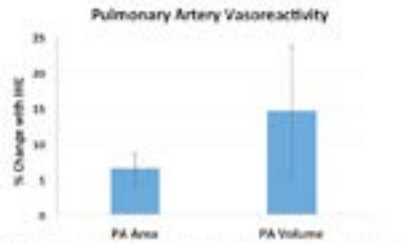

P358

Determinants of Thoracic Aortic Volume: Multi-Ethnic Study of Atherosclerosis

Sreeja Sanampudi, BS[1] Joao A.C. Lima, MD, MBA[2], Bharath Ambale-Venkatesh, PhD[3], Gisela Teixidó-Turà, MD, PhD[4], Tomoki Fujii, MS, RT[2], Alban Redheuil, MD, PhD[5], Colin O. Wu, PhD[6], Antoinette S. Gomes, MD[7], David Bluemke, MD, PhD[8]

1. *University of Kentucky College of Medicine, Lexington, KY*
2. *Johns Hopkins University, Baltimore, MD*
3. *Johns Hopkins University, MD*
4. *Hospital Vall d'Hebron, N/A, Spain*
5. *Sorbonne Universités, UPMC Univ Paris 06, INSERM, CNRS, UMR 7371, UMRS 1146, Laboratoire d'Imagerie Biomédicale, 75013, Paris, France, Ile-de-France, France*
6. *National Institutes of Health, MD*
7. *David Geffen UCLA School of Medicine, Los Angeles,, CA*
8. *NIH, MD*

Background: While previous studies have shown that cross-sectional aortic area and aortic diameters are useful diagnostic tools to distinguish normal states from diseased states, volumetric analysis may potentially provide a more complete assessment of aortic size. This study sought to assess cross-sectional associations of thoracic aortic volume (TAV) assessed by MRI with left ventricular (LV) remodeling and cardiovascular (CV) risk factors in the Multi-Ethnic Study of Atherosclerosis (MESA).

Methods: The MESA study enrolled 6814 participants free of cardiovascular disease at baseline (2000-2002). We included MESA participants who underwent MRI at the follow-up exam at year-10. TAV was measured using transverse bright-blood SSFP (TR/TE = 45/1.05 ms, FA = 65 deg) or black blood TSE (TR/TE = 1 R-R/22 ms, FA = 160 deg) images starting from the level of the arch to the level of the aortic valve (see Figure). The slice thickness was set at 8 mm with 2 mm slice gap, and the in-plane resolution varied from 1.1 to 2.1 mm^2 per pixel. QMass (version 7.5, Medis) was used to calculate TAV using Simpson's method from the transversal cross-sectional areas and was indexed to height^1.7. In all, 1,172 participants had adequate coverage of the aorta and sufficient image quality. Multivariable linear regression models were generated to determine the relationship between demographics, CV risk factors and TAV.

Results: Participants were 69±9 years, 55% female, 38% Caucasian, 20% Chinese, 30% African-American, 11% Hispanic, 60% had hypertension, 19% diabetes, with TAV = 138.64±40.82mL. In multivariable regression, TAV was directly associated with age (betal (b)=0.40,p < 0.001), male gender (b=0.35,p < 0.001), body mass index (b=0.20,p < 0.001), systolic blood pressure (b=0.07,p=0.008), and hypertension medication use (b=0.11,p < 0.001); and inversely associated with lipid medication use (b=-0.06,p=0.038) and treated diabetes (b=-0.10,p < 0.001). Smoking, impaired fasting glucose, HDL cholesterol and total cholesterol were not associated with TAV. Compared to Chinese-Americans, Caucasians (b=-0.15, p < 0.001), African-Americans (b=-0.23,p < 0.001), and Hispanics (b=-0.10,p=0.001) all had lower TAV. LV mass index (b=0.35,p < 0.001), and aortic arch pulse wave velocity (b=0.16,p < 0.001) were directly associated with TAV, while LV ejection fraction (b=-0.07,p=0.006) and ascending aortic distensibility (b=-0.13,p < 0.001) were inversely associated after adjustment for CV risk factors.

Conclusions: Greater TAV is associated with age, hypertension, LV remodeling, and reduced LV function in a large multiethnic population while diabetes and lipid medication use were associated with lower TAV.

Risk Factor	Coefficient	P-value
Age	0.773	<0.001
Gender	9.353	<0.001
Race:		
Chinese American	4.005	<0.001
African American	-3.530	<0.001
Hispanic	0.0435	0.972
BMI	0.565	<0.001
Diastolic blood pressure	0.324	<0.001
Hypertension medication	3.486	<0.001
Lipid medications	-1.495	0.063
Diabetes:		
Impaired fasting glucose	-1.742	0.077
Untreated diabetes	-1.856	0.567
Treated diabetes	-3.170	0.003

P359

Quantitative investigation of abdominal aortic aneurysm growth using registration-based segmentation of 3D black-blood MR images

Yan Wang, Ph.D.[1]Evan Kao, B.S.[2], Florent Seguro, M.D.[2], Farshid Faraji, M.S.[1], Yue Zhang, Ph.D.[3], Michael D. Hope, M.D.[1], Jing Liu, Ph.D.[1], David Saloner, Ph.D.[1]

1. *University of California, San Francisco, CA*
2. *University of California San Francisco, CA*
3. *Northern California Institute for Research and Education, CA*

Background: Analysis of abdominal aortic aneurysm (AAA) geometric features plays an important role in medical treatment. The 3D patient-specific geometries can facilitate the assessment of rupture risk, which is normally based on aneurysm diameter, volume and growth. We propose a reproducible and efficient technique to segment and measure the vessel wall of AAA in 3D black-blood magnetic resonance (MR) imaging.

Methods: Segmentation: The proposed method (Figure 1) consists of co-registering the contrast enhanced MR angiography and black-blood MR images, and segmenting both the inner and outer wall using geometric active contours (GAC) and registration-based geometric active contours (RGAC), respectively. 2) Measurement: Cross sections of the outer wall orthogonal to the vessel centreline were generated at 1mm intervals. The maximum diameter was defined as the maximum distance through each cross section along the ray projected from the centerline. The maximum diameter, area, and volume for each case were calculated. The proposed segmentation technique was evaluated on 9 AAA patients who had follow-up studies. To validate our technique, an experienced radiologist also manually segmented all cases.

Results: Theaverage Dice and CV values reached 89.79±2.46%, which demonstrated that comparable and stable segmentation was achieved with the proposed method compared to manual segmentation. The Bland-Altman and linear regression for the manual and the proposed method generated inner, outer and vessel wall volumes with Bias±1.96std (0.02±0.03, 0.05±0.03 and 0.01±0.07, respectively) and P value (0.85, 0.73 and 0.73, respectively) demonstrating good agreement between manual analysis and the proposed segmentation. The proposed segmentation method requires less time than other semi-automated methods, and is an order of magnitude faster than fully manual segmentation. Measurements including maximum diameter, area and volume are shown in Figure 2, respectively. While the aneurysm size of 2 patients in 9 appeared to decrease at follow-up (6 month after baseline), the reproducibility of measurement must still be established. The average difference of maximum distance, maximum area, and volume between baseline and 6 months follow-up study is 1.65%±16.15%, 1.85%±25.59%, and 1.78%±17.37% in our study.

Conclusions: The proposed segmentation provides a reproducible and efficient way to define the geometrical morphology of AAA, and the measurement gives an accurate and repeatable way to get the maximum AAA diameter, which can be used as a key parameter in surgical planning.

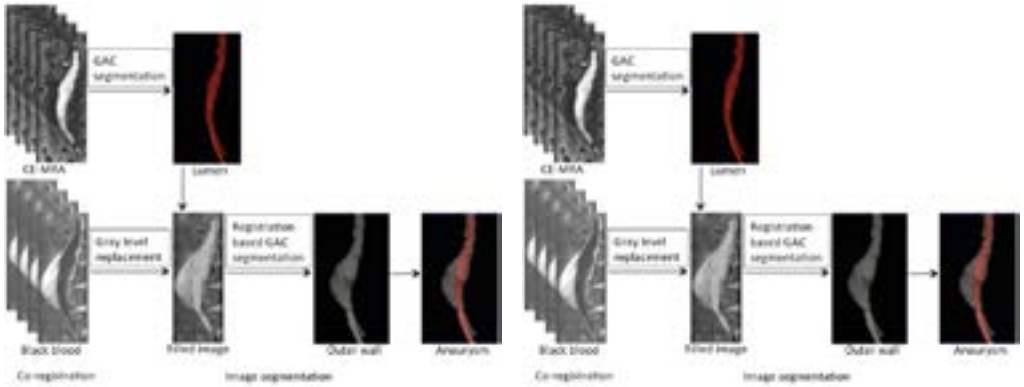

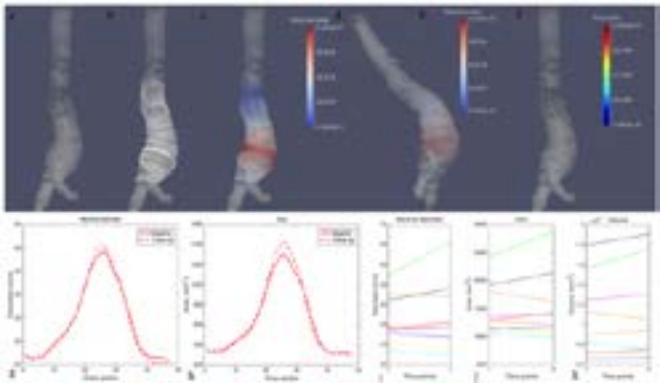

P360

Efficient Pipeline for Patient-Specific Analysis of Intracranial Aneurysm Geometric Parameters Using a Novel Lattice-Boltzmann-Method-based Segmentation

Yue Zhang, Ph.D.1, Yan Wang, PhD[2], Evan Kao, B.S.[2], Bing Tian, M.D.[2], David Saloner, Ph.D.[3], Jing Liu, Ph.D.[3].

1. *Northern California Institute for Research and Education, CA*
2. *University of California San Francisco, CA*
3. *University of California, San Francisco, CA*

Background: Analysis of intracranial aneurysm (IA) geometric features plays a key role in medical treatment planning. The 3D patient-specific geometries can facilitate the assessment of rupture risk, which is normally based on aneurysm diameter, volume and growth. We propose a reproducible and efficient technique to segment and measure the IA from contrast-enhanced magnetic resonance imaging.

Methods: 1)Segmentation: The proposed method segmented IA using region-based active contours (RAC) that were solved with the help of the lattice Boltzmann method, with the aim of being much more efficient than the classic RAC models. 2) Measurements (Figure 1): After the segmentation, the centerline was created based on two seeds that were located respectively at the top and neck of each IA. Cross sections of the IA orthogonal to its centerline were generated at 0.1mm intervals. The diameter was defined as the maximum distance in each cross section along the ray projected from the centerline. The width of the IA was chosen as the maximum diameter of all these cross sections. 3) Growth map: The growth of each voxel was defined as the displacement between the baseline and follow-up study of the segmented IA geometry. The proposed segmentation was tested on 6 IA patients who all had follow-up studies and validated against manual segmentation by an experienced radiologist.

Results: The results demonstrated that comparable and stable segmentation was achieved with the proposed method compared to manual segmentation. Furthermore, the proposed method is an order of magnitude faster than fully manual segmentation. The ranges of length and width of 6 IA cases are 4.4~14.9mm and 3.3~13.4mm, respectively. The volume evolution of 6 IA cases is plotted in Figure 2 along with the growth map of one IA (color coded with increasingly red shades representing regions with faster growth rates).

Conclusions: The proposed segmentation provides a reproducible and efficient way to obtain IA geometry, and the measurements obtained based on this segmentation provide an accurate and repeatable way to produce the IA length, width and volume, which can be used as indicators for the medical treatment planning.

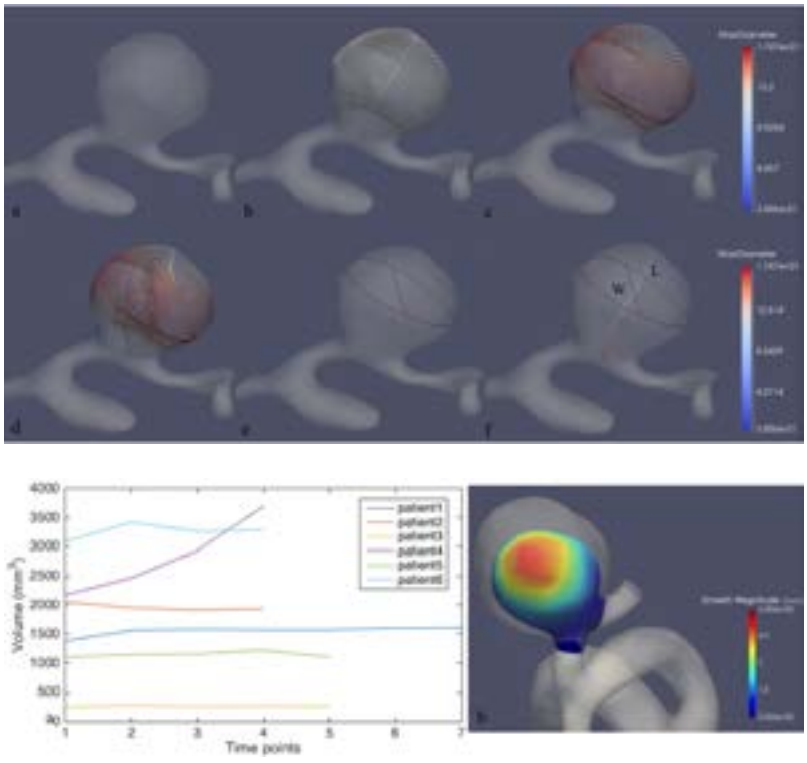

P361

Hemodynamic Differences in Children with Bicuspid and Unicuspid Aortic Valves

Michal Schäfer, MSc[1] Lorna Browne, MD[2], Kendall Hunter, PhD[3], Uyen Truong, MD[2], Alex J. Barker, PhD[4]

1. *University of Colorado Denver | Anschutz Medical Campus; Children's Hospital Colorado, Franktown, CO*
2. *Children's Hospital Colorado, CO*
3. *University of Colorado Denver | Anschutz Medical Campus, CO*
4. *Northwestern University Feinberg School of Medicine, Chicago, IL*

Background: Flow and shear hemodynamic alterations due to altered valve morphology have been strongly associated with aortopathy in adult populations. The objective of this study was to assess flow and wall shear stress (WSS) hemodynamic variations in the ascending aorta among children with anomalous aortic valve morphology including unicuspid and bicuspid aortic valve (UAV and BAV) malformations.

Methods: This is a retrospective study of two-dimensional phase-contrast MRI (PC-MRI) in pediatric patients with unicuspid aortic valve (n=6), right-left (RL) coronary BAV (n=19), and trileaflet controls (n=19) to analyze flow and shear hemodynamic condition in the aorta. The nature of the aortic valve morphology was assessed from SSFP images of aortic root and velocity encoding images. The acquisition plane was positioned approximately one centimeter above the sinotubular junction. The data analysis included comprehensive flow, WSS, and stiffness analysis.

Results: Children with congenitally malformed aortic valves presented with significantly decreased shear with non-uniform circumferential distribution, reduced aortic strain, and regurgitative flow patterns. While children with trileaflet valve had uniformly distributed peak WSS along the vessel circumference, children with RL-BAV revealed peak shear concentration along the posterior wall with directionally reversed WSS along the anterior wall due to flow regurgitation. Children with UAV tend to have maximum WSS localized along right and anterior wall. Comparative analysis revealed significant variability between UAV, RL-BAV, and trileaflet groups in peak WSS (dyne/cm^2) (5.1 ± 1.4, 7.2 ± 3.0, 9.4 ± 2.3), time-averaged WSS (dyne/cm^2) (1.1 ± 0.3, 1.6 ± 0.8, 2.1 ± 0.03), and aortic strain (%) (21 ± 4, 17 ± 8, 30 ± 7). Furthermore, children with RL-BAV presented significantly increased oscillatory shear index (0.06 ± 0.07 vs. 0.02 ± 0.03), increased WSS eccentricity (dyne/cm^2) (15 ± 10), and reduced peak flow (l/min) 13.8 ± 6.3 vs. 17.8 ± 5.8) when compared to trileaflet group.

Conclusions: Children with congenitally altered aortic valve showed variable flow and shear hemodynamic patterns unique to each malformations in specific groups significantly younger than in any previously reported studies. Disturbations within flow patterns and non-uniform WSS already seen in childhood may lead to known vasculopathies frequently observed in adult populations. Future longitudinal studies will focus on flow and WSS effects on overt undesirable signs of aortic remodeling, including vessel dilation, stiffness and degree of regurgitation.

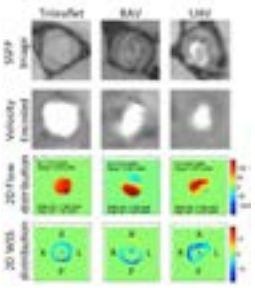

Demographics and Flow/Shear Hemodynamics

K-W p-value	Trileaflet (n=19)	Bicuspid (n=19)	Unicuspid (n=6)	
NS	11.7 ± 2	10.8 ± 5.4	8.3 ± 4.9	Age
NS	2.4 ± 0.3	2.4 ± 0.5	3.3 ± 1.1	Aortic Diameter (cm)
0.002	9.4 ± 2.3	7.2 ± 3.0*	5.1 ± 1.4*‡	Peak WSS (dyne/cm^2)
0.002	2.1 ± 0.6	1.6 ± 0.8*	1.1 ± 0.3*‡	TA WSS (dyne/cm^2)
NS	10	15*	17	WSS eccentricity (dyne/cm^2)
NS	0.02 ± 0.03	0.06 ± 0.07*	0.10 ± 0.08	Oscillatory Shear Index
0.01	17.8 ± 5.8	13.8 ± 6.3*	14.9 ± 12.1	Peak Flow (l/min)
NS	122 ± 16	129 ± 43	131 ± 40	Peak Velocity (cm/s)
0.0002	30 ± 7	17 ± 8*	21 ± 4*	Strain (%)
K-W = Kruskal-Wallis, * = significantly different form trileaflet, ‡ = significantly different from bicuspid				

P362

Arterial Flow Reserve in Patients with Peripheral Artery Disease is Related to Skeletal Muscle Capillary Density and Arterial Stenosis

Tomoki Fujii, MS, RT[1], Bharath Ambale-Venkatesh, PhD[2]Emerson C. Perin, MD, PhD, FACC[3], Alan T. Hirsch, MD, FACC, FAHA, MSVM[4], Joao A.C. Lima, MD, MBA[1]

1. *Johns Hopkins University, Baltimore, MD*
2. *Johns Hopkins University, MD*
3. *Texas Heart Institute, TX*
4. *University of Minnesota, MN*

Background: Peripheral artery disease (PAD) represents a highly prevalent cardiovascular disease, with an associated major limb functional morbidity (claudication). We hypothesized that measures of leg skeletal muscle perfusion and popliteal artery flow reserve, chosen as markers of effective angiogenesis, would be associated with arterial anatomy, particularly arterial stenosis.

Methods: The National Institutes of Health-sponsored ***"Patients with Intermittent Claudication Injected with ALDH Bright Cells"*** (PACE) study is a randomized, double-blind, placebo-controlled multi-center clinical trial that has assessed the clinical safety and efficacy of autologous bone marrow derived aldehyde dehydrogenase-bright cells in symptomatic PAD patients with claudication (with high grade infrainguinal stenosis, and ankle-brachial index < 0.9). A reactive hyperemia (post-occlusive) protocol, in conjunction with dynamic contrast-enhanced (DCE) MRI and phase-contrast (PC) MRI were used to evaluate calf muscle perfusion and popliteal artery flow respectively, using 1.5-T and 3-T scanners (GE, Siemens and Philips) across 9 sites. A 5-minute occlusion of femoral artery flow was achieved by inflating a thigh cuff to suprasystolic pressures on the asymptomatic leg to induce hyperemia. DCE-MRI was performed at mid-calf using 3D SPGR sequences (spatial resolution: 1x1x5 mm, temporal resolution < 5ms) following flow occlusion and 0.05 mmol/kg Magnevist injection. Transfer constant (Ktrans) and fractional blood plasma volume (Vp) were obtained from the modified Tofts' model (with T1 correction) post-hyperemia. PC-MRI measured popliteal artery flow before and after hyperemia. The arterial flow reserve (AFR) was defined as the increment in peak flow after release of thigh occlusion from PC-MRI. Time-to-peak (TTP) was calculated as the time to peak flow after cuff release. Contrast enhanced MR angiography was performed with 0.10 mmol/kg Magnevist to assess the mean stenosis across the superficial femoral artery (SFA, across 3 segments). Parameters were log-transformed as appropriate before assessment of Pearson's correlation.

Results: A total of 82 subjects were include with mean age- 66 ± 9 yrs and they were 75% male` Physiologic measures included Vp= 3.8 ± 3.1%; Ktrans= 0.07 ± 0.05 ml/g/min; AFR= 1.6 ± 2.2 ml/s; and TTP= 130 ± 119 ms. Vp was positively correlated with AFR; TTP was inversely correlated with Vp, and AFR. Mean stenosis at thigh correlated with AFR and TTP, but not Vp. Transfer constant Ktrans was not associated with flow or stenosis.

Conclusions: MR popliteal artery blood flow (AFR and post-reactive hyperemic TTP flow) provides a physiologic correlate that defines the downstream calf muscle capillary density (Vp), and is associated with upstream arterial stenosis severity.

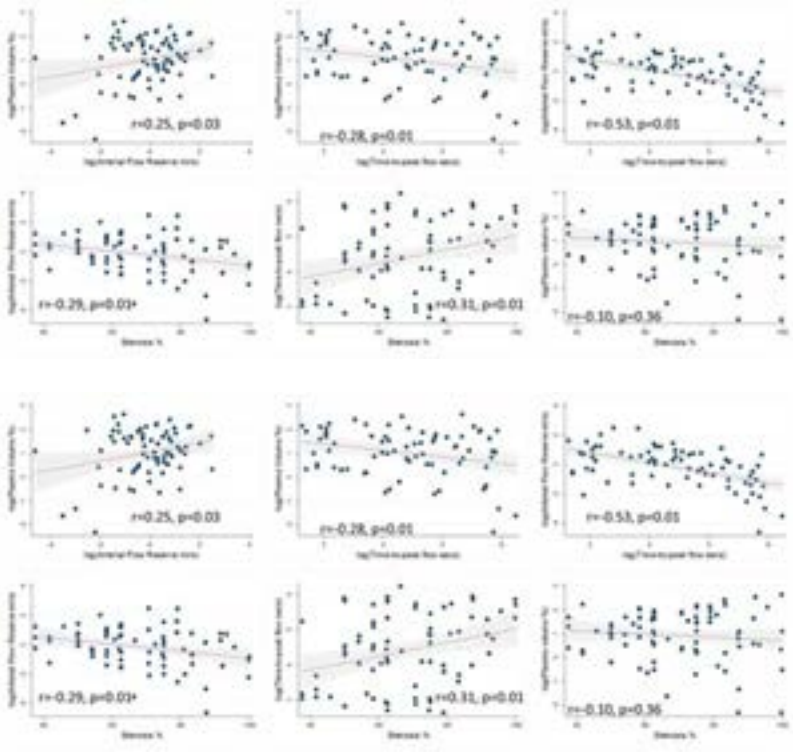

P363

Computer assisted assessment of plaque vulnerability

Andrew Comerford, PhD[1] Rene Michael. Botnar, PhD[2], Alkystis Phinikaridou, PhD[2]

1. King's College London, England, United Kingdom
2. King's College London, London, England, United Kingdom

Background: Atherosclerosis is a major cause of morbidity and mortality. Clinical events, such as heart attacks, can arise from rupture of "vulnerable" plaques. Identification of these plaques remains a clinical challenge. Here we detail a non-invasive approach to determine arterial wall strain, and its potential role in plaque rupture, in a rabbit model by combining biomechanical modeling with elastin-specific molecular MR-imaging. In the long-term the approach could identify patients with high-risk lesions thus reducing clinical complications.

Methods: An existing MR dataset of 14 New Zealand White rabbits with atherosclerosis induced by high cholesterol diet was utilized. Animals were imaged with a 3T MR scanner in the supine position. Late gadolinium enhancement (LGE) inversion-recovery images were obtained 2 hours after administration of 0.2 mmol/kg of the elastin-specific contrast agent, ESMA. Plaque disruption was triggered with Russell's viper venom and histamine. A sub-group of six abdominal aortic walls (one control and five diseased animals) were segmented from ESMA data (0.23 × 0.23-mm resolution; 4-mm-thick slices; 25 slices; range: renal arteries to aortic bifurcation). CINE MR data of the aorta (EGC triggered SSFP images; TR/TE=7.8/3.9ms, FA =60°, resolution=0.5x0.5mm, slice thickness=5mm, slices=11, phases=18) from the same animals were used to determine the luminal shape at peak systole and end diastole. From these data, arterial wall strain was determined using hyperelastic warping in the finite element software, FEBio (see Figure 1). This is a registration approach that utilizes image intensity differences between diastolic and systolic CINE images, and applies this as a force to deform a finite element discretization of the segmented aortic wall geometry (LGE images), thus allowing biomechanical data to be ascertained (e.g. strain). Strain distributions in the simulated aortas were compared with local elastin content - identified from the contrast-to-noise ratio (CNR) of the ESMA data.

Results: Arterial wall deformation was anisotropic and affected by the surrounding tissue. Figure 2 shows the strain and CNR on different cross-sections of the abdominal aorta mapped into cylindrical coordinates for five diseased animals. Elevated strain occurred predominantly in regions adjacent to locations of higher elastin content and aligned in the circumferential direction. In this study, thrombosis occurred only in animal 2 (A2). In this animal, mean CNR was elevated compared to the other animals (A2 CNR=43; A1, A3, A4, A5 & control CNR=29, 22, 28, 11, 12, respectively). Equivalently, mean principal strain was elevated (A2 E=0.22; A1, A3, A4, A5 & control E=0.16, 0.15, 0.16, 0.13, 0.15, respectively).

Conclusions: Our novel assessment of arterial wall biomechanics from MR imaging with an elastin specific contrast agent shows much promise. Currently the dataset is being expanded to more animals with greater occurrence of thrombosis.

http://www.ConferenceAbstracts.com/uploads/cfp2/attachments/LDFAIBDN/LDFAIBDN--220502-1-ANY.pdf

http://www.ConferenceAbstracts.com/uploads/cfp2/attachments/LDFAIBDN/LDFAIBDN--220502-2-ANY.pdf

P364

Thoracic aorta PWV assessment by using 4D Phase Contrast

Gilles Soulat, MD[1] Umit Gencer, -[1], Nadjia Kachenoura, PhD[2], Konstantinos Stampoulis, -[1], Yousef Alattar, -[1], Emmanuel Messas, MD, PhD[1], Olivier Villemain, MD[1], Stéphane Laurent, MD, PhD[1], Elie Mousseaux, MD, PhD[1]

1. European Hospital Georges Pompidou APHP; INSERM U970 PARCC Paris descartes University, Ile-de-France, France
2. Sorbonne Universités, UPMC , INSERM UMRS 1146, Laboratoire d'Imagerie Biomédicale, Ile-de-France, France

Background: In MRI, thoracic aorta pulse wave velocity (TAPWV) is usually estimated by 2D phase contrast (PC) with either in plane or through plane velocity acquisition. Thanks to technological improvement, 4D PC with full coverage of the TA and 3 dimension velocity encoding thought time can be now achievable in 10min. Our aim was to compare estimation of TAPWV using 4DPC or 2DPC on healthy volunteer.

Methods: Acquisitions were performed on a 3 Tesla scanner (GEHC, 750w). 2DPC was done with through plane velocity encoding on an axial oblique slice perpendicular to ascending and descending TA. 4D acquisition covered the full TA volume from the aortic valve to diaphragm. Segmentation and velocity estimates were done by using cloud computing (Arterys, California). Optimal data view sharing was applied to obtain 8ms and 16ms temporal resolution for 2DPC and 4DPC, respectively. Flow data curves where further computed on homemade software (artfun) to assess PWV for both 2D and 4D acquisition.

Results: 57 healthy volunteers (25 male, age 50.9y ±17.3) were included. Correlation coefficient between 4DPC and 2DPC PWV was 0.73 (p

Conclusions: TAPWV can be accurately estimated by 4D flow MRI, since close relation with 2DPC and aging have been obtained. By using the same data set, TAPWV should be estimates in association to other stiffness and geometric parameters of the TA.

P365

Highly Efficient Pulmonary MR Venography using Undersampled Radial QISS: Comparison with CT Angiography

Robert R. Edelman, MD[1] Amit Pursnani, MD[2], Shivraman Giri, PhD[3], Ioannis Koktzoglou, PhD[4]

1. NorthShore University HealthSystem, Evanston, IL
2. 8475702000, IL
3. Siemens Healthcare, IL
4. NorthShore University HealthSystem, IL

Background: Electrical isolation of the pulmonary veins is a useful treatment option for patients with atrial fibrillation who do not respond adequately to medical therapy. Procedure guidance typically involves integration of 3D electro-anatomical maps with pre-procedural contrast-enhanced MRA or CTA. For patients with poor renal function, contrast administration is contraindicated. While traditional multi-shot nonenhanced MRA techniques such as navigator-gated 3D balanced steady-state free precession are a potential option for patients who have a regular heart rhythm, image quality will be degraded in the presence of significant arrhythmias. We hypothesized that a recently developed single-shot nonenhanced technique, undersampled radial quiescent-interval slice-selective (QISS) MR angiography, might provide an efficient means to display the pulmonary venous anatomy while being resistant to image artifacts from the arrhythmia.

Methods: The study was approved by the institutional IRB. Technical optimization was performed in healthy volunteers. Patients in atrial fibrillation scheduled for CTA prior to pulmonary vein isolation underwent nonenhanced MRA on a 1.5 Tesla MAGNETOM Avanto system (Siemens Healthcare, Erlangen, Germany). MRA techniques included: (1) breath-hold radial QISS; (2) free-breathing, navigator-gated radial QISS; (3) navigator-gated, T2-prepared 3D Cartesian bSSFP. Imaging parameters for radial QISS included: slice thickness = 1.6mm – 4mm, in-plane resolution = 1mm, 98 radial views, TI = 550 ms, 1 slice per RR interval; 20 slices per breath-hold. For navigator-gated QISS, 30 slices were acquired, acceptance window = 3mm, scan times of ~2-3 minutes. For navigator-gated 3D bSSFP, slice thickness (before interpolation) was 2mm scan times of ~5-10 minutes.

Results: Single-shot radial QISS depicted the pulmonary veins without significant blurring, flow or off-resonance artifacts in healthy volunteers and patients with atrial fibrillation (Fig. 1). The entire left atrium including the appendage, along with the proximal segments of the pulmonary veins, could be encompassed in a single breath-hold using a slice thickness ≥ 3mm, whereas two breath-holds were required using thinner slices. Reduction of slice thickness was associated with increased off-resonance and flow artifacts in the proximal pulmonary veins. Navigator-gated single-shot radial QISS images showed only slightly increased blurring compared with breath-hold acquisitions. By comparison, navigator-gated 3D bSSFP showed severe motion artifacts in patients with atrial fibrillation. In patients, there was excellent agreement between radial QISS MRA and CT angiography.

Conclusions: Breath-hold single-shot radial QISS shows promise as a highly efficient nonenhanced method for pre-procedural evaluation of pulmonary venous anatomy, with navigator-gated QISS being a viable option for patients who cannot adequately breath-hold.

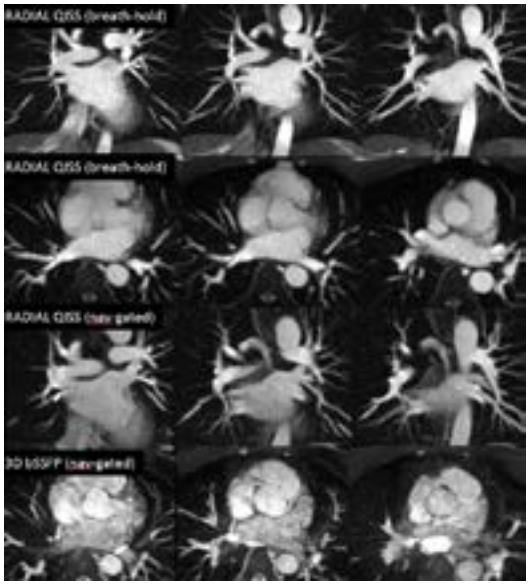

P366

Mixed Multiple T2 preparation modules for high contrast oxygen-sensitive cardiac MRI

Galen D. Reed, PhD[1] William Overall, Ph.D.[2], Michelle Nystrom[3], Okai Addy, Ph.D.[4], Kenneth Johnson, Ph.D.[2], Juan Santos, Ph.D.[2], Bob Hu, MD[2]

1. *HeartVista, San Francisco, CA*
2. *HeartVista, CA*
3. *HeartVista, Los Altos, CA*
4. *HeartVista, Inc, Los Altos, CA*

Background: Oxygen-dependent T_2 changes have been modeled by the Luz-Meiboom (LM) relation which characterizes dependence of T_2 on numerous parameters including echo spacing τ_{esp} [1-4]

$R_2 = R_{20} + K(\tau_{esp})$

$K(\tau_{esp}) = \tau_{ex} H(1-H)[\alpha\omega(1-S)]^2 (1 - (2\tau_{ex}/\tau_{esp}) \tanh(\tau_{esp}/2\tau_{ex}))$

where τ_{ex} is the intra-/extra-cellular water exchange time, H is the hematocrit, $\alpha\omega_0$ is the frequency shift between intra- and extra-cellular environments, and S is the oxygen saturation. This study investigates the feasibility of acquiring oxygen-sensitive images using 2 images acquired at identical echo times but with differing echo spacing. Dividing the images eliminates the background R_{20} contrast thus isolating image contrast to the LM parameters:

$S(\tau_{esp,2})/S(\tau_{esp,1}) = e^{TE(K(\tau_{esp,1}) - K(\tau_{esp,2}))}$

The challenge of sampling a wide range of τ_{esp} values for maximizing contrast is addressed here using a mixed assortment of T_2 preparation modules. Commonly used MLEV super cycles [5] provide robust refocusing to B1 imperfections but necessitate relatively low RF pulse sampling rates. The proposed modification uses SSFP phase cycled hard pulses for short τ_{esp} sampling; this has only a second-order dependence on B_1 variations [6] and a usable bandwidth of $1/\tau_{esp}$. The adiabatic double spin echo module described previously [7] is well suited for long τ_{esp} sampling (Fig 2c) at which point the SSFP bandwith is too narrow (Fig 2b).

Methods: Sequences were implemented on the RTHawk system [8] and data acquired on a GE 1.5T system with healthy volunteers under informed consent. Two single shot SSFP images were acquired during a breath hold with a 4 s delay between images. Each image had TE=100 T_2 prep modules. The first was a hard pulse SSFP (Fig 2a) with 24 180° hard pulses, α/2 excitation and flip-back pulses, 4.2 ms τ_{esp}. The second was an adiabatic double spin echo, τ_{esp} = 50 ms. The long-τ_{esp} image was divided into the short τ_{esp} image and displayed in the colormap (Fig 3).

Results: Figure 3 shows example T_2 prepared images and ratio map. The nearly 2X attenuation difference between the right atrium and aorta indicates that this method may be useful for obtaining a very large effect size.

Conclusions: A T_2 prepared, multiple τ_{esp} sequence was created and tested. Preliminary results indicate this may be useful tool for obtaining high-contrast, oxygen sensitive images in a single breath hold.

References

[1] M. G. Friedrich et al., JCMR 2013;15:43

[2] G. A. Wright et al., JMRI 1991: 1:275-283

[3] Z. Luz. and S. Meiboom., J Chem Phys, 1963;39:366

[4] J. Varghese et al., JCMR 2016 18(Suppl 1):W29.

[5] J. H. Brittain et al., MRM 1995;33:689–696

[6] G. D. Reed et al., Tomography 2016; 2(2): 125-137

[7] R Nezafat et at., MRM 2006;55:858-864

[8] J. M. Santos et al., IEEE EMBS, 2004

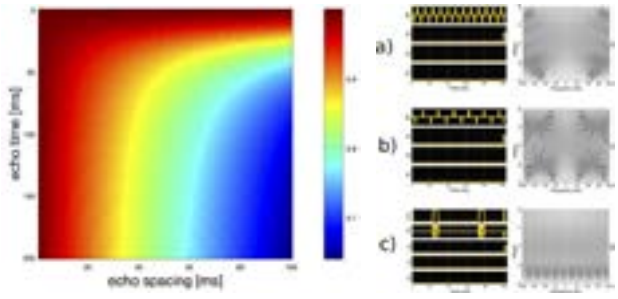

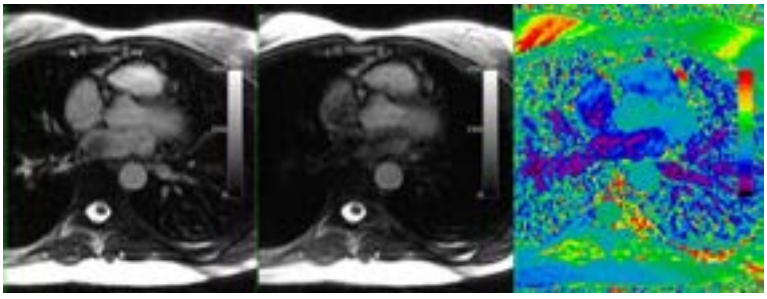

P367

Thoracic aorta flow sensitive 4D MR imaging in hypertension

Lizhen Cao, M.D.[1]Zhiyuan Dong, M.D.[1], Xiangying Du, MD[2], Kuncheng Li, MD[2]

1. Xuanwu Hospital of Capital Medical University, Beijing, China (People's Republic)
2. Xuanwu Hospital, Capital Medical University, Beijing, China (People's Republic)

Background: Previous studies have employed flow sensitive 4D MR imaging to characterize the complex flow patterns in the thoracic aorta of healthy volunteers and patients with aortic pathologies1,2. The purpose of this study was to evaluate the blood flow patterns of thoracic aorta in hypertension using flow sensitive four-dimensional MR imaging at 3T.

Methods: 30 hypertensive patients underwent flow sensitive 4D MR scan after IRB approval and written informed consent. All patients were first diagnosed as hypertension without any medical treatments. According to the 1999 WHO/ISH hypertension guidelines, the patients were grouped as grade 1(n= 14), grade 2 (n= 10) and grade 3 (n= 6). Studies were performed on a 3T scanner (MAGNETOM Verio, Siemens Healthcare, Erlangen, Germany) with a 32-channel body coil. Data preprocessing, quantification and visualization were performed using a prototype 4D-Flow WIP package. On the phase-contrast MR angiograms (PCMRA), six analysis planes transecting the aortic lumen were automatically positioned. The flow data of each plane including flow rate, velocity and pressure was automatically quantified over the cardiac cycle. According to the formula: PI=(Vs–Vd)/Vm and RI=(Vs–Vd)/Vs, pulsatility index (PI) and resistance index (RI) were calculated with Vs, Vd, and Vm representing the systolic, diastolic and mean velocities, respectively. Image quality was independently evaluated by two experienced cardiovascular radiologists based on PCMRA, streamlines and particle traces visualizations using a four-grade scale (1-poor to 4-excellent).

Results: All patients were successfully examined with 4D PC-MRI. PI and RI increased with the growth of hypertensive grades, while mean velocity (Vm), flow rate (F) and pressure (P) decreased with the growth of hypertensive grades. As for PI, RI, Vm, F and P, there were statistical differences among grade 1, 2 and 3 ($P<0.05$). Agreement between the two radiologists was good ($k = 0.78$). The fastest flow was observed in the distal aortic arch (DAoA) in 25/30 cases. Helicity was present in hypertension of grade 2 and 3 in the ascending aorta (AAo) in 13/16 patients, DAoA (6/16) or descending aorta (DAo) (2/16). More helical vectors were observed in higher hypertensive grades.

Conclusions: The findings illustrate that sensitive flow 4D MR imaging can evaluate the hemodynamic patterns of thoracic aorta in hypertension. Future work will focus on the significance of these findings, and then reveal the development of aortic pathologies, such as atherosclerosis and dissection.

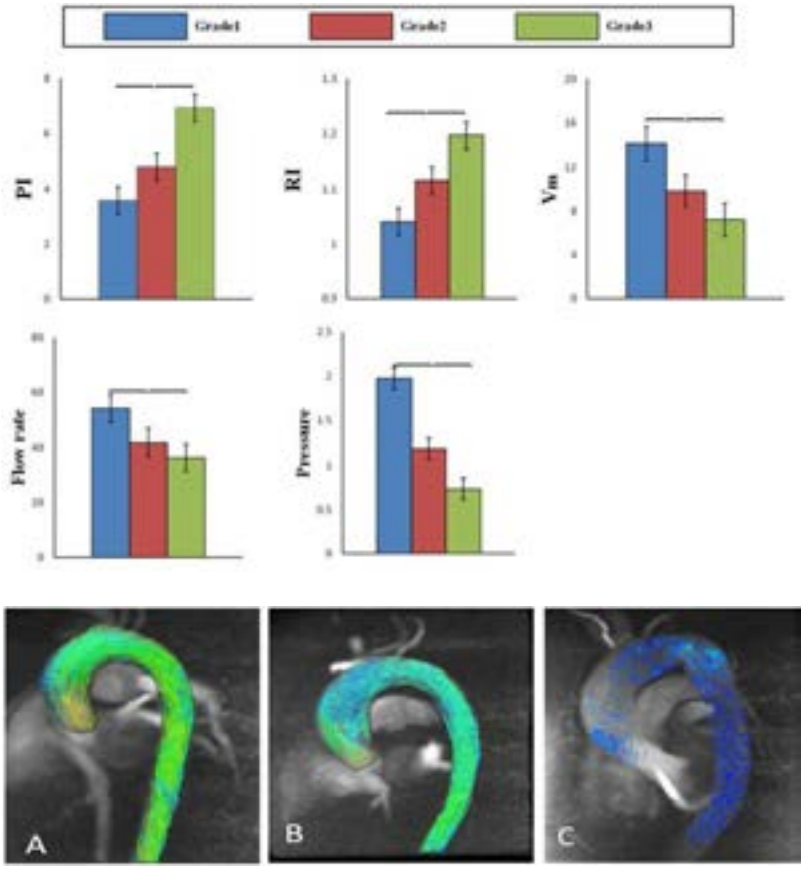

P368

4D Flow Cardiovascular MRI during Exercise

Jacob Macdonald, MS[1] Arij G. Beshish, MBBCH[2], Kristin Haraldsdottir, MS[3], Marlowe Eldridge, MD[4], Christopher J. Francois, MD[1], Oliver Wieben, PhD[5]

1. *University of Wisconsin - Madison, Madison, WI*
2. *University of Wisconsin- Madison, Madison, WI*
3. *University of Wisconsin- Madison, WI*
4. *University of Wisconsin - Madison, WI*
5. *University of Wisconsin-Madison, Madison, WI*

Background: MRI exercise studies can offer many advantages over current clinical techniques. Previous work demonstrated the feasibility of acquiring 2D flow measures across short breath holds following exercise but were limited by motion out of prescribed planes, equipment that limited exercise to low powers, and the need for a breathhold[1]. Utilizing a 4D-flow sequence would allow for flow measurements in multiple vessels from a single acquisition without fear of vessels leaving the imaging window. We investigated the feasibility of using a 4D-flow acquisition (PC-VIPR[2]) in conjunction with an exercise device capable of high exercise powers.

Methods: Seven volunteers (4M,3F; 26±1 years) were imaged on a clinical 3.0T system (Discovery MR750, GE Healthcare). A commercial MR-compatible stepper allowed subjects to exercise in a supine position in the MRI bore (Ergospect, Innsbruck, Austria). 4D-Flow cardiac imaging was performed at both rest and during exercise at 70% of their $VO_{2,max}$ with an ECG-gated, respiratory-averaged, radially-undersampled acquisition (PC-VIPR[2] , TR/TE=6.2/2.0ms; FA=10°; VENC=200cm/s; FOV=32x32x32cm; resolution=1.25mm isotropic; scan time=555s; temporal resolution=58ms). Exercise imaging began when the subject reached a steady-state heart rate. Flow and velocity measurements were made in the great vessels using a customized tool[3]. A paired student's t-test was used to assess statistically significant changes ($p < 0.05$) between rest and stress.

Results: Images acquired during exercise demonstrated increased noise, but sufficient delineation of all major vessels (Fig. 1). The exercise protocol was effective at inducing high exercise stress, as subjects demonstrated a statistically significant increase in cardiac output and significant increases in mean velocity in both the aorta and main pulmonary artery (MPA) (Fig. 2). Only non-significant changes to vessel area were detected. In all subjects, a decreased pulsatility index was measured in the Ao and MPA during exercise due to the decreased length of diastole relative to the cardiac cycle (Fig. 3). Only minimal changes were observed in the superior vena cava with exercise, but statistically significant increases to mean/peak velocity, peak flow, and total flow were observed in the inferior vena cava.

Conclusions: This study demonstrates the feasibility of 4D-flow imaging during high power exercise challenges, as flow and velocity measures in the great vessels responded to stress as expected. Future studies will investigate the capabilities of 4D-Flow MRI exercise studies in quantifying changes in flow characteristics, such as vorticity and helicity.

References

1.Macdonald. JCMR. 2015.

2.Johnson. MRM. 2008.

3.Stalder. MRM. 2008.

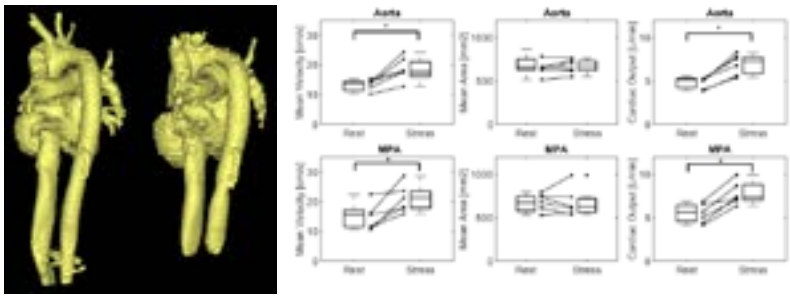

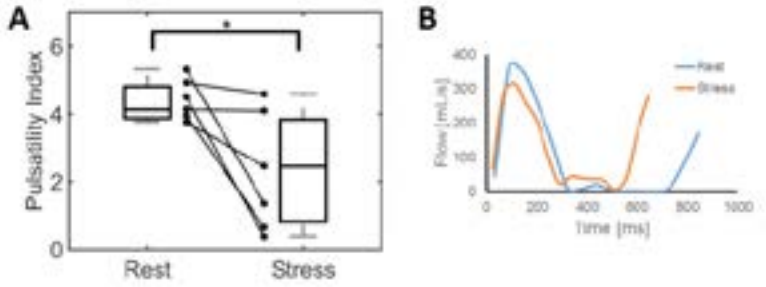

R001

Prognostic Value of Blood Pressure Model in Women Receiving PCI/CABG

Shimaa S. Khidr, MD[1]Mark Doyle, PhD[2], Gerald Pohost, MD, FACC[3], Leslee Shaw, Ph.D.[4], Sheryl Kelsey, Ph.D.[5], William Rogers, MD[6], Geetha Rayarao, MS[2], Barry Sharaf, MD[7], Carl Pepine, MD[8], C. Noel Bairey Merz, MD[9]

1. *Allegheny General Hospital, Pittsburgh, PA*
2. *Allegheny General Hospital, PA*
3. *University of Southern California, CA*
4. *Atlanta Cardiovascular Research Institute, Atlanta, GA*
5. *University of Pittsburgh, Pittsburgh, PA*
6. *University at Alabama at Birmingham, Birmingham, AL*
7. *Brown University, Providence, RI*
8. *University of Florida, Gainesville, FL*
9. *Cedars Sinai Medical Center, Los Angeles, CA*

Background: To examine the prognostic value of a novel model of systolic blood pressure in women with suspected ischemic heart disease receiving PCI/CABG. Previously, we showed that a Flow Index (FI) reveals the presence of several resonance conditions of LV ejection efficiency. The FI is based on aortic morphologic and flow data measured by cardiovascular magnetic resonance imaging (CMRI). Here we show that the FI can be used to model systolic blood pressure in women enrolled in the Women's Ischemia Syndrome Evaluation (WISE) Study and show how the model relates to the success or failure of PCI/CABG.

Methods: Women (n=201), mean age 59±11 yrs, with symptoms suggestive of myocardial ischemia underwent cardiac function evaluation by CMRI and were followed (40±17 months) for time to major adverse cardiac events (MACE) defined as CV death, myocardial infarction, or hospitalization for congestive heart failure. Based on the FI ordered data, Fourier analysis of the variation of systolic blood pressure (SBP) was performed. To reduce noise, 5 unique Fourier coefficients were retained by threshold selection and used to construct a predicted systolic blood pressure for each FI value. Using this model, patients were characterized by Increasing or Decreasing SBP (based on the slope of the FI ordered data and irrespective of their absolute SBP).

Results: MACE occurred in 26 women (13%) and PCI/CABG was performed in 31 (15%) patients. The MACE rate per year and average SBP between the Increasing vs. Decreasing groups were not significantly different (2.6 vs 2.6 and142±25 vs. 140±23, respectively). However, in the Increasing group, 19 (18%) patients received PCI/CABG of which 8 (42%) experienced events. Conversely, in the Decreasing group, 12 (13%) patients received PCI/CABG of which only 1 (8%) suffered an event.

Conclusions: The MACE rate is high for patients undergoing PCI/CABG vs. not receiving PCI/CABG for women in the Increasing group of predicted systolic blood pressure, suggesting that PCI/CABG is contraindicated. However, the MACE rate in the Decreasing group of SBP is lower for those receiving PCI/CABG, suggesting the PCI/CABG is strongly indicated. Further studies are needed to validate and explore this phenomenon.

R002

Associations Between pro-B-Type Natriuretic Peptide and Cardiac Troponin T with Global Systolic Function Measured by MRI: The Multi-Ethnic Study of Atherosclerosis (MESA).

Amir Ali Rahsepar, MD[1]Mohammadali Habibi, MD[2], Cheeling Chan, MS[3], Nadine Kawel-Boehm, MD[4], Kiang Liu, PhD[5], Joao A.C. Lima, MD, MBA[6], James Carr, MD[7]

1. *Northwestern University, Chicago, IL*
2. *Montefiore Hospital/Albert Einstein College of Medicine, NY*
3. *Northwestern University, IL*
4. *Kantonsspital Graubünden, Graubunden, Switzerland*
5. *Northwestern University Feinberg School of Medicine, Chicago, IL*
6. *Johns Hopkins University, Baltimore, MD*
7. *Northwestern Memorial Hospital, Chicago, IL*

Background: Pro-B-Type Natriuretic Peptide (BNP) is a regulator of cardiovascular function, and is elevated in acute myocardial infarction (MI) and heart failure. Troponin T is also associated with myocardial necrosis and elevated levels of troponin are used for detection of MI. Cardiac magnetic resonance imaging (MRI), is known as the gold standard to evaluate cardiac function and structure. We therefore hypothesized that elevated levels of BNP and Troponin would be positively associated with greater burden of subclinical abnormalities in cardiac function and structure.

Methods: Pro-BNP and Troponin levels were measured at baseline (2000-2002) in 4141 (51% female) African American, Caucasian, Chinese, and Hispanic adults (45-84 years) without baseline clinical cardiovascular disease. Left ventricular (LV) end-systolic and -diastolic volumes, ejection fraction (EF), and cardiac output were measured by cardiac MRI. Multiple linear regression analyses were used to investigate the associations of log-BNP and log-TNT with continuous measures of LV function and structure, adjusting for baseline risk factors (RF): age, sex, race, physical activity, smoking, diabetes, body mass index (BMI), blood pressure, anti-hypertensive medication use, lipid profile, statin use, and prevalence of Coronary Artery Calcium (CAC)>10.

Results: The median BNP level (interquartile range) was 53.1 (23.1–107.1) pg/mL and 1.3% of participants had Troponin T >0.01 ng/mL. Individuals with elevated levels of BNP were more likely to be older, female, had higher blood pressure and higher prevalence of CAC>10. In multivariable models adjusted for baseline cardiovascular RF, elevated levels of pro-BNP and Troponin T were positively associated with greater LV dimensions, volumes, and mass and were inversely related to LV ejection fraction (Table). Additional adjustment for C-reactive protein did not change these results.

Conclusions: Elevated levels of BNP and Troponin T were associated with greater subclinical abnormalities in cardiac function and structure in this cross-sectional study of individuals without baseline cardiovascular disease. These population-based findings implicate BNP and Troponin-T not only are useful for acute conditions, but they can also be used for detecting subclinical abnormalities in cardiac function and structure in the pathogenesis of cardiovascular disease.

Table. Regression Coefficients for BNP and Troponin T in relation to Subclinical Abnormalities in Cardiac Function and Structure (N=4141)

Log-transformed BNP/Troponin T (per 1 SD increase)				MRI Cardiac Function/Structure¶
Log NT-proBNP (per 1.18 pg/mL)		Log cardiac Troponin T (per 0.16 ng/mL)		
P-value	Standardized β (SE) ¶¶	P-value	Standardized β (SE) ¶¶	
<0.001	1.96 (0.19)	<0.001	1.21 (0.15)	LV end-diastolic mass index, g
<0.001	2.80 (0.22)	0.004	0.54 (0.19)	LV end-diastolic volume index, mL
<0.001	1.43 (0.12)	<0.001	0.50 (0.10)	LV end-systolic volume index, mL
<0.001	1.38 (0.16)	0.754	0.04 (0.13)	LV stroke volume index, mL
0.040	-0.23 (0.11)	0.033	-0.20 (0.09)	LV ejection fraction, %
0.003	0.09 (0.03)	<0.001	0.14 (0.02)	LV wall thickness, end-diastole, mm
0.223	0.03 (0.02)	0.270	0.02 (0.02)	Cardiac output, L/min

¶All volume and mass measurements were adjusted for body surface area. Each cardiac function/structure represents a separate multiple linear regression model. The regression coefficient (Standardized β) represents the changes in cardiac function/structure per 1 SD (in parentheses) increase in log inflammatory marker, adjusting for all other covariates in the model. ¶¶ Model adjusted for age, sex, race, education, physical activity, cigarette smoking, diabetes, body mass index, systolic blood pressure, anti-hypertensive medication use, HDL cholesterol, total cholesterol, statin use, and prevalence of CAC>10.

Table. Regression Coefficients for BNP and Troponin T in relation to Cardiac Function and Structure (N=4141)

Log-transformed Troponin T/BNP (per 1 SD increase)				MRI Cardiac Function/Structure¶
BNP (per 1.18 pg/mL)		cardiac Troponin T (per 0.16 ng/mL)		
P-value	β (SE) ¶¶	P-value	β (SE) ¶¶	
<0.001	1.96 (0.19)	<0.001	1.21 (0.15)	LV end-diastolic mass index, (g/m^2)
<0.001	2.80 (0.22)	0.004	0.54 (0.19)	LV end-diastolic volume index, (mL/m^2)
<0.001	1.43 (0.12)	<0.001	0.50 (0.10)	LV end-systolic volume index, (mL/m^2)
<0.001	1.38 (0.16)	0.754	0.04 (0.13)	LV stroke volume index, (mL/m^2)
0.040	-0.23 (0.11)	0.033	-0.20 (0.09)	LV ejection fraction, %
0.003	0.09 (0.03)	<0.001	0.14 (0.02)	LV wall thickness, end-diastole, mm
0.223	0.03 (0.02)	0.270	0.02 (0.02)	Cardiac output, L/min

¶All volume and mass measurements were adjusted for body surface area. Each cardiac function/structure represents a separate multiple linear regression model. SD=standard deviation. SE=standard error. The regression coefficient (β) represents the changes in cardiac function/structure per 1 SD (in parentheses) increase in log inflammatory marker, adjusting for all other covariates in the model. ¶¶ Model adjusted for age, sex, race, education, physical activity, cigarette smoking, diabetes, body mass index, systolic blood pressure, anti-hypertensive medication use, HDL cholesterol, total cholesterol, statin use, and prevalence of CAC>10.

R003

Left Atrial Emptying Function Predicts Malignant Ventricular Arrhythmia in Patients with Ischemic Cardiomyopathy Referred for Implantable Cardioverter Defibrillator

Carmen P. Lydell, MD[1] Yoko Mikami, MD, Ph.D[2], Kai Homer[3], Archa Rajagopalan[1], Aidan Cornhill, BMSc, HBA[1], Karen Cowan, RN[4], Andrew Roberts[4], Claire Sumner[4], Derek Exner, MD[4], Bobby Heydari, MD, MPH[1], Andrew Howarth, MD[1], James White, MD, FRCP(C) [5]

1. *Stephenson Cardiac Imaging Centre, Libin Cardiovascular Institute of Alberta, University of Calgary, AB, Canada*
2. *Stephenson Cardiac Imaging Centre, Libin Cardiovascular Institute of Alberta, University of Calgary, Calgary, AB, Canada*
3. *Stephenson Cardiac Imaging Centre, Libin Cardiovascular Institute of Alberta, University of Calgary, Edmonton, AB, Canada*
4. *Libin Cardiovascular Institute of Alberta, University of Calgary, AB, Canada*
5. *Stephenson Cardiovascular Imaging Center, University of Calgary, AB, Canada*

Background: In patients with ischemic cardiomyopathy (ICM), left ventricular ejection fraction (LVEF) continues to be used as a solitary risk marker for the prescription of primary prevention implantable cardioverter-defibrillator (ICD). Function of the left atrium (LA) has also been explored for the prediction of heart failure related events, however, not for arrhythmic outcomes in this population. In this study we evaluate the predictive value of LA function for the prediction of arrhythmic events in patients with ICM.

Methods: 267 patients (mean age 62+/-11, 88% male) with ischemic cardiomyopathy referred for consideration of ICD implantation, were followed for the composite primary outcome of sudden cardiac death or appropriate ICD shock. CMR imaging, including SSFP cine and LGE imaging, was performed using a standard imaging protocol. All image analyses were performed using commercially available software (cvi[42], Circle CVI) by a reader blinded to clinical information. LA maximum volume, LA minimum volume, and LA emptying fraction (LAEF) were measured using the area-length method on long axis cine images of the 2 and 4 chamber view. LV volumes, LVEF and total scar volume (>5SD signal threshold versus remote myocardial SI on LGE imaging) were quantified by a separate blinded reader. Ventricular volumes were indexed by body surface area with scar volume presented as % of LV mass.

Results: The mean LVEF was 29+/-10% with a mean total scar of 22+/-14% of LV mass. During a median follow up of 1134 days, 214 patients had received ICD implantation and 63 patients had suffered a composite primary outcome (12 SCD, 51 shock). In univariable analysis, LVEF, indexed LA minimum volume, and LAEF were each significantly associated with the composite outcome with HR of 0.76 per 10% increase (p=0.04), 1.08 per 10 unit increase (p=0.04) and 0.82 per 10% increase (p=0.01) respectively. Optimal thresholds from ROC analysis for LAEF and LVEF were 33% and 26%, respectively. In multivariable analysis, the thresholds for the respective variables were independently associated with the primary outcome (HR 2.18 (p=0.01), and 1.73 (p=0.049)). Kaplan-Meier analysis showed patients with LAEF < 33% had significantly poorer event free survival (p < 0.001) (Figure 1) with an annual event rate of 9.7% versus 3.7% in those above this threshold (p=0.0004).

Conclusions: CMR-based LAEF is independently associated with SCA or appropriate ICD shock in patients with ICM referred for consideration of ICD. This practical marker provides strong discrimination of patients at low versus high risk of future arrhythmic events.

http://www.ConferenceAbstracts.com/uploads/cfp2/attachments/LDFAIBDN/LDFAIBDN--219858-1-ANY.pdf

R004

The Diagnostic Role of CMR in Survivors of Sudden Cardiac Arrest; 14 year experience from a UK tertiary referral centre

Amrit Lota, BMBCh BA[1]Florence Mouy, BSc[2], Adam Tsao[3], John Baksi, MBBS PhD[4], Rebecca Wassall, BN (Hons), MSc.[5], Brian Halliday, BSc (Hons) MBChB (Hons)[6], Monika Arzanauskaite[7], Evangelia Nyktari, MD[2], Rameen Shakur, BMBCh Mphil[2], Cemil Izgi, MD[8], Francisco Alpendurada, MD PhD[2], Peter D. Gatehouse, PhD[9], Raad Hashem Mohiaddin, MD PhD[10], David N. Firmin, PhD[4], John Cleland, MD PhD[11], Stuart Cook, PhD[11], Dudley J. Pennell, MD[12], Sanjay Prasad, MD[12]

1. *NIHR Royal Brompton Cardiovascular Biomedical Research Unit and National Heart and Lung Institute, Imperial College London, England, United Kingdom*
2. *Royal Brompton Hospital, England, United Kingdom*
3. *Imperial College London, London, England, United Kingdom*
4. *NIHR Cardiovascular Biomedical Research Unit, Royal Brompton Hospital, England, United Kingdom*
5. *Royal Brompton & Harefield NHS Foundation Trust, London, England, United Kingdom*
6. *Royal Brompton Hospital and National Heart and Lung Institute, Imperial College London, London, England, United Kingdom*
7. *Royal Brompton Hospital, London, England, United Kingdom*
8. *Cardiovascular Magnetic Resonance Unit, Royal Brompton Hospital, London, UK, England, United Kingdom*
9. *NIHR Cardiovascular Biomedical Research Unit, Royal Brompton Hospital, London, England, United Kingdom*
10. *Royal Brompton Hospital and Imperial; College London, London, England, United Kingdom*
11. *Imperial College, London, England, United Kingdom*
12. *Royal Brompton Hospital and Imperial College, London, England, United Kingdom*

Background: Successful resuscitation following a sudden cardiac arrest (SCA) has increased due to improvements in prehospital and emergency care. Acute myocardial infarction is considered the predominant cause routine diagnostic tests include ECG, troponin, echocardiography and coronary angiography. Cardiovascular magnetic resonance (CMR) has significant advantages but its routine use is not supported by current guidelines. In this study, we report the diagnostic role of CMR in a large cohorts of survivors of SCA.

Methods: CMR data from consecutive patients referred or admitted to our centre within 6 months of aborted SCA between 2002 and 2016 were retrospectively reviewed. The presenting rhythm abnormality, presence of late gadolinium enhancement and any resulting cardiac diagnoses were recorded.

Results: Of 409 patients (mean age 50±18years, 59% male) undergoing a CMR scan (1.5T) following aborted SCA, the primary rhythm disturbance was ventricular fibrillation in 254 patients (62%), ventricular tachycardia in 33 (8%), pulseless electrical activity and/or asystole in 16 (4%), and information was not available in 106 (26%). Gadolinium contrast was administered in all patients except 6 (1%) due to contraindications. A normal study was reported in 126 patients (31%), whereas cardiac disease was diagnosed in 283 patients (69%). The most common diagnoses were myocardial infarction in 114 patients (40%), dilated cardiomyopathy in 68 (24%), hypertrophic cardiomyopathy in 28 (10%), and myocarditis in 17 (6%). Late gadolinium enhancement was present in 197 patients (49%), including 7 (2%) with an otherwise normal study.

Conclusions: In this cohort of SCA survivors, CMR effectively identified underlying myocardial disease in the vast majority of cases. The exclusion of structural heart disease including myocardial fibrosis known to create a potential arrhythmic substrate remained equally important in risk stratification for further molecular evaluation of ion channel disease. Whilst study limitations included varying time intervals from SCA to CMR and referral bias within a single centre, CMR provided important diagnostic value in the assessment of these SCA survivors.

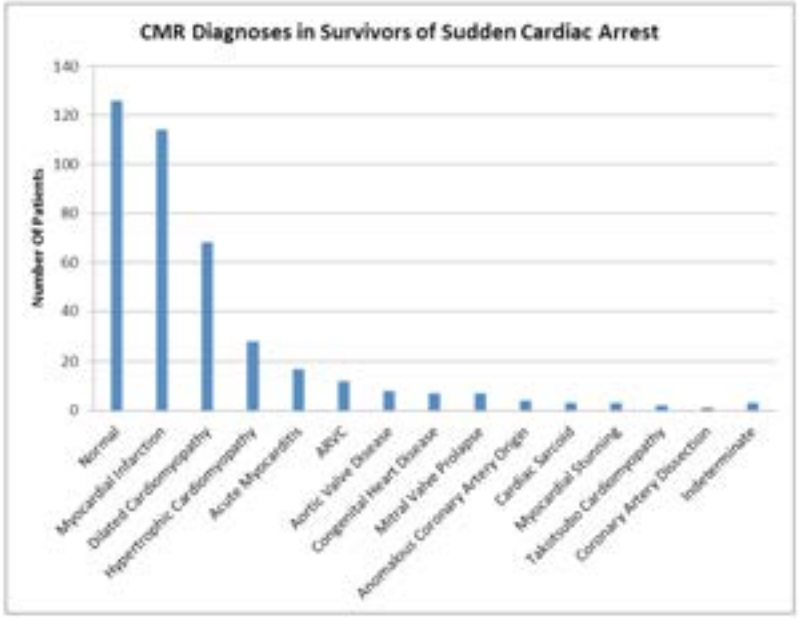

R005

Structure-Function CMR Reveals Altered Myocardial T2 and Strain in Patients after Heart Transplantation

Ryan Dolan, MD[1]Amir Ali Rahsepar, MD[1], Julie Blaisdell[1], Kenichiro Suwa, MD[2], Allen Anderson, MD[3], Jane E. Wilcox, MD, MSc[4], Kambiz Ghafourian, MD, MPH[1], Jeremy D. Collins, MD[5], Michael Markl, PhD[1], James Carr, MD[5]

1. *Northwestern University, Chicago, IL*
2. *Northwestern University Feinberg School of Medicine Department of Radiology, IL*
3. *Northwestern Medicine, Chicago, IL*
4. *Northwestern University Feinberg School of Medicine, Chicago, IL*
5. *Northwestern Memorial Hospital, Chicago, IL*

Background: Acute cardiac allograft rejection (ACAR) occurs in about 25% of cardiac transplant (Tx) recipients within the first year following transplantation and is one of the important causes of mortality post transplantation. The current gold standard screening tool for ACAR is endomyocardial biopsy (EMB), which is invasive and has limited sensitivity due to sampling error. CMR is an alternative due to its capacity to quantify regional changes in ventricular morphology and function. The goal of this study was to apply two CMR techniques, T2-mapping and CINE based left ventricular strain assessment, to test the hypotheses that 1) T2-mapping and strain CMR can detect changes in myocardial structure (elevated myocardial T2 values) and function (reduced myocardial strain) in Tx patients compared to controls, and 2) LV structural abnormalities are associated with impaired LV function.

Methods: Thirty eight patients (age 49.3±15.0,female 37%) within 5 years of Tx and 10 age-matched healthy controls (age 53.1±10.2,female 20%) underwent CMR at 1.5T (MagnetomAera, Siemens, Erlangen, Germany). LV systolic function, T2 (global, segmental peak, average septal, average lateral), and strain (peak strain and time to peak strain (TTP) in radial, circumferential, and longitudinal directions) parameters were calculated using dedicated software (cvi42, version 5.3.6, Circle, Calgary, Canada). ACAR was defined by EMB within one week of CMR with ISHLT grade ≥2. Study was approved by the Northwestern IRB.

Results: Patients had normal global ventricular function parameters following Tx (table 1), but significantly higher myocardial T2 values ($p < 0.01$) and decreased peak strain ($p < 0.01$ except in longitudinal direction) and TTP strain ($p < 0.01$) compared to controls (table 2). Regression analysis revealed a significant inverse correlation between global myocardial T2 and peak strain in the radial (r=-0.321,p=0.03) and circumferential (r=-0.293,p=0.04) directions, indicating a structure-function relationship between elevated T2 and impaired LV function. There was also an inverse correlation between global T2 and TTP in radial (r=-0.366,p=0.01), circumferential (r=-0.341,p=0.02), and longitudinal (r=-0.468,$p < 0.01$) directions. In a subgroup analysis comparing Tx patients with active ACAR (n=4) to patients without ACAR (n=34), global, septal, and lateral T2 were significantly elevated in patients with rejection. There was no difference in strain parameters (table 2).

Conclusions: The correlation between global T2 and strain provides evidence of a relationship between structure (increased T2 with edema/inflammation) and function (decreased peak strain and TTP) following Tx. Additionally, comparison of patients with ACAR to those without demonstrated that T2, but not strain, may be used for detection and monitoring of rejection.

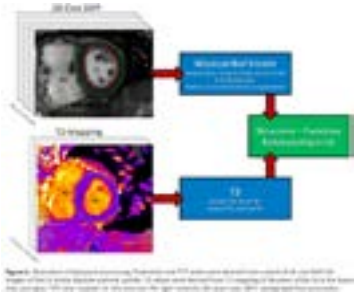

	Controls	Tx Patients
Number of Patients	n=10	n=38
Gender (female)	2 (20%)	14 (37%)
Age at Transplant		47.3 ±14.7
Time from Tx to Scan (yrs)		1.6 ±1.6
Age at Scan	53.1 ±10.3	49.3 ±15.0
Cold Ischemic Time (min)		183.6 ±36.4
Donor Age		28.9 ±13.6
SV (mL)	86.8 ±22.5	67.7 ±18.0
CO (L/min)	4.5 ±1.6	4.5 ±1.7
EF (%)	62.1 ±7.0	58.3 ±9.4
End Diast Myo Mass (gm)	116.2 ±30.7	116.0 ±30.8

Table 1: Patient demographics and global ventricular function. Tx: cardiac transplant, SV: stroke volume, CO: cardiac output, EF: ejection fraction, End diast myo mass: end diastolic myocardial mass.

Table 2: T2 and strain data in controls (column 1) and transplant (column 2) groups. T-tests comparing these groups (none significant) are listed in column 3. T2 parameters and all strain parameters, except peak longitudinal strain (column 5). The transplant group (column 2) is subdivided into patients without active rejection (column 4) and patients with rejection shown on a concomitant biopsy with ISHLT grade ≥2 (column 5). T-tests suggest that patients with rejection have higher T2, but not strain, compared to those without active rejection (column 6). Tx: cardiac transplant, TTP: time to peak strain, Gr: Global, peak R: radial direction, C: circumferential direction, L: longitudinal direction.

R006

Non-invasive assessment for cardiotoxicity from metal-on-metal hip implants using CMR

Amna Abdel-Gadir, MBBS.MRCP(UK)[1]Reshid Berber, MBBS, MRCS[2], Sabrina Nordin, BMBS, MRCP(UK)[3], Veronica Culotta, MD[4], Peter Kellman, PhD[5], Skinner John, FRCS(Orth)[6], Alister Hart, MD, FRCS(Orth)[6], James Moon, MBBS, MD, MRCP[7], Charlotte Manisty, PhD MBBS[8]

1. *University College London and Barts Heart Centre, London, England, United Kingdom*
2. *Royal National Orthopaedic Hospital, England, United Kingdom*
3. *Barts Heart Centre, England, United Kingdom*
4. *Barts Heart Centre, St Bartholomew's Hospital, England, United Kingdom*
5. *Laboratory of Cardiac Energetics, National Institutes of Health/NHLBI, Bethesda, MD, United States., MD*
6. *Royal National Orthopaedic Hospital, Institute of Orthopaedics and Musculoskeletal Sciences, University College London, England, United Kingdom*
7. *Barts Heart Center, The Cardiovascular Magnetic Resonance Imaging Unit and The Center for Rare Cardiovascular Diseases Unit, St Bartholomew's Hospital, West Smithfield, London, UK, England, United Kingdom*
8. *Barts Heart Centre and university college, London, England, United Kingdom*

Background: Metal-on-metal hip prostheses are now known to have high failure rates, resulting in high circulating blood levels of cobalt and chromium. There are now over one million patients worldwide at risk of systemic metal ion deposition, with potentially lethal consequences including cardiomyopathy. Although fulminant cardiotoxicity is rare, concern is growing from clinicians and patients alike that milder forms may be common and under-diagnosed. Currently diagnosis relies on myocardial biopsy or post-mortem analysis, with no non-invasive test available for the detection of metal deposition. T2* quantification has an established role in monitoring for iron overload and, like iron, cobalt is a divalent metal with paramagnetic properties. Based on our previous finding of low T2* signals in a patient with grossly elevated blood metal values and a positive tissue biopsy, this study was designed to explore the effects of long-term metal exposure on cardiac function and volumes, and tissue characterization.

Methods: 90 patients with prosthetic hips were recruited and divided into 3 age and gender-matched groups according to implant type and whole blood metal ion levels: Group A - ceramic-on-ceramic bearing hip implants; Group B – metal-on-metal implants with low whole blood metal ion levels; and Group C - metal-on-metal with high whole blood levels. All patients underwent CMR imaging at 1.5T (Siemens Avanto) for volumes and functional assessment, tissue characterization, and myocardial and hepatic T2*, T1 mapping and ECV. Blood samples for cobalt, chromium, BNP and troponin were also collected. Primary outcomes were pre-specified (clinicaltrials.gov: NCT02331264).

Results: Blood cobalt levels were significantly different between groups (0.17 (SD 0·08), 2·47 (SD 1·81) and 30·0 (SD 29·1) ppb respectively for groups A, B and C). No significant between-group differences were found for LV volumes, ejection fraction, T1 mapping, T2*, ECV, BNP or troponin, with all results within normal ranges (Table). There was no relationship between blood cobalt levels and either ejection fraction or T2* values (r=-0·022 and r=-0·108 respectively). Although small, the study was sufficiently powered to detect, as a minimum, a difference in ejection fraction of 4.8% (Cohen's d effect size 0·8).

Conclusions: Exposure of patients with metal-on-metal hip implants to high (but not extreme) blood cobalt and chromium levels appears to have no significant detectable effect on the heart. CMR with T2* assessment may have new application for screening for cardiomyopathy in at-risk patients with metal-on-metal hip implants.

	C	B	A		
					CMR
p= 0·75	71 ± 5	69 ± 7	70 ± 5	LVEF (%)	
p= 0·86	20 ± 5	21 ± 8	21 ± 6	ESVi (ml/m^2)	
p=0·64	1022 ± 37	1014 ± 33	1030 ± 42	T1 MOLLI (NR 949- 1101ms)	
p= 0.82	956 ± 44	957 ± 30	961 ± 31	T1 ShMOLLI (NR 900- 1020ms)	
p=0·69	32 ± 6	31 ± 6	31 ± 5	T2* (Normal >20ms)	
p=0·28	0.29 ± 0.04	0.27 ± 0.03	0.28 ± 0.03	ECV	
					Blood
p=0·32	25 ± 61	10 ± 8	11 ± 10	BNP (pmol/L)	
p=0.77	8.62 ± 10.2	7.16 ± 5.0	7.38 ± 6.9	Troponin (ng/L)	

Summary of the CMR and Blood Results. Data are Presented as Mean ± SD

R007

Insights from T1-mapping into Left Ventricular Reverse Remodelling in Dilated Cardiomyopathy

Brian Halliday, BSc (Hons) MBChB (Hons)[1]Zohya Khalique, MBBS[2], Andrew D. Scott, PhD[3], Rick Wage, DCR (R)[4], Rebecca Wassall, BN (Hons), MSc.[5], Amrit Lota, BMBCh BA[6], Upasana Tayal, BMBCh[7], Vassilis Vassiliou, MBBS[7], Shivraman Giri, PhD[8], Peter D. Gatehouse, PhD[2], Stuart Cook, PhD[9], Dudley J. Pennell, MD[10], John Cleland, MD PhD[9], Sanjay Prasad, MD[10]

1. *Royal Brompton Hospital and National Heart and Lung Institute, Imperial College London, London, England, United Kingdom*
2. *NIHR Cardiovascular Biomedical Research Unit, Royal Brompton Hospital, London, England, United Kingdom*
3. *NIHR Cardiovascular Biomedical Research Unit, The Royal Brompton Hospital, Sydney Street, London, SW3 6NP, UK, England, United Kingdom*
4. *NIHR Cardiovascular Biomedical Research Unit, Royal Brompton Hospital, England, United Kingdom*
5. *Royal Brompton & Harefield NHS Foundation Trust, London, England, United Kingdom*
6. *NIHR Royal Brompton Cardiovascular Biomedical Research Unit and National Heart and Lung Institute, Imperial College London, England, United Kingdom*
7. *Royal Brompton Hospital, England, United Kingdom*
8. *Siemens Healthcare, IL*
9. *Imperial College, London, England, United Kingdom*
10. *Royal Brompton Hospital and Imperial College, London, England, United Kingdom*

Background: Left ventricular reverse remodelling (LVRR) is well described in dilated cardiomyopathy (DCM) and confers an excellent long-term prognosis. Improved understanding of the tissue and cellular changes that accompany LVRR will help elucidate the underlying mechanisms and offer potential for novel therapeutics. Native T1 times measured using T1-mapping have been shown to correlate with the degree of interstitial fibrosis. We aimed to compare native T1 times in healthy volunteers, patients with DCM and patients with recovered DCM to provide insight into the interstitial abnormalities that accompany LVRR.

Methods: Overall, 20 healthy volunteers without a history of cardiac disease, 21 patients with recovered DCM and 14 patients with DCM underwent native pre-contrast T1-mapping on a 3T system (MAGNETOM Skyra, Siemens Healthineers, Erlangen, Germany) using a MOLLI sequence at mid-ventricular short axis level. Images were analysed using CMR tools (CMRtools, Cardiovascular Imaging Solutions, London, UK). T1 values were measured in a linear region of interest in the septum. Patients with recovered DCM had a previous confirmed diagnosis of DCM with left ventricular ejection fraction (LVEF) < 40% that had subsequently recovered to > 50% with normalisation left ventricular cavity size. Patients with DCM had reduced LVEF and a dilated LV cavity as defined by reference values. Native T1-times were compared between the groups using a one-way ANOVA test with Bonferroni correction applied for multiple comparisons.

Results: In the patients with DCM the median LVEF was 49%. In the patients with recovered DCM the median LVEF was 60% at the time of scan compared to 28% at the time of original diagnosis. The mean (SD) native T1 values in healthy volunteers, patients with DCM and patients with recovered DCM were 1284ms (+/- 40.2), 1345ms (+/- 44.5) and 1292ms (+/- 36.2) respectively (*Figure 1)*. There was a significant difference in native T1 times between the three patient cohorts ($p < 0.001$). This was driven by differences between patients with DCM when compared to those patients with recovered DCM ($p=0.001$) and healthy volunteers ($p < 0.001$) (Figure 1). Patients with recovered DCM had similar native T1 times to healthy volunteers ($p=1.0$) (*Figure 1*).

Conclusions: Patients with recovered DCM have similar native T1 times to healthy volunteers and significantly lower native T1 times compared to patients with DCM. This suggests that patients with recovered DCM either have little interstitial fibrosis or that it reverses as part of left ventricular reverse remodelling.

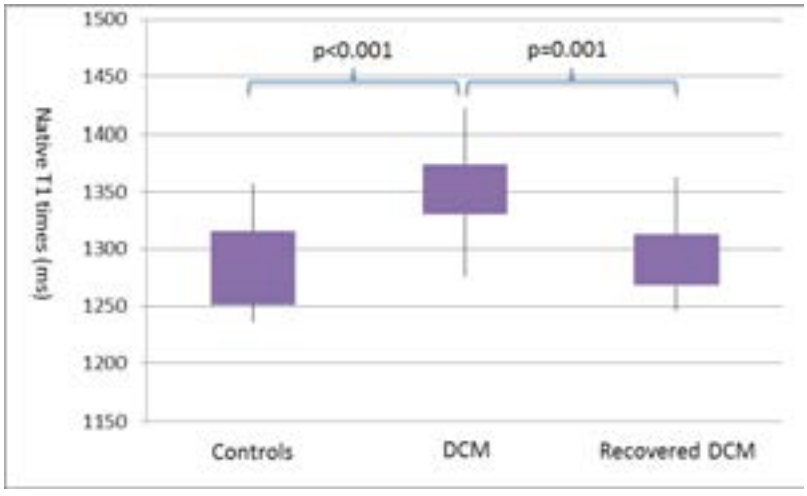

R008

Fractal Dimension as a Biomarker for Left-Ventricular HyperTrabeculation: Effect of Embedding Space and Spatial Resolution

Jaganth Nivas Asok Kumar, M.S[1]Carlo Uribe, MD[2], Anthony Masso, PhD[3], Paolo Angelini, MD[3], Benjamin Cheong, MD[4], Jiming Zhang, PhD[5], Raja Muthupillai, PhD[5]

1. *Department of Biomedical Engineering at University of Houston, Pearland, TX*
2. *Center for coronary artery anomalies at Texas Heart Institute, Houston, TX*
3. *Center for coronary artery anomalies, Texas Heart Institute, Houston, TX, USA, TX*
4. *CHI St.Luke's Health, TX*
5. *Diagnostic and Interventional Radiology, CHI St Luke's Health, TX*

Background: Even expert observers with well-defined classification criteria disagree in their assessment of left ventricular hypertrabeculation or non-compaction in nearly a third of the cases[1]. Recently it has been reported that a fractal dimension (FD) – describes how an object fills space- estimated from steady-state free precession (SSFP) images acquired in short-axis view could serve as a quantitative biomarker of LVHT [2]. It was reported that a maximal apical FD of >= 1.3 can be used to identify subjects with LVHT. In this work we considered the following technical parameters on FD estimation: (a) as the size of the LV cavity in the short axis orientation progressively diminishes from the base to the apex, we sought to evaluate the impact of keeping the embedding space fixed (to the size of the largest LV cavity dimension in the SA stack) versus adaptively varying the embedding space (to the size of the cavity), and (b) as zero-padded reconstruction is commonly used in MRI, we sought to assess the impact of reconstructed pixel size on estimating FD.

Methods: MRI Acquisition: Cine SSFP images of entire LV in the short axis view were acquired at 1.5T using a 32-CH RF coil in 39 subjects. Acquisition parameters: TR/TE/flip angle: 3.5ms/1.75 ms/60°; voxel size: 2x2x8mm^3. All subjects gave written informed consent. **FD analysis**:
The box-counting based method was implemented analogous to that described in ref. [2] in MATLAB™ for FD estimation. We evaluated the effect of the embedding space in relationship to object in both numerical phantoms and human subjects. In human subjects, for each short axis slice we estimated the FD with: (a) a fixed embedding space (FES) dimension that matched the largest cross sectional area among all short-axis slices for a given patient, and (b) an adaptive embedding space (AES) that just encapsulated the anatomy of interest for each slice (Fig. 1). The difference between the two FD metrics is expressed as percent deviation.

Results: FD in a total of 326 slices from 39 subjects was calculated with both FES and AES. (1) Numerical simulations showed that with FES, the FD deviated farther from the true value as the object occupied a smaller fraction of the FES. This deviation was reduced when an AES was used. (2) In clinical subjects, FD values obtained with FES had greater deviation for apical slices (which occupied a smaller fraction of the FES) compared to those obtained with AES (Fig. 2). (3) FD values obtained from images reconstructed at 2x and 3x the base resolution were significantly correlated with those obtained at base resolution (Fig. 3).

Conclusions: FD of short axis cine SSFP slices is strongly influenced by the size of the embedding space in relation to the size of the object. When the size of the embedding space is fixed to the size of the base of the LV cavity, FD of apical slices could deviate substantially from FD estimated with AES. **References: 1.** *JACC,* 8(11)1252-, 2015. 2. *JCMR*, *15*(1)1. 2013

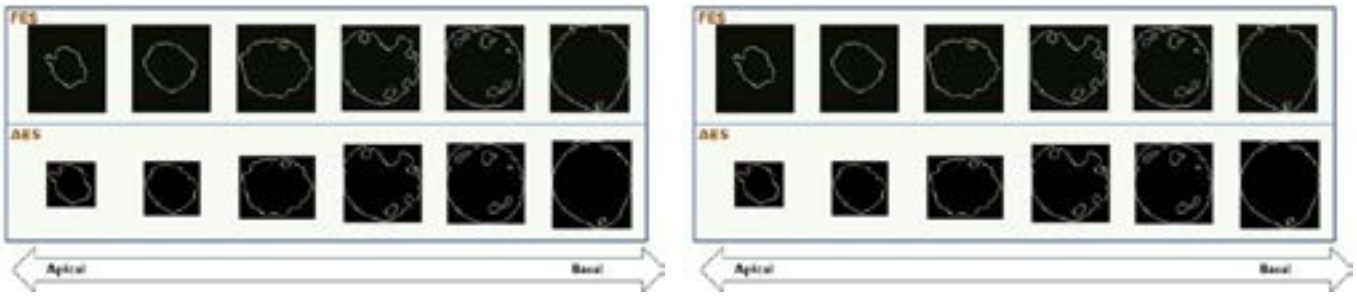

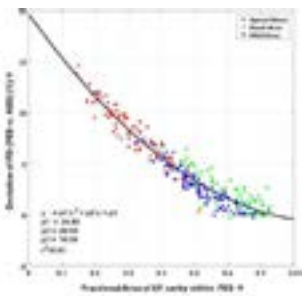

R009

Advanced Structural And Mechanical Myocardial Assessment In Ventricular Fibrillation Cardiac Arrest Survivors

Anna Baritussio, MD[1] Alessandra Scatteia, MD[2], Giovanni Biglino, MD, PhD[3], Amardeep Ghosh Dastidar, MBBS(Hons), MRCP[1], Estefania De Garate, MD[1], Iwan Harries, MD[1], Chiara Bucciarelli-Ducci, MD, PhD[1]

1. *NIHR Bristol Cardiovascular Biomedical Research Unit, Bristol, England, United Kingdom*
2. *Division of Cardiology, Ospedale Medico-Chirurgico Accreditato Villa dei Fiori, Acerra, Naples, Italy. Cardiac Magnetic Resonance Unit, NIHR Bristol Cardiovascular Biomedical Research Unit, Bristol Heart Institute, Bristol UK, Naples, Campania, Italy*
3. *Bristol Heart Institute, School of Clinical Sciences, University of Bristol, Bristol, England, United Kingdom*

Background: Ventricular fibrillation (VF) is the most serious ventricular arrhythmia and causes most of sudden cardiac arrests. Scar quantification and myocardial deformation assessed by cardiovascular magnetic resonance (CMR) have been shown to be powerful predictors of ventricular arrhythmias. We sought to assess scar quantification and myocardial deformation in VF cardiac arrest survivors.

Methods: We retrospectively analysed our CMR registry to enrol VF cardiac arrest survivors. All patients underwent a 1.5 T CMR, comprehensive of long and short-axis cine and late gadolinium enhancement (LGE) sequences. LGE was quantified with a semi-automated software (CVI42, Canada) using the full width at half maximum method. Feature tracking CMR analysis software (CVI42, Canada) was used to assess myocardial deformation.

Results: We consecutively enrolled 129 patients surviving VF cardiac arrest (83% male, mean age 60±14 years). Based on CMR findings, eighty-three patients (64%) had ischemic heart disease (IHD), 20 (16%) had non-ischemic heart disease (NIHD) and 26 (20%) had structurally normal hearts. Mean LVEF was 52±15%. LGE was found in 91 patients (71%, 80/91 being IHD patients) with a mean scar mass of 8.1±11.2 g, which was significantly higher among IHD patients ($p < 0.001$). Global peak systolic strain values were 34.0±12.9% for radial, -15.6±5.0 for circumferential and -15.3±5.2 for longitudinal. Myocardial deformation was significantly different between the three groups ($p < 0.001$), with myocardial strain being more altered among IHD patients. Circumferential, longitudinal and radial strain decreased as the scar mass increased ($p < 0.001$, respectively). On a multivariable regression analysis both the amount of scar (g) and the underlying CMR diagnosis (IHD, NIHD and structurally normal heart) were independent predictors of decreased longitudinal (p=0.001, 95%CI: 0.05- 0.21; p=0.009, 95%CI -2.65 - -0.39, respectively), radial (p=0.002, 95%CI: -0.54- -0.12; p=0.007, 95%CI 1.14-7.03, respectively) and circumferential strain ($p < 0.001$,95%CI 0.09-0.24; p=0.008, 95% CI -2.5- -0.38, respectively).

Conclusions: Among VF cardiac arrest survivors there is a high prevalence of scar and myocardial deformation is altered, despite a nearly normal LVEF. Not only the amount of scar, but also the underlying CMR diagnosis, are independent predictors of decreased myocardial strain. CMR offers an advanced myocardial assessment that might help understand the complex and multi-factorial pathophysiology of ventricular arrhythmias. Further studies are needed to assess the clinical implications on long-term prognosis.

R010

Distinguishing arrhythmogenic right ventricular cardiomyopathy (ARVC) from athlete's heart using cardiac magnetic resonance imaging

Csilla Czimbalmos, MD[1]Hajnalka Vago, MD PhD[2], Ibolya Csecs, MD[2], Attila Toth, MD[2], Róbert Mikle, MD[2], Beata Horvath[2], Zsofia Dohy[2], Tamas Simor, MD PhD DSc[3], David Becker, MD PhD[2], Bela Merkely, MD PhD DSc[2]

1. *Heart and Vascular Center, Semmelweis University, Budapest, Budapest, Hungary*
2. *Heart and Vascular Center, Semmelweis University, Budapest, Hungary*
3. *Heart Institute, University of Pécs, Baranya, Hungary*

Background: ARVC is a major cause of life-threatening arrhythmias in young athletes. However in highly trained athletes the diagnosis is complicated because of overlapping features such as elevated right ventricular end-diastolic volume index (RVEDVi), and the revised Task Force criteria (TFC) contains no cut-off value for professional athletes.
Our goal was to determine CMR parameters and gender-specific cut-off values which can help to differentiate ARVC from athlete's heart.

Methods: Between 2010 and 2015 CMR examination (Philips Achieva 1.5T) was performed on 480 patients due to the suspicion of ARVC. In 45 patients (38±10y,30 male) ECG abnormalities, arrhythmias, family history, histology and/or CMR parameters fulfilled revised TFC. Additionally 80 professional athletes (members of the Hungarian national water polo, canoing or rowing team) free of complaint (26±4y,50 male) were examined by CMR. Right ventricular end-diastolic volume index (RVEDVi), right ventricular ejection fraction (RVEF) and the calculated derived parameters (LVEDV/RVEDV and LVEF/RVEF) were compared. Area under the ROC curves (AUC) of these CMR parameters were analysed, and optimal gender specific cut-off values were established from receiver-operator characteristic (ROC) curves with the highest optimal sensitivity and specificity.

Results: There was no significant difference between RVEDVi of ARVC patients and athletes in both males and females (m:129.2 vs. 129.8ml/m^2;f:125.4 vs. 110.7ml/m^2). RVEF was significantly lower in ARVC patients compared to athletes (m:46 vs. 55.7%;f:44.2 vs. 58.4%). LVEDV/RVEDV and LVEF/RVEF of both male and female patients showed significant difference compared to the athlete's group ($p < 0.01$).

In both gender, AUC of RVEF, LVEF/RVEF and LVEDV/RVEDV shows that these parameters can help to distinguish ARVC and athletes heart heart ($p < 0.01$), but RVEDVi can not (p=NS).

Male cut-off value for ratio of RVEF less than 48.2%, LV/RVEF more than 1.145 and LVEDV/RVEDV < 0.890 discriminated between athlete's heart and ARVC with a sensitivity of 53% and a specificity of 100%. Female cut-off value for ratio of RVEF less than 51%, LV/RVEF more than 1.157 and LVEDV/RVEDV < 0.915 discriminated with a sensitivity of 67%, 66% and 87%; specificity of 93%, 97% and 90%, respectively.

In 6 athletes (28±4y, 5 male) ARVC was diagnosed based on CMR findings (RV wall motion abnormality, late gadolinium enhancement, RVEF), ECG abnormalities, arrhythmias and family history. RVEF, LV/RVEF and LV/RVEDV were in the pathological range in 3, 6 and 5 cases, respectively.

Conclusions: Consequently, in highly trained healthy athletes RVEDVi is in the range of major TFC, while RVEF, LV/RVEDV and LV/RVEF could be useful parameters in differential diagnosis.

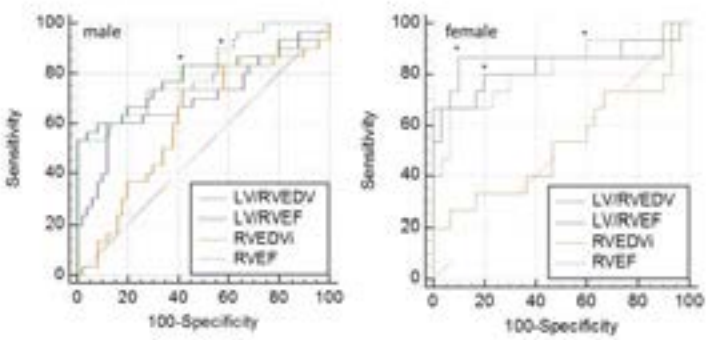

Figure: Receiver Operating Characteristic (ROC) curves visualizing correct identification of ARVC among male and female subjects and comparison between the areas below the ROC curves of different CMR parameters.
* significantly different from RVEDVi

R011

Left ventricular ejection fraction and myocardial necrosis assessed by cardiac magnetic resonance imaging correctly risk stratify patients with coronary artery disease – a multi-center follow-up trial

Dominik Buckert, M.D.[1]Sebastian Kelle, MD, PhD[2], Sebastian Buss, M.D.[3], Grigorios Korosoglou, M.D.[4], Rolf Gebker, MD, PhD[2], Wolfgang Rottbauer, M.D.[5], Hugo Katus, M.D.[6], Burkert Pieske, MD, PhD[2], Peter Bernhardt, M.D.[7]

1. *Dept. Internal Medicine II, University Hospital Ulm, Neu-ulm, Bayern, Germany*
2. *German Heart Institute Berlin, Berlin, Berlin, Germany*
3. *University Hospital Heidelberg, Baden-Wurttemberg, Germany*
4. *Hospital Weinheim, Baden-Wurttemberg, Germany*
5. *Dept. Internal Medicine II, University Hospital Ulm, Baden-Wurttemberg, Germany*
6. *Dept. Internal Medizin III, University Hospital Heidelberg, Baden-Wurttemberg, Germany*
7. *Heart Clinic Ulm, Baden-Wurttemberg, Germany*

Background: Cardiac magnetic resonance imaging (CMR) has become a diagnostic modality that allows for risk stratification of patients with stable coronary artery disease. CMR derived detection of late gadolinium enhancement (LGE) and assessment of left ventricular functional parameters such as left ventricular ejection fraction (LVEF) have been proven to be significantly associated with outcome and prognosis. There still exists inhomogeneity throughout the studies forming the evidence base so the exact role of these parameters and respective thresholds remain to be investigated. Aim was to elaborate thresholds for LVEF assessed by CMR in the specific population of patients with CAD and to elucidate the potential additional prognostic power of LVEF and myocardial necrosis assessed by late gadolinium enhancement (LGE) when combined with traditional risk factors.

Methods: Data from three tertiary high-volume CMR centers have been pooled. Patients referred for viability or stress testing because of known or suspected CAD were enrolled. Assessment of functional parameters of both ventricles and myocardial necrosis by LGE was performed on 1.5-T whole body CMR systems. The primary endpoint was defined as cardiac death and non-fatal myocardial infarction. A multi-model approach was used for the evaluation of predictive power of several LVEF thresholds and LGE.

Results: The study cohort consisted of 2422 patients. Median age was 66 years; about 25% were women. Median follow-up was 2.86 years. During this time, 187 primary endpoints occurred. On multi-model testing, optimal thresholds for LVEF could be defined at 50% and 35%. The addition of LGE as categorical variable further lead to a significant improvement of each risk prediction model, whilst quantification of LGE affection did not.

Conclusions: LVEF thresholds at 50% and 35% in combination with the assessment of LGE allowed for excellent discrimination between low, mid and high risk in patients with stable CAD.

R012

Joint Native Myocardial Fat Fraction, Off-Resonance and R2*/T2* Mapping in Ischemic Cardiomyopathy

James W. Goldfarb, PhD[1] Usama Hasan, MD[2]

1. St Francis Hospital, Roslyn`, NY
2. St Francis Hospital, Roslyn, NY

Background: Multiple gradient echo imaging allows the joint quantification of myocardial T2*/R2*, off -resonance frequency and fat fraction. In a single breath-hold, three native maps of independent MR properties can be obtained. Fatty metaplasia has been shown in chronic myocardial infarction and non-ischemic cardiomyopathies associated with diabetes and obesity. Changes in T2*/R2* and off-resonance frequency due to susceptibility changes have been associated with hemorrhagic myocardial infarction and hemochromatosis. The goal of this study was to obtain normal ranges of the three native parameters maps and investigate their use in acute and chronic myocardial infarction (MI).

Methods: 48 subjects (17 normal control, 11 Acute MI at 3days and 20 Chronic MI >2 yrs) were studied at 1.5T with native joint R2*/T2*, off-resonance and fat fraction mapping using a multipeak model with R2* and B0 corrections in parallel short and long axis slice views spanning the entire the left ventricle. The water-fat separation framework provides four images: water only, fat only, R2* and off-resonance. Additionally, conventional bSSFP CINE and late gadolinium-enhanced (LGE) imaging (0.15 mmol/kg) were obtained. Mean parameter values were measured in the heart (16 segment AHA model). Parameter maps were visually evaluated for focal lesions. Normal segmental differences and associations with LGE presence and age of MI were evaluated with statistical tests.

Results: Focal fatty metaplasia was visualized in a subset of chronic MI patients (n=12). T2* and off-resonance segmental changes were also well visualized in a subset of acute MI patients (n=3) (See Figure 1, red circles). Focal myocardial fat lesions had an admixture of water and fat signal fat fraction =52.8% ± 14.6. Figure 2 shows acute and chronic MI parameters compared with normal values. Fat fraction was significantly higher in chronic myocardial infarction (16.7% ± 12.9 vs 2.8% ± 2.1, $p < 0.001$). Off-resonance frequency was significantly lower in both chronic and acute myocardial infarction (3.2 Hz ± 22.6 vs 20.9 Hz ± 21.6, $p=0.01$). 18 chronic MI patients had fat fractions outside of the normal range (18.4% ± 12.4 vs 2.8% ± 2.1, $p < 0.001$). Three acute MI patients had R2* values and off-resonance frequencies outside of normal ranges and all demonstrated MVO in LGE images consistent with intramyocardial hemorrhage.

Conclusions: Myocardial fat content, R2*/T2* and off-resonance frequency can be measured with high resolution using a native MR water-fat separation imaging technique applied to multiple gradient echo images. Significant differences in myocardial fat fraction were found consistent with fatty metaplasia in a subset of chronic MI patients. Off-resonance and T2* changes consistent with intramyocardial hemorrhage were observed in a subset of acute MI patients.

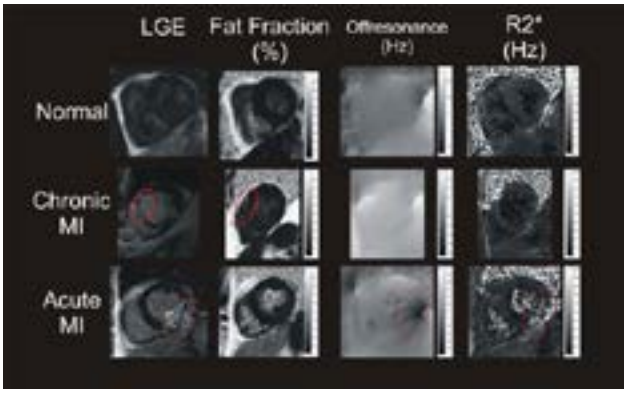

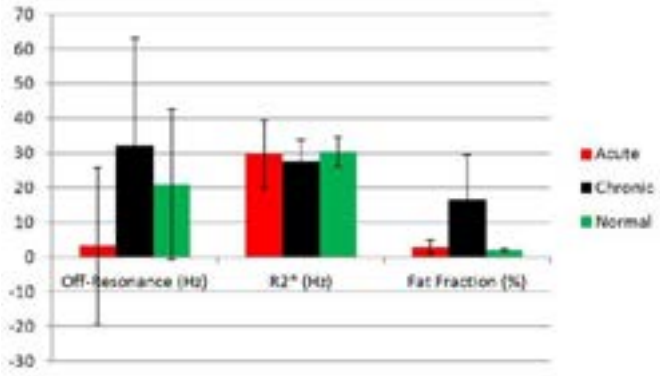

R013

Clinical value of absolute rest myocardial blood flow in STEMI patients in predicting left ventricular dysfunction – an Oxford Acute Myocardial Infarction (OxAMI) study

Alessandra Borlotti, PhD[1] Dan Liu, PhD[2], Dafne Viliani, MD[3], Alessia Bracco, MD[4], Michael Jerosch-Herold, PhD[5], Mohammad Alkhalil, M.D, MRCP[2], Giovanni Luigi De Maria, MD[6], Gregor Fahrni, MD[7], Sam Dawkins, MBBS MRCP[8], Mathias Wolfrum, MD[2], Adrian Banning, MB BS[9], Robin Choudhury, MD[1], Stefan Neubauer, MD, FRCP[2], Keith M. Channon, MD, FRCP[2], Rajesh K. Kharbanda, MBChB, PhD[10], Erica Dall'Armellina, MD, PhD[11]

1. *University of Oxford, Oxford, England, United Kingdom*
2. *University of Oxford, England, United Kingdom*
3. *Division of Cardiovascular Medicine, Radcliffe Department of Medicine, Oxford, Trento, Trentino-Alto Adige, Italy*
4. *University of Oxford, Veneto, Italy*
5. *Department of Radiology, Brigham and Women's Hospital, MA*
6. *Oxford University Hospitals, England, United Kingdom*
7. *Cardiology, University Hospital Basel, Switzerland, Basel-Stadt, Basel-Stadt, Switzerland*
8. *Oxford University Hospitals NHS Trust, Oxford, England, United Kingdom*
9. *Oxford university, N/A, United Kingdom*
10. *Oxford Heart Centre, England, United Kingdom*
11. *Oxford University, England, United Kingdom*

Background: Microvascular obstruction (MO) by late gadolinium enhancement (LGE) CMR is a known poor prognostic factor in ST elevation myocardial infarction (STEMI) patients[1]. First pass perfusion (FFP) CMR allows for accurate quantitative assessment of absolute myocardial blood flow (MBF).[2] The additional diagnostic and predictive value of MBF in patients without MO by LGE in unknown. Our study sought to 1) assess absolute MBF in STEMI patients in relation with the severity of the injury assessed by LGE and T2-weighted (T2W) imaging 2) to investigate the predictive value of absolute MBF in acute for 6 months (6M) myocardial recovery in patients with no/mild MO on LGE.

Methods: 74 STEMI patients underwent PPCI and 3T Siemens VERIO or TRIO CMR scans in acute (within 5 days) and at 6M; the protocol included T2W imaging for oedema quantification, functional imaging, FPP for myocardial perfusion assessment, LGE imaging for infarct and MO determination. MBF was calculated for oedematous ($MBF_{oedema+}$), infarcted (MBF_{LGE+}) and normal remote myocardial segments both in acute and 6 M by deconvolution models using an in-house MatLab software[2]. Receiver-operating characteristic (ROC) analysis was performed per-patient level to assess the diagnostic performance of acute MBF_{LGE+} and LGE in predicting LV dysfunction (EF3. P-values less than 0.05 were considered statistically significant.

Results: Acute $MBF_{oedema+}$ (n=262) was significantly lower than normal remote myocardium (0.96±0.18 ml/min/g vs 1.00±0.21 ml/min/g, poedema+ vs 1.07±0.22 ml/min/g in remote myocardium, p>0.05). Acute MBF_{LGE+} (n=541), progressively decreased with LGE extent and its magnitude of change from acute to 6M was increasingly higher in segments with higher LGE% at baseline (Figure 1). Considering all patients, ROC analysis showed that the diagnostic performance of acute MBF_{LGE+} and LGE in predicting EF 0.05). In the subgroup of patients with no/mild MO (N=43), the AUC of MBF_{LGE+} is significantly higher compared to LGE (0.814 vs 0.527, p < 0.05). A MBF cut-off of 0.72 ml/min/g predicts 6M recovery with a sensitivity of 74% and specificity of 83%.

Conclusions: Following an acute STEMI, myocardial perfusion spontaneously recovers in oedematous myocardium over time. In necrotic myocardium, perfusion improves but remains impaired at 6M compared to remote myocardium. In patients with no/mild MO, absolute rest MBF in the necrotic region assessed acutely might provide important additional predictive information compared to LGE on LV remodelling.

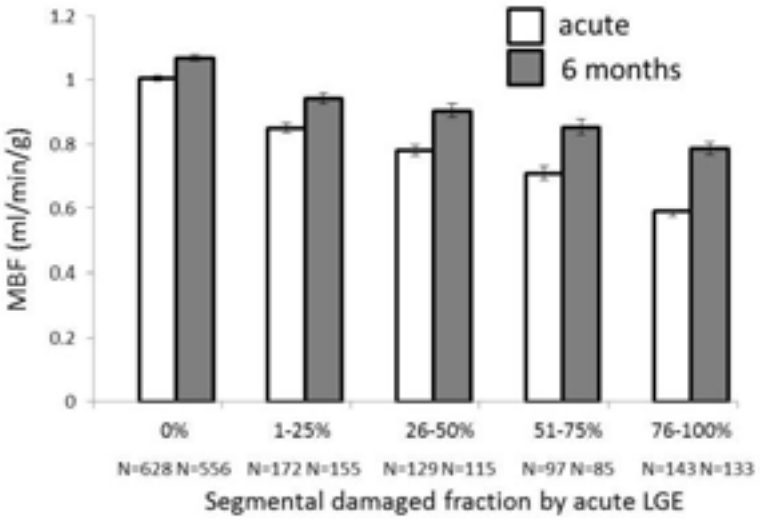

R014

T1 and T2 Mapping cardiovascular magnetic resonance to differentiate acute from chronic myocardial infarction

Enver Guner. Tahir, MD[1]Martin Sinn, student[2], Maxim Avanesov, MD[2], Sebastian Bohnen, MD[2], Kai Muellerleile, MD[2], Christian Stehning, PhD[3], Jitka Starekova, MD[2], Ulf Radunski, MD[2], Bernhard Schnackenburg, PhD[4], Gerhard Adam, MD[2], Gunnar Lund, MD[2]

1. *University Medical Center Hamburg-Eppendorf, Hamburg, Hamburg, Germany*
2. *University Medical Center Hamburg-Eppendorg, Hamburg, Germany*
3. *Philips Research Laboratories, Hamburg, Germany*
4. *Philips GmbH Marked DACH, Hamburg, Germany, Hamburg, Hamburg, Germany*

Background: Quantitative tissue characterization by novel T1 and T2 Mapping CMR techniques could provide incremental information to differentiate acute from chronic myocardial infarction (MI). We investigated the clinical utility of an approach using novel Mapping techniques in comparison to standard T2-weighted CMR to discriminate acute from chronic MI.

Methods: Sixty-seven patients with first reperfused AMI were enrolled. T2w, T2, T1 mapping and late gadolinium enhancement (LGE) CMR were obtained at 2 time points after AMI at 8 ±5 days after infarction (baseline) and 6 ±1.4 months. CMR acquisitions were performed on end-diastolic LV short-axes. Myocardial T2 relaxation times were quantified using a free-breathing, navigator-gated multiecho sequence. Myocardial T1 relaxation times were measured using the modified Look-Locker inversion recovery sequence before and after administration of 0.075 mmol/kg gadobenate dimeglumine. T2, T1, and ECV maps were generated using a plug-in for the OsiriX software (Pixmeo, Bernex, Switzerland). Two experienced observers independently placed regions of interest in the infarcted areas using LGE as a reference standard. A T2w-ratio was generated using the formula: T2w-ratio = Mean SIinfarct / Mean SIremote.

Results: Native T1 had an almost perfect discriminative performance to differentiate between acute (baseline CMR) and the chronic stage (6 months follow-up) with an AUC of 0.984. The AUC of native T1 was significantly superior to the T2w-ratio with an AUC of 0.906 ($P < 0.05$) and to T2 with an AUC of 0.903 ($P < 0.05$). ECV of infarcted myocardium had a poor discriminative performance with an AUC of 0.655, which was significantly inferior compared to native T1, T2w-ratio and T2, respectively ($P < 0.001$). The optimal cutoff of ≥1138 ms for native T1 provided a sensitivity and specificity of 96% and 100%, respectively. The optimal cutoffs for the other CMR parameters were: ≥3.3 for T2w-ratio, ≥69ms for T2 and ≥39% for ECV.

Conclusions: Native T1 of infarcted myocardium is the best discriminator between acute and chronic myocardial infarction and should preferably be used as an objective and truly quantitative parameter to differentiate between the acute and chronic stage of myocardial infarction.

http://www.ConferenceAbstracts.com/uploads/cfp2/attachments/LDFAIBDN/LDFAIBDN--218043-1-ANY.pdf

http://www.ConferenceAbstracts.com/uploads/cfp2/attachments/LDFAIBDN/LDFAIBDN--218043-2-ANY.pdf

http://www.ConferenceAbstracts.com/uploads/cfp2/attachments/LDFAIBDN/LDFAIBDN--218043-3-ANY.pdf

R015

Prognostic value of dipyridamole stress CMR in patients with known or suspected coronary artery disease: a long term follow-up study

Antonella Meloni, PhD[1]Cinzia Nugara, MD[2], Fabiola Cosentino, MD[3], Vincenzo Positano, MSc[4], Giancarlo Todiere, MD[4], Pasquale Assennato, MD[2], Salvatore Novo, MD[2], Alessia Pepe, MD, PhD[4]

1. *Fondazione G. Monasterio CNR Regione Toscana, Pisa, Toscana, Italy*
2. *Università degli Studi di Palermo, Policlinico "Paolo Giaccone", Sicilia, Italy*
3. *Fondazione G. Monasterio CNR Regione Toscana, Sicilia, Italy*
4. *Fondazione G. Monasterio CNR Regione Toscana, Toscana, Italy*

Background: Dipyridamole stress CMR provides detailed information on the key phases (perfusion and wall motion) of the ischemic cascade (myocardial perfusion and segmental kinesis). Although the diagnostic value of stress CMR has been addresed, further studies are needed to evaluate its prognostic role at long-term, specifically using dypiridamol.
The aim of this study wasto determine the long-term prognostic value of dipyridamole stress-CMR in patients with known or suspected coronary artery disease.

Methods: Two hundred and thirty-seven consecutive patients (43 females, 62.57±9.69 years) with known or suspected coronary artery underwent dipyridamole stress-CMR in an high volume CMR Lab. Abnormal wall motion at rest and with dipyridamole, perfusion (at stress first-pass perfusion i and at rest), and delayed enhancement were analyzed.
End points were "major cardiac events" (ventricular arrhitmias, myocardial infarction, acute myocardial infarction, new revascularization) and cardiac death.

Results: Mean follow-up time was 70.46 ±71.88. Seventy-three (30%) patient had major cardiac events and ten (4%) died during the follow-up. At univariate analysis the only predictive variable of death was the presence of late gadolinium enhancement (hazard ratio-HR=7.65, P=0.011), while perfusion deficit was predictor of major cardiac events (HR=1.78, P=0.015). When the composite end-point (cardiac events + death) was considered, both myocardial fibrosis and perfusion deficit resulted to be significant univariate prognosticators, while only perfusion deficit remained significant (HR=1.68, P=0.020) at multivariate analysis.
A positive stress exam (Perfusion and/or motion deficit) was predictor of the composite endpoint (HR=1.57, P= 0.040).

Conclusions: Dipyridamole stress-CMR improves prognostic stratification of patients at long-term follow-up.

R016

Human Heartome Project: Toward a Database of Diffusion CMR of Explanted Human Heart Failure and Autopsy Hearts

Christopher Nguyen, PhD[1] Daniel Berman, MD[1], Daniel Luthringer, MD[2], Jon Kobashigawa, MD[2], Debiao Li, PhD[3]

1. *Cedars-Sinai Medical Center, Los Angeles, CA*
2. *Cedars-Sinai Medical Center, CA*
3. *Biomedical Imaging Research Institute, Cedars-Sinai Medical Center, Los Angeles, CA, CA*

Background: Diffusion tensor magnetic resonance imaging (DT-CMR) is a unique, non-invasive technique capable of mapping human myocardial fiber orientation [1]. However, current technology for in vivo imaging is technically limiting with respect to spatial resolution, spatial coverage, and bulk motion-based artifacts [2]. These technical limitations hinder further progress in revealing the clinical utility of DT-CMR in fundamentally characterizing the perturbation in tissue microstructure of various cardiovascular diseases. Therefore, we propose an ex vivo DT-CMR collection ("Human Heartome Project") of explanted native human heart failure (HF) hearts before radical heart transplantation and normal, age-matched autopsy (NA) hearts with high spatial resolution, full left ventricular coverage, and free of motion-induced artifacts to explore the clinically relevant information DT-CMR may provide.

Methods: High spatial resolution (0.9x0.9x2.5mm^3) ex vivo DT-CMR (single spin echo, 12 directions, b=1000 s/mm^2, TR=4000ms, TE=72ms, scan time=3hrs) was performed on both ventricular chambers for explanted human HF (n = 14, 55±12) and NA (n = 6, 51±9) hearts. All hearts were surgically removed and placed into saline at 4°C for up to 6 hours (4.5±1.1 hours) before being imaged on a 3T scanner (mMR Biograph, Siemens Healthcare). After ex vivo CMR, the hearts were placed in formalin fixation solution and sent back to pathology for routine clinical pathology work-up. DT-CMR images were processed using custom software built on DIPY (www.dipy.org) platform to estimate voxelwise self-diffusion tensors, mean diffusivity (MD), fractional anisotropy (FA), helix angle (HA), and absolute HA transmurality (|HAT|). Unpaired t-test with unequal variances was used to determine statistically significant differences between DT-CMR parameters of HF and NA groups.

Results: Clinical pathology reports the collected HF hearts consistently exhibited the presence of fibrosis while NA hearts did not. MD (HF: 0.64±0.06 um^2/ms vs NA: 0.57±0.02 um^2/ms), FA (HF: 0.37±0.04 vs NA: 0.46±0.05), and |HAT| (HF: 0.85±0.17°/% transmural depth (TD) vs NA: 1.06±0.10°/%TD) were significantly ($p < 0.001$, $p = 0.003$, $p = 0.004$, respectively) when comparing HF with NA groups. The HF subject with the highest MD, lowest FA, and lowest |HAT| was the only subject using a left ventricular assisted device (LVAD) with severe dilated cardiomyopathy. The two HF subjects with MD, FA, and |HAT| within normal range were the youngest patients (27 and 32 y/o) with advanced hypertrophic cardiomyopathy.

Conclusions: Ex vivo DT-CMR in human explanted HF hearts revealed significant differences in MD, FA, and HAT when compared to age-matched NA. Continual recruitment of more HF patients may hopefully provide differences between various etiologies of HF.

References: [1] Sosnovik, et al. Circulation 2012. [2] Nguyen, et al. MRM 2016

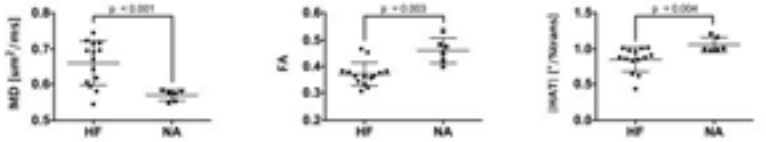

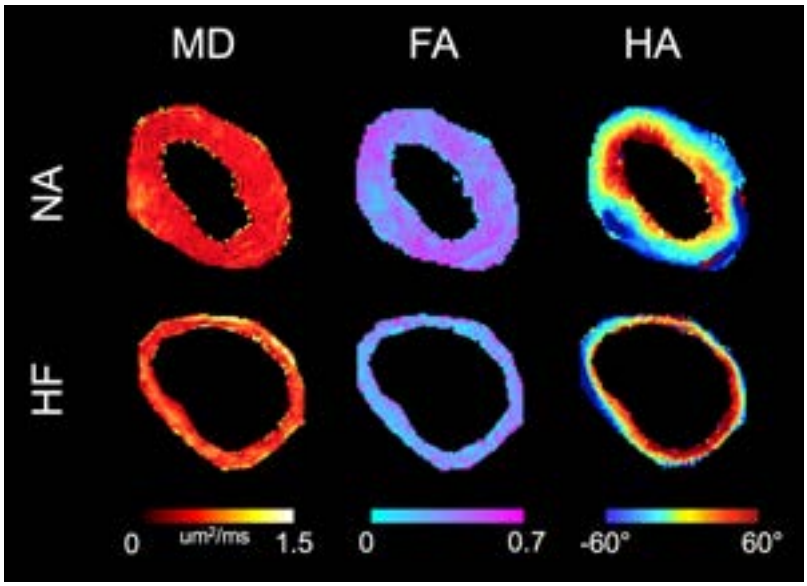

R017

Aortic biomechanics by Cardiac Magnetic Resonance in the development of stent fractures in the Coarctation of the Aorta Stent Trial (COAST)

Lasya Gaur, MD[5]Matthew Woods, BIS[1], Bharath Ambale-Venkatesh, PhD[2], Richard Ringel, MD[3], Joao A.C. Lima, MD, MBA[4]

1. *Johns Hopkins School of Medicine, MD*
2. *Johns Hopkins University, MD*
3. *Johns Hopkins Childrens Center, MD*
4. *Johns Hopkins University, Baltimore, MD*
5. *Johns Hopkins Children's Center, Baltimore, MD*

Background: Stent therapy for Coarctation of the aorta (CoA) is effective for CoA relief as shown by the prospective multicenter Coarctation of the Aorta Stent Trial (COAST). However these stents can be susceptible to fracture. Pulse wave velocity (PWV) and aortic distensibility (AD) measured by cardiac MRI were directly compared in COAST participants who developed stent fractures versus those who did not based on follow up fluoroscopy.

Methods: 104 participants underwent successful implantation of the bare-metal Cheatham Platinum stent for CoA in COAST I. 94 subjects underwent cardiac MRIs at 12 and/or 24 months following stent implantation as part of the COAST I trial. PWV and AD were analyzed by a previously validated semi-automated aorta analysis software (ARTFUN) on phase contrast images obtained at the level of the ascending and descending aorta (distal to the stented coarctation). All measurements were performed by a blinded observer. COAST participants who did not have adequate phase contrast images for analysis were excluded. Comparison between groups was performed by Students t-test (for parametric variables) and the Mann-Whitney U test (for non-parametric variables). Covariate analysis was performed by the analysis of covariance (ANCOVA).

Results: Of the initial 94 CMR studies, 57 studies were adequate for preliminary analysis at either 12 or 24 month follow up. Mean age of participants with stent fractures (Group 1) and those without (Group 2) was 19.6 ± 10.7 years vs 14.7 ± 5.6 years; p = 0.1. PWV was not significantly different in the two groups post stent implantation (Table 1). When adjusted for age, PWV was increased in Group 1 compared with Group 2 (4.2 ± 0.22 vs 3.2 ± 0.38; p = 0.03). AD in the ascending and descending aorta were similar (Table 1).

Conclusions: Vascular profiling of PWV and AD by CMR in CoA post percutaneous Cheatham Platinum bare-metal stent implantation is feasible. PWV and AD were similar in all COAST I participants regardless of development of stent fracture. However when adjusted for age, subjects with stent fractures had increased PWV suggestive of increased wall stiffness. Additional prospective CMR studies are needed to determine whether differences in aortic biomechanics are useful for prediction of stent fractures and whether these represent a change from baseline aortic vascular profiles in CoA prior to stent implantation.

Comparison of Pulse Wave Velocity and Aortic Distensibility between groups

	Group 2 Median (IQR)	Group 1 Median (IQR)	
	43	14	**n**
p = 0.2	3.1 (2.2 – 3.5)	3.3 (3.0 – 4.4)	**PWV (m/s)**
p= 0.5	4.8 (3.4 – 7.0)	4.5 (2.7 – 7.6)	**AD (Asc Ao) (10^{-3}mmHg^{-1})**
p= 0.8	3.9 (3.2 – 7.0)	4.1 (2.8 – 8.6)	**AD (Dsc Ao) (10^{-3}mmHg^{-1})**

IQR = interquartile range; Asc Ao = ascending aorta; Dsc Ao = descending aorta

R018

Tissue phase mapping detects abnormal diastolic function in children with hypertrophic cardiomyopathy but not in non-affected gene mutation carriers

Kristian H. Mortensen, MD, PhD[1] Jennifer Steeden, PhD[2], Vivek Muthurangu, MD[1]

1. Institute of Cardiovascular Science, University College London, England, United Kingdom
2. UCL Centre for Cardiovascular Imaging, Institute of Cardiovascular Science, England, United Kingdom

Background: Diastolic dysfunction may precede myocardial hypertrophy of the left ventricle (LV) in hypertrophic cardiomyopathy (HCM). Consequently, evaluation of diastolic indices may improve risk stratification, particularly in gene mutation carriers. However, evidence of diastolic abnormalities in affected children and those at risk is limited. Tissue phase mapping (TPM) is a CMR technique that accurately measures systolic and diastolic myocardial velocities. In this study, we used a novel accelerated spiral TPM sequence to acquire high-resolution data in a short breath hold manageable in children. The aim was to compare diastolic function in healthy children, phenotype negative gene carriers and pediatric patients with HCM.

Methods: Thirty-six children (12 HCM, 12 gene mutation carriers, and 12 healthy children) were recruited. Myocardial velocities in a mid-ventricular slice were assessed using a spiral UNFOLDed-SENSE TPM sequence (breath hold time 6-8s). TPM data was evaluated using the OsiriX software to assess radial, tangential and longitudinal S, E and A wave velocity. Conventional left ventricular (LV) metrics were measured using a real-time radial SSFP sequence. Measured LV metrics included mass (LVM), maximum wall thickness (LVMWT), volumes (LVEDV, LVESV) and ejection fraction (LVEF). Comparisons were performed using ANOVA with post hoc pairwise comparisons using the Tukey method. Associations were assessed using linear regression.

Results: Peak longitudinal and radial diastolic E wave velocities were significantly lower in children affected by HCM when compared with gene-carriers and healthy volunteers (Table 1). Affected children also had lower peak longitudinal S wave velocities (Table 1). There were no differences in myocardial velocities between healthy children and gene carriers. The LVM and LVMWT were comparable between controls and non-affected gene-carriers, but as expected elevated in affected children. LVEF, LVEDV and LVSV were comparable. Both peak longitudinal and radial E wave velocities were inversely correlated with LVMWT ($P < 0.002$) and LVM ($P < 0.005$).

Conclusions: Indices of diastolic function are normal in phenotype negative children who carry gene mutations associated with HCM. In children affected by HCM diastolic LV function is, however, abnormal and correlates with disease severity. TPM could therefore improve risk stratification in affected children, but currently may have a limited role for risk assessment in phenotype negative, gene mutation carriers.

Table 1. Age, left ventricular morphological indices, and selected myocardial tissue velocities in healthy children, gene mutation carriers for hypertrophic cardiomyopathy, and children with hypertrophic cardiomyopathy.

P value	Phenotype positive (n = 12)	Gene mutation carriers (n = 12)	Controls (n=12)	
0.9	14 ± 2.3	15 ± 1.7	15 ± 1.2	Age (years)
<0.05	109 ± 32	61 ± 12	53 ± 8.6	LVM (g/m^2)
<0.05	22 ± 4.9	9 ± 1.8	8 ± 1.4	LVMWT (mm)
0.7	58 ± 2.1	68 ± 1.1	64 ± 1.1	LVEF (%)
0.10	2.9 ± 1.1	2.6 ± 1.2	2.5 ± 1.2	Radial S wave velocity (cm/sec)
<0.05	2.5 ± 1.1	4.2 ± 1.0	3.8 ± 0.8	Radial E wave velocity (cm/sec)
0.7	1.2 ± 0.5	1.1 ± 0.4	1.2 ± 0.7	Radial A Wave velocity (cm/sec)
<0.05	3.2 ± 1.0	4.2 ± 1.5	4.5 ± 0.9	Longitudinal S wave velocity (cm/sec)
<0.05	4.6 ± 2.6	8.4 ± 2.1	9.3 ± 1.8	Longitudinal E wave velocity (cm/sec)
0.4	2.3 ± 0.9	2.8 ± 0.9	2.8 ± 0.7	Longitudinal A wave velocity (cm/sec)

R019

Does the Electrocardiogram Lead Us Astray in Pulmonary Hypertension; a Cardiac Magnetic Resonance Imaging Cross-Comparison Study?

Matthew S. Tong, D.O.[1]Jose Ricardo Po, M.D[1], Talha Meeran, M.D.[1], Mark Doyle, Ph.D.[1], Geetha Rayarao, MS[2], Shimaa S. Khidr, MD[1]

1. Allegheny General Hospital, Pittsburgh, PA
2. Allegheny General Hospital, PIttsburgh, PA

Background: Right ventricular hypertrophy (RVH) is prevalent in the pulmonary hypertension (PH) population due to increased afterload and is an independent predictor of cardiovascular morbidity and mortality. The use of electrocardiography (ECG) has been the initial screening tool for structural heart disease, including the right ventricle. The role of CMR has become the primary modality for assessment due to its high temporal/spatial resolution and high degree of reproducibility. Limited data on RVH is available as it compares to the ECG, yet the latter is ubiquitous. We aim to correlate the accuracy of ECG criteria for RVH 2009 AHA Recommendations for Standardization and Interpretation of the ECG with CMR quantitative measurements of mass based on the recent consensus statement of normal values for CMR in adults (*JCMR,* 2015).

Methods: A retrospective chart review was performed with consecutive patients in the PH clinic at our institution. Baseline characteristics, PH WHO group classifications, ECGs, and CMR data regarding RV mass (RVM) and volumes were extracted for analysis. ECG diagnosis of RVH followed the 2009 AHA recommendations. Statistical analyses were performed with RVM, RV mass index (RVMI), and RVEDVI against all ECG-RVH diagnoses.

Results: In the cohort of 111, 56% (n=62) were WHO group I PAH, and 37% (n=23) had RVH by RVMI, and 39% (n=24) by ECG. Regarding the other non-WHO group I PH patients (n=49), 31% (n=15) had RVH by RVMI, and 22% (n=11) by ECG. In entire cohort, RVH-ECG had a sensitivity of 50%, specificity of 78% and an accuracy of 68% when compared to RVMI. The ECG was minimally less accurate when comparing only PAH patients (sensitivity = 52%, specificity = 69%, accuracy = 63%). When CMR diagnosed RV dilation was added to the ECG RVH interpretation, sensitivity was lower (47%), but the specificity was higher (84%), with the accuracy essentially unchanged (66%). In light of this potential correlation of mass and volume related ECG vector modulations, an independent analysis was performed for the accuracy of ECG-RVH with RV dilation and normal RVMI by CMR. There were 6 patients (5%) that had RV dilation alone without abnormal RVMI, of which 4 patients had ECG-RVH (67%).

Conclusions: Overall, ECG accuracy for RVH is poorly accurate when compared to CMR RV mass assessment while the addition of CMR RV dilation criteria made the ECG more specific, suggesting perhaps the vector forces from a larger, not necessarily thicker chamber is in part, the explanation of ECG-RVH.

R020

Associations Between Myocardial T1-Mapping and Left Ventricular Strain, Strain Rate, and Dyssynchrony in Patients with Repaired Tetralogy of Fallot

Christopher M. Haggerty, PhD[1] Abba Mejia-Spiegeler, LLB[2], Jonathan D. Suever, PhD[3], Gregory J. Wehner, BS[4], Richard J. Charnigo, PhD[4], Brandon K. Fornwalt, MD, PhD[1], Mark A. Fogel, MD[5]

1. *Geisinger Health System, PA*
2. *Geisinger Health System, Danville, PA*
3. *Geisinger Health System, Bellefonte, PA*
4. *University of Kentucky, KY*
5. *Children's Hospital of Philadelphia, Philadelphia, PA*

Background: Patients with repaired tetralogy of Fallot (TOF) often suffer from progressive, adverse ventricular remodeling, which leads to abnormal contractile mechanics. Defining the mechanisms underlying this dysfunction, such as diffuse myocardial fibrosis, may provide insights into poor long-term outcomes. We hypothesize that left ventricular (LV) diffuse fibrosis is related to impaired LV mechanics (strain/strain rate/dyssynchrony).

Methods: Forty-three patients with TOF were evaluated with cardiovascular magnetic resonance (CMR) in which modified Look-Locker (MOLLI) and spiral cine Displacement Encoding with Stimulated Echoes (DENSE) sequences were each acquired at three LV short-axis positions at 1.5T. From MOLLI, native and post-contrast T1, partition coefficient (λ), and extracellular volume fraction (ECV; using bloodpool T1-derived hematocrit) were computed, while peak mid-wall radial and circumferential strains, circumferential strain rates, and radial and circumferential dyssynchrony were derived from DENSE. Ventricular volumes and ejection fractions (EF) were derived from cine SSFP. Linear mixed modeling was used to predict LV mechanics at a given slice based on diffuse fibrosis measured from the same slice, accounting for age, sex, slice location, and within-patient repeated measures. $P < 0.05$ was defined as significant.

Results: Thirty-nine patients (26±10 years, 56% male) were included, and four patients were excluded due to poor image quality or movement. Right ventricular (RV) indexed end-diastolic volumes were dilated (145±45 mL/m^2), while LV end-diastolic volumes were normal (73±13 mL/m^2); RV and LV EF were both within normal ranges (44±10 and 55±7%, respectively). Neither LV nor RV volumes were significantly associated with any LV fibrosis measures (data not shown). ECV was normal, on average; however, seven patients (18%) had values above normal (>0.28; Figure 1). Similarly, average radial (35±10%) and circumferential (15±3%) strains were normal, although 12 patients (31%) had impaired circumferential strains (< 14.4%). Post-contrast T1, λ, and ECV were individually predictive of peak radial strain (Table 1). While no T1-based measure was predictive of peak circumferential strain, post-contrast T1 was predictive of both systolic and diastolic (Figure 2) strain rates. Finally, ECV was predictive of both radial and circumferential dyssynchrony, while separate associations of λ with radial dyssynchrony and post-contrast T1 with circumferential dyssynchrony were also observed.

Conclusions: After TOF repair, both diffuse fibrosis and impaired mechanics may develop in the left ventricle, even with normal end-diastolic volume and EF. After adjusting for age, sex, and slice location, several moderate associations between diffuse myocardial fibrosis and impaired mechanics were observed. Diffuse fibrosis may therefore be a causal factor for some ventricular dysfunction in these patients.

http://www.ConferenceAbstracts.com/uploads/cfp2/attachments/LDFAIBDN/LDFAIBDN--218650-1-ANY.pdf

http://www.ConferenceAbstracts.com/uploads/cfp2/attachments/LDFAIBDN/LDFAIBDN--218650-2-ANY.pdf

Table 1. Estimates of Mixed Models Effects for LV T1 on Mechanics*

Post-contrast T1 [ms]	λ	ECV	
0.07 (p=0.03)	-74 (p=0.002)	-81 (p=0.02)	Radial strain [%]
0.01 (p=0.07)	-6.1 (p=0.18)	-9.4 (p=0.19)	Circumferential strain [%]
0.10 (p=0.03)	-41 (p=0.14)	-54 (p=0.22)	Systolic circumferential strain rate [%/s]
0.002§ (p=0.002)	-69 (p=0.29)	-179 (p=0.07)	Diastolic circumferential strain rate [%/s]
0.0015† (p=0.02)	-0.36† (p=0.37)	-1.27† (p=0.04)	Circumferential dyssynchrony
0.0003 (p=0.24)	-0.43 (p=0.01)	-0.53 (p=0.03)	Radial dyssynchrony

Data reported are β estimates of individual predictor; *Separate models produced for each predictor/outcome combination, each adjusted for age, sex, slice region; §log transformed dependent variable; † 15th power transformed dependent variable

R021

A comparison of spiral and EPI trajectories for in-vivo cardiac DTI

Margarita Gorodezky, M. Sc.[1] Pedro F. Ferreira, PhD[2], Andrew D. Scott, PhD[3], Sonia Nielles-Vallespin, PhD, MSc[4], Dudley J. Pennell, MD[5], David N. Firmin, PhD[6]

1. *National Heart and Lung Institute, Imperial College, Sydney Street, London, SW3 6NP, UK, England, United Kingdom*
2. *Cardiovascular Biomedical Research Unit, The Royal Brompton Hospital, Sydney Street, London, SW3 6NP, UK, England, United Kingdom*
3. *NIHR Cardiovascular Biomedical Research Unit, The Royal Brompton Hospital, Sydney Street, London, SW3 6NP, UK, England, United Kingdom*
4. *NIH, MD*
5. *Royal Brompton Hospital and Imperial College, London, England, United Kingdom*
6. *NIHR Cardiovascular Biomedical Research Unit, Royal Brompton Hospital, England, United Kingdom*

Background: Stimulated-echo-acquisition-mode (STEAM) echo-planar-imaging (EPI) has proven to be a reliable cardiac-diffusion-tensor-imaging (cDTI) technique[1], however spatial resolution is typically limited. Spiral k-space trajectories are efficient, motion resilient, allow reduced TE relative to EPI and could be used to improve spatial resolution in cDTI[2]. In this work we compare the performance of a novel spiral STEAM cDTI sequence to a standard STEAM EPI sequence.

Methods: An EPI STEAM sequence was modified to have a spiral readout (figure 1) with a reduced excitation field-of-view (FOV) via slice selective RF pulses[3] in both x and y. The first RF pulse is asymmetric (peak at 81% of duration) and second is a time-reversed copy of the first one allowing a sharper slice-profile for an equivalent TE. TE was 12ms and spiral duration 15ms.
The EPI had a reduced FOV in phase direction, used SENSE x2 acceleration, an EPI echo-train length of 24 with a duration of 12ms. TE was 23 ms. 8 volunteers were scanned with both sequences in a mid short-axis slice in peak-systole and the diastolic rest-period during breath-holding (16 RR intervals including 2RR dummy cycle for spiral and 4RR for EPI reference data) on Siemens-Skyra 3T with TR=2RR intervals. Images were acquired with 2.8x2.8x8mm^3 spatial resolution, b_{ref}=150 s/mm^2 and b_{main}=600 s/mm^2 in 6 diffusion directions and 8 averages. The diffusion tensor and derived maps of secondary eigenvector angulation (E2A), fractional anisotropy (FA), mean diffusivity (MD) and helical angle (HA) were calculated with in-house software (MATLAB) and compared between the two sequences. For HA the mean line profile gradient (HAlg) was compared.

Results: Figure 2 shows example parameter maps for a single volunteer in systole and diastole using an EPI and a spiral readout. The mean LV parameters are plotted in figure 3. Systolic FA using EPI (p=0.02) is higher due to a larger primary eigenvector, but the difference is small (9%). HAlg was significantly more negative in both systole (p=0.04) and diastole (p=0.01) using the EPI-sequence due to artefacts in the spiral data. All other plots show no significant differences.

Conclusions: cDTI can be performed with spiral-readouts at the same resolution as current EPI sequences in both systole and diastole with few differences in the parameters derived. Further work will address spiral artefacts and optimise the spiral sequence for high spatial resolutions.

REFERENCES: Nielles-Vallespin S: Magn-Reson-Med2013 Scott A: ISMRM2014:Abstract3968 Scott A: SCMR2016:O50

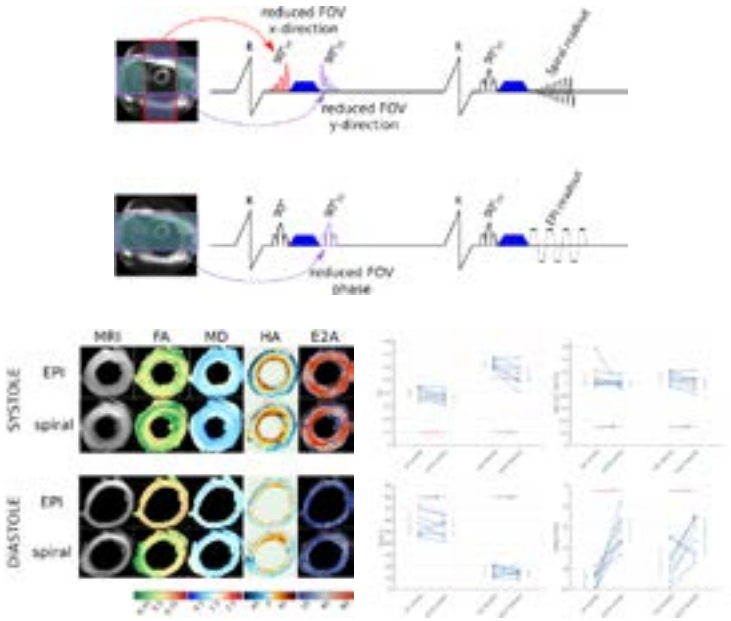

R022

Contact free cardiac gating using the transmit RF coil by monitoring the scattering matrix on a parallel transmit scanner

Sven H.F. Jaeschke[1] Caitlin O'Brien, MSci[2], Aaron T. Hess, PhD[3], Matthew D. Robson, PhD[3]

1. *University of Oxford, Oxford, England, United Kingdom*
2. *University of Oxford, England, United Kingdom*
3. *OCMR, University of Oxford, England, United Kingdom*

Background: ECG remains the go-to method for cardiac MRI synchronisation but requires preparation, electrodes and sometimes expert adjustment. An alternative is proposed requiring no additional hardware other than that provided with a commercial parallel transmit MRI scanner. Forward and return voltages are measured on an RF transmit line by the local SAR monitor. Returned voltages are a function of reflection from the subject and coupling through the subject from other transmitters and it is measured by the scattering (S) matrix. If the objects (and their complex permittivity) change within these RF fields this is detected in the S-matrix. An algorithm to characterise the cardiac cycle from the changing S-matrix is presented and is demonstrated in a cardiac cine acquisition.

Methods: Setup: 7T MRI (VB17, Step 2.3, Siemens), 8 channel PTX, local SAR monitor, 8 channel TEM cardiac transmit/receive coil. S-matrix measurements were made using a frequency multiplexed (2kHz channel spacing) 5ms Gauss RF pulse every TR=10ms. The S-matrix and ECG were recorded in 10 subjects for 165s including an initial 15s breath hold.

A time series of the 8x8 S-matrix was split into real and imaginary components, providing 128 observations per time point. The data was temporally de-trended and the cardiac signal was extracted using an independent component analysis of cardiac band pass filtered data. The cardiac component was identified by a Welch power spectrum density estimate with highest power and the cardiac mixing vector determined. The mixing vector was used to establish a raw, unfiltered scalar signal. Figure 1 shows an example of this raw trace.

The cardiac signal was analysed using a multiresolution discrete wavelet transform (DWT) with a maximal overlap. A mother wavelet with (N=5) vanishing moments of symlets was used. The dominate heart frequency DWT was chosen and a peak detection carried out.

A 2D GRE cardiac cine was acquired and retrospectively gated with this algorithm based on the eight return voltages measured during transmit, these are a row-sum of the S-Matrix.

Results: Using the ECG as a gold standard, the sensitivity and positive predictive value of the feature detection was 100%, the standard deviation of the difference in trigger time between ECG and the new method was 15ms during breath holding and 22ms while free breathing with a mean trigger delay of 302ms and 260ms respectively.

Conclusions: A new method for ECG-free cardiac synchronisation in MRI has been proposed that can be rolled out to PTX cardiac MRI scanners.

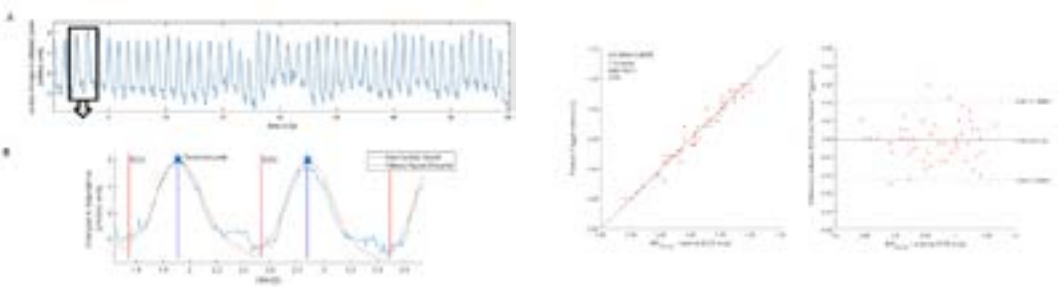

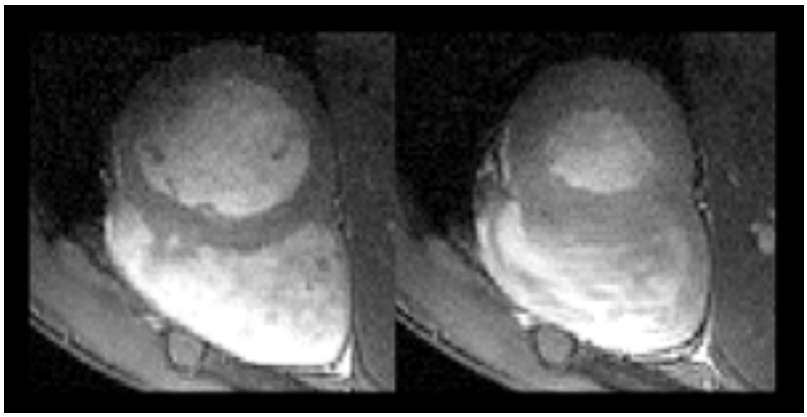

R023

Non-ECG First-Pass Myocardial Perfusion T1 Mapping Using CMR Multitasking

Anthony G. Christodoulou, PhD[1] Jaime L. Shaw, MS[1], Behzad Sharif, PhD[2], Debiao Li, PhD[3]

1. *Cedars-Sinai Medical Center, CA*
2. *Cedars-Sinai Medical Center, Los Angeles, Los Angeles, CA*
3. *Biomedical Imaging Research Institute, Cedars-Sinai Medical Center, Los Angeles, CA, CA*

Background: Quantitative myocardial perfusion MRI is confounded by ECG-triggering misfires and the nonlinear response of signal intensity to contrast agent concentration. Non-ECG, time-resolved T1 mapping could correct for these factors [1] but has previously been too slow to perform myocardial T1 mapping. Here we propose a method for non-ECG, first-pass myocardial perfusion T1 mapping with single-bolus quantification, using the cardiovascular low-rank tensor (LRT) imaging framework [2] for CMR multitasking (simultaneous imaging of multiple dynamics such as cardiac motion, T1 recovery, and contrast agent wash-in/out).

Methods: The proposed method used a continuous-acquisition SR-prepared single-slice 2D radial FLASH sequence with a golden-angle ordering scheme modified to collect LRT subspace training data [2]. Each saturation pulse was followed by 10° FLASH readouts every 3.6 ms throughout the entire 300 ms recovery period. In-plane spatial-resolution was 1.7 mm; scan length was 45 s. Real-time low-rank matrix images [3] were reconstructed first for image-based cardiac binning. LRT image reconstruction was then performed with three time dimensions indexing each heartbeat, 15 cardiac phases, and 42 saturation times (3.6, 10.7, 17.8, ..., 295 ms). Data were collected from n=8 healthy volunteers on a 3T Siemens Verio. To assess repeatability of absolute myocardial blood flow (AMBF) measurements at rest, two 0.1 mmol/kg doses of Gadovist were administered 20 to 30 minutes apart. Subjects were instructed to hold their breath until no longer comfortable, followed by shallow breathing. AMBF was calculated by fitting T1 at the LV blood pool and six myocardial segments, converting to ΔR1, and performing Fermi deconvolution.

Results: Fig. 1 demonstrates imaging of multiple cardiac phases as well as the passage of contrast agent. Fig. 2 demonstrates the calculation of contrast agent concentration from signal intensity surfaces: the large number of saturation times and joint fitting across heartbeats allows measurement of a wide range of blood and myocardial T1's. Table 1 lists measurement statistics aggregated over segments. There was a nonsignificant difference (p=0.40) between the first and second AMBF measurements, and flows were within the normal range from previous literature [4]. The within-segment standard deviation of 0.30 g/mL/min compares favorably with other non-ECG methods [5].

Conclusions: The initial results of non-ECG first-pass myocardial perfusion T1 mapping are promising for single-bolus quantification of myocardial blood flow. AMBF measurements are robust to initial contrast agent concentration, with a nonsignificant difference between first and second boluses. Potential future research involves evaluating the method for stress perfusion, extending it to multi-slice or 3D acquisition, and incorporating motion correction for free-breathing acquisition.

1. Chen *MRM* 2015
2. Christodoulou *ISMRM* 2016
3. Christodoulou *TBME* 2013
4. Muehling *JCMR* 2004
5. Likhite *JMRI* 2015

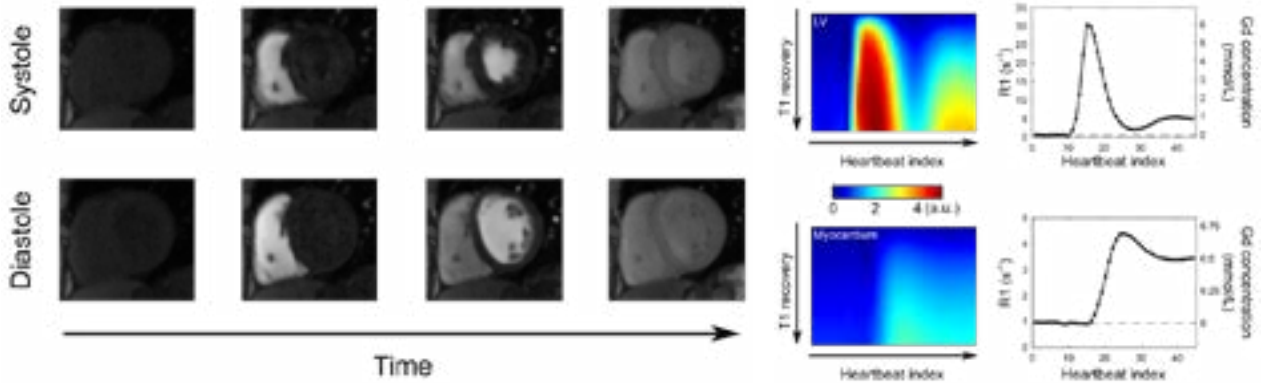

Table 1: Summary of measurement statistics

Coeff. of variation	Within-segment standard deviation	Significance of difference	AMBF values (mL/g/min)	Bolus
25%	0.30 mL/g/min	p = 0.40 (NS)	1.18 ± 0.35	First
			1.23 ± 0.32	Second

R024

Blipped Multiband SSFP: towards band free cine imaging of the whole heart within a single breath-hold

Anthony N. Price, PhDLucilio Cordero-Grande, PhD, Shaihan J. Malik, PhD, Joseph V. Hajnal, PhD

King's College London, London, England, United Kingdom

Background: Multiband (MB) imaging is increasingly used to accelerate multi-slice data due to its SNR advantage over in-plane sub-sampling [1]; when used with controlled aliasing (CAIPIRINHA), separation of simultaneously excited slices is greatly improved [2]. CAIPIRINHA-SSFP typically uses RF phase modulation to shift slices [3,4] but this also shifts the SSFP frequency response which can make banding artefacts more of a challenge for cardiac applications. Applying gradient blips to shift simultaneous slices in SSFP [5], while maintaining standard RF phase alternation, allows the most beneficial aliasing pattern to be used while preserving normal banding properties.
Here we demonstrate preliminary data using this method to accelerate cine SSFP at 3T, and by using MB=4 full LV coverage could be achieved within a single breath-hold.

Methods: Multiband RF capability and flexible gradient blipping scheme was implemented on a 3T Philips Achieva system. Data from 3 healthy adult volunteers was collected with a 32-channel cardiac coil.
Retrospective-gated SSFP cine stacks were collected as standard single-band (SB), and MB=2,3,4 accelerated, each acquired over 6,3,2x(19s) and 1x(28s) breath-holds respectively. Additional parameters: resolution=2x2x8mm, 12 short-axis slices, 30 phases, half-Fourier=0.63, FA=40°, TE/TR=2/4ms.
Images were reconstructed offline utilising ReconFrame (GyroTools) and custom MB-unfolding based on an iterative SENSE approach for joint estimation of sensitivity profiles and unfolded data [6].

Results: All reconstructed images (Fig.1) reveal good SNR and blood-myocardium contrast, with banding artefact locations in all slices unchanged from the single band case. Higher MB stacks require fewer breath-holds and thus generally more consistent in through slice re-formats, aiding segmentation analysis. MB=4 allowed the full acquisition in a single breath-hold, although residual unfold artefacts started to appear.
Improved reconstruction techniques and alternative reference scans are currently being investigated. MB increases peak B1, lengthening TR within fixed SAR constraints, although recent developments in MB pulse design should help to push the boundaries further, also applying at 1.5T could have added benefit.

Conclusions: This pilot study into blipped multiband SSFP for cardiac cine imaging reveals encouraging results suggesting it could provide a valuable additional tool to conventional in-plane and k-t acceleration methods, but with preserved SNR benefits. The use of gradient blips rather than RF phase cycling between slices avoids increasing banding artefacts and is easier to implement. Blipped MB-SSFP could contribute to realising whole heart cine imaging in a single breath-hold.

References:

[1] Barth-(2016)-MRM;75:63–81.

[2] Breuer-(2005)-MRM;53:684–691.

[3] Stäb-(2011)-MRM;65:157–164.

[4] Wang-(2015)-doi:10.1002/mrm.26076

[5] Duerk-(2013)-Patent:US20130271128A1

[6] Cordero-Grande-(2016)-ISMRM:3239

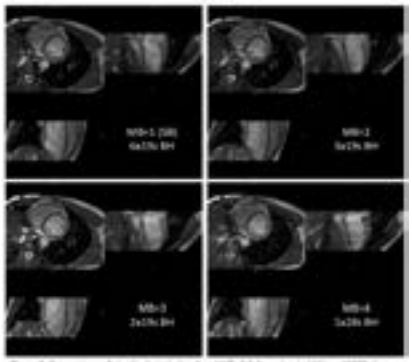

R025

Free-breathing 3D whole-heart stress myocardial perfusion using reordered compressed sensing

Merlin J. Fair, MRes[1], Rick Wage, DCR (R)[2]Eliana Reyes, MD[2], Peter D. Gatehouse, PhD[1], Ganesh Adluru, PhD[3], Jason Mendes, PhD[3], Edward VR. DiBella, PhD[3], David N. Firmin, PhD[2]

1. *NIHR Cardiovascular Biomedical Research Unit, Royal Brompton Hospital, London, England, United Kingdom*
2. *NIHR Cardiovascular Biomedical Research Unit, Royal Brompton Hospital, England, United Kingdom*
3. *UCAIR, University of Utah, UT*

Background: Myocardial first-pass perfusion (FPP) can be extended by 3D imaging to whole-heart coverage in every cardiac cycle with consistent cardiac phase for all reconstructed images[1]. Technical advances have enabled such acquisitions, with recent comparisons in patient cohorts demonstrating strong potential for future clinical application[2][3]. However, extreme sequence acceleration is required to minimise intra-shot cardiac motion. This can make reconstructions sensitive to respiratory motion. In all previous patient validations of 3D FPP techniques, breath-holding was required for accurate reconstruction with temporal parallel imaging techniques. Breath-hold requirements could reduce reliability as patient co-operation during stress is often difficult. Compressed sensing (CS) allows high accelerations of FPP but is also often based on assumed breath-holding – previous 3D FPP work with CS has been performed at rest. This work aims to demonstrate optimised 3D FPP imaging with a modified CS reconstruction algorithm, in free-breathing subjects at both rest and stress.

Methods: 12 3D FPP scans (3 stress, 9 rest) were acquired in consenting patients and volunteers with ethical approval. Each scan was performed during free-breathing, with no instructions issued to the subject. A 3D hybrid Cartesian-radial sequence (Table 1) was utilised, combining the motion-tolerance and CS compatibility of in-plane radial acquisitions with the lower required sampling rate of Cartesian through-plane acquisition. The sequence was optimised with asymmetric echo, slice partial Fourier (75%), and randomised RF spoiling[4], to shorten TR to 1.95ms, combined with variable density undersampling (8-24 rays/partition) for 195ms shot duration. Reconstruction of the ~15x undersampled datasets used a spatially and temporally constrained total variation CS algorithm[5]($\alpha_{temporal}$=3x10^{-5}, $\alpha_{spatial}$=3x10^{-4}, $N_{iterations}$=250). The temporal constraint underwent temporal pixel-wise reordering prior to each iteration, using an initial reconstruction as a prior, improving robustness to motion by better fitting the signal to the constraint[6]. The reconstructions with and without this extra step were compared.

Results: All participants were successfully scanned (examples Fig 1). A wide range of respiratory motions were acquired in rest and stress (see Fig 2) at HR up to 97bpm. Despite this, distortion to the images during the first-pass due to respiratory motion was rarely obvious. Application of the reordering scheme during reconstruction was able to improve the image quality and temporal dynamics of the datasets in all of these cases (e.g. Fig 2).

Conclusions: The feasibility of 3D FPP at stress and rest during free-breathing was demonstrated, and its clinical application in patients with known or suspected coronary artery disease is now being investigated.

References:

1. Fair,JCMR,2015
2. Jogiya,CircCardImag,2015
3. Manka,CircCardImag,2015
4. Roeleffs,MRM,2015
5. Adluru,JMRI,2009
6. Adluru,IntJBioImag,2008

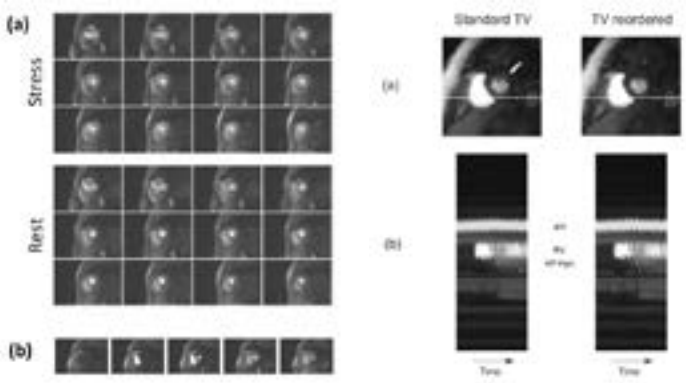

Sequence Parameters

Spoiled-gradient echo	Readout Type
12degrees (hamming-filtered, symmetric n=5 sinc pulse)	Flip Angle
(300x300x80)mm	FOV
(2.1x2.1x10.0)mm	Acquired Resolution
(2.1x2.1x5.0)mm	Reconstructed Resolution
0.98\1.95ms	TE\TR
100 (8/12/16/20/24/20 per partition)	Acquired Rays / Shot
195ms	Acquisition Time / Shot
0.49ms	ADC sampling Time / Ray
Timed to end-systole	Trigger Delay

R026

Typical Readout Durations in Spiral Cine DENSE Produce Blurred Images and Underestimate Radial Strain at Both 3.0T and 1.5T

Gregory J. Wehner, BS[1]Jonathan D. Suever, PhD[2], Samuel W. Fielden, PhD[3], David K. Powell, PhD[1], Sean M. Hamlet, MS[1], Moriel H. Vandsburger, PhD[1], Christopher M. Haggerty, PhD[3], Xiaodong Zhong, PhD[4], Brandon K. Fornwalt, MD, PhD[3]

1. *University of Kentucky, KY*
2. *Geisinger Health System, Bellefonte, PA*
3. *Geisinger Health System, PA*
4. *Siemens Healthcare, GA*

Background: Displacement Encoding with Stimulated Echoes (DENSE) encodes displacements into phase images that can be post-processed to yield cardiac strains. Cine DENSE has often been acquired with a spiral readout in order to optimize signal to noise ratio and temporal resolution. Most implementations have used few spiral interleaves with relatively long readout durations to keep the total scan duration within the length of a breath-hold (e.g. 6 interleaves with 11.1 millisecond readout duration). However, long readout durations can produce blurred images partially due to off-resonance and T2* decay. Importantly, strains are calculated from gradients in measured displacement, and blurred images could corrupt the measured strains. We hypothesized that this typical implementation of spiral cine DENSE is susceptible to spiral artifacts and that acquisitions with shorter readout durations would yield better image quality and more accurate strains.

Methods: To assess the impact of different amounts of off-resonance and T2* decay on image quality and measured strains, simulations were performed on a computational phantom of a deforming short-axis image. The benefit of reduced readout durations was assessed by varying the simulated readout duration between 11.1 and 1.9 milliseconds. The number of spiral interleaves was adjusted between 6 and 36 to hold spatial resolution constant. Spiral cine DENSE in a mid-ventricular image plane was then performed on 5 healthy volunteers at 3.0T and 1.5T (Siemens Trio and Aera, respectively). In both simulations and volunteers, strains were quantified with *DENSEanalysis,* an open-source application. Magnitude images were visually assessed for artifacts while Pearson correlations were used to determine whether measured strains depended on the applied readout duration.

Results: Simulations with longer readout durations were more susceptible to blurring from off-resonance and T2* decay (Figure 1A). Radial strain was the most affected strain component and was underestimated by simulations with longer readout durations in the presence of off-resonance and T2* decay (Figure 1B). Volunteer imaging showed blurring artifacts in the anterior and lateral walls of the left ventricle in acquisitions with longer readout durations at both 3.0T and 1.5T (Figure 2). Measured radial strain in those regions was dependent on the readout duration with underestimation of radial strain by up to 19.5% (absolute) when 11.1 millisecond readouts were used (Figure 3).

Conclusions: Image quality and measured radial strain are dependent on the readout duration of spiral cine DENSE at both 3T and 1.5T. The typical spiral cine DENSE acquisition underestimates radial strain compared to acquisitions with shorter readout durations.

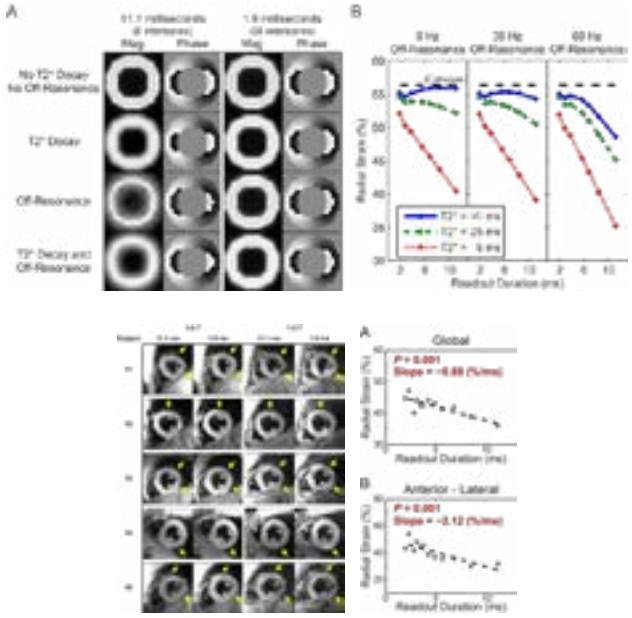

R027

Quantification of myocardial extracellular volume fraction for differentiating between amyloidosis and hypertrophic cardiomyopathy

Lu Lin, M.D.[1] Yining Wang, M.D.[2], Shu Jiang[2], Jian Cao, M.D.[2], Xiao Li, M.D.[2], Jing An, M.D., Ph.D[3], Andreas Greiser, Ph.D[4]

1. *Peking Union Medical Collge Hospital, Beijing, Beijing, China (People's Republic)*
2. *Peking Union Medical College Hospital, Beijing, China (People's Republic)*
3. *MR Collaborations NE Asia, Siemens Healthcare, Beijing, China, Beijing, China (People's Republic)*
4. *Siemens Healthcare GmbH, Erlangen, Germany, Erlangen, Bayern, Germany*

Background: To evaluate the diagnostic performance of using cardiac magnetic resonance (CMR) imaging measurements of extracellular volume (ECV) for differentiating amyloidosis (AL) and hypertrophic cardiomyopathy (HCM).

Methods: In this IRB-approved retrospective case-control study, 11 patients with HCM and 39 patients with AL were included. Patients with AL were confirmed by myocardial biopsy, and patients with HCM met the diagnostic criteria. All participants underwent a 3T (Magnetom Skyra, Siemens Healthcare, Erlangen, Germany) CMR examination including native and post-contrast T1 mapping (prototype modified Look-Locker inversion recovery (MOLLI) sequence with inline motion correction) in identical mid-ventricular short-axis slices of the left ventricle (LV). ECV was analyzed based on the American Heart Association (AHA) 16-segment model using CVI42 software (version 5.3, Circle Cardiovascular Imaging, Canada). ECV of AL and HCM were compared. Receiver-operating characteristic (ROC) analysis was performed, and the area under the ROC curve (AUC) was calculated. Sensitivity (Se), specificity (Sp), positive predictive value (PPV), negative predictive value (NPV) and accuracy were calculated by using the cut-off value of ECV corresponding to the highest AUC.

Results: In comparison to HCM, AL patients had significantly higher ECV at mid short-axis slice (0.45±0.11 vs 0.27±0.05, P < 0.001), interventricular septum (0.45±0.10 vs 0.29±0.07, *P < 0.001*) and anterior wall (0.43±0.12 vs 0.28±0.07, *P* < 0.001) of LV. ECV>0.36 in the mid short-axis slice identified AL from HCM with the highest AUC of 0.93±0.03 (Se=78.1%, Sp=100.0%, PPV=100.0%, NPV=58.8%, Accuracy=76%).

Conclusions: ECV has a potential to differentiate AL from HCM and ECV measured in the mid short-axis slice showed best differential diagnostic performance.

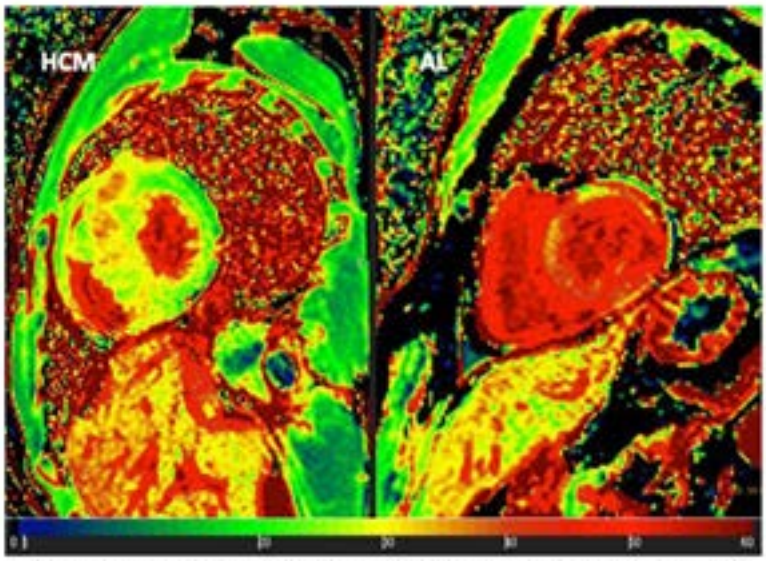

Figure. Two short-axis ECV maps for HCM and AL respectively with elevated ECV illustrated by focal or diffuse red color in the middle slice of left ventricle myocardium.

R028

USPIO-enhanced CMR: comprehensive methodological investigation and application in acute MI

Jakub Lagan, LEKARZ MRCP[1] David Clark, BSc(Hons)[2], Anna Reid, MBChB(Hons) MRCP[2], Gavin Lewis, MBChB[2], Josephine Naish, PhD[3], James E. Fildes, PhD[3], Andrew Trafford, BVSc PhD[3], William Critchley, BSc MRes[3], Erik B. Schelbert, MD, MS[4], Matthias Schmitt, MD PhD[2], Philip Foden, MSc[3], Christopher A. Miller, MBChB PhD[2]

1. *University Hospital of South Manchester, Liverpool, England, United Kingdom*
2. *University Hospital of South Manchester, England, United Kingdom*
3. *University of Manchester, England, United Kingdom*
4. *University of Pittsburgh; Heart and Vascular Institute of UPMC, PA*

Background: Quantification of active myocardial inflammation may improve diagnosis, guide management and provide trial end-points for novel therapies. Ultrasmall particles of iron oxide (USPIO) appear to be phagocytosed by activated leukocytes and USPIO-enhanced CMR is increasingly used to assess tissue inflammation. Typically, imaging is performed using T2* at a single time point post-USPIO. We aimed to; 1. Compare T2* with T1 mapping, which is proposed as an alternative for cardiac iron measurement in iron overload cardiomyopathy; 2. Determine whether imaging at a single time point post-USPIO is sufficient to detect active accumulation in tissue; 3. Determine whether USPIO signal from infarct and remote zones in acute MI reflects active myocardial accumulation as is proposed, or simply slow passive 'wash-through' in edematous myocardium.

Methods: Four healthy volunteers and six patients with acute MI underwent 1.5T CMR, including T1 and T2* mapping, before and at multiple time points following 4mg/kg ferumoxytol.

Results: Normalized T2* of spleen (and liver; not shown), an organ with high active leukocyte activity, dropped post-USPIO and remained low over the study period (Figure 1), with no correlation seen between spleen T2* and blood T1 (rho=-0.43, p=0.875). In comparison, T1 recovery in spleen correlated strongly with T1 recovery in blood (rho=0.924, $p < 0.001$) and there was no correlation between T1 and T2* in spleen (r=0.168, p=0.533). In healthy myocardium, which has low active leukocyte activity, T1 and T2* recovery both correlated strongly with T1 recovery in blood (rho=0.953, $p < 0.001$; rho=0.935, $p < 0.001$ respectively).

In MI, absolute T2* values dropped and remained significantly lower in infarcted (15 vs 27ms, $p < 0.001$, 22 vs 38ms, p=0.001) and remote myocardium (21 vs 27ms, p=0.05, 28 vs 38ms, p=0.024) compared to healthy controls. T2* and T1 recovery curves post-USPIO were significantly different in both infarcted (p=0.028) and remote myocardium (p=0.004; Figures 2a and 2b).

Conclusions: T2* is sensitive to active tissue accumulation of USPIO, likely because T2* reflects field gradients, such as those generated by compartmentalised (phagocytosed) USPIO. T1, which is due to short range dipolar interactions that reduce as USPIOs wash-out, simply tracks passive wash-through. T1 is therefore less suitable for detecting active leukocytes. Measuring T2* at a single time point post-USPIO is insufficient to determine tissue accumulation from passive wash-through. USPIO signal from infarct and remote zones in acute MI appears to genuinely reflect active myocardial accumulation, presumably due to phagocytosis by activated leukocytes. These findings are of fundamental importance.

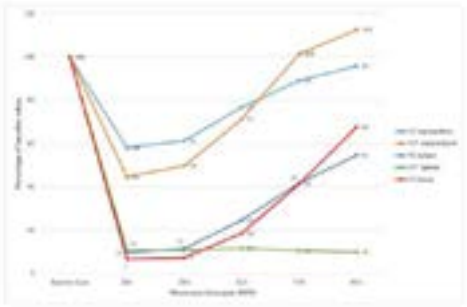

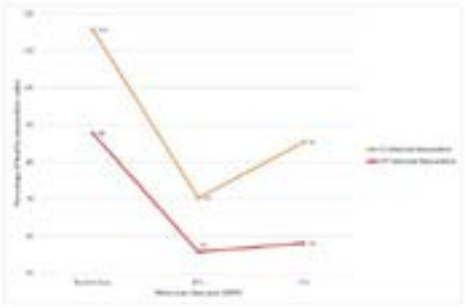

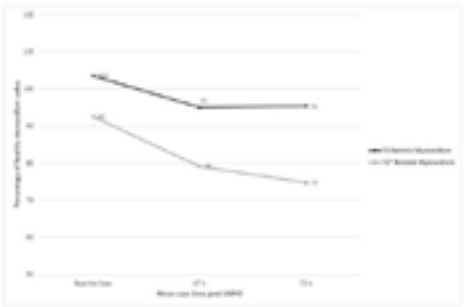

R029

Early Alterations in Myocardial Strain and Native T1 Signal in Patients Receiving Anthracycline, Trastuzumab or Combined Chemotherapeutic Regimens

Alessandro Satriano, Ph.D.[1]Reis Hansen, B.Sc.[2], Joelle Chartrain, B.Sc.[2], Yoko Mikami, MD, Ph.D[1], Nancy Nixon, MD[3], Christina Sheppard, RN MN[4], Andrew Howarth, MD[2], Carmen P. Lydell, MD[2], Bobby Heydari, MD, MPH[2], James McMeekin, MD[3], Douglas A. Stewart, MD[5], Jan-Willem Henning, MBChB, FRCPC[5], Nowell M. Fine, MD M.Sc.[6], Brian Clarke, MD FRCPC FACC[5], James White, MD, FRCP(C) [7]

1. *Stephenson Cardiac Imaging Centre, Libin Cardiovascular Institute of Alberta, University of Calgary, Calgary, AB, Canada*
2. *Stephenson Cardiac Imaging Centre, Libin Cardiovascular Institute of Alberta, University of Calgary, AB, Canada*
3. *University of Calgary, AB, Canada*
4. *South Health Campus, AB, Canada*
5. *University of Calgary, Libin Cardiovascular Institute, AB, Canada*
6. *Libin Cardiovascular Institute, AB, Canada*
7. *Stephenson Cardiovascular Imaging Center, University of Calgary, AB, Canada*

Background: Cancer-therapeutics related cardiac dysfunction (CRTCD) is of growing concern. Early (3-month) alterations in imaging markers across chemotherapeutic regimens remain poorly explored. Both myocardial strain and native T1 can be obtained using a rapid (<15 minute) non-contrast MRI protocol. We report preliminary findings from an ongoing prospective cohort study aimed at assessing its value for the surveillance of cardiotoxicity in patients receiving treatment for Breast cancer or Lymphoma.

Methods: Forty-six patients (35 breast cancer and 11 lymphoma) were enrolled. Cardiac magnetic resonance (CMR) was performed using a 3T scanner (Siemens Prisma or Skyra, Erlangen, Germany) at baseline (pre-exposure), 3 and 6-months following initiation of chemotherapy. A rapid, non-contrast protocol was used inclusive of cine imaging and native T1 mapping using a Shortened Modified Look-Locker Inversion recovery (ShMOLLI) sequence. LV volumes and T1 maps were quantified using commercially available software (cvi[42], Circle Cardiovascular Imaging Inc, Calgary Canada). Three-dimensional strain analysis was performed using a feature-tracking algorithm for the calculation of Global longitudinal strain (GLS) and global longitudinal strain rate (GLSR).

Results: Mean age was 50.8±12.0 years with 5 (11%) male. Chemotherapy was Anthracycline-based (Anth-B) in 18 (39%) (doxorubicin-equivalent dose exposure - DeDE - 228.5±53.2 mg/m^2), Anthracycline-plus-Trastuzumab-based (AnthrTr-B) in 18 (39%) (DeDE 204.0±49.6 mg/m^2) and Trastuzumab alone (Tr-B) in 10 (22%). Baseline LVEF was 63.8±7.1% with mean GLS of -15% and mean T1 of 993±96ms (Figure 1a). At 3-months, significant reductions were seen in GLSR for the AnthTr-B group with non-significant trends in the Anth-B and Tr-B groups. GLS did not change significantly for any group at 3-months. At 6-months, significant reductions were seen for GLSR, GLS, and LVEF in the AnthTr-B group only. Native T1 signal increased significantly for the Anthracycline-containing regimens during the first 6 months. CRTD (defined by drop in LVEF ≥10%) occurred in 13 patients (28%) at 6-months (10 AnthTr-B, 1 Anth-B, 2 Tr-B). This was not predicted by any 3-month marker, inclusive of GLS, GLSR or T1 (Figure 1b). However, absolute LVEF reduction at 6 months was correlated to drop in GLS and GLSR at 3-months (p=0.0032 and p=0.0018, respectively).

Conclusions: CMR identifies changes in GLS, GLSR and native T1 during the first 6 months of exposure to anthracycline-containing regimens. In this preliminary cohort analysis, 3-month changes were not predictive of CRTD at 6 months. However, 3-month GLSR reduction was strongly associated with absolute reduction in LVEF at 6-months. One-year data collection is underway.

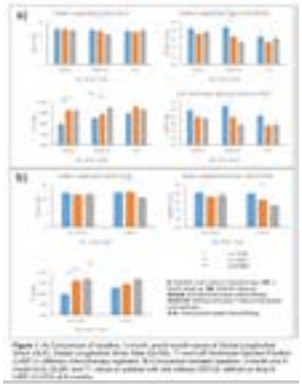

R030

B1+ Mapping of the Heart: Motion-Insensitive Acquisition using Interleaved Bloch-Siegert Shifts

Sebastian Weingärtner, Ph.D.[1]Fabian Zimmer, Ph.D.[2], Gregory J. Metzger, Ph.D.[3], Kâmil Uğurbil, Ph.D.[3], Pierre-Francois Van de Moortele, Ph.D., M.D.[3], Mehmet Akçakaya, Ph.D.[4]

1. *Electrical and Computer Engineering, University of Minnesota; Center for Magnetic Resonance Research, University of Minnesota; Computer Assisted Clinical Medicine, University Medical Center Mannheim, Heidelberg University, Mannheim, Baden-Wurttemberg, Germany*
2. *Computer Assisted Clinical Medicine, University Hospital Mannheim, Heidelberg University, Mannheim, Baden-Wurttemberg, Germany*
3. *Center for Magnetic Resonance Research, University of Minnesota, Minneapolis, MN*
4. *Electrical and Computer Engineering, University of Minnesota; Center for Magnetic Resonance Research, University of Minnesota, Minneapolis, MN*

Background: Quantitative myocardial tissue characterization shows great prognostic and diagnostic value [Salerno et al, JACC2013], but many quantitative techniques, including MOLLI [Messroghli et al, MRM2004] are susceptible to variations in RF transmit field (B_1^+), especially at higher fields. Quantification of B_1^+ field in the heart is challenging due to cardiac and respiratory motions. Saturated double angle method (SDAM) with spiral or EPI readouts during breath-holding is commonly used for cardiac B1+ mapping [Schar et al, MRM2010]. However, acquisition of two separate images with segmented k-space readout causes high sensitivity to motion. In this study, we sought to develop a motion-robust cardiac B_1^+ mapping method using an interleaved Bloch-Siegert (BS) phase shift technique.

Methods: Sequence: B_1^+ maps are acquired by measuring two $|B_1^+|$ dependent BS shifts [Sacolick et al, MRM2010], using off-resonant Fermi pulses (τ_{BS}=8.0 ms, off-resonance shift ω_{BS}=±4.0 kHz, BW of 99% energy=2.1 kHz). Imaging is performed with SPGR readout, and ECG triggering in diastolic quiescence, using a segmented k-space acquisition, with 10 lines/R-R interval for each of the two BS shift images (Figure 1). To minimize motion between these images, positive and negative off-resonance pulses are interleaved for each k-space line.

Imaging: All imaging was performed at 3T. B1+ mapping accuracy of proposed technique was compared to 3D actual flip angle (AFI) method, as gold standard, and to 2D SDAM with EPI readout.

In vivo B1+ mapping was performed in six healthy volunteers using the proposed sequence and SDAM-EPI in short axis (SHAX) and four chamber (4CH) views. Scans were performed twice, during breath-holding and free-breathing. Inter-view consistency was evaluated for each sequence and breathing mode, using an intersection line between views that excludes extracardiac tissue. Consistency was defined as the correlation coefficient between B_1+ profiles along the intersection line in the two views. Statistical significance was assessed for inter-view consistency for a specific breathing mode and sequence, as well as between breathing modes for a given sequence.

Results: Figure 2 depicts measured FA versus nominal FA for each method. Proposed sequence has superior accuracy than SDAM-EPI. Linearity analysis shows excellent correlation for 3D AFI and proposed method, and reduced linearity for SDAM-EPI.

Figure 3a shows in vivo B1+ maps acquired with proposed and SDAM-EPI sequence. Figure 3b depicts results of inter-view consistency analysis, showing superior consistency with the proposed method. No significant difference was found between breath-hold and free breathing for the proposed method.

Conclusions: The proposed interleaved Bloch-Siegert sequence for cardiac B_1^+ mapping shows high resilience to respiratory motion, and robust and consistent B_1^+ map quality at 3T.

Funding: NIH R00HL111410, NIH P41EB015894

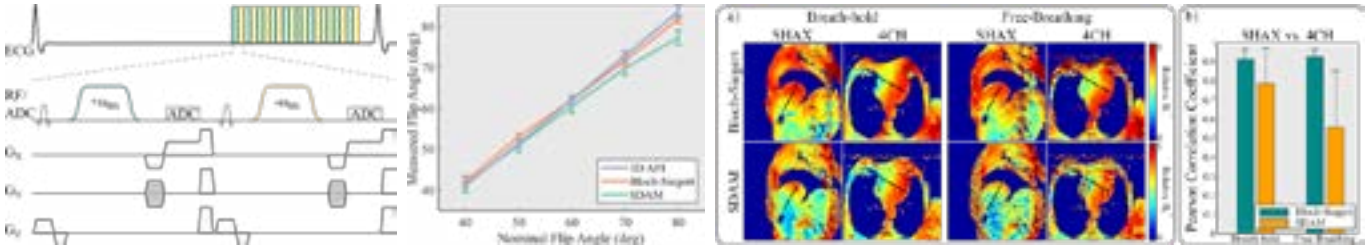

R031

T1 mapping inducible ischemia: pathophysiological insights?

Bashir Alaour, MD, MRCP(UK)[1], Christina Menexi, MBBS [3], Andrew Flett, MBBS, MD (res)[3]Thomas Jackson, MBBS, MRCP(UK)[2], Amanda Murphy[4], Jane Long[3], James Shambrook, BM, FRCR [3], Stephen Harden, MBBS, FRCR [3], Ausami Abbas, MBBS, FRCR [3], Charles Peebles, MBBS, FRCR [3]

1. *University Hospital Southampton, National Health Service UK, Winchester, England, United Kingdom*
2. *University Hospital Southampton, NHS, Southampton, England, United Kingdom*
3. *University Hospital Southampton, England, United Kingdom*
4. *University Hospital Southampton, Southampton, England, United Kingdom*

Background: T1 mapping is a rapidly evolving field and is emerging as a novel quantitative tissue characterisation technique with potential applications in fibrosis, oedema, fat, iron and other patho-physiology. Its significance and value in areas of inducible ischaemia is not yet explored.

Methods: All consenting patients who underwent adenosine perfusion CMR and were found to have a perfusion defect between November 2015 and June 2016 were recruited (n=59). After excluding patients with non-ischaemic wall abnormalities (HCM, DCM and infiltrative disease), patients who had an acute infarct, fixed perfusion defect and those with low suspicion of inducible ischaemia, there were 28 perfusion defects included in the analysis from 25 patients. All patients were scanned on a 1.5T Magnetom Avanto (Siemens Healthcare, Erlangen) using a MOLLI (WIP#448, 5:3:3 acquisition scheme, motion correction and automatically generated T1 map). For the vasodilator stress imaging, a standardized protocol was used with a saturation recovery GRE-EPI sequence. Where a perfusion defect was identified, a slender ROI was drawn on the corresponding pre (native) and post contrast T1 map in the area of maximum ischemia and in the mid wall of the septum (to provide a remote ROI) with meticulous attention to avoid partial volume of blood. If the septum had a perfusion defect, an alternative normal area was selected for control T1 measurement (n=3). ECV was calculated using conventional methods and using the native T1 of blood to estimate the haematocrit. Subjects were grouped by presence of scar in area of perfusion defect (peri-infarct ischaemia) for subgroup analysis. Comparison was performed using ANOVA.

Results: Baseline characteristics are given in table 1. All analyses demonstrated a significant difference between pre-contrast (native) remote T1 and pre-contrast ischaemic T1 (1010±49 vs 1043±69 respectively; p= 0.029), between post contrast T1 remote and post contrast ischaemic T1 (430±38 vs. 399±35 respectively; p < 0.001) and between ECV remote vs ischaemic ECV (0.25 vs. 0.31). In subjects with peri-infarct inducible ischaemia (n=5), there was no difference between pre-contrast (native) remote T1 and pre-contrast ischaemic T1 (1054±24 vs 1076±70 respectively; p=0.346), but the difference remained significant post-contrast (416±77 vs. 370±42; p=0.05). See figure 1.

Conclusions: We have shown that native T1, post contrast T1 and ECV are significantly different in normal vs. ischaemic myocardium. The pathophysiological mechanism and clinical significance of this is yet to be established. One plausible hypothesis is that ischaemia induces diffuse fibrosis.

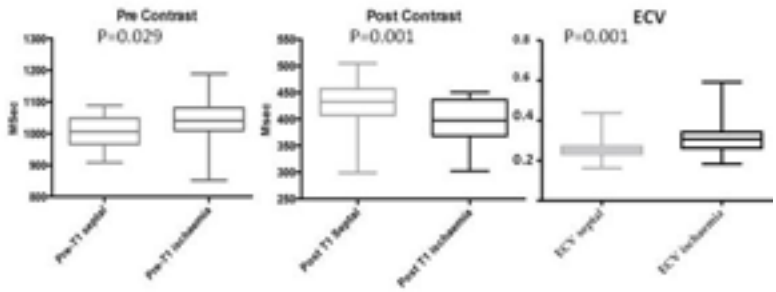

Table 1. Baseline charactarestics

5 (16%)	Female	Genedr
23 (82%)	Male	
Mean (SD)		
67.0 (14.3)	Age	
29.2 (4.7)	BMI	
1.95 (0.24)	BSA	
57.4 (11.2)	EF	
76.0 (17.4)	BSA indexed LV mass (g)	
Median (IQR)		
71 (65, 85)	BSA indexed End Diastlic Volume	

Table 2. Results

All subjects (n=28)			
p-value	Area of inducible ischaemia Mean (SD)	Septum Mean(SD)	
0.029	1043(69)	1010(49)	Pre-contrast T1
<0.001	399(35)	430(38)	Post-contrast T1
0.001	0.31 (0.09)	0.25 (0.04)	ECV
No scar at perfusion defect (n=23)			
p-value	Area of inducible ischaemia Mean (SD)	Septum Mean(SD)	
0.055	1033(66)	1000(48)	Pre-contrast T1
0.001	405(32)	433(25)	Post-contrast T1
0.009	0.3(0.08)	0.25(0.04)	ECV
Scar at perfusion defect(n=5)			
p-value	Area of inducible ischaemia Mean (SD)	Septum Mean(SD)	
0.035	1076(70)	1054(24)	Pre-contrast T1
0.05	370(42)	416(77)	Post-contrast T1
0.18	0.37(0.12)	0.26(0.02)	ECV

R032

Visualization of Acute Edema in the Left Atrial Myocardium after Radiofrequency Ablation: Application of a Novel High-Resolution 3D MRI Sequence (3D-SPACE).

Tarek Zghaib, M.D.[1]Ashkan Malayeri, MD[2], Esra Gucuk Ipek, MD[3], Dong Huang, MD[4], Mohammadali Habibi, MD[5], Muhammad Balouch, MD[6], David Bluemke, MD, PhD[6], Hugh Calkins, MD[6], Saman Nazarian, MD, PhD[7], Stefan L. Zimmerman, MD[8]

1. Johns Hopkins University, Baltimore, MD
2. NIH, MD
3. Johns Hopkins Hospital, MD
4. Johns Hopkins University, MD
5. Montefiore Hospital/Albert Einstein College of Medicine, NY
6. Johns Hopkins Medicine, MD
7. Hospital of the University of Pennsylvania, PA
8. Johns Hopkins University School of Medicine, MD

Background: Reversible ablation induced myocardial edema may result in procedural failure due to the incorrect perception of pulmonary vein exit and entrance block. However, conventional T2 sequences are limited by low spatial resolution and prolonged acquisition time. We sought to evaluate the novel T2-weighted Sampling Perfection with Application optimized Contrasts using different flip angle Evolution (SPACE) sequence for characterization of permanent block with tissue necrosis versus transient block due to edema in the thin myocardium.

Methods: Late Gadolinium Enhancement (LGE) and SPACE cardiac MRI (CMR) were performed before and immediately after an index pulmonary vein (PV) isolation in 8 patients (5 men; mean age 57.5 ± 5 years). Local image intensity ratio (IIR) was defined as signal intensity (SI) for each of 100 myocardial sectors per axial slice divided by the mean SI of the blood pool. Normalized T2 was defined as sector T2 SI divided by para-spinal muscle SI (for SPACE). Ablation points were co-registered with the corresponding image sectors and the change in normalized T2 and IIR signal between pre- and post-ablation scans was measured. The extent of PV encirclement was compared between edema and LGE 3D maps of signal hyperenhancement.

Results: In a mixed effects linear regression model, that accounted for patient clustering of data, both normalized T2 (coefficient= +0.69, p, after adjusting for wall thickness. The extent of encirclement of the right PVs was higher with T2 signal as compared to LGE (Right PVs: 68±19% vs 43±26%, p=0.049; Left PVs: 72±13% vs 51±17%, p=0.12), but the spatial distribution of hyper-enhancement around the PVs appears similar in both modalities (p>0.05 in all quadrants).

Conclusions: The T2 SPACE sequence can be used to map, with near isotropic resolution, the extent of acute edema in the left atrial wall within 24 hours after an ablation procedure.

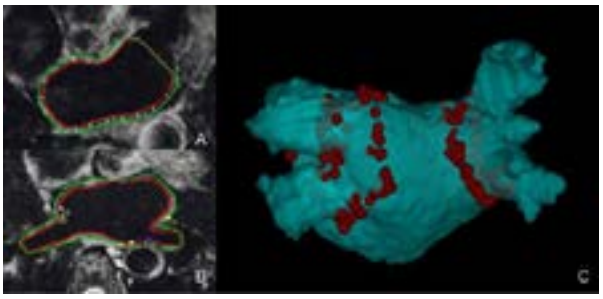

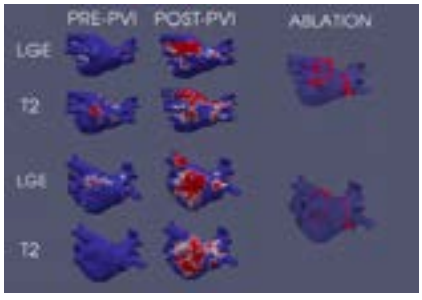

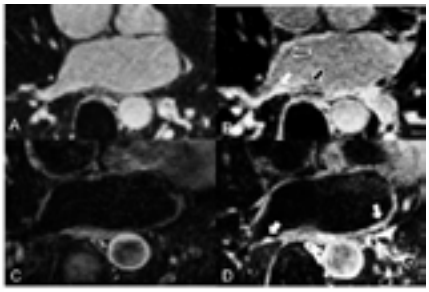

R033

Global myocardial blood perfusion at rest and during various stress protocols in healthy volunteers

Terje H. Larsen, Dr, PhD[1]Kjersti Sellevåg, MD[2], Øyvind Bleie, MD PhD[3], Ståle W Hauge, MD[4], Gottfried Greve, Dr, PhD[1]

1. Department of Heart Disease, Haukeland University Hospital, Bergen, Norway, Bergen, Hordaland, Norway
2. Bergen municipality, Bergen, Hordaland, Norway
3. Dept of Heart Disease, Haukeland University Hospital, Bergen, Norway, Hordaland, Norway
4. Haukeland Universitetssykehus, Hordaland, Norway

Background: Stress-tests are widely used as diagnostic tools to evaluate heart diseases. CMR has the ability of measuring non-invasively total myocardial blood flow by velocity encoded acquisitions of the coronary sinus. Hence, by measuring absolute blood flow in the coronary sinus at rest and during stress, the coronary blood flow reserve capacity is calculated. In young otherwise healthy patients it is a challenge to achieve sufficient stress to establish a maximal coronary flow reserve and cardiac output. To optimize the CMR stress test various techniques were applied.

Methods: The coronary blood flow reserve was measured by 2D velocity PC acquisition directed orthogonally to the blood flow direction of the coronary sinus (CS) close to the entrance into the right atrium. Left ventricular function (cardiac output, CO) was calculated from the area-length product of a 3-chamber view at diastole and systoli. All examinations were performed on a 1.5T scanner (Avanto, Siemens). Ten examinations of healthy volunteers were obtained. Blood velocity acquisitions across the CS were performed sequentially during 1) rest, 2) during adenosine stress (adenosine infusion 140 microg/kg/min), 3) stress by MRI-compatible Lode Supine Ergometer Bicycle, and 4) stress by adenosine combined with Ergometer. For calculation of blood flow commercial software was used (Syngo Via, Siemens).

Results: At rest the the blood flow of CS was 129.9 ml/min (+/- 42.6, SD), 2) adenosine stress 525.7 ml/min (+/-152.9), 3) ergometer stress 346.4 ml/min (+/-133.9), and 4) combined adenosine-ergometer stress 507.1 ml/min (+/-224). All stress tests showed statistically ($p < 00.1$) increase compared to flow at rest. Similarly, CO increased significantly ($p < 00.1$) in all stress tests: (2) 8398.7 ml/min (+/-2937.7), 3) 11306.8 ml/min (+/-4104.2), and 4) 11145.3 ml/min (+/-3877.0) compared to rest 4919.9 ml/min (+/- 1512.8).

A ratio of SC blood flow versus CO was calculated for the various tests, and signifcant ($p>0.05$) changes were shown only for the adenosine test and the combined adensosine-ergometer test compared to the controls.

A ratio of CO versus heart rate showed a significant ($p < 0.05$) increase for adenosine stress compared to rest whereas it was non-significant for the two ergometer tests. Finally, a ratio of SC blood flow and heart rate showed significant increase (p.0.05) for adenosine and combined adenosine-ergometer tests compared with rest, whereas it was non-signifcant for the ergometer stress test.

Conclusions: A combined stress test with adenosine infusion and supine ergometer bicycling is in our data producing both maximum coronary flow reserve and cardiac output. This combination may produce a natural distribution of blood to the heart itself related to the rise in cardiac output. However, these tests were performed on healthy volunteers, and should be repeated for patient groups. Also, the physiological and pathological significance of CS flow versus CO and HR, should be more closely evaluated.

R034

Diagnostic performance of T1-mapping, T2-mapping and bright blood oedema imaging (ACUT2E) in an unselected population of patients with acute STEMI: The British Heart Foundation MR-MI study.

Aidan Morgan, BSc (Med Sci) Hons[1]Colin Berry, PhD FRCP[2], David Carrick, PhD[3], Caroline E Haig, PhD[4], Kenneth Mangion, MD[2], Mark Petrie, MD[5], Margaret McEntegart, MBChB PhD[3], Mitchell Lindsay, MD[6], Keith G. Oldroyd, MD (Hons); FRCP[6], Andrew Davie, MB ChB[6], Stuart Hood, MD FRCP[7], Stuart Watkins, MD, FRCP[3]

1. *University of Glasgow, Aberdeen, Scotland, United Kingdom*
2. *University of Glasgow, Glasgow, Scotland, United Kingdom*
3. *Golden Jubilee National Hospital, Glasgow, Scotland, United Kingdom*
4. *Robertson Centre for Biostatistics, Glasgow, Scotland, United Kingdom*
5. *Glasgow University, Scotland, United Kingdom*
6. *Golden Jubilee National Hospital, Scotland, United Kingdom*
7. *NHS Greater Glasgow and Clyde, Scotland, United Kingdom*

Background: Quantitative parametric mapping of myocardial T1 and T2 relaxation times have emerged as new options to assess the initial extent of oedema after acute ST-segment elevation myocardial infarction (STEMI). Limited information is available on the diagnostic performance of these methods compared with alternative methods such as ACUT2E bright blood oedema imaging.

Methods: 300 patients were enrolled following primary percutaneous coronary intervention (PCI). MRI at 1.5T (Siemens MAGNETOM Avanto) was performed 2 days and 6 months later. LV mass, function and infarct size were assessed using cine-SSFP and late gadolinium enhancement imaging, respectively. The protocol involved pre-contrast native T1 mapping using a Look-locker inversion recovery (MOLLI) prototype sequence, T2 mapping using a prototype T2 prepared (TrueFisp sequence) with motion correction and ACUT2E. Since full volumetric coverage for all modalities is not feasible routinely, in order to limit the scan duration, imaging was limited to 3 slice positions (base, mid and apical). Epicardial and endocardial borders were manually planimetered and a signal intensive threshold of x2SD (remote zone vs. Infarct zone) was used to delineate the extent of the hyper-intense affected area (%LV mass). The angiographic area-at-risk was assessed independently using the APPROACH Lesion Score. The extent of myocardial injury depicted by each modality was assessed independently against LVEF and LVEDV. Summary statistics and Pearson correlation were assessed using SPSS and a $p < 0.05$ was taken as statistically significant.

Results: 272 patients had complete data with all 3 methods, practical limitation prevented all patients from recieving each scan. The rate of non-diagnostic images limited by artefact occurred for T1-mapping, T2-mapping and ACUT2E was 4 (1.5%) of 291, 0% of 300 and 34 (12.7%) of 272 patients, respectively. 291 patients had paired T1 and ACUT2E scans. The extent of oedema revealed by T1-mapping (34.0±14.7%) and T2-mapping (34.0±14.3%) was similar (p=0.98; R=0.94). 272 patients had paired data with T1 maps and ACUT2E bright blood scans. The extent of edema disclosed by ACUT2E (33.7±12.7%) was smaller than with T1 mapping (p=0.02), and the correlation coefficient was also lower (R=0.89). Considering LVEDV at 6 months, univariable associations were observed between the initial extent of oedema revealed by T1 mapping (0.43, 95% CI (0.24, 0.62), p2=0.64), T2 mapping (0.48, 95% CI(0.28, 0.674), p2=0.65) and ACUT2E (0.41, 95% CI(0.18, 0.64), p2=0.68).

Conclusions: T2 mapping with motion correction was not associated with imaging artefacts and in this sense had superior diagnostic performance compared to T1-mapping (without motion correction) and ACUT2E. The extent of oedema revealed by T1-mapping and T2-mapping was similar, implying comparable diagnostic validity, whereas ACUT2E may under-estimate the extent of oedema.

R035

Free breathing motion-corrected single shot phase sensitive inversion recovery sequence in the detection of late gadolinium enhancement in heart failure patients with atrial fibrillation

Jing Wang, doctor[1], Xiangchuang Kong, doctor[2]Xiangquan Kong, doctor[3], Tianjing Zhang, PHD[4]

1. *Deparment of Radiology,Union Hospital,Tongji Medical College,Huazhong University of Science and Technology, Wuhan, Hubei, China (People's Republic)*
2. *Deparment of Radiology,Union Hospital,Tongji Medical College,Huazhong University of Science and Technology, Hubei, China (People's Republic)*
3. *Deparment of Radiology,Union Hospital,Tongji Medical College,Huazhong University of Science and Technology, Hebei, China (People's Republic)*
4. *Siemens Shenzhen Magnetic Resonance Ltd, Beijing, China (People's Republic)*

Background: Atrial fibrillation and congestive heart failure are morbid conditions that share common risk factors and frequently coexist. Atrial fibrillation in Heart failure appears to independently predict death resulting from pump failure and total mortality. Myocardial fibrosis is a fundamental process in pathologic remodeling and is postulated to cause increased cardiac stiffness and poor clinical outcomes. Delayed contrast enhanced CMR (DE-CMR) can be used for non-invasive tissue characterization and may provide a metric of overall disease progression. Many HF patients are unable to perform adequate breath-holding and with arrhythmia which result in poor image quality. Free breathing motion-corrected single shot phase sensitive inversion recovery sequence has been shown to be equal or superior in detecting myocardial fibrosis in vulnerable patients. Moco-LGE sequence may have advantages over conventional breath-held LGE(Bh-LGE) for heart failure patients with arrhythmia or respiratory motions for detection of both ischemic and non-ischemic patterns of delayed enhancement.

Methods: In a consecutive cohort of 46 heart failure patients were referred for late enhancement cardiac MRI, who underwent cardiac MRI on a 1.5T system (Magnetom Aera, Siemens) were imaged with Bh-LGE and FB Moco-LGE. Images were graded by experienced cardiovascular physician for image quality (scale of 1 to 5), diagnostic confidence (scale of 1 to 3) and the localization of LGE (AHA 17-segmented model)

Results: 14 of 46 heart failure patients demonstrated chronic myocardial infarction.12 of 46 heart failure patients showed non-ischemic delayed enhancement (DE), including 8 cases of dilated cardiomyopathy, 3 cases of valvular heart disease and one case of left ventricle non-compaction. FB Moco-LGE and Bh-LGE have high consistency in the detection of DE. The total numbers of involved segments were 59 and 55. Image qualities (4.48±0.6 vs 3.69±0.3 $P<0.05$) and diagnostic confidence (2.85±0.5 vs 2.17±0.8 $P<0.05$) was higher for FB Moco-LGE than Bh-LGE.

Conclusions: FB Moco-LGE and Bh-LGE have high consistency in the detection both of ischemic and non-ischemic delayed enhancement in heart failure patients with AF. More DE segments were identified on FB Moco-LGE then Bh-LGE. Image quality and diagnostic confidence was higher for FB MOCO LGE than BH LGE, and could replace them in clinical application.

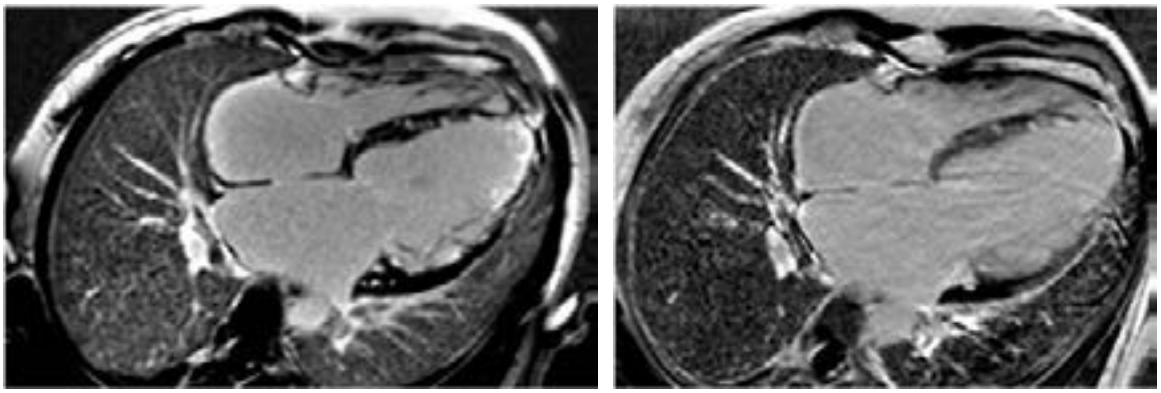

R036

Have we reached Status Quo with Contemporary Pacemaker/ICD in the MRI Environment; a Focused MRI Variability Study

Loretta Gevenosky, R.N.[1]Huma Samar, MD[2], Mark Doyle, PhD[3], Ronald Williams, RT(R)(MR), B.A.[1], Moneal Shah, M.D.[1], Christopher Bonnet, MD[1], Shimaa S. Khidr, MD[1]

1. *Allegheny General Hospital, Pittsburgh, PA*
2. *Loma Linda University Medical Center, Pittsburgh, PA*
3. *Allegheny General Hospital, PA*

Background: There is considerable interest in more clinically routine use of pacemakers/ICD via MRI. However, several limitations to widespread adoption of this concept remain, including the unresolved impact of high magnetic field, RF amplitude and oscillatory forces on sensitive device microcircuitry.

Given recent vender refinements, improved shielding/RF filters/chokes and leads over the last 10 years, we hypothesize that the impact of MRI may be within clinically acceptable limits yet residual issues surrounding sensitive interrogation parameters exist.

Methods: Device interrogation was performed on 94 consecutive patients who underwent clinically indicated MRI in the last 12 months. The cohort comprised of neurology/neurosurgical (64%), orthopedic (9%) and cardiac (26%) cases. Routine device interrogation was performed 10 minutes prior to entry into the bore of a Cardiac MRI scanner (GE,1.5T, Excite, Milwaukee, WI). Following MRI examination, re-interrogation was performed (10 min post MRI). At both pre and post interrogation, an exact but repeat interrogation was performed within 5 minutes such that 2 sets of PM/ICD parameters were obtained pre and post MRI scan(4 total).

Results: No complications to either patient or device occurred during MRI scan. A cardiologist was present and guided interrogation, configuration, and reconfiguration of PM/ICD's as well supervised the entire scan. Altogether, (61%) PM's and (39%) ICD's were studied. Via repeat pre-MRI, repeat post-post or pre-post parameters comparisonsvia ANOVA, there were no significant differences in impedance, amplitude or thresholds at any time period, see Table. Likewise, there was no difference as related to thoracic vs non-thoracic MRI's or PM vs ICD's metrics. Overall, the PM's and ICD's, all after circa 2004, were inert in the MRI field independent of sequence, body part or random chance.

Conclusions: In our experience, intrinsic variability and inherent changes triggered by the MRI environment are statistically and clinically negligible for pacemaker/ICD's when conventional precautions were taken, again, incrementally advancing yet another safety aspect. This allows us to move another step closer towards a more uniform acceptance of this technology for clinically meaningful use and acceptance in the MRI environment.

		Pre	Post	p (Pre-Post)
Atria	Impedance	443±96	439±101	0.23
	Sensing	2.87±1.48	3.41±2.74	0.14
	Threshold (Amplitude)	0.88±0.68	0.9±0.7	0.59
	Threshold (Pulse Width)	0.46±0.13	0.43±0.05	0.32
RV	Impedance	496±118	485±116	0.09
	Sensing	9.42±3.52	20.39±80.56	0.16
	Threshold (Amplitude)	0.83±0.29	0.82±0.3	0.5
	Threshold (Pulse Width)	0.53±0.24	0.52±0.22	0.46
LV	Impedance	637±200	651±208	0.09
	Threshold (Amplitude)	0.96±0.47	0.92±0.43	0.73
	Threshold (Pulse Width)	0.73±0.25	0.62±0.24	0.65

		Pre	Post	p (Pre-Post)
Atria	Impedance	443±96	439±101	0.23
	Sensing	2.87±1.48	3.41±2.74	0.14
	Threshold (Amplitude)	0.88±0.68	0.9±0.7	0.59
	Threshold (Pulse Width)	0.46±0.13	0.43±0.05	0.32
RV	Impedance	496±118	485±116	0.09
	Sensing	9.42±3.52	20.39±80.56	0.16
	Threshold (Amplitude)	0.83±0.29	0.82±0.3	0.5
	Threshold (Pulse Width)	0.53±0.24	0.52±0.22	0.46
LV	Impedance	637±200	651±208	0.09
	Threshold (Amplitude)	0.96±0.47	0.92±0.43	0.73
	Threshold (Pulse Width)	0.73±0.25	0.62±0.24	0.65

R037

Ferumoxytol MRI Across the Age Spectrum: Acute and Short-term Single Center Safety Experience

Kim-Lien Nguyen, M.D.[1]Takegawa Yoshida, M.D.[2], Fei Han, Ph.D.[3], Ihab Ayad, M.D.[4], Gary Satou, M.D.[5], Brian Reemtsen, M.D.[6], Peng Hu, Ph.D.[7], J. Paul Finn, M.D.[2]

1. *Division of Cardiology, David Geffen School of Medicine at UCLA and VA Greater Los Angeles Healthcare System, CA*
2. *Department of Radiology, David Geffen School of Medicine at UCLA, CA*
3. *UCLA, LOS ANGELES, CA*
4. *Department of Anesthesiology, David Geffen School of Medicine at UCLA, CA*
5. *Division of Pediatric Cardiology, David Geffen School of Medicine at UCLA, CA*
6. *Department of Cardiothoracic Surgery, David Geffen School of Medicine at UCLA, CA*
7. *UCLA, CA*

Background: As a theranostic agent, ferumoxytol is FDA-approved for the treatment of anemia secondary to chronic renal disease. However, its unique physiochemical properties and pharmacokinetics can be leveraged for use as a contrast agent in magnetic resonance imaging (MRI), particularly for those with severe renal impairment where gadolinium administration may not be suitable. We aim to summarize our single-center safety experience with the off label use of ferumoxytol for MRI and to compare the effects of ferumoxytol on monitored physiologic indices in patients under anesthesia with those of gadofosveset trisodium.

Methods: Consecutive patients who underwent ferumoxytol-enhanced (FE) MRI exams between 2013 and 2016 were included. Both acute and short-term safety was assessed. Adverse events (AEs) were classified according to the Common Terminology Criteria for Adverse Events v4.0. In a subgroup of patients examined under general anesthesia, recording of blood pressure, heart rate, oxygen saturation and end-tidal CO_2 was performed. For comparison, a comparable group of patients who underwent gadofosveset-enhanced (GE) MRI under anesthesia with similar monitoring was also analyzed.

Results: Two hundred and sitxty-three unique patients (156 adults and 107 children; 291 injections), ages 2 days to 94 years, underwent FE-MRI. No ferumoxytol-related severe, life threatening, or fatal AEs occurred acutely or at short-term follow-up (17.1±9.9 months). Two patients developed ferumoxytol-related nausea, which was classified as a mild AE. In both the ferumoxytol and gadofosveset groups who had anesthesia, no AEs occurred. Between group (FE-MRI vs GE-MRI, Figure 1A) and within group (FE-MRI, Figure 1B) variations of physiologic indices were not statistically different ($p>0.05$). No significant change in blood pressure or heart rate ($p>0.05$) was noted between slow infusion of ferumoxytol (n=113) vs bolus injection (n=145) ($p>0.05$). Twenty-eight patients had at least 2 repeated exams. Five patients had three or more FE-MRI exams.

Conclusions: In our single center experience encompassing 263 unique patients (291 injections) over a period of 3 years, no serious acute or short-term AEs occurred with the diagnostic use of ferumoxytol. Because of the modest population in our single center study, firm conclusions cannot be drawn about the generalizability of our results and thus vigilance and monitoring are recommended to mitigate potential rare adverse reactions.

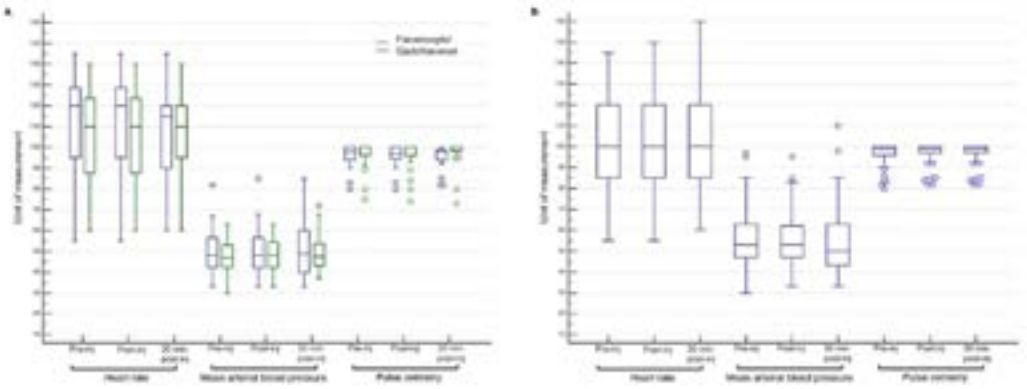

R038

Pacemaker Lead-tip Heating During MRI Exams Depends on Patient Orientation

Jessica A. Martinez Martinez[1] Daniel B. Ennis, PhD[2]

1. University of California, Los Angeles, Los Angeles, CA
2. Department of Radiological Sciences, University of California, Los Angeles, CA, USA., CA

Background: During an MRI exam the induced radiofrequency (RF) electric field can generate a current in the lead of an implanted pacemaker or implantable cardioverter defibrillator (ICD). This can result in tissue heating at the lead-tip due to impedance differences at the tissue interface, which may damage the myocardium or inhibit pacing. Several electromagnetic simulations of the ASTM torso phantom have demonstrated that the induced RF electric field distribution is spatially inhomogeneous {Nordbeck P, et al. MRM 2008}. This electric field asymmetry is greater at the edges of the phantom and the strongest electric field is observed in left-anterior and right-posterior regions when the midpoint of the phantom is positioned at isocenter. This suggests that changing the patient orientation (head-first vs. feet-first) may change lead-tip heating (LTH). Our objective was to evaluate LTH differences in a tissue mimicking ASTM phantom for head-first and a feet-first orientations and to evaluate the impact of placing the device at different anterior-posterior depths.

Methods: A pacemaker connected to a 40 cm lead was paced in an ASTM torso phantom filled with polyacrylic acid with an electrical conductivity of 0.48 S/m. Temperature data at the lead-tip was collected using a fiber optic temperature probe. Two reference readings were obtained from temperature probes positioned 3cm medial to the lead-tip and on the contralateral side. A turbo spin echo sequence (TE/TR = 6.2/110 ms, Flip Angle = 180°) applied 4W/kg for 5 minutes at 1.5T (Siemens Avanto Fit). Temperature increases at the lead-tip (ΔT) were recorded for five different landmarks (LM). LM1 was the middle of the head and LM2 to LM5 were at 18 cm intervals with the lead-tip lying at LM3. Lead-tip heating measurements were acquired for both head-first (HF) and feet-first (FF) orientations and for three anterior-posterior (A-P) depths: posterior at 0 cm(P), middle at 3 cm (M) and anterior at 9 cm (A) (Fig. 1).

Results: ΔT varied with LM, HF vs. FF, and A-P position (Fig. 2). For the anterior depth (Fig. 2-A), the FF approach resulted in a ΔT that was 17x and 2x less than the HF approach at LM2 and LM3 respectively. For the middle depth (Fig. 2-B), ΔT at LM1, LM2 and LM4 was reduced by 1.5x in the FF approach while LM3 was reduced by 2.7x. At the posterior depth (Fig. 2-C), ΔT was smaller in the HF approach for LM1- to LM3, but larger for LM4 and LM5.

Conclusions: Clinically, the patient's orientation within the scanner is determined by the body part under examination. Conventionally, patients with pacemakers are scanned in the same orientation as those without pacemakers. The results presented here, however, suggest that LTH depends on the position of the device within the bore. This suggests that special consideration should be given to patients with pacemakers in order to minimize LTH.

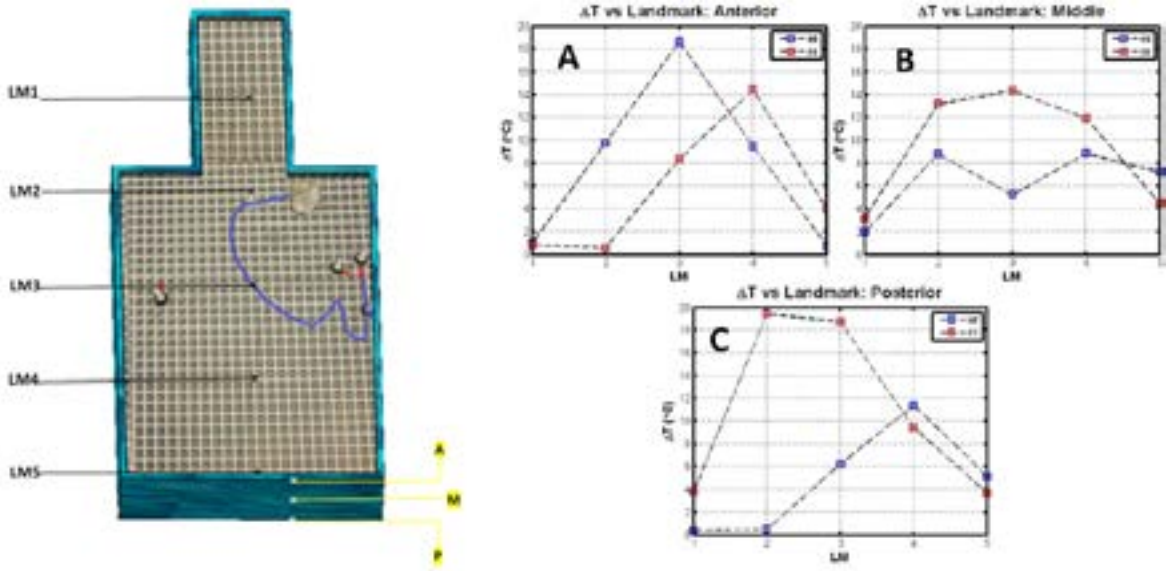

R039

Cardiac Magnetic Resonance Imaging to Diagnose Orthotopic Heart Transplant Rejection

Diego Medvedofsky, MD[1]David M. Tehrani, MD[2], Keigo Kawaji, Ph.D.[3], Victor Mor-Avi, PhD[2], Roberto M. Lang, MD[2], Nir Uriel, MD[2], Amit R. Patel, MD[2]

1. *University of chicago, IL*
2. *University of Chicago, IL*
3. *University of Chicago, Chicago, IL*

Background: The detection of orthotopic heart transplant (OHT) rejection is challenging and the diagnosis often requires endomyocardial biopsy (EMB), which is associated with several complicit risks. There is a need for a non-invasive test that can accurately identify patients most in need of an EMB. Tissue characterization using cardiac magnetic resonance (CMR) has the potential to diagnose early steps of inflammation, edema, and fibrosis, and has been proposed as a gate-keeper for EMB. The goals of this study are to describe the variations in advanced tissue characterization by CMR in a OHT population without evidence of rejection based on EMB.

Methods: We analyzed 27 CMR studies of 17 OHT patients (88% males, age 58.5±11.1) who underwent CMR (1.5T, Achieva, Philips) and had a EBM negative for heart transplant rejection. The CMR protocol included cine-CMR, pre- and post-contrast TI-mapping (modified Look Locker Imaging (MOLLI)) and T1-weighted imaging (DIR prepared T1W Black Blood TFE), T2-weighted imaging (Short Tau Inversion Recovery (T2-STIR), and late gadolinium enhancement ((LGE), phase sensitive inversion recovery (PSIR)). Images were typically acquired in the 2-, 3-, and 4-chamber views and in short axis plane of left ventricle (LV). The following CMR parameters were measured using commercially available software: left and right ventricular (LV, RV) volumes, LV mass, the presence, location and pattern of late gadolinium enhancement (LGE), native and post-contrast myocardial T1-relaxation times, T1 (before and after gadolinium) and T2-weighted signal intensity of the mid-septal myocardial and skeletal muscles. LV and RV ejection fraction (EF), LGE burden, extra-cellular volume (ECV) fraction, global relative enhancement (GRE) and T2-STIR ratio were calculated. EBM results were compared to CMR findings.

Results: Patient characteristics and the median including the 10th, 25th, 75th, and 90th percentiles of each variable are reported in Table 1. The LV was dilated in 11%; 22% had a reduced LVEF, 4% had a dilated RV, 26% had a reduced RVEF, and 30% had LGE. In all cases, the LGE involved the basal lateral, inferolateral, inferior, or inferoseptum walls, and 50% had only one segment involved. The LGE was.non-transmural in 88% and transmural in 12%. Native myocardial T1-relaxation time was normal (≤1050ms) in 20% of the studies, borderline (1050-1100ms) in 10% and increased (≥1100ms) in 70%. The ECV was increased (≥22%) in 22% of the studies. GRE was increased (≥4) in 7% of the studies, T2-STIR ratio was increased (≥2) in 22% of the studies.

Conclusions: Our study shows that a significant proportion of OHT pateints without evidence of acute rejection have abnormalities in various CMR-based tissue characteristic markers. The mechanisms and significance of these abnormalities need to be better understood prior to the routine use of CMR as a gate-keeper for EBM. Further studies are also required to establish the clinical utility and normal ranges of these CMR measurements in OHT patients.

N=27	LVEDVi	LVEF	RVEDVi	RVEF	T2 ratio	GRE	Native Myocardial T1-relaxation time		ECV
	(ml)	(%)	(ml)	(%)	(%)	(%)	(ms)	% of total	(%)
Range criteria	>89	<53	>98	<50	≥2	≥4	<1050	20%	≥30
							1050-1100	10%	
							>1100	70%	
Meet criteria	11%	22%	4%	26%	30%	14%			22%
Median	70	56	67	53	1.7	2.9	1103		27.1
SD	16	9	15	7	0.2	1.6	165		7.9
10% percentile	52	49	52	46	1.4	1.3	966		14.9
25% percentile	61	54	56	50	1.6	1.9	1073		25.5
75% percentile	76	61	73	57	1.9	3.6	1189		32.2
90% percentile	83	65	87	61	2.1	4.3	1244		34.9

R040

Diagnostic Yield of Cardiac MRI for Patients with Ventricular Tachycardia or Premature Ventricular Complexes with Preserved Left Ventricular Function

Ross Roberts-Thomson, MBBS, BMedSci(Hons)[1]Michael B. Stokes, MBBS FRACP[2], Karen S. Teo, MBBS, PhD[3], Adam Nelson, BMedSc MBBS[4], Kurt Roberts-Thomson, MBBS, PhD[5]

1. *Royal Adelaide Hospital, Urrbrae, South Australia, Australia*
2. *Royal Adelaide Hospital, Wayville, South Australia, Australia*
3. *Royal Adelaide Hospital, Adelaide, South Australia, Australia*
4. *Royal Adelaide Hospital, South Australia, Australia*
5. *University of Adelaide, Adelaide, South Australia, Australia*

Background: The prognosis of patients with ventricular arrhythmias is dependent on the underlying substrate. Patients with normal left ventricular (LV) function are thought to be low risk. Cardiac MRI (CMR) can provide a detailed evaluation for the underlying substrate in patients with arrhythmias. The yield in patients with normal LV function remains unknown.

Methods: 100 consecutive patients with normal LV ejection fraction referred for CMR to evaluate ventricular tachycardia (VT) or premature ventricular complexes (PVCs) (48 VT; 52 PVCs) were enrolled in the study. Patients with non-sustained VT were considered part of the PVC group.

Results: Average patient age (VT 57±21 years; PVC 51±15 years; *p=0.26)* and LV ejection fraction on echocardiography (VT 61±7% vs PVC 60±7%; *p=0.5)* were similar between the two groups. For patients with VT, CMR with gadolinium enhancement identified a previously unrecognized substrate more often than in patients with PVCs (38% (18) vs 2% (1); *p=0.001*). In patients without coronary artery disease, VT continued to have a much greater diagnostic yield (27% vs 0%; *p=0.001*). The underlying VT substrates were: five ischemic scar; three cardiac sarcoidosis; three myocarditis; one ARVC; and six non-ischemic non-specific focal fibrosis. The one patient referred for investigation of PVCs who had gadolinium enhancement was found to have ischemic scar.

Conclusions: CMR is a more useful diagnostic tool for patients presenting with VT compared with PVCs, both with and without coronary artery disease. CMR should be considered part of the diagnostic evaluation for all patients presenting with VT and normal LV function.

T001

Pouch in the heart

Yiying HanYi-Hui Hung, BSc

National Heart Centre Singapore, N/A, Singapore

Background: 70 year-old lady with no significant medical history of note presented with an incidental cardiac murmur. Physical examination revealed a soft, grade 3/6 ejection systolic murmur at the left upper sternal edge. A transthoracic echocardiogram showed aortic sclerosis and a small left ventricular (LV) out-pouching arising from the anterolateral LV apex, best seen on contrast-enhanced echocardiography. It has a wide neck, measuring 1cm in diameter and appears dyskinetic. Electrocardiogram showed normal sinus rhythm, no evidence of prior myocardial infarction. A cardiac MRI was ordered.

Methods: -

Results: There is a LV diverticulum, measuring 2.1 x 0.9 cm in size at the LV apex. It has a thin muscular wall and contracts synchronously with the rest of the LV, which distinguishes it from LV aneurysm. The left ventricular systolic function is normal, LV ejection fraction 70%. Early Gadolinium showed no thrombus within the LV cavity and the diverticulum. Late Gadolinium sequences showed no fibrosis or infarction.

Conclusions: Congenital left ventricular diverticulum is a rare cardiac malformation. It can come in the form of fibrous or muscular aneurysm. Usually, fibrous diverticulum is found in children, while muscular diverticulum is found in adults. Muscular diverticulum is generally more common than fibrous diverticulum and has a more benign disease course. Complications such as rupture, arrhythmias and systemic embolism are rare in muscular diverticulum. As the name implies, muscular diverticulum comprises of muscular tissue on the diverticular wall and contracts synchronously with LV, i.e. volume reduction during systole and expands during diastole.

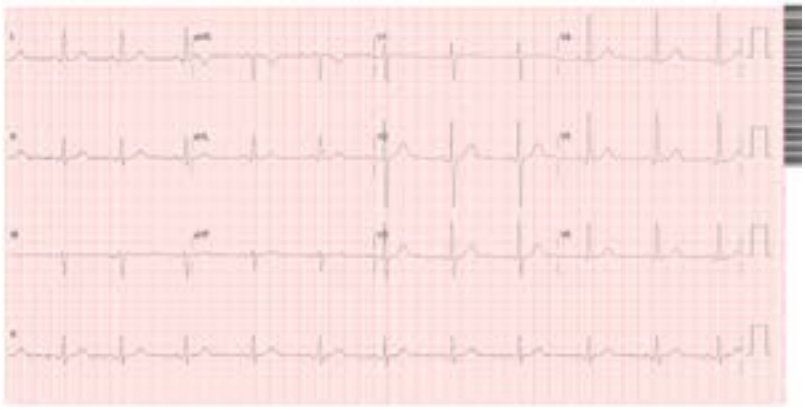

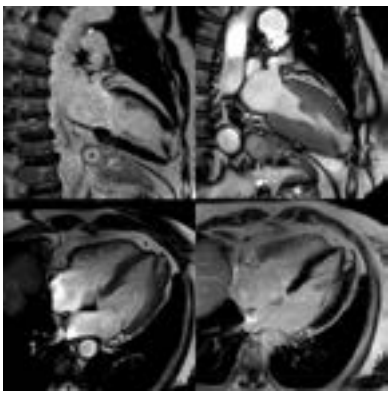

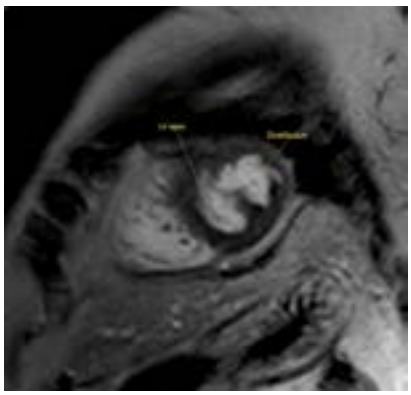

T002

CMR unravels the pathophysiology of heart block in a young woman

Petronella Samuels, B.TECH , NAT DIP RADIOGRAPHY (DIAG)[1] Ashley Chin, MBChB MMed[2], Mpiko Ntsekhe, MD PhD[2], Ntobeko A. B. Ntusi, MD DPhil[2]

1. *UNIVERSITY OF CAPE TOWN, Cape Town, Western Cape, South Africa*
2. *University of Cape Town and Groote Schuur Hospital, Cape Town, Western Cape, South Africa*

Background: Rheumatic heart disease (RHD) remains an important cause of heart failure in sub-Saharan Africa, contributing to significant morbidity and mortality, often affecting young economically active members of society. Due to improved sanitation and public health measures, acute rheumatic fever (ARF) is uncommon in adults and may be associated with PR prolongation on electrocardiography (ECG). We report on an unusual case of ARF in a 34 year old woman, complicated by PR prolongation, an atypical Mobitz 1 atrioventricular block, and evidence of myocarditis and valvulitis on cardiovascular magnetic resonance (CMR).

Methods: CMR was used to investigate the cause of conduction abnormality, including cine, cine tagging, T2-weighted (STIR), precontrast T1 and T2 mapping and late gadolinium enhancement (LGE) imaging.

Results: LV volumes, mass and global biventricular function were normal. However, peak circumferential systolic strain and diastolic strain rates were impaired. The myocardial signal intensity ratio on T2-weighted imaging was increased (2.1). On parametric mapping, evidence of myocardial oedema was supported by elevated T1 (1148 ms) and T2 (56 ms) values. On LGE imaging, there was striking enhancement of mitral and aortic valves suggestive of a valvulitis, but no myocardial enhancement. The diagnosis of acute rheumatic fever was further supported by elevated anti-streptolysin O titre levels (172 mmol/L) and elevated serum anti-DNAse B levels (370 mmol/L).

Conclusions: A multiparametric CMR assessment in a patient with inflammatory heart disease reliably permits the diagnosis of acute rhematic fever. CMR tissue characterisation is important for assessment of disease acuity in inflammatory heart disease.

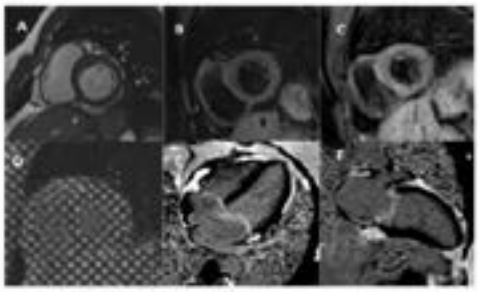

T003

Cocaine-related chest pain; presentations can be deceptive.

Fiona L. Hamilton, PgC Medical Magnetic Resonance, BSc (Hons) Radiography[1] Charlotte Manisty, PhD MBBS[2]

1. Barts Heart Centre, London, England, United Kingdom
2. Barts Heart Centre and university college, London, England, United Kingdom

Background: A 28-year-old male presented to the emergency department with acute chest pain on a background history of cocaine use and smoking. His electrocardiogram showed diffuse ST segment elevation and his troponin was elevated at 4500ng/L. Handheld transthoracic echocardiography showed preserved LV function with no regional wall abnormalities. A coronary angiogram was performed, which showed unobstructed coronary arteries and a presumptive diagnosis was made of cocaine-induced coronary spasm. A cardiovascular magnetic resonance (CMR) scan was requested to assess for evidence of myocardial infarction and to rule out other cardiovascular pathology.

Methods: CMR imaging was performed on a 1.5T Siemens Avanto scanner. The CMR protocol performed included steady-state free precession (SSFP) cines, T2-weighted short tau inversion recovery (STIR) images, native T1 shortened modified look-locker inversion recovery (ShMOLLI), T2 mapping and early and late gadolinium enhanced images.

Results: The CMR scan showed mildly reduced systolic function (LVEF 56%), with hypokinesis and mildly thickened mid and apical LV segments. The T2-weighted STIR images showed high signal in the lateral and mid-inferior wall as well as the apical segments. The native T1 myocardial values were grossly elevated, most notably in the lateral wall – between 1200 and 1400 (normal ShMOLLI 960 +/- 60ms). The T2 values were also elevated in the corresponding segments. There was extensive patchy mid wall late gadolinium enhancement (LGE) segments corresponding to those with abnormal T1 and T2 values. These findings fulfilled the Lake Louise Criteria for diagnosis of acute myocarditis. The patient was discharged, asked to refrain from exercise and started on bisoprolol and ramipril therapy. Follow-up CMR was performed 2 months later which demonstrated normalisation of LV systolic function (LVEF 60%) and a significant reduction in T1 and T2 values, however the late gadolinium enhancement pattern was largely unchanged.

Conclusions: Although cocaine use is commonly associated with coronary spasm, CMR imaging is useful in patients with chest pain, elevated troponin levels and normal coronary arteries on angiography to rule out other pathology. Myocarditis can be difficult to diagnose, but CMR can confirm the diagnosis of myocarditis and quantify the extent and severity of myocardial oedema. This avoids the need for invasive endocardial biopsy. An accurate assessment of LV function can also be made. In the convalescent phase, resolution of myocardial oedema as measured by T1 and T2 mapping techniques can be used to track improvement. The patient received the appropriate treatment and he made a good recovery.

http://www.ConferenceAbstracts.com/uploads/cfp2/attachments/LDFAIBDN/LDFAIBDN--222316-2-ANY.pptx

T004

Hypertension vs Hypertrophic cardiomyopathy: How to distinguish the two by Cardiac MRI

Rick Wage, DCR (R)[1]Brian Halliday, BSc (Hons) MBChB (Hons)[2], Sanjay Prasad, MD[3]

1. NIHR Cardiovascular Biomedical Research Unit, Royal Brompton Hospital, England, United Kingdom
2. Royal Brompton Hospital and National Heart and Lung Institute, Imperial College London, London, England, United Kingdom
3. Royal Brompton Hospital and Imperial College, London, England, United Kingdom

Background: In patients presenting with left ventricular hypertrophy (LVH), establishing the underlying aetiology is important in guiding management. Whilst hypertensive heart disease is the most common cause in older patients, in younger patients, hypertrophy is frequently secondary to hypertrophic cardiomyopathy (HCM). There is however an important subset of patients that fall into a 'grey-zone' with disproportionate LVH in the setting of mild hypertension. In addition, the differential diagnosis includes so called HCM phenocopies such as Fabry's disease, amyloid and endomyocardial fibrosis. We present an overview of 3 cases incorporating CMR to illustrate the determination of the underlying aetiology of LVH. Integral to this is a clinical history in addition to the scan protocol.

Methods: After transverse multi slice imaging, a standard cine stack using steady state free precession (SSFP) imaging is acquired followed by assessment of the left ventricular outflow tract and aortic valve using SSFP imaging and flow mapping. Aortic arch cines are then acquired to exclude coarctation of the aorta, followed by late gadolinium enhancement imaging.

Results: Case 1: the patient presents with mild-moderate HTN with a clinic blood pressure of 150/90mmHg. He is prescribed 2 anti-hypertensive medications. There is no family history of HCM. There is mild LVH with a maximum wall thickness of 13mm, normal indexed dimensions and no late enhancement. These findings are consistent with hypertensive disease. Case 2: A 39-year old lady has an abnormal ECG with t-wave inversion in the lateral leads without a history of hypertension. There is a family history of sudden death. Using a similar protocol, her scan demonstrates asymmetric LVH with a maximum thickness of 15mm in the anteroseptal wall and small indexed volumes. There is patchy mid-wall fibrosis of the anteroseptal wall. These findings are consistent with hypertrophic cardiomyopathy. Case 3: This 70 year old gentleman presents with shortness of breath and reduced exercise capacity. His scan shows concentric hypertrophy with longitudinal function. On late enhancement images, there is a dark blood pool, and near circumferential enhancement of the myocardium with relative hypo-enhancement of the epicardium. These findings are consistent with cardiac amyloid disease.

Conclusions: Combined with clinical history, CMR can distinguish the underlying cause of LVH. A standard protocol that evaluates not only dimensions and function but also the aortic valve, aorta and tissue characteristics of the myocardium following gadolinium contrast is recommended.

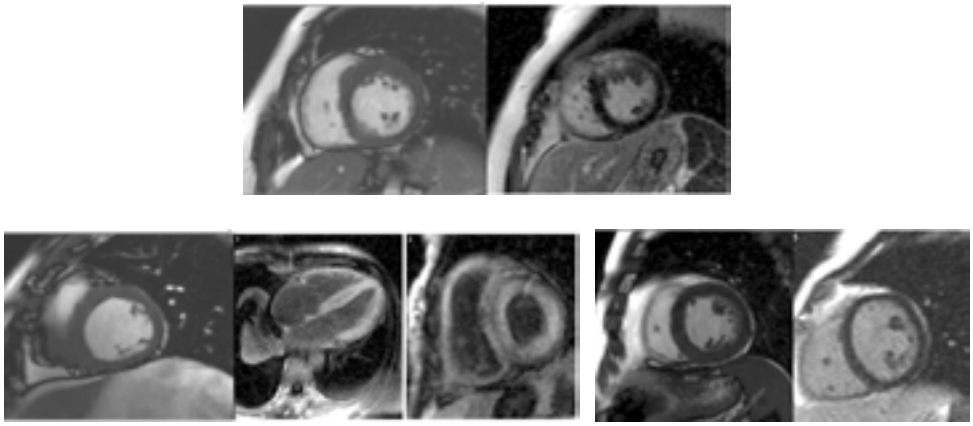

T005

Real time technologist measured T1 values for estimation of diffuse fibrosis.

George L. Mathew, BA[1], Vassilis Vassiliou, MBBS[2]Peter D. Gatehouse, PhD[3]

1. Royal Brompton Hospital, Romford, England, United Kingdom
2. Royal Brompton Hospital, England, United Kingdom
3. NIHR Cardiovascular Biomedical Research Unit, Royal Brompton Hospital, London, England, United Kingdom

Background: New T1-mapping sequences have been introduced in clinical practice in the last few years to estimate diffuse fibrosis. In principle, native T1 values measured by the operator immediately during scanning could be tested against the locally determined normal range before injection of Gadolinium (Gad), and avert the need for injection if found normal. Alternatively, other aims could be for optimisation of late-Gad TI if the TI scout is unclear, or optimising the flip-angle of some post-Gad sequences dependent on the myocardial T1. We therefore aimed to compare native T1 values measured by a CMR experienced technologist during the scan against values measured offline by a CMR accredited cardiologist.

Methods: A small cohort of patients had T1 measured using an 11 heart beat MOLLI sequence (Siemens 448B) in one institution as a feasibility study. Post-Gad values were taken 15 minutes following the intravenous administration of 0.1mmol/kg of gadolinium contrast agent Gadobutrol. The technologist measured the T1 values on the Siemens platform during the scan. The values were later also re-measured by an accredited blinded cardiologist offline (CMR Tools, London, UK). The image display packages were used only for ROI mean value measurement on the T1maps output by the Siemens WIP. No correction for heartrate or any other factors was applied. The circular ROI was positioned in the inner 1/3 of the basal or mid septal wall. The results were compared using intraclass correlation coefficient and Bland-Altman plots.

Results: Thirty-five native T1 maps and 24 post-gad T1 maps were analysed from nine patients (4 women). Mean value for operator 1 (technologist) was 1065 ± 68ms and mean value for operator 2 (cardiologist) was 1068 ± 76ms for native T1, and 432±73 and 433±73 respectively for the post-gad T1 values. There was excellent intraclass correlation between the two operators both for the native values (ICC=0.944 p

Conclusions: Technologist led real time measurement of T1 values is accurate for both native and post-gad states. This could be introduced safely in clinical practice. It might also help reduce the need for gadolinium administration if the native T1 values are measured by the operator and found to be within the locally determined normal range before injection

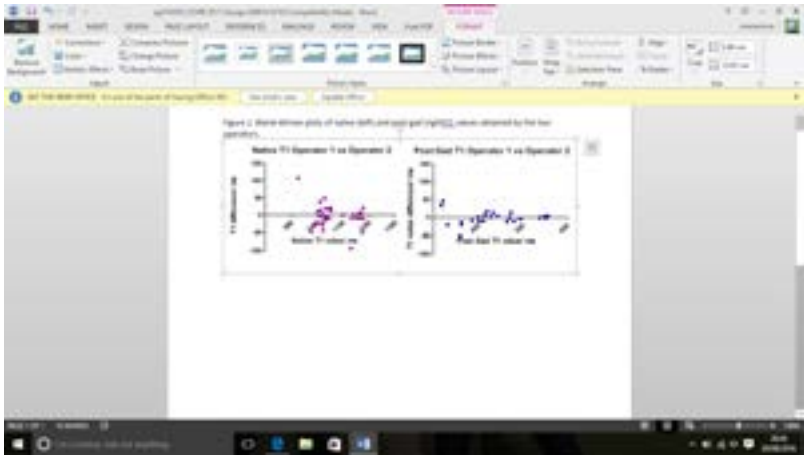

T006

Real time imaging: A new approach in patients in Atrial Fibrillation?

Joana Leal, BSc[1] Betty Raman, MBBS, FRACP[2], Aaron T. Hess, PhD[3], Masliza Mahmod, MBChB, DPhil[4], Matthew D. Robson, PhD[3], Jens Frahm, Prof. Dr.[5], Stefan Neubauer, MD, FRCP[4], Jane M. Francis, DCR(R) DNM[6]

1. *Oxford Centre for Magnetic Resonance Research, Oxford, England, United Kingdom*
2. *University of Oxford, Division of Cardiovascular Medicine, Oxfordshire, England, United Kingdom*
3. *OCMR, University of Oxford, England, United Kingdom*
4. *University of Oxford, England, United Kingdom*
5. *MPI for biophysical Chemistry, Goettingen, Niedersachsen, Germany*
6. *University of Oxford, OX39DU, England, United Kingdom*

Background: Atrial fibrillation (AF) is the most common cardiac arrhythmia characterized by irregular and often rapid ventricular rate. Assessment of cardiac function in patients with AF using Magnetic Resonance Imaging (MRI) is challenging due to poor image quality often necessitating frequent repeat acquisitions. The development and optimisation of real time (RT) imaging has resulted in improved temporal and spatial resolution comparable to standard cine protocols. RT allows for rapid, non-ECG gated and non-breath hold (BH) scans which can shorten the time needed to perform CMR on these patients. Our aim is to compare the results of cardiac mass and function assessment using standard prospective cine steady state free precession (SSFP) and radial RT imaging in a patient with persistent AF with variable ventricular rate.

Methods: We assessed cardiac function of a 62-year-old male with persistent AF and rapid ventricular response (90-115bpm), using both standard prospectively ECG-gated segmented BH SSFP and non-ECG non-BH radial RT sequence with a temporal resolution of 33 ms. The TR and TE were 3,04/1,53 ms and 3/1,14 ms for RT and prospective-gated cine SSFP, respectively. Acquisition times and image quality for both standard BH cine and RT were recorded. Short axis views for both techniques were analysed for cardiac mass, chamber volumes and ejection fraction (LVEF) using an analysis software package (cvi42 version 5.3.4, Circle Cardiovascular Imaging Inc.). Left ventricular parameters were estimated on RT for 3 heart beats and an average was obtained.

Results: Average time to acquire the prospectively gated cine with repeated attempts to optimise image quality was 5 minutes versus 2 minutes for RT imaging (1 attempt). Image quality of prospectively triggered loop was impaired in comparison to RT (Figure 1). LVEF was markedly lower on analysis of prospectively triggered cine loop at 24% compared to 40% on RT imaging (Figure 2). End-diastolic volume (EDV) and stroke volume (SV) were higher in RT than on standard cine with a difference of 14% and 49%, respectively. End-systolic volume (ESV) and mass were relatively similar for both techniques with a difference of only -7% and 1%, respectively.

Conclusions: This case illustrates the limitations of existing prospectively gated cine acquisition in AF as evidenced by clinically significant underestimation of ejection fraction. RT imaging offers the potential to acquire information over several heart beats and account for beat to beat variation in left ventricular volumes in AF, hence representing a more reliable form of left ventricular assessment.

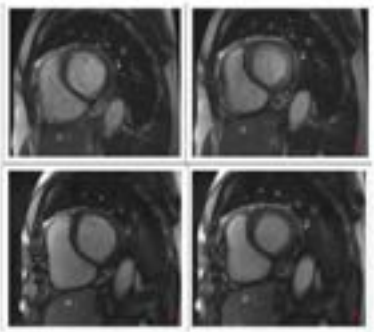

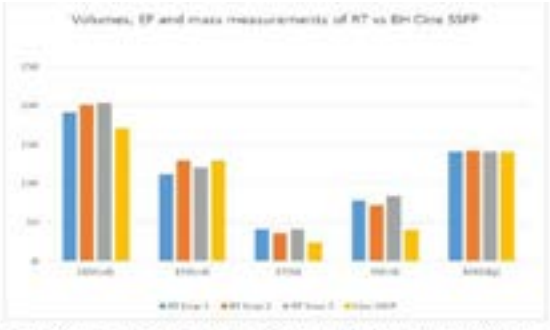

T007

Improving Efficiency in Stress Perfusion CMR with the Use of Regadenoson

Fiona M. McMillan, BSc (Hons) Diagnostic Radiography

OCMR, Thame, England, United Kingdom

Background: Adenosine is typically used in CMR as the stress agent of choice for perfusion imaging. Patients can expect to experience a variety of symptoms and occasionally heart block can be induced. Regadenoson is a selective coronary vasodilator, which is safe and the frequency of adverse events is low. Regadenoson provides diagnostic information comparable to adenosine stress perfusion. There has been a 2.7% increase in clinical scan activity over the past year with a 2% rise in perfusion CMR. Aim To see if using regadenoson instead of adenosine as the stress agent for cardiac perfusion CMR would result in shorter preparation and examination times, resulting in increased capacity.

Methods: Quantifying the time taken to prepare the patient for regadenoson or adenosine stress perfusion CMR. Assessing the time to prepare the stress agent. Retrospective analysis of scan durations. Calculated using the time stamps on the DICOM images for anatomy, function, rest and stress perfusion and late gadolinium.

Results: Patients for adenosine require two cannulas, siting these cannulas take on average 6.25 minutes. Regadenoson administration requires a single canula which takes on average 3.25 minutes to site. An adenosine infusion must be prepared prior to the patient going into the scanner and takes on average 4.52 minutes to prepare. Regadenoson can be prepared by a second operator whist the first operator commences the scan, with no additional preparation time. Scan times for regadenoson perfusion CMR varied between 31 and 40 mins with an average of 37.18 mins. Scan times for adenosine perfusion CMR varied between 35 and 46 minutes with an average of 38 mins.

Conclusions: Patients examined with regadenoson have reduced preparation time due to only siting a single canula with a saving of 3 minutes per patient. As regadenoson can be prepared concurrently whilst scanning the patient there was a saving of 4.52 minutes on drug preparation. There is no significant difference in scanning time between regadenoson and adenosine stress perfusion CMR. Regadenoson has become the stress agent of choice for perfusion CMR in our department due to the ease of patient and drug preparation.

T008

Video information prior to cardiovascular magnetic resonance imaging improves patient experience which still remains more challenging than in myocardial perfusion scintigraphy

Britt-Marie Ahlander, PhD[1] Elisabeth Ericsson, PhD[2], Eva Maret, MD, PhD[3], Jan Engvall, MD, PhD[4]

1. Jonkoping County Hospital, Jonkoping, Jonkopings Lan, Sweden
2. Orebro University, Orebro, Orebro Lan, Sweden
3. Department of Clinical Physiology, Karolinska University Hospital, Stockholm, Stockholms Lan, Sweden
4. Linkoping University, Linkoping, Ostergotlands Lan, Sweden

Background: Cardiovascular magnetic resonance imaging (CMR) and myocardial perfusion scintigraphy (MPS) are two technically advanced methods for imaging cardiac diseases. Although CMR is considered to be painless, considerable patient cooperation is necessary during scanning. Some patients may experience anxiety because of the closed environment of the procedure.

The aims of this paper were to evaluate the potential effect on patient anxiety and on motion artefacts by adding a 5 min video sequence to the standard written information given before CMR. Additionally, the patient experience of CMR was compared to that of MPS.

Methods: The sample (n=146) consisted of 97 patients randomized to receive either video information in addition to standard written information (CMR-video/n=49) or standard written information alone (CMR-standard/n=48). A third group undergoing MPS (n=51) was used to compare CMR-standard and MPS. Anxiety was evaluated before, immediately after the procedure and one week later. Four questionnaires were used: State-Trait-Anxiety Inventory, Hospital-Anxiety and Depression-scale, MRI-Fear-Survey-Schedule and the MRI-Anxiety-Questionnaire (MRI-AQ). Motion artefacts were evaluated by three observers, blinded to the information given. Motion artefacts due to arrhythmia were not considered.

Results: Measured with MRI-AQ, the CMR-video and the CMR-standard groups did not score significantly different on the factor Anxiety. However, CMR-video scored lower (=better) in the factor Relaxation ($p=0.039$). Younger patients and women scored a higher level of anxiety in most scales. Anxiety levels (MRI-AQ) were lower during MPS examinations compared to the CMR-standard group ($p < 0.001$). The presence of motion artefacts was similar in the CMR-video compared to the CMR-standard group.

Conclusions: Patient ability to relax during CMR increased by adding video information prior to the exam. This positive effect on patient experience is important to enable technologists to obtain full patient cooperation. An apparent lack of effect on motion artefact could possibly be due to the addition of compensatory extra scans when a low image quality was recognized by the technologists.

T009

Novel technique for assessing total anatomic coverage of aorta in two short breath-holds with a single contrast injection.

Joanne Wormleighton, DCR(R)[1] Abtehale Al-Hussaini, MBBS[2], Mark Horsfield, PhD[3], Gerry P. McCann, MBChB, MD[4], Abtehale Al-hussaini, MBBS,BSC, MRCP.[2], David Adlam, MD[2]

1. *Glenfield Hospital, University Hospitals of Leicester NHS Trust, Leicester, England, United Kingdom*
2. *Cardiovascular Sciences, Glenfield Hospital, University Hospitals of Leicester NHS Trust, Leicester United Kingdom, Leicester, England, United Kingdom*
3. *Xinapse Systems Ltd, Essex, United Kingdom., Essex, England, United Kingdom*
4. *The University of Leicester, Leicester, United Kingdom, Leicester, England, United Kingdom*

Background: Clinical applications for Magnetic Resonance Angiography (MRA) are rapidly expanding, with recent improvements in hardware and software techniques and the use of higher field strength allowing reduction in exogenous contrast dose. However the use of MRA in situations such as aortopathies often demands total anatomic coverage of aorta, which increases the scan time. We therefore aimed to develop a study protocol which incorporated head and neck angiography, CE-MRA of aorta, cine imaging, and late gadolinium imaging (LGE).

Methods: Imaging of the head & neck vessels were performed using time-of-flight (TOF) non-contrast MRA sequences. Whole aorta MRA was performed using a 3-dimensional T1 gradient echo sequence. Pre-contrast imaging of the aorta was performed in two consecutive stages: i) sagittal oblique of the thoracic aorta including the aortic arch and great vessels (Fig-1); ii) coronal of the abdominal aorta, renal and iliac arteries. A test bolus was acquired in the sagittal oblique plain of the thoracic aorta. A total contrast dose 0.4ml/kg (Dotarem, Gurbet, France), to a maximum of 30ml was then administered in a single injection. For the first part of the CE-MRA, the k-space filling was adjusted to 10 seconds to allow optimal image contrast towards the end of image acquisition time (14 seconds). For the second part of the CE-MRA, the k-space filling was set to 1 second to ensure optimal contrast enhancement. Automatic table movement was set between these two stages of the CE-MRA acquisitions. A stack of short axis SSFP cine series were acquired after the CE-MRA, allowing for an optimal delay for the acquisition of good quality LGE images.

Results: As part of a research study into vascular phenotyping in patients with Spontaneous Coronary Artery Dissection (SCAD) the protocol has been successfully implemented in 150 patients and 30 volunteers. Data was successfully obtained in all cases. The CE-MRA technique allowed imaging of the entire thoracic and abdominal aorta, with coverage from supra-aortic head and neck branches to femoral arteries. In 40% of the SCAD cases we have identified aortic abnormality including aneurysms, fibromuscular dysplasia and tortuosity. The mean total acquisition time for the entire imaging technique was 60 minutes.

Conclusions: We successfully developed and implemented a novel method for assessing total anatomic coverage of the aorta with only two short breath holds in a short acquisition time, and using a single contrast injection. This technique holds promise to facilitate aorta imaging and may broaden the clinical applications of CE-MRA.

Fig 1 represents a sagittal oblique MIP of the thoracic aorta and the great arteries

Fig 1 represents a sagittal oblique MIP of the thoracic aorta and the great arteries

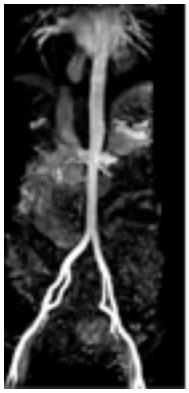

Fig 2 represents a MIP of the same patient in the coronal plane with imaging of abdominal aorta, the renal and iliac arteries.

T010

Comparison of two cardiovascular magnetic resonance feature tracking measurements for the assessment of left ventricular strain

Hong Liu, MS[1] Wei Cheng, BS[2], Dan Yang, msci[3], Bo Jiang, MS[2], Ke Wan, MD[4], Weihao Li, BMSci[5], Yang Dong, BS[6], Yucheng Chen, MD[7]

1. *Cardiology Department West China Hospital Sichuan University, Chengdu, Sichuan, China (People's Republic)*
2. *West China Hospital Sichuan University, Sichuan, China (People's Republic)*
3. *West China Hospital,Sichuan University, Sichuan, China (People's Republic)*
4. *Cardiology Division, West China Hospital, Sichuan University, Guoxue Xiang No. 37, Chengdu, Sichuan Province 610041, China, Sichuan, China (People's Republic)*
5. *West China Hospital / West China School of Medicine, Sichuan University, Chengdu, Sichuan, China (People's Republic)*
6. *Cardiology Department West China Hospital Sichuan University, Sichuan, China (People's Republic)*
7. *West China Hospital, CHENGDU, Sichuan, China (People's Republic)*

Background: Cardiovascular magnetic resonance (CMR) feature tracking (FT) is a reliable and accurate method for measurement of myocardial strain. However, there is no studies performed to evaluate the consistency and reproducibility of two different cardiac magnetic resonance feature tracking software. We evaluated and compared the quantitative strain analysis of using QStrain and TrufiStrain CMR-FT.

Methods: We enrolled 20 patients with acute ST-segment elevation myocardial infarction (STEMI) patients and 20 healthy volunteers. CMR-FT was applied to standard short axis and 2-, 3- and 4-chamber cine images. Global left ventricular (LV) radial strain (Err), circumferential strain (Ecc), and longitudinal strain (Ell) was quantified respectively. Reproducibility of QStrain and TrufiStrain was also determined.

Results: All images satisfied the requirement for strain analysis. There was good correlation of between QStrain and TrufiStrain (Ecc: -18.2±5.8% vs. -14.2±3.7%, r= 0.92; Ell: -13.1±5.1% vs. -11.5±3.7%, r= 0.91, respectively). There was moderate agreement of Err (27.1±10.4 % vs. 32.4±9.5 %, r=0.67). Interclass correlation coefficient (ICC) between software were as follows: Ecc, 0.61; Err, 0.59; LEll, 0.57; REll, 0.23. For MI segments of STEMI patients, moderate to good correlation was found between modalities (Ecc: r=0.56, P=0.0002; Err: r=0.55, P=0.0002; Ell: r=.76, P < 0.001). For NON-MI segments, there were good correlation between measurements (Ecc: r=0.85, P < 0.001; Err: r=0.60, P < 0.001; Ell: r=0.70, P < 0.001). And Intra- and inter-observer variability of QStrain were range from 0.95 to 0.99, with coefficients of variation (CV) range from 3% to 9%. Excellent intra- and inter-observer agreement of TrufiStrain were observed (ICC: 0.92 to 0.99; CV: 2% to 8%).

Conclusions: Quantitative analysis of Ecc and Ell between QStrain and TrufiStrain had high correlation. Both of them has excellent reproducibility of strain measurements.

T011

Gadolinium-Based Contrast Agents: A View from the Dark Side

Ronald Williams, RT(R)(MR), B.A.[1]Richard Lombardi, RT(R)(MR)[1], Moneal Shah, MD[2], Shimaa S. Khidr, MD[1]

1. *Allegheny General Hospital, Pittsburgh, PA*
2. *Allegheny general hospital, pittsburgh, PA*

Background: The use of gadolinium-based contrast agents (GBCAs) began with the introduction and FDA approval of Gadopentetate Dimeglumine (Magnevist, Bayer, Wayne,NJ.) in 1988. Since then 8 additional GBCAs have been introduced. While initially described as the safest of all pharmaceutical agents in the late 1990's, the concern for Nephrogenic Systemic Fibrosis(NSF) exactly 20 years later (2008) in Danish media redefined GBCA's with the resultant wide-spread limitations we have today. Recently, there are reports on increased brain signal on unenhanced T1W who received GBCA's. Taken together, issues of safety remain. Can an examination of the intrinsic physical properties of the GBCA's be made to arrive at a unifying safety statement?

Methods: How does this relate to the GBCA's? The contrast structural stability of different GBCA's is reviewed. The Thermodynamics Constant(TC) and Conditional Stability Constant(CSC) and Kinetic Stability(KS; dissociation rate) are considered. TC(measure of stability, is the energy required for gadolinium-ligand to release Gd3+ ion). If high, the chelate it is less likely to release Gd3+ ion. Most testing is performed in vitro at pH 1; with comparative testing at pH 7. The CSC measured at physiological pH is considered more relevant, although essentially a measure comparative to TC but at body pH. KS of the GBCA describes how fast resting equilibrium is reached and how quickly Gd3+ is released from the GBCA. When the KS is high, the dissociation is considerable slower than the body elimination rate, making the release of Gd3+ negligible.

Results: In vivo, GBCAs dissociation can be facilitated by endogenous metals (e.g. zinc, iron, calcium, copper) all working simultaneously to destabilize the gadolinium complex leading to release of Gd3+. The free Gd3 may then bond with metals surrounding it, resulting in transmetallation and subsequent tissue deposition. Literature describes that 20% of the nonionic linear GBCA's dissociate in human plasma up to 2 weeks after administration1. It is thought that this transmetallation is the preceptor for NSF. The nonionic-linear GBCAs have the most NSF incidences (>330 cases); macrocyclic (3 cases); high relaxivity-protein interacting (zero cases).

Conclusions: Given the known TC, KS and CSC, the physical principles governing each GBCA predict the observed clinical rates of NSF (and potentially the increased T1W brain findings). Moreover, the absence of a single case of NSF in gadobenate (MultiHance, Bracco, NJ) corroborates its physical property while Gadodiamide (Omniscan, GE, Milwaukee, WI) might be predictive of the converse supported by the recent inclusive clinical registries of NSF.

Type of gadolinium	Kinetics	Stability
Gadodiamide Gd-DTPA-BMA	Linear Nonionic	Low
Gadoversetamide Gd-DTPA-BMEA	Linear Nonionic	Low
Gadopentetate Gd-DTPA	Linear Ionic	Low
Gadobenate Gd-BOPTA	Linear Ionic	Medium
Gadoxetic acid Gd-EOB-DTPA	Linear Ionic	Medium
Gadofosveset Gd-DTPA	Linear Ionic	Medium
Gadoteridol Gd-HP-DO3A	Cyclic Nonionic	High
Gadobutrol Gd-BT-DO3A	Cyclic Nonionic	High
Gadoterate Gd-DOTA	Cyclic Ionic	High

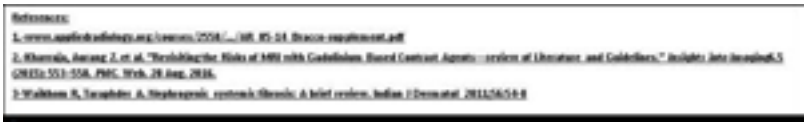

T012

Is the Contemporary Pacemaker/ICD Now Inert in the Magnetic Field; A Focused MRI Variability Study

Loretta Gevenosky, R.N.Ronald Williams, RT(R)(MR), B.A., Christopher Bonnet, M.D., Moneal Shah, M.D., Mark Doyle, Ph.D., Shimaa S. Khidr, MD

Allegheny General Hospital, Pittsburgh, PA

Background: There is considerable interest in more clinically routine use of pacemakers/ICD via MRI. However, several limitations to widespread adoption of this concept remain, including the unresolved impact of high magnetic field, RF amplitude and oscillatory forces on sensitive device microcircuitry.

Given recent vender refinements, improved shielding/RF filters/chokes and leads over the last 10 years, we hypothesize that the impact of MRI may be within clinically acceptable limits yet residual issues surrounding sensitive interrogation parameters exist.

Methods: Device interrogation was performed on 94 consecutive patients who underwent clinically indicated MRI in the last 12 months. The cohort comprised of neurology/neurosurgical (64%), orthopedic (9%) and cardiac (26%) cases. Routine device interrogation was performed 10 minutes prior to entry into the bore of a Cardiac MRI scanner (GE,1.5T, Excite, Milwaukee, WI). Following MRI examination, re-interrogation was performed (10 min post MRI). At both pre and post interrogation, an exact but repeat interrogation was performed within 5 minutes such that 2 sets of PM/ICD parameters were obtained pre and post MRI scan(4 total).

Results: No complications to either patient or device occurred during MRI scan. A cardiologist was present and guided interrogation, configuration, and reconfiguration of PM/ICD's as well supervised the entire scan. Altogether, (61%) PM's and (39%) ICD's were studied. Via repeat pre-MRI, repeat post-post or pre-post parameters comparisonsvia ANOVA, there were no significant differences in impedance, amplitude or thresholds at any time period, see Table. Likewise, there was no difference as related to thoracic vs non-thoracic MRI's or PM vs ICD's metrics. Overall, the PM's and ICD's, all after circa 2004, were inert in the MRI field independent of sequence, body part or random chance.

Conclusions: In our experience, intrinsic variability and inherent changes triggered by the MRI environment are statistically and clinically negligible for pacemaker/ICD's when conventional precautions were taken, again, incrementally advancing yet another safety aspect. This allows us to move another step closer towards a more uniform acceptance of this technology for clinically meaningful use and acceptance in the MRI environment.

		Pre	Post	p (Pre-Post)
Atria	Impedance	443±96	439±101	0.23
	Sensing	2.87±1.48	3.41±2.74	0.14
	Threshold (Amplitude)	0.88±0.68	0.9±0.7	0.59
	Threshold (Pulse Width)	0.46±0.13	0.43±0.05	0.32
RV	Impedance	496±118	485±116	0.09
	Sensing	9.42±3.52	20.39±80.56	0.16
	Threshold (Amplitude)	0.83±0.29	0.82±0.3	0.5
	Threshold (Pulse Width)	0.53±0.24	0.52±0.22	0.46
LV	Impedance	637±200	651±208	0.09
	Threshold (Amplitude)	0.96±0.47	0.92±0.43	0.73
	Threshold (Pulse Width)	0.73±0.25	0.62±0.24	0.65

T013

Novel technique for assessing total anatomic coverage of aorta in two short breath-holds with a single contrast injection.

T014

CMR diagnosis of acute myocarditis in a patient with chest pain following cocaine use

Fiona L. Hamilton, PgC Medical Magnetic Resonance, BSc (Hons) Radiography

Barts Heart Centre, London, England, United Kingdom

T015

This Heart Rocks!

Patricia Feuchter, MSc (MRI) RadiologyAnna Herrey

Barts Heart Centre, London, England, United Kingdom

Background: A 49 year old male presented to his local hospital with recurrent syncope and shortness of breath. His previous medical history included atrial fibrillation, with rapid ventricular rates response, severe LV dysfunction and bipolar affective disorder. Echocardiography performed locally 'showed significant pericardial effusion.' He was referred to our institution for Cardiac Magnetic Resonance (CMR) imaging.

Methods: Initially, segmented SSFP cines were obtained, but later changed to real time SSFP cines because of the varying R-R interval from AF and difficulty with breath holding.

Results: The study confirmed severely reduced systolic function with global severe hypokinesis and a 3cm circumferential pericardial effusion. On the real time free breathing cines, the heart is rocking within the effusion with a degree of RA/RV collapse. On inspiration there is significant septal flattening, indicating constrictive physiology from cardiac tamponade.

Conclusions: On the basis of these findings, the patient was scheduled to undergo pericardial drainage, but took his own discharge against medical advice. Despite his history of psychiatric illness, he was considered to have capacity to make decisions about his admission and treatment.

Technical Points:

- Always look at your images and tailor the protocol to the patient. If they are unwell, scan quickly, if the patient cannott hold their breath, reduce the breath hold time or allow the patient to breathe and freely breathing using real time cines.
- Variable RR intervals cause gating problems: sometimes this can be resolved by prospective gating, but in our case, the patient was too unwell to reliably breath-hold. Therefore, real time cines were used.
- With inspiration, intrathoracic pressure drops. This increases systemic venous return and therefore blood volume within the right side of the heart. If the RV wall cannot expand because of constriction (or in this case, fluid causing tamponade) the interventricular septum flattens and moves across towards the LV during inspiration, causing the LV to have a 'D-shaped' appearance.
- When acquiring real time cines, we increase our acquisition window to 3000ms to obtain more cardiac cycles and therefore enable better visualization of cardiac function and septal motion.

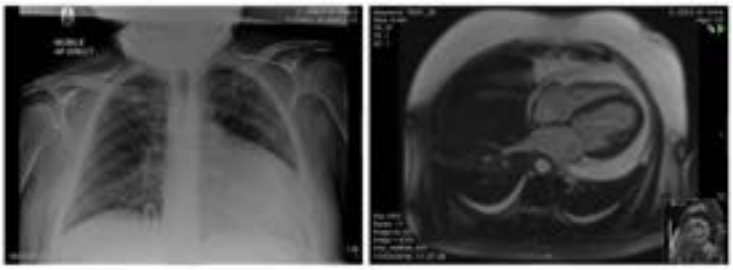

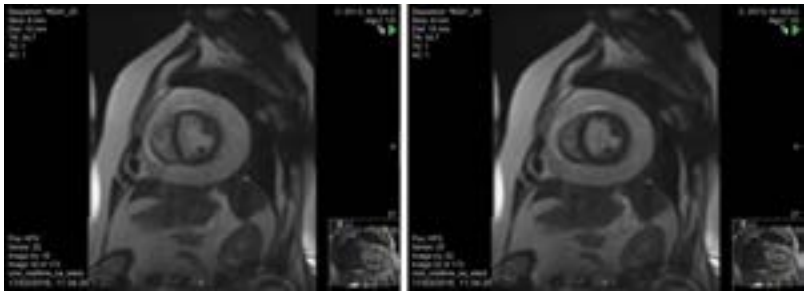

W001

Validation of DTI in Whole Myocardium with Structure Tensor Synchrotron Radiation Imaging

Irvin Teh, PhD[1] Darryl McClymont, PhD[1], Marie-Christine Zdora, MSc[2], Hannah J Whittington, PhD[1], Valentina Davidoiu, PhD[3], Jack Lee, PhD[3], Craig A Lygate, PhD[1], Christoph Rau, PhD[2], Irene Zanette, PhD[2], Jurgen E Schneider, PhD[1]

1. *University of Oxford, England, United Kingdom*
2. *Diamond Light Source, England, United Kingdom*
3. *King's College London, England, United Kingdom*

Background: Diffusion tensor imaging (DTI) is increasingly used to assess the myocardial microstructure. However, relating the diffusion tensor to the complex underlying microstructure is non-trivial. Existing histological validation methods have shown that diffusion principal eigenvectors $\mathbf{v}_{1,DT}$, $\mathbf{v}_{2,DT}$ and $\mathbf{v}_{3,DT}$ generally correspond to the cell,[1,2,3] sheetlet and sheetlet-normal directions.[4,5] However, these methods are destructive, susceptible to tissue distortion, laborious and routinely limited in field-of-view (FOV). Reconstruction of 3D image volumes and tensors from 2D slices with variable distortions remains challenging. X-ray phase contrast synchrotron radiation imaging (SRI) provides both excellent coverage and resolution.[6] Our objective was to validate DTI measurements in the whole heart ex vivo, at high resolution and free of distortion.

Methods: Rat heart (female, Sprague Dawley, N=1) was excised and fixed with isosmotic Karnovsky's fixative and embedded in 1% agarose gel for DTI and SRI. Non-selective 3D fast spin echo DTI was performed on a 9.4 T MRI scanner (Agilent, CA, USA): isotropic resolution=100µm, FOV=21.6×14.4×14.4mm, diffusion-weighted directions=30, b=1000s/mm^2 and acquisition time=6:07h. SRI data were subsequently acquired at beamline I13-2 at Diamond Light Source (Didcot, UK) with a polychromatic beam: X-ray energies~15-30keV, effective isotropic pixel size=3.6µm, FOV=17.3×14.0×14.0mm, and acquisition time=10h. Diffusion tensors (DT) were fit to the DTI data and structure tensors (ST) were derived from signal gradient intensities in the SRI data. The datasets were rigidly registered, the heart was segmented and angle maps were calculated based on local coordinate systems.

Results: Excellent agreement was observed in the orientations of DT primary eigenvectors, $\mathbf{v}_{1,DT}$ and ST tertiary eigenvectors, $\mathbf{v}_{3,ST}$ across the global myocardium. Differences in helix angles (HA) and transverse angles (TA) between methods were $HA_{DTI\text{-}STSRI}$ = -1.3° ± 15.7° and $TA_{DTI\text{-}STSRI}$ = -0.6° ± 18.9° (mean ± 1SD across > 1×10^6 myocardial voxels; Figures 1 & 2). $\mathbf{v}_{2,DT}$ and $\mathbf{v}_{3,DT}$ were found togenerally correspond to $\mathbf{v}_{1,ST}$ and $\mathbf{v}_{2,ST}$ respectively.

Conclusions: The high brilliance in SRI provides far greater flux than X-ray lab sources that enhances resolution, while phase contrast improves soft tissue contrast. STSRI enables resolution of cellular structures in 3D, and novel validation of DTI in the whole myocardium, in the same intact heart without distortion.

Acknowledgements:EPSRC (EP/J013250/1), BBSRC (BB/I012117/1), BHF Centre for Research Excellence (FS/11/50/29038; PG/13/33/30210), Wellcome Trust (090532/Z/09/Z), Diamond Light Source (MT13044-2). **References** [1] Hsu EW., et al. AJP. 1998; [2] Scollan DF., et al. AJP. 1998; [3] Holmes AA., et al. MRM. 2000; [4] Tseng WY., et al. JMRI. 2003; [5] Kung GL., et al. JMRI. 2011; [6] Balicevic V., et al. FIMH. 2015.

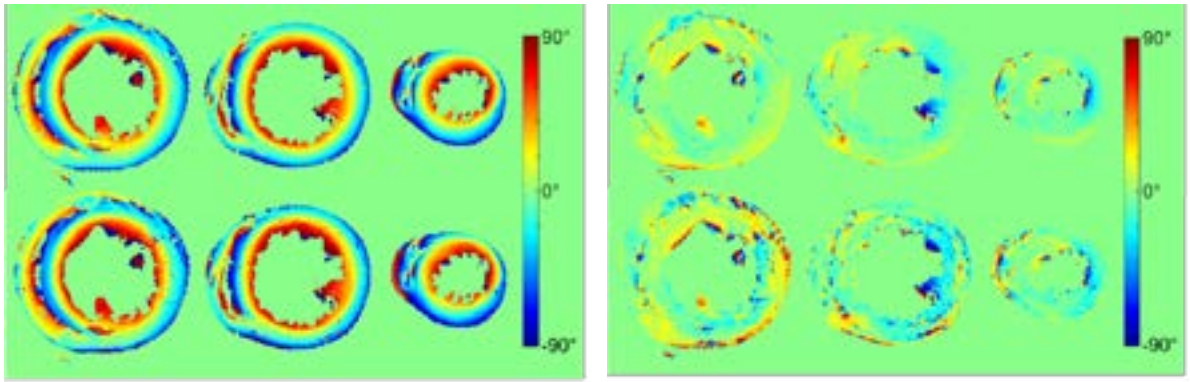

W002

An in-vivo comparison of STEAM and motion compensated spin-echo imaging in cardiac DTI

Andrew D. Scott, PhD[1]Sonia Nielles-Vallespin, PhD, MSc[2], Pedro F. Ferreira, PhD[3], Zohya Khalique, MBBS[4], Dudley J. Pennell, MD[5], David N. Firmin, PhD[6]

1. *NIHR Cardiovascular Biomedical Research Unit, The Royal Brompton Hospital, Sydney Street, London, SW3 6NP, UK, England, United Kingdom*
2. *NIH, MD*
3. *Cardiovascular Biomedical Research Unit, The Royal Brompton Hospital, Sydney Street, London, SW3 6NP, UK, England, United Kingdom*
4. *NIHR Cardiovascular Biomedical Research Unit, Royal Brompton Hospital, London, England, United Kingdom*
5. *Royal Brompton Hospital and Imperial College, London, England, United Kingdom*
6. *NIHR Cardiovascular Biomedical Research Unit, Royal Brompton Hospital, England, United Kingdom*

Background: Stimulated echo acquisition mode (STEAM) cardiac diffusion tensor imaging (cDTI) is robust and reproducible[1,2]. However STEAM is signal to noise ratio (SNR) inefficient and strain affects the measured diffusion. Alternatively, spin-echo (SE) with acceleration and velocity compensated diffusion gradients (M012) has been demonstrated and compared to STEAM at 1.5T in systole[3,4]. In previous work we compared STEAM and M012-SE[5], but subsequent investigations discovered a slice thickness inconsistency between sequences[5].

Methods: STEAM and M012-SE sequences were implemented with identical EPI readouts and matched slice thicknesses(figure 1). Imaging was performed at 2.8x2.8x8mm^3 (1.4x1.4x8mm^3 reconstructed), SENSE x2, field of view 360x135mm^2. Both sequences used water excitation, b_{main}=450smm^{-2}, b_{ref}=150smm^{-2} and 6 directions. STEAM imaging used TE=23ms, TR=2RR-intervals and 8 averages. M012-SE imaging used TE=75ms, TR=1RR-interval and 16 averages. Imaging was performed in an agar phantom (T1= 1090ms, T2=51ms, 50 averages) to compare SNR with theory[4] and in 9 volunteers (5 male, 27±6years). In-vivo data was acquired in a mid-ventricular short-axis slice during breath-holding at end-systole, diastasis and the systolic sweet-spot[6]. Data was processed using Matlab.

Results: The SNR ratio (M012-SE/STEAM) in a phantom of 1.87 was similar to the theoretical value of 1.97. cDTI data was of sufficient quality for analysis in all sweet-spot and systolic acquisitions. In 3/9 subjects, ECG mis-triggering in diastolic M012-SE acquisitions resulted in poor quality data. Figure 2 shows example parameter maps and figure 3 compares average left ventricular values. MD is lower ($p < 0.05$ systole and sweet-spot) and FA is higher using STEAM (p=0.008 sweet-spot). There was a reduction in E2A mobility (systole-diastole median(IQR), 15(15)^o vs. 42(11), p=0.03) using M012-SE; E2A was higher in systole and lower in diastole using STEAM ($p < 0.05$). There were systolic and sweet-spot differences in tensor mode ($p < 0.05$). The standard deviation of the transverse angle was higher at the sweet-spot and diastole using M012-SE ($p < 0.05$) which may suggest uncertainty in the tensor orientation[4].

Conclusions: The previously described systolic differences in MD and FA between STEAM and M012-SE are maintained at 3T in systole, diastasis and sweet-spot. Further work is required to improve M012-SE reliability in diastole and it remains to be seen whether the differences between the sequences provide complementary microstructural information.

References:

1.Reese MRM 1995.DOI:10.1002/mrm.1910340603.

2.Nielles-Vallespin MRM 2012.DOI:2012.10.1002/mrm.24488

3.Stoeck MRM 2015.DOI:10.1002/mrm.25784

4.Von Deuster MRM 2015.DOI:10.1002/mrm.25998

5.Scott SCMR/ISMRM workshop 2016:W19.

6.Tseng MRM 1999.DOI:10.1002/(SICI)1522-2594(199908)42:23.0.CO;2-F

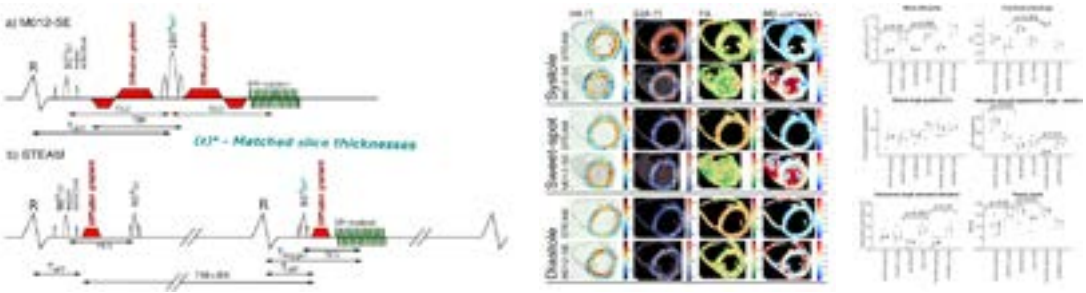

W003

Cardiac Diffusion Tensor Imaging – Comparison of In Vivo Systolic and Diastolic Cardiomyocyte Orientations

Patrick Magrath, M.S.[1]Eric Aliotta, M.S.[2], Kévin Moulin, PhD[3], Daniel B. Ennis, PhD[4]

1. *University of California, Los Angeles, Los Angeles, CA*
2. *UCLA, CA*
3. *UCLA, Los Angeles, CA*
4. *Department of Radiological Sciences, University of California, Los Angeles, CA, USA., CA*

Background: Cardiac diffusion tensor imaging (cDTI) is a promising technique to probe *in vivo* cardiac microstructure. By acquiring diffusion weighted images (DWI) along different encoding directions and reconstructing a diffusion tensor, cDTI is able to measure the local orientations of cardiomyocytes *in vivo* {Tseng *et al*. JMRI 2003}. Diffusion weighted spin echo echo-planar imaging (SE-EPI) methods with first and second order motion compensation mitigate sensitivity to bulk cardiac motion and maintain higher SNR and shortened scan times compared to other methods {Stoek *et al*. MRM 2015}. Convex optimized diffusion encoding (CODE), which reduces TEs in diffusion weighted SE-EPI, boosts SNR while maintaining bulk motion robustness at multiple cardiac phases {Aliotta *et al*. MRM 2016}. The objective of this study was to apply the CODE framework to cDTI and compare cardiomyocyte orientations between systole and diastole via helix angle (HA) maps.

Methods: *Imaging:* Free breathing, two-phase (mid systolic and end diastolic) mid-ventricular short axis cDTI (2x2x5mm, TE/TR=60/4000ms, b-value=[0,350]s/mm^2, N_{avg}=3-5, N_{dir}=12, scan time=~4min/phase) was acquired using CODE cDTI in healthy volunteers (N=5) after obtaining informed consent. Images were acquired at the most quiescent phase, using a mean trigger delay of 100ms was used for mid systolic images and 720ms for end diastolic images. *Post-Processing:* Diffusion tensors were reconstructed from cDTI using a custom Matlab tool. HA maps were generated by calculating the angle between the primary eigenvector of the diffusion tensor and the local circumferential direction. HA was binned into 10 transmural groups (endocardium to epicardium) by percent wall depth for both cardiac phases. Differences in HA distributions between systole and diastole were evaluated within each bin (amongst all volunteers) using a two-sided t-test.

Results: Figure 1 shows cDTI cardiomyocyte orientations (vectors) and HA (color) at systole and diastole in one healthy volunteer. HA increased transmurally in all volunteers from epicardium to endocardium in both systole (-48.7°±10.0° to 37.0°±5.4°) and diastole (-54.2°±6.5° to 37.7°±8.0°). There were no significant differences in HA between mid systole and end diastole at any wall depth ($p \geq 0.2$). The observed transmural HA behavior is in agreement with Nielles-Vallespin *et al.* { Nielles-Vallespin *et al. MRM 2012*} and the cardiac phase invariance is in line with previous reports {Stoek *et al.* MRM 2015}.

Conclusions: CODE cDTI provides end systolic and end diastolic HA distributions that are consistent with known ventricular structure {Lombaert *et al.* IEEE: Trans. Med. Imag.} and previous reports of cDTI in healthy volunteers, which have been shown to be relatively invariant throughout the cardiac cycle {Stoeck *et al*. PLoS 2014}. These results provide additional confidence in CODE cDTI, and further investigation into this new technique is ongoing.

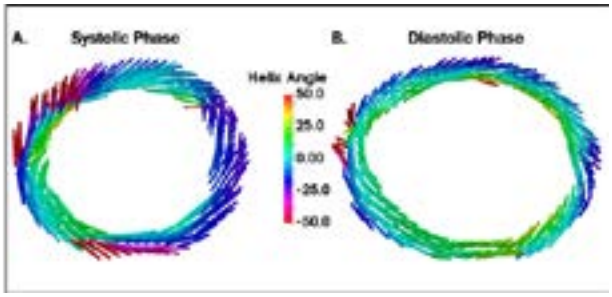

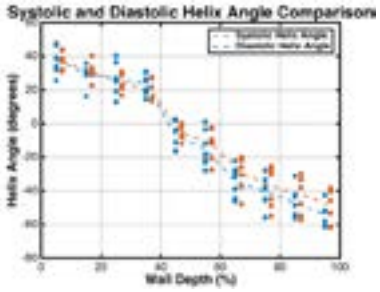

W004

Automatic detection of corrupted frames in cardiac DTI with machine learning

Pedro F. Ferreira, PhD[2]Francesca Cavallo[1], Zohya Khalique, MBBS[3], Andrew D. Scott, PhD[4], Sonia Nielles-Vallespin, PhD, MSc[5], David N. Firmin, PhD[6]

1. *Imperial College London, England, United Kingdom*
2. *Cardiovascular Biomedical Research Unit, The Royal Brompton Hospital, Sydney Street, London, SW3 6NP, UK, England, United Kingdom*
3. *NIHR Cardiovascular Biomedical Research Unit, Royal Brompton Hospital, London, England, United Kingdom*
4. *NIHR Cardiovascular Biomedical Research Unit, The Royal Brompton Hospital, Sydney Street, London, SW3 6NP, UK, England, United Kingdom*
5. *NIH, MD*
6. *NIHR Cardiovascular Biomedical Research Unit, Royal Brompton Hospital, England, United Kingdom*

Background: In vivo cardiac diffusion tensor imaging (DTI) is capable of probing the microstructure of the myocardium and its dynamics throughout the cardiac cycle. A typical DTI study of one mid-ventricular slice scanned at two stages of the cardiac cycle will typically contain more than 180 frames, with approximately 14% of them corrupted by signal loss due to cardiac and respiratory motion. Currently an experienced observer identifies corrupted frames using visual assessment and manually removes them, before the diffusion tensor is calculated. This can take up to 5 minutes per subject. The objective of this work is to accelerate and automate the removal of corrupted frames by machine learning (ML).

Methods: Data from a total of 51 subjects (19 healthy, 32 patients) scanned at systole and diastole were used to assess the accuracy of ML. A visual assessment by two experienced users identified 1407 corrupted frames (figure 1) out of a total of 9651 frames (8% in healthy, 18% in disease). Half of the subjects in both cohorts were randomly selected for machine training. The remaining data were used to determine the accuracy of the algorithm. A machine learning algorithm was used, where images are converted to a vector quantization of affine invariant descriptors [1] before using a quadratic support vector machine classifier (MATLAB). The accuracy of corrupt frame identification by machine learning was compared to the best intrasubject image similarity algorithm we tested, a Pearson correlation coefficient (PCC) test (with the optimum threshold for this data).

Results: The accuracy of corrupt frame identification with ML was higher than that of the PCC tests ($p = 0.058$, Wilcoxon signed rank). The overall confusion matrices are shown in table 1. An intersubject mean+/-SD accuracy of 96+/-4% was achieved with ML, above the mean 88+/-20% accuracy of PCC. Machine learning yielded significantly lower false negatives (figure 2) and a lower inter-subject accuracy variance. An overall average mean difference to the visual assessment of 6% and 9% are observed for ML and PCC respectively when combining multiple DTI parameters. The ML algorithm takes approximately 25 seconds to assess the entire database of 51 subjects.

Conclusions: ML can be used to accurately assess DTI corrupted frames with better efficiency than image similarity measures. Therefore, ML is capable of reducing the user input, accelerating analysis and removing human subjectivity. As the DTI patient database grows, accuracy can potentially improve further.

References: 1 – Csurka et al. ECCV 2004 1-22

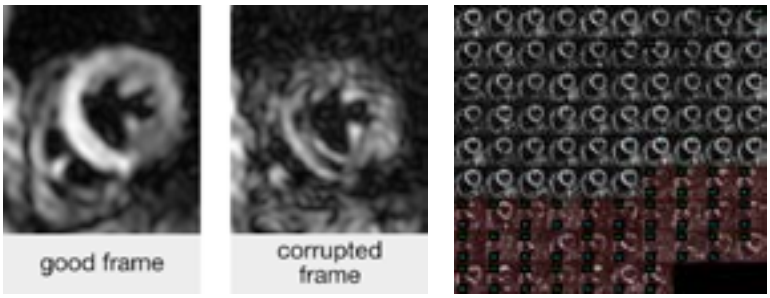

Table 1: Confusion matrices for machine learning and Pearson correlation coefficient test.

Pearson correlation coefficient		machine learning			
predicted		predicted			
bad	good	bad	good		
477	4082	152	4480	good	Known
525	183	556	79	bad	
87%		96%		overall accuracy	

Confusion matrices for machine learning and Pearson correlation coefficient test.

W005

Vasodilator Response in Heart Transplant Recipients using T1-based Myocardial Blood Volume Mapping

Krishna Nayak, PhD[1] Hung Phi Do, MSC[1], Andrew J. Yoon, MD[1], Michael Fong, M.D.[1], Luanda Grazette, MD, MPH[2], Farhood Saremi, MD[3], Mark L. Barr, M.D.[1]

1. *University of Southern California, Los Angeles, CA*
2. *Keck Medical Center of the University of Southern California, Los Angeles, CA*
3. *USC, CA*

Background: Myocardial spin-lattice relaxation time (T1) is sensitive to water content related to fibrosis and to myocardial blood volume (MBV). Previous studies have demonstrated that native T1 is able to differentiate patients in several disease conditions from normal controls. Assessment of fibrosis and blood volume plays an important role in the management of heart transplant recipients where fibrosis formation and reduction in MBV often precede allograft rejection. We hypothesize that native myocardial T1 is higher in transplant recipients due to fibrosis and that this leads to reduced MBV change during vasodilation. This study applies myocardial T1 mapping at rest and adenosine stress to assess native T1 and T1 change (ΔT1) [Liu et al., i*JACC 2016*, *9*(1), 27-36] as potential surrogates of myocardial fibrosis and MBV change in heart transplant recipients.

Methods: This study was approved by our Institutional Review Board and all participants provided written informed consent. MOLLI 5(3s)3 myocardial T1 mapping was performed at rest and during adenosine stress in five heart transplant recipients (4M, age 49 ± 16) and five healthy controls (4M, age 28 ± 4). Imaging parameters: TR/TE = 3.2/1.5 ms, flip angle = 35^0, slice thickness = 10 mm, field-of-view = 160-240 cm, receiver bandwidth = 62.5 kHz, acquisition matrix = 96x96, GRAPPA factor 1.6x. Pixel-by-pixel T1 maps were generated by Levenberg–Marquardt nonlinear curve fitting. Left ventricular myocardium was manually segmented and regional analysis performed using the AHA 6-segment model. ΔT1 was calculated by $100\%*(T1_{stress} - T1_{rest})/T1_{rest}$. Values are reported as mean ± SD. Student's t-test was used to compare regional myocardial T1 and ΔT1 from the two groups.

Results: Figure 1 shows representative pixel-by-pixel T1 maps at rest and stress from a healthy subject and a heart transplant recipient and the corresponding regional ΔT1 maps. **Figure 2** and **Table 1** summarize regional T1 at rest and stress from all subjects and the corresponding regional ΔT1. In healthy subjects, native myocardial T1 and ΔT1 were 1133 ± 84 ms and 5.41 ± 3.12 %, respectively, consistent with literature values. The main findings of this study are 1) native T1 at rest was significantly higher ($P < 0.0001$) in heart transplant recipients consistent with the hypothesis of fibrosis formation; 2) ΔT1 (surrogate for MBV change) was significantly lower ($P = 0.022$) in heart transplant recipients, which may be a consequence of fibrosis and/or impaired vasodilator response.

Conclusions: This study demonstrates that adenosine stress and rest myocardial T1 mapping is potentially able to assess regional MBV change in heart transplant patients without the use of a contrast agent. That would potentially be a useful method for spatial and temporal assessment of myocardial tissue function in patients with cardiovascular disease especially those with renal inefficiency.

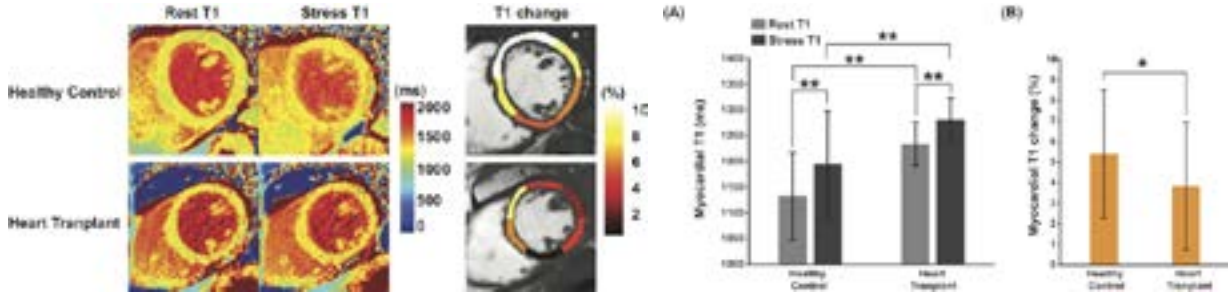

Regional Myocardial T1 and T1 Change (ΔT1) in Heart Transplant Recipients and Healthy Controls

ΔT1 (%)	Stress T1 (ms)	Rest T1 (ms)	
5.41 ± 3.12#	1195 ± 103*	1133 ± 84#	Healthy Control
3.83 ± 3.11	1281 ± 42*	1234 ± 42	Heart Transplant
0.0222	***< 0.0001***	***< 0.0001***	***P-value***

Summary of regional myocardial T1 at rest and stress and regional myocardial ΔT1 measured from healthy controls and heart transplant recipients. (*) indicates significant increase in myocardial T1 with adenosine stress compared to rest ($P < 0.0001$). (#) indicates the resting native T1 and ΔT1 measured from this study are consistent with literature values, which are 1189 ± 34 ms, and 6.2 ± 0.5 % [Liu et al., *JACC: Cardiovascular Imaging 2016*, *9*(1), 27-36], respectively.

W006

Assessing The Repeatability of ECV Mapping Without Hematocrit Measurement at 3T

Michael A. Blatt, B.S.[1] Promporn Suksaranjit, MD, MS[2], Brent Wilson, MD, PhD[3], Edward VR. DiBella, PhD[2]

1. *University of Utah, Slc, UT*
2. *University of Utah, UT*
3. *University of Utah, Salt Lake City, UT*

Background: Through the use of LGE-enhanced T1 mapping, clinicians and researchers have developed and validated a method for mapping extracellular volume (ECV) [1-4]. One of the components for calculating ECV is sampling the blood to determine the hematocrit volume fraction (Hct). Based on the T1-relaxation properties of the blood, Treibel et al. demonstrated that a linear relation between R1 ($T1^{-1}$) and Hct could be derived and applied to generating "synthetic ECV maps"— ECV mapping that required no blood sampling for Hct quantification[5]. In this paper, we expand on the work of [5] by deriving a formula based on [6] and then assessing the interpatient repeatability in comparison to the traditional (or standard) ECV mapping method, which is dependent on blood sampling for quantifying Hct, in addition to assessing the agreeability between the two techniques for ECV mapping at 3T.

Methods: Rearranging the formula correlating T_1 to Hct provided in [6], Hct can be estimated as a function of R_1, $\mathbf{B_0}$, erythrocyte concentration (**[Hb]**), and oxygen saturation (**Y**) as shown in equations (1)-(5). Since Oxygen saturation and Hemoglobin concentration was not measured, **[Hb]** and **Y** were assumed to equal 5.15 $mmol_{Hb\ tetramer}/L_{plasma}$ and 0.68 respectively. The formula was implemented in MATLAB (Natick, Massachusetts). Repeated patient MOLLI studies in 10 subjects, 2-3 slices each, ~10 days apart [7] was then processed to produce sets of traditional and synthetic ECV maps on two separate scan dates (figure 1). To gauge the repeatability of the two methods, a coefficient of variation (COV) was calculated using the standard deviation of the difference in the two scan dates and the mean of the ECV measurement.

Results: The synthetic ECV mapping method correlated relatively well to the standard method ($R^2 = 0.71$). The Bland-Altman plot of the corresponding difference data is shown in figure 2. The average ECV fraction in the standard and synthetic methods was 0.27 ± 0.035 and 0.27 ± 0.039, respectively. The standard method had a COV of 7.5% while the synthetic method had a COV of 9.53%. This difference may be in large part due to an outlier image with a streak artifact. Removing that one (of 26) samples, the COV for the standard and synthetic method became 7.1% and 7.9% respectively and the R^2 increased to 0.77.

Conclusions: This research has demonstrated that an estimation of hematocrit based on R_1 has repeatability similar to the standard method. Larger studies are needed to better determine the accuracy and precision of the synthetic Hct. The advantages from not needing a Hct value could render the synthetic method preferential to clinicians and patients— which does not require blood sampling.

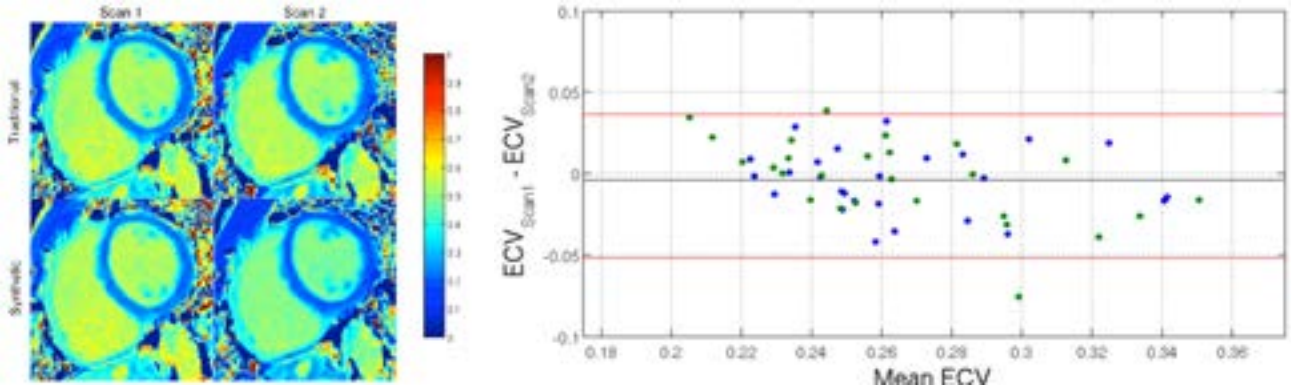

$$\alpha = 1.099 - 0.057B_0 \quad (1)$$

$$\beta = 0.33[\mathrm{Hb}](1 - Y) \quad (2)$$

$$\gamma = 0.496 - 0.023B_0 \quad (3)$$

$$f = \frac{R_1 - \gamma}{\alpha + \beta + \gamma} \quad (4)$$

$$Hct = \frac{0.95f}{0.7 + 0.025f} \quad (5)$$

[1] Sado DM *et al.*: Future Cardiol. 2011, 7 (5): 643-650 [2] Flett AS *et al.*: Circulation. 2010, 122 (2): 138-144 [3] Kellman P *et al.*: JCMR 14:63 [4] Kellman P *et al.*: JCMR 14:64 [5] T.A. Treibel *et al.*: J Am Coll Cardiol Img. 2016 9: 54–63 [6] Hales, Patrick W. *et al.*: Journal of Cerebral Blood Flow & Metabolism. 2016 36.2: 330-374 [7] Likhite, D *et al.*: J. Magn. Reson. Imaging, 43: 1369–1378

W007

Hemorrhage alters remote myocardial response following acute myocardial infarction: A T2-BOLD and T1-ECV study

Nilesh R. Ghugre, PhD[1] Venkat Ramanan, MSc[2], Graham Wright, PhD[3]

1. *Sunnybrook Research Institute, University of Toronto, Toronto, ON, Canada*
2. *Sunnybrook Research Institute, Toronto, ON, Canada*
3. *Sunnybrook Research Institute, University of Toronto, ON, Canada*

Background: Hemorrhage is considered to be a new independent predictor of adverse outcomes following acute myocardial infarction (AMI). It has been suggested that the infarct zone may have translated effects in the distal remote myocardium as well in the form of edema and vasodilator dysfunction. The aim of this study was to evaluate the impact of hemorrhage on remote myocardial remodeling following an ischemic event. To this end, we employed a T2-based blood-oxygen-level-dependent (T2-BOLD) approach to assess vasodilator function and compared this with T1-based extracellular volume fraction (ECV) estimation.

Methods: Hemorrhage was artificially induced in a pig model by direct intracoronary injection of collagenase (col). Animals were subjected to an LAD occlusion followed by reperfusion based on three groups: Group 1 (N=4) 45 min+saline (sal); Group 2 (N=5): 8 min+col; and Group 3 (N=5): 45 min+col. Imaging was performed on a 3T MRI scanner at baseline and up to week 4 post-intervention. Pre- and post-contrast T1 values were quantified using a MOLLI sequence. ECV was estimated from partition coefficient (λ) using the relation:$(1/T1_{myo,post}-1/T1_{myo,pre})/(1/T1_{blood,post}-1/T1_{blood,pre})$. T2 mapping was performed using a T2-prepared spiral sequence; for BOLD response, imaging was repeated with a stress agent. Hemorrhage was assessed from T2* maps obtained using a multi-echo gradient-echo sequence. Infarcted and remote myocardial segments were identified using LGE images.

Results: Infarct size was greater in group 3 compared to group 1 ($p < 0.0001$) and group 2 did not show any infarction on LGE. Low infarct region T2* values confirmed the presence of hemorrhage in the collagenase groups 2 and 3 whereas group 1 was non-hemorrhagic (Figure 1). In group 1, remote T2 was significantly elevated in the stress state at all time points and no changes were noted in the resting state. However, remote resting T2 was significantly elevated at day 1 and week 1 in groups 2 and 3 indicative of edema and this was associated with a transient vasodilator dysfunction (low stress T2) that resolved by week 4; the dysfunction was more persistent in group 3 (Figure 2). In groups 2 and 3, $T1_{post}$ in the remote zone was significantly lower at day 1 compared to group 1, indicative of edema or extracellular matrix (ECM) alterations. Similarly, groups 2 and 3 also demonstrated an elevation in remote zone λ at day 1 and week 1 (only group 3), confirming this response. Interestingly, vasodilator dysfunction and ECM alterations were closely associated responses during the sub acute phase of injury.

Conclusions: Our study demonstrates that T2-BOLD and T1-ECV approaches can identify the contribution of hemorrhage towards remote myocardial remodeling post-AMI; edema, ECM expansion and vasodilator response appear to be inter-linked responses. Early detection of remote tissue alterations will potentially aid better management of the high-risk patients who are prone to adverse long-term consequences.

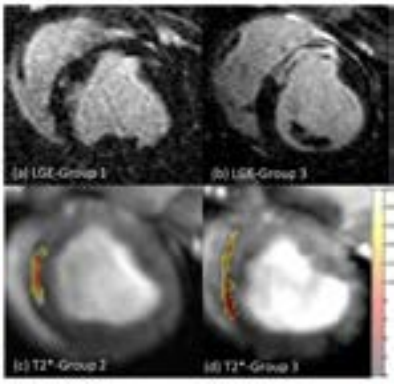

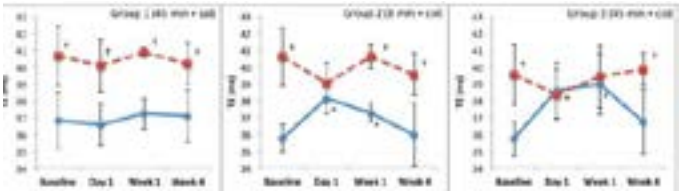

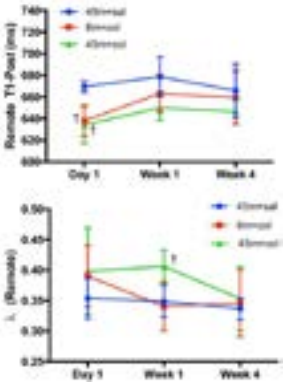

W008

Myocardial T1 and T2 mapping in severe aortic stenosis: novel insights into the pathophysiology of myocardial remodeling?

Bettina Baeßler, M.D.[1]Ana Fehrmann[1], Melanie Treutlein[1], Daniel Giese, PhD[1], Alexander Bunck, M.D.[1], Kilian Weiss, PhD[2], Tanja Rudolph, M.D.[3], Volker Rudolph, M.D.[3], David Maintz, M.D.[1]

1. *University Hospital of Cologne, Department of Radiology, Nordrhein-Westfalen, Germany*
2. *Philips GmbH, Nordrhein-Westfalen, Germany*
3. *University Hospital of Cologne, Department III of Internal Medicine, Heart Center, Nordrhein-Westfalen, Germany*

Background: Severe aortic stenosis (AS) is known to be associated with substantial myocardial remodeling, leading to diffuse myocardial fibrosis. Native myocardial T1 has been shown to correlate with myocardial fibrosis and is emerging as a novel imaging biomarker. In contrast, no studies exist elucidating potential changes of myocardial T2 times reflecting myocardial water content in the presence of myocardial remodeling. The purpose of the present study was to combine native T1 and T2 mapping in a comprehensive CMR examination in order to characterize myocardial tissue changes in the setting of severe AS.

Methods: After obtaining ethical approval and informed consent, 20 patients with severe AS prior to trans-catheter aortic valve replacement (mean age 79 ± 8 years) as well as 15 healthy controls (mean age 62 ± 5 years) underwent a CMR examination on a clinical 3T scanner (Philips Ingenia 3T). The CMR protocol included a Gradient Spin Echo (GraSE) T2-mapping sequence as well as a native Modified Look-Locker (MOLLI) 5-3-3 T1 mapping sequence in a midventricular short-axis slice. After segmentation of T1 and T2 maps using a dedicated Osirix plug-in, myocardial T1 and T2 values were averaged over the entire myocardium. Statistical analysis was performed using Welch's independent T-test and Pearson's correlation coefficient.

Results: Mean native myocardial T1 times were significantly higher in AS patients when compared to controls (1306 ± 44 vs. 1251 ± 30 ms, $p < .001$; Figure 1). In addition, also mean myocardial T2 times were significantly elevated in AS patients (52 ± 7 vs. 46 ± 4 ms, $p < .001$, Figure 1) and showed a moderate correlation ($r=0.5$) with native myocardial T1 values. Only small overlaps were observed for T1 as well as for T2 times between the two groups (Figure 1). 70% (n=14) of AS patients demonstrated native T1 values ≥ 1268 ms combined with T2 values ≥ 48 ms (while none of the controls exhibited this combination), whereas only 10% (n=2) of patients with T1 values ≥ 1268 ms demonstrated T2 values below the 48 ms threshold.

Conclusions: Patients with severe AS exhibit significantly elevated native myocardial T1 times, which has previously been shown to correlate with the amount of myocardial collagen. The present study, however, shows for the first time that native T1 and T2 values in parallel are significantly elevated and correlated in AS patients, pointing towards a potential role of edematous / inflammatory processes in the pathophysiology of myocardial remodeling associated with AS.

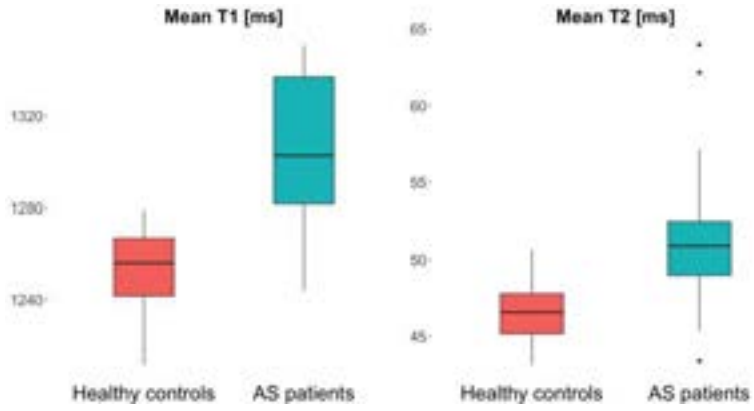

W009

Quantitative Cardiac Mechanics using In Vivo Cine DENSE, Cardiac Diffusion Tensor Imaging, and a Continuum Mechanics Model

Ilya A. Verzhbinsky[1] Luigi E. Perotti, PhD[2], Patrick Magrath, M.S.[1], Eric Aliotta, M.S.[2], Kévin Moulin, PhD[3], Daniel B. Ennis, PhD[4]

1. *University of California, Los Angeles, Los Angeles, CA*
2. *UCLA, CA*
3. *UCLA, Los Angeles, CA*
4. *Department of Radiological Sciences, University of California, Los Angeles, CA, USA., CA*

Background: Quantitative cardiac MRI biomarkers of regional function are sensitive to early changes in cardiac dysfunction. Further insight is gained when cardiomyocyte performance is directly interrogated and distinguished from the extracellular matrix response. In order to do so, our objective was to formulate a continuum mechanics (CM) model that combines *in vivo* cardiac diffusion tensor imaging (cDTI) with regional strains using displacement encoding with stimulated echoes (DENSE).

Methods: Single-slice, cardiac and respiratory triggered cDTI and time-resolved free-breathing DENSE images were acquired in healthy volunteers (N=6) after obtaining informed consent (3T Siemens Prisma). cDTI: 2x2x5mm, TE/TR=60/4000ms, b-value=350s/mm^2, 5 averages, 12 directions, in ~4min; DENSE: 2.5x2.5x8mm, TE/TR=1.04/15ms, encoding strength=0.06cycles/mm, 3 averages, 10 spiral interleaves, in ~5 min. A finite element (FE) mesh was generated using the DENSE magnitude images (Fig. 1a). cDTI and DENSE images were registered using b-splines. Diffusion tensors were reconstructed and interpolated onto the FE mesh (Fig. 1b). To assess DTI registration accuracy, cardiomyocyte helix angles (HA) were calculated and plotted as a function of wall depth before and after image registration. Time-resolved 3D Lagrangian displacements were extracted from DENSE data with an open-source post-processing tool (PPT) [Spottiswoode et al. IEEE TMI 2007] (Fig. 1c). Using FE shape functions, the discrete DENSE Lagrangian displacement field was continuously interpolated. We then computed the deformation gradient **F**, the right Cauchy-Green deformation tensor $\mathbf{C}=\mathbf{F}^T\mathbf{F}$, and its first ($I_1$) and second ($I_2$) isotropic invariants, as well as its fourth (I_4) and fifth (I_5) anisotropic invariants. We validated our CM model by comparing its circumferential strain (E_{cc}) with the ones computed using the DENSE PPT.

Results: Model Validation: There were no significant differences in the HA distributions before and after non-rigid registration ($p=0.09$)(Fig. 2a), suggesting that the non-rigid transformation preserves the HA. Global E_{cc} in the CM and PPT models showed moderate agreement (mean difference=0.018)(Fig. 2b). **Model Output:** Deformation tensor invariant maps were generated at 60 cardiac phases. At peak systole we found: $I_1 = 3.51\pm0.33$; $I_2 = 3.44\pm0.23$; $I_4 = 0.82\pm0.29$; $I_5 = 1.46\pm0.28$, (Fig. 3). I_1 and I_2 characterize the isotropic deformation and are directly linked to the extracellular matrix response, while I_4 and I_5 characterize the anisotropic deformation and are directly linked to myofiber performance.

Conclusions: We have developed a model capable of characterizing myocardial strains using both isotropic and microstructurally based invariants of the deformation tensor **C**. This technique has the potential to directly quantify myofiber performance (I_4 and I_5) and extracellular matrix response (I_1 and I_2), providing novel physiologic insight to regional cardiac performance.

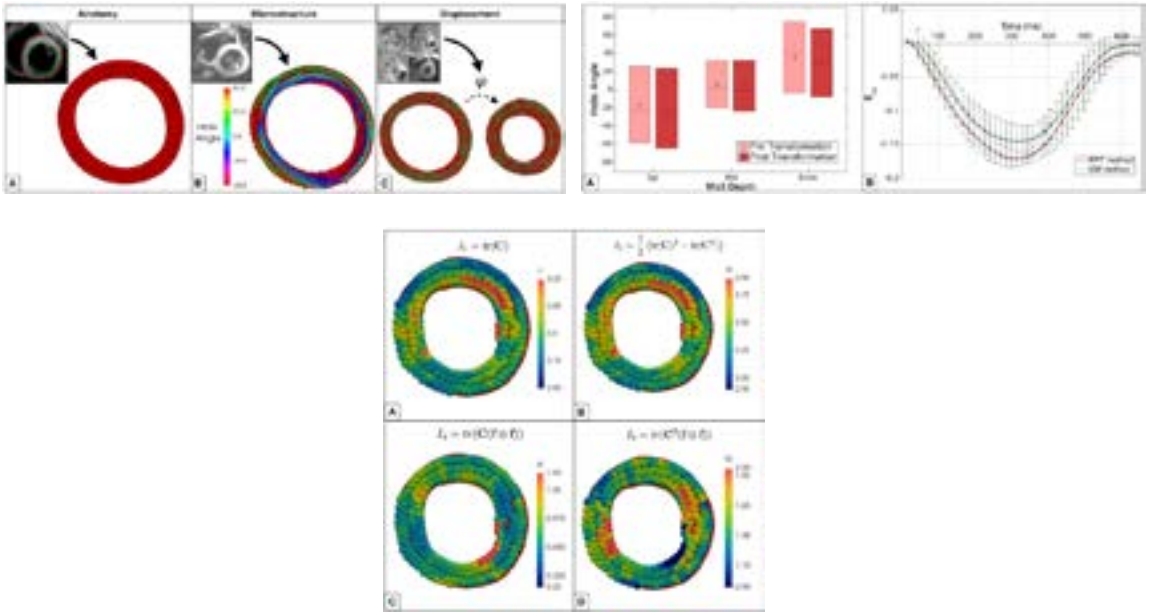

W010

MRI-Based Estimates of Passive Cardiac Mechanics Using A Finite Element Framework

Luigi E. Perotti, PhD[1] Ilya A. Verzhbinsky[2], Patrick Magrath, M.S.[2], Eric Aliotta, M.S.[1], Aditya VS. Ponnaluri, M.S.[3], Daniel B. Ennis, PhD[4]

1. *UCLA, CA*
2. *University of California, Los Angeles, Los Angeles, CA*
3. *University of California, Los Angeles, CA*
4. *Department of Radiological Sciences, University of California, Los Angeles, CA, USA., CA*

Background: Heart Failure with preserved Ejection Fraction (HFpEF) is linked to increased myocardial stiffness during passive filling. Measuring extracellular (isotropic) and cardiomyocyte (anisotropic) differences in passive stiffness is crucial to uncovering the mechanisms underlying HFpEF and diagnosing its onset and therapeutic regression. Current approaches measuring myocardial stiffness: 1) depend on ad hoc assumptions for the stress-free reference state; 2) do not consider myocardial microstructure; and 3) lead to arbitrary stiffness values due to poor problem formulation. Our objective was to overcome these limitations by identifying the most appropriate reference state, acquiring in vivo DENSE and cardiac DTI (cDTI) data, and combining them with our computational framework to robustly identify myocardial isotropic and anisotropic stiffness.

Methods: We acquired cine DENSE MRI [Aletras 1999, JMR], in vivo cDTI [Dou 2002, MRM], and intraventricular pressure in 3 swine experiments, with protocol approved by the Institutional Animal Care and Use Committee.
DENSE displacements were tracked for 2.5x2.5x8mm voxels in a series of 2D short axis slices. The DENSE signal magnitude was used to reconstruct the LV anatomy and generate a finite element (FE) mesh. The voxel displacement data was interpolated to the LV FE mesh using Laplace interpolation.

Cardiomyocyte orientations were mapped in vivo using a custom cDTI sequence [Aliotta 2016 MRM] at a resolution of 2x2x5mm and interpolated to the FE mesh using dyadic tensor interpolation.

Cardiac anatomy and displacements were synchronized with the LV pressure to identify the reference configuration for measuring myocardial stiffness.

The passive myocardial stiffness was identified by minimizing the difference between applied forces (due to the filling pressure) and internal forces computed based on DENSE displacements.

Results: The reference configuration needed to measure myocardial stiffness corresponds to end of diastasis and beginning of atrial systole. During atrial systole, intraventricular pressure and volume increase together (Fig 1). Consequently, the pressure exerts a force against the LV wall, causing its passive deformation. Starting from the identified reference configuration, we combined pressure and LV displacements measured at 5 time points during atrial systole to identify isotropic (0.76 kPa) and anisotropic (0.24 kPa) myocardial stiffness according to a non-linear, finite kinematics, material law (Fig 2).

Conclusions: We have determined that the end of diastasis is the most appropriate reference configuration to measure myocardial stiffness. Identifying this configuration is crucial since all stiffness values are measured with respect to this cardiac phase. Subsequently, we used our computational model to identify the extracellular matrix and myocyte passive stiffness. Our immediate future goal is to characterize the sensitivity of our approach to experimental errors in DENSE and cDTI data.

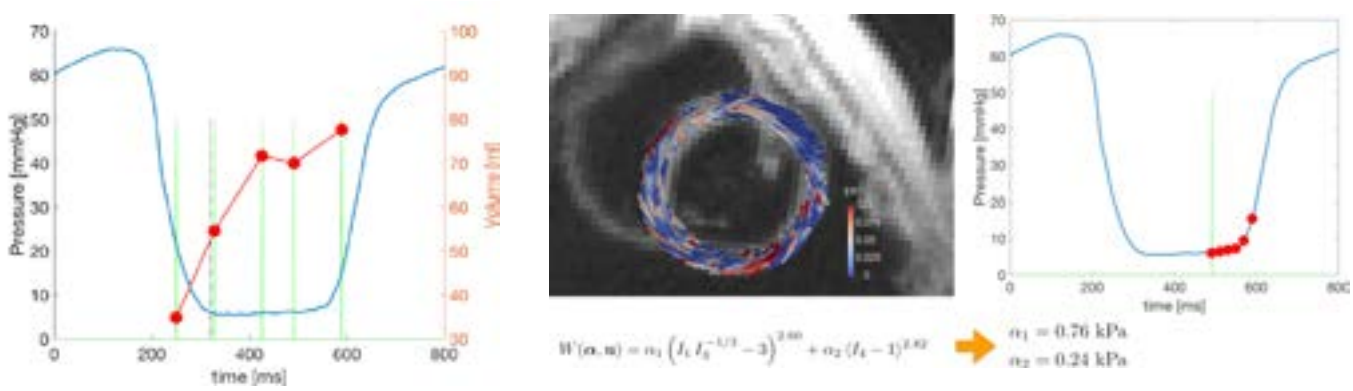

W011

Cine DENSE MRI of cardiac activation: application to cardiac resynchronization therapy

Daniel A. Auger, Ph.D[1] Kenneth C. Bilchick, MD[2], Frederick H. Epstein, PhD[2]

1. University of Virginia, Charlottesville, VA
2. University of Virginia, VA

Background: Electrical delays within the cardiac conduction system manifest as delayed mechanical activation and dyssynchrony. Cardiac resynchronization therapy (CRT) aims to restore synchrony in heart failure (HF) patients, however approximately 40% of HF CRT patients are non-responders. Pre-CRT imaging of delayed activation holds promise for guiding CRT implementation and improving response. While recent studies have assessed the time to peak strain (TPS) as a measure of cardiac activation [1], we hypothesized that the time to the onset of circumferential shortening (TOS) would correlate better with electrical activation and more accurately predict CRT response.

Methods: Data were acquired from 50 HF patients with left bundle branch block (LBBB). Cine DENSE (Displacement Encoding with Stimulated Echoes) and late gadolinium enhancement (LGE) MRI were performed on a 1.5T MRI system prior to CRT. Circumferential strain (E_{cc}) was computed from DENSE images [2, 3], and TPS was defined as the time point where E_{cc} reached its minimum. TOS was computed using an active contour guided by the E_{cc} gradient over space and time (Fig 1(A)). The circumferential uniformity ratio estimate computed with singular value decomposition (CURE-SVD) was used to quantify overall mechanical dyssynchrony, where values near 1 indicate synchrony and lower values indicate dyssynchrony [4]. The electrical activation time (Q-LV) was measured at the CRT left-ventricular (LV) lead position during the CRT procedure, and the LV lead position was identified on MR images using registration methods [5]. CRT response was defined as a 15% reduction in LV end systolic volume (LVESV) based on echocardiography performed before and 6 months after CRT.

Results: Fig 1(B, C) shows bull's eye plots of TOS and TPS, respectively, for a HF-LBBB patient. Fig. 2 shows the correlations of TOS vs. QLV (A, B) and TPS vs. QLV (C, D). TOS correlated better than TPS with Q-LV both in regions of scar and non-scar (Fig. 2). Tables 1 and 2 show results of multivariable linear regression models for TOS/QRS and TPS for predicting CRT response, with adjustment for CURE-SVD and scar at the LV lead position. TOS/QRS was significantly associated with post-CRT LV reverse remodeling ($p < 0.05$), whereas TPS was not ($p = 0.49$).

Conclusions: In HF-LBBB patients, TOS has a better correlation than TPS with the electrical activation time and TOS/QRS at the LV lead position is an independent predictor of LV reverse remodeling whereas TPS is not. Cine DENSE TOS mapping detects regions with late electrical activation and holds promise for identifying optimal LV lead locations for CRT and potentially decreasing the non-responder rate. **References:** [1.] Tanaka et al. Am J Cardiol, 2010; 105:235-42 [2.] Spottiswoode et al. IEEE TMI 2007; 26:15-30. [3.] Spottiswoode et al. MIA 2009; 13:105–115. [4.] Ramachandran et al Radiology 2015; 275(2): 413-20. [5.] Parker et al. PACE, 2014; 37:757-67

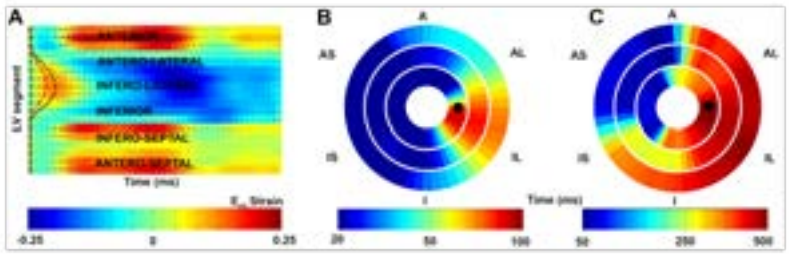

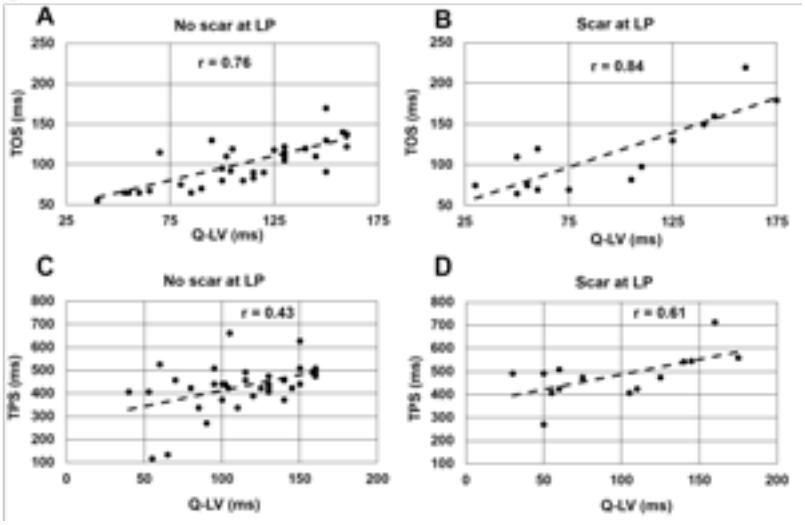

Table 1: Model for Percent Change in LVESV Post-CRT with TOS

Standardized Coefficient	P-Value	t Value	Standard Error	Beta Coefficient	Covariate
0	0.030	-2.24	0.116	-0.259	**Intercept**
0.442	0.0004	3.82	0.123	0.470	**CURE-SVD**
-0.331	0.0046	-2.98	0.145	-0.433	**TOS/QRS Duration**
0.242	0.042	2.09	0.0609	0.127	**LV Pacing Site in Scar**

*R^2=0.44 for model

Table 2: Model for Percent Change in LVESV Post-CRT with TPS

Standardized Coefficient	P-Value	t Value	Standard Error	Beta Coefficient	Covariate
0	0.011	-2.66	0.160	-0.426	**Intercept**
0.481	0.0004	3.84	0.133	0.511	**CURE-SVD**
-0.086	0.49	-0.70	0.000286	-0.000201	**TPS**
0.229	0.079	1.80	0.0671	0.120	**LV Pacing Site in Scar**

*R^2=0.34 for model

W012

Improved free-breathing cine DENSE using image-based navigators with motion compensation and compressed sensing: development and initial evaluation

Xiaoying Cai, BS[1] Yang Yang, PhD[2], Michael Salerno, MD, PhD[2], Christopher M. Kramer, MD[2], Kenneth C. Bilchick, MD[2], Frederick H. Epstein, Ph.D.[2]

1. *University of Virginia, Charlottesville, VA*
2. *University of Virginia, VA*

Background: Cine DENSE images are typically acquired during breathholding, however a reliable free-breathing method would be useful for many patients. Conventional diaphragm-based navigators (dNAVs) have been used, however image quality is variable. We investigated cine DENSE with image-based navigators (iNAVs), motion correction, and compressed sensing (CS).

Methods: A cine DENSE sequence was modified to use variable density spirals, golden angle rotation, and outer volume suppression. A total of 13 subjects (7 volunteers and 6 heart failure patients) were scanned using a 3T system (Skyra, Siemens). Mid-ventricular short-axis slices were acquired during free-breathing using: field-of-view of 160-200 mm, 6 interleaves per image, 2 interleaves per heartbeat, temporal resolution of 30 ms, matrix size of 70x70, 2-point phase cycling, and 4 averages, with a total scan time of 72 heartbeats. dNAVS were collected each heartbeat and used for a conventional dNAV reconstruction. Using the same raw data, we performed iNAV processing and reconstruction. For the iNAV method, iNAV images were reconstructed each heartbeat and image registration was applied to them to measure respiratory movement of the heart. To achieve suppression of the artifact-generating T1-relaxation echo inherent to DENSE, the iNAV algorithm gave high priority to matching respiratory position and direction (inhalation vs. exhalation) to spiral interleaf pairs with opposite polarity of the stimulated echoes (phase-cycling pairs), and subtraction of these matched interleaves was performed to cancel the T1-relaxation echo. After the subtraction, respiratory motion was re-estimated and k-space data were phase-corrected. Interleaves that still had high residual T1-relaxation energy were rejected and final images were reconstructed using CS. Since DENSE utilizes phase-reconstructed images, we compared the iNAV and dNAV reconstructions by calculating phase quality.

Results: Example magnitude (A-D) and phase images (E-L) and x-y-combined phase quality maps (M-P) are shown in Figure 1. The top panel shows an end-systolic frame from a heart failure patient and the bottom panel shows a late-diastolic frame from a volunteer. The iNAV method had less striping artifacts (red arrows) and higher phase quality (N,P vs. M,O). As shown in Figure 2, phase quality of all datasets by iNAV is significantly higher than that of dNAV in both systole (0.853±0.007 vs. 0.837±0.007, $p < 0.001$) and diastole (0.823±0.008 vs. 0.780±0.013, $p < 0.001$).

Conclusions: The proposed iNAV method improves the quality of free-breathing cine DENSE phase images by optimizing the subtraction of phase-cycled interleaf pairs with stimulated echoes of opposite polarity, thereby minimizing the residual artifact-generating T1 relaxation echo. CS regularization may also contribute to the higher phase quality. These methods hold promise for achieving reliable high-quality free-breathing MRI myocardial strain imaging.

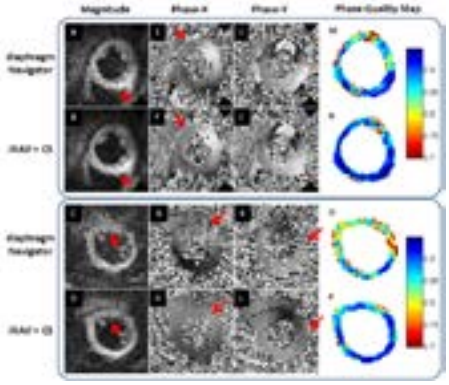

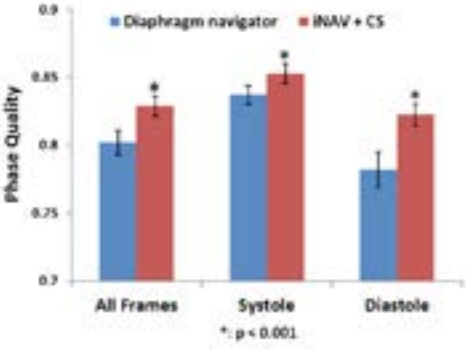

W013

Simulating the Effect of Motion Induced by Systolic Variability in cDTI using STEAM

Andrew D. Scott, PhD[2]Katie Spencer[1], Pedro F. Ferreira, PhD[3], Sonia Nielles-Vallespin, PhD, MSc[4], Dudley J. Pennell, MD[5], David N. Firmin, PhD[6]

1. *University of Manchester, England, United Kingdom*
2. *NIHR Cardiovascular Biomedical Research Unit, The Royal Brompton Hospital, Sydney Street, London, SW3 6NP, UK, England, United Kingdom*
3. *Cardiovascular Biomedical Research Unit, The Royal Brompton Hospital, Sydney Street, London, SW3 6NP, UK, England, United Kingdom*
4. *NIH, MD*
5. *Royal Brompton Hospital and Imperial College, London, England, United Kingdom*
6. *NIHR Cardiovascular Biomedical Research Unit, Royal Brompton Hospital, England, United Kingdom*

Background: The stimulated echo-acquisition mode (STEAM) sequence is a robust and reliable technique for cardiac diffusion tensor imaging (cDTI)[1,2]. However, due to the fixed delay time between the R-wave and application of the diffusion gradients, variability in the systolic timing is a potential source of motion-induced signal loss. Considering both contractile and rotational motion, we simulate errors in mean diffusivity (MD), fractional anisotropy (FA), helical angle (HA) and second eigenvector orientation (E2A) due to systolic variability.

Methods: An existing simulation of short-axis cDTI at end systole[3] (FA=0.42, MD=0.9x10^{-3}mm^2/s, E2A=60^o, HA=-60^o–60^o) was modified to include the effects of motion. Published mid-ventricular strains and rotations[4] were used to create radial and circumferential displacement and velocity-time curves. Normally distributed random beat-to-beat variations in the systolic period of the heart were generated. The systolic variability (SV) was translated into differences in displacements *between* the diffusion encoding gradients (separated by 1000ms) and differences in velocities *during* the two gradients (duration 1.8ms). Transmurally constant radial strain with a fixed epicardium was assumed for contraction and a transmural linear increase in rotation across the myocardium (1.4x larger at endocardium) was simulated. The effects of these movements on the simulated diffusion encoded images were calculated beforecalculating the diffusion tensor and parameter maps. Simulations used b=750s/mm^2, 8 averages, signal-to-noise of 20 per image and 6 diffusion-encoding directions.

Results: Figure 1 shows the effects of contractile motion between and during the diffusion encoding gradients, on the absolute error in the parameters. Figure 2 shows the equivalent results for rotations. In both cases, intra-voxel dephasing due to motion between the gradients causes errors exceeding those caused by image noise at SV >20ms. Figure 3 shows the parameter bias introduced by contractile motion. Increasing SV results in an underestimation of MD, E2A and FA.

Conclusions: The main contributor to parameter error, in relation to SV, is displacement of the heart between the application of the gradients. The additional contribution from motion during the gradients is minimal. Additionally, the contribution to error from contractile motion is approximately double that from rotation in this simple model. For a typical SV of up to ±20ms standard deviation[5], these two types of motion have an acceptably low impact on cDTI parameters.

References

1. Reese: MRM. 1994,doi:10.1002/mrm.1910340603

2. Nielles-Vallespin: JCMR. 2012,doi:10.1186/1532-429X-14-S1-P238

3.Scott: NMR in Biomedicine. 2015,doi:10.1002/nbm.3500

4.Zhong: MRM. 2010,doi:10.1002/mrm.22503

5.Carrasco-Sosa: Computing in Cardiology.2010.

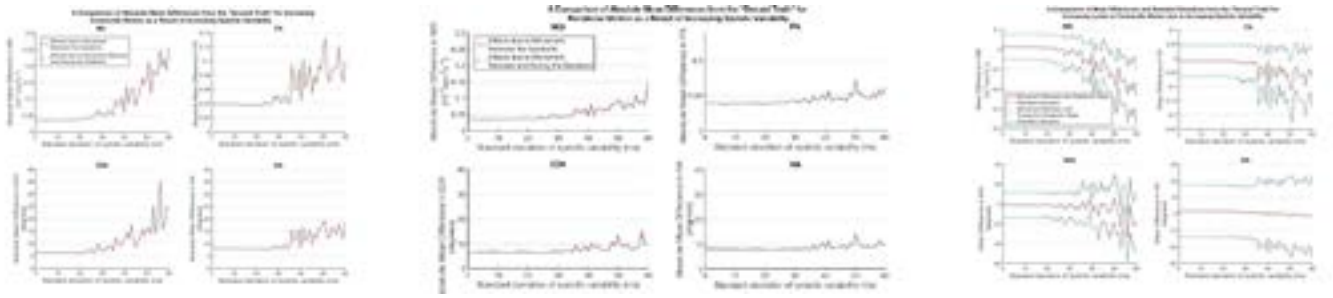

W014

Nonlinear Fitting Improves Precision in Biexponential Joint T2 and Apparent Diffusion Coefficient Mapping in the Heart

Eric Aliotta, M.S.[1] Kévin Moulin, PhD[2], Daniel B. Ennis, PhD[3]

1. *UCLA, CA*
2. *UCLA, Los Angeles, CA*
3. *Department of Radiological Sciences, University of California, Los Angeles, CA, USA., CA*

Background: The diffusion weighted imaging (DWI) signal is typically modeled as mono exponential: $S(b) = S_0 e^{-b*ADC}$ [Eqn 1], where b (b-value) is the diffusion encoding sensitivity, ADC is the underlying apparent diffusion coefficient and S_0 is the signal with b=0. ADC is typically estimated from acquisitions with multiple b-values (with a fixed TE) by performing a linear fit (LF) to the natural log of Eqn 1. Previous work has shown that T_2 can be simultaneously estimated without increasing scan time by varying TE between acquisitions and fitting a bi-exponential model (T_2+ADC): $S(b,TE) = S_0 e^{-TE/T2} e^{-b*ADC}$ [Eqn 2]. (*Aliotta et al*, JCMR 2015). However, fitting an additional parameter introduces noise and reduces precision. The purpose of this study was to apply a non-linear fit (NLF) to the T_2+ADC signal model and evaluate the improvement in T_2 and ADC precision.

Methods: After obtaining informed consent, free-breathing T_2+ADC mapping was performed at 3T (Siemens Prisma) in a single mid-ventricular short-axis slice in healthy volunteers (N=8) using spin echo DWI with motion compensated (M_1=M_2=0) convex optimized diffusion encoding (CODE-M_1M_2) (*Aliotta et al,* MRM 2016) with b=350s/mm^2 and 3 directions (2.0x2.0x5.0mm, TE=65ms, TR≥4s). Ten signal averages were acquired (scan time ~5min) with TE varied between b=0 repetitions: TE_1=25ms (x3 averages), TE_2=65ms (x7 averages). T_2 and ADC maps were then jointly reconstructed from Eqn 2 using both LF and NLF. For comparison, ADC maps were also generated with a conventional DWI reconstruction (b=350s/mm^2, TE=65ms, LF). For each subject and fitting method, mean T_2 (μ_{T2}), T_2 standard deviation (σ_{T2}), mean ADC (μ_{ADC}) and ADC standard deviation (σ_{ADC}) were calculated within the LV.

Results: Example T_2 and ADC maps generated using both fitting algorithms are shown in Figure 1. The fitting algorithm had no significant impact on the population mean or variance of the T_2 maps (LF-μ_{T2}=37.7±3.8ms vs. NLF-μ_{T2}=37.7±3.8ms, p=N.S.; LF-σ_{T2}=6.9±1.1ms vs. NLF-σ_{T2}=6.9±1.1ms, p=N.S.). NLF reported lower (but not significant) mean ADC values (LF-μ_{ADC}=1.45±0.1mm^2/ms vs. NLF-μ_{ADC}=1.38±0.1mm^2/ms, p=N.S.), and significantly lower ADC variance (LF-σ_{ADC}=0.5±0.1mm^2/ms vs. NLF-σ_{ADC}=0.4±0.1mm^2/ms, p=0.04) than LF (Figure 2). With DWI, mean ADC was not significantly different from NLF or LF (μ_{ADC}=1.38±0.1mm^2/ms, p=N.S.), whereas ADC variance was significantly lower than LF (σ_{ADC}=0.4±0.1mm^2/ms, p=0.04) but not different from NLF (p=N.S.).

Conclusions: While T_2+ADC with a linear fit increased ADC variance compared with conventional DWI, the use of a nonlinear fit reduced ADC variance to a level equivalent to DWI (Figure 2). This indicates that T_2 maps can be generated in addition to ADC with little or no cost using joint T_2+ADC.

http://www.ConferenceAbstracts.com/uploads/cfp2/attachments/LDFAIBDN/LDFAIBDN--225476-1-ANY.pdf

http://www.ConferenceAbstracts.com/uploads/cfp2/attachments/LDFAIBDN/LDFAIBDN--225476-2-ANY.pdf

W015

Bringing the T1 mapping sequences together: A study of the T2 and magnetization transfer effects in ex vivo pig hearts

Tarik Hafyane, MSC[1] Catherine Duquette[2], François-Pierre Mongeon, MD[1], Julien Cohen-Adad, PhD[3], Nikola Stikov, PhD[1]

1. Montreal Heart Institute, PQ, Canada
2. École Polytechnique de Montréal, Montréal, PQ, Canada
3. École Polytechnique de Montréal, PQ, Canada

Background: To fully understand native T1 values obtained with inversion recovery (MOLLI, ShMOLLI and IR TSE) or saturation recovery (SASHA) sequences, one needs to consider the T2 relaxation time and magnetization transfer effects. Previous work based on Bloch-McConnell simulations has demonstrated that T1 measured by saturation-recovery single-shot acquisition is insensitive to T2 and magnetization transfer effects. We used ex-vivo pig hearts to demonstrate that the two effects can explain the differences between inversion and saturation recovery T1 mapping sequences.

Methods: Three explanted pig hearts kept in saline solution were imaged right after explantation with a gold-standard inversion-recovery spin-echo (IR-TSE) sequence, and with MOLLI, ShMOLLI and SASHA on a Magnetom Skyra 3T scanner. IR-TSE was implemented with 5 TIs 33-3000ms; TR/TE=5s/12ms, flip angle=90°, turbo factor=7. MOLLI 5(3)3 sequence was implemented with TE/TR=1.07/275 ms, minimum TI=100ms; TI increment=80 ms; flip angle=35°. ShMOLLI was implemented with 7 SSFP readouts; TE/TR=1.07/275 ms, minimum TI=100ms, TI increment=80 ms, flip angle=35°. SASHA was implemented with 11 SSFP readouts; TE/TR=1.07/912 ms, minimum TI=82 ms, TI increment=79 ms, flip angle=70°. T2 mapping was performed using a T2-prepared TrueFISP sequence. Magnetization transfer ratio was computed using CINE b-SSFP acquisitions with low (5°) and high (45°) flip angles as MTR=(S_5°-S_{45}°)/S_5°. T1 measures from a mid ventricular slice were performed by manually delineating the endocardial and epicardial contours of the LV myocardium. Absolute error was computed as the difference between MOLLI, ShMOLLI, SASHA T1 values and the gold standard IR-TSE. Simple and multivariate regression analysis with T2 and MTR as predictor variables and T1 error as dependent variable were applied.

Results: Inversion recovery sequences showed a significant correlation between the absolute error and the MTR values, with r=0.82 for MOLLI (,p < 0.0009) and r=0.79 for ShMOLLI (,p=0.001). The correlation between SASHA and MTR was low (r=0.24, p=0.18) and not significant (Figure 1). Adding T2 to the multivariate linear regression model, the correlation between T1 and MTR increases for MOLLI (r=0.95, p < 0.00015), ShMOLLI (r=0.93, p=0.0003), and SASHA (r=0.39, p=0.23). However, SASHA correlations were not statistically significant, neither for the simple nor for the multivariate linear regression analysis (Figure 2).

Conclusions: Our results demonstrate that inversion recovery sequences are sensitive to changes in magnetization transfer and T2. These results help understand the lower native T1 values obtained by inversion recovery compared to saturation recovery sequences.

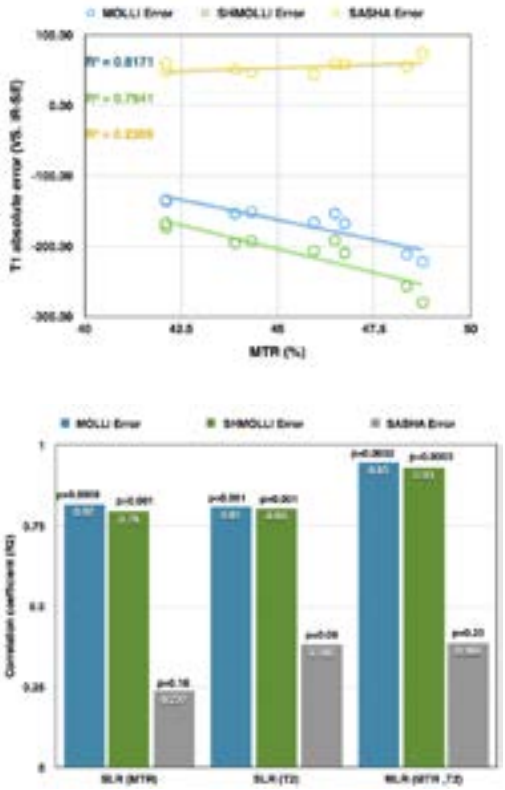

W016

The Influence of the Analysis Technique on Myocardial T1 Measurement Using CMR

El-Sayed H. Ibrahim, PhD[2] Muhammed Hammad[1], Ayman Khalifa, PhD[1]

1. Helwan University, Al Qahirah, Egypt
2. University of Michigan, Ann Arbor, MI

Background: CMR T1 mapping is a valuable technique for myocardial tissue characterization. Nevertheless, various factors can influence the analysis technique and the resulting T1 measurements. These factors include the signal calculation method (signal average (AVG), median (MED), or pixel-wise mapping (MAP)), signal-to-noise ratio (SNR), and size and location of the analyzed region-of-interest (ROI). The effect of these factors on T1 measurement is investigated in this study using numerical and calibrated phantoms.

Methods: A numerical phantom was created to represent a short-axis left-ventricular slice with T1 of 1060ms (~myocardium T1-value at 3.0T). Different levels of noise were included in the simulation to create SNR ranging from 44dB to 7dB. A commercial NIST calibrated phantom with T1 values ranging from 22.6ms to 2048ms (Figure-1) was scanned on a 3.0T MRI scanner using the Modified-Lock-Locker Inversion-recovery (MOLLI) sequence. In-house software was used to estimate T1 of the numerical and calibrated phantoms using different signal calculation methods (AVG, MED, MAP) and Levenberg–Marquardt algorithm. A 1-cm^2 circular ROI was placed at the center of each tube to measure its T1 value. Further, two smaller (0.25-cm^2) circular ROIs, one placed at the tube's center and the other placed closer to the tube's edge, were used in the analysis. Correlation analysis was conducted between T1 values measured by different methods.

Results: Figure-2 shows estimated T1 values for different signal calculation methods in the numerical phantom, and Figure-3 shows percentage measurement error versus SNR. The AVG, MED, and MAP methods resulted in the following T1 ranges: 1060-1093ms, 1060-1085ms, and 1060-1190.3ms, respectively, resulting in percentage measurement error in the following ranges: 0–3.1%, 0–2.3%, and 0–12.28%, respectively, and the three methods finally reached the correct T1 value (1060ms) at SNR of 27.8dB, 17.8dB, and 37.8dB, respectively. The MED method resulted in the smallest measurement error at low-SNR levels, followed by the AVG and then the MAP methods. The large ROI resulted in slightly better correlation between the accurate and estimated T1 values than did the small ROI. The ROI placed closer to the tube's edge resulted in worse T1 correlations (R^2=0.65-0.75) compared to when the ROI was placed at the tube's center (R^2=0.99).

Conclusions: The MED signal calculation method results in smaller T1 measurement error compared to the AVG and MAP methods, especially in images with low SNR. Further, using a large ROI placed at the center of the analyzed region is necessary for accurate T1 estimation.

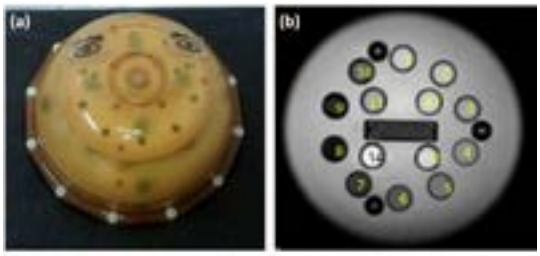

Fig 1. (a) Picture and (b) T1-weighted image of the T1-calibrated phantom with different T1 values ranging from 22.6 to 2048 ms.

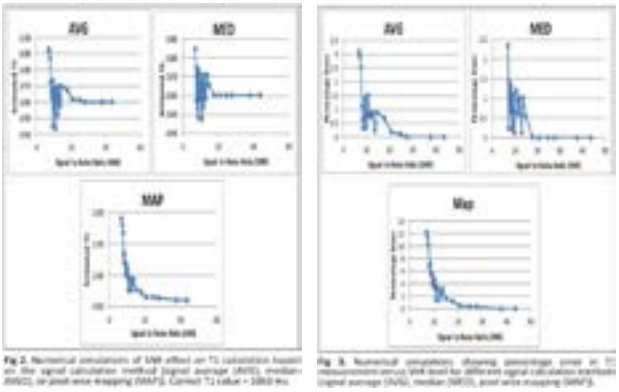

W017

CMR Tissue Characterization for Identifying Obesity Phenotypes in Metabolic Syndrome

Jadranka Stojanovska, MD[1], El-Sayed H. Ibrahim, PhD[2]Thomas Chenevert, PhD[1]

1. *University of Michigan, MI*
2. *University of Michigan, Ann Arbor, MI*

Background: The tissue properties of epicardial and intramyocardial fat in obesity and metabolic-syndrome (MetS) are poorly understood. Emerging evidence suggests that altered fat metabolism and "browning" of white adipose may play a vital role in cardiovascular disease development. The purpose of this study is to identify the feasibility of CMR in identifying tissue fat characteristics in different fat depots, correlated with fat phantom, along with related cardiovascular functional parameters in subjects with and without MetS.

Methods: The study included four normal-weight healthy subjects, two overweight/obese subjects without MetS, and two MetS subjects. All subjects underwent CMR imaging on 3T scanner. Cine, multi-echo Dixon (mDixon), mitral flow, and LGE images were acquired to measure LV function, fat/water quantification, diastolic function (early-to-atrial filling ratio; E/A), and myocardial scar, respectively. Imaging signatures of obesity phenotypes were assessed using water-to-fat ratio (WFR) and %fat in the subcutaneous, epicardial, paraspinal, and myocardial fat-depots. Further, three normal subjects (one normal-weight, one overweight and one obese) were imaged using both mDixon and strain-encoding (SENC) to assess myocardial contractility patterns compared to different fat depositions.

Results: Compared to healthy subjects(Fig-1), MetS subjects had significantly larger epicardial fat-volume (1677±116cm^3 vs. 137±35cm^3), higher epicardial %fat (73±3.5% vs. 52±10%), lower epicardial WFR (0.31±0.05 vs. 0.97±0.3), and higher epicardial-to-subcutaneous %fat ratio (0.97±0.06 vs. 0.62±0.1). Obese subjects without MetS and subjects with MetS had similar epicardial and subcutaneous %fat. Compared to MetS, healthy subjects had significantly different epicardial %fat (52±10%), but similar subcutaneous %fat (82±7%) (Fig-2). Myocardial %fat in healthy and obese subject were minimal, while it was twice more prevalent in MetS (8±2% vs. 16±2%). Similarly, paraspinal muscle %fat was minimal in healthy and obese subjects without MetS, while it was three-times higher in MetS (10±4% vs. 28±10%). LV systolic function was normal in all subjects. Healthy and obese subject without MetS showed normal diastolic function (E/A>1). However, MetS subject had diastolic-dysfunction (E/A < 1). Patchy LGE areas were seen only in MetS, where myocardial fat foci correlated with LGE. Finally, %fat mDixon images correlated well with %fat phantom images from the three healthy volunteers. SENC analysis revealed normal myocardial contractility in the same volunteers regardless of fat deposition in absence of MetS(Fig-3).

Conclusions: CMR tissue characterization allows for assessment of fat tissue properties in different fat-depots by quantifying %fat. These measurements provide unique biosignatures for identifying MetS development, which would allow for earlier intervention and improved outcome.

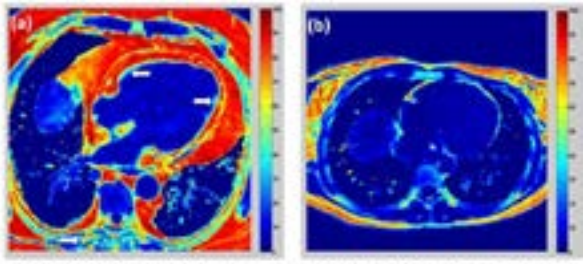

Fig 1. Color-coded mDixon images showing thorax %fat (blue = 0% fat; red = 100% fat) in (a) patient with MetS and (b) healthy volunteer. The MetS patient shows >80% fat in the epicardial, extrapericardial, and subcutaneous tissues, whereas the myocardium and paraspinal muscles (white arrows) show foci of %fat (light blue to yellow color). In comparison, the healthy subject shows %fat (color) difference between subcutaneous (red color) and epicardial depots (green to yellow color). Note blue color of the myocardium and paraspinal muscles in the healthy subject.

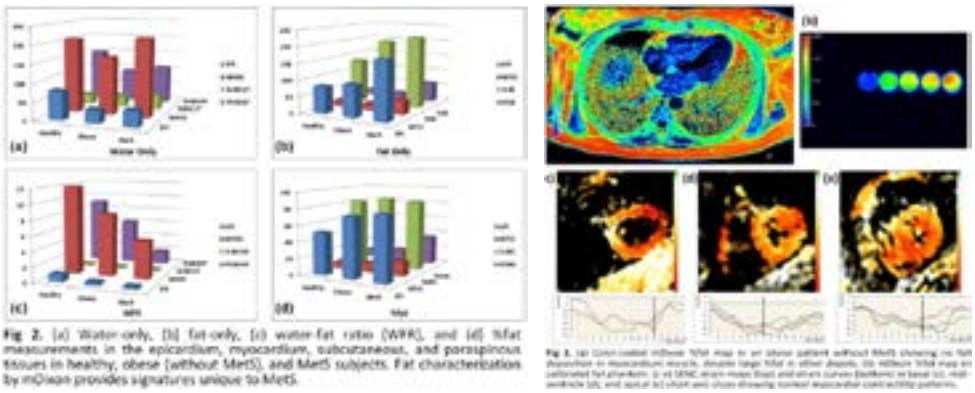

Fig 2. (a) Water-only, (b) fat-only, (c) water-fat ratio (WFR), and (d) %fat measurements in the epicardium, myocardium, subcutaneous, and paraspinous tissues in healthy, obese (without MetS), and MetS subjects. Fat characterization by mDixon provides signatures unique to MetS.

W018

Bright-blood T2STIR-bSSFP has Higher Diagnostic Accuracy Than the Bright-blood T2 pre-bSSFP for Assessment of Area-at-risk in Acute Myocardial Infarction: A New Proposed Bright-blood T2-weighted MRI

Dan Yang, msci[1], Wei Cheng, msci[1] Yanjie Zhu, Ph.D.[2], Yiu-Cho Chung, Ph.D.[3], Yu-Cheng Cheng, MD[4]

1. *West China Hospital,Sichuan University, Sichuan, China (People's Republic)*
2. *shenzhen insitutes of Advanced Technology,Chinese Academy of Science, Guangdong, China (People's Republic)*
3. *Shenzhen Institutes of Advanced Technology, Chinese Academy of Sciences, Guangdong, China (People's Republic)*
4. *West China Hospital ,Sichuan University, Sichuan, China (People's Republic)*

Background: T2-Weighted MRI reveals myocardial edema and enables estimation of the ischemic area at risk in patients with acute myocardial infarction(MI),and dark blood STIR TSE(STIR-TSE) is commonly used. However, dark-blood T2-Weighted MRI may underestimate area at risk and myocardial salvage, Bright-blood T2 weighed has higher diagnostic accuracy than dark-blood. In this study we compared the diagnostic accuracy of a novel bright-blood T2-Weigted by Zhu et al. with single-shot T2-prepared bSSFP(T2p-bSSFP) in one heartbeat.

Methods: A breath-hold, bright-blood T2-weighted, single-short T2-prepared bSSFP(T2p-bSSFP) and a new bright-blood T2-weighted sequence ,which consists of a preparation called"T2-STIR" and a single-shot bSSFP were used to depict the area at risk in 9 consecutive acute MI patients (bright-blood sequences parameters: TR=2.6ms,flip angle=60°, base resolution=256,GRAPPA rate 2, TE_{prep}= 60ms, TI=125ms for T2STIR-bSSFP).Infarct size was measured on gadolinium late contrast enhancement images. A breath-hold dark blood short tau inversion recovery sequence(STIR) –turbo spin echo(TSE) ,T1 and T2 maps were also acquired for better characterize edema. All the sequence mentioned above acquired at the identical locations.T1,T2 value at the remote myocardium and edema region, area-at-risk , infarction size, and CNR were acquired. Paired t test between area-at risk and infarction size.

Results: Compared with T2pre-bSSFP, consensus agreements independent observers for identification of myocardial myocardium were higher with T2STIR-bSSFP when evaluated per patient ($P < 0.001$) and per segment ($P < 0.001$). There was statistical significance between the infarction size and area-at-risk by the new bright-blood T2STIR-bSSFP sequence(26.4±2.2% vs. 36.7±3.3% ,$P = 0.001$), however, bright-blood T2pre-bSSFP underestimated the area-at-risk (25.3±4.5%, $P= 0.795$) (Fig1). Dark-blood STIR-TSE revealed false-negative in 4 patients. the CNR between edema region and remote myocardium in T2STIR-bSSFP is about 1.3-3.3 times higher than that of T2pre-Bssfp($P = 0.007$)

Conclusions: The new bright-blood T2STIR-bSSFP sequence has higher diagnostic accuracy than the bright-blood T2pre-bSSFP. Additionally , bright-blood T2pre-bSSFP may underestimated the area-at-risk

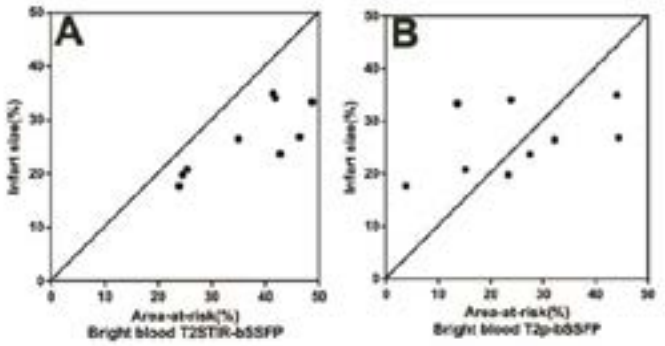

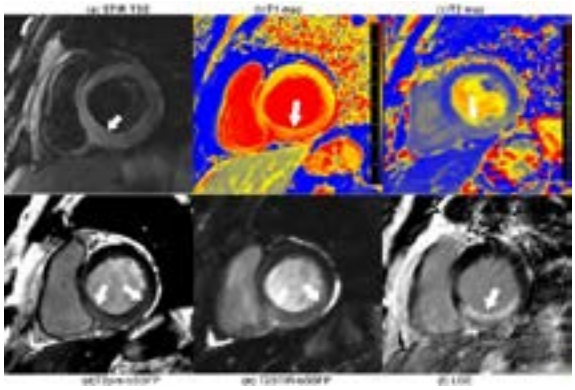

W019

The OS Module: Development and testing of a diagnostic tool that allows for time-efficient analysis of oxygenation-sensitive cardiovascular magnetic resonance.

Thomas Bertrand, B.Sc. (Hons), M.Sc. Student[1] Estee Lee, BSc Electrical Engineering, MSc Biomedical Engineering[2], Philipp Barckow[3], Qiao Wei, PhD[4], Kady Fischer, BHSc[5], Dominik P. Guensch, MD[6], Giulia Vinco, MD[7], Julie Lebel[8], Elizabeth Hillier, B.Sc., M.Sc. Student[9], Matthias G. Friedrich, MD[7]

1. *MUHC, Montreal, PQ, Canada*
2. *Circle Cardiovascular Imaging Inc., AB, Canada*
3. *Circle Cardiovascular Imaging Inc., Berlin, Berlin, Germany*
4. *Circle Cardiovascular Imaging Inc., Calgary, AB, Canada*
5. *McGill University Health Center, Montreal, PQ, Canada*
6. *Department of Anesthesiology and Pain Therapy / Institute for Diagnostic, Interventional and Pediatric Radiology, Bern University Hospital, Inselspital, University of Bern, Switzerland, Bern, Bern, Switzerland*
7. *McGill University Health Centre, PQ, Canada*
8. *Research Institute of the McGill University Health Center, Lachine, PQ, Canada*
9. *McGill University, Montreal, PQ, Canada*

Background: Oxygenation-Sensitive Cardiovascular Magnetic Resonance (OS-CMR) imaging is a non-invasive imaging technique that allows for assessing changes of myocardial oxygenation during vasoactive stimuli based on the BOLD effect of hemoglobin molecules. Similar to injected pharmacological vasodilators, breathing maneuvers such as hyperventilation followed by a long breath-hold lead to coronary vasodilatation and therefore to a strong change of myocardial oxygenation that is detected by CMR. Yet, the analysis of myocardial oxygenation requires time-consuming procedures, involving different post-processing analysis software and lacking clinical practicality. Thus, there is the need for a tool that integrates simplified scientific reports and a quick visual output. In collaboration with Circle Cardiovascular Imaging Inc. (cvi42), the aim was to develop and test a diagnostic tool that performs a rapid analysis of the myocardial oxygenation response during breathing maneuvers.

Methods: Features were developed to allow for quantitative and visual analysis of the myocardial oxygenation response during the vasoactive breathing maneuvers. The module was tested with coronary artery disease patients to demonstrate the feasibility of the analysis using the new features. More intensive testing will be performed to assess whether the tool improves analysis time and visual interpretation. Inter and intra-reader variability of the module will be tested as well as its accuracy by comparing results of automated and manual analyses.

Results: The current version includes automated analysis procedures, graphical parametric recovery curves for customizable myocardial segments and parameters describing dynamic oxygenation response output as a polar map. The myocardial oxygenation response (MORE) was automatically calculated from images acquired during the breathing maneuvers. The polar map (Figure) shows that healthy myocardium (red) could easily be distinguished from myocardium with an oxygenation abnormality (blue) perfused by coronary arteries with significant stenosis (>50% diameter). Initial observations from readers suggest that evaluation time is reduced. Detailed time improvements and inter- and intra-reader analyses are ongoing.

Conclusions: For the evaluation of OS-CMR images acquired during a vasoactive test, automated post-processing significantly reduces analysis time and may improve the interpretation of cardiovascular diseases. The module may significantly increase the clinical feasibility of OS-CMR in a clinical high-throughput setting. A needle free and cost-effective assessment of coronary vascular function will allow for a wider distribution of dynamic coronary vascular tests combining breathing maneuvers and OS-CMR. Further development and testing of the tool are ongoing.

W020

Cardiac viability in the peri-infarct region quantified by T1 mapping following manganese-enhanced MRI (MEMRI) is associated with LV remodeling post-myocardial infarction (MI)

Yuko Tada, MD, PhD[1] Shahriar Heidary, MD, FACC[2], Atsushi Tachibana, RT, MS[3], Hiromi Sano, RT, MT[3], Evgenios Neofytou, MD[2], Rajesh Dash, MD, PhD[3], Joseph Wu, MD, PhD[3], Phillip Yang, MD[3]

1. *Stanford University School of Medicine, Palo Alto, CA*
2. *Stanford University, Stanford, CA*
3. *Stanford University School of Medicine, CA*

Background: Peri-infarct region (PIR), containing injured but viable myocardial cells may play an important role in repairing and remodeling process following myocardial infarction. Accurate quantification of viability based on manganese-specific uptake by the calcium-channels in the metabolically active cardiomyocytes could be more sensitive than the evaluation of cardiac fibrosis and extracellular volume (ECV) fraction to predict future LV remodeling. We quantified myocardial viability in the infarct core (IC) and PIR by post-MEMRI T1 mapping and examined its association with cardiac remodeling following MI and compared to native T1 mapping and ECV values.

Methods: Anterior MI was induced in 15 female swine (30-57kg) by 60 minutes balloon occlusion at the proximal LAD and MRI (GE Signa, 3T) was performed four weeks later. Manganese enhanced MRI (MEMRI) (0.7ml/kg of EVP1001-1) and delayed gadolinium enhanced MRI (DEMRI) (0.2mmol/kg of Gd-DTPA) were acquired on left ventricular (LV) short axis. Areas with DEMRI positive (injury) were divided into non-viable MEMRI negative infarct core (IC) and viable MEMRI positive PIR territories. T1 mapping was performed before contrast, post-manganese and post-gadolinium on the same short axis using smartT1 map sequence. T1 values and ECV fraction were calculated in each territory.

Results: Injury, IC, and PIR size of 15 swine (mean LVEF 27.2±8.8%) were 30.2 ±6.2%, 21.8±5.6%, 8.4±5.9% of total LV mass, respectively. Native T1 value in PIR (1528.7±78.7ms) was significantly lower than the IC T1 (1633.7±89.2ms, p=0.001) and higher than the remote region (RR) T1 (1406.4±37.9ms, p < 0.0001) (figure 1). Post-manganese T1 values demonstrated higher viability in PIR (1135.3±99.6ms) compared to IC (1270.0±138.7ms, p=0.005) and lower viability than the RR (956.7±138.1ms, p=0.0001). ECV in PIR (0.39±0.09) showed significant ECV expansion compared to the RR (0.29±0.08) but comparable to the IC ECV (0.43±0.08, ns). Cardiac viability in PIR was significantly associated with LVEF (p=-0.65, p=0.006) and LVEDV (r=0.65, p=0.006) (figure 2). Cardiac viability in the RR was also significantly associated with LVEDV (r=0.55, p=0.03). However, native T1 values and ECV did not show significant relationship with LVEDV or LVEF.

Conclusions: Cardiac viability in PIR quantified by post-manganese T1 mapping correlates with cardiac remodeling post-MI. Post-MEMRI T1 mapping is more sensitive than the evaluation of cardiac fibrosis or ECV expansion to predict future LV remodeling. Viable but injured cardiomyocytes in the PIR may have a critical role in LV remodeling.

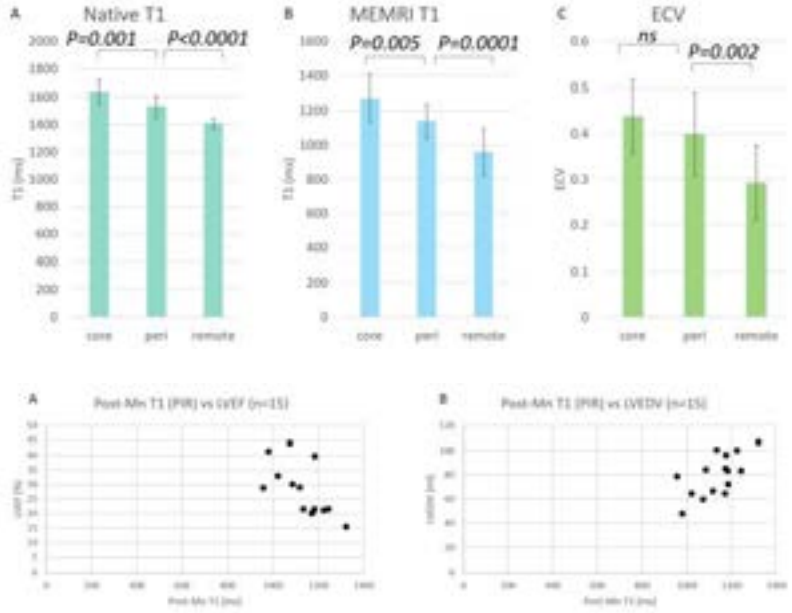

W021

3D Real-Time Cardiac MRI: Preliminary Results on Sheep

Jing Liu, Ph.D.[1] Liang Ge, PhD[2], Henrik Haraldsson, PhD[2], Yan Wang, PhD[2], Li Feng, PhD[3], Yue Zhang, Ph.D.[4], Karen Ordovas, MD, MAS[5], Mark B. Ratcliffe, MD[5], David Saloner, Ph.D.[1]

1. *University of California, San Francisco, CA*
2. *University of California San Francisco, CA*
3. *NYU School of Medicine, NY*
4. *Northern California Institute for Research and Education, CA*
5. *University of California San Francisco, San Francisco, CA*

Background: Left ventricular (LV) pressure-volume relationships provide load-independent measurements of heart function [1], which is usually measured by conductance catheter, based on the observation that conductance is linearly related to LV volume, but requires careful calibration for accurate measurements [2]. Recent work shows that real-time MRI is promising for determining LV pressure-volume loops [3]. Given the requirement of ultra-high temporal resolution, a 2D real-time cardiac MRI protocol was applied to image a single slice for estimating LV volumetric measurement [3]. In this work, we aim to develop 3D real-time cardiac MRI for LV volume measurements with super-high acceleration.

Methods: Our previously developed undersampling strategy, CIRcular Cartesian UnderSampling (CIRCUS) [4], integrates the features of randomization, variable-density and flexible interleaving trajectories on a 3D Cartesian grid. CIRCUS, provides interleaved sampling points through time, which is favorable for dynamic imaging. CIRCUS was implemented in a 3D Gradient Echo sequence. Images were acquired on four Juvenile sheep (weight ~50kg, heart rate ~80-120 bpm) on a 3T MRI scanner (Skyra, Siemens Healthcare) with 24-channel torso coil in short-axis view covering the ventricles. Dilute Ferumoxytol was infused over 20 minutes before MRI scans. A test was done on one sheep by adding three incremental 1.6ml doses of Ferumoxytol (total 5cc) and varying flip angles (15^o, 25^o, 35^o) to optimize the dose and flip angle in terms of achieving good blood signal in LV using 2D real-time imaging. 3D real-time scan parameters were FOV=28x22cm^2, matrix=96x72x10, voxel size=3x3x10mm^3 and TR/TE=3/1.33ms. Data was acquired continuously for ~30s with vena caval occlusion (VCO), and divided into multiple time frames with 60ms footprint and 50 frames per second (fps) by sliding data by 20ms. Undersampled datasets were reconstructed with k-t SPARSE-SENSE [5,6], using a multi-coil compressed sensing reconstruction exploiting joint sparsity along temporal dimension.

Results: Using 3.3cc Ferumoxytol and FA=25^o was found to provide the best SNR of LV blood signal. 3D real-time images of 50frps were achieved with super high acceleration factor of R~50 while visually comparable to the 2D images (Figure 1). 3D real-time imaging can capture the instantaneous change of ventricular volumes during VOC and reduced chamber sizes can be observed (Figure 2). A series of reformatted images acquired with 3D real-time imaging during VCO are shown in Figure 3.

Conclusions: Our preliminary data demonstrate the feasibility of achieving a high frame rate 3D real-time imaging for ventricular volume measurement. Further validation is needed to establish pressure-volume relationships.

References: 1. Baan J. et al. Circulation, 1984. **2**. Pacher P. et al. Nature Protocols, 2008. **3.** Witschey W. et al. Ann Thorac Surg, 2014. **4.** Liu J, et al. QIMS, 2014. **5.** Otazo R et al. MRM, 2010. **6**. Feng L et al, MRM, 2013.

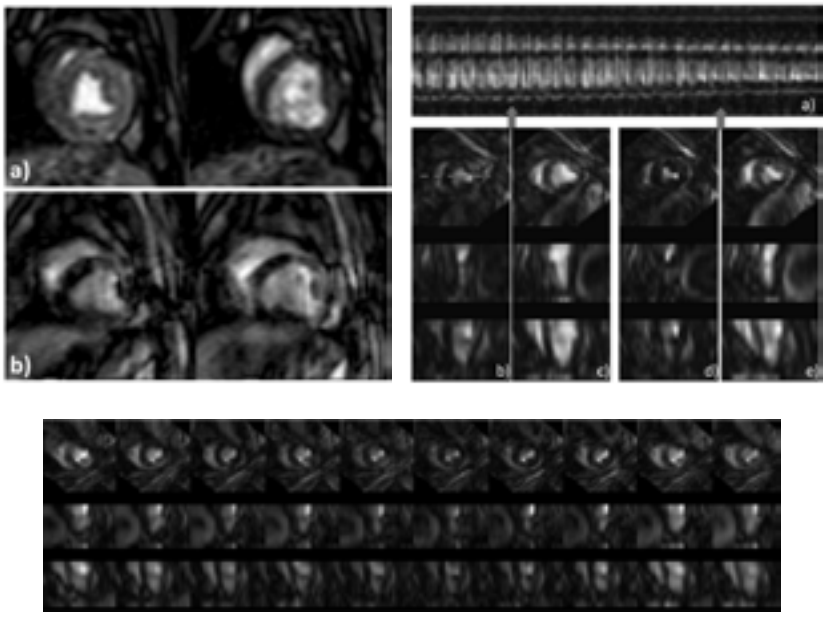

W022

Displacement encoding with Stimulated echoes (DENSE) is superior to feature tracking and tagging to detect abnormal left ventricular wall function by analyzing circumferential strain.

Johan Kihlberg, MSc[1] Vikas Gupta, PhD[2], Henrik Haraldsson, PhD[3], Andreas Sigfridsson, PhD[4], Sebastian Sarvari, MD, PhD[5], Tino Ebbers, PhD[6], Jan Engvall, MD, PhD[6]

1. *CMIV, Linkoping University, Linkoping, Ostergotlands Lan, Sweden*
2. *Linköping University, Linköping, Ostergotlands Lan, Sweden*
3. *University of California San Francisco, San Mateo, CA*
4. *Karolinska Institute, Stockholm, Stockholms Lan, Sweden*
5. *Oslo University Hospital, N/A, Norway*
6. *Linkoping University, Linkoping, Ostergotlands Lan, Sweden*

Background: Regional myocardial function is believed to be an important marker in determining the salvageable myocardium, and several Cardiovascular Magnetic Resonance (CMR) techniques have been developed for its objective assessment, including feature tracking (FT), tagging, and DENSE. FT is an image based technique that requires little user interaction and is performed on cine steady state free precession (SSFP) imaging included in standard CMR protocols. The result is presented on a segmental level and in terms of the endo-epi position of the region of interest. Myocardial tagging has for a long time been the gold standard in deformation imaging and is available in various 2D and 3D techniques. Deformation can be visually assessed and regionally quantified by using tracking softwares, e.g. Harmonic Phase Imaging (HARP). Displacement Encoded Stimulated Echoes (DENSE) shows similarities with tagging but uses the phase of the MRI signal to capture the displacement of the tissue. The advantage of DENSE is a high signal-to-noise-ratio, a high spatial resolution and rather simple post processing. In contrast to FT both tagging and DENSE require a separate acquisition not part of standard CMR protocols.

Methods: 81 patients with symptoms and signs of chronic coronary artery disease underwent CMR including SSFP, tagging and DENSE acquisition. FT analysis was performed on SSFP data using TomTec software, tagging was analyzed by HARP, and DENSE utilized an in-house developed algorithm. Circumferential strain values were used to identify myocardial segments with ≥ 50% transmurality of late gadolinium enhancement (LGE).

Results: Mean age of the patients was 66 ± 6 years [58 (81%) men]. Sixty-four patients (79%) had positive LGE affecting 214 19 patients with transmurality ≥50% (53 segments).The area-under curve (AUC) value from the receiver operating curve (ROC) for detecting ≥50% transmurality was 0.88 for DENSE, 0.73 for FT and 0.69 for HARP. The Pearson Correlation between circumferential strain and ejection fraction was -0.62 (DENSE), -0.13 (HARP) and -0.38 (FT) at a significance level of 0.01.

Conclusions: Circumferential strain assessed by DENSE was better than FT and tagging in detecting regional dysfunction caused by coronary artery disease.

W023

Tissue Tagging Reveals Maternal Nutrient Restriction Induced Alteration of Cardiac Mechanics in the Male Baboon Offspring, Paralleling Effects of Aging

Anderson H. Kuo, MD[1]Hillary Fries. Huber, PhD[2], Cun Li, PhD[2], Peter William. Nathanielsz, MD, PhD[2], Geoffrey David. Clarke, PhD[3]

1. *University of Texas Health Science Center at San Antonio, San Antonio, TX*
2. *University of Wyoming, TX*
3. *University of Texas Health Science Center at San Antonio, TX*

Background: Maternal nutrition restriction (MNR) leads to intrauterine growth restriction (IUGR) and predisposes the offspring to cardiovascular dysfunction. We have previously reported impaired left ventricular (LV) function and morphological changes in our MNR induced IUGR baboons. More specifically, depressed LV ejection fraction, impeded diastolic filling, and increased sphericity indices of the left ventricles are seen in the MNR group, similar to what is observed with aging. We hypothesize that altered cardiac strain is present and contributes to the impaired cardiac function in the MNR baboons.

Methods: Pregnant baboons were fed ad lib or 70% ad lib diets from 0.16 gestation to end of lactation. Three groups of offspring baboons were studied, MNR (N = 16, 8 M, 5.7 yr), age matched controls (CTL, N = 16, 8 M, 5.6 yr), and elderly spontaneously aging baboons (OLD, N = 12, 6 M, 16 yr). Cardiac MRI evaluation of the baboons was then performed under anesthesia to evaluate for systolic LV motion to include tissue-tagging sequence for rotational analysis (Siemens BEAT Tagging module, 45° tag, 13 phases, 256 × 208 matrix, voxel 1.25 × 1.25 x 6 mm^3) using a 3T Siemens MR scanner. Data analysis was performed with Harmonic Phase Flow (Interactive and Augmented Modelling Group, UAB, Barcelona, Spain). Statistical analysis was done by ANOVA and non-linear curve fitting, significance set at $p < 0.05$.

Results: Altered midventricular and basal rotation is seen in the MNR and OLD groups (ANOVA $p < 0.001$, $p < 0.002$). Phase specific analysis reveals changes in rotation during the latter half of systole in both OLD and MNR ($p < 0.05$). A general trend of rotational alteration is seen in the apical segment in the MNR and OLD groups, not reaching significance ($p = 0.06$). No statistically significant difference in torsion or rotation was noted in females.

Conclusions: Altered mid-ventricular and basal myocardial rotation as well as suggestion of abnormal apical torsion is seen in the MNR males, similar to observed in OLD males, further supporting alteration in cardiac physiology with MNR. Lack of statistical significant difference in the females suggests potential sex-dependent responses to the interaction of developmental programming and aging.

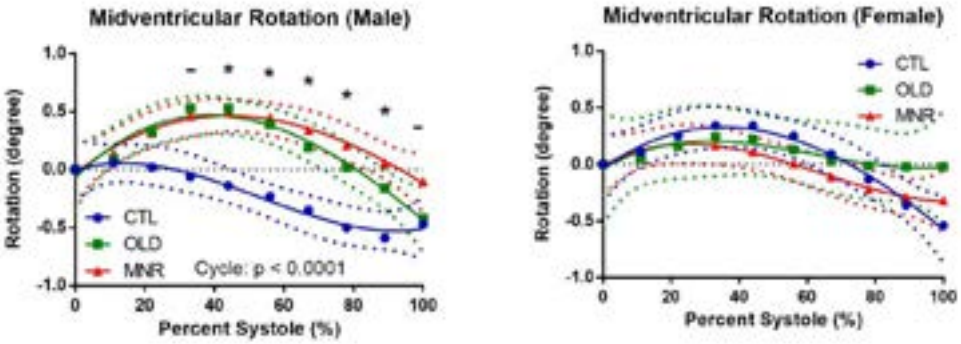

W024

Accurate and rapid longitudinal strain imaging by cine DENSE using one-dimensional longitudinal displacement encoding

Xiaoying Cai, BS[1] Kenneth C. Bilchick, MD[2], Frederick H. Epstein, Ph.D.[2]

1. University of Virginia, Charlottesville, VA
2. University of Virginia, VA

Background: Longitudinal strain is of growing importance for the assessment of left-ventricular function. Cine displacement encoded stimulated echoes (DENSE), an established strain imaging technique, is typically performed using 2D displacement encoding. To reduce the scan time for the assessment of longitudinal strain, we tested the hypothesis that LV long-axis imaging with 1D longitudinal displacement encoding would provide accurate longitudinal strain data.

Methods: MRI was performed on a 3.0T scanner (Skyra, Siemens). Long-axis cine DENSE images were acquired using both 2D in-plane displacement encoding and using 1D displacement encoding. For 2D, displacement encoding was applied in two orthogonal in-plane directions (longitudinal and orthogonal to longitudinal), and for the 1D case displacement encoding was applied in only the longitudinal direction. The scan time is one breathhold for 1D encoding, and two for 2D encoding. Each breathhold is 14 heartbeats long. Four-chamber views were acquired in 7 healthy volunteers and 6 heart failure (HF) patients, and acquisition parameters included: use of outer volume suppression, field-of-view = 160 mm, 6 spiral interleaves per image, 2 interleaves per heartbeat, temporal resolution = 30 ms, slice thickness = 8 mm, spatial resolution = 2.8 mm^2. For each subject, segmental longitudinal strain was calculated using both the 2D-encoded images and the 1D longitudinally-encoded images for 6 segments (excluding the apex). A single mid-wall contour was drawn in less than 5 seconds on an early-systolic frame, and it was automatically propagated to other frames. Strain tangential to the contour was computed. The peak strain values for each segment were compared using Bland-Altman analysis. The peak strain values were compared between HF patients and healthy subjects using two way ANOVA.

Results: Figure 1 shows an example of end-systolic four-chamber DENSE images (A-C) from a healthy volunteer, displacement trajectories at this phase (D, E) and segmental longitudinal strain curves (F,G) from 2D and 1D analyses, respectively. The strain curves in F and G are very similar. Peak strain values from the two analyses are highly correlated (r=0.87, p

Conclusions: Segmental longitudinal strain can be accurately quantified using cine DENSE with (a) a single 14-heartbeat breath-hold with 1D longitudinal displacement encoding and (b) rapid analysis requiring the manual drawing of a single mid-wall contour. Using existing acceleration methods, it will be straightforward to shorten the scan time to eight or even fewer heart beats.

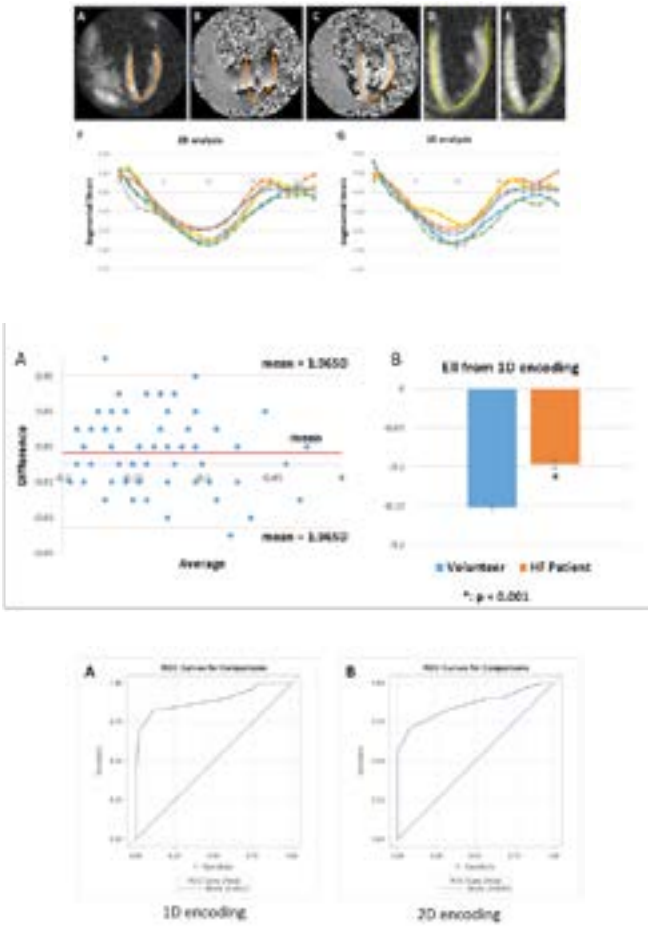

W025

MAPSE and TAPSE for the evaluation of left and right ventricular function in cardiac MR and functional cardiac CT.

Asik Ali Mohamed Ali, MD[1] Tony Sedlic, MD, FRCPC[2], Ana-Maria Bilawich, MD, FRCPC[3], John Mayo, MD, FRCPC[3]

1. *Vancouver General Hospital - University of British Columbia, Vancouver, BC, Canada*
2. *Vancouver General Hospital, BC, Canada*
3. *Vancouver General Hospital - University of British Columbia, BC, Canada*

Background: Cardiac MRI is an established reference standard for quantification of systolic left (LV) and right ventricular(RV) function. LV ejection fraction (EF) is calculated by manually adjusting the software's automated endo and epicardial border on each short axis slice. However, calculation of right ventricular ejection fraction requires manual processing of endocardial border, which is time consuming. The mitral/tricuspid annular plane systolic excursion (MAPSE/TAPSE) on MR has been previously shown to correlate with LVEF and RVEF with heart failure in echocardiographic studies. In this study, we compare the value of MAPSE and TAPSE of CT and MR to the volumetric quantification of LVEF and RVEF assessment in MR.

Methods: A single center study reviewing functional cardiac imaging performed. 15 patients, underwent retrospective functional cardiac CTA and cardiac MRI within 12 months. Retrospectively gated functional CT was performed with 64 slice (Siemens Force, Erlangen, Germany) or 128 slice (Toshiba Aquilion scanner, Japan) scanners. Functional data was processed with Siemens syngo.via automated cardiac analysis software. MRI was performed on a 1.5-T scanner (Magnetom Avanto, Siemens AG, Erlangen, Germany) with CINE sequences acquired in short axis and 4-chamber (horizontal long axis) planes. Functional data was manually processed with the Siemens syngo.via cardiac application. The ejection fraction was calculated by cardiothoracic radiologist blinded to each modality. M/TAPSE were measured on 4-chamber CINE images. Two separate reference lines were drawn in end-diastole and end-systole from the basal lateral tricuspid and the basal anterior mitral leaflet to right and left ventricular apex respectively. TAPSE is calculated as the difference between lengths of line joining the right ventricular apex and tricuspid annulus at end-diastole and end-systole.Similarly, MAPSE is calculated from mitral to left ventricular apex. LV dysfunction is graded as mild (41-51%), moderate (30-40%) and severe (< 30%) of EF. RV dysfunction is graded as mild (35-45%), moderate (25-35%) and severe (< 25%) of EF.

Results: Mean MR-TAPSE for normal RV function is 23 mm, mild-18 mm, moderate-13 mm and severe - 9 mm for dysfunction. Mean CT-TAPSE for normal RV function is 20 mm, mild- 17 mm, moderate-14 mm and severe - 10 mm for dysfunction. Mean MR-MAPSE for normal LV function is 12 mm, mild- 10 mm, moderate-9 mm and severe - 4 mm for dysfunction. Mean CT-MAPSE for normal LV function is 11 mm, mild- 9 mm and severe - 6 mm for dysfunction. MAPSE and TAPSE showed significant correlation with volumetric ejection fraction.

Conclusions: TAPSE and MAPSE assessed with cardiac MR and functional cardiac CT are valid parameters for rapid estimation of RVEF and LVEF.

W026

Stress CMR using Fast-SENC CMR for Predicting Regional Function Abnormalities

El-Sayed H. Ibrahim, PhD[1] Michael Schär, PhD[2], Venkatesh Murthy, MD[3], Jadranka Stojanovska, MD[3]

1. *University of Michigan, Ann Arbor, MI*
2. *Johns Hopkins University, MD*
3. *University of Michigan, MI*

Background: Stress CMR has been incorporated in daily clinical practice for the detection of inducible myocardial ischemia and for risk stratification of patients with coronary artery disease (CAD). However, the detection of inducible ischemia by stress CMR is currently based on assessment of cine images, which is subjective and depends on the experience of the reader. Fast strain-encoding (fast-SENC) is a modified version of the conventional SENC imaging that allows for acquiring strain maps in one heartbeat, which makes it ideal for stress imaging. In this study, we evaluate the feasibility of using fast-SENC CMR for objective detection of myocardial dysfunction in patients evaluated for ischemia.

Methods: Three patients undergoing rest/stress CMR scans for ischemia evaluation were included in the study: one patient with left bundle branch block (LBBB), another with non-compaction cardiomyopathy, and the third with subclinical CAD. The patients were imaged on a 1.5T scanner, and the imaging protocol included cine, fast-SENC, perfusion, and late gadolinium enhancement (LGE) imaging. Rapid intravenous injection of 0.4 mg of regadenoson was conducted, with stress perfusion and fast-SENC imaging performed after 0.1 mmol/kg gadolinium injection. 150 mg of aminophylline was administered intravenously prior to rest imaging. Rest perfusion and fast-SENC imaging was then performed after appropriate delay using an additional gadolinium dose of 0.1 mmol/kg. The cine, fast-SENC, perfusion, and LGE images were analyzed to evaluate ejection fraction (EF), myocardial strain, ischemia, and viability, respectively.

Results: Perfusion and LGE images showed lack of ischemia and delayed hyperenhancement in all patients. Heart rate increased by 33±6% between rest and stress. EF was normal (>55%) in the LBBB and subclinical CAD cases, while it was moderately decreased (45%) in the case of myocardial non-compaction. Fast-SENC provided additional details about regional cardiac function. As shown in Figures 1-3, the generated strain maps showed slightly improved myocardial contractility in LBBB, maintained contractility in subclinical CAD, and slightly depressed contractility as well as regional heterogeneity in non-compaction cardiomyopathy, between rest and stress. The strain curves showed significant mechanical dyssynchrony in LBBB, as measured by the time difference between peak strain in the septal and lateral walls.

Conclusions: Stress SENC CMR is a valuable technique for evaluating regional contractility in ischemia imaging. Fast-SENC allows for generating strain maps in one heartbeat, which makes it ideal for stress imaging and dynamic scans. Adding fast-SENC to the ischemia evaluation protocol allows for detection of subclinical cardiac dysfunction before reduction of global function parameters.

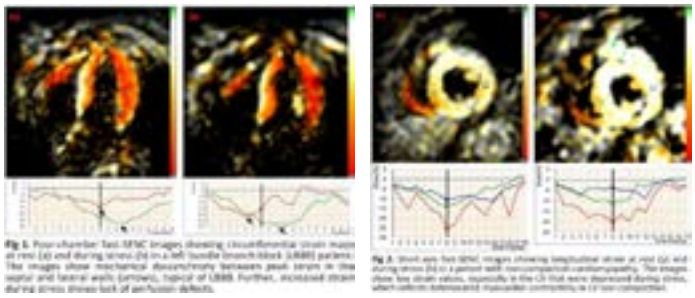

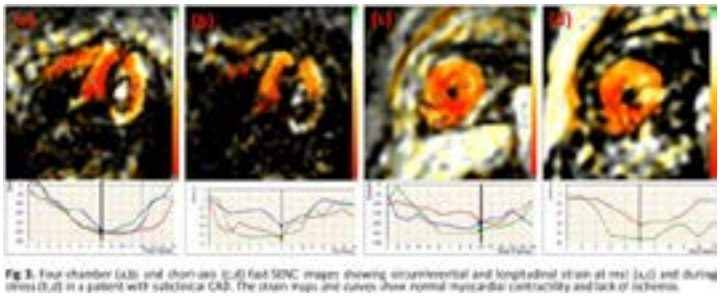

W027

CMR tagging pattern for 3D tracking: Radial-zSPAMM

Abbas Nasiraei Moghaddam, PhD[2] Ali Rezaei, BSc[1]

1. Amirkabir University of Technology, Tehran, Iran
2. Amirkabir University of Technology, Tehran, Tehran, Iran

Background: Using 2D CMR tagging technique to derive 2D strain map were presented in many studies. These patterns give a good insight of regional function of LV but the through-plane motion causes some errors in strain estimation. Tagging with special 3D pattern can be used to overcome these problems. Usually tagging is considered as a binary effect, in which the image is divided to tagged and untagged areas. This approach can give a presentation of in-plane motion in Lagranigian frame work, however, is unable to separate the through-plane motion from in-plane displacement. Therefore, to get a complete Lagrangian displacement field, one needs to exploit other information such as plane-dependent tagging pattern or contrast. We propose a 3D tagging pattern which is radial in SAX and sinosoidal in Longitudinal direction to overcome this problem.

Methods: The proposed tagging sequence, *"Radial-zSPAMM"*, consists of two parts that are separated by spoiler gradients: 1) in-plane Radial Tagging, 2) through-plane SPAMM. The former uses rotating excitation plane in combination with a sinusoidal RF pulse [1] and the latter creates taglines in *z-direction* using two constant RF pulses separated by constant modulation gradient [2]. Detailed sequence parameters are shown in Table 1.

Results: The sequence is simulated using Bloch Simulator MATLAB code for a 3D axisymmetric object in the range of -4*cm* to 4*cm* in each direction (Figure 2). Figure2-A shows high spatial resolution and tagline density relative to previous schemes [3]. Using values in Table 1, distance between taglines in *z-direction* (figure2-B) is set to be around 15*mm* that is more than 2x slice thickness in common CMR imaging sequences. Figure2-B depicts that the thickness of longitudinal taglines changes from 3 to 1.8mm. The contrast of taglines for each transverse slice, with 5 mm thickness, was calculated based on the slice position. Figure 3 shows a plane-dependent contrast in *z-direction* which changes the concept of tagging from binary to gray-scale and provides more infomation to esitmate the through-plane motion.

Conclusions: A special 3D tagging pattern was suggested and simulated that provides plane-dependent contrast as well as variable thickness/location of taglines. The in-plane pattern matches the morphology of the LV and the distance between zSPAMM taglines guarantees the proper visualization of its longitudinal shortening. Combination of these characteristics helps to capture the 3D Lagrangian displacement using 2D imaging and reduce the error caused by through-plane motion in strain calculation. **References**
[1] Nasiraei-Moghaddam and Finn. *MRM* 71.5 (2014): 1750-1759. [2] Axel et al. *Radiology* 171.3 (1989): 841-845. [3] Ryf et al. *MRM* 16.3 (2002): 320-325.

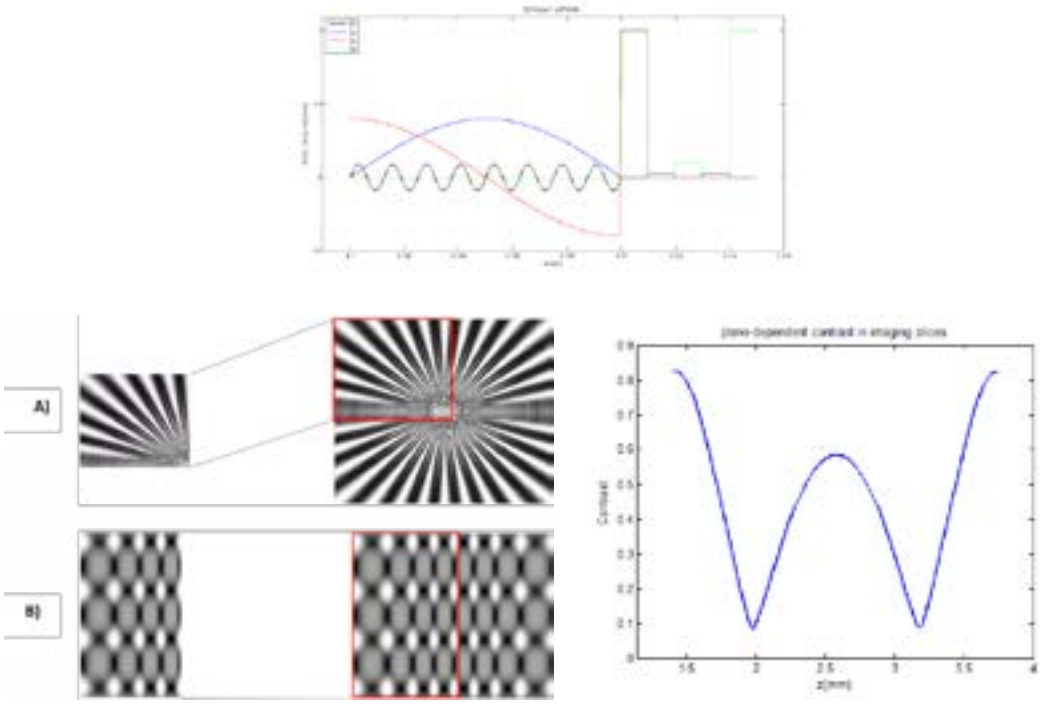

Table 1 – selected parameters for simulation

0.4 G/cm	Max. amplitude of sinusoidal gradients
0.1 G/cm	Amplitude of modulation gradient is SPAMM

W028

Anisotropic Myocardial Stiffness in HFpEF Porcine Hearts: Initial Feasibility

Prateek Kalra, MS[2]Ria Mazumder, PhD[1], Saad Khan, MD[3], Xiaokui Mo, Ph.D.[4], Bradley Clymer, PhD[5], Richard White, MD[2], Arunark Kolipaka, PhD[2]

1. *Widener University, PA*
2. *Department of Radiology, The Ohio State University Wexner Medical Center, Columbus, OH*
3. *Department of Radiology, The Ohio State University Wexner Medical Center, Dublin, OH*
4. *Center for Biostatistics, Department of Biomedical Informatics, The Ohio State University, OH*
5. *The Ohio State University, Columbus, OH*

Background: Myocardial stiffness (MS) estimate is an important determinant of cardiac function and is found to be increased in cardiovascular diseases such as hypertension (HTN) that has potential to trigger heart failure with preserved ejection fraction (HFpEF). Previous studies have shown that MS related to HFpEF has directional dependencies. Anisotropic MS is currently quantified using bi-axial mechanical testing on ex-vivo myocardial strips. However, this method is invasive and only provides global MS estimate. Waveguide magnetic resonance elastography (MRE) is used to estimate anisotropic stiffness non-invasively, which requires both diffusion tensor imaging (DTI) to know the fiber directions and MRE to estimate the displacement field along and across the fibers. The aim of this study is to estimate anisotropic MS in HFpEF using waveguide cardiac MRE (cMRE).

Methods: 6 Yorkshire pigs underwent renal-wrapping surgery to induce chronic systemic arterial hypertension potentially triggering HFpEF. A baseline (Bx_{HTN}) and 8 weeks post surgery scan ($W8_{HTN}$) was acquired. Imaging was performed on 1.5-Tesla clinical MRI scanner (Avanto, Siemens Healthcare, Erlangen, Germany). Axial slices covering the entire left ventricle were obtained using retrospective pulse-gated, segmented multi-phase gradient recalled echo cMRE sequence with TE/TR=9.71/12.5 ms; field of view=384x384 mm^2; matrix size=128x128; slice thickness=8 mm;cardiac phases=8; excitation frequency=80Hz; phase offsets=4; and motion encoding gradient of 160 Hz in x, y and z directions. A 2D spin-echo, echo planar imaging based DTI sequence was performed by euthanizing the animal on the table (*in-vitro*) with TE/TR=70/2000 ms; b0/b1=0/1000 s/mm^2; number of directions=12; and averages=20. cMRE and DTI images were registered to obtain the principal Eigen vectors and displacement field to perform anisotropic inversion.

Results: Figure 1 shows cMRE magnitude image and wave images of a single slice in the same animal at Bx_{HTN} and $W8_{HTN}$. Figure 2 shows box plot of anisotropic stiffness coefficients in 5 animals (1 outlier excluded) at Bx_{HTN} and $W8_{HTN}$ with compressional (C_{11}, C_{22} and C_{33}) (a) and shear stiffness coefficients (C_{44}, C_{55}, and C_{66}) (b). Significant increase in MS at $W8_{HTN}$ compared to Bx_{HTN} was observed for C_{11} ($p=0.05$), C_{44} ($p=0.02$), C_{55} ($p=0.03$) and C_{66} ($p=0.01$). However, C_{22} and C_{33} showed no significant difference.

Conclusions: Despite the limitations of having small sample size (n=5), this study shows that certain anisotropic stiffness directions are affected more than others in HFpEF condition.

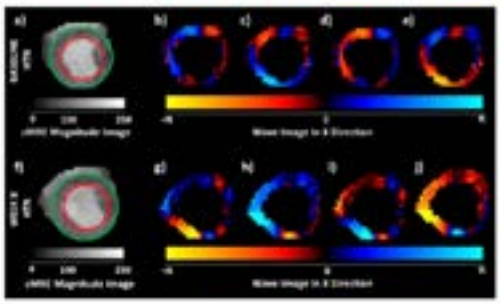

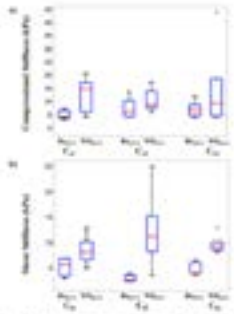

W029

Measuring Left Ventricular Myocardial stiffness using transient intrinsic torsional shear wave propagation: Initial results from phantom study and volunteers

Jessica Webb, BM BCh MRCP[1]Jurgen H. Runge, MD, PhD[1], Jack Lee, PhD[2], Gerald Carr-White, MD, PhD[3], Reza Razavi, MD, PhD[2], Jordi Martorell, PhD[4], David Nordsletten, PhD[1], Ralph Sinkus, PhD[1]

1. *King's College London, London, England, United Kingdom*
2. *King's College London, England, United Kingdom*
3. *St Thomas' Hospital, London, England, United Kingdom*
4. *Department of Chemical Engineering, IQS School of Engineering, Universitat Ramon Llull, Barcelona, Spain, Barcelona, Catalonia, Spain*

Background: It is hypothesized that HFpEF is characterised by increased myocardial stiffness and our preliminary data using transient MR-Elastography utilizing the aortic valve closure as an intrinsic source for the generation of shear waves, has validated this hypothesis. This approach has the drawback that imaging has to be timed minutely to the exact time-point of valve closure and that only one single snap-shot of the propagating wave can be acquired. Thus, only wavelength can be measured and its conversion to shear wave speed and thereby material properties is not evident. To overcome these limitations, we further developed the method to enable the visualization of the torsional aortic wave propagation through the myocardium at temporal resolutions of 0.75ms within 2 consecutive breath-holds.

Methods: This study has 3 parts: sequence development; validation of wave speed measurements in a phantom model; and a volunteer study. We developed an ECG-gated CINE sequence where imaging is done using the phase of the 2D pencil beam navigator (cRNAV, shot duration 30ms). Motion encoding gradients are played during the cRNAV shot enabling the selection of the torsional wave when the navigator is oriented from the aorta towards the apex within the septum. Two consecutive breath holds (each 20secs) provide interleaved 1D phase images (80mm) at a temporal resolution of 0.75ms (=30ms/(20 heartbeats*2 breath holds)). After re-ordering, shear wave speed can be estimated by a fit to the space-time waterfall plot. Increased myocardial stiffness will result in increased speed of shear wave propagation.

Results: Phantom experiments using known material stiffness demonstrated that the 1D CINE cRNAV sequence can measure the correct shear wave speed (1m/s), figure A. 3D finite-element simulations confirmed the existence of a torsional wave generated by aortic valve closure propagating at a speed that corresponds to the true shear stiffness of the myocardium used for the simulation. Torsional waves were observed in two healthy volunteers at around 350ms after the R wave, corresponding to valve closure time. Wave speeds of 5-6m/s were observed resulting in shear modulus estimates of 25-36kPa, figure B.

Conclusions: We have successfully developed and applied a new patient friendly technique to quantify myocardial stiffness in vivo from torsional shear waves generated by aortic valve closure, not requiring any external transducers. Together with our previous preliminary data in HFpEF patients, this method has significant potential to become an important diagnostic tool for the early detection of pathologically altered myocardial stiffness.

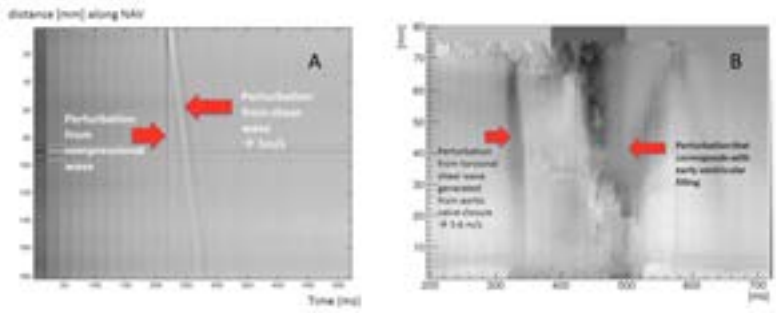

W030

A multi-scale investigation of structural and functional remodelling in heart failure

Vicky Y. Wang, PhD[1] Alexander Wilson[1], Abdallah Hasaballa[1], Gregory Sands, PhD[1], Alistair Young, PhD[2], Ian LeGrice, MD, PhD[1], Martyn Nash, PhD[1]

1. *Auckland Bioengineering Institute, University of Auckland, Auckland, New Zealand*
2. *The University of Auckland, New Zealand, GRAFTON, Auckland, New Zealand*

Background: Conventional clinical diagnosis of heart failure (HF) has primarily focused on cardiac contraction. Whilst failure to pump sufficient blood to meet the body's needs (*systolic HF*) is a hallmark of end-stage failure, impaired ability to relax and fill (*diastolic HF*) has also been found to play an important role in the progression of HF. Structural remodelling of the left ventricle (LV) leads to cardiac dysfunction and subsequent failure. Few studies have characterised the relationship between myocardial structural and functional remodelling during HF.

Methods: A longitudinal animal study was performed to assess this linkage using rat hearts at different stages of HF. Spontaneously hypertensive rats (SHRs) were chosen, since features of their disease resemble those of human HF, and the Wistar Kyoto (WKY) strain was used as the normal control. At each time point, *in vivo* cardiac geometry and motion were derived from cardiac MRI. Subsets of animals were sacrificed at a number of ages and *ex vivo* passive pressure-volume measurements were obtained to provide information on the mechanical behaviour within as well as beyond *in vivo* physiological range. In addition, high resolution extended volume confocal images of excised tissue blocks were used to characterise the 3D reorganisation of extracellular collagen matrix (ECM) and myofibre structure with age and HF development.

Results: In the SHR hearts, micro-scale remodelling of the 3D organisation of the ECM was observed with the myocardium exhibiting planar distributions of collagen as opposed to elongated structures observed in the WKY control groups. Chamber compliance was lower for the SHRs at all study ages compared to the age-matched WKY controls. By performing finite element analysis of ventricular mechanics using 3D models constructed from *in vivo* MRI, our analysis demonstrated that the remodelled ventricular geometry alone could not account for the observed changes in LV function.

Conclusions: We have developed a ventricular mechanics analysis framework that allowed the specific mechanisms of HF to be interrogated and characterised in detail. Microstructural remodelling plays a central role in altering LV mechanical function by adversely influencing myocardial micromechanics.

W031

Feasibility of Cardiac Cine MRI at 0.35T

Shams Rashid, Ph.D.[1] Yingli Yang, Ph.D.[2], Yu Gao, B.S.[3], Fei Han, Ph.D.[4], Peng Hu, Ph.D.[2]

1. Department of Radiological Sciences, UCLA, Los Angeles, CA
2. UCLA, CA
3. UCLA, Los Angeles, CA
4. UCLA, LOS ANGELES, CA

Background: Clinical cardiac magnetic resonance imaging (CMR) is most frequently carried out at a field strength of 1.5T and less frequently at 3T or higher. While higher field strengths boost the baseline SNR, they are often associated with issues such as increased SAR, and generally worse bSSFP banding artifacts. At the other end of the spectrum, low-field MRI ($B_0 < 0.5$T) shows promise for diagnostic imaging [1, 2]. The major advantages of low-field MRI include significantly diminished SAR, increased field homogeneity and generally shorter T1. Furthermore, low-field MRI is preferable to higher field strengths for patients with implants and for interventional MR-guided procedures due to its reduced RF heating in the presence of implanted and interventional devices. In this study, we sought to demonstrate the feasibility of cardiac MRI at 0.35T and compare it with CMR at 1.5T.

Methods: CMR was carried out on an MRIdian system (ViewRay Inc., Oakwood Village, OH), an MR-guided radiation therapy machine which consists of an MRI scanner modified to add radiation sources. Its MRI component is a 0.35T super-conducting actively-shielded magnet with a Siemen software front end. Cardiac cine images were acquired in 3 healthy subjects at 0.35T using a balanced steady state free precession (bSSFP) sequence. Images were acquired for a range of flip angles (FA) from 50-130°. The subjects were also imaged at 1.5T on a Siemens Avanto scanner using a bSSFP cine sequence. All parameters were identical at both field strengths (TR/TE=4/2ms, voxel size 1.25 x 1.25 x 7 mm^3, FOV 32 cm, readout bandwidth 780 Hz/pixel, parallel imaging: GRAPPA).

Results: Fig. 1 top row shows bSSFP cine images acquired on the 0.35T system for FAs from 50° to 130°. For comparison with cine images at 1.5T, Fig. 1 bottom row shows cine images at 1.5T for FAs 50° to 90°. A bSSFP cardiac cine acquisition with FA greater than 90° is generally not possible at 1.5T or higher due to SAR limits. It appears that an FA of about 90° to 110° at 0.35T has improved blood-myocardium contrast and general image quality compared to lower flip angles. Fig. 2 shows cine images of multiple cardiac phases at both field strengths. In general, while the 0.35T images appear grainier due to reduced SNR, the left ventricle myocardium walls can be clearly delineated with good contrast.

Conclusions: This study demonstrates that CMR at 0.35T is highly feasible. Due to reduction in SAR, the maximum achievable flip angle for bSSFP cardiac cine imaging is much higher at 0.35T than 1.5T, which should allow for improved blood-myocardium contrast. Although the SNR at 0.35T is reduced compared to 1.5T, the quality of the cine images is adequate for diagnostic purposes.

References:

[1] Wu et al., PLOS one, May 2016, doi:10.1371/journal.pone.0154711

[2] Rutt et al., JMRI, 1996, 1:57-62

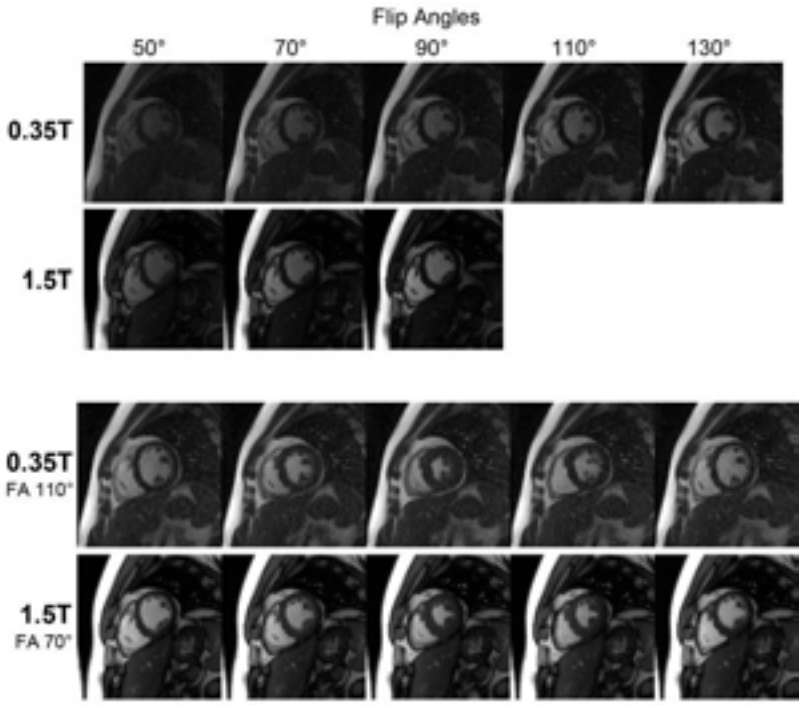

W032

Towards reducing the confounding effect of intra-myocardial blood volume on native T1: Purely-systolic T1 mapping using an ungated spoiled steady-state approach

Behzad Sharif, PhD[1] Zulma Sandoval, PhD[1], Daniel Berman, MD[2], C. Noel Bairey Merz, MD[3]

1. *Cedars-Sinai Medical Center, Los Angeles, Los Angeles, CA*
2. *Cedars-Sinai Medical Center, Los Angeles, CA*
3. *Cedars Sinai Medical Center, Los Angeles, CA*

Background: Recently, it has been established that a major contributor to native myocardial T1 is intra-myocardial water content [1], mainly driven by intra-myocardial blood volume (MBV). MBV depends on various physiologic factors and may act as a confounder for detecting myocardial fibrosis based on native T1. Hence, minimizing the dependence of native T1 on MBV can enhance its role as a reliable marker of fibrosis. To this end, we developed and tested an ungated free-breathing T1 mapping method that, in contrast to MOLLI-based methods, avoids any magnetization preparation – enabling it to capture "purely systolic" T1 maps. Since MBV is reduced during systole vs. diastole, this approach has the potential to reduce its confounding effect on T1.

Methods: Fig. 1 describes the proposed scheme, which continuously acquires data using a spoiled steady-state approach with alternating 3D/2D excitation (see caption) and without ECG gating or breath holding. Data acquisition was performed twice with two different flip angles (FAs) and a fixed TR= 5 ms (FAs = 10° and 3°; scan time for each FA: 45 sec). Image reconstruction employed a self-gating approach using the acquired 3D readouts (separating systolic/diastolic readouts) followed by radial SENSE reconstruction using the 2D readouts (in-plane resolution: 1.8x1.8 mm). FA mapping was performed using an improved version of a previous method [2] to account for B1+ inhomogeneity (12-sec ungated scan). The reconstructed images and the relative FA map were used to generate a pixel-wise T1 map using the DESPOT1 method [3]. Healthy volunteers (n=9) were studied at 3T using the proposed method and the vendor-provided MOLLI sequence for native T1 mapping of the mid ventricular slice in systole and diastole.

Results: Fig. 2 shows representative results for the proposed method including raw images for the two FAs and the FA map in (a), and the T1 maps in (b) with comparison to MOLLI. In the studied subjects, there was a significant difference between systolic vs. diastolic septal T1 for the proposed method (1126 vs. 1233, respectively; $p < 0.01$) consistent with reduced MBV contribution for systolic T1. Overall, the diastolic septal T1 was not significantly different between MOLLI vs. the proposed method (1219 vs. 1233, respectively; p = n.s.).

Conclusions: We have proposed a hybrid 3D/2D *steady-state* approach for T1 mapping that eliminates the need for ECG-gating or breath-holding and, most notably, magnetization preparation. The latter feature has the potential to reduce the confounding effect of MBV on native T1 by *limiting the T1-fitting data to systole* (with lower MBV vs. diastole) and avoiding contamination of the fitting data by diastolic MBV dynamics. The promising results (high image quality and close agreement vs. MOLLI) point to the potential of this approach for accurate ungated free-breathing T1 mapping.

References:

[1] Mahmod & Piechnik et al. JCMR 2014;16.

[2] Chung & Axel et al. MRM 2010;64.

[3] Deoni et al. MRM 2003;49.

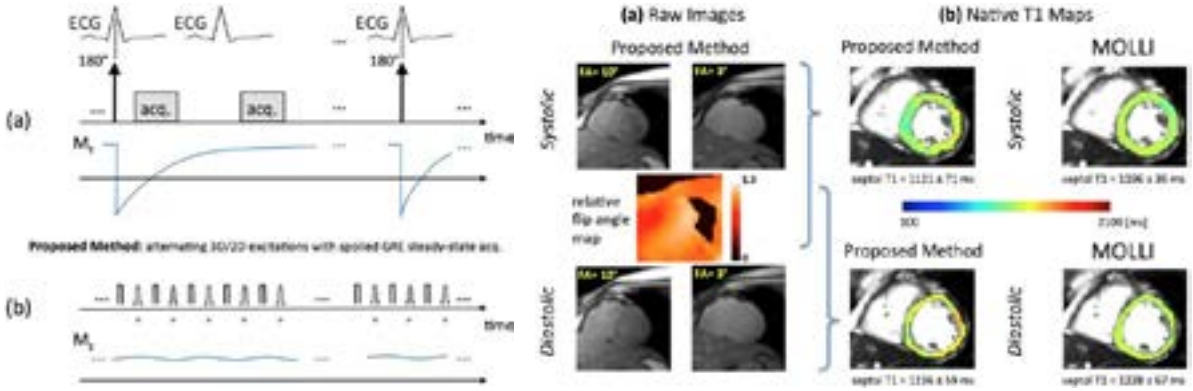

WP01

CMR study of histologically proven primary tumours of the aorta and pulmonary arteries

Monika Arzanauskaite[1] Raad Hashem Mohiaddin, MD PhD[2]

1. *Royal Brompton Hospital, London, England, United Kingdom*
2. *Royal Brompton Hospital and Imperial; College London, London, England, United Kingdom*

Background: Primary tumours of the aorta and pulmonary arteries are extremely rare, but they are being increasingly encountered as cardiovascular imaging accessibility grows every year. Clinical presentation of these tumours is non-specific and the diagnosis is often late. Imaging plays an important part of the diagnosis of these tumours. CMR is particularly useful because of the excellent soft tissue contrast, tissue characterisation, flow assessment and angiography. We report value and features of CMR in the diagnosis of histologically proven spectrum of vascular tumours and discuss the imaging protocol used in these studies.

Methods: 10 patients (9 males, 1 female) with histologically proven primary tumours of the pulmonary arteries and the aorta who had CMR studies at our institution were reviewed. The study included two primary aortic tumours (1 leiomyosarcoma, 1 myxoma) and 8 primary pulmonary tumours (sarcomas). The CMR protocol (see Figure) included T1-weighed, T2W sequences, early and late gadolinium enhanced images for tissue characterisation. MRA and flow measurements for assessment of the haemodynamic impact of the vascular tumour were used. Ventricular function analysis was also performed.

Results: The results of the study are summarised in the Table. Both primary aortic tumours were located in the mid descending aorta. The location of the primary tumours of the pulmonary arteries was variable, nevertheless most of them (5) were found in the right pulmonary artery. The majority (8) of the tumours had an intraluminal component. All of the tumours had high signal intensity of T2-STIR images and enhanced late after contrast administration. None of the ten patients had pericardial effusion.

Conclusions: Aortic and pulmonary artery tumours are rare and mainly malignant. The majority of the neoplasms have intraluminal involvement which results in the symptoms of thromboembolic disease or in direct occlusion of the affected vessel. Contrary to the thrombi, primary tumours show more tissue heterogeneity, are hyperintense on T2-weighted sequences with fat saturation and enhance after contrast administration. Therefore in cases of atypical appearances of thrombi, it is important to suspect primary tumours, to perform a dedicated imaging protocol and to follow-up the patients by CMR after anticoagulation therapy.

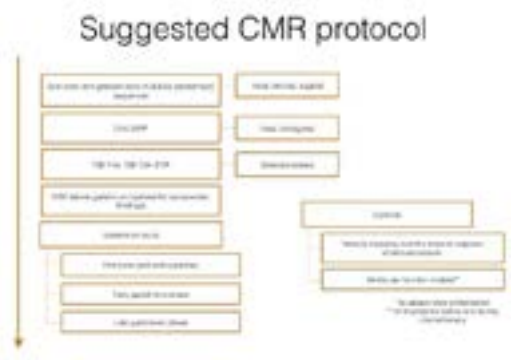

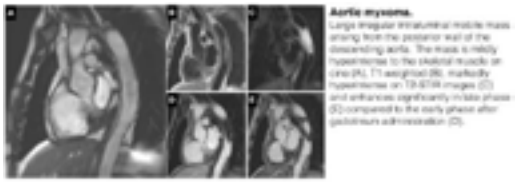

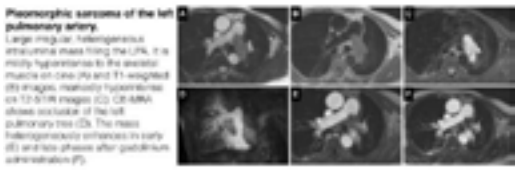

WP02

Cardiac Involvement in Ankylosing Spondylitis: Insights From Cardiac Magnetic Resonance Imaging

Paul S. Biesbroek, MD[1] Sjoerd C. Heslinga, MD[2], Thelma C. Konings, MD[3], Irene E. van der Horst-Bruinsma, MD, PhD[3], Mark B.M. Hofman, PhD[3], Peter M. van de Ven, PhD[3], Otto Kamp, MD, PhD[3], Vokko P. van Halm, MD, PhD[3], Mike J.L. Peters, MD, PhD[3], Yvo M. Smulders, MD, PhD[3], Albert C. van Rossum, MD, PhD[3], Mike T. Nurmohamed, MD, PhD[2], Robin Nijveldt, MD, PhD[1]

1. *VU University Medical Center, Amsterdam, Noord-Holland, Netherlands*
2. *Reade & VU University Medical Center, Noord-Holland, Netherlands*
3. *VU University Medical Center, Noord-Holland, Netherlands*

Background: Ankylosing spondylitis (AS) is a rheumatic inflammatory disease associated with increased cardiovascular morbidity and mortality. Since echocardiography is limited in the ability to characterize myocardial tissue, and studies using cardiac magnetic resonance (CMR) are lacking, it remains uncertain whether and to what extent the myocardium is involved in AS. This study aimed to determine the presence and extent of cardiac involvement in patients with AS using CMR.

Methods: Patients with AS were screened by transthoracic echocardiography (TTE) for study participation. Fifteen consecutive AS patients with an abnormal TTE, including cardiac abnormalities, valvular disease, or aortic root dilatation, were prospectively included. CMR protocol included cine imaging, late gadolinium enhancement (LGE), and T1 mapping with extracellular volume (ECV) calculation. The associations of ECV with log-transformed C-reactive protein (CRP) and erythrocyte sedimentation rate (ESR) were quantified using respectively Pearson's correlation (R) and Spearman's rank correlation (R_S).

Results: Sixty-three patients were screened by TTE when the predefined number of 15 participants was reached, of which one was excluded. In the 14 included AS patients with a complete CMR exam (mean age 62 years, 93% male, and mean disease duration 21 years), left ventricular (LV) diastolic dysfunction was the most common finding on TTE (69%), followed by aortic root dilatation (19%), right ventricular (RV) dilatation (6%), and RV dysfunction (6%). CMR revealed focal hyperenhancement in three patients (21%), all with a particular pattern of enhancement (Figure 1). LVEF was impaired in five patients (36%), and was significantly lower in patients with hyperenhancement (47 ± 8% versus 56 ± 5%, p=0.03). Myocardial ECV was strongly correlated with CRP concentration (R = 0.83, p < 0.01) and ESR level (R_S = 0.69, p < 0.01)(Figure2).

Conclusions: The findings of this first CMR study in AS suggest the presence of cardiac involvement. CMR with cine imaging and LGE identified global LV dysfunction and focal areas of hyperenhancement, while T1 mapping with ECV quantification could discriminate patients with various degrees of disease activity.

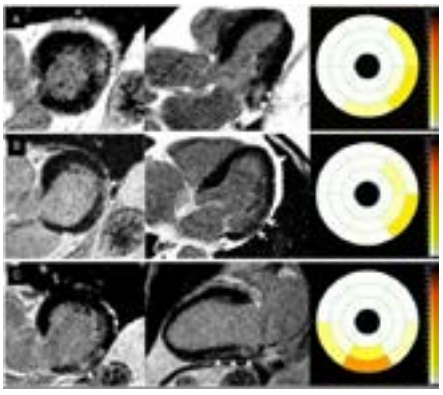

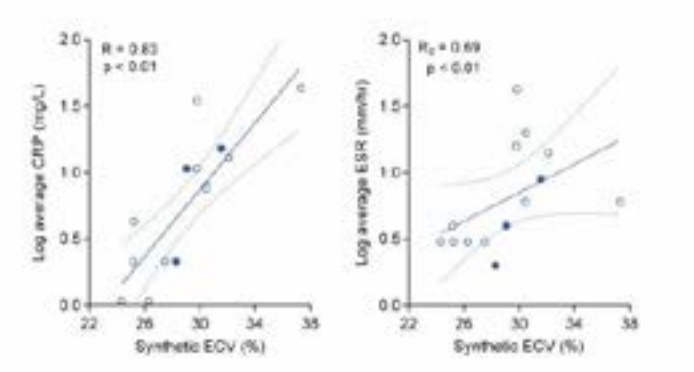

WP03

Pericardial and pleural effusions differ in native T1 mapping and quantitative contrast dynamics

Simon Thalén, None[1]Maren Maanja[2], Andreas Sigfridsson, PhD[3], Peder Sörensson, MD, PhD[4], Martin Ugander, MD, PhD[2]

1. *Karolinska Institutet, Stockholm, Stockholms Lan, Sweden*
2. *Karolinska Institutet, Stockholms Lan, Sweden*
3. *Karolinska Institute, Stockholm, Stockholms Lan, Sweden*
4. *Karolinska University Hospital, Stockholms Lan, Sweden*

Background: Excretion of cardiovascular magnetic resonance (CMR) gadolinium-based contrast agents (GBCA) into pleural and pericardial effusions has been described using T1-weighted imaging. However, the relative T1 mapping characteristics as well as prevalence, magnitude and dynamics of contrast excretion into these effusions is not known. The clinical implications and potential diagnostic utility of such evaluation remains unexplored. The aim of this study is to investigate and compare the differences in T1 mapping characteristics and GBCA excretion dynamics in pleural and pericardial effusions.

Methods: Clinical patients having undergone contrast enhanced CMR who had a minimum of 4 mm pleural and 5 mm pericardial effusion in an end-diastolic cine 4-chamber image, and T1 maps acquired before and after 3 minutes (early) and 27 minutes (late) after admission of a GBCA (0.1-0.2mmol/kg, gadoteric acid, Dotarem) were screened for inclusion. T1 maps were acquired using a MOLLI sequence (1.5 T Siemens Aera). Analyzed variables for both effusions were: native T1 (T1native), T1early, T1late, the difference between T1native and T1early (ΔT1early), the difference between T1native and T1late (ΔT1late), and the effusion-volume-independent early-to-late contrast concentration ratio ΔR1early/ΔR1late, where ΔR1 = 1/T1post-contrast-1/T1native. Data are presented as median [interquartile range (IQR)].

Results: Screening of 1338 consecutive patients undergoing CMR identified a study population of patients with both pleural and pericardial effusion and at least a late post-contrast measurement of T1 (n=22/1338 (1.6%), mean±SD age 57±19 years, 45% female). Native T1 was higher in pleural effusion than in pericardial effusion (3162 [IQR 2620-3566] vs 2572 [IQR 2170-3039] ms, p=0.04). Pleural and pericardial effusion did not differ with regards to T1early (2439[IQR 1377-3067] ms vs. 2014[IQR 1627-2939] ms, p=0.3), T1late (970[IQR 474-1182] vs. 1286[IQR 595-1837] ms, p=0.1), ΔT1early (645[IQR 224-906] ms vs. 493[IQR 252-924] ms, p=0.84), ΔT1late (2093[IQR 1739-2403] ms vs. 2572[IQR 2169-3039] ms, p=0.06) or ΔR1early (0.08[IQR 0.03-0.2] s^-1 vs. 0.07[IQR 0.04-0.2] s^-1, p=0.68). ΔR1late was higher in pleural effusion than in pericardial effusion (0.6[IQR 0.5-0.9] vs. 0.4[IQR 0.2-0.8] s^-1, p = 0.02). ΔR1early/ΔR1late was higher in pleural effusion than in pericardial effusion (0.21[IQR 0.07-0.47] vs. 0.12[IQR 0.04-0.19], p = 0.03.

Conclusions: Quantitative T1 mapping revealed that, compared to pericardial effusions, pleural effusions have a higher native T1 consistent with greater relative fluid content in relation to other components such as proteins, greater ΔR1late indicating greater contrast excretion in relation to fluid volume, and a higher ΔR1early/ΔR1late indicating more prominent early excretion dynamics.

WP04

Potential utility of T1 mapping to characterize pericardial effusions

Hilda M. Gonzalez Bonilla, MD[2] Akanksha N. Thakkar, MD[1], Eric Y. Yang, MD PhD[1], Faisal Nabi, MD[3], Dipan J. Shah, MD[4]

1. *Houston Methodist Hospital, TX*
2. *Houston Methodist Hospital, Houston, TX*
3. *Houston Methodist DeBakey Heart & Vascular Center, Houston, TX*
4. *Houston Methodist DeBakey Heart & Vascular Center, TX*

Background: The diagnostic work-up and management of patients with pericardial effusions hinges on whether the effusion is a transudate or an exudate. Conventionally, this distinction is made based on biochemical and pathological examination of invasively obtained fluid. On non-invasive cardiac magnetic resonance imaging (CMR), the evaluation of pericardial effusions has been limited to qualitative assessment of fluid features. Here, we present a pilot case series to study the diagnostic utility of T1 mapping on CMR for differentiating between transudative and exudative pericardial effusions.

Methods: From 2013 to 2016, we identified 10 patients with pericardial effusions who underwent cardiac T1 mapping using the modified Look-Locker inversion-recovery (MOLLI) technique on clinically ordered CMR studies, followed by biochemical analysis of extracted pericardial fluid. Pericardial fluid for each patient was classified as likely transudative or likely exudative based on biochemical results. Pericardial fluid samples with serum-effusion albumin gradient < 1.2 were considered exudates. If SEAG values were unavailable, we used a ratio of fluid protein to serum protein ≥ 0.6 or fluid LDH to serum LDH ≥ 2.4 to identify an exudate in patients who had not been administered diuretics prior to pericardiocentesis. Then, the T1 relaxation time of the fluid was measured on T1 MOLLI maps to identify a cut-off value that could help distinguish between transudates and exudates.

Results: Of the 10 cases studied, 4 effusions were identified as transudative and 6 were exudative based on biochemical analysis. A receiver operating characteristic curve analysis was performed on the data which showed that a T1 time of < 3093 msec would have 100% sensitivity and specificity to identify an exudate. However, this result must be interpreted with caution due to the small sample size.

Conclusions: For the characterization of pericardial effusions, T1 mapping may offer a noninvasive means to differentiate between exudate and transudate. Further prospective studies may be useful in validating these findings.

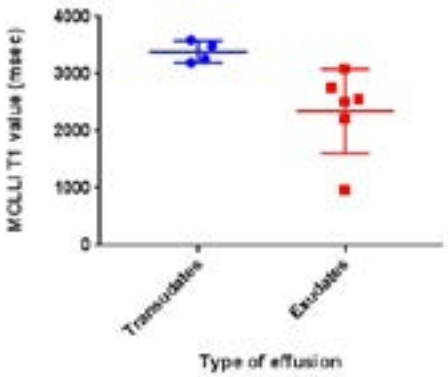

Biochemical and qualitative classification of pericardial fluid samples with T1 times

T1 time range (msec) Min – Max	T1 time (msec) Mean ± SD	Type of scanner used	Biochemical classification	Sr. No.
1849 – 3626	2516 ± 335	3T	Exudate	1
2180 – 3136	2755 ± 148	3T	Exudate	2
862 – 1132	975 ± 34	1.5T	Exudate	3
1970 – 3963	3195 ± 469	1.5T	Transudate	4
2303 – 3979	3268 ± 276	1.5T	Transudate	5
1954 – 2648	2214 ± 95	1.5T	Exudate	6
2848 – 4057	3595 ± 213	3T	Transudate	7
2775 – 3583	3093 ± 87	3T	Exudate	8
1358 – 3737	2568 ± 374	1.5T	Exudate	9
3103 – 3788	3492 ± 67	3T	Transudate	10

T1 time range (msec) Min – Max	T1 time (msec) Mean ± SD	Type of scanner used	Biochemical classification	Sr. No.
1849 – 3626	2516 ± 335	3T	Exudate	1
2180 – 3136	2755 ± 148	3T	Exudate	2
862 – 1132	975 ± 34	1.5T	Exudate	3
1970 – 3963	3195 ± 469	1.5T	Transudate	4
2303 – 3979	3268 ± 276	1.5T	Transudate	5
1954 – 2648	2214 ± 95	1.5T	Exudate	6
2848 – 4057	3595 ± 213	3T	Transudate	7
2775 – 3583	3093 ± 87	3T	Exudate	8
1358 – 3737	2568 ± 374	1.5T	Exudate	9
3103 – 3788	3492 ± 67	3T	Transudate	10

WP05

Ventricular Remodeling and Right Ventricular Involvement in Patients with Early Stage Breast Cancer Receiving Anthracycline Chemotherapy

Mustafa A. Altaha, MBBS[1]Kim Connelly, MD, PhD[2], Eitan Amir, MD, PhD[3], Christine Brezden-Masley, MD PhD[4], Bernd J. Wintersperger, MD[5], Paaladinesh Thavendiranathan, MD, MS[6]

1. *Institute of Medical Science, Faculty of Medicine, University of Toronto, Toronto, ON, Canada*
2. *St. Michaels Hospital and University of Toronto, Toronto, ON, Canada*
3. *Princess Margaret Cancer Centre, ON, Canada*
4. *University of Toronto, ON, Canada*
5. *Department of Medical Imaging, University of Toronto, Toronto, ON, Canada*
6. *Toronto General Hospital and University of Toronto, Toronto, ON, Canada*

Background: Chemotherapy induced cardiac dysfunction is an adverse prognostic marker in women with early stage breast cancer. Patterns of ventricular remodeling and frequency of bi-ventricular involvement during cancer therapy in these patients have not been described. Understanding ventricular remodeling will provide novel knowledge as to the mechanism by which patients eventually develop heart failure (HF). This can help design targeted methods to prevent HF. Describing changes to cardiac function beyond the left ventricle will provide a broader appreciation of cardiac impact of cancer therapy and can have implications for screening of cardiotoxicity.

Methods: Thirty-eight consecutive women (age: 49.6 ± 9.1 years) with early stage HER2+ breast cancer, receiving cancer therapy (anthracyclines followed by trastuzumab) were prospectively recruited. All patients had cardiac MR studies performed pre and post-anthracycline treatment on a 1.5T Siemens Avanto Fit magnet. Short axis SSFP cines with 8mm slice thickness (2mm gap) were acquired for ventricular function analysis. Left and right ventricular (LV/RV) volumes and ejection fraction (EF), and LV mass were measured by an observer blinded to patient identification and imaging time point. A significant change in EF was prospectively defined as a >5% drop after anthracycline therapy based on known reproducibility of cardiac MR measured EF. A paired t-test was used for comparison.

Results: All patients received epirubicin (515.2 mg/m^2 +/- 49.9). Ventricular function and volumetric parameters pre and post epirubicin are summarized in the Table below. Eight (21.0%) patients had a fall in LVEF by >5%, and the primary cause was an increase in end-systolic volume (ESV) as opposed to a change in end-diastolic volume (EDV); Similarly, ten (26.3%) patients had a fall in RVEF by >5% primarily due to an increase in ESV. LVEF and RVEF reduction by >5% occurred concomitantly in four (10.5%) patients. Hypertension was more common in the 14 patients who had a significant drop in LVEF and/or RVEF compared to those who did not (36% versus 17%).

Conclusions: In this study anthracycline exposure resulted in concomitant reduction in LV and RVEF by >5.0% in 10.5% of patients with breast cancer. The main mechanism of reduction in ventricular function was an increase in ESV, which is likely due to a reduction in contractility, as opposed to a fall in EDV which may occur from intravascular volume depletion. The incidence of significant RVEF reduction was similar to LVEF reduction highlighting the importance of following RV function during anthracycline treatment.

Table: Summary of changes in ventricular volume, ejection fraction, and mass between pre-anthracycline and within 3 weeks post anthracycline.

Parameter	Pre Treatment	Post Anthracycline	P value[3]	Mean change in all 38 patients , %	Mean change in patients without >5% drop in LVEF and/or RVEF (n=24), %	Mean change in patients (with >5% drop in LVEF (n=8), %	Mean change in patients with >5% drop in RVEF (n=10), %	Mean change in patients with >5% concomitant drop in LVEF and RVEF (n=4), %
LVEDV (ml/m^2)	75.7 (9.5)	77.4 (12.9)	0.23	2.2	1.2	2.8	4.9	3.4%
LVESV (ml/m^2)	29.3 (5.3)	30.2 (8.2)	0.18	3.0	-1.8	16.4	12.1	19.2%[1]
LVEF (%)	61.5 (3.6)	60.1 (4.4)	0.02	-1.4	0.1	-6.1	-2.9	-6.2%[2]
LVmass (g/m^2)	42.7 (6.1)	40.3 (5.7)	<0.001	-5.4	-5.8	-4	-3.3	0.8%
RVEDV (ml/m^2)	79.1 (12.8)	79.5 (13.4)	0.78	1	2.7	-1.5	-2.4	-2.3%
RVESV (ml/m^2)	35.3 (6.8)	36.4 (7.3)	0.12	3.8	0.1	7.8	13.7	14.1%[1]
RVEF (%)	55.4 (4.2)	54.2 (4.4)	0.09	-1.2	1.1	-4.1	-6.9	-7.2%[2]

LVEDV, left ventricular end-diastolic volume index; LVESV, left ventricular end-systolic volume index; LVEF, left ventricular ejection fraction; LVmass, left ventricular mass index; RVEDV, right ventricular end-diastolic volume index; RVESV, right ventricular end-systolic volume index; RVEF, right ventricular ejection fraction; data presented as mean and standard deviation.
[2]Significant drop in LVEF or RVEF was defined as an absolute reduction of > 5%;
[1]Significant change in indexed end-diastolic and end-systolic volume was defined as a relative increase >5%;
[3]paired t-test.

WP06

Quantitative multiparametric assessment of chemotherapy-associated cardiotoxicity: a cross-sectional cardiovascular magnetic resonance study in cancer survivors

Willeke Naaktgeboren, BSc[1] Jesse Habets, MD, PhD[2], Arco Teske, MD, PhD[3], Maarten-Jan Cramer, MD PHD[4], Tim Leiner, MD, PhD[5]

1. *University Medical Center Utrecht, The Netherlands, Utrecht, Utrecht, Netherlands*
2. *University Medical Center Utrecht, Utrecht, Netherlands*
3. *Univercity Medical Center Utrecht, Utrecht, Utrecht, Netherlands*
4. *University Medical Centre Utrecht, Utrecht, Utrecht, Netherlands*
5. *Utrecht University Medical Center, Utrecht, Utrecht, Netherlands*

Background: In the increasing population of cancer-survivors, chemotherapy-related cardiac dysfunction (CTRCD) is an important clinical problem and associated with clinically relevant morbidity and mortality. The use of type I cardiotoxic agents (i.e. antracyclines) have been shown to cause irreversible cardiac damage in a dose-dependent fashion, whereas myocardial dysfunction due to type II agents (e.g. trastuzumab) is thought to be reversible. The objective of this study was to quantitatively assess the degree of CTRCD using a multiparametric CMR approach in cancer survivors receiving different chemotherapy regimens.

Methods: CMR is routinely performed in our center in cancer survivors with echocardiographically suspected cardiac dysfunction. CMR studies from all patients with suspected CTRCD who underwent imaging between January 2013 and August 2016 were identified. All studies were acquired on a 1.5T clinical MRI-scanner. Quantitative assessment consisted of left ventricular ejection fraction (LVEF), and global longitudinal-, circumferential- and radial strain measurements. In addition, native and post-contrast T1-mapping and extracellular volume (ECV) measurements were obtained in three short-axis slices. Patients were subdivided into three categories based on the chemotherapy received, and categorized as follows: 1) antracycline-group (AC-group); 2) antracycline/trastuzumab-group (ACT-group) and 3) nonantracycline-group (nAC-group). CMR parameters were compared between the chemotherapy regimens with one-way ANOVA's and Kruskal-Wallis test. A p-value < 0.05 was considered significant. Categorical data were presented as number and percentages and continuous data as mean ±standard deviation or median [interquartile range], depending on the data distribution.

Results: Multiparametric CMR data was available from 77 cancer survivors (mean age: 55±15 years; 40 men; 52%). Chemotherapy regimens were as follows: AC-group: n=47; ACT-group: n =8 patients, and nAC-group: n= 22. Results and their corresponding normal values are summarized in the table. In all three chemotherapy regimens LVEF was reduced. GLS-measurements were significantly lower in the AC- and ACT-group. T1-mapping measurements showed elevated native T1-values in all three groups, whereas ECV-values were only borderline abnormal when compared to published reference values.

Conclusions: In the population of cancer survivors with echocardiographically suspected and known cardiac dysfunction, multiparametric CMR shows both structural and functional cardiac abnormalities as a results of all three chemotherapy regimens. However, GLS-measurements was the only parameter to show significant difference in antracycline-based chemotherapy versus nonantracycline-based chemotherapy.

Multiparametric CMR data of patients with suspected chemotherapy-associated cardiotoxicity

Normal values*	p-value	nAC-group (n=22)	ACT-group (n=8)	AC-group (n=47)	
67.0 ± 5.0	0.238	48.0 ± 11.1	41.2 ± 13.0	41.9 ± 14.7	LVEF (%)
NA	0.004	21.0[4.0-40.8]	13.5 [8.5-59.3]	64.0 [18.0-200.0]	First exposure to chemotherapy (months)
-23.0 ± 5.0** NA NA	0.033 0.144 0.071	-17.5 ± 4.7 -27.3 ±8.8 41.1 [26.9-63.0]	-14.1 ± 4.2 -22.5 ± 9.3 37.4 [24.2-43.6]	-14.3 ± 4.7 -22.8 ± 8.7 35.1 [24.1-44.7]	Left ventricular strain: - GLS - GCS - GRS
1003 ± 46 28.0 ± 3.0	0.529 0.672	1135 [1124-1166] 30.0 ± 3.2	1144 [1075-1210] 27.5 ± 2.5	1109 [1050-1190] 28.3 ± 5.5	T1-mapping: - native T1 (ms) - ECV (%)

LVEF, left ventricular ejection fraction; *GLS*, global longitudinal strain; *GCS*, global circumferential strain; *GRS*, global radial strain; *ECV*, extracellular volume fraction; *NA*, not applicable.

*Reference: Kawel Boehm N, Maceira A, Valsangiacomo Buechel E, et al. Normal values for cardiovascular magnetic resonance in adults and children. *J Cardiovasc Magn Reson.* 2015; 17: 29-29. doi:10.1186/s12968-015-0111-7.

** institutional normal value, based on unpublished data from 125 healthy subjects.

WP07

Diffuse Myocardial Fibrosis In Systemic Sclerosis – Quantification Of Progression And Response To Therapy by CMR

Daniel C. Lee, MD, MSc[1]Sanjiv J. Shah, MD, MSc[2], Madeline M. Stark, MD[2], James Carr, MD[3], Benjamin H. Freed, MD[4], Brandon C. Benefield, MS[4], Carol Ann Burns[2], Richard K. Burt, MD[2]

1. *Northwestern University, Feinberg School of Medicine, Chicago, IL*
2. *Northwestern University Feinberg School of Medicine, IL*
3. *Northwestern Memorial Hospital, Chicago, IL*
4. *Northwestern University Feinberg School of Medicine, Chicago, IL*

Background: Systemic sclerosis **(SSc)** is characterized by excessive fibrosis of the skin and internal organs, including the heart. At autopsy, myocardial fibrosis is seen in half of SSc patients, and is associated with an increased risk of cardiac death. Extracellular volume fraction **(ECV)**, a noninvasive marker of diffuse myocardial fibrosis measured by cardiovascular magnetic resonance imaging **(CMR)**, has been shown to correlate with SSc disease severity measured by the modified Rodnan Skin Score **(mRSS)**. We hypothesized that ECV can quantify progression of myocardial fibrosis and response to therapy in SSc patients.

Methods: We identified 21 consecutive SSc patients who were evaluated for hematopoietic stem cell transplantation **(HSCT)** and had ≥2 CMR exams with native and post-contrast T1 mapping. Change in ECV was calculated as second ECV (%) minus first ECV (%). Patients who had HSCT prior to the second CMR were considered HSCT(+), while those who had no HSCT prior to second CMR were HSCT(-). All but one patient also had ≥2 modified Rodnan Skin Score measurements.

Results: For all 21 SSc patients (age 44±13, 86% female, 76%-19%-5% diffuse-limited-CREST), ECV was 28.2±4.2% and mRSS was 17.8±10.7 at baseline. Overall, change in ECV was +0.6±4.4% over 425±315 days in the entire cohort. However, ECV increased in HSCT(-) patients (n=15) by 2.4±3.1 percentage points over 336±311 days, while **ECV decreased in HSCT(+) patients** (n=6) by 4.0±4.1% over 646±210 days (Figure 1). HSCT(-) patients had a statistically significantly greater progression of ECV compared to HSCT(+) patients (p=0.01). Similarly, mRSS increased in HSCT(-) patients by 4.6±9.6 points, but in HSCT(+) patients mRSS decreased by 15.2±7.9 points ($p < 0.001$), Figure 2. Change in ECV correlated with change in mRSS ($R^2 = 0.29$, p=0.015), Figure 3.

Conclusions: Noninvasive quantification of diffuse myocardial fibrosis by CMR measured ECV can detect progression of myocardial fibrosis in HSCT(-) SSc patients and regression of myocardial fibrosis in HSCT(+) SSc patients. The changes in myocardial fibrosis are mirrored by changes in mRSS, a validated measure of disease severity and predictor of prognosis in SSc patients.

http://www.ConferenceAbstracts.com/uploads/cfp2/attachments/LDFAIBDN/LDFAIBDN--220651-1-ANY(1).pdf

http://www.ConferenceAbstracts.com/uploads/cfp2/attachments/LDFAIBDN/LDFAIBDN--220651-1-ANY.pdf

http://www.ConferenceAbstracts.com/uploads/cfp2/attachments/LDFAIBDN/LDFAIBDN--220651-2-ANY.pdf

WP08

DENSE CMR in tuberculous pericardial constriction reveals impaired strain which correlates with late gadolinium enhancement and pericardial thickness and is worse in those with HIV co-infection

Stephen Jermy, M.Eng[1], Ntobeko A. B. Ntusi, MD DPhil[3]Gregori Henryk. Palkowski, MB.ChB FCP(SA)[1], Petronella Samuels, B.Tech Rad[1], Sulaiman Moosa, FFRad Diag(SA)[2], Mpiko Ntsekhe, MD PhD[3], Ernesta Meintjes, PhD[1], Bongani M. Mayosi, FCP(SA) D.Phil[1]

1. *University of Cape Town, Cape Town, Western Cape, South Africa*
2. *2 Military Hospital, Cape Town, Cape Town, Western Cape, South Africa*
3. *University of Cape Town and Groote Schuur Hospital, Cape Town, Western Cape, South Africa*

Background: Tuberculous pericarditis (TBP) is the most common cause of a large pericardial effusion in the developing world. There has been a notable resurgence in TBP in the context of co-infection with the human immunodeficiency virus (HIV). Pericardial constriction (PC) is a serious complication of TBP. Cardiovascular magnetic resonance (CMR) can assess non-invasively cardiac function, myocardial oedema, inflammation and fibrosis. We hypothesised that peak systolic circumferential strain (Ecc) assessed by displacement encoding with stimulated echoes (DENSE) CMR would be impaired in patients tuberculous PC and would be more severely affected in those with HIV co-infection where we have previously demonstrated greater myocardial fibrosis with late gadolinium enhancement (LGE) CMR.

Methods: 39 patients with tuberculous PC (20 female (51%), mean age 41 ± 14) were included in the study. Of these, 22 (56%) were HIV-infected (13 female (59%), mean age 34 ± 7). Assessments included clinical examination, ECG, echocardiography, serum and pericardial biomarkers and CMR (biventricular volumes and function, oedema, and LGE).

Results: HIV infected tuberculous PC patients were younger ($p < 0.001$), had lower serum haemoglobin ($p < 0.001$) and were more likely to have NYHA class III and IV symptoms ($p < 0.001$). There were no differences on ECG and echocardiography between HIV infected and uninfected tuberculous PC patients. On CMR, there were also no differences in global systolic function and left ventricular (LV) mass between HIV infected and uninfected tuberculous PC patients. Ecc was more impaired in those who were HIV infected (-12 ± 3 vs. -14 ± 3 in without HIV infection, p=0.03). Focal fibrosis on LGE was found more commonly in those with HIV infection (p=0.01). Ecc correlated modestly with LGE (R -0.63, p=0.001) and pericardial thickness (R -31, p=0.02).

Conclusions: DENSE CMR reveals more severe myocardial involvement in patients with tuberculous PC and HIV co-infection, which correlates with presence of LGE and pericardial thickness.

Baseline characteristics in patients with pericardial constriction N=39	
41 ± 14	Age, years (mean ± SD)
20 (51)	Female sex (%)
23 ± 5	Body mass index (kg/m2)
22 (56)	Proportion HIV infected
4 (18)	Of HIV infected, proportion of ART
112 968-450)	Of HIV infected, median CD4 count (IQR)
11 (28)	NYHA functional class III or IV at presentation
7 (18)	Presentation with heart failure

CMR findings in patients with pericardial constriction N=39	
63 ± 9	LVEDV indexed, ml/m2 (mean ± SD)
44 ± 7	LVESV indexed, ml/m2 (mean ± SD)
44 ± 5	LVSV indexed, ml/m2 (mean ± SD)
60 ± 7	LV mass indexed, g/m2 (mean ± SD))
74 ± 8	LV ejection fraction,% (mean ± SD)
32 ± 3	LA size, mm (mean ± SD)
-13 ± 3	Mid short axis peak systolic Ecc, % mean ± SD)

WP09

Evaluation of Myocardial Inflammation and Fibrosis with Restricted Diffusion MRI in Non-Human Primate (NHP) Models of AIDS

Yijen L. Wu, Ph.D.[1]Fang-Cheng Yeh, MD, PhD[2], Kevin David Raehtz, MS[3], Cristian Apetrei, MD, PhD[4], George Sebastian Haret Richter, DVM[3], Ranjit Sivanandham, MBBS, MD[5], Noah Krampe, BS[5], Tammy Lynn Dunsmore, BS[3], Ivona Pandrea, MD, PhD[5]

1. *Deapartment of Developmental Biology, University of Pittsburgh and Rangos Research Center Imaging Core, Children's Hospital of Pittsburgh of UPMC, Pittsburgh, PA, USA, Pittsburgh, PA*
2. *Department of Neurological Surgery, University of Pittsburgh, PA*
3. *Department of Pathology, University of Pittsburgh, PA*
4. *Center for Vaccine Research and Department of Microbiology and Molecular Genetics, University of Pittsburgh, PA*
5. *Center for Vaccine Research and Department of Pathology, University of Pittsburgh, PA*

Background: Antiviral therapy dramatically improved survival of HIV-infected patients, yet many develop cardiovascular disease (CVD), the mechanism(s) of which are not understood and whose diagnostic is limited due to the impossibility to perform invasive endomyocardial biopsies (EMB). Cardiac MR (CMR), a noninvasive alternative to EMB, can only measure circumstantial features of myocarditis, such as the nonspecific changes in T1, T2, LGE, and ECV. More specific noninvasive diagnostic approaches are needed. Our goal was to directly image myocardial inflammation and fibrosis in a SIV-infected NHP model, using restricted diffusion imaging (RDI).

Methods: ***Animal model:*** We used the African green monkey (AGM) model of SIV infection which lacks progression to AIDS and CVD. A subset of animals was sacrificed at 28 days post SIV infection (dpi) and used as negative controls. A second subset of the animals was infected with SIV and treated with DSS for >1 year, to induce gut damage and generalized inflammation. We previously showed that inflammation closely correlates with development of CVD in SIV-infected NHPs. ***Diffusion MRI:*** *Ex vivo* diffusion MRI was acquired with Bruker 7-Tesla Avance III system with a quadrature transceiver coil. RDI was acquired with a total of 101 diffusion sampling directions, with 12 b values ranging from 367 to 4000 s/mm2.

Results: Both acute and chronically infected AGMs preserved coherent myocardial fiber integrity (Fig. 1A, B). Focal myocardial lesions with fibrosis can be seen in DSS-treated chronically SIV-infected AGMs (Fig.1D, G, H) as hypointensity in RDI (Fig. 1D) and elevated MD (Fig. 1 G,H) on 804 and 919 dpi. Foci with increased cellular infiltration resulting from inflammation were clearly seen as hyperintensity in RDI in the DSS-treated animals (Fig. 1E). Neither these changes were seen in the negative controls (Fig. 1 C, F). Figure 2 shows quantification of fractional anisotropy (FA, Fig2A), apparent diffusion coefficient (ADC) or mean diffusivity (MD) (Fig2B), axial diffusivity (AD, Fig. 2C) and restricted diffusion (RD, Fig2D) in both heart groups. Lesion sites with fibrosis showed elevation in ADC (Fig. 2B) and decrease in RD (Fig.2D middle right); whereas inflammation site showed increase in RD (Fig. 2D right).

Conclusions: We confirmed that CVD is caused by systemic persistent inflammation in SIV-infected NHPs. Most importantly, we validated a noninvasive imaging method for HHV/SIV-related myocarditis diagnosis. RDI can be used for direct quantification of myocardial inflammation and fibrosis in HIV patients, and can potentially be an alternative to EMB for detecting viral myocarditis.

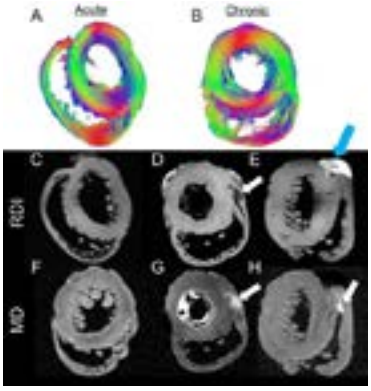

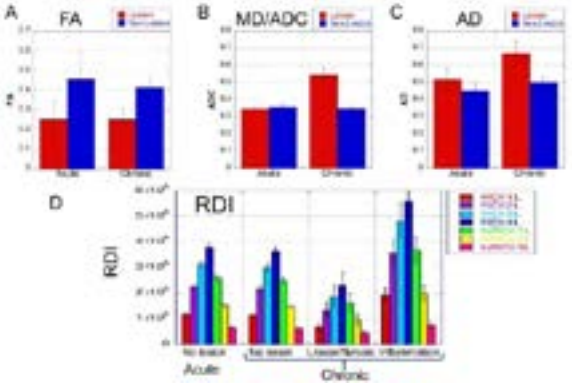

WP10

Cardiac Magnetic Resonance derived Extracellular Volume Fraction as a Marker for Myocardial Fibrosis – The Importance of Coexisting Pathologies

Julia Anna. Lurz, MD[1]Christian Luecke, MD[2], Karl Rommel, MD[3], Christian Besler, MD[4], David Lang[5], Gerhard Hindricks, MD[5], Gerhard Schuler, MD[4], Holger Thiele, MD[6], Matthias Gutberlet, MD[5], Philipp Lurz, MD, PHD[4]

1. *Heart Center Leipzig, Dept. of Electrophysiology, Leipzig, Sachsen, Germany*
2. *Radiology, University Leipzig - Heart Center, Niedersachsen, Germany*
3. *Dept. of Internal Medicine / Cardiology University of Leipzig - Heart Center, Sachsen, Germany*
4. *Leipzig University Heart Center, Department of Cardiology, Sachsen, Germany*
5. *Heart Center Leipzig, Sachsen, Germany*
6. *University Heart Center Luebeck, Sachsen, Germany*

Background: Myocardial fibrosis (MF) is associated with unfavorable outcome in patients with cardiomyopathy and it is of prognostic relevance. Assessment of extracellular volume fraction (ECV) bares the hope for being a non-invasive surrogate parameter for MF. However, ECV may also be altered by other pathologies which are associated with expansion of the extracellular space. The aim of our study was to evaluate whether ECV can reliably inform on the extent of diffuse MF in the simultaneous presence of myocardial inflammation, which has not been verified to date.

Methods: In this prospective study, 107 consecutive patients with clinical suspicion of inflammatory cardiomyopathy were included from August 2012 until May 2015. All patients underwent LV endomyocardial biopsy(EMB) as well as CMR on 1.5 T Scanner. Native and 15 minutes post-contrast T1-mapping was obtained with a MOLLI (3 single slices in VLA, HLA and SA-orientation (3(3)5" scheme). ECV was calculated from T1-times pre- and post-contrast in myocardium. Quantification of fibrosis in EMB was realized by Masson-trichrome staining. Significant inflammation was defined as the presence of ³ 14 infiltrating immune cells/mm^2 on EMB.

Results: Myocardial inflammation was present in 66 patients. 41 patients exhibited no significant inflammation on EMB. Patients with and without inflammation were of similar age (45±15 vs. 45±14 years; p=1.0) and had comparable LV ejection fraction (37±17 vs. 36±18 %; p=0.9) and symptom duration (median 14, IQR 5-36 vs. 14, 7-30 days; p=0.73). Although LV collagen volume percentage was comparable between groups (inflammation 12.3±17.8 vs. non-inflammation 11.4±7.9 %; p=0.577), ECV was significantly higher in patients with inflammation (0.37±0.06 %) than in patients without inflammation (0.33±0.08 %; p=0.02). Importantly, ECV adequately estimated the degree of LV MF percentage only in patients without inflammation (r=0.72; p < 0.0001), but not in those with inflammation (r=0.24; p=0.06, panels).

Conclusions: These findings prove the theoretical concept of ECV as an estimate for MF. This, however, seems only to be accurate in the absence of myocardial inflammation. Fundamentally, ECV is not a direct measure of MF, as it can be increased in other pathologies associated with expansion of the extracellular space which also applies for myocardial inflammation. Assuming that various degrees of myocardial inflammation and fibrosis coexist in such a scenario, the measured ECV will reflect a sum of these different pathologies, but will not inform solely on the extent of MF. When ECV is used as a surrogate parameter of diffuse MF other coexisting pathologies impacting on ECV should be excluded.

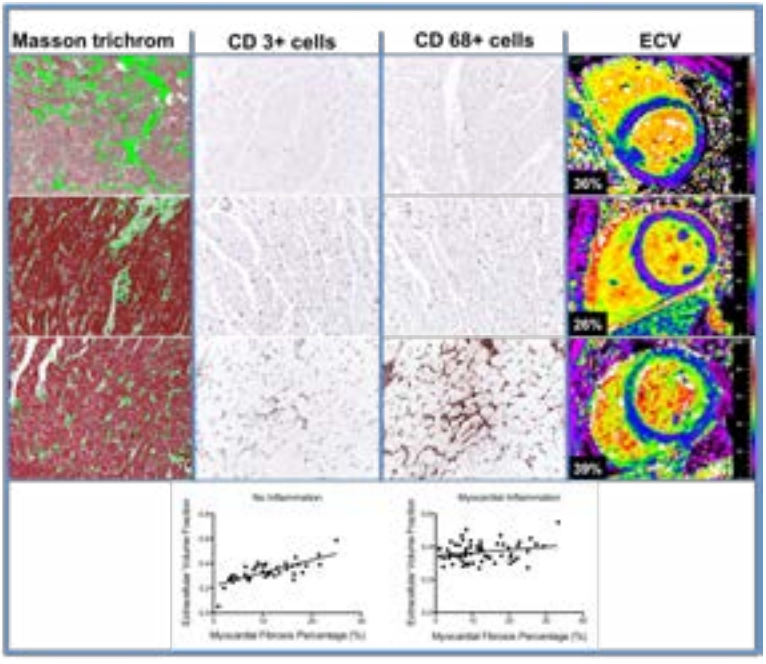

WP11

Fabry disease is a chronic inflammatory cardiomyopathy – insights from multiparametric mapping and blood biomarkers.

Sabrina Nordin, BMBS, MRCP(UK)[1]Rebecca Kozor, MBBS[2], Heerajnarain Bulluck, MBBS[3], Silvia Castelletti, MD[4], Stefania Rosmini, MD, PhD[1], Amna Abdel-Gadir, MBBS.MRCP(UK)[5], Thomas Treibel, MBBS.MRCP(UK)[1], Katia Menacho-Medina, MD[1], Giulia Benedetti, MD[6], Shanat Baig, MBBS[7], Nicola Edwards, PhD[7], Richard Steeds, PhD[7], Atul Mehta, PhD[8], Derralynn Hughes, PhD[8], Peter Kellman, PhD[9], Charlotte Manisty, PhD MBBS[10], James C Moon, MD[1]

1. *Barts Heart Centre, England, United Kingdom*
2. *Royal North Shore Hospital, Sydney, New South Wales, Australia*
3. *University College London, England, United Kingdom*
4. *UCL, N/A, Italy*
5. *University College London and Barts Heart Centre, London, England, United Kingdom*
6. *Barts Heart Centre, London, England, United Kingdom*
7. *University Hospitals Birmingham, England, United Kingdom*
8. *UCL, England, United Kingdom*
9. *NIH, MD*
10. *Barts Heart Centre and university college, London, England, United Kingdom*

Background: Fabry disease (FD) is a rare X-linked lysosomal storage disorder leading to left ventricular hypertrophy (LVH), myocardial fibrosis and heart failure. Cardiovascular Magnetic Resonance (CMR) detects characteristic T1 lowering, thought to be due to intracellular sphingolipid accumulation, and basal inferolateral late gadolinium enhancement (LGE), thought to be extracellular fibrosis. T2 mapping is a sensitive detector of inflammation and oedema but has not been explored in FD. We hypothesised that inflammation plays a role in FD, and investigated this using a combination of imaging (LGE, T1 and T2 mapping) and blood (troponin, NT-proBNP) biomarkers.

Methods: A single time-point cohort study using CMR with T1 mapping (MOLLI, 5s(3s)3s sampling), T2 mapping and LGE. This was performed on 184 patients: 66 FD (genetically confirmed), 28 hypertrophic cardiomyopathy (HCM), 30 chronic myocardial infarcts (cMI, 6 months post ST-elevation MI), plus 60 healthy controls (Figure 1). High sensitivity troponin T and NT-proBNP were prospectively collected for FD cases.

Results: Remote (septal) myocardial T1 was low in FD, but remote T2 was normal. LGE in FD behaved differently compared to HCM and cMI: firstly, it had lower absolute T1 (FD, HCM, cMI: 1098±66ms, 1180±66ms, 1138±52ms; $p < 0.05$), but higher T1 elevation over the low remote T1 (FD, HCM, cMI: 198±90ms, 158±62ms, 135±57ms, $p < 0.05$). Secondly, T2 was very high in FD LGE compared to the other diseases (FD, HCM, cMI: 63±7ms, 55±4ms, 54±3ms, $p < 0.001$,Figure 2), and normal controls (49±2ms).

Troponin elevation was found in 37% of cases where troponin was measured. This was related to LVH (positive vs negative: 72% (21/29) vs 3% (1/30), $p < 0.001$) and the presence of LGE (positive vs negative: 83% (19/23) vs 0% (0/31), $p < 0.001$). However, T2 in the LGE area and basal inferolateral wall was the single best multivariate predictor of troponin elevation in FD (B=2.9, $p < 0.001$), represented also by a strong significant correlation (Figure 3, $R^2=0.66$, $p < 0.001$. NT-proBNP rise was found in 21% of FD cases. T2 in the LGE area and basal inferolateral wall also correlated with the extent of NT-proBNP rise ($R^2=0.49$, $p=0.001$). Multivariate analysis for NT-proBNP revealed only eGFR as a significant predictor (B=-8.2, $p < 0.001$).

Conclusions: Using a combination of blood and CMR multiparametric imaging biomarkers, FD cardiomyopathy (when LGE is present) appears to be a chronic inflammatory cardiomyopathy. These data suggest inflammation links FD intracellular storage to focal extracellular LGE.

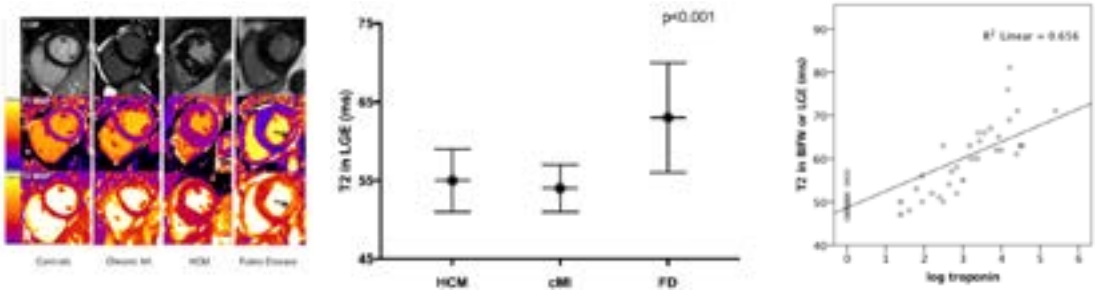

WP12

Cardiovascular magnetic resonance in transthyretin amyloidosis: an under-recognised and emerging cause of heart failure. A 230 patient prospective study

Ana Martinez-Naharro, MD[1] Thomas Treibel, MBBS.MRCP(UK)[2], Amna Abdel-Gadir, MBBS.MRCP(UK)[3], Heerajnarain Bulluck, MBBS[4], Giulia Zumbo, MD[5], Daniel S. Knight, MBBS MRCP(UK)[6], Tushar Kotecha, MBChB[5], Rohin Francis, MBBS[5], David Hutt, BApSc[5], Tamer Rezk, BSc[5], Stefania Rosmini, MD, PhD[2], Cristina Quarta, MD, PhD[5], Carol Whelan, MD[5], Peter Kellman, PhD[7], Julian Gillmore, MD, PhD[5], James Moon, MBBS, MD, MRCP[8], Philip Hawkins, PhD[5], Marianna Fontana, MD, PhD[5]

1. *National Amyloidosis Centre, University College London, London, England, United Kingdom*
2. *Barts Heart Centre, England, United Kingdom*
3. *University College London and Barts Heart Centre, London, England, United Kingdom*
4. *University College London, England, United Kingdom*
5. *National Amyloidosis Centre, University College London, England, United Kingdom*
6. *Royal Free London NHS Foundation Trust, London, England, United Kingdom*
7. *Laboratory of Cardiac Energetics, National Institutes of Health/NHLBI, Bethesda, MD, United States., MD*
8. *Barts Heart Center, The Cardiovascular Magnetic Resonance Imaging Unit and The Center for Rare Cardiovascular Diseases Unit, St Bartholomew's Hospital, West Smithfield, London, UK, England, United Kingdom*

Background: Heart failure caused by transthyretin amyloidosis (ATTR) is an under-appreciated cause of morbidity and mortality. Cardiovascular magnetic resonance (CMR) with T1 mapping and late gadolinium enhancement (LGE) is emerging as a candidate reference standard for non-invasive diagnosis of amyloidosis. The aim of this study was to examine CMR cardiac morphology and tissue characterisation and assess outcomes in the largest CMR ATTR cohort reported to date.

Methods: 230 patients were recruited: 135 with wild-type ATTR and 95 with h. All subjects underwent CMR with standard SSFP-cine imaging, LGE and T1 mapping with extracellular volume fraction (ECV) measurement. All participants also underwent 99mTc-3,3-diphosphono-1,2-propanodicarboxylic acid (Tc-DPD) scintigraphy, the current diagnostic reference standard for ATTR.

Results: ATTR was far less concentric/symmetric than expected with 23.8% symmetric, 46.8% asymmetric septal hypertrophy, 28.9% asymmetric septal hypertrophy with convexity and 0.5% with no LVH – see figure 1 for morphologies. ECV correlated with amyloid burden measured as cardiac uptake on Tc-DPD scintigraphy (pDuring follow-up (23±14months), 56 deaths occurred. ECV predicted death (hazard ratio, 1.13; 95% confidence interval, 1.06-1.20; $p < 0.0001$) and remained independent after adjustment for age, N-terminal pro-brain natriuretic peptide, ejection fraction, E/E' and left ventricular mass index (hazard ratio, 1.13; 95% confidence interval, 1.04-1.23; $P < 0.01$).

Conclusions: Asymmetric LVH, traditionally associated with hypertrophic cardiomyopathy, is the commonest pattern of hypertrophy in ATTR amyloidosis. LGE imaging has a high diagnostic accuracy in all patients with definite cardiac involvement. ECV in ATTR amyloidosis correlates with the amyloid burden and provides incremental information on outcome even after adjustment for known prognostic factors.

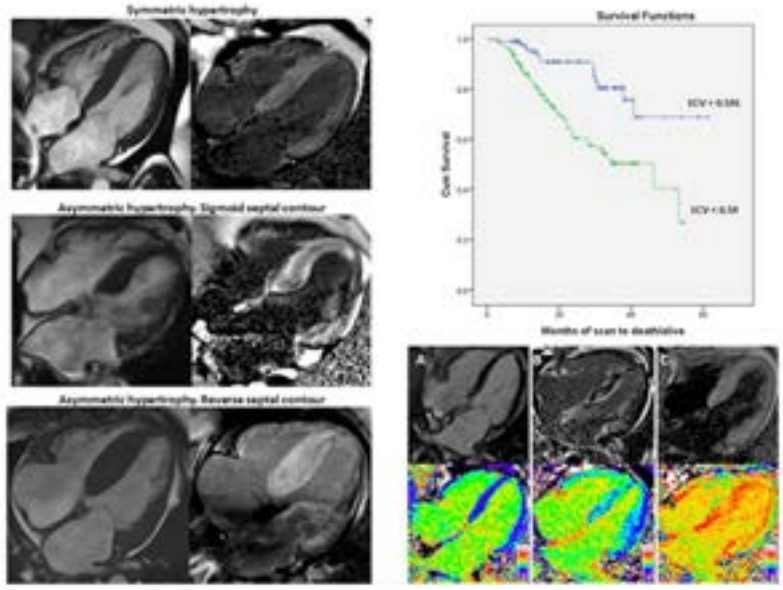

WP13

Extracellular volume fraction may predict outcomes among hypertrophic cardiomyopathy patients without late gadolinium enhancement

Clement F. Cholet, M.D.[1]Mark Kennedy, BS[2], Jeffrey Chung, MD[2], Peter Kellman, PhD[3], Erik B. Schelbert, MD, MS[4], Timothy C. Wong, MD MS[5]

1. *University of Pittsburgh Medical Center, Paris, N/A, France*
2. *University of Pittsburgh Medical Center, PA*
3. *Laboratory of Cardiac Energetics, National Institutes of Health/NHLBI, Bethesda, MD, United States., MD*
4. *University of Pittsburgh; Heart and Vascular Institute of UPMC, PA*
5. *University of Pittsburgh Medical Center, Pittsburgh, PA*

Background: Late gadolinium enhancement (LGE) imaging using cardiovascular magnetic resonance is associated with a higher risk of morbidity and mortality in hypertrophic cardiomyopathy. However, approximately 1/3 of patients do not demonstrate appreciable LGE. Extracellular volume fraction (ECV) utilizing T1 measurement detects fibrosis across the spectrum from focal to diffuse, and also overcomes certain limitations of LGE. We hypothesized that ECV might provide additional prognostic information in the subset of patients without LGE.

Methods: We prospectively consented 234 patients with HCM to research imaging at the time of CMR (1.5 Tesla) at our institution between 2010 and 2015. Systemic disease such as amyloidosis was excluded. Phase sensitive inversion recovery images in the short and long axes were acquired 10 minutes after 0.2 mmol/kg gadolinium contrast administration for LGE evaluation. Native T1 and ~20 minute post contrast T1 were measured using Modified Look-Locker (MOLLI) sequences acquired in the short axis plane (base and mid). ECV was then determined using hematocrit drawn at the time of CMR. All-cause mortality and hospitalization for heart failure (HHF) were determined by electronic medical record review using prespecified criteria. The protocol was approved by the local institutional review board.

Results: In our cohort, 70 patients did not demonstrate LGE; of whom 5 died and 3 had HHF (2 had both) over a median of 2.3 years of follow up from the CMR date. Mean ECV was 34.5% (± 9.2) among those with death or HHF, and 25.5% (± 3.1) among those without events; $p < 0.001$. Among those who died, ECV ranged from 27.8% to 48.3% (see Figure).

Conclusions: ECV in LGE negative patients with HCM associates with outcomes, and may provide additional prognostic information to traditional CMR imaging. Further studies are warranted.

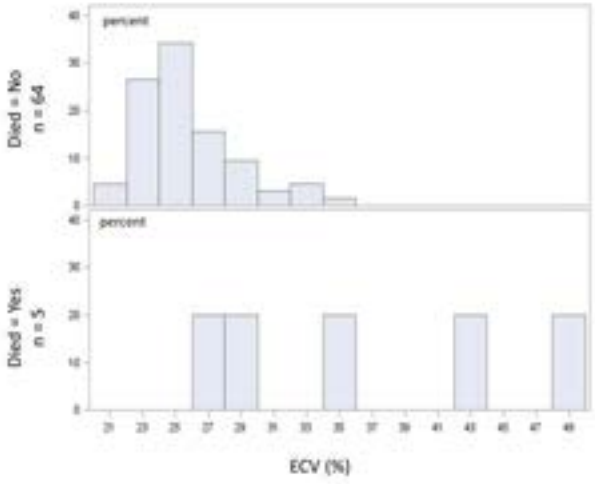

WP14

Predictive role of myocardial fibrosis in thalassemia intermedia patients

Antonella Meloni, PhD[1]Martino Cinquetti, MD[2], Nicola Giunta, MD[3], Pietro Giuliano, MD[3], Laura Pistoia, MSc[4], Carmelo Errigo, MD[5], Pier Paolo Bitti, MD[6], Antonino Vallone, MD[7], Vincenzo Positano, MSc[4], Cristina Salvatori, MSc[4], Gianfranco Sinagra, MD[2], Alessia Pepe, MD, PhD[4]

1. *Fondazione G. Monasterio CNR Regione Toscana, Pisa, Toscana, Italy*
2. *Azienda Ospedaliero-Universitaria "Ospedali Riuniti", Friuli-Venezia Giulia, Italy*
3. *"ARNAS" Civico, Di Cristina Benfratelli, Sicilia, Italy*
4. *Fondazione G. Monasterio CNR Regione Toscana, Toscana, Italy*
5. *Presidio Ospedaliero Locri - A.S.P di Reggio Calabria, Calabria, Italy*
6. *Presidio Ospedaliero "San Francesco" ASL Nuoro, Sardegna, Italy*
7. *Azienda Ospedaliera "Garibaldi" Presidio Ospedaliero Nesima, Sicilia, Italy*

Background: Myocardial fibrosis detected by late gadolinium enhancement (LGE) cardiac magnetic resonance (CMR) is currently used to predict adverse cardiovascular events in different cardiomyopathies. However, its clinical implications in thalassemia intermedia (TI) have not been studied. The aim of this study was to assess the distribution and the predictive value of myocardial fibrosis for future events in TI.

Methods: We considered 218 white TI patients (37.82±11.00 years, 113 females) consecutively enrolled in the Myocardial Iron Overload in Thalassemia (MIOT) network and free of cardiac complications concomitant to CMR. LGE images were acquired to detect myocardial fibrosis and the extent of LGE areas was quantified using a semiautomatic, previously validated software.

Results: Myocardial fibrosis was detected in 46 patients (21.1%). LGE followed a subendocardial ischemic pattern typical of coronary artery disease in two patients. One patient showed both an ischemic and non ischemic pattern. Thirty-two patients had a single focus while 14 had at least two foci. The mean number of LGE segments per patient was 2.70±1.52. LGE involved the septal region in 76.1% of patients. The extent of LGE areas was 2.09±1.77% of the total left myocardial mass. Twenthy-two (47.8%) patients showed fibrosis in the infero- or anteroseptal junction, 18 (39.1%) had a non ischemic no-junctional pattern (intra or subepicardial) and 6 (13.0) had both a junctional and no-junctional pattern. Mean follow-up was 56.76±23.17 months. We recorded 13 cardiac complications: 1 heart failure, 7 arrhythmias and 5 pulmonary hypertension (PH). Myocardial fibrosis was a significant prognosticator for arrhythmias, PH and cardiac complications globally considered (see Table). Number of segments with LGE and extent of myocardial fibrosis were comparable in patients who developed cardiac complications versus the patients who did not.

Conclusions: In TI patients, myocardial fibrosis is a predictor of adverse outcome.

Cardiac complications		PH		Arrhythmias		
HR (95%CI)	N (%)	HR (95%CI)	N (%)	HR (95%CI)	N (%)	
Reference 8.14 (2.51-26.44)	4 (2.3) 9 (19.6)	Reference 14.53 (1.62-130.12)	1 (0.6) 4 (8.7)	Reference 4.84 (1.08-21.63)	3(1.7) 4(8.7)	***Fibrosis*** ***No (N=172)*** Yes (N=46)

WP15

Intermediate Signal Late Gadolinium Enhancement is Predictive of Sudden Cardiac Death and Appropriate ICD Shock in Patients With Non-Ischemic Dilated Cardiomyopathy

Kai Homer[1] Yoko Mikami, MD, Ph.D[2], Steven Dykstra, MSc[3], Aidan Cornhill, BMSc, HBA[3], Andrew Roberts[4], Claire Sumner[4], Karen Cowan, RN[4], Bobby Heydari, MD, MPH[3], Andrew Howarth, MD[3], Carmen P. Lydell, MD[3], Derek Exner, MD[4], James White, MD, FRCP(C) [5]

1. *Stephenson Cardiac Imaging Centre, Libin Cardiovascular Institute of Alberta, University of Calgary, Edmonton, AB, Canada*
2. *Stephenson Cardiac Imaging Centre, Libin Cardiovascular Institute of Alberta, University of Calgary, Calgary, AB, Canada*
3. *Stephenson Cardiac Imaging Centre, Libin Cardiovascular Institute of Alberta, University of Calgary, AB, Canada*
4. *Libin Cardiovascular Institute of Alberta, University of Calgary, AB, Canada*
5. *Stephenson Cardiovascular Imaging Center, University of Calgary, AB, Canada*

Background: Implantable cardioverter defibrillators (ICDs) have been shown to reduce sudden cardiac death (SCD) in patients with non-ischemic dilated cardiomyopathy (NIDCM) and a left ventricular ejection fraction (LVEF) ≤ 35%. However, a majority of patients do not appreciate benefit from their device by 3 years, suggesting modest accuracy and precision for the selection of patients most likely to benefit. We sought to explore the value of intermediate signal intensity Late Gadolinium Enhancement (LGE), a candidate marker of arrhythmogenic substrate, for the prediction of life-threatening arrhythmias in this population.

Methods: Two-hundred patients with NIDCM underwent cardiac magnetic resonance (CMR) with LGE imaging prior to ICD implantation and were followed for the primary outcome of SCD or appropriate ICD shock. Thirty-seven (19%) had a history of prior ventricular arrhythmia (VA). No patients with any known etiology for their cardiomyopathy were included in the study. LV volumes were measured from short-axis cine images using commercially available software (cvi[42], Circle Cardiovascular Imaging Inc. Calgary). LGE images were visually scored for the presence and distribution of LGE followed by signal threshold-based quantification using a >3SD and >5SD signal intensity threshold above the mean signal of reference myocardium, identified on each slice. Dense LGE was defined as tissue with any signal >5SD, and intermediate LGE defined as tissue with signal intensity between >3SD and >5SD thresholds (3-5SD) (Figure 1).

Results: The mean age of the population was 59.3±11.8 years (69.2% male) with a mean LVEF of 26.2±9.8%. A total of 51 primary outcomes occurred during a median follow-up of 1152 days. LGE imaging identified 85 patients (42.5%) with a mid wall septal distribution of LGE. LGE quantification provided a mean extent of dense LGE (>5SD) and intermediate LGE (3-5SD) of 2.7±6.5% and 3.4±3.7% of the LV mass, respectively. Both quantitative LGE markers were associated with the primary outcome ($p < 0.05$) with ROC analysis providing optimal thresholds of 2.5% and 6.6%, respectively. In multivariable analysis adjusted for age, prior VA, LVEF, and mid-wall striae LGE, intermediate LGE >6.6% robustly predicted the primary outcome with an adjusted HR of 3.1 ($p < 0.001$). The same model constructed with Dense LGE >2.5% showed inferior predictive utility (HR 2.3, p=0.006). Intermediate signal LGE >6.6% identified patients at a high (17.7%) versus low (5.8%) annualized risk of SCD or ICD shock.

Conclusions: Intermediate signal LGE is independently associated with sudden cardiac death or appropriate ICD shock in patients with NIDCM.

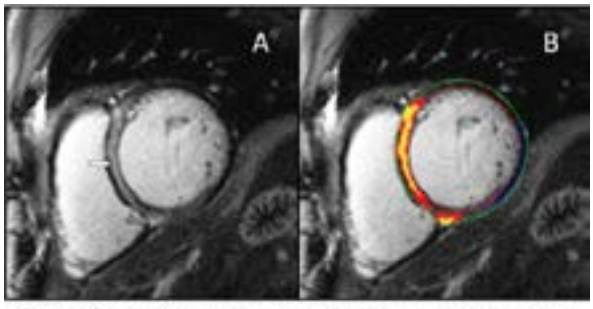

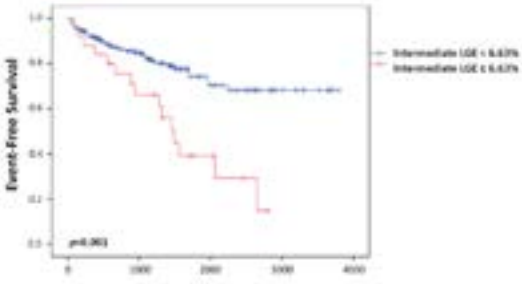

WP16

Native T1 and T2 mapping in recognition of cardiac involvement in systemic sarcoidosis

Valentina O. Puntmann, MD, PhD[1] Alexander Isted, MBBS[2], Rocio Hinojar, MD[3], Lucy Foote, MBBS, BA[4], Gerry Carr-White, MBBS, PhD[2], Eike Nagel, MD, PhD[5]

1. *Institute of experimental and translational cardiovascular imaging, Frankfurt, Hessen, Germany*
2. *Guys and St Thomas's Hospital, England, United Kingdom*
3. *Ramon y Cajal University Hospital, Madrid, Madrid, Madrid, Spain*
4. *King's College London, London, England, United Kingdom*
5. *University Hospital Frankfurt; Institute for Experimental and Translational Cardiovascular Imaging; DZHK Centre for Cardiovascular Imaging, Frankfurt, N/A, Germany*

Background: Cardiac involvement in systemic sarcoidosis has a major prognostic impact. Non-invasive and accurate diagnostic pathways could guide management and improve prognosis. We investigated the comparative ability of T1 and T2 mapping by CMR to Heart Rhythm Society (HRS) and Japanese Ministry of Health and Welfare (JMHW) diagnostic criteria.

Methods: Consecutive subjects with a biopsy-proven extra-cardiac diagnosis of systemic sarcoidosis (n=53) were enrolled. CMR was performed for assessment of cardiac volumes, function and late gadolinium enhancement (LGE), as well as T1 and T2 mapping. A follow-up sub-study was performed in 40 patients (144±35 days); of these 18 subjects received anti-inflammatory treatment for systemic symptoms.

Results: Pulmonary sarcoidosis was the predominant systemic involvement (n=35, 66%) and dyspnoea the most common symptom (n=19, 36%). Compared to controls (n=21), patients had higher ventricular volumes, myocardial T1 and T2 indices, reduced longitudinal strain ($p < 0.05$ for all), but similar ejection fraction (p=0.057). Native T1 and T2 had higher discriminatory accuracy (AUC: 0.96 and 0.86) compared to the JMHW and HRS diagnostic criteria (AUC: 0.61 and 0.67) (Table 1). Native T1 was the independent discriminator between health and disease. Patients receiving anti-inflammatory treatment showed a significant improvement of native T1 and T2 compared to those without treatment ($p < 0.01$).

Conclusions: Novel quantitative myocardial tissue characterization by T1 and T2 mapping can provide accurate non-invasive recognition of cardiac involvement and of myocardial inflammation, over and above LGE, HRS and JMHW criteria. Future studies will confirm their role in risk stratification and clinical management in cardiac sarcoidosis.

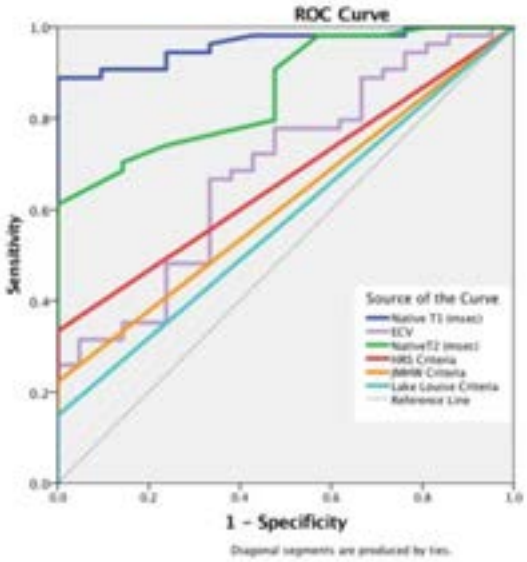

WP17

Extracellular matrix expansion as measured by cardiac MRI impacts diastolic dysfunction

Akira Wada, M.D.[1]Karolina Zareba, M.D.[2], Subha Raman, M.D.[3]

1. *Ohio State University Wexner Medical Center, Columbus, OH*
2. *The Ohio State University Wexner Medical Center, Columbus, OH*
3. *The Ohio State University Wexner Medical Center, OH*

Background: Extracellular matrix expansion has been implicated as a contributor to diastolic dysfunction. Cardiac MRI (CMR) allows quantification of diffuse myocardial fibrosis with extracellular volume fraction (ECV). We sought to evaluate the relationship between diastolic dysfunction as determined by echocardiography and myocardial ECV as measured by CMR.

Methods: We studied 28 patients with an elevated ECV (≥29%) as measured by CMR, and 20 patients with a normal ECV (< 29%) who had a transthoracic echocardiogram with evaluation of diastolic function within 90 days. All patients had preserved systolic function. T1 maps were acquired using a steady state free precession based modified Lock-Locker inversion recovery (MOLLI) sequence. ECV was calculated using pre and post gadolinium T1 values and corrected for hematocrit. Diastolic function was determined based on current standard criteria.

Results: Baseline characteristics did not differ between the elevated and normal ECV groups, including age, gender, hypertension, or presence of late gadolinium enhancement. The mean ECV in patients with abnormal diastolic function was higher compared to those without diastolic dysfunction (31.4% vs 27.4%, p=0.001). As expected, patients with an ECV ≥29% were more likely to have diastolic dysfunction compared to patients with a normal ECV < 29% (71.4% vs 10%, p= < 0.005). In patients with an elevated ECV, E' velocity was lower (9.6 m/sec vs 12.4 m/sec, p= < 0.005), E/E' ratio was higher (10.3 vs 6.5, p=0.003), and left atrial volume index was larger (33.9 ml/m2 vs 25.4 ml/m2, p=0.013) compared to patients with a normal ECV.

Conclusions: Patients with an elevated ECV are more likely to exhibit diastolic dysfunction as measured by echocardiography. Our study highlights that changes in myocardial interstitium adversely affect diastolic function.

WP18

Left atrial dilatation and impaired atrial function are associated with the burden of left ventricular interstitial fibrosis in arterial hypertension

Tamas Erdei, PhD[1]Jonathan C. L. Rodrigues, MBChB (Hons), FRCR[2], Amardeep Ghosh Dastidar, MBBS(Hons), MRCP[3], Amy E. Burchell, MA BMBCh[4], Laura E. K. Ratcliffe, MBBS BSc (Hons)[4], Emma C. Hart, PhD[4], Mark C. K. Hamilton, FRCR[5], Julian F. Paton, PhD[6], Angus K. Nightingale, MD FESC[7], Chiara Bucciarelli-Ducci, MD, PhD[6], Nathan E. Manghat, FRCR, MD[8]

1. *Cardiac MRI Unit, Bristol Heart Institute, Bristol, Bristol, England, United Kingdom*
2. *Bristol Heart Institute, England, United Kingdom*
3. *NIHR Bristol Cardiovascular Biomedical Research Unit, Bristol, England, United Kingdom*
4. *University of Bristol, England, United Kingdom*
5. *Bristol Royal Infirmary, England, United Kingdom*
6. *University of Bristol, Bristol, England, United Kingdom*
7. *Bristol Heart Institute, Bristol, England, United Kingdom*
8. *Bristol Royal Infirmary, Bristol, England, United Kingdom*

Background: In arterial hypertension, left atrial enlargement (LAE) is a significant independent predictor of adverse cardiovascular morbidity and mortality. Impaired left atrial (LA) function also confers poor long-term prognosis. We tested the hypothesis that the burden of left ventricular (LV) interstitial fibrosis is associated with LAE and impaired LA function. We used cardiac magnetic resonance imaging (CMR) T1 mapping sequences to non-invasively quantify the degree of LV myocardial interstitial fibrosis.

Methods: 86 hypertensive patients (49±15 years, 53% male) underwent CMR at 1.5T. LV mass and volumes were measured using validated threshold-detecting software. T1 mapping was performed with a validated modified look-locker inversion-recovery sequence. Extracellular volume fraction (ECV)was calculated: $ECV=(\Delta R1_{myocardium}/\Delta R1_{blood\text{-}pool})x(1\text{-haematocrit})$; where: $\Delta R1=(1/\text{postcontrast T1-1/native T1})$. Indexed interstitial volume was calculated by multiplying ECV by indexed myocardial cell volume (indexed LV mass divided by myocardial specific gravity 1.05 g/mL).
LA volumes were assessed using the biplane area-length method. LA function was assessed by the phasic volumetric method, measuring LA volumes at different points of the cardiac cycle: 1) maximal LA volume (LAVmax) just before mitral valve opening, 2) minimal LA volume (LAVmin) at mitral valve closure and 3) pre-A LA volume (LAVpre-A) preceding LA contraction. LA reservoir function was defined as LA total emptying fraction (LAVmax–LAVmin)/LAVmax). LA conduit function was defined as LA passive emptying fraction (LAVmax–LAVpre-A)/LAVmax. LA pump function was calculated as the LA active emptying fraction (LAVpre-A–LAVmin)/LAVpre-A.

Results: Structurally, there was a significant positive relation between indexed LV mass and LA size (LAVmax: $R = 0.345$, $P < 0.001$).

Functionally, as indexed LV mass increased, there were significant reductions in LA reservoir ($R=-0.439$, $P < 0.0001$) and conduit function ($R=-0.345$, $P < 0.0001$) but not in LA pump function ($R=-0.149$, $P=0.117$).

At the intra/extracellular myocardial structural level, increasing ECV was associated with increasing LA size (LAVmax: $R = 0.359$, $P < 0.001$). Furthermore, increasing indexed myocardial interstitial volume was associated with significant reductions in both LA reservoir ($R=-0.437$, $P < 0.0001$) and conduit function ($R=-0.316$, $P=0.003$) but not in LA pump function ($R=-0.167$, $P=0.125$).

Conclusions: We provide novel insights into atrio-ventricular interaction in arterial hypertension using T1 mapping techniques which support the hypothesis that the burden of LV interstitial fibrosis is associated with LAV enlargement and this impairs reservoir and conduit function. LA pump function is preserved, which offers hope that, if future anti-fibrotic anti-hypertensive agents can reduce LV interstitial fibrosis, the observed LA structural and functional abnormalities may be able to reverse remodel.

WP19

Eplerenone, a mineralocorticoid receptor antagonist, protects the microvasculature and prevents impaired myocardial perfusion reserve in mice fed a high fat diet

Daniel A. Auger, Ph.D[1] Rene J. Roy, BS[1], Franck A. Tonleu, BS[2], Leigh Bradley, B.S.[3], Miranda E. Good, Ph.D[2], Brant E. Isakson, PhD[2], Krister Bamberg[4], Ulrika Johansson, BSc[4], Peter Akerblad[5], Frederick H. Epstein, Ph.D.[3], Matthew Wolf, MD PhD[1]

1. *University of Virginia, Charlottesville, VA*
2. *University of Virginia School of Medicine, VA*
3. *University of Virginia, VA*
4. *AstraZeneca R&D Gothenburg, CVMD iMed, Molndal, N/A, Sweden*
5. *AstraZeneca PLC, England, United Kingdom*

Background: Impaired myocardial perfusion reserve (MPR) is prevalent in obesity and diabetes, can occur in the presence or absence of obstructive coronary artery disease (CAD), and portends a high risk of adverse cardiac events. The mechanisms underlying impaired MPR in the absence of CAD are not completely understood and therapies are not well established. We recently showed that mice fed a high fat diet (HFD) are a model of obesity, diabetes, impaired MPR without obstructive CAD, and coronary microvascular disease (1). Here we used CMR and other methods to test the hypothesis that Eplerenone (EPL), a mineralocorticoid receptor antagonist, protects the microvasculature and prevents impaired MPR in HFD mice.

Methods: Untreated (n=11) and EPL-treated (n=8) HFD mice were studied. HFD (60% calories from fat) was initiated at 6 weeks of age and continued for 24-26 weeks. In the treatment group, EPL (100 mg/kg) was added to the HFD chow. CMR (7T Clinscan, Bruker) was performed at 24 ± 2 weeks after the start of HFD. CMR included multi-slice short-axis cine imaging covering the left ventricle (LV) for the assessment of LV volumes, ejection fraction, LV mass and LV end-diastolic wall thickness (LVWT), short-axis cine DENSE in a mid-ventricular slice for the assessment of strain (Ecc), and first-pass gadolinium-enhanced CMR at rest and after Regadenoson (0.1µg/g body weight) for the assessment of perfusion and MPR. Glucose tolerance tests (GTTs) were also performed. After euthanasia, perivascular fibrosis was quantified using Masson Trichrome staining, and mesenteric arteriolar compliance was measured using pressure arteriography.

Results: No significant differences were found in body weight, glucose tolerance, LV structure and LV systolic function between groups (Table 1). However, parameters related to microvascular disease were different. Specifically, while rest and stress perfusion were not different, MPR was significantly higher for EPL-treated mice (Fig. 1), with a value similar to previously-studied mice fed a low-fat diet (1). Similarly, there was significantly less perivascular fibrosis and greater arteriolar compliance in EPL-treated mice (Fig. 2).

Conclusions: CMR, histology and vascular compliance demonstrate that EPL protects the microvasculature and prevents impairment of MPR in HFD mice. Future studies are warranted to explore treatment with mineralocorticoid receptor antagonism and investigate cellular and molecular mechanisms. **References: (1)** Naresh et al. Cardiac MR Detects the Progression of Impaired Myocardial Perfusion Reserve and Increased LV Mass in Mice Fed a High-fat Diet. JCMR in press. **Acknowledgements:** Funding: NIH R01 EB001763 and AstraZeneca. .

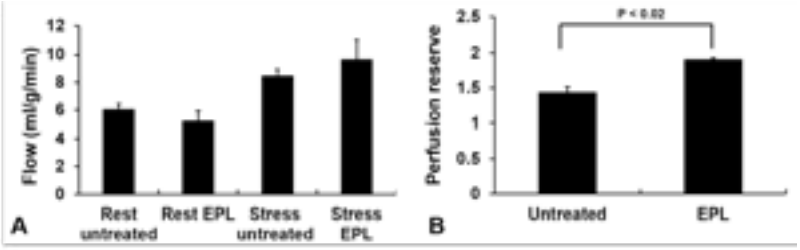

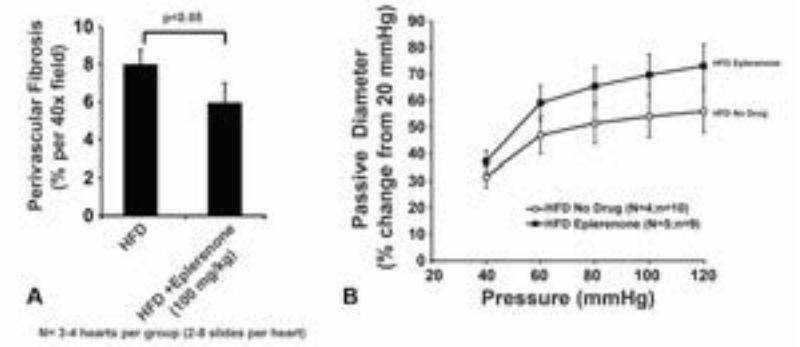

Table 1: Body weight, glucose tolerance, LV structure and LV systolic function parameters in untreated and EPL-treated HFD mice at 24 weeks post diet.

p-value	EPL treated	Untreated	
>0.05	37.19 ± 1.96	39.14 ± 1.19	**Weight (g)**
>0.05	32010 ± 1878	30857 ± 1063	**Glucose intolerance (AUC)**
>0.05	40 ± 3	41 ± 3	**LVEDV (µL)**
>0.05	14 ± 1	15 ± 2	**LVESV (µL)**
>0.05	65.13 ± 1.40	62.95 ± 2.48	**EF (%)**
>0.05	-0.11 ± 0.02	-0.10 ± 0.02	**End-systolic Ecc**
>0.05	89 ± 1	91 ± 1	**LV mass (mg)**
>0.05	0.90 ± 0.11	0.96 ± 0.10	**LVWT (mm)**

WP20

Cardiac magnetic resonance feature tracking (CMR-FT) depicts early changes of myocardial function induced by serelaxin in a mouse model of chronic heart failure

Tomas Lapinskas, MD[1] Sarah Jeuthe, MD[2], Daniel R. Messroghli, MD[3], Heike Meyborg, MD[4], Ulrich Kintscher, MD, PhD[2], Rolf Gebker, MD, PhD[4], Remigijus Zaliunas, MD, PhD[1], Burkert Pieske, MD, PhD[4], Philipp Stawowy, MD, PhD[4], Sebastian Kelle, MD, PhD[4]

1. *Lithuanian University of Health Sciences, Kaunas, Kauno Apskritis, Lithuania*
2. *Charité-Universitätsmedizin Berlin, Berlin, Berlin, Germany*
3. *Charité Universitätsmedizin and Deutsches Herzzentrum Berlin, Berlin, Berlin, Germany*
4. *German Heart Institute Berlin, Berlin, Berlin, Germany*

Background: Initial animal studies have shown that serelaxin (recombinant human relaxin) has positive effects on vascular compliance and ventricular remodeling in heart failure. This study aimed to assess the impact of serelaxin on myocardial deformation using cardiac magnetic resonance feature tracking (CMR-FT) and to elucidate the relationship between myocardial mechanics and histological findings.

Methods: Twenty-eight C57BL/6J male, 8-9 week old mice were subjected to SHAM or transverse aortic constriction (TAC) surgery. After 10 weeks TAC-operated mice were randomized into two groups which received either serelaxin 0.5 mg/kg per day (TAC_Srlxn) or sodium acetate (TAC_Veh) administered as a continuous intravenous infusion using Alzet mini pumps for up to 4 weeks. CMR was performed on a 3 T small-animal MRI system (MRS 3017, MR Solutions, Guildford, UK) at week 10 (before start of study treatment) and 14 (end of study treatment) after surgery. The cine images were used to calculate left ventricular (LV) longitudinal (Ell_{LV}), circumferential (Ecc_{LV}) and radial (Err_{LV}) strain using dedicated software (CMR^{42}, Circle Cardiovascular Imaging Inc., Calgary, Canada). After the 14th week mice were sacrificed and hearts were harvested for histological analysis. Cross-sections of hearts at the mid-ventricular level were fixed in formalin, embedded in paraffin and stained with Picrosirius red for detection of collagen content.

Results: There were no significant differences in LV deformation parameters before randomization in the different groups. All animals which received serelaxin demonstrated significant improvement in all LV strain parameters at week 14 when compared with the TAC_Veh group (Ell_{LV}: -17.5 ± 2.0 % vs. -15.4 ± 2.7 %; p = 0.030; Ecc_{LV}: -17.5 ± 2.1 % vs. -14.2 ± 2.0 %; p = 0.001; Err_{LV}: 34.5 ± 7.3 % vs. 26.3 ± 5.2 %; p = 0.011). There was a significant positive correlation between Ecc_{LV} and the extent of perivascular fibrosis (p = 0.011, r^2 = 0.259).

Conclusions: CMR-FT is a novel and sensitive technique to detect early changes in LV myocardial performance. Myocardial deformation parameters derived from CMR-FT correlate with the histomorphometric findings.

Research was funded by Novartis (Basel, Switzerland).

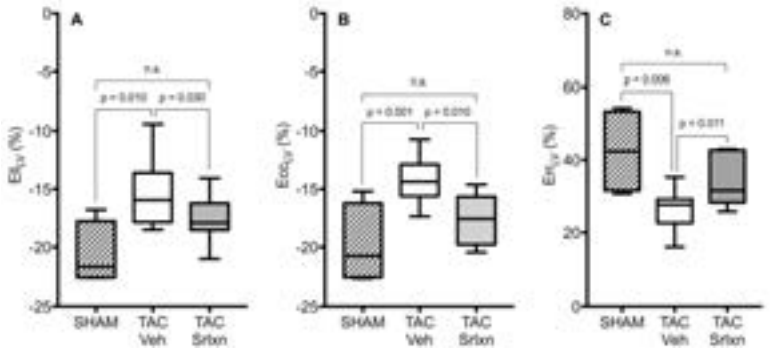

WP21

Intramyocardial Reperfusion Hemorrhage Leads to Infarct Expansion Beyond the Area-At-Risk: Evidence from Cardiac Magnetic Resonance Imaging in Dogs

Andreas Kumar, MD, MSc[1], Rohan Dharmakumar, PhD[2] Avinash Kali, PhD[2], Ivan Cokic, MD[3], Hsin-Jung Yang, PhD[4], Joseph Francis, B.V.Sc., Ph.D[5]

1. *Northern Ontario School of Medicine, Sudbury, ON, Canada*
2. *Cedars-Sinai Medical Center: BIRI, CA*
3. *Cedars-Sinai Medical Center: BIRI, Los Angeles, CA*
4. *Cedars Sinai Medical Center, Los Angeles, CA*
5. *Louisian State University, LA*

Background: Hemorrhage is a consequence of reperfusion injury in some infarcts and most large infarctions are hemorrhagic. However, whether hemorrhage itself can drive infarct expansion has not been investigated. Endothelial nitric oxide can be scavenged by hemoglobin breakdown products from hemorrhage; this leads to oxidative stress. We therefore hypothesized that hemorrhage per se can drive acute infarct size beyond the initial area at risk.

Methods: After ethics approval, forty dogs underwent ischemia by surgical occlusion of the left anterior descending coronary artery. Occlusion was released after 3h (n=20), or maintained indefinitely to create infarction of the entire area-at-risk (control group, n=20). A cardiac 3T MRI study was performed for hemorrhage (T2*-weighted CMR) and infarct size (late gadolinium enhancement), covering the entire left ventricle. Infarct sizes were quantified and compared in the reperfused/ hemorrhagic (R/H+) group, versus the reperfused/ non-hemorrhagic group (R/H-) and the control group (NR).

Results: The reperfused group yielded 9 dogs with hemorrhage (R/H+), and 8 dogs with no hemorrhage (R/H-); 3 dogs died prematurely. In the non-reperfused (NR) group, 16 dogs survived (4 died prematurely). All dogs had MI (Figure, panel A). Acute MI size in R/H+ was more than 2-fold greater than NR and R/H- groups ($p < 0.01$). There was no difference in infarct size between NR and R/H- groups ($p=0.8$). There was a strong correlation between hemorrhage size and acute MI size ($R=0.8$, $p < 0.01$). At 2 month follow-up, chronic MI size in R/H+ was 1.6-fold greater than NR and 1.8-fold greater than R/H- groups ($p < 0.01$). In the chronic phase, again no difference was observed between NR and R/H- groups ($p=0.7$) (Figure, Panel B).

Conclusions: Reperfusion hemorrhage can expand infarct size beyond the area at risk. When validated in patients, this could have major implications for late reperfusion, where reperfusion hemorrhage is an expected complication.

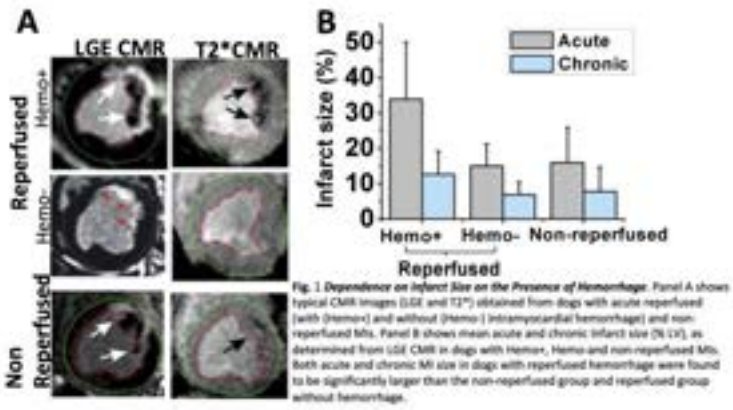

Fig. 1 **Dependence on Infarct Size on the Presence of Hemorrhage**. Panel A shows typical CMR images (LGE and T2*) obtained from dogs with acute reperfused [with (Hemo+) and without (Hemo-) intramyocardial hemorrhage] and non-reperfused MIs. Panel B shows mean acute and chronic infarct size (% LV), as determined from LGE CMR in dogs with Hemo+, Hemo- and non-reperfused MIs. Both acute and chronic MI size in dogs with reperfused hemorrhage were found to be significantly larger than the non-reperfused group and reperfused group without hemorrhage.

WP22

High-resolution late gadolinium enhancement MRI of ex vivo infarcted porcine hearts to characterize the three-dimensional structure of surviving myocardium

Farhad Pashakhanloo, PhD[1] Daniel A. Herzka, PhD[2], Muz Zviman, PhD[3], Henry Halperin, MD, MA[4], Elliot McVeigh, PhD[5], Natalia Trayanova, PhD, FAHA[6]

1. *Johns Hopkins University, MD*
2. *Johns Hopkins University School of Medicine, Baltimore, MD*
3. *Johns Hopkins University School of Medicine, MD*
4. *Johns Hopkins University, Baltimore, MD*
5. *University of California San Diego, CA*
6. *Johns Hopkins Unviersity, Biomedical Engineering and Medicine, Baltimore, MD*

Background: Surviving myocardial fibers surrounding the infarct promote ventricular arrhythmias by providing tortuous conducting pathways for the electrical activation. Therefore, obtaining an accurate knowledge of the three-dimensional structure of surviving myocardium in the zone of infarct is important for understanding the underlying mechanisms of post-infarction arrhythmias and design of improved therapies. We employ an *ex vivo* LGE-MRI technique to image infarcted porcine hearts at a voxel-size more than 400-fold lower than that of clinical-MRI. We next introduce a new metric and apply that to the acquired data to systematically characterize the structure of surviving myocardial tissue in the zone of infarct.

Methods: A 3D T1-W Gradient Echo LGE-MRI was performed *ex vivo* on a clinical scanner to image the whole heart and infarct geometry in 8 intact porcine hearts with chronic infarction (acquired resolution: 0.25×0.25×0.50 mm^3, TE/TR: 2.3/12 ms, flip-angle: 15°, Fig.1). The scar and viable myocardium were segmented from the images using Otsu thresholding, and a 3D finite-element mesh was constructed for each heart (Fig.2A). A local metric was defined on each point of the scar surface that reflects the local structure of surrounding surviving myocardium. It involves finding, for each point, the smallest thickness of surrounding tissue (Fig.2B), and therefore provides an efficient way to characterize the local structure of the tissue. These thickness values were mapped onto the 3D scar geometry, and the corresponding pooled distributions were calculated for all the hearts.

Results: Figure 1 presents a short-axis slice of LGE image, highlighting the scar and surviving surrounding tissue with heterogeneous thickness throughout the infarct. The 3D map of scar geometry color-coded with the thickness metric in Fig.2C illustrates the complex spatial distribution of the sub-endocardial surviving tissue in the same heart. Figure 3 presents pooled histograms of surviving tissue thickness measured over the scar surfaces of all the hearts. The mean value of the thickness metric was 2.0 mm with interquartile interval of [0.57-2.21] mm.

Conclusions: High-resolution LGE-MRI in conjunction with the developed metric unveiled the detailed architecture of scar and the spatial distribution of surviving tissue surrounding the scar. This knowledge may help better understand of the role of infarct structure in the formation of ventricular arrhythmias. In addition, the findings on the distribution of the surviving tissue thickness in the zone of infarct could engender an improved interpretation of data obtained from lower resolution clinical LGE-MRI, and therefore enhance the identification of substrates for ventricular arrhythmias.

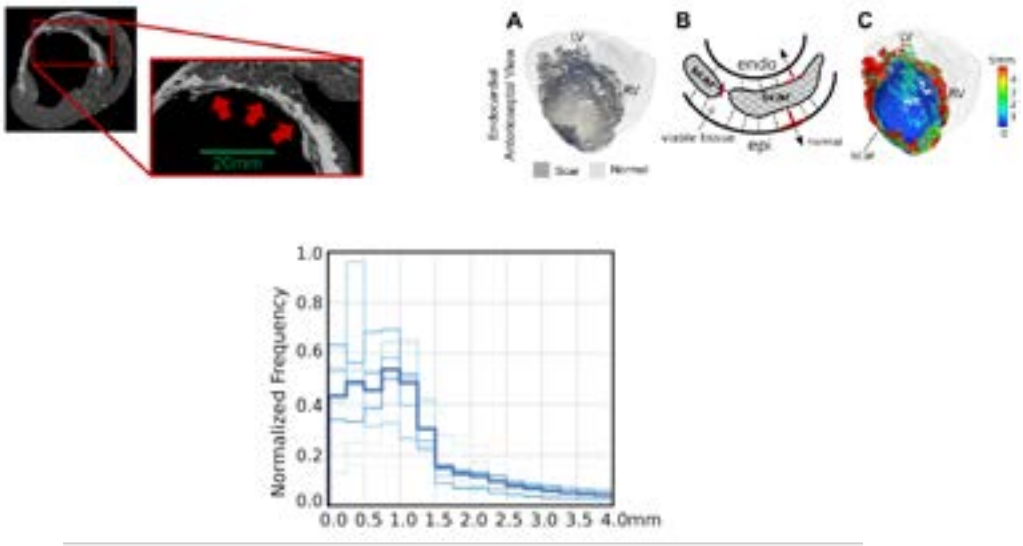

WP23

Characterization of left ventricular injury and remodelling using serial CMR scans in a swine model of myocardial infarction with ventricular arrhythmia

John Whitaker, BM BCh[1]Cory Tschabrunn, PhD[2], Jihye Jang, M.Sc.[3], Eran Leshem, MD[4], Mark O'Neill, MD DPhil[5], Kraig V. Kissinger, BS,RT[6], Warren J. Manning, MD[7], Elad Anter, MD[2], Reza Nezafat, PhD[8]

1. *King's College London/Beth Israel Deaconess Medical Centre, London, England, United Kingdom*
2. *Beth Israel Deaconess Medical Centre, MA*
3. *Beth Israel Deaconess Medical Center and Harvard Medical School, MA*
4. *Beth Israel Deaconess medical center, Boston, Brookline, MA*
5. *King's College London, London, England, United Kingdom*
6. *Beth Israel Deaconess Medical Centre, Dorchester, MA*
7. *Beth Israel Deaconess Medical Center, Boston, MA*
8. *Department of Medicine (Cardiovascular Division) Beth Israel Deaconess Medical Center, Harvard Medical School, Cardiology, East Campus, Room E/SH455, 330 Brookline Ave, Boston, MA, 02215, MA*

Background: Following myocardial infarction (MI) the left ventricle (LV) undergoes a remodelling process from which mature scar may result. Detailed knowledge of this process may elucidate the pathophysiology underlying the development of myocardial scar and formation of substrate for arrhythmia. We used serial cardiac magnetic resonance (CMR) scans to characterize the LV remodelling that follows MI in a swine ischemia-reperfusion model of ventricular arrhythmia.

Methods: 8 Yorkshire swine underwent three-hour occlusion of the mid left anterior descending artery. We performed serial CMR at 15, 30 and 60 days post-MI. Short axis cine-imaging, pre and post contrast T_1 mapping using slice-interleaved T_1 mapping sequence (STONE)(1) and T_2 mapping(2) at 5 ventricular levels were acquired. Extracellular volume (ECV) maps were calculated. Scar was imaged using a dark blood late gadolinium enhanced (DB-LGE) sequence(3). Regions of Interest (ROI) were selected at ischaemic and remote areas on relaxivity maps, guided by LGE distribution, to calculate mean T_1, T_2 and ECV values. Ex vivo LGE imaging was also performed.

Results: Mean LVEF was 32% (day 15), 36% (day 30) and 37% (day 60) with anterospetal hypokinesia in all cases. A region of enhancement in the anterospetum was seen on DB-LGE imaging, corresponding to scar on ex vivo CMR. Mean scar volume was 15ml (day 15), 13ml (day 30) and 15ml (day 60). A core of non-enhancing tissue was observed in scar of all animals at day 15 which reduced in size on subsequent scans. Native T_1 of ischemic myocardium increased between day 30 (mean T_1=1254ms) and day 60 (mean T_1=1332ms) ($p=0.033$). Mean T_2 of ischemic myocardium increased between day 15 (T_2=64ms) and day 30 (T_2=72ms) ($p=0.025$) and then decreased again by day 60 (mean T_2=62ms) ($p=0.018$). Significant differences in T_1 and T_2 measurements were observed between ischaemic and remote regions at each time point ($p < 0.05$). ECV measurements from regions that enhanced on LGE imaging ranged from 0.44–0.75.

Conclusions: The increase in T_1 values with time from MI likely reflects the replacement of necrotic tissue with fibrosis. Elevated T_2 values 60 days post MI may reflect T_2 properties of mature scar rather than persistent edema. The dark core observed on DB-LGE imaging likely represents microvascular obstruction and/or intramyocardial haemorrhage which is common in this model.

1. Weingartner MRM 2014
2. Basha MRM 2015
3. Basha JCMR 2015

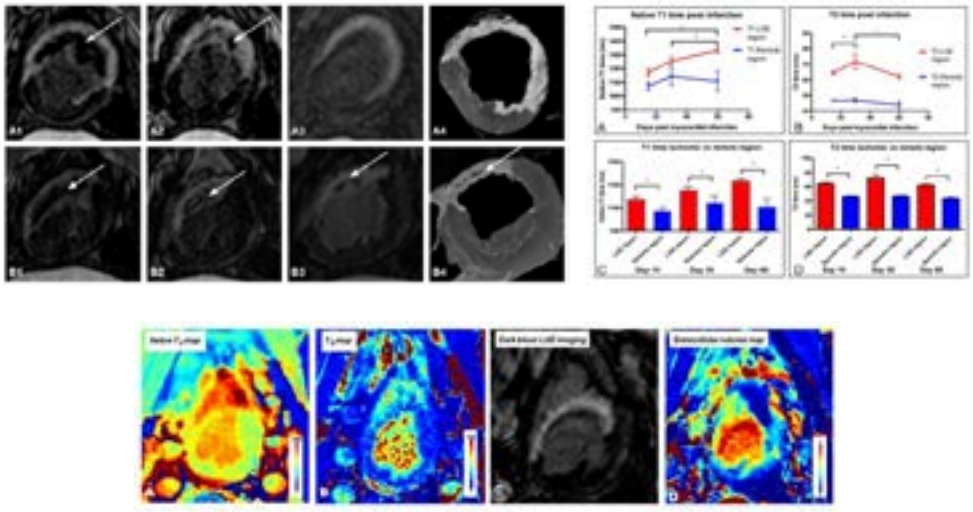

WP24

Measuring extracellular volume (ECV) fraction using T1-mapping - A validation study with radioisotope

David Nordlund, MD[1] Christos Xanthis, PhD[2], Sebastian Bidhult, MSc[3], Robert Jablonowski, MD, PhD[2], Mikael Kanski, MD, PhD[4], Henrik Engblom, MD, PhD[2], Anthony H. Aletras, PhD[5], Håkan Arheden, MD, PhD[6]

1. *Lund University, Lund, Skane Lan, Sweden*
2. *Lund University, Skane Lan, Sweden*
3. *Lund University, Department of Clinical Sciences Lund, Clinical Physiology, Skane University Hospital, Lund, Sweden; Faculty of Engineering, Lund University, Department of Biomedical Engineering, Lund, Sweden, Skane Lan, Sweden*
4. *Lund University, Skåne University Hospital Lund, Skane Lan, Sweden*
5. *Aristotle University of Thessaloniki/Lund University, Thessaloniki, Thessaloniki, Greece*
6. *Lund University, Department of Clinical Sciences Lund, Clinical Physiology, Skane University Hospital, Lund, Sweden, Lund, Skane Lan, Sweden*

Background: Quantitative T1-mapping before and after administration of gadolinium based contrast agent can be used to measure the myocardial extracellular volume (ECV) fraction. Thus, this technique can be used not only to visualize and quantify regional myocardial disease such as myocarditis or myocardial infarction but also diffuse myocardial disease affecting ECV such as storage disease and diffuse myocardial fibrosis of different etiologies. In recent years, technical development using different imaging sequences such as modified Look-Locker inversion recovery (MOLLI)[1] has made T1-mapping and ECV-mapping clinically feasible. However, there is a lack of validation studies. Previous ECV validation studies using T1-measurements were performed on rodents using slow sequences not suited for clinical use[2, 3]. Therefore, the aim of this study was to validate myocardial ECV-measurements based on clinically applicable T1-mapping sequences against ECV-measurements by radioisotope in a large animal model.

Methods: Five healthy pigs were anesthetized and imaged on a 1.5T Aera scanner (Siemens, Erlangen, Germany). Three different MOLLI schemes were acquired before and 15-20 minutes after injection of 0.2 mmol/kg gadolinium-based contrast agent: 1) pre-contrast: 5beat(3sec)3beat [6], post-contrast: 4beat(1sec)3beat(1sec)2beat [6] 2) pre-contrast: 5sec(3sec)3sec [5], post-contrast: 4sec(1sec)3sec(1sec)2sec [5] 3) pre-contrast: 5beat(3beat)3beat [4], post-contrast: 4beat(1beat)3beat(1beat)2beat [5] Regions of interest were defined in the ventricular septum in matching locations for each individual inversion time and T1 was calculated from a 3-parameter nonlinear fit combined with Look-Locker correction [7]. Approximately 10 minutes prior to euthanization, 1000 MBq of an extracellular radioisotope tracer (^{99}Tc-DTPA) was injected. After explantation of the heart, mid-mural samples of myocardium were taken and radioactivity levels in relation to sample weight were measured in a gamma-counter and normalized to radioactivity levels in plasma for calculation of ECV.

Results: Myocardial ECV was 19.6±1.1% (mean±SD) by radioisotope, 23.5±5.7% by scheme 1, 24.3±2.9% by scheme 2 and 26.0±3.6% by scheme 3. There were no significant differences between the methods using ANOVA (p=0.09), but there was a trend towards lower ECV-values by radioisotope compared to those given by the MOLLI-schemes (Figure 1).

Conclusions: In a large animal model, three commonly used MOLLI T1-mapping sequences showed similar ECV-values while there was a trend towards lower ECV by radioisotope tracer measurements.

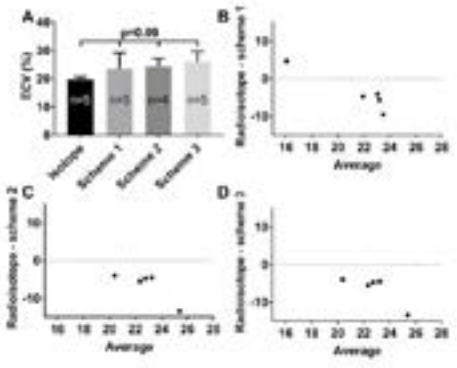

References

Messroghli et al. Magn Reson Med 2004, 52	1
Arheden et al. Radiology 1999, 211	2
Arheden et al. Radiology 2000, 215	3
Kellman et al. J Cardiovasc Magn Reson 2012, 14	4
Kellman et al. J Cardiovasc Magn Reson 2014, 16	5
Kellman et al. J Cardiovasc Magn Reson 2013, 15	6
Deichmann et al. J Magn Reson 1992, 96	7

WP25

In Vivo Quantification of Aortic Stiffness in Abdominal Aortic Aneurysm Porcine Model Using Magnetic Resonance Elastography

Huiming Dong, MS[1] Prateek Kalra, MS[2], Brian Raterman, BSRT[2], Matthew Joseph, BS[3], Richard White, MD[2], Arunark Kolipaka, PhD[2]

1. *Department of Radiology and Department of Biomedical Engineering, The Ohio State University Wexner Medical Center, Upper Arlington, OH*
2. *Department of Radiology, The Ohio State University Wexner Medical Center, Columbus, OH*
3. *Interventional Cardiology Catheter Core Lab-Dorothy M. Davis Heart and Lung Research Institute, The Ohio State University Wexner Medical Center, Columbus, OH*

Background: An abdominal aortic aneurysm (AAA) is an abnormal enlargement of the abdominal aorta which can lead to rupture, making it one of the leading causes of death in the United States. Clinically, AAA diameter is used as gold standard for assessing the rupture risk: a diameter >5.0 cm is considered to be high-risk, indicating the need for surgical or endovascular repair. However, various studies have shown that small AAAs (< 5.0 cm) also rupture while large AAAs (5.0 cm) may remain stable, suggesting that diameter is a poor indicator of rupture potential. Aortic stiffness is an important biomechanical property that is able to provide critical information about the microstructure of aortic wall and extracellular matrix remodeling, potentially providing a more accurate rupture risk assessment. Recent development in magnetic resonance elastography (MRE) has demonstrated that it is feasible to evaluate aortic stiffness in vivo non-invasively. Therefore, the aim of the study is to use MRE to estimate the aortic stiffness in induced AAAs.

Methods: AAA was induced in 4 animals using elastase after mechanically stretching the abdominal aorta wall during the surgery. MRE was performed prior to the surgery (Baseline) and 4 weeks after the surgery (Week 4) on a 1.5T MRI scanner (Avanto, Siemens Healthcare, Erlangen, Germany) in an oblique plane. Imaging parameters included: TR/TE=14.29/10.62 ms; FOV=400x400 mm^2; slice thickness=4-6 mm; acquisition matrix size=128x64; flip angle=15°; mechanical frequency=70 Hz; MEG encoding frequency=120 Hz; phase offsets=4. Images were masked to extract the normal aorta and the AAA region. Consequently, aortic stiffness was obtained using 3D local frequency estimation (LFE).

Results: Figure 1 demonstrates the magnitude, wave images and the corresponding MRE-derived aortic stiffness maps of the same animal at baseline and week 4. Both AAA development and stiffness increase can be clearly observed at week 4. Figure 2 displays the box plot of aortic wall stiffness at baseline and week 4, showing the AAA stiffness is significantly ($p < 0.05$) higher than the normal aorta in the same region of interest. The mean aortic stiffness by pooling all animals at baseline and week 4 are 4.09±0.41 kPa and 6.99±3.93 kPa respectively, demonstrating the reduction of compliance in aortic wall as the disease progresses.

Conclusions: The results of this study demonstrate that MRE-derived aortic stiffness increases with the progression of AAA in a porcine model, suggesting the potential of using MRE as a new tool for AAA diagnosis and accurate rupture risk assessment.

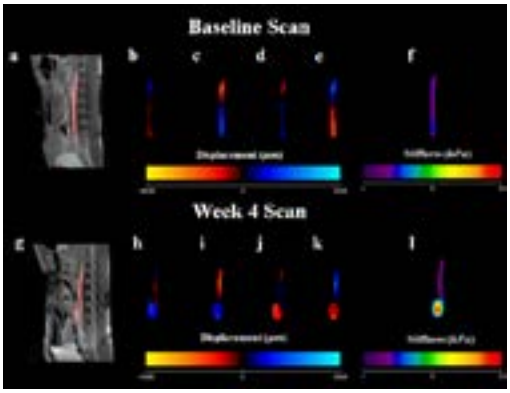

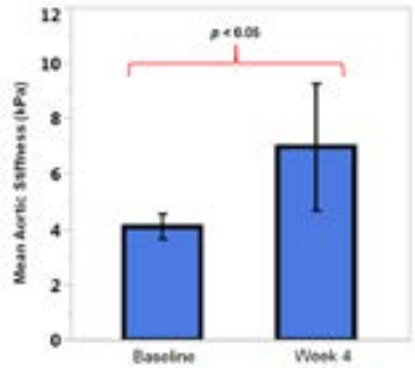

WP26

Strain Derived from Tagging MRI Is More Sensitive Than Ejection Fraction for Detecting Functional Effects of Myocardial Regeneration

Yijen L. Wu, Ph.D.[1]Balakrishnan Ganapathy, MS[2], Niyatie Ammanamanchi, MS[3], Sangita Choudhury, PhD[4], Bernhard Kühn, MD, PhD[5]

1. *Deapartment of Developmental Biology, University of Pittsburgh and Rangos Research Center Imaging Core, Children's Hospital of Pittsburgh of UPMC, Pittsburgh, PA, USA, Pittsburgh, PA*
2. *Department of Pediatrics, University of Pittsburgh, and Richard King Mellon Institute for Pediatric Research and Division of Pediatric Cardiology, Children's Hospital of Pittsburgh of UPMC, Pittsburgh, PA 15224, USA, Pittsburgh, PA*
3. *Department of Pediatrics, University of Pittsburgh, and Richard King Mellon Institute for Pediatric Research and Division of Pediatric Cardiology, Children's Hospital of Pittsburgh of UPMC, Pittsburgh, PA 15224, USA., PA*
4. *Boston Children's Hospital, Harvard Medical School, MA, PA*
5. *Children's hospital f Pittsburgh, McGowan Institute for regenerative Medicine, Pittsburgh, PA 15219, USA., PA*

Background: Cardiac regeneration has the potential for revolutionizing heart failure therapy. It is pivotal to be able to accurately measure the functional effects of the regenerated cardiomyocytes. Here, we evaluate circumferential strain (Ecc) derived from tagging MRI as a sensitive surrogate biomarker for evaluation of myocardial regeneration therapy in a murine neonatal myocardial injury model.

Methods: ***Experimental cardiac regeneration therapy in a neonatal mouse cryoinjury model:*** Adenoviral preparations of LmnB2 (test) and green fluorescent protein (GFP, control) were retro-orbitally injected into pups on the day of birth. Cryoinjury was performed on the next day. ***Echocardiography:*** Tansthoracic echocardiography was used to evaluate ejection fraction (EF) on day post-injury (DPI) 34 with Visual Sonics Vevo 770 system. ***Cardiac MRI and strain analysis:*** Cine and tagging MRI was acquired with **Bruker 7-Tesla** Avance III system on DPI 34. Four short-axis (SA) slices were used to cover the heart from the 1.5 mm below the mitral valve level to apex. Peak circumferential strain (Ecc) was analyzed by HARP software (Myocardial Solutions, Inc.).

Results: Lamin B2 (LmnB2), a nuclear envelope protein, is required for proliferation of fetal and post-natal cardiomyocytes. Here we tested overexpression of LmnB2 as a potential regeneration therapy after cyroinjury in the heart. EF was evaluated by echocardiography and cine MRI on DPI 34 (Fig.1). Adv-LmnB2-treated group showed slightly better EF than the Adv-GFP-treated control group, but the differences observed were not statistically significant. EF is not sensitive in detecting functional improvement by Adv-LmnB2 treatment. Figure 2 shows tagging MRI for an Adv-LmnB2-treated (Fig. 2, A-H) and an Adv-GFP-treated (Fig.2, I-P) heart. Figure 3A shows peak Ecc for 2 Adv-LmnB2-treated (right) and 2 Adv-GFP-treated (left) treated hearts. Both groups received cardiac cyroinjury and displayed impaired Ecc at the injury slice (Fig. 3B,E). On the other hand, 2.2 mm (Fig. 3C, F) and 3.3 mm (Fig. 3D,G) above the injury slice, Adv-LmnB2-treated group showed significantly improved Ecc than the Adv-GFP-treated controls. The Ecc values of the remote zone of the Adv-LmnB2-treated group are in the physiologically normal range. This indicates that as a result of LmnB2 gene therapy, the proliferated cardiomyocytes have functionally integrated for coherent ventricular wall motion, and restricted adverse expansion of the injury to neighboring regions.

Conclusions: Strain analysis derived from tagging MRI is more sensitive than EF in detecting regional functional improvement in ventricular wall and can potentially be a more sensitive quantitative surrogate biomarker for cardiac regeneration therapies.

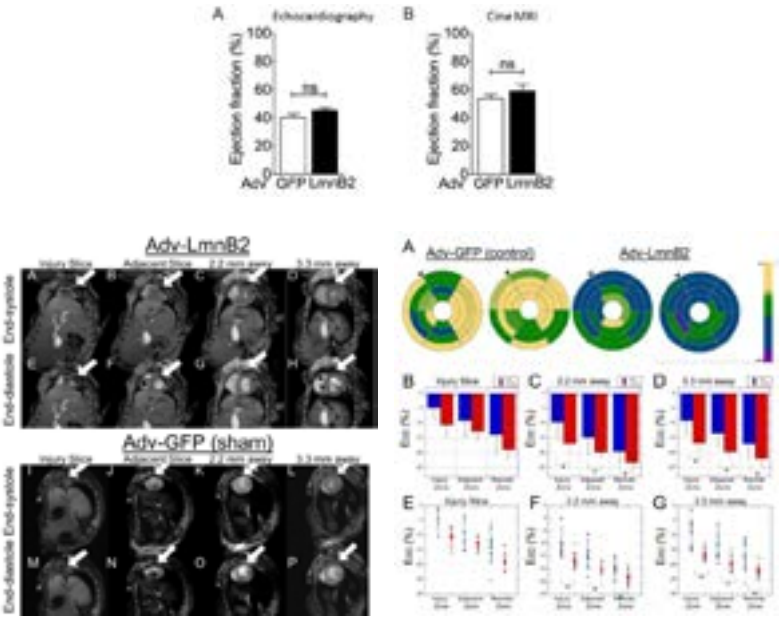

WP27

4D cine strategy for assessment of cardiac function and infarct size in mice on a clinical 3T MR system in a single acquisition

Lindsey A. Crowe, PhD[1] Fabrizio Montecucco, MD PhD[2], Federico Carbone, MD PhD[3], Iris Friedli, MSc[1], Anne-Lise Hachulla, MD[1], Vincent Braunersreuther, PhD[1], Francois Mach, MD PhD[1], Jean-Paul Vallée, MD PhD[1]

1. *Geneva University Hospital, Geneve, Switzerland*
2. *University of Genoa IRCCS AOU San Martino, Liguria, Italy*
3. *University of Genoa, Liguria, Italy*

Background: Small animal cardiac imaging on clinical machines is an important, cost-effective, translational step for new contrast media and sequence development, but suffers hardware limitations compared to dedicated systems. We developed a new single acquisition 4D strategy optimized at 3T to simultaneously assess function and infarct in wild-type mice utilizing improved spatial and temporal resolution.

Methods: Adult C57BL/6J mice underwent 60minutes ischemia then reperfusion. Controls had no surgery. n=14 infarct, 4 control for function, and 6 infarct 6 control for histology/reproducibility. MRI was 24hrs after surgery, with gadolinium (Gd) injection, and sacrifice for post-mortem MRI and histology. The 3D gradient echo cine sequence (ECG/respiratory triggered) had acquired isotropic resolution 344µm, TR/TE 7.8/2.9ms, acquisition time 25-35minutes. The conventional 2D FLASH cine sequence had the same in-plane resolution 344µm, slice thickness 1mm, TR/TE 11/5.4ms, acquisition 20-25minutes (+5minutes planning). Left ventricle (LV) and right ventricle (RV) volumes were measured and statistical comparison was made between 2D and 3D along with inter/intra-observer reproducibility. The physiological equality for left and right ejection volume was verified. MRI infarct volume was compared to histology and function.

Results: Our new '4D strategy' of 3D cine (3D) MRI outperformed 2D cine (2D) for spatial and temporal resolution. 3D required no complex planning. Flow artifacts were significantly reduced in 3D ($p=0.008$). CNR allowed epi/endocardial delineation for 2D and 3D with ICC intra/inter reproducibility of 0.2-0.99 for 2D and 0.6-0.99 for 3D. 3D isotropic coverage improved apex and right ventricle (RV) assessment. All 3D left volumes and right EF showed no difference to 2D ($p>0.05$). Ejection volume was equal for LV and RV.
LV mass correlated 2D to 3D and 3D RV mass correlated with postmortem ($R^2>0.70$) but was not measurable on 2D.
Infarct 'late Gd enhancement' was seen clearly only with 3D and this quantifiable infarct volume correlated to histology ($R^2=0.89$) with both small transmural infarcts (ligature site) and large nontransmural infarcts covering the whole apex. Left ejection fraction and MRI-measured infarct volume correlated ($R^2>0.3$).

Conclusions: In conclusion, we developed a 4D cardiac strategy after contrast media injection in mice. Function and infarct were assessed simultaneously using internal/physiological validation and comparison to 2D and histology. This 4D strategy was faster, easier to use and, due to isotropic resolution, has strong potential for complete LV and RV volume, function, mass and infarct assessment in mice on clinical systems and could replace separate 2D function and infarct MRI techniques.

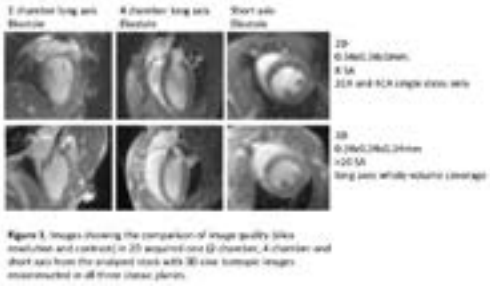

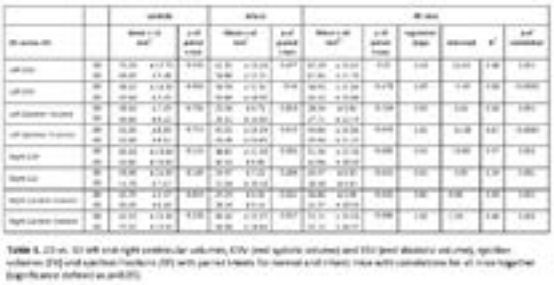

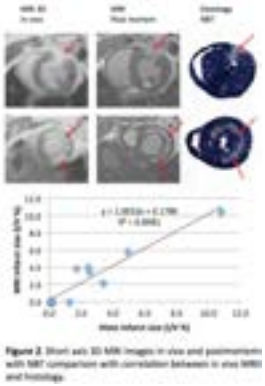

WP28

Sarcopenia, And Not Body Mass Index, Is Associated With Cardiac Remodeling In Elderly Subjects

Angela S. Koh, MBBS; MPH[1] Wan Yi Yew[2], Xiaodan Zhao, Ph.D.[3], Liang Zhong, Ph.D.[4], Yiying Han[3], Fei Gao, PhD[1], Serene Chua[3], Jia Ing Wong[3], Fei Qiong Huang[1], Ru San Tan, MBBS[4], Woon-Puay Koh, MBBS; PhD[5]

1. *National Heart Centre Singapore; Duke-NUS Medical School, N/A, Singapore*
2. *National University of Singapore, N/A, Singapore*
3. *National Heart Centre Singapore, N/A, Singapore*
4. *National Heart Centre Singapore; Duke-NUS Medical School, Singapore, N/A, Singapore*
5. *Duke-NUS Medical School; Saw Swee Hock School of Public Health; National University of Singapore, N/A, Singapore*

Background: Recent studies suggest that muscle mass may mediate cardiac remodeling independent of body mass index (BMI). It is unknown if the association between muscle mass and cardiac remodeling also exists among elderly subjects who have age-related sarcopenia. We hypothesize that even among elderly subjects, muscle mass is independently associated with cardiac remodeling, independent of chronic cardiovascular risk factors.

Methods: This was a prospective community-based cohort study. The participants were those of mean age 72.4 years (SD 4.1) and without any self-reported history of physician-diagnosed coronary heart disease, stroke or cancer thus far. We assessed cardiac remodeling by cardiac magnetic resonance imaging (MRI), and computed geometric remodeling index (left ventricular (LV) mass over LV end diastolic volume (EDV). Inter-observer reproducibility by independent observers in LV mass (intraclass correlation coefficient 0.996, 95%CI 0.989, 0.998) and LV EDV (intraclass correlation coefficient 0.994, 95%CI 0.985, 0.998) were excellent. Sarcopenia was diagnosed using gender-based cut-off values defined by European Working Group on Sarcopenia in Older People (EWGSOP) (appendicular lean mass, ALM/height^2), measured using detailed body composition analyzer for appendicular muscle mass.

Results: In this general population, out of 186 subjects [79 women (42.5%)], 100 subjects (53.8%) were sarcopenic. There were no age (72.6 vs 72.2 years, p=0.54), female gender (37% vs 49%, p=0.14) or risk factor differences in hypertension (50% vs 57%, p=0.38), diabetes mellitus (27% vs 15%, p=0.052) among sarcopenic vs non-sarcopenic patients. Sarcopenic subjects had greater cardiac remodelling compared to individuals who were not sarcopenic (geometric remodelling index 0.775 vs 0.711, p=0.037). By regression analyses, adjusting for hypertension and diabetes mellitus status, sarcopenia, but not BMI, was independently associated with geometric remodelling (β=0.078, SE 0.034, p=0.023).

Conclusions: Among a community cohort of elderly subjects, sarcopenia was associated with geometric cardiac remodeling, a marker of adverse change in cardiac structure. These results support an emerging hypothesis that muscle mass may play an important role in cardiac remodeling independent of traditional pathways represented by BMI or chronic risk factors.

WP29

The leading role of the right ventricle in augmentation of cardiac output during exercise.

Bram Ruijsink, MD[1]Mari Nieves Velasco Forte, MD[1], Muhammad Usman, PhD[1], Miguel S. Vieira, MD[2], Torben Schneider, PhD[3], Claudia Prieto, PhD[1], Alessandra Frigiola, MD, PhD[4], Kuberan Pushparajah, MD[1], David Nordsletten, PhD[1], Reza Razavi, MD, PhD[1]

1. *King's College London, England, United Kingdom*
2. *King's College London, London, England, United Kingdom*
3. *Health Systems, Philips, Guildford, England, United Kingdom*
4. *Guys and St Thomas Hospital NHS Foundation Trust, England, United Kingdom*

Background: Right ventricular (RV) dysfunction significantly impacts exercise capacity –more than left ventricular (LV) dysfunction-, and is independently associated with outcome in a broad range of left ventricular diseases. The RV operates at higher end diastolic and end systolic volumes (EDV, ESV) at rest than the LV and endurance training results in greater RV than LV dilatation. Altogether, this data suggest a key role of the RV in the heart during stress. However, the mechanism involved is unknown. We have recently developed and validated retrospectively gated high temporal resolution CINE and 2D phase contrast flow imaging during strenuous exercise. We aimed to elucidate the difference in RV and LV function under stress by investigating the RV/LV adaption to acute selective heart rate modulation (lower heart rate, but similar bodily demand for cardiac output (CO)) during exercise in healthy volunteers.

Methods: 10 healthy volunteers underwent cardiac exercise MRI before and after a single dose of 7.5mg ivabradine (I_f inhibitor). Ivabradine selectively slows sinus node depolarisation, without influencing cardiac contractility and relaxation. Cardiac volumes and aortic flow were measured at rest and during moderate and high exercise using retrospectively cardiac and respiratoiry gated real time highly accelerated balanced SSFP. Exercise levels (cycling wattage) were obtained from previous cardiopulmonary exercise testing for each participant and kept constant between the two tests. All participants underwent training on the supine bicycle prior to start of the study to prevent training-effect on outcomes.

Results: At baseline, RV-ESV was significantly higher at each stage of exercise than LV-ESV (31ml/m^2 vs 20ml/m^2, $p < .01$). HR significantly decreased after ivabradine (peak HR 155±9, mean effect -11±4% $p < .01$). CO was maintained at all exercise levels (peak CO at baseline 14.4±2.1 L/min, after ivabradine 14.8±1.8 L/min reflecting similar bodily demand of CO (similar workload). Preservation of CO was accomplished by increased RV contraction: ESV decreased from 28±2 to 19±4 ml/m^2 $p < .01$, whereas EDV did not change. In the LV, ESV did not decrease but EDV increased (71±9 to 81±9 ml/m^2 p=.03) in response to increased RV-SV. Systolic and mean blood pressure response during exercise did not significantly change after ivabradine administration.

Conclusions: This is the first study that elucidates the mechanism behind and impact of right ventricular systolic function on CO augmentation during high intensity exercise in the healthy heart. Despite HR reduction obtained with ivabradine, healthy volunteers were able to maintain the same cardiac output during exercise. This was the result of increased RV contraction to lower ESV and subsequent improved left ventricular filling. The RV-ESV decreased to values of LV-ESV (19 vs 20 ml/m^2) suggest an bigger 'reserve' ESV in the RV that is utilized during peak exercise.

http://www.ConferenceAbstracts.com/uploads/cfp2/attachments/LDFAIBDN/LDFAIBDN--222739-1-ANY.pdf

http://www.ConferenceAbstracts.com/uploads/cfp2/attachments/LDFAIBDN/LDFAIBDN--222739-2-ANY.pdf

http://www.ConferenceAbstracts.com/uploads/cfp2/attachments/LDFAIBDN/LDFAIBDN--222739-3-ANY.pdf

WP30

Improved workflow for quantification of right ventricular volumes and mass using free-breathing motion corrected cine imaging

Anthony C. Merlocco, M.D.[1]Russell Cross, M.D.[2], Laura Olivieri, M.D.[1], Peter Kellman, Ph.D.[3], Hui Xue, PhD[3], Michael Hansen, Ph.D.[3]

1. *Children's National Medical Center, Washington, DC*
2. *Children's National Medical Center, DC*
3. *National Heart, Lung, and Blood Institute, Bethesda, MD*

Background: Cardiac functional assessment by MRI traditionally requires breath-holding for cine imaging. Development of free-breathing techniques has allowed for use of cine imaging in populations which may be younger, less able to follow instruction, or less stable; however, the images can be spatially and/or temporally blurred. One novel approach has been to acquire real-time images over multiple cardiac cycles and apply motion correction and reformatting to display one cardiac cycle with high temporal and spatial resolution, known as re-binning. Significant reconstruction time,however,limits feasibility. Distributed computing has recently been shown to reduce formatting time significantly and to improve workflow. It has been used in motion corrected re-binning imaging and compares favorably to breath-held SSFP for quantification of left ventricular volumetry. However, its utility in quantification of the right ventricle has not been established. In this study we deployed a distributed computing version of motion corrected re-binning reconstruction for free-breathing evaluation of right ventricular function.

Methods: Twenty five patients and 25 volunteers underwent cardiovascular magnetic resonance (CMR) for evaluation of right ventricular end-systolic volume (ESV), end-diastolic volume (EDV), and end-diastolic mass. Measurements using motion corrected re-binning were compared to those using breath-held SSFP. Pearson correlation coefficients and Bland-Altman plots tested agreement across techniques. Total scan plus reconstruction times were tested for significant differences using paired t-test.

Results: Measured volumes and mass obtained by motion corrected re-binning compared favorably to those obtained by breath-held SSFP ($r = 0.9820$ for EDV, 0.9678 for ESV, 0.9470 for mass, 0.9600 for stroke volume). Motion corrected re-binning reconstruction times were shorter than breath-held SSFP techniques ($p < 0.0001$). On average, motion corrected re-binning required 3 min less than breath-held SSFP imaging, a 37 % reduction in acquisition and reconstruction time.

Conclusions: The motion corrected re-binning image reconstruction technique provides robust cardiac imaging that can be used for quantification of the right ventricular mass and volume that compares favorably to breath-held SSFP, but can be obtained in a fraction of the time when using cloud-based distributed computing reconstruction. Combined with previous findings validating this method for left ventricular quantification, these findings provide support for the clinical use of this novel method.

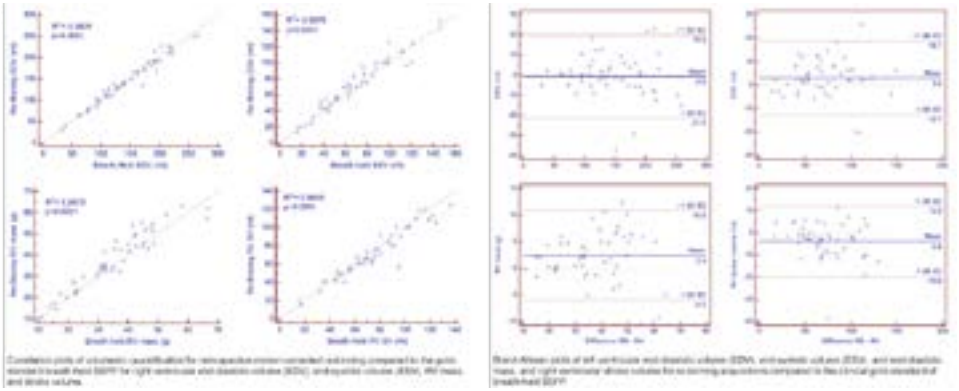

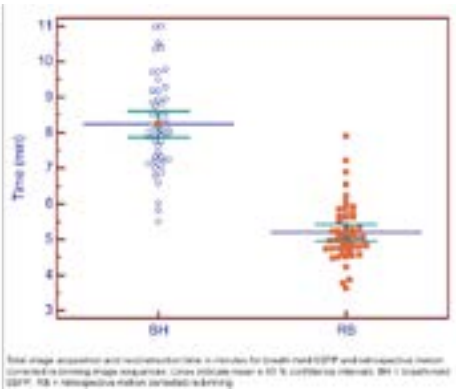

WP31

Association of ambulatory blood pressure and insulin resistance with cardiac remodeling in obese children

Linyuan Jing, PhD[1] Christopher Nevius, BT[2], Cassi Friday, M.S.[3], Jonathan D. Suever, PhD[4], Abba Mejia-Spiegeler, LLB[2], Gregory J. Wehner, BS[5], Aftab S. Chishti, MD, FAAP, FASN, CCST[5], Christopher M. Haggerty, PhD[6], Brandon K. Fornwalt, MD, PhD[6]

1. *Geisinger Health System, State College, PA*
2. *Geisinger Health System, Danville, PA*
3. *University of Kentucky, Junction city, KS*
4. *Geisinger Health System, Bellefonte, PA*
5. *University of Kentucky, KY*
6. *Geisinger Health System, PA*

Background: Children with obesity have been shown to have cardiac remodeling. Hypertension and insulin resistance are two common comorbidities in pediatric obesity, both of which may independently contribute to cardiac remodeling. We aimed to explore the relationship between cardiac remodeling, ambulatory blood pressure (BP) and insulin resistance in obese children using cardiac magnetic resonance (CMR) imaging.

Methods: Children, aged 8-17 years, were prospectively enrolled and underwent CMR. Left ventricular mass indexed to height$^{2.7}$ (LVMI), myocardial thickness and end-diastolic volume were quantified from a reconstructed 3D LV mesh using cine SSFP images. Ambulatory BP was measured every 30 minutes for 24 hours. Fasting blood samples were collected in a subgroup to measure insulin resistance using the homeostatic model assessment (HOMA-IR). In addition to discretizing presence of concentric hypertrophy based on cutoff values for LVMI and mass/volume from a previous CMR study, principal component analysis was used to define a continuous variable (as a linear function of LVMI and mass/volume) where lower values corresponded to a more normal geometry and higher values corresponded to more concentric hypertrophy. Univariate linear regression was used to assess correlations between measures of cardiac remodeling, BP and insulin resistance. Independent predictors for cardiac remodeling were determined using stepwise linear regression.

Results: Twenty healthy weight and 26 obese/overweight children underwent CMR. Obese/overweight children had increased LVMI (26±4 vs 22±4 g/m$^{2.7}$, $p < 0.001$), myocardial thickness (5.4±0.7 vs 5.0±0.8 mm, p=0.001) and mass/volume (0.66±0.08 vs 0.60±0.05, p=0.002), and 19% of them had concentric hypertrophy based on cutoff values. 38% of the obese/overweight children had masked hypertension, 4% had pre-hypertension, and 19% had ambulatory hypertension. Body mass index z-score (BMIz), 24-hour systolic BP (SBP), systolic load and systolic dipping all correlated with LVMI, thickness, mass/volume and concentric hypertrophy (Table 1). Multivariate analysis showed BMIz and 24-hour SBP were the strongest predictors of LVMI (β=0.52 and 0.34), thickness (β=0.33 and 0.51) and concentric hypertrophy (β=0.48 and 0.41) (Table 2). BMIz, systolic load and systolic dipping were independent predictors for mass/volume (β=0.37, 0.34 and 0.25). In 29 subjects with blood samples, HOMA-IR correlated with LVMI, mass/volume and concentric hypertrophy in univariate regression. When adding HOMA-IR to the multivariate model, HOMA-IR (β=0.36) and systolic load (β=0.38) became the strongest predictors of concentric hypertrophy.

Conclusions: In children, both the degree of obesity and ambulatory blood pressure are independently associated with cardiac remodeling (LVMI). Ambulatory blood pressure and insulin resistance are both independent predictors for the presence of concentric hypertrophy in obese children.

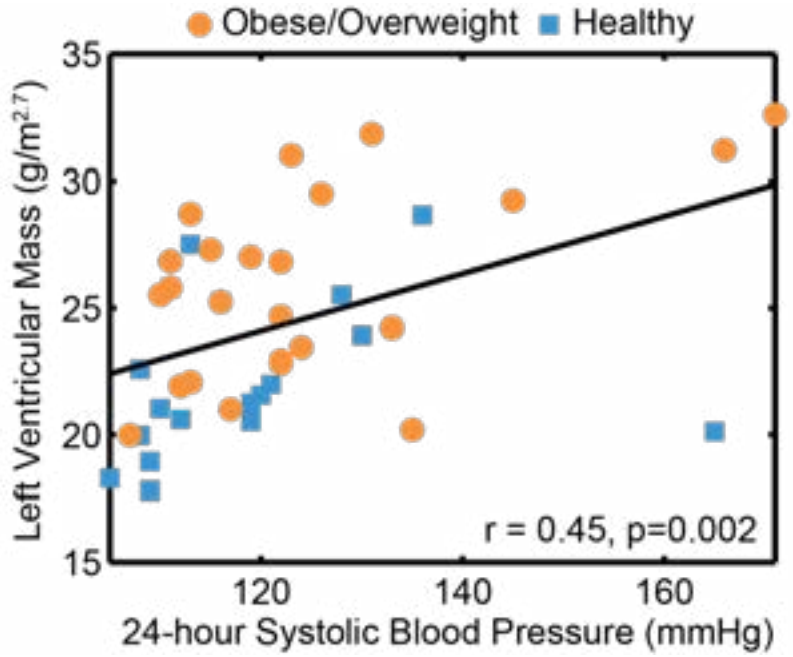

Table 1: Linear correlations between blood pressure, insulin resistance and cardiac remodeling

Concentric Hypertrophy[2]		Mass/Volume		Thickness		LVMI		
P	r	p	r	p	r	p	r	
<0.001	0.54	0.005	0.42	0.006	0.42	<0.001	0.57	BMI z-score
				0.003	0.42	0.03	0.33	Clinical SBP
				0.006	0.40			Clinical MAP
0.002	0.46	0.007	0.41	<0.001	0.59	0.002	0.45	24-hour SBP
				0.03	0.33			24-hour MAP
<0.001	0.49	0.002	0.47	<0.001	0.53	0.003	0.44	Systolic load
0.01	-0.39	0.01	-0.38			0.02	-0.35	Systolic dipping
0.05	-0.36					0.05	-0.36	HDL Cholesterol[1]
0.01	0.45	0.04	0.37			0.03	0.39	HOMA-IR[1]

[1]subset of n = 29 out of 46 subjects were included in the analysis; [2]quantified as a continuous variable as described in the methods

Table 2: Multivariate analysis with BP measurements and BMI z-score, sex adjusted

Concentric Hypertrophy[1]		Mass/Volume		Thickness		LVMI		
p	β	p	β	p	β	p	β	
<0.001	0.48	0.005	0.37	0.008	0.33	<0.001	0.52	BMI z-score
0.001	0.41			<0.001	0.51	0.005	0.34	24-hour SBP
		0.008	0.34					Systolic Load
		0.04	-0.25					Systolic Dipping

[1]quantified as a continuous variable as described in the methods.

WP32

Tricuspid valve displacement analysis using Cardiac MRI feature tracking provides a simple correlate of RV function in Tetralogy of Fallot

Edythe Tham, MBBS[1] Benjamin Goot, MD[1], Kumaradevan Punithakumar, PhD[2], Michelle Noga, MD, FRCP(C)[2]

1. Stollery Children's Hospital, University of Alberta, AB, Canada
2. University of Alberta, Edmonton, AB, Canada

Background: Impaired longitudinal strain in tetralogy of Fallot (TOF) has been associated with adverse clinical outcome. Assessment of myocardial deformation using novel CMR software may provide prognostic information in TOF. We aimed to determine correlates of RV function using TV displacement analysis in patients with repaired TOF.

Methods: A retrospective analysis of 62 CMR studies in patients (14±5 years) with repaired TOF (35 transannular patch, 14 RV-PA conduit, 8 valve-sparing repair, 5 pulmonary valve replacement). Right ventricular volumes and ejection fraction were recorded. Peak RV longitudinal strain and strain rate (SR) were measured from the 4-chamber cine view using in-house developed CMR software that utilizes a semi-automatic feature tracking program. Tricuspid valve (TV) displacement was measured at end-systole as the shortest distance between both anterior and septal leaflet hinge points relative to the RV apex, and the velocity of shortening in systole and early diastole (e') was computed (Figure). Pearson's correlation coefficient was calculated between RV volumes, RVEF, RV strain, and SR, with TV displacement parameters.

Results: Increased anterior and septal distance (i.e. decreased shortening) was associated with larger RV volumes, decreased RVEF and longitudinal strain; but showed no relationship to SR. Increased anterior displacement velocities were associated with increased longitudinal strain, SR and EDSR, while septal velocity correlated with SR only. Both anterior and septal e' velocities increased with increasing RVEF, strain, SR and EDSR (Table).

Conclusions: Decreased TV shortening in systole is associated with larger RV volumes and decreased RV function. Greater anterior displacement velocities in systole and early diastole are associated with improved RV function, contractility and early filling rate. TV displacement analysis provides a simple correlate of RV function, and may be a quicker, serial method to estimate RV myocardial mechanics in TOF.

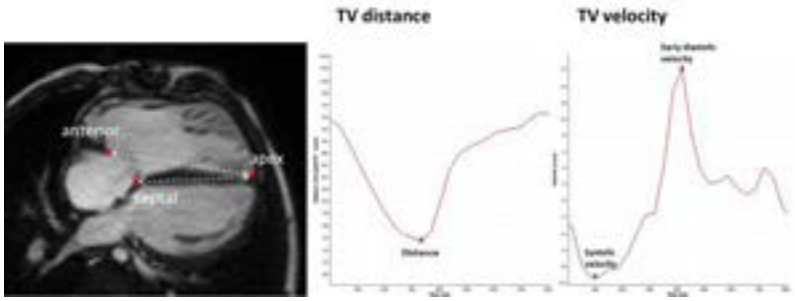

Pearson's correlation coefficient between RV volumes, strain parameters and TV displacement parameters with significant correlations highlighted in bold.

EDSR	SR	Strain	RVEF	RVESV	RVEDV	
-0.24	0.21	**0.32**	**-0.48**	**0.83**	**0.81**	anterior distance
-0.30	**-0.30**	**0.56**	**-0.39**	0.03	-0.18	anterior velocity
0.52	**-0.51**	**-0.62**	**0.47**	-0.11	0.08	anterior e' velocity
-0.20	0.16	**0.26**	**-0.38**	**0.76**	**0.79**	septal distance
-0.06	**0.33**	0.19	-0.13	0.03	-0.02	septal velocity
0.50	**-0.46**	**-0.53**	**0.31**	-0.03	0.10	septal e' velocity

WP33

A clinically applicable method for time-resolved measurements of the atrioventricular plane displacement in CMR – validated in patients with myocardial infarction, athletes, and healthy controls

Felicia Seemann, MSc[1] Ulrika Pahlm, MD[2], Katarina Steding-Ehrenborg, PhD[3], Ellen Ostenfeld, M.D., Ph.D.[4], David Erlinge, MD, PhD[5], Jean-Luc Dubois-Rande, MD, PhD[6], Svend Eggert Jensen, MD, PhD[7], Dan Atar, MD, PhD[8], Håkan Arheden, MD, PhD[9], Marcus Carlsson, MD, PhD[10], Einar Heiberg, PhD[11]

1. *Lund University, Skane University Hospital, Dept of Clinical Physiology, Lund, Sweden; Lund University, Faculty of Engineering, Dept of Numerical Analysis, Lund, Sweden; Lund University, Faculty of Engineering, Dept of Biomedical Engineering, Lund, Skane Lan, Sweden*
2. *Lund University, Skane University Hospital, Department of Clinical Physiology, Lund, Sweden, Skane Lan, Sweden*
3. *Lund University, Skane University Hospital, Department of Clinical Physiology, Lund, Sweden; Lund University, Department of Health Sciences, Physiotherapy, Lund, Sweden, Skane Lan, Sweden*
4. *Lund University, Dept of Clinical Sciences, Clinical Physiology, Lund, and Skane University Hospital, Lund, Skane Lan, Sweden*
5. *Lund University, Department of Cardiology, Clinical Sciences, Lund, Sweden, Lund, Skane Lan, Sweden*
6. *Assistance Publique Hôpitaux de Paris, Hôpital Henri Mondor, Créteil, N/A, France*
7. *Aalborg University Hospital, Aalborg, N/A, Denmark*
8. *Department of Cardiology B, Oslo University Hospital Ullevål and Faculty of Medicine, University of Oslo, Oslo, Norway, N/A, Norway*
9. *Lund University, Department of Clinical Sciences Lund, Clinical Physiology, Skane University Hospital, Lund, Sweden, Lund, Skane Lan, Sweden*
10. *Lund University, Department of Clinical Sciences Lund, Clinical Physiology, Skane University Hospital, Lund, Sweden, Skane Lan, Sweden*
11. *Lund University, Department of Clinical Sciences Lund, Clinical Physiology, Skane University Hospital, Lund, Sweden; Lund University, Faculty of Engineering, Department of Biomedical Engineering, Lund, Sweden, Skane Lan, Sweden*

Background: Atrioventricular plane displacement (AVPD) accounts for 60% of the stroke volume in the left ventricle (LV) and 80% in the right ventricle (RV), and a reduced AVPD have prognostic significance for future clinical events. In echocardiography, it is clinical standard to measure AVPD as mitral and tricuspid annular plane systolic excursion (MAPSE and TAPSE) [Lang et al., J Am Soc Echocardiogr, 2015, 28:1]. However, in cardiovascular magnetic resonance (CMR), AVPD is rarely evaluated clinically, and is not implemented in the CMR assessment consensus [Schulz-Menger et al. J Cardiovasc Magn Reson, 2013, 15:352].

Time-resolved AVPD in CMR allow computation over the cardiac cycle, creating a curve from which peak emptying rate, peak filling rate, and atrial contraction can be derived (Fig.1), but manual measurements are time consuming. Automatic tracking reduces subjectivity of observers, as well as time spent on manual image analysis.

Therefore, this study aimed to develop, validate and provide an automatic method for tracking AVPD in CMR, which can be used clinically or in cardiovascular research in multi-center studies.

Methods: The algorithm is based on normalized cross-correlation and a priori information by principal component analysis, using cine images of the 2, 3, and 4-chamber views. A total of 153 subjects from 10 centers underwent CMR scanning in a 1.5T Philips, Siemens or GE scanner. Subjects consisted of 32 athletes, 81 first time ST-elevation myocardial infarction patients, and a total 40 healthy controls, out of which 14 were elderly healthy controls. Subjects were divided into a training set (n=40) and a test set (n=113). Manual AVPD measurements were used as reference standard. The whole test set was used for end systolic validation and a subset of the test set (n=20) was used for time-resolved validation. Inter-observer variability was analyzed for end systolic AVPD (n=20).

Results: Similarity of a corresponding manual and tracked AVPD-curve is shown in Fig. 1. The difference in mm between the algorithm and reference standard in all timeframes was (mean±SD) -0.3±1.7, R=0.95, in the LV, and -0.7±2.3, R=0.94, in the RV (Fig. 2). In end systole the difference in LV was -0.7±1.7, R=0.85, and -1.2±2.2, R=0.88, in RV. Inter-observer variability in LV was -0.6±0.7, R=0.95, and -0.5±1.4, R=0.95, in RV.

Conclusions: The proposed algorithm performs well compared to manual measurements in data from multi-center and multi-vendor, yielding results in parity with inter-observer variability. Therefore, a tracking algorithm using a priori information may be introduced as a method for measuring the AVPD in CMR.

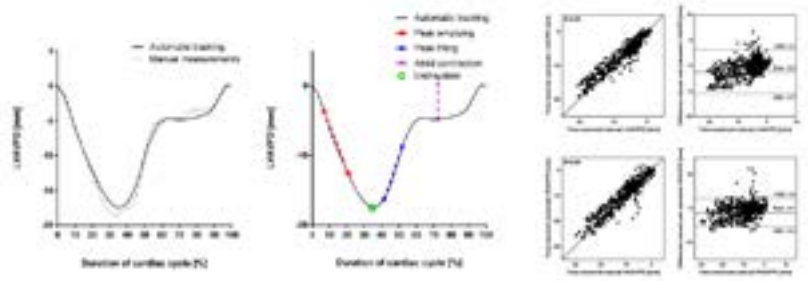

WP34

In Vivo Cardiomyocyte Strain Using Combined Cardiac DENSE and cDTI

Patrick Magrath, M.S.[1]Luigi E. Perotti, PhD[2], Eric Aliotta, M.S.[2], Ilya A. Verzhbinsky[1], Kévin Moulin, PhD[3], Daniel B. Ennis, PhD[4]

1. *University of California, Los Angeles, Los Angeles, CA*
2. *UCLA, CA*
3. *UCLA, Los Angeles, CA*
4. *Department of Radiological Sciences, University of California, Los Angeles, CA, USA., CA*

Background: Quantitative MRI biomarkers of regional myocardial performance may outperform global measurements of ventricular function (e.g. ejection fraction, EF) in diagnosing the earliest signs of cardiac disease. Displacement Encoding with Stimulated Echoes (DENSE) has shown particular promise, reporting changes in mid-wall circumferential strain (E_{cc}) in acute MI {Aletras *et al*. Circ. 2006} and hypertrophic cardiomyopathy {Aletras *et al*. Circ. Img. 2011}. LV mid-wall E_{cc} is commonly reported because mid-wall cardiomyocytes align with the local circumferential direction {Ennis *et al*. J Biomech 2008}. However, E_{cc} increases from epicardium to endocardium and does not accord with the local cardiomyocyte direction at all wall depths. This limits the precision and repeatability of mid-wall E_{cc} measurements and confounds clinical interpretations of strains near the endo- and epicardium.

Cardiac diffusion tensor imaging (cDTI) directly measures *in vivo* cardiomyocyte orientations {Tseng *et al*. JMRI 2003, Aliotta *et al.* MRM 2016}. Our objectives were: 1) to combine cDTI cardiomyocyte orientations with local DENSE strains to measure regional cardiomyocyte strain ("myofiber" strain, E_{ff}); and 2) to compare the transmural variability of E_{ff} and E_{cc}. We hypothesize that measuring E_{ff} will reduce transmural variability in E_{cc}.

Methods: *Imaging:* A single mid-ventricular short-axis slice was acquired with cDTI and DENSE in healthy volunteers (N=6) (3T Siemens Prisma) with informed consent. Imaging parameters were: cDTI (2x2x5mm, TE/TR=60/4000ms, b-value=[0,350]s/mm^2, N_{avg}=5, N_{dir}=12, dur.=4min); DENSE (bal. 4-pt., 2.5x2.5x8mm, TE/TR=1.04/15, K_e=0.06cycles/mm, N_{avg}=3, spiral interleaves=10, dur.=5min).

Post-processing: Figure 1 summarizes the steps needed to calculate E_{ff}. Lagrangian displacements were extracted from DENSE data with custom software {Spottiswoode *et al.* IEEE TMI 2007}. cDTI and DENSE registration and E_{ff} calculations were performed with custom Matlab code.

Strain Analysis: Peak systolic E_{ff} and E_{cc} for each volunteer were binned in 20% increments from epi- (0%) to endocardium (100%). Each bin was averaged across subjects and the transmural gradients of E_{ff} and E_{cc} were estimated with linear regression and compared using a 1-sided, paired t-test.

Results: Figure 2 shows cDTI cardiomyocyte orientations and peak E_{ff} for a single healthy volunteer. Corresponding circumferential vectors and E_{cc} are shown for comparison. E_{cc} has a larger transmural gradient than E_{ff} (-8.1±2.9 vs. 0.03±0.06 (unitless). E_{cc} values are consistent with previous reports {Moore *et al.* Rad. 2000}. Globally, E_{ff} is 23% lower than midwall E_{cc}, which is consistent with Dou *et al.* {MRM 2003}.

Conclusions: Here we report, for the first time, the calculation of E_{ff} using co-registered *in vivo* cDTI and DENSE. These results agree with literature and indicate that E_{ff} is a more consistent, spatially uniform measurement of cardiac performance than E_{cc}.

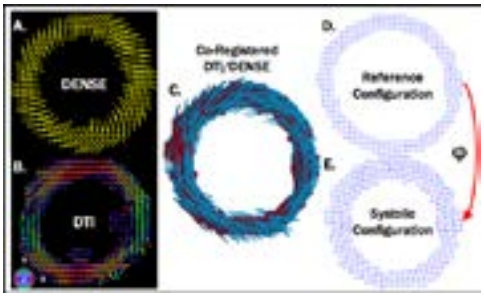

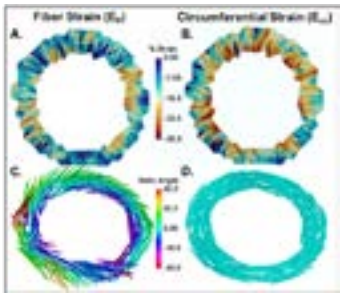

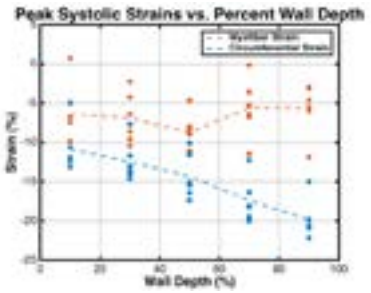

WP35

Evidence for Right Ventricular Resonance

Victor Farah, MD[1]Shimaa Sayed. Khidr, MD[1], Mark Doyle, PhD[2], Geetha Rayarao, MS[3], Ronald Williams, RT(R)(MR), B.A.[1], Moneal Shah, MD[4], Shimaa S. Khidr, MD[1], Shimaa Khidr, MD[2]

1. *Allegheny General Hospital, Pittsburgh, PA*
2. *Allegheny General Hospital, PA*
3. *Allegheny General Hospital, PIttsburgh, PA*
4. *Allegheny general hospital, pittsburgh, PA*

Background: EF is an indicator of the cardiovascular efficiency: 45% is considered normal. Recently, we have shown that the LV demonstrates a resonance phenomena whereby key resonance conditions correspond to high efficiency conditions and indicate prognosis for EF's above or below the single 45% threshold. This observation suggests an as yet, unexpected periodicity governs certain LV mechanical characteristics well beyond classical EF constructs. However, these resonance phenomena have not been demonstrated for the RV. The objective is to demonstrate the resonance response in the RV and its relationship to RVEF.

Methods: The resonance model considers the LV as a pulse generator ejecting/transmitting blood through the aorta and for the RV through the pulmonary artery (PA). Pulse waves are most efficiently transmitted when the pulse wavelength has a ratio to the transmitting vessel diameter of unity. We formed a flow index (FI) to represent the efficiency of blood transmission using CMR measures of the PA and PA flow: FI = PA area * Average PA flow velocity / systolic duration The EF was measured by 3D volumetric extraction of RV volume via Simpsons Rule. The population consisted of 56 consecutive pts undergoing routine CMR-RV metrics.

Results: The FI relates to EF using the formula $EF = Base^{(FI * Power)}$ Where Base has values of 0.3 for EF < 45 and .5 for EF > 45, with corresponding values of Power 0.2 and 0.1, respectively, Fig 1. The fit of the FI modeled EF to the measured EF has a correlation of 0.82 ($p < 0.05$).

Conclusions: The RV demonstrates a resonance phenomena for blood ejection but unlike the LV which has several bands of resonance, the RV only demonstrates two resonance bands. Resonance conditions corresponding to the central value of the FI for each band. Further work is required to demonstrate the prognostic value of this observation but initial observations support a periodicity governing RV contractility with a frequency dissimilar to the LV.

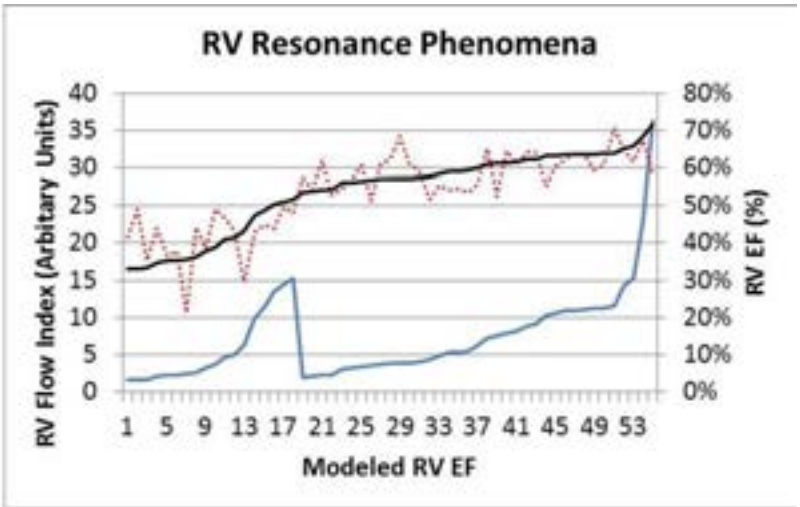

Figure 1: RV Flow Index (solid blue) demonstrates 2 bands, corresponding to measured EF (Doted red) and modeled EF (solid black)

WP36

Biventricular Remodelling After Pulmonary Valve Replacement: Does Type Of Right Ventricular Loading Influence The Outcome?

Francesca Romana Pluchinotta, MD[1] Michiel M. Winter, MD, PhD[2], Francesco Secchi, MD[1], Luciane Piazza, MD[3], Mario Carminati, MD[4], Massimo Lombardi, MD[4]

1. *IRCCS Policlinico San Donato, Milan, Italy, Milano, Lombardia, Italy*
2. *Academic Medical Center, Amsterdam, the Netherlands, Amsterdam, Noord-Holland, Netherlands*
3. *IRCCS Policlinico San Donato, Milan, Italy, San Donato Milanese, MI, Lombardia, Italy*
4. *IRCCS Policlinico San Donato, Milan, Italy, Lombardia, Italy*

Background: In patients with severe pulmonary valve regurgitation or stenosis, pulmonary valve replacement (PVR) has a positive effect on the right ventricle (RV), diminishing progression of RV dilation and/or hypertrophy. However, it remains unknown whether the loading conditions of the RV prior to PVR influence post-treatment ventricular remodeling.

Methods: We evaluated 103 patients who have been evaluated with cardiac magnetic resonance (CMR) before and after PVR between 2010 and 2015. Comparisons were made according to the RV loading conditions prior to PVR, i.e. isolated volume-loaded (iPR, n = 41), combined volume- and pressure-loaded (cPR/PS, n = 35), and isolated pressure-loaded RVs (iPS n = 27). The main study outcome was the change in the RV and left ventricular (LV) end-diastolic volume (ΔRVED, ΔLVED) and ejection fraction (EF) before and after PVR, measured on CMR.

Results: The majority of patients had pulmonary stenosis (52%) or pulmonary atresia (9%) associated with ventricular septal defect, isolated pulmonary stenosis (10%), or underwent Ross operation (15%). After PVR, the RVEDV and RVESV decreased respectively with 27 ml/m2 and 16 ml/m2 ($P < 0.001$). The change in the RVEDV after PVR was different according to the pre-implantation loading condition: iPR -48 ml/m2 ($P < 0.05$), cPR/PS -22 ml/m2 ($P < 0.05$) and iPS: -2 ml/m2 (P ns). RVEF significantly improved only in the cPR/PS group (2%, $P < 0.001$). In addition, in the total population the LVEDV and LVESD increased with 7 ml/m2 and 2.5 ml/m2 ($P < 0.05$) respectively, while LVEF showed only minor changes. However, there was an important trend in positive remodeling of the LV in patients with severe iPS (ΔLVEDV -10 ml/m2; ΔLVESV -5 ml/m2, $P < 0.05$).

Conclusions: Patients who undergo PVR seem to benefit from biventricular remodeling. The type of RV loading (pressure versus volume) before PVR affects the RV and LV remodelling pattern. Resolution of RV volume load has a positive effect on RV remodeling but did not significantly affect LV. On the other hand RV pressure-load relieve allows for better expansion of the LV, with subsequent positive effect on LV volumes and function.

WP37

Non-invasive assessment of aortic coarctation severity using computational fluid dynamics: a feasibility study

Piero Triverio, PhD Electrical Engineering[6]Zihan Chen, Master of Applied Science[1], Francesco Ballarin, PhD Applied Mathematics[2], Gianluigi Rozza, PhD Mathematics[3], Andrew M. Crean, MD, MRCP[4], Laura Jimenez-Juan, MD[5]

1. *Department of Electrical and Computer Engineering, University of Toronto, Toronto, ON, Canada*
2. *SISSA mathLab, International School for Advanced Studies, Trieste, Friuli-Venezia Giulia, Italy*
3. *SISSA, Int. School for Advanced Studies, Trieste, Trieste, Friuli-Venezia Giulia, Italy*
4. *Toronto General Hospital, Toronto, ON, Canada*
5. *Sunnybrook Health Sciences Centre, Toronto, ON, Canada*
6. *University of Toronto, Toronto, ON, Canada*

Background: Aortic coarctation (CoA) is a common congenital lesion with potentially serious consequences. Complications after repair, such as recoarctation, aneurysm formation and systemic hypertension are encountered in more than one third of adult patients throughout their lives, and need to be closely monitored. Cardiovascular MRI (CMR) is widely used for follow-up, but mainly provides anatomical information. Obtaining hemodynamic information is more challenging but very valuable to detect complications. The gold standard to assess CoA severity is the pressure drop across the narrowing measured with catheterization. Unfortunately, catheterization is an invasive procedure with a 1 in a 1000 risk of patient death or serious injury. Intervention is recommended if the pressure gradient exceeds 20 mmHg. Computational fluid dynamics (CFD) is a promising non-invasive method to calculate the pressure drop across the CoA, based on CMR images. The aim of this study was to evaluate the performance of a CMR-based CFD approach using catheterization as the reference standard.

Methods: Adult patients with a history of CoA who had CMR with contrast-enhanced 3D MR angiography and catheterization were identified from an institutional database. Images were acquired in parasagittal orientation (spatial resolution = 0.9-1.1mm x 1.0-1.1mm x 1.2-2.4mm), 19-24 s post-injection of 0.15-0.2 mmol/kg gadobutrol (Bayer Healthcare, Berlin, Germany), using bolus triggering in the ascending aorta. Images were processed using VMTKlab (Orobix srl, Bergamo, Italy) to reconstruct the geometry of the aorta in 3D. The geometry was then used to perform a patient-specific CFD simulation using Simvascular (Standford University, simvascular.github.io) (Figure 1). The pressure drop across the CoA was extracted and correlated with catheterization using Fisher's exact test. A pressure gradient >20 mmHg was considered the cut off value for significant CoA. Cohen's kappa statistic was used to measure the agreement between the two methods.

Results: Twelve CoA patients (3 female, mean age 38±17.2 years) were included. Six (50%) patients had native and 6 (50%) post repaired CoA. A significant pressure gradient (>20mmHg) was found in 7 (58%) patients by catheterization. In 10 (83%) patients, the CFD method was in agreement with catheterization (p=0.02). In only 2 (17%) patients the CFD method underestimated the CoA severity (Table 1). A good agreement between the two methods (kappa=0.68) was obtained.

Conclusions: The results of our pilot study suggest that CFD has the potential to become a non-invasive alternative to evaluate the severity of CoA.

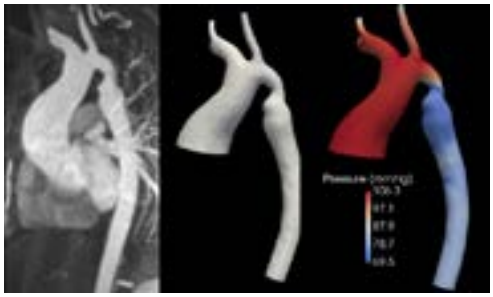

Table 1. Relationship between catheterization and computational fluid dynamics-derived pressure drop

Total	Pressure drop >20 mmHg (catheterization)	Pressure drop ≤20 mmHg (catheterization)	
7 (58%)	2 (29%)	5 (71%)	Pressure drop ≤20 mmHg (CFD)
5 (42%)	5 (100%)	0	Pressure drop >20 mmHg (CFD)
12	7 (58%)	5 (42%)	Total

WP38

Comparison of Non-Contrast Cardiovascular Magnetic Resonance and Computed Tomography Angiography for Aortic Annular Sizing before Transcatheter Aortic Valve Replacement

Yuchi Han, MD[2]Jing Wang, MD[1], Dinesh Jagasia, MD[1], Yamuna Kondapally, MD[1], Howard Herrmann, MD[1]

1. *University of Pennsylvania, PA*
2. *University of Pennsylvania, Philadelphia, PA*

Background: Accurate measurement of aortic annulus is crucial before transcatheter aortic valve replacement (TAVR). CT angiography is the most commonly utilized method, but requires contrast administration. CMR is a promising alternative modality to provide aortic annulus measurements. We aim to evaluate and compare the clinical feasibility and accuracy of a fast non-contrast cardiac magnetic resonance (CMR) protocol for the measurement of aortic annular dimensions compared with computed tomography (CT) angiography in order to provide a non-contrast alternative to CT annular sizing.

Methods: We prospectively imaged 21 consecutive patients (mean age 85.7±5.2 years) with severe aortic stenosis (mean aortic valve area= 0.6±0.1 cm^2) who were undergoing pre-TAVR CT angiography. We performed non-contrast CMR using cine SSFP and slabs of 3D navigator gated whole heart SSFP sequences covering the aortic root during systole and diastole at 1.5T (Avanto, Siemens, Germany). We performed annular measurements comparing both modalities during systole. CMR measurements were also performed during diastole and included 3- dimensional (3D) and 2-dimensional (2D) methods. The results were compared using Pearson correlation and Bland-Altman analyses.

Results: The mean systolic annular area was not significantly different between CT and 3D CMR (480.0±77.9 mm^2 vs 479.4±66.2 mm^2, P=0.98) in systole (images shown in Figure 1). There was no clinically relevant systematic difference between area measurements [mean difference 0.6 mm^2 (limits of agreement -38.2 mm^2; 39.3 mm^2)] using Bland-Altman analyses. The time for 3D CMR aortic annulus imaging by obtaining two separate systolic and diastolic imaging slabs covering the aortic root was 9.1 ± 5.3 min. There was no significant statistical difference between mean systolic and diastolic 3D CMR annular area measurements (479.4±66.2mm^2 vs. 470.8±71.2 mm^2, P =0.71) and 2D CMR annular area measurements (479.2±71.1 mm^2 vs. 465.2±70.3mm^2, P =0.56). However, the 3D diastolic CMR measurements and 2D CMR measurements were lower in numerical value as compared to the 3D CT measurements.

Conclusions: Non-contrast CMR protocol for the measurement of aortic annulus area is feasible and accurate. 3D CMR could provide an alternative for annular sizing pre TAVR.

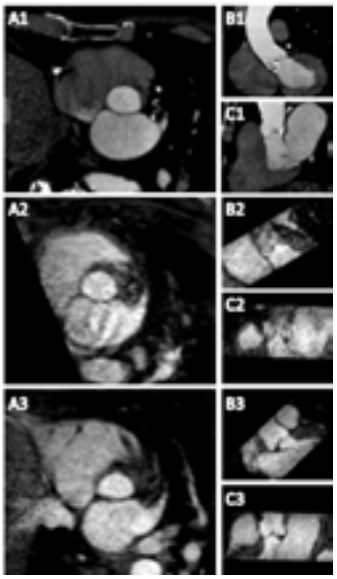

WP39

The Summed Kinetic Energy of the Residual Volume 4D Flow Component Represents a Novel Imaging Biomarker in the Evaluation of Patients with Left Ventricular Thrombus

Victoria Stoll, DPhil, BMBCh[1] Aaron T. Hess, PhD[2], Jonatan Eriksson, PhD[3], Malenka Bissell, DPhil[4], Petter Dyverfeldt, PhD[5], Tino Ebbers, PhD[6], Saul Myerson, MD, FRCP[7], Carl-Johan G. Carlhäll, MD, PhD[8], Stefan Neubauer, MD, FRCP[9]

1. *Oxford University, Oxford, England, United Kingdom*
2. *OCMR, University of Oxford, England, United Kingdom*
3. *Divsion of Cardiovascular Medicine, Department of Medical and Health Sciences, Linköping University, Linköping, Sweden, Ostergotlands Lan, Sweden*
4. *Oxford University, England, United Kingdom*
5. *Linköping University, Linköping, Ostergotlands Lan, Sweden*
6. *Linkoping University, Linkoping, Ostergotlands Lan, Sweden*
7. *NA, Oxford, England, United Kingdom*
8. *Linköping university, Ostergotlands Lan, Sweden*
9. *University of Oxford, England, United Kingdom*

Background: Ventricular thrombus is a serious complication in a subgroup of left ventricular dysfunction patients. Thrombus occurs as a consequence of stasis, hypercoagulability and endothelial injury (Virchow's triad). There are no reliable predictors for which patients will develop thrombus. 4D flow CMR may allow insights into thrombus by intra-cardiac blood flow visualisation.

We hypothesise that in patients with LV dysfunction and thrombus, compared to those without thrombus, the residual volume would constitute a similar proportion of the LV end diastolic volume (EDV) but possess less kinetic energy, thereby predisposing the blood to stasis and therefore thrombus formation.

Methods: 100 participants (47 LV dysfunction but no thrombus (LVD), 17 LV dysfunction and thrombus and 36 controls underwent CMR (Table 1). The LV flow was analysed as 4 components; direct flow, retained inflow, delayed ejection flow and residual volume. Each components' volume was calculated in proportion to the EDV. The kinetic energy of the blood per millilitre was summed throughout the cardiac cycle and divided by the cycle length to calculate the summed kinetic energy. 25 controls, 14 LVD and 14 thrombus patients returned for an interval scan to assess flow parameter stability.

Results: Both patient groups had significantly increased residual volume (LVD 50±10%, thrombus 51±12% vs 30±4% controls, p 0.001) and decreased direct flow (LVD 11±7%, thrombus 16±10% vs 38±4% controls, p 0.001). There was no difference between the 2 patient groups (Fig 1A). The summed kinetic energy of the residual volume was significantly higher in the LVD group (0.55±0.30 microJ/ml/s) compared to the thrombus group (0.38±0.16 microJ/ml/s, p 0.02) (Fig 1B). No difference between patient groups was seen for the direct flow summed kinetic energy (Fig 1C). 4D flow parameters were similar between visits with no significant change on paired t-tests (Table 2). The summed kinetic energy of the residual volume was higher in the LV dysfunction than thrombus group at visit 1 and 2, but failed to reach significance with the smaller cohorts.

Conclusions: The residual volume blood of LV thrombus patients possessed significantly less summed kinetic energy per mL than that of LV dysfunction patients with a well matched degree of LV size, impairment and similar proportion of residual volume. Residual volume blood resides within the ventricle for at least two cardiac cycles; reduced movement of this blood component may be a contributing factor to stasis and hence thrombus formation. Similar results at interval studies propose that the residual volume summed kinetic energy is a stable parameter over time. This study suggests that the summed kinetic energy of the residual volume is a novel imaging biomarker which may allow identification, monitoring of patients with LV dysfunction at higher risk of thrombus formation, and may in future guide treatment decisions on anticoagulation.

http://www.ConferenceAbstracts.com/uploads/cfp2/attachments/LDFAIBDN/LDFAIBDN--216555-1-ANY(2).pdf

http://www.ConferenceAbstracts.com/uploads/cfp2/attachments/LDFAIBDN/LDFAIBDN--216555-2-ANY(2).pdf

http://www.ConferenceAbstracts.com/uploads/cfp2/attachments/LDFAIBDN/LDFAIBDN--216555-3-ANY.pdf

WP40

CMR and Computational Flow Dynamics for Assessing Cardiovascular Aortic Remodeling Following Endovascular Aortic Repair

El-Sayed H. Ibrahim, PhD[1] Foeke Nauta, MD[2], Prachi Agarwal, MD[2], Allen Jin, PhD[2], Carlos Alberto Figueroa, PhD[3]

1. *University of Michigan, Ann Arbor, MI*
2. *University of Michigan, MI*
3. *University of Michigan & King's College London, MI*

Background: Current thoracic aortic endografts are several orders of magnitude stiffer than the native aorta. These devices are associated with acute hypertension, elevated pulse pressure, cardiac remodeling, and reduced coronary perfusion. Nevertheless, a systematic assessment of the deleterious effects of thoracic endovascular aortic repair (TEVAR) is still missing. In this abstract, we present the CardiOvascular aortic Remodeling following Endovascular aortic repair (CORE) study, which aims to: 1) quantify cardiovascular remodeling following TEVAR; and 2) validate computational modeling of thoracic aortic hemodynamics following TEVAR using clinical measurements.

Methods: The study population consists of adult patients with descending thoracic aortic aneurysm (TAA) or penetrating aortic ulcer (PAU) managed with TEVAR (TEVAR group, n=12) or with optimal medical treatment (control group, n=12). CMR imaging and vascular computational flow dynamic (CFD) simulations are conducted on both groups prior to treatment and at one-year follow-up. The CMR exam consists of the following sequences (Table-1): cine, trans-mitral velocity-encoding, velocity-encoding across the aorta, strain-encoding (SENC), and perfusion. Using CMR images and clinical data, CFD simulations are performed to obtain highly detailed descriptions of blood velocity, flow, pressure, and wall shear-stress. The CFD image-based modeling paradigm uses anatomical data to create a 3D computer model of the aorta (Figure-1a), where hemodynamics simulation is performed (Figure-1b). Additional physiological measurements of flow (from velocity-encoded images), wall motion (from cine images), or pressure (acquired during TEVAR) are used to inform the simulation boundary conditions.

Results: Although the CORE study is still in progress, we present here preliminary results of the feasibility of the implemented techniques for assessing the impact of systemic, i.e. aging, and localized stiffening, i.e. ascending aortic endograft repair, on cardiac function (Figure-2), where the results demonstrated that acute increases in left-ventricle contractility (20% for old-age, 8.5% for stent-repair) and work (11% for old-age, 5% for stent-repair) are required to maintain the pre-operative cardiac output. These results highlight that alterations in stiffness in a relatively short segment of the aorta have comparable impacts to those induced by generalized age-induced stiffening.

Conclusions: Although the TEVAR procedure is increasingly used, and patients are being treated at younger age, assessment of deleterious effects of TEVAR is still missing. The CORE study represented here helps assess the impact of thoracic aortic stent grafts on the cardiovascular system by providing unique data, including intraluminal pressure measurements, CMR imaging, and computational modeling. Future patients would benefit from better patient management with improved aortic endograft designs and long-term outcomes.

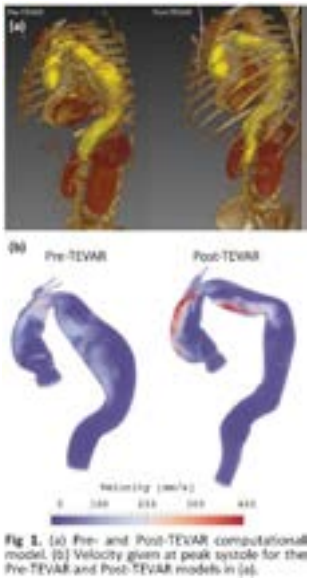

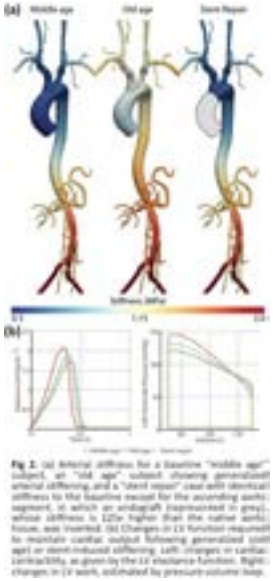

WP41

Longitudinal Changes in Cardiac-MRI derived Segmental Aortic Stiffness in Children and Young Adults with Connective Tissue Disorders

Anthony C. Merlocco, M.D.[1] Ronald Lacro, M.D.[2], Kimberlee Gauvreau, Sc.D.[2], Nicole Rabideau, RDCS[2], Michael Singh, M.D.[2], Ashwin Prakash, M.D.[2]

1. *Children's National Medical Center, Washington, DC*
2. *Boston Children's Hospital, Boston, MA*

Background: Surgical guidelines for aortic root replacement in CTDs are based on aortic diameter, an imperfect predictor of risk of dissection. Aortic stiffness has emerged as a novel marker of vascular phenotype. Stiffness measured by cardiac magnetic resonance (CMR) in CTD patients is abnormal and associated with adverse aortic outcomes. However, longitudinal changes in aortic stiffness in CTD patients have not been well characterized.

Methods: Retrospective analysis of 50 children and young adults (median age 20, range 0.2-49) with a CTD with at least 2 CMR examinations (total 152 examinations) over a median duration of 3.9 (1-13.2) years was performed. Aortic stiffness measures (area strain, distensibility, and β stiffness index) were calculated on each examination at the aortic root (AoR), ascending (AAO) and descending aorta (DAO). Longitudinal changes in stiffness parameters were analyzed using linear mixed models.

Results: All CMR parameters of aortic stiffness increased with age at the AoR, AAO and DAO (Table). Interobserver reliability for measurement of stiffness parameters was acceptable (mean difference between observers 0.1±7 for AAO strain). No significant associations were found between the longitudinal rate of increase in aortic stiffness and the rates of aortic root dilation or surgical aortic root replacement.

Conclusions: Children and young adults with CTD demonstrate progressive increase in aortic stiffness with increasing age. Further research is warranted to compare the rate of increase in stiffness in CTD patients with normal subjects and to determine if longitudinal changes in aortic stiffness are important in the pathogenesis of aortic complications such as dissection.

Longitudinal measures of aortic stiffness

Parameter	Number of CMR studies	Number of patients	Average change per 10 year increase in age	P Value
Aortic Root				
Strain (%)	145	50	-1.9(-1.3, -2.6)	<0.001
Distensibility (x10-3mmHg-1)	144	50	-0.7(-0.5, -0.9)	<0.001
β-stiffness index	144	50	1.91 (1.11, 2.71)	<0.001
AAO				
Strain (%)	127	47	-3.7(-2.0, -5.3)	<0.001
Distensibility (x10-3mmHg-1)	126	47	-1.3(-0.9, -1.8)	<0.001
β-stiffness index	126	47	0.60 (0.22, 0.103)	0.007
DAO				
Strain (%)	128	47	-2.5(-1.3, -3.7)	<0.001
Distensibility (x10-3mmHg-1)	127	47	-1.0(-0.6, -1.3)	<0.001
β-stiffness index	127	47	0.40 (0.23, 0.57)	<0.001

Average changes are shown with 95% confidence intervals

AAO = Ascending aorta; DAO = Descending aorta

WP42

4D Flow MRI Image Quality and Cardiac Volumetric Data Depends on Contrast Agent Used

Kanae Mukai, MD[1] Nicholas Burris, MD[2], Karen Ordovas, MD, MAS[3], Michael D. Hope, M.D.[4]

1. *UCSF, Palo Alto, CA*
2. *University of Michigan, Ann Arbor, MI*
3. *University of California San Francisco, San Francisco, CA*
4. *University of California, San Francisco, CA*

Background: Prior studies suggest that 4D Flow MRI data can be used for standard cardiac volumetric analysis. The purpose of this study was to assess the impact of MRI contrast agent on 4D Flow image quality and volume measurements compared with the standard MRI technique (CINE steady state free precession (SSFP)).

Methods: Adult patients referred for clinical cardiac MRI/MRA (n=22) were prospectively and consecutively recruited for 4D Flow imaging after completion of their clinical exam. Patients with renal failure (n=10) received ferumoxytol, an investigative contrast agent and the rest (n=12) received gadolinium. Image quality was assessed with 1) signal-to-noise ratio (SNR); 2) contrast-to-noise ratio (CNR); 3) ventricular blood pool:myocardial signal ratio; and 4) a 5-point Likert scale based on the definition of the endocardial border (1=none; 2=partial but unable to draw border; 3=able to roughly estimate the border; 4=visible for most of the cardiac cycle; 5=excellent definition in systole and diastole). A subset (n=15) had CINE SSFP imaging for standard volumetric analysis (gadolinium=11, ferumoxytol=4). CINE SSFP and 4D Flow volumes were compared for the 2 contrast agents.

Results: 4D Flow studies using ferumoxytol demonstrated higher SNR, CNR, and bloodpool:myocardial signal ratio compared to those using gadolinium (7.3 vs. 3.3, 4.8 vs. 1.3, and 2.8 vs. 1.4, respectively, $p < 0.005$). Excellent definition of myocardial contours (Likert=5) was more frequently noted with ferumoxytol than with gadolinium (8/10 vs. 0/12), with higher average Likert scores (4.8 versus 3.0). Very strong correlation was seen between ventricular volumes measured using SSFP and 4D Flow with ferumoxytol (R^2=0.997, mean=1.2, LOA=-7.3 to 9.7), with significant improvement compared to gadolinium (R^2=0.872, mean=-4.3, LOA=-12.7 to 34.0).

Conclusions: Ferumoxytol (FDA-approved for iron replacement) used off-label for patients with renal failure can substantially improve the image quality of 4D Flow MRI relative to gadolinium-based contrast, allowing cardiac volumetric measurements that correlate well with the standard MRI technique.

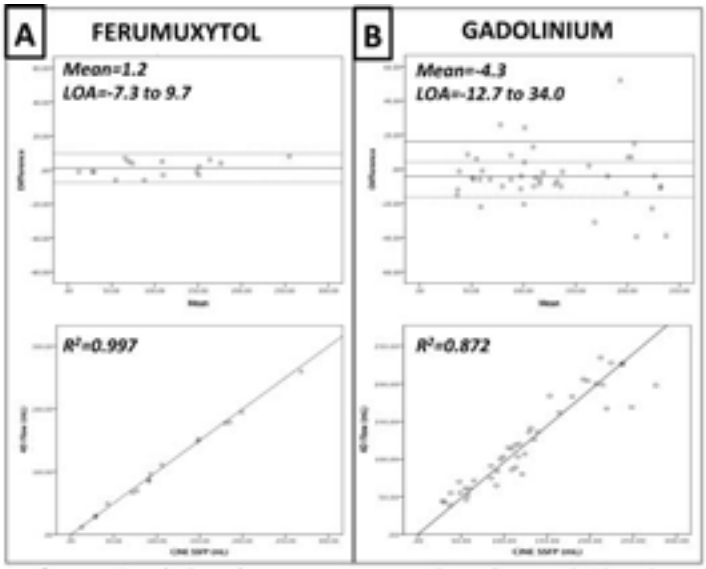

Figure 1: Comparison of volumes (LVEDV, LVESV, RVEDV, and RVESV) measured with 4D Flow and CINE SSFP. (A)= Ferumoxytol (N=4). (B)= Gadolinium (N=11).

WP43

Association between pulmonary artery pulse wave velocity and packyears of smoking. The Multi-Ethnic Study of Atherosclerosis (MESA) COPD Study

Roy Huurman, BSc[1] Bharath Ambale-Venkatesh, PhD[2], Yoshiaki Ohyama, MD, PhD[3], Chikara Noda, PhD[4], So-Yeon Lim, MD[2], Colin O. Wu, PhD[5], Eliseo Guallar, MD, DrPH[6], Russell Tracy, PhD[7], Martin R. Prince, MD, PhD[8], R. Graham Barr, MD, DrPH[9], David Bluemke, MD, PhD[10], Joao A.C. Lima, MD, MBA[11]

1. Erasmus Medical Center, Rotterdam, Zuid-Holland, Netherlands
2. Johns Hopkins University, MD
3. Johns Hopkins Hospital, MD
4. Showa University, Tokyo, Japan
5. National Institutes of Health, MD
6. Johns Hopkins Bloomberg School of Public Health, MD
7. University of Vermont, VT
8. Cornell University, NY
9. Columbia University, NY
10. NIH, MD
11. Johns Hopkins University, Baltimore, MD

Background: Pulse wave velocity (PWV), defined as the rate at which pressure waves propagate along the artery after ventricular contraction, is a marker for arterial stiffness strongly correlated with cardiovascular events and mortality. Data on pulmonary artery (PA) PWV is lacking, although small studies have examined PA PWV using cardiac magnetic resonance (CMR) imaging, obtaining relatively positive results. We aimed to further explore the use of CMR for PA PWV measurement in a larger group of patients. As smoking is a major contributor to vascular stiffness, we also assessed the relation between smoking packyears and PA PWV.

Methods: In the Multi-Ethnic Study of Atherosclerosis (MESA) Chronic Obstructive Pulmonary Disease (COPD) Study, 325 patients with or without COPD were enrolled predominantly from two prospective population-based cohorts (MESA and Emphysema and Cancer Action Project; EMCAP). All participants were free of overt cardiovascular disease, were 50-79 years old and had smoked 10 or more packyears. All cases that underwent MRI to measure PA PWV were included (n=270). 115 were excluded because of insufficient image quality or missing data (30 aliasing and 36 breathing artifacts, 49 incomplete cases). Phase contrast cross-sectional images of the main, left and right pulmonary artery (MPA, LPA, RPA) were obtained. The vessel contours were tracked semi-automatically for each subject and super-imposed on the corresponding velocity-encoded images to obtain flow data using ARTFUN (INSERM, France). Transit time was calculated using least squares minimization. The distance between the MPA and either branch was measured using axial images displaying the pulmonary system. PA PWV was calculated by dividing distance by time for both branches. Data was log transformed before analysis. Univariable and multivariable regression assessed the association of PA PWV and demographics, vascular risk factors, COPD stage and ankle-brachial index (ABI). To assess reproducibility, 40 studies were analyzed by two readers and compared with the concordance correlation coefficient (CCC).

Results: The population was age 68±7, 65% male, had smoked 30±24 packyears; 36% had COPD. Median (IQR) LPA and RPA PWV was 3.5 (2.1-5.3) and 3.1 (2.1-5.2) m/s. No association was found between log mean PA PWV (LMPP) and age, systolic blood pressure (SBP) and COPD stage. One packyear increase was associated with an increase in LMPP of 0.006 ($p<0.01$). This association persisted after adjustment for demographics, vascular risk factors, COPD stage and ABI ($\beta=0.006$, $p<0.01$). CCC of LMPP was 0.937 (mean difference -0.517±1.05).

Conclusions: In our population of ever-smoking elderly free of cardiovascular disease, PA PWV had a positive association with cumulative smoking, after adjustment for demographics, vascular risk factors, COPD stage and ABI. No association was found between PA PWV and age, SBP or COPD. Inter-reader reproducibility was good. This method may be used to investigate the mechanics underlying PA stiffness.

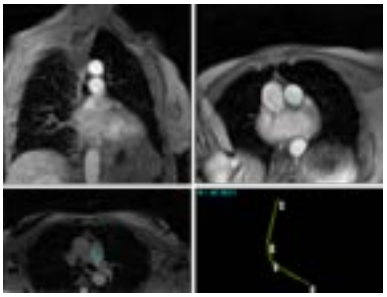

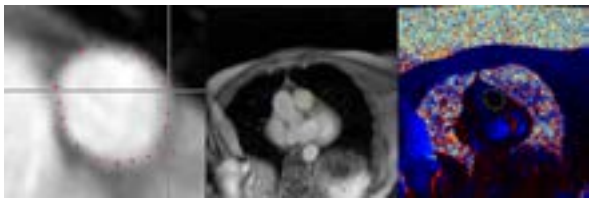

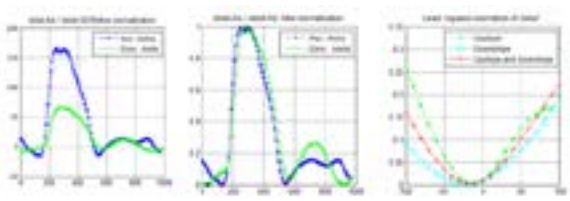

WP44

Scan-rescan reproducibility of Left Ventricular Stroke Volume Assessment by 4D-Flow CMR with Retrospective Valve Tracking and Particle Tracing versus Planimetry in Healthy Volunteers.

Vivian P. Kamphuis, MD[1]Roel L.F. van der Palen, MD[2], Rob J. van der Geest, PhD[3], Patrick J.H. de Koning, MSc[3], Pieter J. van den Boogaard, BSc[3], Albert de Roos, MD, PhD[3], Nico A. Blom, MD, PhD[4], Arno A.W. Roest, MD, PhD[4], Jos J.M. Westenberg, PhD[5]

1. *Division of Pediatric Cardiology, Department of Pediatrics, Leiden University Medical Center, Leiden, The Netherlands and Netherlands Heart Institute, Utrecht, The Netherlands, Den Haag, Zuid-Holland, Netherlands*
2. *Division of Pediatric Cardiology, Department of Pediatrics, Leiden University Medical Center, Leiden, The Netherlands, Zuid-Holland, Netherlands*
3. *Department of Radiology, Leiden University Medical Center, Leiden, The Netherlands, Zuid-Holland, Netherlands*
4. *Division of Pediatric Cardiology, Department of Pediatrics, Leiden University Medical Center, Leiden, The Netherlands and Netherlands Heart Institute, Utrecht, The Netherlands, Zuid-Holland, Netherlands*
5. *Department of Radiology, Leiden University Medical Center, Leiden, The Netherlands, Leiden, Zuid-Holland, Netherlands*

Background: 4D-flow cardiovascular magnetic resonance (CMR) with retrospective valve tracking is the most accurate CMR method to assess multi-trans-valvular flow. However, the reproducibility from a scan-rescan test is not known. Therefore, we aimed to assess the scan-rescan reproducibility of left ventricular (LV) stroke volume (SV) assessment by 2D-planimetry and 4D-flow CMR.

Methods: Ten healthy volunteers (age 27±3 years) underwent whole-heart 4D-flow CMR at a 3T MRI scanner (VENC =150cm/s, spatial resolution 3×3×3mm^3, temporal resolution 40ms and 30 phases retrospectively reconstructed phased over one cardiac cycle, free-breathing with Echo-Planar-Imaging factor 5 and Sensitivity-Encoding factor 2). All volunteers were scanned with the same protocol twice in one session (± 10 minutes between scans). SV was obtained by 1) 2D-planimetry from cine short-axis (multi-slice multi-phase steady-state free-precession gradient-echo), 2) 4D-flow CMR with retrospective valve tracking over mitral valve (MV) and aortic valve (AV) and 3) particle tracing evaluating LV inflow through the MV and outflow through the AV. For particle tracing, the LV was filled with particles (one per voxel) at end-diastole; AV outflow particles were counted by forward tracing over systole and MV inflow particles were counted by backward tracing over diastole. Figure 1 shows the three methods that were used. Mean differences were determined for inter-scan comparison and significance was tested by paired-samples t test. Correlation and agreement was tested by Pearson correlation coefficient (R), intraclass correlation coefficients (ICC) and coefficient of variation (CV).

Results: Scan-rescan assessment of SV by 2D planimetry shows strong correlation between flow volumes measured in both scans (R=0.95, P < 0.001) with a strong ICC and small CV indicating good reproducibility. Also, scan-rescan assessment of MV and AV SV by retrospective valve tracking from 4D-flow CMR shows good reproducibility with strong scan-rescan correlation (MV R=0.90, P < 0.001, AV R=0.83, P < 0.001) and a strong ICC. CV for assessment by retrospective valve tracking is small, but slightly higher than CV for SV assessment by planimetry (CV 11-12% vs. 7%, respectively). However, particle tracing from 4D-flow CMR shows lowest reproducibility. Detailed results are shown in table 1.

Conclusions: SV by 2D-planimetry and 4D-flow CMR with retrospective valve tracking shows strong reproducibility, but 4D-flow CMR with particle tracing is less reliable for SV assessment, possibly due to the required integration procedures on noisy data.

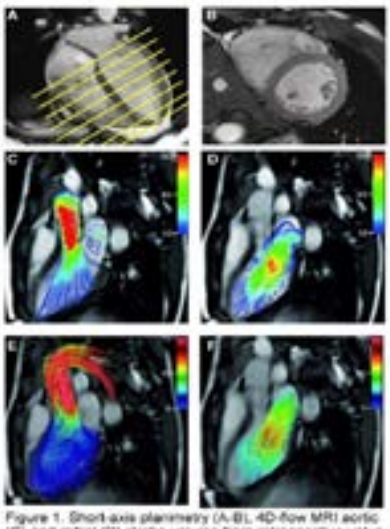

Figure 1. Short-axis planimetry (A-B), 4D-flow MRI aortic (C) and mitral (D) stroke volume from retrospective valve tracking and from forward (E) and backward (F) particle tracing.

Statistics for Comparison of 2D Stroke Volume and Net Flow Through the Mitral and Aortic Valve

AV particle tracing	MV particle tracing	AV retrospective valve tracking	MV retrospective valve tracking	SV 2D planimetry	
15.01 ± 29.70	-1.52 ± 29.52	2.58 ± 11.70	2.23 ± 11.33	0.81 ± 7.00	Mean difference (mL)
0.2	0.9	0.5	0.5	0.7	P-value*
0.70	0.77	0.83	0.90	0.95	Pearson correlation coefficient
0.038	0.015	0.003	<0.001	<0.001	P-value
0.80	0.88	0.89	0.92	0.98	Intraclass correlation coefficient
0.013	0.005	0.002	<0.001	<0.001	P-value
23%	28%	12%	11%	7%	Coefficient of variation
*P-values were calculated with the paired-samples t test					

WP45

Biventricular hemodynamic forces in healthy volunteers and elite athletes quantified with 4D flow MRI

Per M. Arvidsson, MD[1]Johannes Töger, PhD[2], Marcus Carlsson, MD, PhD[3], Katarina Steding-Ehrenborg, PhD[4], Gianni Pedrizzetti, PhD[5], Einar Heiberg, Ph.D.[6], Håkan Arheden, MD, PhD[7]

1. *Lund University, Department of Clinical Sciences Lund, Clinical Physiology, Skane University Hospital, Lund, Sweden, Luns, Skane Lan, Sweden*
2. *Lund University, Lund, N/A, Sweden*
3. *Lund University, Department of Clinical Sciences Lund, Clinical Physiology, Skane University Hospital, Lund, Sweden, Skane Lan, Sweden*
4. *Lund University, Skane University Hospital, Department of Clinical Physiology, Lund, Sweden; Lund University, Department of Health Sciences, Physiotherapy, Lund, Sweden, Skane Lan, Sweden*
5. *University of Trieste, Trieste, Toscana, Italy*
6. *Lund University, Dept. of clinical sciences, Clinical Physiology, Lund, Skane Lan, Sweden*
7. *Lund University, Department of Clinical Sciences Lund, Clinical Physiology, Skane University Hospital, Lund, Sweden, Lund, Skane Lan, Sweden*

Background: Intracardiac blood flow is driven by hemodynamic forces that are exchanged between the blood and myocardium, and which reflect the functional performance of the ventricles. Previous studies have been limited to 2D measurements using echocardiography or have investigated only left ventricular (LV) forces. Right ventricular (RV) forces and their contribution to asymmetric redirection of flow in the RV have not been measured. We therefore aimed to quantify three-dimensional hemodynamic forces in both ventricles in a cohort of healthy subjects.

Methods: 25 controls and 14 elite endurance athletes (total n=39) were included. 4D flow (SENSE=2, 50 ms temporal resolution, 3 mm isotropic) and bSSFP imaging was performed during supine rest at 1.5T or 3T (Philips Achieva). Ventricular endocardial borders were segmented semi-automatically over the cardiac cycle. 4D flow data was used as input for the Navier-Stokes equations to compute hemodynamic forces over the entire cardiac cycle for each ventricle separately. Global hemodynamic forces were decomposed into three components: longitudinal (apical-basal), and two transversal directions at right angles to each other. The ratio between longitudinal and transversal forces was computed for each ventricle separately.

Results: Hemodynamic force patterns were consistent in all subjects, with variations in amplitude (Figure 1). LV forces were mainly aligned along the apical-basal longitudinal axis (Figure 2), with an additional lateral component aimed towards the aortic valve during systole. In contrast, RV forces were found in both the longitudinal direction and in the transversal directions, with a systolic force component redirecting blood flow around the interventricular septum towards the pulmonary valve. Spatial downsampling of 4D data resulted in similar quantitative results (Figure 3).

Conclusions: Normal cardiac pumping is associated with highly specific force patterns in both ventricles, and deviation from these forces may be a sensitive marker of ventricular dysfunction. Right ventricular forces drive a slingshot-like redirection of blood flow along the interventricular septum, which illustrates its importance for RV pumping. Hemodynamic forces are not strongly influenced by low spatial resolution, enabling faster scan times and potentially facilitating clinical use.

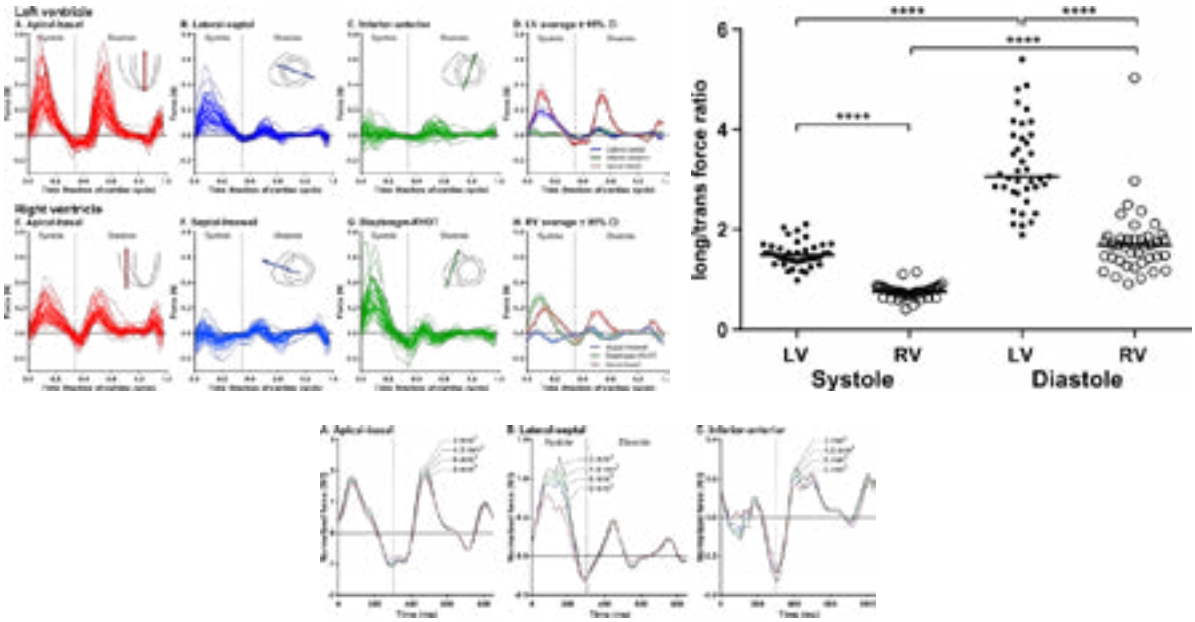

WP46

Validation of a novel cine-derived b-spline deformable strain method against reference measurements with DENSE in a group of healthy volunteers at 1.5T.

Kenneth Mangion, MD[1] Hao Gao, PhD[2], Christie McComb, PhD[3], David Carrick, PhD[4], Guillaume Clerfond, MD[5], Xiaodong Zhong, PhD[6], Xiaoyu Luo, PhD, MSc [1], Caroline E Haig, PhD[7], Colin Berry, PhD FRCP[1]

1. *University of Glasgow, Glasgow, Scotland, United Kingdom*
2. *School of Mathematics and Statistics, University of Glasgow, Scotland, United Kingdom*
3. *NHS Greater Glasgow and Clyde / University of Glasgow, Glasgow, Scotland, United Kingdom*
4. *Golden Jubilee National Hospital, Glasgow, Scotland, United Kingdom*
5. *University Hospital of Clermont Ferrand, France, Clermont Ferrand, Auvergne, France*
6. *Siemens Healthcare, GA*
7. *Robertson Centre for Biostatistics, Glasgow, Scotland, United Kingdom*

Background: Cine-derived methods of estimating myocardial strain avoid the penalty of additional breath-holds for dedicated strain-acquisitions, however, diagnostic accuracy may be a trade-off. We have developed a novel method for estimation of E_{cc} derived from an intensity-based b-spline deformable registration method. This technique called deformation tracking, derives strain from across the entire myocardial wall, rather than the endocardial border and associated features, as is the case with feature-tracking. We aimed to compare peak circumferential strain derived with deformation tracking, feature-tracking and a reference method (Displacement ENcoding with Stimulated Echoes (DENSE)) for estimating peak circumferential strain (E_{cc}). We hypothesised that strain estimated with deformation tracking would be more closely associated with strain from the reference method (DENSE), than strain derived from a standard method for feature-tracking in healthy volunteers.

Methods: Healthy adults across a broad age range (18-85 years) with a normal ECG but without any history of cardiovascular disease or treatment underwent MRI at 1.5T (MAGNETOM Avanto, Siemens Healthcare, Erlangen, Germany) including b-SSFP cines, 2D cine-EPI-DENSE (work-in-progress sequence 611, Siemens Healthcare, Erlangen, Germany), and late gadolinium enhancement (0.15mmol/kg gadolinium diethyltriaminepentaacetic acid, Magnevist, Bayer Healthcare, Berlin, Germany) in subjects >45 years. Mid-left ventricular acquisitions were divided into 6 segments, and global and segmental E_{cc} were derived and analysed by age and sex using an in-house software application for cine-derived deformation tracking commercial feature-tracking software (TomTec Imaging Systems, Germany), and 2D-DENSE (University of Auckland, New Zealand). Statistical analysis was performed using SPSS software (SPSS Inc, Chicago, IL, USA, version 22) and directed by a statistician who was independent of the research group. All subjects gave written informed consent (ethics reference 11/AL/0190).

Results: Eighty one healthy adults (44.6±17.7 years old, 47% male) underwent CMR at 1.5T. E_{cc} differed between the 3 methods: (deformation tracking: -16.8 ± 2.4 %; FT: -28.7 ± 4.8%; DENSE: -19.4 ± 4.8 %) (ANOVA with Tukey post-hoc, F-value 279.93, p< 0.01). Deformation tracking E_{cc} (Pearson co-efficient = 0.41, pcc (Pearson co-efficient = 0.46, pcc. Regional differences in strain were observed with all 3 methods (Table 1). Deformation tracking and DENSE disclosed more sex-related and regional differences in peak E_{cc} than feature-tracking.

Conclusions: Peak E_{cc} revealed by deformation tracking and 2D-DENSE were similar, suggesting E_{cc} may be over-estimated with feature-tracking. Deformation tracking resolved differences in strain related to sex and myocardial region whereas feature tracking did not. Further research is warranted.

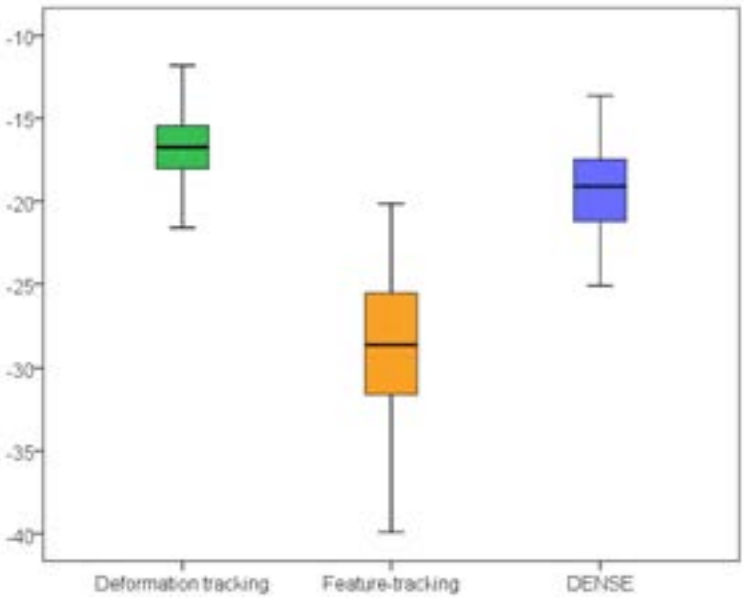

Table 1. Circumferential strain utilising DENSE, cine-derived and feature-tracking

Feature-tracking			**B-spline deformable registration method**			**DENSE**			
p-value	Female	Male	p-value	Female	Male	p-value	Female	Male	Parameter
	(n=42)	(n=39)		(n=42)	(n=39)		(n=42)	(n=39)	E_{cc}
0.262	-29.2 ± 4.8	-28.0 ± 4.8	**0.005**	-17.5 ± 2.7	-16.0 ± 1.7	**0.014**	-20.1 ± 2.7	-18.7 ± 2.2	Global (%)
0.501	-28.1 ± 8.9	-29.6 ± 10.1	**0.053**	-16.1 ± 3.8	-14.2 ± 3.8	0.153	-21.6 ± 4.2	-20.3 ± 3.5	Anterior (%)
0.388	-26.9 ± 12.1	-24.8 ± 9.0	**0.009**	-20.2 ± 3.8	- 17.9 ± 3.9	0.667	-17.9 ± 3.3	-18.2 ± 3.7	Antero-septal (%)
0.891	22.9 ± 11.1	-23.2 ± 8.8	0.179	-20.6 ± 2.1	-19.4 ± 3.3	**0.055**	-17.4 ± 3.0	-16.0 ± 3.6	Infero-septal (%)
0.139	-24.5 ± 7.6	-26.9 ± 6.1	0.141	-16.4 ± 3.8	-15.3 ± 2.2	**0.003**	-20.8 ± 3.6	-18.5 ± 3.3	Inferior (%)
0.019	-30.9 ± 9.5	-26.2 ± 7.6	**0.005**	-19.7 ± 3.8	-18.9 ± 3.1	**0.030**	-22.7 ± 3.7	-21.1 ± 2.9	Infero-lateral (%)
0.72	-26.0 ± 7.7	-22.5 ± 9.0	0.501	-14.7 ± 3.1	-14.0 ± 3.2	**0.047**	-22.3 ± 3.2	-20.9 ± 3.2	Antero-lateral (%)

Mean (±SD); E_{cc}: Circumferential strain

WP47

Using a Respiratory Navigator Significantly Reduces Variability when Quantifying Left Ventricular Torsion from CMR

Sean M. Hamlet, MS[1] Christopher M. Haggerty, PhD[2], Jonathan D. Suever, PhD[3], Gregory J. Wehner, BS[1], Kristin N. Andres, BS[1], David K. Powell, PhD[1], Richard J. Charnigo, PhD[1], Brandon K. Fornwalt, MD, PhD[2]

1. *University of Kentucky, KY*
2. *Geisinger Health System, PA*
3. *Geisinger Health System, Bellefonte, PA*

Background: Left ventricular (LV) torsion is an important indicator of cardiac function, however its quantification is limited by high inter-test variability. Torsion is typically quantified using two short-axis images acquired during separate end-expiratory breath-holds. Unfortunately, the exact breath-hold position may differ by up to 13mm between breath-holds resulting in differences in heart position between acquisitions. We believe that inconsistent breath-hold positions during serial image acquisitions accounts for a substantial portion of variability in measured LV torsion. We hypothesized that this variability could be substantially reduced by using a respiratory navigator to minimize differences in breath-hold position.

Methods: Ten healthy subjects and seven patients with heart disease underwent navigator-gated 2D spiral cine displacement encoding with stimulated echoes (DENSE) to measure LV twist at basal and apical short-axis planes. Variability in the quantification of LV torsion due to inconsistent breath-hold positions was simulated using three steps: 1) a respiratory navigator was used to measure subject-specific maximum, middle, and minimum breath-hold positions (Figure 1) over 10 consecutive breath-holds; 2) DENSE data were acquired with the navigator acceptance window positioned at each of the three subject-specific breath-hold positions; and 3) LV torsion was computed for all permutations of slice pairs and breath-hold position. To assess inter-test reproducibility with consistent breath-holds, image acquisitions at the middle position were repeated. To quantify the variability introduced by inconsistent breath-holds, the root mean squared error (RMSE) of torsion due to consistent and inconsistent breath-holds was compared. To determine the reduction in sample size required to detect a clinically meaningful change in LV torsion by using a respiratory navigator, theoretical study sample sizes were computed.

Results: With a consistent breath-hold position enforced by using a respiratory navigator, the variability in measured LV torsion was reduced by 56% (RMSE: 0.7±0.3 °/cm vs 0.3±0.2 °/cm, $p < 0.001$). Furthermore, the sample size required to detect a 10% relative difference in LV torsion was reduced from 34 to 16. There was a positive correlation between the RMSE from inconsistent breath-hold positions and the individual subject-specific range of breath-hold positions ($r=0.50$ $p=0.049$) (Figure 2). The range of breath-hold positions over 10 breath-holds was 10±4 mm on average across all subjects.

Conclusions: Inconsistent breath-hold positions contribute to significant variability in the quantification of LV torsion. Using a respiratory navigator to ensure a consistent breath-hold position between image acquisitions can reduce the variability in quantifying LV torsion by 56%.

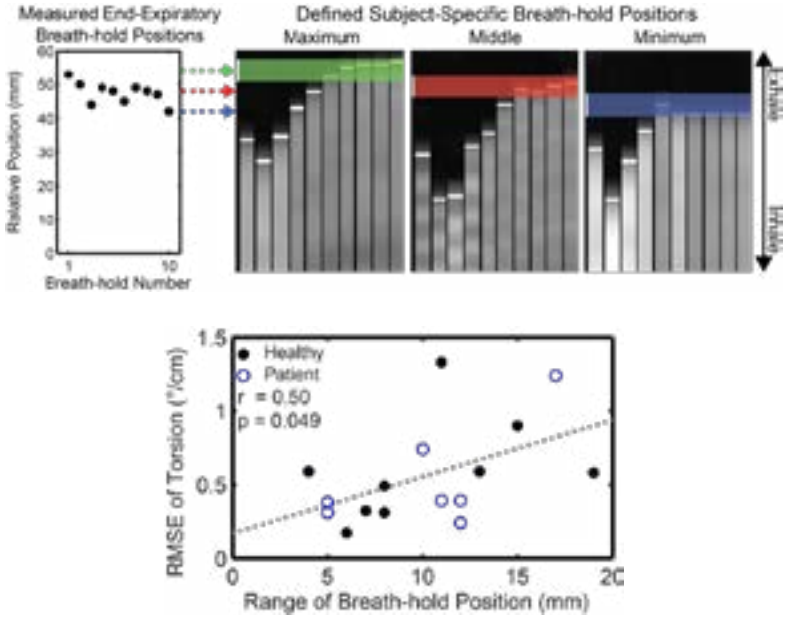

WP48

Novel approach to CMR T1 and T2 maps based on texture analysis

Nadjia Kachenoura, PhD[4] Tania-Marina Bacoyannis, MS[1], Adrian Huber, MD[2], Jérôme Lamy, MS[2], Alain De Cesare, PhD[3], Philippe Cluzel, MD, PhD[1], Alban Redheuil, MD, PhD[1]

1. *Sorbonne Universités, UPMC Univ Paris 06, INSERM, CNRS, UMR 7371, UMRS 1146, Laboratoire d'Imagerie Biomédicale, 75013, Paris, France, Ile-de-France, France*
2. *Sorbonne Universités, UPMC Univ Paris 06, INSERM, CNRS, UMR 7371, UMRS 1146, Laboratoire d'Imagerie Biomédicale, 75013, Paris, France, Paris, Ile-de-France, France*
3. *Sorbonne Université, Université Pierre et Marie Curie, Laboratoire d'Imagerie Biomédicale, UMRS 1146 INSERM-CNRS, Paris, France, Ile-de-France, France*
4. *Sorbonne Universités, UPMC , INSERM UMRS 1146, Laboratoire d'Imagerie Biomédicale, Ile-de-France, France*

Background: Myocardial fiber disarray is a characteristic feature of hypertrophic cardiomyopathy (HCM) in pathology. We hypothesized that texture indices related to local image homogeneity and dissimilarity when calculated from T1 and T2 maps can reveal and quantify such disarray at the macroscopic level.

Methods: We studied 12 healthy subjects (40y±13, 3 females) and 10 patients with HCM (49y±16, 4 females) who had a CMR exam on a 1.5T magnet withT2 and native T1 mapping imaging. After myocardial delineation global mean T1 and T2 values were measured. Furthermore, in the same myocardial regions of interest, new texture indices were extracted from the T1 and T2 maps, including: 1) homogeneity (local similarity of signal within the myocardium), 2) entropy, (local randomness of signal within the myocardium). Finally, a receiver operating characteristic (ROC) analysis has been performed to assess the ability of myocardial T1, T2 as well as texture indices to detect myocardial alteration secondary to HCM. Sensitivity, specificity and the area under the ROC curve (AUC) were provided.

Results: Native myocardial T1 values were higher for HCM subjects and were able to characterize HCM with a sensitivity of 70%, a specificity of 91% and an AUC of 0.84. Myocardial T2 was also higher in HCM and was able to separate between the two groups with a sensitivity of 90%, a specificity of 91% and an AUC of 0.90. ROC performance was higher for texture indices when compared to myocardial T1 and T2 values thanks to a lower overlap in myocardial texture values between HCM and controls (Homogeneity from T1 maps: sensitivity = 90%, specificity = 100% and AUC = 0.92 ; Homogeneity from T2 maps: sensitivity = 100%, specificity = 90% and AUC = 0.96 ; Entropy from T1 maps: sensitivity = 90%, specificity = 100% and AUC = 0.93 ; Entropy from T2 maps: sensitivity = 100%, specificity = 91% and AUC = 0.96).

Conclusions: New texture indices have been applied to T1 and T2 maps and proved their ability to detect myocardial alterations with higher sensitivity and specificity than native T1 and T2 values. Their clinical usefulness needs to be confirmed on a larger population.

WP49

Fat Suppressed Dark-Blood Delayed-Enhancement

Elizabeth Jenista, Ph.D.[1] Wolfgang Rehwald, PhD[2], David Wendell, PhD[3], Stephen Darty, RT-N,MR; BSRS[3], Han Kim, MD[1], Enn-Ling Chen, PhD[3], Michele Parker, MS[4], Raymond j. Kim, MD[3]

1. *Duke University, Durham, NC*
2. *Siemens Healthcare, NC*
3. *Duke University Medical Center, NC*
4. *Duke Cardiovascular MR Center, Durham, NC*

Background: The diagnosis of myocardial infarction is crucial in determining clinical management and prognosis. Delayed-enhancement MRI (DE-MRI) is the current in vivo reference standard, with excellent delineation of bright infarct from dark normal myocardium. However, it can be difficult to distinguish infarct from other bright tissues, such as blood and fat. We recently developed FIDDLE[1] (flow-independent dark-blood delayed-enhancement) to provide robust black blood DE-MRI, and DSPAIR (Double SPAIR[2]) for fat suppressed DE-MRI. We hypothesized the combination would provide fat suppressed, black-blood DE-MRI.

Methods: The combination of DSPAIR and FIDDLE is not straightforward as both use PSIR to render certain tissues black based on the tissue T_1 and inversion time. In order to produce both dark fat and dark blood, a balance must be maintained between the T_1 of fat and blood and the separate inversion times of DSPAIR (TI_{DSPAIR}) and FIDDLE (TI_{FIDDLE}). In addition, as shown in Fig 1a, there is limited time for 2 SPAIR pulses and TI_{DSPAIR} within TI_{FIDDLE}.

The interaction between TI_{DSPAIR} and TI_{FIDDLE} and the effect of SPAIR inversion quality were simulated and optimized then prospectively tested in 10 patients. FIDDLE and fat suppressed FIDDLE (fs-FIDDLE) images were acquired 10-20 mins after gadolinium administration (0.15 mmol/kg) using identical parameters. Images were visually graded for overall quality (artifacts, sharpness, black-blood, etc), and fat suppression quality on a 0-3 scale (poor-to-excellent). Quantitative ROI analyses were also performed.

Results: Simulations demonstrated that longer TI_{FIDDLE} increased the available range of TI_{DSPAIR} that produced black fat (Fig 2a, left). Reduced SPAIR inversion efficiency greatly reduced the available range of TI_{DSPAIR} with efficiencies below 60% no longer resulting in black fat (Fig 2a, right). This is shown schematically in Fig. 1a; magnetization with a reduced SPAIR efficiency is equivalent to the case without fat suppression. Moving the first SPAIR pulse before the IR pulse provides more recovery time, and compensates for SPAIR inefficiencies (Fig 1b). The latter configuration was prospectively in 10 patients, all of whom demonstrated fat suppressed FIDDLE images (Fig 3).

Visual scoring of the images demonstrated excellent image quality for both fs-FIDDLE and FIDDLE (2.5 ± 0.6 vs 2.6 ± 0.6, $p = 0.3$). Only fs-FIDDLE had significant fat suppression (2.2 ± 0.6 vs. 0 ± 0, $p < 0.001$). Similarly, quantitative analysis showed a significant signal reduction in fat signal relative to normal myocardium (fat/myocardium: 0.7 ± 0.2 fs-FIDDLE, 1.2 ± 0.1 for FIDDLE $p < 0.001$).

Conclusions: A modified DSPAIR module can be combined with FIDDLE to provide excellent fat suppressed black blood DE-MRI to improve discrimination of infarct from other bright tissues (e.g. blood, fat).

References: 1. Kim, HW et al JCMR 2016 18(supp1):O55 2. Rehwald, WG et al JCMR 2012 14(Supp1):O53.

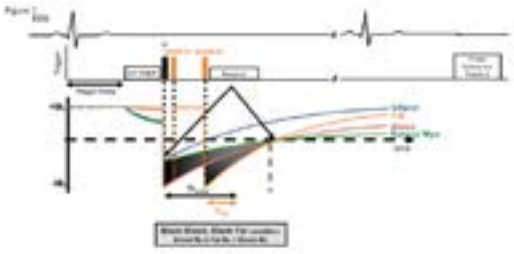

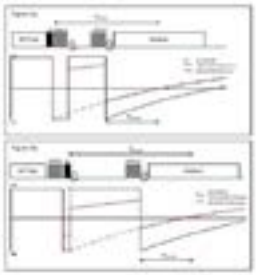

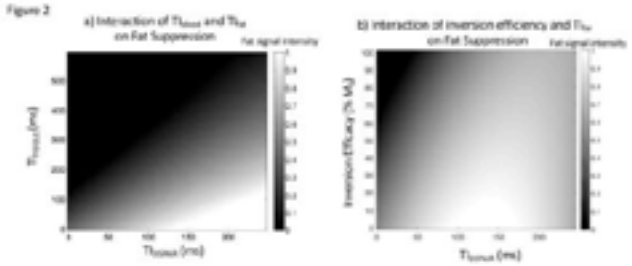

WP50

Contact free respiratory monitoring using the RF transmit scattering on a parallel transmit scanner

Aaron T. Hess, PhDMatthew D. Robson, PhD

OCMR, University of Oxford, England, United Kingdom

Background: Respiratory motion remains a limiting factor to increased cardiac MRI resolution. Navigators whether diaphragm-, image- or self-navigators can have a lag of ~1s. Respiratory bellows precision is limited to providing respiratory phase. An alternative method (Hess, ISMRM2016) measures respiration in mm units of diaphragm position using measurements based on the RF power reflected from the coil during transmission on a parallel transmit system (PTX). One measurement is made every TR (usually ~5ms) and allows for online measurement of respiration and cardiac motion.

Methods: The return voltage on an RF transmit line results from RF reflected back to a transmitter and RF coupled from other transmitters, this is called scatter and each is quantified by the scattering (S) matrix. Complex permittivity of the tissue in the fields of the transmitters modulates the magnitude and phase of the scatter. The forward and return voltages were measured by the scanners local-SAR-monitor. The ratio of returned voltage to expected returned voltage on eight transmit lines were linearly combined and scaled into a diaphragm position in mm. A 30s diaphragm-navigated learning cycle was used to calculate the transformation to diaphragm position using linear regression. A 7T MRI (Siemens 8 channel PTX step 2.3) with a local cardiac TEM transmit/receive coil was used. For validation a pulse sequence that images the diaphragm at 3 Hz at 1.4x1.4x8mm resolution for 165s and recorded the scatter measurements was acquired on 7 healthy volunteers. Velocity was measured using a Kalman filter on both the scatter and MRI measurements. To explore the practicalities of this approach in a prospective pulse sequence, a 2D free-breathing cine gradient echo pulse sequence was gated to end expiration using position and velocity.

Results: Figure 1 plots the position and velocity and the difference of this measure to that made by imaging, showing the increased sampling rate of 5ms compared to 330ms from imaging. Figure 2 shows a single cine-frame from the free-breathing scan. Across all subjects the standard deviation of the difference between image and scatter measured position was 1.1±0.3mm, and velocity was 1.5±0.4 mm/s. Across all subjects when using this measure to establish a prospective gating window resulted in the gate being open in error 3.6±2.8% and closed in error 2.1±1.9% of the time compared to the same using the images.

Conclusions: The measurement of respiration with this method enables accurate measurement of respiratory velocity and diaphragm position and produces good image quality with minimal artefact.

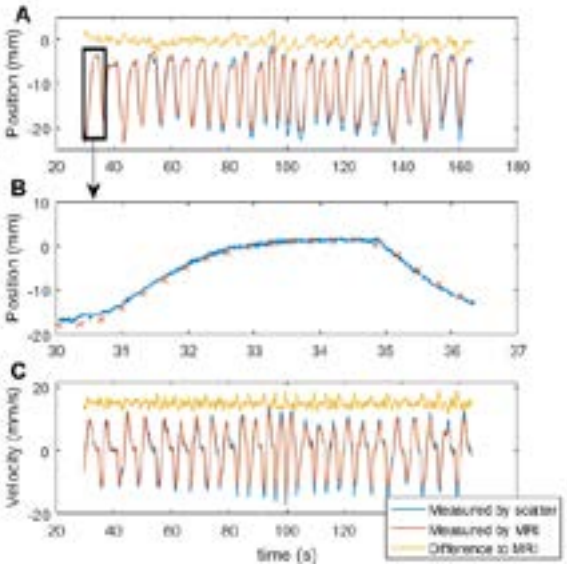

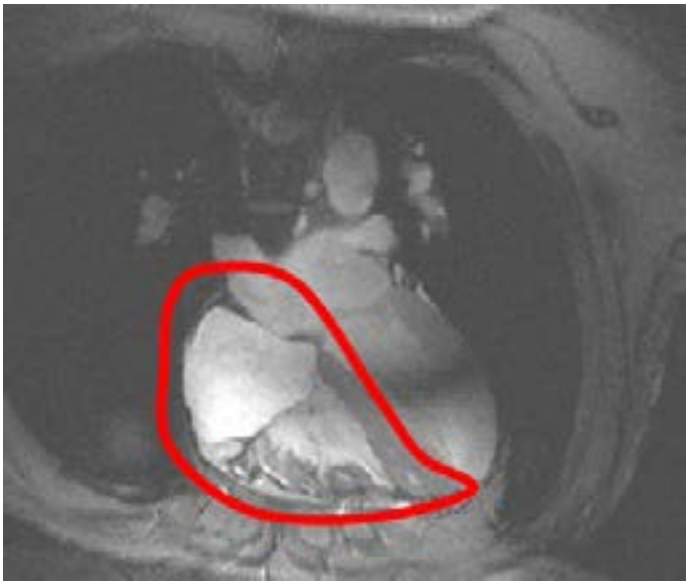

WP51

A novel low powered wideband inversion pulse for Delayed Enhancement Imaging at 3T

David Wendell, PhD[1] Elizabeth Jenista, Ph.D.[2], Enn-Ling Chen, PhD[1], Wolfgang Rehwald, PhD[3], Han Kim, MD[1], Michele Parker, MS[4], Raymond j. Kim, MD[1]

1. *Duke University Medical Center, NC*
2. *Duke University, Durham, NC*
3. *Siemens Healthcare, NC*
4. *Duke Cardiovascular MR Center, Durham, NC*

Background: Cardiac MRI at 3T is more prevalent and, with it, increased disturbances in B0 and B1, particularly in patients with implanted metallic devices causing image artifacts and tissue contrast variability due to uneven RF deposition across the body. Wideband hyperbolic secant (wide-HS) inversion pulses provide improved delayed enhancement (DE) imaging in patients with devices (i.e. ICDs)(1). However, the HS waveform requires high peak power (i.e. B1 amplitude) due to inefficient RF power distribution(2), which is particularly important at 3T. We developed a low-power, wideband inversion pulse for use at 3T, based on a constant amplitude linear sweep for the central region which can be "stretched" to achieve the desired effective inversion bandwidth (BW)(2). In this study we compared the performance of our novel low power stretched adiabatic (SA) inversion to wide-HS and the conventional narrow band HS pulse (narrow-HS, spectral BW=1kHz).

Methods: The SA and wide-HS inversion pulses were designed with a spectral BW of 3kHz. The 3 inversion pulses were evaluated in simulations (frequency profile and inversion efficiency), phantoms, and in 27 patients. We tested the B1 required to invert on-resonance, and swept the scanner frequency from ±2kHz to determine the off-resonance frequency performance in a T1-phantom. We embedded a MitraClip into the center of a spherical Agarose mold to test image homogeneity near (2-5 cm) the edge of the MitraClip for the 3 DE-MRI variants. DE-MRI was compared in 27 patients (sternal wires: 8, prosthetic valves: 5, others: 5) using the 3 pulses. Images were graded for image quality, metal bloom artifact, and homogeneity (0=poor, 3=excellent). Image homogeneity was quantified by CoV of subcutaneous fat at the 4 corners of the image on both magnitude and PSIR images.

Results: Fig 1A shows the inversion efficiency and frequency profile of the 3 pulses. The SA pulse required 50% and 68% of the peak power needed for the wide-HS to invert >150° and >175°, respectively. The SA pulse was flat throughout the inversion band with slightly more rounded shoulders than wide-HS. Experimentally, the frequency profile was consistent with simulations (**Fig 1B**), and the SA pulse required less power to invert on-resonance (F**ig 1B**). Wide-HS and SA improved DE-MRI image homogeneity in the mitraClip phantom compared to narrow-HS (**Fig 2**). Patient images showed reduction in metal bloom artifacts (**Fig 3A**, yellow arrows, score: $p < 0.05$), and improved overall image homogeneity (**Fig 3A**, red arrows) with wideband pulses in both magnitude ($p < 0.05$) and PSIR ($p < 0.005$) images. The CoV was significantly improved for the SA pulse in magnitude images and wide-HS and SA pulses for PSIR (**Fig 3B**).

Conclusions: We have implemented a novel wideband inversion pulse for DE-MRI. It proved to be more efficient and evenly homogeneous in simulations, phantoms, and patients suggesting its usefulness as an everyday inversion pulse for DE-MRI at 3T.

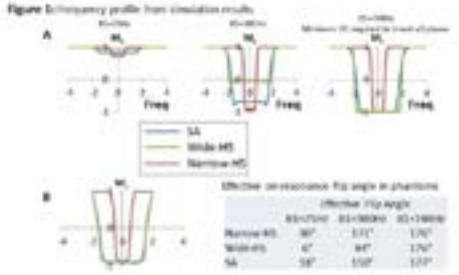

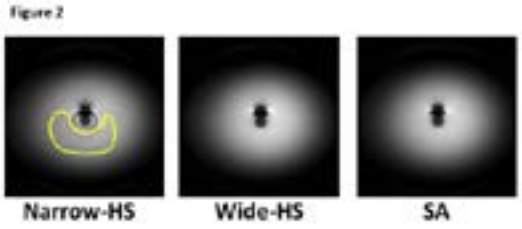

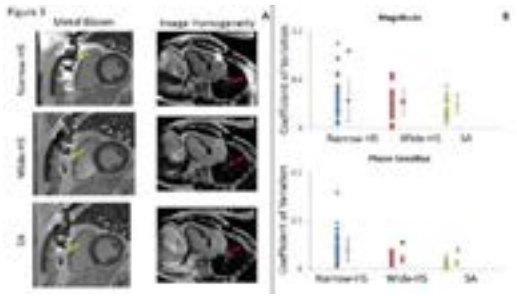

WP52

Imaging Sequence for Joint Myocardial T1 Mapping and Fat/Water Separation

Maryam Nezafat, MRes[1] Tamer Basha, PhD[2], Rene Michael. Botnar, PhD[3]

1. *King's College London, Auburndale, MA*
2. *BIDMC, Revere, MA*
3. *King's College London, London, England, United Kingdom*

Background: T_1 time changes due to diffuse myocardial fibrosis can be measured using T_1 mapping sequences. The presence of epicardial fat has been shown to have prognostic value but it also can lead to altered T_1 myocardial values in the vicinity of fat making assessment of diffuse fibrosis more challenging. Therefore, assessment of accurate myocardial T_1 with simultaneous fat quantification would be advantageous. In this study, we therefore aimed to develop an imaging sequence that allows simultaneous imaging of epicardial fat and myocardial T_1 quantification.

Methods: In this study, we devised and validated a novel simultaneous myocardial T_1 maps and fat/water separation sequence (**Figure1a**) by combining a slice-interleaved (STONE) T_1 mapping sequence [1] with a dual echo gradient echo acquisition and 2-point Dixon reconstruction [2]. Similar to STONE sequence, an inversion pulse is applied, but then two echo images are acquired in each cardiac cycle. The two echo images are then used to separate the water and fat components. A two parameter fit model was used to calculate the T_1 maps from the water images. The accuracy and precision of the proposed sequence was investigated in a phantom consisting of: vials with different T_1/T_2 values and a bottle of oil by comparison with an inversion recovery spin echo sequence (inversion times: 50 to 3000ms). In-vivo validation was performed in: 8 healthy subjects and 14 patients (4 hypertrophic cardiomyopathy, 5 atrial fibrillation, 1 non-ischemic cardiomyopathy, 1 normal, 2 arrhythmogenic right ventricular cardiomyopathy and 1 left ventricular noncompaction patients) to evaluate the sequence. Imaging performed using 1.5T Philips Achieva scanner equipped with a 32-element cardiac coil with the following imaging parameters for STONE: TR/TE=4.5/2.2 ms, and joint T_1-Fat/Water separation sequence: TR/TE1/TE2=7.1/2/4.9 ms, flip angle=10°, FOV=300×300mm^2, voxel size=2×2mm^2, slice thickness=8mm and SENSE factor=2.

Results: Figure1b shows the fat image and the T_1 maps reconstructed from both imaging techniques. No difference was found between the measured T_1 of the STONE and joint T_1-Fat/Water separation sequence (p=0.1) (**Figure1c**). The measured T_1 in healthy subjects with STONE and joint T_1-Fat/Water separation sequence was 1083±25ms and 1057±19ms (p=0.01), respectively. In patients, the measured T_1 (**Figure2**) with STONE and proposed sequence was 1104±22ms and 1084±31ms (p=0.003), respectively.

Conclusions: We introduced a joint T_1-Fat/Water separation sequence which quantifies the myocardial T_1 value while simultaneously provides images of fat with no penalty in terms of imaging time. The sequence provided similar accuracy and precision compared to the STONE sequence in a T_1/T_2 phantom. In-vivo, myocardial T_1 was slightly lower compared to the STONE sequence which requires further investigation.

Reference: [1] Weingartner, MRM, 2014. [2] Dixon, Radiology, 1984.

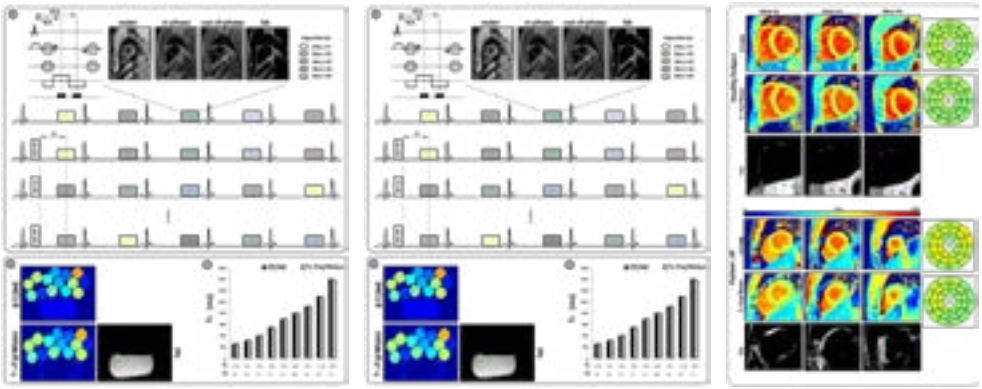

WP53

Free-Breathing Diffusion Tensor Imaging in Patients with Severe Cardiopulmonary Disease Using Simultaneous Multislice Acceleration and Enhanced Retrospective Image Selection

Choukri Mekkaoui, Ph.D.[1] Timothy G. Reese, Ph.D.[2], Marcel P. Jackowski, Ph.D.[3], David E. Sosnovik, M.D.[1]

1. *Harvard Medical School - Massachusetts General Hospital, Charlestown, MA*
2. *Harvard Medical School - Massachusetts General Hospital, MA*
3. *University of São Paulo, Sao Paulo, Sao Paulo, Brazil*

Background: Diffusion tensor imaging (DTI) of the heart, performed with multiple breath-holds, precludes its application in patients with severe cardiopulmonary compromise. Recently we reported free-breathing DTI of the entire heart in healthy individuals using simultaneous multislice (SMS) acceleration and entropy-based retrospective image selection **[1,2]**. Here, we use SMS-accelerated free-breathing DTI, combined with improved retrospective image selection (RIS), to demonstrate reliable quantification of left ventricular (LV) changes in patients with pulmonary hypertension.

Methods: DTI was performed in seven healthy volunteers and three subjects with advanced pulmonary fibrosis complicated by pulmonary hypertension. All three patients were on home oxygen and had deep and irregular breathing patterns. Subjects were imaged on a clinical 3T scanner (Siemens Skyra) with an ECG-gated STE sequence, volume selected in the phase-encode axis. Acquisition parameters were: FOV=360x200mm^2, resolution 2.5x2.5mm^2, slice thickness=8mm, in-plane GRAPPA rate 2, TE=34ms, b-values=0 and 500s/mm^2, 10 diffusion-encoding directions, and 8 magnitude averages. Twelve short-axis slices were acquired at the systolic sweet spot (160ms after R-wave), mitigating strain effects **[3]**. Rate 2 SMS excitation was followed by a blipped-CAIPI readout. Previously, RIS utilized an entropy-based metric, which exhibited insufficient range for patients with highly variable breathing patterns. A novel criterion based on SNR of the myocardium compared to the SNR context of the entire image was developed to determine image acceptance. Mean diffusivity (MD), fractional anisotropy (FA), helix angle (HA), and tractograms were compared between patients and normal subjects.

Results: Free-breathing DTI was performed and evaluated on patients and normal subjects. **Figure 1** shows clinical anatomical images from one of these patients with advanced pulmonary fibrosis complicated by pulmonary hypertension, right ventricular (RV) volume overload, and septal flattening. **Figure 2** shows HA maps and tractograms, depicting a rightward realignment of the myofibers in the septum of the patient *vs*. normal, confirmed by the differences in HA profiles as well as in MD (0.74±0.14 *vs*. 0.89±0.09) and FA (0.59±0.12 *vs*. 0.42±0.06) measurements.

Conclusions: Despite the difficulty posed by these patients' deep and irregular respiratory patterns, cardiac DTI of the entire LV was successfully performed. The marked RV enlargement and diastolic flattening of the septum, consistent with the patient's pulmonary hypertension, was characterized by a change in transmural HA associated with an increase in FA and a decrease in MD. Tractography exhibited fiber reorganization in the septum, indicating remodeling of the septum due to RV overload. Our ability to image these difficult patients presages the clinical translation of cardiac DTI.

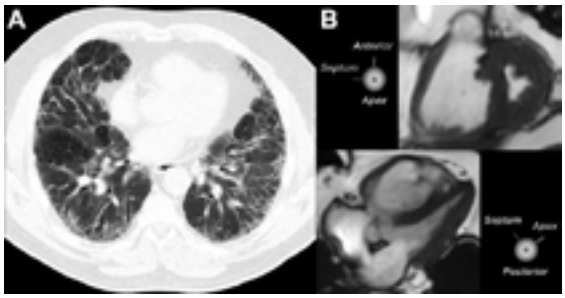

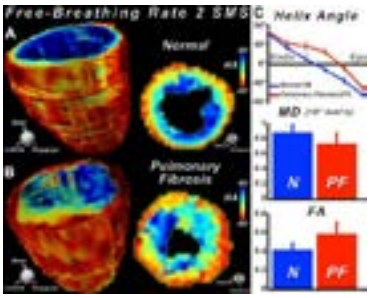

WP54

4-Dimensional Multiphase Steady State Imaging of Contrast Enhancement (MUSIC): Value-Based Imaging in Neonates with Congenital Heart Disease

Kim-Lien Nguyen, M.D.[1]Fei Han, Ph.D.[2], Daniel Brunengraber, M.D.[3], Ziwu Zhou, B.S.[4], Ihab Ayad, M.D.[5], Gary Satou, M.D.[6], Brian Reemtsen, M.D.[7], Peng Hu, Ph.D.[8], J. Paul Finn, M.D.[4]

1. *Division of Cardiology, David Geffen School of Medicine at UCLA and VA Greater Los Angeles Healthcare System, CA*
2. *UCLA, LOS ANGELES, CA*
3. *Department of Radiology at David Geffen School of Medicine at UCLA, CA*
4. *Department of Radiology, David Geffen School of Medicine at UCLA, CA*
5. *Department of Anesthesiology, David Geffen School of Medicine at UCLA, CA*
6. *Division of Pediatric Cardiology, David Geffen School of Medicine at UCLA, CA*
7. *Department of Cardiothoracic Surgery, David Geffen School of Medicine at UCLA, CA*
8. *UCLA, CA*

Background: Although echocardiography is the clear first line test in congenital heart disease (CHD), it may not always be definitive. In these cases, cardiovascular magnetic resonance (CMR) imaging may play a vital role without ionizing radiation. Recently, a 4D (MUSIC) technique has been described [1,2], which generates high-resolution 3D images of the beating heart during uninterrupted ventilation. We evaluated the diagnostic performance and clinical impact of 4D MUSIC in a clinical cohort of neonates with congenital heart disease (CHD).

Methods: Twenty consecutive neonates with CHD (age range 2 to 25 days, weight 1 to 4 kg) underwent CMR with ferumoxytol (FE) at 3.0T and were prospectively enrolled. Two readers graded the diagnostic image quality of intra-cardiac structures and vascular segments using a four-point scale. Correlation of CMR findings with other imaging modalities and/or surgical reports was performed. Clinical impact was assessed on a five-point scale (one point per key measure): 1) change in overall surgical management, 2) change in surgical approach, 3) elimination of need for diagnostic catheterization, 4) improved assessment of risk-to-benefit for planned intervention and discussion with parents, and 5) accurate pre-procedural roadmap with reduction of procedure time.

Results: All studies were technically successful and there were no adverse events. On a four-point scale, the average FE-MUSIC image quality scores were >3.5 for intra-cardiac structures and >3.0 for coronary arteries. Intra-cardiac morphology and vascular anatomy were visualized with good interobserver agreement (r=0.46). Concordance with correlative imaging, surgical, and /or autopsy results was excellent. In two patients with discordant findings between echo and catheter angiography, findings on FE-MUSIC were shown to be accurate by surgical reports (n = 2). The clinical impact score was 4.1±0.8. Surgical management was affected in all cases. In 75% of cases, clinical impact was affected across more than four key outcome measures.

Conclusions: FE-MUSIC enables non-breath-held, high-resolution, 3D cine imaging of cardiac and vascular anatomy in neonates with CHD, providing highly diagnostic and value-added studies without the need for prospective customized imaging planes. The overall clinical impact of FE-MUSIC is substantial with implications for value-based imaging.

References:

1. Fei Han, et al. *4-Dimensional, Multiphase, Steady-state Imaging with Contrast Enhancement (MUSIC) in the Heart; a Feasibility Study in Children*. Mag Reson Med 2015 Oct;74(4):1042-9.
2. Fei Han, et al. *Cardiac and Respiratory Self-Gated 4D Multiphase Steady-State Imaging with Ferumoxytol Contrast (MUSIC).* ISMRM 24th Annual Conference Proceedings. May 2016. Singapore.

WP55

Correcting for off-resonance error to improve myocardial T1 mapping in patients with implanted cardiac devices

Anish N. Bhuva, MRCP MBBS[1] Thomas Treibel, MBBS.MRCP(UK)[2], Camilla Torlasco, MD[3], Andrew D'Silva, MRCP[4], Redha Boubertakh, PhD[5], Charlotte Manisty, MBBS PhD[6], Peter Kellman, PhD[7], James Moon, MBBS, MD, MRCP[8]

1. *Barts Heart Centre and Institute of Cardiovascular Science, UCL., London, England, United Kingdom*
2. *Barts Heart Centre, England, United Kingdom*
3. *Barts Heart Center. St Bartholomew's Hospital, West Smithfield, London, EC1A 7BE, England, United Kingdom*
4. *Cardiovascular Sciences Research Centre, St. George's, University of London, London, United Kingdom, London, England, United Kingdom*
5. *Barts Health NHS Trust, London, England, United Kingdom*
6. *Barts Heart Centre and University College London, England, United Kingdom*
7. *Laboratory of Cardiac Energetics, National Institutes of Health/NHLBI, Bethesda, MD, United States., MD*
8. *Barts Heart Center, The Cardiovascular Magnetic Resonance Imaging Unit and The Center for Rare Cardiovascular Diseases Unit, St Bartholomew's Hospital, West Smithfield, London, UK, England, United Kingdom*

Background: Many patients with infiltrative diseases have implantable cardiac devices and T1 mapping is important for diagnostic and therapeutic pathways. The significant artifact resulting from the generator and lead(s) however means that many operators feel that the T1 values measured are unreliable. Regional variations in T1 due to incomplete shimming can be quantified by field maps to measure the off-resonance effect: The T1 error at 1000ms with an off-resonance of 50Hz is 10ms, whereas this rises rapidly to a 50ms T1 error at 100Hz.

We aim to quantify the off resonance error in T1 and to apply a correction for MOLLI in patients with implanted cardiac devices.

Methods: Shimmed native MOLLI and paired single breath-hold ECG gated field maps were acquired in 30 healthy volunteers (Age 30±3 years), and 24 patients with implanted cardiac devices (Age 54±19 years; 8 ILRs; 11 pacemakers; 3 defibrillators; 2 cardiac resynchronisation devices; 20 MR conditional). T1 and frequency shift were measured segmentally in the mid myocardial short axis. Segments with visual artifact on MOLLI were excluded from analysis. T1 maps were then corrected for off-resonance error up to 160Hz using previously calculated Bloch simulated correction.

Results: Peak off-resonance in controls was 43±17 Hz. Compared with controls, patients with implanted devices had significantly higher peak off-resonance frequencies (median 96Hz, interquartile range 99Hz; p=0.004). Artifact was greatest with CRT-D followed by ICD, PPM then ILR (R^2 0.48, $p < 0.01$). Generator proximity to the heart and the presence of an RV lead correlated with the degree of artifact in closest segments (R^2 0.22, p=0.02; and R^2 0.20, p=0.03 respectively). T1 correction based on off-resonance was calculated from field maps and integrated into an off line tool (Figure 1). Correction of off-resonance in patients with devices resulted in an average maximal change in T1 of 65±60ms per patient. Figure 2 illustrates the effect in one patient.

Conclusions: Myocardial segments with no obvious artifact on visual inspection still have device artifact on T1 maps despite shimming. Field map correction improves this, and may be needed for accurate T1 measurement in patients with implanted cardiac devices.

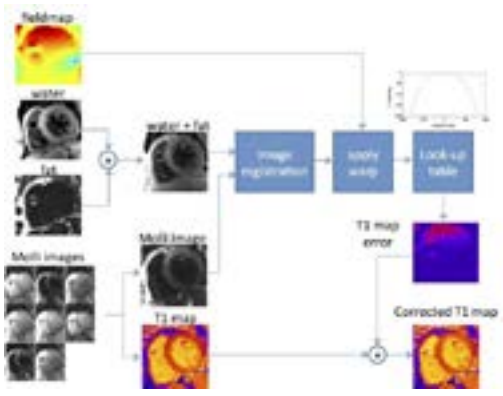

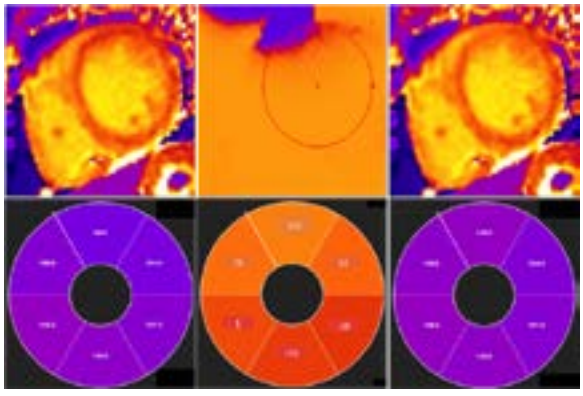

WP56

Derivation and Validation of Synthetic ECV Calculation from Blood Pool T1 values at 3T MRI

Ozair Rahman, MD[1] Kelvin Chow, PhD[2], Alex J. Barker, PhD[3], Michael Markl, PhD[4], James Carr, MD[5], Jeremy D. Collins, MD[5]

1. *Northwestern University, Feinberg School of Medicine, Chicago, IL*
2. *Siemens Medical Solutions, Chicago, IL*
3. *Northwestern University Feinberg School of Medicine, Chicago, IL*
4. *Northwestern University, Chicago, IL*
5. *Northwestern Memorial Hospital, Chicago, IL*

Background: Myocardial gadolinium extracellular volume fraction (ECV) quantification with T1 mapping is a clinically useful tool in diagnosis and prognosis of cardiac pathology. As originally described ECV calculation requires a recent laboratory hematocrit (HCT_{lab}), which is impractical in the clinical routine and has slowed adoption of this technique. Recently, Treibel described a relationship between blood pool T1 values and the hematocrit using 1.5T MRI.

Methods: A retrospective study was conducted on 95 consecutive patients (mean age 59.1±25.1 yrs, 45 men) who underwent cardiac MR (CMR) with native T1 and 15-20 minute post-contrast T1 mapping using a modified Look-Locker inversion recovery (MOLLI) sequence using a 5(3)3 scheme with single shot steady state diastolic readouts at a single center between April 4th, 2015 to February 3rd, 2016. Patients were randomly divided into derivation and validation subgroups with equal health and disease representation. Imaging was performed at 3T (Magnetom Skyra, Siemens Medical Systems, Erlangen, Germany). T1 parametric maps quantified T1 values in the Left Ventricle (LV). ECV quantification was performed with HCT_{lab} obtained at the time of the CMR (ECV_{lab}) and HCT_{syn} (ECV_{syn}) using the suggested in the consensus statement by Moon et al.

Results: Proof of concept, 95 subjects (28 women), were randomly assigned to derivation (N=70, mean age 63± 25.8 years) and validation (N=25, mean age 59.1±25 years) cohorts. A linear relationship between HCT_{lab} and Left Ventricle $R1_{Blood}$ (R^2=0.09) was used to derive the HCT_{syn}: $(239\times[1/T1_{Blood}]) + 0.2815$, and applied to the validation cohort. Myocardial ECV_{syn} was similar to ECV_{lab} derived from laboratory-determined hematocrit. Bland-Altman plots demonstrated excellent agreement between ECV_{syn} and ECV_{lab} and HCT_{syn} vs HCT_{lab} in the validation cohort (Figure 1).

Conclusions: HCT_{syn} derived from pre-contrast blood pool T1 values at 3T demonstrated excellent agreement compared to HCT_{lab} in a separate validation cohort. ECV_{syn} and ECV_{lab} were similar, suggesting that Hematocrit estimation using HCT_{syn} may obviate the need for same-day hematocrits in patients undergoing cardiac imaging at 3T (Figure 1).

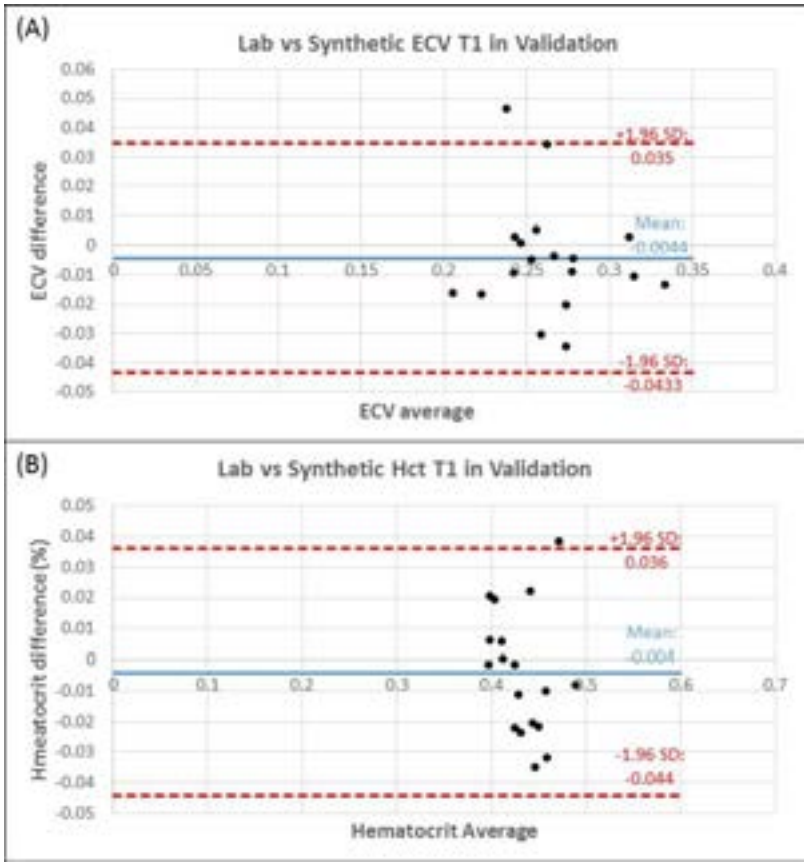

WP57

Improving the Optimized Sampling Point Selection for Saturation-Recovery T1 Mapping of the Heart

Glenn Slavin, Ph.D.

GE Healthcare, MD

Background: Saturation-recovery (SR) T1 mapping methods such as SASHA and SMART1Map typically sacrifice precision for accuracy. Recent studies have sought to improve the precision of SR by optimizing the sampling of the T1 magnetization recovery curve. These studies suggest repeatedly sampling fixed saturation delay times (TS), including the minimum TS (TS_{min}), an intermediate TS (TS_{int}) near the expected T1, and an infinite TS (TS_{∞}). For current SR techniques, the optimal TS_{int} is not achievable because the maximum intra-heartbeat TS is limited by the trigger delay (TD). In this work, we propose sampling in a heretofore unexplored area of the relaxation curve where $TD < TS < T_{RR}$. This longer delay time (TS_{RR}), which is limited by the R-R interval (T_{RR}) rather than TD, should provide better precision for longer T1s (e.g., native myocardium) and can be attained by performing the saturation immediately after data acquisition in one heartbeat and subsequently acquiring data in the next heartbeat (Figure 1).

Methods: We attempted to maximize the precision by optimizing the sample times based on practical boundary conditions: a single expected T1 of 1200ms (native myocardium at 1.5T), a limited set of potential TS times, and a scan time of 13 heartbeats, where every heartbeat is used for data acquisition. The Monte Carlo method was used to calculate the standard deviation of T1 for various sampling schemes with the following four options for TS: TS_{min}; TS_{TD} (TS_{int} limited by TD); the proposed TS_{RR}; and TS_{∞} (acquired once). Values between TS_{TD} and TS_{RR} would not improve precision. Because TS_{RR} is dependent on heart rate, simulations were also performed with heart rate variations of up to 20% during the scan. Phantom experiments at 1.5T were conducted to validate the simulations and to compare TS_{TD}, TS_{RR}, SASHA, and SMART1Map.

Results: For simulations using a 60 bpm heart rate, optimal precision was achieved by acquiring 5 samples at TS_{min}, 7 samples at TS_{RR}, and 1 sample at TS_{∞}, which is consistent with prior studies. Simulation and phantom results are shown in Table 1, with precision measured using the coefficient of variation. The use of TS_{RR} improved the precision by 8% vs. the currently used TS_{TD}, and by 27% and 34% vs. SASHA and SMART1Map, respectively. The effect of variable heart rates on TS_{RR} had a negligible impact (< 1%) on precision.

Conclusions: Sampling at TS_{RR} provides better precision than TS_{TD} for measuring longer T1 values. While modest at 1.5T, the improvement is expected to be more substantial at 3T, and there is no apparent disadvantage or scan time penalty, despite the saturation and acquisition occurring in different heartbeats. A further benefit of this approach is that TS_{RR} is decoupled from TD because the saturation timing is not determined by the ECG. Since TS_{RR} remains effectively constant, systolic acquisitions are therefore possible without the concomitant reduction of TS_{TD} and precision (Figure 1).

http://www.ConferenceAbstracts.com/uploads/cfp2/attachments/LDFAIBDN/LDFAIBDN--216520-1-ANY(1).pdf

Table 1. Results of Sampling Schemes for Saturation-Recovery T1 Mapping at 1.5T

Coeff of Variation (%)		Sampled Points TS (msec)	Sampling Scheme
1.030	simulation	{130, 130, 130, 130, 130, 902, 902, 902, 902, 902, 902, 902, ∞}	TS_{RR} (Proposed)
1.029	phantom		
1.114	simulation	{130, 130, 130, 130, 130, 664, 664, 664, 664, 664, 664, 664, ∞}	TS_{TD}
1.129	phantom		
1.444	simulation	{130, 179, 227, 276, 324, 373, 421, 470, 518, 567, 615, 664, ∞}	SASHA (13 points)
1.419	phantom		
1.582	simulation	{130, 307, 485, 663, 1657, 2653, 3649, ∞}	SMART1Map
1.567	phantom		

Coefficient of Variation for T1 = std dev/mean. Mid-diastolic trigger delay (TD)=674 ms, TS_{min}=130ms, TS_{TD}=664ms, TS_{RR}=902ms. Phantom T1 = 1150ms. Scan time: 13 heartbeats for TS_{RR}, TS_{TD}, and SASHA; 14 heartbeats for SMART1Map. Each scheme was scanned 10 times. A 3-parameter fit to $A - B\, e^{-TS/T1}$ was used.

WP58

Native ShMOLLI T1 mapping to differentiate reversible vs. irreversible myocardial damage in STEMI patients

Alessandra Borlotti, PhD[2]Dan Liu, PhD[1], Dafne Viliani, MD[3], Michael Jerosch-Herold, PhD[4], Mohammad Alkhalil, M.D, MRCP[5], Giovanni Luigi De Maria, MD[6], Gregor Fahrni, MD[5], Sam Dawkins, MBBS MRCP[7], Rohan S. Wijesurendra, MB BCHIR MA(Cantab) MRCP[2], Jane M. Francis, DCR(R) DNM[8], Vanessa M. Ferreira, MD, DPhil[5], Stefan K. Piechnik, PhD, MScEE[5], Matthew D. Robson, PhD[9], Adrian Banning, MD[10], Robin Choudhury, MD[2], Stefan Neubauer, MD, FRCP[5], Keith M. Channon, MD, FRCP[5], Rajesh K. Kharbanda, MBChB, PhD[11], Erica Dall'Armellina, MD, PhD[12]

1. *University of Oxford, London, England, United Kingdom*
2. *University of Oxford, Oxford, England, United Kingdom*
3. *Division of Cardiovascular Medicine, Radcliffe Department of Medicine, Oxford, Trento, Trentino-Alto Adige, Italy*
4. *Department of Radiology, Brigham and Women's Hospital, MA*
5. *University of Oxford, England, United Kingdom*
6. *Oxford University Hospitals, England, United Kingdom*
7. *Oxford University Hospitals NHS Trust, Oxford, England, United Kingdom*
8. *University of Oxford, OX39DU, England, United Kingdom*
9. *OCMR, University of Oxford, England, United Kingdom*
10. *Oxford heart center, England, United Kingdom*
11. *Oxford Heart Centre, England, United Kingdom*
12. *Oxford University, England, United Kingdom*

Background: Native T1 mapping may serve as a quantitative diagnostic tool to allow the assessment of myocardial injury early after ST elevation myocardial infarction (STEMI). In this study we are aiming to define the diagnostic T1 thresholds to assess irreversible injury and relate these to imaging measures of infarct size, and 6 month (6M) LV function.

Methods: Sixty STEMI patients post primary percutaneous coronary intervention (PPCI) underwent acute (42 ± 19 hours) and 6 months (6M) CMR including cine, native Shortened Modified Look-Locker Inversion recovery (ShMOLLI) T1 mapping, and LGE at 3T (Siemens MAGNETOM TIMTrio or Verio). Troponin I AUC was assessed using measurements at time of admission, 6h, 24h, and 48h post PPCI. Region of interest (ROI) based T1 analysis was implemented to determine a T1 cut-off value to discriminate reversible (oedematous) versus irreversible (necrotic) injury. Segmental analysis was performed on all patients to explore association between mean T1 values and left ventricle (LV) functional recovery on matching short axis slices.

Results: ShMOLLI T1 cut-off values for progressive detection of oedematous versus necrotic myocardium were identified as 1251msec and 1400msec respectively (Figure 1) with prediction accuracy of 96.7% (95% confidence interval 82.8~99.9%). Troponin I measurements at 4 time points were available in 46 patients, out of which 20 patients had full LV T1 map coverage. For these 20 patients, using the proposed threshold, the volume of irreversibly damaged tissue was in good agreement with the 6M LGE volume ($r=0.99$, $p < 0.001$) and correlated significantly with the log AUC Troponin ($r=0.80$, $p < 0.001$), and 6M ejection fraction ($r=-0.73$, $p < 0.001$) (Figure 2). Receiver-operating characteristic (ROC) analysis indicates that acute T1 values can predict 6M wall thickening (area under the curve AUC=0.71) as well as LGE (AUC=0.72).

Conclusions: Native ShMOLLI T1 mapping performed in the early hours post MI differentiates reversible and irreversible myocardial damage and it is a strong predictor of LV remodelling at 6M. By allowing assessment of myocardial necrosis and salvage myocardium acutely without need for contrast, native T1 mapping could potentially represent a valid alternative to LGE and allow for shorter scanning protocols in acutely ill patients with kidney impairment.

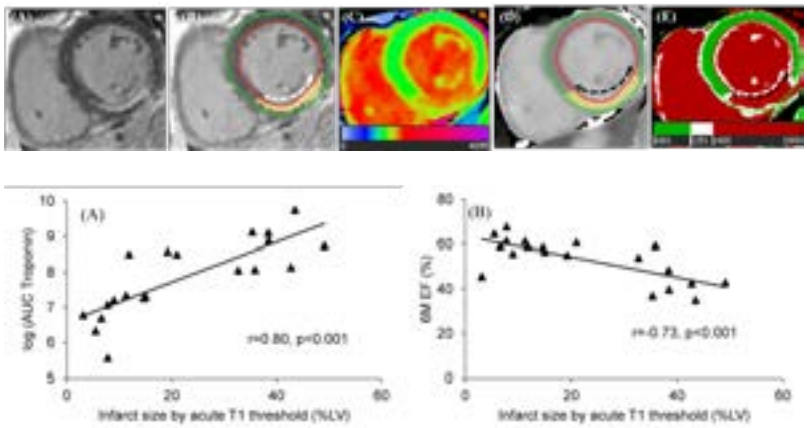

WP59

A Non-contrast CMR Index Can Detect Myocardial Fibrosis with Superior Sensitivity and Specificity

Jiayu Sun, MS[1] Simeng Wang, BS[1], Robert O'Connor, PhD[2], David Muccigrosso, BS[3], Wei Cheng, BS[1], Yucheng Chen, MD[1], Sharon Cresci, MD[3], Jie Zheng, PhD[4], Fabao Gao, MD,PHD[1]

1. *China West Hospital, Sichuan, China (People's Republic)*
2. *NIH/NIDDK, MD*
3. *Washington University in St. Louis, MO*
4. *Washington University in St. Louis, Saint Louis, MO*

Background: Myocardial fibrosis can be assessed by the administration of gadolinium contrast agent in cardiac magnetic resonance imaging (CMR). However, patients with renal dysfunction or pediatric patients for surveillance studies are contraindicated for contrast injection. The purpose of this project is to develop and evaluate a non-contrast cardiac imaging approach for the sensitive and quantitative assessment of myocardial fibrosis.

Methods: Eighteen patients with a variety of cardiac disorders (myocardial infarction, dilate and hypertrophic cardiomyopathy, alcoholic cardiomyopathy) were prospectively scanned on a clinical 3T MRI system (Siemens Medical Solution). CMR protocol included non-contrast spin-locking T1ρ–based imaging at two different spin-locking frequencies, native and post-contrast T1 mapping, and late gadolinium enhancement imaging. A myocardial fibrosis index (mFI) and a pseudo-ECV were derived from the T1ρ dispersion data and compared with extracellular volume (ECV) determined by the contrast study.

Results: There was strong correlations between ECV and fibrosis index mFI or pseudo-ECV on a patient basis, with a Pearson correlation coefficient *(r)* of 0.95 and 0.82, respectively; whereas *r* was 0.87 for native T1ρ and 0.33 for native T1. The receiver operating characteristic analysis revealed 100% in both sensitivity and specificity for mFI to differentiate healthy from diseased myocardium (Table). The corresponding sensitivity and specificity were 83.3% and 75% (T1ρ), respectively; and 50% and 87.5% (native T1), respectively. The Figure demonstrates one example of various images and maps obtained from a patient with alcoholic cardiomyopathy, showing very similar enhancement distribution between non-contrast mFI and ECV maps.

Conclusions: This study is the first to introduce a non-contrast CMR fibrosis index for the detection of myocardial fibrosis, especially diffuse fibrosis, in cardiac patients with superior sensitivity and specificity. The non-contrast approach may have important implications for the diagnosis and management of patients with cardiomyopathy and heart failure, particularly if they have impaired renal function or require frequent surveillance for medical treatment.

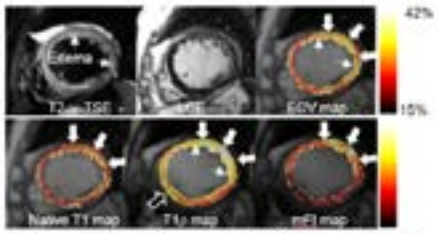

Figure. Different cardiac magnetic resonance images and calculated maps acquired from a patient with alcoholic cardiomyopathy. The late gadolinium enhancement image (LGE) shows slightly enhanced signals in the endocardium of the anterior and lateral regions, which suggests diffuse fibrosis. The ECV map shows enhancement in the same regions (solid arrows). The maps in the bottom row show various enhancements in these regions. Note that the mFI map shows much higher contrast than the native T1 map. The mismatched areas between the ECV and myocardial fibrosis index maps are in the anterior and inferolateral regions where edema possibly existed (thin arrows), as shown in the T2-WI image. Open arrows point to areas with inhomogeneity artifacts. The color scale bars varied for the different maps in the bottom row.

Table. The Sensitivity and Specificity of Various CMR Parameters for the Detection of Myocardial Fibrosis on a Patient basis

Specificity	Sensitivity	Cutoff values	CMR Parameters
100%	100%	18.9	mFI (a.u.)
100%	83.3%	36.9	pseudo-ECV (x 100)
75%	83.3%	46.5	T1p (ms)
87.5%	50%	1366	Native T1 (ms)
25%	100%	552	Post-contrast T1 (ms)

WP60

Native T1 value in the myocardial areas without scar on LGE is independently associated with left ventricular dysfunction in patients with prior myocardial infarction

Shiro Nakamori, MD, PhD[1]Javid Alakbarli, MD[1], Steven Bellm, MD[1], Gifty Addae, BS[1], Warren J. Manning, MD[2], Reza Nezafat, PhD[3]

1. *Beth Israel Deaconess Medical Center, MA*
2. *Beth Israel Deaconess Medical Center, Boston, MA*
3. *Department of Medicine (Cardiovascular Division) Beth Israel Deaconess Medical Center, Harvard Medical School, Cardiology, East Campus, Room E/SH455, 330 Brookline Ave, Boston, MA, 02215, MA*

Background: Left ventricular (LV) remodeling after myocardial infarction (MI) is a complex process. Areas remote from the scar region undergo structural and molecular changes to compensate for scarred region and LV dysfunction. However, the importance of remote areas away from scar as a pathogenic mechanism for LV dysfunction after MI is incompletely understood. Furthermore, association of diffuse fibrosis in the remote myocardium and LV dysfunction after MI is unknown. This prospective study sought to elucidate T_1 map-derived diffuse myocardial fibrosis in the remote myocardium, and to assess its relation to LV function in patients with prior MI.

Methods: A total of 41 chronic myocardial infarction patients (63 ± 9 yrs, 30 male) and 15 age-matched healthy control subjects (62 ± 8 yrs, 5 male) were studied. Native T_1 map was performed using free-breathing slice-interleaved T_1 mapping sequence at 1.5 T [1]. 3D Late gadolinium enhanced (LGE) was acquired to assess infarct size. To evaluate inter-observer reproducibility, measurements of native T_1 from 10 patients with prior MI were independently taken by two observers. One of the two observers measured native T_1 twice to assess intra-observer reproducibility.

Results: The mean native T_1 time in the remote myocardium was significantly elevated in patients with prior MI, compared to healthy controls, regardless of anterior MI vs. non-anterior MI (anterior MI:1099 ± 30, non-anterior MI:1097 ± 39, controls:1068 ± 25 msec, $p < 0.05$ after Bonferroni correction, respectively) (Figure 1). Native T_1 was moderately correlated with LV volume, mass index and LV ejection fraction (LVEF) (r=0.38, 0.50, -0.49, respectively, all $p < 0.05$). Hyperenhancement of LGE image was observed in all chronic MI patients; transmural LGE in 13 patients, and subendocardial LGE in 28 patients. Similarly, infarct size was 13.2 ± 7.6 g and had moderate correlation with reduced LVEF ($r=-0.33$, $p < 0.05$), while there was no significant association between native T_1 and infarct size. Native T_1time in the remote myocardium was independently associated with reduced LVEF, after adjusting for age, gender, infarct size and comorbidity ($\beta=-0.34$, $p=0.03$). The intraclass coefficients for the interobserver and intraobserver measurements of native T_1 were 0.88 (95% confidence interval [CI]: 0.72 to 0.94) and 0.91 (95% CI: 0.82 to 0.96), respectively.

Conclusions: LV systolic dysfunction after MI was independently associated with diffuse myocardial fibrosis in the remote myocardium. Larger, multicenter studies are needed to investigate the clinical implications of abnormal T_1in the remote myocardium in patients with chronic myocardial infarction.

Reference: [1] Weingartner S et al., MRM, 2014.

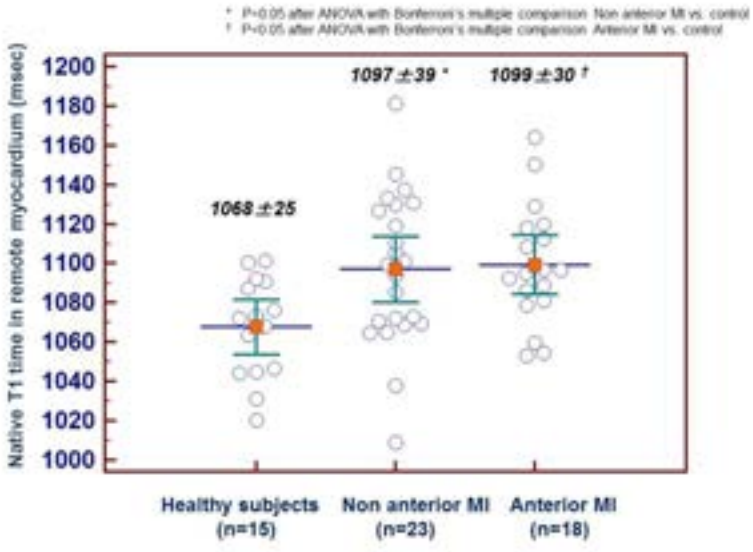

WP61

Simultaneous Multi-Slice Imaging For Myocardial T1 Mapping In A Single Breath-Hold

Sebastian Weingärtner, Ph.D.[1] Mehmet Akçakaya, Ph.D.[2]

1. *Electrical and Computer Engineering, University of Minnesota; Center for Magnetic Resonance Research, University of Minnesota; Computer Assisted Clinical Medicine, University Medical Center Mannheim, Heidelberg University, Mannheim, Baden-Wurttemberg, Germany*
2. *Electrical and Computer Engineering, University of Minnesota; Center for Magnetic Resonance Research, University of Minnesota, Minneapolis, MN*

Background: Myocardial T1 mapping is commonly performed with 3 slices covering the base, middle and apex of the LV in short-axis view for comprehensive T1 characterization and one breath-hold per slice. This leads to patient discomfort and long scan times due to rest-periods between breath-holds [Makowski et al, JCMR2012]. Simultaneous multi-slice (SMS) or multi-band (MB) imaging offers a method for accelerating acquisitions by extending coverage, where the only SNR reduction compared to single slice imaging is due to coil geometry. In this study, we sought to employ MB imaging for myocardial T1 mapping to enable myocardial tissue characterization with 3-slice coverage in a single breath-hold.

Methods: Sequence and Imaging: Myocardial T1 mapping was performed using SAPPHIRE [Weingärtner et al, MRM2014] (Fig. 1a). For MB imaging, phase-cycled multiband RF pulses were utilized with FLASH imaging, as proposed in [Breuer et al, MRM2005]. Additionally, an optimized constant RF phase was added to each baseline pulse to reduce peak B1 amplitude. MB factor = 3 and uniform in-plane acceleration = 2 were utilized. For MB reconstruction, a 1 second MB-reference scan with no breath-holding or ECG gating was implemented to acquire low-resolution images (6x6 mm^2) of the 3 slices, prior to T1 mapping acquisitions.

Phantom and in vivo imaging in 5 healthy subjects was performed at 3T. MB imaging was performed in a single breath-hold, and single band (SB) multi-slice imaging was performed in 3 breath-holds with imaging parameters: FOV=320x320mm^2, resolution=2x2mm^2, slice thickness=10mm, partial Fourier = 6/8, TR/TE/FA=4/2ms/10°. **Reconstruction:** Multi-slice unaliasing (Fig. 1b) was performed using slice-GRAPPA [Setsompop et al, MRM2012] using [5,5] kernels, calibrated from the MB-reference scan. Following slice unaliasing, in-plane GRAPPA [Griswold et al, MRM2002] was performed with [5,4] kernels, also calibrated from the MB-reference scans. Individual coil images were combined using coil sensitivity profiles, and T1 fitting was then performed on these images.

Results: Phantom results (Fig. 2) show good agreement (normalized RMSE: 1.7%) for T1 estimation between SB and MB imaging. However, there is a 2.4-fold loss of precision when using MB compared to SB imaging. An example in vivo acquisition is depicted in Fig. 3. All slices are recovered with similar T1 values (relative difference: -0.9%). However, there is a 1.4-fold loss of precision for MB myocardial T1 maps, due to coil geometry.

Conclusions: The proposed MB T1 mapping sequence allows for myocardial tissue characterization with 3-slice coverage in a single breath-hold, albeit at a loss of precision in T1 maps compared to single-slice imaging. Linear reconstruction methods used here suffer from noise amplification due to coil geometry, which have overlapping coverage for cardiac MRI. Alternative reconstruction methods may provide additional benefits for SMS imaging of the myocardium.

Funding: NIH R00HL111410, P41EB015894.

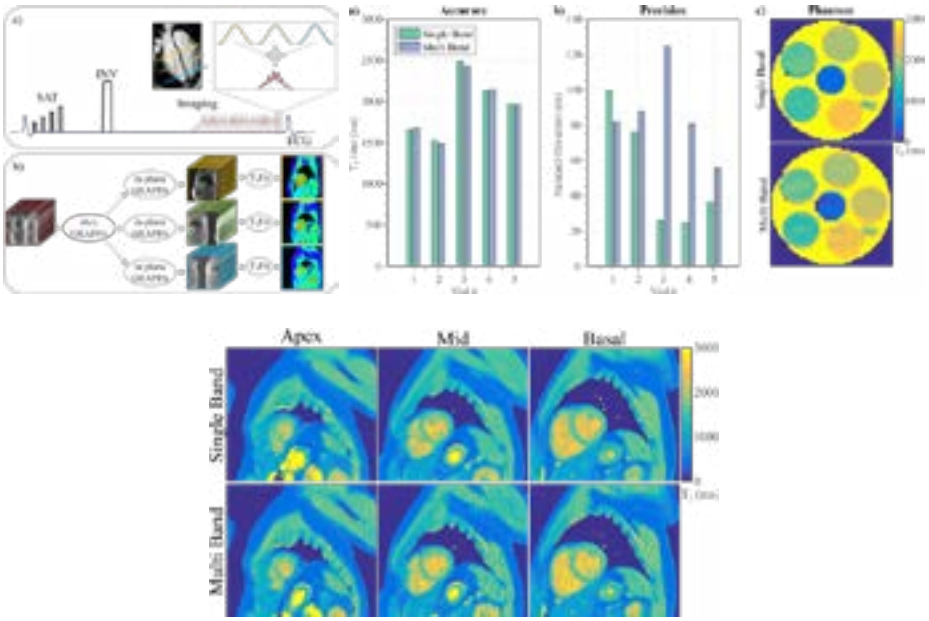

WP62

Quantification of myocardial blood volume reserve by adenosine stress native T1 mapping – validation with adenosine stress ECV mapping

Jannike Nickander, MD[1]Raquel Themudo, MD, PhD[2], Vivianne Jakobsson[3], Peter Kellman, PhD[4], Hui Xue, PhD[5], Andreas Sigfridsson, PhD[1], Martin Ugander, MD, PhD[6]

1. *Karolinska Institute, Stockholm, Stockholms Lan, Sweden*
2. *Department of Clinical Physiology, Karolinska Institutet and Karolinska University Hospital, Stockholms Lan, Sweden*
3. *Karolinska Institute, Stockholms Lan, Sweden*
4. *Laboratory of Cardiac Energetics, National Institutes of Health/NHLBI, Bethesda, MD, United States., MD*
5. *National Heart, Lung, and Blood Institute, Bethesda, MD*
6. *Karolinska Institutet, Stockholms Lan, Sweden*

Background: Coronary artery disease (CAD) and several non-ischemic heart diseases effect the myocardial microcirculation, and can affect the change in myocardial blood volume (MBV) that occurs during adenosine stress, also referred to as the MBV reserve (MBVR). Adenosine stress native T1 mapping could potentially be used to quantify the MBVR. However, it is not known what a possible change in T1 values signifies. Therefore, this study aimed to validate the quantification of MBVR by adenosine stress native T1 mapping, compared to adenosine stress extracellular volume fraction (ECV) mapping.

Methods: Healthy volunteers (n=23, age 26±6 years, 40% females) underwent CMR (1.5T Siemens Aera). A midventricular short axis T1 map (MOLLI) was acquired before and during adenosine stress (140 microg/kg/min infusion), and following an intravenous contrast bolus (0.2 mmol/kg, gadobutrol, Gadovist®) rendering native rest and stress T1 maps, and rest and stress ECV maps. Myocardial T1 and ECV values were acquired by contouring left ventricular epi- and endocardium borders in the respective maps both at rest and stress. LV blood pool T1* was measured in the corresponding T1* map. MBVR was calculated as MBVR = (myocardialR1rest-myocardialR1stress)/ LV blood pool R1*, where R1= 1/T1. Values are reported as mean ± SD. The MBVR by T1 maps was compared to the increase in ECV in percentage points during stress (ΔECV) by linear regression.

Results: Native T1 increased from rest (mean±SD) 993±39 ms to stress 1058±51 ms ($p < 0.001$) and ΔT1 was 62±25 ms. ECV also increased from rest 26.7±2.5% to stress 30.6±3.1% ($p < 0.001$) and ΔECV was 4.0±2.5%. MBVR by stress/rest native T1 mapping was 9.6±3.3%, and correlated with ΔECV (R^2=0.43, p=0.001) (Figure).

Conclusions: Quantification of MBVR with stress/rest native T1 mapping is feasible, and correlates with the increase in percentage points in ECV during adenosine stress. The increase in ECV during stress is due to the increase in plasma volume during adenosine stress, and this correlates with the increase in whole blood by native adenosine stress T1 mapping. This confirms that MBVR reflects the increase in intramyocardial blood during adenosine stress. Therefore, imaging with T1 mapping before and during adenosine stress is valid for quantification of MBVR.

http://www.ConferenceAbstracts.com/uploads/cfp2/attachments/LDFAIBDN/LDFAIBDN--220080-1-ANY(3).pdf

WP63

Normative Native Myocardial T1 and ECV Values in Healthy Children

Joseph J. Pagano, MD[1] Deane Yim, MBchB[2], Christopher Lam, MD[3], Mike Seed, MBBS[4], Shi-Joon Yoo, MD[5], Lars Grosse-Wortmann, MD[1]

1. *The Hospital for Sick Children, ON, Canada*
2. *The Hospital for Sick Children, Toronto, ON, Canada*
3. *The Hospital for Sick Children, University of Toronto, ON, Canada*
4. *SickKids, Toronto, ON, Canada*
5. *Hospital for Sick Children, Toronto, ON, Canada*

Background: The use of magnetic resonance T1 relaxometry, particularly native T1 and extracellular volume (ECV) for myocardial tissue characterization has increased in recent years. However, the applicability of T1 relaxometry in pediatric populations, both clinically and in research, is hampered by the lack of normal values. The aim of this study was to establish a reference range of values for myocardial T1 and ECV using the modified Look-Locker inversion recovery (MOLLI) approach.

Methods: Healthy subjects were identified through the cardiac magnetic resonance (CMR) database at The Hospital for Sick Children in Toronto. Subjects were included if the CMR study was requested for screening purposes and all other tests, including genetic testing, were normal. Indications for CMR included family history of cardiomyopathy and atypical chest pain with inability to visualize the coronary arteries by echocardiography. Studies were performed on a 1.5T Siemens system ('Avanto'), using gadobenate dimeglumine contrast. T1 quantification was obtained at a mid-ventricular location in diastasis, using a 5(nHB)3 MOLLI sequence with 35° flip angle and in-line motion correction, where nHB was 3 to 5 heart beats depending on the heart rate. T1 analysis was performed in Qmap (MedisSuite 2.1). Left ventricular (LV) endo- and epicardial borders were contoured on the motion corrected T1-weighted images, including only the inner 50% of myocardium to avoid partial volume errors (Fig1). T1 values were calculated using average ROI signal and a curve fitting algorithm, and corrected by a factor of 1.0365 for imperfect inversion pulse efficiency. ECV was calculated using pre- and post-contrast T1 times and the subject's hematocrit, drawn immediately prior to the CMR. Values are reported for the entire LV myocardium, interventricular septum, LV free wall, and blood.

Results: 40 subjects (age 14±3 years; 20 male) were included, with 27 subjects receiving gadolinium. Average values for whole LV native myocardial T1, blood T1, and ECV were 1004±40 ms, 1561±79 ms, and 23±4%, respectively. Septal T1 values were increased compared to the free wall (1026±41 vs. 1008±61 ms, p=0.03), however not for ECV (24±4 vs. 23±5%, p=0.27). There were no differences between gender for age, hematocrit, or native myocardial T1; however native blood T1, and ECV in the whole LV and free wall were higher in females (Table 1).

Conclusions: In this study we provide normative values for myocardial T1 and ECV in healthy children using the MOLLI sequence at 1.5T, demonstrating increased native blood T1 and LV myocardial ECV values in young healthy females.

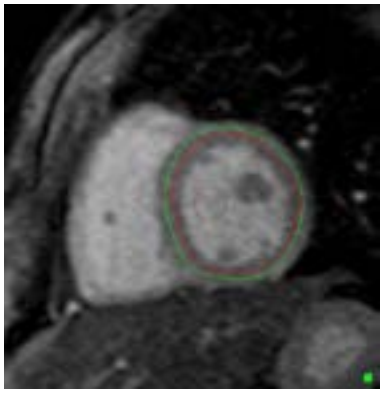

Native T1 and ECV Data for the Healthy Pediatric Cohort, Including by Gender

	Female	Male	All	
p-value*	n=20	n=20	n=40	
0.51	14±2	14±3	14±3	Age (years)
Native T1 (ms)				
0.43	1009±36	999±44	1004±40	Whole LV
0.24	1034±36	1018±46	1026±41	IVS
0.54	1014±57	1003±66	1008±61	Free wall
0.047	1585±80	1536±72	1561±79	Blood (ms)
	n=14	n=13	n=27	Hematocrit available
0.08	0.41±0.04	0.43±0.04	0.42±0.04	Hematocrit
ECV (%)				
0.048	24±4	21±3	23±4	Whole LV
0.06	25±4	22±3	24±4	IVS
0.01	25±5	21±3	23±5	Free wall

LV = left ventricle, IVS = interventricular septum, ECV = extracellular volume fraction
*p-values represent comparisons between male and female subjects

WP64

Qualitative perfusion assessment by CMR and invasive coronary angiography is not enough when evaluating patients with coronary artery disease - a cardiac positron emission tomography study

Shahnaz Akil, Master of Science[1]Fredrik Hedeer, MD[2], Marcus Carlsson, MD, PhD[3], Håkan Arheden, MD, PhD[4], Jenny Oddstig, PhD[5], Cecilia Hindorf, PhD[5], Henrik Engblom, MD, PhD[6]

1. *Lund University, Lund University Hospital, Lund, Skane Lan, Sweden*
2. *Lund University, Skane Univeristy Hospital, Lund, Skane Lan, Sweden*
3. *Lund University, Department of Clinical Sciences Lund, Clinical Physiology, Skane University Hospital, Lund, Sweden, Skane Lan, Sweden*
4. *Lund University, Department of Clinical Sciences Lund, Clinical Physiology, Skane University Hospital, Lund, Sweden, Lund, Skane Lan, Sweden*
5. *Skane University Hospital, Lund, Skane Lan, Sweden*
6. *Lund University, Skane Lan, Sweden*

Background: Evaluation of stress-induced myocardial ischemia is essential and also recommended in ESC/AHA guidelines for decision making regarding revascularization, in patients with stable coronary disease. Still, coronary intervention is currently performed in many patients without prior assessment of myocardial perfusion. First-pass perfusion cardiac magnetic resonance (CMR) imaging is one of several methods currently available for qualitative assessment of myocardial perfusion distribution. Cardiac positron emission tomography (PET) is another method which enables assessment of absolute myocardial blood flow and coronary flow reserve (CFR). The aim of this prospective study was to relate findings on first-pass perfusion CMR and coronary angiography (CA) to regional CFR as assessed by cardiac PET, in patients with stable coronary artery disease.

Methods: Twenty-five patients with suspected stable ischemic heart disease, referred for CA with suspected coronary artery disease, performed adenosine stress/rest first-pass perfusion CMR (1.5 T) as well as ^{13}N-NH_3 cardiac PET on the same day, 1-4 weeks before CA. Angiographers were blinded to cardiac PET and CMR results. Presence of stress-induced ischemia in the LAD, LCX and RCA vessel territories was evaluated by CMR by qualitatively comparing the first-pass perfusion at stress and rest for perfusion defects. Presence of significant coronary stenosis by CA was visually evaluated by the angiographer performing the CA. CFR < 2.0 was considered pathological and was calculated by dividing stress by the rest regional myocardial blood flow in ml/min/g from the dynamically acquired cardiac PET images.

Results: There was significantly lower CFR in vessel territories with stress-induced myocardial ischemia by CMR compared to those with no regional stress-induced ischemia ($p< 0.001$, Figure 1a). Furthermore, there was significantly lower CFR in vessel territories supplied by arteries evaluated to have significant coronary stenosis compared to arteries with no significant stenosis ($p=0.01$, Figure 1b). There were, however, several vessel territories with decreased CFR but normal first-pass perfusion (26/64, 41%) and non-significant coronary stenosis (19/50, 38%). Furthermore, several coronaries that underwent intervention, after being evaluated as having significant stenosis, had a normal CFR (Figure 1b).

Conclusions: Qualitative assessment of myocardial perfusion by first-pass CMR and invasive angiography have limited diagnostic accuracy with regard to CFR. Thus, there is a need for quantitative assessment of myocardial perfusion by CMR to increase the diagnostic accuracy of this technique in patients with stable coronary artery disease.

http://www.ConferenceAbstracts.com/uploads/cfp2/attachments/LDFAIBDN/LDFAIBDN--205205-1-ANY.pdf

WP65

Prognostic significance of heart rate response to regadenoson during stress cardiovascular magnetic resonance imaging

Jennifer Jue, MDSimone Romano, MD, Brent White, MD, Raksha Indorkar, MD, Afshin Farzaneh-Far, MD, PhD

University of Illinois at Chicago, Chicago, IL

Background: Regadenoson is a selective adenosine receptor agonist, which is increasingly used as a coronary vasodilator during CMR stress perfusion imaging. Regadenoson also increases heart rate by both direct and indirect stimulation of the sympathetic nervous system via A2A receptor activation. It has been shown that cardiac autonomic dysfunction and decreased heart rate variability are associated with adverse outcomes in patients with CAD. We hypothesized that abnormal cardiac autonomic function as reflected by a decreased heart rate response to regadenoson may be a predictor of adverse cardiovascular outcomes in patients undergoing stress CMR and may provide additive prognostic information.

Methods: 303 consecutive patients referred for suspected myocardial ischemia underwent a CMR stress-rest perfusion protocol. Perfusion imaging was performed at 1-minute and 15-minutes after administration of 0.4 mg of regadenoson. Heart rate was measured just before (baseline) and during stress perfusion (peak). Heart rate response (HRR) was calculated as 100 x (peak stress heart rate – baseline heart rate)/(baseline heart rate). Patients were followed for occurrence of major adverse cardiac events (all-cause mortality, nonfatal myocardial infarction, late revascularization, and hospitalization for heart failure).

Results: Baseline characteristics of the study population are shown in Table 1. Median HRR was 33.8%. By Kaplan-Meier analysis, patients with HRR ≤ median experienced significantly more adverse cardiac events than patients with HRR > median (p=0.037) (Figure 1). Cox proportional hazard modeling showed that HRR was significantly associated with adverse cardiac events (Hazard ratio=1.23 per 10% decrease in HRR, p=0.04) even when adjusted to known clinical markers of cardiac autonomic dysfunction (age, diabetes, smoking) (Table 2).

Conclusions: A blunted heart rate response to regadenoson during stress CMR is a significant predictor of major adverse cardiac events.

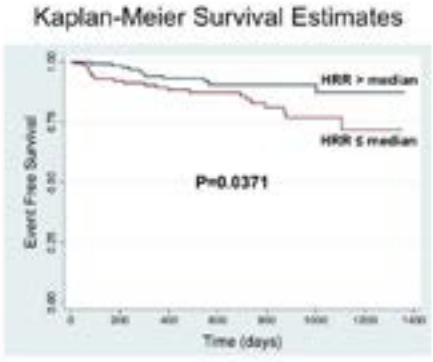

Baseline Patient Characteristics

Total Population (N = 303)	Characteristics
58.5 ± 13.5	Age (years)
45%	Male
30.6 ± 5.8	BMI (kg/m^2)
55%	Hyperlipidemia
45%	Smoking
31%	Known CAD
33%	Diabetes
76%	Hypertension
61.4 ± 12.7	LVEF (%)

Multivariable Analysis

P Value	Hazard Ratio (95% CI)	Variables
0.174	0.982 (0.956-1.008)	Age
0.337	1.413 (0.698-2.862)	Diabetes
0.721	1.165 (0.505-2.687)	Smoking
0.041	1.229 (1.008-1.494)	HRR

HRR = Heart rate response per 10% decrease

WP66

Safety and Feasibility of Breathing Maneuvers to detect Inducible Ischemia in Patients with Coronary Artery Disease - A Pilot Study using Oxygenation-Sensitive CMR

Dominik P. Guensch, MD[1]Kady Fischer, BHSc[2], Kyohei Yamaji, MD, PhD[3], Bernd Jung, PhD[4], Stephan Windecker, MD[5], Johannes Heverhagen, PhD, MD[6], Balthasar Eberle, MD[7], Matthias G. Friedrich, MD[8]

1. *Department of Anesthesiology and Pain Therapy / Institute for Diagnostic, Interventional and Pediatric Radiology, Bern University Hospital, Inselspital, University of Bern, Switzerland, Bern, Bern, Switzerland*
2. *McGill University Health Center, Montreal, PQ, Canada*
3. *Inselspital, Bern, Switzerland*
4. *Inselspital Bern, Institute for Diagnostic, Interventional and Pediatric Radiology, Bern, Switzerland*
5. *Department Cardiology, University Hospital Bern, Bern Switzerland, Bern, Bern, Switzerland*
6. *University of Bern, Bern, Switzerland*
7. *Department of Anesthesiology, Inselspital / University Hospital Bern, Bern, Bern, Switzerland*
8. *McGill University Health Centre, PQ, Canada*

Background: Oxygenation-sensitive (OS-)CMR is an emerging technique that uses the BOLD effect to detect changes in myocardial oxygenation. Recently, the vasomotor effect of breathing maneuvers has been proposed as an alternative to pharmacologic vasodilators in controlled animal models as well as in human studies to investigate changes in myocardial oxygenation in different pathologies. In an animal model hyperventilation (hypocapnic vasoconstriction) followed by a breath-hold (hypercapnic vasodilation) has been shown to be able to detect acute regional ischemia and has also been successfully performed in obstructive sleep apnea syndrome patients. The aim of this study is to assess if combined vasoactive breathing maneuvers can be performed in patients with coronary artery disease (CAD) to detect changes in myocardial oxygenation.

Methods: Six healthy volunteers and seven multi-vessel CAD patients (stenosis of 50-70% by quantitative coronary angiography, QCA) performed a controlled 60s hyperventilation followed by maximal apnea in a clinical 3T scanner. After a baseline oxygenation-sensitive cine sequence had been acquired in a basal and mid-ventricular short axis slice, images were recorded during the entire breath-hold. Changes in myocardial oxygenation were calculated as a %-change between the baseline and after hyperventilation and changes in SI during apnea were related to post-hyperventilation images. Global changes in myocardial oxygenation were compared to healthy controls and intra-individual changes were assessed between stenosed and healthy remote myocardium in the CAD patients.

Results: Myocardial oxygenation in healthy volunteers significantly decreased after 60s hyperventilation and increased after 30s of apnea (Fig. 1, *p < 0.05). These effects were significantly attenuated in CAD patients (#p < 0.05). One patient showed an oxygenation response similar to that of healthy subjects. Four patients showed a regional oxygenation deficit, while 2 patients showed a global decrease in SI (Fig. 2). The regional decrease in myocardial oxygenation during apnea can be explained by a hypercapnic myocardial steal in the affected territories caused by apnea. Participants only reported three types of adverse effects during the breathing maneuvers: tingling in the extremities (healthy: n=2, CAD: n=2), temporary headache (healthy: n=1) and dizziness (healthy: n=1), while three healthy participants and five CAD patients reported no side effects. The breath-hold time in the CAD patients was comparable to that of the controls (healthy 63+25s, CAD 69+37s). However, 30s of apnea were sufficient to unmask oxygenation deficits.

Conclusions: Breathing maneuvers can potentially identify abnormal oxygenation responses in patients with coronary artery disease. Hyperventilation and breath-holding appear to be associated with minimal side effects in our preliminary sample.

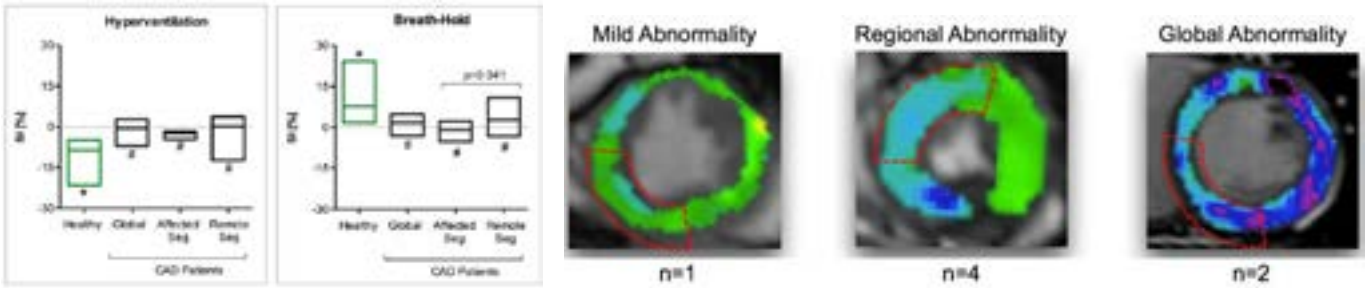

WP67

Multi-fold Amplification of Myocardial BOLD Sensitivity Through Coronary Relaxation Mapping Following Regadenoson Injection: Early Findings

Hsin-Jung Yang, PhD[1] Jane Sykes, BS[2], John Butler, BSc MRT(MR)[3], Damini Dey, PhD[4], Xiaoming Bi, PhD[5], Behzad Sharif, PhD[6], Ivan Cokic, MD[4], Sotirios Tsaftaris, PhD[7], Debiao Li, PhD[8], Piotr Slomka, PhD[4], Frank S Prato, PhD[9], Rohan Dharmakumar[10]

1. *Cedars Sinai Medical Center, Los Angeles, CA*
2. *Lawson Health Research Institute, ON, Canada*
3. *Lawson Health Research Institute, London, ON, Canada*
4. *Cedars Sinai Medical Center, CA*
5. *Siemens Healthcare, CA*
6. *Cedars-Sinai Medical Center, Los Angeles, Los Angeles, CA*
7. *The University of Edinburgh, Scotland, United Kingdom*
8. *Biomedical Imaging Research Institute, Cedars-Sinai Medical Center, Los Angeles, CA, CA*
9. *Lawson Health Research Institute, University of Western Ontario, ON, Canada*
10. *Cedars-Sinai Medical, CA*

Background: In the past two decades BOLD CMR has seen major advances. Yet, the reliability of BOLD CMR remains a major weakness for clinical use. A key unresolved obstacle with BOLD CMR is the artifactual signal changes that are typically observed during vasodilator stress. We hypothesized that if BOLD images could be repeatedly acquired under stress, they could be used to improve the reliability of BOLD CMR. We tested our hypothesis by acquiring multiple BOLD images post regadenoson (which extends vasodilation to tens of minutes) and estimate the BOLD response with a coronary relaxation model (CRM) based on the pharmacokinetics of regadenoson. We validated our findings with $^{13}N\text{-}NH_3$ PET perfusion images.

Methods: Intact (n=7) and infarcted (n=2) dogs were studied in a PET/MR system. BOLD (T_2 maps), LGE and $^{13}N\text{-}NH_3$ PET images were acquired pre- and post-regadenoson administration (p.r.a). T_2 maps p.r.a were repeatedly acquired over 30 mins and were registered to T_2 maps at rest. These time-dependent T_2 maps were then used to model the coronary relaxation as $T_2(t)=T_{2o}+\Delta T_{2max}\exp(-t/\tau)$, where T_{2o}, ΔT_{2max} and τ are fit parameters with $T_{2o}=T_2$ at rest; ΔT_{2max}=maximal T_2 change from rest; and τ=time constant of coronary relaxation. Maximum BOLD response from CRM was estimated ($MBR_{CRM}=\Delta T_{2max}/T_{2o}x100\%$) and compared to conventional myocardial BOLD response [$MBR_{con}= (T_2^{2min}\text{-}Rest\ T_2)/Rest\ T_2 x100\%$, where T_2^{2min}= mycoardial T_2 at 2 min p.r.a and *Rest* T_2=T_2 prior to regadenoson injection] using a regression model. In infarcted dogs, affected zones were identified using LGE. BOLD contrast-to-noise ratio between remote and affected zones (CNR= $(\mu MBR_{Remote}-\mu MBR_{Affect})/\sigma MBR_{Remote}$, where μ and σ are the mean and std dev) were estimated for MBR_{CRM} and MBR_{con} and compared. MBRs were validated with perfusion reserve from PET (MPR).

Results: In intact dogs, T_2 dynamics was nicely fitted with CRM (R=0.92 ±0.06). Parameters estimated from CRM (T_{2o}:44.2±6.7ms; ΔT_{2max}:14.7±5.8ms; τ:35.5±26.8min) were in agreement with previous reports. Both MBRs (MBR_{CRM}=27±16% and MBR_{con}=12±6%) were consistent with p.r.a PET (MPR=3.0±0.6). MBR_{CRM} and MBR_{con} were highly correlated(R=0.93; $MBR_{CRM}=2.83MBR_{con}-0.27$, indicating that MBR_{CRM} was ~2.8-fold higher than the MBR_{con}. In infarcted dogs, significantly higher MBRs in the remote and lower MBRs in the affected regions were observed with both methods (Remote: MBR_{CRM}=27±6%, MBR_{con}=15±5%; Affected: MBR_{CRM}=1±10%, MBR_{con}=5±7%; both MPR_{remote}=3.7±0.6; $MPR_{affected}$=1.9±0.7;). Mean CNR based on CRM were ~2-fold larger than the conventional approach (CNR_{CRM}=3.7±0.6; CNR_{con}=1.9±0.7).

Conclusions: Repeatedly acquired BOLD CMR p.r.a can be used to significantly improve the reliability limitations of current myocardial BOLD CMR.

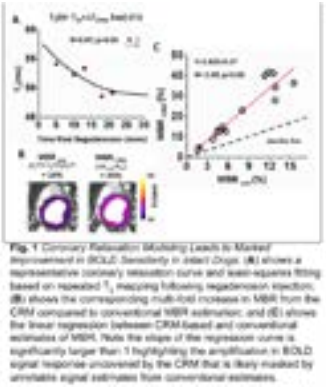

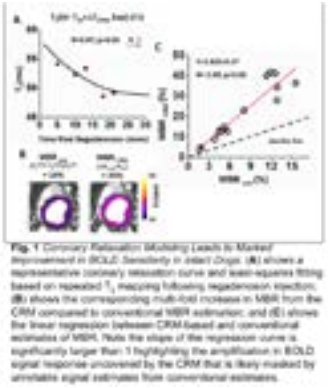

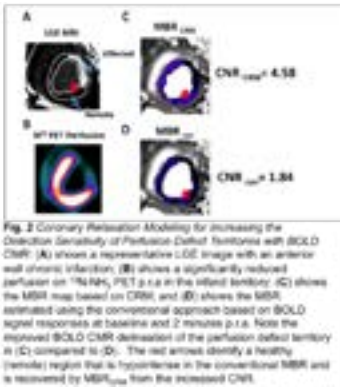

WP68

Prognostic value of perfusion cardiovascular magnetic resonance

Eva Sammut, MD[1] Adriana Villa, MD[2], Gabriella Di Giovine, MD[3], Luke H. Dancy, MD[4], Filippo Bosio, Radiographer[5], Thomas Gibbs[3], Swarna Jeyabraba[3], Susanne Schwenke, Dipl-Stat[6], Steven Williams, MD PhD[7], Khaled Alfakih, MD[3], Tevfik Ismail, PhD MRCP[8], Reza Razavi, MD[3], Amedeo Chiribiri, MD, PhD[2]

1. *King's College London / Bristol Heart Institute, Bristol, England, United Kingdom*
2. *King's College London, England, United Kingdom*
3. *Kings College London, England, United Kingdom*
4. *Kings College Hospital, London, England, United Kingdom*
5. *Kings College London, London, England, United Kingdom*
6. *SCO:SSiS, Berlin, Germany*
7. *Kings College Londin, England, United Kingdom*
8. *St. Thomas' Hospital, London; King's College London, England, United Kingdom*

Background: The use of cardiac magnetic resonance (CMR) continues to increase due to its suitability for multi-parametric assessment of patients with known or suspected coronary artery disease. Specifically, perfusion CMR is increasingly used to identify myocardial ischemia with studies demonstrating non-inferiority to other techniques. However, there are limited data on the prognostic value of visual assessment of myocardial ischemic burden by CMR and no previous prognostic studies on quantitative perfusion CMR analysis. In this study we sought to evaluate the prognostic utility of visual and quantitative CMR ischemic burden and furthermore to assess the validity of consensus-based ischemic burden thresholds in the setting of CMR.

Methods: Patients with suspected coronary artery disease (CAD) referred for adenosine-stress perfusion CMR were included (n=395, 70% male, age 58±13 years). The primary endpoint was a composite of cardiovascular death, non-fatal myocardial infarction, aborted sudden death, and revascularization after 90 days. Patients were censored at the point of last follow up. Perfusion scans were assessed with both visual and quantitative analysis, using a threshold of either >2 segments or >10% myocardium with myocardial perfusion reserve (MPR)

Results: After a median 460 days [IQR 190-869] follow-up, 52 patients reached the primary endpoint. On univariate analysis, there were significant differences using both visual and quantitative perfusion analysis when comparing patients with versus without events (HR visual 3.009 (1.506-6.012) versus quantitative 16.048 (6.898-37.336, p=0.002 versus p=

Conclusions: This study is the first to support the use of ischemic burden at accepted consensus-based thresholds by perfusion CMR for prognostic evaluation of patients with suspected CAD. We show that the use of perfusion CMR provides additional prognostic information over well-recognized variables and suggests superiority of a quantitative approach. This study represents an important step forward in the translation of quantitative analysis to the clinical setting.

http://www.ConferenceAbstracts.com/uploads/cfp2/attachments/LDFAIBDN/LDFAIBDN--223039-1-ANY.pdf

P value	Total (N=395)	Event (N=52)	No event(N-343)	Variable
0.019*	58.3+-13.1	63.3+-11.8	57.6+-13.2	Age, years
<0.001*	277 (70.1)	51 (98.1)	226 (65.9)	Gender, male (%)
0.612	1.96+-0.23	2.00+-0.20	1.95+-0.23	Body mass index (kg/m^2)
0.575	78 (19.7)	12 (23.5)	66 (19.2)	Diabetes mellitus (%)
0.368	235 (59.5)	33 (66.7)	201 (58.6)	Hypertension (%)
0.025*	216 (54.7)	36 (72)	180 (52.5)	Hypercholesterolaemia (%)
0.849	73 (18.5)	10 (19.2)	63 (18.4)	Smoker (%)
0.100	46 (11.6)	10 (19.2)	36 (10.5)	Atrial fibrillation (%)
0.804	40 (10.1)	4 (7.7)	36 (10.5)	Revascularisation <90 days (%)
0.121	60 (52-66)	59 (44-67)	60 (53-66)	LV Ejection Fraction (%)
0.790	79 (67-91)	79 (65-96)	78 (67-91)	Indexed LV EDV (ml/m$^{2)}$
0.374	31 (24-41)	32 (22-47)	30 (24-40)	Indexed LV ESV (ml/m$^{2)}$
0.075	56 (47-56)	115 (97-134)	45 (46-66)	Indexed LV mass (g/m$^{2)}$
<0.001*	17.2+-29.7, 0-25 (0)	26.9+-28.2, 0-50 (25)	14.7+-29.2, 0-12.5 (0)	Visual Ischaemic Burden (%)
<0.001*	8.35+-16.7, 0-8.5 (0)	25.1+-22.0, 1.3-39.0 (23.4)	6.09+-14.6, 0-4.9 (0)	MPR Ischaemic Burden (%)

Univariate predictors of outcome

P value	*Hazard ratio (95% CI)*	
		Univariate
0.006*	1.033 (1.010-1.057)	Age 1.033 (1.010-1.057)0.006*
0.002*	0.201 (0.075-0.542)	Gender
0.102	0.983 (0.963-1.003)	LV Ejection Fraction
<0.001*	0.343 (0.196-0.600)	Late Gadolinium Enhancement
0.002*	3.009 (1.506-6.012)	Visual Ischaemic Burden
<0.001*	16.048 (6.898-37.336)	MPR Ischaemic Burden
		Multivariate
0.02* 0.002* 0.038* <0.001*	1.027 (1.004-1.051) 0.212 (0.078-0.573) 1.847 (1.036-3.292) 4.125 (1.934-8.799)	Age Gender Late Gadolinium Enhancement Visual Ischaemic Burden
0.100 0.007* 0.009* <0.001*	1.020 (0.996-1.043) 0.257 (0.095-0.696) 2.184 (1.214-3.931) 12.87 (4.965-33.365)	Age Gender Late Gadolinium Enhancement MPR Ischaemic Burden

WP69

Whole-Heart Quantitative Adenosine Stress CMR with Motion-Compensated CS Reconstruction Accurately Detects CAD: Initial Clinical Evaluation

Michael Salerno, MD, PhD[1] Yang Yang, PhD[1], Stephen C. McHugh, MS[1], Eric Holland, M.D.[1], Peter W. Shaw, MD[2], Jonathan A. Pan, BS[3], Craig H. Meyer, PhD[3], Angela Taylor, MD[1], Christopher M. Kramer, MD[1]

1. *University of Virginia, VA*
2. *Berkshire Medical Center, Lenox, MA*
3. *University of Virginia, Charlottesville, VA*

Background: Adenosine stress CMR imaging has become an important tool for diagnosing coronary artery disease (CAD). However, clinically available techniques are limited by dark-rim artifact, have limited spatiotemporal resolution, and incomplete ventricular coverage. We have recently demonstrated a dual-sequence variable density (VD) spiral pulse sequence which can acquire 8 short-axis slices with 2mm in-plane resolution at heart rates up to 125 bpm providing whole-heart quantitative assessment of perfusion. The purpose of this study was to assess the clinical performance of this new technique to detect obstructive CAD using both visual and quantitative assessment.

Methods: CMR perfusion imaging was performed during adenosine stress (140µg/kg-min) and at rest on a Siemens 1.5T Avanto scanner in 20 subjects with chest pain scheduled for coronary angiography (CA) Images were acquired during injection of 0.075mmol/kg Gd-DTPA at 8 short-axis locations using a 2D saturation recovery (SR) accelerated VD spiral pulse sequence and reconstructed using rigid-motion compensated L1-SPIRiT. Quantification was performed using Fermi-function deconvolution in a custom MATLAB program. A significant stenosis was defined as >50% by quantitative CA (QCA). Two blinded reviewers evaluated the spiral perfusion images for the presence of adenosine-induced perfusion abnormalities and assessed image quality using a 5 point scale (1-poor to 5-excellent).

Results: Patients had a mean age of 62±11, 80% were male, 45% had a smoking history 30% had diabetes, 60% had hypertension and 85% had hyperlipidemia. 30% of the patients had known CAD. QCA demonstrated obstructive CAD in 12 patients (60%). Figure 1 shows (a) stress and (b) rest spiral perfusion images from a subject who had normal cardiac function and no LGE. Perfusion defects are seen in all territories consistent with 3 vessel disease at CA (Fig 1 c-d). Pixel-wise quantification of perfusion (Fig 2) demonstrated reduced stress flow in all territories in this subject. Figure 3 shows (a) stress and (b) rest perfusion images, and (c) stress and (d) rest quantitative perfusion maps from another subject who had a 100% stenosis of the mid LAD. For the detection of a 50% stenosis by QCA the average sensitivity, specificity, and accuracy of the two readers were 88%, 86%, and 87% respectively, with a positive predictive value (PPV) and negative predictive value (NPV) of 91% and 80% respectively. The overall image quality score was 4.5±0.8. Global quantitative stress perfusion performed similarly to visual analysis on a per-patient basis with a sensitivity, specificity, and accuracy of 83%, 86%, and 81%. PPV and NPV were 91% and 75% respectively.

Conclusions: Clinical assessment of the diagnostic performance of whole-heart spiral perfusion imaging using motion compensated compressed sensing for detection of CAD demonstrated good image quality, minimal motion artifacts, and high diagnostic accuracy for both visual and quantitative evaluation.

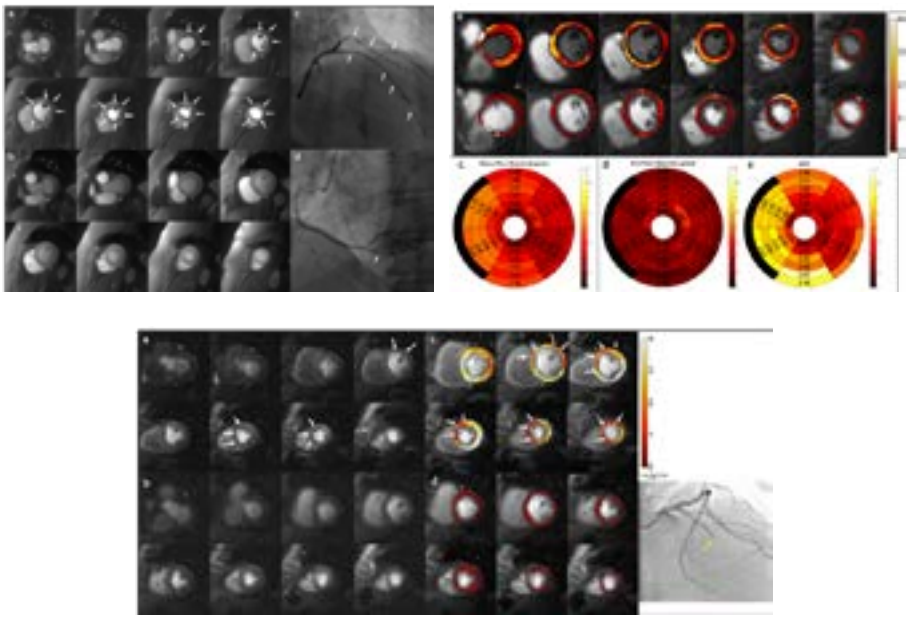

WP70

Contrast free assessment of vasodilator response using myocardial T2 BOLD and Arterial Spin Labeled CMR

Nilesh R. Ghugre, PhD[1]Hung Phi Do, MSC[2], Venkat Ramanan, MSc[3], Krishna Nayak, PhD[2], Graham Wright, PhD[4]

1. *Sunnybrook Research Institute, University of Toronto, Toronto, ON, Canada*
2. *University of Southern California, Los Angeles, CA*
3. *Sunnybrook Research Institute, Toronto, ON, Canada*
4. *Sunnybrook Research Institute, University of Toronto, ON, Canada*

Background: Following acute myocardial infarction (AMI), many patients experience compromised microvascular integrity and function. This is manifested in the form of 'no-reflow' or microvascular obstruction (MVO) in the infarcted territory and as impaired vasodilator response in the remote myocardium. Our study explored the utility of two contrast free CMR techniques to assess vasodilator response in a porcine model of AMI: Arterial spin labeled CMR (ASL-CMR) to quantify myocardial blood flow (MBF) and a T2-based blood-oxygen-level-dependent (T2-BOLD) approach to detect oxygenation changes.

Methods: Animals were imaged on a 3T scanner in healthy state (N=13) and at 1-2 weeks following a 90 min reperfused LAD occlusion (N=4). ASL-CMR was performed using a flow-sensitive alternating inversion recovery (FAIR) labeling scheme and SSFP image acquisition. T2-BOLD was achieved using a validated T2-prepared spiral imaging sequence. ASL-CMR and T2-BOLD were acquired on two mid-ventricular slices in each animal. The two sequences were repeated following an intravenous injection of Dipyridamole to assess vasodilator function. First-pass perfusion and LGE imaging were performed following injection of gadolinium-DTPA to identify perfusion abnormalities and necrosis. Segmental MBF, myocardial perfusion reserve ($MPR=MBF_{stress}/MBF_{rest}$), T2 values and %T2 change ($100*[T2_{stress}-T2_{rest}]/T2_{rest}$) were reported as mean±SD. For ASL, segments with temporal signal-to-noise ratio < 2 were excluded from the analysis.

Results: In healthy animals, global stress MBF and T2 were significantly elevated compared to rest: (MBF_{stress} = 1.4±0.5 vs. MBF_{rest} = 0.95±0.5 ml/g/min; p< 0.0001); and ($T2_{stress}$ = 44.6±2.7 vs. $T2_{rest}$ = 39.9±2.5 ml/g/min; p< 0.0001). A global MPR of 1.9±1.2 was found equivalent to a global %T2 change of 12.0±5.4. The rest-stress response for both perfusion and T2-BOLD were consistent with prior findings in the literature. **Figure 1** shows the regional stress response in all the AHA-defined segments. At week 1 post-AMI, all animals exhibited a perfusion deficit on first-pass imaging and an anteroseptal infarction with MVO on LGE; this is consistent with a 90 min LAD ischemia-reperfusion model. Both MBF and T2 measurements indicated a blunted stress response in the infarcted region compared to remote tissue (see **Figure 2**), indicating severe ischemia-induced microvascular damage. The vasodilator response assessed using both contrast free techniques agreed well with the region of perfusion abnormality on first pass imaging and MVO on LGE.

Conclusions: This study demonstrates that ASL-CMR and T2-BOLD techniques offer a contrast free alternative to evaluate vasodilator function in heart disease. Taken together, they can potentially provide complementary insights into the myocardial remodeling process; particularly in the remote territory, which develops hypertrophy and fibrosis in the high-risk patients in the chronic stage.

http://www.ConferenceAbstracts.com/uploads/cfp2/attachments/LDFAIBDN/LDFAIBDN--219275-1-ANY(1).pdf

http://www.ConferenceAbstracts.com/uploads/cfp2/attachments/LDFAIBDN/LDFAIBDN--219275-2-ANY(2).pdf

WP71

Stress Cardiac MRI for Evaluation of Nonspecific Allograft Dysfunction in Heart-Transplant Patients

Paul J. Kim, MD[1]Francisco Contijoch, PhD[2], Reeve Ingle, PhD[3], Albert Hsiao, MD, PhD[2], Juan Santos, Ph.D.[3], Darrin Wong, MD[2], Andrew Kahn, MD,PhD[2], Michael Pham, MD[4], Patricia Nguyen, MD[4]

1. *University of California, San Diego, San Diego, CA*
2. *University of California, San Diego, CA*
3. *HeartVista, CA*
4. *Stanford University, CA*

Background: Despite our improved understanding of rejection, a significant percentage of heart-transplant patients have graft dysfunction with reduced left ventricular ejection fraction (LVEF) without a clear cause. These patients are categorized as nonspecific graft dysfunction (NGD) and represent 20 to 36 percent of patients with graft dysfunction. Cardiac MRI (CMR) can provide a comprehensive evaluation of the transplanted heart including extracellular volume (ECV), myocardial scar via late gadolinium enhancement (LGE), and myocardial perfusion reserve. We hypothesized patients with NGD may show decreased myocardial perfusion reserve due to undiagnosed microvascular allograft vasculopathy. Additionally, we expect the ECV and myocardial scar to be increased in NGD patients compared to those with normal graft function.

Methods: 18 heart-transplant patients were enrolled over 6 months that comprised of three groups: normal graft function (n=8), NGD (n=6) and graft dysfunction due to allograft vasculopathy (n=4). Stress CMR with regadenoson that included T1 mapping and LGE was performed. ECV and LGE are expressed in terms of percent myocardial mass. Patients with signs/symptoms of myocardial ischemia, recent biopsy proven acute rejection and known contraindications to stress CMR were excluded.

Results: As expected, both NGD and allograft vasculopathy patients demonstrated decreased LVEF that was significant compared to those with normal graft function (52±8% and 52±3% vs 61±5%, $P < 0.05$). NGD patients showed significantly increased myocardial scar compared to normal (5.7±2.6% vs 1.8±0.8%, $P < 0.05$). Allograft vasculopathy patients showed a trend towards increased myocardial scar (4.1±2.1% vs 1.8±0.8%, P=0.10). There was a trend towards increasing ECV in NGD and allograft vasculopathy patients. NGD patients demonstrated a trend towards decreased rest perfusion compared to normal (6.65±2.38 vs 7.67±2.91, NS). Allograft vasculopathy patients did show significantly decreased rest perfusion compared to normal (3.04±2.02 vs 7.67±2.91, $P < 0.05$). After stress, both NGD and allograft vasculopathy patients showed significantly decreased perfusion compared to control (18.67±5.35 and 11.37±7.68 vs 33.53±12.38, $P < 0.05$). Accordingly, myocardial perfusion reserve was significantly decreased in NGD patients compared to normal (3.2±1.3 vs 4.6±0.7, $P < 0.05$).

Conclusions: In addition to demonstrating decreased LVEF, patients with NGD show decreased myocardial perfusion reserve. This finding suggests that patients with NGD may have low-level allograft vasculopathy detectable by stress CMR but not by angiography or intravascular ultrasound, which may contribute to graft dysfunction. Furthermore, patients with NGD show significantly increased myocardial scar compared to normal subjects, supporting this hypothesis.

http://www.ConferenceAbstracts.com/uploads/cfp2/attachments/LDFAIBDN/LDFAIBDN--219520-1-ANY(2).pdf

http://www.ConferenceAbstracts.com/uploads/cfp2/attachments/LDFAIBDN/LDFAIBDN--219520-2-ANY(1).pdf

http://www.ConferenceAbstracts.com/uploads/cfp2/attachments/LDFAIBDN/LDFAIBDN--219520-3-ANY.pdf

WP72

Splenic 'switch-off' as a marker of inadequate adenosine stress using fractional flow reserve to define flow-limiting coronary artery disease and its relationship with serum caffeine levels

David Corcoran, BSc (Hons), MBChB, MRCP[1] Kenneth Mangion, MD[2], Andrew Saul, BAppSci(Medical Radiation Science)[3], Colin Berry, PhD FRCP[2], Keith G. Oldroyd, MD (Hons); FRCP[3], Stuart Watkins, MD, FRCP[4]

1. *University of Glasgow, Scotland, United Kingdom*
2. *University of Glasgow, Glasgow, Scotland, United Kingdom*
3. *Golden Jubilee National Hospital, Scotland, United Kingdom*
4. *Golden Jubilee National Hospital, Glasgow, Scotland, United Kingdom*

Background: Magnetic Resonance Myocardial Perfusion Imaging (MRMPI) is well-established for the diagnosis of myocardial ischemia. Sensitivity of MRMPI is limited by the adequacy of vasodilator stress with adenosine. Adenosine results in reduced splenic perfusion, and splenic 'switch-off' has been proposed as a marker of adequate vasodilator stress. Stress perfusion studies have traditionally been compared to invasive coronary angiography (ICA). However, there is a well-recognized discordance between the functional significance of a coronary stenosis with fractional flow reserve (FFR) measurement and degree of stenosis (%) on ICA.

Methods: 103 patients with chest pain referred for ICA were enrolled. MRMPI (Siemens Sonata 1.5T) was performed prior to ICA. Stress and rest acquisitions were obtained 20 minutes apart. Vasodilator stress was induced using IV adenosine (140µg/kg/min), and hemodynamic and symptomatic responses were recorded. Venous blood was obtained for serum caffeine levels prior to ICA and MRMPI. At ICA, FFR was measured in at least the 3 main epicardial coronary arteries, with values ≤0.80 indicative of significant flow-limiting CAD.

Myocardial perfusion defects were assessed qualitatively by 2 observers blinded to the invasive data. Splenic switch-off was assessed qualitatively by 2 different blinded observers (Figure). Semi-quantitative indices of splenic switch-off were measured offline (Medis QMass). ROIs were contoured within the splenic tissue on the stress and rest perfusion sequences, and SI/time curves derived. Percentage SI reduction from rest-to-stress, and stress-to-rest SI ratios were calculated. Data were compared using the Chi-square test. A p-value < 0.05 was considered significant.

Results: Of the 103 patients (Table), 101 (98%) had complete FFR data, the spleen was not visible in 16 (16%) MRMPI scans, leaving 85 patients with complete data. 78 patients had concordant FFR and MRMPI results (i.e. true positive/true negative). 7 participants had false negative scans, with no false positives.

Significantly more participants with false-negative scans demonstrated failed splenic switch-off assessed qualitatively (p=0.001). Mean splenic SI reduction from rest-to-stress and stress-to-rest SI ratios were reduced in participants demonstrating splenic switch-off compared to those with failed switch-off (47.36% vs. 9.36% and 0.53 vs. 0.90 respectively). No significant relationship was demonstrated between dual hemodynamic/symptomatic response to adenosine (p=0.71), or detectable serum caffeine levels (p=0.58), and failed splenic switch-off.

Conclusions: Using FFR as the gold standard for the diagnosis of significant myocardial ischemia, failed splenic switch-off is an excellent sign of possible inadequate adenosine stress producing a false-negative perfusion scan result. Serum caffeine level alone was unable to explain the occurrence of failed splenic switch-off.

http://www.ConferenceAbstracts.com/uploads/cfp2/attachments/LDFAIBDN/LDFAIBDN--222597-1-ANY(2).pdf

Detectable serum caffeine level	Dual hemodynamic and symptomatic adenosine response	Stress-rest SI ratio	Percentage splenic SI reduction from rest-stress	Qualitative splenic switch-off	Patients (n=85)	MRMPI test result
8/43 (19%) 4/17 (24%)	39/43 (91%) 15/17 (88%)	0.53 0.83	47% 17%	Yes: 43 (72%) No: 17 (28%)	60 (71%)	True Positive
-	-	-	-	-	0 (0%)	False Positive
2/14 (14%) 1/1 (25%)	13/14 (93%) 4/4 (100%)	0.51 1.00	49% 0%	Yes: 14 (78%) No: 4 (22%)	18 (21%)	True Negative
0/1 (0%) 1/6 (17%)	1/1 (100%) 5/6 (83%)	0.53 0.97	47% 3%	Yes: 1 (14%) No: 6 (86%)	7 (8%)	False negative

Data are expressed as mean values for each group. SI = signal intensity.